NBSIR 83-2742

Photonuclear Data - Abstract Sheets 1955 - 1982 Volume XV (Thorium - Americium)

E. G. Fuller, Henry Gerstenberg

U.S. DEPARTMENT OF COMMERCE
National Bureau of Standards
National Measurement Laboratory
Center for Radiation Research
Gaithersburg, MD 20899

February 1986

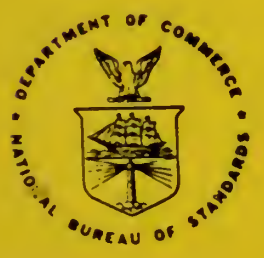

U.S. DEPARTMENT OF COMMERCE
NATIONAL BUREAU OF STANDARDS

NBSIR 83-2742

PHOTONUCLEAR DATA - ABSTRACT SHEETS 1955 - 1982 VOLUME XV (THORIUM - AMERICIUM)

E. G. Fuller, Henry Gerstenberg

U.S. DEPARTMENT OF COMMERCE
National Bureau of Standards
National Measurement Laboratory
Center for Radiation Research
Gaithersburg, MD 20899

February 1986

U.S. DEPARTMENT OF COMMERCE, Malcolm Baldrige, *Secretary*
NATIONAL BUREAU OF STANDARDS, Ernest Ambler, *Director*

TABLE OF CONTENTS

Photonuclear Data-Abstract Sheets
1955-1982

I. Introduction

As used in connection with this collection of data-abstract sheets, the term photonuclear data is taken to mean any data leading to information on the electromagnetic matrix element between the ground state and excited states of a given nuclide. The most common types of reactions included in this compilation are: (e,e'), (γ,γ), (γ,γ'), (γ,n), (γ,p), etc. as well as ground-state particle capture reactions, e.g. (α,γ_0). Two reactions which fit the matrix element criterion are not included in the compilation because of their rather special nature. These are heavy particle Coulomb excitation and the thermal neutron capture reaction (n,γ_0). While the energy region of particular interest extends from 0 to 150 MeV, papers are indexed which report measurements in the region from 150 MeV to 4 GeV. Most of the experiments listed are concerned with the excitation energy range from 8 to 30 MeV, the region of the photonuclear giant resonance.

The hierarchical grouping of the photonuclear data-abstract sheets within the file is by: 1. Target Element, 2. Target Isotope, and 3. by the Bibliographic Reference Code assigned to the paper from which the data on the sheet were abstracted. In this file, colored pages are used to mark the beginning and end of the sheets for each chemical element. A brief historical sketch of the element is given on the divider sheet marking the start of each section; the information for this sketch was derived from references such as the Encyclopaedia Britannica. In those cases where the sheets for a given element make up a major part of a volume, colored pages are also used to delineate sections pertaining to the individual isotopes of the element. Each of the sections of the file, as delineated by two colored divider sheets, represents a 27 year history of the study of electromagnetic interactions in either a specific nuclide or a specifc element.

The data-abstract sheets are filed under the element and/or isotope in which the ground-state electromagnetic transition takes place. For example, the abstract sheet for a total neutron yield measurement for a naturally occurring copper sample would appear in the elemental section of the copper file. On the other hand, a measurement of the ^{62}Cu 9.73 minute positron activity produced in the same sample by photons with energies below the three-neutron separation energy for ^{65}Cu (28.68 MeV) would be filed with the sheets for ^{63}Cu. Similarly a measurement of the ground-state neutron capture cross section in ^{12}C would be filed under ^{13}C while the corresponding ground-state alpha-particle capture cross section would be filed under ^{16}O.

At the end of this volume there is a master list of the abbreviations that have been used in the index section of the abstract sheets. The listings are those used in the final published index, Photonuclear Data Index, 1973-1981, NBSIR 82-2543, issued in August 1982 by the U. S. Department of Commerce, National Bureau of Standards, Washington, DC 20234. In some cases two notations are entered for the same quantity. The second entry is the abbreviation that was used in one or more of the earlier published editions of the index.

# THORIUM
Z=90

J. Berzelius, in 1815, obtained a material which he regarded as a new earth. He gave the oxide and metal names which intended to honor Thor, the ancient Scandinavian god of thunder. Seven years later he showed the "new earth" to be yttrium phosphate. Four years later, the Rev. H. Esmark discovered a black mineral on the island of Lövö in Norway; he gave a sample of the material to his father, Professor J. Esmark, a well known mineralogist. He in turn, not being able to identify the material, sent a sample of it to Berzelius. A chemical analysis by Berzelius showed it contained 60% of a new earth. This discovery of the new material called thorium, was announced by Berzelius in a publication in 1829.

TH
A=232

Little interest was shown in thorium until Auer von Welsbach patented the incandescent gaslight mantle in which thorium oxide played an important role. The brilliant white light from this mantle, when contrasted with the weak light from the flickering gas or kerosene lamp, was considered a major breakthrough in lighting technology. The mantle industry grew to its peak in the 20th century but decreased due to the advent of electricity and the electric lightbulb. A more recent use of thorium has been for the production of thorium–magnesium alloys for jet turbines and rockets. A few percent of thorium in such an alloy gives to the magnesium an increased strength that remains effective above normal temperatures.

TH
A=232

REF. L. E. Lazareva, B.S. Ratner and I.V. Shtranikh
J. Exper. Theoret. Phys. USSR 29, 274 (1955)
Soviet Phys. JETP 2, 301 (1956)

ELEM. SYM.	A	Z
Th	232	90

METHOD

REF. NO. 55 La 2 EGF

REACTION	RESULT	EXCITATION ENERGY	SOURCE		DETECTOR		ANGLE
			TYPE	RANGE	TYPE	RANGE	
G,F	RLY	THR-18.5	C	18.5	BF3-I		4PI

DELAYED NEUTRON

Delayed neutron 0.18±0.01% of total neutrons from bremsstrahlung absorption.

Ref. B.I. Gavrilov, L.E. Lazareva
Zhur. Eksp. i Teoret. Fiz. 30, 855 (1956);
Soviet Phys. JETP 3, 871 (1957)

Elem. Sym.	A	Z
Th	232	90

Method γ-Bremsstrahlung; synchrotron; BF_3 counter

Ref. No. 56 Ga 1 EGF

Reaction	E or ΔE	E_0	Γ	$\int \sigma dE$	Jπ	Notes (562)
(γ,xn)	5-27	14.5	5.6	6.33 MeV-b		

Figure 2: Photoneutron cross section σ_n, computed from the yield curves by the "photon difference method." "●" -- cross sections obtained in Ref. 9 [Nathans and Halpern, Phys. Rev. 93, 437 (1954)].

TABLE I. Fundamental characteristics of photoneutron cross sections.

Element	$E_{\sigma_n max}$ in mev	$\sigma_{n max}$ in barns	dart width in mev	$\frac{\int_{E_s}^{E_s+5} \sigma_n(E)dE}{5}$	$\frac{E_0}{\int_{E_s}^{E_0} \sigma_n(E)dE}$ on max
Copper	[illegible]	0.125	[illegible]	[illegible]	[illegible]
Zinc	[illegible]	0.[illegible]	[illegible]	[illegible]	8.1
Cadmium	[illegible]	0.[illegible]	[illegible]	[illegible]	8.4
Iodine	[illegible]	0.[illegible]	[illegible]	[illegible]	8.2
Platinum	[illegible]	0.[illegible]	[illegible]	[illegible]	8.6
Gold	[illegible]	0.[illegible]	[illegible]	[illegible]	7.6
Thallium	[illegible]	0.[illegible]	[illegible]	[illegible]	7.6
Bismuth	[illegible]	0.[illegible]	[illegible]	[illegible]	7.4
Thorium	[illegible]	0.[illegible]	[illegible]	[illegible]	8.0
Uranium	[illegible]	1.15	[illegible]	[illegible]	10.6

Ref. J.E. Gindler, J.R. Huizenga
Phys. Rev. 104, 425 (1956)

Elem. Sym.	A	Z
Th	232	90

Method: Chemical activity

Ref. No.: 56 Gi 1 | EGF

Reaction	E or ΔE	E_0	Γ	$\int \sigma dE$	Jπ	Notes
(γ,n)	Bremss.					
(γ,f)	8-20					

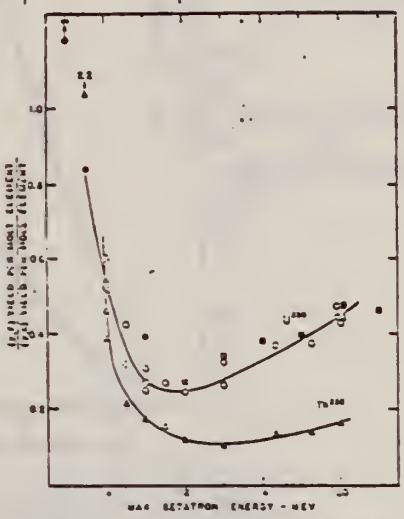

FIG. 1. Ratios of the total number of photofission events per mole element to the number of residual (γ,n) atoms per mole element as a function of maximum betatron energy. Uranium determinations: ○, x-ray, this work; ◎, probe target, this work; □, x-ray, reference 4. Thorium irradiations: ▲, x-ray, this work; △, probe target, this work. The broken circles represent uranium data having errors of approximately ±10% because of low U^{237} counting rates. The broken triangle represents a weighting error of ±25% in the determination of the thorium fission yield.

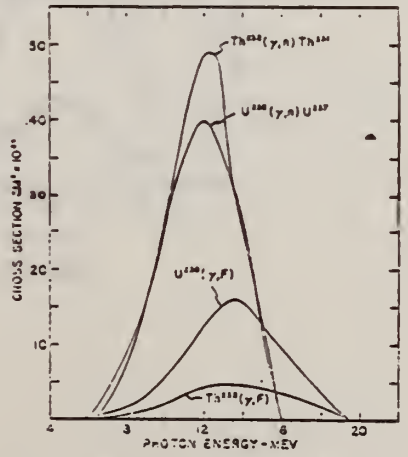

FIG. 2. Photoneutron and photofission cross sections of Th and U obtained from analysis of the corresponding activation functions of Fig. 3 by the photon difference method.

TABLE I. Characteristics of photofission and neutron emission excitation functions for thorium and uranium.

Reaction	σ_{max} (barns)	$E(\sigma_{max})$ (Mev)	Half-width[d] (Mev)	$\int \sigma dE$ (Mev barns)	Reference
$U^{238}(\gamma,F)$[a]		16[e]	5[e]		a
$U^{238}(\gamma,F)$		15	8[e]		b
$U^{238}(\gamma,F)$		14.6	6.8		i
$U^{238}(\gamma,F)$	0.13	14	7.6	1.2(0–20)	j
$U^{238}(\gamma,F)$	0.125	14	8.8	1.1(0–24)	k
$U^{238}(\gamma,F)$	0.20±0.03	14.0	6.7	1.71±0.14(0–25)	g
$Th^{232}(\gamma,F)$	0.051±0.007	14.1	7.0	0.64±0.06(0–25)	l
$U^{238}(\gamma,n)U^{237}$	0.53	11	3.6	2.6(0–20)	g
$U^{238}(\gamma,n)$[b]		15.8	7.1		i
$U^{238}(\gamma,N)$	1.8	13	(5)	11.4(0–27.5)	m
$U^{238}(\gamma,N)$	0.96	14	6.4	7.1(0–25)	n
$U^{238}(\gamma,N)$	1.15±0.15	14.9	6.8	12.0±1.0(0–28)	l
$Th^{232}(\gamma,N)$	0.80±0.10	14.5	5.6	6.61±0.60(0–28)	l

[a] (γ,F) indicates all processes initiated by a photon in which fission occurs.

[b] (γ,N) indicates the total number of neutrons produced by the nuclear absorption of a photon. Because of the low probability of charged particle emission, the cross section for the (γ,N) process may be represented by

$$\sigma_{(\gamma,N)} = \sigma_{(\gamma,n)} + 2\sigma_{(\gamma,2n)} + 3\sigma_{(\gamma,3n)} + \cdots + \nu\sigma_{(\gamma,F)},$$

where ν represents the average number of neutrons produced by a photon-excited nucleus which eventually fissions. These neutrons may be emitted before fission occurs, may be a result of the fission process, or may be a combination of the two.

[c] Although the authors of reference 1 state that "no significance can be given to the shape of the curve of σ vs E_0" the characteristics of their excitation function, given above, compare favorably with later analyses.

[d] Half-width is defined as the full width at half σ_{max}.

[e] This value represents the half-width of the sigma function of reference 2.

[f] Integration limits in Mev are given in parentheses following the integrated value.

[g] See reference 1.
[h] See reference 2.
[i] See reference 3.
[j] See reference 4.
[k] See reference 5.
[l] See reference 6.
[m] See reference 7.
[n] See reference 8.

[a] G. C. Baldwin and G. S. Klaiber, Phys. Rev. 71, 3 (1947).
[b] W. H. Ogle and J. McElhinney, Phys. Rev. 91, 344 (1951).
[c] R. B. Anderson and R. R. Duffield, Phys. Rev. 85, 728 (1952); R. R. Anderson, M. S. thesis, University of Illinois, 1951 (unpublished).
[d] R. B. Duffield and J. R. Huizenga, Phys. Rev. 89, 1042 (1953).
[e] Katz, Kavanagh, Cameron, Bailey, and Spinks, Phys. Rev. 99, 95 (1955).
[f] Lazareva, Gavrilov, Valuev, Zatsepina, and Stavinsky, *Conference of the Academy of Sciences of the U.S.S.R. on the Peaceful Uses of Atomic Energy*, July 1–5, 1955, Session of the Division of Physical and Mathematical Sciences (Consultants Bureau, New York, 1955), p. 217.
[g] T. W. Jones and K. M. Terwilliger, Phys. Rev. 91, 699 (1953).
[h] R. Nathans and J. Halpern, Phys. Rev. 93, 437 (1954).

REF.

V. A. Korotkova, P. A. Cherenkov and I. V. Chuvilo
Dokl. Akad. Nauk SSSR 106, 633 (1956)
Soviet Phys. Doklady 1, 77 (1956)

ELEM. SYM.	A	Z
Th	232	90

METHOD

REF. NO.	
56 Ko 2	EGF

REACTION	RESULT	EXCITATION ENERGY	SOURCE		DETECTOR		ANGLE
			TYPE	RANGE	TYPE	RANGE	
G,F	ABX	8-24	C	8-24	ION-I		

Monitor-graphite ion chamber

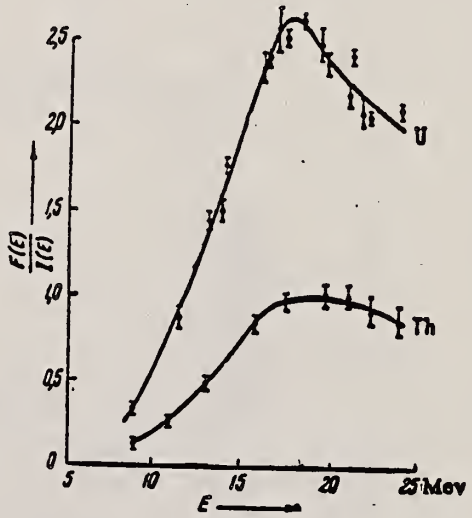

Figure 1.

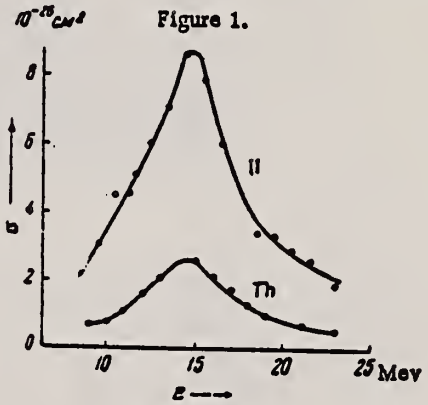

Figure 2.

REF.

V. A. Korotkova, P. A. Cherenkov, I. V. Chuvilo
Dokl. Akad. Nauk SSSR 106, 811 (1956)
Soviet Phys. Doklady 1, 104 (1956)

ELEM. SYM.	A	Z
Th	232	90

METHOD

REF. NO.	
56 Ko 3	EGF

REACTION	RESULT	EXCITATION ENERGY	SOURCE		DETECTOR		ANGLE
			TYPE	RANGE	TYPE	RANGE	
G,F	SPC	THR - 18	C	18	ION-D	50-100	4PI

E_o = 17.6 MeV

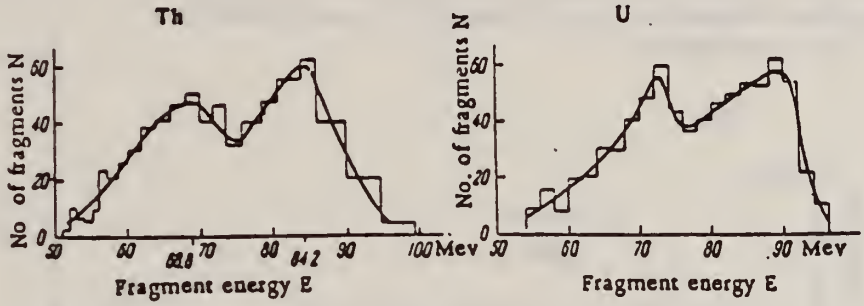

Figure 1.

Table 1
Most Probable Energy Values (in Mev)

Element	E_L	E_H	E_S
Uranium	86.5 ± 4	72.5 ± 3	159
Thorium	84.2 ± 4	68.8 ± 4	153

REF.	ELEM. SYM.	A	Z
L. Katz, K. G. McNeill, M. LeBlanc and F. Brown Can. J. Phys. 35, 470 (1957)	Th	232	90
METHOD	REF. NO.		
	57 Ka 1		JOC

REACTION	RESULT	EXCITATION ENERGY	SOURCE		DETECTOR		ANGLE
			TYPE	RANGE	TYPE	RANGE	
G,XN	ABX	6 - 23	C	6 - 23	BF3-I		4PI

Fig. 1. Yield and cross section curves for the total neutron emission (γ,N), from Th^{232} under betatron X-ray irradiation.

FIG. 1

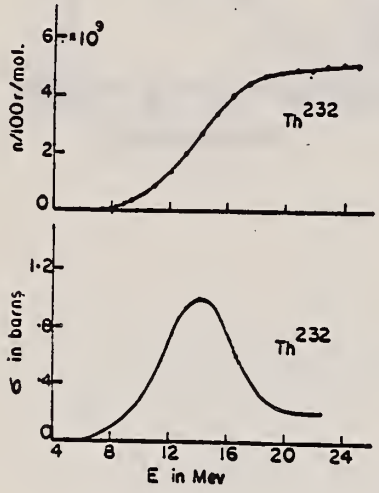

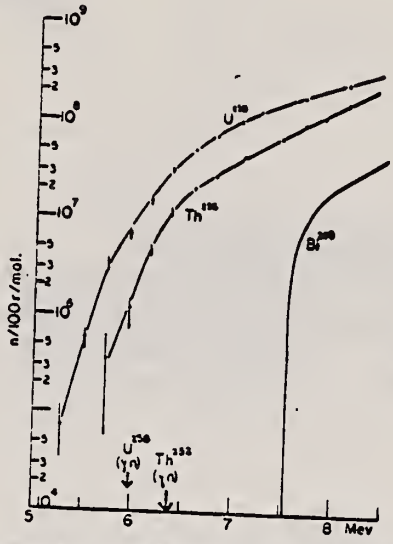

FIG. 5. The low energy section of the U^{238}, Th^{232}, and Bi^{209} neutron yield curves plotted on a logarithmic scale. Compared with the previous figures, the energy scale is expanded.

REF.

R. A. Schmitt and R. B. Duffield
Phys. Rev. 105, 1277 (1957)

ELEM. SYM.	A	Z
Th	232	90

METHOD

REF. NO. 57 Sc 2 EGF

REACTION	RESULT	EXCITATION ENERGY	SOURCE		DETECTOR		ANGLE
			TYPE	RANGE	TYPE	RANGE	
G,F	RLY	THR - 15	C	4 - 16	ACT-I		4PI

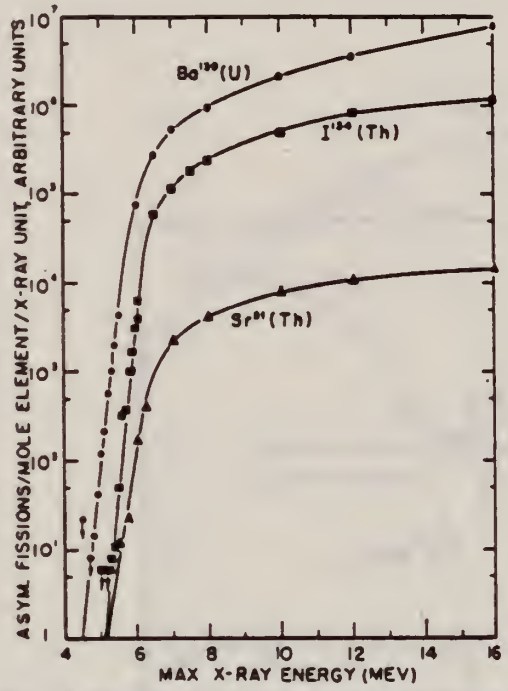

FIG. 1. Semilogarithmic plot of the asymmetric photofissions in natural uranium and natural thorium as a function of increasing betatron energy. ●, Ba^{139} isolated from uranium probe target; ▲, Sr^{91} and ■, I^{134} isolated from thorium probe target. Arrows indicate upper limits. Ordinates for Ba^{139}, Sr^{91}, and I^{134} are unrelated. See footnote 22 for absolute values of the fission yield obtained from thin-target bremsstrahlung spectrum.

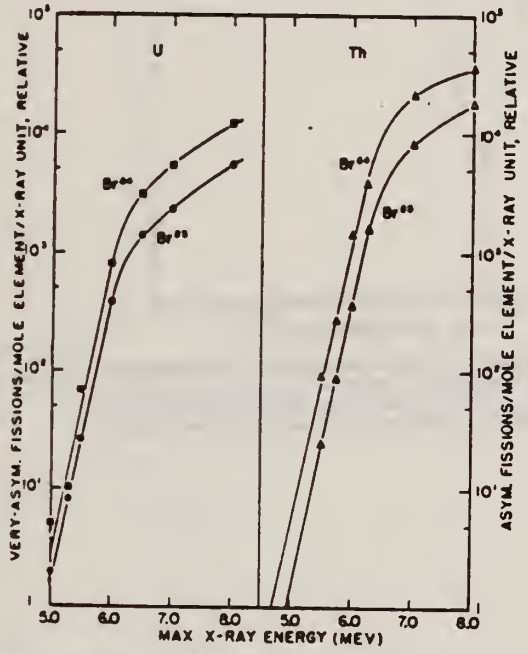

FIG. 2. Semilogarithmic plots of the very-asymmetric and asymmetric photofissions in natural uranium and natural thorium, respectively, as a function of increasing betatron energy. ●, Br^{83} and ■, Br^{84} isolated from uranium probe target; △, Br^{83} and ▲, Br^{84} isolated from thorium probe target. Arrows indicate upper limits. Uranium and thorium ordinates are unrelated.

REF.

R. A. Schmitt and R. B. Duffield
Phys. Rev. 105, 1277 (1957)

ELEM. SYM.	A	Z
Th	232	90

METHOD

[Page 2 of 2]

REF. NO. 57 Sc 2 EGF

REACTION	RESULT	EXCITATION ENERGY	SOURCE		DETECTOR		ANGLE
			TYPE	RANGE	TYPE	RANGE	

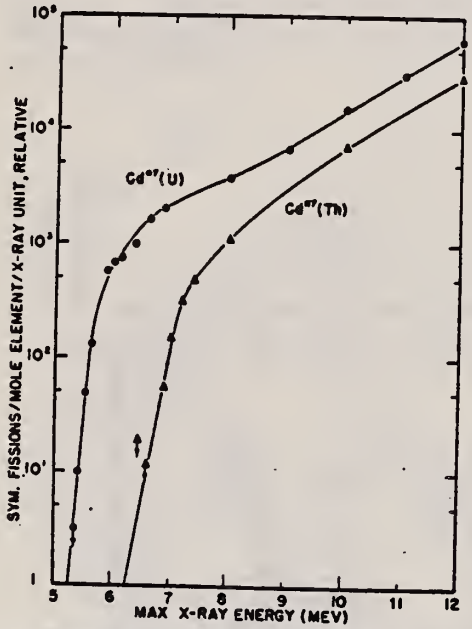

FIG. 3. Semilogarithmic plot of the symmetric photofissions in natural uranium and natural thorium as a function of increasing betatron energy. ●, Cd^{117} isolated from uranium probe target; ▲, Cd^{117} isolated from thorium probe target. Arrows indicate upper limits.

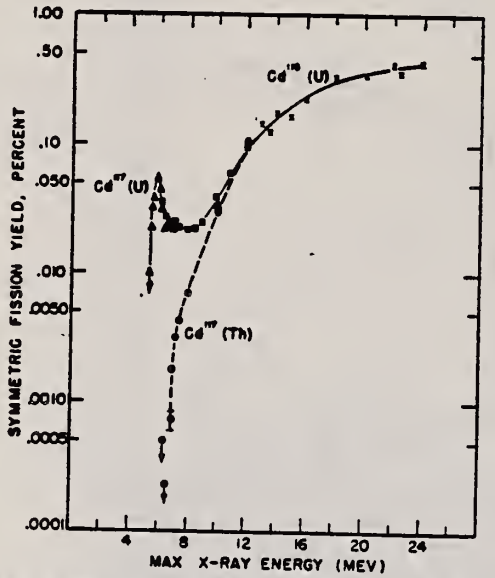

FIG. 4. Symmetric photofission yields of uranium and thorium relative to the 6.0% yields of the asymmetric mode of fission. ✕, uranium external samples, Cd^{115} and Ba^{139} were separated by Katz *et al.* (reference 8); ■, uranium external samples, Cd^{117} and Ba^{139} were separated; ▲, uranium probe targets, Cd^{117} and Ba^{139} were separated; and ●, thorium probe targets, Cd^{117} and Sr^{91} were separated. All Cd^{117} yields have a normalization factor which was calculated by assuming that the Cd^{115} yield equals the Cd^{117} yield for the 12-Mev x-ray fission of uranium. Downward directed arrows indicate absence of detectable activity and are the calculated upper limits. The 6.9-Mev thorium value of 0.00073 ± 0.00008 is the mean of two irradiations.

REF.

H. Faissner und F. Gönnenwein
Z. Physik 153, 257 (1958)

ELEM. SYM.	A	Z
Th	232	90

METHOD

REF. NO.	
58 Fa 2	EGF

REACTION	RESULT	EXCITATION ENERGY	SOURCE		DETECTOR		ANGLE
			TYPE	RANGE	TYPE	RANGE	
G,F	NØX	THR-16	C	16	EMU-I		DST

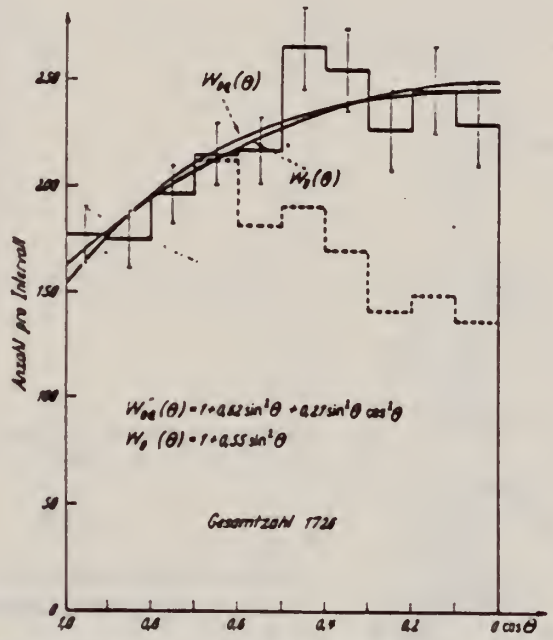

Fig. 4. Verteilung der wahren Winkel θ. Gestrichelt eingezeichnetes Histogramm: Unmittelbar beobachtete Verteilung. Ausgezogenes Histogramm: Gemäß (7) korrigierte Verteilung. Die Kurven wurden nach der Methode der kleinsten Quadrate berechnet

REF. L. Katz, A. P. Baerg and F. Brown
Peaceful Uses of Atomic Energy, Switzerland 1958

ELEM. SYM.	A	Z
Th	232	90

METHOD
Fission chamber

[Page 1 of 2]

REF. NO. 58 Ka 2 EGF

REACTION	RESULT	EXCITATION ENERGY	SOURCE		DETECTOR		ANGLE
			TYPE	RANGE	TYPE	RANGE	
G,F	ABX	5-18	C	5-18	ION-I		DST

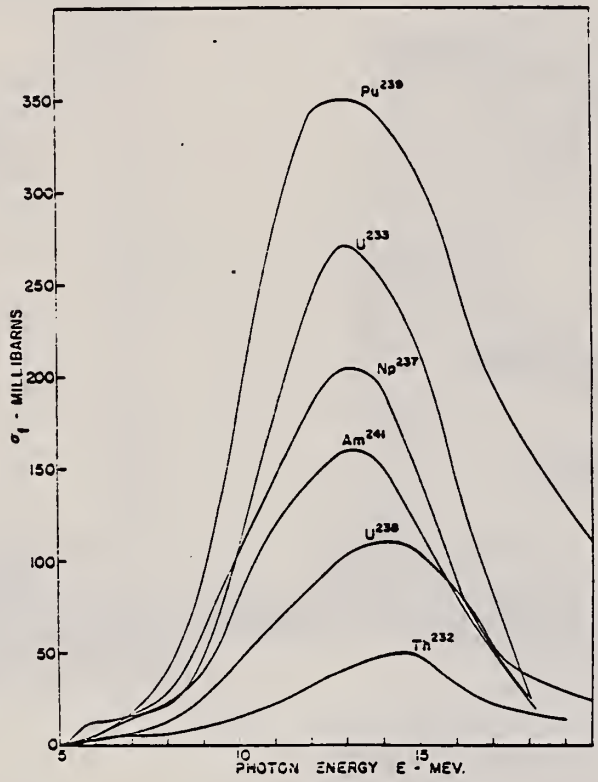

Fig. 5 - Photofission cross sections versus photon energy

REF.

L. Katz, A. P. Baerg and F. Brown
Peaceful Uses of Atomic Energy, Switzerland 1958

ELEM. SYM.	A	Z
Th	232	90

METHOD

Fission chamber

[Page 2 of 2]

REF. NO.

58 Ka 2

EGF

ION Y	SOURCE TYPE	SOURCE RANGE	DETECTOR TYPE	DETECTOR RANGE	ANGLE

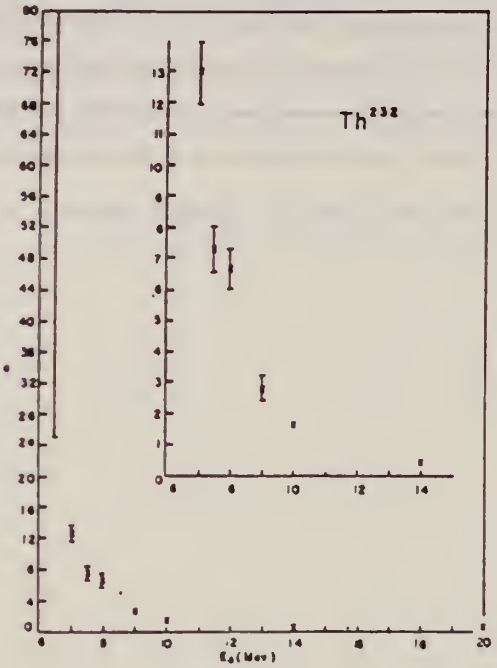

Figure 9

Anisotropy versus maximum bremsstrahlung energy:
Th-232

The ordinate is a in the expression $W(\theta) = 1 + a \sin^2 \theta$.
The values are corrected for resolution.

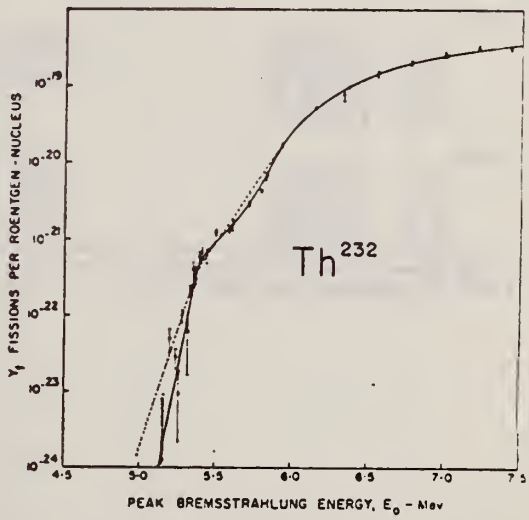

Fig. 7 - Low-energy-yield curves: fissions per roentgen-nucleus versus maximum bremsstrahlung energy. (The solid and dotted lines are samples of smoothed yield curves which fit the experimental data.)

A. P. Baerg, R. M. Bartholomew, F. Brown, L. Katz, and S. B. Kowalski
Can. J. Phys. 37, 1418 (1959) (A.E.C.L. No. 896)

Th	232	90

METHOD

Betatron with ionization chamber detector, enriched samples.

REF. NO. 59 Ba 4 EGF

REACTION	RESULT	EXCITATION ENERGY	SOURCE TYPE	SOURCE RANGE	DETECTOR TYPE	DETECTOR RANGE	ANGLE
G,F	RLY	THR - 20	C	6-20	ION-I		DST

TABLE II

Angular distributions

Relative fission fragment yields as a function of peak bremsstrahlung energy E_0 and angle θ to X-ray beam

E_0, Mev	Angle θ 0	25	45	60	90
Th-232					
6.5	1.00±0.3				20±5
7.0	1.00±0.04		4.1±0.2	6.7±0.3	8.4±0.3
7.5	1.00±0.1		5.1±0.4	6.0±0.4	7.9±0.5
8.0	1.00±0.09		2.4±0.2	3.6±0.3	5.1±0.3
9.0	1.00±0.1				3.4±0.3
10.0	1.00±0.04	1.16±0.05	1.67±0.08	1.97±0.08	2.4±0.1
14.0	1.00±0.05				1.43±0.08
20.0	1.00±0.05				1.13±0.06
U-238					
6.0	1.00±0.3				6.0±1.4
6.3	1.00±0.1		3.6±0.4		5.9±0.6
6.5	1.00±0.2				4.5±0.7
7.0	1.00±0.08	1.5±0.1	2.0±0.2	2.4±0.2	2.9±0.2
8.0	1.00±0.06				2.1±0.1
9.4	1.00±0.023	1.094±0.029	1.224±0.029	1.274±0.034*	1.452±0.033
10.0	1.00±0.04				1.38±0.04
14.0	1.00±0.04				1.08±0.04
20.0	1.00±0.03				1.05±0.03
	*θ = 65° in this case				
U-236					
6.0	1.00±0.25				4.6±0.8
6.5	1.00±0.1		2.06±0.2		2.55±0.25
7.0	1.00±0.06		1.65±0.10		2.11±0.12
8.0	1.00±0.04		1.39±0.06		1.66±0.07
9.0	1.00±0.04	1.10±0.07	1.15±0.04	1.31±0.08*	1.46±0.05
10.0	1.00±0.03		1.07±0.03		1.28±0.04
14.0	1.00±0.02				1.03±0.02
	*θ = 65° in this case				
U-234					
6.5	1.00±0.1		1.41±0.14		1.98±0.20
7.0	1.00±0.05		1.19±0.06		1.53±0.08
8.0	1.00±0.03		1.11±0.03		1.30±0.04
10.0	1.00±0.03				1.12±0.03
15.0	1.00±0.03				1.01±0.03
Pu-240					
6.5	1.00±0.10		1.49±0.15		1.55±0.16
7.0	1.00±0.06		1.03±0.06		1.35±0.08
8.0	1.00±0.03		1.01±0.03		1.21±0.04
15.0	1.00±0.02				1.01±0.02

The values quoted are counts observed for unit X-ray dose normalized to unit yield at θ = 0°. No corrections have been applied.

TABLE VI

Corrected values of α in $W(\theta) = 1+\alpha \sin^2\theta$

E_0	Th-232	U-238	U-236	U-234	Pu-240
6.0		6.6±2	6.0±2.3		
6.3		6.7±1.1			
6.5	>25	4.4±1.0	2.1±0.4	2.3±0.6	0.65±0.20
7.0	11.0±0.8	2.05±0.24	1.33±0.17	0.90±0.16	0.49±0.12
7.5	10.3±1.6				
8.0	4.9±0.6	1.3±0.1	0.79±0.09	0.44±0.08	0.29±0.07
9.0	2.8±0.4		0.51±0.07		
9.4		0.44±0.04			
10.0	1.61±0.12	0.41±0.05	0.32±0.06	0.17±0.07	
14.0	0.46±0.09	0.09±0.04	0.01±0.03		
15.0				0.02±0.04*	0.01±0.03*
20.0	0.14±0.06	0.05±0.03			

*These values, which do not differ from zero, have not been corrected for isotopic composition.

REF.

L. I. Prokhorova, G. N. Smirenkin
Atom. Energiya 8, 457 (1960)
[See also AEC-tr-8966]

ELEM. SYM.	A	Z
Th	232	90

METHOD

$F^{19}(p,\alpha\gamma)$ source

REF. NO.: 60 Pr 2 JOC

REACTION	RESULT	EXCITATION ENERGY	SOURCE		DETECTOR		ANGLE
			TYPE	RANGE	TYPE	RANGE	
G,F	NOX	6	D	6	BF_3-I		4PI

Average number of neutrons per photofission.

Ref. E. Bethel, A.E. Mann
Phys. Rev. 118, 701 (1960)

Elem. Sym.	A	Z
Th	232	90

Method: γ's from $F^{19}(p,\alpha\gamma)$ reaction; protons from Vande Graaff; NaI.

Ref. No.: 60 Re 1 JHH

Reaction	E or ΔE	E_o	Γ	$\int \sigma dE$	Jπ	Notes
(γ,γ)	~7 ?					$\langle\bar{\sigma}\rangle$ (E_p = 2.05 MeV) = 0.86 ± 0.13 mb

REF.

R.G. Baker, K.G. McNeill
Can. J. Phys. 39, 1158 (1961)

ELEM. SYM.		
Th	232	90

METHOD

Betatron; fast neutron yield, angular distribution; Si threshold detector; ion chamber

REF. NO. 61 Ba 2 NVB

REACTION	RESULT	EXCITATION ENERGY	SOURCE		DETECTOR		ANGLE
			TYPE	RANGE	TYPE	RANGE	
G,XN	ABY	THR-22	C	22	THR-I	5-+	DST

In Table 4:

$\bar{\sigma}$ = average cross section of detector weighted with neutron spectrum

$\bar{\nu}$ = neutrons/100 roentgen/mole

$$W(\theta) = a_o \sum_{n=1}^{\infty} [1 + A_n P_n (\cos \theta)]$$

TABLE IV

I Element	II a_0	III a_1	IV a_2	V $(\bar{\sigma}\Phi)\times10^{26}$	VI Φ_{total} (22 Mev)$\times10^{9}$	VII $\Phi_{1.67}/\Phi_{total}$
Vanadium	245 (1±0.06)	0.01±0.08	−0.00±0.10	6.05	0.21	0.12
Chromium	164 (1±0.03)	0.04±0.04	−0.05±0.05	4.05	0.17	0.10
Manganese	308 (1±0.02)	0.07±0.03	−0.09±0.04	7.61	0.25	0.12
Iron	200 (1±0.03)	0.05±0.04	−0.17±0.05	4.94	0.18	0.11
Cobalt	390 (1±0.02)	0.08±0.03	−0.22±0.04	9.63	0.20	0.15
Nickel	145 (1±0.05)	0.07±0.07	−0.23±0.09	3.58	0.12	0.12
Copper	347 (1±0.02)	0.05±0.03	−0.29±0.04	8.57	0.30	0.12
Arsenic	482 (1±0.03)	0.11±0.04	−0.24±0.05	11.91	0.33	0.15
Rubidium	638 (1±0.05)	0.13±0.06	−0.14±0.08	15.76		
Strontium	409 (1±0.05)	0.10±0.06	−0.17±0.08	10.10		
Yttrium	290 (1±0.10)	0.08±0.12	−0.12±0.15	7.16		
Silver	590 (1±0.04)	0.10±0.06	−0.22±0.08	14.57	0.87	0.07
Cadmium	905 (1±0.02)	0.02±0.02	−0.26±0.03	22.35		
Iodine	1133 (1±0.03)	0.04±0.04	−0.29±0.05	27.99	1.42	0.08
Barium	1048 (1±0.04)	0.10±0.06	−0.38±0.08	25.89		
Lanthanum	1595 (1±0.02)	0.02±0.03	−0.42±0.04	39.40	1.04	0.15
Cerium	1316 (1±0.05)	0.05±0.06	−0.39±0.08	32.50		
Dysprosium	1652 (1±0.03)	0.04±0.10	−0.34±0.13	40.80		
Tantalum	1558 (1±0.02)	0.04±0.03	−0.22±0.04	38.48	2.50	0.06
Tungsten	1365 (1±0.02)	−0.07±0.03	−0.24±0.04	33.71		
Mercury	1345 (1±0.02)	0.04±0.03	−0.31±0.04	33.22		
Lead	2274 (1±0.01)	0.02±0.02	−0.42±0.03	56.17	2.72	0.08
Bismuth	2162 (1±0.02)	0.05±0.03	−0.45±0.04	53.40	3.36	0.06
Thorium	3031 (1±0.04)	0.00±0.05	−0.32±0.07	74.87		
Uranium	4630 (1±0.02)	0.05±0.03	−0.17±0.04	114.36		

*$(\bar{\sigma}\Phi)$ = 2.47×10⁹ coulombs-millibarn-neutron. Errors are standard errors due to counting statistics only.

REF.

B. A. Bochagov, A. P. Komar, G. E. Solyakin, V. I. Fadeev
Atom. Energiya 11, 540 (1961)

ELEM. SYM.	A	Z
Th	232	90

METHOD

REF. NO.	
61 Bo 2	JOC

REACTION	RESULT	EXCITATION ENERGY	SOURCE		DETECTOR		ANGLE
			TYPE	RANGE	TYPE	RANGE	
G,F	SPC	THR - 70	C	70	EMU-D		

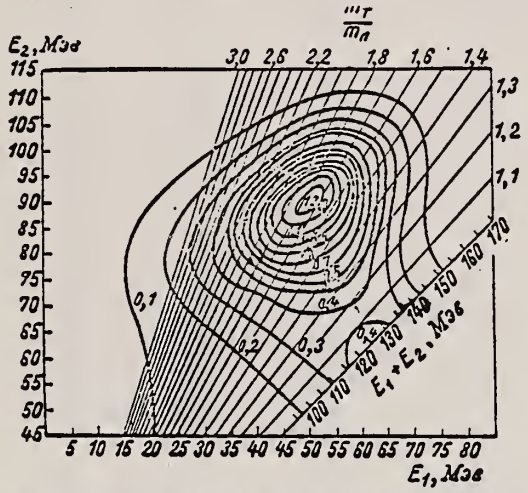

Рис. 1. Контурная диаграмма энергетического распределения осколков фотоделения ядер Th^{232} при $E_{\gamma\ макс.} = 70$ *Мэв*.

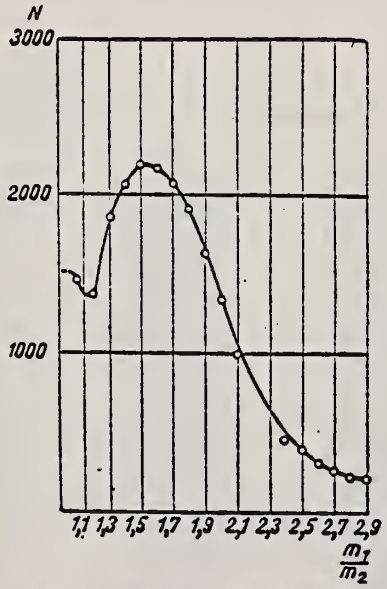

Рис. 2. Массовое распределение осколков фотоделения ядер Th^{232}.

Ref. H.G. DeCarvalho, A. Celano, G. Cortini, R. Rinzivillo, G. Ghigo
Nuovo Cimento 19, 187 (1961)

Elem. Sym.	A	Z
Th	232	90

Method: Synchrotron; emulsions

Ref. No.: 61 De 2 JS | JHH

Reaction	E or ΔE	E_o	Γ	$\int \sigma dE$	Jπ	Notes
Th (γ, f)	300-1000 MeV					Slope = $\frac{d\,\sigma_Q\,F}{d\,\ell n\,E}$ = 36×10^{-27} cm^2 ± 10% over range 300-1000 MeV

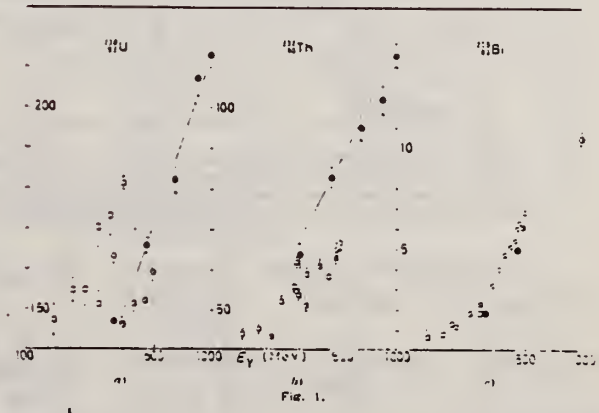

Fig. 1.

Ref.	Elem. Sym.	A	Z
H.G. DeCarvalho, A. Manfredini, M. Muchnik, M. Severi, H. Bösch, J. Lang, R. Müller, W. Wölfli Nuovo Cimento 25, 534 (1962) ERRATUM: Nuovo Cimento 29, 475 (1963)	Th	232	90

Method	Ref. No.	
Reactor; monoenergetic γ's from Ti(n,γ) reaction; emulsions; NaI monitor	62 De 3 cs	JHH

Reaction	E or ΔE	E_o	Γ	$\int \sigma dE$	Jπ	Notes
$Th^{232}(\gamma, f)$	$6.61^{+0.14}_{-0.20}$ MeV					In Table III, $\sigma_{f(Th)}/\sigma_{f(U)} = 0.92$ should be 0.85.

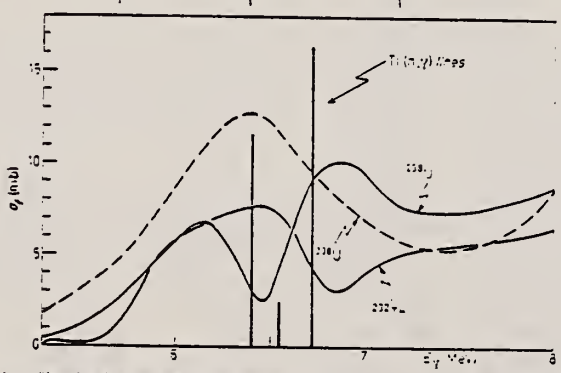

Fig. 2. – Sketch of preceeding experimental results for the photofission cross-section of ^{238}U (—— Katz *et al.* [3]; – – – Schmitt *et al.* [2]) and of ^{232}Th (— — Katz *et al.* [3]). Schmitt's results have been normalized to those of Katz at 5 MeV. Shown in the figure also the three main lines of the Ti(n, γ) process with their corresponding intensities in arbitrary units.

TABLE III.

	σ_{Th} (mb)	σ_U (mb)	$\sigma_{f(Th)}/\sigma_{f(U)}$
Present work	4.73±0.50	7.89±0.83	0.600±0.005
Katz *et al.* [3].	5.6	6.6	0.92 *
Schmitt *et al.* [2]	—	10.7	—

[2] R. A. Schmitt and R. B. Duffield: *Phys. Rev.*, 105, 1277 (1957).

[3] L. Katz, A. P. Baerg and F. Brown: *Second U.N. International Conference on the Peaceful Uses of Atomic Energy*, vol. 45 (1958), p. 188.

[4] A. I. Baz, N. M. Kulikova, L. E. Lazareva, N. V. Nikitina and V. A. Semenov: *Second U.N. International Conference on the Peaceful Uses of Atomic Energy*, vol. 15 (1958), p. 184.

Ref. J.R. Huizenga, K.M. Clarke, J.E. Gindler, R. Vandenbosch
Nuclear Phys. 34, 439 (1962)

Elem. Sym.	A	Z
Th	232	90

Method Monoergic γ's from $F^{19}(p,\alpha\gamma)O^{16}$ reaction; fission fragment ionization chamber.

Ref. No. 62 Hu 1 JHH

Reaction	E or ΔE	E_o	Γ	$\int \sigma dE$	Jπ	Notes
$Th^{232}(\gamma,f)$	6.14					
	7.0					

TABLE 3

Photofission cross sections obtained with mono-energetic gamma rays from the $F^{19}(p,\alpha\gamma)O^{16}$ reaction

Target	$\sigma_{\gamma,a}/\sigma_{\gamma,10}$	$\sigma_{\gamma,a}$(mb)	$\sigma_{\gamma,10}$(mb)	B_a(MeV) [a]	E_f(MeV) [b]
Th^{232}	1.00 ± 0.13	9 ± 3	9 ± 3	6.34	5.5
U^{233}	1.12 ± 0.15	15 ± 5	13 ± 4	6.04	5.3
U^{235}	0.80 ± 0.10	28 ± 9	33 ± 11	6.40	5.2
U^{238}	2.06 ± 0.33	33 ± 10	16 ± 5	5.24	5.5
U^{238}	10.0 ± 3.0	52 ± 16	5^{+10}_{-4}	6.77	5.1
U^{238}	3.24 ± 0.79	44 ± 14	13 ± 4	5.90	5.4
Np^{237}	1.43 ± 0.21	45 ± 14	31 ± 10	6.76	5.3

[a]) From the compilation of ref [20])
[b]) From the compilation of ref [26])

Ref 20: Everling, König, Mattauch & Wapstra - Nuclear Phys. 18, 529 (1960)

Ref 26: Vandenbasch & Seaborg - Phys. Rev. 110, 507 (1958)

Ref. J.A.Michel, E.V.March, M.Lindner, R.J.Nagle
Phys.Rev. 128, 2717 (1962)

Elem. Sym.	A	Z
Th	232	90

Method
Li(p,n)F or T(p,n) - NaI(Tl)

Ref. No.
62M11

Reaction	E or ΔE	E_o	Γ	$\int \sigma dE$	Jπ	Notes
(n,γ)	E_n = .030-4.0					Observed activities converted to disintegration rates, extrapolated in time to end of irradiation and corrected for decay during bombardment. Activation cross section calculated. (data given in article). $S_J = D_J/2\pi\Gamma_\gamma$, D_J is the spacing between levels of same spin and parity. Fig. 10 : $\rho_n = C_n[\exp 2(aE)^{1/2}]$, C_n values obtained from fit of calculated and measured cross section above 1 MeV (listed in article).

REF.

G. Moscati, J. Goldemberg
Phys. Rev. 126, 1098 (1962)

ELEM. SYM.	A	Z
Th	232	90

METHOD Betatron; fission, delayed neutron yield; BF_3 counters

REF. NO. 62 Mo 3 NVB

REACTION	RESULT	EXCITATION ENERGY	SOURCE		DETECTOR		ANGLE
			TYPE	RANGE	TYPE	RANGE	
G,F	ABY	THR-20	C	12, 20	BF3-I		4PI

DELAYED N YIELDS

Delayed means > 3000 μ sec.

TABLE I. Experimental results. The errors in columns 3 and 4 are statistical. The errors in column 5 represent extreme values using plausible estimates for $\sigma(\gamma,n)$ and $\sigma(\gamma,2n)$, and $\bar{\nu}$ from Gindler *et al.*[3] and Leachman.[4]

Element	Energy (Mev)	(Relative counts/pulse)/monitor unit Prompt	Delayed	Delayed neutrons/fission
U^{238}	12	620±25	3.2 ±0.2	$0.036^{+0.008}_{-0.007}$
	20	2545±100	13.6 ±0.5	$0.035^{+0.010}_{-0.009}$
Th^{232}	12	225±12	0.55±0.04	$0.027^{+0.008}_{-0.007}$
	20	995±40	2.2 ±0.1	$0.030^{+0.012}_{-0.006}$

[3] J. E. Gindler, J. R. Huizenga, and R. A. Schmitt, Phys. Rev. 104, 425 (1956).
[4] R. B. Leachman, *Proceedings of the Second United Nations International Conference on the Peaceful Uses of Atomic Energy, Geneva, 1958* (United Nations, Geneva, 1958), Paper P/2467, Vol. 15, p. 229.

REF.

M.V. Ballariny
Notas de Fisica 10 (No. 12), 205 (1963)

ELEM. SYM.	A	Z
Th	232	90

METHOD

Betatron; fission fragment angular distribution; nuclear emulsion; ion chamber

REF. NO.	
63 Ba 3	NVB

REACTION	RESULT	EXCITATION ENERGY	SOURCE		DETECTOR		ANGLE
			TYPE	RANGE	TYPE	RANGE	
G,F	RLY	0-12	C	12	EMU-I		DST

In Figure 1, $W(\theta) = a + b \sin^2\theta$

In Figure 2, $W(\theta) = 1 + 0.73 \sin^2\theta$

TABLE I

Th_{232} angular distribution at 12,4 MeV

θ Interval	15° - 30° 165°-150°	30° - 45° 150°-135°	45° - 60° 135°-120°	60° - 75° 120°-105°	75° - 90° 105°- 90°
θ̄ (average)	22,5°	37,5°	52,5°	67,5°	82,5°
relative yield per unity of solid angle	1,09 ± 0,08	1,12 ± 0,10	1,30 ± 0,09	1,45 ± 0,09	1,54 ± 0,08

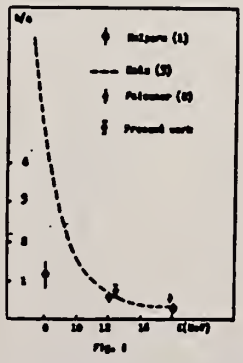

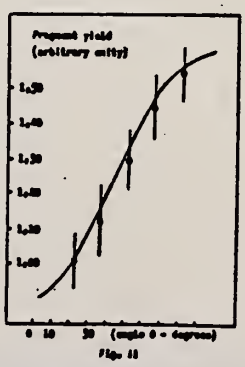

Ref. H.G. DeCarvalho, A. Manfredini, M. Muchnik, M. Severi, R. Bosch, W. Wolfli
Nuovo Cimento 29, 463 (1963)

Elem. Sym.	A	Z
Th	232	90

Method: Reactor; monoenergetic γ's from Ti(n,γ) reaction; emulsions; NaI monitor

Ref. No.: 63 De 1 cs — JHH

Reaction	E or ΔE	E_0	Γ	$\int \sigma dE$	Jπ	Notes
$Th^{232}(\gamma, f)$	$6.61^{+0.14}_{-0.20}$ MeV					Parameters for angular distribution function, $W(\theta) = a + b \sin^2\theta + c \sin^2\theta \cos^2\theta$ are given in Table II.

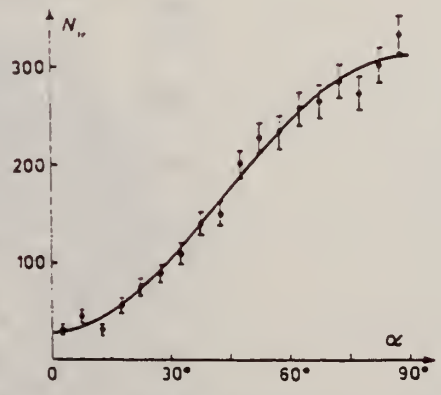

Fig. 3. - Angular distribution $W(\alpha, \beta_0 = 15°)$ of fission fragments from ^{232}Th. $E_\gamma = 6.61$ MeV.

TABLE II.

	E_γ(*) MeV	γ-ray source	b/a	c/a	c/b
Th	6.5	bremss. (1)	> 25	—	—
	6.61 (**)	Ti(n, γ)	11 ± 3	1 ± 1	0.1 ± 0.1
	7.0 (***)	bremss. (1)	10.6 ± 2.1	−2.1 ± 1.6	−0.20 ± 0.16
U	6.1	F(p, γ) (2)	14 ± 14	21 ± 21	1.4 ± 0.2
	6.5	bremss. (1)	4.4 ± 1.0	—	—
		bremss. (3)	4.2 ± 1.3	3.1 ± 3.2	0.75 ± 0.71
	6.61 (**)	Ti(n, γ)	2.0 ± 0.2	0.6 ± 0.3	0.3 ± 0.2
	6.9	F(p, γ) (2)	0.7 ± 0.3	0.2 ± 0.3	0.3 ± 0.5
		bremss. (4)	2.80 ± 0.44	0.34 ± 0.35	0.12 ± 0.30
	7.0 (***)	bremss. (1)	2.11 ± 1.24	0.90 ± 0.38	0.43 ± 0.49

(*) As indicate either the maximum bremsstrahlung energy or the energy of the monoenergetic beam, as the case may be. Only those points of other authors are quoted whose energy lies within 0.5 MeV from our energy (6.61 MeV).
(**) We give the values obtained by means of the Fourier analysis on the data (see Table I).
(***) For purposes of comparison we quote the values given in the paper of Bishop et al.(3), including the coefficient c, although the authors assume in their discussion c = 0.

TABLE III (*).

Nucleus	σ_f (mb) (from part I) (**)	$\sigma_{(\gamma,n)}$ (mb)	σ_a (mb)	σ_γ (mb)
^{232}Th	5.3 ± 0.6	0.7 ± 0.2	4.8 ± 0.6	0.1 ± 0.1
^{238}U	9.2 ± 0.9	3.7 ± 0.4	5.1 ± 0.6	0.3 ± 0.2

(*) The values of σ_γ, σ_a and σ_γ have been computed using the Fourier analysis results for a, b and c (see Table I).
(**) An error on the dose measurement has been detected since the publication of Part I of this paper. Instead of $(2.6 \cdot 10^{11} \pm 10\%)$ quanta/cm² the dose was $(1.72 \cdot 10^{11} \pm 10\%)$ quanta/cm² accordingly the cross-sections reported in Part I should be changed to the values shown in the present Table III.

(1) A. BOHR: *International Conference on the Peaceful Uses of Atomic Energy*, vol. 2 p. 911, (1956).

REF.

A.P. Komar, B.A. Bochagov, V.I. Fadeev
Dokl. Akad. Nauk SSSR 152, 858 (1963); Soviet Phys. Doklady 8, 978 (1964)

ELEM. SYM.	A	Z
Th	232	90

METHOD

Synchrotron; Fission; ion chamber

REF. NO. 63 Ko 1 | NVB

REACTION	RESULT	EXCITATION ENERGY	SOURCE		DETECTOR		ANGLE
			TYPE	RANGE	TYPE	RANGE	
G,F	SPC	THR - 90	C	90	IØN - D		DST

E = total energy of fragment pair
m_H/m_L = mass ratio of fragments

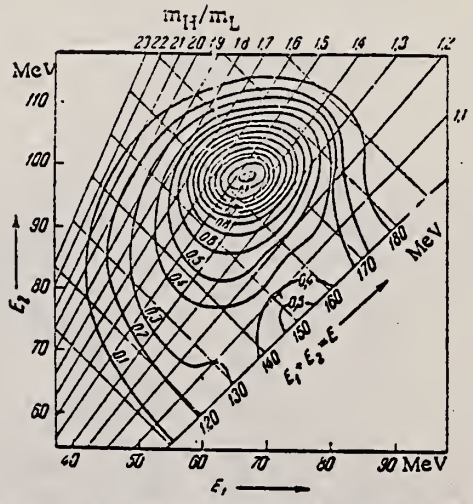

Fig. 2. Contour diagram for the fission of Th^{232} by photons with $E_{\gamma max}$ = 90 MeV.

REF.

M. Langevin, J. M. Loiseaux et J. M. Maison
Nucl. Phys. 54, 114-124 (1964)

ELEM. SYM.	A	Z
Th	232	90

METHOD

Bremsstrahlung scattering

REF. NO.	
64 La 1	JOC

REACTION	RESULT	EXCITATION ENERGY	SOURCE		DETECTOR		ANGLE
			TYPE	RANGE	TYPE	RANGE	
G,G	ABX	10-25	C		NAI-D		DST

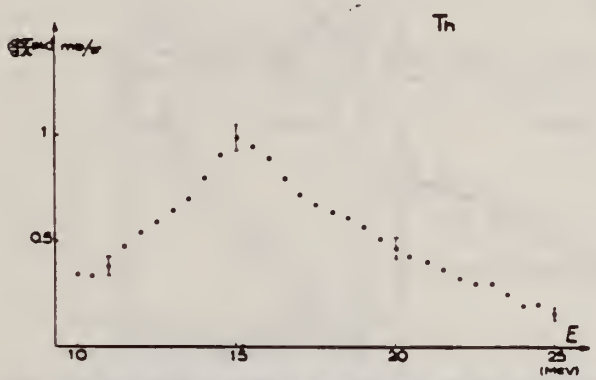

Fig. 7. Sections efficaces différentielles obtenues pour le thorium.

REF.

E. Albertsson and B. Forkman
Nuclear Phys. 70, 209(1965)

ELEM. SYM.	A	Z
Th	232	90

METHOD

$^{19}F(p,\alpha\gamma)^{16}O$ radiation

[Page 1 of 2]

REF. NO. 65 A1 1

EGF

REACTION	RESULT	EXCITATION ENERGY	SOURCE		DETECTOR		ANGLE
			TYPE	RANGE	TYPE	RANGE	
G,F	RLX	6-7	D	6-7	EMU-D		DST

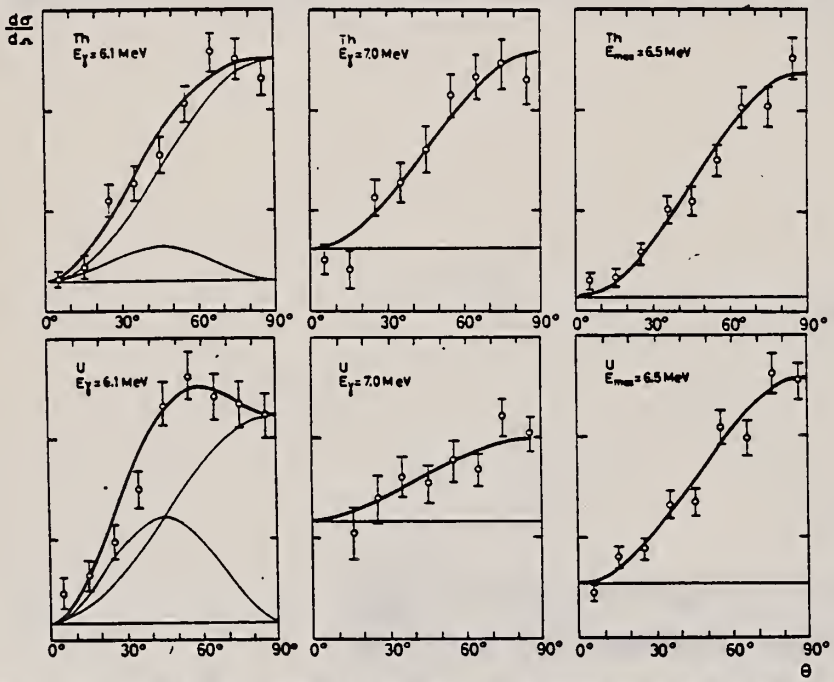

Fig. 1. Angular distributions from pure 6.1 MeV and 7.0 MeV photon excitation and from 6.5 MeV bremsstrahlung excitation in the present work and in ref. [a]).

TABLE 2

Coefficients in the angular distribution $W(\theta) = a + b\sin^2\theta + c\sin^2 2\theta$ in photofission of thorium and uranium

Element	Photon energy (MeV)	a	b	c
Th^{232}	6.1	0.12±0.03	0.89±0.05	0.14±0.06
	7.0	0.25±0.04	0.78±0.06	
	6.5 (bremsstr.)	0±0.05	1.27±0.07	
U^{238}	6.1 [a])	0.07±0.08	1.00±0.10	0.50±0.12
	7.0 [a])	1.00±0.22	0.70±0.22	0.05±0.20
	6.5 (bremsstr.)	0.17±0.03	0.93±0.05	

[a]) Ref. [a]).

REF.

E. Albertsson and B. Forkman
Nuclear Phys. 70, 209 (1965)

ELEM. SYM.	A	Z
Th	232	90

METHOD

$^{19}F(p,a\gamma)^{16}O$ radiation

REF. NO. 65 Al 1 EGF

REACTION	RESULT	EXCITATION ENERGY	SOURCE		DETECTOR		ANGLE
			TYPE	RANGE	TYPE	RANGE	

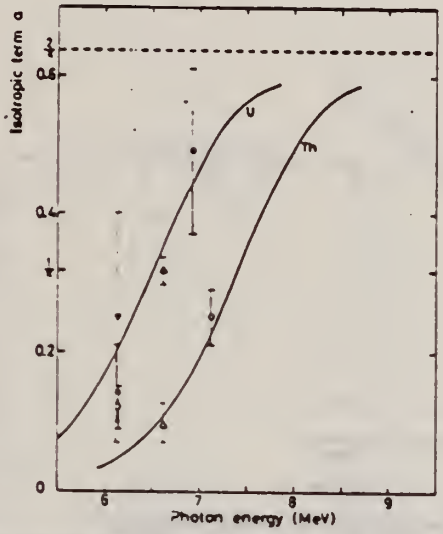

Fig. 3. Increase of the isotropic term a in $W(\theta)$ with photon energy. The curve is the function $f(E) = 2/\pi(1+\exp([B-E)/E_0))^{-1}$ with $B = 7.4$ for thorium and $B = 6.5$ MeV for uranium and $E_0 = 0.5$ MeV for both. The experimental points are from the following papers: ○(Th) present work; ● (U) Forkman *et al.* [6]); ▼ (U) Takekoshi [9]); △▲ (Th, U) Carvalho *et al.* [10]).

REF.

F. Carbonara, H.G. DeCarvalho, R. Rinzivillo, E. Sassi and G.P. Murtas.
Nucl. Phys. 73, 385 (1965)

ELEM. SYM.	A	Z
Th	232	90

METHOD

REF. NO. 65 Ca 3 JOC

REACTION	RESULT	EXCITATION ENERGY	SOURCE		DETECTOR		ANGLE
			TYPE	RANGE	TYPE	RANGE	
G,F	ABY	300-1000	C	1 BEV	EMU-I		4PI

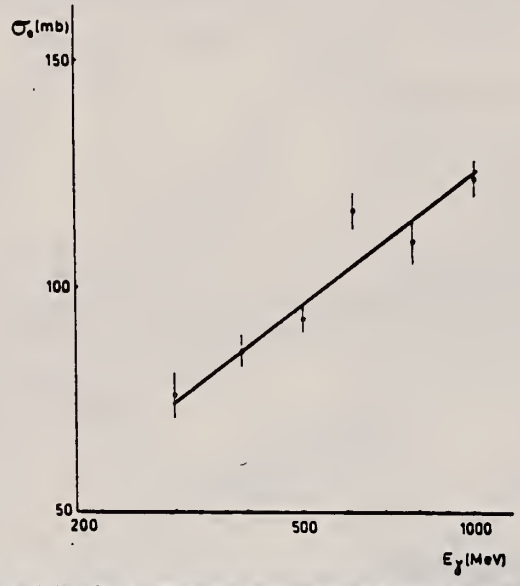

Fig. 5. The experimental data for the Th fission cross-section per equivalent quantum σ_0 are plotted against the maximum energy of the γ beam. The solid line is the result of a least-squares calculation.

TABLE I

Some fissility values

Particle	Energy (MeV)	Nucleus		
		^{238}U	^{232}Th	^{209}Bi
Photons	300÷1000	0.84±0.13	0.47±0.10	0.12±0.02
Protons	600 [a])	0.65	0.40	0.13
Protons	200 [b])	0.80	0.47	0.09

[a]) Ref. [16]). [b]) Ref. [17]).

REF.

C. P. Sargent, W. Bertozzi, P. T. Demos, J. L. Matthews and W. Turchinetz
Phys. Rev. 137, B89 (1965)

ELEM. SYM.	A	Z
Th	232	90

METHOD

MIT Linac

REF. NO.

65 Sa 1 EGF

REACTION	RESULT	EXCITATION ENERGY	SOURCE		DETECTOR		ANGLE
			TYPE	RANGE	TYPE	RANGE	
G,F	SPC	THR - 8.0	C	7.8	TØF	1-8	77,157

Measured neutron spectra at two angles.
Analyzes data in terms of neutron distribution from recoiling fission fragments.
Concludes that fraction of neutrons not emitted from fully accelerated fragments is 0.07 ± 0.09.

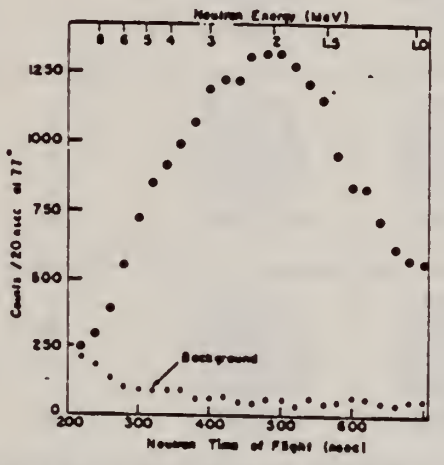

FIG. 4. Thorium photoneutron time-of-flight spectrum observed at 77° with 7.75-MeV bremsstrahlung. The points labeled "background" are the normalized result of a run with a bismuth target.

REF.

A.S. Soldatov, Z.A. Aleksandrova, L.D. Gordeeva, and G.N. Smirenkin
Sov. J. of Nuclear Phys. 1, 335 (1965)

ELEM. SYM.	A	Z
Th	232	90

METHOD

$F^{19}(p,\alpha\gamma)O^{16}$ E_γ = 6.1, 6.9, 7.1 MeV

REF. NO. 65 So 1 JOC

REACTION	RESULT	EXCITATION ENERGY	SOURCE		DETECTOR		ANGLE
			TYPE	RANGE	TYPE	RANGE	
G,F	RLX	6-7	D	6-7			DST

TRACKS IN GLASS

$\sigma(\theta) = (0.07 \pm 0.01) + (0.93 \pm 0.03)\ \sin^2\theta + (0.12 \pm 0.04)\ \sin^2 2\theta.$

I(6.1 MeV): I(6.9 MeV): I(7.1 MeV) = 1.00:0.15:0.17.

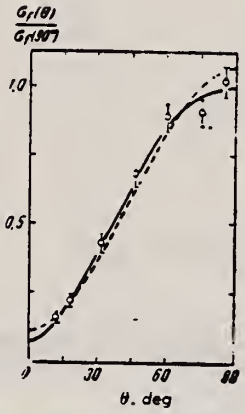

Fig. 3. Angular distribution of fragments from photofission of Th^{232}. The solid and broken curves describe the results of analysis of the experimental data by the method of least squares with the respective assumptions $c \neq 0$, and $c = 0$, where c is the coefficient of $\sin^2 2\theta$.

REF. O. P. Nikotin and K. A. Petrzhak
Atomnaya Energiya 20, 268 (1966)
UDC 539.173.84, p. 300

ELEM. SYM.	A	Z
Th	232	90

METHOD

REF. NO. 66 Ni 1 egf

REACTION	RESULT	EXCITATION ENERGY	SOURCE		DETECTOR		ANGLE
			TYPE	RANGE	TYPE	RANGE	
G,F	RLY	THR-15	C	10-15	TRK-D	0-1	4PI
						(.1-1.0)	

Delayed Neutrons from Photofission ($E_{\gamma\,max}$ = 15 MeV)

DELAYED N YIELDS

Total yield of delayed neutrons, neutrons/100 fissions	Neutron group	$T_{1/2}$, sec	Relative yield of group, %	Absolute yield of group, neutrons per 100 fissions
3,8±0,6 (Th^{232})	1	55,6±1,5	4,40±0,20	0,17±0,03
	2	20,3±0,8	16,3±1,0	0,62±0,10
	3	5,45±0,50	15,9±1,5	0,60±0,10
	4	1,98±0,20	37,5±3,0	1,43±0,20
	5	0,43±0,10	17,2±2,0	0,66±0,10
	6	0,18±0,03	$8,7^{+2,0}_{-4,0}$	$0,33^{+0,10}_{-0,20}$
0,96±0,13 (U^{234})	1	54,7±2,5	5,4±0,5	0,052±0,010
	2	20,3±1,0	20,0±2,0	0,193±0,040
	3	5,45±0,60	15,2±2,0	0,146±0,030
	4	2,01±0,25	36,9±4,0	0,354±0,070
	5	0,50±0,10	13,9±2,0	0,134±0,030
	6	0,19±0,04	$8,6^{+2,0}_{-5,0}$	$0,083^{+0,025}_{-0,050}$
3,1±0,4 (U^{235})	1	56,2±0,8	1,98±0,08	0,061±0,010
	2	21,3±0,3	15,7±0,5	0,489±0,070
	3	5,50±0,20	17,5±0,7	0,545±0,070
	4	2,15±0,10	31,1±0,8	0,970±0,150
	5	0,70±0,06	17,7±0,9	0,552±0,080
	6	0,19±0,02	$16,1^{+2,0}_{-5,0}$	$0,502^{+0,120}_{-0,200}$
0,36±0,06 (Pu^{239})	1	54,0±3,0	6,05±0,60	0,022±0,004
	2	20,6±1,0	20,6±2,0	0,075±0,018
	3	5,7±0,7	18,3±3,0	0,066±0,015
	4	1,94±0,30	29,5±4,0	0,105±0,020
	5	0,58±0,10	14,9±3,0	0,054±0,012
	6	0,20±0,04	$10,6^{+2,0}_{-5,0}$	$0,038^{+0,012}_{-0,025}$

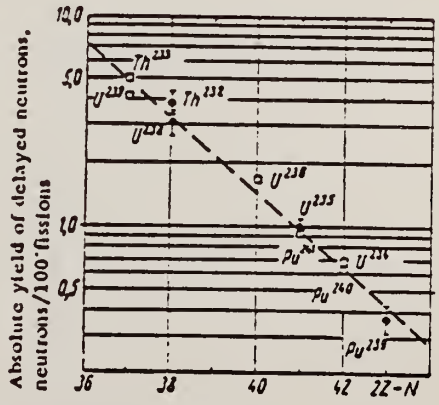

Fig. 3. Absolute yields of delayed neutrons from fission of nuclei: □) [7]; ●) present authors.

REF.	ELEM. SYM.	A	Z
N. S. Rabotnov, G. N. Smirenkin, A. S. Soldatov, L. N. Ysachev, S. P. Kapitza and Yu. M. Tsipeniuk Phys. Letters 26B, 218 (1968)	Th	232	90

METHOD	REF. NO.	
	68 Ra 1	EGF

REACTION	RESULT	EXCITATION ENERGY	SOURCE		DETECTOR		ANGLE
			TYPE	RANGE	TYPE	RANGE	
G,F	NOX	. THR-8	C	5-8	FRG-I		DST

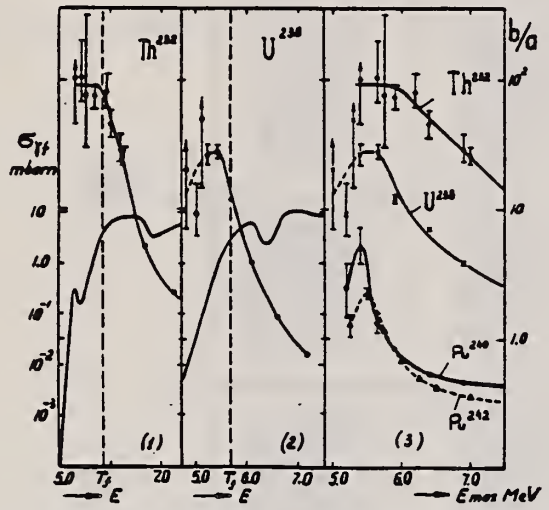

Fig. 1. The measured value of b/a as a function of energy. Photofission cross sections taken from ref. 1 are also shown for ^{232}Th and ^{238}U. E is the average excitation energy of the fissioning nuclei and T_f the observable fission threshold.

S. P. Kapitza, N. S. Rabotnov, G. N. Smirenkin, A. S. Soldatov, L. N. Usachev, Yu. M. Ysipenyuk
ZhETF Pis. Red. 9, 128 (1969)
JETP Letters 9, 73 (1969)

Th	232	90

METHOD

REF. NO. 69 Ka 1 hmg

REACTION	RESULT	EXCITATION ENERGY	SOURCE TYPE	SOURCE RANGE	DETECTOR TYPE	DETECTOR RANGE	ANGLE
G,F	ABX	THR-8	C	5-8	TRK-I		DST

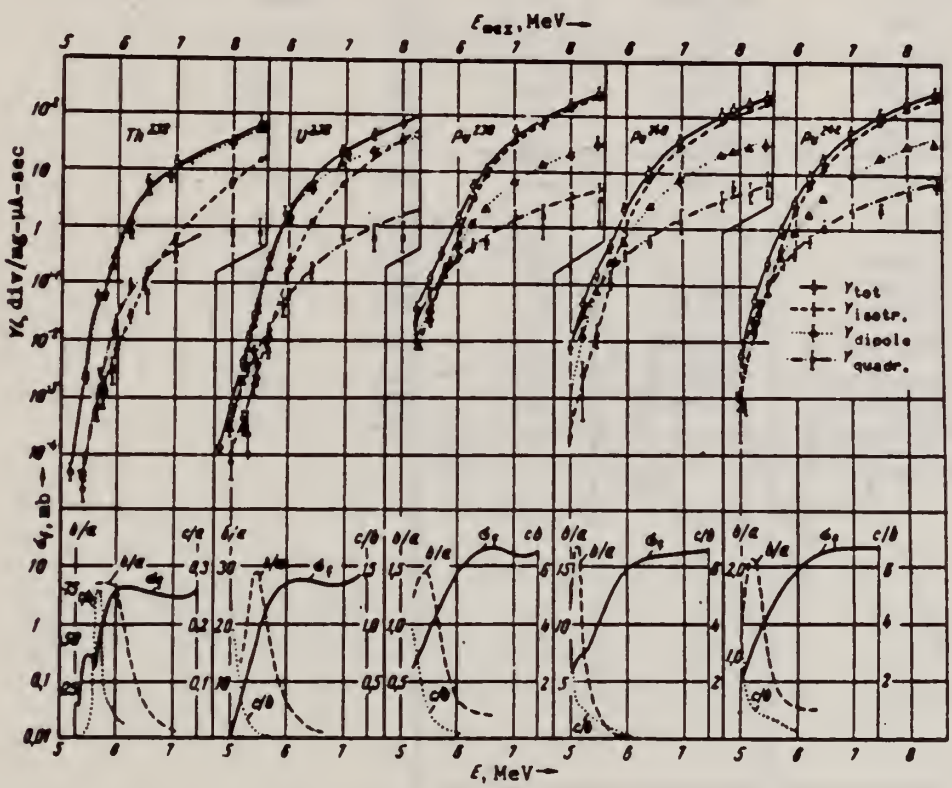

Fig. 2. Results of measurements of the fragment yields corresponding to different components of the angular distribution, as functions of the end-point energy of the bremsstrahlung spectrum (upper plots) and fission cross section and values of the ratios b/a and c/b as functions of the energy of the γ quanta, obtained as a result of the reduction of the experimental data (lower plots).

REF.

A. Manfredini, L. Fiore, C. Ramorino, H. G. De Carvalho and W. Wolfli
Nucl. Phys. A127, 687 (1969)

ELEM. SYM.	A	Z
Th	232	90

METHOD

REF. NO.	
69 Ma 2	egf

REACTION	RESULT	EXCITATION ENERGY	SOURCE		DETECTOR		ANGLE
			TYPE	RANGE	TYPE	RANGE	
G,F	ABX	5-9	D	5-9	EMU-I		4PI

Source n-capture gamma rays.

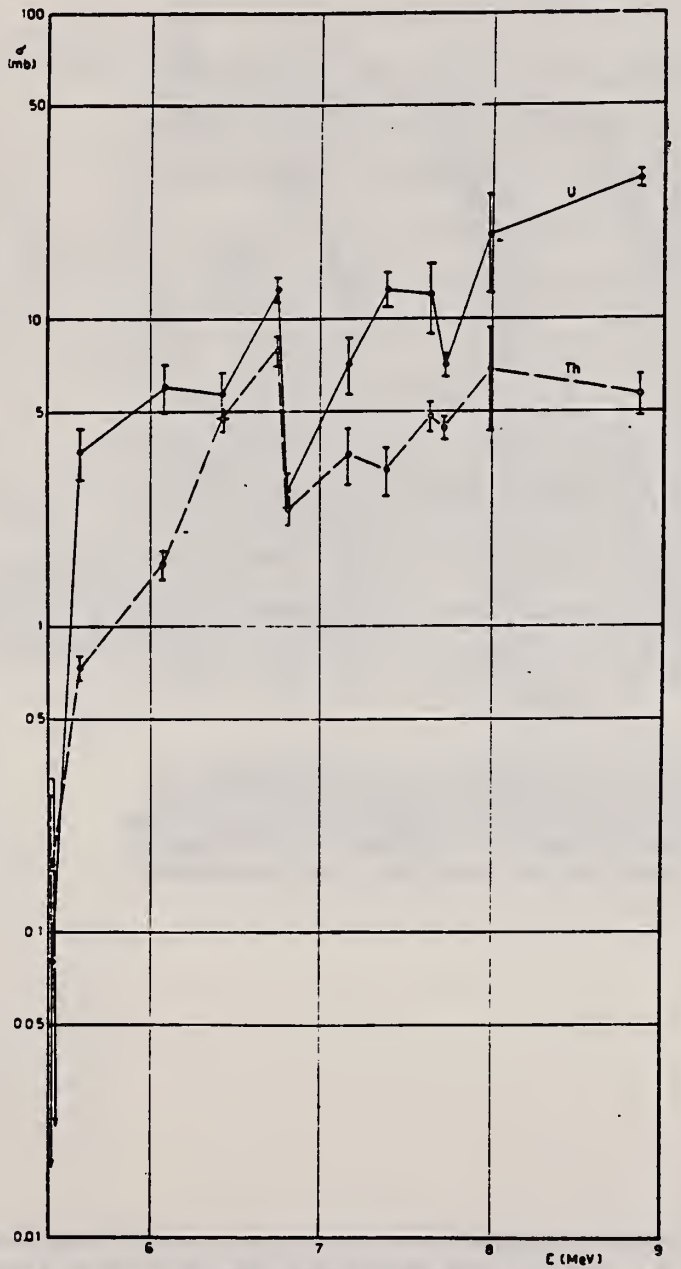

Fig. 1. Experimental results of photofission cross section for ^{238}U and ^{232}Th.

[over]

TABLE 1

Experimental data

Target	E_γ (MeV)	Φ_a ($10^{10} \cdot cm^{-2}$)	$N_f/(\Phi_a Th)$ (mb)	$\sigma_f(Th)$ (mb)	$\sigma_f(U)$ (mb)
S	5.43	3.32	0.59±0.16	0.16±0.16	0.08±0.20
Dy	5.58	2.62	0.79±0.07	0.73±0.07	3.73±0.70
Y	6.07	2.18	1.90±0.15	1.60±0.16	5.99±1.05
Ca	6.42	2.16	5.13±0.44	4.73±0.44	5.88±1.06
Ti	6.75	9.21 1.16	12.20±0.82	7.94±0.89	12.5 ±1.1
Be	6.80	1.01 0.96	2.40±0.25	2.40±0.25	2.73±0.32
Mn	7.16	2.39	7.14±1.11	3.67±0.74	7.17±1.50
Pb	7.38	0.65	3.81±0.56	3.25±0.56	12.6 ±1.6
Fe	7.64	1.40	6.38±0.51	4.86±0.53	12.1 ±3.1
Al	7.72	5.11 3.14	5.45±0.34	4.47±0.34	7.15±0.56
Cu	7.91	0.71	12.31±2.53	6.89±2.55	18.9 ±6.7
Ni	8.86	1.29	12.05±1.03	5.79±0.91	29.0 ±1.8

REF.

Y. Wakuta, M. Sonoda, A. Katase, H. Tawara, M. Hyakutake
J. Phys. Soc. Japan 26, 851 (1969)

Th	232	90

METHOD

REF. NO. 69 Wa 1 hmg

REACTION	RESULT	EXCITATION ENERGY	SOURCE		DETECTOR		ANGLE
			TYPE	RANGE	TYPE	RANGE	
G,F	RLX	0-999	C	200-999	SCD-D		DST

-999=1.2 GEV

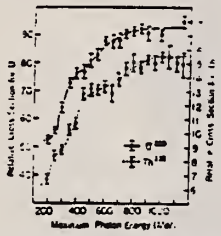

Fig. 1. Relative photofission cross section per equivalent quantum as a function of maximum photon energy for U^{238} and Th^{232}.

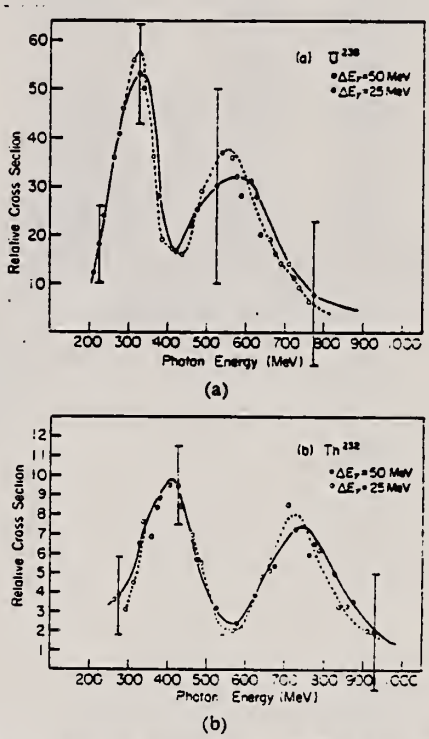

Fig. 2. Relative photofission cross section for two values of bin width as a function of photon energy. (a) for U^{238} and (b) for Th^{232} respectively.

REF.

D. C. Aumann and J. E. Gindler
J. inorg. nucl. Chem. 32, 731 (1970)

ELEM. SYM.	A	Z
Th	232	90

METHOD

REF. NO.	
70 Au 1	egf

REACTION	RESULT	EXCITATION ENERGY	SOURCE		DETECTOR		ANGLE
			TYPE	RANGE	TYPE	RANGE	
G,F	RLY	THR-17	C	14-17	ACT-I		4PI

Data ratio of isomer to ground state yields.

ISOMER YIELDS

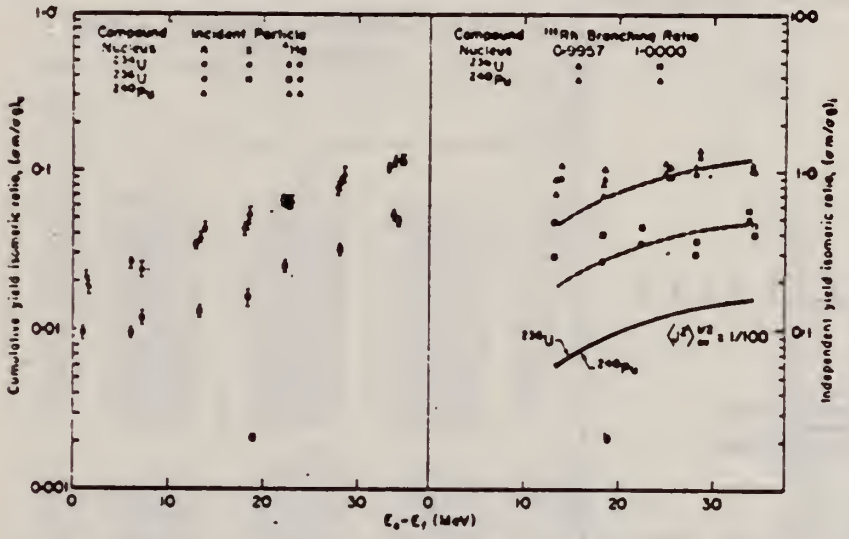

Fig. 3. Cumulative (a) and independent (b) yield ^{111}Pd isomeric ratios as a function of excitation energy above the fission barrier for several compound nuclei. The solid curves in 3b represent the root-mean-square average angular momenta of the compound nuclei indicated. The dashed curves are the solid curves displaced to pass approximately through the respective isomeric ratio data.

Table 3. Cumulative yield isomeric ratios of ^{111}Pd formed in photofission

Target	E_γ MeV) 13·8	16·6–17·0	17·1
^{232}Th	0·0040 ± 0·0004	0·0056 ± 0·0006	
^{238}U	0·0053 ± 0·0004	0·0054 ± 0·0005	0·0066 ± 0·0007
^{236}U	0·0095 ± 0·0007		0·0119 ± 0·0012
^{235}U	0·0125 ± 0·0009	0·0130 ± 0·0013	
^{234}U	0·0261 ± 0·0019		0·0235 ± 0·0024
^{233}U	0·0304 ± 0·0022	0·0380 ± 0·0038	0·0454 ± 0·0045

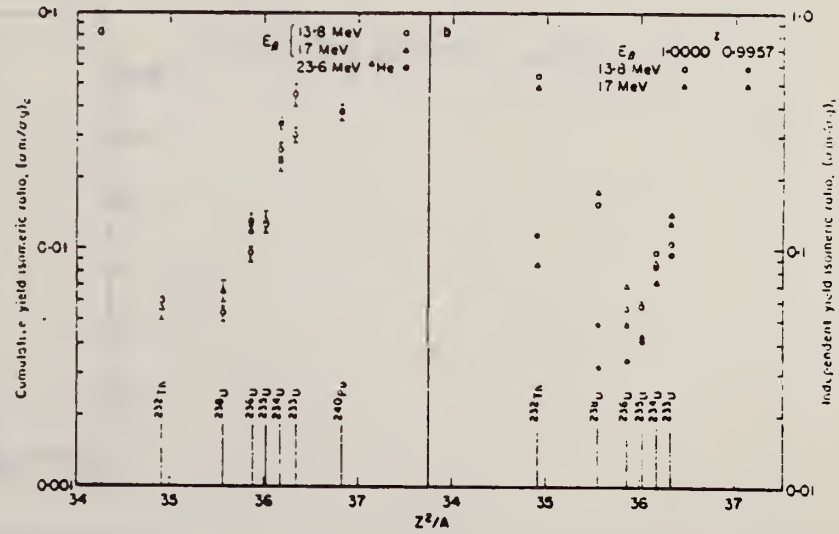

Fig. 5. Cumulative (a) and independent (b) yield ^{111}Pd isomeric ratios as a function of Z^2/A for the compound nucleus.

REF.

T. Methasiri
Nucl. Phys. A158, 433 (1970)

ELEM. SYM.	A	Z
Th	232	90

METHOD

REF. NO.: 70 Me 5 egf

REACTION	RESULT	EXCITATION ENERGY	SOURCE		DETECTOR		ANGLE
			TYPE	RANGE	TYPE	RANGE	
G,F	ABY	THR-900	C	200-900	TRK		4PI

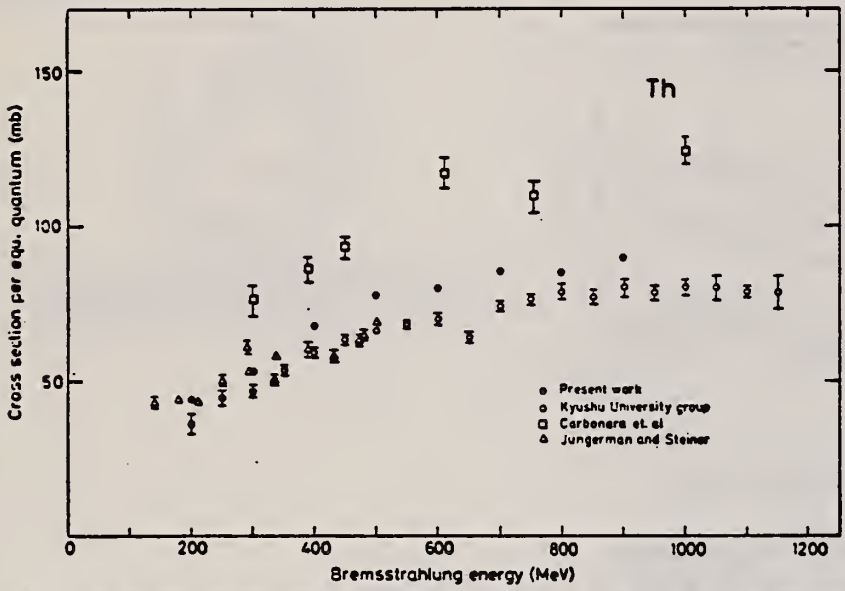

Fig. 3. Cross sections per equivalent quantum $\sigma_q(\hat{E})$ of thorium as a function of bremsstrahlung maximum energy ($\hat{E}$).

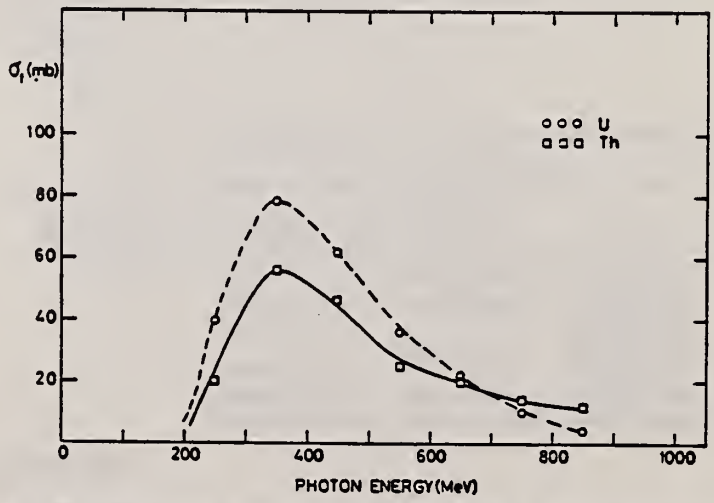

Fig. 4. Photofission cross sections of uranium and thorium as a function of photon energy.

REF. N.S. Rabotnov, G.N. Smirenkin, A.S. Soldatov, L.N. Usachev, S.P. Kapitza, and Yu. M. Tsipenyuk
Yad. Fiz. 11, 508 (1970)
Sov. J. Nucl. Phys. 11, 285 (1970)

ELEM. SYM.	A	Z
Th	232	90

METHOD

REF. NO.: 70 Ra 1 | hmg

REACTION	RESULT	EXCITATION ENERGY	SOURCE TYPE	SOURCE RANGE	DETECTOR TYPE	DETECTOR RANGE	ANGLE
G,F	ABX	THR-9	C	5-10	TRK-D		DST

SEE 68RA1, 69KA1

Table II. Parameters of angular distributions of the fragments

E_{max}, MeV	a	b	c	Y, fission / mg·μ·sec
		Th^{232}		
5.2	—	—	—	$4.5\cdot10^{-6}$
5.4	0.000±0.009	0.991±0.027	0.020±0.025	0.0024
5.65	0.011±0.005	0.989±0.007	−0.005±0.006	0.059
5.75	0.015±0.010	0.985±0.034	0.013±0.031	0.062
5.9	0.010±0.005	0.990±0.016	0.041±0.015	0.20
6.05	0.014±0.004	0.986±0.009	0.075±0.010	0.32
6.2	0.012±0.003	0.988±0.010	0.079±0.010	0.79
6.5	0.022±0.005	0.978±0.015	0.022±0.014	5.5
6.7	0.023±0.002	0.977±0.009	0.009±0.008	9.8
6.9	0.032±0.007	0.968±0.024	0.024±0.022	7.7
7.0	0.036±0.004	0.964±0.013	0.038±0.012	13.5
7.3	0.056±0.006	0.944±0.020	0.031±0.017	19.5
7.7	0.088±0.015	0.912±0.015	0.029±0.013	30.5
8.0	0.109±0.008	0.891±0.013	0.026±0.012	35
8.5	0.164±0.004	0.836±0.008	0.017±0.008	71
10.0	0.301±0.000	0.698±0.014	−0.031±0.014	—
		U^{238}		
5.0	0.052±0.100	0.948±0.161	1.296±0.245	0.00071
5.2	0.100±0.038	0.900±0.061	0.910±0.090	0.0042
5.3	0.020±0.035	0.980±0.061	0.566±0.078	0.0120
5.4	0.007±0.021	0.993±0.050	0.312±0.066	0.040
5.45	0.038±0.019	0.962±0.017	0.155±0.021	0.014
5.65	0.034±0.005	0.966±0.011	0.060±0.010	0.27
5.95	0.078±0.005	0.922±0.014	0.039±0.014	1.7
6.4	0.127±0.004	0.873±0.009	0.035±0.008	6.0
6.95	0.213±0.004	0.787±0.008	0.037±0.006	24.0
7.5	0.261±0.006	0.739±0.010	0.021±0.011	47.0
8.0	0.401±0.005	0.599±0.006	0.014±0.007	74.0
9.25	0.570±0.006	0.430±0.007	0.013±0.007	—
		Pu^{240}		
5.25	0.408±0.103	0.592±0.130	1.412±0.120	0.031
5.5	0.320±0.063	0.680±0.044	1.513±0.112	0.15
5.75	0.311±0.017	0.688±0.016	0.655±0.055	0.47
6.0	0.326±0.011	0.674±0.016	0.370±0.018	1.7
6.25	0.666±0.008	0.334±0.011	0.180±0.013	5.9
6.5	0.731±0.012	0.269±0.016	0.080±0.018	11
7.0	0.772±0.011	0.228±0.016	0.068±0.017	56
7.5	0.785±0.012	0.215±0.017	0.032±0.019	90
8.0	0.813±0.013	0.187±0.017	0.029±0.018	160
8.5	0.828±0.015	0.172±0.020	0.023±0.022	270
		Pu^{242}		
5.0*	0.000±0.200	0.000±0.200	1±0.200	0.0031
5.2	0.115±0.107	0.885±0.111	2.58±0.15	0.047

*In this case W(θ) is described by a pure quadrupole distribution, ~$\sin^2 2\theta$, and therefore the coefficient c is meaningless in the employed normalization and is assumed equal to unity.

Table II (cont.)

E_{max}, MeV	a	b	c	Y, Y, fission / mg·μ·sec
		Pu^{239}		
5.15	0.102±0.014	0.898±0.056	1.147±0.070	0.15
5.7	0.222±0.034	0.778±0.012	0.710±0.052	0.49
5.95	0.533±0.010	0.467±0.011	0.331±0.011	2.3
6.4	0.670±0.012	0.330±0.012	0.096±0.013	11.5
6.95	0.689±0.025	0.311±0.027	0.067±0.029	40
7.7	0.716±0.012	0.284±0.016	0.055±0.017	115
7.9	0.725±0.012	0.275±0.016	0.074±0.018	145
8.2	0.762±0.010	0.238±0.014	0.068±0.015	180
8.5	0.779±0.020	0.221±0.027	0.057±0.029	210
8.7	0.791±0.009	0.209±0.012	0.032±0.014	230
9.5	0.822±0.011	0.178±0.014	0.019±0.016	650
5.0	0.532±0.308	0.468±0.372	3.702±0.424	0.0055
5.25	0.448±0.051	0.552±0.068	0.965±0.042	0.056
5.75	0.418±0.026	0.582±0.050	1.018±0.060	—
5.5	0.310±0.022	0.690±0.029	0.735±0.034	0.28
5.75	0.488±0.008	0.512±0.010	0.122±0.012	1.0
6.0	0.598±0.011	0.402±0.016	0.207±0.018	2.7
6.25	0.669±0.012	0.331±0.017	0.138±0.019	8.8
6.5	0.700±0.009	0.300±0.013	0.122±0.014	17
7.0	0.740±0.005	0.260±0.007	0.075±0.008	50
7.5	0.754±0.005	0.246±0.007	0.046±0.008	105
8.0	0.766±0.008	0.234±0.008	0.047±0.009	175
8.5	0.814±0.005	0.186±0.007	0.012±0.008	225

$$W(\theta) = a + b \sin^2\theta + c \sin^2 2\theta$$

[over]

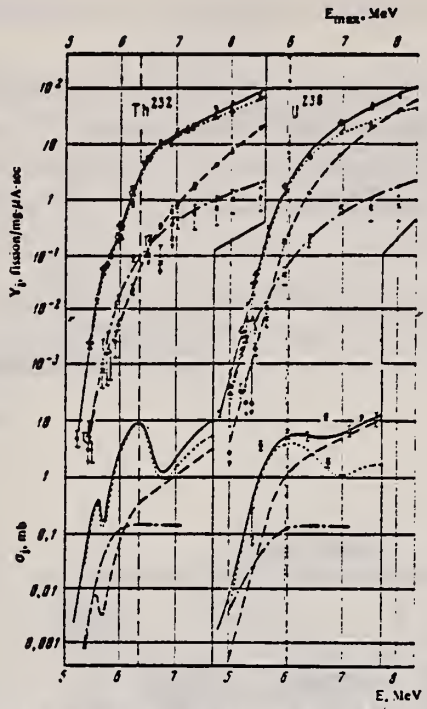

FIG. 3. Energy dependence of the total yield $Y(E_{max})$ (○) and its angular components $Y_a(E_{max})$ (●), $Y_b(E_{max})$ (▲), and $Y_c(E_{max})$ (×). Below—plots of the total cross section $\sigma_{\gamma f}(E)$ (solid curve) and its angular components $\sigma_a(E)$ (long dashes), $\sigma_b(E)$ (short dashes), and $\sigma_c(E)$ (dash-dot), obtained by solving Eq. (5), vs. the γ-quantum energy. The points for $\sigma_{\gamma f}$ for U^{238} were taken from [10]. The vertical dashed line denotes the binding energies of the neutron in the corresponding nucleus.

Anguiar components of the yieid. Knowledge of the coefficients a, b, and c makes it possible to determine the contribution of the individual components of the yield Y_a, Y_b, and Y_c, the angular dependence of which corresponds to three components in the expression (2): isotropic, dipole, and quadrupole. Their meaning can be understood from the following definitions:

$$Y = Y_a + Y_b + Y_c; \quad \frac{dY}{d\Omega} = \frac{1}{4\pi\nu} YW(\vartheta);$$

$$Y_a = \frac{a}{\nu} Y; \quad Y_b = \frac{2}{3}\frac{b}{\nu} Y; \quad Y_c = \frac{8}{15}\frac{c}{\nu} Y. \qquad (4)$$

Plots of Y_i and E_{max} are shown in Fig. 3 together with the data on the total yield. The experimental points $Y_i(E_{max})$ were determined by means of formulas (4) from the coefficients $W(\vartheta)$ listed in Table II and from the totai yield. The error of Y_i indicated in Fig. 3 does not include the error in the measurement of $Y(E_{max})$ (~10%).

B. Schröder, G. Nydahl and B. Forkman
Nucl. Phys. A143, 449 (1970)

ELEM. SYM.	A	Z
Th	232	90

METHOD

REF. NO.: 70 Sc 1 | egf

REACTION	RESULT	EXCITATION ENERGY	SOURCE TYPE	SOURCE RANGE	DETECTOR TYPE	DETECTOR RANGE	ANGLE
G,F	RLY	THR-999	C	300-999	ACT-I		4PI

999 = 1100 MEV

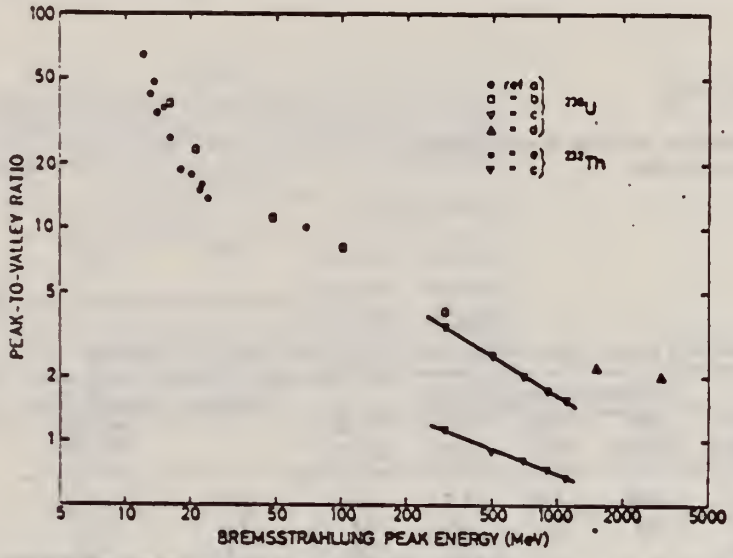

Fig. 4. Published data on peak-to-valley ratio of ^{238}U and ^{232}Th. ref. a, see ref. [3]); ref. b, see ref. [3]); ref. c, see this work; ref. d, see ref. [4]); ref. e, see ref. [7]).

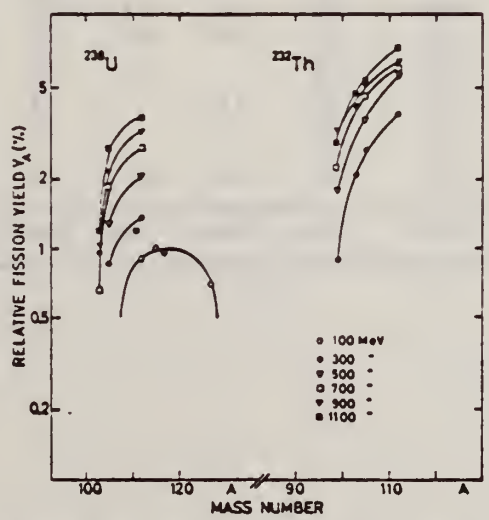

Fig. 5. Symmetric high-energy mass distributions from ^{238}U and ^{232}Th. The data at 100 MeV are those reported by Schmitt and Sugarman [3]).

[over].

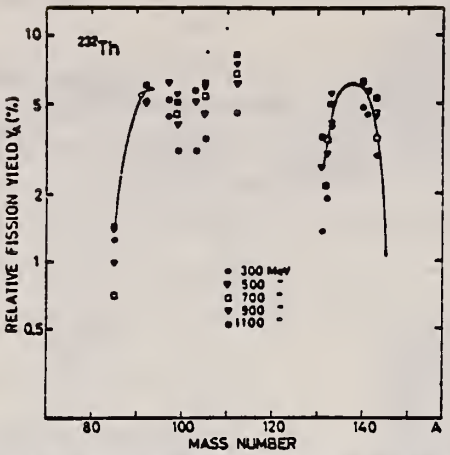

Fig. 6. Relative fission yields of ^{232}Th at different irradiation energies. All yields normalized to $Y_{91} = 5.5\,\%$ (○). The curve shows the average values.

TABLE 3

Measured cumulative fission yields relative to $A = 91$ (^{232}Th) and $A = 105$(^{209}Bi)

Mass number	Thorium fission yield (%)					Average	Bismuth fission yield (%)
	300 (MeV)	500 (MeV)	700 (MeV)	900 (MeV)	1100 (MeV)		700 MeV
85	1.3	0.98	0.70	1.4	1.4	1.1	0.46
91	5.5	5.5	5.5	5.5	5.5	5.5	2.1
92	5.3			5.2	6.0	5.5	3.2
95							4.8
97	4.4			6.2	5.2	5.3	5.1
99	3.1	4.0	4.5	5.5	5.1		4.9
103	3.1			5.2	5.8		5.1
105	3.5	4.5	5.4	6.0	6.0		5.0
112	4.6	6.2	6.8	7.5	8.3		4.0
131	1.3			2.7	3.5	2.5	
132	1.9		3.5	3.0	2.2	2.6	
133	4.0	4.1		5.5	5.0	4.7	
140	4.9			6.0	6.2	5.7	
141	4.5				5.6	5.1	
143	2.9	4.6	3.5	4.5	5.3	4.2	
detector	30 cm³	7 mm	7 mm	7 mm	30 cm³		30 cm³

REF.

M. Hass, R. Moreh, and D. Salzmann
Phys. Letters 36B, 68 (1971)

ELEM. SYM.	A	Z
Th	232	90

METHOD

REF. NO. 71 Ha 1 egf

REACTION	RESULT	EXCITATION ENERGY	SOURCE		DETECTOR		ANGLE
			TYPE	RANGE	TYPE	RANGE	
G,G	ABX	8-9	D	8-9	SCD-D	7-9	90

Table 1
Measured differential cross sections (μb/sr) for elastic and Raman scattering from U and Th targets at an angle of 140°. The calculated values for ^{238}U using the GDR parameters of ref. [6] and a set of tentative parameters are shown.

	Experiment				Calculated (^{238}U)			
E_γ	^{232}Th		^{238}U		Ref. [6]		Tentative	
(keV)	Elastic	Raman	Elastic	Raman	Elas-tic	Ra-man	Elas-tic	Ra-man
8533	7± 3	7± 3	8± 3	8± 3	17	15	11	10
8998	24± 7	15± 5	27± 6	18± 4	38	28	27	18
9298	37±10	25± 8	42± 9	27± 7	62	43	44	28

REF.

A.V. Ignatyuk, N.S. Rabotnov, G.N. Smirenkin, A.S. Soldatov, and Yu. M. Tsipenyuk
Zh. Eksp. Teor. Fiz. 61, 1284 (1971)
Sov. Phys. JETP 34, 684 (1972)

ELEM. SYM.	A	Z
Th	232	90

METHOD

REF. NO.	
71 Ig 1	egf

REACTION	RESULT	EXCITATION ENERGY	SOURCE		DETECTOR		ANGLE
			TYPE	RANGE	TYPE	RANGE	
G,F	ABX	5 - 7	C	5 - 7	TRK-I		DST

Table I. Angular-distribution parameters a_f and c_f and yield of the photofission reaction, obtained in measurements with metallic foils. The isotropic component $W(\theta)$, obtained with layers (a_f), is compared with the value of a obtained from (13)

E_{max}, MeV	a_f	a	a_f	c_f	Y, fiss/mg·μA·sec
			Th^{232}		
5.36	0.042±0.019	0.019±0.019	—	0.022±0.046	$1.45\cdot10^{-4}$
5.65	0.041±0.014	0.017±0.014	0.016±0.008	0.038±0.025	$5.1\cdot10^{-4}$
5.93	0.031±0.012	0.010±0.013	0.013±0.010	0.027±0.007	$6.2\cdot10^{-4}$
6.20	0.024±0.009	0.006±0.009	0.015±0.010	0.013±0.025	$8.3\cdot10^{-4}$
6.80	0.024±0.004	−0.004±0.005	0.014±0.005	0.044±0.011	0.21
6.80	0.024±0.004	0.004±0.005	0.012±0.003	0.042±0.011	0.70
6.80	0.044±0.003	0.021±0.003	0.022±0.003	0.059±0.005	4.0
6.80	0.060±0.003	0.034±0.004	0.023±0.003	−0.006±0.010	9.8
7.08	0.056±0.004	0.030±0.005	0.026±0.004	0.027±0.012	16.5
7.35	0.075±0.003	0.054±0.004	—	−0.005±0.011	17.6
7.35	0.070±0.003	0.047±0.004	0.026±0.005	0.031±0.004	19.5
7.35	0.111±0.005	0.091±0.006	0.044±0.005	0.021±0.013	60.5
8.00	0.135±0.004	0.113±0.005	0.107±0.016	0.007±0.011	80
8.36	0.161±0.005	0.161±0.005	0.164±0.006	0.015±0.012	88
			U^{238}		
4.83	0.255±0.175	0.211±0.210	—	1.057±0.334	$1.2\cdot10^{-4}$
4.8	0.241±0.077	0.260±0.078	—	0.921±0.118	$2\cdot10^{-4}$
4.85	0.321±0.078	0.291±0.078	—	1.340±0.134	$3\cdot10^{-4}$
4.93	0.171±0.032	0.171±0.033	—	1.320±0.068	$4.7\cdot10^{-4}$
5.0	0.211±0.047	0.153±0.050	0.062±0.026	1.137±0.062	$8.4\cdot10^{-4}$
5.13	0.126±0.031	0.162±0.033	—	1.026±0.054	$2.7\cdot10^{-4}$
5.11	0.174±0.023	0.098±0.024	0.108±0.025	1.107±0.045	$6.3\cdot10^{-4}$
5.4	0.074±0.011	0.024±0.012	0.038±0.009	0.306±0.026	$2.1\cdot10^{-4}$
5.5	0.021±0.003	0.040±0.004	—	0.161±0.007	$7.4\cdot10^{-4}$
5.6	0.048±0.005	0.024±0.005	—	0.071±0.012	0.16
5.65	0.057±0.005	0.034±0.006	0.038±0.005	0.064±0.011	0.27
5.7	0.017±0.003	0.014±0.004	—	0.041±0.009	0.34
5.8	0.052±0.005	0.046±0.007	—	0.052±0.014	0.68
5.8	0.079±0.003	0.054±0.004	0.078±0.005	0.058±0.007	0.91
6.0	0.122±0.005	0.094±0.006	—	0.064±0.012	1.8
6.1	0.149±0.014	0.124±0.015	—	0.034±0.034	3.0
6.2	0.141±0.004	0.124±0.005	—	0.013±0.007	36
6.4	0.141±0.005	0.126±0.007	—	0.009±0.010	45
6.5	0.154±0.004	0.139±0.010	0.104±0.005	0.027±0.013	47

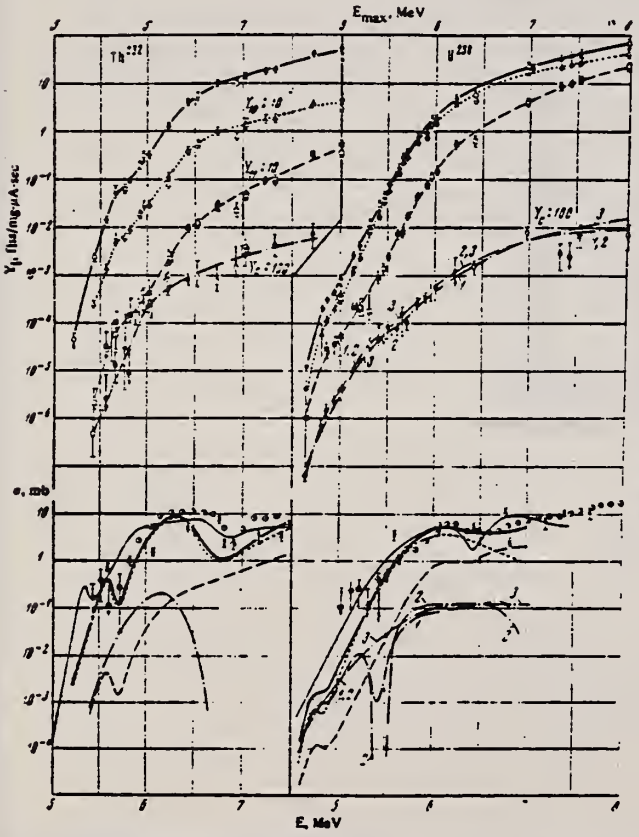

FIG. 4. Top—Energy dependences of the total yield $Y(E_{max})$—○, ● and its components $Y_{10}(E_{max})$—△, ▲, $Y_{11}(E_{max})$—□, ■) and $Y_C(E_{max})$—◇, ◇. The light circles represent the results of measurements with thin layers of Th^{232} and U^{238}, and the dark ones correspond to metallic foils. Bottom—plots of the photofission total cross section $\sigma_f(E)$ and of its components $\sigma_{10}(E)$, $\sigma_{11}(E)$, and $\sigma_C(E)$. The points X and ◑ represent respectively the results of [10] and [12]. The thin solid line shows plots of the total cross section $\sigma_f(E)$ obtained in [8].

REF. A. Manfredini, L. Fiore, C. Ramorino, and W. Wolfli
Nuovo Cimento 4A, 421 (1971)

ELEM. SYM.	A	Z
Th	232	90

METHOD

REF. NO. 71 Ma 3 hmg

REACTION	RESULT	EXCITATION ENERGY	SOURCE		DETECTOR		ANGLE
			TYPE	RANGE	TYPE	RANGE	
G,F	NOX	5-9	D	5-9	EMU-I		DST

$$W(\theta) = a + b \sin^2\theta + c \sin^2\theta \cos^2\theta$$

$$\int_0^{\pi/2} W(\theta)\sin\theta\, d\theta = 1$$

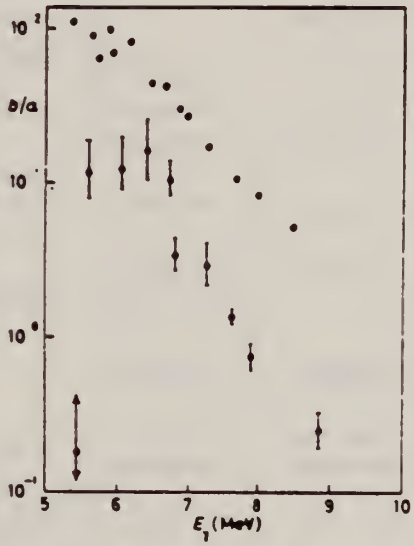

Fig. 1. – Experimental ratio b/a as a function of E_γ. Black points are our experimental data; white points are RABOTNOV *et al.* (6) results and are plotted as a function of E_{max} of the bremsstrahlung spectrum.

TABLE I. – *Values of the a, b, and c parameters of the angular distribution.*

Target	E_γ	a	b	c	Target	E_γ	a	b	c
Dy	5.61	0.10±0.07	1.12±0.05	1.15±0.44	S	5.43	0.48±0.63	0.09±0.54	3.47±2.60
Y	6.14	0.10±0.03	1.22±0.02	0.61±0.23	Dy	5.58	0.10±0.07	1.11±0.06	1.19±0.47
Ca	6.42	0.09±0.02	1.16±0.02	1.03±0.18	Y	6.07	0.10±0.04	1.21±0.03	0.72±0.28
Ti	6.66	0.12±0.02	1.20±0.01	0.20±0.15	Ca	6.42	0.07±0.03	1.18±0.02	1.03±0.20
Be	6.80	0.29±0.07	0.95±0.10	0.50±0.49	Ti	6.75	0.13±0.03	1.36±0.03	0.26±0.26
Pb	7.38	0.26±0.07	0.92±0.06	0.93±0.01	Be	6.82	0.29±0.07	0.95±0.10	0.59±0.49
S	7.33	0.59±0.17	0.39±0.15	1.13±0.69	Pb	7.38	0.29±0.09	0.84±0.07	1.14±0.72
Cu	7.60	0.50±0.03	0.66±0.02	0.49±0.23	Fe	7.63	0.51±0.04	0.68±0.03	0.23±0.27
Fe	7.63	0.50±0.03	0.69±0.02	0.29±0.20	Cu	7.91	0.62±0.06	0.50±0.04	0.54±0.45
Ni	8.27	0.74±0.03	0.38±0.02	0.03±0.24	Ni	8.86	0.89±0.05	0.22±0.03	−0.24±0.36

REF.

O. Y. Mafra and S. Kuniyoshi
An. Acad. Brasil. Cienc. 43, 571 (1971)

ELEM. SYM.	A	Z
Th	232	90

METHOD

REF. NO.	
71 Ma 6	egf

REACTION	RESULT	EXCITATION ENERGY	SOURCE		DETECTOR		ANGLE
			TYPE	RANGE	TYPE	RANGE	
G,F	ABX	5- 10	D	5- 10	ION-I		4PI

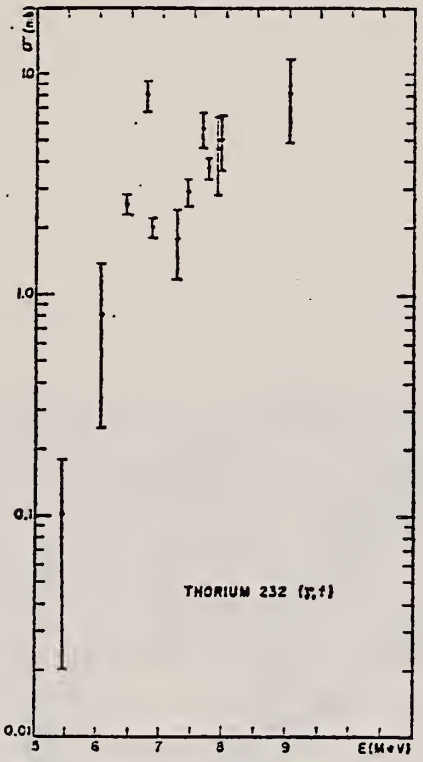

Fig. 2 — Experimental photofission cross section for Thorium.

REF.

G.A. Vartapetyan, N.A. Demekhina, V.I. Kasilov, Yu. N. Ranyuk, P.V. Sorokin and A.G. Khudaverdyan
Yad. Fiz. 14, 65 (1971)
Sov. J. Nucl. Phys. 14, 37 (1972)

ELEM. SYM.	A	Z
Th	232	90

METHOD

REF. NO.: 71 Va 4 egf

REACTION	RESULT	EXCITATION ENERGY	SOURCE		DETECTOR		ANGLE
			TYPE	RANGE	TYPE	RANGE	
G,F	ABX	100-999	C	100-999	TRK-I		4PI

999 = 5 GEV

$E_{\gamma\,max}$, MeV	Photofission yields per cm³ per equivalent photon					
	U^{238}	U^{235}	Th^{232}	Bi^{209}	Au^{197}	Ta^{181}
100	$(226 \pm 20) \cdot 10^{-27}$	$(120 \pm 12) \cdot 10^{-27}$	$(50 \pm 5) \cdot 10^{-27}$	$(0.70 \pm 0.08) \cdot 10^{-27}$	$(3.0 \pm 0.4) \cdot 10^{-27}$	
120				$(1.5 \pm 0.2) \cdot 10^{-27}$	$(1.6 \pm 0.2) \cdot 10^{-27}$	
140				$2.0 \pm 0.2) \cdot 10^{-27}$	$(2.0 \pm 0.2) \cdot 10^{-27}$	
150	$(240 \pm 20) \cdot 10^{-27}$		$(63 \pm 7) \cdot 10^{-27}$			
160				$(3.1 \pm 0.3) \cdot 10^{-27}$	$(3.7 \pm 0.4) \cdot 10^{-27}$	
180				$(4.6 \pm 0.5) \cdot 10^{-27}$	$(5.5 \pm 0.6) \cdot 10^{-27}$	
200	$(268 \pm 30) \cdot 10^{-27}$	$(150 \pm 15) \cdot 10^{-27}$	$(72 \pm 7) \cdot 10^{-27}$	$(6.1 \pm 0.6) \cdot 10^{-27}$	$(6.2 \pm 0.8) \cdot 10^{-27}$	$(4.9 \pm 0.5) \cdot 10^{-27}$
220				$(8.3 \pm 0.8) \cdot 10^{-27}$	$(9.1 \pm 0.9) \cdot 10^{-27}$	$(8.2 \pm 0.8) \cdot 10^{-27}$
240				$(1.2 \pm 0.1) \cdot 10^{-26}$	$(1.5 \pm 0.2) \cdot 10^{-26}$	$(1.2 \pm 0.1) \cdot 10^{-26}$
215		$(156 \pm 16) \cdot 10^{-27}$				
260				$(1.5 \pm 0.2) \cdot 10^{-26}$	$(1.8 \pm 0.2) \cdot 10^{-26}$	$(1.5 \pm 0.2) \cdot 10^{-26}$
280		$(160 \pm 16) \cdot 10^{-27}$	$(85 \pm 9) \cdot 10^{-27}$			
300				$(2.2 \pm 0.2) \cdot 10^{-26}$	$(2.8 \pm 0.2) \cdot 10^{-26}$	
320				$(3.5 \pm 0.4) \cdot 10^{-26}$	$(4.4 \pm 0.4) \cdot 10^{-26}$	
340				$(4.2 \pm 0.4) \cdot 10^{-26}$	$(5.0 \pm 0.5) \cdot 10^{-26}$	
360	$(318 \pm 30) \cdot 10^{-27}$	$(175 \pm 20) \cdot 10^{-27}$				
420			$(105 \pm 11) \cdot 10^{-27}$			$(7.0 \pm 0.7) \cdot 10^{-26}$
440				$(5.4 \pm 0.5) \cdot 10^{-26}$	$(6.9 \pm 0.7) \cdot 10^{-26}$	
460				$(6.7 \pm 0.7) \cdot 10^{-26}$	$(8.1 \pm 0.9) \cdot 10^{-26}$	
500		$(190 \pm 20) \cdot 10^{-27}$	$(115 \pm 12) \cdot 10^{-27}$	$(8.0 \pm 0.8) \cdot 10^{-26}$	$(9.0 \pm 1) \cdot 10^{-26}$	
520				$(7.8 \pm 0.8) \cdot 10^{-26}$	$(1.1 \pm 0.1) \cdot 10^{-25}$	
540	$(348 \pm 35) \cdot 10^{-27}$					
560				$(7.7 \pm 0.8) \cdot 10^{-26}$	$(1.0 \pm 0.1) \cdot 10^{-25}$	$(1.7 \pm 0.2) \cdot 10^{-26}$
645				$(8.8 \pm 0.9) \cdot 10^{-26}$	$(1.1 \pm 0.1) \cdot 10^{-25}$	
700		$(200 \pm 20) \cdot 10^{-27}$	$(120 \pm 12) \cdot 10^{-27}$	$(8.5 \pm 0.9) \cdot 10^{-26}$	$(1.3 \pm 0.1) \cdot 10^{-25}$	
750				$(9.2 \pm 0.9) \cdot 10^{-26}$	$(1.2 \pm 0.1) \cdot 10^{-25}$	
800						$(2.4 \pm 0.2) \cdot 10^{-26}$
850				$(10.4 \pm 1) \cdot 10^{-26}$	$(1.3 \pm 0.2) \cdot 10^{-25}$	
900		$(230 \pm 23) \cdot 10^{-27}$	$(135 \pm 14) \cdot 10^{-27}$			
950	$(386 \pm 40) \cdot 10^{-27}$					
1000		$(224 \pm 23) \cdot 10^{-27}$	$(140 \pm 14) \cdot 10^{-27}$			
1015						$(2.9 \pm 0.3) \cdot 10^{-26}$
1050				$(11.3 \pm 1.1) \cdot 10^{-26}$	$(1.9 \pm 0.2) \cdot 10^{-25}$	
1100	$(440 \pm 40) \cdot 10^{-27}$					
1150	$(390 \pm 40) \cdot 10^{-27}$	$(217 \pm 23) \cdot 10^{-27}$	$(136 \pm 14) \cdot 10^{-27}$			
1170				$(12.5 \pm 1.3) \cdot 10^{-26}$	$(1.9 \pm 0.2) \cdot 10^{-25}$	
1200						$(3.3 \pm 0.3) \cdot 10^{-26}$
1250				$(13.8 \pm 1.4) \cdot 10^{-26}$	$(2.1 \pm 0.2) \cdot 10^{-25}$	
1300	$(376 \pm 40) \cdot 10^{-27}$	$(193 \pm 20) \cdot 10^{-27}$	$(125 \pm 15) \cdot 10^{-27}$			
1350				$(14.3 \pm 1.4) \cdot 10^{-26}$	$(2.0 \pm 0.2) \cdot 10^{-25}$	
1400	$(445 \pm 45) \cdot 10^{-27}$	$(238 \pm 24) \cdot 10^{-27}$	$(155 \pm 15) \cdot 10^{-27}$			
1450				$(13.9 \pm 1.4) \cdot 10^{-26}$	$(2.1 \pm 0.2) \cdot 10^{-25}$	
1500				$(15.5 \pm 1.6) \cdot 10^{-26}$	$(2.2 \pm 0.2) \cdot 10^{-25}$	
1550	$(440 \pm 45) \cdot 10^{-27}$	$(207 \pm 21) \cdot 10^{-27}$	$(141 \pm 14) \cdot 10^{-27}$			
1600	$(435 \pm 45) \cdot 10^{-27}$	$(242 \pm 24) \cdot 10^{-27}$	$(155 \pm 16) \cdot 10^{-27}$			
1650	$(491 \pm 50) \cdot 10^{-27}$	$(245 \pm 25) \cdot 10^{-27}$	$(152 \pm 15) \cdot 10^{-27}$	$(18.1 \pm 1.8) \cdot 10^{-26}$	$(2.3 \pm 0.3) \cdot 10^{-25}$	
1700	$(455 \pm 45) \cdot 10^{-27}$	$(230 \pm 23) \cdot 10^{-27}$	$(146 \pm 15) \cdot 10^{-27}$			
1750	$(500 \pm 50) \cdot 10^{-27}$	$(251 \pm 25) \cdot 10^{-27}$	$(148 \pm 15) \cdot 10^{-27}$		$(3.0 \pm 0.3) \cdot 10^{-25}$	$(6.4 \pm 0.6) \cdot 10^{-26}$
1800				$(15.6 \pm 1.6) \cdot 10^{-26}$	$(3.0 \pm 0.3) \cdot 10^{-25}$	$(6.6 \pm 0.7) \cdot 10^{-26}$
1850	$(476 \pm 50) \cdot 10^{-27}$	$(264 \pm 27) \cdot 10^{-27}$	$(183 \pm 18) \cdot 10^{-27}$			
1900	$(477 \pm 50) \cdot 10^{-27}$			$(20.2 \pm 2) \cdot 10^{-26}$	$(2.9 \pm 0.3) \cdot 10^{-25}$	$5.8 \pm 0.7) \cdot 10^{-26}$
1950	$(495 \pm 50) \cdot 10^{-27}$			$(20.2 \pm 2) \cdot 10^{-26}$	$(2.8 \pm 0.3) \cdot 10^{-25}$	$(6.3 \pm 0.6) \cdot 10^{-26}$

REF.	ELEM. SYM.	A	Z
Yoshihisa Wakuta . J. Phys. Soc. Japan 31, 12 (1971)	Th	232	90

METHOD	REF. NO.	
	71 Wa 1	egf

REACTION	RESULT	EXCITATION ENERGY	SOURCE		DETECTOR		ANGLE
			TYPE	RANGE	TYPE	RANGE	
G,F	ABX	THR-999	C	200-999	SCD-I		DST

Emulsion for angular distribution measurements. 999=1150 MEV 460

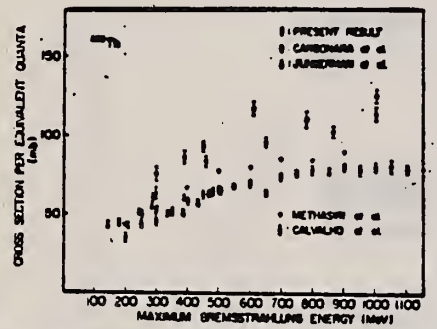

Fig. 4. Photofission cross section per equivalent quanta of Th as a function of maximum bremsstrahlung energy.

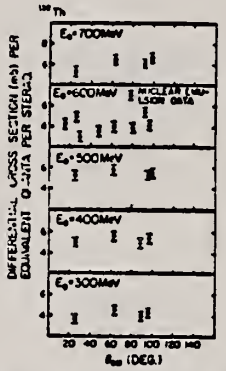

Fig. 10. Angular distribution of fragment in photofission of Th.

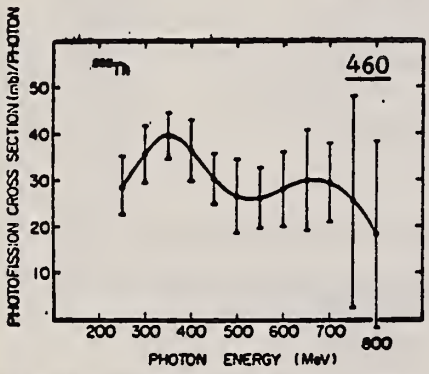

Fig. 8. Photofission cross section of Th as a function of photon energies up to 800 MeV.

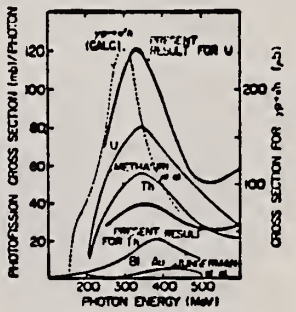

Fig. 13. Photofission cross sections for several nuclei as a function of photon energy. A theoretical curve obtained for $\gamma p \rightarrow \pi^+ n$ reaction is also shown for comparison.

REF.	ELEM. SYM.	A	Z
R. Bergere, H. Beil, P. Carlos, A. Veyssiere, A. Lepretre PICNS-72, p.273 Sendai	Th	232	90

METHOD	REF. NO.	
	72 Be 15	hvm

REACTION	RESULT	EXCITATION ENERGY	SOURCE		DETECTOR		ANGLE
			TYPE	RANGE	TYPE	RANGE	
G,N	ABX	9- 16	D	9- 16	MOD-I		4PI
G,2N	ABX	9- 16	D	9- 16	MOD-I		4PI
G,F	ABX	9- 16	D	9- 16	MOD-I		4PI

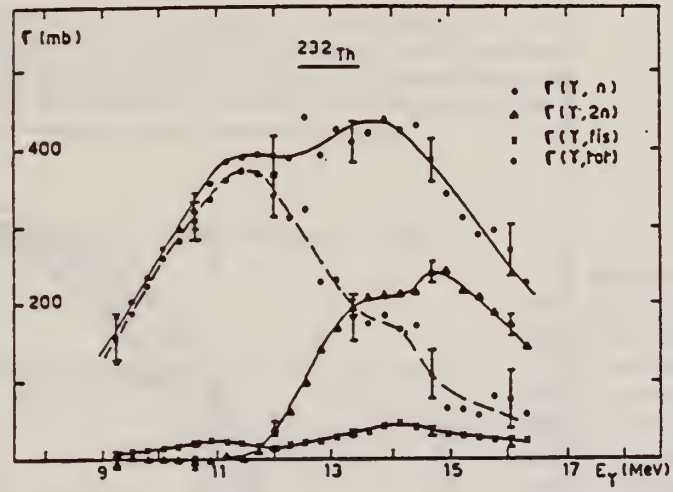

Fig. 3

TABLE 1

LORENTZ LINE PARAMETRS AND INTRINSIC QUADRUPOLE MOMENTS

Target nucleus	E_1 MeV	σ_1 mb	Γ_1 MeV	E_2 MeV	σ_2 mb	Γ_2 MeV	$R = \frac{\sigma_2 \Gamma_2}{\sigma_1 \Gamma_1}$	Q_0 barns *	Q_0 barns **
$^{232}_{90}Th$	11.08 ±0.12	268 ± 7	3.37 ±0.22	14.07 ±0.14	349 ± 9	4.62 ±0.16	1.8 ± 0.15	10.2 ± 1	9.86 ±0.1
$^{238}_{92}U$	10.96 ±0.09	301 ± 6	2.96 ±0.14	14.04 ±0.13	369 ± 6	4.53 ±0.13	1.9 ± 0.1	11 ± 1	11.3 ±0.1
$^{237}_{93}Np$	11.06 ±0.12	251 ± 7	3.16 ±0.27	14.21 ±0.14	380 ± 9	5.12 ±0.3	2.4 ± 0.3	11.3 ± 1	10.9 ±0.7

I/ LORENTZ LINES PARAMETERS

* this experiment

** —. E.E.O. [illegible], E. [illegible], V. [illegible]. – Nuclear data tables, Vol. 7, 5 (1570).

REF.

R.L. Bramblett, T. Gozani, R.O. Ginaven, D.E. Rundquist
Nucl. Technology 13, 33 (1972)

ELEM. SYM.	A	Z
Th	232	90

METHOD

REF. NO. 72 Br 8 egf

REACTION	RESULT	EXCITATION ENERGY	SOURCE		DETECTOR		ANGLE
			TYPE	RANGE	TYPE	RANGE	
G,F	RLY	THR-11	C	5-11	TRK-I		4PI
G,XN	RLY	THR-11	C	5-11	BF3-I		4PI

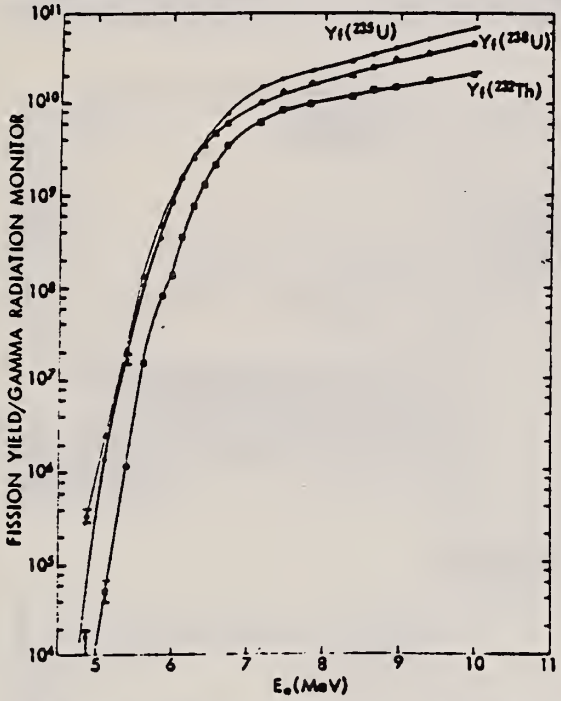

Fig. 7. Bremsstrahlung photofission yields from ^{232}Th, ^{235}U, and ^{238}U obtained using solid-state track detectors (from Gozani et al.[15]).

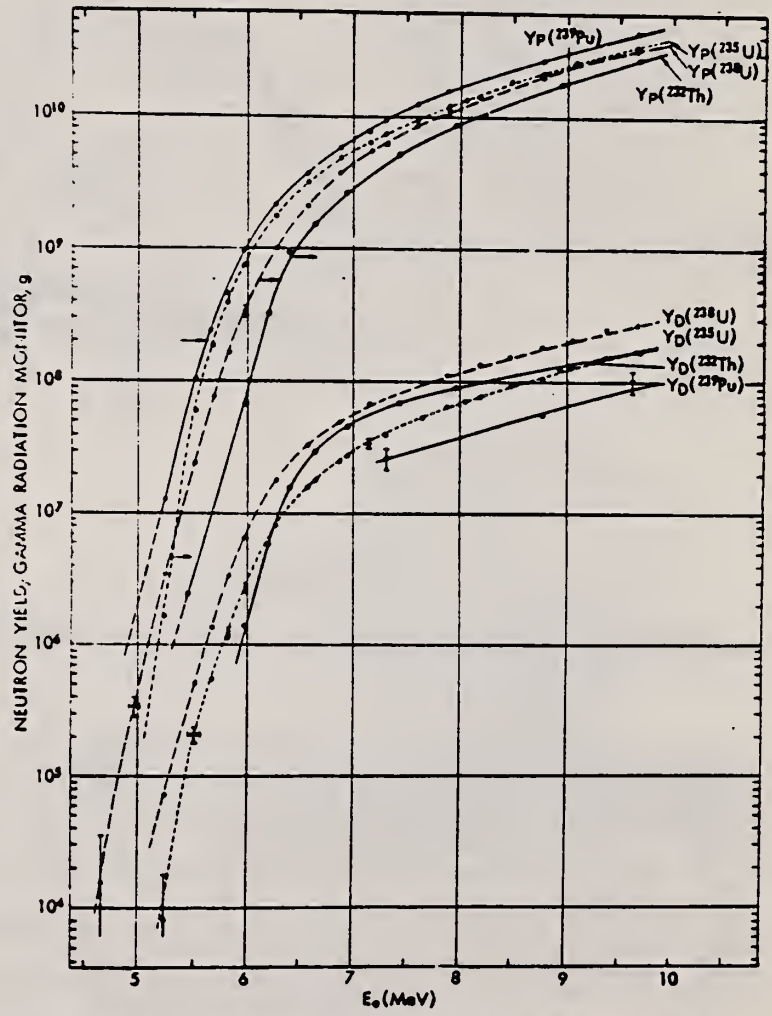

Fig. 8. Prompt- and delayed-neutron yields induced by electron bremsstrahlung for ^{232}Th, ^{235}U, ^{238}U, and ^{239}Pu.

REF.

H. E. Jackson and K. J. Wetzel
Phys. Rev. Letters 28, 513 (1972)

ELEM. SYM.	A	Z
Th	232	90

METHOD

REF. NO.: 72 Ja 1 hmg

REACTION	RESULT	EXCITATION ENERGY	SOURCE		DETECTOR		ANGLE
			TYPE	RANGE	TYPE	RANGE	
G,G	RLX	10	D	10	SCD-D		90
		(10.83)		(10.83)			

RATIO: RAMAN/ELASTIC

We have measured the differential cross sections for the elastic scattering of 10.83-MeV photons by U, Th, and Bi targets and for inelastic scattering to the first excited states of the residual nuclei over a range of scattering angles. The inelastic scattering is found to be significantly weaker than predicted by currently accepted models of the giant dipole resonance.

To establish that the anomaly we observe was not limited to uranium, we repeated the measurements on a second deformed actinide target (^{232}Th) and also on a spherical nucleus (^{209}Bi) for which no observable Raman component was expected. For ^{232}Th at 90° the observed ratio is 0.7 ± 0.1, while for ^{209}Bi no inelastic scattering to the first excited state was observed; i.e., the experimental ratio is ≤ 0.1. Thus the evidence suggests that the Raman to elastic ratio we find may be characteristic of the deformed actinide nuclei.

REF.

A. M. Khan and J. W. Knowles
Nucl. Phys. A179, 333 (1972)

ELEM. SYM.	A	Z
Th	232	90

METHOD

REF. NO. 72 Kh 1 egf

REACTION	RESULT	EXCITATION ENERGY	SOURCE		DETECTOR		ANGLE
			TYPE	RANGE	TYPE	RANGE	
G,F	ABX	THR-9	D	5-9	ION-I		4PI

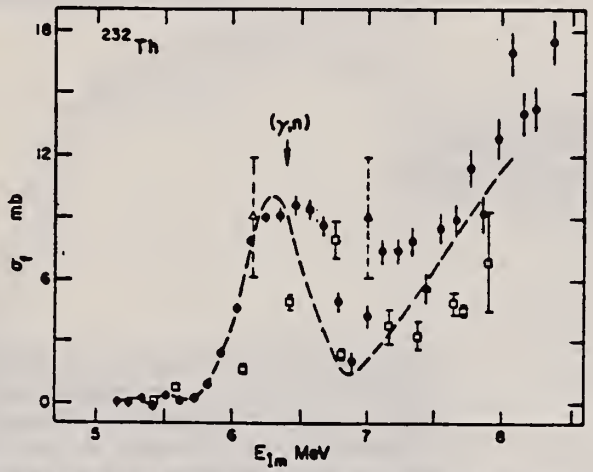

Fig. 9. Absolute photofission cross-section measurements σ_f of ^{232}Th as a function of γ-radiation energy E_{1m}. The error bars, estimated from the statistical count, indicate relative precision only. The photoneutron separation energy is indicated by (γ, n). The broken line is the corresponding photofission cross-section spectrum of Rabotnov *et al.*[8]); the points □ and △ are measurements of Manfredini *et al.*[7]) and Huizenga *et al.*[14]) respectively.

[7] A. Manfredini, L. Fiore, C. Ramorino, H.G. DeCarvalho & W. Wolfli, Nucl. Phys. A127 (1969) 637.

[8] N.S. Rabotnov, G.N. Smirenkin & A.S. Soldatov et al., Proc. Symp. on phys. and chem. of fission, SM 60/81, Vienna, 1965, p.135.

[14] A.S. Soldatov, Z.A. Aleksandrova, L.D. Gordeeva & G.N. Smirenkin, Sov. J. Nucl. Phys. 1 (1965) 335.

REF.

O.Y. Mafra, S. Kuniyoshi and J. Goldemberg
Nucl. Phys. A186, 110 (1972)

ELEM. SYM.	A	Z
Th	232	90

METHOD

REF. NO.: 72 Ma 1 | egf

REACTION	RESULT	EXCITATION ENERGY	SOURCE		DETECTOR		ANGLE
			TYPE	RANGE	TYPE	RANGE	
G,F	ABX	5-9	D	5-9	ION-I		4PI
G,N	ABX	5-9	D	5-9	BF3-I		4PI

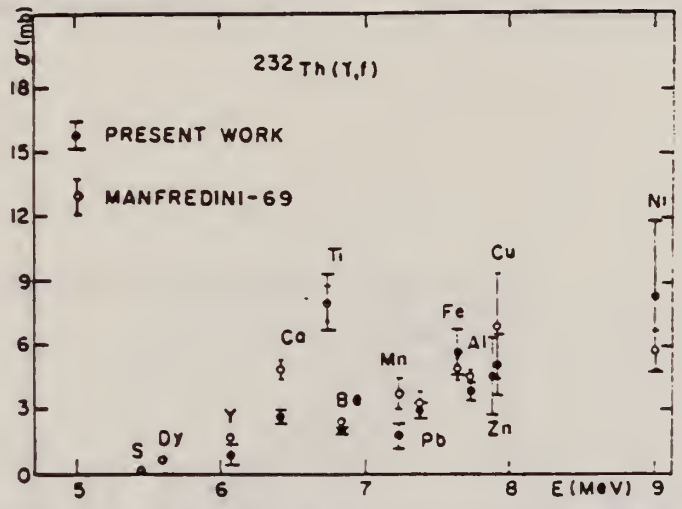

Fig. 7. Photofission cross sections of ^{232}Th compared with Manfredini's results. Element symbols indicate the sources of neutron capture γ-rays whose energies are listed in table 1.

TABLE 4
Principal γ-ray energies and uranium and thorium Γ_γ/Γ_f ratios

E(MeV)	Uranium Γ_γ/Γ_f	Thorium Γ_γ/Γ_f
6.07	1.3±0.4	
6.42	1.1±0.5	2.0±0.8
6.73	2.1±0.6	3.2±0.6
6.83	1.9±0.6	
7.23	1.7±1.1	2.9±1.4
7.38	2.1±0.5	5.5±1.0
7.64	2.2±0.8	3.8±0.9
7.72	2.1±0.4	5.1±1.0
7.88	2.3±0.7	5.1±1.0
9.00	2.5±0.7	8.3±2.0

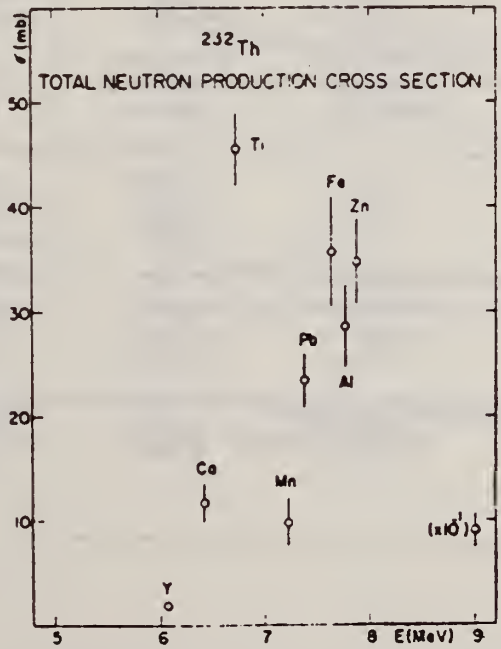

Fig. 9. Total neutron production cross section for ^{232}Th. Element symbols indicate the sources of neutron capture γ-rays whose energies are listed in table 1.

REF. J.T. Caldwell, G.M. Worth, and E.J. Dowdy
PICNS-73, Vol.I, p.651 Asilomar

ELEM. SYM.	A	Z
Th	232	90

METHOD

REF. NO.: 73 Ca 2 hmg

REACTION	RESULT	EXCITATION ENERGY	SOURCE		DETECTOR		ANGLE
			TYPE	RANGE	TYPE	RANGE	
G, N	NOX	THR- 12	C	8- 12	BF3-I		4PI
G,F	NOX	THR- 12	C	8- 12	BF3-I		4PI

TABLE I

Low Energy Photoneutron and Photofission
Parameters Deduced from this Experiment

Isotope	E_c (MeV)	Prompt $\bar{\nu}$	Γ_n / Γ_f	Delayed Neutrons Per Photofission
^{238}U	8	2.683±.094	1.765±.136	0.0355±.0015
^{238}U	10	2.861±.037	2.313±.161	0.0358±.0023
^{238}U	12	3.087±.079	3.250±.150	0.0319±.0028
^{235}U	8	2.675±.095	1.061±.103	0.0101±.0011
^{235}U	10	2.936±.085	1.161±.087	0.0121±.0017
^{235}U	12	3.086±.079	1.224±.079	0.0110±.0020
^{232}Th	8	2.091±.112	1.086±.147	0.0324±.0017
^{232}Th	10	1.980±.115	4.017±.266	0.0309±.0019
^{232}Th	12	2.226±.113	6.781±.577	0.0292±.0038
^{239}Pu	10	3.605±.083	----------	----------
^{239}Pu	12	3.733±.075	0.7±0.4	----------

REF.	ELEM. SYM.	A	Z
T. Gozani, R.L. Bramblett, R.O. Ginaven, and D.E. Rundquist PICNS-73, Vol.I, p.649 Asilomar	Th	232	90

METHOD	REF. NO.	
	73 Go 2	hmg

REACTION	RESULT	EXCITATION ENERGY	SOURCE		DETECTOR		ANGLE
			TYPE	RANGE	TYPE	RANGE	
G,N	RLY	THR- 7	C	5- 7	BF3-I		4PI

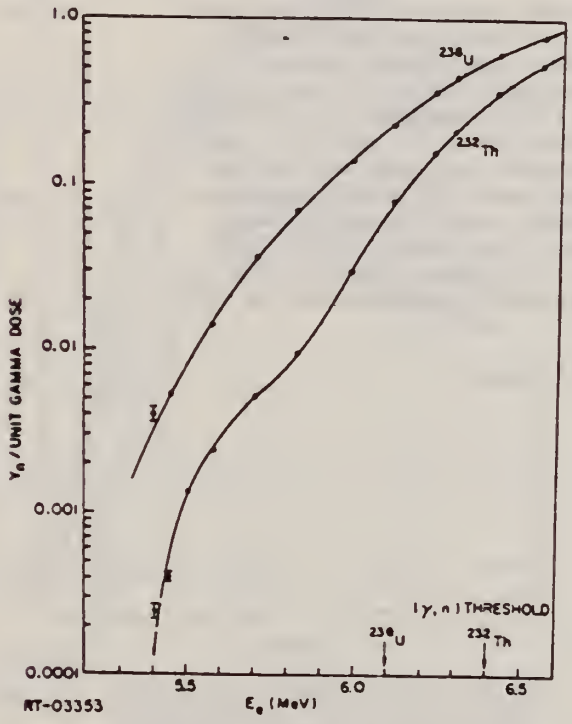

FIG. 1. Prompt neutron yields induced by low-energy electron bremsstrahlung in ^{238}U and ^{232}Th (the statistical errors are shown when larger than the drawn points)

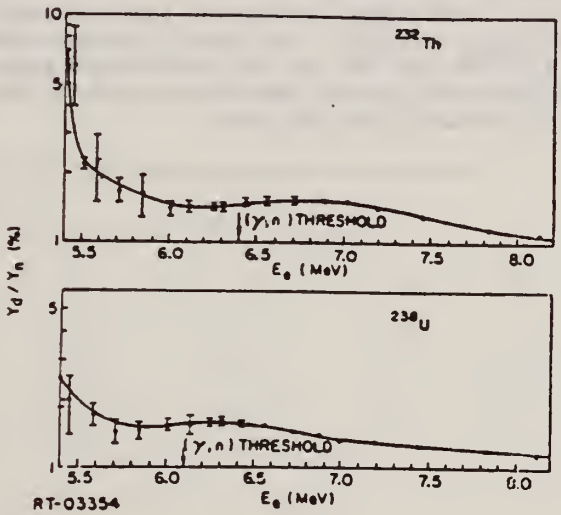

FIG. 2. Bremsstrahlung-averaged delayed neutron fraction

(over)

Since 1968 effort has been devoted at Radiation Technology to measurements of some basic integral quantities related to the low-energy photofission phenomena. The interest in this domain evolves from the application of photoinduced reactions to the nondestructive assay of nuclear materials. The most sensitive energy region for the identification of the various isotopes is around and below the photofission barrier (about 6 MeV). In this region, slight differences in the barrier height or width will cause large differences in the photofission cross sections. The only practical intense source of low-energy photons is bremsstrahlung from low-energy electron accelerators. With such devices the measured quantities are yields. However, in the energy region of importance, especially below the fission barrier, the fission cross section is a very steep function of energy; its integrated product with the bremsstrahlung spectrum, $\phi_B(E,E_e)$, rather closely resembles the fission cross section itself with an effective resolution which broadens as the energy increases. The fission yields were measured[1] simultaneously with the prompt (Y_n) and delayed (Y_d) neutron yields in a moderated neutron detector:

$$Y_n \propto \int_0^{E_e} \left[\nu(E)\sigma_{\gamma,f}(E) + \sigma_{\gamma,n}(E)\right]\phi_B(E,E_e)dE$$

and

$$Y_d \propto \int_0^{E_e} \beta(E)\nu(E)\sigma_{\gamma,f}(E)\phi_B(E,E_e)dE$$

where β is the fractional yield of delayed neutrons per prompt neutrons, while the other symbols are the usual ones. The delayed neutron yield, as well as the prompt neutron yield (Fig. 1), indicates the existence of a structure in the subthreshold region of ^{232}Th. This agrees well with Rabotnov *et al.*[2] measurement and our previous fission yield measurement.[1] A plausible explanation[2] for this structure is the existence of a vibrational resonance in this region creating a shallow double hump potential barrier. Ratios of the various yields furnish important integral quantities such as the bremsstrahlung-averaged, effective delayed neutron yield, $\beta(E)$, and averaged number of prompt neutrons, $\nu(E)$, per fission. The former is shown in Fig. 2, which shows a substantial increase toward low excitation energies. Similarly, a certain amount of structure in $\nu(E)$ has been observed in ^{232}Th and ^{238}U in the subthreshold region. This paper presents the techniques used and the complete results obtained, as well as an intercomparison to the small amount of available previous data.

REF.	ELEM. SYM.	A	Z
David E. Rundquist PICNS-73, Vol.I, p.619 Asilomar	Th	232	90

METHOD	REF. NO.
	73 Ru 1 hmg

REACTION	RESULT	EXCITATION ENERGY	SOURCE		DETECTOR		ANGLE
			TYPE	RANGE	TYPE	RANGE	
G,XN	RLY	THR- 10	C	5- 10	BF3-I		4PI

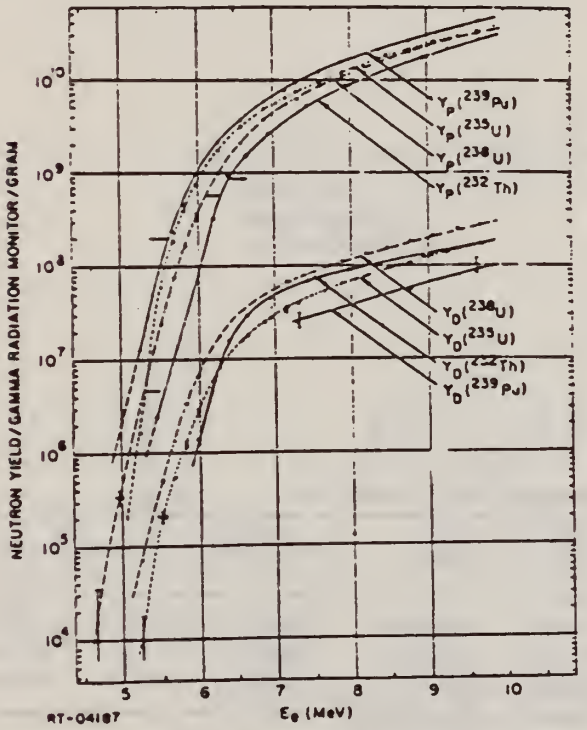

Fig. 1. Prompt and delayed neutron yields in fissile and fertile material produced by bremsstrahlung from electrons of energy E_e

REF. A. Veyssiere, H. Beil, R. Bergere, P. Carlos, A. Lepretre and K. Kernbath
Nucl. Phys. A199, 45 (1973)

ELEM. SYM.	A	Z
Th	232	90

METHOD

REF. NO. 73 Ve 1 egf

REACTION	RESULT	EXCITATION ENERGY	SOURCE		DETECTOR		ANGLE
			TYPE	RANGE	TYPE	RANGE	
G,N	ABX	9- 17	D	9- 17	MOD-I		4PI
G,2N	ABX	9- 17	D	9- 17	MOD-I		4PI
G,F	ABX	9- 17	D	9- 17	MOD-I		4PI

(γ,n) 503+
(γ,2n) 504+
(γ,f) 505+
(γ,tot) 506

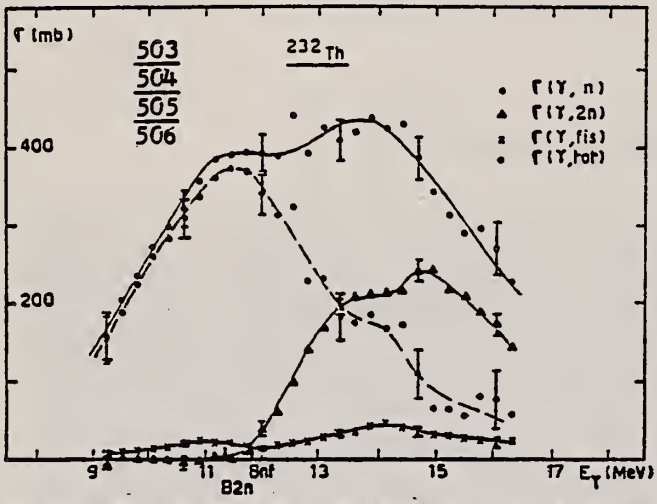

Fig. 6. Partial and total photonuclear cross sections $\sigma(\gamma, n)$, $\sigma(\gamma, 2n)$, $\sigma(\gamma, F)$ and $\sigma_{tot} = \sigma(\gamma, n)+\sigma(\gamma, 2n)+\sigma(\gamma, F)$ of $^{232}_{90}$Th.

TABLE 3
Lorentz line parameters and quadrupole moments for ^{232}Th, ^{238}U and ^{237}Np

	E_1 (MeV)	σ_1 (mb)	Γ_1 (MeV)	E_2 (MeV)	σ_2 (mb)	Γ_2 (MeV)	$R = \frac{\frac{1}{2}\pi\sigma_2\Gamma_2}{\frac{1}{2}\pi\sigma_1\Gamma_1}$	Q_0 [a]	Q_0 [b]
$^{232}_{90}$Th	11.08±0.12	268±7	3.37±0.22	14.07±0.14	349±9	4.62±0.16	1.8±0.15	10.2±1	9.66±0.1
$^{238}_{92}$U	10.96±0.09	301±6	2.90±0.14	14.04±0.13	369±6	4.53±0.13	1.9±0.1	11 ±1	11.3 ±0.1
$^{237}_{93}$Np	11.06±0.12	251±7	3.16±0.27	14.21±0.14	380±9	5.12±0.3	2.4±0.3	11.3±1	10.9 ±0.7

[a]) This experiment.
[b]) Ref. [21]).

[21] K.E.G. Löbner et al., Nucl. Data Tables 7, 5 (1970).

TABLE 4
Integrated cross sections of ^{232}Th, ^{238}U and ^{237}Np

	σ_0 [a]) (MeV · b)	σ_{-1} [a]) (mb)	σ_{-2} [a]) (mb · MeV^{-1})	$\sigma'_0 = \frac{1}{2}\pi(\sigma_1\Gamma_1+\sigma_2\Gamma_2)$ [b]) (MeV · b)	0.06 NZ/A (MeV · b)	$\frac{\sigma_0}{0.006\,NZ/A}$	$\frac{\sigma'_0}{0.006\,NZ/A}$
$^{232}_{90}$Th	2.50±0.25	198±20	16±2	3.95±0.3	3.31	0.76±0.07	1.19±0.08
$^{238}_{92}$U	2.98±0.15	235±15	19±1.5	3.99±0.15	3.39	0.88±0.05	1.18±0.04
$^{237}_{93}$Np	2.60±0.35	204±30	16±3	4.30±0.4	3.39	0.77±0.12	1.27±0.1

[a]) Values obtained by integrating $\sigma(\gamma, \text{total})$ from 8 to 18 MeV for ^{238}U and from 9 to 16 MeV for ^{232}Th and ^{237}Np.
[b]) Surface under the two Lorentz lines.

REF. M. V. Yester, R. A. Anderl, R. C. Morrison
Nucl. Phys. A206, 593 (1973)

ELEM. SYM.	A	Z
Th	232	90

METHOD

REF. NO. 73 Ye 2 egf

REACTION	RESULT	EXCITATION ENERGY	SOURCE		DETECTOR		ANGLE
			TYPE	RANGE	TYPE	RANGE	
G,F	ABX	5- 8	D	5- 8	SCD-I		4PI

COMPTON SCD G-SOURCE

Incident spectrum is result of Compton scattering of Ni n-capture gammas. Spectrum is flat with peak at high energy end. Cross section obtained by unfolding yield curve.

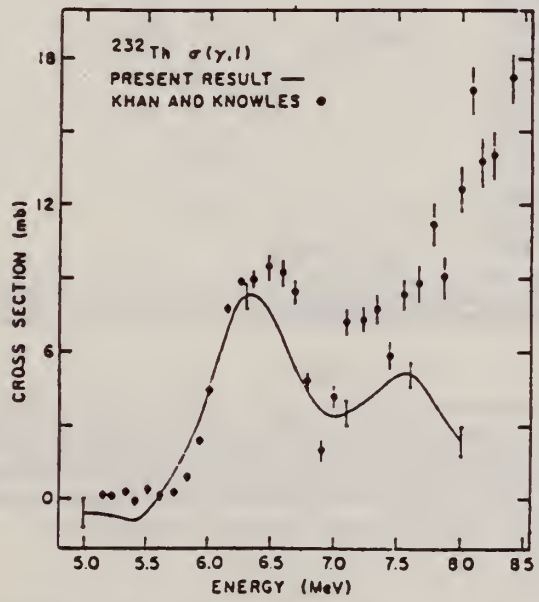

Fig. 10. The photofission cross section of ^{232}Th. The results of the present measurement (smooth curve) are shown along with the data of Khan and Knowles.

[10] A. M. Khan and J. W. Knowles, Nucl. Phys. A179 (1972) 333.

(over)

TABLE I

Photofission cross sections of ^{232}Th and ^{236}U

Energy (MeV)	^{232}Th cross section (mb)	^{236}U cross section (mb)
5.0	−0.6±0.6 [a])	−2.6±1.3 [a])
5.1	−0.6±0.5	−2.0±1.1
5.2	−0.7±0.3	−1.1±0.8
5.3	−0.8±0.3	−0.1±0.7
5.4	−0.9±0.4	0.2±0.7
5.5	−0.6±0.4	0.7±0.8
5.6	0.1±0.5	1.3±0.9
5.7	0.9±0.5	2.1±1.0
5.8	1.7±0.5	3.2±1.0
5.9	2.9±0.5	4.2±1.0
6.0	4.5±0.5	4.7±1.0
6.1	6.2±0.5	4.9±1.0
6.2	7.6±0.5	4.9±1.0
6.3	8.3±0.5	5.0±1.0
6.4	8.2±0.5	5.3±1.0
6.5	7.5±0.5	5.7±1.1
6.6	6.4±0.5	5.7±1.1
6.7	5.2±0.5	5.5±1.1
6.8	4.2±0.5	5.3±1.1
6.9	3.6±0.5	5.0±1.1
7.0	3.4±0.5	5.4±1.1
7.1	3.5±0.5	6.4±1.1
7.2	3.9±0.5	8.0±1.1
7.3	4.3±0.5	10.1±1.1
7.4	4.7±0.5	11.9±1.1
7.5	5.1±0.5	12.6±1.1
7.6	5.1±0.5	12.6±1.1
7.7	4.7±0.5	12.1±1.1
7.8	3.9±0.5	11.5±1.1
7.9	3.1±0.5	10.7±1.1
8.0	2.4±0.6	9.8±1.3

[a]) These are the relative errors only. The ±30% error in the absolute scale has not been included.

REF. T. Bar-Noy and R. Moreh
Nucl. Phys. A229, 417 (1974)

EL.EM. SYM.	A	Z
Th	232	90

METHOD

REF. NO. 74 Ba 6 egf

REACTION	RESULT	EXCITATION ENERGY	SOURCE TYPE	SOURCE RANGE	DETECTOR TYPE	DETECTOR RANGE	ANGLE
G,G	ABX	8- 11	D	8- 11	SCD-D		DST

RAMAN SCTNG

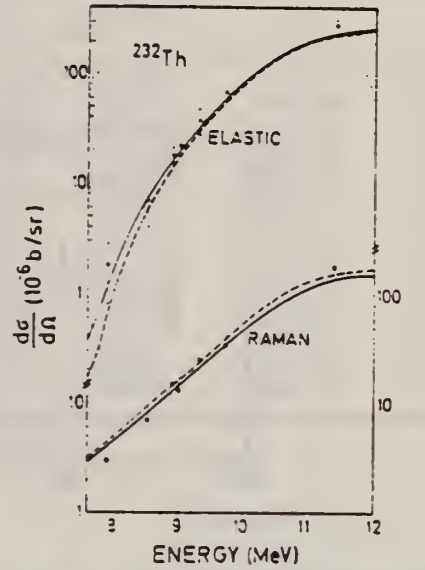

Fig. 4. Differential elastic and Raman photon scattering cross sections for ^{232}Th. The solid curves represent the results of the SRM and the dashed curves the results of the DCM. See caption to fig. 3.

ENERGY (MeV)

Fig. 3. Differential elastic and Raman photon scattering cross sections for ^{238}U. For the elastic cross section, the solid curve represents the values obtained by including the amplitudes of Thomson, nuclear resonance (according to the SRM) and the imaginary part only of Delbruck scattering (the contribution of the real Delbruck amplitudes was excluded). Dashed curves are similar results with the nuclear resonance amplitudes calculated by the DCM. For Raman scattering, the solid curve represents the results of both the SRM and the DCM.

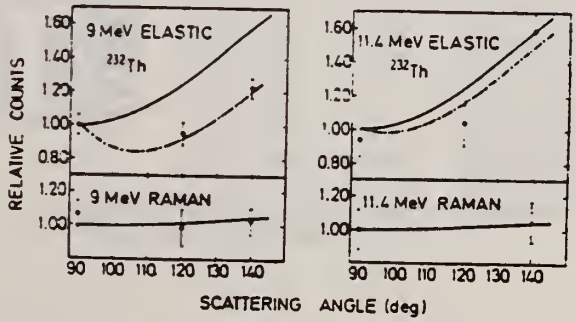

Fig. 5. Angular distributions of elastic and Raman scattered lines from ^{232}Th. The solid curves of the elastic and Raman lines have the forms: $W(\theta) = 1+\cos^2\theta$ and $W(\theta) = 1+\frac{1}{13}\cos^2\theta$ respectively. The dashed curves include contributions of nuclear resonance, nuclear Thomson and the imaginary part of Delbruck scattering and are normalised to a value 1.00 at 90°.

REF.		EL EM. SYM.	A	Z
	G.M. Gurevich, L.E. Lazareva, V.M. Mazur, and G.V. Solodukhov ZhETF Pis. Red. 20, 741 (1974) JETP Lett. 20, 343 (1974)	Th	232	90
METHOD		REF. NO.		
		74 Gu 11		hmg

REACTION	RESULT	EXCITATION ENERGY	SOURCE		DETECTOR		ANGLE
			TYPE	RANGE	TYPE	RANGE	
G,MU-T	ABX	7- 19	C	35	NAI-D		4PI

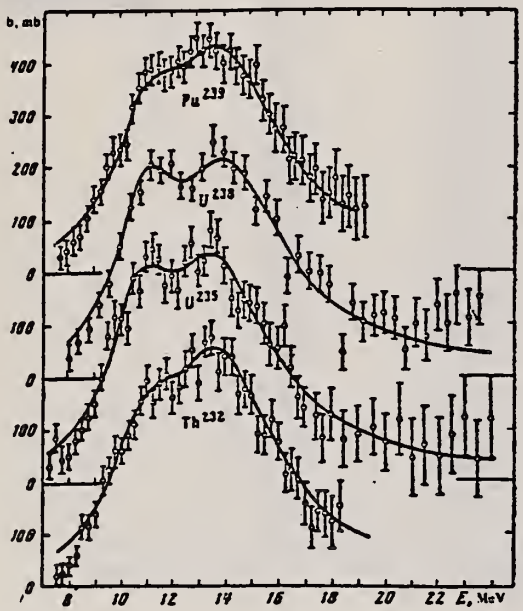

FIG. 1.

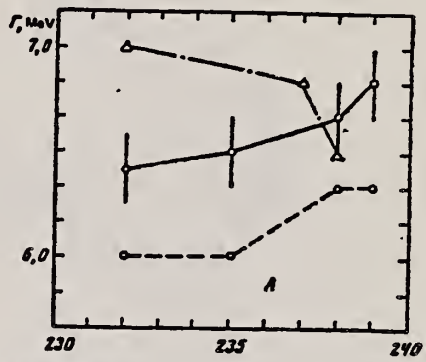

FIG. 2.

TABLE. Parameters for the approximation of the cross section by Lorentz lines.

Nucleus	σ_1 mb	Γ_1 MeV	E_1 MeV	σ_2 mb	Γ_2 MeV	E_2 MeV	$\frac{\sigma_2\Gamma_2}{\sigma_1\Gamma_1}$	β	Q
Th^{232}	247	3.90	10.99	362	4.67	13.9	1.75	0.28	10.0
U^{235}	283	3.23	10.74	354	4.92	13.77	1.91	0.30	11.0
U^{238}	286	2.99	10.97	351	5.10	14.25	2.09	0.31	11.7
Pu^{239}	227	3.47	11.05	362	5.23	14.01	2.40	0.29	11.0

REF.

E. Hayward, W.C. Barber, and J.J. McCarthy
Phys. Rev. C10, 2652 (1974)

ELEM. SYM.	A	Z
Th	232	90

METHOD

REF. NO.: 74 Ha 4 hmg

REACTION	RESULT	EXCITATION ENERGY	SOURCE TYPE	SOURCE RANGE	DETECTOR TYPE	DETECTOR RANGE	ANGLE
$ G,G	ABX	15	D	15	NAI-D		90
		(15.1)		(15.1)			

POL PHOTONS

TABLE I. Results.

Target	$d\sigma^{\parallel}/d\Omega_F$ (Arbitrary units)	$d\sigma^{\perp}/d\Omega_F$ (Arbitrary units)	η_F	η	η(DCM)
Cd	0.042 ± 0.028	0.39 ± 0.05	0.11 ± 0.07	0.09 ± 0.07	0.19
In [a]	0.026 ± 0.020	0.54 ± 0.04	0.05 ± 0.04	0.03 ± 0.04	0.19
Sn	0.084 ± 0.036	0.65 ± 0.06	0.13 ± 0.06	0.11 ± 0.06	0.07
Sb [a]	0.14 ± 0.030	0.77 ± 0.05	0.18 ± 0.05	0.16 ± 0.05	
Nd [a]	0.14 ± 0.07	1.03 ± 0.10	0.14 ± 0.07	0.12 ± 0.07	
Ta	0.24 ± 0.10	1.47 ± 0.14	0.16 ± 0.07	0.14 ± 0.07	0.20
W	0.52 ± 0.10	1.66 ± 0.12	0.31 ± 0.07	0.29 ± 0.07	0.20
Pt	0.23 ± 0.08	1.94 ± 0.13	0.12 ± 0.04	0.10 ± 0.04	0.08
Au	0.39 ± 0.11	2.08 ± 0.15	0.19 ± 0.06	0.17 ± 0.06	0.07
Hg [a]	0.33 ± 0.09	2.16 ± 0.15	0.15 ± 0.04	0.13 ± 0.04	0.03
Pb [a]	0.19 ± 0.14	2.42 ± 0.19	0.08 ± 0.06	0.06 ± 0.06	0
Bi	0.10 ± 0.15	2.65 ± 0.26	0.04 ± 0.06	0.02 ± 0.06	0
Th [a]	0.31 ± 0.12	2.26 ± 0.19	0.14 ± 0.05	0.12 ± 0.05	0.07
U [a]	0.21 ± 0.11	2.38 ± 0.19	0.09 ± 0.05	0.07 ± 0.05	0.08

[a] Data not previously reported.

TABLE II. Comparison with Saclay data.

Target	$\lvert A_0\rvert^2$ This experiment (Arbitrary units)	$\lvert A_0\rvert^2$ Saclay (mb)	Ratio
Cd	0.337 ± 0.058	0.508	0.663 ± 0.114
In [a]	0.507 ± 0.046	0.591	0.859 ± 0.078
Sn	0.550 ± 0.072	0.822	0.669 ± 0.096
Sb [a]	0.590 ± 0.061	0.794	0.743 ± 0.077
Nd [a]	0.837 ± 0.100	1.170	0.715 ± 0.086
Ta	1.19 ± 0.18	1.88	0.633 ± 0.096
W	1.05 ± 0.17	2.05	0.512 ± 0.083
Pt	1.67 ± 0.16	2.70	0.619 ± 0.059
Au	1.62 ± 0.20	2.92	0.555 ± 0.068
Hg [a]	2.16 ± 0.20	3.29	0.540 ± 0.060
Pb [a]	2.20 ± 0.27	3.43	0.641 ± 0.078
Bi	2.53 ± 0.31	3.43	0.737 ± 0.090
Th [a]	1.89 ± 0.22	2.73	0.692 ± 0.080
U [a]	2.13 ± 0.22	2.83	0.754 ± 0.077
			0.656 ± 0.021

[a] Data not previously reported.

REF. K.N. Ivanov and K.A. Petrzhak
At. Energ. 36, 404 (1974)
Sov. J. At. Energy 36, 515 (1974)

ELEM. SYM.	A	Z
Th	232	90

METHOD

REF. NO. 74 Iv 2 egf

REACTION	RESULT	EXCITATION ENERGY	SOURCE		DETECTOR		ANGLE
			TYPE	RANGE	TYPE	RANGE	
G,F	RLY	5- 12	C	5- 12	TRK-I		4PI

YIELD REL U-238

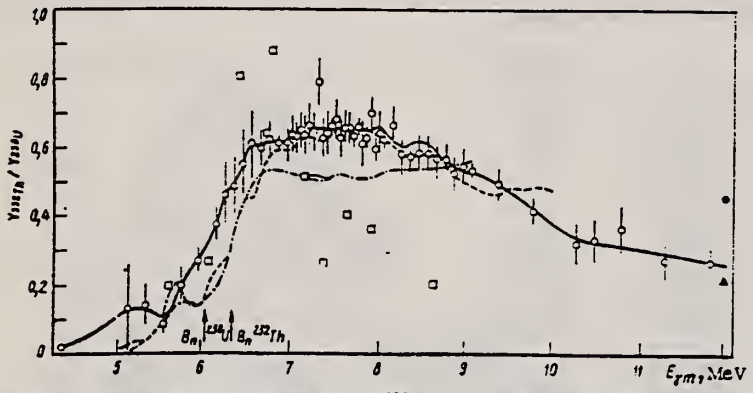

Fig. 1. Relative photofissility of ^{232}Th: ○) present work; – – –, ▲, ●, □, –·–·–) data from [3-7], respectively.

3. A. V. Ignatyuk et al., Yad. Fiz., 11, No. 5, 992 (1970).
4. J. McElhinney and W. Ogle, Phys. Rev., 81, 342 (1951).
5. J. Huizenga et al., Phys. Rev., 95, 1009 (1954).
6. A. Manfredini, Nuovo Cimento, 4A, No. 2, 421 (1971).
7. T. Gozani, Atomkernenergie, 19, 63 (1972).

The curves for the relative photofission yield functions $Y_i(E_{\gamma m})/Y_{^{238}U}(E_{\gamma m})$ were obtained from experimental ratios by least-square analysis. This method of analysis smooths out observed structure but maxima are seen in the curves (with an accuracy of ±0.16 MeV) at the following values of maximum bremsstrahlung energy:

Nucleus	Position of Maximum, MeV
^{232}Th	5.3; 6.3; 6.6; 7.5; 10.8.
^{235}U	5.1; 6.6; 8.4.
^{237}Np	5.5; 6.0; 7.1; 8.35; 9.8.
^{239}Pu	6.5.

REF.

H.E. Jackson, G.E. Thomas, and K.J. Wetzel
Phys. Rev. C9, 1153 (1974)

ELEM. SYM.	A	Z
Th	232	90

METHOD

REF. NO.	
74 Ja 2	hmg

REACTION	RESULT	EXCITATION ENERGY	SOURCE		DETECTOR		ANGLE
			TYPE	RANGE	TYPE	RANGE	
G,G	ABX	10	D	10	SCD-D		90
		(10.83)		(10.83)			

TABLE I. Differential cross sections measured for elastic and inelastic scattering of 10.83-MeV photons. State or states populated by inelastic scattering are indicated in parentheses below the target. The errors given result from the statistical error in the measurement of the cross section relative to the calibration value, the 90° uranium inelastic cross section.

Nucleus	θ (deg)	$d\sigma/d\omega$ (elastic) (mb/sr)	$d\sigma/d\omega$ (inelastic) (mb/sr)
^{238}U			
(2$^+$, 45 keV)	20	1.72 ± 0.17	
	30	0.97 ± 0.12	
	50	0.334 ± 0.039	
	60	0.23 ± 0.04	
	70	0.245 ± 0.024	0.136 ± 0.015
	90	0.182 ± 0.017	0.154 ± 0.012
	120	0.189 ± 0.017	0.160 ± 0.013
	150	0.303 ± 0.016	0.160 ± 0.015
^{232}Th			
(2$^+$, 45 keV)	90	0.129 ± 0.015	0.103 ± 0.007
Pb	20	1.28 ± 0.12	
	30	0.55 ± 0.07	
	50	0.289 ± 0.051	
	60	0.20 ± 0.04	
	70	0.087 ± 0.014	
	90	0.079 ± 0.005	
	120	0.060 ± 0.004	
	150	0.127 ± 0.008	
^{209}Bi			
($\frac{1}{2}^-$, 910 keV)	90	0.101 ± 0.0062	~0
^{181}Ta			
($\frac{9}{2}^-$, 136 keV)	90	0.0370 ± 0.003	0.006 56 ± 0.0015
^{159}Tb			
($\frac{3}{2}^+$, 58 keV)	90	0.0314 ± 0.003	0.0110 ± 0.0016
$\frac{7}{2}^+$, 138 keV)			0.005 11 ± 0.0011

TABLE III. Comparison of calculated and observed values of the 90° cross sections for elastic scattering and of the ratio at 90° of Raman to elastic scattering by various nuclei for 10.83-MeV photons. The parameters used in the calculations are given in Table II.

Target	$d\sigma_{elas}(90°)/d\Omega$ (mb/sr) Calc	Exp	$d\sigma^{(90°)}_{Raman}/d\sigma^{(90°)}_{elas}$ Calc	Exp
Tb	0.036	0.031 ± 0.003	0.80	0.51 ± 0.06
Ta	0.055	0.037 ± 0.003	0.28	0.18 ± 0.04
Pb	0.076	0.079 ± 0.005	0	
Bi		0.101 ± 0.006	0	~0
Th	0.128	0.129 ± 0.015	0.91	0.80 ± 0.08
U	0.157[a]	0.182 ± 0.017	1.03	0.85 ± 0.08

[a] If the Livermore parameters (Ref. 33) for ^{235}U are used then this calculated value would be 0.210 mb/sr.

33
C.D. Bowman, G.F. Auchampaugh, and S.C. Fultz, Phys. Rev. 133, B676 (1964).

REF. O.Y. Mafra, M.F. Cesar, C. Renner, and J. Goldemberg
Nucl. Phys. A236, 1 (1974)

ELEM. SYM.	A	Z
Th	232	90

METHOD

REF. NO. 74 Ma 9 egf

REACTION	RESULT	EXCITATION ENERGY	SOURCE		DETECTOR		ANGLE
			TYPE	RANGE	TYPE	RANGE	
G,N	ABX	6- 11	D	6- 11	ACT-I		4PI

CAPTURE GAMMAS

U-238 re-analysis of data in 72Mal (O.Y. Mafra, S. Kuniyoshi, J. Goldemberg, Nucl. Phys. A186, 110 (1972).

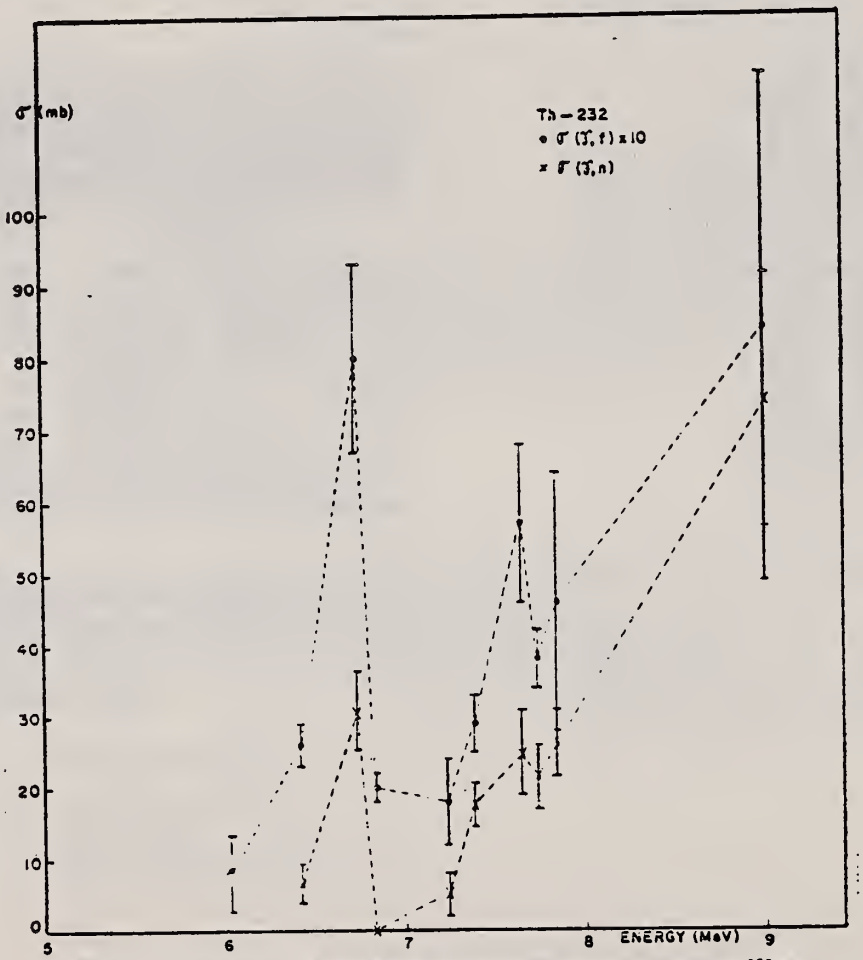

Fig. 4. Comparison of the photofission and photoneutron cross sections of ^{232}Th.

(over)

TABLE 3

Principal γ-ray energies and thorium and uranium photoneutron cross section measured by activation

E (MeV)	$\sigma_{\gamma,n}$ (mb)	
	^{238}U	^{232}Th
6.07	18.0 ±4.8	3.4 ± 0.9
6.42	2.4 ±0.8	1.4 ± 0.4
6.73	22.7 ±1.4	27.8 ± 1.7
6.83	2.35±0.09	1.38± 0.05
7.23	1.3 ±0.7	0 ± 4
7.38	14.5 ±0.2	16.1 ± 0.2
7.64	13.3 ±4.4	10.4 ± 3.4
7.73	15.3 ±2.8	13.0 ± 2.4
7.88	23.6 ±5.0	18.0 ± 3.8
7.91		18.0 ± 3.9
9.00		28.6 ± 8.5
9.72		53.4 ±14.8
10.83		158.3 ±78.8

TABLE 4

Photoneutron cross section of ^{238}U and ^{232}Th recalculated using Caldwell's results for $\bar{\nu}_p$

E (MeV)	$\sigma_{\gamma,n}$ (mb)	
	^{238}U	^{232}Th
6.07	10.6± 3.2	
6.42	2.4± 1.2	6.7± 2.6
6.73	23.2± 6.4	30.5± 4.8
6.83	3.8± 1.2	
7.23	6.3± 3.9	6.3± 3.0
7.38	21.9± 5.4	17.7± 2.9
7.64	21.9± 6.9	24.8± 6.1
7.73	18.8± 4.1	21.4± 4.3
7.88	25.4± 6.4	25.9± 4.6
7.91		
9.00	85.1±23.2	73.8±17.4
9.72		
10.83		

REF.

P. Rasch, G. Fiedler, and E. Konecny
Nucl. Phys. A219, 397 (1974)

ELEM. SYM.	A	Z
Th	232	90

METHOD

REF. NO.: 74 Ra 1 | egf

REACTION	RESULT	EXCITATION ENERGY	SOURCE		DETECTOR		ANGLE
			TYPE	RANGE	TYPE	RANGE	
E,F	NOX	0- 30	D	8- 30	TRK-I		DST

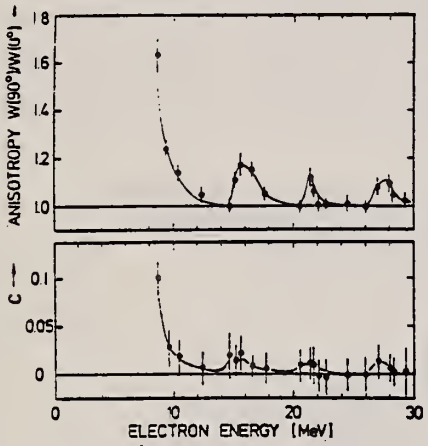

Fig. 3. Top: Anisotropies $A = W(90°)/W(0°)$ corresponding to the fitted curves in fig. 2, as a function of electron energy. The bumps in the anisotropy at about $E_e = 15.2$, 21.5, and 27 MeV correspond to the onset of second-, third- and fourth-chance fission, respectively. Bottom: Relative contribution C of the $\sin^2(2\theta)$ term in the angular distribution (integrated over θ and φ) as a function of electron energy.

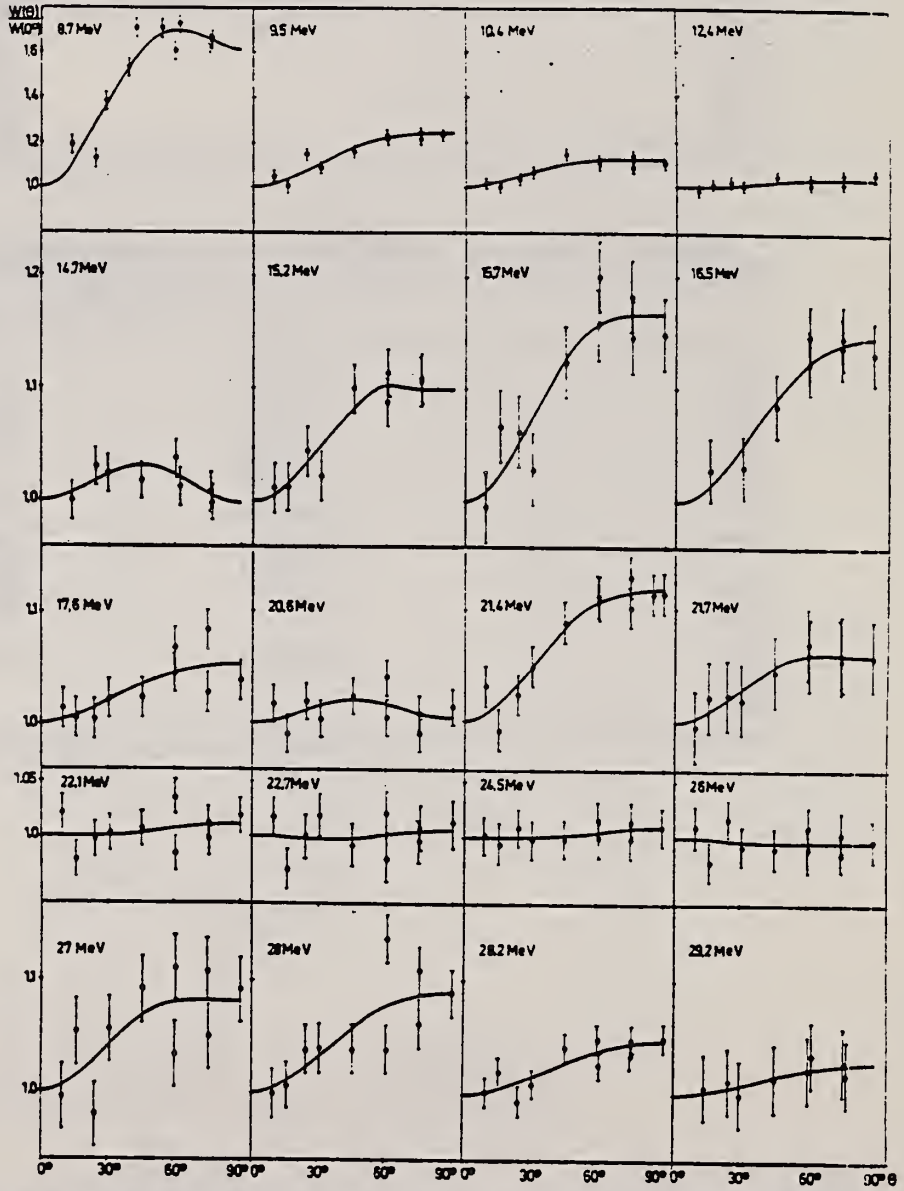

Fig. 2. Fragment angular distributions in fission induced by electrons of different energies between 8.7 and 29.2 MeV. The solid lines correspond to least squares fits to

$$W(\theta) = a + b \sin^2\theta + c \sin^2(2\theta).$$

REF. J.T. Caldwell and E.J. Dowdy
Nucl. Sci. & Eng. 56, 179 (1975)

ELEM. SYM.	A	Z
Th	232	90

METHOD

REF. NO. 75 Ca 5 egf

REACTION	RESULT	EXCITATION ENERGY	SOURCE		DETECTOR		ANGLE
			TYPE	RANGE	TYPE	RANGE	
G,F	NOX	6- 13	C	8- 13	MOD-I		4PI

NEUTRON MULTIPLICITIES

The prompt- and delayed-neutron multiplicities for photofission of the eight isotopes, ^{232}Th, ^{233}U, ^{234}U, ^{235}U, ^{236}U, ^{238}U, ^{237}Np, and ^{239}Pu, have been measured using bremsstrahlung with end-point energies ranging from 8 to 13 MeV. The measured multiplicities are compared with those from the same compound nucleus formed in neutron-induced fission where such data exist.

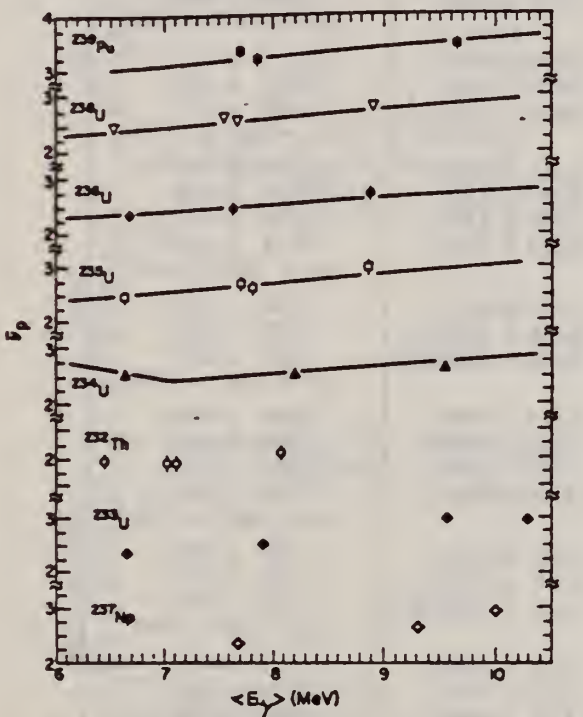

Fig. 5. $\bar{\nu}_p$ versus excitation energy for the eight isotopes studied in this experiment. The full curves shown are from the evaluations of Davey[2] with the excitation energy determined as described in the text. For the lower three isotopes shown, no previous experimental values for $\bar{\nu}_p$ exist.

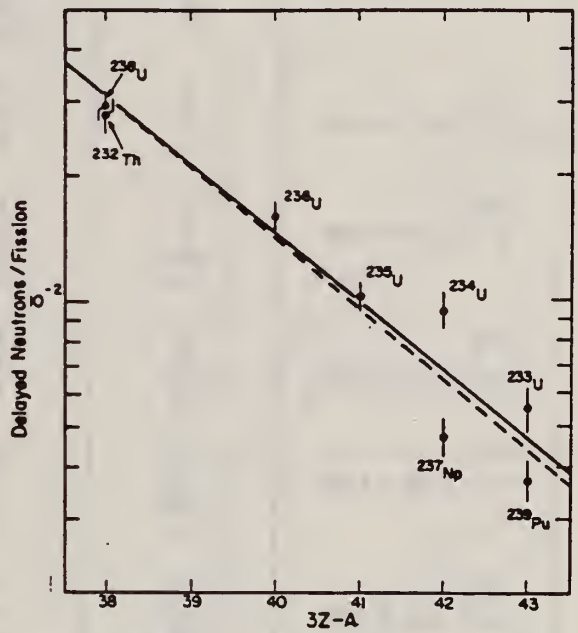

Fig. 6. Delayed neutrons per fission versus the parameter 3Z-A of the compound nucleus. The full curve shown is the least-squares fit to the data shown with $\ln Y_0 = 10.61$, $K = -0.372$. The dashed curve is the least-squares fit to the data provided by Tomlinson[6] with $\ln Y_0 = 11.35$, $K = -0.39$.

TABLE IV

Least-Squares Linear Fit Expressions for $\bar{\nu}_p(\langle E_\gamma \rangle)$

Isotope	$\bar{\nu}_p(\langle E_\gamma \rangle) = \bar{\nu}_0 + d\bar{\nu}_p/dE\,\langle E_\gamma \rangle$	Correlation Coefficient
^{232}Th	$\bar{\nu}_p(\langle E_\gamma \rangle) = 1.310 + 0.090\ \langle E_\gamma \rangle$	0.675
^{233}U	$\bar{\nu}_p(\langle E_\gamma \rangle) = 1.200 + 0.1709\ \langle E_\gamma \rangle$	0.947
^{234}U	$\bar{\nu}_p(\langle E_\gamma \rangle) = 2.222 + 0.0399\ \langle E_\gamma \rangle$	0.741
^{235}U	$\bar{\nu}_p(\langle E_\gamma \rangle) = 0.9034 + 0.2292\ \langle E_\gamma \rangle$	0.967
^{236}U	$\bar{\nu}_p(\langle E_\gamma \rangle) = 1.140 + 0.1788\ \langle E_\gamma \rangle$	0.986
^{238}U	$\bar{\nu}_p(\langle E_\gamma \rangle) = 1.502 + 0.1458\ \langle E_\gamma \rangle$	0.984
^{237}Np	$\bar{\nu}_p(\langle E_\gamma \rangle) = 0.4027 + 0.2505\ \langle E_\gamma \rangle$	0.967
^{239}Pu	$\bar{\nu}_p(\langle E_\gamma \rangle) = 2.526 + 0.0930\ \langle E_\gamma \rangle$	0.777

[2] W.G. Davey, Nucl. Sci. Eng., 44, 345 (1971)

[6] L. Tomlinson, "Delayed Neutrons from Fission: A Compilation and Evaluation of Experimental Data," AERE-R-6993, Atomic Energy Research Establishment, Harwell (1972)

over

TABLE III

Prompt- and Delayed-Neutron Yields

	E_n, MeV	$\langle E_\gamma \rangle$, MeV	ν_p	Delayed Neutrons per 100 Fissions
^{232}Th	8	6.44	1.96 ± 0.11	3.10 ± 0.28
(σ = 1.15 ± 0.05)	10	7.02	1.89 ± 0.11	3.06 ± 0.31
	10.2	7.10	1.89 ± 0.11	2.67 ± 0.21
	12	8.06	2.08 ± 0.11	2.59 ± 0.31
				av = 2.80 ± 0.28
^{233}U	8	6.68	2.350 ± 0.112	0.455 ± 0.040
(σ = 1.25 ± 0.05)	10	7.90	2.498 ± 0.108	0.518 ± 0.040
	12	9.55	2.960 ± 0.096	0.640 ± 0.044
	13	10.27	2.870 ± 0.099	0.598 ± 0.051
				av = 0.553 ± 0.044
^{234}U	8	(6.67)[a]	2.536 ± 0.112	---
(σ = 1.13 ± 0.05)	10	8.69	2.499 ± 0.107	0.92 ± 0.06
	12	9.54	2.623 ± 0.105	0.97 ± 0.12
				av = 0.94 ± 0.094
^{235}U	8	6.67	2.456 ± 0.086	0.90 ± 0.08
(σ = 1.20 ± 0.05)	10	7.70	2.697 ± 0.081	0.88 ± 0.08
	10.2	7.81	2.612 ± 0.079	1.13 ± 0.07
	12	8.86	2.963 ± 0.072	1.12 ± 0.08
				av = 1.02 ± 0.08
^{236}U	8	6.66	2.357 ± 0.111	1.43 ± 0.14
(σ = 1.20 ± 0.05)	10	7.63	2.470 ± 0.105	1.73 ± 0.12
	12	8.86	2.744 ± 0.095	1.64 ± 0.10
				av = 1.60 ± 0.13
^{238}U	8	6.53	2.457 ± 0.088	3.06 ± 0.24
(σ = 1.22 ± 0.05)	10	7.54	2.628 ± 0.083	2.76 ± 0.17
	10.2	7.66	2.585 ± 0.082	3.06 ± 0.14
	12	8.88	2.802 ± 0.078	2.75 ± 0.19
				av = 2.91 ± 0.20
^{237}Np	10	7.68	2.35 ± 0.11	0.38 ± 0.04
(σ = 1.20 ± 0.05)	12	9.31	2.65 ± 0.10	0.50 ± 0.04
	13	9.92	2.95 ± 0.10	0.54 ± 0.04
				av = 0.47 ± 0.04
^{239}Pu	10	7.69	3.32 ± 0.08	---
(σ = 1.18 ± 0.10)	10.2	7.84	3.17 ± 0.14	0.37 ± 0.04
	12	9.65	3.43 ± 0.10	0.37 ± 0.04
				av = 0.37 ± 0.04

[a]Estimated value.

REF. P. A. Dickey and P. Axel
Phys. Rev. Lett. 35, 501 (1975)

ELEM. SYM.	A	Z
Th	232	90

METHOD

REF. NO. 75 Di 2 hmg

REACTION	RESULT	EXCITATION ENERGY	SOURCE TYPE	SOURCE RANGE	DETECTOR TYPE	DETECTOR RANGE	ANGLE
G,F	ABX	THR- 8	C	8, 10	TOF-D		135

Variable-energy photons defined to 100 keV were used to study ^{238}U and ^{232}Th from 5 to 8 MeV. The inferred fission transmission indicates (a) that the lowest 1$^-$ fission barrier is about 6.5 MeV in ^{238}U and 6.3 MeV in ^{232}Th, and (b) that there is an energy gap before the rapid opening of additional fission channels above 7 MeV in ^{238}U.

1066

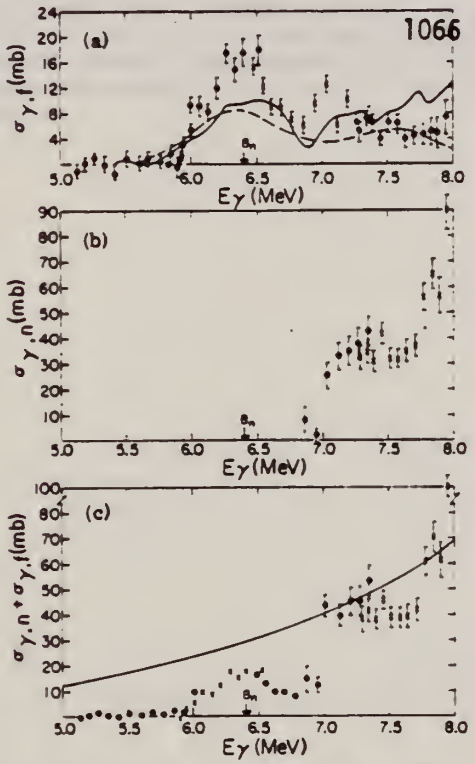

FIG. 2. Photon-induced cross sections for ^{232}Th. All of the points come from this experiment. In (b), (c), and the high-energy portion of (a), the different symbols identify different runs. The spacing of the points in a single run is equal to the photon-energy resolution. (a) Photofission cross sections. The curves correspond to measurements with poorer resolution; the solid curve is from Ref. 12 and the dashed curve is from Ref. 13. (b) Photoneutron cross sections inferred by measuring only neutrons with energy above 300 keV. (c) Below 6.9 MeV the points represent $\sigma_{\gamma f}$ only. Above 6.9 MeV, the points are the sum, $\sigma_{\gamma f} + \sigma_{\gamma n}$, with statistical errors shown. The line is the extrapolation of the Lorentzian curves which have been fitted to the giant dipole resonance as reported in Ref. 19.

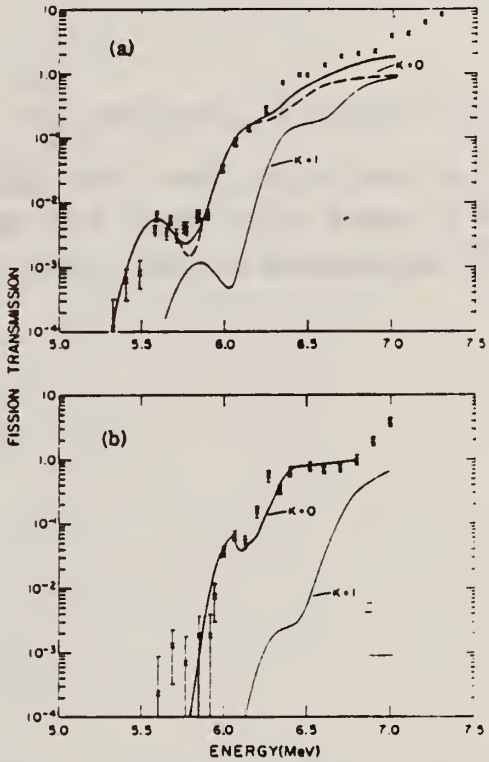

FIG. 3. Fission transmissions: (a) ^{238}U. The upper solid curve is the sum of the $K=0$ and $K=1$ transmissions calculated with the parameters in Table I. The dashed curve shows the $K=0$-barrier contribution when it is noticeably lower than the sum. (b) ^{232}Th. The curves are calculated transmissions for $K=0$ and $K=1$ using the barrier parameters listed in Table I.

(over)

TABLE I. Fission-barrier parameters (energies given in MeV).

	J^π	K	E_A	E_{min}	E_B	$\hbar\omega_A$	$\hbar\omega_{min}$	$\hbar\omega_B$
^{238}U	0^+	0	5.9[a]	2.0	6.1[a]	1.0[a]	0.9	0.6[a]
	1^-	0	6.5	2.35	6.1	1.0	0.9	0.6
	1^-	1	6.7	2.55	6.6	1.0	0.9	0.6
^{232}Th	0^+	0	< 5.5[a]	3.0	6.1[a]	0.9[a]	1.5	0.5[a]
	1^-	0	6.3	3.1	6.3	0.9	1.0	0.45
	1^-	1	6.5	3.3	6.9	0.9	1.0	0.5

[a]Values taken from Ref. 4.

[4] B.B. Back et al., Phys. Rev. C9, 1924 (1974)

[12] A.M. Khan et al., Nucl. Phys. A179, 333 (1972)

[13] M.V. Yester et al., Nucl. Phys. A206, 593 (1973)

[19] A. Veyssiere et al., Nucl. Phys. A199, 45 (1973)

REF.

V. S. Evseev, T. N. Mamedov, O. V. Selyugin
Yad. Fiz. 21, 245 (1975)
Sov. J. Nucl. Phys. 21, 129 (1975).

EL. SYM.	A	Z
Th	232	90

METHOD

REF. NO. 75 Ev 1 hmg

REACTION	RESULT	EXCITATION ENERGY	SOURCE		DETECTOR		ANGLE
			TYPE	RANGE	TYPE	RANGE	
G,N	SPC	6- 31	C	31	SCI-D		140

Neutron energy spectra have been measured in the energy range $2 \leq E_n \leq 5$ MeV for photoexcitation of the nuclei Ta, Pb, Bi, and Th by bremsstrahlung with maximum energy 31 MeV. From the neutron spectra we have determined values of the nuclear temperature T after emission of the first neutron: 1.01 ± 0.04, 1.12 ± 0.04, 1.11 ± 0.04, and 1.25 ± 0.05 MeV respectively for Ta, Pb, Bi, and Th. Comparison of the values obtained for the nuclear level-density parameter with the predictions of the statistical theory of nuclear reactions shows that this theory does not describe the decay of collective nuclear states of the giant dipole resonance type.

REF.	ELEM. SYM.	A	Z
H. E. Jackson, G. E. Thomas, K. J. Wetzel Phys. Rev. C11, 1664 (1975)	Th	232	90

METHOD	REF. NO.
	75 Ja 1 hmg

REACTION	RESULT	EXCITATION ENERGY	SOURCE		DETECTOR		ANGLE
			TYPE	RANGE	TYPE	RANGE	
G,G	ABX	11	D	11	SCD-D		150
		(11.387)		(11.387)			

RATIO RAMAN/ELASTIC

TABLE I. Differential cross sections measured for elastic and inelastic scattering of 11.39-MeV photons. State or states populated by inelastic scattering are indicated in parentheses beside the target. The errors given result from the statistical error in the measurement of the cross section relative to the calibration value, the 90° uranium elastic cross section.

θ (deg)	$d\sigma/d\omega$ (elastic) (mb/sr)	$d\sigma/d\omega$ (inelastic) (mb/sr)
	^{238}U (2$^+$, 45 keV)	
90	0.169 ± 0.011	0.173 ± 0.016
150	0.355 ± 0.041	0.236 ± 0.24
	^{232}Th (2$^+$, 45 keV)	
150	0.331 ± 0.035	0.210 ± 0.022
	^{181}Ta ($\frac{9}{2}^+$, 136 keV) ($\frac{11}{2}^+$, 301 keV)	
90	0.073 ± 0.008	0.020 ± 0.004 0.009 ± 0.004
150	0.145 ± 0.015	0.017 ± 0.004 0.017 ± 0.004
	^{165}Ho ($\frac{9}{2}^+$, 95 keV) ($\frac{11}{2}^+$, 210 keV)	
150	0.141 ± 0.014	0.022 ± 0.004 0.013 ± 0.004
	^{159}Tb ($\frac{5}{2}^+$, 58 keV) ($\frac{7}{2}^+$, 138 keV)	
90	0.062 ± 0.006	0.024 ± 0.003 0.013 ± 0.003
150	0.134 ± 0.012	0.042 ± 0.004 0.019 ± 0.004
	^{141}Pr	
150	0.030 ± 0.008	...

TABLE II. Comparison of calculated and observed values of the cross sections for elastic scattering and of the ratio of Raman to elastic scattering by various nuclei for 11.387-MeV photons at 90 and 150°. The parameters used in the calculations for column 5 are given in Table II. Column 4 describes results obtained by perturbing those parameter to meet the constraint of Eq. (3) (see text).

Target	$d\sigma(\theta)d\Omega$ (mb/sr) Calc.	Exp.	$d\sigma_{Raman}(\theta)/d\sigma_{elastic}(\theta)$		
		$\theta = 150°$			
Pr	0.025	0.030 ± 0.008		0.0	0.0
Tb	0.094	0.134 ± 0.012	0.53	0.57	0.46 ± 0.04
Ho	0.170	0.141 ± 0.014	0.28	0.28	0.25 ± 0.04
Ta	0.160	0.145 ± 0.015	0.23	0.22	0.23 ± 0.04
Th	0.253	0.331 ± 0.035	0.59	0.63	0.64 ± 0.08
U	0.289	0.355 ± 0.041	0.78	0.73	0.67 ± 0.07
		$\theta = 90°$			
Tb	0.062	0.062 ± 0.006	0.76	0.82	0.60 ± 0.07
Ta	0.109	0.074 ± 0.008	0.32	0.30	0.38 ± 0.07
U	0.172	0.169 ± 0.008	1.29	1.15	1.03 ± 0.10

REF. H. Jungclas, R. Brandt, and G. Stark
Phys. Rev. C12, 1834 (1975)

ELEM. SYM.	A	Z
Th	232	90

METHOD

REF. NO. 75 Ju 3 hmg

REACTION	RESULT	EXCITATION ENERGY	SOURCE		DETECTOR		ANGLE
			TYPE	RANGE	TYPE	RANGE	
G,4N	NOX	23- 55	C	55	ACT-I		4PI
G,5N	NOX	30- 55	C	55	ACT-I		4PI
G,6N	NOX	36- 55	C	55	ACT-I		4PI

Photonuclear recoil studies with thick ThF_4 targets and thick catcher foils for the emitted products after neutron evaporation were carried out with bremsstrahlung of a 55 MeV electron beam. The hypothetical range (R_0) of the $^{232}Th(\gamma, xn)^{232-x}Th$ reaction recoils (x = 5,6) in the target material was found to be about 12 $\mu g/cm^2$ (in the frame of the moving compound nucleus). The effective ranges in beam and in the opposite direction (R_+ and R_-) lead to forward-backward recoil ratios (R_+/R_-) of 2–4, increasing with the number of evaporated neutrons (x = 4,5,6). The reaction kinematics are discussed in the compound nucleus model, first by a step-by-step Monte Carlo calculation, then by a mean value analysis. The calculated mean ranges and forward-backward recoil ratios agree satisfactorily with the experimental results for most residual nuclei studied.

ALPHA SPECTROSCOPY

TABLE IV. Summary of results for the range calculations: (1) Step-by-step Monte Carlo calculation; (2) mean-value analysis; (3) corresponding experimental values.

		Residual nucleus ^{228}Th	^{227}Th	^{226}Th
Most probable momentum of compound nucleus $\bar{p}_{CN}$ (in MeV/c)	(1)	31.0	36.7	46.3
	(2)	34	43	52
Standard deviation of momentum distribution σ_x (in MeV/c)	(1)	68.5	80.1	83.2
	(2)	71.2	79.7	87.3
Mean forward range in target material $\langle R_+ \rangle$ (in $\mu g/cm^2$) respectively effective range	(1)	4.6	5.8	6.6
	(2)	5.7	7.0	8.3
	(3)	···	4.2 ± 1.0	5.4 ± 0.5
Mean backward range in target material $\langle R_- \rangle$ (in $\mu g/cm^2$) respectively effective range	(1)	2.4	2.8	2.9
	(2)	3.1	3.5	3.9
	(3)	···	1.7 ± 0.4	1.1 ± 0.2
Forward-backward recoil ratio $\langle R_+ \rangle / \langle R_- \rangle$ respectively A_{C_+}/A_{C_-}	(1)	1.9	2.1	2.3
	(2)	1.8	2.0	2.1
	(3)	2.0 ± 0.5	2.7 ± 0.3	3.8 ± 0.5

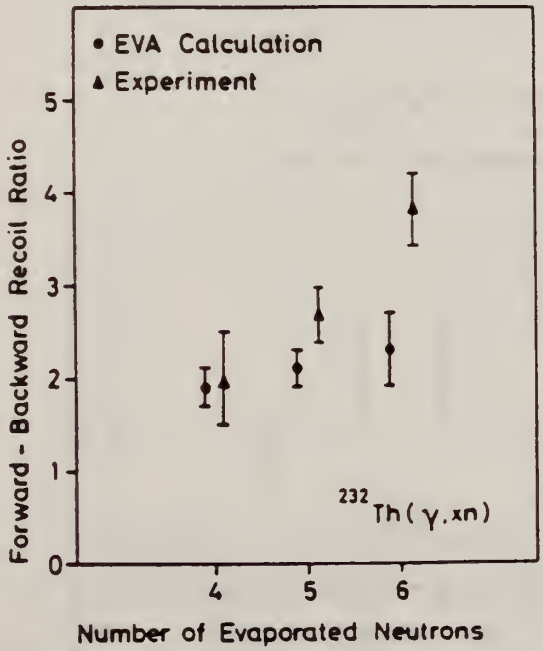

FIG. 8. Forward-backward recoil ratio in the $^{232}Th-(\gamma, xn)^{232-x}Th$ reactions for x = 4, 5, and 6; comparison of $(F/B)_{exp}$ with $(F/B)_{theo}$.

REF. V.E. Zhuchko, A.V. Ignatyuk, Yu. B. Ostapenko, G.N. Smirenkin, A.S. Soldatov, Yu.M. Tsipenyuk
ZhETF Pis. Red. 22, 255 (1975)
JETP Lett. 22, 118 (1975)

EL EM. SYM.	A	Z
Th	232	90

METHOD

REF. NO.	
75 Zh 1	hmg

REACTION	RESULT	EXCITATION ENERGY	SOURCE		DETECTOR		ANGLE
			TYPE	RANGE	TYPE	RANGE	
G,F	NOX	THR- 6	C	3- 6	TRK-I		4PI
		(Thr-5.5)		(3.8-5.5)			

For the isotopes ^{232}Th, ^{237}Np, and ^{238}U, in the deep subbarrier region, we observed an abrupt decrease of the slope of the energy dependence of the photofission cross section, called the isomer shelf. An investigation of this phenomenon uncovers a number of new possibilities for the refinement of our concepts concerning the structure of the fission barrier of heavy nuclei.

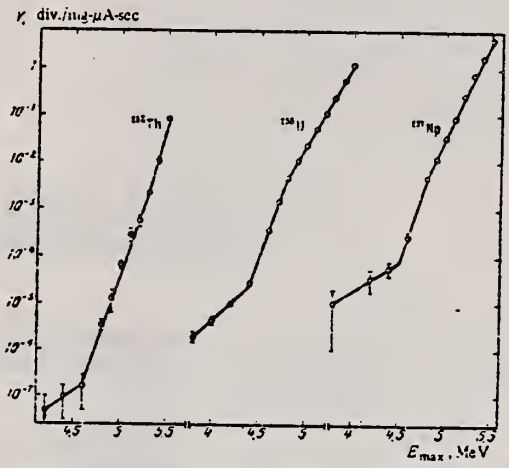

Energy dependence of the photofission yield of ^{232}Th, ^{238}U, and ^{237}Np.

REF. J. Aschenbach, G. Fiedler, E. Konecny
Nucl. Phys. A260, 287 (1976)

ELEM. SYM.	A	Z
Th	232	90

METHOD

REF. NO. 76 As 1 egf

REACTION	RESULT	EXCITATION ENERGY	SOURCE		DETECTOR		ANGLE
			TYPE	RANGE	TYPE	RANGE	
E,F	NOX	THR- 66	D	7- 66	TRK-I		DST

FISSION K.E.

Abstract: We have measured fragment kinetic energies in electron induced fission of ^{232}Th for electron energies in the range 7 MeV $\leq E_e \leq$ 66 MeV. The relative contribution of the distribution peak associated with high fragment kinetic energies decreases continuously with electron energy. This is interpreted as a relative increase of the symmetric fission yield as compared to the asymmetric fission yield; this fact in turn indicates a non-negligible increase in the average excitation of the fissioning nucleus, with the energy of the bombarding electrons, even above the giant dipole resonance.

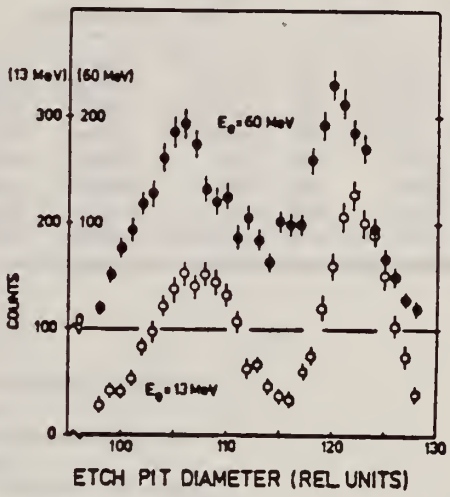

Fig. 1. Fission fragment etch pit diameters for electron energies E_e = 13 and 60 MeV for the 90° detector (open and full circles, respectively).

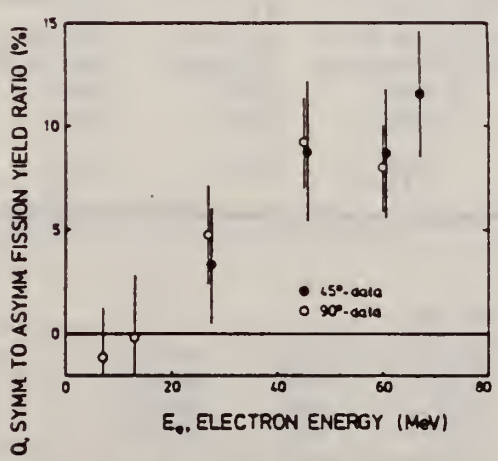

Fig. 2. Symmetric to asymmetric fission yield ratio as a function of electron energy.

REF.		ELEM. SYM.	A	Z
	T. Cooper, W. Bertozzi, J. Heisenberg, S. Kowalski, W. Turchinetz, C. Williamson, L. Cardman, S. Fivozinsky, J. Lightbody, Jr., and S. Penner Phys. Rev. C13, 1083 (1976)	Th	232	90
METHOD		REF. NO.		
		76 Co 3		hmg

REACTION	RESULT	EXCITATION ENERGY	SOURCE		DETECTOR		ANGLE
			TYPE	RANGE	TYPE	RANGE	
E,E/	FMF	1, 1	D	44-101	MAG-D		DST

LEVELS .048,.157

TABLE VI. Cross sections of ^{232}Th.

Elastic

Energy (MeV)	Angle (deg)	q_{eff} (fm^{-1})	$\frac{d\sigma}{d\Omega}_{exp}$ (mb)	$\frac{d\sigma}{d\Omega}_{bestfit}$ (mb)	Ratio σ_2^+/σ elastic	$\frac{d\sigma}{d\Omega}^{4^+}_{exp}$ (mb)
44.61	92.42	0.546	0.138×10^{2} ±3%	0.141×10^{2}	0.013 23	0.615×10^{-2} ±40%
53.31	92.39	0.609	0.518×10 ±4%	0.489×10	0.024 32	0.389×10^{-2} ±42%
64.99	92.39	0.695	0.151×10 ±3%	0.146×10	0.033 77	0.471×10^{-2} ±14.4%
77.37	145.28	0.990	0.198×10^{-1} ±4%	0.203×10^{-1}	0.083 67	0.150×10^{-3} ±14.4%
75.09	92.42	0.769	0.637 ±4%	0.662	0.029 11	0.414×10^{-2} ± 9.9%
84.92	92.39	0.841	0.364 ±6%	0.347	0.029 45	0.340×10^{-2} ± 7%
95.33	92.42	0.917	0.164 ±3%	0.168	0.053 11	0.199×10^{-2} ± 5.7%
100.45	145.28	1.262	0.107×10^{-2} ±4%	0.105×10^{-2}	0.098 66	0.281×10^{-4} ± 9.1%

TABLE VIII. Deformed Fermi best fit parameters.

	Units	^{152}Sm	^{154}Sm	^{232}Th	^{233}U
c_0	fm	5.8044	5.9387	6.7915	6.8054
t	fm	0.5814	0.5223	0.5713	0.6049
β_2		0.237 ± 0.003	0.311 ± 0.003	0.233 ± 0.002	0.261 ± 0.002
β_4		0.070 ± 0.003	0.087 ± 0.002	0.101 ± 0.003	0.087 ± 0.003
β_6		−0.0120	−0.180	0.0	0.0
$B(E2)$	e^2b^2	3.38 ±0.07	4.40 ±0.09	9.21 ±0.09	11.70 ±0.15
$B(E4)$	e^2b^4	0.136 ± 0.013	0.221 ± 0.010	1.16 ±0.05	1.20 ±0.06
rms radius	fm	5.0922	5.126	5.7723	5.842
ρ_2 Transition radius	fm	6.937	6.950	7.895	7.979
ρ_4 Transition radius	fm	7.757	7.704	8.540	8.748

REF. G. M. Gurevich, L. E. Lazareva, V. M. Mazur, G. V. Solodukhov, B. A. Tulupov
Nucl. Phys. A273, 326 (1976)

ELEM. SYM.	A	Z
Th	232	90

METHOD

REF. NO. 76 Gu 2 egf

REACTION	RESULT	EXCITATION ENERGY	SOURCE		DETECTOR		ANGLE
			TYPE	RANGE	TYPE	RANGE	
G,MUT	ABX	7- 19	C	UKN	NAI-D		4PI

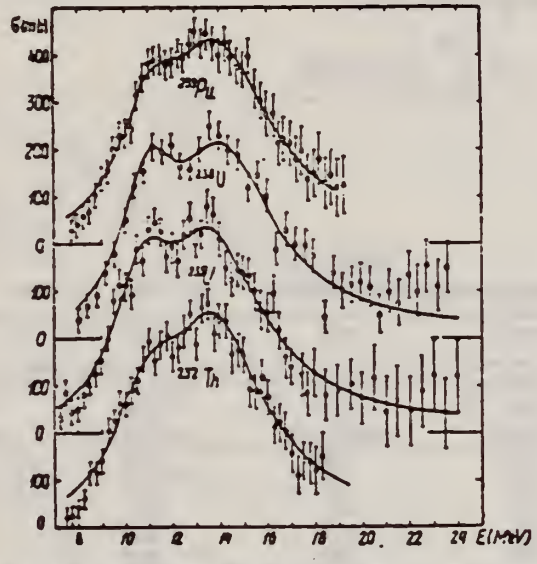

Fig. 2. Total photoabsorption cross sections for ^{232}Th, ^{235,238}U and ^{239}Pu and their respective best two Lorentz line fits.

TABLE 1

Lorentz line parameters for ^{232}Th, ^{235,238}U and ^{239}Pu

Nucleus	E_1 (MeV)	σ_1 (mb)	Γ_1 (MeV)	E_2 (MeV)	σ_2 (mb)	Γ_2 (MeV)
^{232}Th	10.99±0.16	247±26	3.90±0.4	13.9 ±0.13	362±26	4.67±0.38
^{235}U	10.74±0.18	283±39	3.23±0.55	13.77±0.23	354±33	4.92±0.58
^{238}U	10.97±0.13	286±30	2.99±0.48	14.25±0.18	351±25	5.10±0.63
^{239}Pu	11.05±0.13	227±39	3.47±0.57	14.01±0.21	362±31	5.23±0.59

TABLE 2

Deformation parameters and quadrupole moments for ^{232}Th, ^{235,238}U and ^{239}Pu

Nucleus	β_{exp}	β	Q_0 (b)		
			this work	refs. [5,6])	ref. [14])
^{232}Th	0.28±0.03	0.274	10.0±0.8	10.2±1	9.66±0.1
^{235}U	0.30±0.03	0.285	11.0±0.9	12.8±1.3	11.12±0.2
^{238}U	0.31±0.03	0.300	11.7±0.9	11 ±1	11.3 ±0.1
^{239}Pu	0.29±0.03	0.302	11.0±0.9		11.02±0.3

(over)

TABLE 3

Integrated cross sections and mean energies of the dipole absorption

Nucleus	σ_0 (MeV · b)	σ_{-1} (mb)	σ_{-2} (mb · MeV^{-1})	E (MeV)	E_H (MeV)	E_M (MeV)	E' (MeV)
^{232}Th	2.92±0.32	231±24	19±2	13.08	12.64	12.40	12.16
^{235}U	2.99±0.39	238±31	20±2.5	12.91	12.56	12.23	11.90
^{238}U	2.95±0.29	229±22	18±1.8	13.34	12.88	12.80	12.72
^{239}Pu	2.97±0.34	232±26	19±2	13.28	12.80	12.50	12.21

In table 3 various integrated cross sections are defined by the relations

$$\sigma_0 = \int_{S}^{18} \sigma_{tot}(E)dE, \qquad \sigma_{-1} = \int_{S}^{18} \frac{1}{E}\sigma_{tot}(E)dE, \qquad \sigma_{-2} = \int_{S}^{18} \frac{1}{E^2}\sigma_{tot}(E)dE.$$

TABLE 4

Comparison of various integrated cross sections for ^{232}Th, ^{235,238}U and ^{239}Pu

	^{232}Th	^{235}U	^{238}U	^{239}Pu
σ_{0L} (MeV · b)	4.17	4.17	4.16	4.21
0.06 NZ/A (MeV · b)	3.31	3.36	3.39	3.42
$\sigma_0/(0.06\ NZ/A)$	0.88±0.1	0.89±0.12	0.87±0.09	0.87±0.1
$\sigma_{0L}/(0.06\ NZ/A)$	1.26	1.24	1.23	1.23
$\sigma_2\Gamma_2/\sigma_1\Gamma_1$	1.75	1.91	2.09	2.40
σ_{-1L} (mb)	294	298	288	289
$\sigma_{-1L}/A^{4/3}$	0.21	0.21	0.20	0.20
σ_{-2L} (mb · MeV^{-1})	26.3	26.9	25.0	25.3
$\sigma_{-2L} \times 10^3/A^{5/3}$	3.00	3.01	2.74	2.76

[5] C. D. Bowman et al., Phys. Rev. 133 (1964) B676
[6] A. Veyssiere et al., Nucl. Phys. A199 (1973) 45
[14] K.E.G. Lobner et al., Nucl. Data Tables 7 (1970)495

REF.

U. Kneissl, G. Kuhl, K. H. Leister, A. Weller
Nucl. Phys. A256, 11 (1976)

ELEM. SYM.	A	Z
Th	232	90

METHOD

REF. NO.: 76 Kn 1 egf

REACTION	RESULT	EXCITATION ENERGY	SOURCE		DETECTOR		ANGLE
			TYPE	RANGE	TYPE	RANGE	
E,F	RLX	THR- 40	D	10- 40	TRK-I		2PI

SIGMA(E-)/SIGMA(E+)

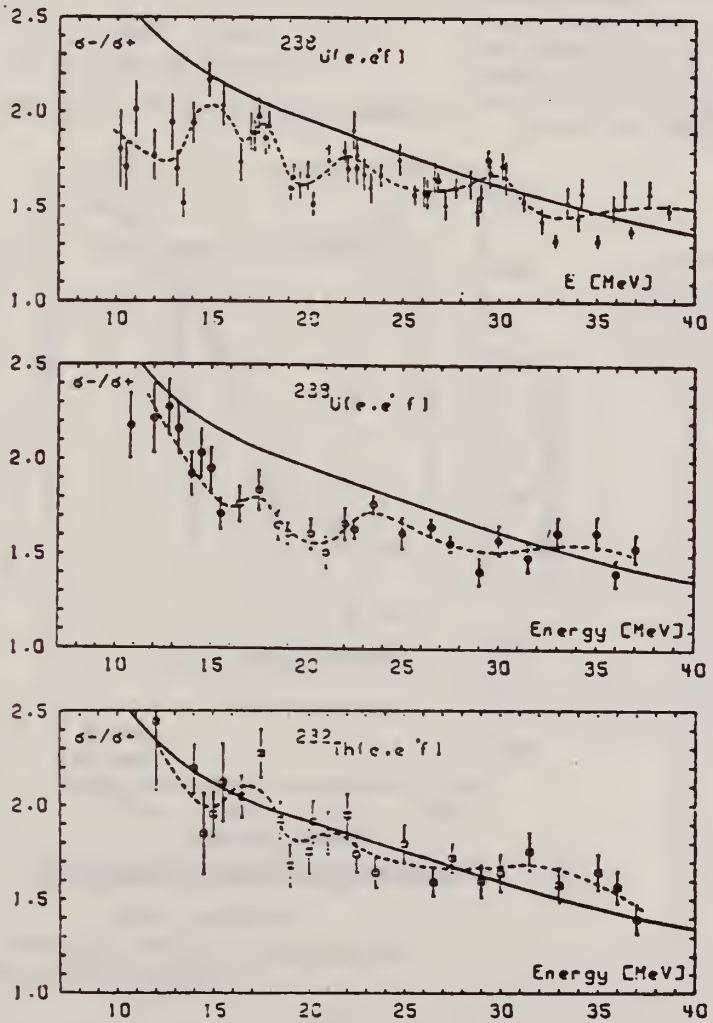

Fig. 2. Experimental results for σ^-/σ^+. Full lines: DW calculations for pure E1 excitation according to ref. [8]). Dashed lines are to guide the eye. The upper part shows the results for uranium (detectors at 90°) with crosses and triangles representing earlier results [7]) with glass detectors and surface barrier detectors, and circles representing new results with glass detectors. The middle and lower parts show the results for uranium and thorium with the 2π arrangement and Macrofol detectors.

[7] U. Kneissl, G. Kuhl, and A. Weller; Phys. Lett. 49B, 440 (74).

[8] D.S. Onley (Ohio Univ. priv. comm; I.C. Nascimento et al., Nucl. Phys. A246, 210 (75).

REF. J.C. Hogan, A.E. Richardson, J.L. Meason and H.L. Wright
Phys. Rev. C 16, 2296 (1977)

ELEM. SYM.	A	Z
Th	232	90

METHOD

REF. NO. 77 Ho 3 hmg

REACTION	RESULT	EXCITATION ENERGY	SOURCE TYPE	SOURCE RANGE	DETECTOR TYPE	DETECTOR RANGE	ANGLE
G,F	RLY	5- 38	C	9- 38	ACT-I		UKN
		(5.4-38)					

MASS YLD DISTRIB

The mass-yield distribution of fission products following photofission of ^{232}Th using peak bremsstrahlung energies of 9, 15, and 38 MeV were measured by γ spectrometry for 25 mass chains in the light and heavy mass wings. Fission yields for mass chains 85, 87, 88, 138, and 146 were measured for the first time for the photofission of ^{232}Th in this work. Several fractional chain yields were measured and various postulates of charge distribution were tested to correlate the experimental data. The Nethaway modified empirical Coryell method showed the best correlation with the observed charge distributions. Evidence for fine structure was observed from the 9 and 15 MeV irradiations in both the heavy and light mass wings with peaks occurring at A = 134 and 93, respectively. The inner portions of the mass wings both exhibited increasing splay as the irradiation energy was increased, indicating that symmetric fission was enhanced with increased energy.

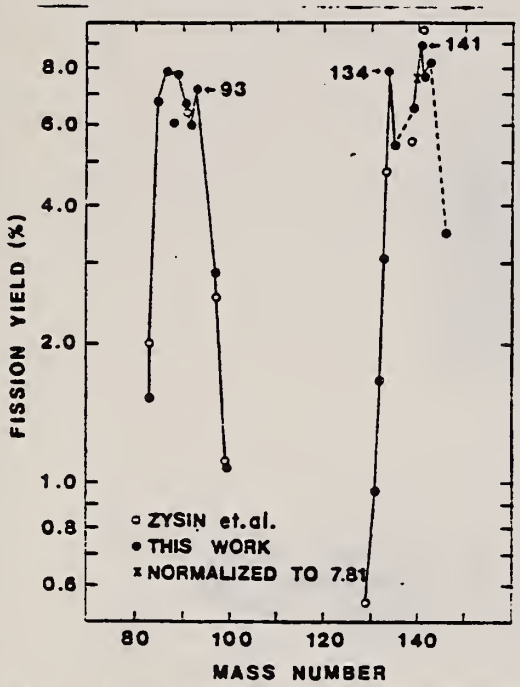

FIG. 1. Photofission of ^{232}Th with 9 MeV bremsstrahlung.

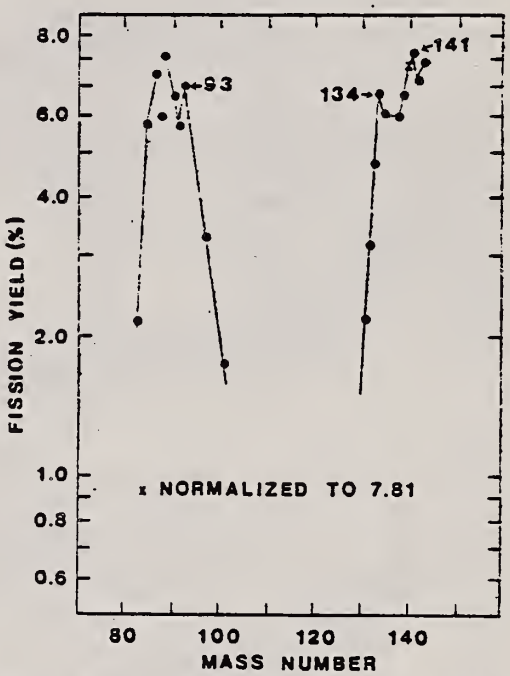

FIG. 2. Photofission of ^{232}Th with 15 MeV bremsstrahlung.

over

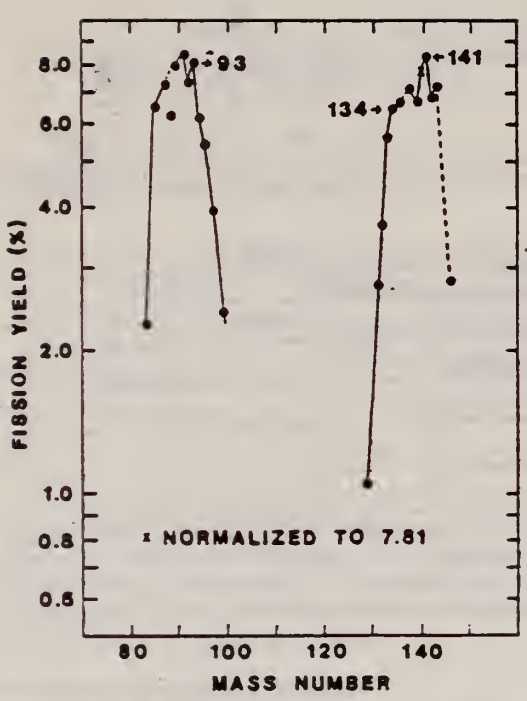

FIG. 3. Photofission of ^{232}Th with 38 MeV bremsstrahlung.

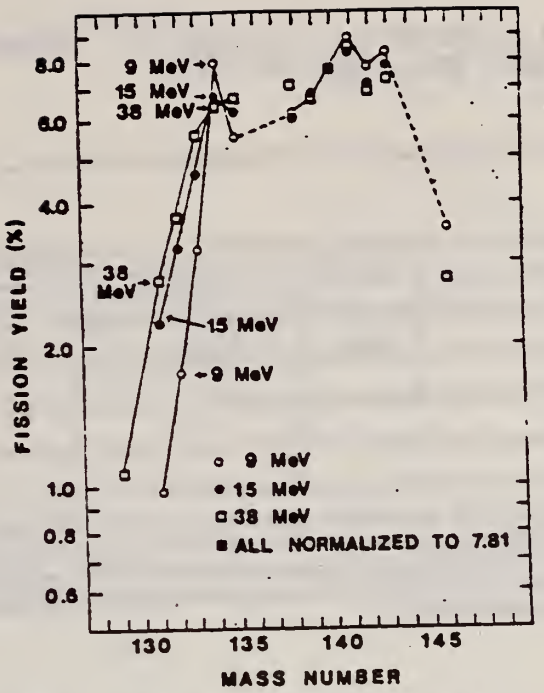

FIG. 4. Photofission of ^{232}Th with 9, 15, and 38 MeV bremsstrahlung (heavy mass wing).

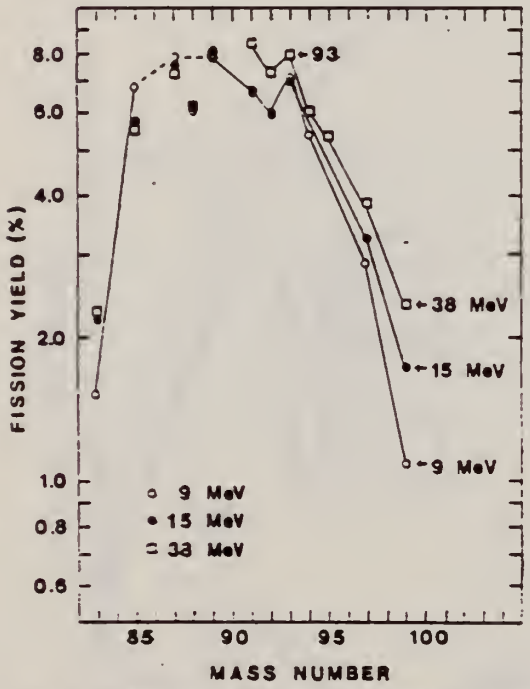

FIG. 5. Photofission of ^{232}Th with 9, 15, and 38 MeV bremsstrahlung (light mass wing).

TABLE V. Photofission yields of ^{232}Th determined in present work normalized to ^{140}Ba.

Mass no.	9 MeV	15 MeV	38 MeV
83	1.52 ± 0.16	2.15 ± 0.13	2.24 ± 0.16
85	6.75 ± 0.75	5.75 ± 0.53	5.50 ± 0.50
87	7.87 ± 0.65	7.43 ± 0.53	7.20 ± 0.53
88	6.09 ± 0.55	6.00 ± 0.40	6.16 ± 0.48
89	7.81 ± 0.71	8.25 ± 0.85	7.92 ± 0.30
91	6.75 ± 0.32	6.61 ± 0.31	8.37 ± 0.40
92	5.99 ± 0.39	5.88 ± 0.43	7.33 ± 0.50
93	7.21 ± 0.65	7.03 ± 0.60	8.02 ± 0.53
94	5.42 ± 0.54		6.10 ± 0.38
95			5.39 ± 0.60
97	2.90 ± 0.14	3.26 ± 0.13	3.88 ± 0.21
99	1.09 ± 0.10	1.73 ± 0.09	2.40 ± 0.13
129			1.04 ± 0.16
131	0.95 ± 0.08	2.20 ± 0.20	2.74 ± 0.13
132	1.69 ± 0.10	3.20 ± 0.13	3.71 ± 0.21
133	3.22 ± 0.18	4.53 ± 0.25	5.61 ± 0.37
134	7.90 ± 0.72	6.75 ± 0.61	6.46 ± 0.38
135	5.43 ± 0.49	6.08 ± 0.55	6.70 ± 0.55
136	6.09 ± 0.50	6.00 ± 0.54	7.16 ± 0.75
139	6.62 ± 0.71	6.70 ± 0.77	6.75 ± 0.70
140	7.31	7.31	7.81
141	9.06 ± 0.51	8.26 ± 0.61	8.40 ± 0.62
142	7.87 ± 0.71	7.20 ± 0.71	6.86 ± 0.57
143	8.53 ± 0.41	7.89 ± 0.37	7.30 ± 0.42
146	3.57 ± 0.41		2.80 ± 0.40

REF. A.C. Shotter, D. Branford, J.C. McGeorge and J.M. Reid
Nucl. Phys. A290, 55 (1977)

ELEM. SYM.	A	Z
Th	232	90

METHOD

REF. NO. 77 Sh 9

REACTION	RESULT	EXCITATION ENERGY	SOURCE		DETECTOR		ANGLE
			TYPE	RANGE	TYPE	RANGE	
E,F	ABX	C-120	D	20-120	SCD-I		DST

Abstract: Measurements of the electrofission cross section for ^{232}Th, ^{238}U and ^{237}Np have been made for an electron energy range from 20 to 120 MeV. A comparison is made between the electrofission and photofission cross sections using the concept of virtual photons. It is deduced that the electrofission reaction for these elements proceeds through a significant E2 contribution as well as an E1 transition mode.

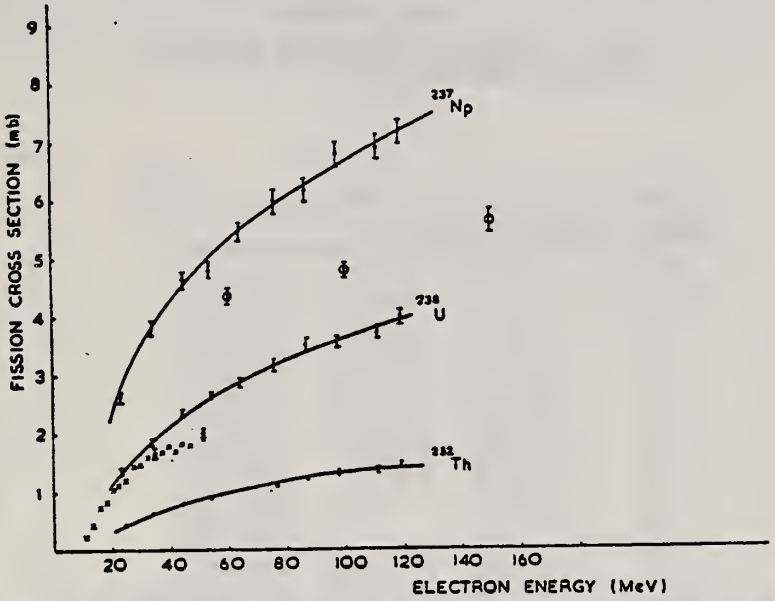

Fig. 1. Total electrofission cross sections versus electron energy. The solid circles are from the present work. Data on ^{238}U from ref. [1]) (open circles) and ref. [3]) (crosses) are also shown. The curves are the best fit to the data as described in the text. The errors shown for the present data are relative only.

[1] L.G. Morretto, R.C. Gatti, S.G. THompson, J.T. Routti, J.H. Heisenberg, L.M. Middleman, M.R. Yearian and R. Hofstadter, Phys. Rev. 179 (1969) 1176

[3] J.D.T. Arruda Neto, S.B. Herdade, B.S. Bhandari and I.C. Niscimento, Universidade de Sao Paulo, report no. IFUSP/P-76 (1976); J.C. Nascimento, S.B. Herdade and J.D.T. Arruda Neto, Proc. Int. Conf. on Photonuclear reactions and applications, Asilomar, 1973, ed. B.L. Berman (Lawrence Livermore Laboratory, Livermore, California) contributed paper, 5D10

USCOMM-NBS-DC

TABLE 1

Nucleus	Normalisation		$\int\sigma_{E2(\gamma n)}(E_\gamma)dE_\gamma$	
	9 MeV	22 MeV	9 MeV	22 MeV
^{232}Th	1.17	1.81	2.5 mb · MeV	12.8 mb · MeV
^{238}U	1.00	1.30	6.4 mb · MeV	38.8 mb · MeV
^{237}Np	1.12	1.34	7.9 mb · MeV	52.3 mb · MeV

From table 1 it is observed that the normalisation factors for $E_g = 22$ MeV are higher than would be expected from the absolute experimental errors (± 20 %). This may indicate a preferential concentration of E2 strength at 9 MeV.

PHO 88

REF. V.E. Zhuchko, S.P. Kapitza, Yu.B. Ostapenko, G.N. Smirenkin, A.S. Soldatov, Yu.M. Tsipenyuk
JETP Lett. 26, 553 (1977)

ELEM. SYM.	A	Z
Th	232	90

METHOD

REF. NO. 77 Zh 3 hg

REACTION	RESULT	EXCITATION ENERGY	SOURCE		DETECTOR		ANGLE
			TYPE	RANGE	TYPE	RANGE	
G,F	ABY	THR-7	C	5-7	TRK-D		DST

An increase in the quadrupole component of the angular distribution of the fragments was observed deep below the photofission barrier of ^{232}Th. We discuss the influence of the symmetry of the saddle configurations in the double-hump-barrier model on the spectrum of the fission channels of even-even nuclei and the resonant structure of the cross section.

PACS numbers: 25.85.Jg, 27.90.+b

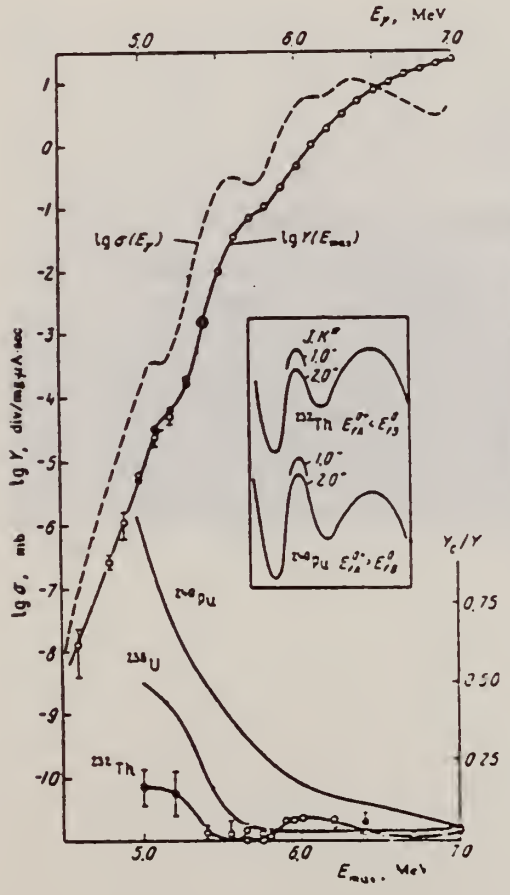

FIG. 1. Bottom: dependence of the relative contribution Y_c/Y of the quadrupole component to the total yield; for ^{232}Th: (●)—data of present paper, (○)—data of[2,3]; for ^{238}U and ^{240}Pu—dependence in accordance with the data of[2,3]. Top: dependence of the yield of the reaction ^{232}Th(γ,f) on the end-point energy of the bremmstrahlung spectrum: (○)—data of[4], (●)—data of present paper; the dashed curve shows the dependence of the photofission cross section $\sigma_f(E_\gamma)$ obtained by te method of[5]. Insert: schematic representation of the structure of the ^{232}Th and ^{240}Pu fission barriers.

REF. C.D. Bowman, I.G. Schroder, K.C. Duvall and C.E. Dick
Phys. Rev. C 17, 1086 (1978)

ELEM. SYM.	A	Z
Th	232	90

METHOD

REF. NO. 78 Bo 8 hg

REACTION	RESULT	EXCITATION ENERGY	SOURCE		DETECTOR		ANGLE
			TYPE	RANGE	TYPE	RANGE	
G,F	ABX	THR- 6	C	3- 6	TRK-I		4PI
		(THR-5.75)		(3.2-5.75)			

Photofission cross sections for ^{232}Th, and ^{236}U have been measured in the energy range from 3.25 to 5.75 MeV and for ^{234}U and ^{236}U at 3.5 MeV. The cross sections change by over seven orders of magnitude for this energy range. Cross section shapes are significantly different for different isotopes indicating a strong sensitivity to fission barrier parameters.

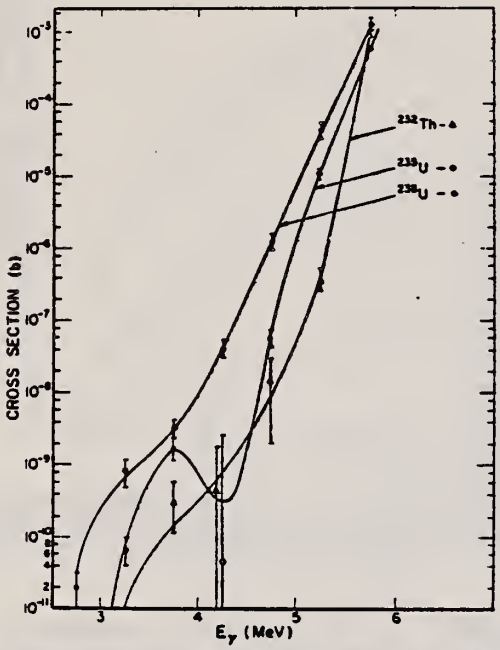

FIG. 1. The photofission cross sections of ^{232}Th, ^{235}U, and ^{238}U. The uncertainty shown includes only track counting statistics propagated through the unfolding process. A systematic uncertainty in the cross section scale might be as large as a factor of 2. The lines through the data are included to guide the eye.

TABLE III. Photofission cross sections for ^{232}Th and ^{235}U.

Photon energy (MeV)	Cross section ^{235}U (b)	Cross section ^{232}Th (b)
3.25	$6.8 \pm 2.6 \times 10^{-11}$	$7.4 \pm 129 \times 10^{-13}$
3.75	$170 \pm 47 \times 10^{-11}$	$3.3 \pm 2.2 \times 10^{-10}$
4.25	$4.9 \pm 248 \times 10^{-11}$	$4.4 \pm 10.7 \times 10^{-10}$
4.75	$6.3 \pm 1.9 \times 10^{-8}$	$1.6 \pm 1.4 \times 10^{-8}$
5.25	$1.1 \pm 0.08 \times 10^{-5}$	$4.2 \pm 1.1 \times 10^{-7}$
5.75	$5.6 \pm 0.11 \times 10^{-4}$	$8.6 \pm 0.25 \times 10^{-4}$

REF. V.E. Zhuchko, Yu.B. Ostapenko, G.N. Smirenkin, A.S. Soldatov, Yu.M. Tsipenyuk
Yad. Fiz. 28, 1185 (1978)
Sov. J. Nucl. Phys. 28, 611 (1978)

ELEM. SYM.	A	Z
Th	232	90

METHOD

REF. NO. 78 Zh 6 hg

REACTION	RESULT	EXCITATION ENERGY	SOURCE		DETECTOR		ANGLE
			TYPE	RANGE	TYPE	RANGE	
G,F	RLY	THR-5	C	3-5	TRK-D		4PI
		(THR-4.6)		(3.5-4.6)			

Yield measurements are reported for photofission of ^{232}Th, ^{236}U, ^{238}U, and ^{237}Np in the deep sub-barrier energy region 3.5–4.6 MeV where anomalies in the cross section—isomeric shelfs—were previously observed [Phys. Rev. C, 12, 863 (1975)]; Pis'ma. Zh. Eksp. Teor. Fiz. 22, 255 (1975), [JETP Lett. 22, 118 (1975)]. The various sources of background arising in this energy region, which is only with difficulty accessible for measurements, are analyzed in detail. Analysis of the anomalies in the behavior of the integrated photofission yields in the case of the two nuclei ^{236}U and ^{238}U most favorable for study indicates a resonance nature of the cross sections for delayed fission and a substantially more complicated physics of the phenomenon than the simplified interpretation of Bowman [Phys. Rev. C, 12, 863 (1975)].

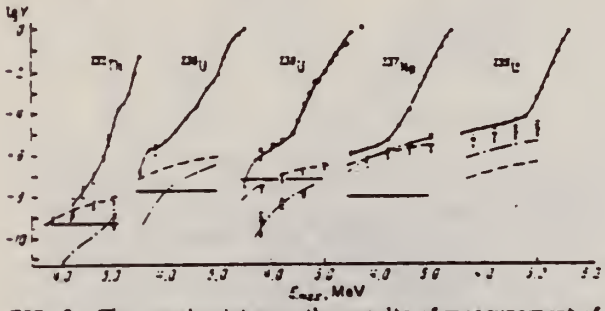

FIG. 2. The round points are the results of measurement of the yields $Y(E_{max})$ in fissions/mg-μC of the photofission reaction: ●—present work and Ref. 7; ○—Ref. 8. ⁻ and dashed lines—respectively the experimental and theoretical estimates of the background due to fissions by neutrons from the reaction Be(γ,n); ⊏ and dot-dash lines—the same for the D(γ,n) reaction. The shaded sections show the level of background from spontaneous fission and fission induced by cosmic rays.

REF. V.E. Zhuchko, Yu.B. Ostapenko, G.N. Smirenkin, A.S. Soldatov, Yu.M. Tsipenyuk
Yad. Fiz. 28, 1170 (1978)
Sov. J. Nucl. Phys. 28, 602 (1978)

ELEM. SYM.	A	Z
Th	232	90

METHOD

REF. NO. 78 Zh 7 hg

REACTION	RESULT	EXCITATION ENERGY	SOURCE		DETECTOR		ANGLE
			TYPE	RANGE	TYPE	RANGE	
G,F	ABX	THR-7	C	4-7	TRK-D		4PI
				(4.4-7.)			

The bremsstrahlung beam of the microtron at our Institute has been used to measure photofission yields of nine nuclei—^{232}Th, ^{233,235,236,238}U, ^{237}Np, ^{239,241}Pu, and ^{241}Am in the energy region 4.4–7.0 MeV. The method of minimization of the directed deviation was used to reproduce the photofission cross sections from the integrated yields. The following problems are discussed in terms of the experimental data: resonance structure of the cross sections, effects of a two-humped shape of the fission barrier, and comparison of the fissility in the (γ,f) and (n,f) reactions and in direct reactions.

PACS numbers: 25.85.Jg

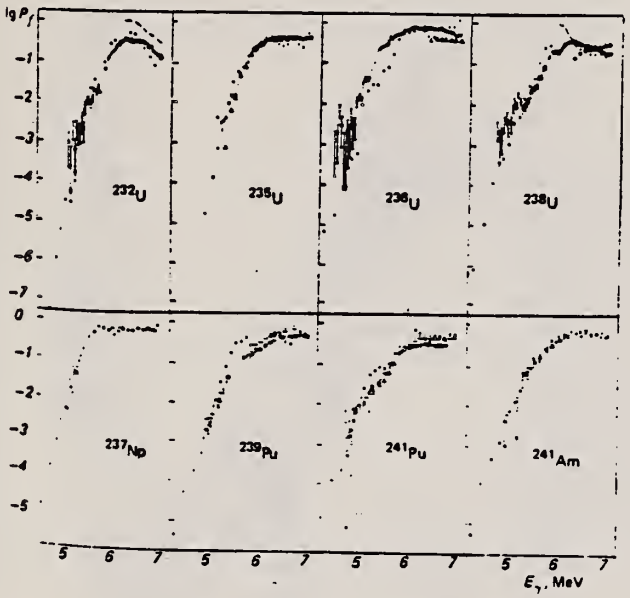

FIG. 4. Fissility P_f in the reactions (γ,f)—●, (n,f)—△ (Ref. 14), and in direct reactions—○.[2] The dashed curve shows the results of evaluation of P_f in accordance with Eq. (9).

(over)

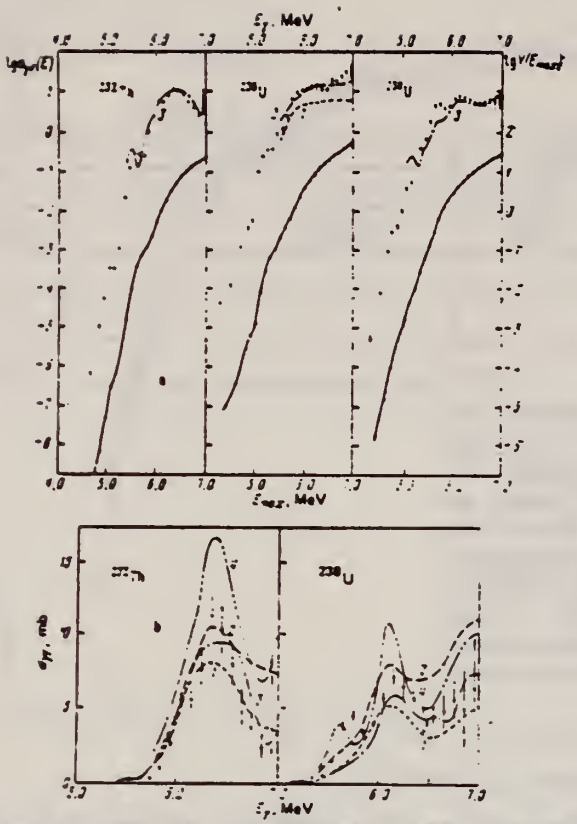

FIG. 2. Yields $Y(E_{max})$, fissions/mg-μC (lower curve), and cross sections $\sigma_{\gamma f}(E_\gamma)$, mb (upper curve), of the photofission reaction for even-even isotopes—a; comparison of the functions $\sigma_{\gamma f}(E_\gamma)$ obtained in the present work for ^{232}Th and ^{238}U with data obtained in quasimonochromatic γ rays—b. Curves: solid lines (and points)—results of the present work, 1—data of Ref. 5, 2—data of Ref. 6, 3—data of Ref. 7, 4—data of Ref. 8.

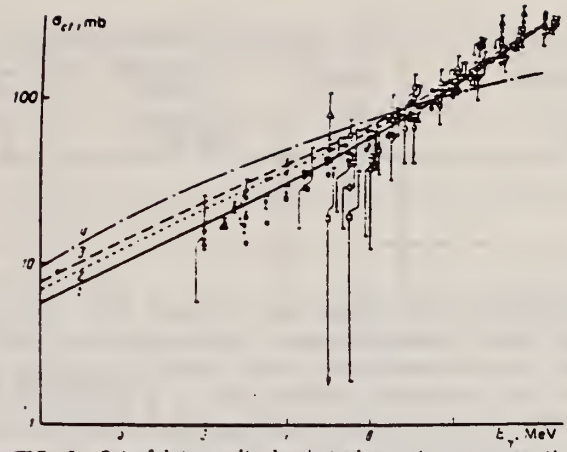

FIG. 6. Set of data on dipole photoabsorption cross sections σ_{c1}. The solid line (1)—the present work—is the result of fitting the data of Ref. 6 by Eq. (2) in the region $E_\gamma = 6$–10 MeV. Curves 2 and 3 are an extrapolation of the fit from Ref. 16 (2) and Ref. 17 (3) for ^{238}U; curve 4 is an estimate by means of Axel's formula.[15] Points: □, ■—^{232}Th; △, ▲—^{235}U; ♦—^{236}U; ○, ●—^{238}U; ▽, ▼—^{237}Np; ◇—^{239}Pu. The hollow points are from Refs. 16 and 17; the solid points are from Ref. 6.

REF. J. Aschenbach, R. Haag, H. Krieger
Z. Phys. A292, 285 (1979)

ELEM. SYM.	A	Z
TH	232	90

METHOD

REF. NO. 79As4 hg

REACTION	RESULT	EXCITATION ENERGY	SOURCE		DETECTOR		ANGLE
			TYPE	RANGE	TYPE	RANGE	
E,F	ABX	THR-65	D	7-65	TRK-D		DST

Absolute electrofission cross sections for ^{238}U and ^{232}Th in the energy region $E_e = 7 - 65$ MeV and fission fragment angular distributions for $E_e = 7 - 30$ MeV have been measured. The angular distributions show strong anisotropies for low energies. The relative dipole and quadrupole contributions as a function of excitation energy are discussed in terms of the low lying fission transition states above the fission barriers. The cross sections show significant deviations from the results of some earlier measurements, in particular in the energy region above the giant dipole resonance. From the difficulties of absolute electrofission cross section measurements and the ambiguities in their interpretation it is concluded that by this time the quantitative analysis of electrofission cross sections with respect to the contributions of the giant quadrupole resonances to the fission decay channel should be regarded as rather tentative.

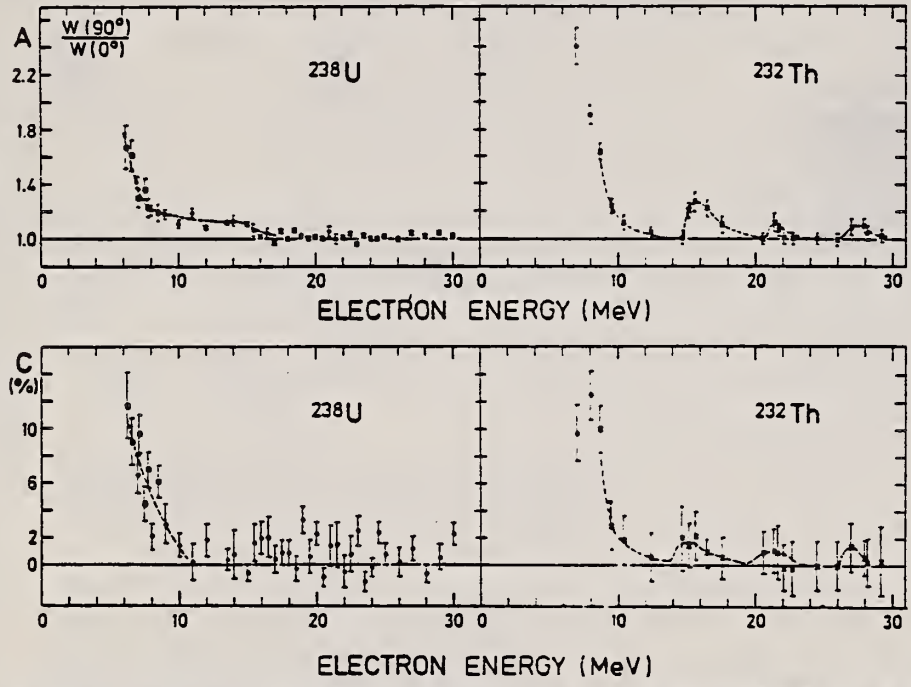

Fig. 2. Top: Anisotropies $A = W(90°)/W(0°)$ corresponding to the least squares fit results from Fig. 1 in the electrofission of ^{238}U and ^{232}Th. Bottom: Relative quadrupole contributions C as described in the text. Circles this work, squares [8], crosses [6]

$$C = (8c/15)/(a + 2b/3 + 8c/15) \qquad (2)$$

over

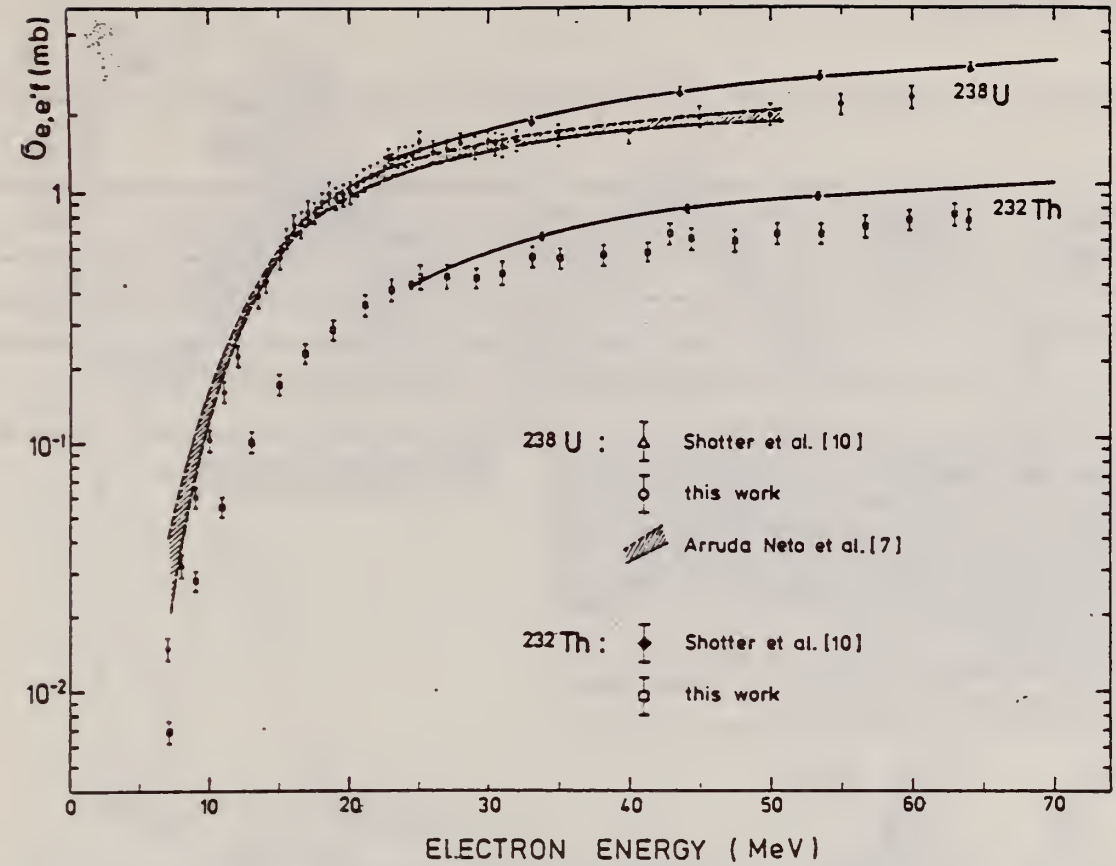

Fig. 4. Absolute electrofission cross sections of ^{238}U and ^{232}Th from this work in comparison with the data of Shotter et al. [10] and Arruda Neto et al. [7]

REF. J. C. McGeorge, A. C. Shotter, D. Branford, J. M. Reid
Nucl. Phys. A326, 108 (1979)

ELEM. SYM.	A	Z
Th	232	90

METHOD

REF. NO. 79Mc2 hg

REACTION	RESULT	EXCITATION ENERGY	SOURCE		DETECTOR		ANGLE
			TYPE	RANGE	TYPE	RANGE	
E, F.	NOX	THR-110	D	110	SCD-D	115-190	90

Abstract: Fission of ^{232}Th, ^{237}Np, ^{209}Bi, ^{235}U and ^{238}U induced by 110 MeV electrons has been studied by means of surface barrier detectors. The resulting mass and kinetic energy distributions are presented. Comparison with the liquid drop model predictions shows reasonable agreement in the case of ^{209}Bi. The data are analysed in terms of a two component model of fission and the mean total kinetic energies of the components are shown to depend linearly on $Z_1Z_2(A_1^{1/3}+A_2^{1/3})$. Interesting differences are found when the present results are compared with the recent photofission experiments of Areskoug *et al.* and features in both sets of data correlate with changes of fragment deformation implied by the calculations of Wilkins *et al.*

MASS AND EGY DISTRIB

E NUCLEAR REACTIONS ^{237}Np, ^{232}Th, ^{209}Bi, ^{238}U, ^{235}U(e, f), E = 110 MeV; measured fission fragment E, deduced mass.

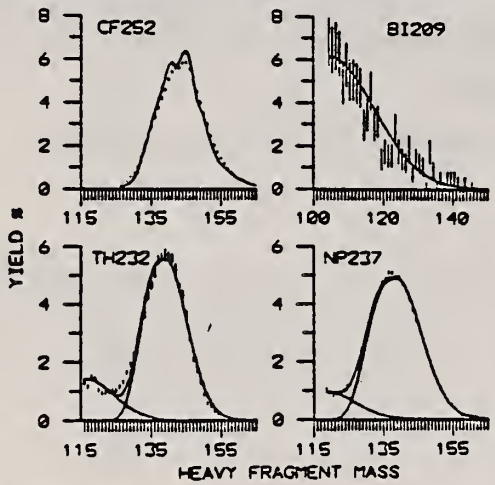

Fig. 1. The HFM yield distributions for electrofission of ^{209}Bi, ^{232}Th and ^{237}Np and spontaneous fission of ^{252}Cf. Statistical uncertainties are shown where larger than the size of the points in this and succeeding diagrams. The solid line in the ^{252}Cf case represents the experimental results of Schmidt *et al.* [12]). In the ^{209}Bi case the solid line represents a Gaussian fit to the data while the solid lines in the other two cases are the result of a two component analysis (see text).

TABLE 2

Target	Mean total KE (MeV)			Width
	present work	semi-empirical [ref. [14])]		present work
		[a])	[b])	
^{238}U	171.8±3.4	168.5	169.4	11.6±0.1
^{235}U	171.3±3.4	169.1	170.1	10.8±0.1
^{232}Th	167.0±3.3	163.4	163.5	9.6±0.1
^{237}Np	174.3±3.0	171.9	173.3	11.5±0.1
^{209}Bi	140 ±4	146.5	143.9	11.5±0.4

[a]) $0.1071Z^2/A^{1/3}+22.2$.
[b]) $0.1240Z^2/A^{1/3}$.

over

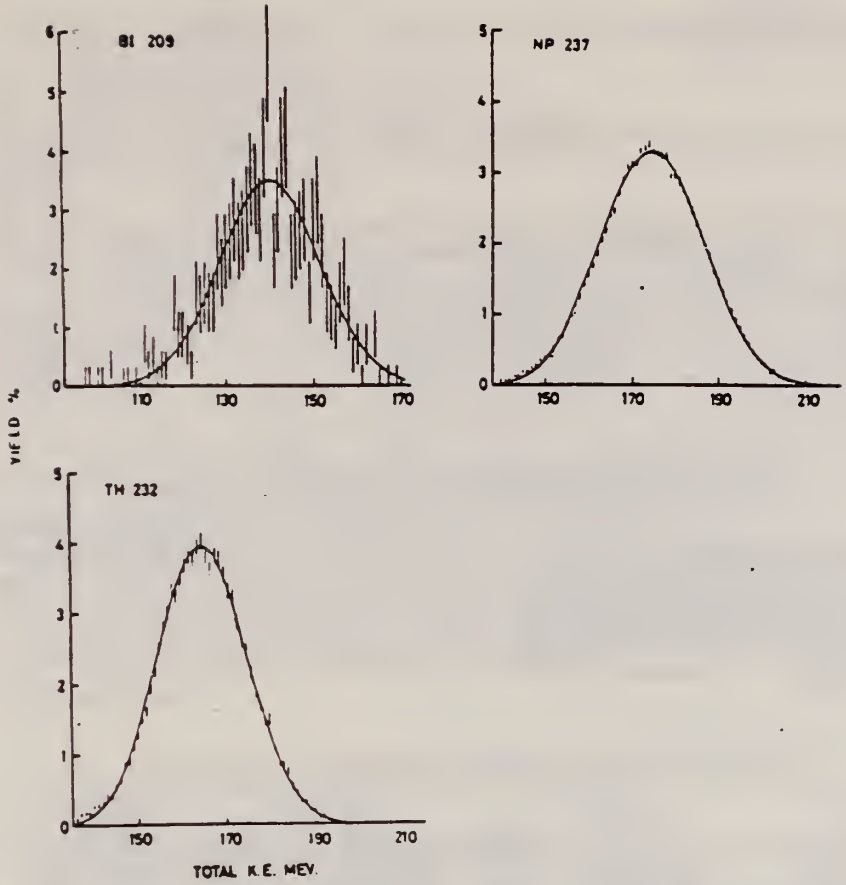

Fig. 2. Total fragment kinetic energy distributions in the electrofission of ^{209}Bi, ^{237}Np and ^{232}Th. The solid lines result from fitting a single Gaussian to the data in the ^{209}Bi case and a double Gaussian in the other cases.

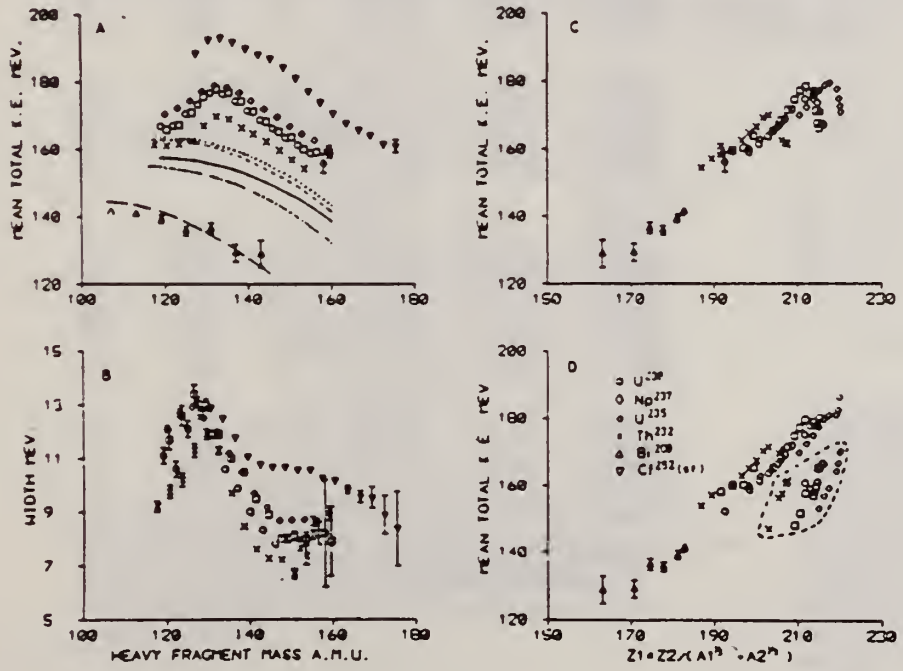

Fig. 3. Total fragment kinetic energy data from electrofission of ^{238}U, ^{235}U, ^{237}Np, ^{232}Th, ^{209}Bi and for spontaneous fission of ^{252}Cf. (A) Mean TKE versus HFM. The lines represent the LDM calculations of Nix and Swiatecki [13] – solid ^{238}U, short dash ^{235}U, long dash ^{209}Bi, dot ^{237}Np and dot dash ^{232}Th. (B) Width of the TKE distribution versus heavy fragment mass. (C) Mean total fragment kinetic energy versus $Z_1Z_2/(A_1^{1/3}+A_2^{1/3})$. (D) Mean total fragment kinetic energy of the symmetric (enclosed by the dashed line) and asymmetric components versus $Z_1Z_2/(A_1^{1/3}+A_2^{1/3})$. In (A)(C) and (D) the relative uncertainties between targets are ±3 MeV and the absolute uncertainties are ±4 MeV.

REF. J. Visser, G.A. Brinkman, Cees N.M. Bakker
Int. J. Appl. Rad. Isotopes 30, 745 (1979)

ELEM. SYM.	A	Z
Th	232	90

METHOD

REF. NO. 79 Vi 1 hg

REACTION	RESULT	EXCITATION ENERGY	SOURCE		DETECTOR		ANGLE
			TYPE	RANGE	TYPE	RANGE	
G,SPL	ABY	THR-350	C	250-350	ACT-I		4PI
G,F	RLY	THR-350	C	250,350	ACT-I		4PI

Yield (cross section per equivalent quantum) for
A=135 (presumably photofission): at .25 GeV 1.96±0.18mb
.35 GeV 2.53 mb

Photospallation cross sections of ^{232}Th with bremsstrahlung beams of 0.25, 0.30 and 0.35 GeV maximum energies have been determined for ^{209}At (66, 87 and 280 μb), ^{210}At (74, 98 and 230 μb) and ^{211}Rn (28, 40 and 130 μb). These yields are an order of magnitude lower than predicted by the Rudstam CDMD formula, possibly as a consequence of the rather thick Cu converter that was used. Irradiation of UO_2 at 0.3 GeV resulted in cross sections for ^{209}At: 15.8 μb and for ^{210}At: 17.9 μb. Cumulative photofission cross sections have been determined for $A = 135$ at 0.25 GeV (1.96 mb) and at 0.35 GeV (2.53 mb). Half-lives were measured for ^{207}Po (6.7 h) and ^{211}Rn (14.6 h).

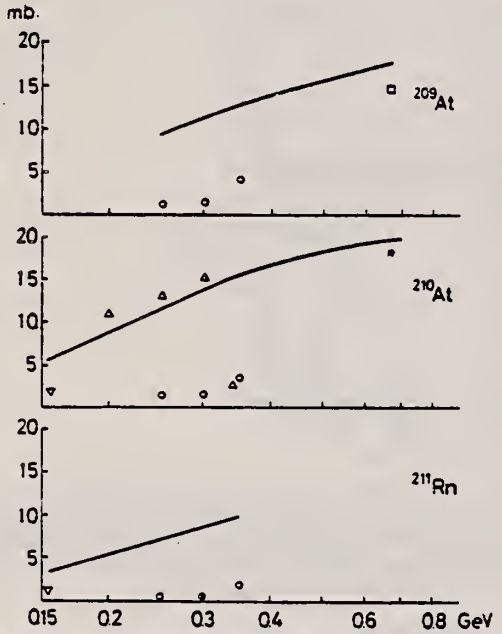

FIG. 1. Spallation cross sections for ^{232}Th. Protons: □ (Ref. 14), ▽ (Ref. 15), △ (Ref. 12), • (Ref. 2); Photons: ○ (this work) multiplied by 0.49 $\hat{\sigma}_\gamma/\hat{\sigma}_q$ ——: calculated from proton Rudstam formula,[18] multiplied by 0.49.

TABLE I. Experimental and calculated* σ_q values (mb) for the photospallation of ^{232}Th

E_0	0.25 GeV Exp.†	0.25 GeV Calc.	0.3 GeV Exp.†	0.3 GeV Calc.	0.35 GeV Exp.‡	0.35 GeV Calc.
^{209}At	0.066 ± 0.003	0.50	0.087 ± 0.003	0.69	0.28	0.90
^{210}At	0.074 ± 0.003	0.60	0.098 ± 0.006	0.84	0.23	1.06
^{211}Rn	0.028 ± 0.001	0.37	0.040 ± 0.005	0.52	0.13	0.66

* References (10) and (11). To correct for the nuclear fissility, the σ_q values were multiplied by 0.49.
† Average of three experiments.
‡ One experiment.

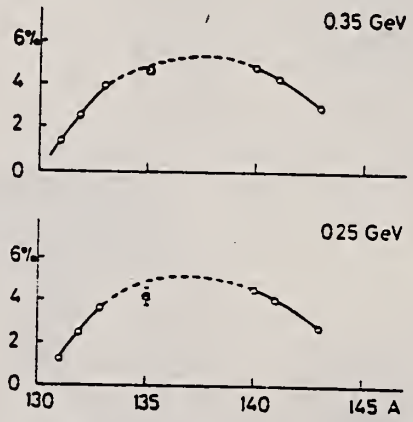

FIG. 2. Cumulative $A = 135$ chain yield for photofission: ○ (Ref. 9), □ (this work).

REF. V.E. Zhuchko, Yu.B. Ostapenko, G.N. Smirenkin, A.S. Soldatov, Yu.M. Tsipenyuk
Yad. Fiz. 30, 634, (1979)
Sov. J. Nucl. Phys. 30, 326 (1979)

ELEM. SYM.	A	Z
Th	232	90

METHOD

REF. NO.	
79 Zh 3	hg

REACTION	RESULT	EXCITATION ENERGY	SOURCE		DETECTOR		ANGLE
			TYPE	RANGE	TYPE	RANGE	
G,F	YLD	THR-7	C	5-7	TRK-D		DST
				(5.2-6.4)			

We report the method and results of measurements of angular distributions of fragments in the (γ,f) reaction for ^{232}Th, ^{236}U, and ^{238}U carried out in connection with the investigation of the properties of deep sub-barrier photofission: the isomeric shelf phenomenon, disappearance of the angular anisotropy ($^{236,238}U$), and the absence of this effect and of the sub-barrier enhancement of quadrupole photofission in ^{232}Th. The experimental data presented permit an understanding of the nature and relation of these properties in terms of the concept of a two-humped fission-barrier structure.

PACS numbers: 25.85.Jg

TABLE I. Parameters of the angular distributions of photofission fragments.

E_{max}, MeV	N, no.	$J\Delta t$, μC	$a \pm \Delta a$	$b \pm \Delta b$	$c \pm \Delta c$
		^{232}Th (δ = 200 mg/cm^2)			
5.0	552	$8.9 \cdot 10^6$	0.000±0.06	1.000±0.06	0.250±0.080
5.2	758	$1.0 \cdot 10^6$	0.001±0.08	1.000±0.08	0.225±0.100
6.4	48 940	510	0.08±0.03	0.94±0.03	0.08±0.04
6.4 •	29 340	10 900	0.014±0.002	0.956±0.003	0.028±0.006
		^{236}U (δ = 1.7 mg/cm^2)			
4.3	168	$9.8 \cdot 10^6$	0.72±0.25	0.28±0.28	1.71±0.35
4.75	2543	$2.0 \cdot 10^6$	0.17±0.20	0.83±0.20	0.18±0.15
5.0	3441	$10.5 \cdot 10^6$	0.10±0.10	0.90±0.10	0.20±0.15
5.1 •	852	$0.9 \cdot 10^6$	0.04±0.02	0.96±0.05	0.167±0.048
5.25	23 630	$0.1 \cdot 10^6$	0.06±0.03	0.94±0.03	0.12±0.04
5.5	16 580	$1.5 \cdot 10^6$	0.11±0.08	0.89±0.09	0.42±0.08
5.6 •	4623	$0.17 \cdot 10^6$	0.040±0.012	0.960±0.024	0.503±0.028
		^{238}U (δ = 0.8 mg/cm^2)			
4.5	812	$8.9 \cdot 10^6$	1.000±0.3	0.000±0.3	2.800±0.35
5.0	3917	$1.0 \cdot 10^6$	0.20±0.1	0.800±0.1	0.250±0.15
5.5	12 800	$2.0 \cdot 10^6$	0.150±0.07	0.850±0.07	0.500±0.13
5.5 •	12 760	$1.8 \cdot 10^6$	0.068±0.008	0.952±0.014	0.479±0.016
5.75 •	7605	$2.0 \cdot 10^6$	0.027±0.005	0.973±0.013	0.452±0.015
6.0 •	7681	$4.0 \cdot 10^6$	0.042±0.005	0.958±0.013	0.166±0.013
6.25 •	9431	$2.0 \cdot 10^6$	0.069±0.005	0.931±0.013	0.110±0.013
6.5 •	10 150	$1.0 \cdot 10^6$	0.112±0.008	0.888±0.013	0.080±0.014
6.75 •	10 090	5000	0.199±0.008	0.801±0.013	0.051±0.015
7.0 •	7762	2500	0.257±0.008	0.743±0.014	0.071±0.015
7.25 •	4790	1000	0.320±0.010	0.680±0.014	0.038±0.015
		^{238}U (δ = 200 mg/cm^2)			
4.15	130	$12.6 \cdot 10^6$	1.000±0.2	0.000±0.2	0.230±0.20
4.4	434	$9.5 \cdot 10^6$	0.930±0.35	0.070±0.35	2.500±0.50
4.8	7252	$1.0 \cdot 10^6$	0.490±0.04	0.510±0.04	2.840±0.03
5.4	449 050	$0.4 \cdot 10^6$	0.020±0.002	0.980±0.002	0.240±0.02
5.6 •	5781	$0.5 \cdot 10^6$	0.094±0.011	0.906±0.015	0.308±0.028

Note. N is the total number of tracks recorded by the detectors; $J\Delta t$ is the integral of the current of accelerated electrons at the bremsstrahlung target; δ is the thickness of the fissile target. The results marked by an asterisk were obtained by the circular glass plate technique[2]; the remaining results are in the 4π geometry.

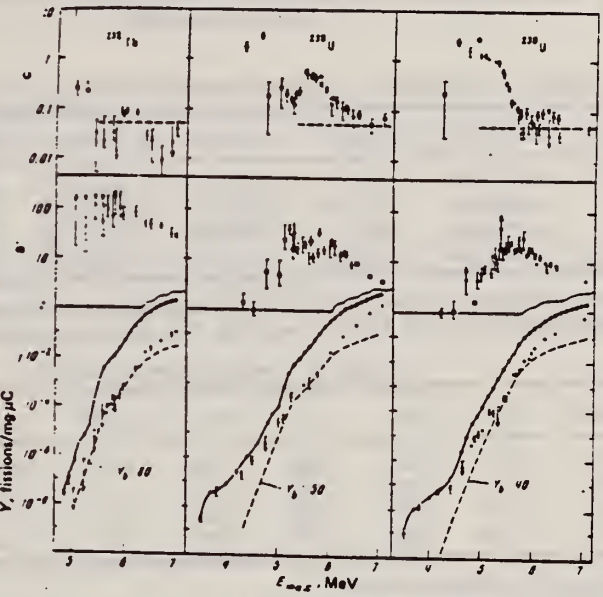

FIG. 3. In the upper and central parts we have shown the parameters of the angular distributions of fragments from photofission of ^{232}Th, ^{236}U, and ^{238}U as a function of E_{max}. Points: ■—results of the present work, ●—results of Refs. 2 and 15, ○—results of Ref. 13. In the lower part; the hollow circles and their connecting solid lines are the total yield of photofissions of the corresponding nuclei,[6,10] the solid circles are the isotropic component of the yield—Y_s, and the dashed line is the component Y_a which has been normalized to Y_s in the region of maximum anisotropy. The dashed line in the upper part of the figure shows the asymptotic value of the coefficient $c \approx c/b \approx 0.05$ for energies above the barrier [see Eq. (3)].

REF. J. T. Caldwell, E.J. Dowdy, B. L. Berman, R. A. Alvarez, P. Meyer
Phys. Rev. C21, 1215 (1980)

ELEM. SYM.	A	Z
Th	232	90

METHOD

REF. NO. 80Cal egf

REACTION	RESULT	EXCITATION ENERGY	SOURCE		DETECTOR		ANGLE
			TYPE	RANGE	TYPE	RANGE	
G,1N	ABX	6-18	D	5-18	BF3 - I		4PI
G,2N	ABX	10-18	D	5-18	BF3 - I		4PI
G,F	ABX	5-18	D	5-18	BF3 - I		4PI

The photoneutron cross sections $\sigma(\gamma,n)$ and $\sigma(\gamma,2n)$, and total photofission cross sections $\sigma(\gamma,F)$ have been measured for ^{235}U, ^{236}U, ^{238}U, and ^{232}Th from threshold to 18.3 MeV using monoenergetic photons from the annihilation in flight of fast positrons and neutron-multiplicity detection in an efficient 4π neutron detector. Use of the ring-ratio technique allowed both the average photofission neutron energy for each nucleus to be obtained as a function of photon energy and, for ^{236}U and ^{238}U, the determination of the partial cross sections for first-chance $\sigma(\gamma,f)$ and second-chance $\sigma(\gamma,nf)$ photofission as well. Information extracted from the data includes integrated cross sections and their moments, giant-resonance parameters, deformation and radius parameters, and relative and absolute neutron and fission probabilities.

[NUCLEAR REACTIONS $^{235,236,238}U$ and ^{232}Th $(\gamma,n,2n,F)$, $E_\gamma = 5$–18.3 MeV; measured 4π neutron yield, neutron multiplicities, and average energies for monoenergetic photons; $\sigma(E_\gamma,1n)$, $\sigma(E_\gamma,2n)$, $\sigma(E_\gamma,F)$, integrated cross sections and moments, GDR parameters, nuclear shape parameters, neutron and fission probabilities.]

TABLE II. Parameters of Lorentz-curve fits to the giant dipole resonance.[a]

Nucleus	$E_m(1)$ (MeV)	$\sigma_m(1)$ (mb)[b]	$\Gamma(1)$ (MeV)	$E_m(2)$ (MeV)	$\sigma_m(2)$ (mb)[b]	$\Gamma(2)$ (MeV)
^{235}U	10.90±0.05	328±19	2.30±0.15	13.96±0.09	459±10	4.75±0.32
^{236}U	10.92±0.04	271±16	2.55±0.17	13.78±0.08	415±10	4.88±0.24
^{238}U	10.77±0.04	311±20	2.37±0.13	13.80±0.09	459± 9	5.13±0.35
^{232}Th	11.03±0.04	302±19	2.71±0.13	13.87±0.08	449± 9	4.77±0.28

[a] Lorentz parameters defined by Eq. (1); the fitting interval for all cases is 9 to 18 MeV.
[b] Uncertainties for σ_m given here are relative. The absolute uncertainties are 7%.

TABLE IV. Nuclear shape parameters.

Nucleus	R_A[a]	η[b]	ϵ[c]	β_2[d]	Q_0 (b)[e]	Q_0 (b)[f]	Q_0 (b)[g]
^{235}U	0.35	1.308	0.595	0.315	12.0	10.6 ±0.2	11.0±0.5
^{236}U	0.34	1.287	0.556	0.295	11.2	10.75±0.7	10.3±0.4
^{238}U	0.31	1.309	0.596	0.316	12.1	11.3 ±0.1	11.1±0.5
^{232}Th	0.38	1.283	0.547	0.290	10.7	9.8 ±0.1	9.8±0.4

[a] Area ratio, defined by Eq. (6).
[b] Deformation parameter, computed from Eq. (3).
[c] Nuclear eccentricity, computed from Eq. (4).
[d] Deformation parameter, computed from Eq. (7).
[e] Intrinsic quadrupole moment, computed from Eq. (8), with R_0 taken to be 1.20 fm.
[f] Intrinsic quadrupole moment, taken from Ref. 47.
[g] "Best value" for Q_0, computed from Eq. (8), with R_0 taken to be 1.15 fm (see text).

TABLE V. Integrated cross sections.[a]

Nucleus	$\sigma_{int}(\gamma,n)$ (MeV b)	$\sigma_{int}(\gamma,2n)$ (MeV b)	$\sigma_{int}(\gamma,F)$ (MeV b)	$\frac{\frac{1}{2}\pi(\sigma_m(1)\Gamma(1)+\sigma_m(2)\Gamma(2)]^b}{0.06NZ/A}$
^{235}U	1.14	0.20	2.16	1.37
^{236}U	1.26	0.45	1.45	1.26
^{238}U	1.36	1.13	1.09	1.43
^{232}Th	1.66	1.45	0.37	1.41

[a] $\sigma_{int}(\gamma,x) = \int \sigma(\gamma,x)dE_\gamma$, integrated from threshold to the maximum experimental energy $E_{\gamma max} = 18.3$ MeV.
[b] Uncertainties given here are relative. The absolute uncertainties are 7%.

SEE ALSO 80CA2

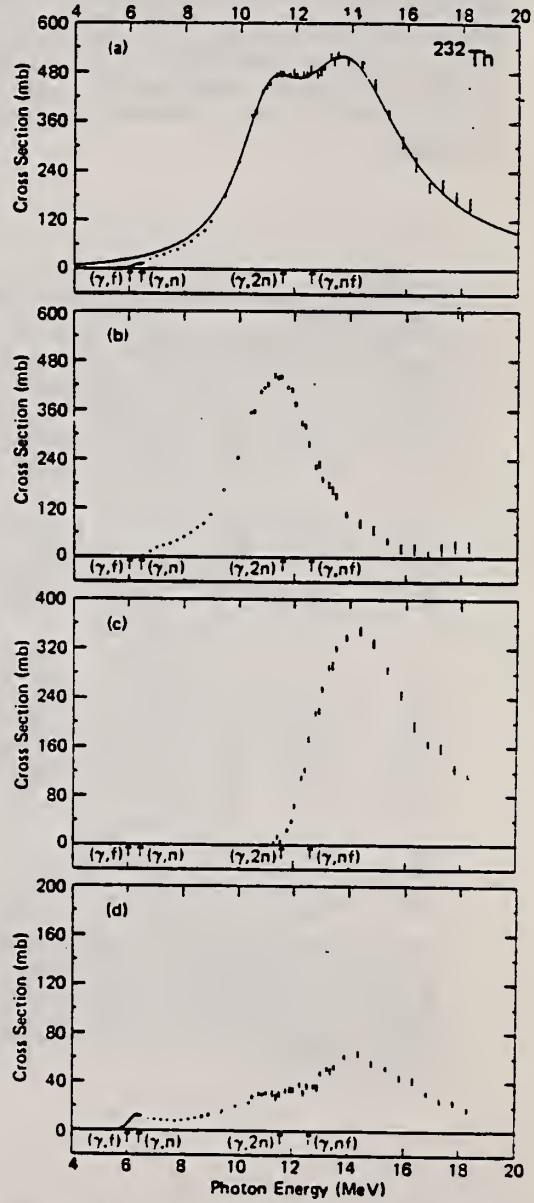

FIG. 5. Photonuclear cross sections for ^{232}Th: (a) $\sigma(\gamma,\text{tot})$, with a Lorentz-curve fit; (b) $\sigma(\gamma,n)$; (c) $\sigma(\gamma,2n)$; (d) $\sigma(\gamma,F)$.

over

TABLE VI. Integrated cross-section moments.[a]

Nucleus	σ_{-1} (mb)	$\sigma_{-1}A^{-4/3}$ (mb)	σ_{-2} (mb MeV^{-1})	$\frac{\sigma_{-2}}{0.00225\,A^{5/3}}$	$\frac{\sigma_{-1}K}{0.05175^{5/3}}$	$\frac{0.05175\,A^{5/3}}{\sigma_{-2}}$ (MeV)
^{235}U	278	0.191	23.1	1.15	1.36	20.1
^{236}U	252	0.173	21.0	1.04	1.21	22.2
^{238}U	286	0.194	24.0	1.17	1.38	19.7
^{232}Th	276	0.194	22.8	1.16	1.35	19.9

[a] $\sigma_{-1} = \int \sigma(\gamma, \text{tot})\, E_\gamma^{-1}\, dE_\gamma$ and $\sigma_{-2} = \int \sigma(\gamma, \text{tot}) E_\gamma^{-2}\, dE_\gamma$, integrated from threshold to $E_{\gamma\,\max}$ = 18.3 MeV.

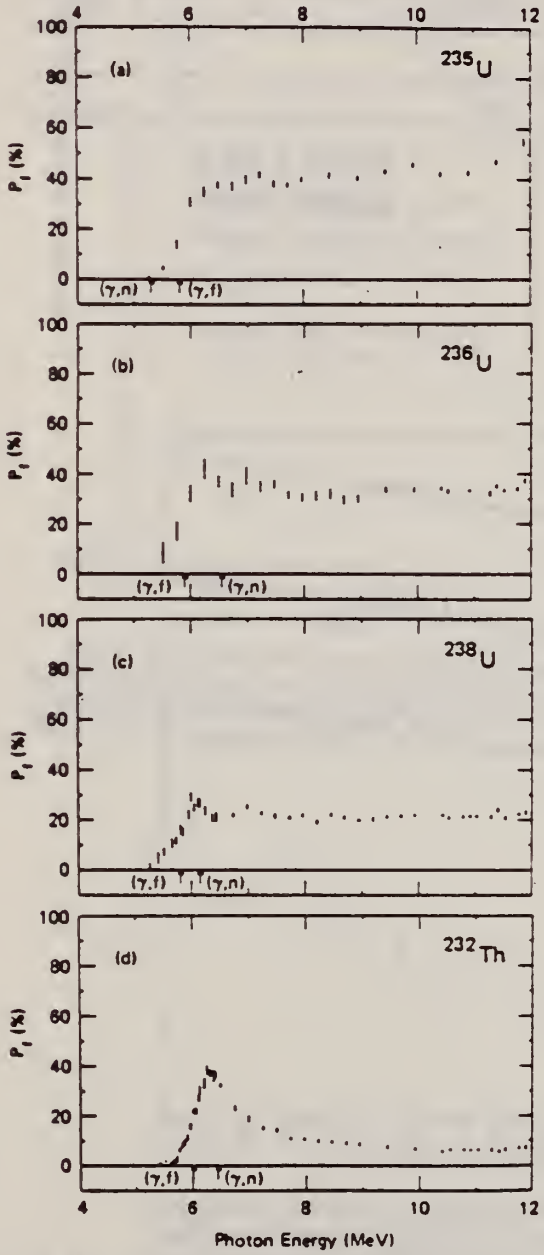

FIG. 15. Fission probability P_f from the ratio of $\sigma(\gamma f)$ to the value at each energy of the two-component Lorentz-curve fits to the GDR shown in Figs. 3-5: (a) for ^{235}U, (b) for ^{236}U, (c) for ^{238}U, (d) for ^{232}Th.

REF. J. T. Caldwell, E. J. Dowdy, R. A. Alvarez, B. L. Berman, P. Meyer
Nucl. Sci. Eng. 73, 153 (1980)

ELEM. SYM.	A	Z
Th	232	90

METHOD

REF. NO.: 80Ca2 egf

REACTION	RESULT	EXCITATION ENERGY	SOURCE		DETECTOR		ANGLE
			TYPE	RANGE	TYPE	RANGE	
G,F	NOX	5-18	D	5-18	BF3-I	D	4PI
G,F	NOX	11,17	D	5-18	BF3-I	D	4PI

The prompt neutron multiplicities for photofission of the four isotopes ^{235}U, ^{236}U, ^{238}U, and ^{232}Th have been measured with monoenergetic photons over the energy range from 5.5 to 18 MeV using the annihilation in flight of fast positrons. The delayed neutron yield has been measured for all four isotopes at 10.9- and 16.8-MeV photon energies. The ratio of first- to second-chance fission has been measured as a function of energy up to 17-MeV excitation energy for ^{236}U and ^{238}U photofission.

PROMPT N MULT

DELAYED N YLD

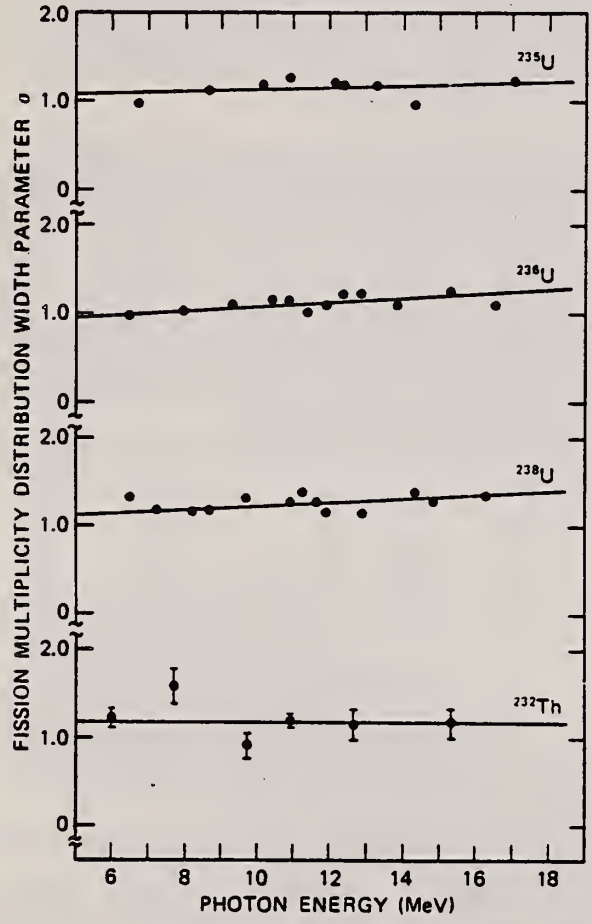

Fig. 6. Prompt neutron multiplicity width parameter data as a function of excitation energy. Solid circles are experimental data, and straight lines are the least-squares fits to these data (see Table II).

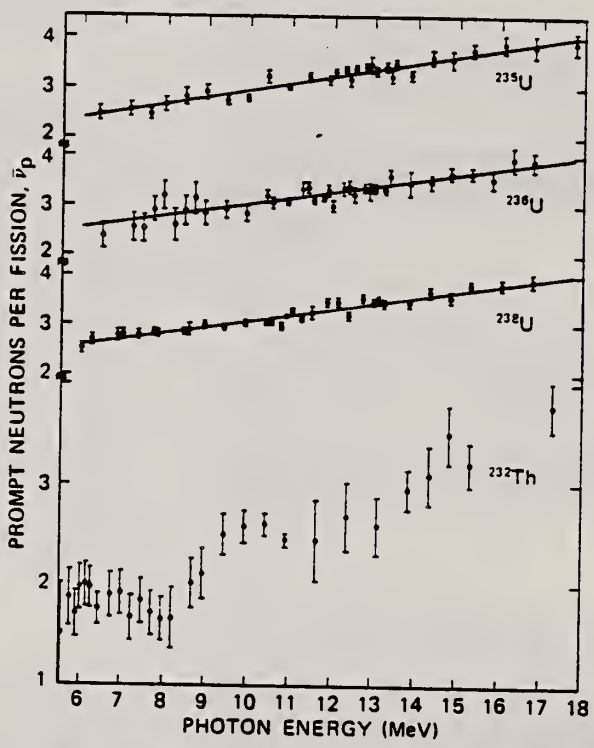

Fig. 7. Prompt neutron $\bar{\nu}_p$ data as a function of excitation energy. Solid circles are experimental data, and the straight lines are the least-squares fits (see Table IV) to these data. A single straight line fit was not obtainable for ^{232}Th.

over

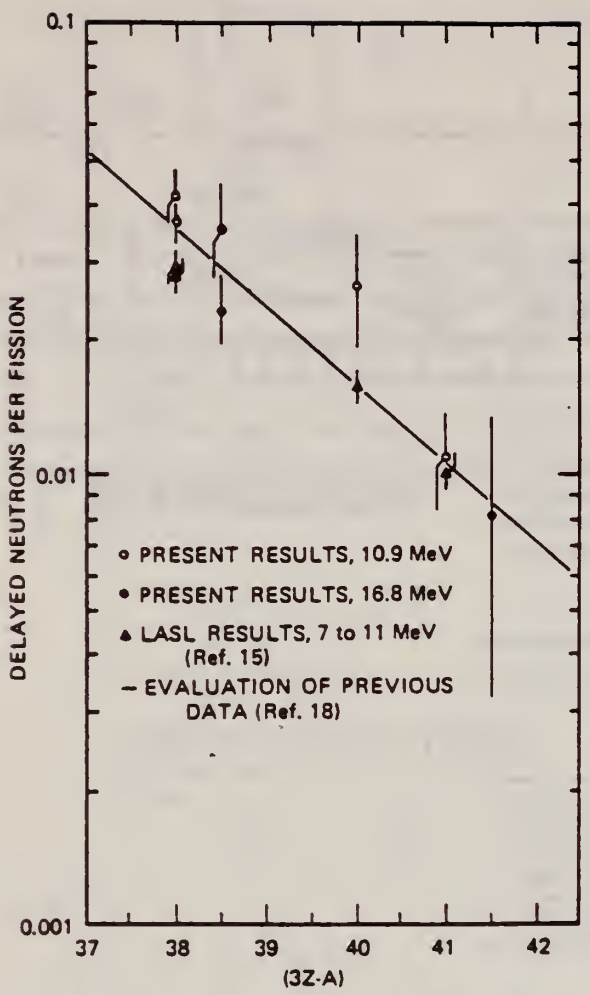

Fig. 9. Yield of delayed neutron from photofission as a function of $3Z\text{-}A$. Solid line is an evaluated least-squares fit to existing data as of 1975 (Ref. 18). Solid circles are the present results. Solid squares are from Ref. 15.

TABLE II

Multiplicity Width Parameter

Isotope	Least-Squares Fit
^{235}U	$\sigma = 1.009 + 0.0110\,E$
^{236}U	$\sigma = 0.840 + 0.0253\,E$
^{238}U	$\sigma = 1.003 + 0.0227\,E$
^{232}Th	$\sigma = 1.183$

TABLE IV

Prompt Neutrons per Photofission, $\bar{\nu}_p(E)$

Isotope	Least-Squares Fit	Correlation Coefficient
^{235}U	$\bar{\nu}_p = 1.610 + 0.133\,E$ (all data)	0.965
^{236}U	$\bar{\nu}_p = 1.881 + 0.116\,E$ (all data)	0.906
^{238}U	$\bar{\nu}_p = 1.862 + 0.123\,E$ (all data)	0.969
^{232}Th	$\bar{\nu}_p = 2.826 - 0.143\,E$ $(6.0 < E < 8.2$ MeV)	0.819
	$\bar{\nu}_p = 0.453 + 0.175\,E$ $(E > 8.5$ MeV)	0.927

TABLE V

Prompt Neutrons per Photofission at 8.5 MeV

Isotope	From Ref. 15	Present Data
^{235}U	2.85 ± 0.09	2.74 ± 0.10
^{236}U	2.66 ± 0.11	2.71 ± 0.10
^{238}U	2.74 ± 0.09	2.91 ± 0.10
^{232}Th	2.07 ± 0.11	1.94 ± 0.08

REF. W. Günther, K. Huber, U. Kneissl, H. Krieger, H.J. Maier
Z. Phys. A 295, 333 (1980)

ELEM. SYM.	A	Z
Th	232	90

METHOD

REF. NO. 80 Gu 4 hg

REACTION	RESULT	EXCITATION ENERGY	SOURCE		DETECTOR		ANGLE
			TYPE	RANGE	TYPE	RANGE	
G,F	RLY	THR-55	C	15-55	SCD-D		90

Measurements are presented for the mass and energy distributions of fragments from the photofission of ^{232}Th, ^{235}U, ^{238}U and ^{239}Pu. The experiments were performed for bremsstrahlung endpoint energies between 15 and 55 MeV, using silicon surface barrier detectors. The results are discussed with respect to the competition between the symmetric and asymmetric fission modes.

M,E DST, SYM/ASYM YLD

Table 2. Most probable heavy masses, most probable total kinetic energies and their variances (The variances have been corrected for the detector resolution and for γ- and electron pile up)

Nucleus	$[m]_{heavy}$	$[E_k]_{syst}$ a)	$[E_k]_{syst}$ b)	$[E_k]_{exp}$	σ_{E_k}
^{232}Th	(141.7 ± 2) amu	163.3 MeV	163.5 MeV	(159.5 ± 4) MeV	(9.0 ± 0.8) MeV
^{235}U	(138.5 ± 2) amu	169.1 MeV	170.1 MeV	(168 ± 3) MeV	(11.1 ± 1) MeV
^{238}U	(140.3 ± 2) amu	168.5 MeV	169.4 MeV	(164.5 ± 4) MeV	(11.7 ± 1) MeV
^{239}Pu	(137.2 ± 2) amu	174.7 MeV	176.6 MeV	(174 ± 3) MeV	(11.9 ± 1) MeV
^{252}Cf[c]				185.5 MeV	11.6 MeV

[a] $[E_k] = (0.1071 \cdot Z^2/A^{1/3} + 22.2)$ MeV
[b] $[E_k] = (0.1240 \cdot Z^2/A^{1/3})$ MeV
[c] Calibration measurement

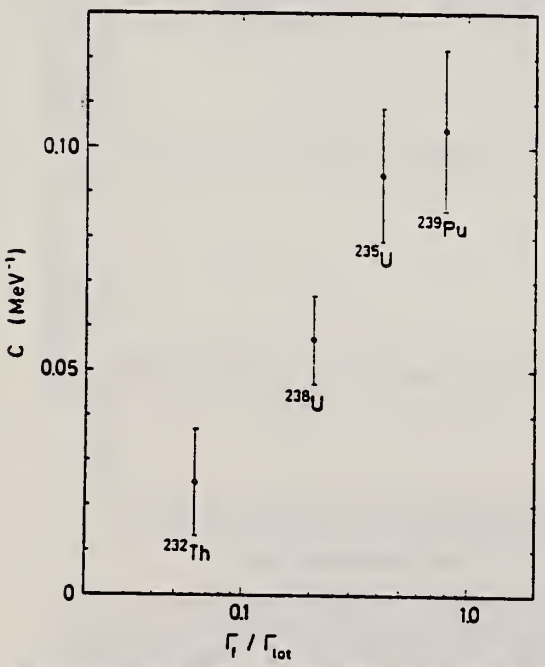

Fig. 5. Saturation parameter c as a function of the fission probability Γ_f/Γ_{tot}

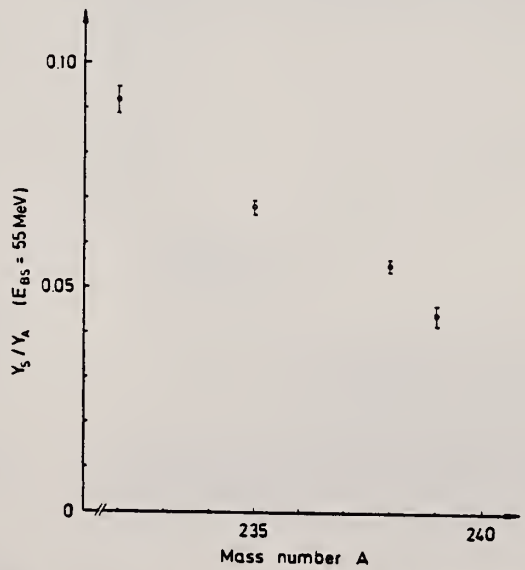

Fig. 6. Y_S/Y_A at $E_{BS} = 55$ MeV as a function of the mass number A

(OVER)

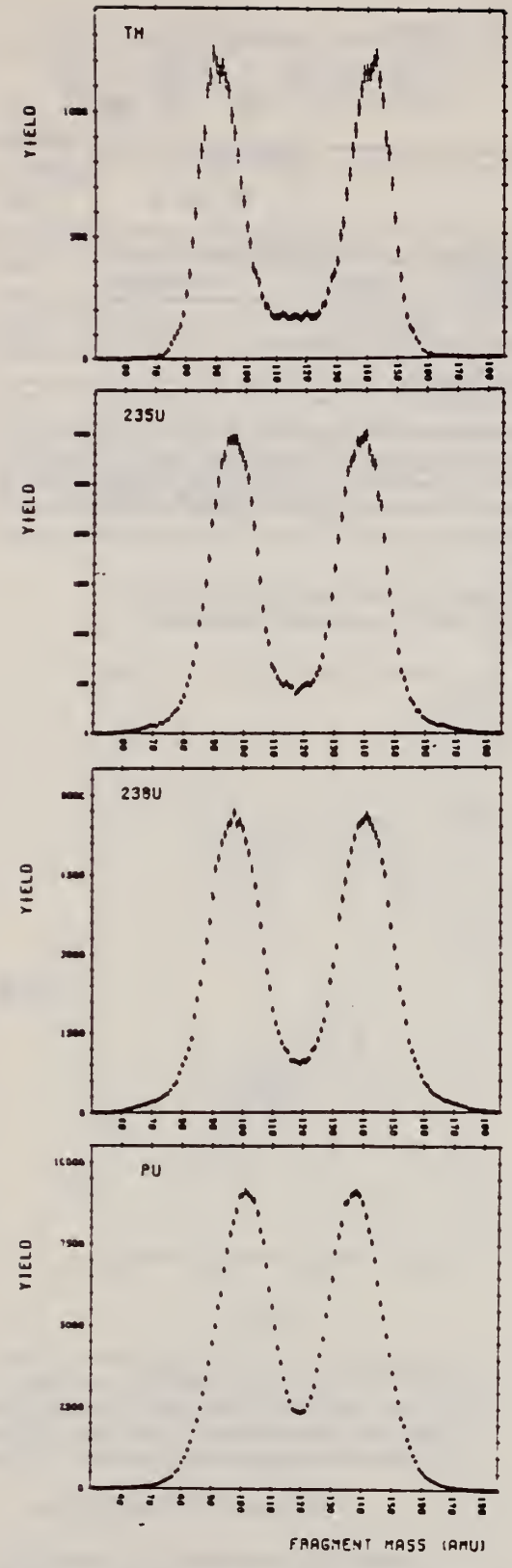

Fig. 1. Mass distributions for the photofission of ^{232}Th, ^{235}U, ^{238}U and ^{239}Pu (Bremsstrahl endpoint energy E_{gs} = 45 MeV).

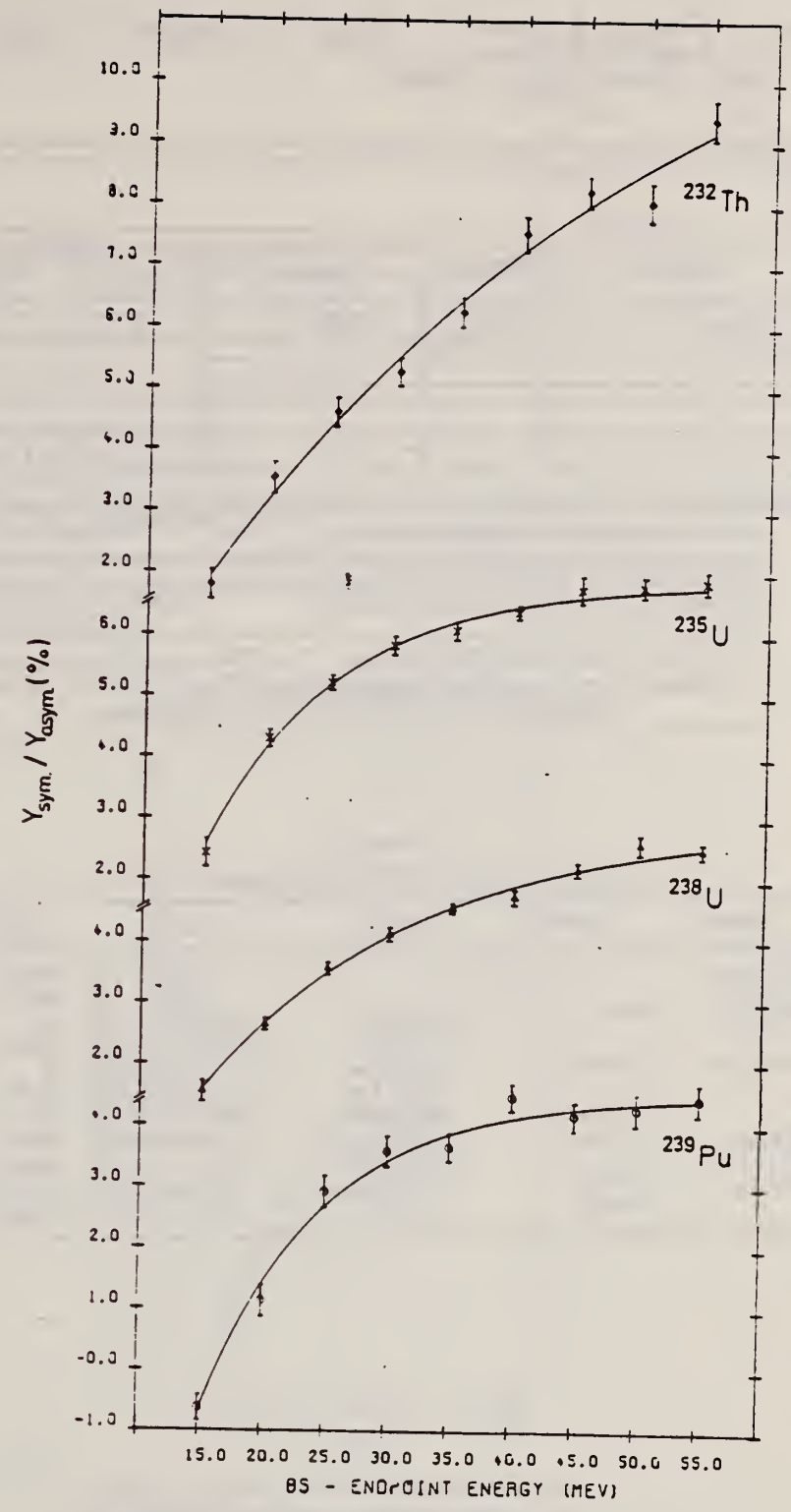

Fig. 4. Symmetric to asymmetric fission yield ratio as a function of E_{gs}. The lines are fits with an empirical function $Y_s/Y_a = a + be^{-c\,E_{ex}}$ (s. text).

REF. W. Günther, K. Huber, U. Kneissl, H. Krieger, H. Ries, H. Ströher, W. Wilke, H.J. Maier
Nucl. Phys. A350, 1 (1980)

ELEM. SYM.	A	Z
Th	232	90

METHOD

REF. NO. 80 Gu 5 hg

REACTION	RESULT	EXCITATION ENERGY	SOURCE TYPE	SOURCE RANGE	DETECTOR TYPE	DETECTOR RANGE	ANGLE
G,XN	RLY	THR-	C		SPK-I		90

YLD FISSION ISOMERS

Abstract: Half-lives and yields in photonuclear reactions have been measured for shape isomers in U and Pu isotopes by pulsed-beam techniques bombarding ^{235,238}U and ^{239,240,242}Pu targets with bremsstrahlung. Isomeric fission cross sections have been deduced from the measured isomeric to prompt yield ratios within an evaporation model using absolute prompt fission data. The results are compared with data from particle-induced reactions.

E NUCLEAR REACTIONS ^{240}Pu^{235}U(γ, xn), ^{238}U, ^{239}Pu(γ, 2n), ^{242}Pu(γ, n); bremsstrahlung; measured $T_{1/2}$, isomeric to prompt yield ratios, ^{236}U, ^{237}Pu, ^{239}Pu, ^{241}Pu levels, deduced σ for isomeric fission. Natural and enriched targets.

TABLE 2

Results of isomeric fission experiments performed at Giessen

Reaction	Isomer	Half-life	Y_{iso}/Y_{pr}	Detector
^{232}Th(γ, xn)			$<10^{-6}$	PPAD
^{235}U (γ, xn)			$<10^{-4}$	PPAD
^{238}U (γ, 2n)	^{236}U	115 ± 5 ns	$(2.02\pm0.16)\times10^{-5}$	Si
		118 ± 7 ns	$(2.10\pm0.16)\times10^{-5}$	PPAD
^{239}Pu (γ, 2n)	^{237m_1}Pu	77 ± 16 ns	$(6.4\pm1.7)\times10^{-6}$	Si
		87 ± 11 ns	$(4.9\pm0.7)\times10^{-6}$	PPAD
	^{237m_2}Pu	1050 ± 400 ns	$(0.83\pm0.22)\times10^{-6}$	Si
^{240}Pu (γ, n)	^{239m_1}Pu	6.5 ± 0.4 μs	$(7.9\pm0.4)\times10^{-5}$	PPAD
^{240}Pu(γ, xn)	?	4.5 ± 1.5 ns	$<1.1\times10^{-4}$	PPAD
^{242}Pu(γ, n)	^{241m_1}Pu	20.5 ± 2.5 μs	$(9.2\pm0.8)\times10^{-5}$	PPAD
	^{241m_2}Pu	34 ± 7 ns	$(3.7\pm0.7)\times10^{-5}$	PPAD

REF. G. Bellia, L. Calabretta, A. Del Zoppo, E. Migneco, G. Russo, R.C. Barna, D. De Pasquale
Phys. Rev. C24, 2762 (1981)

ELEM. SYM.	A	Z
Th	232	90

METHOD

REF. NO. 81 Be 12 hg

REACTION	RESULT	EXCITATION ENERGY	SOURCE TYPE	SOURCE RANGE	DETECTOR TYPE	DETECTOR RANGE	ANGLE
G,F	ABX	THR-7	C	5-7	TRK-I		DST
		(THR-6.4)		(5.4-6.4)			

Angular distributions of photofission of ^{232}Th have been measured using bremsstrahlung γ beams in the (5.4–6.4) MeV range. With decreasing energy below 6 MeV the angular anisotropy decreases strongly and, moreover, a shelf appears in the isotropic component of the yield. These effects are interpreted in terms of a competition between prompt and delayed fission. Vibrational resonances in the 1^-0 and 2^+0 channels are detected.

[NUCLEAR REACTIONS, FISSION Angular distributions and yields of subthreshold photofission of ^{232}Th in the (5.4–6.4) MeV range.]

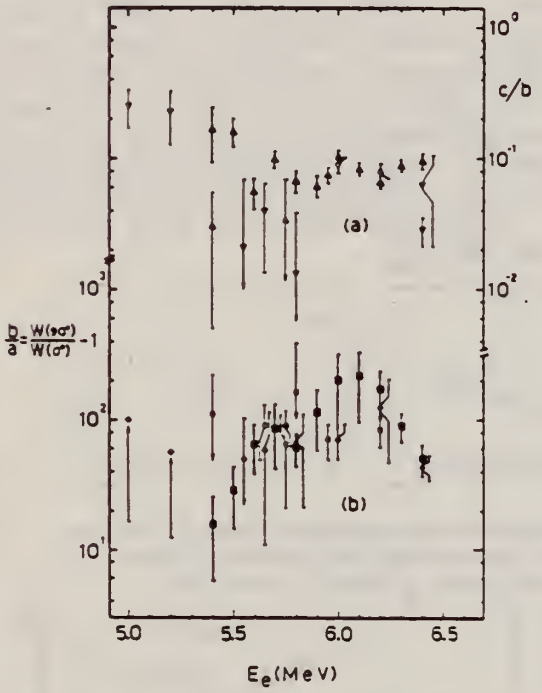

FIG. 1. (a) c/b ratio as a function of electron energy. (▲) present work, (△) from Ref. 13, and (▽) from Ref. 14. (b) b/a ratio as a function of electron energy. (●) present work, (○) from Ref. 13 (target thickness 1.35 mg/cm^2), and (◇) from Ref. 14 (target thickness 200 mg/cm^2).

$$W(\theta)=a+b\sin^2\theta+c\sin^2 2\theta$$

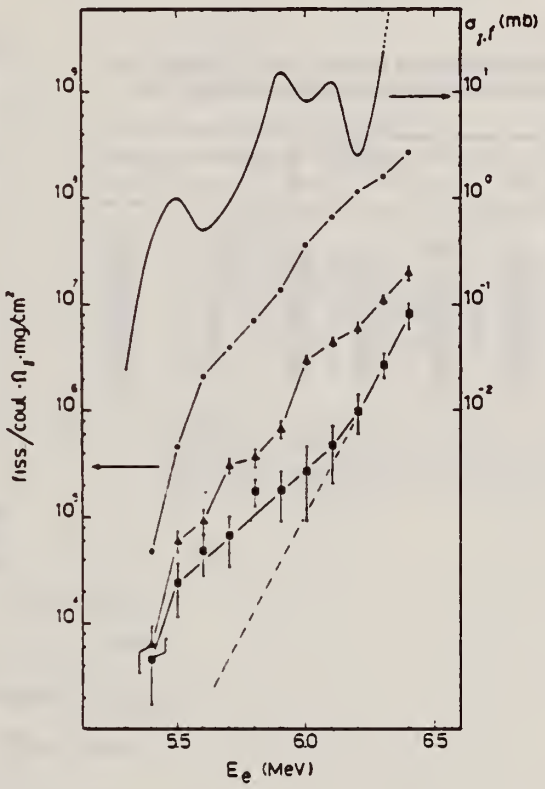

FIG. 2. The figure shows the experimental yields (●) Y_a, (◆) Y_b, and (▲) Y_c as functions of electron energy. The upper solid curve is our unfolded total photofission cross-section. Yields are normalized to the solid angle Ω_γ subtended from the target to the bremsstrahlung converter.

[13]N. S. Rabinov, G. N. Smirenkin, A. S. Soldatov, L. N Usachev, S. P. Kapitza, and Yu. M. Tsipenyuk, Yad. Fiz. 11, 508 (1970) [Sov. J. Nucl. Phys. 11, 285 (1970)] Ra 1

[14]A. V. Ignatyuk, N. S. Rabotnov, G. N. Smirenkin, A. S. Soldatov, and Yu. M. Tsipenyuk, Zh. Eksp Teor Fiz. 61, 1284 (1971) [Sov. Phys. JETP 34, 684 (1972)], V. E. Zhucho, Yu. B. Ostapenko, G. N. Smirenkin, A. S. Soldatov, and Yu. M. Tsipenyuk, Sov. J. Nucl. Phys. 30, 326 (1979). Ig 1

REF. A.S. Voronin, I.S. Koretskaya, V.L. Kuznestsov, V.G. Nedorezov, N.V. Nikitina, V.I. Noga, S.A. Pashchuk, Yu.N. Ranyuk, S.M. Solov'ev
Yad. Fiz. 34, 1439 (1981)
Sov. J. Nucl. Phys. 34, 797 (1981)

ELEM. SYM.	A	Z
Th	232	90

METHOD

REF. NO.	
81 Vo 3	egf

REACTION	RESULT	EXCITATION ENERGY	SOURCE		DETECTOR		ANGLE
			TYPE	RANGE	TYPE	RANGE	
E,F	ABX	4-275	D	97-275	TRK-I		45

Results are presented of cross-section measurements for the fission of ^{232}Th, ^{233}U, ^{235}U, ^{236}U, ^{238}U, ^{237}Np, and ^{239}Pu by electrons with energies between 100 and 275 MeV; photofission and electrofission cross-section ratios for the same nuclei are given as well.

PACS numbers: 25.85.Jg, 27.90. + b, 25.85.Ge

TABLE II. Electrofission cross sections (mb) for nuclei with $Z \geq 90$ measured for electron energies between 100 and 275 MeV.

E_e, MeV	Nucleus						
	^{232}Th	^{233}U	^{235}U	^{236}U	^{238}U	^{237}Np	^{239}Pu
97	1.24	8.12	5.66	4.55	3.23	6.22	7.26
134	1.47	9.17	6.08	4.74	3.42	6.83	7.98
149	1.42	9.75	6.17	5.50	3.39	7.16	8.39
166	1.63	10.36	7.01	5.29	4.15	7.70	9.18
184	1.78	9.61	7.13	5.64	4.17	7.92	8.92
201	1.54	9.84	6.53	6.10	4.56	7.49	9.31
217	1.73	10.91	7.73	6.14	4.77	7.99	9.56
250	1.91	10.25	7.26	5.92	4.49	7.84	9.13
253	1.85	9.89	7.00	6.17	4.76	7.50	9.78
278	2.22	10.50	8.15	6.66	5.26	9.68	10.50

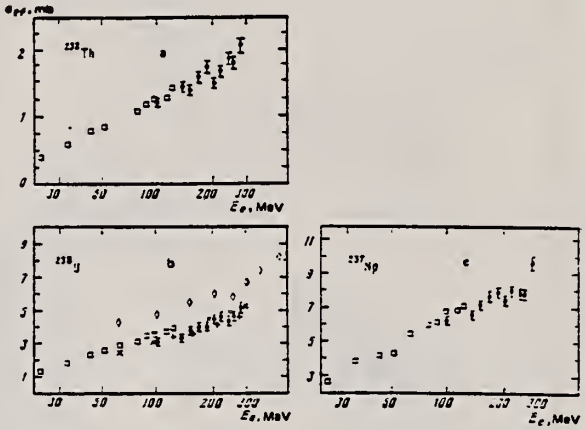

FIG. 2. Electrofission cross section for ^{232}Th (a), ^{238}U (b), and ^{237}Np (c). The points represent data as follows: □—Ref. 3, ●—present work, ◇—Ref. 1, ×—Ref. 2, and +—Ref. 4.

REF. T.R. Yeh, H. Lancman
IEEE Trans. Nucl. Sci. NS-28, 1289 (1981)

ELEM. SYM.	A	Z
Th	232	90

METHOD

REF. NO. 81 Ye 1 egf

REACTION	RESULT	EXCITATION ENERGY	SOURCE		DETECTOR		ANGLE
			TYPE	RANGE	TYPE	RANGE	
G,F	ABX	5-11	D	5-11			4PI

Summary

High intensity proton beams from the Dynamitron at Brooklyn College are used to generate monochromatic gamma rays from known (p,γ) resonances in various nuclei. The gamma rays, whose energy varies continuously as a function of the angle with the proton beam, are used in turn to measure photofission cross sections in ^{238}U and ^{232}Th. The number of suitable (p,γ) resonances is sufficient to cover the 5 - 13 MeV range of excitation energy with an average step of ~100 keV. For a resonance of average strength the yield is 10^3 photons per μA of protons on target. The energy spread is typically 20 - 40 keV and a gamma ray energy resolution of 200 eV can easily be reached. This resolution is adequate for investigating structure in the photofission cross sections resulting from class II states in the second well of the fission barrier.

PHOTONS FROM P,G

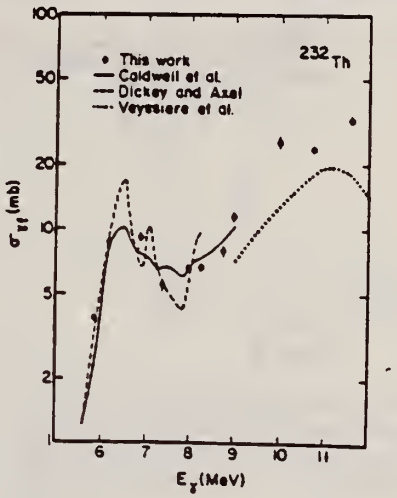

Fig. 4 Averaged photofission cross section $\sigma_{\gamma f}(E_\gamma)$ for ^{232}Th. The results of Caldwell et al.[10], Dickey and Axel[4] and Veyssiere et al.[12] are shown for comparison.

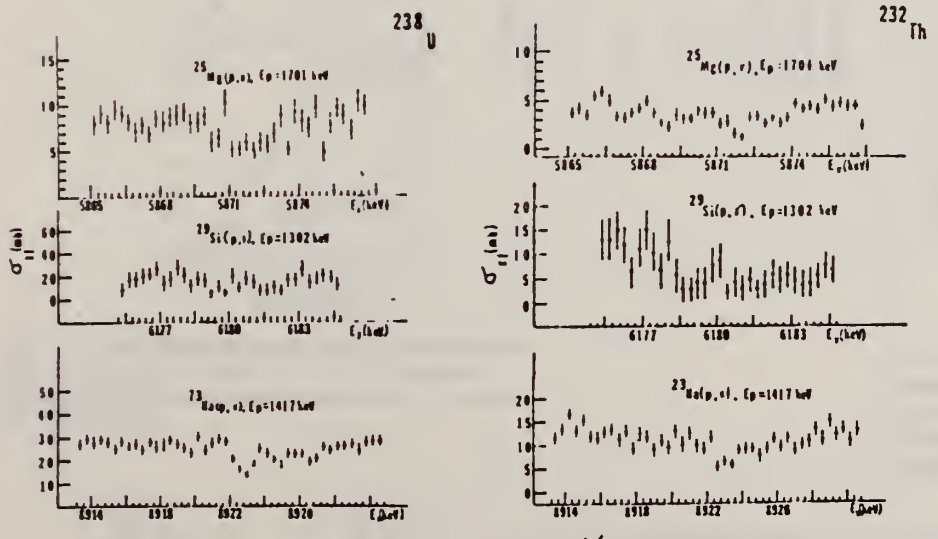

Fig. 2 Photofission fragment spectra at several (p,γ) resonances.

(over)

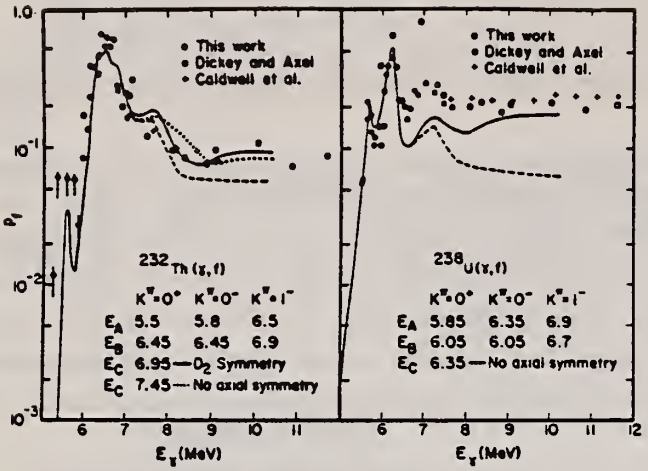

Fig. 5 Comparison of the fission probabilities of ^{238}U and ^{232}Th with results of statistical model calculations.

REF. J.D.T. Arruda-Neto, M.F.B.M. Vannucci, S.B. Herdade, A. Vanucci, I.C. Nascimento
Phys. Rev. C25, 1689 (1982)

ELEM. SYM.	A	Z
Th	232	90

METHOD

REF. NO. 82 Ar 2 egf

REACTION	RESULT	EXCITATION ENERGY	SOURCE		DETECTOR		ANGLE
			TYPE	RANGE	TYPE	RANGE	
E,F	ABX	5-7	D	5-7	TRK-I		DST

The electrofission angular distribution of ^{232}Th, in the energy interval 5.5–7 MeV, was measured. The analysis of the $E2$ coefficient of the angular distribution revealed that a substantial amount of $E2$ fission strength is concentrated near the fission barrier, corresponding to (8 ±2)% of one energy-weighted sum-rule unity.

[NUCLEAR REACTIONS ^{232}Th(e,f), E = 5.5–7 MeV, with electrons; measured fission-fragment angular distributions; deduced $E2$ fission strength. Natural target.]

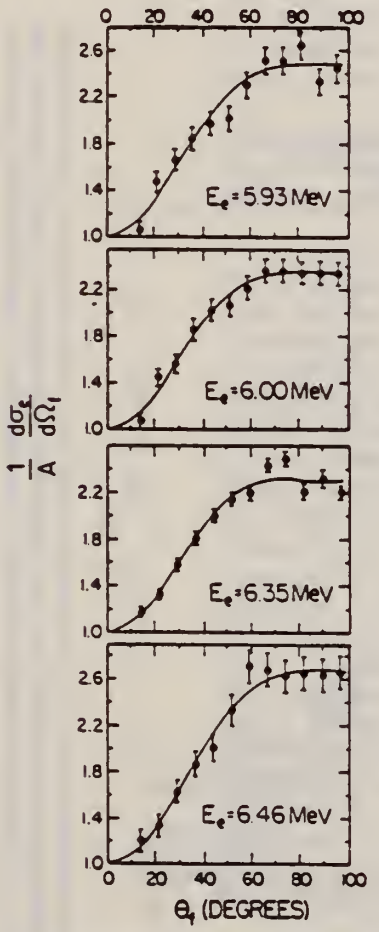

FIG. 1. Electrofission-fragments angular distributions for ^{232}Th. $[1/A(E_e)](d\sigma_e/d\Omega_f)(E_e,\theta_f)$. The curves are least-squares fits of the function defined in Eq. (3) to the experimental points.

TABLE I. $E1$ and $E2$ fission probabilities, and percent of EWSR, for ^{232}Th and ^{238}U, between 5 and 7 MeV.

Nucleus	EWSR ($E2$) (%)	$P_f(E2)$ (%)	$P_f(E1)$ (%)
^{232}Th	8 ± 2[a]	...	~40[d]
^{238}U	6 ± 1[b]	80 ± 10[c]	~25[d]

[a]Present work.
[b]Reference 2, and (7 ± 1) as deduced from Ref 16.
[c]Reference 2.
[d]Reference 19 at $\omega \cong 6.3$.

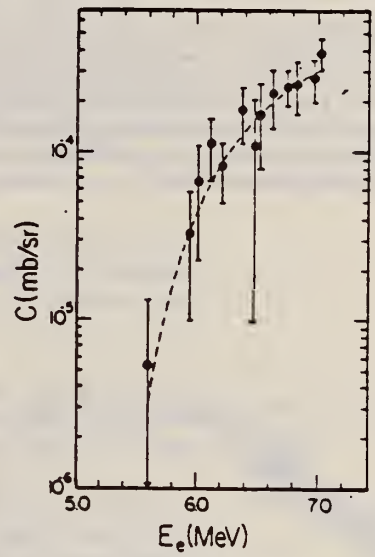

FIG. 2. Absolute values for the coefficient of the $\sin^2 2\theta_f$ term in the electrofission differential cross section $C(E_e)$ [Eq. (3)], obtained from the measured angular distributions for ^{232}Th. The dashed curve is the fold-back of $\sigma_{\gamma,f}(2^+,0)$ in Eq. (6).

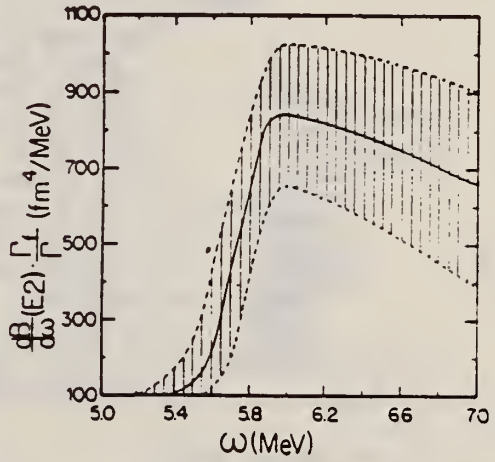

FIG. 3. $E2$ fission strength function deduced from the experimentally determined photofission cross section $\sigma_{\gamma,f}(2^+,0)$ [obtained by solving the integral equation (6), as explained in the text]. Both systematic and statistical uncertainties are included in the error band.

$$\frac{d\sigma_e}{d\Omega_f}(E_e,\theta_f)=\sum_{J^\pi=1^-,2^+}\sum_{K=0}^{\pm J}\frac{d\sigma_e}{d\Omega_f}(J^\pi,K;E_e,\theta_f)=A(E_e)+B(E_e)\sin^2\theta_f+C(E_e)\sin^2(2\theta_f) \qquad (3)$$

REF. J.W. Knowles, W.F. Mills, R.N. King, B.O. Pich, S. Yen, R. Sobie, L. Watt, T.E. Drake, L.S. Cardman, R.L. Gulbranson
Phys. Lett. 116B, 315 (1982)

ELEM. SYM.	A	Z
Th	232	90

METHOD

REF. NO.: 82 Kn 3 | egf

REACTION	RESULT	EXCITATION ENERGY	SOURCE TYPE	SOURCE RANGE	DETECTOR TYPE	DETECTOR RANGE	ANGLE
G,F	ABX	5-7	D	5-7	ION*I		4PI

The Chalk River bremsstrahlung monochromator at the University of Illinois Microtron Laboratory has been used with a multiwire fission chamber to measure the photofission cross section of ^{232}Th between 4.95 and 6.76 MeV with a resolution of 12–14 keV. This cross section, which on the average increases exponentially with photon energy, shows three plateaus 5.20 to 5.80, 5.90 to 6.15, and above 6.30 MeV respectively. Structure is observed on eached plateau. In particular there appear to be well-resolved peaks, separated by ≈100 keV, at 5.50 and 5.60 MeV on the lowest plateau and other prominent peaks are observed at 5.92, 6.03 and 6.11 MeV on the middle plateau. The closely spaced structure in each region might be interpreted as evidence for the excitation of vibrational states in shallow outer wells of a multiwell potential.

*FISSION CHAMBER

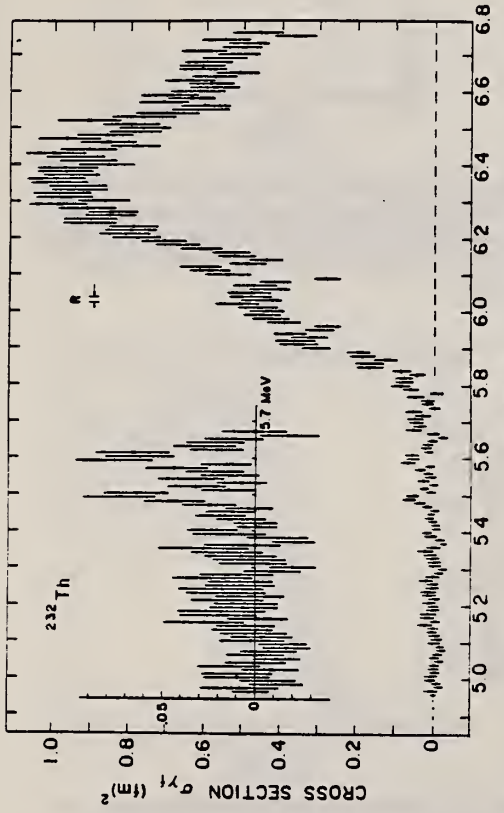

Fig. 2. The photofission cross section $\sigma_{\gamma f}$ of ^{232}Th between 4.95 and 6.76 MeV as a function of the photon energy E_γ. The peaks, at 5.50 and 5.60 MeV, are shown more clearly in the inset where they are magnified by a factor of 5. The resolution is R = 12–14 keV.

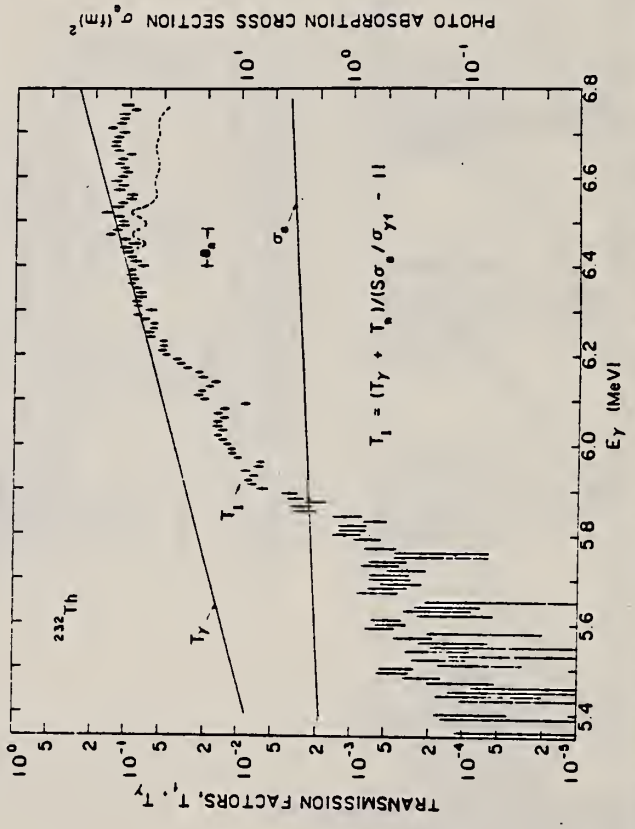

Fig. 3. The photofission transmission factor T_f of ^{232}Th between 5.35 and 6.76 MeV calculated from the $\sigma_{\gamma f}$ measurements and from estimates of the total absorption cross section σ_a and γ-ray and neutron transmission factors T_γ and T_n, respectively, using $T_f = (T_\gamma + T_n)/(S\sigma_a/\sigma_{\gamma f} - 1)$. The statistical factor S is estimated [21] assuming a Porter–Thomas distribution of level widths. The range of values are $0.74 < S < 1$. The broken line, above the neutron separation energy B_n, is the estimate of T_f assuming $T_n = 0$.

URANIUM
Z=92

A richly colored glass mosaic mural was excavated from the Bay of Naples by R. T. Gunther of Oxford University. Archaeological and historical reasons indicate that the glass dates from approximately 79 A. D. Analysis of the glass in 1912 showed that it contained more than 1% of an oxide of uranium. A careful study of the evidence indicates that the addition of the uranium mineral to the glass was probably intentional. This is the first known use of uranium in a man-made product.

The element was discovered in 1789 by the German chemist M. S. Klaproth from the pitchblende ores; he named it uranium in honor of the planet Uranus which had been discovered just eight years earlier.

The following paragraph, written in 1940, gives some idea of the excitement of the period when it was first realized that nuclear energy could possibly be of great importance to man:

"The release of the tremendous storehouse of energy which large atoms represent has long been an intriguing field of speculation. At a conference in February 1939 at Washington a report was given of the work of Drs. Hahn, Meitner and Strassman in Berlin in which neutrons have been used to liberate energy from the nuclei of uranium atoms. The amount of energy liberated is stated to be 175,000,000 electron volts for each atom of uranium which is split. There is also a delayed reaction resulting in the emission of other neutrons which are believed to be capable of producing a chain reaction upon other atoms, thus liberating atomic energy equal to twice that already reported. So important is this accomplishment that its comfirmation was hastily sought in several directions. These results are said to have been confirmed in Niels Bohr's laboratory in Copenhagen; by Professor Enrico Fermi and a group of associates at Columbia University; by Dr. John A. Fleming and associates at the Carnegie Institution at Washington; and by Dr. R. D. Fowler of Johns Hopkins University. Slow neutrons have been found to be highly efficient in splitting uranium. The method is not efficient as yet, but these experiments may lead to developments of great importance."[1]

[1]Chapters in the Chemistry of the Less Familiar Elements, Chapter 18, Uranium, B. S. Hopkins, Copyright 1940, Stipes Publishing Co., Champaign, Illinois.

REACTION	RESULT	EXCITATION ENERGY	SOURCE TYPE	SOURCE RANGE	DETECTOR TYPE	DETECTOR RANGE	ANGLE
G,F	RLX	0-999	C	200-999	SCD-D		DST

999=1.2 GEV

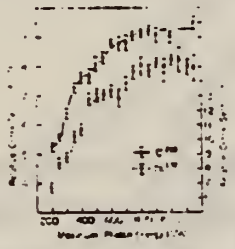

Fig. 1. Relative photofission cross section per equivalent quantum as a function of maximum photon energy for U^{238} and Th^{232}.

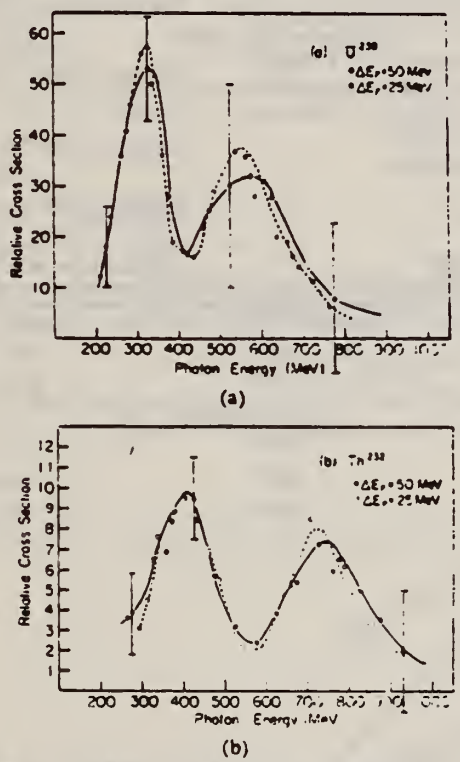

Fig. 2. Relative photofission cross section for two values of bin width as a function of photon energy. (a) for U^{238} and (b) for Th^{232} respectively.

REF.

I. Kimura, S.A. Hayashi, K. Kobayashi, S. Yamamoto & T. Shibata
J. Nucl. Sci. & Tech. 8, 173 (1971)

ELEM. SYM.	A	Z
U		92

METHOD

REF. NO.	
71 Ki 1	egf

REACTION	RESULT	EXCITATION ENERGY	SOURCE		DETECTOR		ANGLE
			TYPE	RANGE	TYPE	RANGE	
G,XN	SPC	5-23	C	15-23	TOF-D		90

Table 1 Comparison of nuclear temperatures of neutrons from natural uranium target bombarded with high energy electrons

Electron energy E_e(MeV)	Nuclear temperature (MeV)	Reference
18.5	$T_1=0.88\pm0.01$ ($E<3.5$ MeV) $T_2=1.50\pm0.02$ ($E>3.5$ MeV)	Present work
20	$T_1=0.92\pm0.01$ ($E<3.2$ MeV) $T_2=1.51\pm0.01$ ($E>3.2$ MeV)	Present work
23	$T_1=1.08\pm0.01$ ($E<3.0$ MeV) $T_2=1.63\pm0.01$ ($E>3.0$ MeV)	Present work
16	$T=0.33\pm0.03$ $T_f=1.05\pm0.04$	Glazunov *et al.*[9]*
30	$T=1.5$	Kramer-Ageev & Troshin[10]**
55	$T=1.53$**	Augustson *et al.*[11]

* Neutron spectrum is assumed to be the sum of fission and evaporation spectra with nuclear temperature T
** The assumption that the nuclear temperature of uranium is 1.5 MeV has been shown to be valid for some threshold detectors
*** Calculated from the data given by Augustson *et al.*[11]

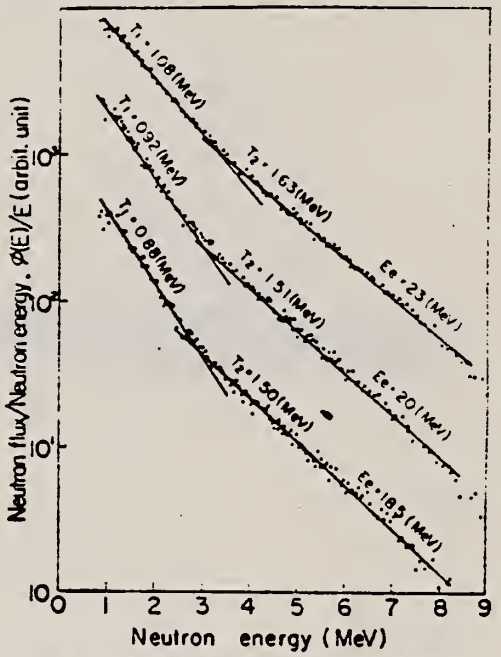

Fig. 3 Fast neutron spectra from natural uranium target, plotted in log $\phi(E)/E$ *vs.* E representation
(Annotations represent the nuclear temperatures determined from the gradients.)

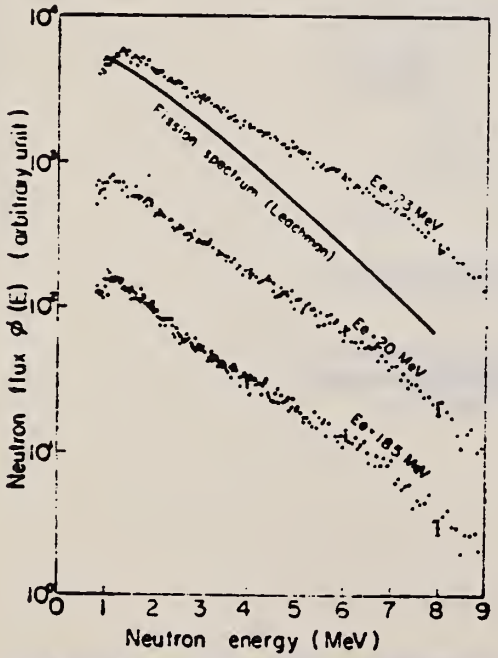

Fig. 2 Fast neutron spectra from natural uranium target bombarded with electrons of three different energies E_e = 23, 20 and 18.5 MeV

(9) Glaznov, Yu. Ya., Savin, M.V., Safina, I.N., *et al.*: *Soviet Phys. JETP.* **19**, 1284 (1964).
(10) Kramer-Ageev, E.A., Troshin, V.S.: *Vop. Dozimetr Zashch. Izluch., Moskov Inzh. Fiz. Inst.*, Sb. St. **3**, 12 (1964).
(11) Augustson, R.H., Gaerttner, E.R., Gozani,

U.S. DEPARTMENT OF COMMERCE
NATIONAL BUREAU OF STANDARDS

REF.

J. Maly
Phys. Letters 35B, 148 (1971)

ELEM. SYM.	A	Z
U		92

METHOD

REF. NO. 71 Ma 2 egf

REACTION	RESULT	EXCITATION ENERGY	SOURCE		DETECTOR		ANGLE
			TYPE	RANGE	TYPE	RANGE	
E,F	SPC	THR-999	D	500,999	FRG-I		4PI

999 = 1.3 GEV

Table 1
Estimated energies and cross-sections of fission fragment formations produced by 1300 MeV electrons (detected on (D) foils)

Range in mylar (μm) (passing foil No.)	Estimated energy of fragment in MeV				Cross section in μb		
	$A = 25$ $Z = 10$	$A = 50$ $Z = 20$	$A = 75$ $Z = 30$	$A = 100$ $Z = 40$	U	Pb	W
(0.foil)					3×10^5	6×10^3	400
53 μm (4. foil)	79	185	294	391	1.7	2.2	4.1
67 μm (5. foil)	89	222	362	484	1.8	1.0	1.2
79 μm (6. foil)	105	260	422	576	3.6	1.2	1.8
E_{kin} from Q values (MeV)	23.6	60.1	60.0	49.8	Kinetic energy from fission of: ^{186}W		
	22.4	61.6	80.0	66.9	^{208}Pb		
	49.2	92.0	111.0	111.3	^{238}U		
E_{Lab} (MeV)	92.6	192	302	433	E_{lab} for fusion with: ^{186}W		
	99.7	203.5	315	442	^{208}Pb		
	107	209	334	462	^{238}U		

[over]

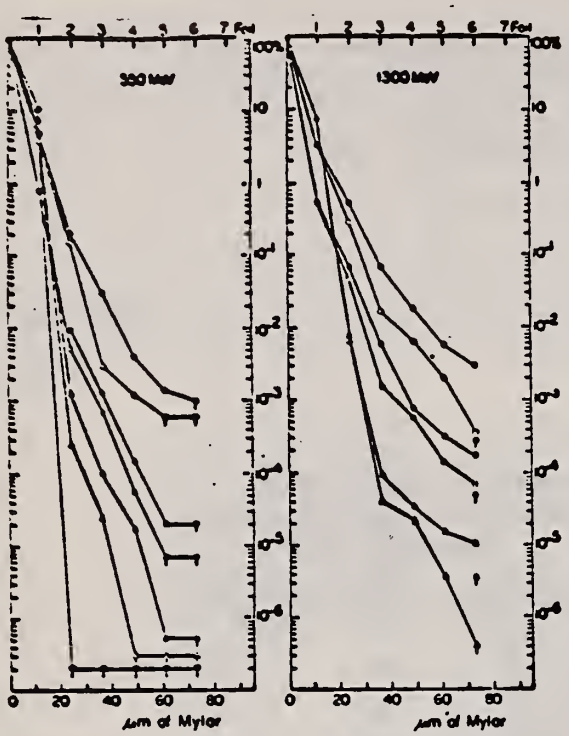

Fig. 1. Penetration of fission fragments through mylar foils from fission induced in U, Pb and W by electrons and bremsstrahlung. Explanation of symbols: Cf spontaneous fission ○; U fission front foils △ and back foils ▲; Pb fission front foils □ and back foils ■; W fission front foils ○ and back foils ○ .
Symbols with arrows (e.g. ⊖) denote background level.

REF.	ELEM. SYM.	A	Z
I.C. Nascimento, S.B. Herdade, and J.D. T. Arruda Neto PICNS-73, Vol.I, p.653 Asilomar	U		92

METHOD	REF. NO.
	73 Na 3 hmg

REACTION	RESULT	EXCITATION ENERGY	SOURCE		DETECTOR		ANGLE
			TYPE	RANGE	TYPE	RANGE	
E,F	ABX	THR- 50	D	8- 50	TRK-I		4PI
G,F	ABX	THR- 50	C	8- 50	TRK-I		4PI

GIVES G,F/E,F RATIO

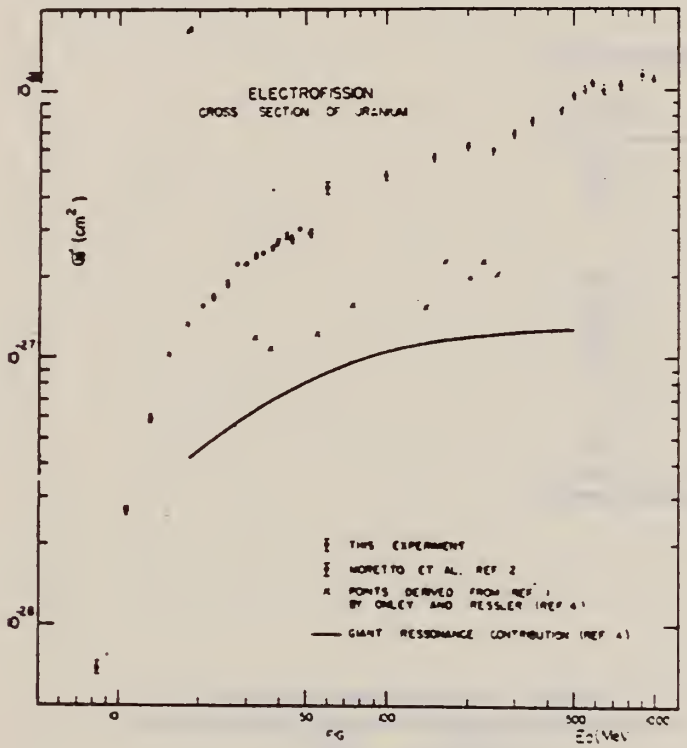

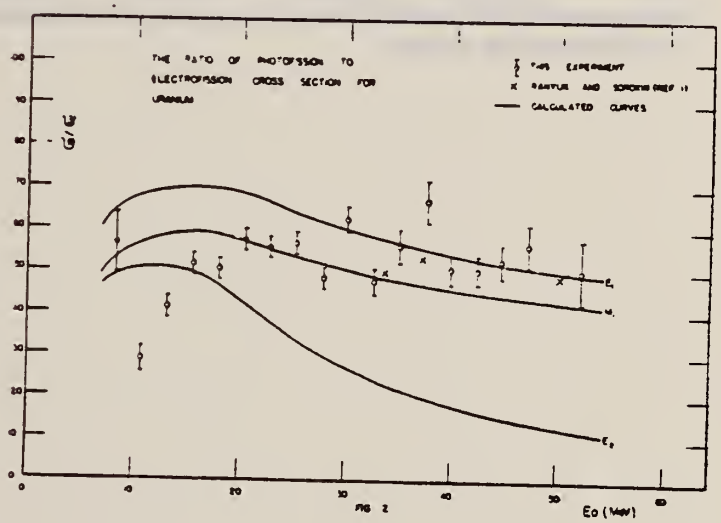

REFERENCES

1. Y.N.Ranyuk and P.V.Sorokin, Soviet J.Nucl.Phys. 5:377 (1967)
2. L.G.Moretto et al , Phys.Rev. 179:1176 (1969)
3. W.C.Barber, Phys.Rev. 111, 1642 (1958)
4. D.S.Onley and G.M.Ressler, Phys.Rev.Letters 22:236 (1969)
5. L.Katz, A.P.Baerg and F.Brown, II Int. Conf. on the Peaceful Uses of Atomic Energy, A/Conf. 15/p/200, (1958), p.31
6. H.W.Koch and J.M.Motz, Rev.Mod.Phys. 31, 920 (1959)

REF.

E. Hayward, W.C. Barber, and J.J. McCarthy
Phys. Rev. C10, 2652 (1974)

ELEM. SYM.	A	Z
U		92

METHOD

REF. NO.: 74 Ha 4 hmg

REACTION	RESULT	EXCITATION ENERGY	SOURCE		DETECTOR		ANGLE
			TYPE	RANGE	TYPE	RANGE	
$ G,G	ABX	15	D	15	NAI-D		90
		(15.1)		(15.1)			

POL PHOTONS

TABLE I. Results.

Target	$d\sigma^{\parallel}/d\Omega_F$ (Arbitrary units)	$d\sigma^{\perp}/d\Omega_F$ (Arbitrary units)	η_F	η	η (DCM)
Cd	0.042 ± 0.028	0.39 ± 0.05	0.11 ± 0.07	0.09 ± 0.07	0.19
In [a]	0.026 ± 0.020	0.54 ± 0.04	0.05 ± 0.04	0.03 ± 0.04	0.19
Sn	0.084 ± 0.036	0.65 ± 0.06	0.13 ± 0.06	0.11 ± 0.06	0.07
Sb [a]	0.14 ± 0.030	0.77 ± 0.05	0.18 ± 0.05	0.16 ± 0.05	
Nd [a]	0.14 ± 0.07	1.03 ± 0.10	0.14 ± 0.07	0.12 ± 0.07	
Ta	0.24 ± 0.10	1.47 ± 0.14	0.16 ± 0.07	0.14 ± 0.07	0.20
W	0.52 ± 0.10	1.66 ± 0.12	0.31 ± 0.07	0.29 ± 0.07	0.20
Pt	0.23 ± 0.08	1.94 ± 0.13	0.12 ± 0.04	0.10 ± 0.04	0.08
Au	0.39 ± 0.11	2.08 ± 0.15	0.19 ± 0.06	0.17 ± 0.06	0.07
Hg [a]	0.33 ± 0.09	2.16 ± 0.15	0.15 ± 0.04	0.13 ± 0.04	0.03
Pb [a]	0.19 ± 0.14	2.42 ± 0.19	0.08 ± 0.06	0.06 ± 0.06	0
Bi	0.10 ± 0.15	2.65 ± 0.26	0.04 ± 0.06	0.02 ± 0.06	0
Th [a]	0.31 ± 0.12	2.26 ± 0.19	0.14 ± 0.05	0.12 ± 0.05	0.07
U [a]	0.21 ± 0.11	2.38 ± 0.19	0.09 ± 0.05	0.07 ± 0.05	0.08

[a] Data not previously reported.

TABLE II. Comparison with Saclay data.

Target	$\lvert A_0\rvert^2$ This experiment (Arbitrary units)	$\lvert A_0\rvert^2$ Saclay (mb)	Ratio
Cd	0.337 ± 0.058	0.508	0.663 ± 0.114
In [a]	0.507 ± 0.046	0.591	0.859 ± 0.078
Sn	0.550 ± 0.072	0.822	0.669 ± 0.096
Sb [a]	0.590 ± 0.061	0.794	0.743 ± 0.077
Nd [a]	0.837 ± 0.100	1.170	0.715 ± 0.086
Ta	1.19 ± 0.18	1.88	0.633 ± 0.096
W	1.05 ± 0.17	2.05	0.512 ± 0.083
Pt	1.67 ± 0.16	2.70	0.619 ± 0.059
Au	1.62 ± 0.20	2.92	0.555 ± 0.068
Hg [a]	2.16 ± 0.20	3.29	0.540 ± 0.060
Pb [a]	2.20 ± 0.27	3.43	0.641 ± 0.078
Bi	2.53 ± 0.31	3.43	0.737 ± 0.090
Th [a]	1.89 ± 0.22	2.73	0.692 ± 0.080
U [a]	2.13 ± 0.22	2.83	0.754 ± 0.077
			0.656 ± 0.021

[a] Data not previously reported.

U
A=233

U
A=233

U
A=233

REF.

L. Katz, K. G. McNeill, M. LeBlanc and F. Brown
Can. J. Phys. 35, 470 (1957)

ELEM. SYM.	A	Z
U	233	92

METHOD

REF. NO. 57 Ka 1 JOC

REACTION	RESULT	EXCITATION ENERGY	SOURCE		DETECTOR		ANGLE
			TYPE	RANGE	TYPE	RANGE	
G,XN	ABX	6 - 23	C	6 - 23	BF3-I		4PI

Fig. 2. (γ,N) yield and cross section curves for U^{233}.

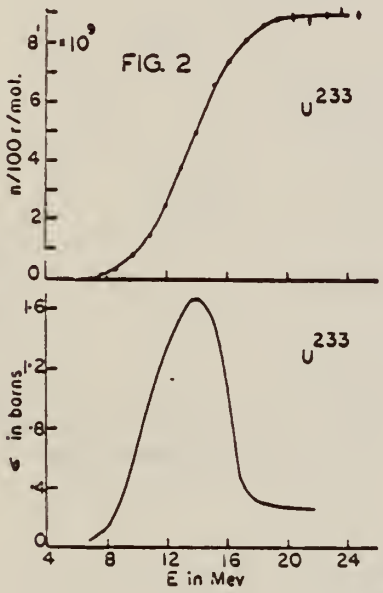

REF.

L. Katz, A. P. Baerg, and F. Brown
Peaceful Uses of Atomic Energy, Switzerland 1958

ELEM. SYM.	A	Z
U	233	92

METHOD

Fission chamber

[Page 1 of 2]

REF. NO. 58 Ka 2 EGF

REACTION	RESULT	EXCITATION ENERGY	SOURCE		DETECTOR		ANGLE
			TYPE	RANGE	TYPE	RANGE	
G,F	ABX	5-18	C	5-18	ION-I		DST

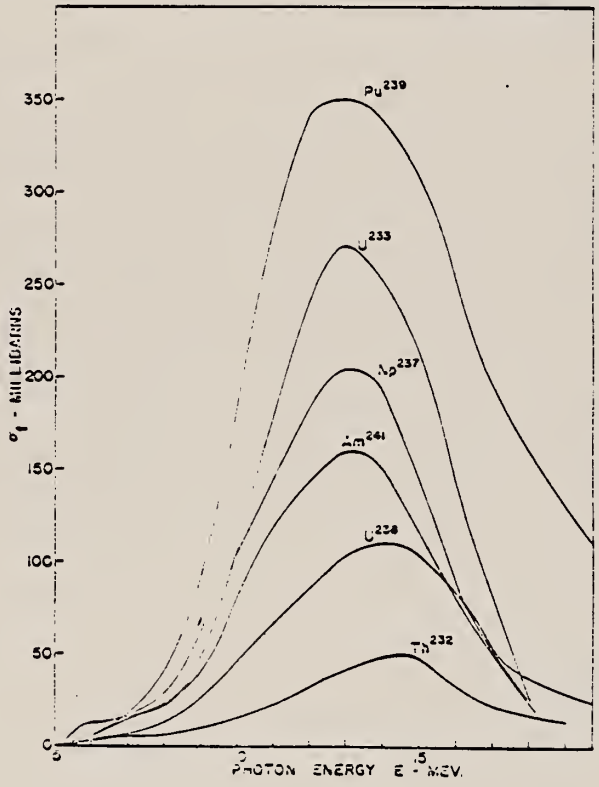

Fig. 5 - Photofission cross sections versus photon energy

REF.	ELEM. SYM.	A	Z
L. Katz, A. P. Baerg, and F. Brown Peaceful Uses of Atomic Energy, Switzerland 1958	U	233	92

METHOD	REF. NO.	
Fission chamber [Page 2 of 2]	58 Ka 2	EGF

REACTION	RESULT	EXCITATION ENERGY	SOURCE		DETECTOR		ANGLE
			TYPE	RANGE	TYPE	RANGE	

Fig. 7 - Low-energy-yield curves: fissions per roentgen-nucleus versus maximum bremsstrahlung energy. (The solid and dotted lines are samples of smoothed yield curves which fit the experimental data.)

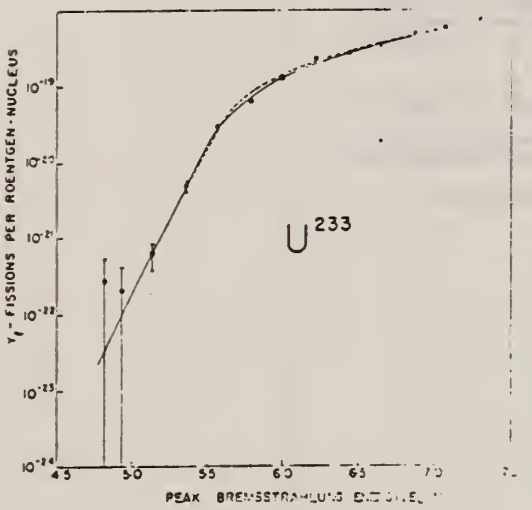

Table 4

Angular Distributions

	Ratio, (Counts at 90°)/(Counts at 0°)[a]		
	E_0 = 8.0 Mev[b]	E_0 = 10.0 Mev	E_0 = 20.0 Mev
U-233	1.043 ± 0.07	1.032 ± 0.04	0.994 ± 0.03
U-235	1.024 ± 0.05		
Np-237	1.024 ± 0.10		
Pu-239	1.002 ± 0.06	1.013 ± 0.05	0.952 ± 0.03
Pu-240	0.956 ± 0.07		

[a] This is the number of counts observed at 90° per unit X-ray dose divided by the number observed at 0° for the same dose.

[b] E_0 is the maximum energy of the bremsstrahlung spectrum.

REF.

A. P. Baerg, R. M. Bartholomew, F. Brown, L. Katz, and S. B. Kowalski
Can. J. Phys. 37, 1418 (1959) (A.E.C.L. No. 896)

ELEM. SYM.	A	Z
U	233	92

METHOD

Betatron with ionization chamber detector, enriched samples.

REF. NO. 59 Ba 4 EGF

REACTION	RESULT	EXCITATION ENERGY	SOURCE		DETECTOR		ANGLE
			TYPE	RANGE	TYPE	RANGE	
G,F	RLY	THR - 20	C	6-20	ION-I		DST

TABLE I

Angular distributions
Ratio, counts at 90°/counts at 0°*

Nuclide	E_0† = 6.0	E_0 = 6.5	E_0 = 8.0	E_0 = 10.0	E_0 = 20.0
U-233			1.048±0.07	1.032±0.04	0.994±0.03
U-235			1.024±0.05		
Np-237			1.024±0.10		
Pu-239‡	1.034±0.26	0.927±0.12	1.002±0.06	1.013±0.05	0.952±0.03
Am-241			0.958±0.07		

*The ratio is the number of counts observed at 90° per unit X-ray dose divided by the number observed at 0° for the same dose.
†E_0 is the maximum energy in million electron volts of the bremsstrahlung spectrum.
‡The 45°/0° ratio at E_0 = 6.5 Mev was 1.09±0.23.

Ref. J.R. Huizenga, K.M. Clarke, J.E. Gindler, R. Vandenbosch
Nuclear Phys. 34, 439 (1962)

Elem. Sym.	A	Z
U	233	92

Method: Monoergic γ's from $F^{19}(p,\alpha\gamma)$ reaction; fission fragment ionization chamber.

Ref. No.: 62 Hu 1 JHH

Reaction	E or ΔE	E_o	Γ	$\int \sigma dE$	Jπ	Notes
$U^{233}(\gamma,f)$	6.14 7.0					

TABLE 1
Isotopic content of uranium targets in mass per cent

Target \ A	233	234	235	236	238
[illegible]	98.33	0.010	0.627		1.03
[illegible]		93.44	4.87		1.69
[illegible]		0.022	99.04		0.938
[illegible]		0.07	4.02	94.27	1.64
[illegible]			0.04		99.96

TABLE 3
Photofission cross sections measured with monoenergetic gamma rays [illegible]

Target	$\sigma_{\gamma,f}/\sigma_{\gamma,fis}$	$\sigma_{\gamma,f}$ mb	$\sigma_{\gamma,fis}$ mb	E_γ MeV	[illegible]
Th^{232}	1.00 ± 0.13	9 ± 3	9 ± 3	6.34	5.5
[illegible]	1.12 ± 0.15	15 ± 5	13 ± 4	6.04	5.3
[illegible]	0.80 ± 0.10	28 ± 9	35 ± 11	6.40	5.2
[illegible]	2.06 ± 0.33	33 ± 10	16 ± 5	5.24	5.5
[illegible]	10.0 ± 3.0	52 ± 16	5 +10 -4	6.77	5.1
U^{238}	3.21 ± 0.70	44 ± 14	13 ± 4	5.90	5.4
Np^{237}	1.43 ± 0.21	45 ± 14	31 ± 10	6.76	5.1

a: From the computation of ref. 20)
b: From the extrapolation of ref. 26)

Ref 20: Everling, König, Mattauch, & Wapstra - Nuclear Phys. 18, 529 (1960)

Ref 26: Vandenbosch & Seaborg - Phys. Rev. 110, 507 (1958)

REF.

D. C. Aumann and J. E. Gindler
J. inorg. nucl. Chem. 32, 731 (1970)

ELEM. SYM.	A	Z
U	233	92

METHOD

REF. NO.	
70 Au 1	egf

REACTION	RESULT	EXCITATION ENERGY	SOURCE		DETECTOR		ANGLE
			TYPE	RANGE	TYPE	RANGE	
G,F	RLY	THR-17	C	14-17	ACT-I		4PI

Data ratio of isomer to ground state yields.

ISOMER YIELDS

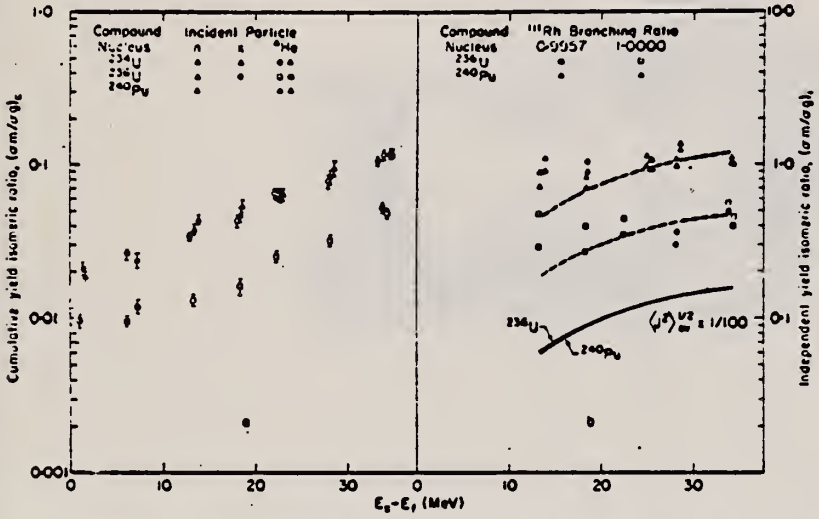

Fig. 3. Cumulative (a) and independent (b) yield ^{111}Pd isomeric ratios as a function of excitation energy above the fission barrier for several compound nuclei. The solid curves in 3b represent the root-mean-square average angular momenta of the compound nuclei indicated. The dashed curves are the solid curves displaced to pass approximately through the respective isomeric ratio data.

Table 3. Cumulative yield isomeric ratios of ^{111}Pd formed in photofission

Target	13·8	E_γ(MeV) 16·6–17·0	17·1
^{232}Th	0·0060 ± 0·0004	0·0056 ± 0·0006	
^{235}U	0·0053 ± 0·0004	0·0054 ± 0·0005	0·0066 ± 0·0007
^{236}U	0·0095 ± 0·0007		0·0119 ± 0·0012
^{233}U	0·0125 ± 0·0009	0·0130 ± 0·0013	
^{234}U	0·0261 ± 0·0019		0·0235 ± 0·0024
^{238}U	0·0304 ± 0·0022	0·0380 ± 0·0038	0·0454 ± 0·0045

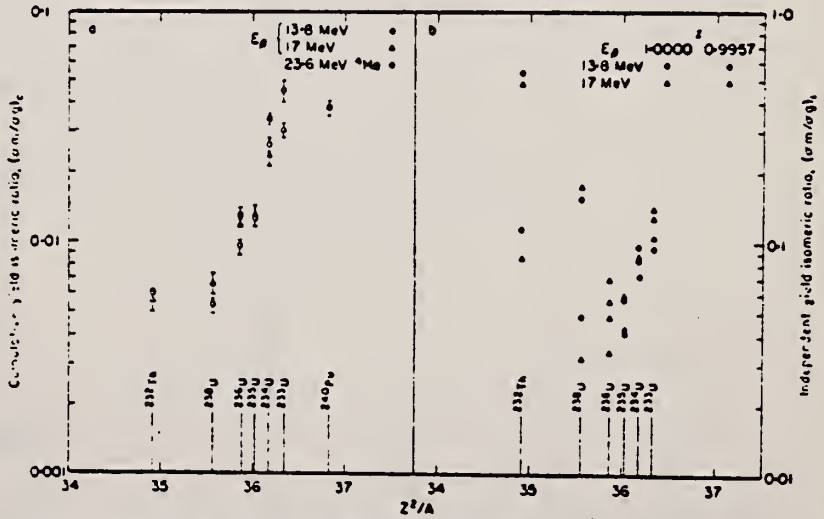

Fig. 5. Cumulative (a) and independent (b) yield ^{111}Pd isomeric ratios as a function of Z^2/A for the compound nucleus.

REF. J.T. Caldwell and E.J. Dowdy
Nucl. Sci. & Eng. 56, 179 (1975)

ELEM. SYM.	A	Z
U	233	92

METHOD

REF. NO. 75 Ca 5 egf

REACTION	RESULT	EXCITATION ENERGY	SOURCE TYPE	SOURCE RANGE	DETECTOR TYPE	DETECTOR RANGE	ANGLE
G,F	NOX	6- 13	C	8- 13	MOD-I		4PI

NEUTRON MULTIPLICITIES

The prompt- and delayed-neutron multiplicities for photofission of the eight isotopes, ^{232}Th, ^{233}U, ^{234}U, ^{235}U, ^{236}U, ^{238}U, ^{237}Np, and ^{239}Pu, have been measured using bremsstrahlung with end-point energies ranging from 8 to 13 MeV. The measured multiplicities are compared with those from the same compound nucleus formed in neutron-induced fission where such data exist.

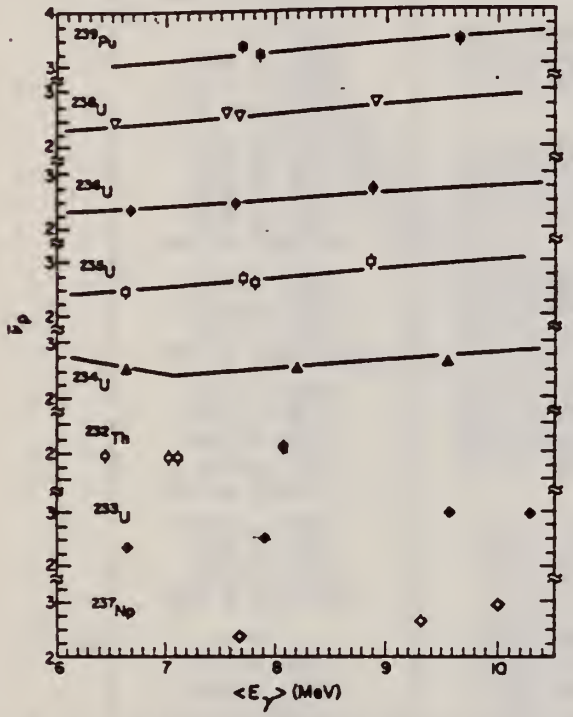

Fig. 5. $\bar{\nu}_p$ versus excitation energy for the eight isotopes studied in this experiment. The full curves shown are from the evaluations of Davey[2] with the excitation energy determined as described in the text. For the lower three isotopes shown, no previous experimental values for $\bar{\nu}_p$ exist.

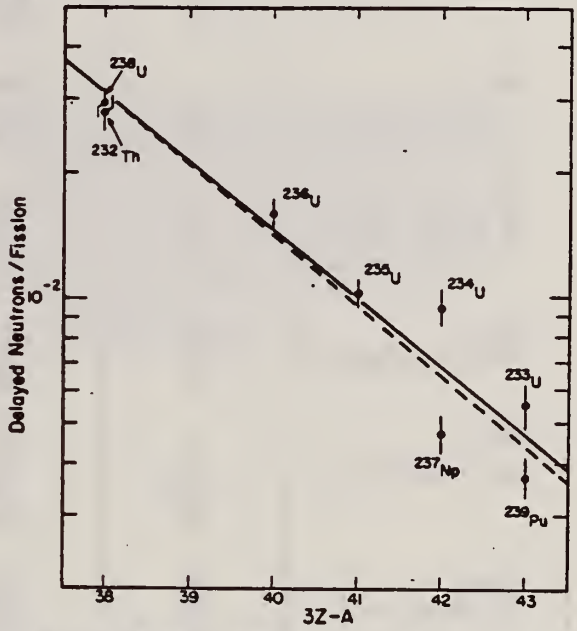

Fig. 6. Delayed neutrons per fission versus the parameter 3Z-A of the compound nucleus. The full curve shown is the least-squares fit to the data shown with $\ln Y_0 = 10.61$, $K = -0.372$. The dashed curve is the least-squares fit to the data provided by Tomlinson[6] with $\ln Y_0 = 11.35$, $K = -0.39$.

TABLE IV

Least-Squares Linear Fit Expressions for $\bar{\nu}_p(\langle E_\gamma \rangle)$

Isotope	$\bar{\nu}_p(\langle E_\gamma \rangle) = \bar{\nu}_0 + d\bar{\nu}_p/dE\,\langle E_\gamma \rangle$	Correlation Coefficient
^{232}Th	$\bar{\nu}_p(\langle E_\gamma \rangle) = 1.310 + 0.090\ \langle E_\gamma \rangle$	0.675
^{233}U	$\bar{\nu}_p(\langle E_\gamma \rangle) = 1.200 + 0.1709\ \langle E_\gamma \rangle$	0.947
^{234}U	$\bar{\nu}_p(\langle E_\gamma \rangle) = 2.222 + 0.0399\ \langle E_\gamma \rangle$	0.741
^{235}U	$\bar{\nu}_p(\langle E_\gamma \rangle) = 0.9034 + 0.2292\ \langle E_\gamma \rangle$	0.967
^{236}U	$\bar{\nu}_p(\langle E_\gamma \rangle) = 1.140 + 0.1788\ \langle E_\gamma \rangle$	0.986
^{238}U	$\bar{\nu}_p(\langle E_\gamma \rangle) = 1.502 + 0.1458\ \langle E_\gamma \rangle$	0.984
^{237}Np	$\bar{\nu}_p(\langle E_\gamma \rangle) = 0.4027 + 0.2505\ \langle E_\gamma \rangle$	0.967
^{239}Pu	$\bar{\nu}_p(\langle E_\gamma \rangle) = 2.526 + 0.0930\ \langle E_\gamma \rangle$	0.777

[2] W.G. Davey, Nucl. Sci. Eng., 44, 345 (1971)

[6] L. Tomlinson, "Delayed Neutrons from Fission: A Compilation and Evaluation of Experimental Data," AERE-R-6993, Atomic Energy Research Establishment, Harwell (1972)

TABLE III

Prompt- and Delayed-Neutron Yields

	E_n, MeV	$\langle E_\gamma \rangle$, MeV	ν_p	Delayed Neutrons per 100 Fissions
^{232}Th	8	6.44	1.96 ± 0.11	3.10 ± 0.28
(σ = 1.15 ± 0.05)	10	7.02	1.89 ± 0.11	3.06 ± 0.31
	10.2	7.10	1.89 ± 0.11	2.67 ± 0.21
	12	8.06	2.08 ± 0.11	2.59 ± 0.31
				av = 2.80 ± 0.28
^{233}U	8	6.68	2.350 ± 0.112	0.455 ± 0.040
(σ = 1.25 ± 0.05)	10	7.90	2.498 ± 0.108	0.518 ± 0.040
	12	9.55	2.960 ± 0.096	0.640 ± 0.044
	13	10.27	2.870 ± 0.099	0.598 ± 0.051
				av = 0.553 ± 0.044
^{234}U	8	(6.67)[a]	2.536 ± 0.112	---
(σ = 1.13 ± 0.05)	10	8.69	2.499 ± 0.107	0.92 ± 0.06
	12	9.54	2.623 ± 0.105	0.97 ± 0.12
				av = 0.94 ± 0.094
^{235}U	8	6.67	2.456 ± 0.086	0.90 ± 0.08
(σ = 1.20 ± 0.05)	10	7.70	2.697 ± 0.081	0.88 ± 0.08
	10.2	7.81	2.612 ± 0.079	1.13 ± 0.07
	12	8.86	2.963 ± 0.072	1.12 ± 0.08
				av = 1.02 ± 0.08
^{236}U	8	6.66	2.357 ± 0.111	1.43 ± 0.14
(σ = 1.20 ± 0.05)	10	7.63	2.470 ± 0.105	1.73 ± 0.12
	12	8.86	2.744 ± 0.095	1.64 ± 0.10
				av = 1.60 ± 0.13
^{238}U	8	6.53	2.457 ± 0.088	3.06 ± 0.24
(σ = 1.22 ± 0.05)	10	7.54	2.628 ± 0.083	2.76 ± 0.17
	10.2	7.66	2.585 ± 0.082	3.06 ± 0.14
	12	8.88	2.802 ± 0.078	2.75 ± 0.19
				av = 2.91 ± 0.20
^{237}Np	10	7.68	2.35 ± 0.11	0.38 ± 0.04
(σ = 1.20 ± 0.05)	12	9.31	2.65 ± 0.10	0.50 ± 0.04
	13	9.92	2.95 ± 0.10	0.54 ± 0.04
				av = 0.47 ± 0.04
^{239}Pu	10	7.69	3.32 ± 0.08	---
(σ = 1.18 ± 0.10)	10.2	7.84	3.17 ± 0.14	0.37 ± 0.04
	12	9.65	3.43 ± 0.10	0.37 ± 0.04
				av = 0.37 ± 0.04

[a]Estimated value.

REF. M. Ya. Kondrat'ko, V. N. Korinets, and K. A. Petrzhak
Sov. Atomic Energy 40, 83 (1976)
Atomnaya Energiya 40, 72 (1976)

ELEM. SYM.	A	Z
U	233	92

METHOD

REF. NO. 76 Ko 8 hmg

REACTION	RESULT	EXCITATION ENERGY	SOURCE		DETECTOR		ANGLE
			TYPE	RANGE	TYPE	RANGE	
G,F	RLY	THR- 24	C	10- 24	ACT-I		4PI

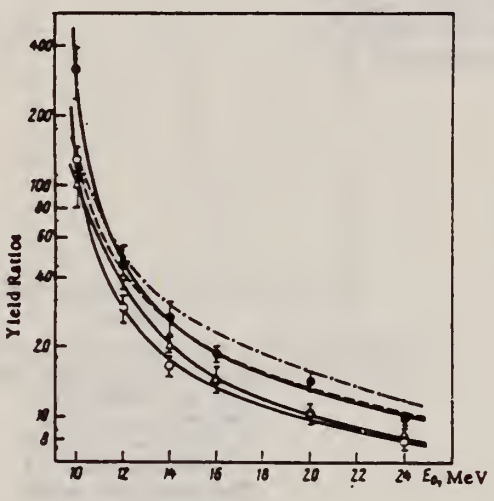

Fig. 1. Yield ratios "peak to trough" for photofission. Data of present paper for the reaction ^{233}U (γ, f): ○) $Y_{140}Ba/Y_{115}Cd$; ●) $Y_{140}Ba/Y_{111}Ag$; for the reaction ^{239}Pu (γ, f): △) $Y_{140}Ba/Y_{117}Cd$. Data in [1] for the reaction ^{235}U (γ, f): – – –) $Y_{140}Ba/Y_{115}Cd$; in [6] for the reaction ^{238}U (γ, f): —·—·—·) $Y_{140}Ba/Y_{115}Cd$.

TABLE 1. Relative Yields of ^{233}U Photofission Products

E_γ, MeV	Y_{111Ag}/Y_{140Ba}	Y_{115Cd}/Y_{140Ba}	Y_{117Cd}/Y_{140Ba}
10	0,0031±0,0008	0,0078±0,0010	0,005±0,001
12	0,022±0,005	0,034±0,002	0,032±0,002
14	0,037	0,060	0,060
16	0,053	0,068	0,061
20	0,068	0,095	0,086
24	0,100	0,126	0,128

REF. V.E. Zhuchko, Yu.B. Ostapenko, G.N. Smirenkin, A.S. Soldatov, Yu.M. Tsipenyuk
Yad. Fiz. 28, 1170 (1978)
Sov. J. Nucl. Phys. 28, 602 (1978)

ELEM. SYM.	A	Z
U	233	92

METHOD

REF. NO.	
78 Zh 7	hg

REACTION	RESULT	EXCITATION ENERGY	SOURCE		DETECTOR		ANGLE
			TYPE	RANGE	TYPE	RANGE	
G,F	ABX	THR-7	C	4-7	TRK-D		4PI
				(4.4-7.)			

The bremsstrahlung beam of the microtron at our Institute has been used to measure photofission yields of nine nuclei—^{232}Th, ^{233,235,236,238}U, ^{237}Np, ^{239,241}Pu, and ^{241}Am in the energy region 4.4–7.0 MeV. The method of minimization of the directed deviation was used to reproduce the photofission cross sections from the integrated yields. The following problems are discussed in terms of the experimental data: resonance structure of the cross sections, effects of a two-humped shape of the fission barrier, and comparison of the fissility in the (γ,f) and (n,f) reactions and in direct reactions.

PACS numbers: 25.85.Jg

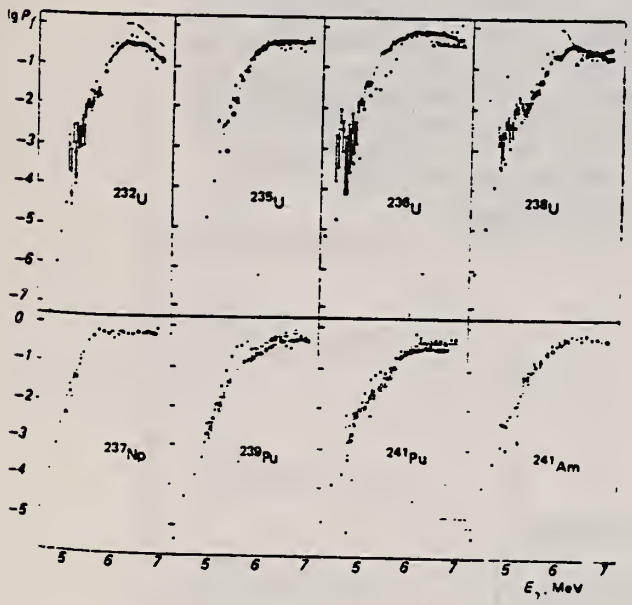

FIG. 4. Fissility P_f in the reactions (γ,f)—●, (n,f)—Δ (Ref. 14), and in direct reactions—○.[2] The dashed curve shows the results of evaluation of P_f in accordance with Eq. (9).

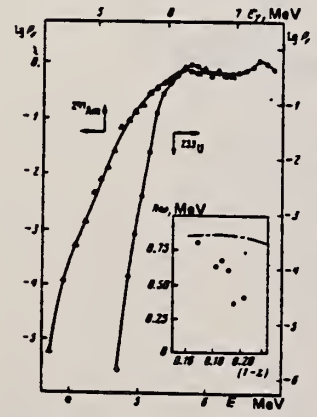

FIG. 8. Comparison of energy dependences of the fissilities of ^{233}U and ^{241}Am. In the insert is a comparison of the effective curvature parameters (10) (points) with calculations according to the liquid-drop model[25] (dot-dash curve).

(over)

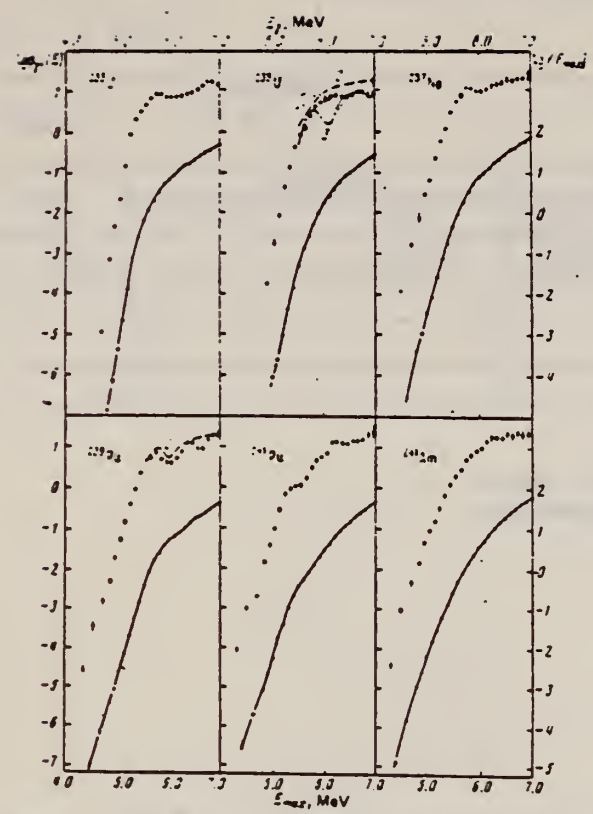

FIG. 3. Yields $Y(E_{max})$, fissions/mg-μC, and cross sections $\sigma_{\gamma f}(E_\gamma)$, mb, for odd isotopes. The designations are the same as in Fig. 2.

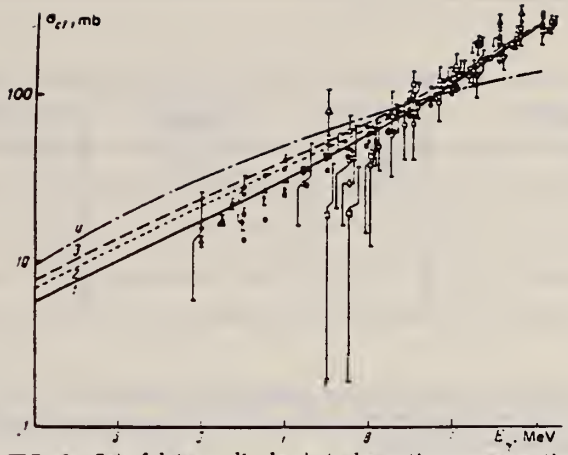

FIG. 6. Set of data on dipole photoabsorption cross sections σ_{c1}. The solid line (1)—the present work—is the result of fitting the data of Ref. 6 by Eq. (2) in the region $E_\gamma = 6$–10 MeV. Curves 2 and 3 are an extrapolation of the fit from Ref. 16 (2) and Ref. 17 (3) for ^{238}U; curve 4 is an estimate by means of Axel's formula.[15] Points: □, ■—^{232}Th: △, ▲—^{235}U: ♦—^{236}U; C, ●—^{238}U; ▽, ▼—^{237}Np; ◇—^{239}Pu. The hollow points are from Refs. 16 and 17: the solid points are from Ref. 6.

REF. A.S. Voronin, I.S. Koretskaya, V.L. Kuznetsov, V.G. Nedorezov, N.V. Nikitina, V.I. Noga, S.A. Pashchuk, Yu.N. Ranyuk, S.M. Solov'ev
Yad. Fiz. 34, 1439 (1981)
Sov. J. Nucl. Phys. 34, 797 (1981)

ELEM. SYM.	A	Z
U	233	92

METHOD

REF. NO.	
81 Vo 3	egf

REACTION	RESULT	EXCITATION ENERGY	SOURCE		DETECTOR		ANGLE
			TYPE	RANGE	TYPE	RANGE	
E,F	ABX	4-275	D	97-275	TRK-I		45

Results are presented of cross-section measurements for the fission of ^{232}Th, ^{233}U, ^{235}U, ^{236}U, ^{238}U, ^{237}Np, and ^{239}Pu by electrons with energies between 100 and 275 MeV; photofission and electrofission cross-section ratios for the same nuclei are given as well.

PACS numbers: 25.85.Jg, 27.90. + b, 25.85.Ge

TABLE II. Electrofission cross sections (mb) for nuclei with $Z \geq 90$ measured for electron energies between 100 and 275 MeV.

E_0, MeV	Nucleus						
	^{232}Th	^{233}U	^{235}U	^{236}U	^{238}U	^{237}Np	^{239}Pu
97	1.24	8.12	5.66	4.55	3.23	6.22	7.26
134	1.47	9.17	6.08	4.74	3.42	6.63	7.98
149	1.42	9.75	6.17	5.50	3.39	7.16	8.39
166	1.63	10.36	7.01	5.29	4.15	7.70	9.18
184	1.78	9.61	7.13	5.64	4.17	7.92	8.92
201	1.54	9.84	6.53	6.10	4.76	7.49	9.31
217	1.73	10.91	7.73	6.14	4.77	7.99	9.56
240	1.91	10.25	7.26	5.92	4.49	7.54	9.43
253	1.85	9.89	7.09	6.17	4.76	7.50	9.78
275	2.22	10.53	8.15	6.68	5.26	9.63	10.50

U
A=234

U
A=234

U
A=234

REF.

A. P. Baerg, R. M. Bartholomew, F. Brown, L. Katz, and S. B. Kowalski
Can. J. Phys. 37, 1418 (1959) (A.E.C.L. No. 896)

ELEM. SYM.	A	Z
U	234	92

METHOD

Betatron with ionization chamber detector, enriched samples.

REF. NO. 59 Ba 4 EGF

REACTION	RESULT	EXCITATION ENERGY	SOURCE		DETECTOR		ANGLE
			TYPE	RANGE	TYPE	RANGE	
G,F	RLY	THR - 20	C	6-20	ION-I		DST

TABLE II

Angular distributions
Relative fission fragment yields as a function of peak bremsstrahlung energy E_0 and angle θ to X-ray beam

E_0, Mev	Angle θ 0	25	45	60	90
Th-232					
6.5	1.00±0.3				20±5
7.0	1.00±0.04		4.1±0.2	6.7±0.3	8.4±0.3
7.5	1.00±0.1		5.1±0.4	6.0±0.4	7.9±0.5
8.0	1.00±0.09		2.4±0.2	3.6±0.3	5.1±0.3
9.0	1.00±0.1				3.4±0.3
10.0	1.00±0.04	1.16±0.05	1.67±0.08	1.97±0.08	2.4±0.1
14.0	1.00±0.05				1.43±0.08
20.0	1.00±0.05				1.13±0.06
U-238					
6.0	1.00±0.3				6.0±1.4
6.3	1.00±0.1		3.6±0.4		5.9±0.6
6.5	1.00±0.2				4.5±0.7
7.0	1.00±0.08	1.5±0.1	2.0±0.2	2.4±0.2	2.9±0.2
8.0	1.00±0.05				2.1±0.1
9.4	1.00±0.023	1.094±0.029	1.224±0.020	1.274±0.034*	1.452±0.033
10.0	1.00±0.04				1.38±0.04
14.0	1.00±0.04				1.08±0.04
20.0	1.00±0.03				1.05±0.03
	*θ = 65° in this case				
U-236					
6.0	1.00±0.25				4.6±0.8
6.5	1.00±0.1		2.06±0.2		2.55±0.25
7.0	1.00±0.05		1.65±0.10		2.11±0.12
8.0	1.00±0.04		1.39±0.06		1.66±0.07
9.0	1.00±0.04	1.10±0.07	1.15±0.04	1.31±0.08*	1.46±0.05
10.0	1.00±0.03		1.07±0.03		1.28±0.04
14.0	1.00±0.02				1.03±0.02
	*θ = 65° in this case				
U-234					
6.5	1.00±0.1		1.41±0.14		1.98±0.20
7.0	1.00±0.05		1.19±0.06		1.53±0.08
8.0	1.00±0.03		1.11±0.03		1.30±0.04
10.0	1.00±0.03				1.12±0.03
15.0	1.00±0.03				1.01±0.03
Pu-240					
6.5	1.00±0.10		1.49±0.15		1.55±0.16
7.0	1.00±0.06		1.03±0.06		1.35±0.08
8.0	1.00±0.03		1.01±0.03		1.21±0.04
15.0	1.00±0.02				1.01±0.02

The values quoted are counts observed for unit X-ray dose normalized to unit yield at $\theta = 0°$. No corrections have been applied.

REACTION	RESULT	EXCITATION ENERGY	SOURCE		DETECTOR		ANGLE
			TYPE	RANGE	TYPE	RANGE	

TABLE IV

Relative fissionabilities, U-238 = 100 at 20 Mev

E_0	U-234	U-235	U-236	U-238	Pu-239	Pu-240
6.0		0.45±0.05	0.303±0.013	0.387±0.040		
6.5	1.165±0.033	1.134±0.025	1.159±0.026	1.08±0.07	0.239±0.024	1.145±0.051
7.0	2.515±0.053	2.282±0.038	2.358±0.037	2.14±0.14	4.50±0.22	2.528±0.075
8.0	6.285±0.085	5.519±0.067	5.285±0.056	4.87±0.24	11.35±0.34	6.09±0.12
9.0		11.00±0.33	8.94±0.13	8.65±0.26		
10.0	17.36±0.53	18.75±0.30	14.29±0.20	14.41±0.28	45.1±2.2	
14.0		88.0±4.5	43.11±0.53	57.7±1.4		
15.0	84.3±1.9	119.0±0.9	73.58±0.78	70.5±1.8	255.0±7.6	82.3±1.8
20.0	127.5±2.5	180.8±2.2	109.4±1.0	100±2.5	352±10	120.8±2.3

TABLE VI

Corrected values of α in $W(\theta) = 1+\alpha \sin^2\theta$

E_0	Th-232	U-238	U-236	U-234	Pu-240
6.0		6.6±2	6.0±2.3		
6.3		6.7±1.1			
6.5	>25	4.4±1.0	2.1±0.4	2.3±0.6	0.65±0.20
7.0	11.0±0.8	2.05±0.24	1.83±0.17	0.90±0.16	0.49±0.12
7.5	10.3±1.6				
8.0	4.9±0.6	1.3±0.1	0.79±0.09	0.44±0.08	0.29±0.07
9.0	2.8±0.4		0.51±0.07		
9.4		0.41±0.04			
10.0	1.61±0.12	0.41±0.05	0.32±0.06	0.17±0.07	
14.0	0.46±0.09	0.09±0.01	0.04±0.03		
15.0				0.02±0.04*	0.01±0.03*
20.0	0.14±0.06	0.05±0.03			

*These values, which do not differ from zero, have not been corrected for isotopic composition.

Ref. J.R. Huizenga, K.M. Clarke, J.E. Gindler, R. Vandenbosch
Nuclear Phys. 34, 439 (1962)

Elem. Sym.	A	Z
U	234	92

Method: Monoergic γ's from $F^{19}(p,\alpha\gamma)$ reaction; fission fragment ionization chamber.

Ref. No.: 62 Hu 1 | JHH

Reaction	E or ΔE	E_o	Γ	$\int \sigma dE$	Jπ	Notes
$U^{234}(\gamma, f)$	6.14 7.0					

TABLE 1
Isotopic content of uranium targets in mass per cent

Target	233	234	235	236	238
	98.33	0.010	0.0127		1.33
		93.44	4.87		1.69
		0.022	99.94		0.038
		0.07	4.62	94.77	0.54
			0.134		99.96

TABLE 3
Photofission cross sections obtained with mono-energetic gamma rays from the $F^{19}(p, \alpha\gamma)O^{16}$ reaction

Target	$\sigma_{f,a}/\sigma_{a,\gamma}$	$\sigma_{f,a}$(mb)	$\sigma_{a,\gamma}$(mb)	B_a(MeV) [a]	E_f(MeV) [b]
Th^{232}	1.00 ± 0.13	9 ± 3	9 ± 3	6.34	5.5
U^{233}	1.12 ± 0.15	15 ± 5	13 ± 4	6.04	5.3
U^{234}	0.80 ± 0.10	28 ± 9	35 ± 11	6.40	5.2
U^{235}	2.06 ± 0.23	33 ± 10	16 ± 5	5.24	5.5
U^{236}	10.0 ± 5.0	52 ± 16	5^{+10}_{-4}	6.77	5.1
U^{238}	3.24 ± 0.79	44 ± 14	13 ± 4	5.90	5.4
Np^{237}	1.43 ± 0.21	45 ± 14	31 ± 10	6.76	5.3

[a] From the compilation of ref. [25])
[b] From the compilation of ref. [26])

Ref 20: Everling, König, Mattauch, & Wapstra - Nuclear Phys. 18, 529 (1960)

Ref 26: Vandenbosch & Seaborg - Phys. Rev. 110, 507 (1958)

REF.

D. C. Aumann and J. E. Gindler
J. inorg. nucl. Chem. 32, 731 (1970)

ELEM. SYM.	A	Z
U	234	92

METHOD

REF. NO.	
70 Au 1	egf

REACTION	RESULT	EXCITATION ENERGY	SOURCE		DETECTOR		ANGLE
			TYPE	RANGE	TYPE	RANGE	
G,F	RLY	THR-17	C	14-17	ACT-I		4PI

Data ratio of isomer to ground state yields.

ISOMER YIELDS

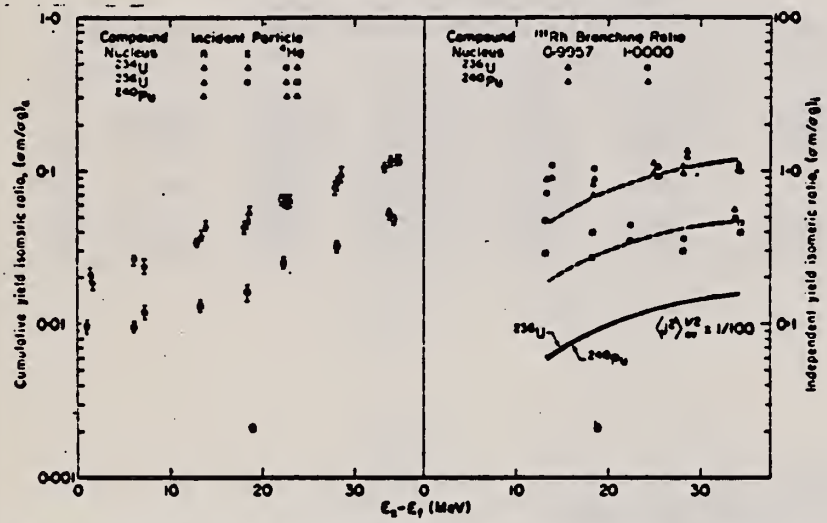

Fig. 3. Cumulative (a) and independent (b) yield ^{111}Pd isomeric ratios as a function of excitation energy above the fission barrier for several compound nuclei. The solid curves in 3b. represent the root-mean-square average angular momenta of the compound nuclei indicated. The dashed curves are the solid curves displaced to pass approximately through the respective isomeric ratio data.

Table 3. Cumulative yield isomeric ratios of ^{111}Pd formed in photofission

Target	E_γ(MeV) 13·8	16·6–17·0	17·1
^{232}Th	0·0060 ± 0·0004	0·0056 ± 0·0006	
^{236}U	0·0053 ± 0·0004	0·0054 ± 0·0005	0·0066 ± 0·0007
^{235}U	0·0095 ± 0·0007		0·0119 ± 0·0012
^{233}U	0·0125 ± 0·0009	0·0130 ± 0·0013	
^{234}U	0·0261 ± 0·0019		0·0235 ± 0·0024
^{238}U	0·0304 ± 0·0022	0·0380 ± 0·0038	0·0454 ± 0·0045

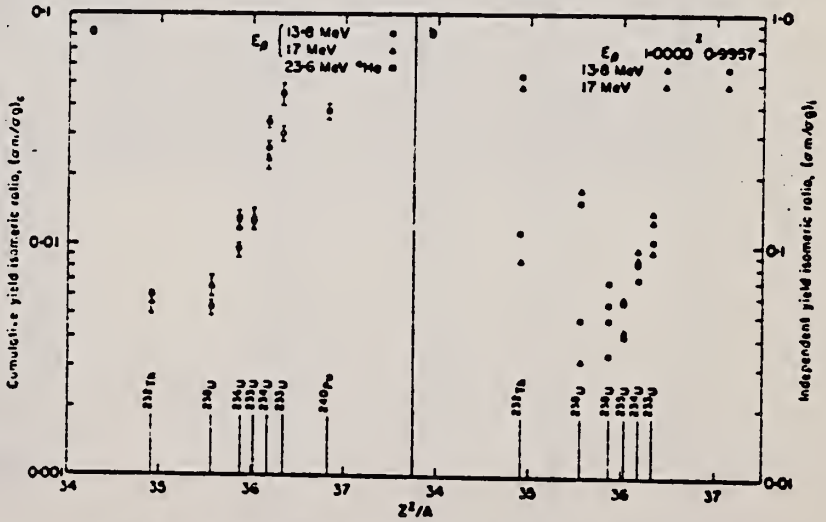

Fig. 5. Cumulative (a) and independent (b) yield ^{111}Pd isomeric ratios as a function of Z^2/A for the compound nucleus.

REF.

J.T. Caldwell and E.J. Dowdy
Nucl. Sci. & Eng. 56, 179 (1975)

ELEM. SYM.	A	Z
U	234	92

METHOD

REF. NO. 75 Ca 5 egf

REACTION	RESULT	EXCITATION ENERGY	SOURCE TYPE	SOURCE RANGE	DETECTOR TYPE	DETECTOR RANGE	ANGLE
G,F	NOX	6- 13	C	8- 13	MOD-I		4PI

NEUTRON MULTIPLICITIES

The prompt- and delayed-neutron multiplicities for photofission of the eight isotopes, ^{232}Th, ^{233}U, ^{234}U, ^{235}U, ^{236}U, ^{238}U, ^{237}Np, and ^{239}Pu, have been measured using bremsstrahlung with end-point energies ranging from 8 to 13 MeV. The measured multiplicities are compared with those from the same compound nucleus formed in neutron-induced fission where such data exist.

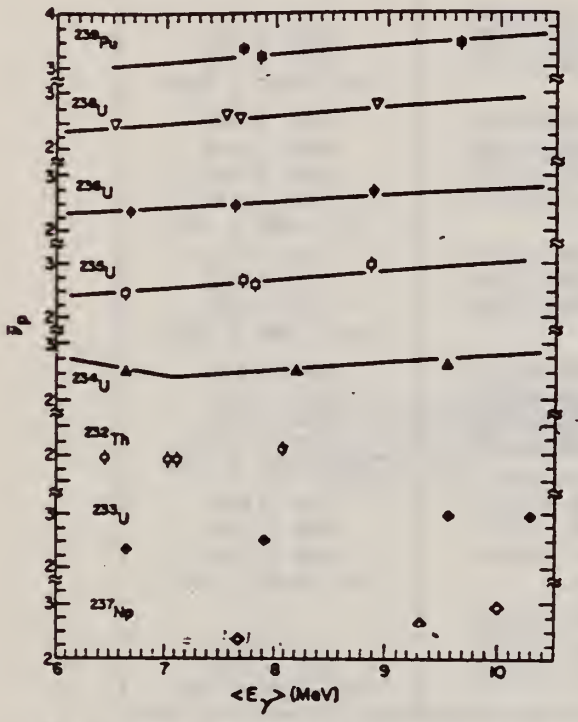

Fig. 5. $\bar{\nu}_p$ versus excitation energy for the eight isotopes studied in this experiment. The full curves shown are from the evaluations of Davey[2] with the excitation energy determined as described in the text. For the lower three isotopes shown, no previous experimental values for $\bar{\nu}_p$ exist.

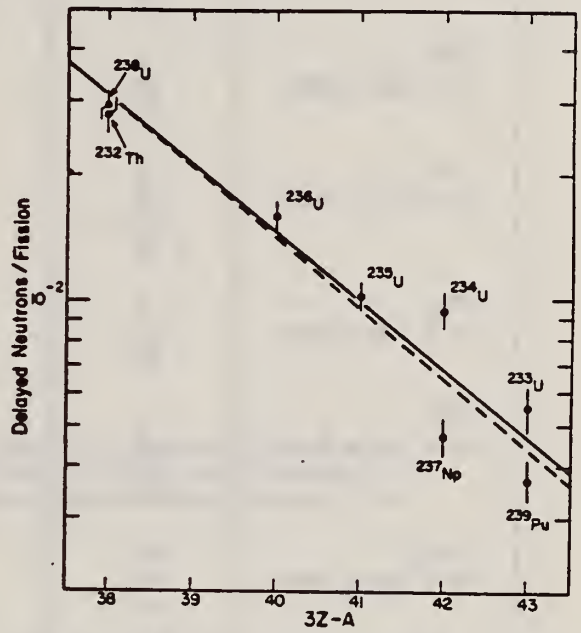

Fig. 6. Delayed neutrons per fission versus the parameter 3Z-A of the compound nucleus. The full curve shown is the least-squares fit to the data shown with $\ln Y_0 = 10.61$, $K = -0.372$. The dashed curve is the least-squares fit to the data provided by Tomlinson[6] with $\ln Y_0 = 11.35$, $K = -0.39$.

TABLE IV

Least-Squares Linear Fit Expressions for $\bar{\nu}_p(\langle E_\gamma \rangle)$

Isotope	$\bar{\nu}_p(\langle E_\gamma \rangle) = \bar{\nu}_0 + d\bar{\nu}_p/dE\,\langle E_\gamma \rangle$	Correlation Coefficient
^{232}Th	$\bar{\nu}_p(\langle E_\gamma \rangle) = 1.310 + 0.090\ \langle E_\gamma \rangle$	0.675
^{233}U	$\bar{\nu}_p(\langle E_\gamma \rangle) = 1.200 + 0.1709\ \langle E_\gamma \rangle$	0.947
^{234}U	$\bar{\nu}_p(\langle E_\gamma \rangle) = 2.222 + 0.0399\ \langle E_\gamma \rangle$	0.741
^{235}U	$\bar{\nu}_p(\langle E_\gamma \rangle) = 0.9034 + 0.2292\ \langle E_\gamma \rangle$	0.967
^{236}U	$\bar{\nu}_p(\langle E_\gamma \rangle) = 1.140 + 0.1788\ \langle E_\gamma \rangle$	0.986
^{238}U	$\bar{\nu}_p(\langle E_\gamma \rangle) = 1.502 + 0.1458\ \langle E_\gamma \rangle$	0.984
^{237}Np	$\bar{\nu}_p(\langle E_\gamma \rangle) = 0.4027 + 0.2505\ \langle E_\gamma \rangle$	0.967
^{239}Pu	$\bar{\nu}_p(\langle E_\gamma \rangle) = 2.526 + 0.0930\ \langle E_\gamma \rangle$	0.777

[2] W.G. Davey, Nucl. Sci. Eng., 44, 345 (1971)

[6] L. Tomlinson, "Delayed Neutrons from Fission: A Compilation and Evaluation of Experimental Data," AERE-R-6993, Atomic Energy Research Establishment, Harwell (1972)

over

TABLE III

Prompt- and Delayed-Neutron Yields

	E_n, MeV	$\langle E_\gamma \rangle$, MeV	$\bar{\nu}_p$	Delayed Neutrons per 100 Fissions
^{232}Th	8	6.44	1.96 ± 0.11	3.10 ± 0.28
(σ = 1.15 ± 0.05)	10	7.02	1.89 ± 0.11	3.06 ± 0.31
	10.2	7.10	1.89 ± 0.11	2.67 ± 0.21
	12	8.06	2.08 ± 0.11	2.59 ± 0.31
				av = 2.80 ± 0.28
^{233}U	8	6.68	2.350 ± 0.112	0.455 ± 0.040
(σ = 1.25 ± 0.05)	10	7.90	2.498 ± 0.108	0.518 ± 0.040
	12	9.55	2.960 ± 0.096	0.640 ± 0.044
	13	10.27	2.870 ± 0.099	0.598 ± 0.051
				av = 0.553 ± 0.044
^{234}U	8	(6.67)[a]	2.536 ± 0.112	---
(σ = 1.13 ± 0.05)	10	8.69	2.499 ± 0.107	0.92 ± 0.06
	12	9.54	2.623 ± 0.105	0.97 ± 0.12
				av = 0.94 ± 0.094
^{235}U	8	6.67	2.456 ± 0.086	0.90 ± 0.08
(σ = 1.20 ± 0.05)	10	7.70	2.697 ± 0.081	0.88 ± 0.08
	10.2	7.81	2.612 ± 0.079	1.13 ± 0.07
	12	8.86	2.963 ± 0.072	1.12 ± 0.08
				av = 1.02 ± 0.08
^{236}U	8	6.66	2.357 ± 0.111	1.43 ± 0.14
(σ = 1.20 ± 0.05)	10	7.63	2.470 ± 0.105	1.73 ± 0.12
	12	8.86	2.744 ± 0.095	1.64 ± 0.10
				av = 1.60 ± 0.13
^{238}U	8	6.53	2.457 ± 0.088	3.06 ± 0.24
(σ = 1.22 ± 0.05)	10	7.54	2.628 ± 0.083	2.76 ± 0.17
	10.2	7.66	2.585 ± 0.082	3.06 ± 0.14
	12	8.88	2.802 ± 0.078	2.75 ± 0.19
				av = 2.91 ± 0.20
^{237}Np	10	7.68	2.35 ± 0.11	0.38 ± 0.04
(σ = 1.20 ± 0.05)	12	9.31	2.65 ± 0.10	0.50 ± 0.04
	13	9.92	2.95 ± 0.10	0.54 ± 0.04
				av = 0.47 ± 0.04
^{239}Pu	10	7.69	3.32 ± 0.08	---
(σ = 1.18 ± 0.10)	10.2	7.84	3.17 ± 0.14	0.37 ± 0.04
	12	9.68	3.43 ± 0.10	0.37 ± 0.04
				av = 0.37 ± 0.04

[a]Estimated value.

REF. C.D. Bowman, I.G. Schroder, K.C. Duvall and C.E. Dick
Phys. Rev. C 17, 1086 (1978)

ELEM. SYM.	A	Z
U	234	92

REF. NO. 78 Bo 8 hg

Upper limit of σ at 3.5 MeV is 0.3 ± 2.5 x 10^{-10} b

REACTION	RESULT	EXCITATION ENERGY	SOURCE		DETECTOR		ANGLE
			TYPE	RANGE	TYPE	RANGE	
G,F	ABX	THR- 4	C	4	TRK-I		4PI
		(THR-3.5)		(3.5)			

Upper limit for SIGMA

Photofission cross sections for ^{232}Th, and ^{236}U have been measured in the energy range from 3.25 to 5.75 MeV and for ^{234}U and ^{236}U at 3.5 MeV. The cross sections change by over seven orders of magnitude for this energy range. Cross section shapes are significantly different for different isotopes indicating a strong sensitivity to fission barrier parameters.

REF. L.J. Lindgren, A. Alm and A. Sandell
Nucl. Phys. A298, 43 (1978)

ELEM. SYM.	A	Z
U	234	92

METHOD

REF. NO. 78 Li 1 rs

REACTION	RESULT	EXCITATION ENERGY	SOURCE		DETECTOR		ANGLE
			TYPE	RANGE	TYPE	RANGE	
G,F	RLX	5- 6	C	0- 6	TRK-D		DST

Abstract: A measurement of the angular distributions and yields of fission fragments in the photofission of ^{234}U has been performed between 5.2 and 6.4 MeV. As γ-source, the bremsstrahlung from a microtron was used. For the detection of the fission fragments, solid-state track detectors were used. The present data for ^{234}U have been analysed together with earlier obtained data for ^{236}U and ^{238}U. The values of the fission barrier parameters obtained are compared to results in theoretical macroscopic and microscopic fission potential energy calculations.

See figure on other side

over

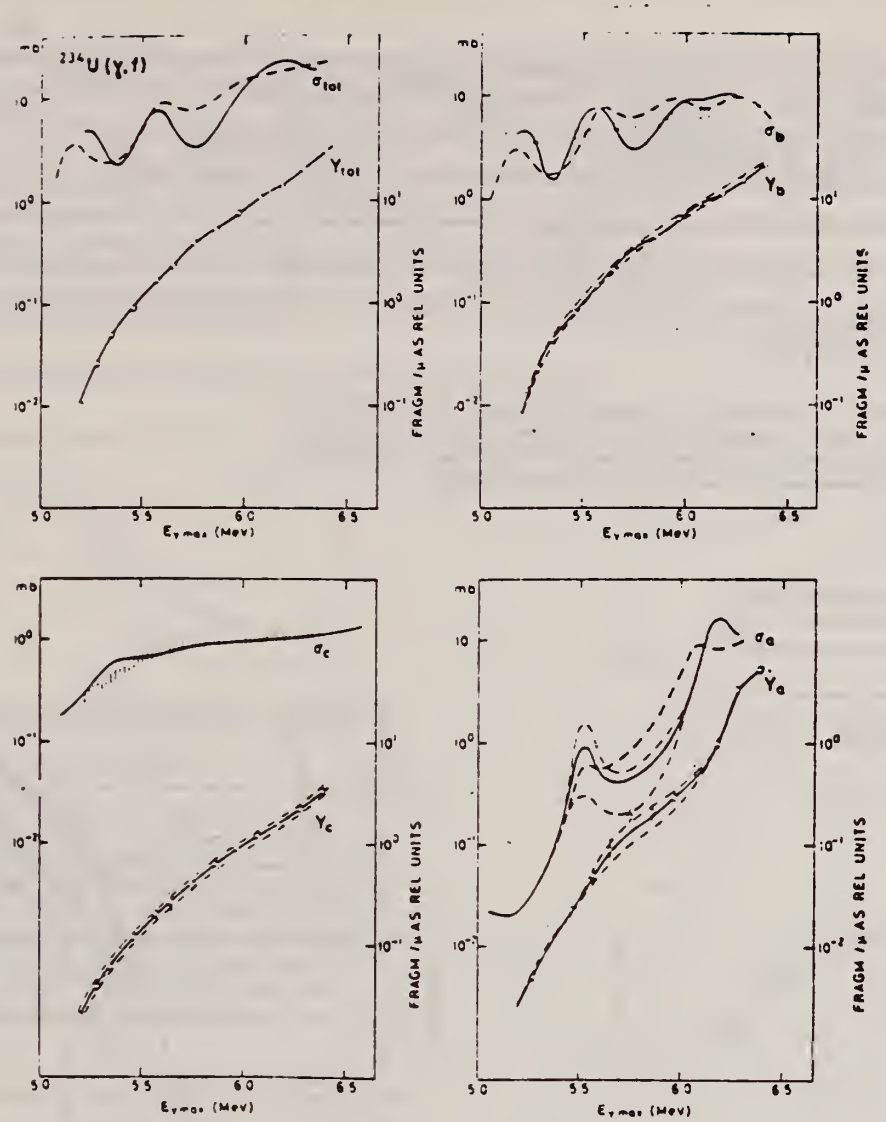

Fig. 1. *Upper left*: σ_{tot}, "experimental" (solid curve) and model calculated (dashed curve) total cross sections. Y_{tot}, experimental yield points (○) with the yield curve assumed (solid curve). *Upper right*: σ_b, "experimental" (solid curve) and model calculated (dashed curve) cross sections, and mean cross section (shaded band). Y_b, experimental yield points (○) with the yield curve assumed (solid curve). Dashed lines correspond to the mean cross section band above. *Lower left*: σ_c, "mean experimental" (shaded band) and model calculated (solid curve) cross sections. Y_c, experimental yield points (○) with the yield assumed (solid curve). The dashed lines correspond to the mean cross-section band above. *Lower right*: σ_a, "experimental" (solid curve and fine dashed lines) and model calculated cross sections (dashed curve). Y_a, experimental points (○) with three different yield curves (solid and dashed curves).

REF. L.J. Lindgren, A.S. Soldatov, Yu.M. Tsipenyuk
Sov. J. Nucl. Phys. 32, 173 (1980)
Yad. Fiz. 32, 335 (1980)

ELEM. SYM.	A	Z
U	234	92

METHOD

REF. NO.	
80 Li 5	hg

REACTION	RESULT	EXCITATION ENERGY	SOURCE		DETECTOR		ANGLE
			TYPE	RANGE	TYPE	RANGE	
G,F	ABX	THR-6.5	C	4-6	TRK-I		DST
				(4-5.7)			

$$W(\theta) = a + b \sin^2\theta + c \sin^2 2\theta$$

Measurements of the integrated yield of ^{234}U photofission are reported in the range of bremsstrahlung maximum energies E_{max} = 4–5.7 MeV, and also angular distributions of fragments for E_{max} = 5.1 and 5.6 MeV. On the basis of these data, total and partial cross sections for fission of ^{234}U have been obtained. The qualitative differences of ^{234}U from the heavier isotopes of uranium 236 and 238 are discussed.

PACS numbers: 25.85.Jg, 27.90. + b

TABLE I. Coefficients of the angular distribution of fragments from photofission of ^{234}U.

E_{max}, MeV	a	b	c
5.1	0.023±0.036	0.977±0.06	1.146±0.079
5.6	0.032±0.008	0.968±0.016	0.195±0.018

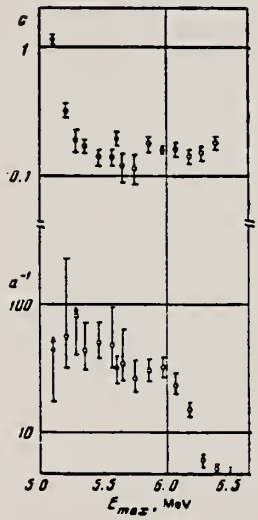

FIG. 1. Dependence of the coefficient a and c of the angular distribution $W(\theta)$ on the energy obtained in the present work (●) and in Ref. 5 (□).

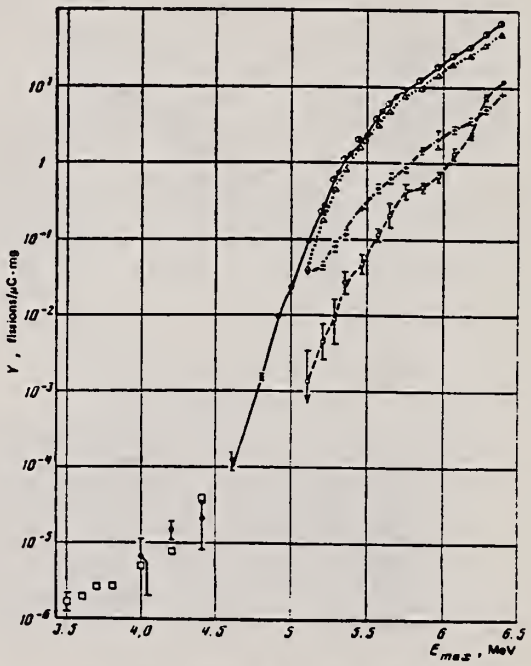

FIG. 2. Integrated yield Y in photofission of ^{234}U and its angular components Y_a(○), Y_b(Δ), and Y_c (+): ●—results of the present work, ○—Ref. 5, □—data on ^{237}Np.[10]

REF. J.D.T. Arruda-Neto, B.L. Berman, S.B. Herdade, I.C. Nascimento
Phys. Rev. C23, 2595 (1981)

ELEM. SYM.	A	Z
U	234	92

METHOD

REF. NO.: 81 Ar 4 | egf

REACTION	RESULT	EXCITATION ENERGY	SOURCE TYPE	SOURCE RANGE	DETECTOR TYPE	DETECTOR RANGE	ANGLE
E,F	ABX	5-25	D	5-25	TRK-I		4PI

The electrofission cross section for ^{234}U from 5.5 to 25.4 MeV has been measured. From a combined analysis of it and the previously measured photofission cross section, using virtual-photon spectra calculated in the distorted-wave Born approximation, the $E2$ photofission cross section has been determined. Parameters of the fission-decay branch of the giant quadrupole resonance for this nucleus have been obtained. A comparison of the $E2$ and $E1$ integrated photofission cross sections for the even uranium isotopes shows that the $E1$ fission channel increases in strength more rapidly with fissility than does the $E2$ channel.

G,F VIA VIRTUAL PHOT

[NUCLEAR REACTIONS Measured $\sigma(e,f)$ for ^{234}U; deduced $\sigma^{E2}(\gamma,f)$.]

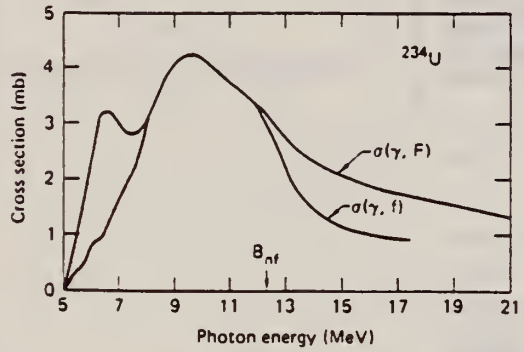

FIG. 3. The upper curve is σ_γ^{2dd} from Fig. 2. Subtraction of the $M1$ contribution, represented by the shaded region (see text) yields the lower curve below ~8 MeV. Subtraction of the second-chance photofission cross section $\sigma(\gamma, nf)$ from the total photofission cross section $\sigma(\gamma, F)$ yields the first-chance photofission cross section $\sigma(\gamma, f)$ which is the lower curve above the (γ, nf) threshold B_{nf} =12.3 MeV. Thus, the lower curve represents the fission-decay branch of the GQR.

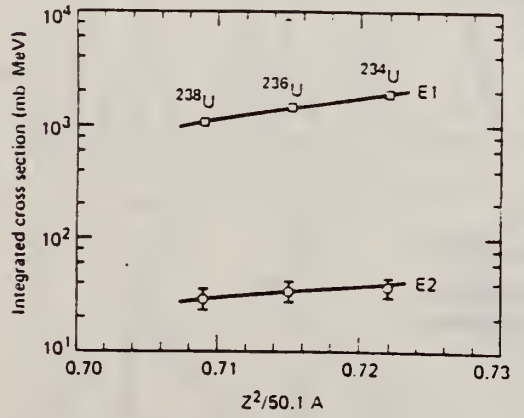

FIG. 4. The data points are the integrated photofission cross sections for the $E1$ and $E2$ multipolarities for the even uranium isotopes, as labeled. The lines illustrate the steeper dependence of the $E1$ strength of the fissility Z^2/A than that of the $E2$ strength.

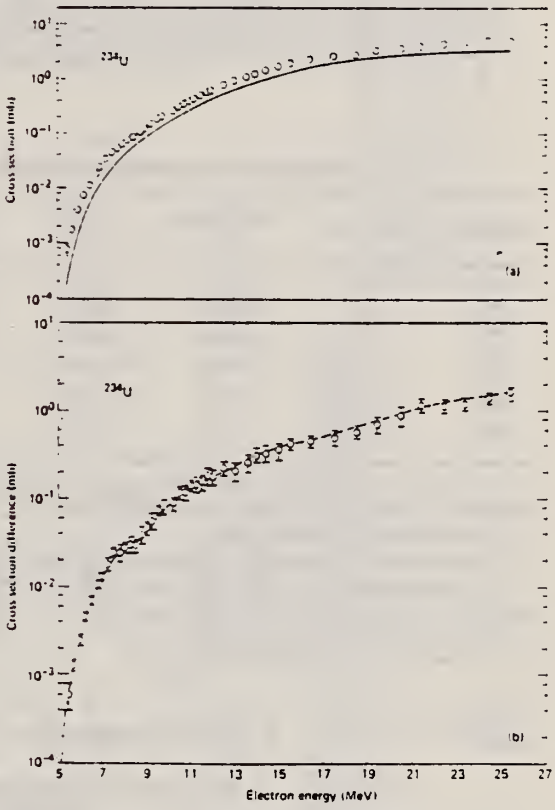

FIG. 1. (a) The data points are the present measured electrofission cross section $\sigma_e(E_0)$ for ^{234}U. Except for the point at 5.5 MeV, the statistical uncertainties are smaller than the plotted symbols. The solid curve is $\sigma_e^s(E_0)$, which was obtained by integrating the measured photofission cross section of Ref. 9 with the $E1$ virtual-photon spectrum of Ref. 8; it represents mainly the $E1$ component. (b) The data points (with error flags) are the electrofission cross-section differences $\Delta\sigma_e(E_0)$ between the data points and the curve of part (a). The dashed curve is the foldback of σ_γ^{2dd} (shown in Fig. 2) in Eq. (3).

REF. J.D. T. Arruda-Neto, S.B. Herdade, I.C. Nascimento, B.L. Berman, Nucl. Phys. A389, 378 (1982)

ELEM. SYM.	A	Z
U	234	92

METHOD

REF. NO. 82 Ar 3 egf

REACTION	RESULT	EXCITATION ENERGY	SOURCE		DETECTOR		ANGLE
			TYPE	RANGE	TYPE	RANGE	
E,F	ABX	5-25	D	5-25	TRK-I		DST

Reanalysis of data from ref. 2-5 also given

Abstract: The electrofission angular distributions for ^{234}U in the energy range 5.5 to 25 MeV were measured and are analyzed together with those obtained previously for ^{236}U and ^{238}U. The competition between the $K = 0$ and $K = 1$ fission channels following E2 excitation is established, showing a dominance of the $K = 0$ channel for near-barrier fission. The E2 fission strength functions for ^{234}U, ^{236}U and ^{238}U are deduced as well, and the E2 fission probabilities (at energies below the pairing gap) are estimated. A substantial concentration of E2 strength near the fission barrier is found, in good agreement with earlier photofission angular-distribution studies.

TABLE 1

First-chance fission-decay parameters of the GQR strength function*

Nucleus	Reaction	Peak energy (MeV)	FWHM (MeV)	EWSR (%)	P_f(E2) (%)	Ref.
^{234}U	(e, f)	8.2 ± 0.4	4.8 ± 1.0	87 ± 14	70 ± 15 [a])	this work
^{236}U	(e, f)	8.9 ± 0.4	4.7 ± 1.0	72 ± 10	60 ± 10 [a])	this work
^{238}U	(e, f)	8.3 ± 0.4	5.0 ± 1.0	55 ± 10	40 ± 10 [a])	this work
^{238}U	(e, e'f)	8.8 ± 0.2	~3/4.5 ± 0.5 [b])	[c])	[c])	[6])
^{238}U	(α,α'f)	~11 [d])	4.0 ± 0.5 [d])		<10	[7])
^{238}U	(α, α'f)	10.6	2.2 ± 0.2 [e])		25 ± 10	[8])
^{238}U	(^{6}Li, ^{6}Li'f)	~10.5	~7 [d])		≥20	[9])

* In our early work we published [2,4,5]) results derived simply from the cross sections and not the parameters of the strength functions obtained therefrom.

[a]) As determined at the peak energy.

[b]) Without and with the inclusion of the peak at ~6 MeV, respectively.

[c]) No definitive figures at the present stage of the data analysis can be given but they are at *least* equivalent to the (γ, f) results [23]) for GDR fission decay at ~9 MeV, and larger near ~6 MeV.

[d]) From the published singles spectrum.

[e]) For the $K = 0$ component only [see ref. [8])].

$$\frac{d\sigma_e}{d\Omega_f}(E_e, \theta_f) = \sum_{J^\pi=1^-}^{\ } \sum_{K=0}^{\infty J} \frac{d\sigma_e}{d\Omega_f}(J^\pi, K; E_e, \theta_f)$$

$$= A_e(E_e) + B_e(E_e) \sin^2 \theta_f + C_e(E_e) \sin^2 2\theta_f . \qquad (13)$$

2) J.D.T. Arruda-Neto, S.B., Herdade, B.S. Bhandari and I.C. Nascimento, Phys. Rev. C18 (1978) 863
3) J.D.T. Arruda-Neto and B.L. Berman, Nucl. Phys. A349 (1980) 483
4) J.D.T. Arruda-Neto, B.L. Berman, S.B. Herdade and I.C. Nascimento, Phys. Rev. C22 (1980) 1996
5) J.D.T. Arruda-Neto, B.L. Berman, S.B. Herdade and I.C. Nascimento, Phys. Rev. C23 (1981) 2595

(OVER)

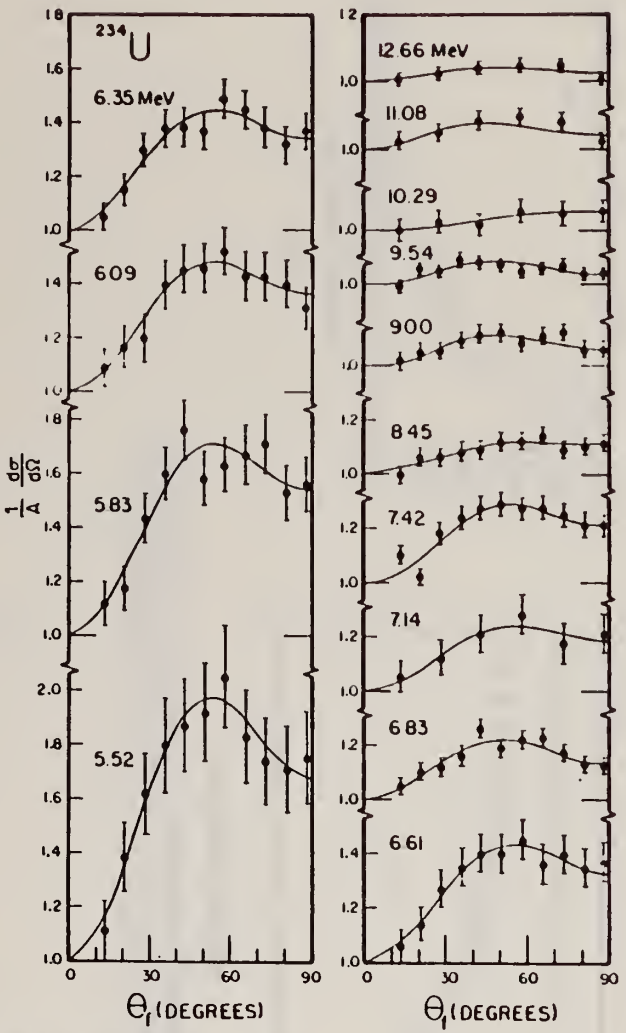

Fig. 4. Electrolission-fragment angular distributions $(1/A_c(E_e))(d\sigma/d\Omega_f)(E_e, \theta_f)$ for ^{234}U, for incident electrons having energies from 5.5 to 12.7 MeV. The curves are weighted least-squares fits of the function defined in eq. (13) to the experimental points. Both systematic and statistical uncertainties are included in the error flags (and were used in the fitting procedure).

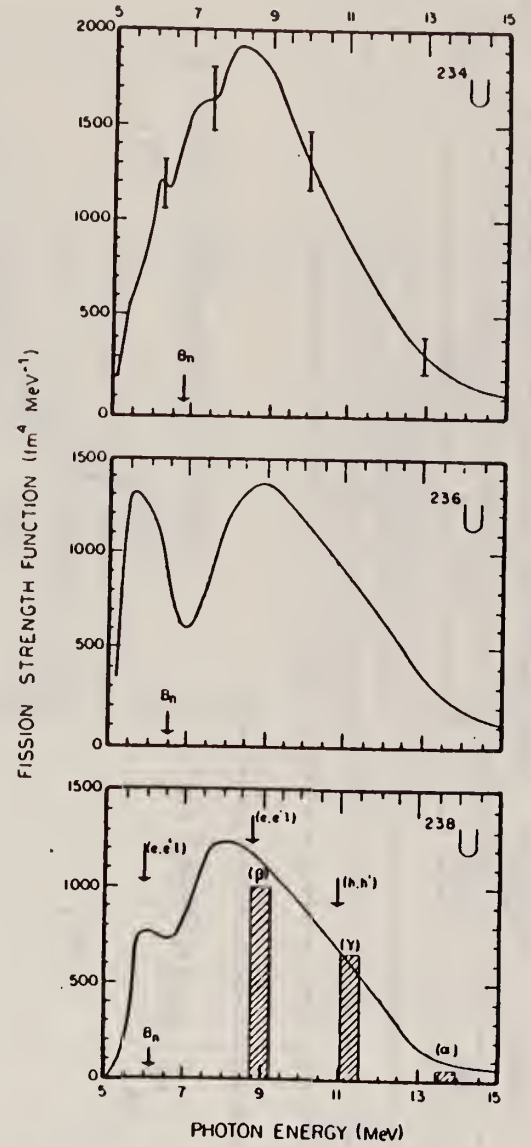

Fig. 6. Experimentally determined fission strength functions $(dB/d\omega)(\Gamma_f/\Gamma)$ for the GQR for the even uranium isotopes, derived from the (e, f) cross sections. The error flags shown on the curve for ^{234}U (which are the same percent errors associated with the cross sections $\sigma_{\gamma,f}(E2, \omega)$ [refs. [2,4,5]] used in the present derivation of the strength-function curve) are roughly the same as those for ^{236}U and ^{238}U. The shaded bands represent the fragmentation of the GQR as calculated in ref. [15]). The arrows indicate the energy of the structures in the E2 strength as determined from (e, e'f) and (h, h') experiments for ^{238}U (see text).

ELEM. SYM.	A	Z
U	234	92

METHOD

REF. NO. 82 Ar 3 egf

REACTION	RESULT	EXCITATION ENERGY	SOURCE		DETECTOR		ANGLE
			TYPE	RANGE	TYPE	RANGE	
E,F	ABX	5-25	D	5-25	TRK-I		DST

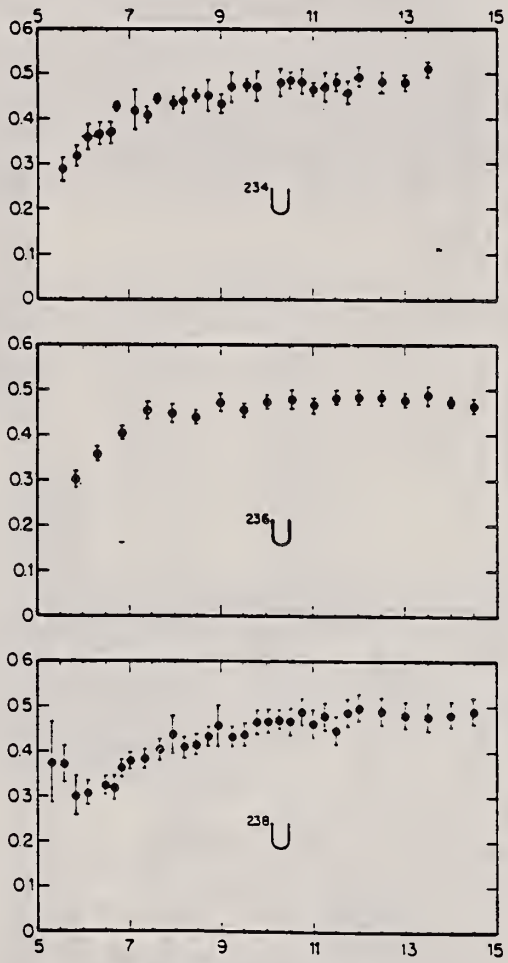

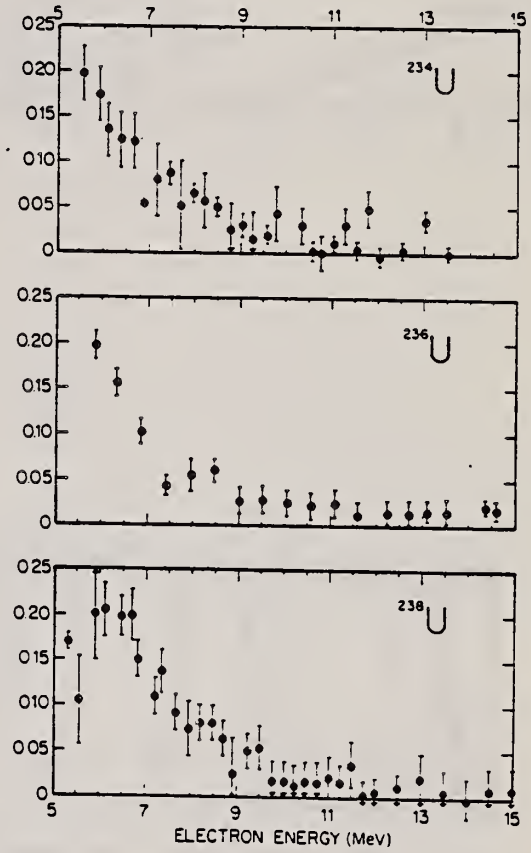

Fig. 5b.

Fig. 5. (a) Coefficient A of the angular-distribution function [eq. (13)] divided by the quantity $[2A - \frac{4}{3}B + \frac{16}{15}C]$ (which is proportional to the total electrofission cross section), as a function of the incident electron energy. (b) Same as in fig. 5a, for the coefficient B. (c) Same as in fig. 5a, for the coefficient C.

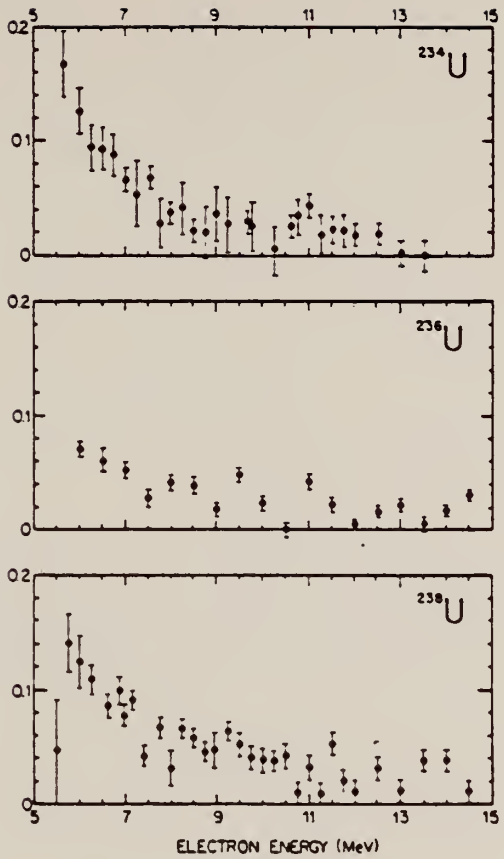

Fig. 5c.

U
A=235

U
A=235

REF.

A. P. Baerg, R. M. Bartholomew, F. Brown, L. Katz, and S. B. Kowalski
Can. J. Phys. 37, 1418 (1959) (A.E.C.L. No. 396)

ELEM. SYM.	A	Z
U	235	92

METHOD

Betatron with ionization chamber detector, enriched samples.

REF. NO. 59 Ba 4 EGF

REACTION	RESULT	EXCITATION ENERGY	SOURCE		DETECTOR		ANGLE
			TYPE	RANGE	TYPE	RANGE	
G,F	RLY	THR - 20	C	6-20	ION-I		DST

TABLE I

Angular distributions

Ratio, counts at 90°/counts at 0°*

Nuclide	E_0† = 6.0	E_0 = 6.5	E_0 = 8.0	E_0 = 10.0	E_0 = 20.0
U-233			1.048±0.07	1.032±0.04	0.994±0.03
U-235			1.024±0.05		
Np-237			1.024±0.10		
Pu-239‡	1.034±0.26	0.927±0.12	1.002±0.06	1.013±0.05	0.952±0.03
Am-241			0.958±0.07		

*The ratio is the number of counts observed at 90° per unit X-ray dose divided by the number observed at 0° for the same dose.
†E_0 is the maximum energy in million electron volts of the bremsstrahlung spectrum.
‡The 45°/0° ratio at E_0 = 6.5 Mev was 1.09±0.23.

TABLE IV

Relative fissionabilities, U-238 = 100 at 20 Mev

E_0	U-234	U-235	U-236	U-238	Pu-239	Pu-240
6.0		0.45±0.05	0.303±0.013	0.387±0.040		
6.5	1.165±0.033	1.134±0.025	1.139±0.026	1.08±0.07	0.239±0.024	1.145±0.051
7.0	2.515±0.053	2.282±0.038	2.358±0.037	2.11±0.14	4.50±0.22	2.528±0.075
8.0	6.285±0.085	5.519±0.067	5.285±0.056	4.87±0.21	11.35±0.34	6.09±0.12
9.0		11.00±0.33	8.94±0.33	8.65±0.26		
10.0	17.30±0.53	18.75±0.30	14.29±0.20	14.11±0.28	45.1±2.2	
14.0		88.0±4.5	43.11±0.54	37.7±1.4		
15.0	84.3±1.9	119.0±0.9	73.58±0.78	70.5±1.8	255.0±7.6	82.3±1.8
20.0	127.5±2.5	180.8±2.2	109.4±1.0	100±2.5	352±10	120.8±2.3

Ref. J.R. Huizenga, K.M. Clarke, J.E. Gindler, R. Vandenbosch
Nuclear Phys. 34, 439 (1962)

Elem. Sym.	A	Z
U	235	92

Method: Monoergic γ's from $F^{19}(p,\alpha\gamma)$ reaction; fission fragment ionization chamber.

Ref. No.: 62 Hu 1 JHH

Reaction	E or ΔE	E_o	Γ	$\int \sigma dE$	Jπ	Notes
$U^{235}(\gamma, f)$	6.14 7.0					

TABLE 1
Isotopic content of uranium targets in mass per cent

Target \ A	233	234	235	236	238
U^{233}	98.33	0.010	0.0127		1.53
U^{234}		93.44	4.87		1.69
U^{235}		0.022	99.94		0.038
U^{236}		0.07	4.62	94.77	0.54
U^{238}			0.04		99.96

TABLE 3
Photofission cross sections obtained with mono-energetic gamma rays from the $F^{19}(p, \alpha\gamma)O^{16}$ reaction

Target	$\sigma_{\gamma,f}/\sigma_{\gamma,n}$	$\sigma_{\gamma,f}$(mb)	$\sigma_{\gamma,n}$(mb)	B_n(MeV) [a]	E_f(MeV) [b]
Th^{232}	1.00 ± 0.13	9 ± 3	9 ± 3	6.34	5.5
U^{233}	1.12 ± 0.15	15 ± 5	13 ± 4	6.04	5.3
U^{235}	0.80 ± 0.10	28 ± 9	35 ± 11	6.40	5.2
U^{236}	2.06 ± 0.33	33 ± 10	16 ± 5	5.24	5.5
U^{238}	10.0 ± 5.0	52 ± 16	5^{+10}_{-4}	6.77	5.1
U^{233}	3.24 ± 0.79	44 ± 14	13 ± 4	5.90	5.4
Np^{237}	1.43 ± 0.21	45 ± 14	31 ± 10	6.76	5.3

[a]) From the compilation of ref. [20])
[b]) From the compilation of ref. [26])

Ref 20: Everling, König, Mattauch, & Wapstra - Nuclear Phys. 18, 529 (1960)

Ref 26: Vandenbosch & Seaborg - Phys. Rev. 110, 507 (1958)

REF.
C.D. Bowman, G.F. Auchampaugh, S. C. Fultz
Phys. Rev. 133, B676-83 (1964)

ELEM. SYM.	A	Z
U	235	92

METHOD
Positron annihilation, linac; ion chamber monitor

REF. NO.
64 Bo 3
NVB

REACTION		RESULT	EXCITATION ENERGY	SOURCE TYPE	SOURCE RANGE	DETECTOR TYPE	DETECTOR RANGE	ANGLE
G,F	425	ABX	6 - 19	D	6 - 19	IØN-I		4PI
G,N	424+	ABX	8 - 21	D	8 - 21	BF3-I		4PI
G,2N	442	ABX	8 - 21	D	8 - 21	BF3-I		4PI

423+

Target enriched to 93% U^{235}.

$$\int_{9}^{18.5\ \text{MeV}} \sigma(\gamma,f)dE = 1.07\ \text{MeV-barns}$$

$$\int_{9}^{18.5\ \text{MeV}} \sigma(\gamma,n)dE = 1.00\ \text{MeV-barns}$$

$$\int_{9}^{18.5\ \text{MeV}} \sigma(\gamma,2n)dE = 1.49\ \text{MeV-barns}$$

On Danos' theory, find quadrupole moment = 12.8 ± 1.3 barns.

E_{th} 10.85 E_b: 14.1

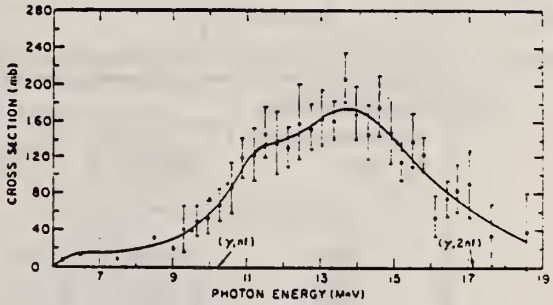

FIG. 2. Photofission cross section $\sigma(\gamma,F)$ of U^{235}. The data denoted by dots represent the fission cross section as measured with the annihilation photons. Error bars give standard deviation in the positron data. The crosses represent normalized bremsstrahlung data obtained with the spark chamber. The solid line through the data represents the photofission cross section used in the analysis for the formation cross section.

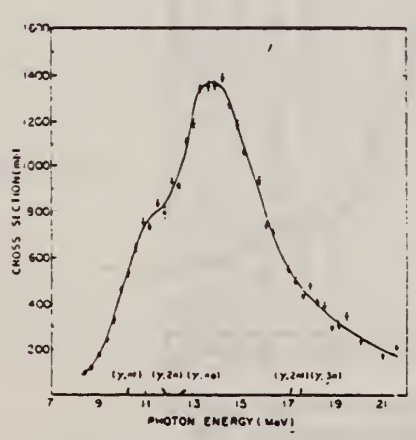

FIG. 5. Total neutron-emission cross section $\sigma(\gamma,V)$ for U^{235}. These data were obtained by taking the difference between the neutron-yield curves of Fig. 4. The statistical errors on the points represent the standard deviation of the measurements with positrons. The thresholds for various reactions which emit neutrons are also shown.

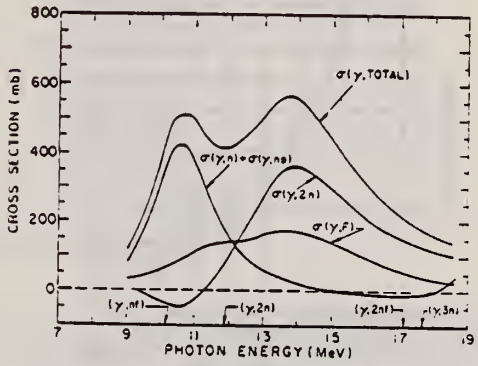

FIG. 8. The compound-nucleus-formation cross section $\sigma(\gamma,\text{total})$ and its components. The formation cross section was obtained by dividing $\sigma(\gamma,V)$ by μ. The (γ,n) and $(\gamma,2n)$ cross sections computed from Eqs. (14) are also shown. The (γ,F) cross section of Fig. 2 is included for comparison. The negative cross sections arise mainly from inaccuracies in the determination of μ and $\sigma(\gamma,F)$.

REF. M. Ya. Kondrat'ko and K. A. Petrzhak
Atomnaya Energiya 20, 514 (1966)
Atomic Energy 20, 594 (1966)

ELEM. SYM.	A	Z
U	235	92

METHOD: Betatron

REF. NO.: 66 Ko 3 | JDM

REACTION	RESULT	EXCITATION ENERGY	SOURCE TYPE	SOURCE RANGE	DETECTOR TYPE	DETECTOR RANGE	ANGLE
G,F	RLY	THR-25	C	10-25	ACT-I		4PI

Maximum energy of Bremsstrahlung E_0, MeV	Ratios of yields for U^{235} (γ, f)					Ratios of yields for U^{238} (γ, f)
	$\frac{Y_{Ba^{139}}}{Y_{Cd^{115}}}$	$\frac{Y_{Ba^{140}}}{Y_{Cd^{115}}}$	$\frac{Y_{Ba^{139}}}{Y_{Cd^{117m}}}$	$\frac{Y_{Ba^{140}}}{Y_{Cd^{117m}}}$	$\frac{Y_{Sr^{91}}}{Y_{Cd^{115}}}$ [4]	$\frac{Y_{Ba^{139}}}{Y_{Cd^{115}}}$ [5]
10,0	131±28	124±22	134±25	127±18	—	150
12,0	52,2±8,3	50,8±8,1	60,1±8,0	58,5±7,9	—	—
14,0	30,8±3,4	28,5±3,2	35,6±2,1	33,1±1,8	—	—
16,0	21,6±2,4	20,4±1,9	26,4±2,0	25,0±1,1	—	25
18,0	20,3±2,8	16,5±1,7	22,7±2,4	18,5±0,9	—	—
20,0	13,7±1,1	13,6±1,0	17,0±0,9	16,9±0,8	20	—
22,0	13,2±1,7	11,9±1,3	16,7±1,4	15,0±0,7	—	14
25,2	11,3±1,6	10,3±0,9	15,6±1,9	14,2±0,7	—	—

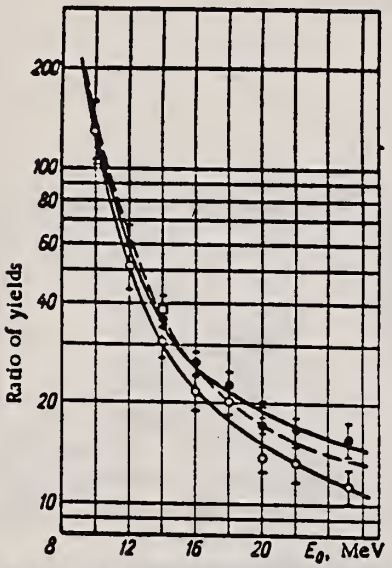

Fig. 1. "Peak-to-trough" ratio for the photofission of uranium isotopes: ○ $Y_{Ba^{139}}/Y_{Cd^{115}}$, ● $Y_{Ba^{139}}/Y_{Cd^{117m}}$, □ $Y_{Ba^{139}}/Y_{Ag^{113}}$ [for U^{235} (γf) data of the present investigation]; × $Y_{Sr^{91}}/Y_{Cd^{115}}$ for U^{235} (γf) [4]; – – – $Y_{Ba^{139}}/Y_{Cd^{115}}$ for U^{238} (γf) [5].

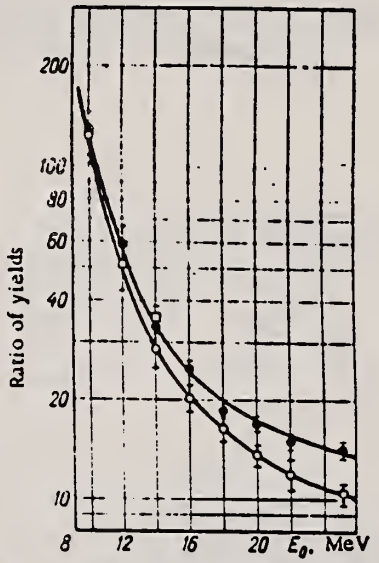

Fig. 2. "Peak-to-trough" ratio for the photofission of isotope U^{235} (data of present investigation): ○ $Y_{Ba^{140}}/Y_{Cd^{115}}$; ● $Y_{Ba^{140}}/Y_{Cd^{117m}}$; □ $Y_{Ba^{140}}/Y_{Ag^{115}}$.

REF. O. P. Nikotin and K. A. Petrzhak
Atomnaya Energiya 20, 268 (1966)
UDC 539.173.84, p. 300

ELEM. SYM.	A	Z
U	235	92

METHOD

REF. NO.	
66 Ni 1	egf

REACTION	RESULT	EXCITATION ENERGY	SOURCE		DETECTOR		ANGLE
			TYPE	RANGE	TYPE	RANGE	
G,F	RLY	THR-15	C	10-15	TRK-D	0-1	4PI
						(.1-1.0)	

Delayed Neutrons from Photofission ($E_{\gamma\,max}$ = 15 MeV)

Total yield of delayed neutrons, neutrons/100 fissions	Neutron group	$T_{1/2}$, sec	Relative yield of group, %	Absolute yield of group, neutrons per 100 fissions
3,8±0,6 (Th^{232})	1	55,6±1,5	4,48±0,20	0,17±0,03
	2	20,3±0,8	16,3±1,0	0,62±0,10
	3	5,45±0,50	15,9±1,5	0,60±0,10
	4	1,98±0,20	37,5±3,0	1,43±0,30
	5	0,43±0,10	17,2±2,0	0,66±0,10
	6	0,18±0,03	$8,7^{+2,0}_{-4,0}$	$0,33^{+0,10}_{-0,20}$
0,96±0,13 (U^{233})	1	54,7±2,5	5,4±0,5	0,052±0,010
	2	20,3±1,0	20,0±2,0	0,193±0,040
	3	5,45±0,60	15,2±2,0	0,146±0,030
	4	2,01±0,25	36,9±4,0	0,354±0,070
	5	0,50±0,10	13,9±2,0	0,134±0,030
	6	0,19±0,04	$8,6^{+2,0}_{-3,0}$	$0,083^{+0,025}_{-0,050}$
3,1±0,4 (U^{238})	1	56,2±0,8	1,98±0,08	0,061±0,010
	2	21,3±0,3	15,7±0,5	0,489±0,070
	3	5,50±0,20	17,5±0,7	0,545±0,070
	4	2,15±0,10	31,1±0,8	0,970±0,150
	5	0,70±0,06	17,7±0,9	0,552±0,080
	6	0,19±0,02	$16,1^{+2,0}_{-3,0}$	$0,502^{+0,120}_{-0,200}$
0,36±0,06 (Pu^{239})	1	54,0±3,0	6,05±0,60	0,022±0,004
	2	20,6±1,0	20,6±2,0	0,075±0,018
	3	5,7±0,7	18,3±3,0	0,066±0,015
	4	1,94±0,30	29,5±4,0	0,105±0,020
	5	0,58±0,10	14,9±3,0	0,054±0,012
	6	0,20±0,04	$10,6^{+2,0}_{-3,0}$	$0,038^{+0,012}_{-0,025}$

DELAYED N YIELDS

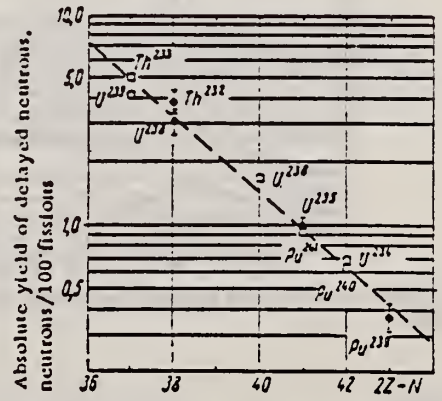

Fig. 3. Absolute yields of delayed neutrons from fission of nuclei: □) [7]; ●) present authors.

REF. K. A. Petrzhak and G. A. Tutin
Yad. Fiz. 7, 970 (1968)
Sov. J. Nucl. Phys. 7, 584 (1968)

ELEM. SYM.	A	Z
U	235	92

METHOD

REF. NO.	
68 Pe 2	hmg

REACTION	RESULT	EXCITATION ENERGY	SOURCE		DETECTOR		ANGLE
			TYPE	RANGE	TYPE	RANGE	
G,F	NOX	THR-25	C	25	ION-D		4PI

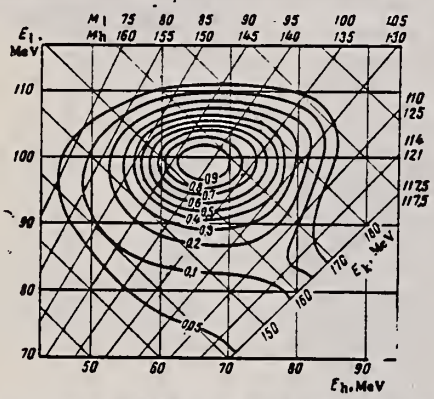

FIG. 1. Contour diagram of the distribution of the kinetic energy of the paired photofission fragments of U^{235} at $E_{\gamma max}$ = 25 MeV (E_l, E_h – kinetic energy of the light and heavy fragments, respectively; $E_k = E_l + E_h$ – summary kinetic energy of the fragments; M_l, M_h – mass of heavy and light fragments).

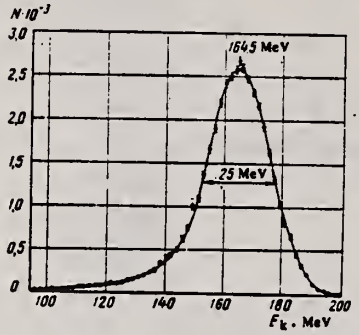

FIG. 2. Distribution of the total kinetic energy of the fragments of photofission of U^{235}

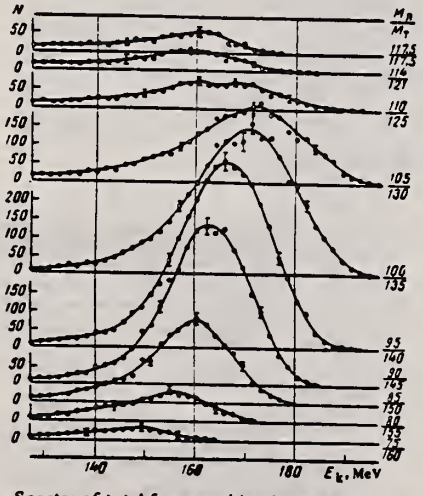

FIG. 4. Spectra of total fragment kinetic energy for different mass ratios.

REF.

K. A. Petrzhak and G. A. Tutin
Yad. Fiz. 9, 949 (1969)
Sov. J. Nucl. Phys. 9, 556 (1969)

ELEM. SYM.	A	Z
U	235	92

METHOD

REF. NO. 69 Pe 1 egf

REACTION	RESULT	EXCITATION ENERGY	SOURCE		DETECTOR		ANGLE
			TYPE	RANGE	TYPE	RANGE	
G,F	SPC	THR-12	C	12	ION-D	50-110	4PI

MASS, ENERGY SPC

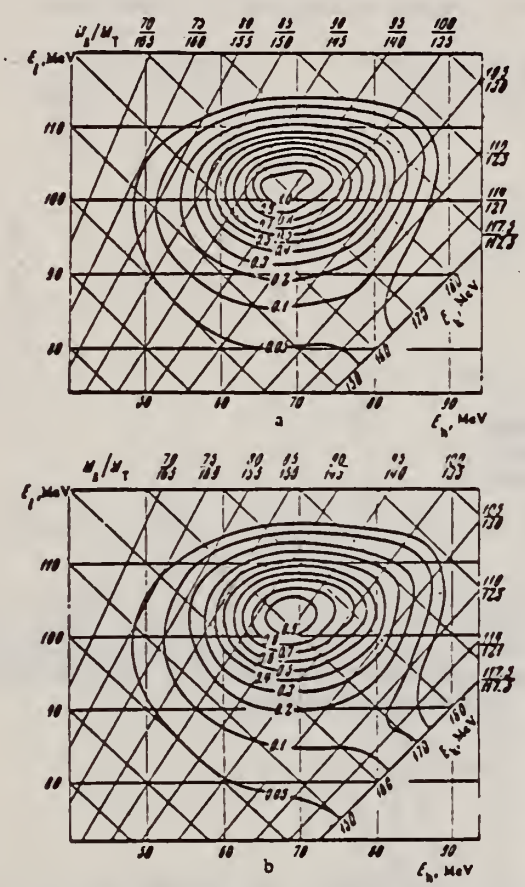

FIG. 1. Contour diagram of fragment kinetic energy distribution in the photofission of U^{235} at $E\gamma max$ = 12.1 MeV. The contour 1.0 corresponds to an event probability density 2.72 X 10^{-3} [fission-MeV^2]$^{-1}$ –a; b–E_{max} = 25 MeV (corrected data of [1]).

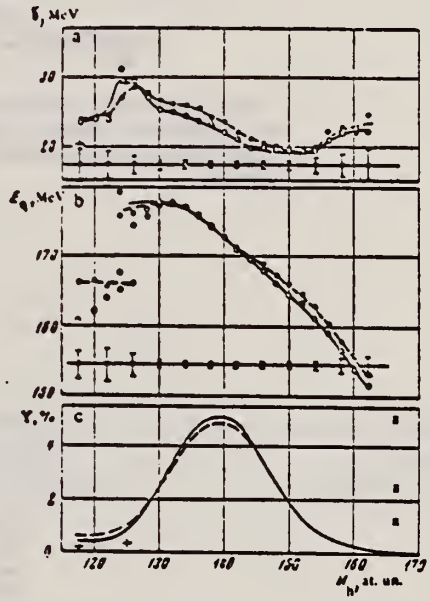

FIG. 2. Dependence of the width of the distribution of a summary kinetic energy of the fragments δ at half the height (a), of the most probable summary kinetic energy of the fragments E_q (b), and of the fragment yield Y (c) on the mass of the heavy fragment in the fission of U^{235} by bremsstrahlung with maximum energy 12.1 MeV (O) and 25 MeV (●). Only the statistical errors are indicated.

over

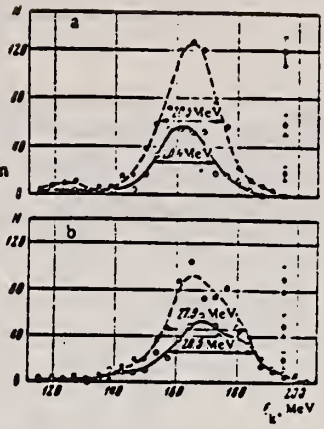

FIG. 3. Corrected distribution of the summary kinetic energy of U^{235} photofission fragments for a selected heavy-fragment mass interval: a—117.5—123 at. un., b—123—127 at. un. Points: O—$E\gamma_{max}$ = 12.1 MeV, ●—25 MeV. Statistical errors are indicated.

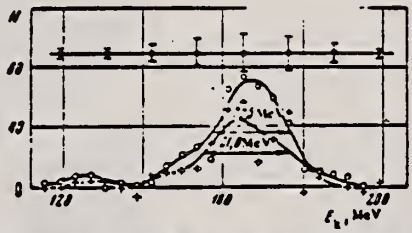

FIG. 4. Difference distributions of the summary kinetic energy of the U^{235} photofission fragments for selected heavy-fragment mass intervals: 117.5—123 at. un. (O) and 123—127 at. un. (+). The statistical errors are indicated.

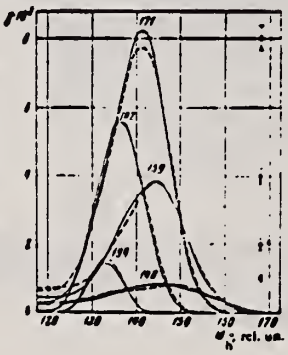

FIG. 5. Mass distributions of the U^{235} photofission fragments at $E\gamma$ max = 12.1 MeV (solid lines) and $E\gamma$ max = 25 MeV (dashed line) for selected values of the summary kinetic energy of the fragments. The corresponding values of the summary kinetic energy in MeV are indicated in the diagrams by arrows in units (fission-at. un. × 4 MeV).[10] The statistical errors are indicated.

REF.

D. C. Aumann and J. E. Gindler
J. inorg. nucl. Chem. 32, 731 (1970)

ELEM. SYM.	A	Z
U	235	92

METHOD

REF. NO. 70 Au 1 egf

REACTION	RESULT	EXCITATION ENERGY	SOURCE		DETECTOR		ANGLE
			TYPE	RANGE	TYPE	RANGE	
G,F	RLY	THR-17	C	14-17	ACT-I		4PI

Data ratio of isomer to ground state yields.

ISOMER YIELDS

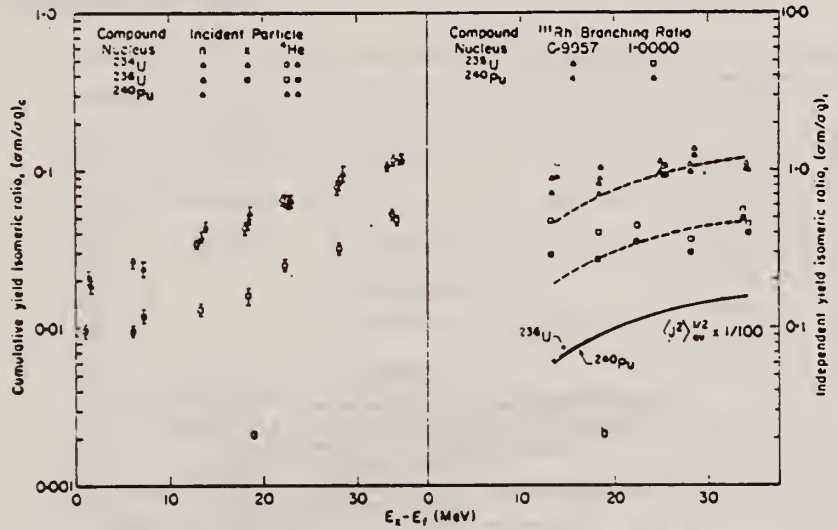

Fig. 3. Cumulative (a) and independent (b) yield ^{111}Pd isomeric ratios as a function of excitation energy above the fission barrier for several compound nuclei. The solid curves in 3b represent the root-mean-square average angular momenta of the compound nuclei indicated. The dashed curves are the solid curves displaced to pass approximately through the respective isomeric ratio data.

Table 3. Cumulative yield isomeric ratios of ^{111}Pd formed in photofission

Target	E_γ(MeV) 13·8	16·6–17·0	17·1
^{232}Th	0·0060 ± 0·0004	0·0056 ± 0·0006	
^{238}U	0·0053 ± 0·0004	0·0054 ± 0·0005	0·0066 ± 0·0007
^{236}U	0·0095 ± 0·0007		0·0119 ± 0·0012
^{235}U	0·0125 ± 0·0009	0·0130 ± 0·0013	
^{234}U	0·0261 ± 0·0019		0·0235 ± 0·0024
^{233}U	0·0304 ± 0·0022	0·0380 ± 0·0038	0·0454 ± 0·0045

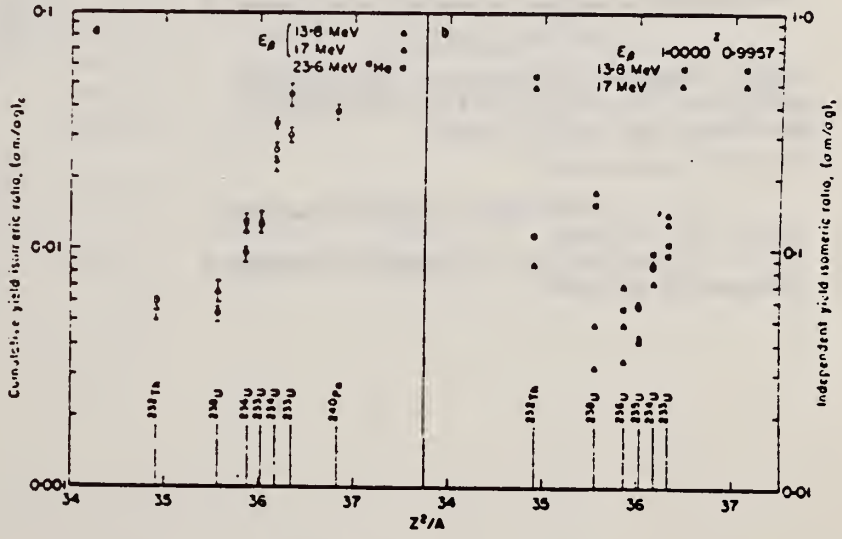

Fig. 5. Cumulative (a) and independent (b) yield ^{111}Pd isomeric ratios as a function of Z^2/A for the compound nucleus.

REF. L. A. Kull, R. L. Bramblett, T. Gozani, D. E. Rundquist
Nucl. Sci. & Eng. 39, 163 (1970)

ELEM. SYM.	A	Z
U	235	92

METHOD

REF. NO. 70 Ku 2 egf

REACTION	RESULT	EXCITATION ENERGY	SOURCE		DETECTOR		ANGLE
			TYPE	RANGE	TYPE	RANGE	
G,F	NOX	5-10	C	8,10	BF3-I		4PI

DELAYED NEUT YLDS

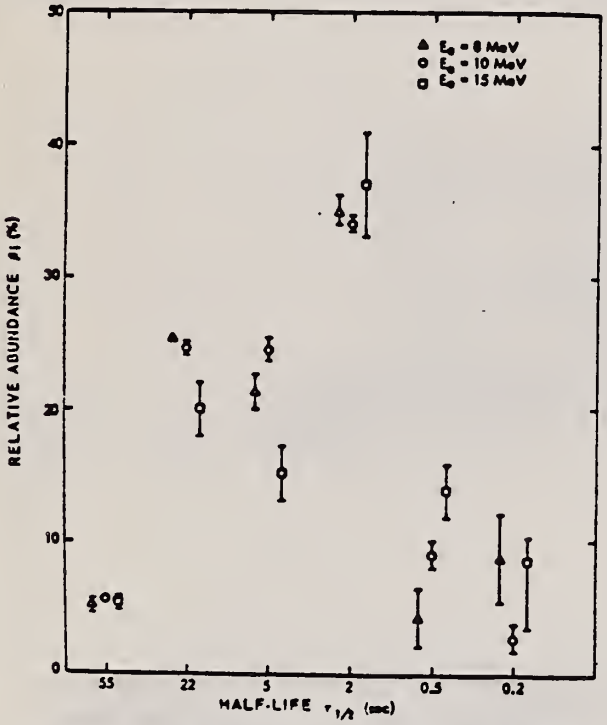

Fig. 7. Relative abundances of the delayed neutron groups (β_i) for $^{235}U(\gamma,f)$ at E_e = 8 and 10 MeV together with the data of Ref. 3 at E_e = 15 MeV.

TABLE I

Relative Abundances for the Photofission of ^{238}U and ^{235}U with Bremsstrahlung at Endpoint Energies of 8 and 10 MeV Actual Half-Lives Used in the Analyses were Taken from Ref. 4

Half-Life (sec)	Relative Abundance (percent)			
	^{238}U (8 MeV)	^{238}U (10 MeV)	^{235}U (8 MeV)	^{235}U (10 MeV)
55	2.5 ± 0.1	2.1 ± 0.1	5.2 ± 0.5	5.6 ± 0.2
20	17.3 ± 0.4	16.3 ± 0.1	25.3 ± 0.3	24.5 ± 0.5
5	17.0 ± 1.1	16.7 ± 0.3	21.3 ± 1.3	24.4 ± 0.9
2	36.1 ± 0.9	36.4 ± 0.4	35.0 ± 1.2	33.7 ± 0.5
0.6	17.9 ± 1.1	18.1 ± 1.0	4.4 ± 2.2	9.1 ± 1.0
0.2	9.2 ± 1.4	10.5 ± 1.1	8.8 ± 3.2	2.8 ± 1.1

[3] B. P. MAKSYUTENKO, *J. Exptl. Theoret. Phys.* (USSR), 135, 415 (1958).
[4] O. P. NIKOTIN, K. A. PETRZHAK, *Atomnaya Energiya*, 20, 268 (1966).

REF.

G.A. Vartapetyan, N.A. Demekhina, V.I. Kasilov, Yu. N. Ranyuk, P.V. Sorokin and A.G. Khudaverdyan
Yad. Fiz. 14, 65 (1971)
Sov. J. Nucl. Phys. 14, 37 (1972)

ELEM. SYM.	A	Z
U	235	92

METHOD

REF. NO.: 71 Va 4 egf

REACTION	RESULT	EXCITATION ENERGY	SOURCE		DETECTOR		ANGLE
			TYPE	RANGE	TYPE	RANGE	
G,F	ABX	100-999	C	100-999	TRK-I		4PI

999= 5GEV

$E_{\gamma\,max}$, MeV	Phototissue yields per cm^3 per equivalent photon					
	U^{238}	U^{235}	Th^{232}	Bi^{209}	Au^{197}	Ta^{181}
100	$(226 \pm 20) \cdot 10^{-27}$	$(120 \pm 12) \cdot 10^{-27}$	$(50 \pm 5) \cdot 10^{-27}$	$(0.70 \pm 0.08) \cdot 10^{-27}$	$(3.0 \pm 0.4) \cdot 10^{-27}$	
120				$(1.5 \pm 0.2) \cdot 10^{-27}$	$(11.0 \pm 0.2) \cdot 10^{-27}$	
140				$(2.9 \pm 0.2) \cdot 10^{-27}$	$(20 \pm 0.2) \cdot 10^{-27}$	
150	$(240 \pm 24) \cdot 10^{-27}$		$(63 \pm 7) \cdot 10^{-27}$			
160				$(3.1 \pm 0.3) \cdot 10^{-27}$	$(3.7 \pm 0.4) \cdot 10^{-27}$	
180				$(4.6 \pm 0.5) \cdot 10^{-27}$	$(5.5 \pm 0.6) \cdot 10^{-27}$	
200	$(265 \pm 30) \cdot 10^{-27}$	$(150 \pm 15) \cdot 10^{-27}$	$(72 \pm 7) \cdot 10^{-27}$	$(6.1 \pm 0.6) \cdot 10^{-27}$	$(8.2 \pm 0.8) \cdot 10^{-27}$	$(4.9 \pm 0.5) \cdot 10^{-27}$
220				$(8.3 \pm 0.8) \cdot 10^{-27}$	$(11.1 \pm 0.1) \cdot 10^{-27}$	$(8.2 \pm 0.8) \cdot 10^{-27}$
240				$(11.2 \pm 0.1) \cdot 10^{-27}$	$(15 \pm 0.2) \cdot 10^{-27}$	$(12 \pm 0.1) \cdot 10^{-27}$
215		$(156 \pm 16) \cdot 10^{-27}$				
260				$(1.5 \pm 0.2) \cdot 10^{-27}$	$(1.8 \pm 0.2) \cdot 10^{-27}$	$11.6 \pm 0.2) \cdot 10^{-27}$
280		$(160 \pm 16) \cdot 10^{-27}$	$(85 \pm 9) \cdot 10^{-27}$			
300				$(2.2 \pm 0.2) \cdot 10^{-27}$	$(2.7 \pm 0.2) \cdot 10^{-27}$	
320				$(3.5 \pm 0.4) \cdot 10^{-27}$	$(4.4 \pm 0.4) \cdot 10^{-27}$	
340				$(4.2 \pm 0.4) \cdot 10^{-27}$	$(5.0 \pm 0.5) \cdot 10^{-27}$	
360	$(318 \pm 30) \cdot 10^{-27}$	$(175 \pm 20) \cdot 10^{-27}$				
380			$(106 \pm 11) \cdot 10^{-27}$			$(7.0 \pm 0.7) \cdot 10^{-27}$
400				$(5.4 \pm 0.5) \cdot 10^{-27}$	$(6.9 \pm 0.7) \cdot 10^{-27}$	
420				$(6.7 \pm 0.7) \cdot 10^{-27}$	$(9.1 \pm 0.9) \cdot 10^{-27}$	
440		$(190 \pm 20) \cdot 10^{-27}$	$(115 \pm 12) \cdot 10^{-27}$	$(8.5 \pm 0.8) \cdot 10^{-27}$	$(10.6 \pm 1) \cdot 10^{-27}$	
460				$(9.8 \pm 0.8) \cdot 10^{-27}$	$(11.3 \pm 0.1) \cdot 10^{-27}$	
480	$(346 \pm 35) \cdot 10^{-27}$					
500				$(7.2 \pm 0.8) \cdot 10^{-27}$	$(1.4 \pm 0.1) \cdot 10^{-27}$	$(1.7 \pm 0.2) \cdot 10^{-27}$
520				$(8.5 \pm 0.9) \cdot 10^{-27}$	$(1.1 \pm 0.1) \cdot 10^{-27}$	
540						
560		$(200 \pm 20) \cdot 10^{-27}$	$(120 \pm 12) \cdot 10^{-27}$	$(8.5 \pm 0.9) \cdot 10^{-27}$	$(1.3 \pm 0.1) \cdot 10^{-27}$	
580				$(9.2 \pm 0.9) \cdot 10^{-27}$	$(1.2 \pm 0.1) \cdot 10^{-27}$	
600						$(2.4 \pm 0.2) \cdot 10^{-27}$
620				$(10.4 \pm 1) \cdot 10^{-27}$	$(1.7 \pm 0.2) \cdot 10^{-27}$	
640		$(220 \pm 22) \cdot 10^{-27}$	$(135 \pm 14) \cdot 10^{-27}$			
660	$(386 \pm 40) \cdot 10^{-27}$					
680		$(224 \pm 23) \cdot 10^{-27}$	$(140 \pm 14) \cdot 10^{-27}$			
700						$(2.9 \pm 0.3) \cdot 10^{-27}$
720				$(11.3 \pm 1.1) \cdot 10^{-27}$	$(1.9 \pm 0.2) \cdot 10^{-27}$	
740	$(410 \pm 40) \cdot 10^{-27}$					
760	$(390 \pm 40) \cdot 10^{-27}$	$(217 \pm 23) \cdot 10^{-27}$	$(136 \pm 14) \cdot 10^{-27}$			
780				$(12.5 \pm 1.3) \cdot 10^{-27}$	$(1.9 \pm 0.2) \cdot 10^{-27}$	
800						$(3.3 \pm 0.3) \cdot 10^{-27}$
820				$(13.5 \pm 1.4) \cdot 10^{-27}$	$(2.1 \pm 0.2) \cdot 10^{-27}$	
840	$(376 \pm 40) \cdot 10^{-27}$	$(193 \pm 20) \cdot 10^{-27}$	$(132 \pm 15) \cdot 10^{-27}$			
860				$(14.3 \pm 1.41) \cdot 10^{-27}$	$(2.2 \pm 0.2) \cdot 10^{-27}$	
880	$(445 \pm 45) \cdot 10^{-27}$	$(239 \pm 24) \cdot 10^{-27}$	$(155 \pm 15) \cdot 10^{-27}$			
900				$(15.3 \pm 1.4) \cdot 10^{-27}$	$(2.3 \pm 0.2) \cdot 10^{-27}$	
920				$(15.5 \pm 1.6) \cdot 10^{-27}$	$(2.2 \pm 0.2) \cdot 10^{-27}$	
940	$(491 \pm 45) \cdot 10^{-27}$	$(207 \pm 21) \cdot 10^{-27}$	$(149 \pm 14) \cdot 10^{-27}$			
960	$(435 \pm 45) \cdot 10^{-27}$	$(242 \pm 24) \cdot 10^{-27}$	$(155 \pm 16) \cdot 10^{-27}$			
980	$(479 \pm 50) \cdot 10^{-27}$	$(235 \pm 23) \cdot 10^{-27}$	$(152 \pm 15) \cdot 10^{-27}$	$(16.1 \pm 1.6) \cdot 10^{-27}$	$(3.0 \pm 0.3) \cdot 10^{-27}$	
1000	$(455 \pm 45) \cdot 10^{-27}$	$(230 \pm 23) \cdot 10^{-27}$	$(146 \pm 15) \cdot 10^{-27}$			
1020	$(498 \pm 50) \cdot 10^{-27}$	$(251 \pm 25) \cdot 10^{-27}$	$(145 \pm 15) \cdot 10^{-27}$			
1040				$(15.6 \pm 1.6) \cdot 10^{-27}$	$(3.0 \pm 0.3) \cdot 10^{-27}$	$(5.4 \pm 0.6) \cdot 10^{-27}$
1060	$(476 \pm 50) \cdot 10^{-27}$	$(264 \pm 27) \cdot 10^{-27}$	$(163 \pm 18) \cdot 10^{-27}$		$(2.9 \pm 0.3) \cdot 10^{-27}$	$(5.6 \pm 0.6) \cdot 10^{-27}$
1080	$(477 \pm 50) \cdot 10^{-27}$	$(249 \pm 25) \cdot 10^{-27}$		$(15.2 \pm 2) \cdot 10^{-27}$	$(2.8 \pm 0.3) \cdot 10^{-27}$	$(5.8 \pm 0.6) \cdot 10^{-27}$
1100	$(495 \pm 50) \cdot 10^{-27}$	$(274 \pm 28) \cdot 10^{-27}$	$(166 \pm 21) \cdot 10^{-27}$	$(15.2 \pm 2) \cdot 10^{-27}$	$(2.8 \pm 0.3) \cdot 10^{-27}$	$(6.3 \pm 0.6) \cdot 10^{-27}$

REF.

R.L. Bramblett, T. Gozani, R.O. Ginaven, D.E. Rundquist
Nucl. Technology 13, 33 (1972)

ELEM. SYM.	A	Z
U	235	92

METHOD

REF. NO. 72 Br 8 egf

REACTION	RESULT	EXCITATION ENERGY	SOURCE		DETECTOR		ANGLE
			TYPE	RANGE	TYPE	RANGE	
G,F	RLY	THR-11	C	5-11	TRK-I		4PI
G,XN	RLY	THR-11	C	5-11	BF3-I		4PI

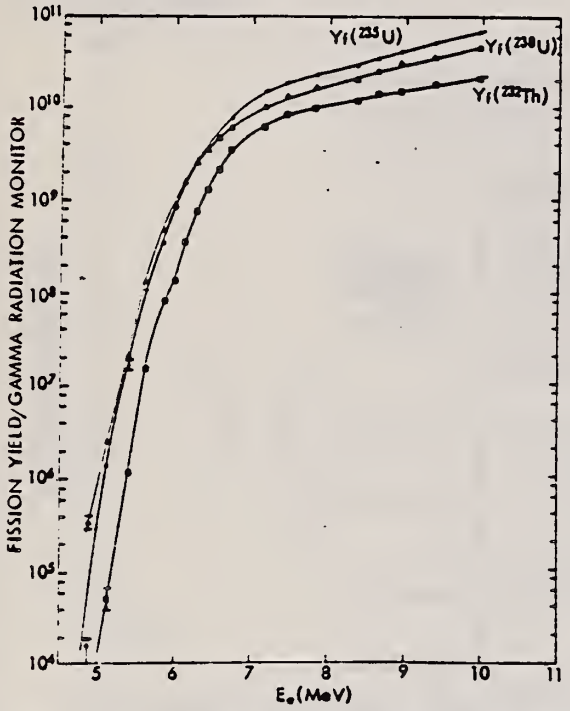

Fig. 7. Bremsstrahlung photofission yields from ^{232}Th, ^{235}U, and ^{238}U obtained using solid-state track detectors (from Gozani et al.[13]).

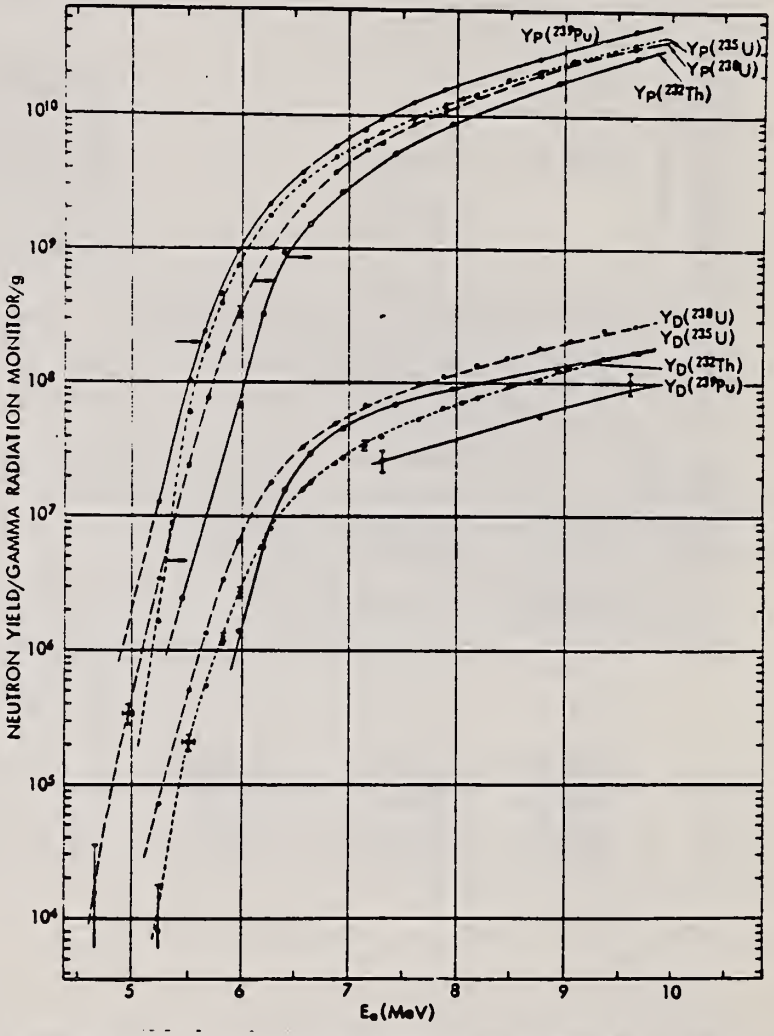

Fig. 8. Prompt- and delayed-neutron yields induced by electron bremsstrahlung for ^{232}Th, ^{235}U, ^{238}U, and ^{239}Pu.

REF.

A. M. Khan and J. W. Knowles
Nucl. Phys. A179, 333 (1972)

ELEM. SYM.	A	Z
U	235	92

METHOD

REF. NO. 72 Kh 1 egf

REACTION	RESULT	EXCITATION ENERGY	SOURCE		DETECTOR		ANGLE
			TYPE	RANGE	TYPE	RANGE	
G,F	ABX	THR-9	D	5-9	ION-I		4PI

543

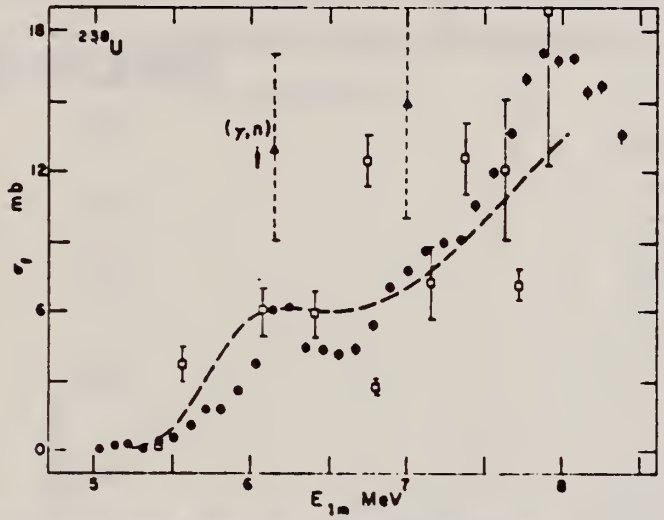

Fig. 10. Absolute photofission cross-section measurements σ_f of ^{238}U as a function of E_{1m}. The broken line represents measurements of Rabotnov *et al.*[8]); the points □ and △ are measurements of Manfredini *et al.*[7]) and Huizenga *et al.*[14]) respectively.

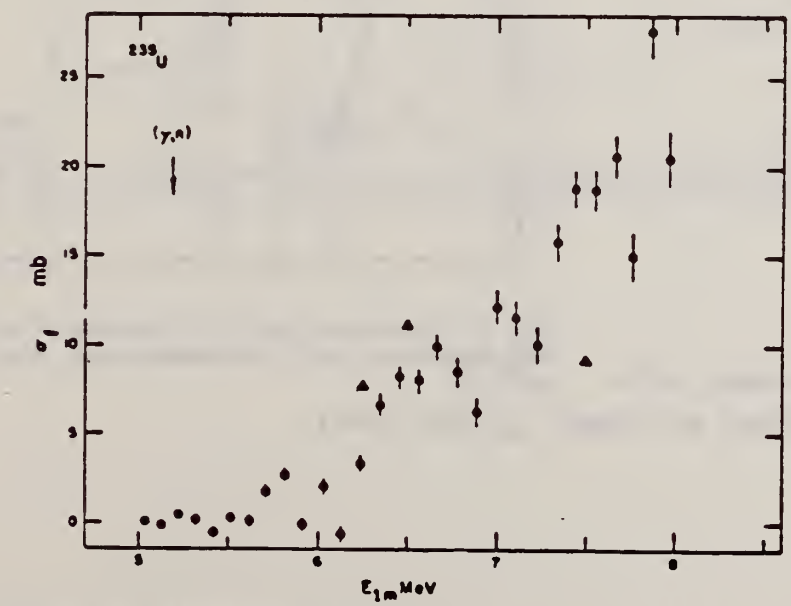

Fig. 11. Absolute photofission cross-section measurements σ_f of ^{239}U as a function of E_{1m}. The points △ are measurements of Bowman *et al.*[13]).

[7] A. Manfredini, L. Fiore, C. Ramorino, H.G. DeCarvalho & W. Wolfli, Nucl. Phys. A127 (1969) 637.

[8] N.S. Rabotnov, G.N. Smirenkin & A.S. Soldatov et al., Proc. Symp. on phys. and chem. of fission, SM 60/81, Vienna, 1965, p.135.

[13] J. R. Huizenga, K.M. Clarke, J.E. Gindler and R. Vandenbosch, Nucl. Phys. 34 (1962) 439.

[14] A.S. Soldatov, Z.A. Aleksandrova, L.D. Gordeeva & G.N. Smirenkin, Sov. J. Nucl. Phys. 1 (1965) 335.

REF. M.Ya. Kondrat'ko, V.N. Korinets, and K.A. Petrzhak
At. Energ. 35, 214 (1972)
Sov. J. At. Energy 35, 866 (1973)

ELEM. SYM.	A	Z
U	235	92

METHOD

REF. NO. 72 Ko 10 egf

REACTION	RESULT	EXCITATION ENERGY	SOURCE		DETECTOR		ANGLE
			TYPE	RANGE	TYPE	RANGE	
G,F	RLY	THR- 14	C	14	ACT-I		4PI

FISSION PROD YIELD

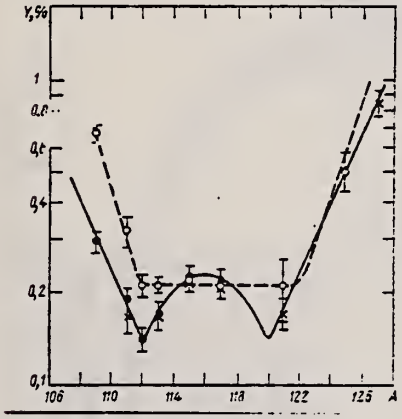

Fig. 1. Distribution of masses of fragments in the region of symmetric photofission; —●—) data of the present study; —×—) data of [9] for U^{235}; —○—) data of [1] for Np^{237}.

TABLE 1. Yields of Fragments for Photofission of U^{235} ($E_{\gamma 0}$ = 14 MeV)

Mass number	Isotope	Present study	Data from [9]
109	Pd^{109}	0,292±0,030	—
111	Ag^{111}	0,189±0,020	0,165±0,020
112	Pd^{112}	0,142±0,013	—
113	Ag^{113}	0,170±0,020	0,166±0,015
115	Cd^{115}	0,224±0,020	0,214±0,020
117	Cd^{117}	0,218±0,021	0,208±0,020*
121	Sn^{121}	—	0,169±0,020
127	Sb^{127}	—	0,87±0,05

*Value reduced to total yield of chain.

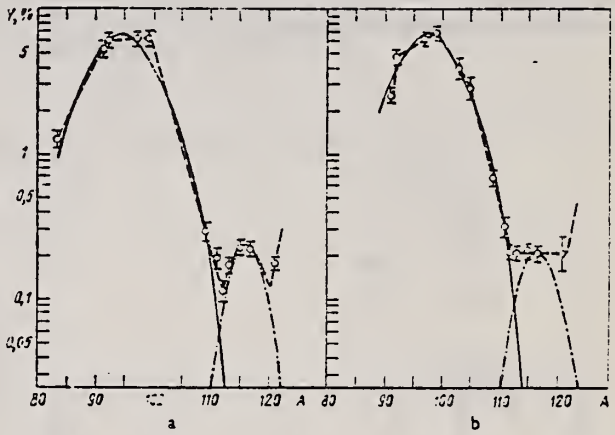

Fig. 2. Distribution curves for the yields of photofission fragments: a) U^{235} (the present study, [9]); b) Np^{237} [1].

[1] M. Ya. Kondrat'ko et al., this issue, p.862.

[9] M. Ya. Kondrat'ko and K.A. Petrzhak, At. Energ., 23, 559 (1967).

REF.

R.A. Anderl, M.V. Yester, and R.C. Morrison
Nucl. Phys. A212, 221 (1973)

ELEM. SYM.	A	Z
U	235	92

METHOD

REF. NO. 73 An 13 egf

REACTION	RESULT	EXCITATION ENERGY	SOURCE		DETECTOR		ANGLE
			TYPE	RANGE	TYPE	RANGE	
G,F	ABX	5- 8	D	5- 8	SCD-I		4PI

834

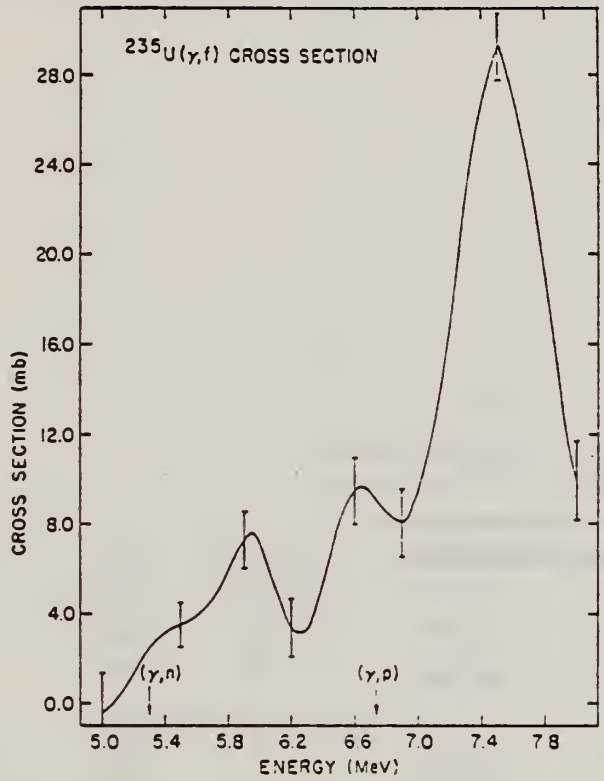

Fig. 7. The ^{235}U photofission cross section. Vertical error bars indicate uncertainty in the relative cross section. Vertical arrows near the abscissa indicate the threshold for competing reactions.

(over)

TABLE 1

Photofission cross sections of ^{238}U and ^{235}U

Energy (MeV)	^{238}U cross section (mb)	^{235}U cross section (mb)
5.0	−0.8±0.6	−0.4±1.9
5.1	−0.9±0.5	0.3±1.6
5.2	−0.9±0.4	1.4±1.3
5.3	−0.5±0.4	2.5±1.0
5.4	0.2±0.5	3.2±0.9
5.5	0.9±0.5	3.6±1.0
5.6	1.2±0.6	3.9±1.1
5.7	1.4±0.6	4.6±1.3
5.8	2.1±0.5	6.0±1.3
5.9	3.2±0.5	7.3±1.3
6.0	4.6±0.5	6.9±1.3
6.1	5.4±0.6	5.1±1.3
6.2	5.2±0.6	3.4±1.3
6.3	4.5±0.6	3.4±1.3
6.4	3.6±0.6	5.4±1.4
6.5	3.1±0.6	8.1±1.4
6.6	3.2±0.6	9.5±1.5
6.7	3.7±0.6	9.4±1.5
6.8	4.3±0.6	8.6±1.5
6.9	4.9±0.6	8.1±1.5
7.0	5.3±0.5	9.5±1.5
7.1	5.9±0.6	12.7±1.5
7.2	6.6±0.6	17.2±1.5
7.3	7.7±0.6	22.6±1.5
7.4	8.9±0.6	26.9±1.5
7.5	9.5±0.6	28.4±1.5
7.6	9.6±0.6	27.0±1.5
7.7	9.5±0.6	23.3±1.4
7.8	9.0±0.5	18.4±1.5
7.9	8.2±0.5	13.6±1.6
8.0	7.2±0.6	10.0±1.8

The relative errors only are given. The ±30% error in the absolute scale has not been included.

REF. J.T. Caldwell, G.M. Worth, and E.J. Dowdy
PICNS-73, Vol.I, p.o51 Asilomar

ELEM. SYM.	A	Z
U	235	92

METHOD

REF. NO. 73 Ca 2 hmg

REACTION	RESULT	EXCITATION ENERGY	SOURCE		DETECTOR		ANGLE
			TYPE	RANGE	TYPE	RANGE	
G,N	NOX	THR- 12	C	8- 12	BF3-I		4PI
G,F	NOX	THR- 12	C	8- 12	BF3-I		4PI

TABLE I

Low Energy Photoneutron and Photofission Parameters Deduced from this Experiment

Isotope	E_c (MeV)	Prompt $\bar{\nu}$	Γ_n / Γ_f	Delayed Neutrons Per Photofission
^{238}U	8	2.603±.094	1.765±.136	0.0355±.0015
^{238}U	10	2.861±.037	2.813±.161	0.0308±.0023
^{238}U	12	3.087±.079	3.250±.150	0.0319±.0048
^{235}U	8	2.675±.093	1.061±.103	0.0101±.0011
^{235}U	10	2.936±.085	1.161±.087	0.0121±.0017
^{235}U	12	3.086±.079	1.224±.079	0.0110±.0020
^{232}Th	8	2.091±.112	1.086±.147	0.0324±.0017
^{232}Th	10	1.980±.115	4.017±.266	0.0309±.0019
^{232}Th	12	2.226±.113	6.784±.577	0.0292±.0038
^{239}Pu	10	3.603±.033	----------	----------
^{239}Pu	12	3.738±.075	0.7±0.4	----------

REF.

K. N. Ivanov, Yu. A. Solov'ev and K. A. Petrzhak
ZhETF Pis. Red. 17, 610 (1973)
JETP Letters (USSR) 17, 429 (1973)

ELEM. SYM.	A	Z
U	235	92

METHOD

REF. NO.: 73 Iv 5 | hmg

REACTION	RESULT	EXCITATION ENERGY	SOURCE TYPE	SOURCE RANGE	DETECTOR TYPE	DETECTOR RANGE	ANGLE
G,F	RLX	THR- 15	D	THR- 15	TRK-I		DST

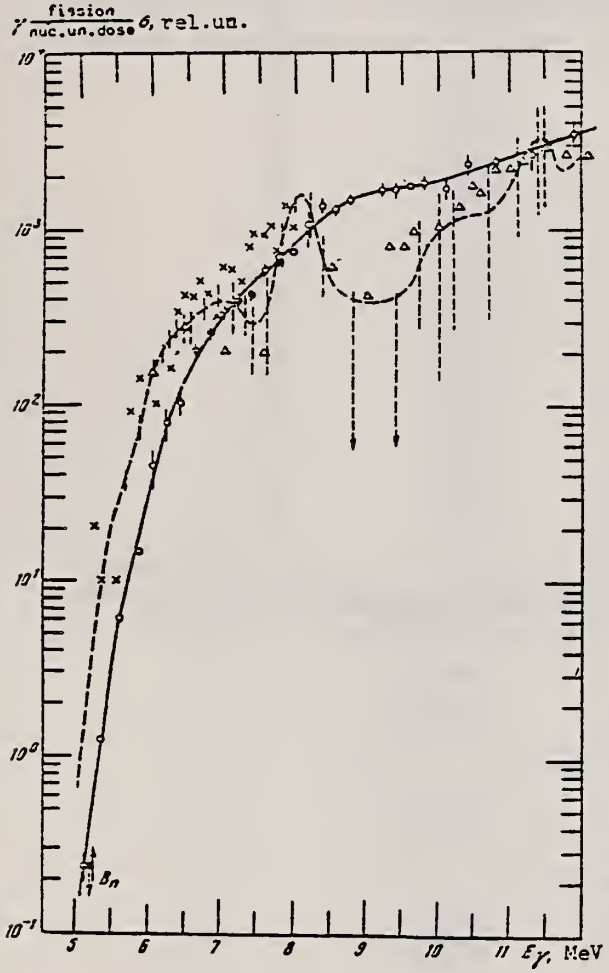

Fig. 1. Circles – energy dependence of total photofission yield of U^{235}; dashed – energy dependence of photofission cross section $\sigma_{\gamma f}$; the crosses and triangles show the results of [3] and [2], respectively; the arrow denotes the neutron detachment energy

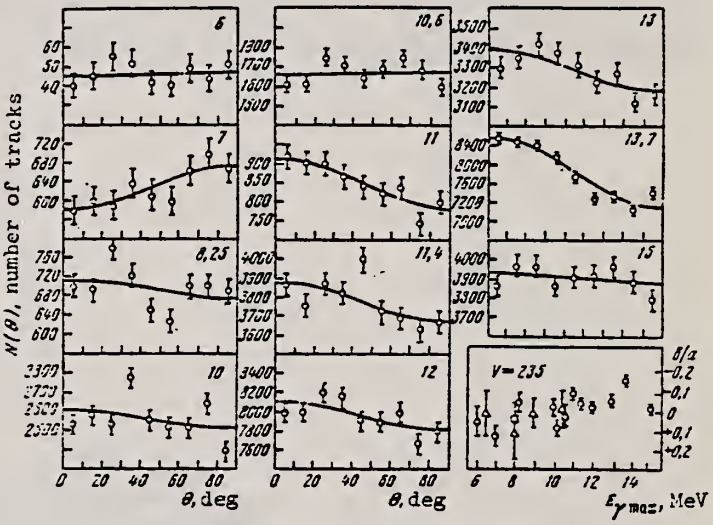

Fig. 2. Angular distributions of the U^{235} fission fragments and of the values of b/a. The numbers on the plots show the maximum bremsstrahlung energy. The squares and triangles denote the data of [8] and [9], respectively.

2) A.M. Khan et al., Nucl. Phys. A119, 333 (1972).
3) C. D. Bowman et al., Phys. Rev. B133, 676 (1964).
8) A.P. Baerg et al., Can. J. Phys. 37, 1418 (1959).
9) E.J. Winhold et al., Phys. Rev. 103, 990 (1956).

REF.	David E. Rundquist PICNS-73, Vol.I, p.619 Asilomar	ELEM. SYM.	A	Z
		U	235	92
METHOD		REF. NO.		
		73 Ru 1		hmg

REACTION	RESULT	EXCITATION ENERGY	SOURCE		DETECTOR		ANGLE
			TYPE	RANGE	TYPE	RANGE	
G,XN	RLY	THR- 10	C	5- 10	BF3-I		4PI

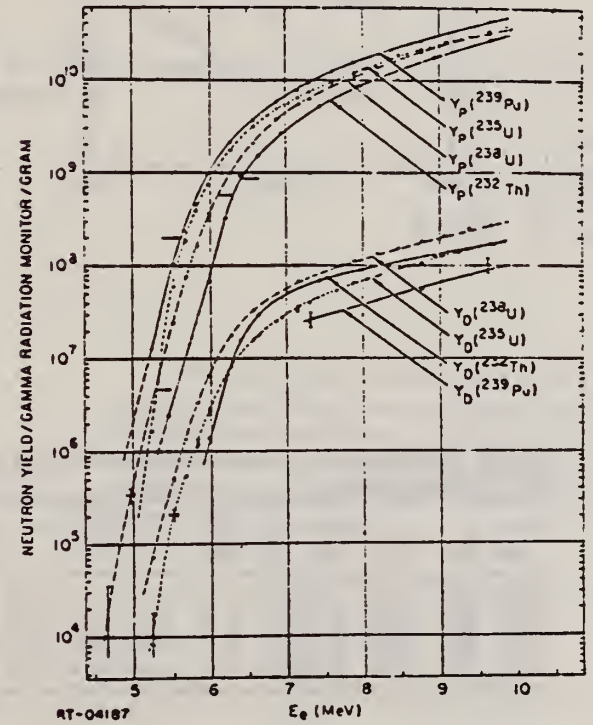

Fig. 1. Prompt and delayed neutron yields in fissile and fertile material produced by bremsstrahlung from electrons of energy E_e

REF. G.M. Gurevich, L.E. Lazareva, V.M. Mazur, and G.V. Solodukhov
ZhETF Pis. Red. 20, 741 (1974)
JETP Lett. 20, 343 (1974)

ELEM. SYM.	A	Z
U	235	92

METHOD

REF. NO.	
74 Gu 11	hmg

REACTION	RESULT	EXCITATION ENERGY	SOURCE		DETECTOR		ANGLE
			TYPE	RANGE	TYPE	RANGE	
G,MU-T	ABX	7- 24	C	35	NAI-D		4PI

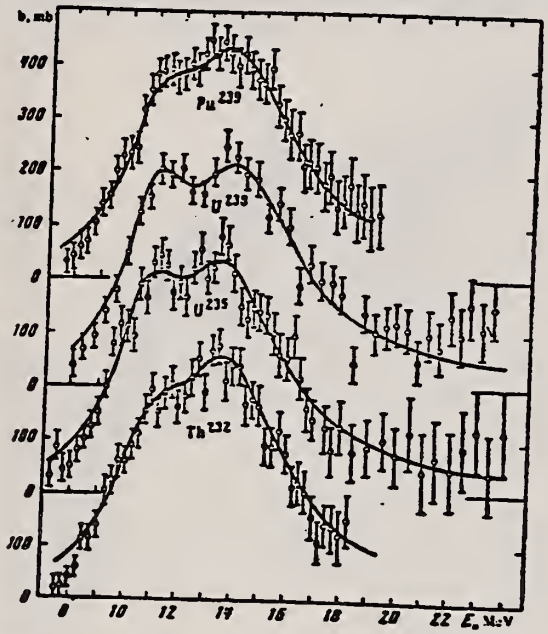

FIG. 1.

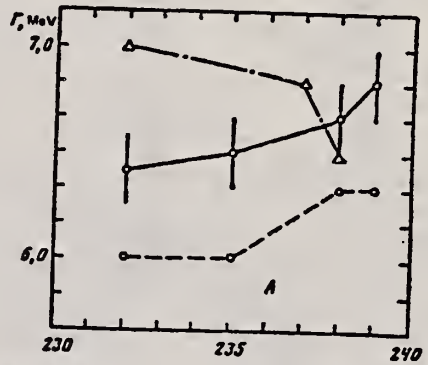

FIG. 2.

TABLE. Parameters for the approximation of the cross section by Lorentz lines.

Nucleus	σ_1 mb	Γ_1 MeV	E_1 MeV	σ_2 mb	Γ_2 MeV	E_2 MeV	$\frac{\sigma_2\Gamma_2}{\sigma_1\Gamma_1}$	β	Q
Th^{232}	247	3.90	10.99	362	4.67	13.9	1.75	0.28	10.0
U^{235}	283	3.23	10.74	354	4.92	13.77	1.91	0.30	11.0
U^{238}	286	2.99	10.97	351	5.10	14.25	2.09	0.31	11.7
Pu^{239}	227	3.47	11.05	362	5.23	14.01	2.40	0.29	11.0

REF. K.N. Ivanov and K.A. Petrzhak
At. Energ. 36, 404 (1974)
Sov. J. At. Energy 36, 515 (1974)

ELEM. SYM.	A	Z
U	235	92

METHOD

REF. NO. 74 Iv 2 egf

REACTION	RESULT	EXCITATION ENERGY	SOURCE		DETECTOR		ANGLE
			TYPE	RANGE	TYPE	RANGE	
G,F	RLY	5- 12	C	5- 12	TRK-I		4PI

YIELD REL U-238

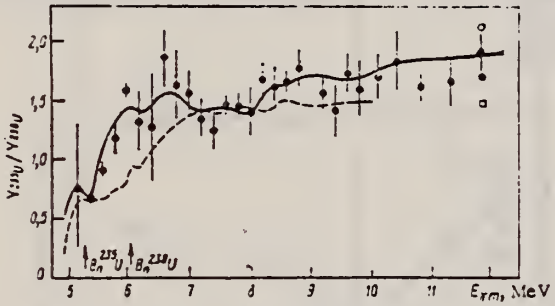

Fig. 2

Fig. 2. Relative photofissility of ^{235}U: ●) present work; □, C, – – –) data from [4, 5, 7], respectively.

4. J. McElhinney and W. Ogle, Phys. Rev., 81, 342 (1951).
5. J. Huizenga et al., Phys. Rev., 95, 1009 (1954).
6. A. Manfredini, Nuovo Cimento, 4A, No. 2, 421 (1971).
7. T. Gozani, Atomkernenergie, 19, 63 (1972).

The curves for the relative photofission yield functions $Y_i(E_{\gamma m})/Y_{^{235}U}(E_{\gamma m})$ were obtained from experimental ratios by least-square analysis. This method of analysis smooths out observed structure but maxima are seen in the curves (with an accuracy of ±0.16 MeV) at the following values of maximum bremsstrahlung energy:

Nucleus	Position of Maximum, MeV
^{232}Th	5.3; 6.3; 6.6; 7.5; 10.8.
^{235}U	5.1; 6.6; 8.4.
^{237}Np	5.5; 6.0; 7.1; 8.35; 9.8.
^{239}Pu	6.5.

REF. J.T. Caldwell and E.J. Dowdy
Nucl. Sci. & Eng. 56, 179 (1975)

ELEM. SYM.	A	Z
U	235	92

METHOD

REF. NO. 75 Ca 5 egf

REACTION	RESULT	EXCITATION ENERGY	SOURCE		DETECTOR		ANGLE
			TYPE	RANGE	TYPE	RANGE	
G,F	NOX	6- 13	C	8- 13	MOD-I		4PI

The prompt- and delayed-neutron multiplicities for photofission of the eight isotopes, ^{232}Th, ^{233}U, ^{234}U, ^{235}U, ^{236}U, ^{238}U, ^{237}Np, and ^{239}Pu, have been measured using bremsstrahlung with end-point energies ranging from 8 to 13 MeV. The measured multiplicities are compared with those from the same compound nucleus formed in neutron-induced fission where such data exist.

NEUTRON MULTIPLICITIES

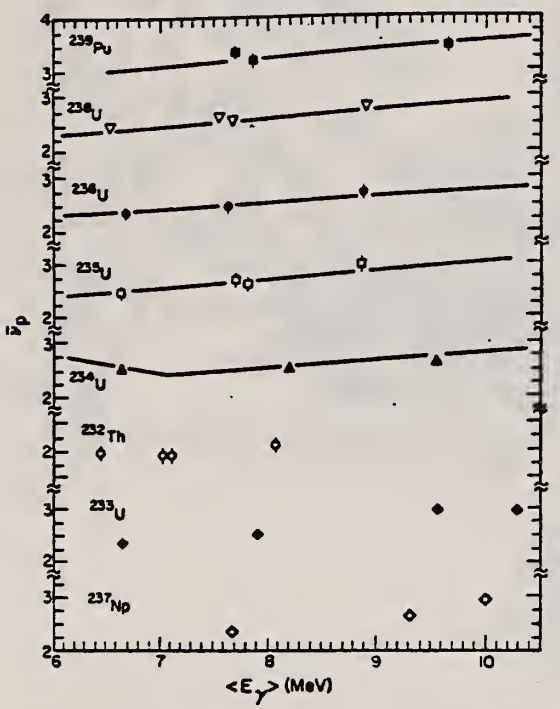

Fig. 5. $\bar{\nu}_p$ versus excitation energy for the eight isotopes studied in this experiment. The full curves shown are from the evaluations of Davey[2] with the excitation energy determined as described in the text. For the lower three isotopes shown, no previous experimental values for $\bar{\nu}_p$ exist.

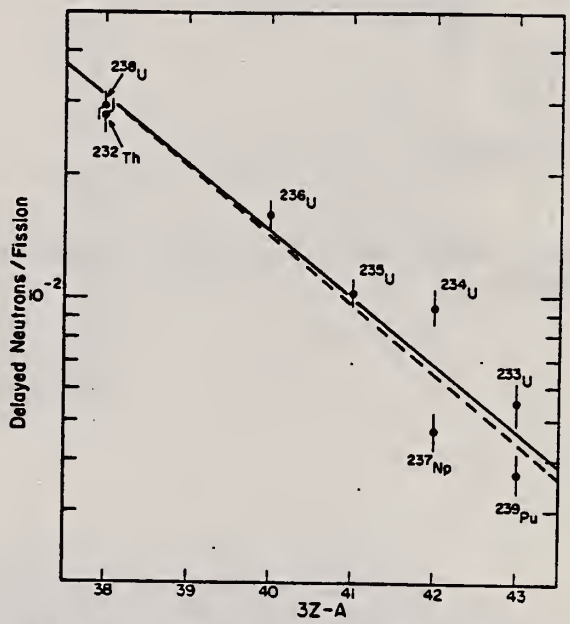

Fig. 6. Delayed neutrons per fission versus the parameter 3Z-A of the compound nucleus. The full curve shown is the least-squares fit to the data shown with ln Y_0 = 10.61, K = -0.372. The dashed curve is the least-squares fit to the data provided by Tomlinson[6] with ln Y_0 = 11.35, K = -0.39.

TABLE IV

Least-Squares Linear Fit Expressions for $\bar{\nu}_p(\langle E_\gamma \rangle)$

Isotope	$\bar{\nu}_p(\langle E_\gamma \rangle) = \bar{\nu}_0 + d\bar{\nu}_p/dE \langle E_\gamma \rangle$	Correlation Coefficient
^{232}Th	$\bar{\nu}_p(\langle E_\gamma \rangle) = 1.310 + 0.090 \langle E_\gamma \rangle$	0.675
^{233}U	$\bar{\nu}_p(\langle E_\gamma \rangle) = 1.200 + 0.1709 \langle E_\gamma \rangle$	0.947
^{234}U	$\bar{\nu}_p(\langle E_\gamma \rangle) = 2.222 + 0.0399 \langle E_\gamma \rangle$	0.741
^{235}U	$\bar{\nu}_p(\langle E_\gamma \rangle) = 0.9034 + 0.2292 \langle E_\gamma \rangle$	0.967
^{236}U	$\bar{\nu}_p(\langle E_\gamma \rangle) = 1.140 + 0.1788 \langle E_\gamma \rangle$	0.986
^{238}U	$\bar{\nu}_p(\langle E_\gamma \rangle) = 1.502 + 0.1458 \langle E_\gamma \rangle$	0.984
^{237}Np	$\bar{\nu}_p(\langle E_\gamma \rangle) = 0.4027 + 0.2505 \langle E_\gamma \rangle$	0.967
^{239}Pu	$\bar{\nu}_p(\langle E_\gamma \rangle) = 2.526 + 0.0930 \langle E_\gamma \rangle$	0.777

[2] W.G. Davey, Nucl. Sci. Eng., 44, 345 (1971)

[6] L. Tomlinson, "Delayed Neutrons from Fission: A Compilation and Evaluation of Experimental Data," AERE-R-6993, Atomic Energy Research Establishment, Harwell (1972)

TABLE III

Prompt- and Delayed-Neutron Yields

	E_n, MeV	$\langle E_\gamma \rangle$, MeV	$\bar{\nu}_p$	Delayed Neutrons per 100 Fissions
^{232}Th	8	6.44	1.96 ± 0.11	3.10 ± 0.28
(σ = 1.15 ± 0.05)	10	7.02	1.89 ± 0.11	3.06 ± 0.31
	10.2	7.10	1.89 ± 0.11	2.67 ± 0.21
	12	8.06	2.08 ± 0.11	2.59 ± 0.31
				av = 2.80 ± 0.28
^{233}U	8	6.68	2.350 ± 0.112	0.455 ± 0.040
(σ = 1.25 ± 0.05)	10	7.90	2.498 ± 0.108	0.518 ± 0.040
	12	9.55	2.960 ± 0.096	0.640 ± 0.044
	13	10.27	2.870 ± 0.099	0.598 ± 0.051
				av = 0.553 ± 0.044
^{234}U	8	(6.67)[a]	2.536 ± 0.112	---
(σ = 1.13 ± 0.05)	10	8.69	2.499 ± 0.107	0.92 ± 0.06
	12	9.54	2.623 ± 0.105	0.97 ± 0.12
				av = 0.94 ± 0.094
^{235}U	8	6.67	2.456 ± 0.086	0.90 ± 0.08
(σ = 1.20 ± 0.05)	10	7.70	2.697 ± 0.081	0.88 ± 0.08
	10.2	7.81	2.612 ± 0.079	1.13 ± 0.07
	12	8.86	2.963 ± 0.072	1.12 ± 0.08
				av = 1.02 ± 0.08
^{236}U	8	6.66	2.357 ± 0.111	1.43 ± 0.14
(σ = 1.20 ± 0.05)	10	7.63	2.470 ± 0.105	1.73 ± 0.12
	12	8.86	2.744 ± 0.095	1.64 ± 0.10
				av = 1.60 ± 0.13
^{238}U	8	6.53	2.457 ± 0.088	3.06 ± 0.24
(σ = 1.22 ± 0.05)	10	7.54	2.628 ± 0.083	2.76 ± 0.17
	10.2	7.66	2.585 ± 0.082	3.06 ± 0.14
	12	8.88	2.802 ± 0.078	2.75 ± 0.19
				av = 2.91 ± 0.20
^{237}Np	10	7.68	2.35 ± 0.11	0.38 ± 0.04
(σ = 1.20 ± 0.05)	12	9.31	2.65 ± 0.10	0.50 ± 0.04
	13	9.92	2.95 ± 0.10	0.54 ± 0.04
				av = 0.47 ± 0.04
^{239}Pu	10	7.69	3.32 ± 0.08	---
(σ = 1.18 ± 0.10)	10.2	7.84	3.17 ± 0.14	0.37 ± 0.04
	12	9.65	3.43 ± 0.10	0.37 ± 0.04
				av = 0.37 ± 0.04

[a]Estimated value.

REF.	ELEM. SYM.	A	Z
G. M. Gurevich, L. E. Lazareva, V. M. Mazur, G. V. Solodukhov, B. A. Tulupov Nucl. Phys. A273, 326 (1976)	U	235	92

METHOD	REF. NO.
	76 Gu 2 egf

REACTION	RESULT	EXCITATION ENERGY	SOURCE		DETECTOR		ANGLE
			TYPE	RANGE	TYPE	RANGE	
G,MUT	ABX	7- 24	C	UKN	NAI-D		4PI

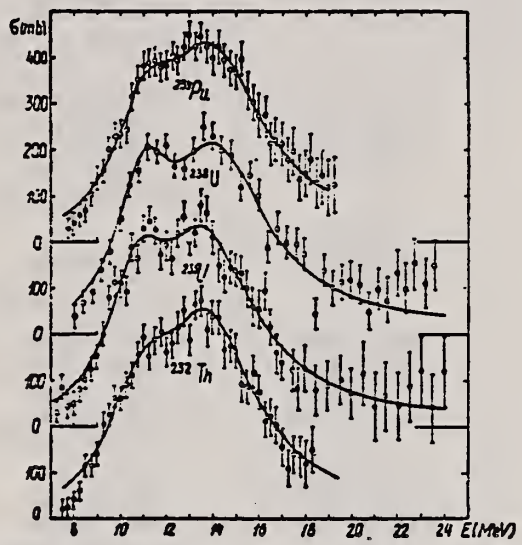

Fig. 2. Total photoabsorption cross sections for ^{232}Th, ^{235,238}U and ^{239}Pu and their respective best two Lorentz line fits.

TABLE 1

Lorentz line parameters for ^{232}Th, ^{235,238}U and ^{239}Pu

Nucleus	E_1 (MeV)	σ_1 (mb)	Γ_1 (MeV)	E_2 (MeV)	σ_2 (mb)	Γ_2 (MeV)
^{232}Th	10.99±0.16	247±26	3.90±0.4	13.9 ±0.13	362±26	4.67±0.38
^{235}U	10.74±0.18	283±39	3.23±0.55	13.77±0.23	354±33	4.92±0.58
^{238}U	10.97±0.13	286±30	2.99±0.48	14.25±0.18	351±25	5.10±0.63
^{239}Pu	11.05±0.13	227±39	3.47±0.57	14.01±0.21	362±31	5.23±0.59

TABLE 2

Deformation parameters and quadrupole moments for ^{232}Th, ^{235,238}U and ^{239}Pu

Nucleus	β_{exp}	$\bar{\beta}$	Q_0 (b)		
			this work	refs. [5,6])	ref. [14])
^{232}Th	0.28±0.03	0.274	10.0±0.8	10.2±1	9.66±0.1
^{235}U	0.30±0.03	0.285	11.0±0.9	12.8±1.3	11.12±0.2
^{238}U	0.31±0.03	0.300	11.7±0.9	11 ±1	11.3 ±0.1
^{239}Pu	0.29±0.03	0.302	11.0±0.9		11.02±0.3

(over)

TABLE 3

Integrated cross sections and mean energies of the dipole absorption

Nucleus	σ_0 (MeV · b)	σ_{-1} (mb)	σ_{-2} (mb · MeV^{-1})	$\bar{E}$ (MeV)	E_H (MeV)	E_M (MeV)	E^* (MeV)
^{232}Th	2.92 ± 0.32	231 ± 24	19 ± 2	13.08	12.64	12.40	12.16
^{235}U	2.99 ± 0.39	238 ± 31	20 ± 2.5	12.91	12.56	12.23	11.90
^{238}U	2.95 ± 0.29	229 ± 22	18 ± 1.8	13.34	12.83	12.80	12.72
^{239}Pu	2.97 ± 0.34	232 ± 26	19 ± 2	13.28	12.80	12.50	12.21

In table 3 various integrated cross sections are defined by the relations

$$\sigma_0 = \int_8^{18} \sigma_{tot}(E)\mathrm{d}E, \qquad \sigma_{-1} = \int_8^{18} \frac{1}{E}\sigma_{tot}(E)\mathrm{d}E, \qquad \sigma_{-2} = \int_8^{18} \frac{1}{E^2}\sigma_{tot}(E)\mathrm{d}E.$$

TABLE 4

Comparison of various integrated cross sections for ^{232}Th, ^{235,238}U and ^{239}Pu

	^{232}Th	^{235}U	^{238}U	^{239}Pu
σ_{0L} (MeV · b)	4.17	4.17	4.16	4.21
0.06 NZ/A (MeV · b)	3.31	3.36	3.39	3.42
$\sigma_0/(0.06\ NZ/A)$	0.88 ± 0.1	0.89 ± 0.12	0.87 ± 0.09	0.87 ± 0.1
$\sigma_{0L}/(0.06\ NZ/A)$	1.26	1.24	1.23	1.23
$\sigma_2\Gamma_2/\sigma_1\Gamma_1$	1.75	1.91	2.09	2.40
σ_{-1L} (mb)	294	298	288	289
$\sigma_{-1L}/A^{4/3}$	0.21	0.21	0.20	0.20
σ_{-2L} (mb · MeV^{-1})	26.3	26.9	25.0	25.3
$\sigma_{-2L} \times 10^3/A^{5/3}$	3.00	3.01	2.74	2.76

[5] C. D. Bowman et al., Phys. Rev. 133 (1964) B676

[6] A. Veyssiere et al., Nucl. Phys. A199 (1973) 45

[14] K.E.G. Lobner et al., Nucl. Data Tables 7 (1970) 495

REF. A.C. Shotter, J.M. Reid, J.M. Hendry, D. Branford, J.C. McGeorge, J.S. Barton
J. Phys. G: Nucl. Phys. 2, 769 (1976)

ELEM. SYM.	A	Z
U	235	92

METHOD

REF. NO. 76 Sh 12 hg

REACTION	RESULT	EXCITATION ENERGY	SOURCE		DETECTOR		ANGLE
			TYPE	RANGE	TYPE	RANGE	
E,F	RLY	THR-120	D	30-120	SCD-D		90

Abstract. Measurements are presented for the mass and energy distributions of fragments from the fission of ^{235}U and ^{238}U, induced by electrons in the energy range 30–120 MeV. Solid state detectors were used to detect the fragments. Both the mass and energy distributions suggest that the fission process has two distinct components. The change in the distributions for different electron energies indicate that the components are associated with different regions of excitation energy in the fissioning nucleus.

NUCLEAR REACTIONS, FISSION ^{235}U(e,F), ^{238}U(e,F), E = 30, 50, 115 MeV; FF coin; measured $\sigma(E;E_F,M_F)$. Enriched targets, semiconductor detectors.

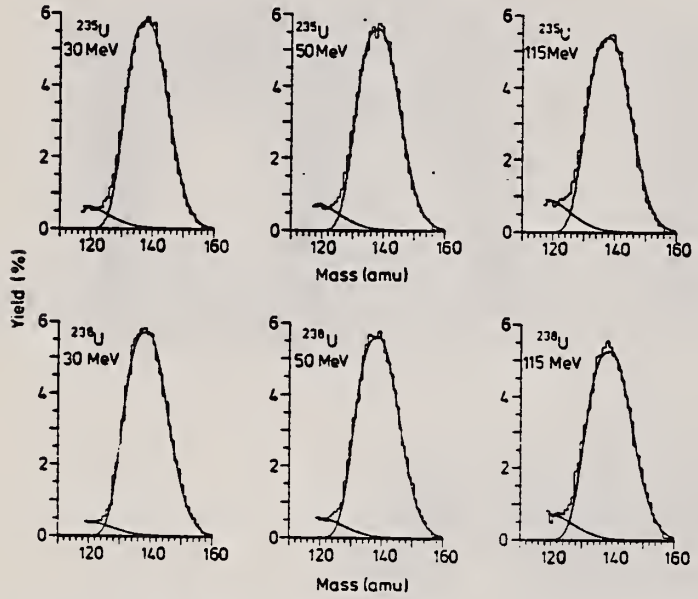

Figure 2. Mass yields for ^{235}U and ^{238}U at 30, 50 and 115 MeV electron energies. Histograms show experimental yields; curves are least-squares fits determining the division of fission into two components. Only the heavy fragment masses are shown.

(over)

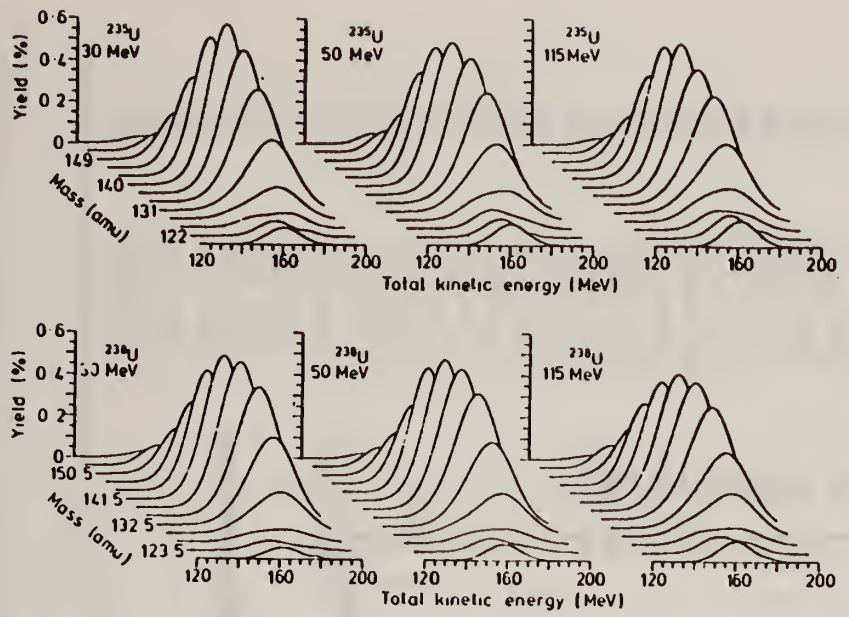

Figure 4. Total kinetic energy yields for ^{235}U and ^{238}U at 30, 50 and 115 MeV electron energies. Curves are least-squares fits to yields for heavy fragment masses in bins of 3 amu. The lowest curve in each set corresponds to symmetric mass division.

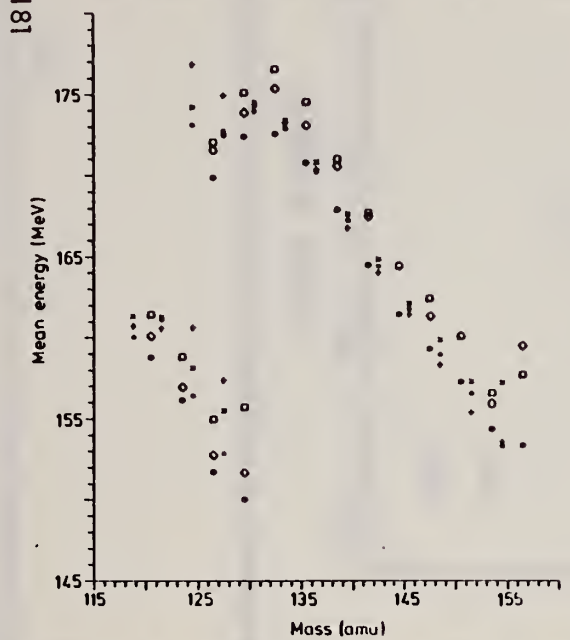

Figure 7. Mean energies of symmetric and asymmetric modes of fission versus heavy fragment mass for ^{235}U and ^{238}U at 30, 50 and 115 MeV electron energies. ●, ^{235}U(30 MeV); +, ^{235}U(50 MeV); ×, ^{235}U(115 MeV); □, ^{238}U(30 MeV); •, ^{238}U(50 MeV); ◇, ^{238}U(115 MeV).

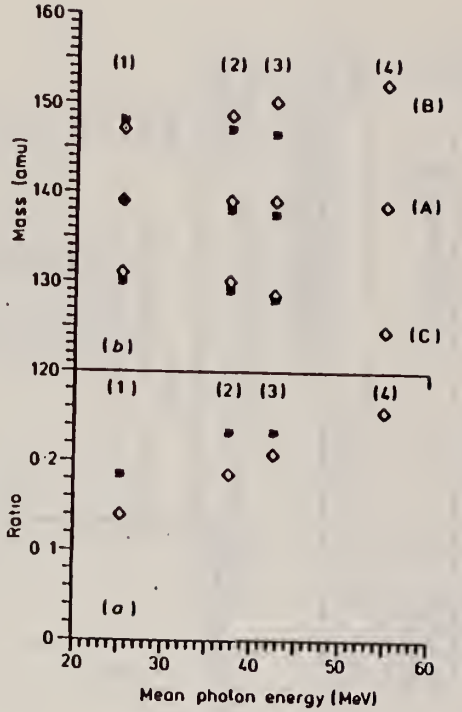

Figure 8. (*a*) Ratio of peak symmetric mass yields to peak asymmetric mass yield against mean photon energy. The data points shown correspond to the difference spectra (1) 50 MeV − 30 MeV; (2) 115 MeV − 30 MeV; (3) 115 MeV − 50 MeV; (4) (115 MeV − 50 MeV) − (50 MeV − 30 MeV). (*b*) (A), mass values of maximum fission yields for the heavy fragment. (B) and (C), mass values corresponding to half of the maximum yields for same difference spectra as (*a*). •, ^{235}U; ◇, ^{238}U.

REF. H. Thierens, D. De Frenne, E. Jacobs, A. De Clercq, P. D'hondt, A. J. Deruytter
Phys. Rev. C14, 1058 (1976)

ELEM. SYM.	A	Z
U	235	92

METHOD

REF. NO. 76 Th 1 hmg

REACTION	RESULT	EXCITATION ENERGY	SOURCE		DETECTOR		ANGLE
			TYPE	RANGE	TYPE	RANGE	
G,F	RLY	THR- 25	C	25	ACT-I		4PI

FISSION PROD YIELD

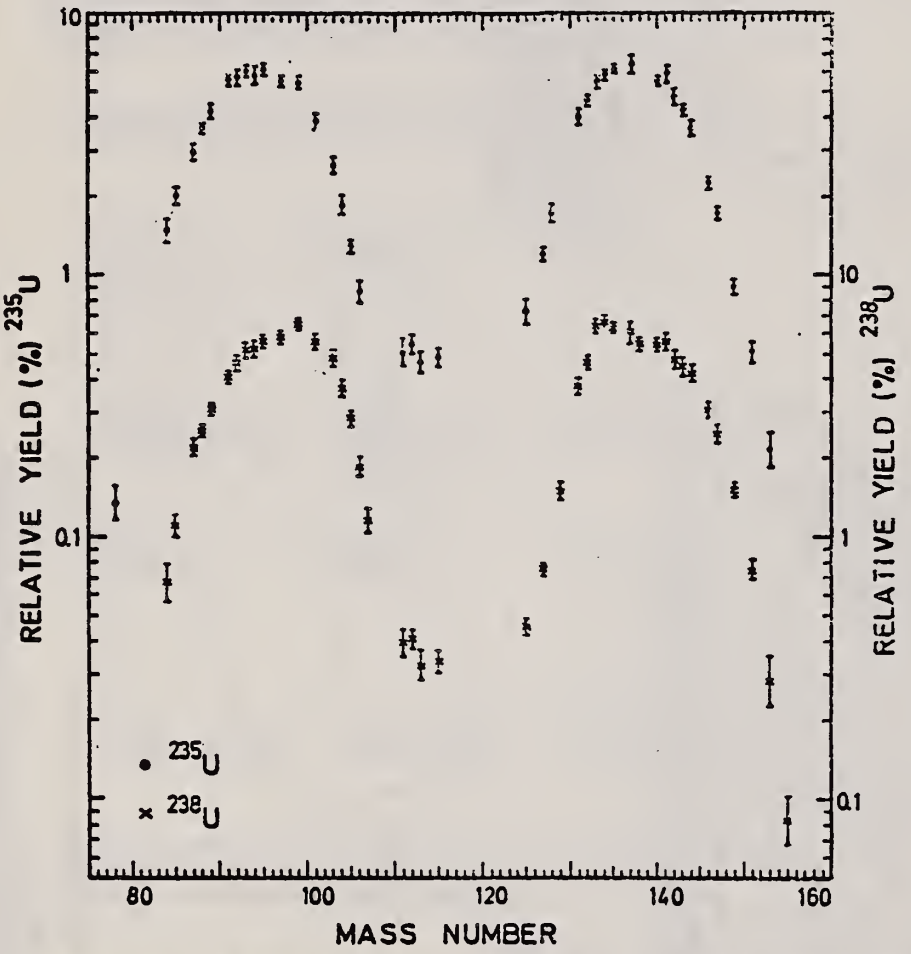

FIG. 1. Postneutron mass distributions for the photofission of ^{235}U and ^{238}U with 25-MeV bremsstrahlung.

(over)

TABLE VII. Independent isomeric yield ratios in fission.

Target	Projectile	Projectile energy (MeV)	Isomeric pair	Spin	$\frac{\sigma_m}{\sigma_m+\sigma_g}$	Ref.
^{233}U	γ (bremsstrahlung)	16	$^{134}Cs^m$-$^{134}Cs^g$	8-4	0.43	37
	n	Thermal	$^{131}Te^m$-$^{131}Te^g$	$\frac{11}{2}-\frac{3}{2}$	0.66±0.03	36
^{235}U	γ (bremsstrahlung)	25	$^{126}Sb^m$-$^{126}Sb^g$	5-8	0.53±0.05	This work
			^{128}Sb(10 min)-^{128}Sb(9 h)	5, 6, 7-8	0.45±0.09	This work
			$^{131}Te^m$-$^{131}Te^g$	$\frac{11}{2}-\frac{3}{2}$	0.58±0.06	This work
	n	Thermal	$^{131}Te^m$-$^{131}Te^g$	$\frac{11}{2}-\frac{3}{2}$	0.64±0.05	36
			$^{133}Te^m$-$^{133}Te^g$	$\frac{11}{2}-\frac{3}{2}$	0.61±0.010	36
^{238}U	γ (bremsstrahlung)	25	^{128}Sb(10 min)-^{128}Sb(9 h)	5, 6, 7-8	0.62±0.22	This work
			$^{131}Te^m$-$^{131}Te^g$	$\frac{11}{2}-\frac{3}{2}$	0.45±0.09	This work
^{239}Pu	n	Thermal	$^{131}Te^m$-$^{131}Te^g$	$\frac{11}{2}-\frac{3}{2}$	0.77±0.04	36

TABLE II. Cumulative chain yields for the photofission of ^{235}U.

Mass chain	Yield This experiment	Kondrat'ko
78	0.136±0.018	...
84	1.47 ±0.15	...
85	2.01 ±0.15	...
87	2.97 ±0.21	...
88	3.61 ±0.14	...
89	4.21 ±0.23	...
91	5.57 ±0.23	...
92	5.69 ±0.31	...
93	5.98 ±0.33	...
94	5.78 ±0.42	...
95	6.06 ±0.25	...
97	5.47 ±0.27	...
99	5.39 ±0.24	...
101	3.84 ±0.25	...
103	2.60 ±0.18	...
104	1.84 ±0.14	...
105	1.29 ±0.05	...
106	0.854±0.080	...
111	0.511±0.061	0.561±0.040
112	0.542±0.039	...
113	0.466±0.041	0.454±0.050
115	0.486±0.036	0.528±0.040
125	0.726±0.073	...
127	1.20 ±0.06	...
128	1.72 ±0.14	...
131	4.00 ±0.29	...
132	4.66 ±0.18	...
133	5.45 ±0.29	...
134	5.82 ±0.17	...
135	6.08 ±0.22	...
137	6.34 ±0.48	...
139	...	5.90 ±0.70
140	5.46 ±0.20	5.39 ±0.30
141	5.83 ±0.41	...
142	4.80 ±0.36	...
143	4.23 ±0.22	...
144	3.62 ±0.26	...
146	2.25 ±0.12	...
147	1.71 ±0.10	...
149	0.899±0.058	...
151	0.509±0.041	...
153	0.217±0.031	...

[36] D.G. Sarantites, G.E. Gordon, C.D. Coryell, Phys. Rev. 138, B353 (1965).

[37] H. Warhanek and R. Vandenbosch, J. Inorg. Chem. 26, 669 (1964).

REF. V.E. Zhuchko, Yu.B. Ostapenko, A.S. Soldatov, Yu.M. Tsipenyuk
Nucl. Inst. Meth. 136, 373 (1976)

ELEM. SYM.	A	Z
U	235	92

METHOD

REF. NO.: 76 Zh 2 hg

REACTION	RESULT	EXCITATION ENERGY	SOURCE		DETECTOR		ANGLE
			TYPE	RANGE	TYPE	RANGE	
G,F	ABX	THR-7	C	3-7	TRK-D		90

UNFOLDING SIGMA SOLUT.

Three methods for the solution of experimental subthreshold photofission yield functions for cross-sections of ^{235}U and ^{238}U in the energy range 3.6–7 MeV are presented. Comparison of the resulting cross-sections with the data obtained from reactions with monochromatic photons and charged particles is given.

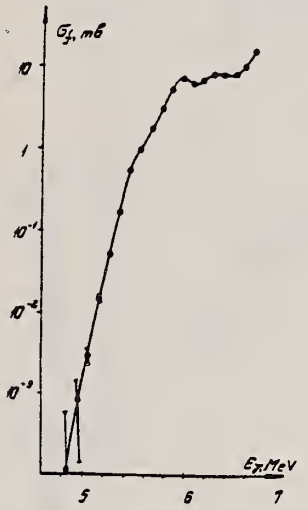

Fig. 4. The photofission cross-section of ^{235}U.

REF. B.M. Aleksandrov, A.S. Krivokhatskii, V.L. Kuznetsov, L.E. Lazareva, V.G. Nedorezov, N.V. Nikitina, Yu.N. Ranyuk
Yad. Fiz. 28, 1165 (1978)
Sov. J. Nucl. Phys. 28, 600 (1978)

ELEM. SYM.	A	Z
U	235	92

METHOD

REF. NO. 78 A1 5 hg

REACTION	RESULT	EXCITATION ENERGY	SOURCE TYPE	SOURCE RANGE	DETECTOR TYPE	DETECTOR RANGE	ANGLE
G,F	RLY	THR-999	C	100-999	TRK-D		4PI

The 300- and 2000-MeV electron linear accelerators have been used to measure the relative fissilities of the nuclei ^{235}U, ^{238}U, ^{237}Np, ^{239}Pu, ^{241}Am, and ^{243}Am. Fragments were detected by glass detectors. Photofission yields were obtained for the nuclei indicated at maximum bremsstrahlung energies 100, 240, 400, and 1200 MeV.

999=1.2 GEV

PACS numbers: 25.85.Jg

TABLE I. Relative photofission yields for $E_{\gamma max}$ = 100, 240, 400, and 1200 MeV.

Nucleus	Fissility of nuclei in the excitation-energy range ~5–12 MeV: $D_f = \Gamma_f/(\Gamma_f + \Gamma_n)$	Fissility of nuclei in the excitation-energy range ~5–12 MeV: Relative fissility	Ratio of fragment yields $Y/Y(^{238}U)$ for different maximum energies $E_{\gamma max}$: 100 MeV	240 MeV	400 MeV	1200 MeV
^{235}U	0.38(b)	1.45(a) 1.38(b) 2.15(f)	2.22±0.16	2.15±0.15	1.70±0.13	1.74±0.12
^{238}U	0.22±0.01 *	1.00	1.00	1.00	1.00	1.00
^{237}Np	0.51(b) 0.53(d)	2.33(b) 2.16(e) 2.34(d) 2.93(f)	1.89±0.14	1.92±0.13	1.67±0.12	1.81±0.10
^{239}Pu	0.70(b)	2.70(a) 3.51(b) 3.51(e) 3.45(f)	2.10±0.15	2.10±0.15	1.80±0.13	1.83±0.12
^{241}Am	0.53(e)	1.68(e) ** 2.42(e) 3.27(f)	1.91±0.14	1.77±0.13	1.48±0.10	1.44±0.10
^{243}Am	0.62(e)	2.30(e) 2.59(f)	1.81±0.13	1.81±0.13	1.52±0.11	1.44±0.10

Note. *a*, *b*, *c*, *d*, and *e* denote that the data have been taken respectively from the photofission studies of Refs. 16, 17, 18, 19, and 15. *f* are the average values for the data of a given study on fission by neutrons[20] at nuclear excitation energy ~8 MeV.

*The number given is an average over the results of a large number of studies on photofission of ^{238}U.

**The authors of Ref. 18 point out that the value obtained by them for ^{241}Am is obviously underestimated.

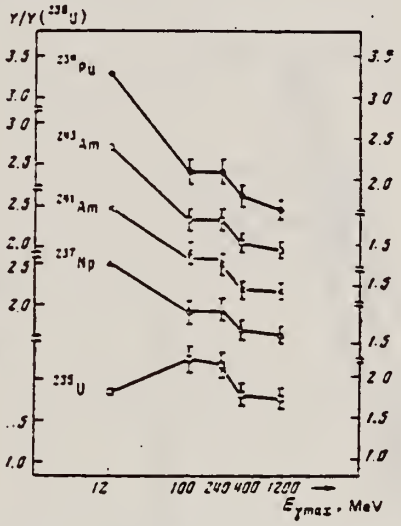

FIG. 2. Relative yields $Y/Y(^{238}U)$ for the nuclei ^{235}U (□), ^{237}Np (△), ^{239}Pu (●), ^{241}Am (×), and ^{243}Am (○) for maximum bremsstrahlung energies $E_{\gamma max}$ ~12, 100, 240, 400, and 1200 MeV.

[15]Yu. A. Vinogradov, V. I. Kasilov, L. E. Lazareva, V. G. Nedorezov, N. V. Nikitina, N. M. Parovik, Yu. N. Ranyuk, and P. V. Sorokin. Yad. Fiz. 24, 686 (1976) Sov. J. Nucl. Phys. 24, 357 (1976).
[16]J. McElhinney and W. E. Ogle. Phys. Rev. 81, 342 (1951).
[17]J. R. Huizenga, Phys. Rev. 109, 484 (1953).
[18]L. Katz, A. P. Baerg, and F. Brown, Proc. of the Second Intern. Conf. on the Peaceful Uses of Atomic Energy, Geneva, 1958, United Nations, Geneva, 1958, Vol. 15, p. 200.
[19]A. Veyssiere, H. Beil, R. Bergere, P. Carlos, A. Lepretre, and K. Kernbath, Nucl. Phys. A199, 45 (1973).

REF. C.D. Bowman, I.G. Schroder, K.C. Duvall and C.E. Dick
Phys. Rev. C 17, 1086 (1978)

ELEM. SYM.	A	Z
U	235	92

METHOD

REF. NO. 78 Bo 8 hg

REACTION	RESULT	EXCITATION ENERGY	SOURCE		DETECTOR		ANGLE
			TYPE	RANGE	TYPE	RANGE	
G,F	ABX	THR- 6	C	3- 6	TRK-I		4PI
		(THR-5.75)		(3.2-5.75)			

Photofission cross sections for ^{232}Th, and ^{236}U have been measured in the energy range from 3.25 to 5.75 MeV and for ^{234}U and ^{236}U at 3.5 MeV. The cross sections change by over seven orders of magnitude for this energy range. Cross section shapes are significantly different for different isotopes indicating a strong sensitivity to fission barrier parameters.

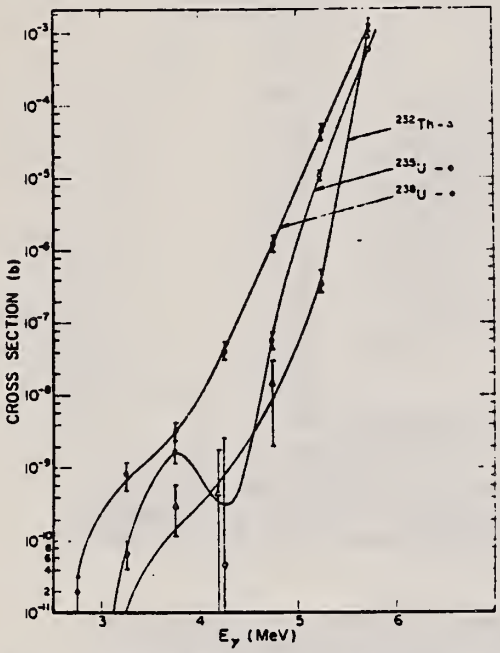

FIG. 1. The photofission cross sections of ^{232}Th, ^{235}U, and ^{238}U. The uncertainty shown includes only track counting statistics propagated through the unfolding process. A systematic uncertainty in the cross section scale might be as large as a factor of 2. The lines through the data are included to guide the eye.

TABLE III. Photofission cross sections for ^{232}Th and ^{235}U.

Photon energy (MeV)	Cross section ^{235}U (b)	Cross section ^{232}Th (b)
3.25	$6.8 \pm 2.6 \times 10^{-11}$	$7.4 \pm 129 \times 10^{-13}$
3.75	$170 \pm 47 \times 10^{-11}$	$3.3 \pm 2.2 \times 10^{-10}$
4.25	$4.9 \pm 248 \times 10^{-11}$	$4.4 \pm 10.7 \times 10^{-10}$
4.75	$6.3 \pm 1.9 \times 10^{-8}$	$1.6 \pm 1.4 \times 10^{-8}$
5.25	$1.1 \pm 0.08 \times 10^{-5}$	$4.2 \pm 1.1 \times 10^{-7}$
5.75	$5.6 \pm 0.11 \times 10^{-4}$	$8.6 \pm 0.25 \times 10^{-5}$

REF. V.E. Zhuchko, Yu.B. Ostapenko, G.N. Smirenkin, A.S. Soldatov, Yu.M. Tsipenyuk
Yad. Fiz. 28, 1185 (1978)
Sov. J. Nucl. Phys. 28, 611 (1978)

ELEM. SYM.	A	Z
U	235	92

METHOD

REF. NO. 78 Zh 6 hg

REACTION	RESULT	EXCITATION ENERGY	SOURCE		DETECTOR		ANGLE
			TYPE	RANGE	TYPE	RANGE	
G,F	RLY	THR-5	C	3-5	TRK-D		4PI
		(THR-4.6)		(3.5-4.6)			

Yield measurements are reported for photofission of ^{232}Th, ^{236}U, ^{238}U, and ^{237}Np in the deep sub-barrier energy region 3.5–4.6 MeV where anomalies in the cross section—isomeric shelfs—were previously observed [Phys. Rev. C, 12, 863 (1975)]; Pis'ma. Zh. Eksp. Teor. Fiz. 22, 255 (1975), [JETP Lett. 22, 118 (1975)]. The various sources of background arising in this energy region, which is only with difficulty accessible for measurements, are analyzed in detail. Analysis of the anomalies in the behavior of the integrated photofission yields in the case of the two nuclei ^{236}U and ^{238}U most favorable for study indicates a resonance nature of the cross sections for delayed fission and a substantially more complicated physics of the phenomenon than the simplified interpretation of Bowman [Phys. Rev. C, 12, 863 (1975)].

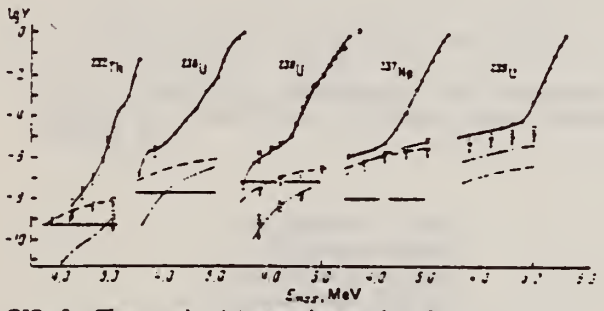

FIG. 2. The round points are the results of measurement of the yields $Y(E_{max})$ in fissions/mg-μC of the photofission reaction: ●—present work and Ref. 7; ○—Ref. 8. ⊤ and dashed lines—respectively the experimental and theoretical estimates of the background due to fissions by neutrons from the reaction Be(γ, n); ⊏ and dot-dash lines—the same for the D(γ, n) reaction. The shaded sections show the level of background from spontaneous fission and fission induced by cosmic rays.

REF. V.E. Zhuchko, Yu.B. Ostapenko, G.N. Smirenkin, A.S. Soldatov, Yu.M. Tsipenyuk
Yad. Fiz. 28, 1170 (1978)
Sov. J. Nucl. Phys. 28, 602 (1978)

ELEM. SYM.	A	Z
U	235	92

METHOD

REF. NO. 78 Zh 7 hg

REACTION	RESULT	EXCITATION ENERGY	SOURCE TYPE	SOURCE RANGE	DETECTOR TYPE	DETECTOR RANGE	ANGLE
G,F	ABX	THR-7	C	4-7	TRK-D		4PI
				(4.4-7.)			

The bremsstrahlung beam of the microtron at our Institute has been used to measure photofission yields of nine nuclei—^{232}Th, ^{233,235,236,238}U, ^{237}Np, ^{239,241}Pu, and ^{241}Am in the energy region 4.4–7.0 MeV. The method of minimization of the directed deviation was used to reproduce the photofission cross sections from the integrated yields. The following problems are discussed in terms of the experimental data: resonance structure of the cross sections, effects of a two-humped shape of the fission barrier, and comparison of the fissility in the (γ,f) and (n,f) reactions and in direct reactions.

PACS numbers: 25.85.Jg

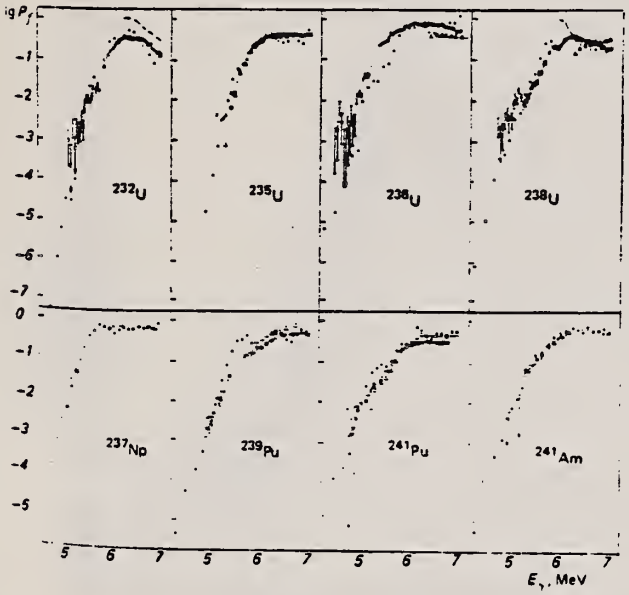

FIG. 4. Fissility P_f in the reactions (γ,f)—●, (n,f)—△ (Ref. 14), and in direct reactions—○.[2] The dashed curve shows the results of evaluation of P_f in accordance with Eq. (9).

(over)

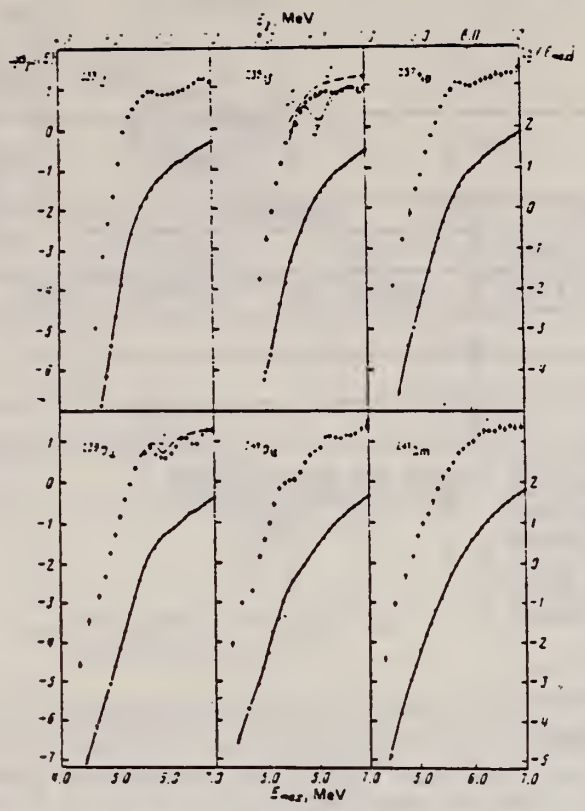

FIG. 3. Yields $Y(E_{max})$, fissions/mg-μC, and cross sections $\sigma_{\gamma f}(E_\gamma)$, mb, for odd isotopes. The designations are the same as in Fig. 2.

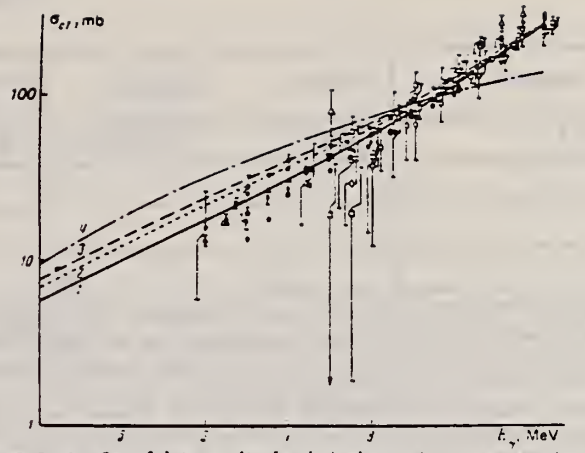

FIG. 6. Set of data on dipole photoabsorption cross sections σ_{c1}. The solid line (1)—the present work—is the result of fitting the data of Ref. 6 by Eq. (2) in the region $E_\gamma = 6$–10 MeV. Curves 2 and 3 are an extrapolation of the fit from Ref. 16 (2) and Ref. 17 (3) for ^{238}U; curve 4 is an estimate by means of Axel's formula.[15] Points: □, ■—^{232}Th; △, ▲—^{235}U; ♦—^{236}U; ○, ●—^{238}U; ▽, ▼—^{237}Np; ◇—^{239}Pu. The hollow points are from Refs. 16 and 17; the solid points are from Ref. 6.

REF. J. C. McGeorge, A. C. Shotter, D. Branford, J. M. Reid
Nucl. Phys. A326, 108 (1979)

EL EM. SYM.	A	Z
U	235	92

METHOD

REF. NO. 79Mc2 hg

REACTION	RESULT	EXCITATION ENERGY	SOURCE		DETECTOR		ANGLE
			TYPE	RANGE	TYPE	RANGE	
E,F	NOX	THR-110	D	110	SCD-D	120-160	90

Abstract: Fission of ^{232}Th, ^{237}Np, ^{209}Bi, ^{233}U and ^{238}U induced by 110 MeV electrons has been studied by means of surface barrier detectors. The resulting mass and kinetic energy distributions are presented. Comparison with the liquid drop model predictions shows reasonable agreement in the case of ^{209}Bi. The data are analysed in terms of a two component model of fission and the mean total kinetic energies of the components are shown to depend linearly on $Z_1Z_2(A_1^{1/3}+A_2^{1/3})$. Interesting differences are found when the present results are compared with the recent photofission experiments of Areskoug *et al.* and features in both sets of data correlate with changes of fragment deformation implied by the calculations of Wilkins *et al.*

MASS AND EGY DISTRIB

E NUCLEAR REACTIONS ^{237}Np, ^{232}Th, ^{209}Bi, ^{238}U, ^{235}U(e, f), E = 110 MeV; measured fission fragment E, deduced mass.

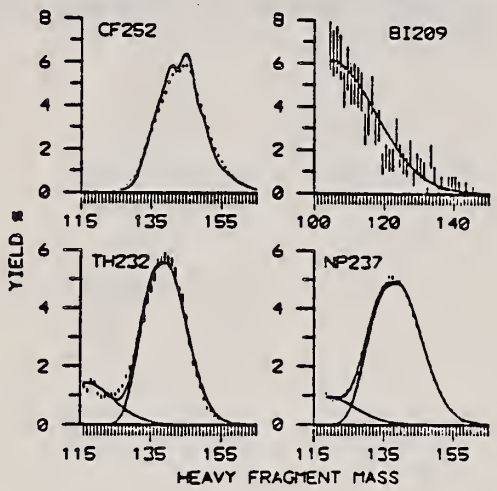

Fig. 1. The HFM yield distributions for electrofission of ^{209}Bi, ^{232}Th and ^{237}Np and spontaneous fission of ^{252}Cf. Statistical uncertainties are shown where larger than the size of the points in this and succeeding diagrams. The solid line in the ^{252}Cf case represents the experimental results of Schmidt *et al.* [12]). In the ^{209}Bi case the solid line represents a Gaussian fit to the data while the solid lines in the other two cases are the result of a two component analysis (see text).

TABLE 2

Target	Mean total KE (MeV) present work	semi-empirical [ref [14])] a)	b)	Width present work
^{238}U	171.8±3.4	168.5	169.4	11.6±0.1
^{235}U	171.3±3.4	169.1	170.1	10.8±0.1
^{232}Th	167.0±3.3	163.4	163.5	9.6±0.1
^{237}Np	174.3±3.0	171.9	173.3	11.5±0.1
^{209}Bi	140 ±4	146.5	143.9	11.5±0.4

a) $0.1071Z^2/A^{1/3}+22.2$.
b) $0.1240Z^2/A^{1/3}$

over

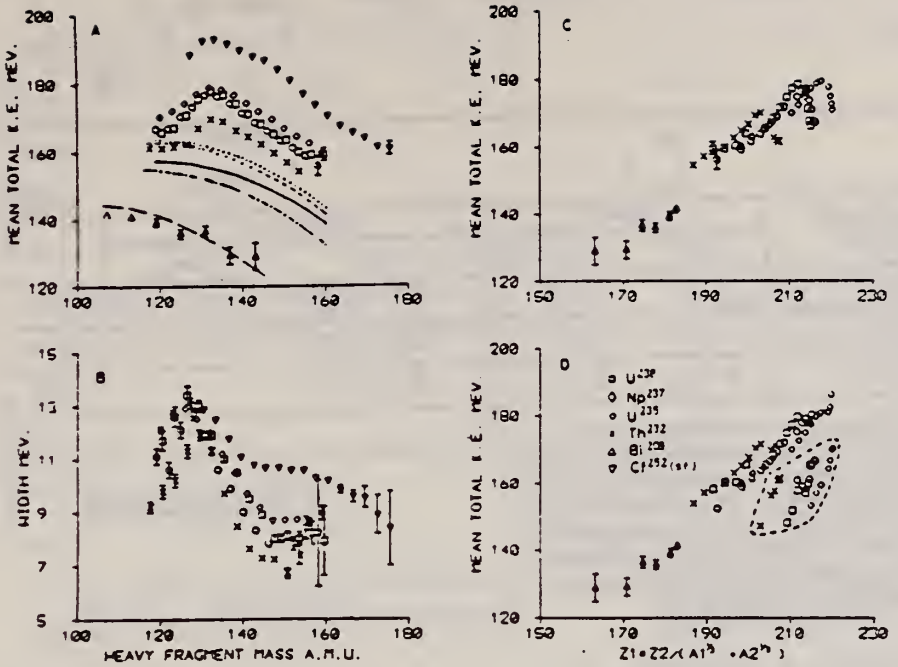

Fig. 3 Total fragment kinetic energy data from electrofission of ^{238}U, ^{235}U, ^{237}Np, ^{232}Th, ^{209}Bi and for spontaneous fission of ^{252}Cf. (A) Mean TKE versus HFM. The lines represent the LDM calculations of Nix and Swiatecki [13]) – solid ^{238}U, short dash ^{235}U, long dash ^{209}Bi, dot ^{237}Np and dot dash ^{232}Th. (B) Width of the TKE distribution versus heavy fragment mass. (C) Mean total fragment kinetic energy versus $Z_1Z_2/(A_1^{1/3}+A_2^{1/3})$. (D) Mean total fragment kinetic energy of the symmetric (enclosed by the dashed line) and asymmetric components versus $Z_1Z_2/(A_1^{1/3}+A_2^{1/3})$. In (A)(C) and (D) the relative uncertainties between targets are ±3 MeV and the absolute uncertainties are ±4 MeV.

REF. J. T. Caldwell, E. J. Dowdy, B. L. Berman, R. A. Alvarez, P. Meyer
Phys. Rev. C21, 1215 (1980)

ELEM. SYM.	A	Z
U	235	92

METHOD

REF. NO.	
80Cal	egf

REACTION	RESULT	EXCITATION ENERGY	SOURCE		DETECTOR		ANGLE
			TYPE	RANGE	TYPE	RANGE	
G,1N	ABX	5-18	D	5-18	BF3 - $\mathcal{I}$	I	4PI
G,2N	ABX	11-18	D	5-18	BF3 - $\mathcal{I}$	I	4PI
G,F	ABX	5-18	D	5-18	BF3 - $\mathcal{I}$	I	4PI

The photoneutron cross sections $\sigma(\gamma,n)$ and $\sigma(\gamma,2n)$, and total photofission cross sections $\sigma(\gamma,F)$ have been measured for ^{235}U, ^{236}U, ^{238}U, and ^{232}Th from threshold to 18.3 MeV using monoenergetic photons from the annihilation in flight of fast positrons and neutron-multiplicity detection in an efficient 4π neutron detector. Use of the ring-ratio technique allowed both the average photofission neutron energy for each nucleus to be obtained as a function of photon energy and, for ^{236}U and ^{238}U, the determination of the partial cross sections for first-chance $\sigma(\gamma,f)$ and second-chance $\sigma(\gamma,nf)$ photofission as well. Information extracted from the data includes integrated cross sections and their moments, giant-resonance parameters, deformation and radius parameters, and relative and absolute neutron and fission probabilities.

SEE ALSO 80CA2

[NUCLEAR REACTIONS ^{235,236,238}U and ^{232}Th ($\gamma,n,2n,F$), E_γ = 5–18.3 MeV; measured 4π neutron yield, neutron multiplicities, and average energies for monoenergetic photons; $\sigma(E_\gamma,1n)$, $\sigma(E_\gamma,2n)$, $\sigma(E_\gamma,F)$, integrated cross sections and moments, GDR parameters, nuclear shape parameters, neutron and fission probabilities.]

TABLE II. Parameters of Lorentz-curve fits to the giant dipole resonance.[a]

Nucleus	$E_m(1)$ (MeV)	$\sigma_m(1)$ (mb)[b]	$\Gamma(1)$ (MeV)	$E_m(2)$ (MeV)	$\sigma_m(2)$ (mb)[b]	$\Gamma(2)$ (MeV)
^{235}U	10.90 ± 0.05	328 ± 19	2.30 ± 0.15	13.96 ± 0.09	459 ± 10	4.75 ± 0.32
^{236}U	10.92 ± 0.04	271 ± 16	2.55 ± 0.17	13.78 ± 0.08	415 ± 10	4.88 ± 0.24
^{238}U	10.77 ± 0.04	311 ± 20	2.37 ± 0.13	13.80 ± 0.09	459 ± 9	5.13 ± 0.35
^{232}Th	11.03 ± 0.04	302 ± 19	2.71 ± 0.13	13.87 ± 0.08	449 ± 9	4.77 ± 0.28

[a] Lorentz parameters defined by Eq. (1); the fitting interval for all cases is 9 to 18 MeV.
[b] Uncertainties for σ_m given here are relative. The absolute uncertainties are 7%.

TABLE IV. Nuclear shape parameters.

Nucleus	R_A[a]	η[b]	ϵ[c]	β_2[d]	Q_0 (b)[e]	Q_0 (b)[f]	Q_0 (b)[g]
^{235}U	0.35	1.308	0.595	0.315	12.0	10.6 ± 0.2	11.0 ± 0.5
^{236}U	0.34	1.287	0.556	0.295	11.2	10.75 ± 0.7	10.3 ± 0.4
^{238}U	0.31	1.309	0.596	0.316	12.1	11.3 ± 0.1	11.1 ± 0.5
^{232}Th	0.38	1.283	0.547	0.290	10.7	9.8 ± 0.1	9.8 ± 0.4

[a] Area ratio, defined by Eq. (6).
[b] Deformation parameter, computed from Eq. (3).
[c] Nuclear eccentricity, computed from Eq. (4).
[d] Deformation parameter, computed from Eq. (7).
[e] Intrinsic quadrupole moment, computed from Eq. (8), with R_0 taken to be 1.20 fm.
[f] Intrinsic quadrupole moment, taken from Ref. 47.
[g] "Best value" for Q_0, computed from Eq. (8), with R_0 taken to be 1.15 fm (see text).

TABLE V. Integrated cross sections.[a]

Nucleus	$\sigma_{int}(\gamma,n)$ (MeV b)	$\sigma_{int}(\gamma,2n)$ (MeV b)	$\sigma_{int}(\gamma,F)$ (MeV b)	$\frac{\frac{1}{2}\pi[\sigma_m(1)\Gamma(1) + \sigma_m(2)\Gamma(2)]}{0.06NZ/A}$[b]
^{235}U	1.14	0.20	2.16	1.37
^{236}U	1.26	0.45	1.45	1.26
^{238}U	1.36	1.13	1.09	1.43
^{232}Th	1.66	1.45	0.37	1.41

[a] $\sigma_{int}(\gamma,x) = \int \sigma(\gamma,x)dE_\gamma$, integrated from threshold to the maximum experimental energy $E_{\gamma max}$ = 18.3 MeV.
[b] Uncertainties given here are relative. The absolute uncertainties are 7%.

TABLE VI. Integrated cross-section moments.[a]

Nucleus	σ_{-1} (mb)	$\sigma_{-1}A^{-4/3}$ (mb)	σ_{-2} (mb MeV^{-1})	$\frac{\sigma_{-2}}{0.00225\,A^{5/3}}$	$\frac{\sigma_{-2}K}{0.05175^{5/3}}$	$\frac{0.05175\,A^{5/3}}{\sigma_{-2}}$ (MeV)
^{235}U	278	0.191	23.1	1.15	1.36	20.1
^{236}U	252	0.173	21.0	1.04	1.21	22.2
^{238}U	286	0.194	24.0	1.17	1.38	19.7
^{232}Th	276	0.194	22.8	1.16	1.35	19.9

[a] $\sigma_{-1} = \int \sigma(\gamma,tot)\,E_\gamma^{-1}\,dE_\gamma$ and $\sigma_{-2} = \int \sigma(\gamma,tot)E_\gamma^{-2}\,dE_\gamma$, integrated from threshold to $E_{\gamma max}$ = 18.3 MeV.

over

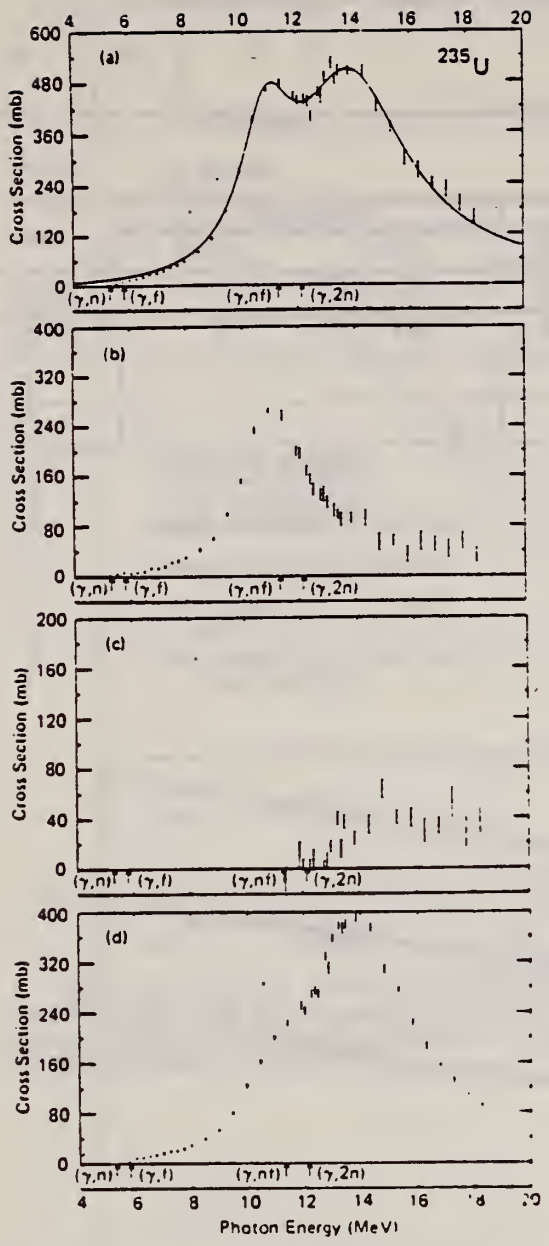

FIG. 2. Photonuclear cross sections for [illegible]: (a) total photonuclear cross section $\sigma(\gamma,\text{tot}) = [\sigma(\gamma,n) + \sigma(\gamma,2n) + \sigma(\gamma,F)]$, together with a two-component Lorentz-curve fit to the data in the GDR energy region; (b) single-photoneutron cross section $\sigma(\gamma,n)$; (c) double-photoneutron cross section $\sigma(\gamma,2n)$; (d) photofission cross section $\sigma(\gamma,F)$.

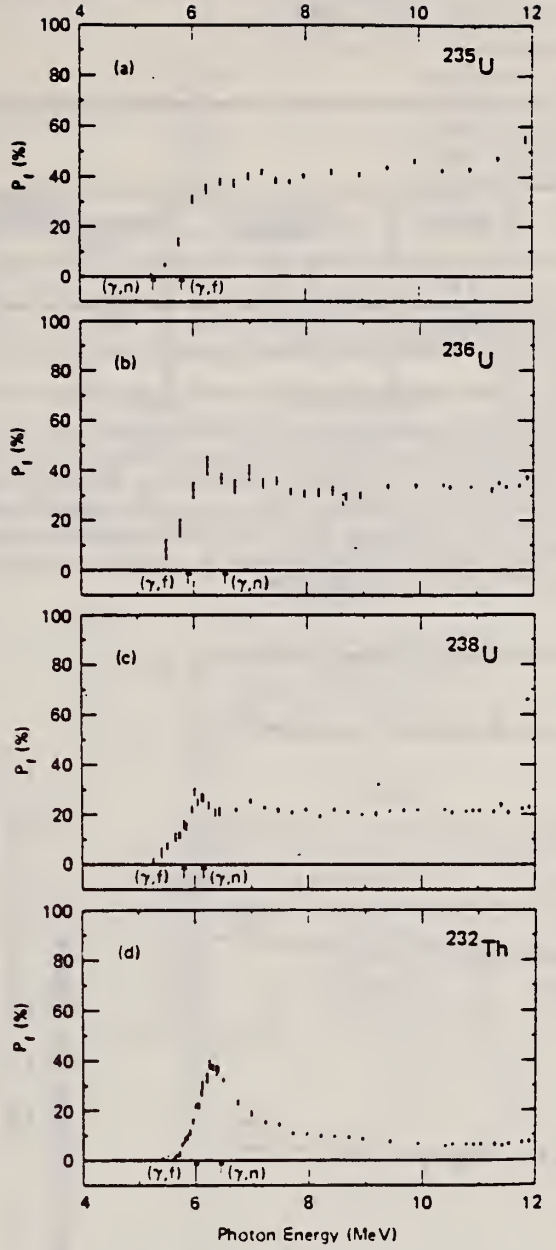

FIG. 13. Fission probability P_f from the ratio of $\sigma(\gamma,f)$ to the value at each energy of the two-component Lorentz-curve fits to the GDR shown in Figs. 2–5: (a) for [illegible]U, (b) for ^{236}U, (c) for [illegible]U, (d) for ^{232}Th.

REF. J. T. Caldwell, E. J. Dowdy, R. A. Alvarez, B.L. Berman, P. Meyer
Nucl. Sci. Eng. 73, 153 (1980)

ELEM. SYM.	A	Z
U	235	92

METHOD

REF. NO.: 80Ca2 egf

REACTION	RESULT	EXCITATION ENERGY	SOURCE		DETECTOR		ANGLE
			TYPE	RANGE	TYPE	RANGE	
G,F	NOX	5-18	D	5-18	BF3 - I	D	4PI
G,F	NOX	11,17	D	5-18	BF3 - I	D	4PI

The prompt neutron multiplicities for photofission of the four isotopes ^{235}U, ^{236}U, ^{238}U, and ^{232}Th have been measured with monoenergetic photons over the energy range from 5.5 to 18 MeV using the annihilation in flight of fast positrons. The delayed neutron yield has been measured for all four isotopes at 10.9- and 16.8-MeV photon energies. The ratio of first- to second-chance fission has been measured as a function of energy up to 17-MeV excitation energy for ^{236}U and ^{238}U photofission.

PROMPT N MULT

DELAYED N YLD

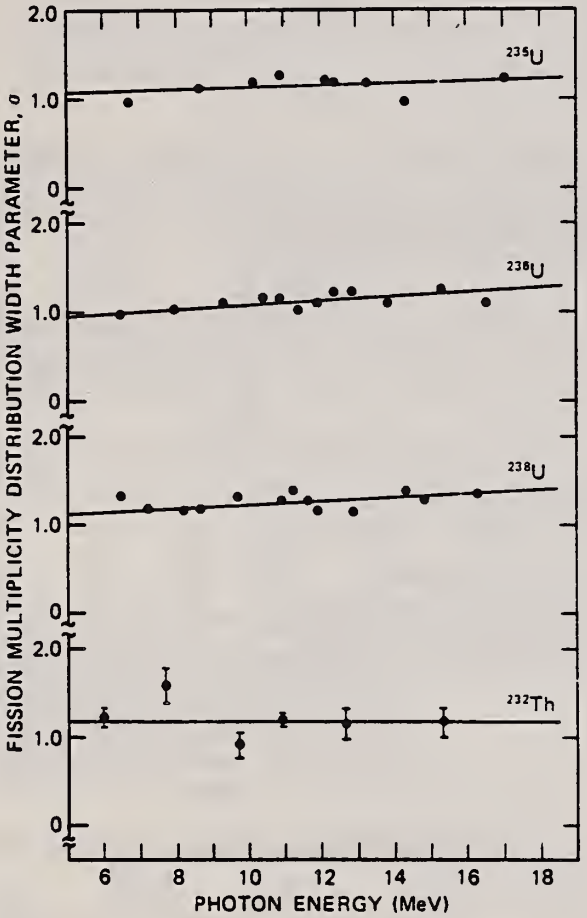

Fig. 6. Prompt neutron multiplicity width parameter data as a function of excitation energy. Solid circles are experimental data, and straight lines are the least-squares fits to these data (see Table II).

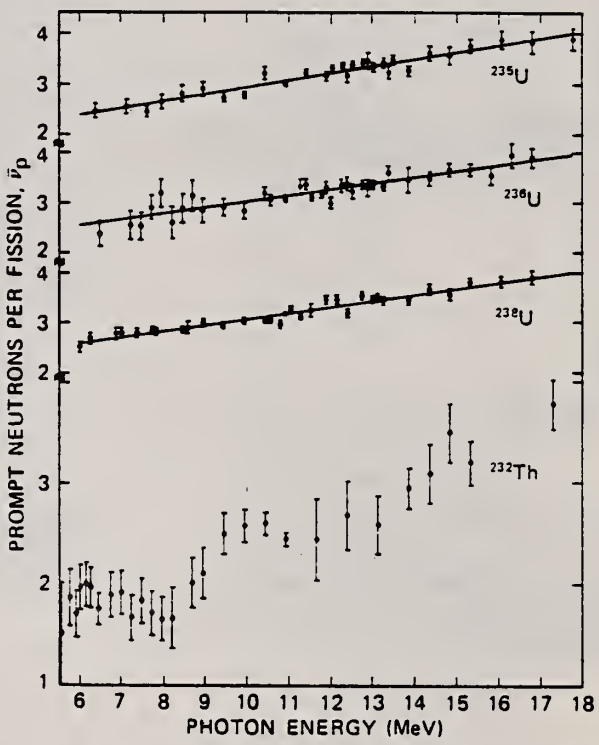

Fig. 7. Prompt neutron $\bar{\nu}_p$ data as a function of excitation energy. Solid circles are experimental data, and the straight lines are the least-squares fits (see Table IV) to these data. A single straight line fit was not obtainable for ^{232}Th.

over

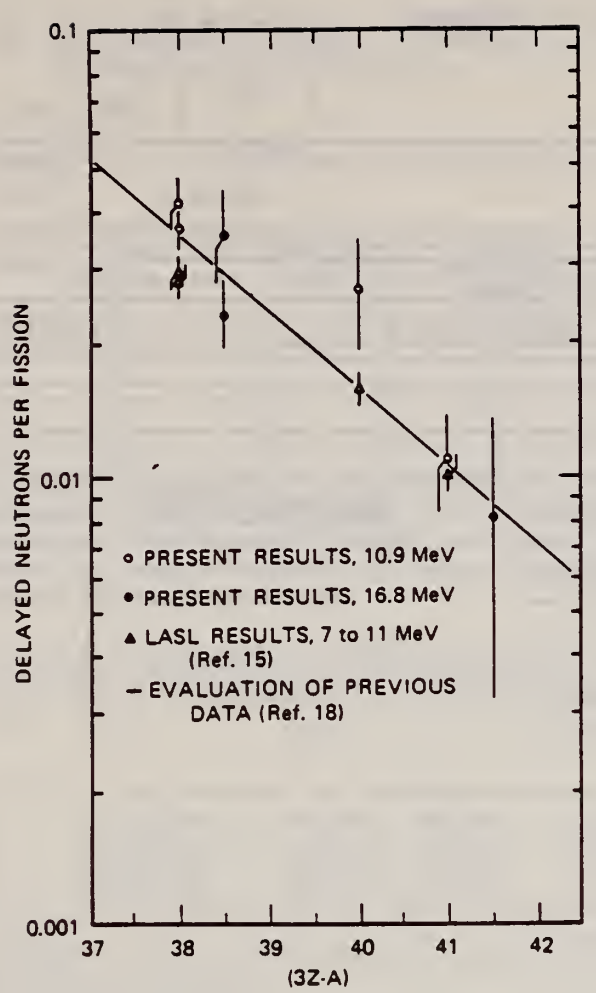

Fig. 9. Yield of delayed neutron from photofission as a function of $3Z\text{-}A$. Solid line is an evaluated least-squares fit to existing data as of 1975 (Ref. 18). Solid circles are the present results. Solid squares are from Ref. 15.

TABLE II

Multiplicity Width Parameter

Isotope	Least-Squares Fit
^{235}U	$\sigma = 1.009 + 0.0110\ E$
^{236}U	$\sigma = 0.840 + 0.0253\ E$
^{238}U	$\sigma = 1.003 + 0.0227\ E$
^{232}Th	$\sigma = 1.183$

TABLE IV

Prompt Neutrons per Photofission, $\bar{\nu}_p(E)$

Isotope	Least-Squares Fit	Correlation Coefficient
^{235}U	$\bar{\nu}_p = 1.610 + 0.133\ E$ (all data)	0.965
^{236}U	$\bar{\nu}_p = 1.881 + 0.116\ E$ (all data)	0.906
^{238}U	$\bar{\nu}_p = 1.862 + 0.123\ E$ (all data)	0.969
^{232}Th	$\bar{\nu}_p = 2.826 - 0.143\ E$ ($6.0 < E < 8.2$ MeV)	0.819
	$\bar{\nu}_p = 0.453 + 0.175\ E$ ($E > 8.5$ MeV)	0.927

TABLE V

Prompt Neutrons per Photofission at 8.5 MeV

Isotope	From Ref. 15	Present Data
^{235}U	2.85 ± 0.09	2.74 ± 0.10
^{236}U	2.66 ± 0.11	2.71 ± 0.10
^{238}U	2.74 ± 0.09	2.91 ± 0.10
^{232}Th	2.07 ± 0.11	1.94 ± 0.08

REF. P. D'hondt, E. Jacobs, A. De Clercq, D. De Frenne, H. Thierens, P. De Gelder, A. J. Deruytter
Phys. Rev. C21, 963 (1980)

ELEM. SYM.	A	Z
U	235	92

METHOD

REF. NO. 80 Dh 3 hg

REACTION	RESULT	EXCITATION ENERGY	SOURCE		DETECTOR		ANGLE
			TYPE	RANGE	TYPE	RANGE	
G, A	SPC	THR-20	C	20	TEL-D		UKN

Binary fission to Long Range Alpha particle emission is 580±50

LONG-RANGE ALPHAS

Long-range alpha particles emitted in the photofission of ^{235}U with 20-MeV bremsstrahlung were measured. The binary to long-range alpha particle ratio, $\langle E_\alpha \rangle$, and full width at half maximum (E_α) were deduced.

[NUCLEAR REACTIONS, FISSION $^{235}U(\gamma, F)$, $E_{\gamma max} = 20$ MeV, measured: Long-range α spectrum.]

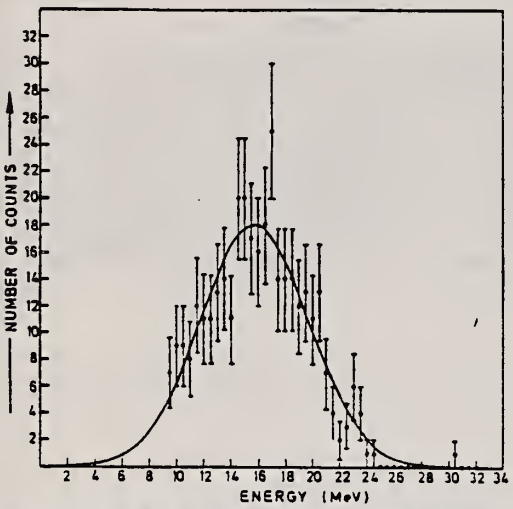

FIG. 2. The spectrum, corrected for energy losses, of the LRA particles emitted in the photofission of ^{235}U with 20-MeV bremsstrahlung.

REF. W. Günther, K. Huber, U. Kneissl, H. Krieger, H.J. Maier
Z. Phys. A 295, 333 (1980)

ELEM. SYM.	A	Z
U	235	92

METHOD

REF. NO. 80 Gu 4 hg

REACTION	RESULT	EXCITATION ENERGY	SOURCE		DETECTOR		ANGLE
			TYPE	RANGE	TYPE	RANGE	
G,F	RLY	THR-55	C	15-55	SCD-D		90

M,E DST, SYM/ASYM YLD

Measurements are presented for the mass and energy distributions of fragments from the photofission of ^{232}Th, ^{235}U, ^{238}U and ^{239}Pu. The experiments were performed for bremsstrahlung endpoint energies between 15 and 55 MeV, using silicon surface barrier detectors. The results are discussed with respect to the competition between the symmetric and asymmetric fission modes.

Table 2. Most probable heavy masses, most probable total kinetic energies and their variances (The variances have been corrected for the detector resolution and for γ- and electron pile up)

Nucleus	$[m]_{heavy}$	$[E_k]_{exp}$ a)	b)	$[E_k]_{calc}$	σ_{E_k}
^{232}Th	(141.7 ± 2) amu	163.3 MeV	163.5 MeV	(159.5 ± 4) MeV	(9.0 ± 0.8) MeV
^{235}U	(138.5 ± 2) amu	169.1 MeV	170.1 MeV	(168 ± 3) MeV	(11.1 ± 1) MeV
^{238}U	(140.3 ± 2) amu	168.5 MeV	169.4 MeV	(164.5 ± 4) MeV	(11.7 ± 1) MeV
^{239}Pu	(137.2 ± 2) amu	174.7 MeV	176.6 MeV	(174 ± 3) MeV	(11.9 ± 1) MeV
^{252}Cf[c]				185.5 MeV	11.6 MeV

[a] $[E_k] = (0.1071 \cdot Z^2 A^{1/3} + 22.2)$ MeV
[b] $[E_k] = (0.1240 \cdot Z^2 A^{1/3})$ MeV
[c] Calibration measurement

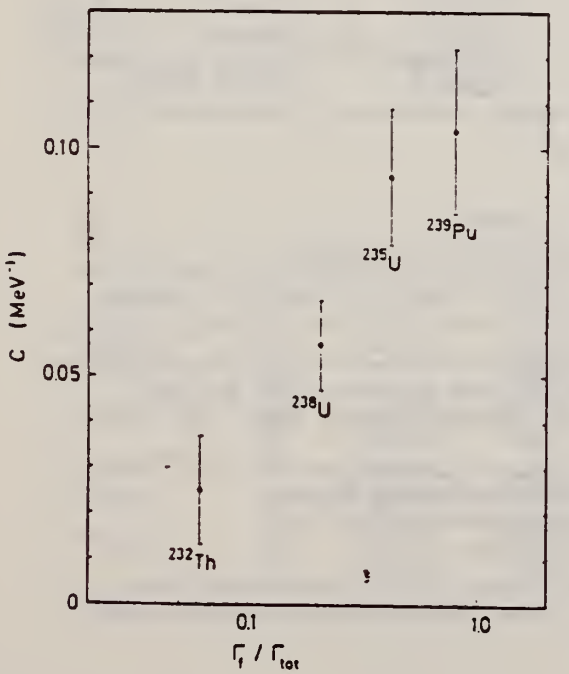

Fig. 5. Saturation parameter c as a function of the fission probability Γ_f/Γ_{tot}

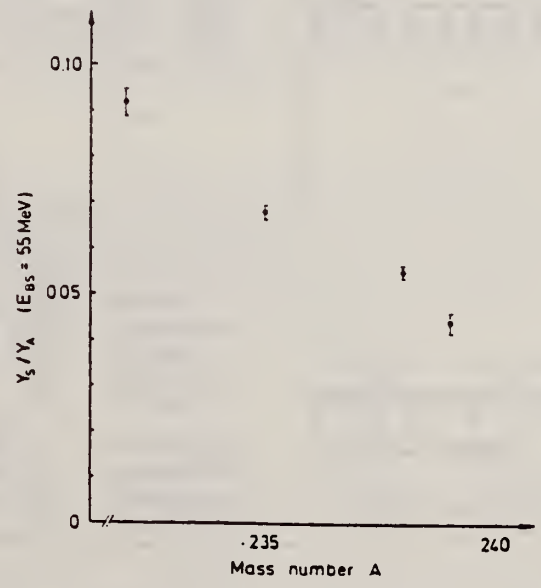

Fig. 6. $Y_S\ Y_A$ at $E_{BS} = 55$ MeV as a function of the mass number A

(OVER)

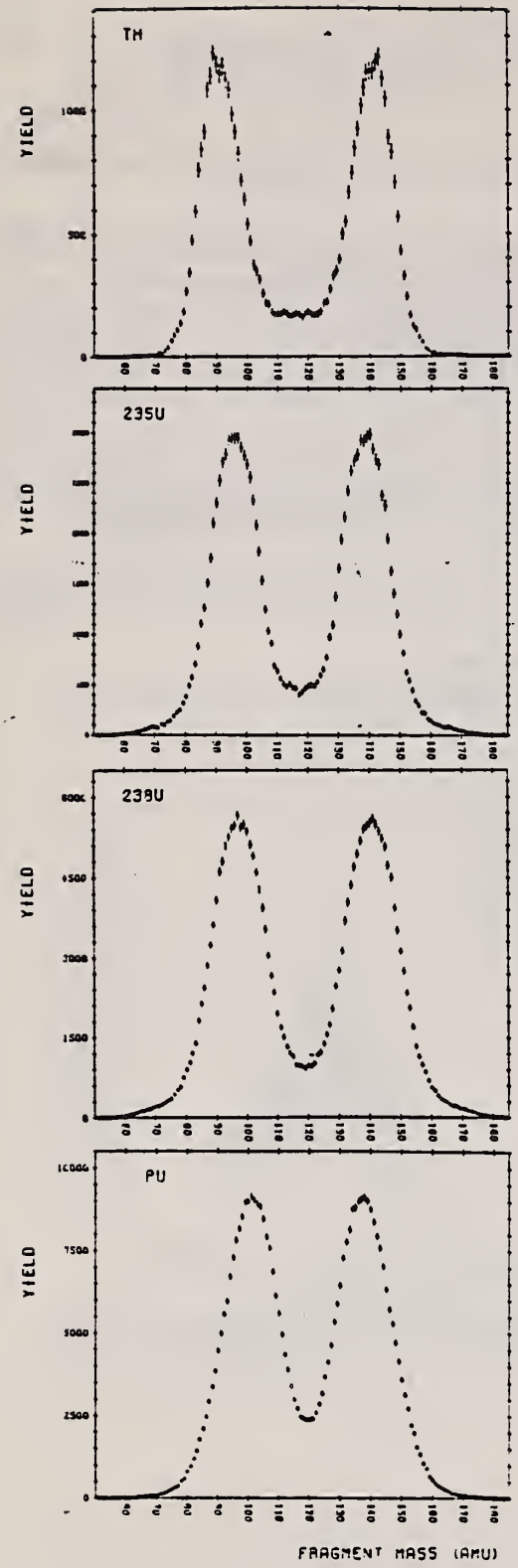

Fig. 1. Mass distributions for the photofission of ^{232}Th, ^{235}U, ^{238}U and ^{239}Pu (Bremsstrahl endpoint energy E_{BS} = 45 MeV)

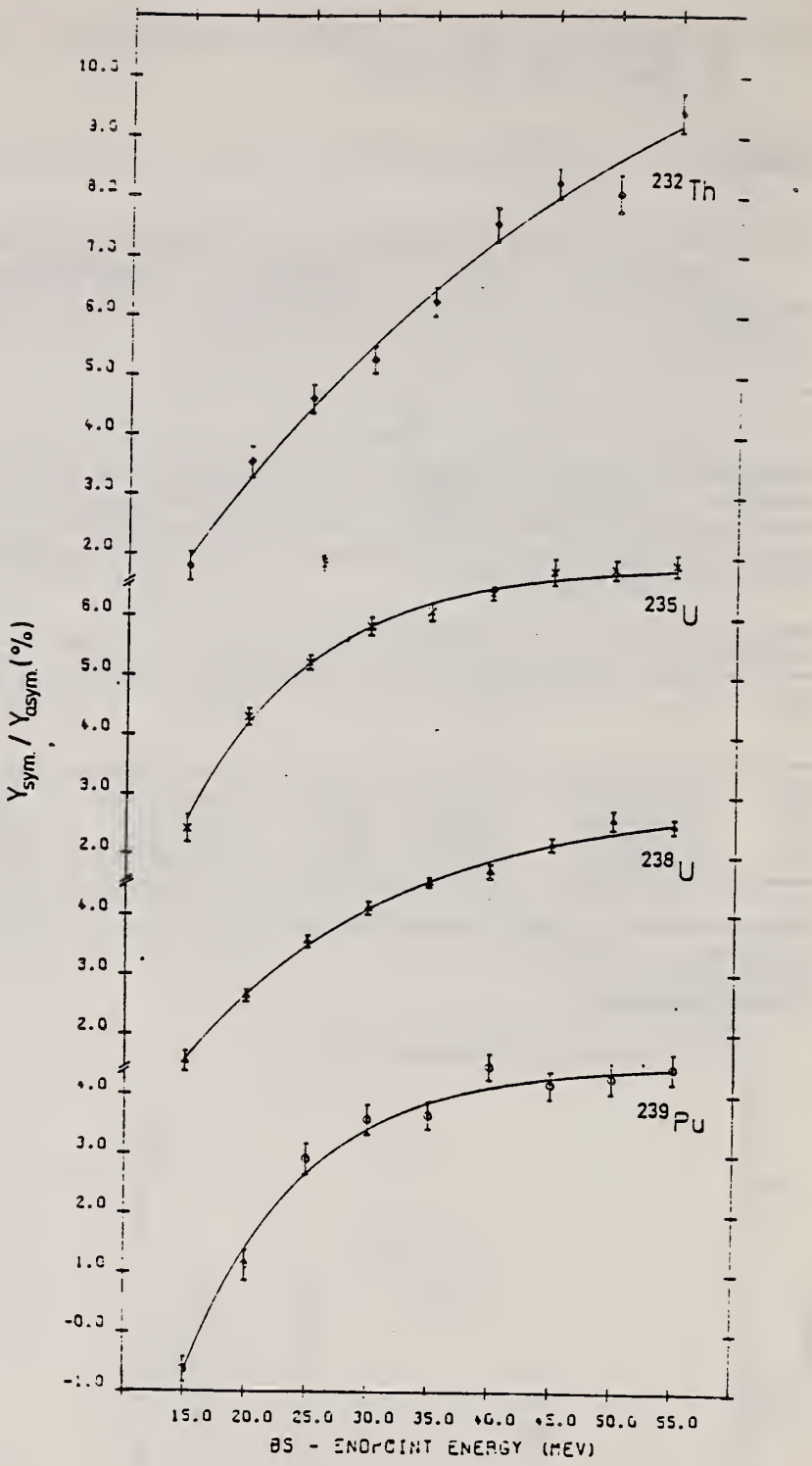

Fig. 4. Symmetric to asymmetric fission yield ratio as a function of E_{BS}. The lines are fits with an empirical function Y_S: $Y_S = a + be^{-cE_{BS}}$ (s. text)

REF. W. Günther, K. Huber, U. Kneissl, H. Krieger, H. Ries, H. Ströher, W. Wilke, H.J. Maier
Nucl Phys. A350, 1 (1980)

ELEM. SYM.	A	Z
U	235	92

METHOD

REF. NO. 80 Gu 5 hg

REACTION	RESULT	EXCITATION ENERGY	SOURCE		DETECTOR		ANGLE
			TYPE	RANGE	TYPE	RANGE	
G,XN	RLY	THR-45	C	45	SPK-$\mathcal{L}$		90

Abstract: Half-lives and yields in photonuclear reactions have been measured for shape isomers in U and Pu isotopes by pulsed-beam techniques bombarding ^{235,238}U and ^{239,240,242}Pu targets with bremsstrahlung. Isomeric fission cross sections have been deduced from the measured isomeric to prompt yield ratios within an evaporation model using absolute prompt fission data. The results are compared with data from particle-induced reactions.

YLD FISSION ISOMERS

E NUCLEAR REACTIONS ^{240}Pu^{235}U(γ, xn), ^{238}U, ^{239}Pu(γ, 2n), ^{242}Pu(γ, n); bremsstrahlung; measured $T_{1/2}$, isomeric to prompt yield ratios, ^{236}U, ^{237}Pu, ^{239}Pu, ^{241}Pu levels, deduced σ for isomeric fission. Natural and enriched targets.

TABLE 2

Results of isomeric fission experiments performed at Giessen

Reaction	Isomer	Half-life	Y_{iso}/Y_{pr}	Detector
^{232}Th(γ, xn)			$<10^{-6}$	PPAD
^{235}U (γ, xn)			$<10^{-7}$	PPAD
^{238}U (γ, 2n)	^{236}U	115 ± 5 ns	$(2.02\pm0.16)\times10^{-5}$	Si
		118 ± 7 ns	$(2.10\pm0.16)\times10^{-5}$	PPAD
^{239}Pu (γ, 2n)	^{237m_1}Pu	77 ± 16 ns	$(6.4\pm1.7)\times10^{-6}$	Si
		87 ± 11 ns	$(4.9\pm0.7)\times10^{-6}$	PPAD
	^{237m_2}Pu	1050 ± 400 ns	$(0.83\pm0.22)\times10^{-6}$	Si
^{240}Pu (γ, n)	^{239m_1}Pu	6.5 ± 0.4 μs	$(7.9\pm0.4)\times10^{-5}$	PPAD
^{240}Pu(γ, xn)	?	4.5 ± 1.5 ns	$<1.1\times10^{-4}$	PPAD
^{242}Pu(γ, n)	^{241m_1}Pu	20.5 ± 2.5 μs	$(9.2\pm0.8)\times10^{-5}$	PPAD
	^{241m_2}Pu	34 ± 7 ns	$(3.7\pm0.7)\times10^{-5}$	PPAD

TABLE 5

Isomeric fission cross sections for (γ, n) reactions

Reaction	E_0 (MeV)	$Y_{iso}/Y_{pr}\times10^5$	σ_{iso}^{max} (μb)	E_{max} (MeV)	Ref.
^{235}U(γ, n)	45	≤0.01	<0.05	11.4†	this work
^{240}Pu(γ, n)	15.5		170 ± 60	11.5	Gangrsky *et al.* [3])
	45	7.9 ± 0.4	49 ± 3	12.3†	this work
^{242}Pu(γ, n)^{241m_1}Pu	12.5	115 ± 25	200 ± 60	10.5	Gangrsky *et al.* [3])
	40	9.2 ± 0.8	54 ± 5	12.0†	this work
^{242}Pu(γ, n)^{241m_2}Pu	48	3.7 ± 0.7			
^{241}Am(γ, n)	13	40 ± 10	150 ± 50	11.2	Gangrsky *et al.* [3])
	41	13 ± 1.5	60 ± 8	12.0	Kuznetsov *et al.* [4])
^{243}Am(γ, n)	12.5	70 ± 20	130 ± 50	10.6	Gangrsky *et al.* [3])
	41	18.5 ± 2.5	80 ± 10	12.0	Kuznetsov *et al.* [4])

† The shape of the cross section was calculated (see text).

REF. E. Jacobs, H. Thierens, D. De Frenne, A. De Clercq, P. D'hondt, P. De Gelder, A.J. Deruytter
Phys. Rev. C21, 237 (1980)

ELEM. SYM.	A	Z
U	235	92

METHOD

REF. NO.: 80 Ja 3 hg

REACTION	RESULT	EXCITATION ENERGY	SOURCE TYPE	SOURCE RANGE	DETECTOR TYPE	DETECTOR RANGE	ANGLE
G,F	RLY	THR-7Ø	C	12-7Ø	ACT-I		4PI

Detailed yield data given in tables.

MASS YLDS, ISM RATIOS

The mass distributions for the photofission of ^{235}U using bremsstrahlung with end-point energy of 12, 15, 20, 30, and 70 MeV were determined by γ spectrometry of fission product catcher foils. Smoothly varying curves without fine structure were obtained. A third hump in the symmetric region is not present. Several fractional independent chain yields in the mass region 126–140 were measured and the corresponding most probable charges $Z_p(E_e)$ were deduced. A comparison with the charge expected from the unchanged charge density hypothesis is made and an influence of the 50-proton shell on the behavior of the Z_p function is observed. Except in this mass region the determined $Z_p(E_e)$ values are very well described by the empirical relation of Nethaway. From the isomeric ratios of $^{126}Sb^g$-$^{126}Sb^m$, $^{128}Sb^g$-$^{128}Sb^m$, and $^{131}Te^g$-$^{131}Te^m$ average initial fragment spins are calculated using a statistical model analysis. The values increase with increasing end-point energy of the bremsstrahlung.

[NUCLEAR REACTIONS, FISSION $^{235}U(\gamma,F)$, $E_{\gamma max}$=12, 15, 20, 30, 70 MeV; measured: fragment γ-ray spectra; deduced: mass distributions, most probable charges, isomeric ratios, average initial fragment spins.]

TABLE II. Mass distribution characteristics.

E_e (MeV)	12	15	20	30	70
P/V	37 ± 5	22 ± 2	15.5 ± 1.4	11.7 ± 0.8	8.4 ± 0.6
MLM[a]	94.85 ± 0.07	94.70 ± 0.07	94.80 ± 0.07	94.68 ± 0.07	94.77 ± 0.07
MHM[a]	137.28 ± 0.07	137.24 ± 0.07	137.09 ± 0.07	137.15 ± 0.07	137.14 ± 0.07
FWHM	14.7 ± 0.4	15.0 ± 0.4	15.0 ± 0.4	15.0 ± 0.4	15.2 ± 0.4
$\langle\mu\rangle$[a]	2.78 ± 0.12	3.06 ± 0.12	3.15 ± 0.11	3.25 ± 0.11	3.26 ± 0.11

[a]Uncertainties on MLM, MHM, and $\langle\mu\rangle$ were obtained by a statistical treatment of the uncertainties of the yields.

TABLE IV. $Z_p(E_e)$ values for the photofission of ^{235}U.

M_{post} \ E_e (MeV)	12	15	20	30
126		49.82 ± 0.09	49.89 ± 0.06	49.97 ± 0.06
128		50.21 ± 0.12	50.24 ± 0.11	50.32 ± 0.11
130		$50.89^{+0.09}_{-0.13}$	50.97 ± 0.05	51.04 ± 0.05
131	51.24 ± 0.11	51.34 ± 0.07	51.45 ± 0.08	51.47 ± 0.08
132	$51.51^{+0.10}_{-0.15}$	51.60 ± 0.03	51.65 ± 0.03	51.68 ± 0.04
134	52.41 ± 0.10	52.50 ± 0.04	52.55 ± 0.04	52.60 ± 0.04
135	52.93 ± 0.06	53.04 ± 0.04	53.08 ± 0.03	53.10 ± 0.02
136		53.28 ± 0.06	53.37 ± 0.05	53.40 ± 0.04
140		55.01 ± 0.07	55.02 ± 0.06	55.09 ± 0.04

(OVER)

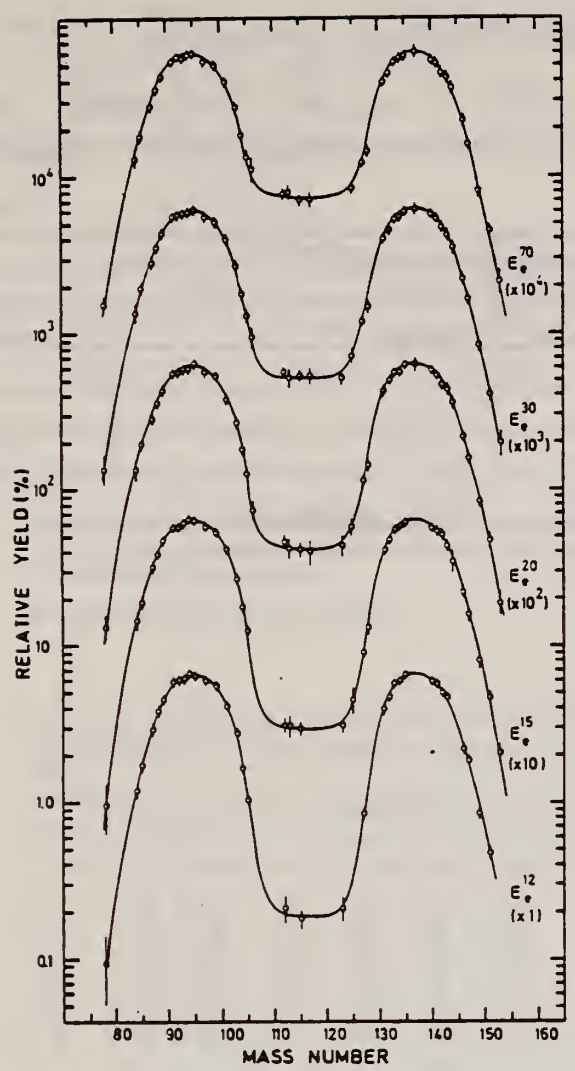

FIG. 1. Postneutron mass distributions for the photofission of ^{235}U with 12-, 15-, 20-, 30-, and 70-MeV bremsstrahlung. The yields have been multiplied by the scale factor given in parentheses.

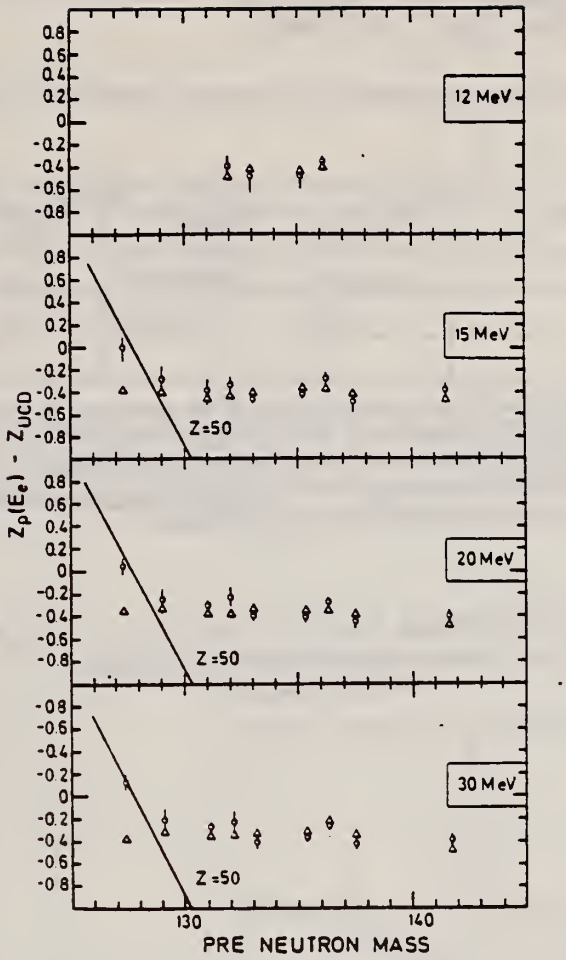

FIG. 2. $Z_p(E_e)$-Z_{UCD} versus fragment mass number for the photofission of ^{235}U with 12-, 15-, 20-, and 30-MeV bremsstrahlung. The open circles represent the $Z_p(E_e)$ values deduced from the measured independent yields, the triangles the Z_p values calculated following Nethaway (Ref. 6).

TABLE V. Isomeric ratios $\sigma_m/(\sigma_g+\sigma_m)$.

Isomeric pair \ E_e (MeV)	12	15	20	30	70
$^{126}Sb^m(5^+)$-$^{126}Sb^g(8^-)$		0.52 ± 0.12	0.45 ± 0.08	0.42 ± 0.07	0.34 ± 0.05
$^{128}Sb^m(5^+)$-$^{128}Sb^g(8^-)$		0.53 ± 0.10	0.49 ± 0.10	0.45 ± 0.11	0.39 ± 0.08
$^{131}Te^m(\frac{11}{2}^-)$-$^{131}Te^g(\frac{3}{2}^+)$	0.59 ± 0.11	0.59 ± 0.06	0.61 ± 0.05	0.62 ± 0.07	0.61 ± 0.05

REF. E. Jacobs, A. De Clercq, H. Thierens, D. De Frenne, P. D'hondt, P. De Gelder, A.J. Deruytter
Phys. Rev. C24, 1795 (1981)

ELEM. SYM.	A	Z
U	235	92

METHOD

REF. NO.: 81 Ja 2 hg

REACTION	RESULT	EXCITATION ENERGY	SOURCE TYPE	SOURCE RANGE	DETECTOR TYPE	DETECTOR RANGE	ANGLE
G,F	NOX	THR-70	C	12-70	SCD-D		90

Energy correlation measurements were performed for the photofission of ^{235}U with 12-, 15-, 20-, 30-, and 70-MeV bremsstrahlung. Overall fragment mass and kinetic energy distributions are deduced. The behavior of the total fragment kinetic energy as a function of the fragment mass and excitation energy of the compound nucleus is studied. The results are interpreted in terms of the scission-point model of Wilkins *et al.*

MASS, ENERGY DIST.

[NUCLEAR REACTIONS, FISSION $^{235}U(\gamma,f)$, $E_{\gamma max}$ = 12, 15, 20, 30, and 70 MeV; measured fragment energies E_1, E_2; deduced $N(\mu,E_K)/\langle E_{exc}(E_e)\rangle$.]

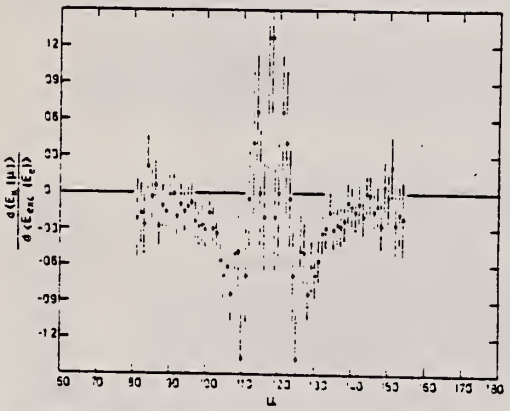

FIG. 1. Compound nucleus excitation energy dependence of the total fragment kinetic energy $d\langle E_K(\mu)\rangle/d\langle E_{exc}(E_e)\rangle$ as a function of the provisional mass μ for the photofission of ^{235}U.

TABLE I. Parameters of the overall kinetic energy and provisional mass distributions for the photofission of ^{235}U.

E_e(MeV)	12	15	20	30	70
$\langle E_{exc}(E_e)\rangle$ (MeV)	9.7	11.6	13.1	14.1	
NEV	16.10^3	99.10^3	241.10^3	113.10^3	145.10^3
$\langle \mu_L \rangle$ (u)	96.89 ± 0.35	96.96 ± 0.16	97.23 ± 0.16	97.41 ± 0.24	97.75 ± 0.15
$\langle \mu_L \rangle_{3/4}$ (u)	97.00	96.87	96.96	96.87	96.99
$\langle \mu_H \rangle$ (u)	138.11 ± 0.16	138.04 ± 0.11	137.77 ± 0.20	137.59 ± 0.31	137.25 ± 0.22
$\langle \mu_H \rangle_{3/4}$ (u)	138.00	138.13	138.04	138.13	138.01
$\sigma(\mu_L) = \sigma(\mu_H)$ (u)	6.15 ± 0.31	6.47 ± 0.26	6.79 ± 0.20	7.05 ± 0.20	7.33 ± 0.22
FW($\frac{1}{4}$) (u)	10.39	10.69	10.80	10.93	11.11
P/V	41 ± 4	24 ± 1	14.2 ± 0.3	10.7 ± 0.4	7.5 ± 0.3
$\langle E_k \rangle$ (MeV)	171.03 ± 0.65	170.50 ± 0.30	169.97	169.64 ± 0.13	169.36 ± 0.30
$\sigma(E_k)$ (MeV)	10.43 ± 0.10	10.63 ± 0.10	10.81 ± 0.10	10.94 ± 0.11	11.35 ± 0.33

REF. A.S. Voronin, I.S. Koretskaya, V.L. Kuznetsov, V.G. Nedorezov, N.V. Nikitina, V.I. Noga, S.A. Pashchuk, Yu.N. Ranyuk, S.M. Solov'ev
Yad. Fiz. 34, 1439 (1981)
Sov. J. Nucl. Phys. 34, 797 (1981)

ELEM. SYM.	A	Z
U	235	92

METHOD

REF. NO.: 81 Vo 3 | egf

REACTION	RESULT	EXCITATION ENERGY	SOURCE TYPE	SOURCE RANGE	DETECTOR TYPE	DETECTOR RANGE	ANGLE
E,F	ABX	4-275	D	97-275	TRK-I		45
G,F	RLY	4-275	D	184-275	TRK-I		45

RELATIVE BRMS/E YLD

Results are presented of cross-section measurements for the fission of ^{232}Th, ^{233}U, ^{235}U, ^{236}U, ^{238}U, ^{237}Np, and ^{239}Pu by electrons with energies between 100 and 275 MeV; photofission and electrofission cross-section ratios for the same nuclei are given as well.

PACS numbers: 25.85.Jg, 27.90. + b, 25.85.Ge

TABLE II. Electrofission cross sections (mb) for nuclei with $Z \geq 90$ measured for electron energies between 100 and 275 MeV.

E_e, MeV	Nucleus						
	^{232}Th	^{233}U	^{235}U	^{236}U	^{238}U	^{237}Np	^{239}Pu
97	1.24	8.12	5.66	4.55	3.23	6.22	7.26
134	1.47	9.17	6.08	4.74	3.42	6.63	7.98
149	1.42	9.75	6.17	5.59	3.59	7.16	8.39
168	1.63	10.26	7.01	5.20	4.15	7.79	9.18
184	1.78	9.61	7.13	5.04	4.17	7.92	8.92
201	1.54	9.84	6.53	6.10	4.56	7.49	9.31
217	1.73	10.91	7.73	6.14	4.77	7.29	9.56
240	1.91	10.25	7.26	5.92	4.49	7.54	9.43
253	1.85	9.89	7.01	6.17	4.78	7.59	9.78
275	2.22	10.50	8.15	6.68	5.26	9.68	10.50

TABLE IV. Cross sections (mb) for photo- and electrofission ($\sigma_{Qf}\Delta t + \sigma_{ef}$) obtained in measurements with aluminum radiators with a thickness of $0.023t_0$ for ^{235}U, ^{236}U, ^{238}U, and ^{237}Np and of $0.011t_0$ for ^{239}Pu.

E_e, MeV	Nucleus					E_e, MeV	Nucleus				
	^{235}U	^{236}U	^{238}U	^{237}Np	^{239}Pu		^{235}U	^{236}U	^{238}U	^{237}Np	^{239}Pu
184	13.33	10.48	7.37	13.49	11.65	240	14.02	10.37	8.13	11.62	13.23
201	14.10	11.50	8.82	12.79	12.16	253	14.17	10.96	8.11	11.95	12.90
217	14.36	10.76	8.07	12.94	12.96	275	15.22	12.00	9.29	12.92	13.83

TABLE V. Cross-section ratios for photo- and electrofission (σ_{Qf}/σ_{ef}) for energies between 184 and 275 MeV.

Nucleus	σ_{Qf}/σ_{ef}	Nucleus	σ_{Qf}/σ_{ef}
^{235}U	40±8	^{237}Np	24±5
^{236}U	35±7	^{239}Pu	30±6
^{238}U	35±7		
	Average	33±3	
	Theoretical	35.3	

REF. D. DeFrenne, H. Thierens, B. Proot, E. Jacobs, P. DeGelder, A. DeClercq, W. Westmeier
Phys. Rev. C26, 1356 (1982)

ELEM. SYM.	A	Z
U	235	92

METHOD

REF. NO. 82 De 4 egf

REACTION	RESULT	EXCITATION ENERGY	SOURCE		DETECTOR		ANGLE
			TYPE	RANGE	TYPE	RANGE	
G,F	RLY	5-30	C	12-30	ACT-I		4PI

FRAG YLDS

A systematic study of the charge distribution for bremsstrahlung-induced photofission of ^{235}U and ^{238}U with the end point energies ranging from 12 to 30 MeV was performed using direct γ-ray spectrometry of irradiated uranium samples or of fission product catcherfoils, and also employing chemical separation techniques. For both fissioning systems the width of the charge distribution was found to be practically independent of the average excitation energy and the values obtained are in very good agreement with those reported in the literature for low-energy fission. The deviation of the most probable charge Z_p from the unchanged charge density value Z_{UCD} as a function of the fragment mass shows the influence of the 50-proton shell in the charge distributions and a higher charge-to-mass ratio of the light fragments independent of the compound nucleus excitation energy. For the necessary conversion of postneutron into preneutron masses, neutron emission curves, $\nu(m^*)$, were deduced from previously measured postneutron and provisional mass distributions. Calculations following the scission-point model of Wilkins *et al.* and the predictions of the empirical relation of Nethaway reproduce very well the experimentally determined Z_p behavior, except in the mass region affected by the $Z = 50$ closed shell.

NUCLEAR REACTIONS, FISSION $^{235,238}U(\gamma,F)$, E_{max} = 12, 15, 20, 30 MeV; measured product γ-ray spectra deduced charge distributions, width, and most probable charges; calculated $\nu(m^*)$ from measured provisional and postneutron mass distributions.

TABLE IV. Values of the width parameter c determined for the photofission of ^{235}U. M_{post} denotes the postneutron mass.

M_{post} \ E_e (MeV)	12	15	20	30
130		0.86±0.09	[illegible]	0.90±0.04
131	0.92±0.14	1.02±0.13	[illegible]	1.45±0.19
132	0.72±0.12	0.71±0.05	[illegible]	0.76±0.05
133	0.66±0.10	0.68±0.08	[illegible]	0.79±0.21
134	0.67±0.07	0.63±0.06	[illegible]	0.55±0.08
135	0.86±0.14	0.82±0.09	[illegible]	1.00±0.13
136		0.76±0.05	[illegible]	0.87±0.03
140	0.92±0.35	0.94±0.23	[illegible]	1.14±0.35
$\langle c \rangle$	0.78±0.12	0.80±0.14	[illegible]	0.93±0.27
$\langle E_{exc} \rangle$ (MeV)	9.7	11.6	[illegible]	14.1

(OVER)

TABLE II. Fractional independent and cumulative chain yields for the photofission of ^{235}U. (c) denotes the fractional cumulative chain yield.

Nuclide \ E_γ (MeV)	12	15	20	30
$^{88}Br(c)$	0.434±0.042	0.427±0.042	0.396±0.035	0.408±0.040
$^{89}Kr(c)$	0.870±0.084	0.842±0.079	0.852±0.079	0.867±0.084
$^{90}Kr(c)$	0.595±0.076	0.628±0.079	0.599±0.075	0.602±0.076
$^{91}Kr(c)$	0.372±0.037	0.377±0.124	0.342±0.035	0.304±0.033
$^{93}Rb(c)$	0.441±0.089	0.482±0.066	0.419±0.103	
$^{94}Sr(c)$	0.802±0.099	0.817±0.088	0.762±0.080	0.787±0.083
$^{95}Sr(c)$	0.641±0.063	0.634±0.056	0.579±0.053	0.625±0.058
$^{100}Zr(c)$	0.704±0.091	0.677±0.102	0.604±0.076	0.598±0.108
$^{126}Sb^g$		$(5.9 \pm 2.2)\times 10^{-2}$	$(8.2 \pm 1.7)\times 10^{-2}$	0.110±0.017
$^{126}Sb^m$		$(6.4 \pm 2.0)\times 10^{-2}$	$(6.7 \pm 1.7)\times 10^{-2}$	$(8.0 \pm 1.9)\times 10^{-2}$
$^{128}Sn(c)$		0.685±0.053	0.661±0.046	0.611±0.049
$^{129}Sb^A(\frac{11}{2}^-)(c)$	0.253±0.020	0.196±0.012	0.186±0.013	0.180±0.016
$^{129}Sb^B(\frac{3}{2}^+)(c)$	0.151±0.011	0.146±0.009	0.133±0.009	0.123±0.009
$^{130}Sn(c)$	0.258±0.020	0.236±0.019	0.241±0.034	0.173±0.020
$^{130}Sb^A(5^+)$	0.293±0.137	0.248±0.072	0.220±0.059	0.250±0.063
$^{130}Sb^B(8^-)$	0.331±0.030	0.281±0.020	0.296±0.016	0.275±0.011
^{130}I		$(3.6 \pm 1.7)\times 10^{-3}$	$(5.7 \pm 1.0)\times 10^{-3}$	$(9.8 \pm 1.6)\times 10^{-3}$
$^{131}Sn(c)$	0.119±0.010	0.110±0.006	0.114±0.007	0.122±0.007
^{131}Sb	0.549±0.066	0.485±0.045	0.416±0.047	0.410±0.040
$^{131}Te^g$	0.125±0.052	0.151±0.034	0.167±0.028	0.168±0.037
$^{131}Te^m$	0.180±0.023	0.215±0.019	0.263±0.026	0.270±0.023
^{132}Sn	$(3.2 \pm 1.8)\times 10^{-2}$	$(2.2 \pm 0.7)\times 10^{-2}$	$(2.5 \pm 0.7)\times 10^{-2}$	$(3.0 \pm 0.8)\times 10^{-2}$
$^{132}Sb^g$	0.138±0.017	0.100±0.010	$(7.5 \pm 0.9)\times 10^{-2}$	$(9.8 \pm 1.3)\times 10^{-2}$
$^{132}Sb^m$	0.202±0.054	0.214±0.023	0.187±0.020	0.192±0.022
^{132}Te	0.562±0.094	0.602±0.052	0.629±0.065	0.592±0.028
^{132}I	$(4.6 \pm 1.9)\times 10^{-2}$	$(6.2 \pm 0.6)\times 10^{-2}$	$(7.6 \pm 0.8)\times 10^{-2}$	$(9.1 \pm 0.9)\times 10^{-2}$
^{133}Sb	0.196±0.019	0.175±0.017	0.162±0.013	0.179±0.018
$^{133}Te^g$	0.203±0.043	0.214±0.032	0.175±0.072	0.167±0.038
$^{133}Te^m$	0.473±0.062	0.471±0.040	0.454±0.042	0.404±0.041
^{133}I	0.118±0.042	0.153±0.034	0.180±0.025	0.181±0.035
^{134}Sb	$(3.6 \pm 0.6)\times 10^{-2}$	$(3.0 \pm 0.2)\times 10^{-2}$	$(2.3 \pm 0.4)\times 10^{-2}$	$(2.3 \pm 0.4)\times 10^{-2}$
^{134}Te	0.52 ±0.05	0.51 ±0.05	0.48 ±0.05	0.53 ±0.10
^{134}I	0.36 ±0.07	0.40 ±0.06	0.40 ±0.05	0.42 ±0.08
^{135}Te	0.237±0.006	0.171±0.035	0.147±0.031	0.203±0.040
^{135}I	0.603±0.083	0.623±0.056	0.625±0.050	0.562±0.052
^{135}Xe	0.160±0.021	0.206±0.017	0.228±0.016	0.245±0.012
^{136}Te	$(6.4 \pm 0.5)\times 10^{-2}$	$(5.7 \pm 0.9)\times 10^{-2}$	$(5.3 \pm 0.7)\times 10^{-2}$	$(7.0 \pm 0.4)\times 10^{-2}$
$^{136}I^g$	$(8.9 \pm 1.4)\times 10^{-2}$	$(7.1 \pm 2.3)\times 10^{-2}$	$(7.7 \pm 1.3)\times 10^{-2}$	$(8.3 \pm 1.2)\times 10^{-2}$
$^{136}I^m$	0.212±0.018	0.225±0.014	0.199±0.017	0.207±0.017
^{136}Cs		$(2.0 \pm 0.5)\times 10^{-2}$	$(2.9 \pm 0.5)\times 10^{-2}$	$(3.6 \pm 0.5)\times 10^{-2}$
$^{137}I(c)$	0.334±0.045	0.326±0.075	0.294±0.069	0.364±0.068
^{137}Xe	0.567±0.114	0.548±0.070	0.483±0.087	0.455±0.078
$^{138}Xe(c)$	0.725±0.115	0.679±0.079	0.589±0.091	0.613±0.093
^{138}Cs	0.250±0.070	0.350±0.078	0.360±0.062	0.390±0.071
$^{139}Xe(c)$	0.547±0.074	0.447±0.065	0.380±0.048	0.418±0.053
$^{140}Xe(c)$	0.248±0.025	0.245±0.025	0.218±0.018	0.223±0.019
^{140}Cs	0.583±0.098	0.576±0.063	0.538±0.081	0.524±0.085
$^{141}Cs(c)$	0.611±0.040	0.643±0.056	0.610±0.082	0.629±0.070
$^{142}Ba(c)$		0.894±0.096	0.866±0.053	0.846±0.091
$^{143}Ba(c)$	0.775±0.105	0.782±0.061	0.685±0.060	0.666±0.055

U
A=236

U
A=236

U
A=236

REACTION	RESULT	EXCITATION ENERGY	SOURCE TYPE	SOURCE RANGE	DETECTOR TYPE	DETECTOR RANGE	ANGLE
G,F	RLY	THR -20	C	6-20	ION-I		DST

TABLE II

Angular distributions

Relative fission fragment yields as a function of peak bremsstrahlung energy E_0 and angle θ to X-ray beam

E_0, Mev	Angle θ 0	25	45	60	90
Th-232					
6.5	1.00±0.3				20±5
7.0	1.00±0.04		4.1±0.2	6.7±0.3	8.4±0.3
7.5	1.00±0.1		5.1±0.4	6.0±0.4	7.9±0.5
8.0	1.00±0.09		2.4±0.2	3.6±0.3	5.1±0.3
9.0	1.00±0.1				3.4±0.3
10.0	1.00±0.04	1.16±0 05	1.67±0.08	1.97±0.08	2.4±0.1
14.0	1.00±0.05				1.43±0.08
20.0	1.00±0.05				1.13±0.06
U-238					
6.0	1.00±0.3				6.0±1.4
6.3	1.00±0.1		3.6±0.4		5.9±0.6
6.5	1.00±0.2				4.5±0.7
7.0	1.00±0.08	1.5±0 1	2.0±0.2	2.4±0.2	2.9±0.2
8.0	1.00±0.06				2.1±0.1
9.4	1.00±0.023	1.094±0.029	1.224±0.029	1.274±0.034*	1.452±0.033
10.0	1.00±0.04				1.38±0.04
14.0	1.00±0.04				1.08±0.04
20.0	1.00±0.03				1.05±0.03
	*θ = 65° in this case				
U-236					
6.0	1.00±0.25				4.6±0.8
6.5	1.00±0.1		2.06±0.2		2.55±0.25
7.0	1.00±0.06		1.65±0.10		2.11±0.12
8.0	1.00±0.04		1.39±0.06		1.66±0.07
9.0	1.00±0.04	1.10±0 07	1.15±0.04	1.31±0.08*	1.46±0.05
10.0	1.00±0.03		1.07±0.03		1.28±0.04
14.0	1.00±0.02				1.03±0.02
	*θ = 65° in this case				
U-234					
6.5	1 00±0.1		1 41±0.14		1.98±0.20
7.0	1 00±0.05		1 19±0.06		1.53±0.08
8.0	1.00±0.03		1.11±0.03		1.30±0.04
10.0	1.00±0.03				1.12±0.03
15.0	1.00±0.03				1.01±0.03
Pu-240					
6.5	1.00±0 10		1.49±0 15		1.55±0.16
7.0	1.00±0 06		1.03±0.06		1.35±0.08
8.0	1.00±0.03		1.01±0.03		1.21±0.04
15.0	1.00±0.02				1.01±0.02

The values quoted are counts observed for unit X-ray dose normalized to unit yield at θ = 0°. No corrections have been applied.

REACTION	RESULT	EXCITATION ENERGY	SOURCE		DETECTOR		ANGLE
			TYPE	RANGE	TYPE	RANGE	

TABLE IV

Relative fissionabilities, U-238 = 100 at 20 Mev

E_0	U-234	U-235	U-236	U-238	Pu-239	Pu-240
6.0		0.45±0.05	0.303±0.013	0.387±0.040		
6.5	1.165±0.033	1.134±0.025	1.159±0.026	1.08±0.07	0.239±0.024	1.145±0.051
7.0	2.515±0.053	2.282±0.038	2.358±0.037	2.14±0.14	4.50±0.22	2.528±0.075
8.0	6.285±0.085	5.519±0.067	5.285±0.056	4.87±0.21	11.35±0.34	6.09±0.12
9.0		11.00±0.33	8.94±0.13	8.65±0.26		
10.0	17.30±0.53	18.75±0.30	14.29±0.20	14.41±0.28	45.1±2.2	
14.0		88.0±4.5	43.11±0.53	57.7±1.4		
15.0	84.3±1.9	119.0±0.9	73.58±0.78	70.5±1.8	235.0±7.6	82.3±1.8
20.0	127.5±2.5	180.8±2.2	109.4±1.0	100±2.5	352±10	120.8±2.3

TABLE VI

Corrected values of α in $W(\theta) = 1+\alpha \sin^2\theta$

E_0	Th-232	U-238	U-236	U-234	Pu-240
6.0		6.6±2	6.0±2.3		
6.3		6.7±1.1			
6.5	>25	4.4±1.0	2.1±0.4	2.3±0.6	0.65±0.20
7.0	11.0±0.8	2.05±0.24	1.33±0.17	0.90±0.16	0.49±0.12
7.5	10.3±1.6				
8.0	4.9±0.6	1.3±0.1	0.79±0.09	0.44±0.08	0.20±0.07
9.0	2.8±0.4		0.51±0.07		
9.4		0.41±0.01			
10.0	1.61±0.12	0.41±0.05	0.22±0.06	0.17±0.07	
14.0	0.46±0.09	0.09±0.04	0.04±0.03		
15.0					
20.0	0.14±0.06	0.05±0.03		0.02±0.04*	0.01±0.03*

*These values, which do not differ from zero, have not been corrected for isotopic composition.

Ref. J.R. Huizenga, K.M. Clarke, J.E. Gindler, R. Vandenbosch
Nuclear Phys. 34, 439 (1962)

Elem. Sym.	A	Z
U	236	92

Method: Monoergic γ's from $F^{19}(p,\alpha\gamma)$ reaction; fission fragment ionization chamber.

Ref. No.: 62 Hu 1 JHH

Reaction	E or ΔE	E_o	Γ	$\int \sigma dE$	Jπ	Notes
$U^{236}(\gamma,f)$	6.14 7.0					

Table 1
Isotopic content of uranium targets in mass per cent

Target	233	234	235	236	238
U[233]	98.33	0.010	0.0127		1.53
U[234]		93.44	4.87		1.69
U[235]		0.022	99.94		0.038
U[236]		0.07	4.62	94.77	0.54
U[238]			0.04		99.96

Table 3
Photofission cross sections obtained with mono-energetic gamma rays from the $F^{19}(p,\alpha\gamma)O^{16}$ reaction

Target	$\sigma_{\gamma,a}/\sigma_{a,1a}$	$\sigma_{\gamma,a}$(mb)	$\sigma_{a,1a}$(mb)	B_a(MeV) a)	E_f(MeV) b)
Th^{232}	1.00 ± 0.13	9 ± 3	9 ± 3	6.34	5.5
U^{233}	1.12 ± 0.15	15 ± 5	13 ± 4	6.04	5.3
U^{235}	0.80 ± 0.10	28 ± 9	35 ± 11	6.40	5.2
U^{236}	2.00 ± 0.33	33 ± 10	16 ± 5	5.24	5.5
U^{238}	10.0 ± 5.0	52 ± 16	5^{+10}_{-5}	6.77	5.1
U^{233}	3.25 ± 0.79	44 ± 14	13 ± 4	5.90	5.4
Np^{237}	1.43 ± 0.21	45 ± 14	31 ± 10	6.78	5.3

a) From the compilation of ref [20]
b) From the compilation of ref [26]

Ref 20: Everling, König, Mattauch, & Wapstra - Nuclear Phys. 18, 529 (1960)

Ref 26: Vandenbosch & Seaborg - Phys. Rev. 110, 507 (1958)

REF.

D. C. Aumann and J. E. Gindler
J. inorg. nucl. Chem. 32, 731 (1970)

ELEM. SYM.	A	Z
U	236	92

METHOD

REF. NO.	
70 Au 1	egf

REACTION	RESULT	EXCITATION ENERGY	SOURCE		DETECTOR		ANGLE
			TYPE	RANGE	TYPE	RANGE	
G,F	RLY	THR-17	C	14-17	ACT-I		4PI

Data ratio of isomer to ground state yields.

ISOMER YIELDS

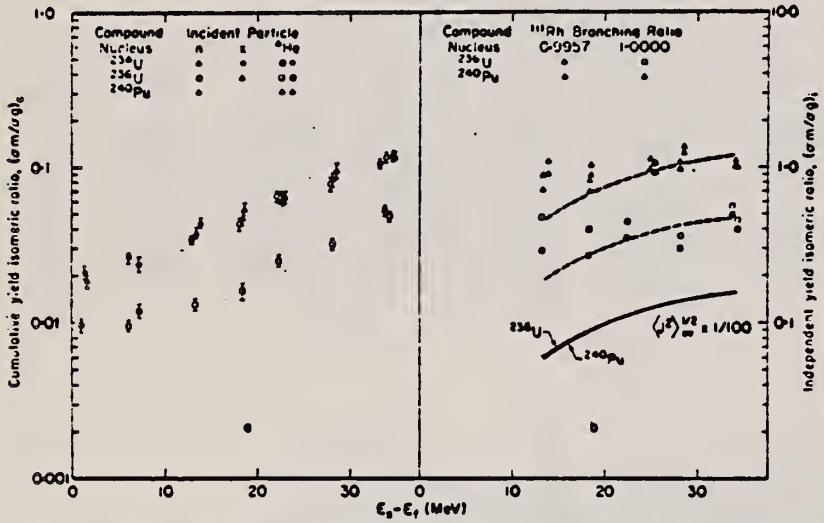

Fig. 3. Cumulative (a) and independent (b) yield ^{111}Pd isomeric ratios as a function of excitation energy above the fission barrier for several compound nuclei. The solid curves in 3b represent the root-mean-square average angular momenta of the compound nuclei indicated. The dashed curves are the solid curves displaced to pass approximately through the respective isomeric ratio data.

Table 3. Cumulative yield isomeric ratios of ^{111}Pd formed in photofission

Target	E_γ(MeV) 13·8	16·6–17·0	17·1
^{232}Th	0·0060 ± 0·0004	0·0056 ± 0·0006	
^{235}U	0·0053 ± 0·0004	0·0054 ± 0·0005	0·0066 ± 0·0017
^{238}U	0·0095 ± 0·0007		0·0119 ± 0·0012
^{233}U	0·0125 ± 0·0009	0·0130 ± 0·0013	
^{234}U	0·0261 ± 0·0019		0·0235 ± 0·0024
^{239}U	0·0304 ± 0·0022	0·0380 ± 0·0038	0·0454 ± 0·0045

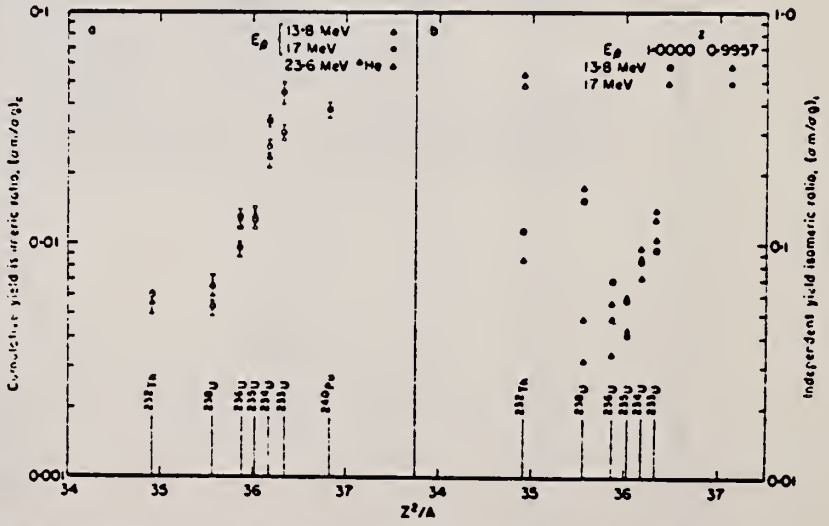

Fig. 5. Cumulative (a) and independent (b) yield ^{111}Pd isomeric ratios as a function of Z^2/A for the compound nucleus.

REF. M.V. Yester, R.A. Anderl, R.C. Morrison
Nucl. Phys. A206, 593 (1973)

ELEM. SYM.	A	Z
U	236	92

METHOD

REF. NO. 73 Ye 2 egf

REACTION	RESULT	EXCITATION ENERGY	SOURCE TYPE	SOURCE RANGE	DETECTOR TYPE	DETECTOR RANGE	ANGLE
G,F	ABX	5- 8	D	5- 8	SCD-I		4PI

COMPTON SCD G-SOURCE

Incident spectrum is result of Compton scattering of Ni n-capture gammas. Spectrum is flat with peak at high energy end. Cross section obtained by unfolding yield curve.

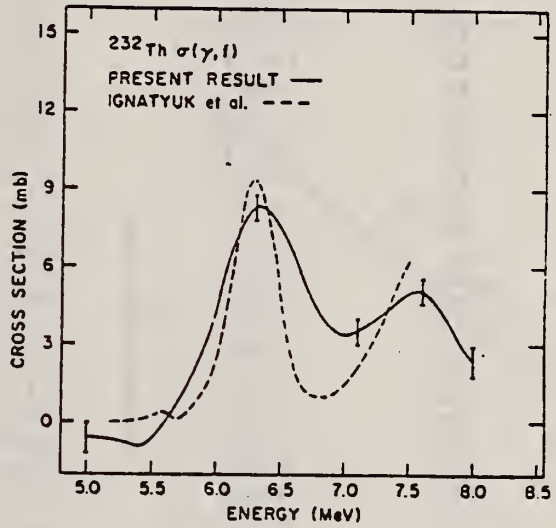

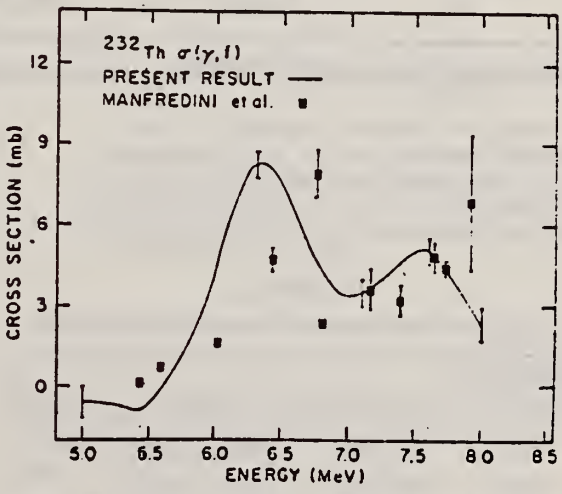

Fig. 11. Comparison of the ^{232}Th photofission cross section measured in the present work (a) with the data obtained by Ignatyuk *et al.* [6]) using bremsstrahlung, and (b) with the data of Manfredini *et al.* [8]) obtained with discrete lines from neutron-capture γ-sources.

[6] A.V. Ignatyuk, N.S. Rabotnov, G.N. Smirenkin, A.S. Soldatov, Yu. M. Tsipenyuk, JETP (Sov. Phys.) 34 (1972) 684

[8] A. Manfredini, L. Fiore, C. Ramorino, H. G. De Carvalho and W. Wolfli, Nucl. Phys. A127 (1969) 68

(over)

TABLE I

Photofission cross sections of ^{232}Th and ^{236}U

Energy (MeV)	^{232}Th cross section (mb)	^{236}U cross section (mb)
5.0	−0.6±0.6 [a])	−2.6±1.3 [a])
5.1	−0.6±0.5	−2.0±1.1
5.2	−0.7±0.3	−1.1±0.8
5.3	−0.8±0.3	−0.1±0.7
5.4	−0.9±0.4	0.2±0.7
5.5	−0.6±0.4	0.7±0.8
5.6	0.1±0.5	1.3±0.9
5.7	0.9±0.5	2.1±1.0
5.8	1.7±0.5	3.2±1.0
5.9	2.9±0.5	4.2±1.0
6.0	4.5±0.5	4.7±1.0
6.1	6.2±0.5	4.9±1.0
6.2	7.6±0.5	4.9±1.0
6.3	8.3±0.5	5.0±1.0
6.4	8.2±0.5	5.3±1.0
6.5	7.5±0.5	5.7±1.1
6.6	6.4±0.5	5.7±1.1
6.7	5.2±0.5	5.5±1.1
6.8	4.2±0.5	5.3±1.1
6.9	3.6±0.5	5.0±1.1
7.0	3.4±0.5	5.4±1.1
7.1	3.5±0.5	6.4±1.1
7.2	3.9±0.5	8.0±1.1
7.3	4.3±0.5	10.1±1.1
7.4	4.7±0.5	11.9±1.1
7.5	5.1±0.5	12.6±1.1
7.6	5.1±0.5	12.6±1.1
7.7	4.7±0.5	12.1±1.1
7.8	3.9±0.5	11.5±1.1
7.9	3.1±0.5	10.7±1.1
8.0	2.4±0.6	9.8±1.3

[a]) These are the relative errors only. The ±30% error in the absolute scale has not been included.

REF. J.T. Caldwell and E.J. Dowdy
Nucl. Sci. & Eng. 56, 179 (1975)

EL EM. SYM.	A	Z
U	236	92

METHOD

REF. NO. 75 Ca 5 egf

REACTION	RESULT	EXCITATION ENERGY	SOURCE		DETECTOR		ANGLE
			TYPE	RANGE	TYPE	RANGE	
G,F	NOX	6- 13	C	8- 13	MOD-I		4PI

The prompt- and delayed-neutron multiplicities for photofission of the eight isotopes, ^{232}Th, ^{233}U, ^{234}U, ^{235}U, ^{236}U, ^{238}U, ^{237}Np, and ^{239}Pu, have been measured using bremsstrahlung with end-point energies ranging from 8 to 13 MeV. The measured multiplicities are compared with those from the same compound nucleus formed in neutron-induced fission where such data exist.

NEUTRON MULTIPLICITIES

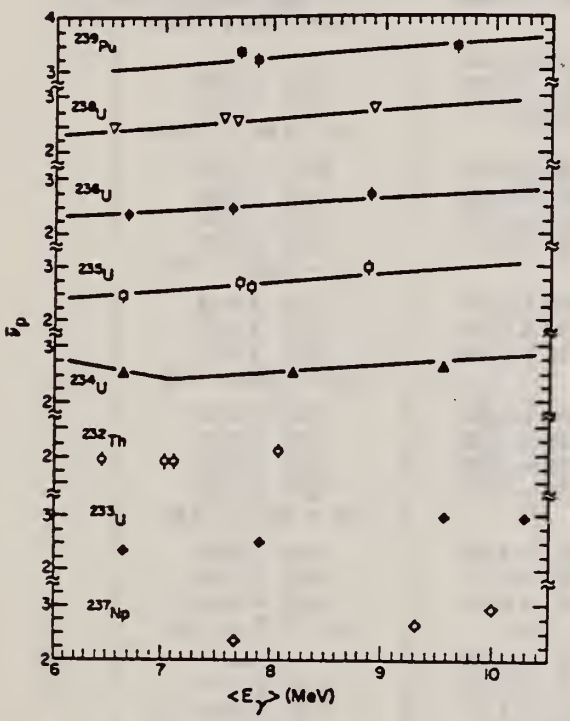

Fig. 5. $\bar{\nu}_p$ versus excitation energy for the eight isotopes studied in this experiment. The full curves shown are from the evaluations of Davey[2] with the excitation energy determined as described in the text. For the lower three isotopes shown, no previous experimental values for $\bar{\nu}_p$ exist.

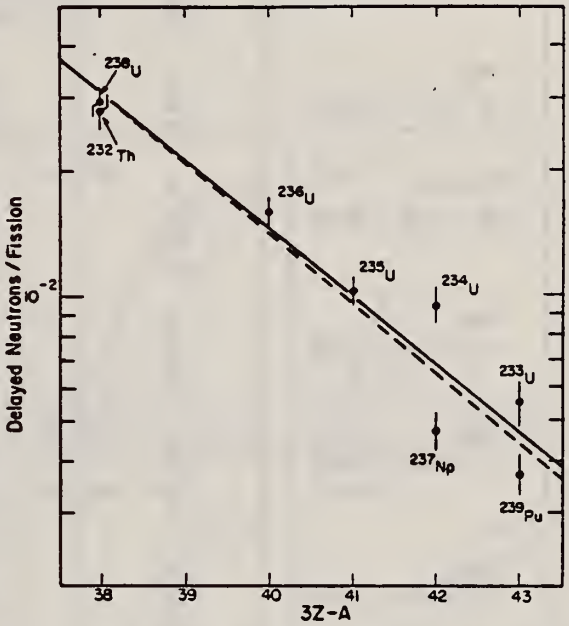

Fig. 6. Delayed neutrons per fission versus the parameter 3Z-A of the compound nucleus. The full curve shown is the least-squares fit to the data shown with ln Y_0 = 10.61, K = -0.372. The dashed curve is the least-squares fit to the data provided by Tomlinson[6] with ln Y_0 = 11.35, K = -0.39.

TABLE IV

Least-Squares Linear Fit Expressions for $\bar{\nu}_p(\langle E_\gamma \rangle)$

Isotope	$\bar{\nu}_p(\langle E_\gamma \rangle) = \bar{\nu}_0 + d\bar{\nu}_p/dE\,\langle E_\gamma \rangle$	Correlation Coefficient
^{232}Th	$\bar{\nu}_p(\langle E_\gamma \rangle) = 1.310 + 0.090\ \langle E_\gamma \rangle$	0.675
^{233}U	$\bar{\nu}_p(\langle E_\gamma \rangle) = 1.200 + 0.1709\ \langle E_\gamma \rangle$	0.947
^{234}U	$\bar{\nu}_p(\langle E_\gamma \rangle) = 2.222 + 0.0399\ \langle E_\gamma \rangle$	0.741
^{235}U	$\bar{\nu}_p(\langle E_\gamma \rangle) = 0.9034 + 0.2292\ \langle E_\gamma \rangle$	0.967
^{236}U	$\bar{\nu}_p(\langle E_\gamma \rangle) = 1.140 + 0.1788\ \langle E_\gamma \rangle$	0.986
^{238}U	$\bar{\nu}_p(\langle E_\gamma \rangle) = 1.502 + 0.1458\ \langle E_\gamma \rangle$	0.984
^{237}Np	$\bar{\nu}_p(\langle E_\gamma \rangle) = 0.4027 + 0.2505\ \langle E_\gamma \rangle$	0.967
^{239}Pu	$\bar{\nu}_p(\langle E_\gamma \rangle) = 2.526 + 0.0930\ \langle E_\gamma \rangle$	0.777

[2] W.G. Davey, Nucl. Sci. Eng., 44, 345 (1971)

[6] L. Tomlinson, "Delayed Neutrons from Fission: A Compilation and Evaluation of Experimental Data," AERE-R-6993, Atomic Energy Research Establishment, Harwell (1972)

over

TABLE III

Prompt- and Delayed-Neutron Yields

	E_n, MeV	$\langle E_\gamma \rangle$, MeV	ν_p	Delayed Neutrons per 100 Fissions
^{232}Th	8	6.44	1.96 ± 0.11	3.10 ± 0.28
(σ = 1.15 ± 0.05)	10	7.02	1.89 ± 0.11	3.06 ± 0.31
	10.2	7.10	1.89 ± 0.11	2.67 ± 0.21
	12	8.06	2.08 ± 0.11	2.59 ± 0.31
				av = 2.80 ± 0.28
^{233}U	8	6.68	2.350 ± 0.112	0.455 ± 0.040
(σ = 1.25 ± 0.05)	10	7.90	2.498 ± 0.108	0.518 ± 0.040
	12	9.55	2.960 ± 0.096	0.640 ± 0.044
	13	10.27	2.870 ± 0.099	0.598 ± 0.051
				av = 0.553 ± 0.044
^{234}U	8	(6.67)[a]	2.536 ± 0.112	---
(σ = 1.13 ± 0.05)	10	8.69	2.499 ± 0.107	0.92 ± 0.06
	12	9.54	2.623 ± 0.105	0.97 ± 0.12
				av = 0.94 ± 0.094
^{235}U	8	6.67	2.456 ± 0.086	0.90 ± 0.08
(σ = 1.20 ± 0.05)	10	7.70	2.697 ± 0.081	0.88 ± 0.08
	10.2	7.81	2.612 ± 0.079	1.13 ± 0.07
	12	8.86	2.963 ± 0.072	1.12 ± 0.08
				av = 1.02 ± 0.08
^{236}U	8	6.66	2.357 ± 0.111	1.43 ± 0.14
(σ = 1.20 ± 0.05)	10	7.63	2.470 ± 0.105	1.73 ± 0.12
	12	8.86	2.744 ± 0.095	1.64 ± 0.10
				av = 1.60 ± 0.13
^{238}U	8	6.53	2.457 ± 0.088	3.06 ± 0.24
(σ = 1.22 ± 0.05)	10	7.54	2.628 ± 0.083	2.76 ± 0.17
	10.2	7.66	2.585 ± 0.082	3.06 ± 0.14
	12	8.88	2.802 ± 0.078	2.75 ± 0.19
				av = 2.91 ± 0.20
^{237}Np	10	7.68	2.35 ± 0.11	0.38 ± 0.04
(σ = 1.20 ± 0.05)	12	9.31	2.65 ± 0.10	0.50 ± 0.04
	13	9.92	2.95 ± 0.10	0.54 ± 0.04
				av = 0.47 ± 0.04
^{239}Pu	10	7.69	3.32 ± 0.08	---
(σ = 1.18 ± 0.10)	10.2	7.84	3.17 ± 0.14	0.37 ± 0.04
	12	9.65	3.43 ± 0.10	0.37 ± 0.04
				av = 0.37 ± 0.04

[a]Estimated value.

REF.

A. Alm, L. J. Lindgren
Nucl. Phys. A271, 1 (1976)

ELEM. SYM.	A	Z
U	236	92

METHOD

REF. NO. 76 Al 4 egf

REACTION	RESULT	EXCITATION ENERGY	SOURCE TYPE	SOURCE RANGE	DETECTOR TYPE	DETECTOR RANGE	ANGLE
G,F	RLY	THR- 7	C	5- 7	TRK-I		DST

Abstract: A measurement of the angular distribution and yield of fission fragments from photofission of ^{236}U has been performed between 5.2 MeV and 6.4 MeV. As γ-source the bremsstrahlung from a microtron has been used. For the detection of the fission fragments, solid-state track detectors were used. The experimental data were analyzed within the framework of the double-hump fission barrier model.

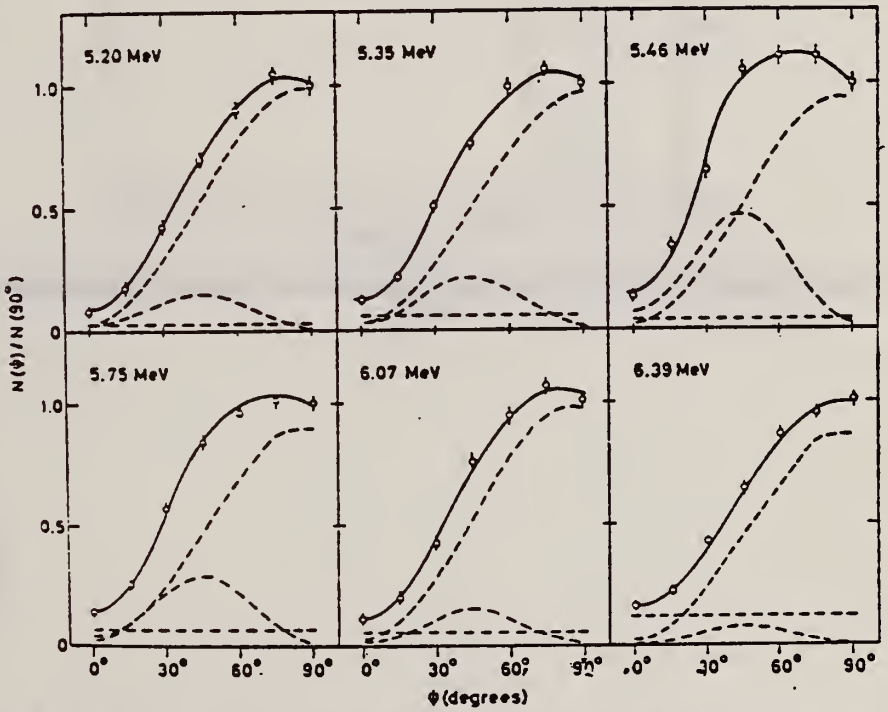

Fig. 3. Some typical angular distributions (circles) normalized to the value in the 90° direction. The dashed curves represent the components of the angular distribution, as given by the best fit of the constants *a*, *b* and *c*. The solid curve is the sum of these components. Actually, both the experimental values and the calculated components represent histograms, the width of each angular bin being 15°, but for greater clarity, the curves are drawn.

(over)

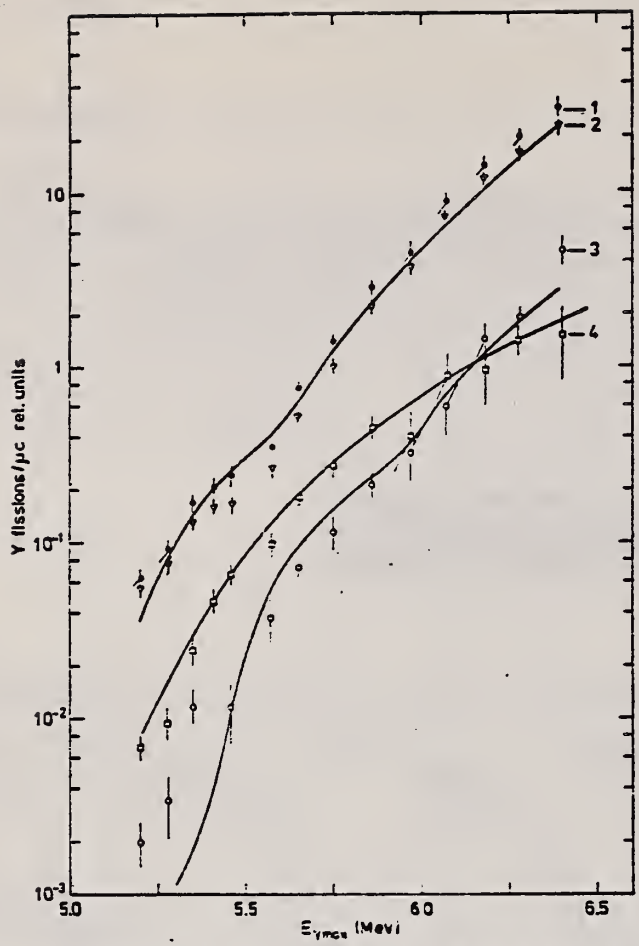

Fig. 4. The yields $Y(1)$, $Y_a(3)$, $Y_b(2)$ and $Y_c(4)$. The curves represent the best fit for the experimental points.

REF. V.E. Zhuchko, A.V. Ignatyuk, Yu.B. Ostapenko, G.N. Smirenkin, A.S. Soldatov and Yu.M. Tsipenyuk
Phys. Lett. 68B, 323 (1977).

ELEM. SYM.	A	Z
U	236	92

METHOD

REF. NO. 77 Zh 1 egf

REACTION	RESULT	EXCITATION ENERGY	SOURCE		DETECTOR		ANGLE
			TYPE	RANGE	TYPE	RANGE	
G,F	ABX	3- 7	C	3- 7	TRK-I		DST

Experimental data on yields and angular distributions of photofission fragments of ^{236}U and ^{238}U are presented. The anomalies caused by delayed fission from the low-lying isomer states of the second well have been clearly observed in the energy dependence of the yields of the isotropic component. Characteristic features of the observed phenomena have been analyzed.

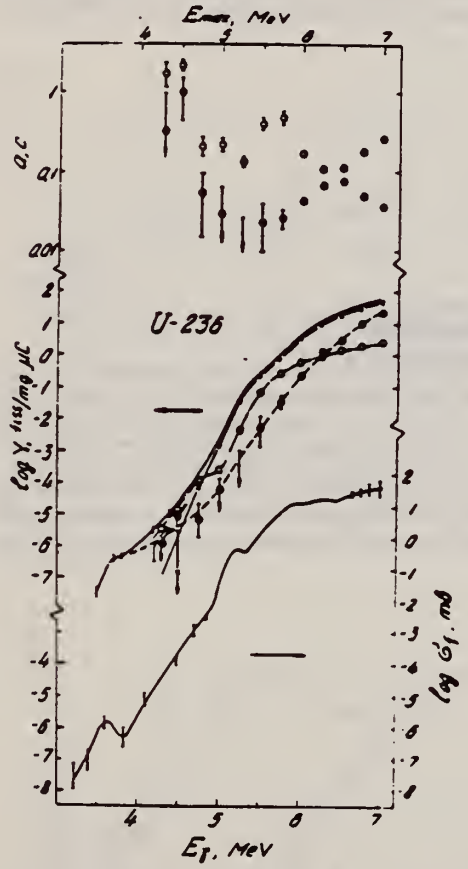

Fig. 2. The coefficients of the fragment angular distributions, the integral yields and the photofission cross sections for ^{236}U. The symbols are the same as in fig. 1.

REF. C.D. Bowman, I.G. Schroder, K.C. Duvall and C.E. Dick
Phys. Rev. C 17, 1086 (1978)

ELEM. SYM.	A	Z
U	236	92

~~METHOD~~

Upper limit of σ at 3.5 MeV is 1.2 ± 1.7 x 10^{-10} b

REF. NO. 78 Bo 8

hg

REACTION	RESULT	EXCITATION ENERGY	SOURCE		DETECTOR		ANGLE
			TYPE	RANGE	TYPE	RANGE	
G,F	ABX	THR- 4	C	4	TRK-I		4PI
		(THR-3.5)		(3.5)			

Upper limit for SIGMA

Photofission cross sections for ^{232}Th, and ^{236}U have been measured in the energy range from 3.25 to 5.75 MeV and for ^{234}U and ^{236}U at 3.5 MeV. The cross sections change by over seven orders of magnitude for this energy range. Cross section shapes are significantly different for different isotopes indicating a strong sensitivity to fission barrier parameters.

REF. V.E. Zhuchko, Yu.B. Ostapenko, G.N. Smirenkin, A.S. Soldatov, Yu.M. Tsipenyuk
Yad. Fiz. 28, 1185 (1978)
Sov. J. Nucl. Phys. 28, 611 (1978)

ELEM. SYM.	A	Z
U	236	92

METHOD

REF. NO. 78 Zh 6

REACTION	RESULT	EXCITATION ENERGY	SOURCE		DETECTOR		ANGLE
			TYPE	RANGE	TYPE	RANGE	
G,F	ABX	THR-5	C	3-5	TRK-D		4PI
		(THR-4.6)		(3.5-4.6)			

Yield measurements are reported for photofission of ^{232}Th, ^{236}U, ^{238}U, and ^{237}Np in the deep sub-barrier energy region 3.5–4.6 MeV where anomalies in the cross section—isomeric shelfs—were previously observed [Phys. Rev. C, 12, 863 (1975)]; Pis'ma. Zh. Eksp. Teor. Fiz. 22, 255 (1975), [JETP Lett. 22, 118 (1975)]. The various sources of background arising in this energy region, which is only with difficulty accessible for measurements, are analyzed in detail. Analysis of the anomalies in the behavior of the integrated photofission yields in the case of the two nuclei ^{236}U and ^{238}U most favorable for study indicates a resonance nature of the cross sections for delayed fission and a substantially more complicated physics of the phenomenon than the simplified interpretation of Bowman [Phys. Rev. C, 12, 863 (1975)].

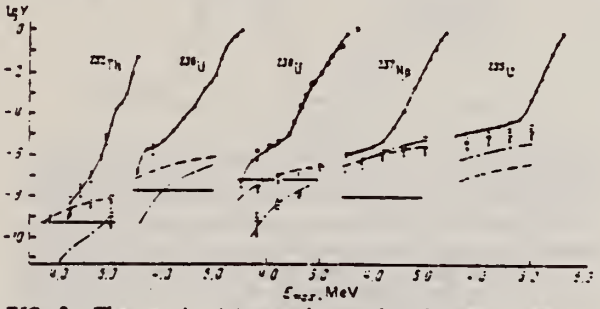

FIG. 2. The round points are the results of measurement of the yields $Y(E_{max})$ in fissions/mg-μC of the photofission reaction: ●—present work and Ref. 7; ○—Ref. 8. ⁻ and dashed lines—respectively the experimental and theoretical estimates of the background due to fissions by neutrons from the reaction Be(γ,n); ○ and dot-dash lines—the same for the D(γ,n) reaction. The shaded sections show the level of background from spontaneous fission and fission induced by cosmic rays.

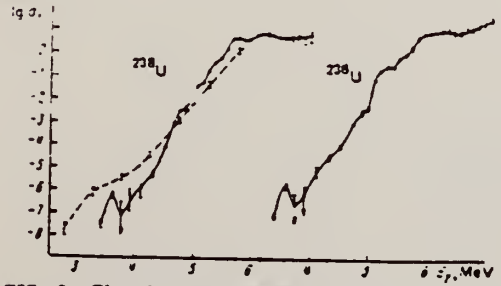

FIG. 3. Photofission cross sections $\sigma_f(E_\gamma)$ in mb for ^{236}U and ^{238}U: ●—results of the present work and Ref. 7; ○ data of Ref. 2.

REF. V.E. Zhuchko, Yu.B. Ostapenko, G.N. Smirenkin, A.S. Soldatov,
Yad. Fiz. 28, 1170 (1978)
Sov. J. Nucl. Phys. 28, 602 (1978)

ELEM. SYM.	A	Z
U	236	92

METHOD

REF. NO. 78 Zh 7 hg

REACTION	RESULT	EXCITATION ENERGY	SOURCE		DETECTOR		ANGLE
			TYPE	RANGE	TYPE	RANGE	
G,F	ABX	THR-7	C	4-7	TRK-D		4PI
				(4.4-7.)			

The bremsstrahlung beam of the microtron at our Institute has been used to measure photofission yields of nine nuclei—^{232}Th, ^{233,235,236,238}U, ^{237}Np, ^{239,241}Pu, and ^{241}Am in the energy region 4.4–7.0 MeV. The method of minimization of the directed deviation was used to reproduce the photofission cross sections from the integrated yields. The following problems are discussed in terms of the experimental data: resonance structure of the cross sections, effects of a two-humped shape of the fission barrier, and comparison of the fissility in the (γ,f) and (n,f) reactions and in direct reactions.

PACS numbers: 25.85.Jg

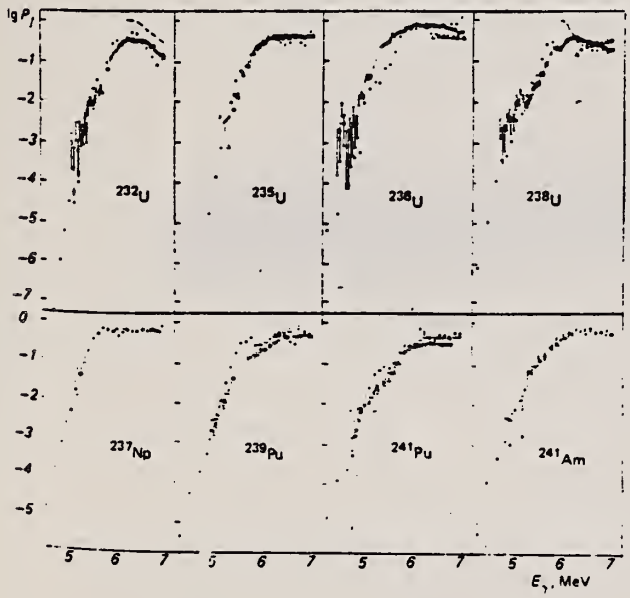

FIG. 4. Fissility P_f in the reactions (γ,f)—●, (n,f)—△ (Ref. 14), and in direct reactions—○.[2] The dashed curve shows the results of evaluation of P_f in accordance with Eq. (9).

(over)

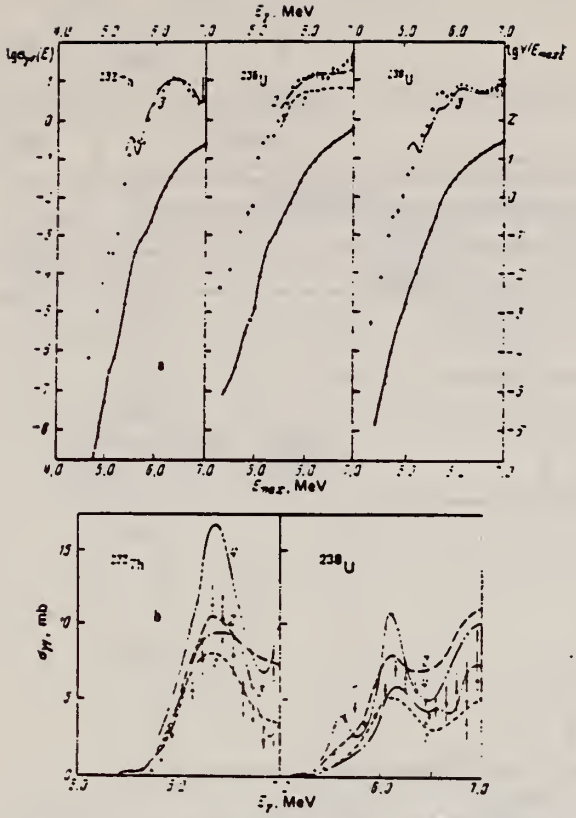

FIG. 2. Yields $Y(E_{max})$, fissions/mg-μC (lower curve), and cross sections $\sigma_{ff}(E_\gamma)$, mb (upper curve), of the photofission reaction for even-even isotopes—a: comparison of the functions $\sigma_{ff}(E_\gamma)$ obtained in the present work for ^{232}Th and ^{238}U with data obtained in quasimonochromatic γ rays—b. Curves: solid lines (and points)—results of the present work, 1—data of Ref. 5, 2—data of Ref. 6, 3—data of Ref. 7, 4—data of Ref. 8.

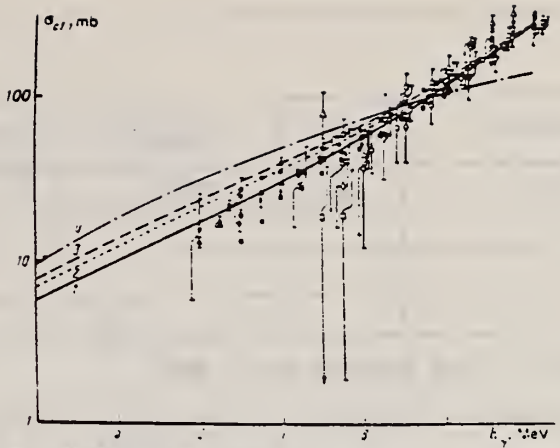

FIG. 6. Set of data on dipole photoabsorption cross sections σ_{ct}. The solid line (1)—the present work—is the result of fitting the data of Ref. 6 by Eq. (2) in the region $E_\gamma = 6$–10 MeV. Curves 2 and 3 are an extrapolation of the fit from Ref. 16 (2) and Ref. 17 (3) for ^{238}U; curve 4 is an estimate by means of Axel's formula.[15] Points: □, ■—^{232}Th; △, ▲—^{235}U; ♦—^{236}U; ○, ●—^{238}U; ▽, ▼—^{237}Np; ◇—^{239}Pu. The hollow points are from Refs. 16 and 17; the solid points are from Ref. 6.

REF. J.D.T. Arruda Neto, B.L. Berman, S.B. Herdade, I.C. Nascimento
Lett. al Nuovo Cimento 26, 487 (1979)

ELEM. SYM.	A	Z
U	236	92

METHOD

REF. NO. 79 Ar 7 hg

REACTION	RESULT	EXCITATION ENERGY	SOURCE		DETECTOR		ANGLE
			TYPE	RANGE	TYPE	RANGE	
G,F	ABX	THR-7	C	11-19	TRK-D		4PI

See 80Ar15. Data entered to 33 MeV.

VIRTUAL PHOTONS, GQR

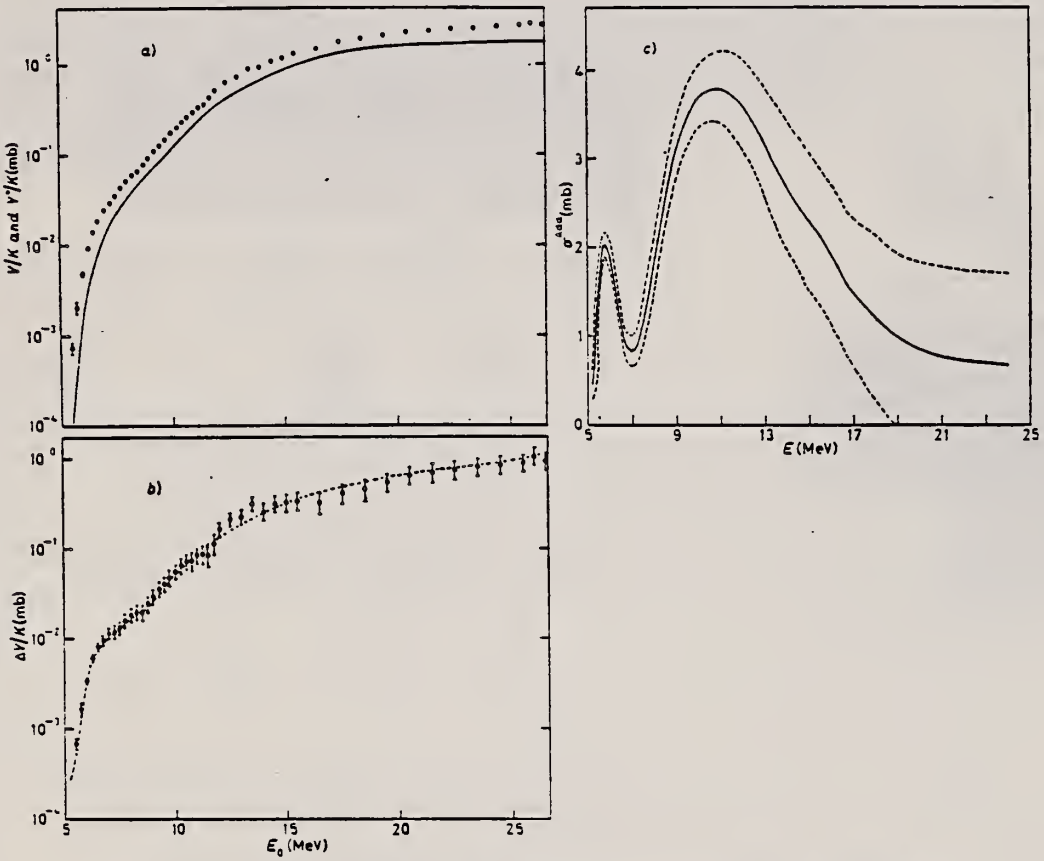

Fig. 1. – *a*) Normalized electronfission yield for ^{238}U (data points). The solid curve represents the yield which would result from the *E*1 component only, obtained by integrating the photofission cross-section data of ref. (7). *b*) Normalized electrofission yield difference between the data and the curve of fig. 1*a*) (data points). The solid curve is the fold-back of σ^{Add} in eq. (3). *c*) Photofission cross-section obtained from the yield analysis (σ^{Add}). The dashed curves determine the error limits for σ^{Add}.

(over)

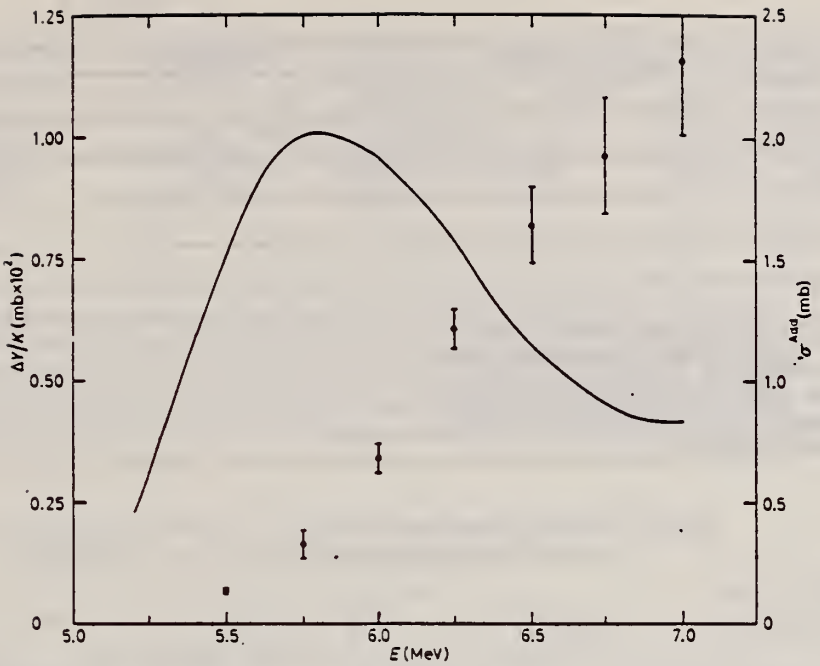

Fig. 2. – Data points represent the same yield differences of fig. 1*b*) in linear plot (left scale), and the solid curve is the σ^{Add} of fig. 1*c*) (right scale).

REF. V.E. Zhuchko, Yu.B. Ostapenko, G.N. Smirenkin, A.S. Soldatov, Yu.M. Tsipenyuk
Yad. Fiz. 30, 634 (1979)
Sov. J. Nucl. Phys. 30, 326 (1979)

ELEM. SYM.	A	Z
U	236	92

METHOD

REF. NO. 79 Zh 3 hg

REACTION	RESULT	EXCITATION ENERGY	SOURCE TYPE	SOURCE RANGE	DETECTOR TYPE	DETECTOR RANGE	ANGLE
G,F	YLD	THR-7	C	4-7	TRK-D		DST
				(4.3-7)			

We report the method and results of measurements of angular distributions of fragments in the (γ,f) reaction for ^{232}Th, ^{236}U, and ^{238}U carried out in connection with the investigation of the properties of deep sub-barrier photofission: the isomeric shelf phenomenon, disappearance of the angular anisotropy ($^{236,238}U$), and the absence of this effect and of the sub-barrier enhancement of quadrupole photofission in ^{232}Th. The experimental data presented permit an understanding of the nature and relation of these properties in terms of the concept of a two-humped fission-barrier structure.

PACS numbers: 25.85.Jg

TABLE I. Parameters of the angular distributions of photofission fragments.

E_{max}, MeV	N, no.	$J\Delta t$, μC	$c \pm \Delta c$	$b \pm \Delta b$	$c \pm \Delta c$
		^{232}Th (δ=200 mg/cm^2)			
5.0	552	$8.9\cdot10^6$	0.000±0.06	1.000±0.06	0.250±0.080
5.2	758	$1.0\cdot10^6$	0.000±0.08	1.000±0.08	0.225±0.100
6.4	48 940	510	0.06±0.03	0.94±0.03	0.06±0.04
6.4 •	29 340	10 900	0.044±0.002	0.956±0.003	0.028±0.006
		^{236}U (δ=1.7 mg/cm^2)			
4.3	168	$9.6\cdot10^6$	0.72±0.25	0.28±0.26	1.71±0.35
4.75	2543	$2.0\cdot10^6$	0.17±0.20	0.83±0.20	0.18±0.15
5.0	3441	$0.5\cdot10^6$	0.10±0.10	0.90±0.10	0.20±0.15
5.1 •	852	$0.9\cdot10^6$	0.04±0.02	0.96±0.05	0.187±0.048
5.25	23 630	$0.1\cdot10^6$	0.06±0.03	0.94±0.03	0.12±0.04
5.5	16 580	$1.5\cdot10^6$	0.11±0.08	0.89±0.08	0.42±0.08
5.8 •	4623	$0.17\cdot10^6$	0.040±0.012	0.960±0.024	0.503±0.028
		^{238}U (δ=0.8 mg/cm^2)			
4.5	612	$8.9\cdot10^6$	1.000±0.3	0.000±0.3	2.800±0.35
5.0	3917	$1.0\cdot10^6$	0.200±0.1	0.800±0.1	0.250±0.15
5.3	12 800	$2.0\cdot10^6$	0.150±0.07	0.850±0.07	0.549±0.13
5.5 •	12 760	$1.6\cdot10^6$	0.048±0.006	0.952±0.014	0.479±0.016
5.75 •	7695	$2.0\cdot10^6$	0.027±0.005	0.973±0.013	0.432±0.015
6.0 •	7681	$4.0\cdot10^6$	0.042±0.005	0.958±0.013	0.186±0.013
6.25 •	9831	$2.0\cdot10^6$	0.069±0.005	0.931±0.013	0.110±0.013
6.5 •	10 150	$1.0\cdot10^6$	0.112±0.008	0.868±0.013	0.080±0.013
6.75 •	10 080	5000	0.199±0.008	0.801±0.014	0.051±0.015
7.0 •	7762	2500	0.257±0.008	0.743±0.014	0.071±0.015
7.25 •	4790	1000	0.320±0.009	0.680±0.014	0.035±0.015
		^{238}U (δ=200 mg/cm^2)			
4.15	130	$12.8\cdot10^6$	1.000±0.2	0.000±0.2	0.230±0.20
4.4	434	$9.5\cdot10^6$	0.940±0.35	0.060±0.35	2.500±0.40
4.8	7252	$1.0\cdot10^6$	0.490±0.04	0.510±0.04	2.400±0.04
5.4	449 050	$0.4\cdot10^6$	0.020±0.02	0.980±0.02	0.400±0.02
5.4 •	5781	$0.5\cdot10^6$	0.094±0.011	0.906±0.015	0.306±0.016

Note. N is the total number of tracks recorded by the detectors; $J\Delta t$ is the integral of the current of accelerated electrons at the bremsstrahlung target; δ is the thickness of the fissile target. The results marked by an asterisk were obtained by the circular glass plate technique[2]; the remaining results are in the 4π geometry.

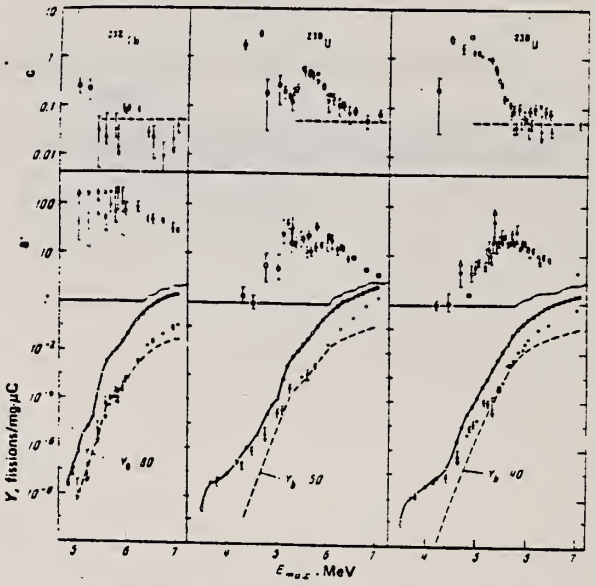

FIG. 3. In the upper and central parts we have shown the parameters of the angular distributions of fragments from photofission of ^{232}Th, ^{236}U, and ^{238}U as a function of E_{max}. Points: ■—results of the present work, ●—results of Refs. 2 and 15, ○—results of Ref. 13. In the lower part: the hollow circles and their connecting solid lines are the total yield of photofissions of the corresponding nuclei,[6,10] the solid circles are the isotropic component of the yield—Y_a, and the dashed line is the component Y_b which has been normalized to Y_a in the region of maximum anisotropy. The dashed line in the upper part of the figure shows the asymptotic value of the coefficient $c \approx c/b \approx 0.05$ for energies above the barrier [see Eq. (3)].

REF. J.D.T. Arruda-Neto, S.B. Herdade, B.L. Berman, I.C. Nascimento
Phys. Rev. C22, 1996 (1980)

ELEM. SYM.	A	Z
U	236	92

METHOD

REF. NO. 80 Ar 7 hg

REACTION	RESULT	EXCITATION ENERGY	SOURCE		DETECTOR		ANGLE
			TYPE	RANGE	TYPE	RANGE	
E,F	ABX	6-33	D	6-33	TRK-D		DST
G,F	ABX	THR-19	C	9-19	TRK-D		2PI

Electrofission and photofission yields and electrofission-fragment angular distributions for ^{236}U have been measured with fission-track detectors for incident electron energies from 5.5 to 33.0 MeV. Analysis of these data with the use of virtual-photon spectra calculated in distorted-wave Born approximation, combined with the known photofission cross section, results in the simultaneous determination for this nucleus of (a) a giant isoscalar $E2$ resonance located at 10.8±0.4 MeV, having a width of 6±1 MeV, and exhausting ~70% of the isoscalar energy-weighted sum rule, and (b) a small $M1$ component located at 5.8±0.2 MeV whose strength is <2% of that of the giant isoscalar $E2$ resonance. No evidence is seen for a giant isovector $E2$ resonance between 22 and 30 MeV.

SEE ALSO 78AR11, 79AR7

[NUCLEAR REACTIONS $^{236}U(e,f)$; measured fission-fragment yields and angular distributions, 5.5 to 33.0 MeV; deduced GQR characteristics.]

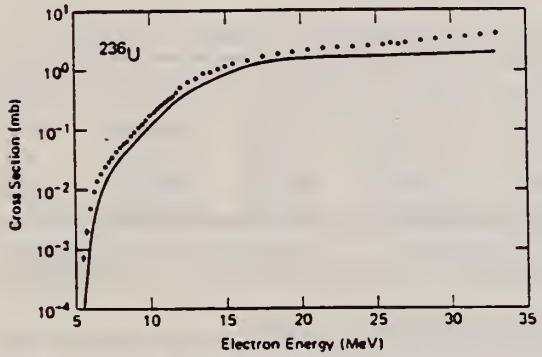

FIG. 2. Measured electrofission cross section σ_e for ^{236}U (data points). Except for the two lowest-energy points, the statistical uncertainties are smaller than the plotted symbols. The solid curve represents the cross section σ_e^* which would result from the $E1$ component only, obtained by integrating the photofission cross section $\sigma(E)$ of Ref. 18 with the $E1$ virtual-photon spectrum. The uncertainty here is of the order of the thickness of the line.

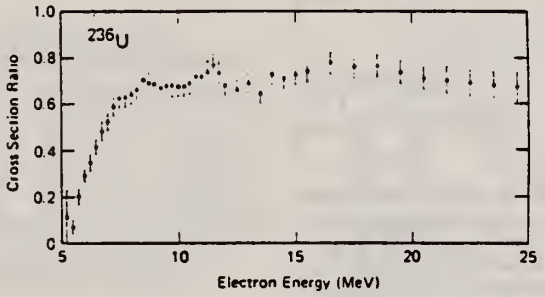

FIG. 4. The ratio of the $E1$ electrofission cross section and the total electrofission cross section for ^{236}U.

TABLE I. Parameters for first-chance fission decay of the GQR.

Nucleus	Peak energy (MeV)	FWHM (MeV)	% EWSR 1 Unit[a]	% EWSR 1.3 Units[b]	Reference
^{236}U	10.8±0.4	~6	72±10	≈55	Present work
^{238}U	9.9±0.4	~5	≥55	≥42	5, 17

[a] Assumes that the total $E2$-photoabsorption strength exhausts one isoscalar EWSR unit.
[b] Assumes that 1.3 EWSR units (130% of the isoscalar $E2$ sum rule) are exhausted (see text).

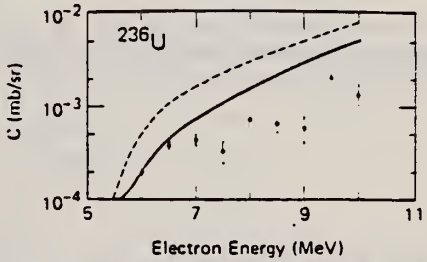

FIG. 8. Absolute values for the coefficient of the $\sin^2 2\theta$ term in the electrofission differential cross section $C(E_0)$ [Eq. (11)], obtained from the measured angular distributions for ^{236}U (data points). The solid curve represents this coefficient as computed, using Eq. (13), from σ^{Add} after $M1$ subtraction; the dashed curve assumes there to be no $M1$ component in σ^{Add}.

(OVER)

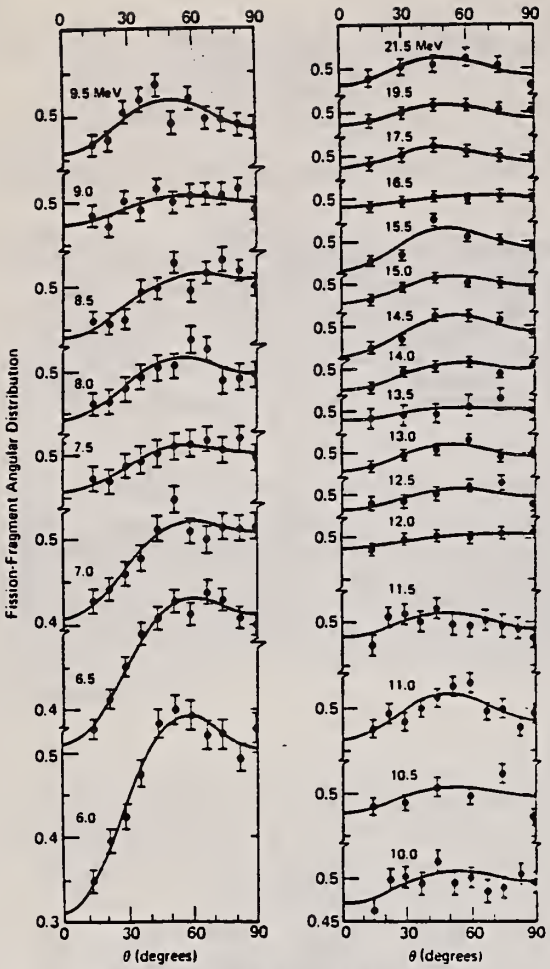

FIG. 7. Electrofission-fragment angular distributions for ^{236}U for incident electrons having energies from 6.0 to 21.5 MeV. The curves are least-square fits of the function $W(\theta)$ [Eq. (12)] to the experimental points. Both systematic and statistical uncertainties are included in the error flags, and were used in the fitting procedure. The redundant data points at 97.5° are not shown.

REF. J. T. Caldwell, E. J. Dowdy, B. L. Berman, R. A. Alvarez, P. Meyer
Phys. Rev. C21, 1215 (1980)

EL EM. SYM.	A	Z
U	236	92

METHOD

REF. NO. 80Cal egf

REACTION	RESULT	EXCITATION ENERGY	SOURCE		DETECTOR		ANGLE
			TYPE	RANGE	TYPE	RANGE	
G,1N	ABX	5-18	D	5-18	BF3 - I	I	4PI
G,2N	ABX	11-18	D	5-18	BF3 - I	I	4PI
G,F	ABX	5-18	D	5-18	BF3 - I	I	4PI

The photoneutron cross sections $\sigma(\gamma,n)$ and $\sigma(\gamma,2n)$, and total photofission cross sections $\sigma(\gamma,F)$ have been measured for ^{235}U, ^{236}U, ^{238}U, and ^{232}Th from threshold to 18.3 MeV using monoenergetic photons from the annihilation in flight of fast positrons and neutron-multiplicity detection in an efficient 4π neutron detector. Use of the ring-ratio technique allowed both the average photofission neutron energy for each nucleus to be obtained as a function of photon energy and, for ^{236}U and ^{238}U, the determination of the partial cross sections for first-chance $\sigma(\gamma,f)$ and second-chance $\sigma(\gamma,nf)$ photofission as well. Information extracted from the data includes integrated cross sections and their moments, giant-resonance parameters, deformation and radius parameters, and relative and absolute neutron and fission probabilities.

[NUCLEAR REACTIONS $^{235,236,238}U$ and ^{232}Th $(\gamma,n,2n,F)$, E_γ = 5–18.3 MeV; measured 4π neutron yield, neutron multiplicities, and average energies for monoenergetic photons; $\sigma(E_\gamma,1n)$, $\sigma(E_\gamma,2n)$, $\sigma(E_\gamma,F)$, integrated cross sections and moments, GDR parameters, nuclear shape parameters, neutron and fission probabilities.]

SEE ALSO 80CA2

TABLE II. Parameters of Lorentz-curve fits to the giant dipole resonance.[a]

Nucleus	$E_m(1)$ (MeV)	$\sigma_m(1)$ (mb)[b]	$\Gamma(1)$ (MeV)	$E_m(2)$ (MeV)	$\sigma_m(2)$ (mb)[b]	$\Gamma(2)$ (MeV)
^{235}U	10.90 ± 0.05	328 ± 19	2.30 ± 0.15	13.96 ± 0.09	459 ± 10	4.75 ± 0.32
^{236}U	10.92 ± 0.04	271 ± 16	2.55 ± 0.17	13.78 ± 0.08	415 ± 10	4.88 ± 0.24
^{238}U	10.77 ± 0.04	311 ± 20	2.37 ± 0.13	13.80 ± 0.09	459 ± 9	5.13 ± 0.35
^{232}Th	11.03 ± 0.04	302 ± 19	2.71 ± 0.13	13.87 ± 0.08	449 ± 9	4.77 ± 0.28

[a] Lorentz parameters defined by Eq. (1); the fitting interval for all cases is 9 to 18 MeV.
[b] Uncertainties for σ_m given here are relative. The absolute uncertainties are 7%.

TABLE IV. Nuclear shape parameters.

Nucleus	R_A[a]	η[b]	ϵ[c]	β_2[d]	Q_0 (b)[e]	Q_0 (b)[f]	Q_0 (b)[g]
^{235}U	0.35	1.308	0.595	0.315	12.0	10.6 ± 0.2	11.0 ± 0.5
^{236}U	0.34	1.287	0.556	0.295	11.2	10.75 ± 0.7	10.3 ± 0.4
^{238}U	0.31	1.309	0.596	0.316	12.1	11.3 ± 0.1	11.1 ± 0.5
^{232}Th	0.38	1.283	0.547	0.290	10.7	9.8 ± 0.1	9.8 ± 0.4

[a] Area ratio, defined by Eq. (6).
[b] Deformation parameter, computed from Eq. (3).
[c] Nuclear eccentricity, computed from Eq. (4).
[d] Deformation parameter, computed from Eq. (7).
[e] Intrinsic quadrupole moment, computed from Eq. (8), with R_0 taken to be 1.20 fm.
[f] Intrinsic quadrupole moment, taken from Ref. 47.
[g] "Best value" for Q_0, computed from Eq. (8), with R_0 taken to be 1.15 fm (see text).

TABLE V. Integrated cross sections.[a]

Nucleus	$\sigma_{int}(\gamma,n)$ (MeV b)	$\sigma_{int}(\gamma,2n)$ (MeV b)	$\sigma_{int}(\gamma,F)$ (MeV b)	$\frac{\frac{1}{2}\pi[\sigma_m(1)\Gamma(1)+\sigma_m(2)\Gamma(2)]}{0.06NZ/A}$[b]
^{235}U	1.14	0.20	2.16	1.37
^{236}U	1.26	0.45	1.45	1.26
^{238}U	1.36	1.13	1.09	1.43
^{232}Th	1.66	1.45	0.37	1.41

[a] $\sigma_{int}(\gamma,x)=\int\sigma(\gamma,x)dE_\gamma$, integrated from threshold to the maximum experimental energy $E_{\gamma max}$ = 18.3 MeV.
[b] Uncertainties given here are relative. The absolute uncertainties are 7%.

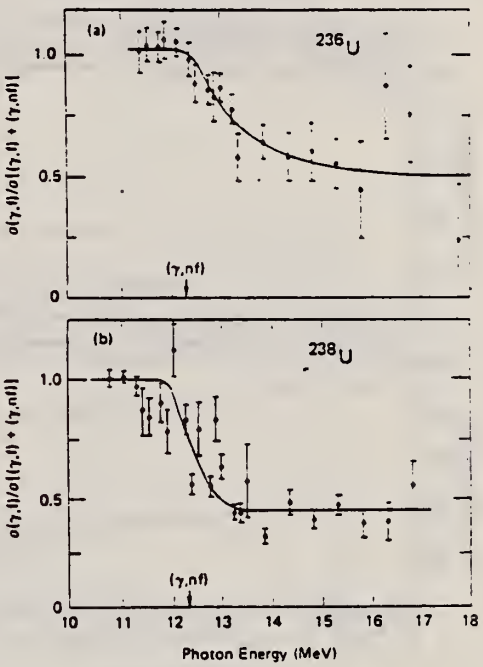

FIG. 12. Ratios of the first-chance photofission cross section $\sigma(\gamma,f)$ to the total photofission cross section $\sigma(\gamma,F)=\sigma[(\gamma,f)+(\gamma,nf)]$: (a) for ^{236}U, (b) for ^{238}U.

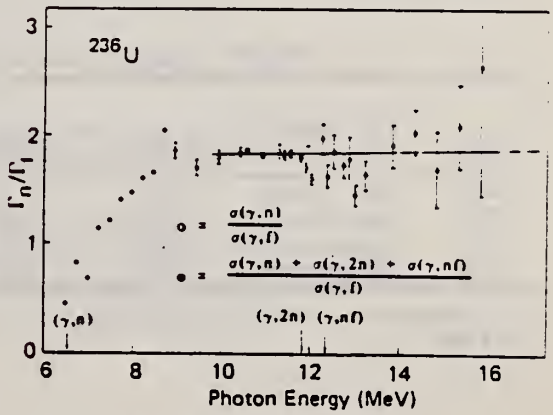

FIG. 13. Neutron-to-fission branching ratio Γ_n/Γ_f versus photon energy for ^{236}U.

over

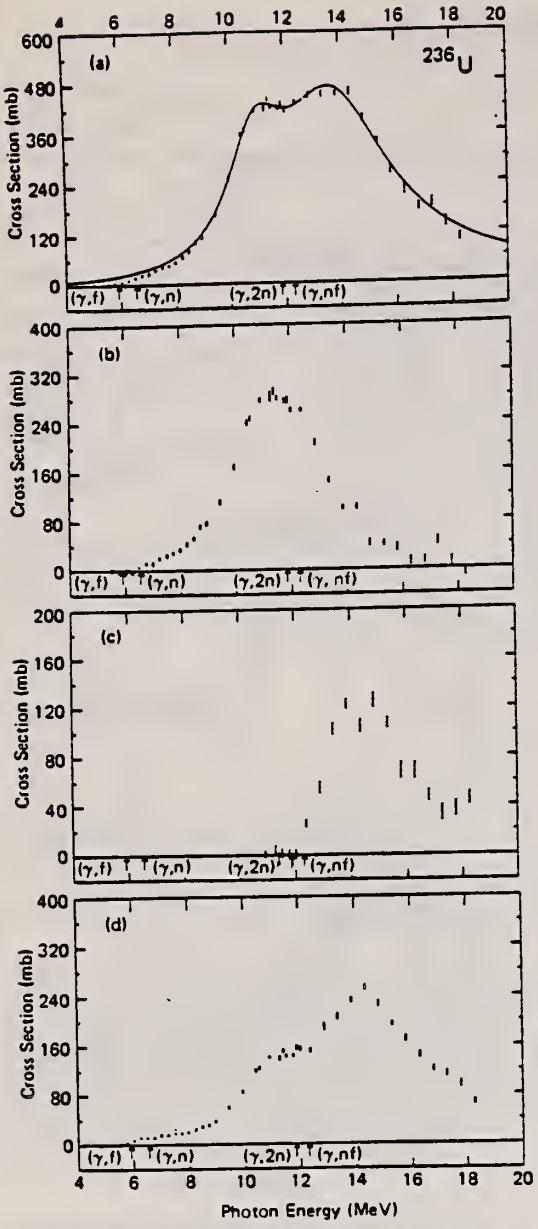

FIG. 3. Photonuclear cross sections for ^{236}U: (a) $\sigma(\gamma,\text{tot})$, with a Lorentz-curve fit; (b) $\sigma(\gamma,n)$; (c) $\sigma(\gamma,2n)$; (d) $\sigma(\gamma,F)$.

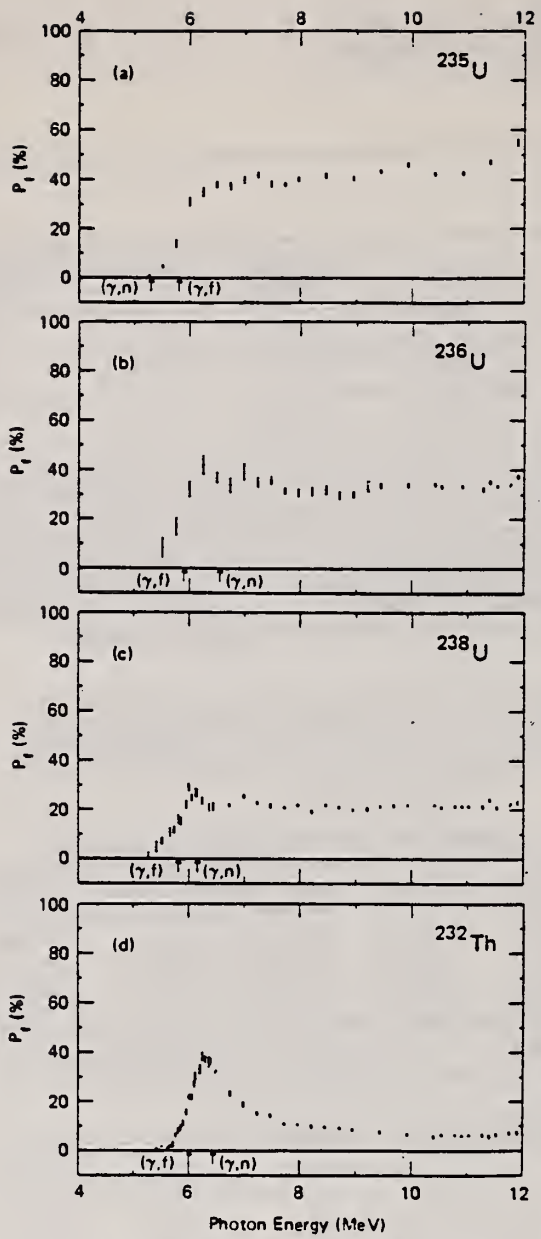

FIG. 13. Fission probability P_f from the ratio of $\sigma(\gamma,f)$ to the value at each energy of the two-component Lorentz-curve fits to the GDR shown in Figs. 2–5: (a) for ^{235}U, (b) for ^{236}U, (c) for ^{238}U, (d) for ^{232}Th.

TABLE VI. Integrated cross-section moments.[a]

Nucleus	σ_{-1} (mb)	$\sigma_{-1}A^{-4/3}$ (mb)	σ_{-2} (mb MeV^{-1})	$\frac{\sigma_{-2}}{0.00225\,A^{5/3}}$	$\frac{\sigma_{-2}K}{0.05173^{5/3}}$	$\frac{0.05175\,A^{5/3}}{\sigma_{-2}}$ (MeV)
^{235}U	278	0.191	23.1	1.15	1.36	20.1
^{236}U	252	0.173	21.0	1.04	1.21	22.2
^{238}U	286	0.194	24.0	1.17	1.38	19.7
^{232}Th	276	0.194	22.8	1.16	1.35	19.9

[a] $\sigma_{-1}=\int\sigma(\gamma,\text{tot})\,E_\gamma^{-1}\,dE_\gamma$ and $\sigma_{-2}=\int\sigma(\gamma,\text{tot})E_\gamma^{-2}\,dE_\gamma$. Integrated from threshold to $E_{\gamma\max}=18.3$ MeV.

REF. J. T. Caldwell, E. J. Dowdy, R. A. Alvarez, B. L. Berman, P. Meyer
Nucl. Sci. Eng. 73, 153 (1980)

ELEM. SYM.	A	Z
U	236	92

METHOD

REF. NO. 80Ca2 egf

REACTION	RESULT	EXCITATION ENERGY	SOURCE TYPE	SOURCE RANGE	DETECTOR TYPE	DETECTOR RANGE	ANGLE
G,F	NOX	5-18	D	5-18	BF3 - I	D	4PI
G,F	NOX	11 17	D	5-18	BF3 - I	D	4PI
G,F	RLX	5-17	D	5-18	BF3 - I	D	4PI

The prompt neutron multiplicities for photofission of the four isotopes ^{235}U, ^{236}U, ^{238}U, and ^{232}Th have been measured with monoenergetic photons over the energy range from 5.5 to 18 MeV using the annihilation in flight of fast positrons. The delayed neutron yield has been measured for all four isotopes at 10.9- and 16.8-MeV photon energies. The ratio of first- to second-chance fission has been measured as a function of energy up to 17-MeV excitation energy for ^{236}U and ^{238}U photofission.

PROMPT N MULT
DELAYED N YLD
RATIO 1-/2=-CHANCE F

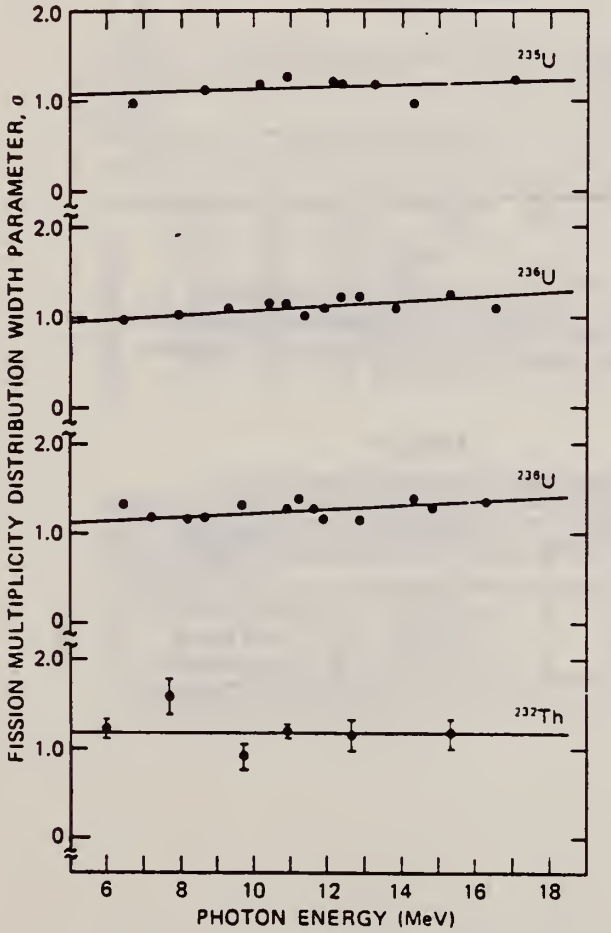

Fig. 6. Prompt neutron multiplicity width parameter data as a function of excitation energy. Solid circles are experimental data, and straight lines are the least-squares fits to these data (see Table II).

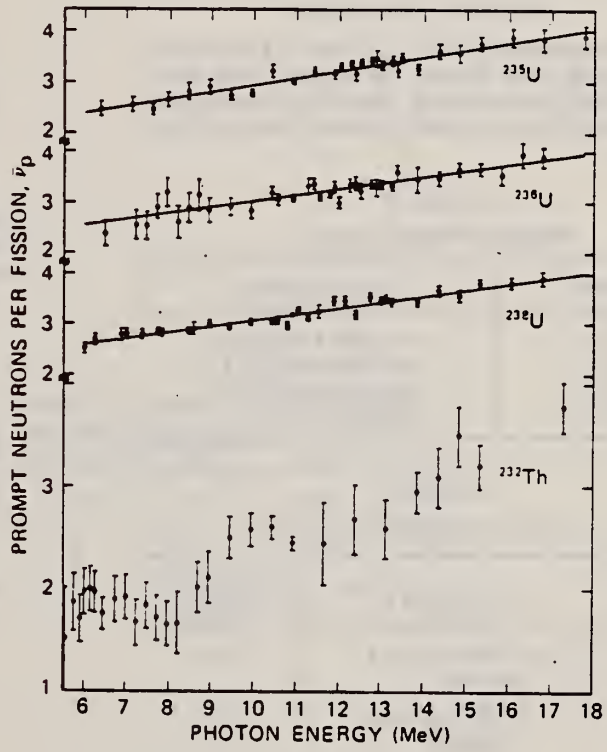

Fig. 7. Prompt neutron $\bar{\nu}_p$ data as a function of excitation energy. Solid circles are experimental data, and the straight lines are the least-squares fits (see Table IV) to these data. A single straight line fit was not obtainable for ^{232}Th.

over

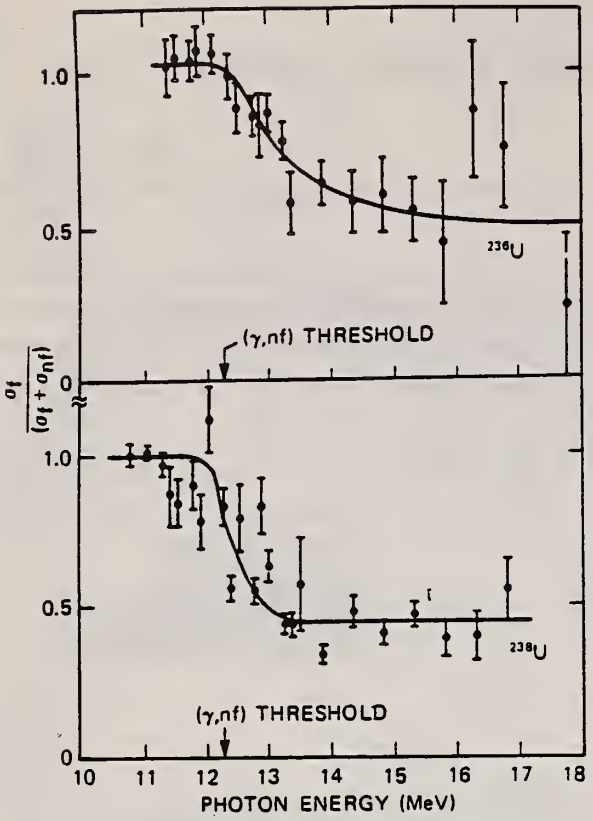

Fig. 8. Experimental $\sigma_f/(\sigma_f + \sigma_{nf})$ data as a function of excitation energy (solid circles). The smooth curves drawn through the data are intended to guide the eye and are not based on analytic fits to the data. Threshold values are from Ref. 15.

TABLE II

Multiplicity Width Parameter

Isotope	Least-Squares Fit
^{235}U	$\sigma = 1.009 + 0.0110\ E$
^{236}U	$\sigma = 0.840 + 0.0253\ E$
^{238}U	$\sigma = 1.003 + 0.0227\ E$
^{232}Th	$\sigma = 1.183$

TABLE IV

Prompt Neutrons per Photofission, $\bar{\nu}_p(E)$

Isotope	Least-Squares Fit	Correlation Coefficient
^{235}U	$\bar{\nu}_p = 1.610 + 0.133\ E$ (all data)	0.9[illegible]
^{236}U	$\bar{\nu}_p = 1.881 + 0.116\ E$ (all data)	0.9[illegible]
^{238}U	$\bar{\nu}_p = 1.862 + 0.123\ E$ (all data)	0.9[illegible]
^{232}Th	$\bar{\nu}_p = 2.826 - 0.143\ E$ ($6.0 < E < 8.2$ MeV)	0.8[illegible]
	$\bar{\nu}_p = 0.453 + 0.175\ E$ ($E > 8.5$ MeV)	0.9[illegible]

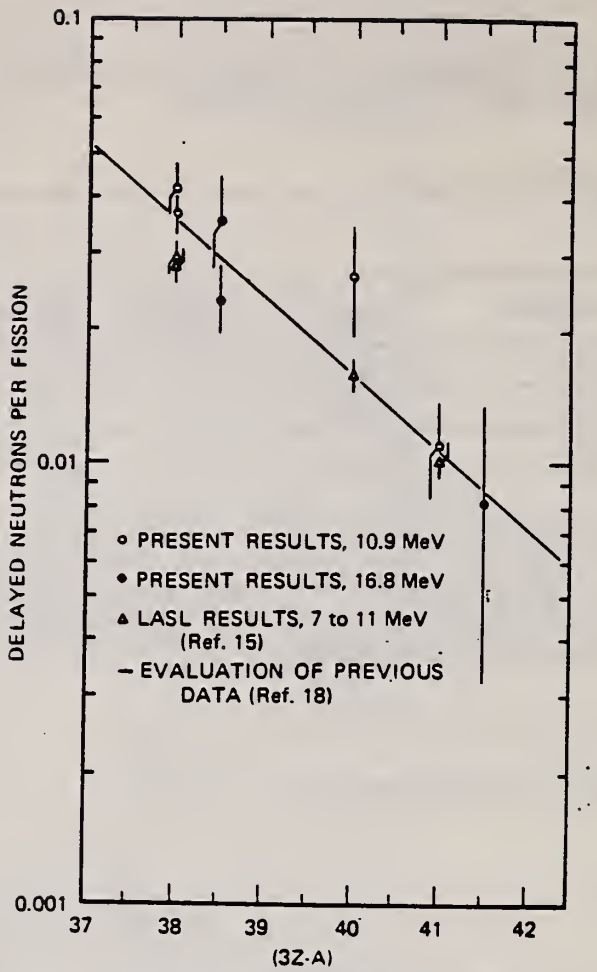

Fig. 9. Yield of delayed neutron from photofission as a function of $3Z$-A. Solid line is an evaluated least-squares fit to existing data as of 1975 (Ref. 18). Solid circles are the present results. Solid squares are from Ref. 15.

TABLE V

Prompt Neutrons per Photofission at 8.5 MeV

Isotope	From Ref. 15	Present Data
^{235}U	2.85 ± 0.09	2.74 ± 0.10
^{236}U	2.66 ± 0.11	2.71 ± 0.10
^{238}U	2.74 ± 0.09	2.91 ± 0.10
^{232}Th	2.07 ± 0.11	1.94 ± 0.08

REF. A.S. Voronin, I.S. Koretskaya, V.L. Kuznetsov, V.G. Nedorezov, N.V. Nikitina, V.I. Noga, S.A. Pashchuk, Yu.N. Ranyuk, S.M. Solov'ev
Yad. 34, 1439 (1981)
Sov. p. Nucl. Phys. 34, 797 (1981)

ELEM. SYM.	A	Z
U	236	92

METHOD

REF. NO. 81 Vo 3 egf

REACTION	RESULT	EXCITATION ENERGY	SOURCE		DETECTOR		ANGLE
			TYPE	RANGE	TYPE	RANGE	
E,F	ABX	4-275	D	97-275	TRK-I		45
G,F	RLY	4-275	D	184-275	TRK-I		45

RELATIVE BRMS/E YLD

Results are presented of cross-section measurements for the fission of ^{232}Th, ^{233}U, ^{235}U, ^{236}U, ^{238}U, ^{237}Np, and ^{239}Pu by electrons with energies between 100 and 275 MeV. photofission and electrofission cross-section ratios for the same nuclei are given as well.

PACS numbers: 25.85.Jg, 27.90. + b, 25.85.Ge

TABLE II. Electrofission cross sections (mb) for nuclei with $Z \geq 90$ measured for electron energies between 100 and 275 MeV.

E_e, MeV	Nucleus						
	^{232}Th	^{233}U	^{235}U	^{236}U	[illegible]	[illegible]	^{239}Pu
97	1.24	8.12	5.66	4.55	[illegible]	[illegible]	7.26
134	1.47	9.17	6.05	4.74	[illegible]	[illegible]	7.98
149	1.42	9.75	6.17	5.59	[illegible]	[illegible]	8.39
166	1.63	10.36	7.01	5.29	[illegible]	[illegible]	9.18
184	1.78	9.61	7.13	5.65	[illegible]	[illegible]	8.92
201	1.54	9.84	6.53	6.10	[illegible]	[illegible]	9.31
217	1.73	10.91	7.73	6.13	[illegible]	[illegible]	9.56
240	1.91	10.25	7.26	5.92	[illegible]	[illegible]	9.13
253	1.85	9.89	7.09	6.17	[illegible]	[illegible]	9.78
275	2.22	10.50	8.15	6.66	[illegible]	[illegible]	10.50

TABLE IV. Cross sections (mb) for photo- and electrofission ($\sigma_{Qf}\Delta t + \sigma_{ef}$) obtained in measurements with aluminum radiators with a thickness of $0.023t_0$ for ^{235}U, ^{236}U, ^{238}U, and ^{237}Np and of $0.011t_0$ for ^{239}Pu.

E_e, MeV	Nucleus					E_e, MeV	[illegible]						
	^{235}U	^{236}U	^{238}U	^{237}Np	^{239}Pu							Np	Pu
154	13.33	10.48	7.57	13.40	11.65	[illegible]	[illegible]	[illegible]	[illegible]	[illegible]	[illegible]	[illegible]	[illegible]
201	14.10	11.50	8.82	12.79	12.16	[illegible]	[illegible]	[illegible]	[illegible]	[illegible]	[illegible]	[illegible]	[illegible]
217	14.36	10.76	8.07	12.94	12.98	275	[illegible]	[illegible]	[illegible]	[illegible]	[illegible]	[illegible]	13.63

TABLE V. Cross-section ratios for photo- and electrofission (σ_{Qf}/σ_{ef}) for energies between 184 and 275 MeV.

Nucleus	σ_{Qf}/σ_{ef}	Nucleus	σ_{Qf}/σ_{ef}
^{233}U	40±8	^{237}Np	24±5
^{235}U	37±7	^{239}Pu	30±6
^{238}U	35±7		
	Average	33±3	
	Theoretical	35.3	

U
A=238

U
A=238

U
A=238

REFL

L. Katz, T. M. Kavanagh, A. G. W. Cameron, E. C. Bailey, and J. W. T. Spinks
Phys. Rev. 99, 98 (1955)

ELEM. SYM.	A	Z
U	238	92

METHOD

REF. NO. 55 Ka 1 EGF

REACTION	RESULT	EXCITATION ENERGY	SOURCE		DETECTOR		ANGLE
			TYPE	RANGE	TYPE	RANGE	
G, F	ABX	THR - 26	C	12-26	ACT-I		4PI

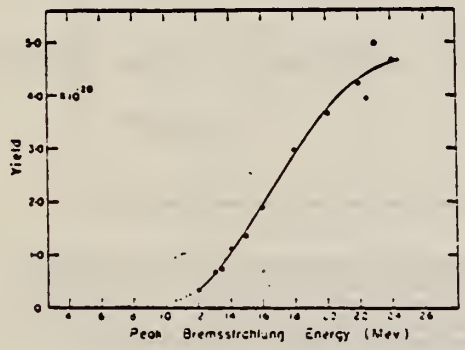

FIG. 1. Yield of mass chain 115 resulting from photofission of U^{238} as indicated by the yield of the 54-hr Cd^{115} beta-ray activity. The yield is expressed in nuclei of mass 115 per irradiated U^{238} nucleus per roentgen of irradiation.

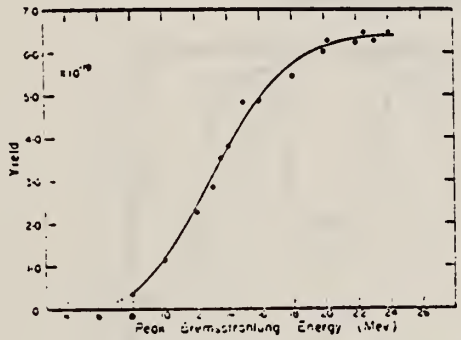

FIG. 2. Yield of mass chain 139 resulting from photofission of U^{238} as indicated by the yield of 85-min Ba^{139}. The yield is expressed in nuclei of mass 139 per irradiated U^{238} nucleus per roentgen of irradiation.

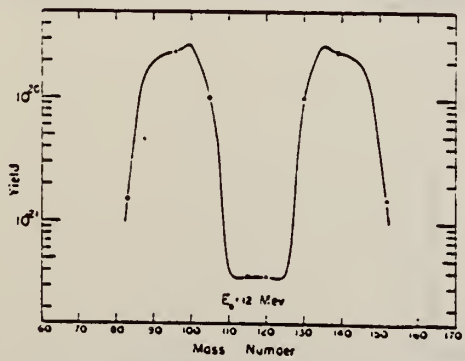

FIG. 3. Yield of mass chains 83, 105, 115, and 139 at a betatron operating energy of 12 Mev. The measurements are indicated by the circles and reflection of these about mass 117.5 are indicated by crosses. The curve drawn through these points was made to correspond in shape to those shown in Figs. 4 and 5.

Ref. L. Katz, T. M. Kavanagh, A. G. W. Cameron, E. C. Bailey, and J. W. T. Spinks
Phys. Rev. 99, 98 (1955)

Elem. Sym.	A	Z
U	238	92

Method

Ref. No. 55 Ka 1 EGF

Reaction	Result	Excitation Energy	Source Type	Source Range	Detector Type	Detector Range	Angle

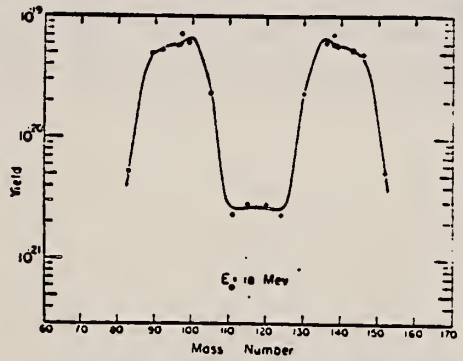

FIG. 4. Yield of mass chains 83, 89, 97, 99, 105, 111, 115, 138, 139, and 143 at a betatron operating energy of 18 Mev. The measurements are indicated by the circles and reflection of these about mass 117.5 are indicated by crosses.

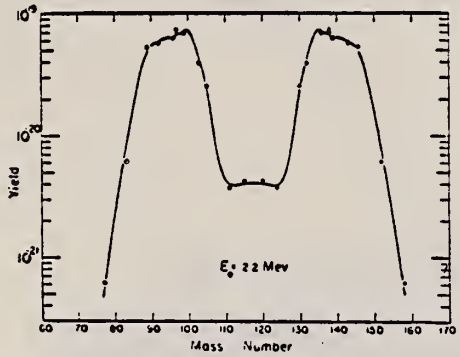

FIG. 5. Yield of mass chains 77, 83, 89, 97, 99, 103, 105, 111, 115, 138, 139, and 143 at a betatron operating energy of 22 Mev. The measurements are indicated by the circles and reflection of these about mass 117.5 are indicated by crosses.

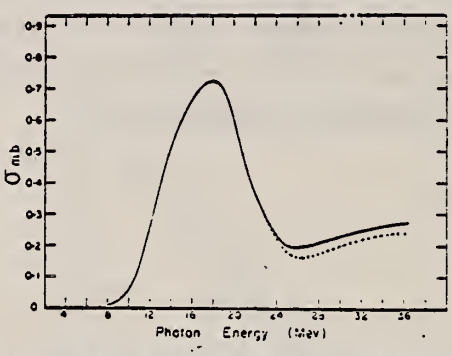

FIG. 8. Cross section for symmetric fission obtained from analysis of Fig. 1 by the photon difference method. The cross section above 24 Mev was obtained from the analysis of the ratio of Fig. 7 as outlined in the text. The dashed curve is obtained if the asymmetric cross section is assumed zero above 24 Mev.

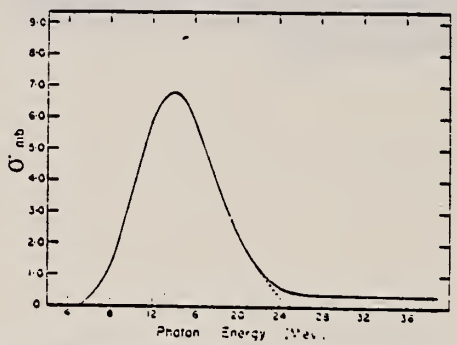

FIG. 9. Cross section for asymmetric fission obtained from analysis of Fig. 2 by the photon difference method. The cross section above 24 Mev was obtained from the analysis of the ratio of Fig. 7 as outlined in the text.

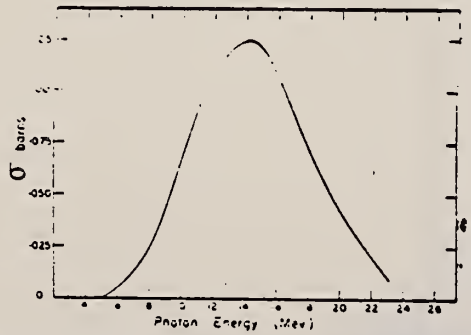

FIG. 14. Total photofission cross section as a function of photon energy. This curve can be obtained from Fig. 13 by the photon difference method, or since Fig. 13 is similar to Fig. 2 then this cross section is similar to that of Fig. 9 except that each ordinate is 18.4 times larger.

REF. L. E. Lazareva, B.S. Ratner and I.V. Shtranikh
J. Exper. Theoret. Phys. USSR 29, 274 (1955)
Soviet Phys. JETP 2, 301 (1956)

ELEM. SYM.	A	Z
U	238	92

METHOD -

REF. NO. 55 La 2 EGF

REACTION	RESULT	EXCITATION ENERGY	SOURCE		DETECTOR		ANGLE
			TYPE	RANGE	TYPE	RANGE	
G,F	RLY	THR- 18.5	C	18.5	BF3-I		4PI

DELAYED NEUTRON

Delayed neutron 0.41±0.02% of total neutrons from bremsstrahlung absorption.

Ref. E.G. Fuller, E. Hayward
Phys. Rev. 101, 692 (1956)

Elem. Sym.	A	Z
U	238	92

Method: Betatron; photon scattering; NaI spectrometer

Ref. No.: 56 Fu 1 | NVB

Reaction	E or ΔE	E_o	Γ	$\int \sigma dE$	Jπ	Notes
U (γ,γ)	Bremss. 4-40					Detector at 120°. Cross sections given here are 13% too high due to erroneous cos β factor in denominator of Eq. 5. [See footnote 8 in Phys. Rev. 106, 993 (1957)].

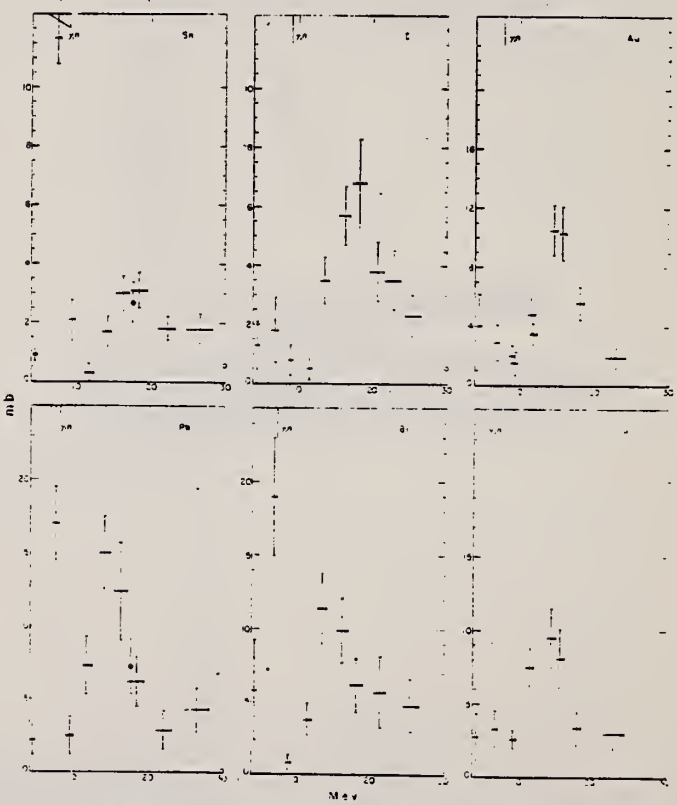

Fig. 6. The ...astic scatter... ...ections for Sn, I, Au, Pb, Bi, and U. The points at 17.6 Mev are those of Stearns.[6]

[4] E. R. Gaerttner and G. L. Yeater, Phys. Rev. 76, 363 (1949).
[5] Dressel, Goldhaber, and Hanson, Phys. Rev. 77, 754 (1950).
[6] M. B. Stearns, Phys. Rev. 87, 706 (1952).

Ref. B.I. Gavrilov, L.E. Lazareva
Zhur. Eksp. i Teoret. Fiz. 30, 855 (1956);
Soviet Phys. JETP 3, 871 (1957)

Elem. Sym.	A	Z
U	238	92

Method γ-Bremsstrahlung; synchrotron; BF_3 counter

Ref. No. 56 Ga 1 EGF

Reaction	E or ΔE	E_0	Γ	∫σdE	Jπ	Notes	SSO
(γ,xn)	5-27	14.9	6.8	12.5 MeV-b			

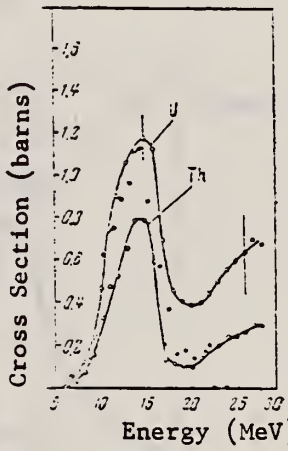

Figure 2: Photoneutron cross section σ_n, computed from the yield curves by the "photon difference method." "●" -- cross sections obtained in Ref. 9 [Nathans and Halpern, Phys. Ref. 93, 437 (1954)].

TABLE I. . . . cross sections.

Element		
Copper		7.6
Zinc		8.1
Cadmium		8.2
Iodine		8.4
Tantalum		8.6
Gold		7.6
Thallium		7.6
Uranium		8.0
Thorium		8.0
Uranium		12.6

Ref. J.E. Gindler, J.R. Huizenga
Phys. Rev. 104, 425 (1956)

Elem. Sym.	A	Z
U	238	92

Method: Chemical activity

Ref. No.: 56 Gi 1 | EGF

Reaction	E or ΔE	E_o	Γ	$\int \sigma dE$	Jπ	Notes
(γ,n)	Bremss. 8-20					
(γ,f)						

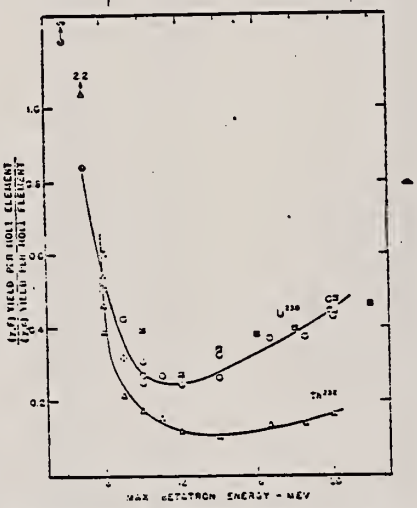

FIG. 1. Ratios of the total number of photofission events per mole element to the number of residual (γ,n) atoms per mole element as a function of maximum betatron energy. Uranium irradiations: ○, x-ray, this work; ●, probe target, this work; ⊡, x-ray, reference ⁴; thorium irradiations: △, x-ray, this work; ▲, probe target, this work. The broken circles represent uranium data having errors of approximately ±40% because of low U^{237} counting rates. The broken triangle represents a weighting error of ±25% in the determination of the thorium fission yield.

TABLE I. Characteristics of photofission and neutron emission excitation functions for thorium and uranium.

Reaction	σ_{max} (barns)	$E(\sigma_{max})$ (Mev)	Half-width (Mev)	$\int \sigma dE$ (Mev barns)	Reference
$U^{238}(\gamma,f)$[a]		16[a]	5[a]		4
$U^{238}(\gamma,2n)$		15	5[a]		a
$U^{238}(\gamma,f)$		14.6	6.8		a
$U^{238}(\gamma,f)$	0.18	14	7.6	1.2(0–20)	c
$U^{238}(\gamma,f)$	0.125	14	8.8	1.1(0–24)	d
$U^{238}(\gamma,f)$	0.20≡0.03	14.0	6.7	1.71≡0.14(0–28)	b
$Th^{232}(\gamma,F)$	0.051≡0.007	14.1	7.0	0.64≡0.09(0–28)	b
$U^{238}(\gamma,pn),U^{237}$	0.53	11	3.6	2.6(0–20)	e
$U^{238}(\gamma,n)^{237}U$		15.8	7.1		a
$U^{238}(\gamma,n)$	1.8	13	(5)	11.2(0–27.3)	a
$U^{238}(\gamma,n)$	0.96	14	6.4	7.1(0–25)	b
$U^{238}(\gamma,n)$	1.15≡0.15	14.9	6.5	12.9≡1.0(0–28)	b
$Th^{232}(\gamma,n)$	0.80≡0.10	14.5	5.6	6.61≡0.60(0–28)	b

[a] (γ,F) indicates all processes initiated by a photon in which neutron emission is involved. (γ,xn) indicates the total number of neutrons produced by the nuclear absorption of a photon, irrespective of the relative probability of charged particle emission. In this reaction the (γ,xn) process may be represented by

$$\sigma_{\gamma,xn} = \sigma_{\gamma,n} + \sigma_{\gamma,2n} + \sigma_{\gamma,3n} + \cdots + \sigma_{\gamma,pn} + \cdots$$

where $\sigma_{\gamma,xn}$ is the cross section for the production of neutrons produced by a photon-excited nucleus without restriction to the number of neutrons emitted. Each neutron emitted before the final one may be a result of the known processes, or may be a combination of the two.

[b] Although the authors in reference 1 state that the significance can be given to the shape of the curve of σ vs E_o, the characteristics of their excitation curves, when compared favorably with later measurements, [illegible] the half-width at half maximum.

[c] These values represent the integration of the sigma function of reference 2.

[d] The limits in Mev are given in parentheses following the integrated value.

[e] See reference 3. [f] See reference 5. [g] See reference 6. [h] See reference 7. [i] See reference 4. [j] See reference 8.

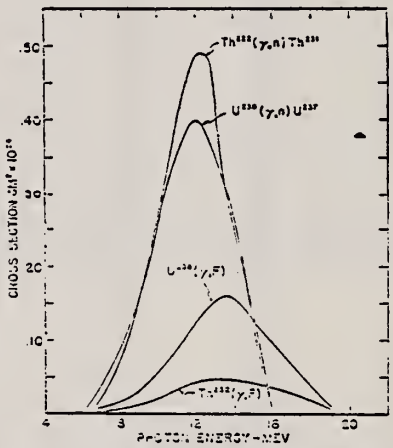

FIG. 2. Photoneutron and photofission cross sections of Th^{232} and U^{238} obtained from analysis of the corresponding activation functions of Fig. 3 by the photon difference method.

[1] G. C. Baldwin and G. S. Klaiber, Phys. Rev. 71, 3 (1947).
[2] W. E. Ogle et al., Phys. Rev. 81, 344 (1951).
[3] E. E. Anderson and R. ... Duffield, Phys. Rev. 85, 728 (1952).
[4] E. E. Anderson, M. S. Thesis, University of Illinois, 1951 (unpublished).
[5] R. L. Gluckstern and J. S. Huizenga, Phys. Rev. 89, 1042 (1953).
[6] Katz, Kavanagh, Cameron, Bailey, and Spinks, Phys. Rev. 99, 93 (1955).
[7] [illegible]eva, Varfolov, Vatsenina, and Stavinsky, Conference on the Academy of Sciences of the U.S.S.R. on the Peaceful Uses of Atomic Energy, July 1-5, 1955, Session of the Division of Physical and Mathematical Sciences (Consultants Bureau, New York, 1955), p. 217.
[8] W. Jones and K. M. Terwilliger, Phys. Rev. 91, 650 (1953).
[9] R. Nathans and J. Halpern, Phys. Rev. 93, 437 (1954).

REF.

V. A. Korotkova, P. A. Cherenkov and I. V. Chuvilo
Dokl. Akad. Nauk SSSR 106, 633 (1956)
Soviet Phys. Doklady 1, 77 (1956)

ELEM. SYM.	A	Z
U	238	92

METHOD

REF. NO.	
56 Ko 2	EGF

REACTION	RESULT	EXCITATION ENERGY	SOURCE		DETECTOR		ANGLE
			TYPE	RANGE	TYPE	RANGE	
G,F	ABX	8-24	C	8-24	ION-I		

Monitor-graphite ion chamber

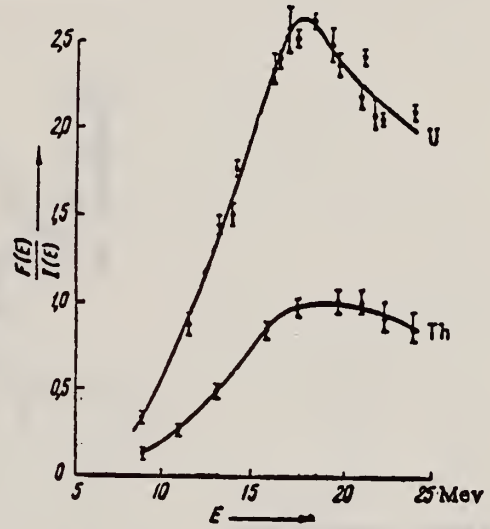

Figure 1.

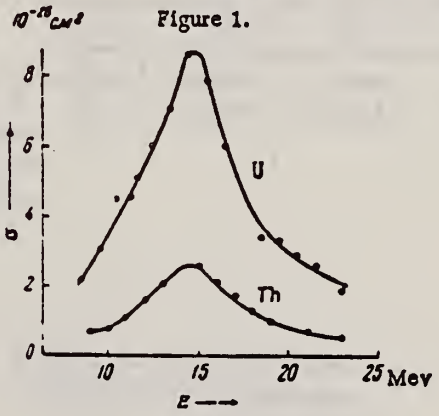

Figure 2.

REF.
V. A. Korotkova, P. A. Cherenkov, I. V. Chuvilo
Dokl. Akad. Nauk SSSR 106, 811 (1956)
Soviet Phys. Doklady 1, 104 (1956)

ELEM. SYM.	A	Z
U	238	92

METHOD

REF. NO.	
56 Ko 3	EGF

REACTION	RESULT	EXCITATION ENERGY	SOURCE		DETECTOR		ANGLE
			TYPE	RANGE	TYPE	RANGE	
G,F	SPC	THR - 18	C	18	ION-D	50-100	4PI

E_o = 17.6 MeV

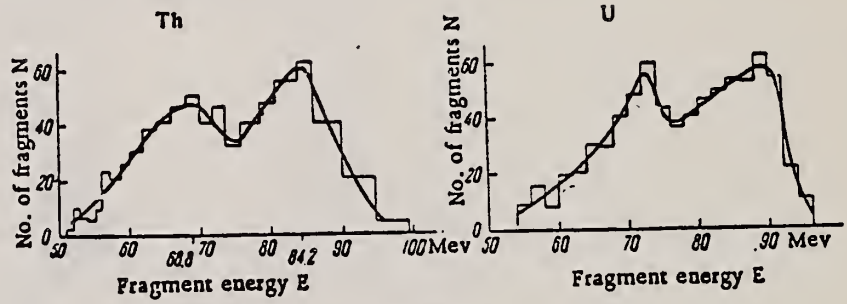

Figure 1.

Table 1
Most Probable Energy Values (in Mev)

Element	E_L	E_H	E_S
Uranium	86.5 ± 4	72.5 ± 3	159
Thorium	84.2 ± 4	68.8 ± 4	153

REF. B. P. Bannik, N. M. Kulikova, L. E. Lazareva and V. A. Iakovlev
J. Exptl. Theoret. Phys.(USSR) 33, 53 (1957)
Soviet Phys. JETP 6, 39 (1958)

ELEM. SYM.	A	Z
U	238	92

METHOD

REF. NO. 57 Ba 4 JOC

REACTION	RESULT	EXCITATION ENERGY	SOURCE		DETECTOR		ANGLE
			TYPE	RANGE	TYPE	RANGE	
G,F	NOX	THR-27	C	9 - 27	EMU-D		DST

TABLE I. Angular distribution of photofission fragments from U^{238}

Maximum x-ray energy, E_{max} Mev	Number of tracks	Distribution of tracks (per steradian)		
		0—30° 180—150°	30—60° 150—120°	60—90° 120—90°
9.4	3901	1∓0.03	1.35∓0.04	1.36∓0.04
12	2053	1∓0.04	1.09∓0.04	1.16∓0.04
26.5	2507	1∓0.04	1.10∓0.04	1.06∓0.04

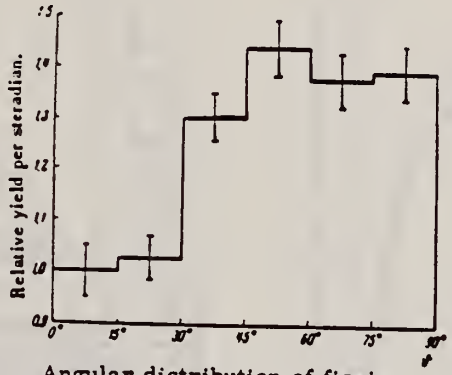

Angular distribution of fission fragments from irradiation with x-rays of maximum energy E_{max} = 9.4 Mev

TABLE II. Anisotropy coefficients for U^{238} photofission

E_{max} Mev	b/a	Ratio of anisotropic and isotropic fission yields $\left(\frac{2}{3}\frac{b}{a}+\frac{2}{15}\frac{c}{a}\right)$
9.4	0.55∓0.09	0.55∓0.09
12	0.20∓0.07	0.13∓0.05
26.5	0.07∓0.06	0.05∓0.04

REF.

L. Katz, K. G. McNeill, M. LeBlanc and F. Brown
Can. J. Phys. 35, 470 (1957)

ELEM. SYM.	A	Z
U	238	92

METHOD

REF. NO.	
57 Ka 1	JOC

REACTION	RESULT	EXCITATION ENERGY	SOURCE		DETECTOR		ANGLE
			TYPE	RANGE	TYPE	RANGE	
G,XN	ABX	6 - 23	C	6 - 23	BF3-I		4PI

Fig. 3. (γ,N) yield and cross section curves for U^{238}.

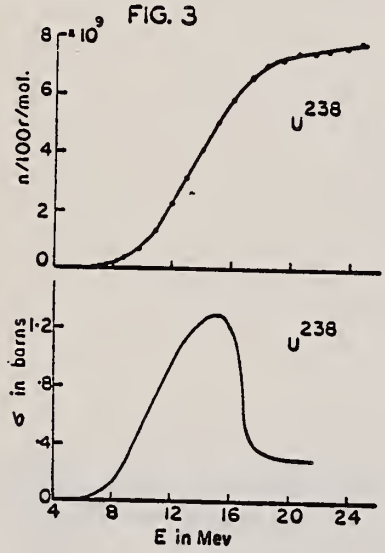

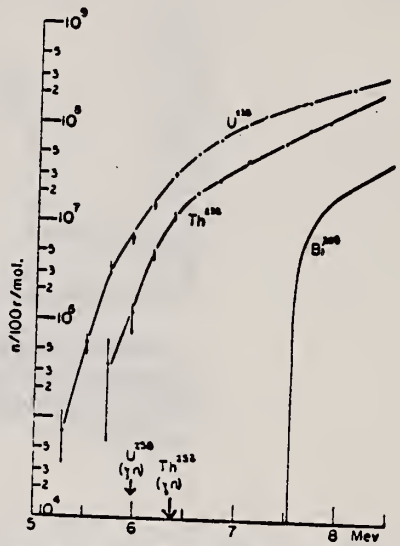

FIG. 5. The low energy section of the U^{238}, Th^{232}, and Bi^{209} neutron yield curves plotted on a logarithmic scale. Compared with the previous figures, the energy scale is expanded.

REF.

R. A. Schmitt and R. B. Duffield
Phys. Rev. 105, 1277 (1957)

ELEM. SYM.	A	Z
U	238	92

METHOD

[Page 1 of 2]

REF. NO. 57 Sc 2 EGF

REACTION	RESULT	EXCITATION ENERGY	SOURCE TYPE	SOURCE RANGE	DETECTOR TYPE	DETECTOR RANGE	ANGLE
G,F	RLY	THR - 15	C	4 -16	ACT-I		4PI

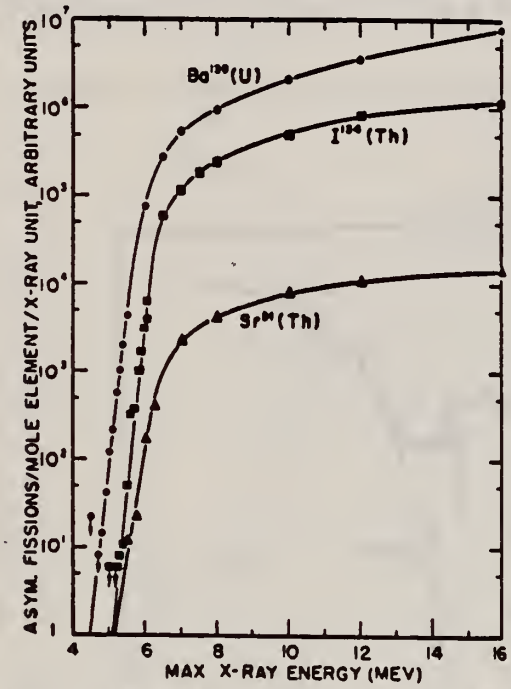

FIG. 1. Semilogarithmic plot of the asymmetric photofissions natural uranium and natural thorium as a function of increas betatron energy. ●, Ba^{139} isolated from uranium probe targ ▲, Sr^{91} and ■, I^{134} isolated from thorium probe target. Arr indicate upper limits. Ordinates for Ba^{139}, Sr^{91}, and I^{134} are u related. See footnote 22 for absolute values of the fission yiel obtained from thin-target bremsstrahlung spectrum.

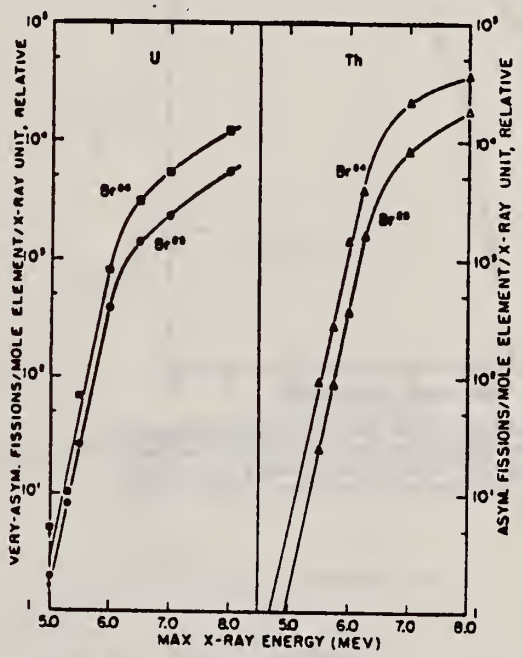

FIG. 2. Semilogarithmic plots of the very-asymmetric and asymmetric photofissions in natural uranium and natural thorium, respectively, as a function of increasing betatron energy. ●, Br^{82} and ■, Br^{83} isolated from uranium probe target; △, Br^{82} and ▲, Br^{83} isolated from thorium probe target. Arrows indicate upper limits. Uranium and thorium ordinates are unrelated.

REF.

R.A. Schmitt and R. B. Duffield
Phys. Rev. 105, 1277 (1957)

ELEM. SYM.	A	Z
U	238	92

METHOD

[Page 2 of 2]

REF. NO. 57 Sc 2 EGF

REACTION	RESULT	EXCITATION ENERGY	SOURCE		DETECTOR		ANGLE
			TYPE	RANGE	TYPE	RANGE	

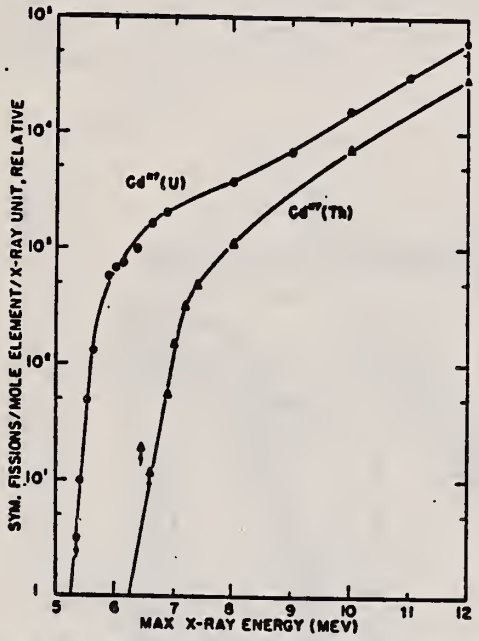

FIG. 3. Semilogarithmic plot of the symmetric photofissions in natural uranium and natural thorium as a function of increasing betatron energy. ●, Cd^{117} isolated from uranium probe target; ▲, Cd^{117} isolated from thorium probe target. Arrows indicate upper limits.

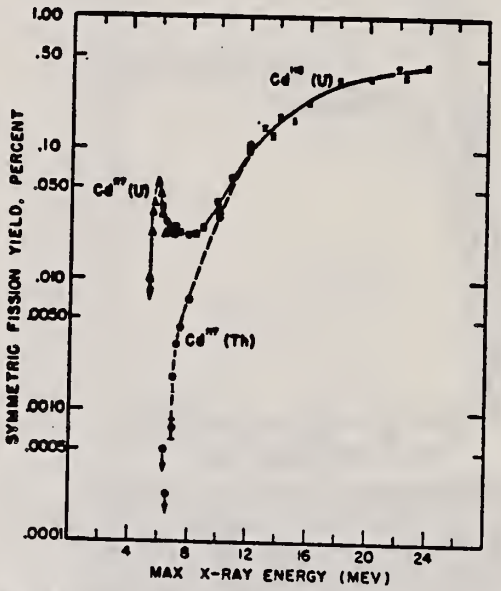

FIG. 4. Symmetric photofission yields of uranium and thorium relative to the 6.0% yields of the asymmetric mode of fission. ×, uranium external samples, Cd^{115} and Ba^{139} were separated by Katz *et al.* (reference 8); ■, uranium external samples, Cd^{117} and Ba^{139} were separated; ▲, uranium probe targets, Cd^{117} and Ba^{139} were separated; and ●, thorium probe targets, Cd^{117} and Sr^{91} were separated. All Cd^{117} yields have a normalization factor which was calculated by assuming that the Cd^{115} yield equals the Cd^{117} yield for the 12-Mev x-ray fission of uranium. Downward directed arrows indicate absence of detectable activity and are the calculated upper limits. The 6.9-Mev thorium value of 0.00073 ± 0.00008 is the mean of two irradiations.

REF.

A. I. Baz, N. M. Kulikova, L. E. Lazareva, N. V. Nikitina and V. A. Semenov
Int. Conf. Peaceful Uses of Atomic Energy 15, 2037 (1958)

ELEM. SYM.	A	Z
U	238	92

METHOD

REF. NO. 58 Ba 7 EGF

REACTION	RESULT	EXCITATION ENERGY	SOURCE		DETECTOR		ANGLE
			TYPE	RANGE	TYPE	RANGE	
G,F	NOX	THR - 27	C	6 - 27	EMU-I		DST

Determine $I(\theta) + I(\pi - \theta) = a + b \sin^2\theta + C \sin^2\theta \cos^2\theta$.

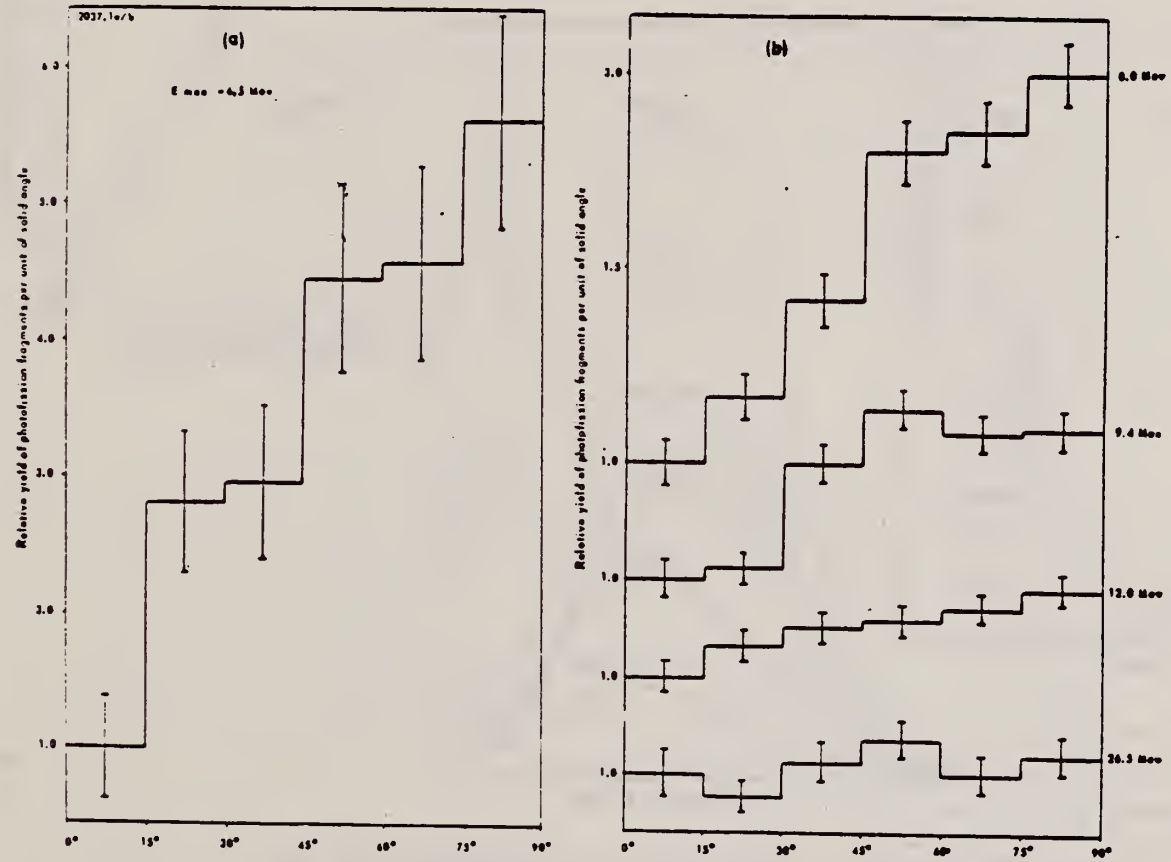

Figure 1. The angular distribution of photofission fragments from U^{238} at E_{max} = 6.5, 8, 9.4, 12 and 26.5 Mev

Table 2. Values of Ratios Calculated by Least-Squares Method for Distribution of Table 1

Maximum X-ray energy E_{max} (Mev)	b/a	c/a	c/b	σ_{fa}/σ_{fa}
6.5	4.2 ± 1.8	3.1 ± 3.2	0.75 ± 0.71	0.15 ± 0.14
8.0	1.12 ± 0.12	0.60 ± 0.38	0.54 ± 0.34	0.11 ± 0.07
9.4	0.54 ± 0.08	1.34 ± 0.34	2.46 ± 0.68	0.49 ± 0.14
12.0	0.20 ± 0.05	—	—	—
26.5	0.07 ± 0.6	—	—	—

REF. L. Katz, A. P. Baerg and F. Brown
Peaceful Uses of Atomic Energy, Switzerland 1958

ELEM. SYM.	A	Z
U	238	92

METHOD: Fission chamber

[Page 1 of 2]

REF. NO.: 58 Ka 2

EGF

REACTION	RESULT	EXCITATION ENERGY	SOURCE		DETECTOR		ANGLE
			TYPE	RANGE	TYPE	RANGE	
G,F	ABX	5-18	C	5-18	ION-I		DST

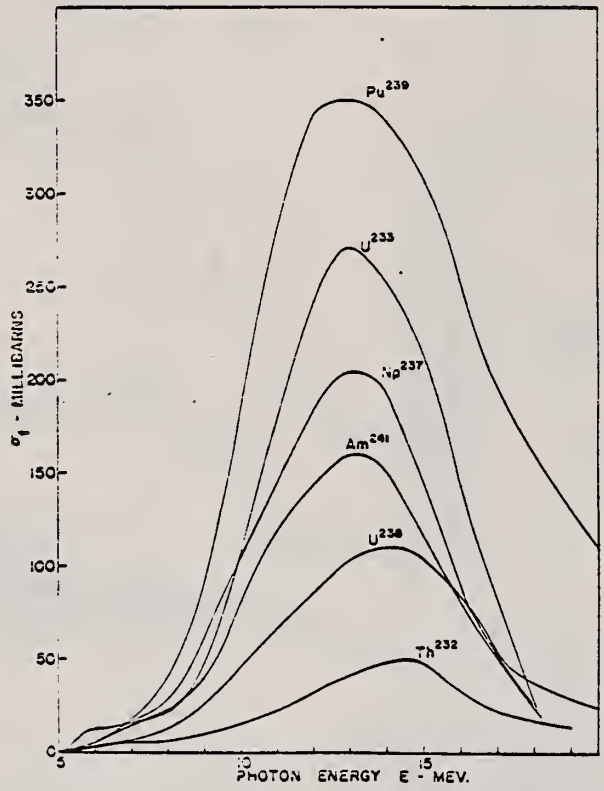

Fig. 5 - Photofission cross sections versus photon energy

Fig. 7 - Low-energy-yield curves: fissions per roentgen-nucleus versus maximum bremsstrahlung energy. (The solid and dotted lines are samples of smoothed yield curves which fit the experimental data.)

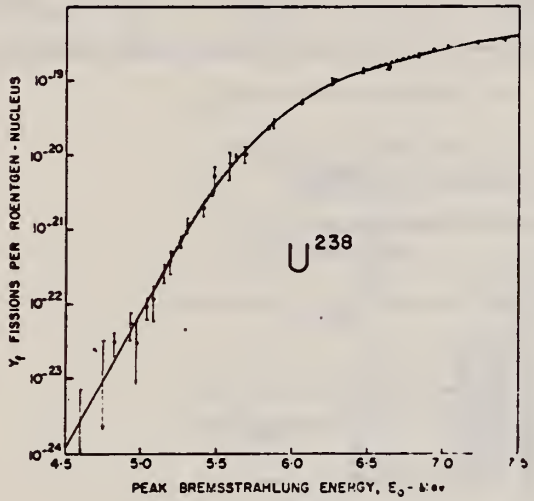

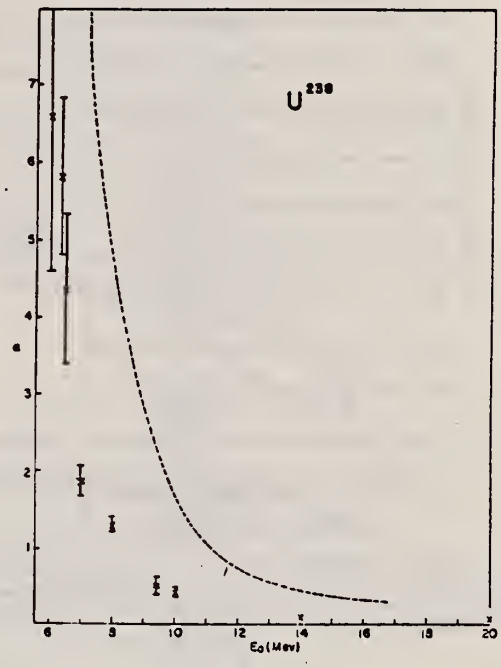

Figure 10

Anisotropy versus maximum bremsstrahlung energy: U-238

The ordinate is a in the expression $W(\theta) = 1 + a \sin^2 \theta$. The values are corrected for resolution.

The dotted line represents the results for Th-232 and corresponds to the data given in Figure 9. The points are the U-238 data.

REF.

W. C. Barber and W. D. George
Phys. Rev. 116, 1551 (1959)

ELEM. SYM.	A	Z
U	238	92

METHOD

REF. NO. 59 Ba 3 EGF

REACTION	RESULT	EXCITATION ENERGY	SOURCE		DETECTOR		ANGLE
			TYPE	RANGE	TYPE	RANGE	
E,N	ABY	THR - 36	D	10 - 36	BF3-I		4PI

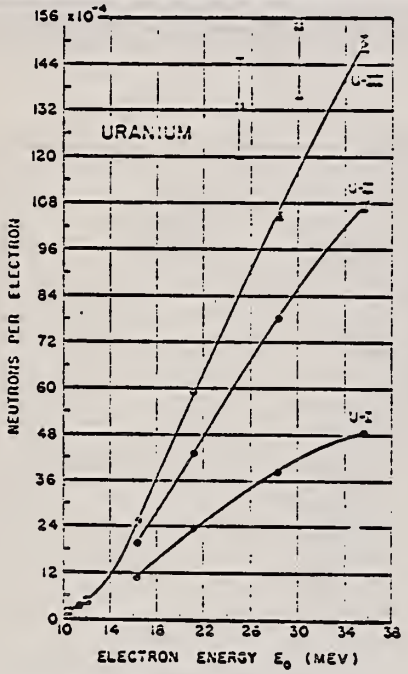

FIG. 10. Yield of neutrons per incident electron as a function of electron energy for natural uranium targets of various thicknesses. The results of the calculation by Biram (reference 1) are shown by solid squares.

TABLE I. Thicknesses of the targets used in the experiment, with the exception of heavy water, all targets contained isotopes in their naturally-occurring proportions.

Target	Thickness (g/cm²)	Thickness (radiation lengths)
Heavy water	0.698	"thick"
Be	0.589	0.00867
C-I	38.91	0.88
Al-I	24.19	1.00
Cu-A	1.372	0.108
Cu-I	13.26	1.04
Cu-II	26.56	2.08
Cu-III	39.86	3.13
Cu-IV	53.15	4.17
Ta-I	6.21	0.98
Pb-I	5.88	1.00
Pb-II	11.42	1.97
Pb-III	17.30	2.98
Pb-IV	22.89	3.94
Pb-VI	34.42	5.93
U-I	6.17	1.14
U-II	12.42	2.30
U-III	18.61	3.46
Concrete	28.5	1.19

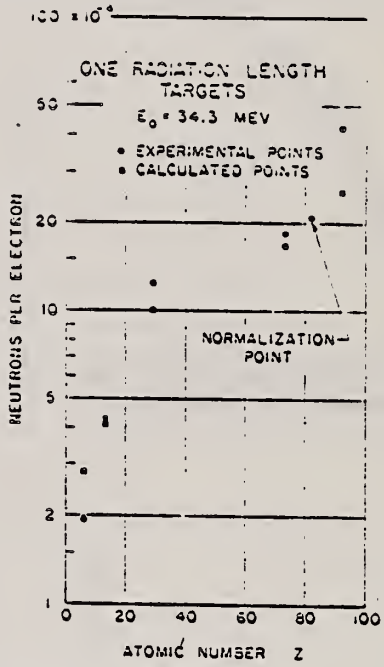

FIG. 14. Experimental and expected yields of neutrons per incident electron for 1-radiation-length targets at 34.3 Mev, as a function of atomic number Z. The experimental yields were obtained by dividing the measured yields from the targets listed by the actual target thicknesses listed in Table I. The expected yields were calculated from expression (8).

U.S. DEPARTMENT OF COMMERCE
NATIONAL BUREAU OF STANDARDS

REF.

A. P. Baerg, R. M. Bartholomew, F. Brown, L. Katz, and S. B. Kowalski
Can. J. Phys. 37, 1418 (1959) (A.E.C.L. No. 896)

ELEM. SYM.	A	Z
U	238	92

METHOD [Page 1 of 2]

Betatron with ionization chamber detector, enriched samples.

REF. NO. 59 Ba 4 EGF

REACTION	RESULT	EXCITATION ENERGY	SOURCE		DETECTOR		ANGLE
			TYPE	RANGE	TYPE	RANGE	
G,F	RLY	THR- 20	C	6-20	ION-I		DST

TABLE II

Angular distributions

Relative fission fragment yields as a function of peak bremsstrahlung energy E_0 and angle θ to X-ray beam

E_0, Mev	Angle θ 0	25	45	60	90
Th-232					
6.5	1.00±0.3				20±5
7.0	1.00±0.04		4.1±0.2	6.7±0.3	8.4±0.3
7.5	1.00±0.1		5.1±0.4	6.0±0.4	7.9±0.5
8.0	1.00±0.09		2.4±0.2	3.6±0.3	5.1±0.3
9.0	1.00±0.1				3.4±0.3
10.0	1.00±0.04	1.16±0.05	1.67±0.08	1.97±0.08	2.4±0.1
14.0	1.00±0.05				1.43±0.08
20.0	1.00±0.05				1.13±0.06
U-238					
6.0	1.00±0.3				6.0±1.4
6.3	1.00±0.1		3.6±0.4		5.9±0.6
6.5	1.00±0.2				4.5±0.7
7.0	1.00±0.08	1.5±0.1	2.0±0.2	2.4±0.2	2.9±0.2
8.0	1.00±0.06				2.1±0.1
9.4	1.00±0.023	1.094±0.029	1.224±0.029	1.274±0.034*	1.452±0.033
10.0	1.00±0.04				1.38±0.04
14.0	1.00±0.04				1.08±0.04
20.0	1.00±0.03				1.05±0.03
		*θ = 65° in this case			
U-236					
6.0	1.00±0.25				4.6±0.8
6.5	1.00±0.1		2.06±0.2		2.55±0.25
7.0	1.00±0.06		1.65±0.10		2.11±0.12
8.0	1.00±0.04		1.39±0.06		1.66±0.07
9.0	1.00±0.04	1.10±0.07	1.15±0.04	1.31±0.08*	1.46±0.05
10.0	1.00±0.03		1.07±0.03		1.28±0.04
14.0	1.00±0.02				1.03±0.02
		*θ = 65° in this case			
U-234					
6.5	1.00±0.1		1.41±0.14		1.98±0.20
7.0	1.00±0.05		1.19±0.06		1.53±0.08
8.0	1.00±0.03		1.11±0.03		1.30±0.04
10.0	1.00±0.03				1.12±0.03
15.0	1.00±0.03				1.01±0.03
Pu-240					
6.5	1.00±0.10		1.49±0.15		1.55±0.16
7.0	1.00±0.06		1.03±0.06		1.35±0.08
8.0	1.00±0.03		1.01±0.03		1.21±0.04
15.0	1.00±0.02				1.01±0.02

The values quoted are counts observed for unit X-ray dose normalized to unit yield at θ = 0°. No corrections have been applied.

REACTION	RESULT	EXCITATION ENERGY	SOURCE		DETECTOR		ANGLE
			TYPE	RANGE	TYPE	RANGE	

TABLE IV

Relative fissionabilities, U-238 = 100 at 20 Mev

E_n	U-234	U-235	U-236	U-238	Pu-239	Pu-240
6.0		0.45±0.05	0.303±0.013	0.387±0.040		
6.5	1.165±0.033	1.134±0.025	1.159±0.026	1.08±0.07	0.239±0.024	1.145±0.051
7.0	2.515±0.053	2.282±0.038	2.358±0.037	2.14±0.14	4.50±0.22	2.528±0.075
8.0	6.285±0.085	5.519±0.067	5.285±0.056	4.87±0.24	11.35±0.34	6.09±0.12
9.0		11.00±0.33	8.94±0.13	8.65±0.26		
10.0	17.36±0.53	18.75±0.30	14.29±0.20	14.41±0.28	45.1±2.2	
14.0		88.0±4.5	43.11±0.53	57.7±1.4		
15.0	84.3±1.9	119.0±0.9	73.58±0.78	70.5±1.8	253.0±7.6	82.3±1.8
20.0	127.5±2.5	180.8±2.2	109.4±1.0	100±2.5	352±10	120.8±2.3

TABLE VI

Corrected values of α in $W(\theta) = 1+\alpha \sin^2\theta$

E_n	Th-232	U-238	U-236	U-234	Pu-240
6.0		6.6±2	6.0±2.3		
6.3		6.7±1.1			
6.5	>25	4.4±1.0	2.1±0.4	2.3±0.6	0.65±0.20
7.0	11.0±0.8	2.05±0.24	1.33±0.17	0.90±0.16	0.49±0.12
7.5	10.3±1.6				
8.0	4.9±0.6	1.3±0.1	0.79±0.09	0.44±0.08	0.29±0.07
9.0	2.8±0.4		0.51±0.07		
9.4		0.44±0.04			
10.0	1.61±0.12	0.41±0.05	0.32±0.06	0.17±0.07	
14.0	0.46±0.09	0.09±0.04	0.04±0.03		
15.0				0.02±0.04*	0.01±0.03*
20.0	0.14±0.06	0.05±0.03			

*These values, which do not differ from zero, have not been corrected for isotopic composition.

Ref. B.A. Bochagov, A.P. Komar, G.E. Solyakin
Zhur. Eksp. i Teoret. Fiz. 38, 1374 (1960);
Soviet Phys. JETP 11, 990 (1960)

Elem. Sym.	A	Z
U	238	92

Method: 70 MeV synchrotron; 2 pulse ion chambers with electron collection

Ref. No.: 60 Bo 1 JHH

Reaction	E or ΔE	E_0	Γ	$\int \sigma dE$	Jπ	Notes
$U^{238}(\gamma, f)$	Bremss. 70					

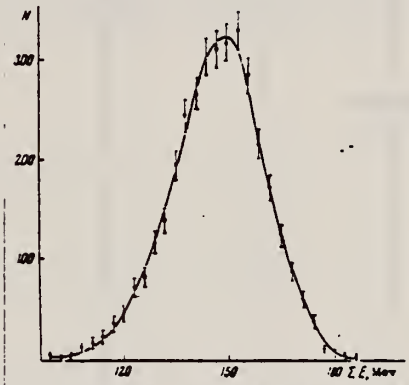

FIG. 6. Total fragment energy from photofission of U^{238}.

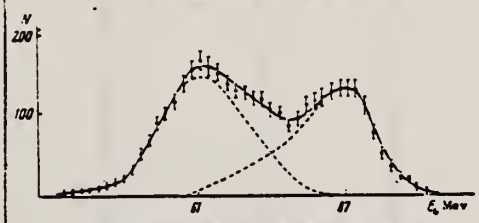

FIG. 7. U^{238} photofission fragment energy E_1 measured with a single chamber. The dashed curves represent light and heavy fragment energies measured separately by means of two chambers.

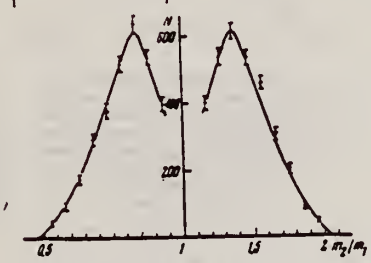

FIG. 4. Photofission fragment yield of U^{238} as a function of the mass ratio $m_1/m_1 = E_1/E_2$.

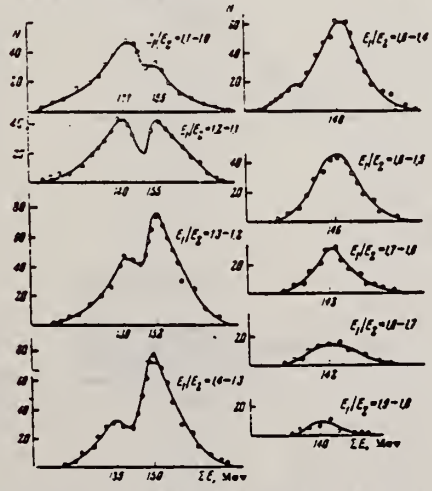

FIG. 5. Total fragment (kinetic) energy $\Sigma E = E_1 + E_2$ in U^{238} photofission for different mass ratios E_1/E_2.

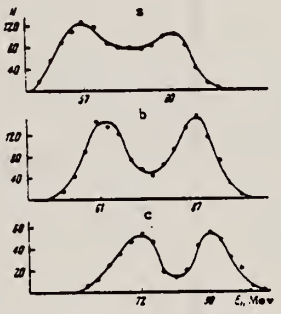

FIG. 8. U^{238} photofission fragment energy E_1 in one chamber for three different intervals of total fragment energy: a – $105 < \Sigma E < 135$ Mev; b – $135 < \Sigma E < 165$ Mev; c – $165 < \Sigma E < 195$ Mev.

No.	Experimental quantities	Uncorrected	Corrected for source thickness	Correction for ionization defect
1	Most probable light-fragment energy, Mev	87±1	91.5±1	+5.6
2	Most probable heavy-fragment energy, Mev	61±1	64.5±1	+6.8
3	Ratio of most probable energies	1.43±0.04	1.42±0.04	
4	Most probable mass ratio	1.36±0.04	1.36±0.04	
5	Half-width of high-energy peak, Mev	17		
6	Half-width of low-energy peak, Mev	19		
7	Valley-to-peak ratio for high-energy peak	0.7		
8	Most probable total (kinetic) energy ΣE, Mev	150±2	157.5±2	+12.4
9	Half-width of total energy peak, Mev	31		

Ref. B. Forkman, S.A.E. Johansson
Nuclear Phys. 20, 136 (1960)

Elem. Sym.	A	Z
U	238	92

Method: Synchrotron; $F^{19}(p,\alpha\gamma)O^{16}$ reaction; photo-fission angular distribution; nuclear emulsions; scintillator

Ref. No.: 60 Fo 1 2S NVB

Reaction	E or ΔE	E_o	Γ	$\int \sigma dE$	Jπ	Notes
U(γ, f)	Bremss.					Natural uranium.
	E_γ max:					
	10					
	20					
	E_γ discrete:					
	6.1					
	6.9					
	7.1					

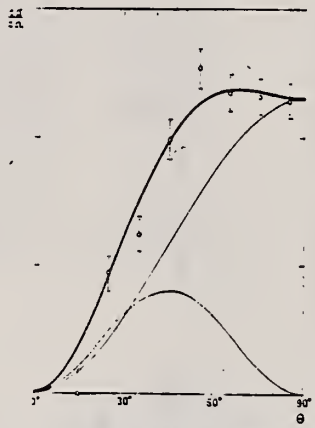

Fig. 7. Angular distribution obtained by the 6.1 MeV gamma rays with the emulsion mounted perpendicular to the incident radiation. The distribution is corrected for the 7 MeV component of the radiation. The fitted curve (heavy line) has the equation $\sin^2\theta - 0.35$ 2θ. The fine lines show the curve resolved in its two components.

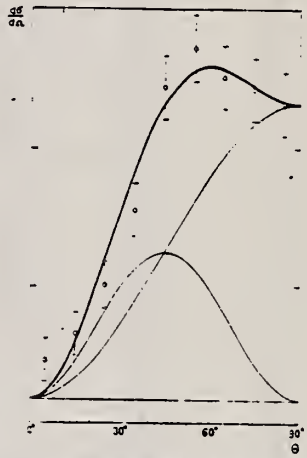

Fig. 8. Angular distribution obtained by the 6.1 MeV gamma rays with the emulsion mounted parallel to the incident radiation. The distribution is corrected for the 7 MeV component of the radiation. The fitted curve (heavy line) has the equation $0.07 - \sin^2\theta - 0.50 \sin^4 2\theta$. The fine lines show the three components of the curve.

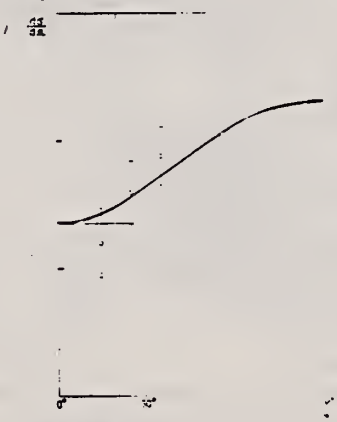

Fig. 9. Angular [illegible] 6.9 MeV gamma [illegible] rected for the [illegible] radiation. The [illegible] the equation [illegible] fine line shows [illegible]

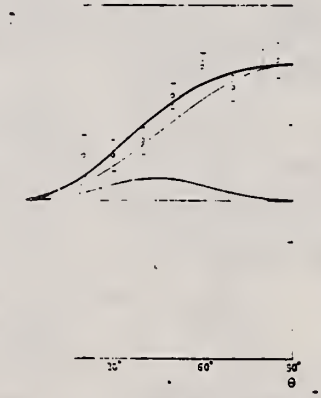

Fig. 10. Angular distribution obtained by 10 [illegible] bremsstrahlung. The fitted curve (heavy [illegible] the equation $1 - 0.85 \sin^2\theta - 0.13$ [illegible] 2θ. The fine lines show the components of the curve.

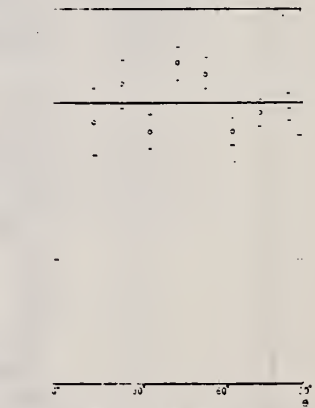

Fig. 11. Angular distribution obtained by 20 MeV bremsstrahlung.

REF. L. I. Prokhorova, G. N. Smirenkin
Atom. Energiya 8, 457 (1960)

[See also AEC-tr-8966]

ELEM. SYM.	A	Z
U	238	92

METHOD

$F^{19}(p,\alpha\gamma)$ source

REF. NO. 60 Pr 2 JOC

REACTION	RESULT	EXCITATION ENERGY	SOURCE		DETECTOR		ANGLE
			TYPE	RANGE	TYPE	RANGE	
G,F	NOX	6	D	6	BF3-I		4PI

Average number of neutrons per photofission.

REF.

E. Takekoshi
J. Phys. Soc. Japan 15, 2129 (1960)

ELEM. SYM.	A	Z
U	238	92

METHOD: Van de Graaff; fission spectrum; nuclear emulsion

REF. NO.: 60 Ta 3 NVB

REACTION	RESULT	EXCITATION ENERGY	SOURCE TYPE	SOURCE RANGE	DETECTOR TYPE	DETECTOR RANGE	ANGLE
G,F	SPC	6	D	6	EMU-D		DST
				(6.13)			

$F(p,\alpha\gamma)$ source of γ rays.

Angular distribution:

$$I(\theta) + I(\pi-\theta) = a + b \sin^2\theta + c \sin^2\theta \cos^2\theta$$

Theoretical attempts at evaluating ratio of quadrupole cross section to dipole cross section are made.

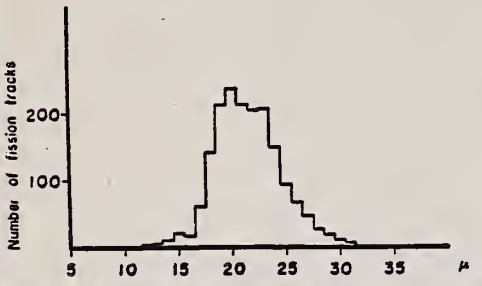

Fig. 3. Range distribution of fission tracks in uranium-impregnated nuclear plates, exposed to γ rays.

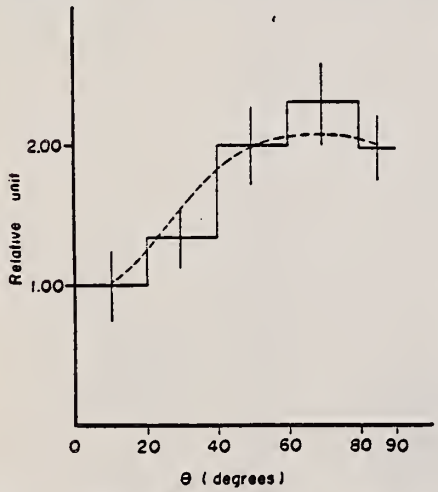

Fig. 4. Angular distribution for the fission tracks longer than 21 μ. Dotted line curve was calculated by least square fitting; this is expressed by

$$I(\theta)=1+(1.02\pm0.49)\sin^2\theta + (1.63\pm0.52)\sin^2\theta\cdot\cos^2\theta .$$

Table I. Comparison with the ratios b/a, c/a and c/b produced by $F(p, \alpha\gamma)$ γ rays and bremsstrahlung.

E_γ	b/a	c/a	c/b	Reference
$E_{\gamma\,Max}$ =6.5 MeV	4.2 ±1.8	3.1 ±3.2	0.75 ±0.71	A. I. Baz *et al.*
$E_{\gamma\,Max}$ =8.0 MeV	1.12 ±0.12	0.60 ±0.38	0.54 ±0.34	"
$E_{\gamma\,Max}$ =9.4 MeV	0.54 ±0.08	1.34 ±0.34	2.46 ±0.68	"
$F(p\,\alpha\gamma)$ γ rays E_γ =6.13 MeV	1.02 ±0.49	1.63 ±0.52	1.59 ±0.49	Present Experiment

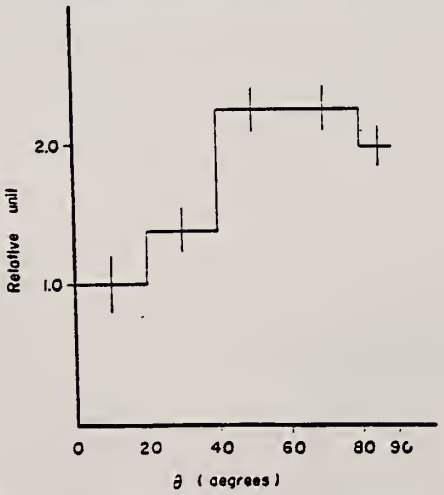

Fig. 5. Angular distribution for the fission tracks longer than 22 μ.

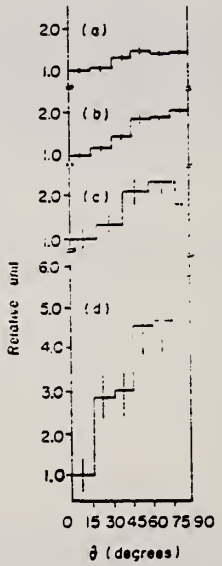

Fig. 7. Comparison of the angular distributions. (*a*), (*b*) and (*d*) show the results obtained by Baz *et al.*, and (*c*) shows the results obtained in the present experiment.

5) A. I. Baz, N. M. Klikova, L. E. Lazareva, N. V. Nikitina and V. A. Semenov: Geneva Conf. A/Conf. 15/P/2037 USSR. (1958).

REF.	ELEM. SYM.	A	
R.G. Baker, K.G. McNeill Can. J. Phys. 39, 1158 (1961)	U	238	92

METHOD	REF. NO.	
Betatron; fast neutron yield, angular distribution; Si threshold detector; ion chamber	61 Ba 2	NVB

REACTION	RESULT	EXCITATION ENERGY	SOURCE		DETECTOR		ANGLE
			TYPE	RANGE	TYPE	RANGE	
G,XN	ABY	THR-22	C	22	THR-I	[illegible]	DST

In Table 4:

$\bar{\sigma}$ = average cross section of detector weighted with neutron spectrum

$\bar{q}$ = neutrons/100 roentgen/mole

$$W(\theta) = a_o \sum_{n=1}^{\infty} [1 + A_n P_n (\cos \theta)]$$

TABLE IV

I Element	II a_0	III a_1	IV a_2	V $(\bar{\sigma}\Phi)\times10^{26}$	VI Φ_{total} (22 Mev)$\times10^{8}$	VII Φ_{fast}/Φ_{total}
Vanadium	245(1±0.06)	0.01±0.08	−0.00±0.10	6.05	0.21	0.12
Chromium	164(1±0.03)	0.04±0.04	−0.05±0.05	4.05	0.17	0.10
Manganese	308(1±0.02)	0.07±0.03	−0.09±0.04	7.61	0.25	0.12
Iron	200(1±0.03)	0.05±0.04	−0.17±0.05	4.94	0.18	0.11
Cobalt	390(1±0.02)	0.08±0.03	−0.22±0.04	9.63	0.26	0.15
Nickel	145(1±0.05)	0.07±0.07	−0.23±0.09	3.58	0.12	0.12
Copper	347(1±0.02)	0.05±0.03	−0.29±0.04	8.57	0.30	0.12
Arsenic	482(1±0.03)	0.11±0.04	−0.24±0.05	11.91	0.33	0.15
Rubidium	638(1±0.05)	0.13±0.06	−0.14±0.08	15.76		
Strontium	409(1±0.05)	0.10±0.06	−0.17±0.08	10.10		
Yttrium	290(1±0.10)	0.08±0.12	−0.12±0.15	7.16		
Silver	590(1±0.04)	0.10±0.06	−0.22±0.08	14.57	0.87	0.07
Cadmium	905(1±0.02)	0.02±0.02	−0.26±0.03	22.35		
Iodine	1133(1±0.03)	0.04±0.04	−0.29±0.05	27.99	1.42	0.08
Barium	1048(1±0.04)	0.10±0.06	−0.38±0.08	25.89		
Lanthanum	1595(1±0.02)	0.02±0.03	−0.42±0.04	39.40	1.04	0.15
Cerium	1316(1±0.05)	0.05±0.06	−0.39±0.08	32.50		
Dysprosium	1652(1±0.03)	0.04±0.10	−0.34±0.13	40.80		
Tantalum	1558(1±0.02)	0.04±0.03	−0.22±0.04	38.48	2.50	0.06
Tungsten	1365(1±0.02)	0.07±0.03	−0.24±0.04	33.71		
Mercury	1345(1±0.02)	0.04±0.03	−0.31±0.04	33.22		
Lead	2274(1±0.01)	0.02±0.02	−0.42±0.03	56.17	2.72	0.08
Bismuth	2162(1±0.02)	0.05±0.03	−0.45±0.04	53.40	3.36	0.06
Thorium	3031(1±0.04)	0.00±0.05	−0.32±0.07	74.87		
Uranium	4630(1±0.02)	0.05±0.03	−0.17±0.04	114.36		

*$(\bar{\sigma}\Phi)$ = 2.47×10⁷ ex millibarn-neutron. Errors are standard errors due to counting statistics only.

Ref. H.G. DeCarvalho, A.G.-DaSilva, J. Goldemberg
Nuovo Cimento 19, 1131 (1961)

Elem. Sym.	A	Z
U	238	92

Method: Betatron; uranium-loaded emulsions

Ref. No.: 61 De 1 JHH

Reaction	E or ΔE	E_0	Γ	$\int \sigma dE$	Jπ	Notes
U(γ, f)	Bremss. 6.9 8.1 9.4 12.5 20					Angular distribution of photofission fragments: $\theta = a + b \sin^2\theta + c \sin^2\theta \cos^2\theta$ (see Table II), indicates mostly electric dipole photon absorption.

TABLE II.

Maximum X-ray energy (MeV)	$\frac{b}{a}$	$\frac{c}{a}$
6.9	2.80 ± 0.44	0.34 ± 0.85
8.1	1.18 ± 0.14	0.52 ± 0.32
9.4	0.62 ± 0.12	0.60 ± 0.56
15.5	0.09 ± 0.14	—
20.0	0.08 ± 0.13	—

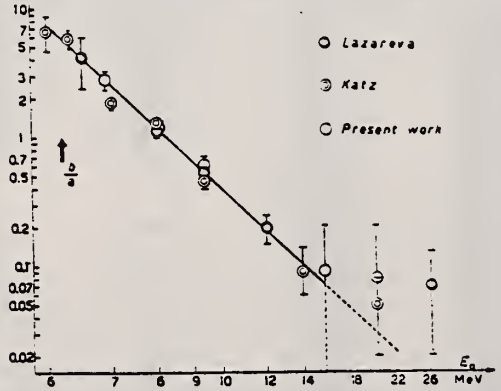

Fig. 1. – Variation with the maximum bremsstrahlung energy E_0 (in MeV) of ratio b/a, between the coefficients «a» related to the isotropic part of the angular distribution and «b» the anisotropic part related to the dipole photon absorption. The solid line represents the empirical equation $\log(b/a) = (1.676 \pm 0.24) - (2.66 \pm 0.10) \log(E_0 - 4)$ obtained from a least square fitting of the results of KATZ, LAZAREVA and the present work.

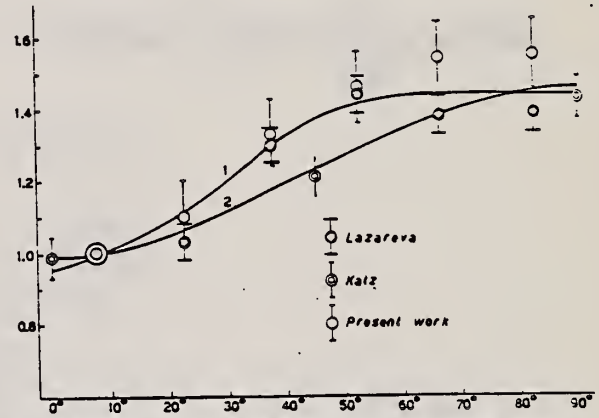

Fig. 2. – Angular distribution for 9.4 MeV bremsstrahlung showing the data of KATZ, LAZAREVA and the present work, normalized to 7.5°. Curve 1 corresponds to the best fitting of the data of LAZAREVA and the present work together $(1 + 0.47 \sin^2\theta + 0.30 \sin^2\theta \cos^2\theta)$, curve 2 is a fitting of KATZ's results with a pure dipole photon absorption curve $(1 + 0.46 \sin^2\theta)$.

(2) L. KATZ, A. P. BAERG and F. BROWN: *Second United Nations International Conference on Peaceful Uses of Atomic Energy*, Geneve P/266, 15, 188 (1958).

(3) B. P. BANNIK, N. M. KULIKOVA, L. E. LAZAREVA and V. A. IAKOVLEV: *Sov. Phys. J.E.T.P.*, 6, 39 (1958); A. I. BRAZ, N. M. KULIKOVA, L. E. LAZAREVA, N. V. NIKITINA and V. A. SEMENOV: *Second United Nations International Conference on the Peaceful Uses of Atomic Energy*, Geneve P/2037, 15, 184 (1958).

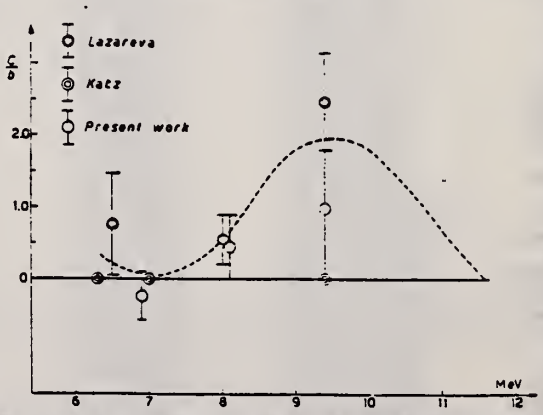

Fig. 3. – Variation of the ratio c/b with the peak bremsstrahlung energy.

Ref. H.G. DeCarvalho, A. Celano, G. Cortini, R. Rinzivillo, G. Ghigo
Nuovo Cimento 19, 187 (1961)

Elem. Sym.	A	Z
U	238	92

Method: Synchrotron; emulsions

Ref. No.: 61 De 2 ds | JHH

Reaction	E or ΔE	E_o	Γ	$\int \sigma dE$	Jπ	Notes
U (γ, f)	300-1000 MeV					Slope = $\frac{d\,\sigma_Q\,F}{d\,\ell n\,E}$ = 60×10^{-27} cm^2 ± 10% over range 300-1000 MeV.

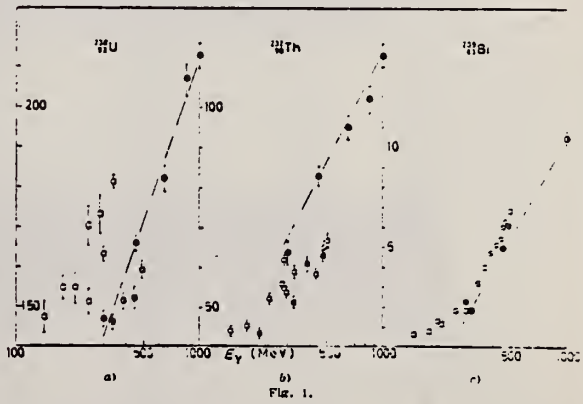

Fig. 1.

Ref. F. Tagliabue, J. Goldemberg
Nuclear Phys. 27, 144 (1961)

Elem. Sym.	A	Z
U	238	92

Method 22 MeV betatron; $Si^{28}(n,p)Al^{28}$ threshold detector.

Ref. No. 61 Ta 1 JHH

Reaction	E or ΔE	E_o	Γ	$\int \sigma dE$	Jπ	Notes
(γ,n)	Bremss. 22					$E_n > 6$ MeV. $W(\theta_n) = A + B \sin^2\theta$ where B/A = 0.41±0.21

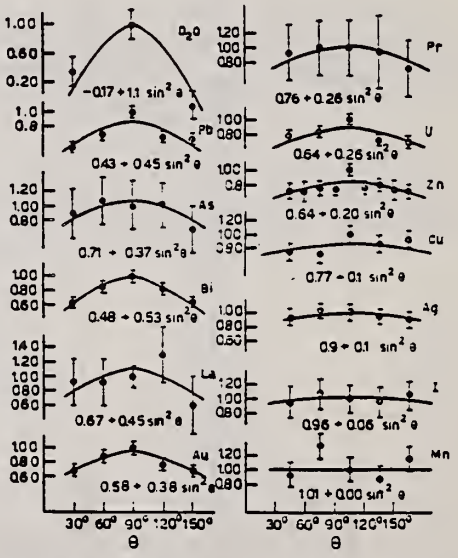

Figure 4: Angular distribution of fast photoneutrons as observed with the $Si^{28}(n,p)Al^{28}$ detector. Data normalized at 90° in each case.

REF. B.A. Bochagov, A.P. Komar, G.E. Solyakin
Zhur. Eksp. i Teoret. Fiz. 43, 1611 (1962); Soviet Phys. JETP 16, 1135 (1963)

ELEM. SYM.	A	Z
U	238	92

METHOD
Synchrotron; fission energy distribution; ion chamber

REF. NO. 62 Bo 8 NVB

REACTION	RESULT	EXCITATION ENERGY	SOURCE TYPE	SOURCE RANGE	DETECTOR TYPE	DETECTOR RANGE	ANGLE
G,F	SPC	THR-50	C	17-50	ION-D		90
				(17.5, 30, 50)			

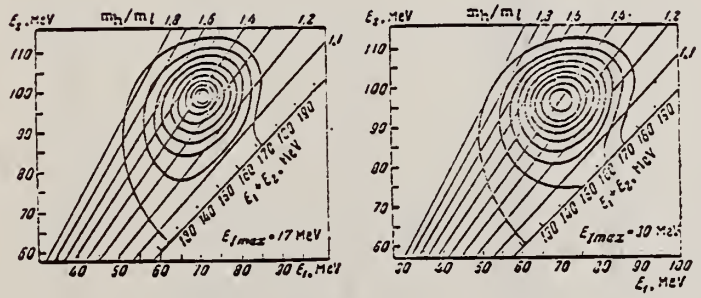

FIG. 2. Contour diagrams for the kinetic energy distribution of fragments for two values of the bremsstrahlung maximum energy. Each contour line corresponds to an increase in the fission probability by 0.1 (m_h and m_l are the masses of the heavy and light fragments)

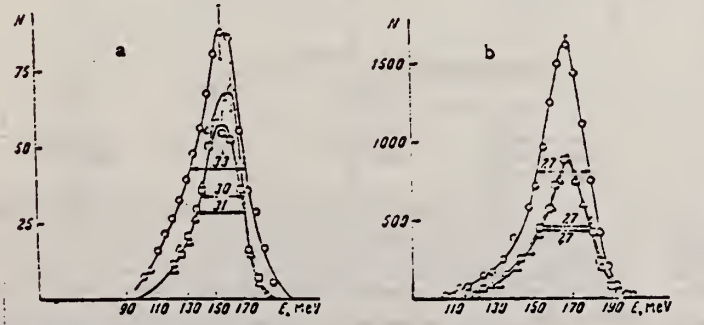

FIG. 3. Spectra of the total kinetic energy of photofission fragments for various brehmsstrahlung energies (the numbers indicate the half-widths of the peaks): a – symmetric (in mass) fission, b – asymmetric fission, □ – $E_{\gamma max}$ = 17.5 MeV, ○ – $E_{\gamma max}$ = 30 MeV, Δ – $E_{\gamma max}$ = 50 MeV.

Ref.	Elem. Sym.	A	Z
H.G. DeCarvalho, A. Manfredini, M. Muchnik, M. Severi, H. Bösch, J. Lang, R. Müller, W. Wölfli Nuovo Cimento 25, 534 (1962) ERRATUM: Nuovo Cimento 29, 475 (1963)	U	238	92

Method	Ref. No.
Reactor; monoenergetic γ's from Ti(n,γ) reaction; emulsions; NaI monitor	62 De 3 cs JHH

Reaction	E or ΔE	E_o	Γ	$\int \sigma dE$	Jπ	Notes
$U^{238}(\gamma, f)$	$6.61^{+0.14}_{-0.20}$ MeV					In Table II, $\sigma_{f(Th)}/\sigma_{f(U)} = 0.92$ should be 0.85.

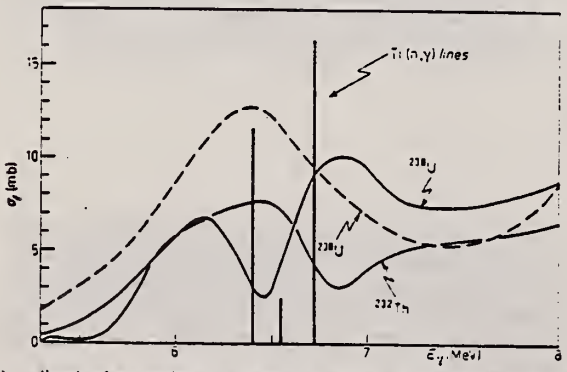

Fig. 2. – Sketch of preceding experimental results for the photofission cross-section of ^{238}U (—— Katz *et al.* [3]; - - - Schmitt *et al.* [2]) and of ^{232}Th (—— Katz *et al.* [3]). Schmitt's results have been normalized to those of Katz at 8 MeV. Shown in the figure also the three main lines of the Ti(n, γ) process with their corresponding intensities in arbitrary units.

Table III.

	σ_{Th} (mb)	σ_U (mb)	$\sigma_{f(Th)}/\sigma_{f(U)}$
Present work	4.73 ± 0.30	7.89 ± 0.83	0.600 ± 0.005
Katz *et al.* [3]	5.6	6.6	0.92 *
Schmitt *et al.* [2]	—	10.7	—

(*) Normalized to Katz *et al.* [3] at 8 MeV.

[2] R. A. Schmitt and R. B. Duffield: *Phys. Rev.*, 105, 1277 (1957).

[3] L. Katz, A. P. Baerg and F. Brown: *Second U.N. International Conference on the Peaceful Uses of Atomic Energy*, vol. 15 (1958), p. 184.

[4] A. I. Baz, N. M. Kulkova, L. E. Lazareva, N. V. Nikitina and V. A. Semenov: *Second U.N. International Conference on the Peaceful Uses of Atomic Energy*, vol. 15 (1958), p. 184.

Ref. J.R. Huizenga, K.M. Clarke, J.E. Gindler, R. Vandenbosch
Nuclear Phys. 34, 439 (1962)

Elem. Sym.	A	Z
U	238	92

Method: Monoergic γ's from $F^{19}(p,\alpha\gamma)$ reaction; fission fragment ionization chamber.

Ref. No.: 62 Hu 1 | JHH

Reaction	E or ΔE	E_o	Γ	$\int \sigma dE$	Jπ	Notes
	6.14					
	7.0					
$U^{238}(\gamma, f)$						

TABLE 1

Isotopic content of uranium targets in mass per cent

Target	233	234	235	236	238
U[233]	98.33	0.010	0.0127		1.53
U[234]		93.44	4.87		1.69
U[235]		0.022	99.94		0.038
U[236]		0.07	4.62	94.77	0.54
U[238]			0.04		99.96

TABLE 3

Photofission cross sections obtained with mono-energetic gamma rays from the $F^{19}(p, \alpha\gamma)O^{16}$ reaction

Target	$\sigma_{\gamma,f}/\sigma_{\gamma,16}$	$\sigma_{\gamma,f}$(mb)	$\sigma_{\gamma,16}$(mb)	B_n(MeV) [a]	E_t(MeV) [b]
Th^{232}	1.00 ± 0.13	9 ± 3	9 ± 3	6.34	5.5
U^{233}	1.12 ± 0.15	15 ± 5	13 ± 4	6.04	5.3
U^{235}	0.80 ± 0.10	28 ± 9	33 ± 11	6.40	5.2
U^{236}	2.08 ± 0.33	33 ± 10	16 ± 5	5.24	5.5
U^{238}	10.0 ± 5.0	52 ± 16	5^{+30}_{-4}	6.77	5.1
U^{238}	3.24 ± 0.79	44 ± 14	13 ± 4	5.90	5.4
Np^{237}	1.43 ± 0.21	45 ± 14	31 ± 10	6.76	5.3

[a]) From the compilation of ref. [20])
[b]) From the compilation of ref. [20])

Ref 20: Everling, König, Mattauch, & Wapstra - Nuclear Phys. 18, 529 (1960)

Ref 26: Vandenbosch & Seaborg - Phys. Rev. 110, 507 (1958)

REF.

A.P. Komar, B.A. Bochagov, V.I. Fadeev
Dokl. Akad. Nauk SSSR 146, 1051 (1962); Soviet Phys. Doklady 7, 913 (1963)

ELEM. SYM.	A	Z
U	238	92

METHOD: Synchrotron; fission fragment mass distribution; ion chamber

REF. NO.: 62 Ko 4 | NVB

REACTION	RESULT	EXCITATION ENERGY	SOURCE TYPE	SOURCE RANGE	DETECTOR TYPE	DETECTOR RANGE	ANGLE
G,F	NΦX	THR-35	C	35	IΦN-D		DST

m_h/m_l = ratio of fragments

MASS DISTRIBUTION

I: θ = 0-34°
II: θ = 34-48°
III: θ = 48-60°
IV: θ = 60-70°
V: θ = 70-80°

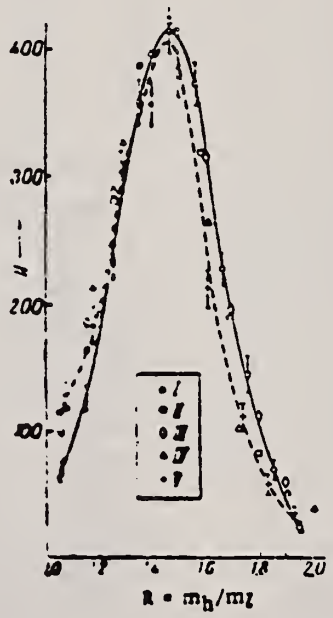

Fig. 2. Mass distribution of fragments resulting from the splitting of the U^{238} nucleus by photons with $E_{\gamma max}$ = 35 MeV in the I-V range of angles.

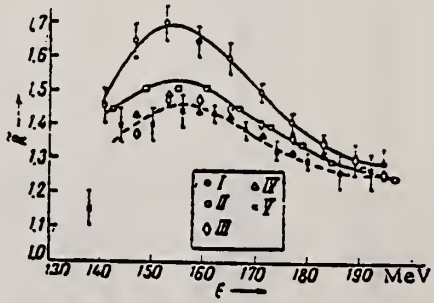

Fig. 3. Dependence of the most probable ratio of the masses of fragments on total kinetic energy in the case of the splitting of U^{238} nuclei by 14-MeV neutrons in the I-V range of angles.

REF.
G. Moscati, J. Goldemberg
Phys. Rev. 126, 1098 (1962)

ELEM. SYM.	A	Z
U	238	92

METHOD
Betatron; fission, delayed neutron yield; BF_3 counters

REF. NO.
62 Mo 3 NVB

REACTION	RESULT	EXCITATION ENERGY	SOURCE		DETECTOR		ANGLE
			TYPE	RANGE	TYPE	RANGE	
G,F	ABY	THR-20	C	12,20	BF3-I		4PI

DELAYED N YIELDS

Delayed means > 3000 μ sec.

TABLE I. Experimental results. The errors in columns 3 and 4 are statistical. The errors in column 5 represent extreme values using plausible estimates for $\sigma(\gamma,n)$ and $\sigma(\gamma,2n)$, and $\bar{\nu}$ from Gindler *et al.*[3] and Leachman.[4]

Element	Energy (Mev)	(Relative counts/pulse)/monitor unit Prompt	Delayed	Delayed neutrons/fission
U^{238}	12	620±25	3.2 ±0.2	$0.036^{+0.008}_{-0.007}$
	20	2545±100	13.6 ±0.5	$0.036^{+0.010}_{-0.009}$
Th^{232}	12	223±12	0.55±0.04	$0.027^{+0.008}_{-0.007}$
	20	995±40	2.2 ±0.1	$0.030^{+0.012}_{-0.006}$

[3] J. E. Gindler, J. R. Huizenga, and R. A. Schmitt, Phys. Rev. 104, 425 (1956).
[4] R. B. Leachman, *Proceedings of the Second United Nations International Conference on the Peaceful Uses of Atomic Energy, Geneva, 1958* (United Nations, Geneva, 1958), Paper P/2467, Vol. 15, p. 229.

REF.	ELEM. SYM.	A	Z
R. Bosch, J. Lang, R. Muller, W. Wolfli Helva. Phys. Acta 36, 625 (1963)	U	238	92

METHOD	REF. NO.
n capture source; photon scattering; NaI spectrometer	63 Bo 2

REACTION	RESULT	EXCITATION ENERGY	SOURCE		DETECTOR		ANGLE
			TYPE	RANGE	TYPE	RANGE	
G,G	ABX	9	D	9	NAI - D		DST

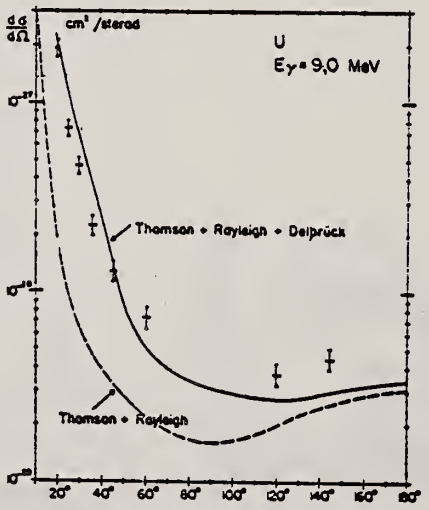

Fig. 11.

Experimentell bestimmte Wirkungsquerschnitte für die Streuung von 9-MeV-Quanten an Uran. Die gestrichelte Kurve gibt den theoretischen Wert für Thomson- und Rayleighstreuung (nach BETHE); in der ausgezogenen Kurve ist zudem der Delbrückeffekt (nach einer Extrapolation aus den Werten ZERNIKS) mit einbezogen.

REF.

B.A. Bochagov, A.P. Komar, V.I. Fadeev
Atomnaya Energiya 15, 191 (1963); Soviet Atomic Energy 15, 891 (1963)

ELEM. SYM.	A	Z
U	238	92

METHOD: Synchrotron; fission angular, energy distribution; ion chamber

REF. NO.: 63 Bo 6 NVB

REACTION	RESULT	EXCITATION ENERGY	SOURCE		DETECTOR		ANGLE
			TYPE	RANGE	TYPE	RANGE	
G,F	NΦX	THR-35	C	35	IΦN-D		DST

$R = \frac{m_H}{m_L}$ = mass ratio of fragments

$\bar{E}_{max}$ = 171±3 MeV at R = 1.25 - 1.30, independent of angle.

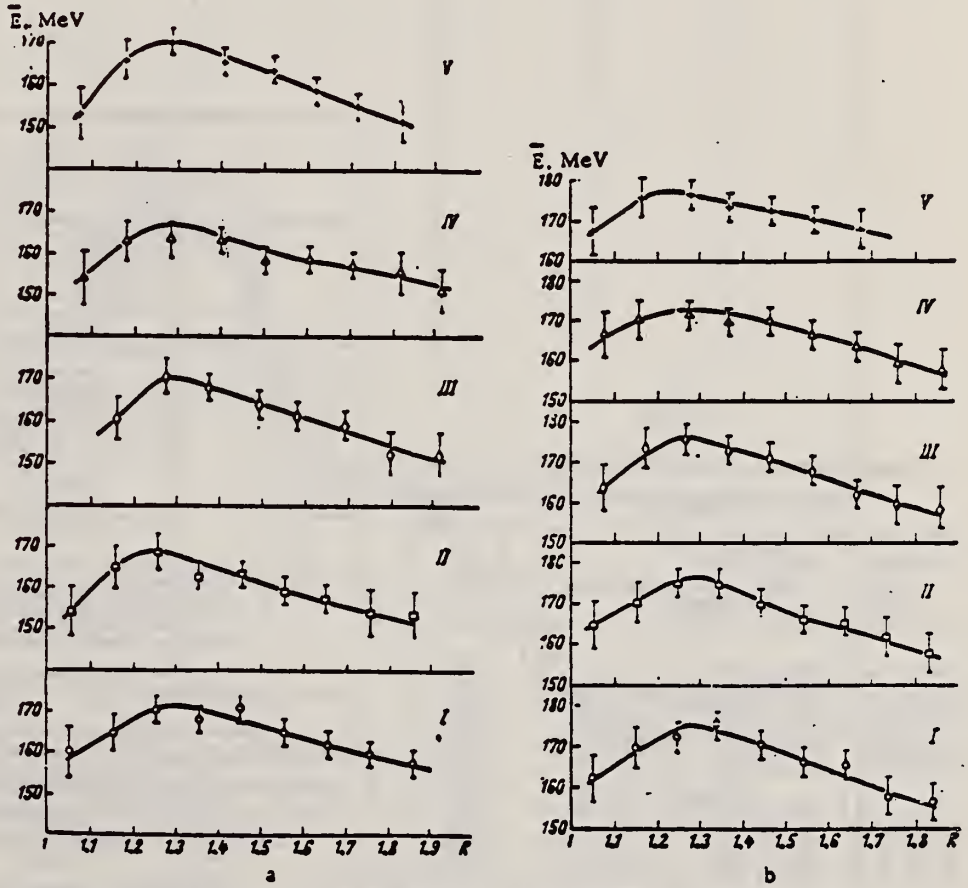

Fig. 2. Most probable total kinetic energy of the fragments, $\bar{E}$, at fixed mass ratios for different angular ranges in the case of 14 MeV neutron fission (a) and photofission with $E_{\gamma max}$ = 35 MeV (b). (I-V angular range numbers).

Ref. H.G. DeCarvalho, A. Manfredini, M. Muchnik, M. Severi, R. Bosch, W. Wolfli
Nuovo Cimento 29, 463 (1963)

Elem. Sym.	A	Z
U	238	92

Method
Reactor; monoenergetic γ's from Ti(n,γ) reaction; emulsions; NaI monitor

Ref. No. 63 De 1 c s | JHH

Reaction	E or ΔE	E_0	Γ	$\int \sigma dE$	Jπ	Notes
$U^{238}(\gamma, f)$	$6.61^{+0.14}_{-0.20}$ MeV					Parameters for angular distribution function, $W(\theta) = a + b \sin^2\theta + c \sin^2\theta \cos^2\theta$ are given in Table II.

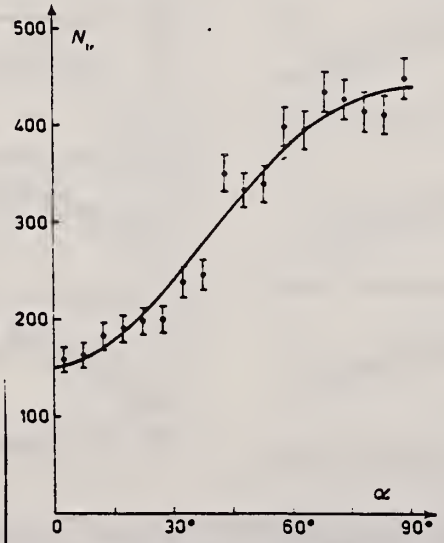

Fig. 4. – Angular distribution $W(\alpha, \beta_0 = 15°)$ of fission fragments from ^{238}U.

TABLE II.

	E_γ(*) MeV	γ-ray source	b/a	c/a	c/b
Th	6.5	bremss. (2)	> 25	—	—
	6.61 (**)	Ti(n, γ)	11 ± 3	1 ± 1	0.1 ± 0.1
	7.0 (***)	bremss. (2)	10.6 ± 2.1	−2.1 ± 1.6	−0.20 ± 0.16
U	6.1	F(p, γ) (7)	14 ± 14	21 ± 21	1.4 ± 0.2
	6.5	bremss. (2)	4.4 ± 1.0	—	—
		bremss. (3)	4.2 ± 1.3	3.1 ± 3.2	0.75 ± 0.71
	6.61 (**)	Ti(n, γ)	2.0 ± 0.2	0.6 ± 0.3	0.3 ± 0.2
	6.9	F(p, γ) (7)	0.7 ± 0.3	0.2 ± 0.3	0.3 ± 1.1
		bremss. (4)	2.80 ± 0.44	0.34 ± 0.35	0.12 ± 0.30
	7.0 (***)	bremss. (2)	2.11 ± 1.24	0.96 ± 0.88	0.45 ± 0.49

(*) E_γ indicates either the maximum bremsstrahlung energy or the energy of the monoenergetic beam, as the case may be. Only those points of other authors are quoted whose energy lies within 0.5 MeV from our energy (6.61 MeV).
(**) We give the values obtained by means of the Fourier analysis of the data (see Table I).
(***) For purposes of comparison we quote the values given in the paper of BATHO *et al.* (4), including the coefficient c, although the authors assume in their discussion $c = 0$.

(2) A. BOHR: *International Conference on the Peaceful Uses of Atomic Energy*, vol. 2 p. 911, (1956).

TABLE III (*).

Nucleus	σ_f (mb) (from part I) (**)	σ_{te} (mb)	σ_d (mb)	σ_q (mb)
^{238}Th	5.3 ± 0.6	0.7 ± 0.2	4.8 ± 0.6	0.1 ± 0.1
^{238}U	9.2 ± 0.9	3.7 ± 0.4	5.1 ± 0.6	0.3 ± 0.2

(*) The values of σ_f, σ_e and σ_q have been computed using the Fourier analysis results for a, b and c (see Table I).
(**) An error on the dose measurement has been detected since the publication of Part I of this paper. Instead of $(2.0 \cdot 10^{11} \pm 10\%)$ quanta/cm² the dose was $(1.72 \cdot 10^{11} \pm 10\%)$ quanta/cm²: accordingly the cross-sections reported in Part I should be changed to the values shown in the present Table III.

REF.	ELEM. SYM.	A	Z
K.A. Petrzhak, R.V. Sedletskii Atomnaya Energiya 15, 308 (1963); Soviet Atomic Energy 15, 1025 (1963)	U	238	92

METHOD	REF. NO.	
Betatron; fission yield, mass distribution; radio-chemical separation (activation)	63 Pe 2	NVB

REACTION	RESULT	EXCITATION ENERGY	SOURCE		DETECTOR		ANGLE
			TYPE	RANGE	TYPE	RANGE	
G, F	RLY	THR-14	C	14	ACT-I		4PI

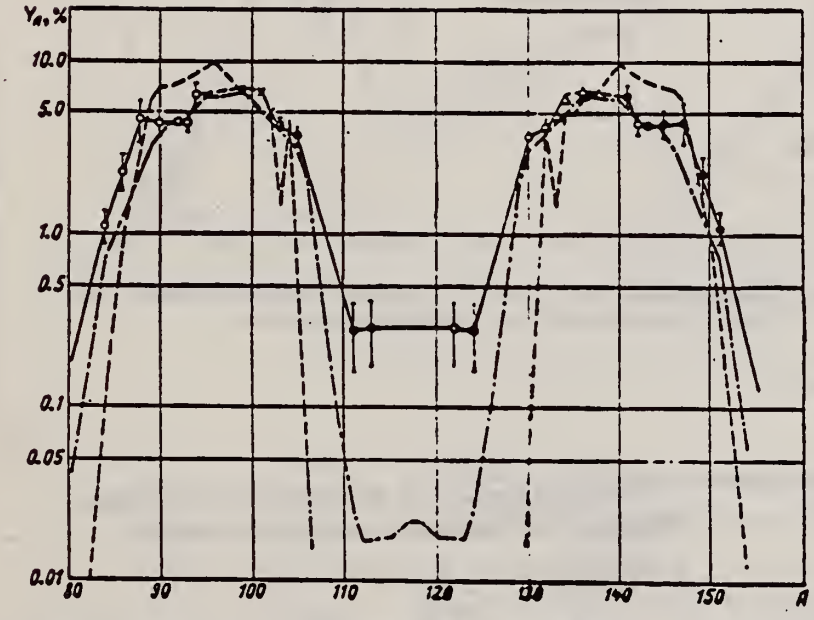

Relation between fission fragment yields and mass number: ⊖) main points; ○) mirror points (our results for U^{238} photofission at 14 MeV); ×) main points; △) mirror points (results in [22] for U^{238} photofission at 13 MeV); – · – · –) U^{238} photofission at 8 MeV [1]; ——) spontaneous fission of U^{238} [19-21].

19. P. Kuroda and M. Menon. Nucl. Sci. Engng., 10, 70 (1961).
20. B. Young and H. Thode. Canad. J. Phys., 38, 1 (1960).
21. G. Wetherill. Phys. Rev., 92, 907 (1953).
22. D. Wiles and C. Coryell. Phys. Rev., 96, 696 (1954).

TABLE 1. Yields of U^{238} Photofission Fragments at a Maximum Bremsstrahlung Energy of 14 MeV

Fragment	Half-life.	Ratio of fragment yield to Ce^{143} yield	Only one experiment
Y^{93}	11 h	0.996±0.096	4.3 ±0.4
Ru^{103}	39.8 days	0.955±0.028	4.11±0.12
Ru^{106}	4.4 h	0.832±0.020	3.59±0.09
Ag^{111} •	7.6 days	0.064±0.025	0.27±0.11
Ag^{112} •	5.3 h	0.066±0.025	0.28±0.11
La^{141}	3.7 h	1.45 ±0.21	6.2 ±0.9
Co^{143}	33.4 h	1.0	4.3
Pr^{148}	6.0 h	0.989±0.167	4.2 ±0.7
Nd^{147}	11.3 days	1.03 ±0.28	4.4 ±1.2
Nd^{149}	1.8 h	0.52 ±0.12	2.2 ±0.5
Pm^{151}	27.5 h	0.25 ±0.05	1.1 ±0.2

• Only one experiment.

REF.	ELEM. SYM.	A	Z
Yu.Ya. Glazunov, M.V. Savin, I.N. Safina, E.F. Fomushkin, Yu.A. Khokhlov Zhur. Eksp. i Teoret. Fiz. 46, 1906-08 (1964) Soviet Phys. JETP 19, 1284 (1964)	U	238	92

METHOD	REF. NO.	
Linac	64 G1 1	NVB

REACTION	RESULT	EXCITATION ENERGY	SOURCE		DETECTOR		ANGLE
			TYPE	RANGE	TYPE	RANGE	
G,N	SPC	16	D	16	TØF-D	0-5	90

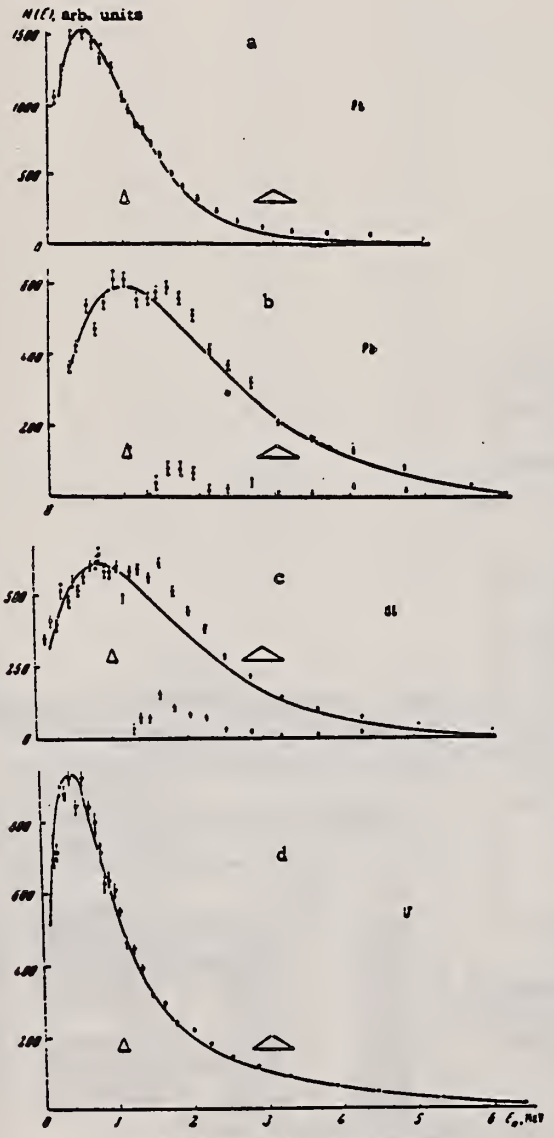

Photoneutron energy distributions.

shown in the figure. The solid curves a, b, and c are the evaporation spectra

$$N(E) \sim \frac{E}{T} \exp\left(-\frac{E}{T}\right)$$

with the temperature T = 0.48 ± 0.03 MeV for platinum, 0.84 ± 0.04 MeV for Bi, and 0.98 ± 0.04 MeV for lead.

The solid curve d is the sum of the evaporation spectrum and the fission spectrum of uranium:

$$N(E) = \alpha \frac{E}{T} \exp\left(-\frac{E}{T}\right) + (1-\alpha) \exp\left(-\frac{E}{T}\right) \times \frac{1}{\sqrt{\pi\omega T_f}} \exp\left(-\frac{E}{T_f}\right) \sinh \frac{\sqrt{\omega E}}{T_f}$$

with the parameters: T = 0.33 ± 0.03 MeV, T_f = 1.05 ± 0.04 MeV, ω = 0.5 MeV, α = 0.49 ± 0.01.

REF.

E. Albertsson and B. Forkman
Nuclear Phys. 70, 209 (1965)

ELEM. SYM.	A	Z
U	238	92

METHOD

$^{19}F(p,\alpha\gamma)^{16}O$ radiation

[Page 1 of 2]

REF. NO. 65 Al 1 EGF

REACTION	RESULT	EXCITATION ENERGY	SOURCE		DETECTOR		ANGLE
			TYPE	RANGE	TYPE	RANGE	
G,F	RLX	6-7	D	6-7	EMU-D		DST

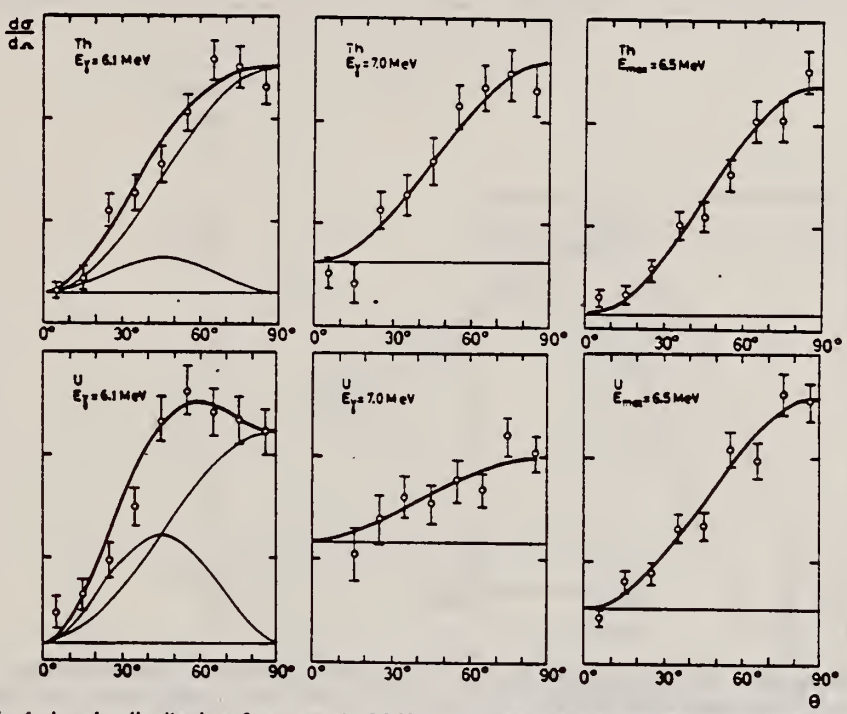

Fig. 1. Angular distributions from pure 6.1 MeV and 7.0 MeV photon excitation and from 6.5 MeV bremsstrahlung excitation in the present work and in ref. [a]).

TABLE 2

Coefficients in the angular distribution $W(\theta) = a + b\sin^2\theta + c\sin^2 2\theta$ in photofission of thorium and uranium

Element	Photon energy (MeV)	a	b	c
Th^{228}	6.1	0.12±0.03	0.89±0.05	0.14±0.06
	7.0	0.25±0.04	0.78±0.06	
	6.5 (bremsstr.)	0±0.05	1.27±0.07	
U^{236}	6.1 [a])	0.07±0.08	1.00±0.10	0.50±0.12
	7.0 [a])	1.00±0.22	0.70±0.22	0.05±0.20
	6.5 (bremsstr.)	0.17±0.03	0.93±0.05	

[a]) Ref. [a]).

REF.

E. Albertsson and B. Forkman
Nuclear Phys. 70, 209 (1965)

ELEM. SYM.	A	Z
U	238	92

METHOD

$^{19}F(p,a\gamma)^{16}O$ radiation

REF. NO. 65 A1 1 EGF

REACTION	RESULT	EXCITATION ENERGY	SOURCE		DETECTOR		ANGLE
			TYPE	RANGE	TYPE	RANGE	

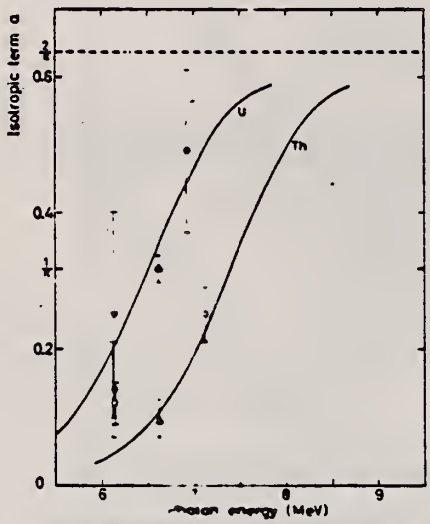

Fig. 3. Increase of the isotropic term a in $W(\theta)$ with photon energy. The curve is the function $f(E) = 2/\pi\{1+\exp([B-E)/E_p)\}^{-1}$ with B = 7.4 for thorium and B = 6.5 MeV for uranium and E_p = 0.5 MeV for both. The experimental points are from the following papers: ○(Th) present work; ● (U) Forkman *et al.*[8]); ▼ (U) Takeshita[9]); △▲ (Th, U) Carvalho *et al.*[10]).

REF.

F. Carbonara, H.G. DeCarvalho, R. Rinzivillo, E. Sassi and G.P. Murtas
Nucl. Phys. 73, 385 (1965)

ELEM. SYM.	A	Z
U	238	92

METHOD

REF. NO.	
65 Ca 3	JOC

REACTION	RESULT	EXCITATION ENERGY	SOURCE		DETECTOR		ANGLE
			TYPE	RANGE	TYPE	RANGE	
G,F	ABY	300-1000	C	1 BEV	EMU-I		4PI

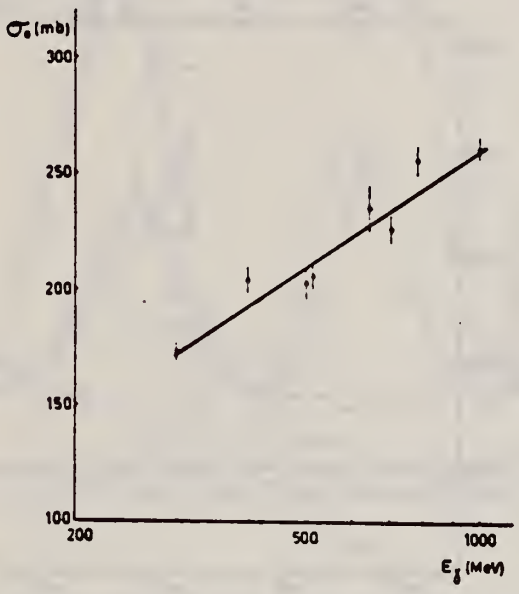

Fig. 4. The experimental data for the U fission cross-section per equivalent quantum σ_0 are plotted against the maximum energy of the γ beam. The solid line is the result of a least-squares calculation.

TABLE 1
Some fissility values

Particle	Energy	Nucleus		
	(MeV)	^{238}U	^{232}Th	^{209}Bi
Photons	300÷1000	0.84±0.13	0.47±0.10	0.12±0.02
Protons	600 [a])	0.65	0.40	0.13
Protons	200 [b])	0.80	0.47	0.09

[a]) Ref. [16]). [b]) Ref. [17]).

REF.

G. R. Hogg
Nuclear Phys. 72, 167 (1965)

ELEM. SYM.	A	Z
U	238	92

METHOD

[Page 1 of 3]

REF. NO. 65 Ho 1

EGF

REACTION	RESULT	EXCITATION ENERGY	SOURCE		DETECTOR		ANGLE
			TYPE	RANGE	TYPE	RANGE	
G,F	RLY	THR - 33	C	33	SCD-D	100 - 200	90

MASS DISTRIBUTION

$\bar{E}_k$ is mean total KE released

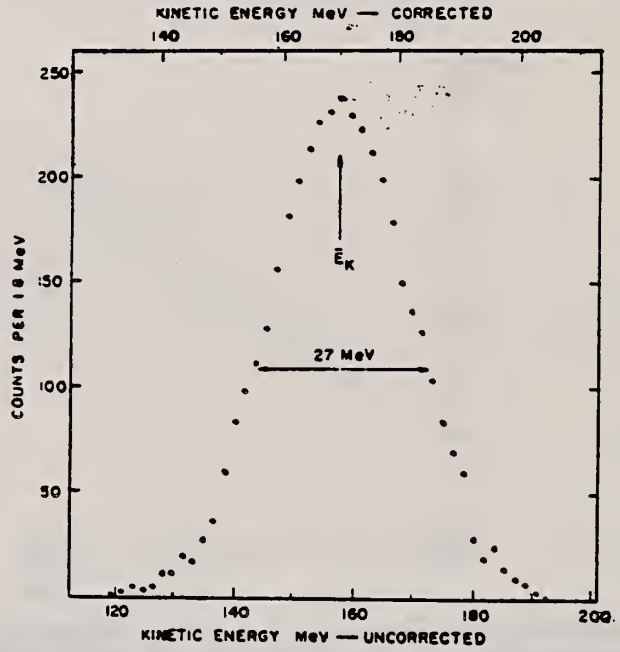

Fig. 2. The total fragment kinetic energy release spectrum. The corrected energy scale has been corrected for the detector pulse height defect and fragment energy loss in the target, but not for prompt neutron emission effects.

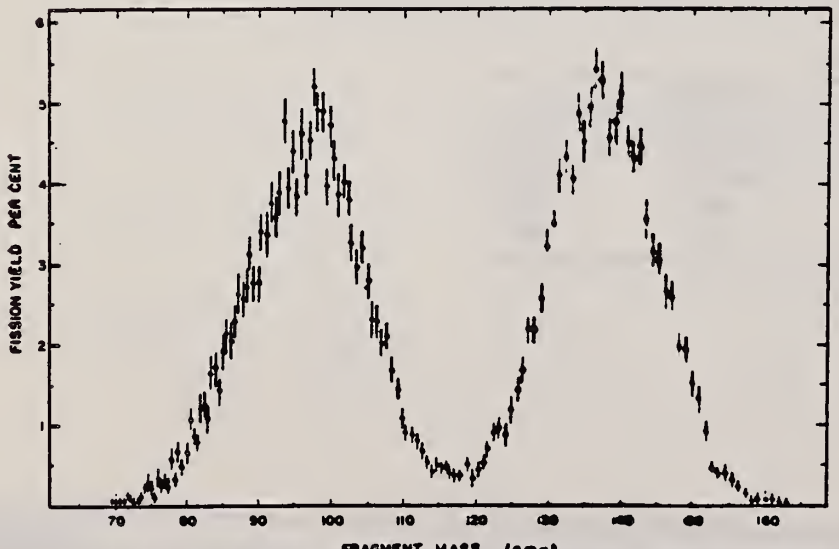

Fig. 3. Total mass distribution of the fragments from the photofission of ^{238}U with 33 MeV bremsstrahlung. The error bars are statistical.

REACTION	RESULT	EXCITATION ENERGY	SOURCE TYPE	SOURCE RANGE	DETECTOR TYPE	DETECTOR RANGE	ANGLE

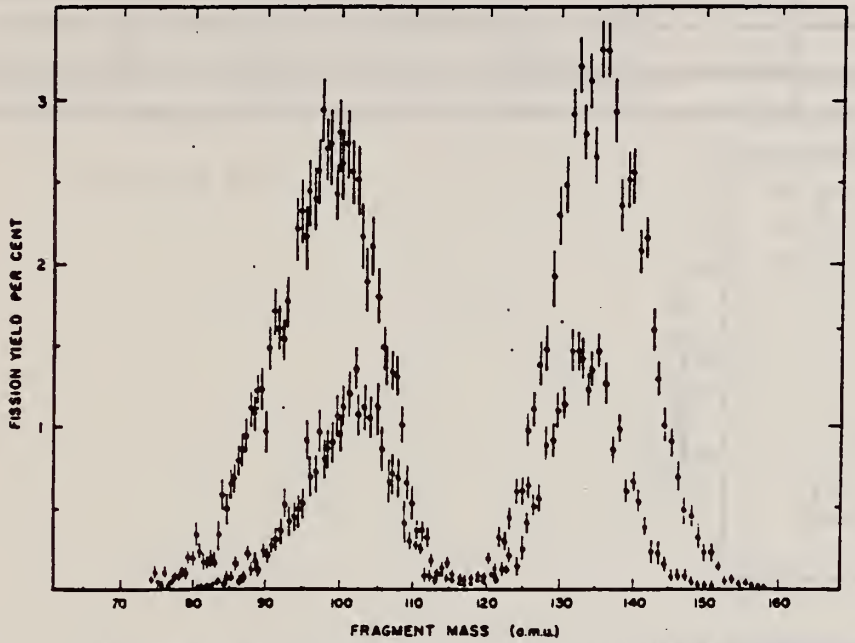

Fig. 4. Partial mass distribution for total fragment kinetic energy release $E_K > \bar{E}_K$ (closed circles) and $E_K > \bar{E}_K + 10$ MeV (open circles). The error bars are statistical.

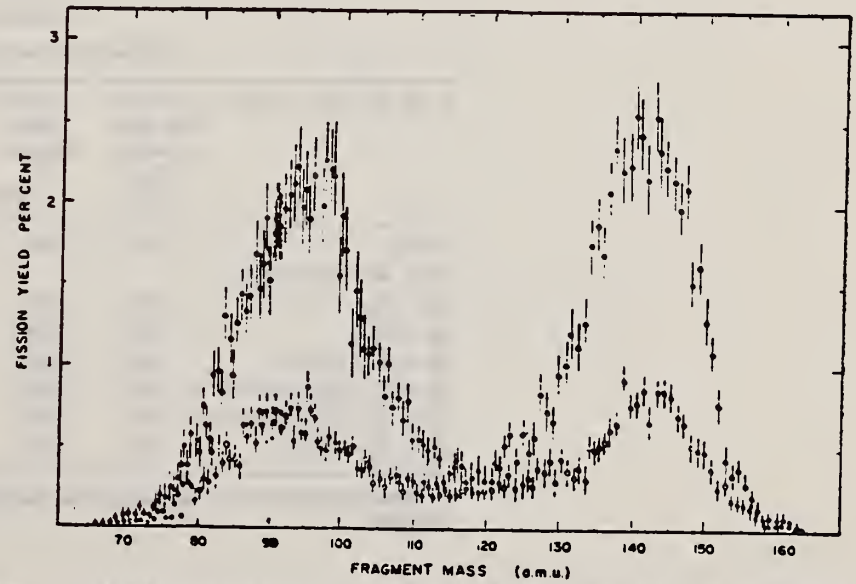

Fig. 5. Partial mass distributions for total fragment kinetic energy release $E_K < \bar{E}_K$ (closed circles) and $E_K < \bar{E}_K - 10$ MeV (open circles). The error bars are statistical.

REACTION	RESULT	EXCITATION ENERGY	SOURCE		DETECTOR		ANGLE
			TYPE	RANGE	TYPE	RANGE	

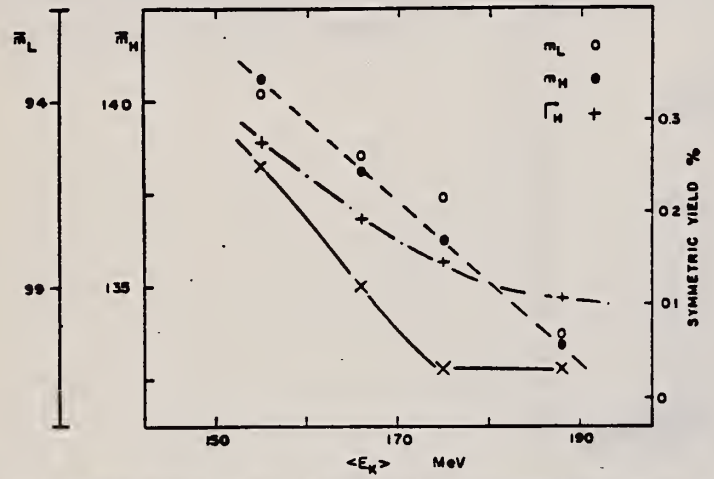

Fig. 6. Graphical summary of the parameters of the mass distributions (cf. table 1).

TABLE 1

Parameters of the mass distributions

Range of energy release	Average total kinetic energy $\langle E_K \rangle$ (MeV)	Mean mass light fragment $\bar{m}_L$ a.m.u.	Mean mass heavy fragment $\bar{m}_H$ a.m.u.	Calculated width light fragment Γ_L a.m.u.	Calculated width heavy fragment Γ_H a.m.u.	Yield at symmetry (%)
All E_K (total mass distribution)	170	96.4	137.8	7.95	7.65	0.43
$E_K > \hat{E}_K$	180	98.3	135.5	7.1	6.2	0.06
$E_K < \hat{E}_K$	160	94.5	139.7	9.1	8.5	0.37
$E_K > \hat{E}_K + 10$ MeV	188	101.6	133.4	6.0	5.3	0.03
$\hat{E}_K < E_K < \hat{E}_K + 10$ MeV [a])	175	96.4	136.2	7.3	6.4	0.03
$\hat{E}_K > E_K > \hat{E}_K - 10$ MeV [a])	166	95.5	138.2	8.4	7.6	0.12
$E_K < \hat{E}_K - 10$ MeV	156	93.8	140.6	9.3	9.6	0.25

[a]) These distributions were determined from the difference between the appropriate measured distributions.

REF.

M. Holmberg and H. Condé
Arkiv for Fysik 29, 301 (1965)

ELEM. SYM.	A	Z
U	238	92

METHOD

$F^{19}(p,a\gamma)$

REF. NO. 65 Ho 2 JOC

REACTION	RESULT	EXCITATION ENERGY	SOURCE		DETECTOR		ANGLE
			TYPE	RANGE	TYPE	RANGE	
G,F	NOX	7	D	7	SCI-I		4PI

$\bar{\nu} = 2.77 \pm 0.13$

REF.

T. Kivikas and B. Forkman
Nuclear Physics 64, 420 (1965)

ELEM. SYM.	A	Z
U	238	92

METHOD

[Page 1 of 2]

REF. NO. 65 Ki 1

EGF

REACTION	RESULT	EXCITATION ENERGY	SOURCE		DETECTOR		ANGLE
			TYPE	RANGE	TYPE	RANGE	
G,F	ABY	6-7	C	5-7	ACT-I		4PI

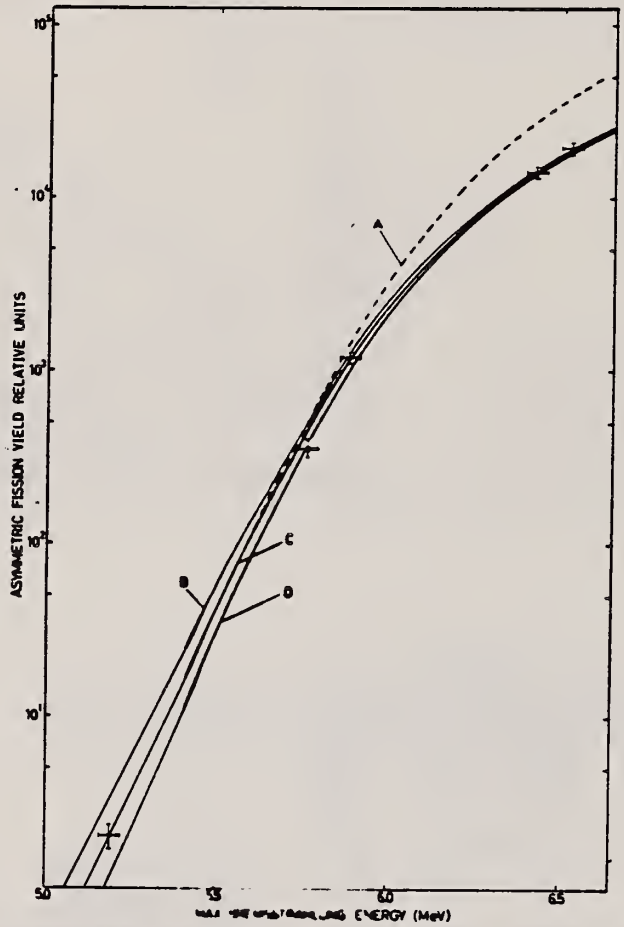

Fig. 3. Semilogarithmic plot of the asymmetric photofission yield as a function of maximum bremsstrahlung energy. Theoretical yields eq. (3) are given with the parameters

A: (T = 0.6 MeV, B_f = 5.9 MeV, E_0 = 85 keV),
B: (T = 0.6 MeV, B_f = 5.8 MeV, E_0 = 90 keV),
C: (T = 0.6 MeV, B_f = 5.8 MeV, E_0 = 85 keV),
D: (T = 0.6 MeV, B_f = 5.8 MeV, E_0 = 80 keV).

REF.

T. Kivikas and B. Forkman
Nuclear Phys. 64, 420 (1965)

ELEM. SYM.	A	Z
U	238	92

METHOD

[Page 2 of 2]

REF. NO. 65 K1 1 EGF

REACTION	RESULT	EXCITATION ENERGY	SOURCE		DETECTOR		ANGLE
			TYPE	RANGE	TYPE	RANGE	

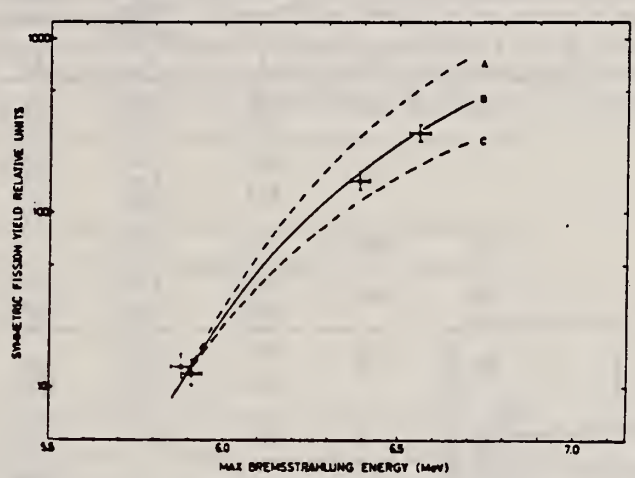

Fig. 4. Semilogarithmic plot of the symmetric photofission yield as a function of maximum bremsstrahlung energy. Theoretical yields (eq. (3)) are given with the parameters

A: (T = 0.6 MeV, B_f = 6.0 MeV, E_p = 85 keV),
B: (T = 0.6 MeV, B_f = 5.9 MeV, E_p = 85 keV),
C: (T = 0.6 MeV, B_f = 5.8 MeV, E_p = 85 keV).

REF.

A. Manfredini, M. Muchnik, L. Fiore, C. Ramorino, H. G. De Carvalho
J. Lang and R. Müller
Nuclear Phys. 74, 377 (1965)

ELEM. SYM.	A	Z
U	238	92

METHOD

Several (n,γ) sources

REF. NO.

65 Ma 3

EGF

REACTION	RESULT	EXCITATION ENERGY	SOURCE		DETECTOR		ANGLE
			TYPE	RANGE	TYPE	RANGE	
G,F	ABX	5 - 8	D	5 - 8	EMU-D		4PI

n-capture gamma rays

TABLE 2

Experimental data

Reactor target[a])	Mean energy (MeV)	Main line dose ($10^{16}\gamma$ cm^{-2})	U (10^{16} cm^{-2}) Weight ratio method	U (10^{16} cm^{-2}) Density method	Total number of fissions counted	$\langle \frac{N_t}{\phi_m U} \rangle$ (mb)	σ (mb)
1	2	3	4	5	6	7	8
S	5.43	3.32 5.56	9.59 10.14	11.18	2580 2799	1.44	0.70±0.11
Y	6.07	6.80 2.18	8.64 8.89 9.69	11.40 7.56 8.35	2400 1654 3225	6.82	6.38±0.69
Ti	6.44	7.99	6.38		3324	17.0	13.9 ±2.6
Be	6.80	1.01 0.96	8.95 9.31	12.35 8.20	1965 1658	4.64	3.81±0.46
Pb	7.38	0.65 0.67	9.23 9.79 9.41	8.60 8.28	2035 1895	13.2	12.8 ±1.5
Al	7.72	5.11	10.0	9.25	3538	7.65	5.25±0.61
				Total	27073		

[a]) Exposures to some other elements have also been performed but will be repeated in the near future to ascertain the validity of the results.

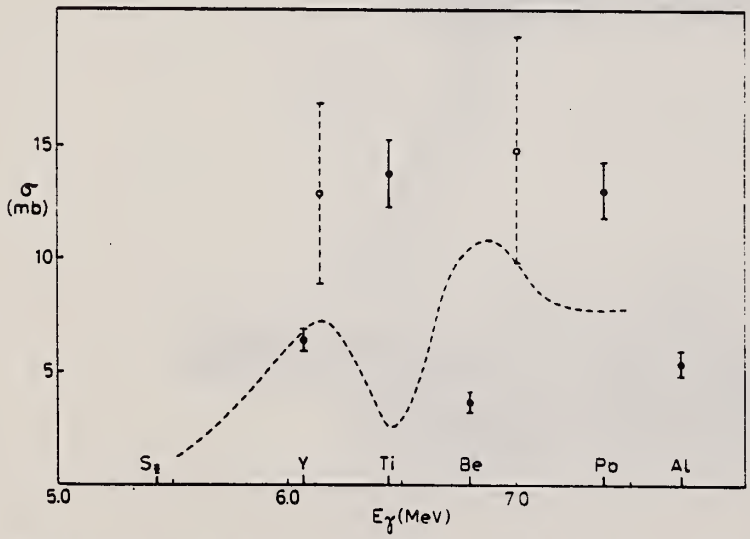

Fig. 1. Photofission cross-section of ^{238}U at low energies. Dashed curve behaviour obtained from bremsstrahlung exposures, by the photon difference method by Katz *et al.*[6]), ⊖ experimental points obtained from F(p, αγ)O radiation by Huizenga *et al.*[5]); ⊕ results obtained from monochromatic radiation from (n, γ) reactions of the present work.

REF.	ELEM. SYM.	A	Z
O. P. Nikotín and K. A. Petrzhak Atom. Energ. 19, 185 (1965) Sov. At. Energy. 19, 1080 (1965)	U	238	92

METHOD	REF. NO.	
Betatron	65 Ni 1	JDM

REACTION	RESULT	EXCITATION ENERGY	SOURCE		DETECTOR		ANGLE
			TYPE	RANGE	TYPE	RANGE	
G,F	RLY	· THR-15	C	10-15	BF3-I		4PI

The time distribution of delayed neutron activity, measured in 20-50 experiments, was summed, and the sum curves were analyzed graphically to separate the groups of delayed neutrons. We give the results of more than 700 irradiations. For U^{238} we observed six groups of delayed neutrons with half-lives of 55.0 ± 2.0; 21.0 ± 0.6; 5.4 ± 0.3; 2.2 ± 0.2; 0.7 ± 0.2 and 0.18 ± 0.03 sec. The relative yields of these groups at maximum energy of bremsstrahlung radiation 14.0 MeV were 0.020 ± 0.001; 0.158 ± 0.008; 0.142 ± 0.012; 0.340 ± 0.014; 0.180 ± 0.010 and 0.160 ± 0.020 respectively.

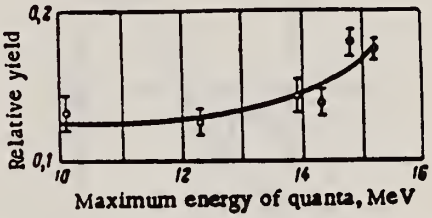

Fig. 2. Variation of relative yield of third group of delayed neutrons with maximum energy of bremsstrahlung radiation.

REF.

A.S. Soldatov, Z.A. Aleksandrova, L.D. Gordeeva, and G.N. Smirenkin
Sov. J. of Nuclear Phys. 1, 335 (1965)

ELEM. SYM.	A	Z
U	238	92

METHOD

$F^{19}(p,\alpha\gamma)O^{16}$ E_γ = 6.1,6.9,7.1 MeV

REF. NO. 65 So 1

JOC

REACTION	RESULT	EXCITATION ENERGY	SOURCE		DETECTOR		ANGLE
			TYPE	RANGE	TYPE	RANGE	
G,F	RLX	6-7	D	6-7			DST

TRACKS IN GLASS

$\sigma(\theta) = (0.22 \pm 0.02) + (0.78 \pm 0.03)\ \sin^2\theta + (0.04 \pm 0.04)\ \sin^2 2\theta.$

I(6.1 MeV): I(6.9 MeV): I(7.1 MeV) = 1.00:0.15:0.17.

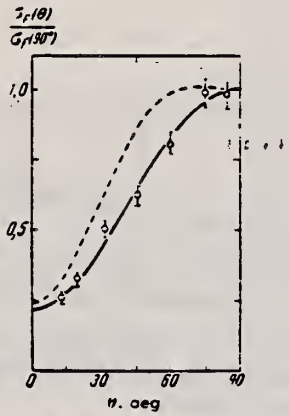

Fig. 2. Angular distribution of fragments from [illegible] of U^{238}. The solid curve was obtained by analysis of the experimental data by the method of least squares; the broken curve describes the data of Forkman and Johansson.

REF. A. S. Soldatov, G. N. Smirenkin, S. P. Kapitza and Y. M. Tsipeniuk
Phys. Letters 14, 217 (1965)

ELEM. SYM.	A	Z
U	238	92

METHOD

REF. NO. 65 So 2 EGF

REACTION	RESULT	EXCITATION ENERGY	SOURCE		DETECTOR		ANGLE
			TYPE	RANGE	TYPE	RANGE	
G,F	NOX	THR-9	C	5-9	EMU-I		DST

Angular distribution of fragments fitted to $W(\theta) = a + b \sin^2\theta + c \sin^2 2\theta$.

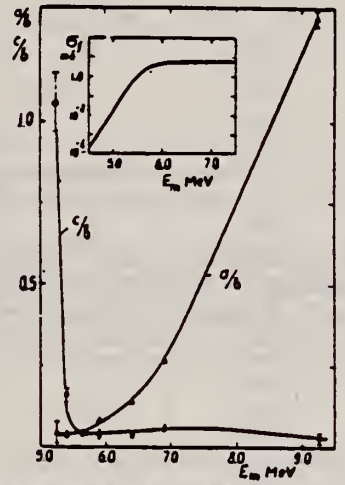

Fig. 1. Energy dependence of a/b and c/b and total photofission cross section of U^{238} (insert).

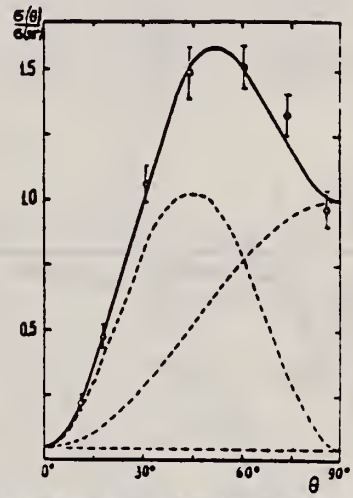

Fig. 2. Angular distribution of fragments of U^{238} at $E_m = 5.2$ MeV; dashed lines show three terms of (1), where $a = 0.04 \pm 0.04$; $b = 0.96 \pm 0.05$; $c = 1.02 \pm 0.07$.

REF. I.E. Bocharova, V.G. Zolotukhin, S.P. Kapitza, G.N. Smirenkin, A.S. Soldatov, and Yu. M. Tsipenyuk
J. Exptl. Theoret. Phys. (USSR) 49, 476 (1965)
Sov. Phys. JETP 22, 335 (1966)

ELEM. SYM.	A	Z
U	238	92

METHOD

12 MeV Microtron; Angular Distribution

REF. NO. 66 Bo 1 JDM

REACTION	RESULT	EXCITATION ENERGY	SOURCE TYPE	SOURCE RANGE	DETECTOR TYPE	DETECTOR RANGE	ANGLE
G,F	NOX	THR - 9	C	5 - 9	D		DST

$W(90^\circ) = a + b = 1$

$W(\theta) = a + b \sin^2\theta + c \sin^2 2\theta$

Coefficients obtained as the result of analyzing the experimental data by the method of least squares, with representation of the angular distributions in the form $W(\theta) = a + b \sin^2\theta + c \sin^2 2\theta$

E_{max}, MeV	a	b	c
5.2	0.012±0.005	0.938±0.050	..015±..
...	0.038±0.003	0.962±0.017	...
...	0.021±0.005	0....	0.0...
...	0.073±0.005	0.922±0....	0.0...
...	...±0.00...	0.873±0....	...
...	0.213±0.00...	...737±0.008	0.0...
6.25	0.370±0.008	0.430±0.007	0.0...3

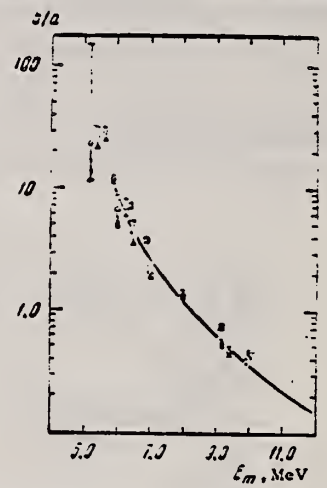

FIG. 5. Fission anisotropy b/a = W(90°)/W(0°) - 1 as a function of bremsstrahlung maximum energy E_{max}: Δ – results of Terg et al.[3], o – results of the present work, obtained with a target 1 mm thick, ● – point obtained with a target 0.05 mm thick.

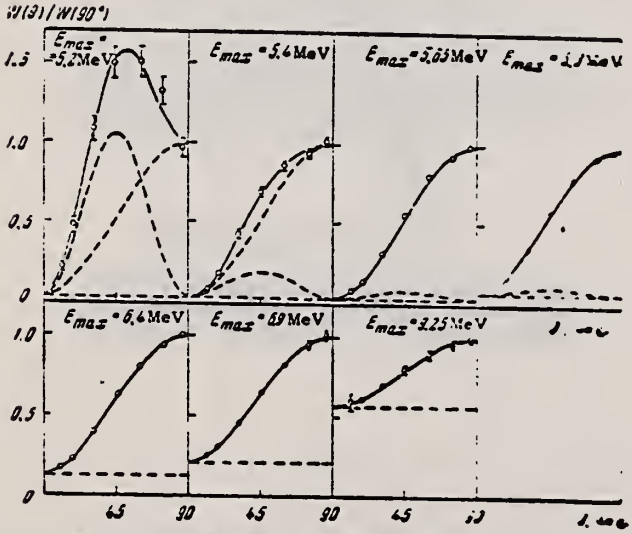

FIG. 4. Angular distributions of fragments in photofission of U^{238}.

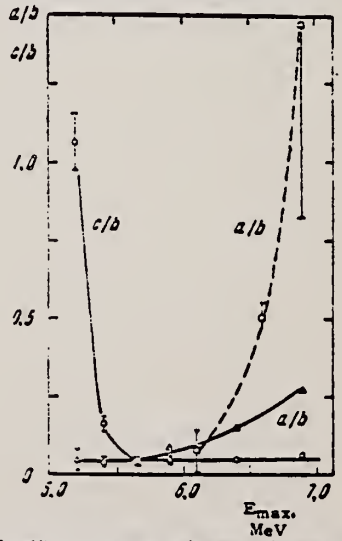

FIG. 6. Coefficient ratios a/b and c/b as a function of bremsstrahlung maximum energy.

REF. A. Manfredini, M. Muchnik, L. Fiore, C. Ramorino, H. G. DeCarvalho, R. Bosch and W. Wolfli
Nuovo Cimento 44B, 218 (1966)

ELEM. SYM.	A	Z
U	238	92

METHOD

REF. NO. 66 Ma 3 JDM

REACTION	RESULT	EXCITATION ENERGY	SOURCE		DETECTOR		ANGLE
			TYPE	RANGE	TYPE	RANGE	
G,F	ABX	5-9	D	5-9	EMU-I		DST

TABLE I.

Reactor target	Main-line energy (MeV)	Main-line dose (10^{19} γ cm^{-2})	$N_f/\Phi_m U$ (mb)	σ (mb)
1	2	3	4	5
S	5.43	3.32 5.56	1.40±0.11	0.08±0.20
Dy	5.58	2.62	3.96±0.34	3.73±0.70
Y	6.07	6.80 2.18	6.54±0.37	5.99±1.05
Ca	6.42	4.51 2.16	7.20±0.54	5.68±1.02
Ti	6.75	7.99 1.49 1.16	18.5±0.9	12.5±1.1
Be	6.80	1.01 0.96	1.92±0.35	1.92±0.35
Mn	7.16	2.39	9.46±1.50	7.17±1.50
Pb	7.38	0.65 0.67	13.5±0.9	12.6±1.6
Fe	7.64	21.5 1.40	18.7±1.3	12.1±3.1
Al	7.72	5.11 3.14	9.28±0.55	7.15±0.56
Cu	7.91	7.05	31.3±6.4	18.9±6.7
Ni	8.86	24.6 1.00 1.29	35.2±1.8	29.0±1.8

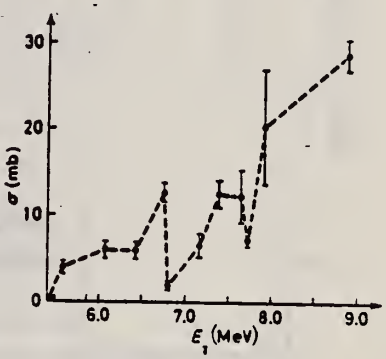

Fig. 1.

REF.	ELEM. SYM.	A	Z
J. L. Meason and P. K. Kuroda Phys. Rev. 142, 691 (1966)	U	238	92

METHOD	REF. NO.	
Monoenergetic x-rays from $^{7}Li(p,\gamma)2^{4}He$	66 Me 2	JDM

REACTION	RESULT	EXCITATION ENERGY	SOURCE		DETECTOR		ANGLE
			TYPE	RANGE	TYPE	RANGE	
G,F	ABY	17	D	17	ACT-I		4PI

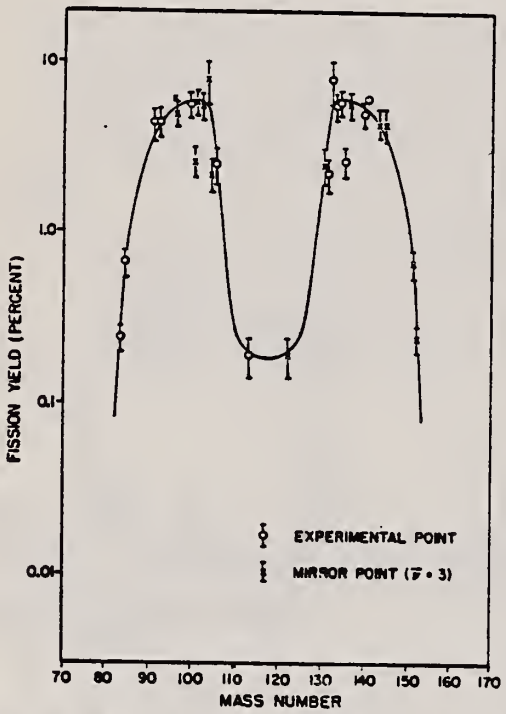

FIG. 1. The mass-yield curve for 17.5-MeV photofission of U^{238}. The mirror points were calculated for $\bar{\nu}=3$.

TABLE I. 17.5-MeV photofission chain yields of U^{238} measured in this work.

Nuclide	Percent yield
Br^{88}	0.24±0.04
Br^{84}	0.66±0.12
Sr^{91}	4.3 ±0.9
Sr^{92}	4.4 ±0.9
Mo^{99}	5.6 ±1.0
Ru^{106}	2.5 ±0.6[a]
Ag^{113}	0.19±0.05[a]
I^{131}	2.2 ±0.5
I^{132}	7.8 ±2.2
I^{133}	5.5 ±1.0
I^{134}	5.7 ±1.0
I^{135}	2.6 ±0.5
Ba^{139}	4.9 ±0.8
Ba^{140}	6.00

[a] Data obtained by R. Ganapathy.

REF. O. P. Nikotin and K. A. Petrzhak
Atomnaya Energiya 20, 268 (1966)
UDC 539.173.84, p. 300

ELEM. SYM.	A	Z
U	238	92

METHOD

REF. NO.: 66 Ni 1 | egf

REACTION	RESULT	EXCITATION ENERGY	SOURCE TYPE	SOURCE RANGE	DETECTOR TYPE	DETECTOR RANGE	ANGLE
G,F	RLY	THR-15	C	10-15	TRK-D	C-1	4PI
						(.1-1.0)	

DELAYED N YIELDS

Delayed Neutrons from Photofission ($E_{\gamma\,max}$ = 15 MeV)

Total yield of delayed neutrons, neutrons/100 fissions	Neutron group	$T_{1/2}$, sec	Relative yield of group, %	Absolute yield of group, neutrons per 100 fissions
3,8±0,6 (Th^{232})	1	55,6±1,5	4,40±0,20	0,17±0,03
	2	20,3±0,8	16,3±1,0	0,62±0,10
	3	5,45±0,50	15,9±1,5	0,60±0,10
	4	1,98±0,20	37,5±3,0	1,43±0,30
	5	0,43±0,10	17,2±2,0	0,66±0,10
	6	0,18±0,03	$8,7^{+2,0}_{-4,0}$	$0,33^{+0,10}_{-0,20}$
0,96±0,13 (U^{235})	1	54,7±2,5	5,4±0,5	0,052±0,010
	2	20,3±1,0	20,0±2,0	0,193±0,050
	3	5,45±0,60	15,2±2,0	0,146±0,030
	4	2,03±0,25	36,9±4,0	0,354±0,070
	5	0,50±0,10	13,9±2,0	0,134±0,030
	6	0,19±0,04	$8,6^{+2,0}_{-3,0}$	$0,083^{+0,025}_{-0,050}$
3,1±0,4 (U^{238})	1	56,2±0,8	1,98±0,08	0,061±0,010
	2	21,3±0,3	15,7±0,5	0,489±0,070
	3	5,50±0,20	17,5±0,7	0,545±0,070
	4	2,15±0,10	31,1±0,8	0,970±0,150
	5	0,70±0,06	17,7±0,9	0,552±0,080
	6	0,19±0,02	$16,1^{+2,0}_{-3,0}$	$0,502^{+0,120}_{-0,200}$
0,36±0,06 (Pu^{239})	1	54,0±3,0	6,05±0,60	0,022±0,004
	2	20,6±1,0	20,6±2,0	0,075±0,018
	3	5,7±0,7	18,3±3,0	0,066±0,015
	4	1,94±0,30	29,5±4,0	0,105±0,020
	5	0,58±0,10	14,9±3,0	0,054±0,012
	6	0,20±0,04	$10,6^{+2,0}_{-3,0}$	$0,038^{+0,012}_{-0,025}$

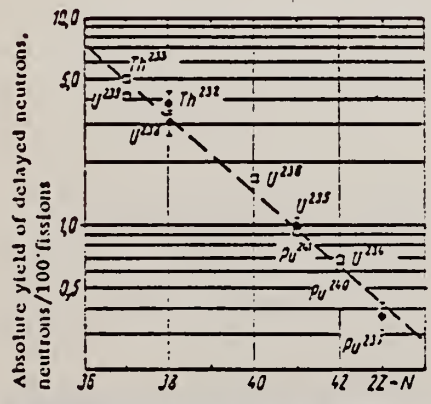

Fig. 3. Absolute yields of delayed neutrons from fission of nuclei: □) [7]; ●) present authors.

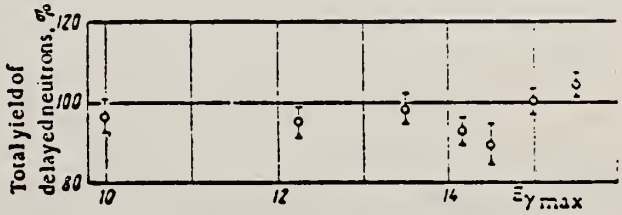

Fig. 2. Total yields of delayed neutrons from photofission of U^{238}. The yield $E_{\gamma\,max}$ = 15 MeV is taken as 100%.

U.S. DEPARTMENT OF COMMERCE
NATIONAL BUREAU OF STANDARDS

REF. K. Sakamtoto and P. K. Kuroda
J. Inorg. Nucl. Chem. 28, 679 (1966)

ELEM. SYM.	A	Z
U	238	92

METHOD
1.3 BeV. electron synchrotron

REF. NO. 66 Sa 1 JDM

REACTION	RESULT	EXCITATION ENERGY	SOURCE		DETECTOR		ANGLE
			TYPE	RANGE	TYPE	RANGE	
G,F	RLY	THR - 650	C	650	ACT-I		4PI

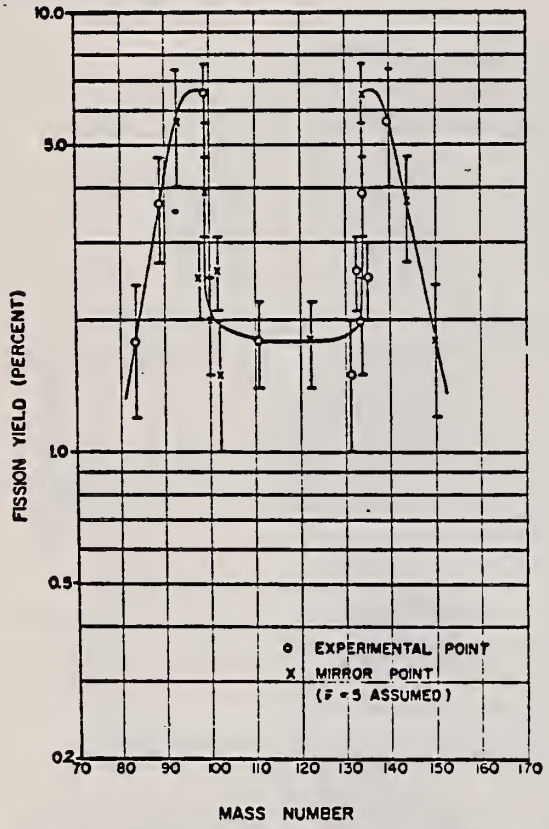

FIG. 1.—Mass-yield curve for 650-MeV photofission of U^{238}.

REF.	ELEM. SYM.	A	Z
S.P. Kapitsa, V.I. Novgorodtseva, V.A. Pchelin, G.N. Smirenkin, Yu. M. Tsipenyuk, and V.M. Shubko ZhETF Pis'ma 6, 495 (1967) JETP Letters 6, 27 (1967)	U	238	92

METHOD	REF. NO.	
	67 Ka 1	hmg

REACTION	RESULT	EXCITATION ENERGY	SOURCE		DETECTOR		ANGLE
			TYPE	RANGE	TYPE	RANGE	
G,F	RLY	THR-7	C	5 - 7	ACT-I		4PI
				(5.4-6.5)			

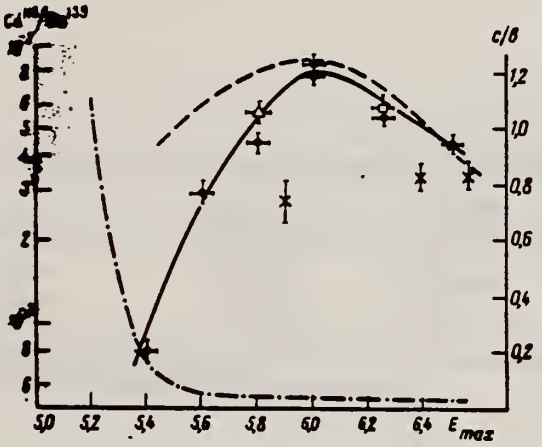

Relative yield Cd^{115}/Ba^{139} vs. the maximum γ-quantum energy. o - present work, Δ - with W target, □ - in front part of U-block, --- - results of [1], × - results of [5], -·-·- - relative probability of quadrupole photofission [6].

REF. Yu. N. Ranyuk and P. V. Sorokin
J. Nucl. Phys. (USSR) 5, 531 (1967)
Sov. J. Nucl. Phys. 5, 377 (1967)

ELEM. SYM.	A	Z
U	238	92

METHOD

REF. NO. 67 Ra 3 HMG

REACTION	RESULT	EXCITATION ENERGY	SOURCE		DETECTOR		ANGLE
			TYPE	RANGE	TYPE	RANGE	
E,F	RLX	THR- 260	D	25-260	EMU-I		4PI
G,F	RLX	THR- 260	C	25-260	EMU-I		4PI

σ_q/σ_e = ratio of bremsstrahlung yield to electron yield.

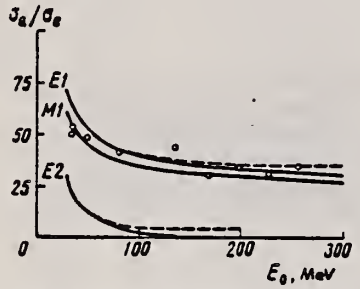

Fig. 3. The ratio of σ_q/σ_e as a function of electron energy.

REF. H. R. Bowman, R. C. Gatti, R. C. Jared, G. Kilian, L. G. Moretto, S. G. Thompson, M. R. Croissiaux, J. H. Heisenberg, R. Hofstadter, L. M. Middleman, and M. R. Yearian
Phys. Rev. 168, 1396 (1968)

ELEM. SYM.	A	Z
U	238	92

METHOD

REF. NO.	
68 Bo 1	HMG

REACTION	RESULT	EXCITATION ENERGY	SOURCE		DETECTOR		ANGLE
			TYPE	RANGE	TYPE	RANGE	
E,F	ABI	THR-40	D	250,500	EMU-I		DST
					(MICA)		

Angular distribution showed less than 10% deviation from isotropy for 250 MeV electrons. Angular distribution and energy spectra also made using semiconductor detectors.

TABLE I. Experimental results.

Target	Thickness	Method used	Fission cross section 250 MeV σ^- (cm^2)	500 MeV σ^- (cm^2)
$_{92}U^{238}$ [a]	85 μg/cm^2	Mica	$(6.0\pm1.2)\times10^{-27}$	$(9.4\pm1.9)\times10^{-27}$
$_{92}U^{238}$	162 μg/cm^2	Counter	$(5.0\pm1.0)\times10^{-27}$	$(7.0\pm1.4)\times10^{-27}$
$_{83}Bi^{209}$	1 mg/cm^2	Mica	$(2.3\pm0.5)\times10^{-28}$	$(1.4\pm0.3)\times10^{-28}$
$_{73}Ta^{181}$	4 mg/cm^2	Mica		3.9×10^{-31} [b]

[a] U^{234}/U^{238} was 1.12×10^{-4} in target sample.
[b] Not corrected for photofission contribution [see (4) in text].

REF. N. N. Kaushal, E. J. Winhold, P. F. Yergin, H. A. Medicus and R. H. Augustson
Phys. Rev. 175, 1330 (1968)

ELEM. SYM.	A	Z
U	238	92

METHOD

REF. NO. 68 Ka 1 HMG

REACTION	RESULT	EXCITATION ENERGY	SOURCE		DETECTOR		ANGLE
			TYPE	RANGE	TYPE	RANGE	
G,N	ABX	50-85	C	55,85	TOF-D	10-85	67
							(67.5)

NEUT ENGY SPEC

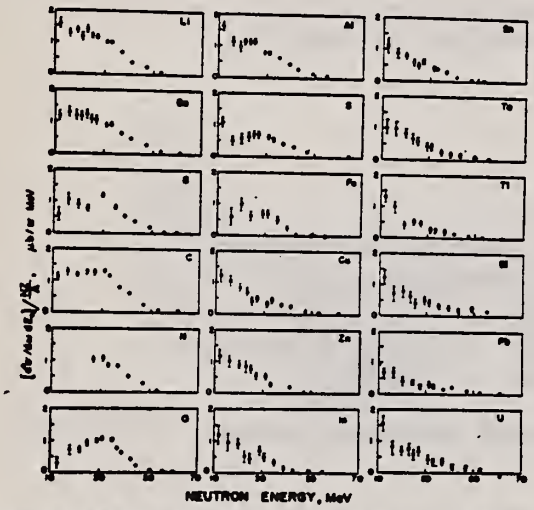

FIG. 6. Observed neutron spectra due to 55–85-MeV difference photon spectra. The effective cross sections have been divided by NZ/A.

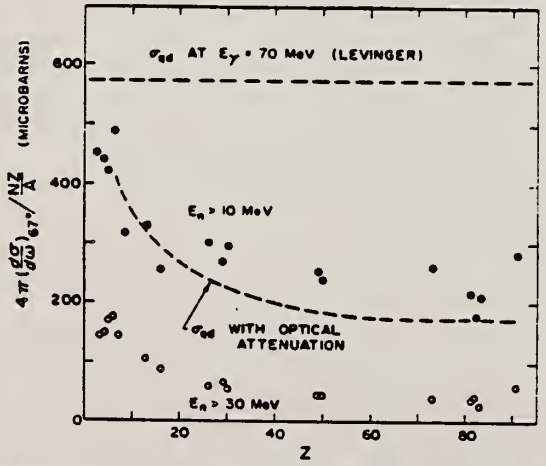

FIG. 7. Effective cross sections for production of fast neutrons with energies greater than 10 MeV (solid circles) and 30 MeV (open circles) by the 55–85-MeV photon difference spectrum. The dashed curves are modified quasideuteron model predictions as discussed in the text.

TABLE I. Comparison of present cross-section values in mb for production of high-energy photoneutrons by 55–85-MeV photons with measured cross sections $\sigma(\gamma,Tn)$, also in mb, for total photoneutron production. The present cross-section values are uncertain by 8 to 10% because of counting statistics and normalization errors; in addition all values depend on an absolute normalization in terms of the deuteron photodisintegration cross section, which is known to about 10% at these energies.

Target	$4\pi(d\sigma/d\omega)_{90°}$ ($E_n>10$ MeV) [Present experiment]	$\sigma(\gamma,Tn)$ Jones and Terwilliger[a]	$\sigma(\gamma,Tn)$ Costa *et al.*[b]	Other results
Li	0.75		1.0	
Be	1.0	2.7	2.3	2.3[c]
B	1.0		1.4	
C	1.5	1.3	1.4	2.4[d]
O	1.3		1.6	
Al	2.8	5.5	4.6	8[d]
S	2.1		4.4	6.5[d]
Fe	4.2	16	12	
Cu	4.3	20	19	
Zn	4.4		15	
In	7.4			
Sn	7.0			
Ta	10.7	95		
Tl	10.7			
Pb	8.3	100		
Bi	13			
U	16	65		

[a] Average cross sections between 55 and 85 MeV, as read from Figs. 4 and 5 of Ref. 6.
[b] $\int_0^{\infty}\sigma dE - \int_0^{30}\sigma dE/50$, as taken from Fig. 4 of Ref. 5 and Table I of Ref. 6.
[c] S. Costa, L. Pasqualini, G. Piragino, and L. Roasio, Nuovo Cimento 42, 306 (1966).
[d] G. Bishop, S. Costa, S. Ferroni, R. Malvano, and G. Ricco, Nuovo Cimento 42, 148 (1966).

REF. B. V. Kurchatov, V. I. Novgorodtseva, V. A. Pchelin, G. N. Smirenkin, Yu. M. Tsipenyuk, and V. M. Shubko
Yad. Fiz. 7, 521 (1968)
Sov. J. Nucl. Phys. 7, 326 (1968)

ELEM. SYM.	A	Z
U	238	92

METHOD

REF. NO.	
68 Ku 1	hmg

REACTION	RESULT	EXCITATION ENERGY	SOURCE		DETECTOR		ANGLE
			TYPE	RANGE	TYPE	RANGE	
G,F	ABY	THR-7	C	4-7	ACT-I		4PI
				(4.5-6.5)			

E_{max}, MeV	Fragment yields, averaged over the runs, referred to a current of 50 μA at infinite irradiation time					
	Decays per minute (x 10^{-6})			Decays per minute (x 10^{-6})		
	Ba^{139}	Ba^{140}	Mo^{99}	Cd^{117}	Cd^{115}	Ag^{111}
6.5	320	310	348	1700	1400	1800
6.25	215	212	217	1400	1200	1600
6.0	79	83	89	640	610	--
5.8	25	25	24	145	130	165
5.6	6	6	7.1	22	18	24
5.4	1.9	1.5	1.75	1.2	1.2	2.3
5.3	0.55	0.44	0.55	0.11	0.11	0.40
5.2	0.13	0.13	0.13	0.04	0.05	—
5.1	0.06	0.064	0.066	0.03	0.02	—
5.0	0.029	0.036	0.027	0.011	0.02	—
4.75	0.004	—	0.004	—	—	—
4.5	0.001	—	0.001	—	—	—

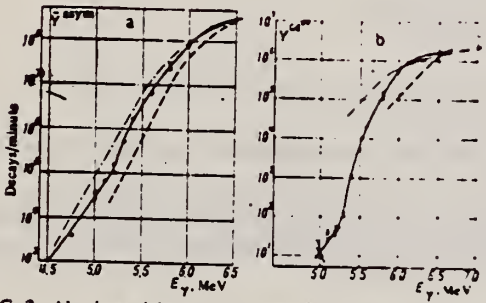

FIG. 2. Absolute yield: a – asymmetrical fragments, averaged over the nuclei Ba^{139}, Ba^{140}, and Mo^{99}; b – of Cd^{117} as a function of the end-point energy of the bremsstrahlung spectrum. Points - our data, dashed curves – data of [4] (Ba^{139}), dash-dot curves - data of [3] (Ba^{139}). The normalization is performed at E_γ = 6.5 MeV

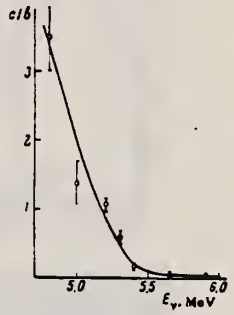

FIG. 4. Relative probability of quadrupole fission vs. energy E_γ.

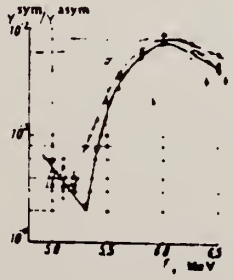

FIG. 3. Ratio of the yields of symmetrical and asymmetrical fragments. Points: ○ – yield of Cd^{115}, × – Cd^{117}, ○ – Ag^{111}; △ – results of [4]; □ – results of [3].

REF. N. S. Rabotnov, G. N. Smirenkin, A. S. Soldatov, L. N. Ysachev, S. P. Kapitza and Yu. M. Tsipeniuk
Phys. Letters 26B, 218 (1968)

ELEM. SYM.	A	Z
U	238	92

METHOD

REF. NO. 68 Ra 1 EGF

REACTION	RESULT	EXCITATION ENERGY	SOURCE		DETECTOR		ANGLE
			TYPE	RANGE	TYPE	RANGE	
G,F	NOX	THR-8	C	5-8	FRG-I		DST

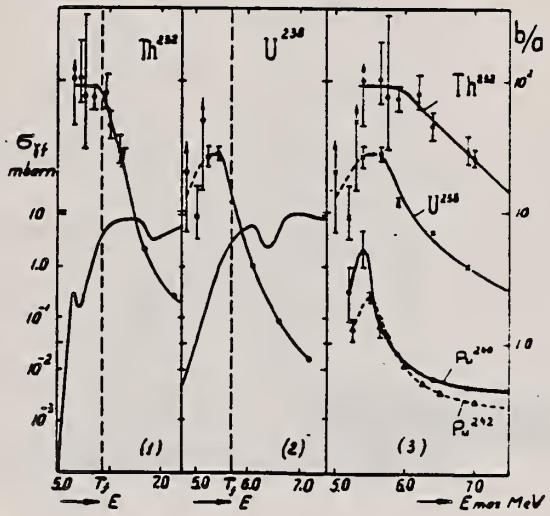

Fig. 1. The measured value of b/a as a function of energy. Photofission cross sections taken from ref. 1 are also shown for ^{232}Th and ^{238}U. E is the average excitation energy of the fissioning nuclei and T_f the observable fission threshold.

REF.	ELEM. SYM.	A	Z
H. G. De Carvalho, V. Di Napoli, D. Margadonna and F. Salvetti and K. Tesch Nucl. Phys. A126, 505 (1969)	U	238	92

METHOD	REF. NO.
	69 De 1 egf

REACTION	RESULT	EXCITATION ENERGY	SOURCE		DETECTOR		ANGLE
			TYPE	RANGE	TYPE	RANGE	
G,N	ABY	THR-999	C	1-6	ACT-I		4PI
				(1.0-5.5)			

Yield per equivalent quantum.

999 = 5.5 GEV

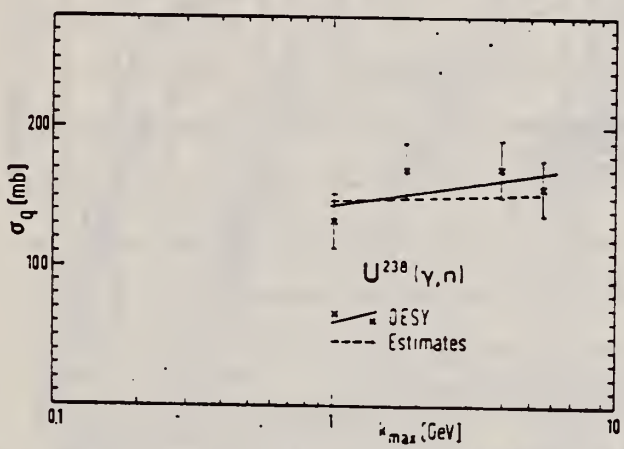

Fig. 5. See caption to fig. 1. The errors are high because of the natural radioactivity of ^{238}U.

Cross sections per equivalent quantum for (γ, n) reactions as a function of the maximum bremsstrahlung energy. A straight line is adjusted to the experimental points by means of a least-squares fit. The indicated errors are due to the γ-ray spectroscopy. The dashed line gives the result of simple estimates.

REF.

I.A. Grishaev, V.P. Efimov, V.I. Kasilov, V.I. Noga,
Yu. N. Ranyuk, P.V. Sorokin, A.N. Fisun
Ukr. Fiz. Zhur. 14, 1818 (1969)

ELEM. SYM.	A	Z
U	238	92

METHOD

REF. NO. 69 Gr 2 egf

REACTION	RESULT	EXCITATION ENERGY	SOURCE		DETECTOR		ANGLE
			TYPE	RANGE	TYPE	RANGE	
E,F	RLY	THR-999	C	70-999	ACT-I		4PI

RLY E-/E+ 999= 1 GEV

DISINTEGRATION OF HEAVY NUCLEI BY ELECTRONS AND POSITRONS

I. A. Grishaev, V. P. Efimov, V. I. Kasilov, V. I. Noga, Yu. N. Ranyuk, P. V. Sorokin, A. N. Fisun

Summary

Gross-section ratio for the uranium and tantalum disintegration by electrons and positrons is equal to unity within the experimental errors over the investigated energy range from 70 to 1000 MeV and is in agreement with Barber's measurements and Rodenberg's calculations.

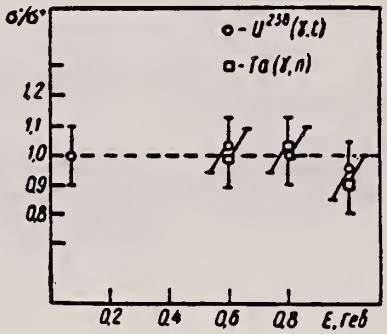

REF.

S. P. Kapitza, N. S. Rabotnov, G. N. Smirenkin, A. S. Soldatov
L. N. Usachev, Yu. M. Ysipenyuk
ZhETF Pis. Red. 9, 128 (1969); JETP Letters 9, 73 (1969)

ELEM. SYM.	A	Z
U	238	92

METHOD

REF. NO.	
69 Ka 1	hmg

REACTION	RESULT	EXCITATION ENERGY	SOURCE		DETECTOR		ANGLE
			TYPE	RANGE	TYPE	RANGE	
G,F	ABX	THR-8	C	5-8	TRK-I		DST

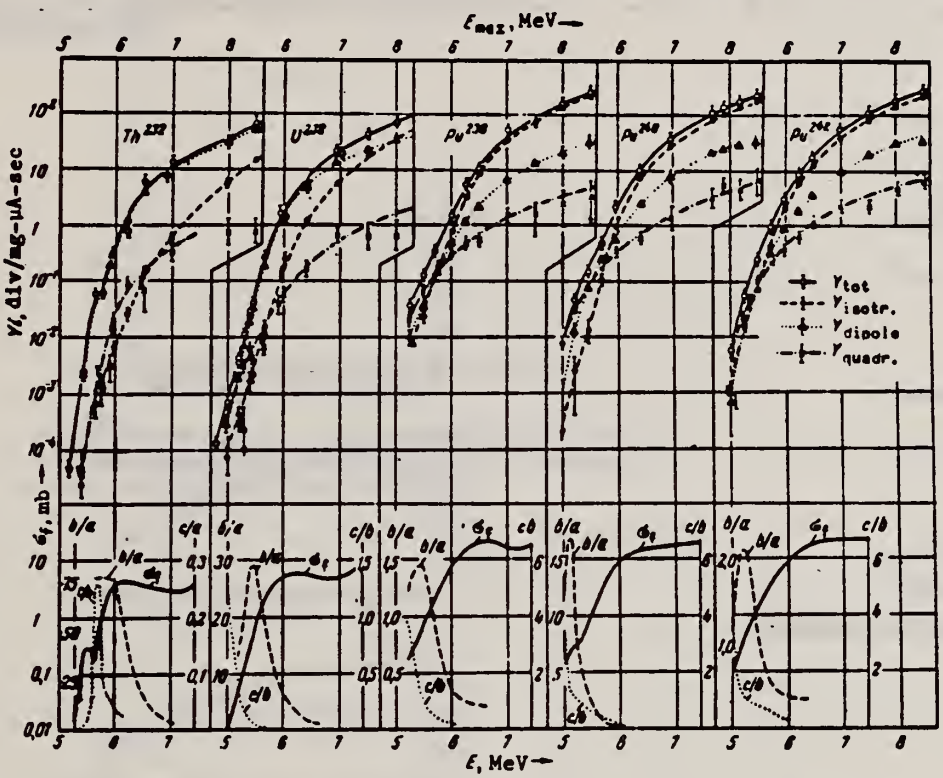

Fig. 2. Results of measurements of the fragment yields corresponding to different components of the angular distribution, as functions of the end-point energy of the bremsstrahlung spectrum (upper plots) and fission cross section and values of the ratios b/a and c/b as functions of the energy of the γ quanta, obtained as a result of the reduction of the experimental data (lower plots).

REF. A. P. Komar, B. A. Bochagov, A. A. Kotov, Yu. N. Ranyuk, G. G. Semenchuk, G. E. Solyakin, and P. V. Sorokin
Yad. Fiz. 10, 51 (1969)
Sov. J. Nucl. Phys. 10, 30 (1970)

ELEM. SYM.	A	Z
U	238	92

METHOD

REF. NO. 69 Ko 2 | egf

REACTION	RESULT	EXCITATION ENERGY	SOURCE		DETECTOR		ANGLE
			TYPE	RANGE	TYPE	RANGE	
G,F	SPC	THR-999	C	250-999	SCD-D		DST
		(1000)		(1000)			

999 = 1000 MEV

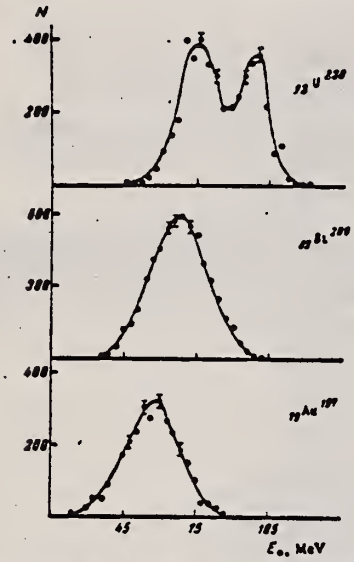

FIG. 2. Single-ended energy spectra of fragments from photofission of $_{92}U^{238}$, $_{83}Bi^{209}$, and $_{79}Au^{197}$.

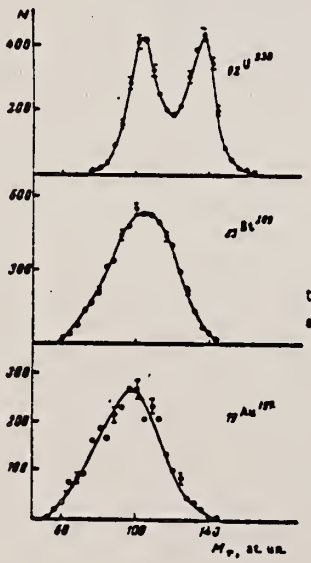

FIG. 3. Fragment mass distributions from photofission of $_{92}U^{238}$, $_{83}Bi^{209}$, and $_{79}Au^{197}$.

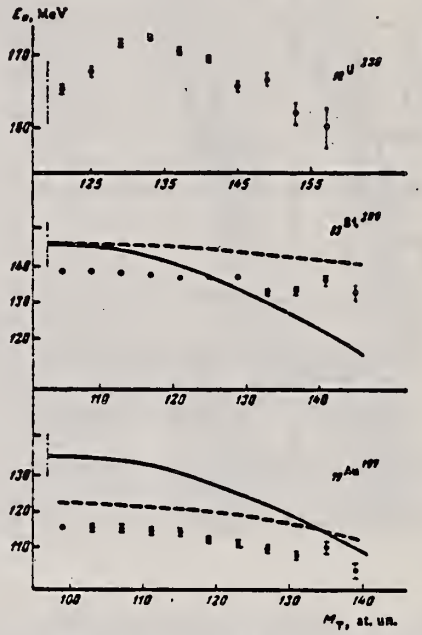

FIG. 4. Average total kinetic energies $\bar{E}_k$ of fragments from photofission of $_{92}U^{238}$, $_{83}Bi^{209}$, and $_{79}Au^{197}$, as a function of the heavy fragment mass. Points—experiment; solid curves—theory; dashed curves—experiment with inclusion of a correction for neutron emission from the fragments.

[over]

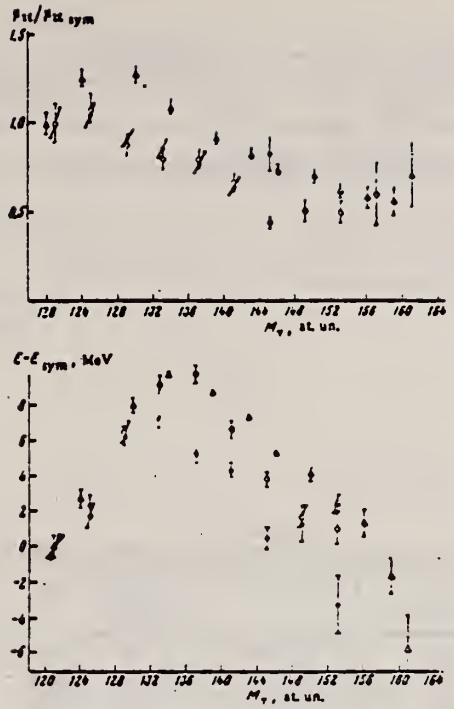

FIG. 6. The ratio $\mu_{2E}/\mu_{2E_{sym}}$ and the difference $\overline{E} - \overline{E}_{sym}$, as a function of heavy fragment mass for photofission of $_{92}U^{238}$ for three values of $E_{\gamma max}$: Δ–250 MeV, O–600 MeV, ●–1000 MeV.

REF.

A. Manfredini, L. Fiore, C. Ramorino, H. G. De Carvalho, and W. Wölfli
Nucl. Phys. A123, 664 (1969)

ELEM. SYM.	A	Z
U	238	92

METHOD

REF. NO.: 69 Ma 1 egf

REACTION	RESULT	EXCITATION ENERGY	SOURCE		DETECTOR		ANGLE
			TYPE	RANGE	TYPE	RANGE	
G,F	ABX	5-9	D	5-9	EMU-I		DST

$W(\theta) = a + b \sin^2\theta + c \sin^2\theta \cos^2\theta$.

N-CAPTURE G'S

TABLE 1
Values of the a-, b- and c-parameters of the angular distribution for different γ-ray energies

Target	$\bar{E}$ (MeV)	a	b	c	E (MeV)	a	b	c
Dy	5.60	0.05 ±0.06	1.37 ±0.05	0.30 ±0.21	5.58	0.05 ±0.06	1.36 ±0.14	0.26 ±0.23
Y	6.09	0.01 ±0.03	1.34 ±0.03	0.74 ±0.13	6.07	−0.02 ±0.03	1.38 ±0.09	0.79 ±0.16
Ca	6.37	0.23 ±0.04	1.04 ±0.04	0.53 ±0.18	6.42	0.25 ±0.06	1.02 ±0.11	0.52 ±0.24
Ti	6.71	0.40 ±0.03	0.85 ±0.03	0.23 ±0.14	6.75	0.45 ±0.06	0.80 ±0.09	0.09 ±0.23
Be	6.80	0.55 ±0.11	0.41 ±0.10	1.11 ±0.41	6.80	0.55 ±0.11	0.41 ±0.10	1.11 ±0.41
Mn	6.94	0.63 ±0.04	0.56 ±0.04	−0.04 ±0.18	7.16	0.75 ±0.14	0.44 ±0.13	−0.32 ±0.25
Pb	7.34	0.65 ±0.06	0.41 ±0.06	0.61 ±0.23	7.38	0.66 ±0.08	0.38 ±0.07	0.64 ±0.25
Fe	7.71	0.63 ±0.05	0.45 ±0.05	0.49 ±0.23	7.64	0.67 ±0.11	0.40 ±0.10	0.47 ±0.36
Al	7.41	0.75 ±0.05	0.30 ±0.05	0.37 ±0.21	7.72	0.91 ±0.09	0.08 ±0.08	0.32 ±0.29
Cu	7.66	0.62 ±0.06	0.49 ±0.06	0.38 ±0.24	7.91	0.63 ±0.24	0.48 ±0.20	0.39 ±0.43
S	7.96	0.69 ±0.06	0.33 ±0.06	0.71 ±0.24	8.16	0.79 ±0.11	0.15 ±0.09	0.81 ±0.32
Ni	8.63	0.83 ±0.05	0.20 ±0.06	0.30 ±0.19	8.86	0.88 ±0.08	0.13 ±0.07	0.24 ±0.24

Column 2 gives the mean energy of the γ-ray spectrum and column 6 the energy of the main line.

[over]

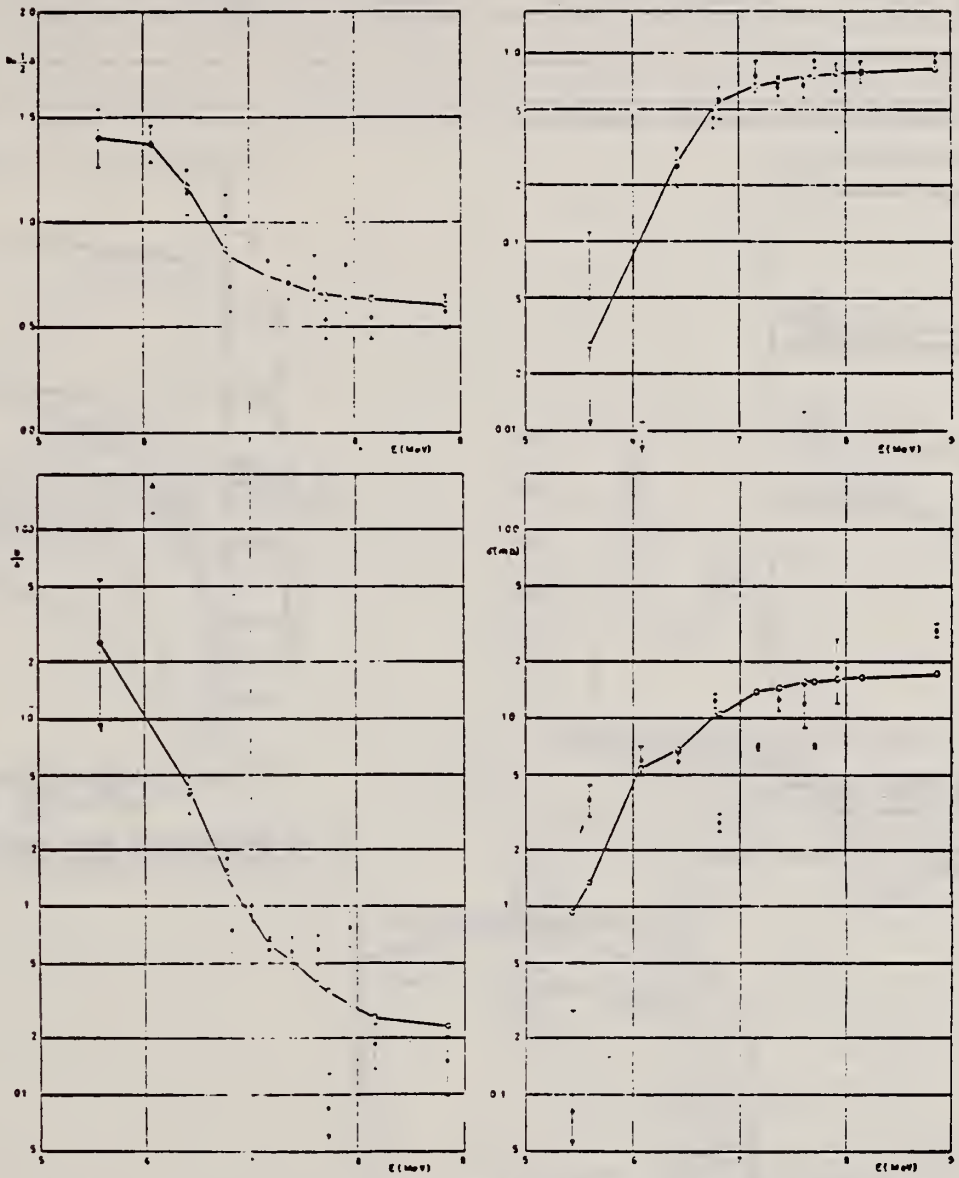

Fig. 4. Dependence of the measured parameters a, $b+\frac{1}{2}a$ and b/a and the photofission cross section σ as a function of γ-ray energy. The solid lines shows the theoretical functions deduced from the fission barrier penetration using the values of the T, B and E_b parameters reported in table 2. Black dots - experimental values, white dots - calculated values.

REF.

L. G. Moretto, R. C. Gatti, S. G. Thompson, J. T. Routti, J. H. Heisenberg, L. M. Middleman, M. R. Yearian, R. Hofstadter
Phys. Rev. 179, 1176 (1969)

ELEM. SYM.	A	Z
U	238	92

METHOD

REF. NO.: 69 Mo 1 hmg

REACTION	RESULT	EXCITATION ENERGY	SOURCE TYPE	SOURCE RANGE	DETECTOR TYPE	DETECTOR RANGE	ANGLE
E,F	ABX	THR-999	D	60-999	TRK-I		DST
G,F	ABX	THR-999	C	60-999	TRK-I		DST

Tabular data given; angular distribution isotopes

999= 1 GEV

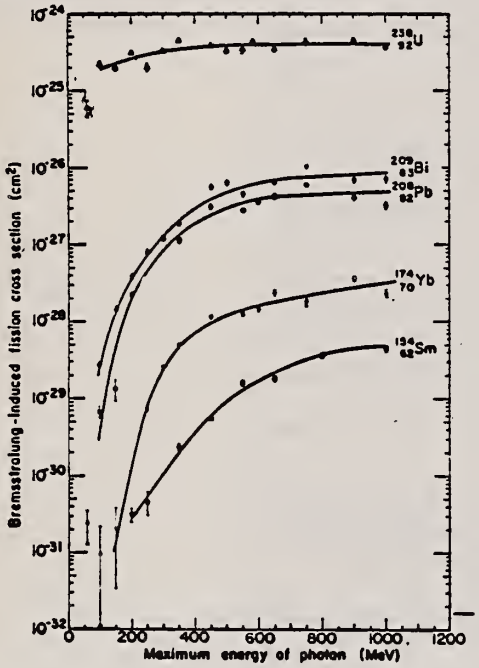

FIG. 4. Bremsstrahlung-induced fission cross section per equivalent quantum.

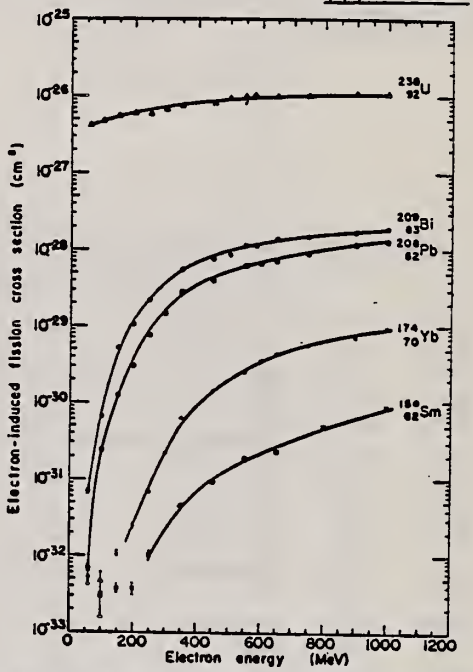

FIG. 2. Electron-induced fission cross-section data. Different symbols for the same isotope refer to different targets.

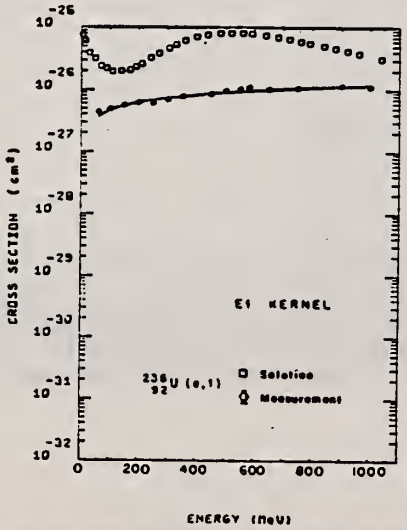

FIG. 6. Photofission cross section as a function of energy for $_{92}^{238}U$ (open squares) as obtained by unfolding the electron-induced fission cross-section data (diamonds) with the $E1$ kernel. The solid line is the fit to the electron-induced fission cross sections which is obtained by folding back the photofission cross section into the $E1$ kernel.

REF.

Y. Wakuta, M. Sonoda, A. Katase, H. Tawara, M. Hyakutake
J. Phys. Soc. Japan 26, 851 (1969)

ELEM. SYM.		
U	238	92

METHOD

REF. NO.	
69 Wa 1	hmg

REACTION	RESULT	EXCITATION ENERGY	SOURCE		DETECTOR		ANGLE
			TYPE	RANGE	TYPE	RANGE	
G,F	RLX	0-999	C	200-999	SCD-D		DST

999=1.2 GEV

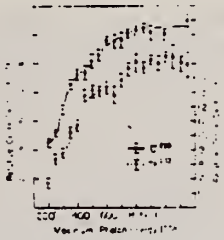

Fig. 1. Relative photofission cross section per equivalent quantum as a function of maximum photon energy for U^{238} and Th^{232}.

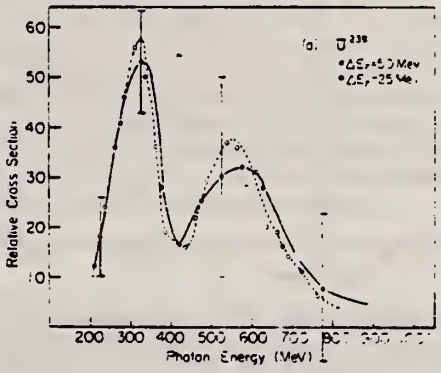

(a)

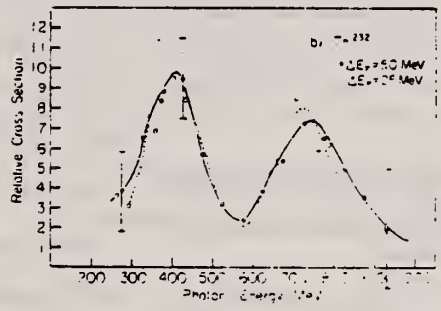

(b)

Fig. 2. Relative photofission cross section for two values of bin width as a function of photon energy. (a) for U^{238} and (b) for Th^{232} respectively.

REF.

D. C. Aumann and J. E. Gindler
J. inorg. nucl. Chem. 32, 731 (1970)

ELEM. SYM.	A	Z
U	238	92

METHOD

REF. NO. 70 Au 1 egf

REACTION	RESULT	EXCITATION ENERGY	SOURCE		DETECTOR		ANGLE
			TYPE	RANGE	TYPE	RANGE	
G,F	RLY	THR-17	C	14-17	ACT-I		4PI

Data ratio of isomer to ground state yields.

ISOMER YIELDS

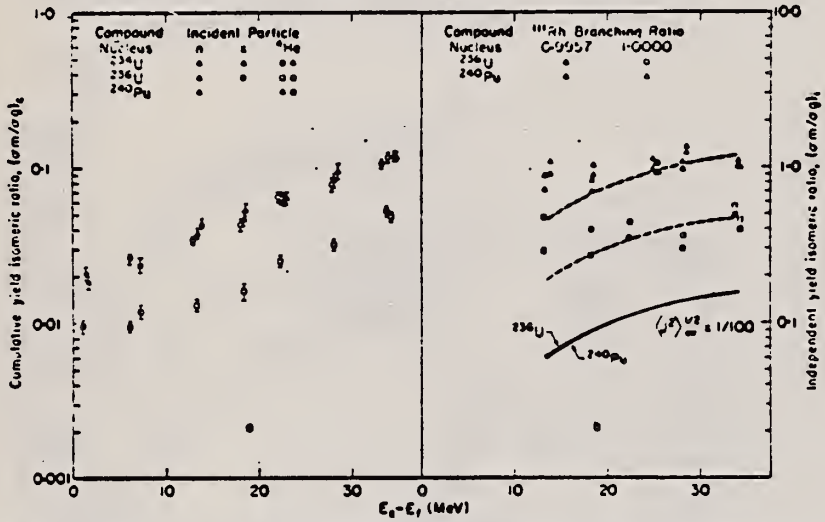

Fig. 3. Cumulative (a) and independent (b) yield ^{111}Pd isomeric ratios as a function of excitation energy above the fission barrier for several compound nuclei. The solid curves in 3b represent the root-mean-square average angular momenta of the compound nuclei indicated. The dashed curves are the solid curves displaced to pass approximately through the respective isomeric ratio data.

Table 3. Cumulative yield isomeric ratios of ^{111}Pd formed in photofission

Target	13·8	E_γ(MeV) 16·6–17·0	17·1
^{232}Th	0·0060 ± 0·0004	0·0056 ± 0·0006	
^{238}U	0·0053 ± 0·0004	0·0054 ± 0·0005	0·0066 ± 0·0017
^{236}U	0·0095 ± 0·0007		0·0119 ± 0·0012
^{235}U	0·0125 ± 0·0009	0·0130 ± 0·0013	
^{234}U	0·0261 ± 0·0019		0·0235 ± 0·0124
^{233}U	0·0304 ± 0·0022	0·0380 ± 0·0038	0·0454 ± 0·0045

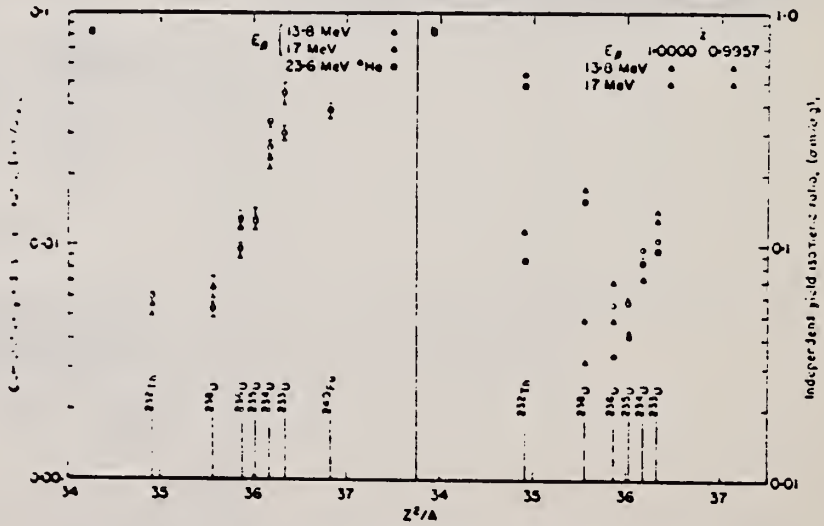

Fig. 5. Cumulative (a) and independent (b) yield ^{111}Pd isomeric ratios as a function of Z^2/A for the compound nucleus.

REF. V. I. Kasilov, Yu. N. Ranyuk, and P. V. Sorokin
Yad. Fiz. 11, 1324 (1970)
Sov. J. Nucl. Phys. 11, 736 (1970)

ELEM. SYM.	A	Z
U	238	92

METHOD

REF. NO. 70 Ka 1 hmg

REACTION	RESULT	EXCITATION ENERGY	SOURCE		DETECTOR		ANGLE
			TYPE	RANGE	TYPE	RANGE	
E,F	ABX	THR-500	C	25-500	TRK-D		4PI
G,F	ABY	THR-500	C	25-500	TRK-D		4PI

ONLEY and Ressler[1] have calculated theoretically the cross section for electrofission of U^{238} in the electron-energy range E_0 = 25–500 MeV. The cross section σ_e for electrofission of U^{238} has been measured experimentally by Bowman et al.[2] for $E_0 \geq 250$ MeV. For $E_0 < 250$ MeV, σ_e has not been measured directly. Onley and Ressler[1] estimate σ_e in this energy range by using data on the ratio of the cross sections σ_Q/σ_e,[3] where σ_Q is the cross section for photofission per equivalent photon. σ_Q is determined by integration of the uranium photofission cross section[4] over the photon spectrum. The value of σ_e obtained turned out to be close to that calculated theoretically, but differed considerably from that measured by Bowman et al.[2] at E_0 = 250 MeV. The contradiction between the data of the two experiments apparently arose from the uncertainties associated with calculation of σ_Q. In order to check this assumption we have measured the yield of the U^{238} photofission reaction by a technique previously described by two of us.[5] The result is shown in Fig. 1. Using these data and also the value of σ_Q/σ_e from [3], we determined the electrofission cross section of uranium. The value of σ_Q/σ_e for $E_0 > 250$ MeV was taken as 30 ± 5.

The values obtained for the U^{238} electrofission cross section are shown in Fig. 2 by the circles. Also shown in this figure are the results of Bowman et al.[2] and the theoretical curve of Onley and Ressler[1] (solid line). It is apparent that the cross sections obtained by us are in good agreement with those of Bowman et al.[2] The experimental values of the cross sections are greater than the theoretical values.

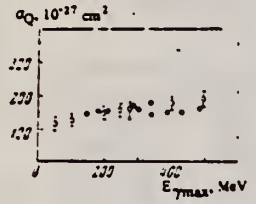

FIG. 1

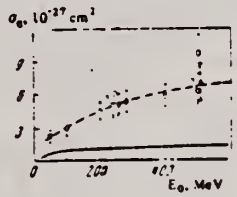

FIG. 2

FIG. 1. U^{238} photofission yield per equivalent photon as a function of bremsstrahlung maximum energy. Points ○–present work, ●–data of Jungerman and Steiner. [6] The errors in ref. 6 are smaller than the size of the points.

FIG. 2. Cross section for electrofission of U^{238} as a function of electron energy. Points: □, ■–data of Bowman et al. [2] ○–present work. The solid curve is taken from ref. 1. The dashed curve was drawn visually.

[1]The article was transmitted from the editor of the journal Pisma Zh. Eksp. Teor. Fiz., where it was received July 30, 1969

[1] D. S. Onley and G. M. Ressler, Phys. Rev. Letters 22, 236 (1969).

[2] H. R. Bowman, R. C. Gattl, R. C. Jared, G. Kiliam, et al., Phys. Rev. 168, 1396 (1968).

[3] Yu. N. Ranyuk and P. V. Sorokin, Yad. Fiz. 5, 531 (1967) [Sov. J. Nucl. Phys. 5, 377 (1967)].

[4] L. Katz, A. P. Baerg, and F. Brown, Proceedings of the Second United Nations International Conference on the Peaceful Uses of Atomic Energy, United Nations, Geneva, 1958.

[5] Yu. N. Ranyuk and P. V. Sorokin, Yad. Fiz. 5, 531 (1967) [Sov. J. Nucl. Phys. 5, 377 (1967)].

[6] J. A. Jungerman and H. M. Steiner, Phys. Rev. 106, 585 (1957).

Translated by C. S. Robinson
180

REF. L. A. Kull, R. L. Bramblett, T. Gozani, D. E. Rundquist
Nucl. Sci. & Eng. 39, 163 (1970)

ELEM. SYM.	A	Z
U	238	92

METHOD

REF. NO. 70 Ku 2 egf

REACTION	RESULT	EXCITATION ENERGY	SOURCE		DETECTOR		ANGLE
			TYPE	RANGE	TYPE	RANGE	
G,F	NOX	5-10	C	8,10	BF3-I		4PI

DELAYED NEUT YLDS

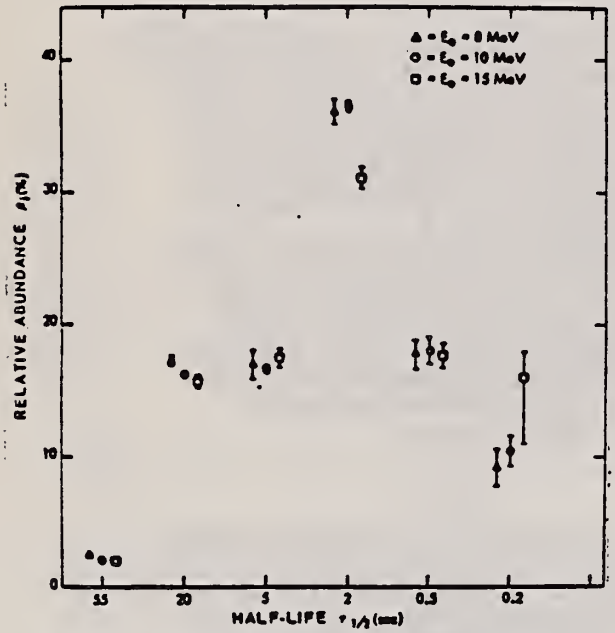

Fig. 5. Relative abundances of the delayed-neutron groups (β_i) (specified by their approximate half-lives) for $^{238}U(\gamma,f)$ at E_e = 8 and 10 MeV. The error bars only represent statistics. The data at E_e = 15 MeV of Ref. 3 is also shown.

TABLE I

Relative Abundances for the Photofission of ^{235}U and ^{238}U with Bremsstrahlung at Endpoint Energies of 8 and 10 MeV Actual Half-Lives Used in the Analyses were Taken from Ref. 4

Half-Life (sec)	Relative Abundance (percent)			
	^{238}U (8 MeV)	^{238}U (10 MeV)	^{235}U (8 MeV)	^{235}U (10 MeV)
55	2.5 ± 0.1	2.1 ± 0.1	5.2 ± 0.5	5.6 ± 0.2
20	17.3 ± 0.4	16.3 ± 0.1	25.3 ± 0.3	24.5 ± 0.5
5	17.0 ± 1.1	16.7 ± 0.3	21.3 ± 1.3	24.4 ± 0.9
2	36.1 ± 0.9	36.4 ± 0.4	35.0 ± 1.2	33.7 ± 0.5
0.6	17.9 ± 1.1	18.1 ± 1.0	4.4 ± 2.2	9.1 ± 1.0
0.2	9.2 ± 1.4	10.5 ± 1.1	8.8 ± 3.2	2.8 ± 1.1

[3] B. P. MAKSYUTENKO, *J. Exptl. Theoret. Phys.* (USSR), 135, 815 (1958).
[4] O. P. NIKOTIN, K. A. PETRZHAK, *Atomnaya Energiya*, 20, 268 (1966).

REF. T. Methasiri
Nucl. Phys. A158, 433 (1970)

ELEM. SYM.	A	Z
U	233	92

METHOD

REF. NO. 70 Me 5 egf

REACTION	RESULT	EXCITATION ENERGY	SOURCE		DETECTOR		ANGLE
			TYPE	RANGE	TYPE	RANGE	
G,F	ABY	THR-900	C	200-900	TRK		4PI

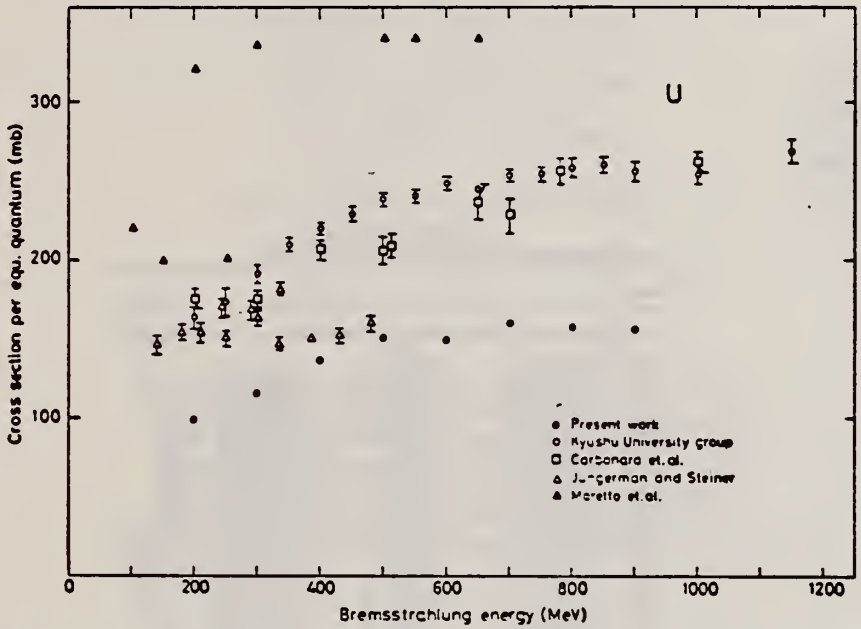

Fig. 2. Cross sections per equivalent quantum $\sigma_e(E)$ of uranium as a function of bremsstrahlung maximum energy (E).

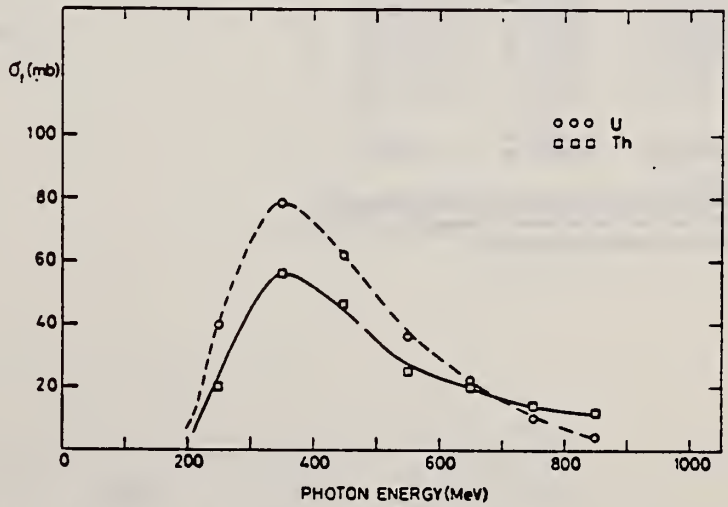

Fig. 4. Photofission cross sections of uranium and thorium as a function of photon energy.

REF. N.S. Rabotnov, G.N. Smirenkin, A.S. Soldatov, L.N. Usachev, S.P. Kapitza, and Yu. M. Tsipenyuk
Yad. Fiz. 11, 508 (1970)
Sov. J. Nucl. Phys. 11, 285 (1970)

ELEM. SYM.	A	Z
U	238	92

METHOD

REF. NO. 70 Ra 1 hmg

REACTION	RESULT	EXCITATION ENERGY	SOURCE		DETECTOR		ANGLE
			TYPE	RANGE	TYPE	RANGE	
G,F	ABX	THR-9	C	5-10	TRK-D		DST

SEE 68RA1, 69KA1

Table II. Parameters of angular distributions of the fragments

E_{max}, MeV	a	b	c	Y, fission mg·μ·sec
		Th^{232}		
5.2	—	—	—	$4.5\cdot10^{-4}$
5.4	0.009±0.009	0.931±0.027	0.030±0.025	0.0025
5.65	0.011±0.005	0.980±0.007	0.005±0.006	0.059
5.75	0.015±0.010	0.985±0.014	0.003±0.013	0.062
5.9	0.010±0.005	0.990±0.016	0.084±0.014	0.21
5.95	0.014±0.004	0.986±0.009	0.074±0.010	0.32
6.2	0.012±0.003	0.988±0.010	0.079±0.010	0.79
6.5	0.022±0.005	0.978±0.015	0.022±0.015	3.1
6.7	0.023±0.002	0.977±0.009	0.069±0.008	9.8
6.9	0.032±0.007	0.968±0.024	0.029±0.022	7.7
7.0	0.036±0.005	0.964±0.013	0.038±0.012	13.5
7.1	0.056±0.006	0.944±0.020	0.031±0.017	19.5
7.7	0.088±0.005	0.912±0.015	0.024±0.013	30.5
8.0	0.109±0.006	0.891±0.013	0.026±0.012	35
8.5	0.164±0.004	0.836±0.008	0.017±0.008	71
10.0	0.304±0.009	0.696±0.014	−0.031±0.014	—
		U^{238}		
5.0	0.052±0.100	0.948±0.164	1.296±0.265	0.00071
5.2	0.100±0.025	0.900±0.061	0.910±0.060	0.032
5.3	0.020±0.035	0.980±0.065	0.566±0.076	0.0120
5.4	0.007±0.021	0.993±0.050	0.412±0.066	0.06
5.45	0.038±0.009	0.962±0.017	0.155±0.021	0.033
5.65	0.034±0.005	0.966±0.011	0.059±0.010	0.27
5.95	0.078±0.005	0.922±0.014	0.039±0.014	1.7
6.4	0.127±0.004	0.873±0.009	0.034±0.008	6.0
6.95	0.213±0.005	0.787±0.008	0.037±0.008	24.0
7.5	0.364±0.006	0.636±0.009	0.024±0.011	47.9
8.0	0.401±0.005	0.599±0.006	0.014±0.007	74.0
9.25	0.570±0.008	0.430±0.007	0.013±0.007	—
		Pu^{239}		
5.25	0.408±0.103	0.592±0.139	1.512±0.139	0.011
5.5	0.330±0.063	0.670±0.084	1.513±0.112	0.15
5.75	0.344±0.047	0.656±0.066	0.654±0.055	0.37
6.0	0.526±0.011	0.474±0.016	0.376±0.018	1.7
6.25	0.666±0.008	0.334±0.011	0.180±0.013	5.9
6.5	0.733±0.012	0.267±0.016	0.180±0.018	11
7.0	0.772±0.011	0.228±0.016	0.064±0.017	36
7.5	0.785±0.012	0.215±0.017	0.032±0.019	50
8.0	0.813±0.013	0.187±0.017	0.029±0.018	136
8.5	0.828±0.015	0.172±0.020	0.021±0.022	270
		Pu^{240}		
5.0*	0.000±0.200	0.000±0.200	1±0.200	0.0001
5.2	0.115±0.097	0.885±0.111	2.58±0.15	0.47

*In this case W(ϑ) is described by a pure quadrupole distribution, ~$\sin^2 2\vartheta$, and therefore the coefficient c is meaningless in the employed normalization and is assumed equal to unity.

Table II (cont.)

E_{max}, MeV	a	b	c	Y, fission mg·μ·sec
		Pu^{242}		
5.45	0.102±0.014	0.898±0.056	1.147±0.070	0.15
5.7	0.222±0.034	0.778±0.062	0.710±0.052	0.49
5.95	0.533±0.010	0.467±0.011	0.331±0.013	2.3
6.4	0.870±0.012	0.130±0.012	0.096±0.013	11.5
6.95	0.680±0.025	0.331±0.027	0.097±0.029	30
7.7	0.716±0.012	0.284±0.006	0.055±0.017	115
7.9	0.725±0.012	0.275±0.006	0.075±0.018	135
8.2	0.762±0.010	0.238±0.015	0.046±0.015	180
8.5	0.779±0.020	0.221±0.027	0.057±0.029	230
8.7	0.791±0.009	0.209±0.002	0.032±0.014	230
9.5	0.822±0.011	0.178±0.013	0.019±0.016	680
5.0	0.502±0.303	0.498±0.372	3.702±0.424	0.0055
5.25	0.448±0.053	0.552±0.085	0.965±0.052	0.056
5.5	0.418±0.046	0.582±0.060	1.018±0.069	—
5.5	0.310±0.022	0.690±0.029	0.735±0.034	0.26
5.75	0.488±0.004	0.512±0.010	0.422±0.012	1.9
6.0	0.598±0.011	0.402±0.016	0.207±0.018	2.7
6.25	0.669±0.012	0.331±0.017	0.138±0.019	8.8
6.5	0.709±0.009	0.291±0.013	0.122±0.014	17
7.0	0.730±0.005	0.269±0.007	0.075±0.004	50
7.5	0.754±0.005	0.246±0.007	0.046±0.004	105
8.0	0.766±0.006	0.234±0.008	0.037±0.000	175
8.5	0.814±0.005	0.186±0.007	0.042±0.008	225

$$W(\vartheta) = a + b \sin^2\vartheta + c \sin^2 2\vartheta$$

[over]

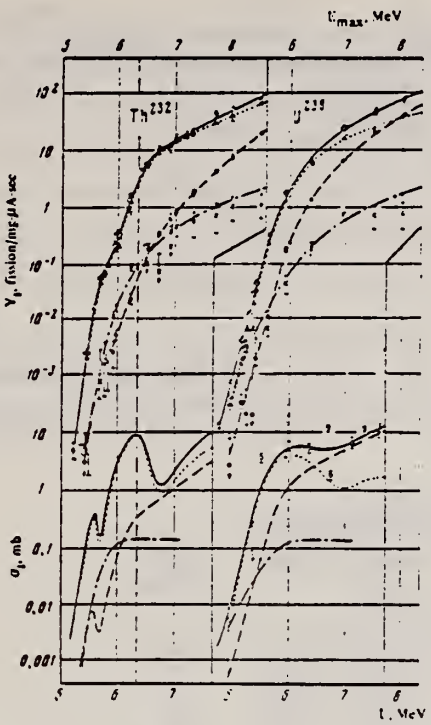

FIG. 3. Energy dependence of the total yield $Y(E_{max})$ (○) and its angular components $Y_a(E_{max})$ (●), $Y_b(E_{max})$ (▲), and $Y_c(E_{max})$ (×). Below—plots of the total cross section $\sigma_{\gamma f}(E)$ (solid curve) and its angular components $\sigma_a(E)$ (long dashes), $\sigma_b(E)$ (short dashes), and $\sigma_c(E)$ (dash-dot), obtained by solving Eq. (5), vs. the γ-quantum energy. The points for $\sigma_{\gamma f}$ for U^{238} were taken from [10]. The vertical dashed line denotes the binding energies of the neutron in the corresponding nucleus.

Angular components of the yield. Knowledge of the coefficients a, b, and c makes it possible to determine the contribution of the individual components of the yield Y_a, Y_b, and Y_c, the angular dependence of which corresponds to three components in the expression (2): isotropic, dipole, and quadrupole. Their meaning can be understood from the following definitions:

$$Y = Y_a + Y_b + Y_c; \quad \frac{dY}{d\Omega} = \frac{1}{4\pi\nu} YW(\vartheta);$$

$$Y_a = \frac{a}{\nu} Y; \quad Y_b = \frac{2}{3}\frac{b}{\nu} Y; \quad Y_c = \frac{8}{15}\frac{c}{\nu} Y. \qquad (4)$$

Plots of Y_i and E_{max} are shown in Fig. 3 together with the data on the total yield. The experimental points $Y_i(E_{max})$ were determined by means of formulas (4) from the coefficients $W(\vartheta)$ listed in Table II and from the total yield. The error of Y_i indicated in Fig. 3 does not include the error in the measurement of $Y(E_{max})$ (~10%).

REF.

B. Schrøder and G. Nydahl and B. Forkman
Nucl. Phys. A143, 449 (1970)

ELEM. SYM.	A	Z
U	238	92

METHOD

REF. NO.	
70 Sc 1	egf

REACTION	RESULT	EXCITATION ENERGY	SOURCE		DETECTOR		ANGLE
			TYPE	RANGE	TYPE	RANGE	
G,F	RLY	THR-999	C	300-999	ACT-I		4PI

999 = 1100 MEV

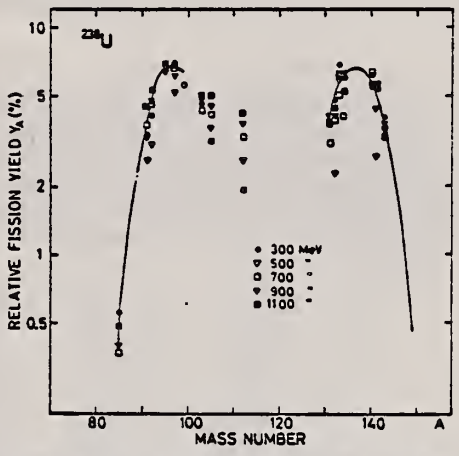

Fig. 2. Relative fission yields of ^{238}U at different irradiation energies. All yields normalized to $Y_{99} = 5.6\,\%$ (o). The curve shows the average values.

humps A_L and A_H, the number of neutrons emitted $n = A_{target} - (A_L + A_H)$ and the values of the peak-to-valley ratios defined by Y_{97}/Y_{112}. The last-named quantities are plotted in fig. 4.

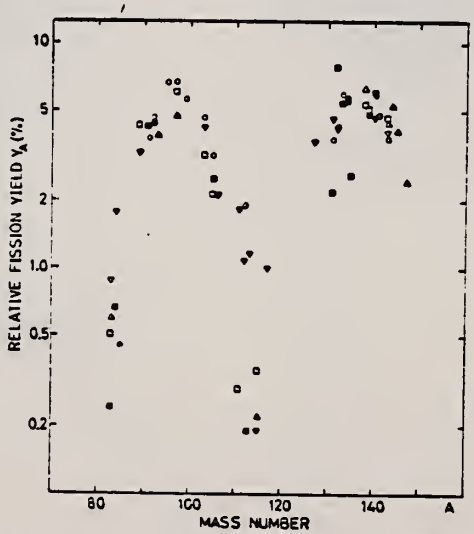

Fig. 3. Published data on the relative fission yields of ^{238}U at different irradiation energies. Black squares, 17.5 MeV monoenergetic, ref. [5]); open squares, 22 MeV bremsstrahlung, ref. [3]); triangles, Δ 23 MeV bremsstrahlung, ref. [6]); triangles ▽, 300 MeV bremsstrahlung, ref. [2]); open circles ○, 300 MeV bremsstrahlung, this work. All yields were normalized to $Y_{99} = 5.6\,\%$.

[over]

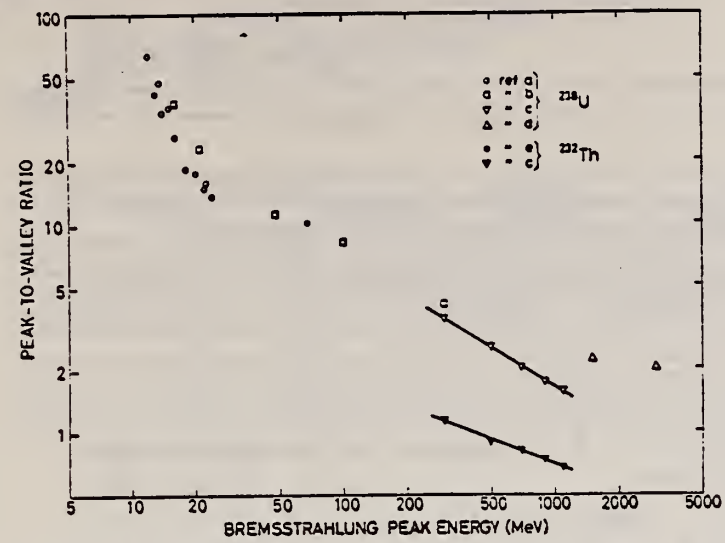

Fig. 4. Published data on peak-to-valley ratio of ^{238}U and ^{232}Th. ref. a, see ref. [3]); ref. b, see ref. [3]); ref. c, see this work; ref. d, see ref. [4]); ref. e, see ref. [7]).

TABLE 1

Measured cumulative fission yields relative to $A = 99$ (^{238}U)

Mass number	Nucleide	Gamma line (keV)	Uranium fission yield (%)					Average
			300 (MeV)	500 (MeV)	700 (MeV)	900 (MeV)	1100 (MeV)	
85	^{85m}Kr	150	0.55		0.37	0.39	0.48	0.45
91	^{91}Sr	753	3.4	2.6	3.7	3.3	4.5	3.7
92	^{92}Y	934	4.1	3.1	4.6	4.7	5.3	4.7
95	^{95}Zr	759				6.5	6.9	6.7
97	^{97}Zr	744	7.0	5.2	6.6	6.3	6.8	6.7
97	^{97}Nb	658	6.2		5.8	5.3	5.7	
99	^{99m}Tc	142	5.6	5.6	5.6	5.6	5.6	
103	^{103}Ru	497	4.6		4.4	4.7	5.0	
105	^{105}Rh	319	3.1	3.6	4.2	4.5	5.0	
112	^{112}Ag	618	1.9	2.6	3.3	3.8	4.2	
131	^{131}I	366	4.0		3.1	4.1	3.8	3.8
132	^{132}Te	229	4.8	2.3	2.9	4.1	4.5	4.3
133	^{133}I	532	6.9	5.7	5.0	6.0	6.0	6.0
134	^{134}I	848	6.1		4.2	6.0	5.2	5.8
140	^{140}La	487	6.2		6.2	5.5	5.5	5.9
141	^{141}Ce	145	5.4		2.7	4.4	4.6	4.8
143	^{143}Ce	293	4.0	3.3	3.3	3.8	3.6	3.8
detector			30 cm³	5 mm	7 mm	7 mm	30 cm³	

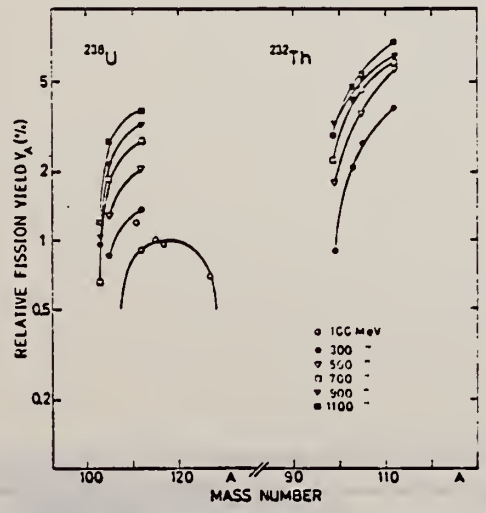

Symmetric high-energy mass distributions from ^{238}U and ^{232}Th. The data at 100 MeV are those reported by Schmitt and Sugarman [2]).

REF. V. Di Napoli, F. Salvetti, H. G. De Carvalho, J. Benuzzi Martins
Lettere al Nuovo Cimento 1, 538 (1971)

ELEM. SYM.	A	Z
U	238	92

METHOD

REF. NO. 71 Di 2 egf

REACTION	RESULT	EXCITATION ENERGY	SOURCE TYPE	SOURCE RANGE	DETECTOR TYPE	DETECTOR RANGE	ANGLE
G,N	ABY	7-999		300-999	ACT-I		4PI

999 = 1 GEV

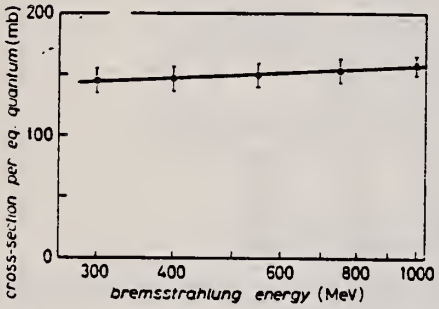

Fig. 1.

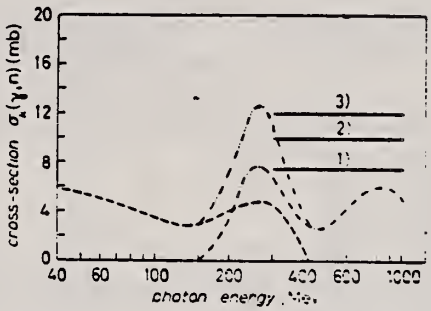

Fig. 2.

Fig. 1. – Cross-sections per equivalent quantum σ_Q are plotted vs. the natural logarithm of the maximum energy of the bremsstrahlung. Circles: Frascati data. Triangle: average value of Frascati and DESY (*) data at 1000 MeV. The straight line is a least-squares fit of the experimental points.

Fig. 2. – The dashed line represents $\sigma_x(\gamma, n)$ calculated by the expression (1). The dash-dotted line represents $\sigma_x(\gamma, n)$ calculated by the expression (2). The dash-two-dot line represents the total $\sigma_x(\gamma, n)$. The solid line 1) represents the average value σ_x obtained with a factor of 1.26 for the transparency. The solid line 3) is the average value with a factor 2 for the transparency. The solid line 2) is the experimental value of the present work.

REF.

E. J. Dowdy and T. L. Krysinski
Nucl. Phys. A175, 501 (1971)

ELEM. SYM.	A	Z
U	238	92

METHOD

REF. NO.	
71 Do 1	egf

REACTION	RESULT	EXCITATION ENERGY	SOURCE		DETECTOR		ANGLE
			TYPE	RANGE	TYPE	RANGE	
G,F	NOX	6-9	D	6-9	FRG-I		DST

$$W(\theta) = a + b \sin^2\theta + c \sin^2 2\theta$$

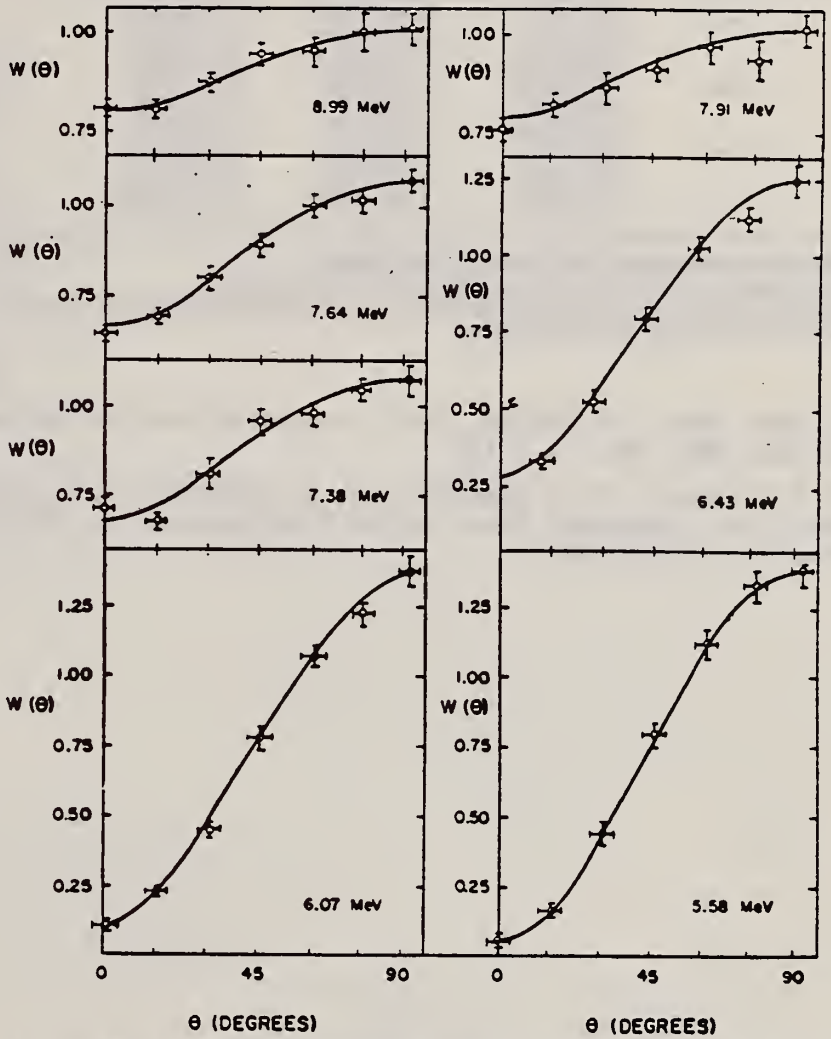

Fig. 3. Fission-fragment angular distributions for the several discrete excitation energies. The full curves are the least-squares fits of eq. (1) to the data.

(over)

TABLE 2

Values of the coefficients a, b and c as a function of energy for the best fit of the assumed angular distribution [eq. (1)] to the experimental data

Photon energy (MeV)	a	b	c
(5.58)	0.057±0.006 [a])	1.34 ±0.04	0.083±0.008
	0.05 ±0.06 [b])	1.36 ±0.14	0.26 ±0.23
	0.041±0.013 [c])	0.965±0.023	0.102±0.009
(6.07)	0.083±0.015	1.33 ±0.04	0.051±0.009
	−0.02 ±0.03	1.38 ±0.09	0.79 ±0.16
	0.136±0.007	1.31 ±0.02	0.068±0.010
(6.42)	0.29 ±0.03	1.02 ±0.08	0.058±0.013
	0.25 ±0.06	1.02 ±0.11	0.52 ±0.24
	0.165±0.005	1.13 ±0.01	0.044±0.010
(7.38)	0.708±0.013	0.392±0.042	0.057±0.008
	0.66 ±0.08	0.38 ±0.07	0.64 ±0.25
	0.31 ±0.04	0.786±0.008	0.044±0.008
(7.64)	0.689±0.008	0.424±0.024	0.051±0.004
	0.67 ±0.11	0.40 ±0.10	0.47 ±0.36
	0.359±0.004	0.750±0.007	0.041±0.008
(7.91)	0.832±0.018	0.217±0.054	0.04 ±0.01
	0.63 ±0.24	0.48 ±0.20	0.39 ±0.43
	0.382±0.006	0.641±0.007	0.033±0.007
(8.99)	0.839±0.007	0.215±0.021	0.033±0.004
	0.88 ±0.08	0.13 ±0.07	0.24 ±0.24
	0.554±0.007	0.495±0.008	0.017±0.008

[a]) Results of this study appear in the first row for each energy.
[b]) The constants appearing in the second row for each energy are from ref. [1]).
[c]) The constants appearing in the third row for each energy are interpolated from the data in ref. [5]).
Included are results of previous measurements.

1 A. Bohr, Proc. of the Int. Conf. on peaceful uses of atomic energy, Geneva, 1955, vol. 2, p. 151.

5 N. S. Rabotnov, G. N. Smirenkin, A. S. Soldatov, L. N. Usachev, S. P. Kapitsa and Iu. M. Tsipeniuk. Proc. of the IAEA Symposium on physics and chemistry of fission 1 (1965) 135.

REF.

M. Hass, R. Moreh, and D. Salzmann
Phys. Letters 36B, 68 (1971)

ELEM. SYM.	A	Z
U	238	92

METHOD

REF. NO. 71 Ha 1 egf

REACTION	RESULT	EXCITATION ENERGY	SOURCE		DETECTOR		ANGLE
			TYPE	RANGE	TYPE	RANGE	
G,G	ABX	8-9	D	8-9	SCD-D	7-9	90

Table 1
Measured differential cross sections (μb/sr) for elastic and Raman scattering from U and Th targets at an angle of 140°. The calculated values for ^{238}U using the GDR parameters of ref. [6] and a set of tentative parameters are shown.

	Experiment				Calculated (^{238}U)			
E_γ	^{232}Th		^{238}U		Ref. [6]		Tentative	
(keV)	Elastic	Raman	Elastic	Raman	Elas-tic	Ra-man	Elas-tic	Ra-man
8533	7± 3	7± 3	8± 3	8± 3	17	15	11	10
8998	24± 7	15± 5	27± 6	18± 4	38	28	27	18
9298	37±10	25± 8	42± 9	27± 7	62	43	44	28

REF.

A.V. Ignatyuk, N.S. Rabotnov, G.N. Smirenkin, A.S. Soldatov, and Yu. M. Tsipenyuk
Zh. Eksp. Teor. Fiz. 61, 1284 (1971)
Sov. Phys. JETP 34, 684 (1972)

ELEM. SYM.	A	Z
U	238	92

METHOD

REF. NO. 71 Ig 1 | egf

REACTION	RESULT	EXCITATION ENERGY	SOURCE TYPE	SOURCE RANGE	DETECTOR TYPE	DETECTOR RANGE	ANGLE
G,F	ABX	5-8	C	5-8	TRK-I		DST

Table I. Angular-distribution parameters a_f and c_f and yield of the photofission reaction, obtained in measurements with metallic foils. The isotropic component $W(\theta)$, obtained with layers (a_l), is compared with the value of a obtained from (13)

E_{max}, MeV	a_f	a	a_l	c_f	Y, fiss/mg·μA·sec
			Th^{232}		
5.55	0.022±0.019	0.019±0.019	—	0.022±0.016	$1.45\cdot10^{-8}$
5.65	0.041±0.014	0.017±0.014	0.010±0.005	0.024±0.013	$5.1\cdot10^{-8}$
5.75	0.031±0.002	0.019±0.003	0.015±0.010	0.004±0.007	$6.2\cdot10^{-8}$
5.90	0.024±0.004	0.008±0.004	0.011±0.010	0.013±0.025	$11.3\cdot10^{-8}$
6.00	0.026±0.005	0.004±0.005	0.014±0.003	0.021±0.011	0.31
6.20	0.034±0.004	0.009±0.005	0.015±0.003	0.005±0.011	0.73
6.40	0.044±0.002	0.021±0.003	0.022±0.005	0.028±0.006	4.0
6.60	0.049±0.003	0.022±0.004	0.022±0.002	−0.006±0.010	9.4
6.80	0.058±0.004	0.026±0.005	0.029±0.004	0.037±0.012	14.5
7.00	0.075±0.003	0.034±0.004	—	−0.005±0.011	17.8
7.20	0.070±0.003	0.047±0.004	0.038±0.006	0.021±0.004	19.5
7.40	0.111±0.005	0.096±0.006	0.064±0.005	0.022±0.013	40.5
7.60	0.124±0.004	0.115±0.005	0.109±0.008	0.007±0.011	50
9.50	0.181±0.005	0.161±0.006	0.164±0.004	0.015±0.012	89
			U^{238}		
4.63	0.334±0.195	0.215±0.220	—	1.657±0.336	$1.2\cdot10^{-8}$
4.8	0.441±0.077	0.270±0.078	—	0.971±0.110	$2\cdot10^{-8}$
4.95	0.359±0.078	0.231±0.079	—	1.340±0.134	$3\cdot10^{-8}$
4.72	0.250±0.042	0.171±0.043	—	1.300±0.049	$4.7\cdot10^{-8}$
5.0	0.241±0.017	0.133±0.020	0.052±0.008	1.139±0.031	$8.4\cdot10^{-8}$
5.13	0.256±0.031	0.162±0.033	—	1.026±0.046	$2.7\cdot10^{-8}$
5.2	0.173±0.023	0.060±0.024	0.100±0.035	0.107±0.043	$4.3\cdot10^{-8}$
5.4	0.074±0.011	0.050±0.012	0.038±0.009	0.306±0.018	$2.4\cdot10^{-8}$
5.5	0.073±0.003	0.040±0.005	—	0.161±0.007	$7.4\cdot10^{-8}$
5.6	0.090±0.005	0.054±0.005	—	0.071±0.012	0.15
5.65	0.082±0.005	0.035±0.006	0.034±0.005	0.055±0.011	0.37
5.7	0.077±0.003	0.054±0.004	—	0.041±0.009	0.24
5.8	0.092±0.006	0.068±0.007	—	0.052±0.014	0.69
5.9	0.079±0.003	0.054±0.004	0.078±0.005	0.056±0.007	0.91
6.0	0.102±0.005	0.069±0.006	—	0.048±0.012	1.8
6.1	0.149±0.018	0.124±0.019	—	0.034±0.009	3.0
6.3	0.141±0.004	0.126±0.005	—	0.013±0.007	34
6.5	0.351±0.006	0.338±0.007	—	0.009±0.010	40
7.5	0.334±0.004	0.333±0.010	0.304±0.006	0.027±0.013	47

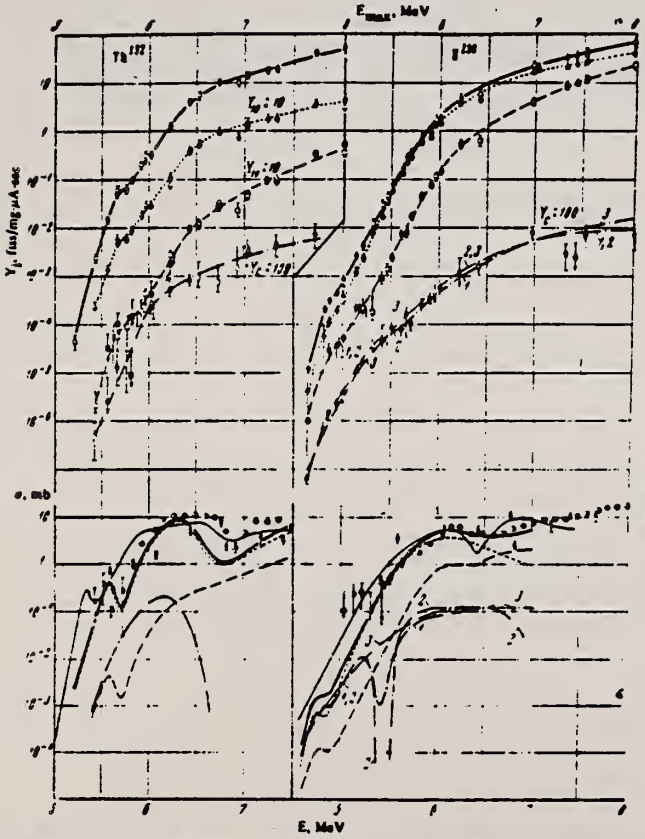

FIG. 4. Top—Energy dependences of the total yield $Y(E_{max})$—○, ● and its components Y_{10} (E_{max})—△, ▲, Y_{11}(E_{max})—□, ■) and $Y_C(E_{max})$—◇, ◇. The light circles represent the results of measurements with thin layers of Th^{232} and U^{238}, and the dark ones correspond to metallic foils. Bottom—plots of the photofission total cross section $\sigma_f(E)$ and of its components $\sigma_{10}(E)$, $\sigma_{11}(E)$, and $\sigma_C(E)$. The points X and ◑ represent respectively the results of [10] and [12]. The thin solid line shows plots of the total cross section $\sigma_f(E)$ obtained in [8].

REF.

O. Y. Mafra and S. Kuniyoshi
An. Acad. Brasil. Cienc. 43, 571 (1971)

ELEM. SYM.	A	Z
U	238	92

METHOD

REF. NO.	
71 Ma 6	egf

REACTION	RESULT	EXCITATION ENERGY	SOURCE		DETECTOR		ANGLE
			TYPE	RANGE	TYPE	RANGE	
G,F	ABX	5- 10	D	5- 10	ION-I		4PI

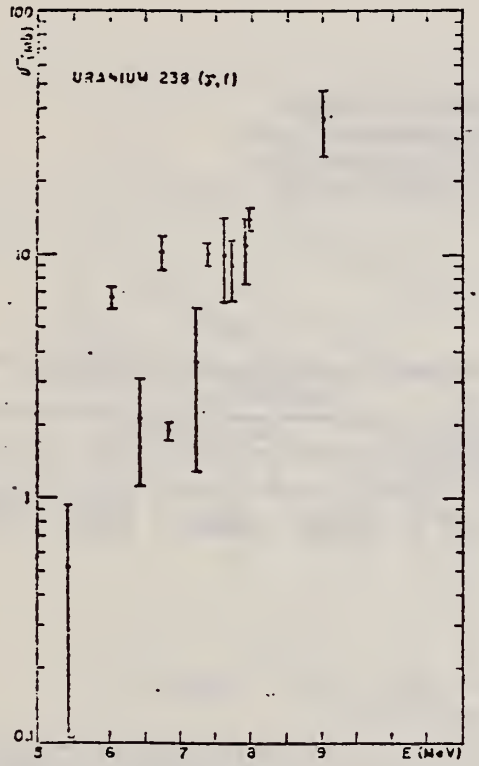

Fig. 1 — Experimental photofission cross section for Uranium.

REF.

K.A. Petrzhak, V.F. Teplykh, M.G. Pan yan, V.A. Demin
Yad. Fiz. 14, 950 (1971)
Sov. J. Nucl. Phys. 14, 532 (1972)

ELEM. SYM.	A	Z
U	238	92

METHOD

REF. NO. 71 Pe 1 hmg

REACTION	RESULT	EXCITATION ENERGY	SOURCE		DETECTOR		ANGLE
			TYPE	RANGE	TYPE	RANGE	
G,F	RLY	THR-25	C	15,25	MSP-I		4PI

XE 131-136 YIELDS

A high-frequency mass spectrometer has been used to measure the relative yields of the isotopes Xe^{131}, Xe^{132}, Xe^{134}, and Xe^{136} in photofission of U^{238} for bremsstrahlung maximum energies of 15 and 25 MeV It has been established that for both energies the fine-structure peak of the fragment-yield curve is at A = 134. The experimental results are compared with those obtained by other workers for spontaneous fission of the same nucleus.

Relative content of xenon isotopes in U^{238} photofission products

Bremsstrahlung maximum energy, MeV	U^{238} excitation energy, MeV	Isotopic composition, %			
		Xe^{131}	Xe^{132}	Xe^{134}	Xe^{136}
15	10.3	17.20±0.50	24.30±0.52	30.70±0.66	27.60±0.74
25	13.1	18.60±0.57	24.60±0.64	30.70±0.68	26.10±0.56

REF.

B. Tamain, B. Pfeiffer, H. Wollnik, E. Konecny
Nucl. Phys. A173, 465 (1971)

ELEM. SYM.	A	Z
U	238	92

METHOD

REF. NO. 71 Ta 1 egf

REACTION	RESULT	EXCITATION ENERGY	SOURCE		DETECTOR		ANGLE
			TYPE	RANGE	TYPE	RANGE	
G,F	LFT	THR-53	C	53	SCD-I		90

DELAYED FISSION

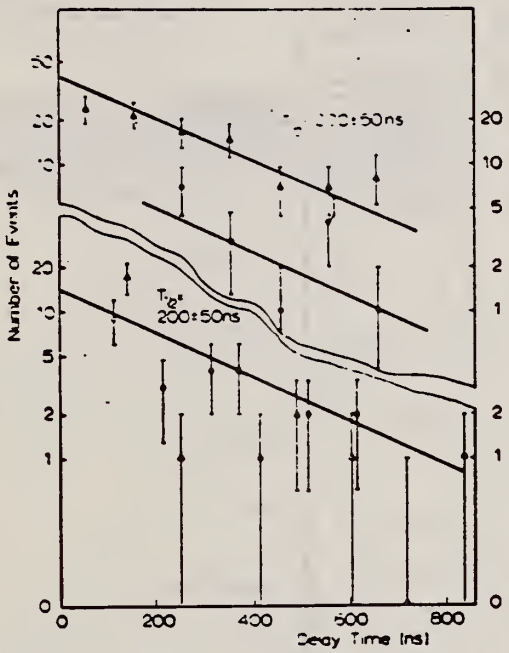

Fig. 6. Decay curves for delayed fission of $^{238}U-\gamma$. Four different curves are shown: △ and ○ refer to single fission pulses obtained by method A in detectors 1 and 2, respectively; ● and ▲ refers to events recorded by method B in one detector only and in both detectors in coincidence, respectively. All decay curves are consistent with a half-life of 200 ± 50 ns.

REF.

G.A. Vartapetyan, N.A. Demekhina, V.I. Kasilov, Yu. N. Ranyuk, P.V. Sorokin and A.G. Khudaverdyan
Yad. Fiz. 14, 65 (1971)
Sov. J. Nucl. Phys. 14, 37 (1972)

ELEM. SYM.	A	Z
U	238	92

METHOD

REF. NO.	
71 Va 4	egf

REACTION	RESULT	EXCITATION ENERGY	SOURCE		DETECTOR		ANGLE
			TYPE	RANGE	TYPE	RANGE	
G,F	ABX	100-999	C	100-999	TRK-I		4PI

999= 5 GEV

E_{max} MeV	Photofission yields per cm³ per equivalent photon					
	U^{238}	U^{235}	Th^{232}	Bi^{209}	Au^{197}	Ta^{181}
100	$(226 \pm 20) \cdot 10^{-27}$	$(120 \pm 12) \cdot 10^{-27}$	$(50 \pm 5) \cdot 10^{-27}$	$(0.70 \pm 0.08) \cdot 10^{-25}$	$(3.0 \pm 0.4) \cdot 10^{-25}$	
120				$(1.5 \pm 0.2) \cdot 10^{-25}$	$(1.4 \pm 0.2) \cdot 10^{-25}$	
140				$(2.0 \pm 0.2) \cdot 10^{-25}$	$(2.0 \pm 0.2) \cdot 10^{-25}$	
150	$(240 \pm 20) \cdot 10^{-27}$		$(61 \pm 7) \cdot 10^{-27}$			
160				$(3.1 \pm 0.3) \cdot 10^{-25}$	$(3.7 \pm 0.4) \cdot 10^{-25}$	
180				$(4.0 \pm 0.5) \cdot 10^{-25}$	$(5.5 \pm 0.6) \cdot 10^{-25}$	
200	$(265 \pm 30) \cdot 10^{-27}$	$(150 \pm 15) \cdot 10^{-27}$	$(72 \pm 7) \cdot 10^{-27}$	$(6.1 \pm 0.6) \cdot 10^{-25}$	$(8.2 \pm 0.8) \cdot 10^{-25}$	$(4.9 \pm 0.5) \cdot 10^{-25}$
220				$(8.3 \pm 0.8) \cdot 10^{-25}$	$(1.1 \pm 0.1) \cdot 10^{-24}$	$(8.2 \pm 0.8) \cdot 10^{-25}$
240				$(1.2 \pm 0.1) \cdot 10^{-24}$	$(1.5 \pm 0.2) \cdot 10^{-24}$	$(1.2 \pm 0.1) \cdot 10^{-24}$
245		$(156 \pm 16) \cdot 10^{-27}$				
260				$(1.5 \pm 0.2) \cdot 10^{-24}$	$(1.9 \pm 0.2) \cdot 10^{-24}$	$(1.6 \pm 0.2) \cdot 10^{-24}$
280		$(160 \pm 16) \cdot 10^{-27}$	$(85 \pm 9) \cdot 10^{-27}$			
300				$(2.2 \pm 0.2) \cdot 10^{-24}$	$(2.3 \pm 0.2) \cdot 10^{-24}$	
320				$(3.5 \pm 0.4) \cdot 10^{-24}$	$(4.4 \pm 0.4) \cdot 10^{-24}$	
340				$(4.2 \pm 0.4) \cdot 10^{-24}$	$(5.0 \pm 0.5) \cdot 10^{-24}$	
360	$(318 \pm 30) \cdot 10^{-27}$	$(175 \pm 20) \cdot 10^{-27}$				
380			$(106 \pm 11) \cdot 10^{-27}$			$(7.0 \pm 0.7) \cdot 10^{-24}$
400				$(5.4 \pm 0.5) \cdot 10^{-24}$		
420				$(6.7 \pm 0.7) \cdot 10^{-24}$		
440		$(189 \pm 20) \cdot 10^{-27}$	$(115 \pm 12) \cdot 10^{-27}$	$(7.9 \pm 0.8) \cdot 10^{-24}$		
460						
480	$(546 \pm 35) \cdot 10^{-27}$					
500						
520						
540						
560						
580						
600		$(200 \pm 20) \cdot 10^{-27}$	$(120 \pm 12) \cdot 10^{-27}$			
620						
640						
660						
680						
700		$(220 \pm 22) \cdot 10^{-27}$	$(135 \pm 14) \cdot 10^{-27}$			
720	$(386 \pm 40) \cdot 10^{-27}$	$(224 \pm 23) \cdot 10^{-27}$	$(140 \pm 14) \cdot 10^{-27}$			
740						
760						
780	$(440 \pm 40) \cdot 10^{-27}$					
800	$(390 \pm 40) \cdot 10^{-27}$	$(217 \pm 23) \cdot 10^{-27}$	$(136 \pm 14) \cdot 10^{-27}$			
820						
840				$(12.5 \pm 1.3) \cdot 10^{-24}$		
860						
880				$(13.5 \pm 1.4) \cdot 10^{-24}$		
900	$(471 \pm 50) \cdot 10^{-27}$	$(193 \pm 20) \cdot 10^{-27}$	$(152 \pm 15) \cdot 10^{-27}$			
920				$(14.3 \pm 1.4) \cdot 10^{-24}$		
940	$(445 \pm 45) \cdot 10^{-27}$	$(238 \pm 24) \cdot 10^{-27}$	$(155 \pm 15) \cdot 10^{-27}$			
960				$(15.2 \pm 1.4) \cdot 10^{-24}$		
980				$(15.5 \pm 1.6) \cdot 10^{-24}$		
1000	$(480 \pm 45) \cdot 10^{-27}$	$(207 \pm 21) \cdot 10^{-27}$	$(145 \pm 14) \cdot 10^{-27}$			
1050	$(445 \pm 45) \cdot 10^{-27}$	$(242 \pm 24) \cdot 10^{-27}$	$(155 \pm 16) \cdot 10^{-27}$			
1100	$(495 \pm 50) \cdot 10^{-27}$	$(245 \pm 25) \cdot 10^{-27}$	$(172 \pm 15) \cdot 10^{-27}$	$(16.1 \pm 1.6) \cdot 10^{-24}$	$(2.0 \pm 0.2) \cdot 10^{-23}$	
1150	$(455 \pm 45) \cdot 10^{-27}$	$(230 \pm 23) \cdot 10^{-27}$	$(149 \pm 15) \cdot 10^{-27}$			
1200	$(541 \pm 50) \cdot 10^{-27}$	$(251 \pm 25) \cdot 10^{-27}$	$(178 \pm 15) \cdot 10^{-27}$			
1250					$(3.0 \pm 0.3) \cdot 10^{-23}$	$(6.4 \pm 0.6) \cdot 10^{-24}$
1300	$(476 \pm 50) \cdot 10^{-27}$	$(264 \pm 27) \cdot 10^{-27}$	$(184 \pm 18) \cdot 10^{-27}$	$(15.6 \pm 1.6) \cdot 10^{-24}$	$(3.0 \pm 0.3) \cdot 10^{-23}$	$(6.6 \pm 0.7) \cdot 10^{-24}$
1350	$(477 \pm 50) \cdot 10^{-27}$	$(260 \pm 26) \cdot 10^{-27}$				
1400	$(515 \pm 50) \cdot 10^{-27}$	$(274 \pm 28) \cdot 10^{-27}$	$(204 \pm 20) \cdot 10^{-27}$	$(20.2 \pm 2) \cdot 10^{-24}$	$(4.2 \pm 0.4) \cdot 10^{-23}$	$(8.5 \pm 0.9) \cdot 10^{-24}$
1450				$(20.2 \pm 2) \cdot 10^{-24}$	$(4.2 \pm 0.4) \cdot 10^{-23}$	$(8.3 \pm 0.8) \cdot 10^{-24}$

(over)

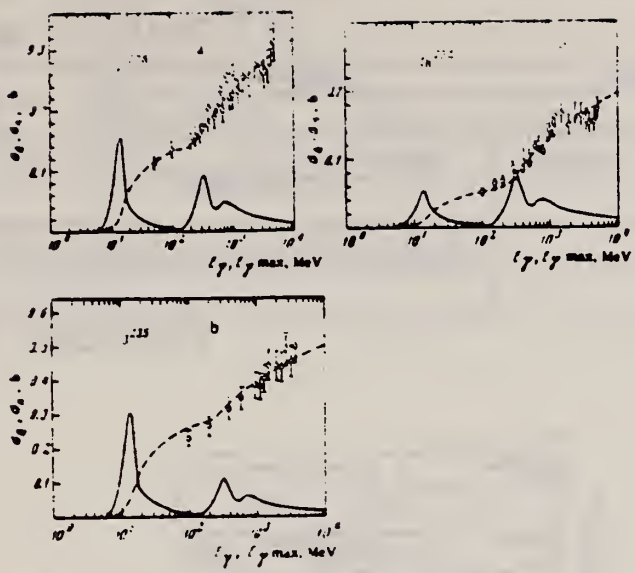

FIG. 1. Solid curve – cross section for photofission of U^{238} as a function of photon energy. Dashed line – the same cross section, integrated over the Schiff bremsstrahlung spectrum (yield per equivalent photon as a function of bremsstrahlung end-point energy). Points ○ – present work; □ – data of Carbonara et al. [*]. a – U^{238}, b – U^{235}, c – Th^{232}

REF.

Yoshihisa Wakuta
J. Phys. Soc. Japan 31, 12 (1971)

ELEM. SYM.	A	Z
U	238	92

METHOD

REF. NO. 71 Wa 1 egf

REACTION	RESULT	EXCITATION ENERGY	SOURCE		DETECTOR		ANGLE
			TYPE	RANGE	TYPE	RANGE	
G,F	ABX	THR-999	C	200-999	SCD-I		DST

Emulsion for angular distribution measurements. 999=1150 MEV 461

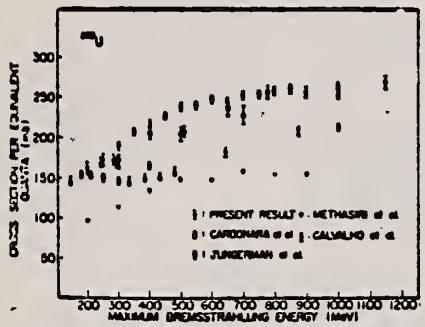

Fig. 3. Photofission cross section per equivalent quanta of U as a function of maximum bremsstrahlung energy.

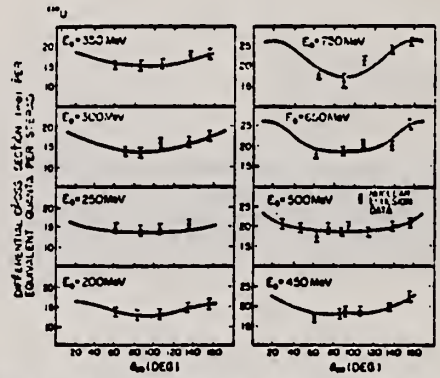

Fig. 9. Angular distribution of fragment in photofission of U.

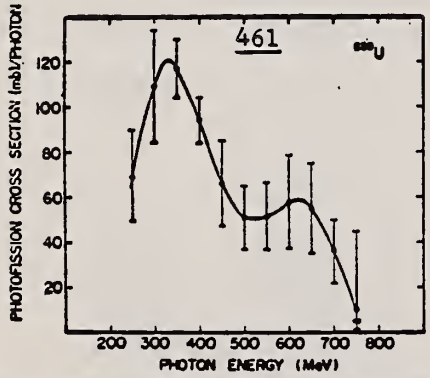

Fig. 7. Photofission cross section of U as a function of photon energies up to 750 MeV.

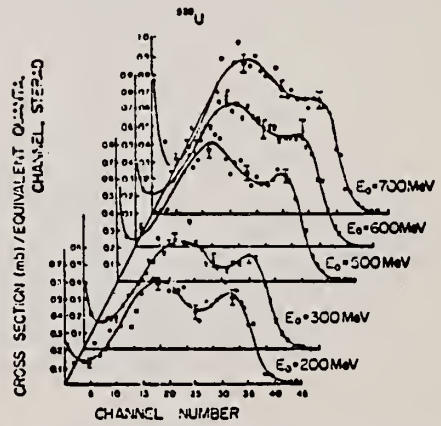

Fig. 11. Single kinetic energy distribution of fragment in photofission of ^{238}U as a function of maximum bremsstrahlung energy.

(over)

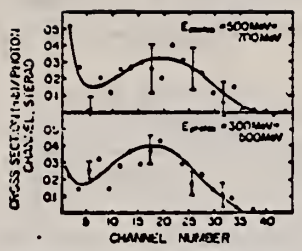

Fig. 12. Single kinetic energy distribution of fragment in photofission of U as a function of photon energy.

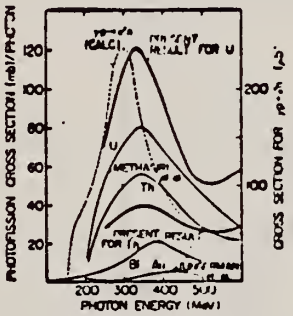

Fig. 13. Photofission cross sections for several nuclei as a function of photon energy. A theoretical curve obtained for $\gamma p \rightarrow \pi^+ n$ reaction is also shown for comparison.

Table I. Expansion coefficient of even Legendre polynomials obtained from a least-square fit to the experimental data of U shown in Fig. 13. (The errors are less than ±0.001)

Maximum Energy of Bremsstrahlung (MeV)	a_2/a_0	a_4/a_0	a_6/a_0
200	0.174	−0.016	−0.005
250	0.065	0.079	0.114
300	0.169	0.046	0.022
350	0.029	0.024	−0.270
450	0.140	0.067	0.018
500	0.120	0.046	−0.004
650	0.237	0.071	−0.091
750	0.334	−0.075	0.000

REF.

R.A. Anderl, J.E. Hall, R.C. Morrison, R.G. Struss, M.V. Yester and D.J. Zaffarano
Nucl. Instr. & Methods 102, 101 (1972)

ELEM. SYM.	A	Z
U	238	92

METHOD

REF. NO. 72 An 2 egf

REACTION	RESULT	EXCITATION ENERGY	SOURCE		DETECTOR		ANGLE
			TYPE	RANGE	TYPE	RANGE	
G,F	RLX	5-8	D	5-8	SCD-I		4PI

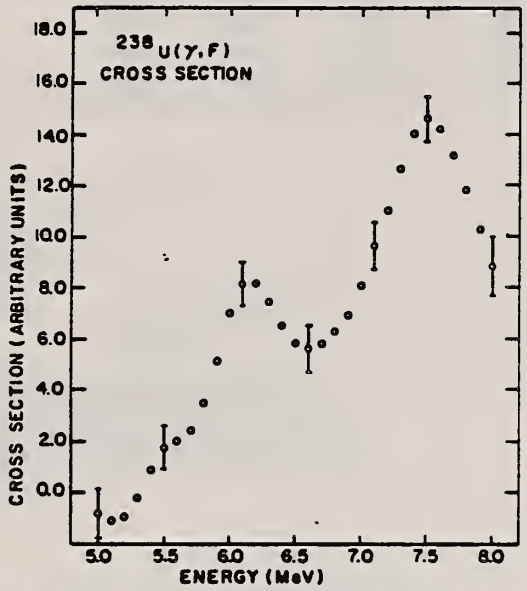

Fig. 7. Relative cross section for photofission of ^{238}U from 5.0 MeV to 8.0 MeV.

REF.	R. Bergere, H. Beil, P. Carlos, A. Veyssiere, A. Lepretre PICNS-72, p. 273 Sendai	ELEM. SYM.	A	Z
		U	238	92
METHOD		REF. NO.		
		72 Be 15		hvm

REACTION	RESULT	EXCITATION ENERGY	SOURCE		DETECTOR		ANGLE
			TYPE	RANGE	TYPE	RANGE	
G,N	ABX	8- 18	D	8- 18	MOD-I		4PI
G,2N	ABX	8- 18	D	8- 18	MOD-I		4PI
G,F	ABX	8- 18	D	8- 18	MOD-I		4PI

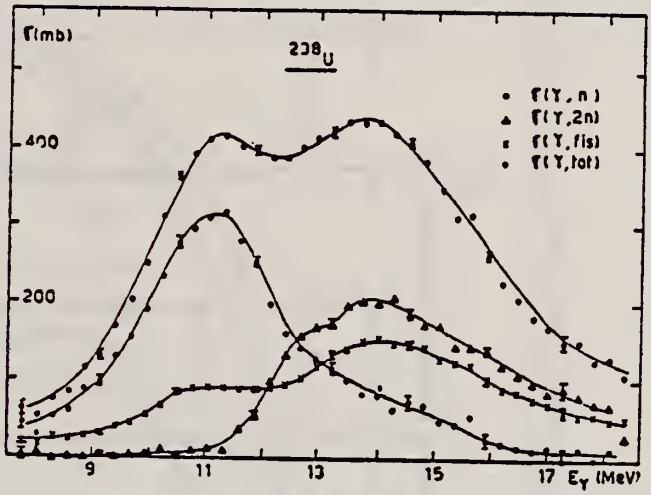

Fig. 4

TABLE I

LORENTZ LINE PARAMETRS AND INTRINSIC QUADRUPOLE MOMENTS

Target nucleus	E_1 MeV	σ_1 mb	Γ_1 MeV	E_2 MeV	σ_2 mb	Γ_2 MeV	$R = \frac{\sigma_2 \Gamma_2}{\sigma_1 \Gamma_1}$	Q_0 barns *	Q_0 barns **
$^{232}_{90}Th$	11.08 ±0.12	268 ± 7	3.37 ±0.22	[illegible]	[illegible]	[illegible]	1.8 ± 0.15	10.2 ± 1	9.66 ±0.1
$^{238}_{92}U$	10.96 ±0.09	301 ± 6	2.90 ±0.14	[illegible]	[illegible]	[illegible]	1.9 ± 0.1	11 ± 1	11.3 ±0.1
$^{237}_{93}Np$	11.06 ±0.12	251 ± 7	3.16 ±0.27	[illegible]	[illegible]	[illegible]	2.4 ± 0.3	11.3 ± 1	10.9 ±0.7

I/ [illegible] LINES PARAMETERS

* this experiment

** [illegible] - Nuclear data tables, Vol. 7, 5 (1970).

REF.

R.L. Bramblett, T. Gozani, R.O. Ginaven, D.E. Rundquist
Nucl. Technology 13, 33 (1972)

ELEM. SYM.	A	Z
U	238	92

METHOD

REF. NO.
72 Br 8 egf

REACTION	RESULT	EXCITATION ENERGY	SOURCE		DETECTOR		ANGLE
			TYPE	RANGE	TYPE	RANGE	
G,F	RLY	THR-11	C	5-11	TRK-I		4PI
G,XN	RLY	THR-11	C	5-11	BF3-I		4PI

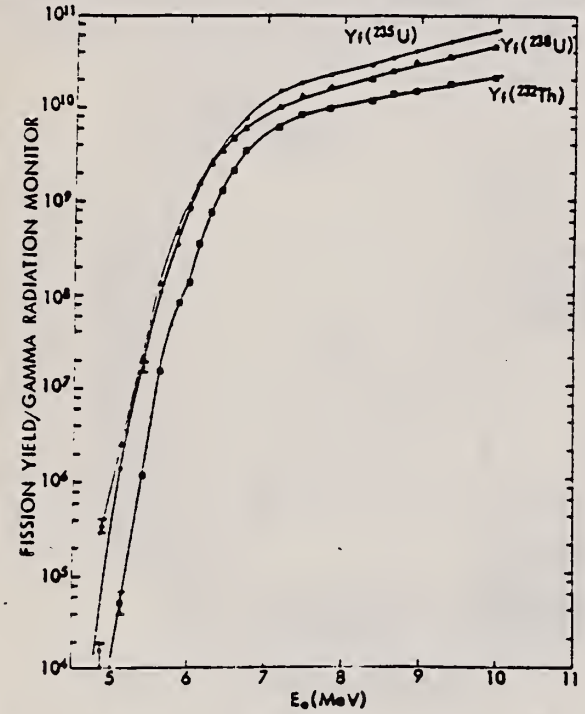

Fig. 7. Bremsstrahlung photofission yields from ^{232}Th, ^{235}U, and ^{238}U obtained using solid-state track detectors (from Gozani et al.[13]).

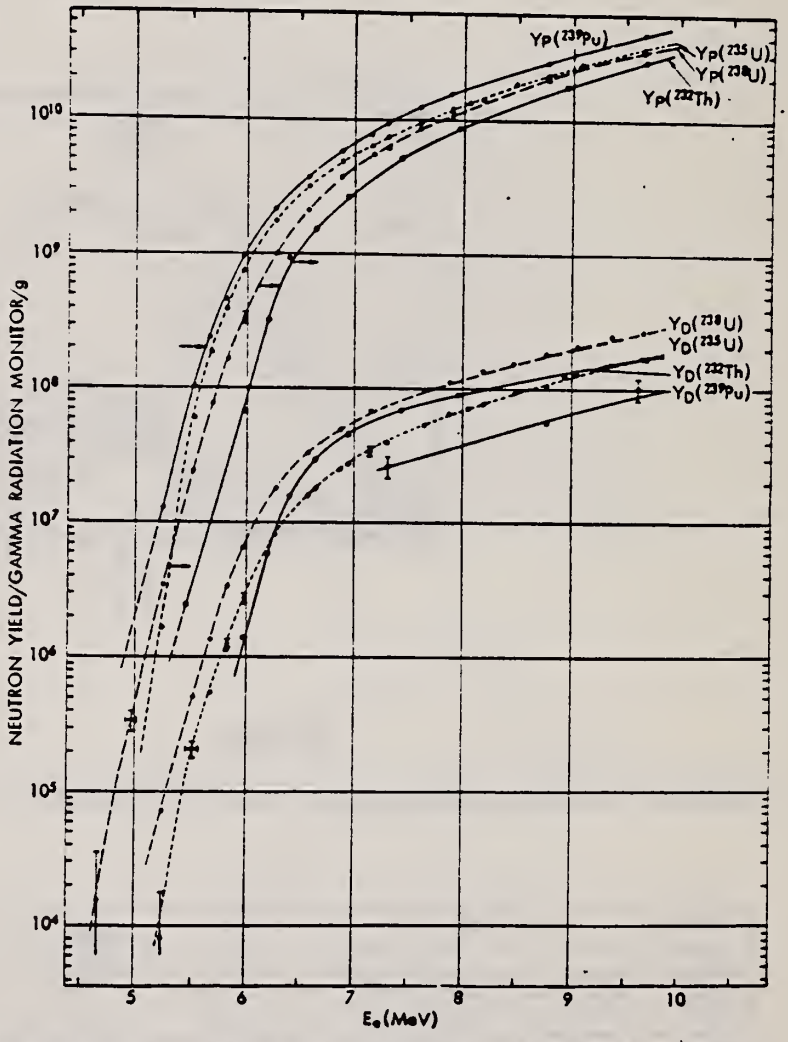

Fig. 8. Prompt- and delayed-neutron yields induced by electron bremsstrahlung for ^{232}Th, ^{235}U, ^{238}U, and ^{239}Pu.

REF.

P. David, J. Debrus, U. Kim, G. Kumbartzki, H. Mommsen, W. Soyez, K. H. Speidel and G. Stein
Nucl. Phys. A197, 163 (1972)

ELEM. SYM.	A	Z
U	238	92

METHOD

REF. NO.	
72 Da 6	egf

REACTION	RESULT	EXCITATION ENERGY	SOURCE		DETECTOR		ANGLE
			TYPE	RANGE	TYPE	RANGE	
G,F	ABY	THR-999	C	800-999	TRK-I		DST

999=2.2 GEV

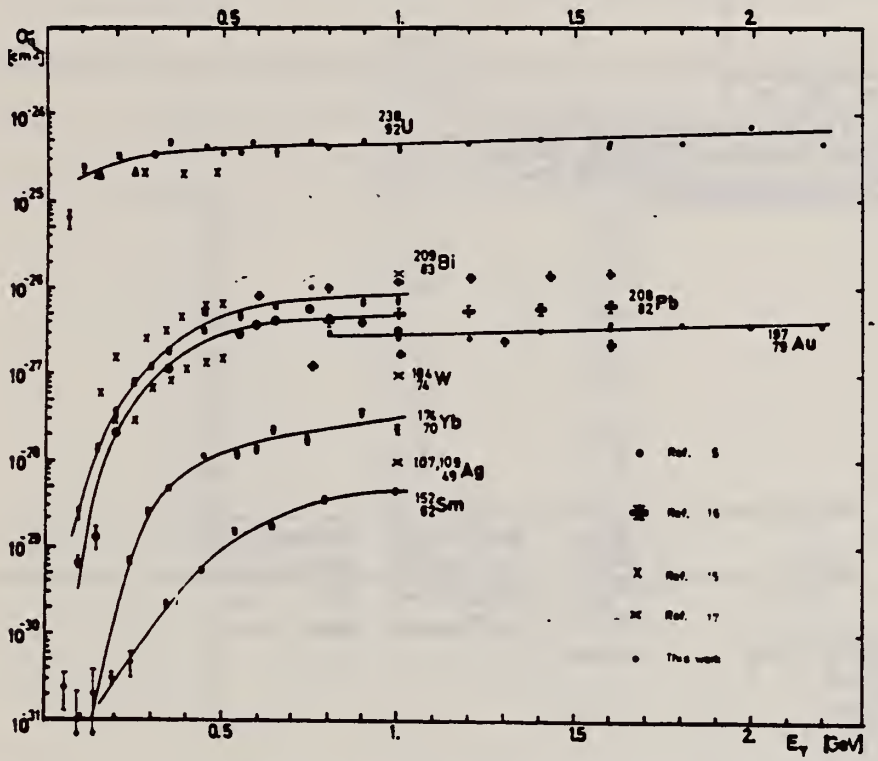

Fig. 3. The bremsstrahlung induced total fission cross section per number of equivalent quanta for uranium and gold in comparison to previous measurements.

TABLE 2

Peak-to-valley ratios for asymmetric fission of ^{238}U by bremsstrahlung with maximum energy E_γ^{max}

E_γ^{max} (GeV)	Y_{97}/Y_{112}
0.8	2.98±0.26
1.2	2.74±0.09
1.5	2.50±0.25
1.8	2.44±0.18
2.0	2.37±0.15
2.2	2.14±0.12

(over)

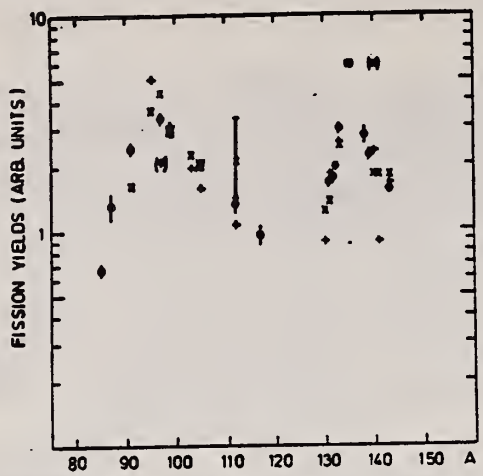

Fig. 5. Comparative display of our cumulative yields (●) obtained in the reaction $^{238}U(\gamma, f)$ at $E_\gamma^{max} = 1.5$ GeV and of the data of Williams *et al.* [10]) from the reaction $^{238}U(e^-, f)$ at electron energies of 1.5 GeV (×) and 3.0 GeV (+). The yields are normalised (■) to each other at $A = 135$, the position of the maximum of the heavy-mass peak.

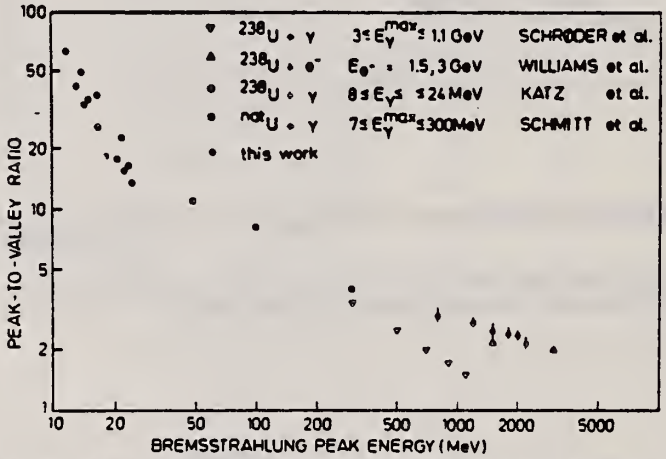

Fig. 10. Peak-to-valley ratios for the fission of ^{238}U as a function of the maximum bremsstrahlung energy, for γ-rays and electrons. For comparison the results of Schrøder *et al.* [11]), Williams *et al.* [10]), Katz *et al.* [9]) and Schmitt *et al.* [12]) are also displayed.

REACTION	RESULT	EXCITATION ENERGY	SOURCE		DETECTOR		ANGLE
			TYPE	RANGE	TYPE	RANGE	

TABLE 3

Forward-backward ratios of the observed cumulative activities for two maximum bremsstrahlung energies

Isotope	Forward-backward ratio	
	0.8 GeV	2.0 GeV
^{85}Kr	1.18	1.05
^{87}Kr	1.12	1.11
^{91}Sr	1.15	1.05
^{97}Zr	1.09	
^{97}Nb		1.03
^{99}Mo	1.10	1.05
^{105}Ru	1.12	1.05
^{112}Ag	1.07	1.06
^{117}In	1.12	
^{132}Te	1.14	1.09
^{133}J	1.15	1.09
^{135}Xe	1.03	1.09
^{138}Cs	1.04	
^{139}Ba	1.14	
^{143}Ce	1.16	1.04

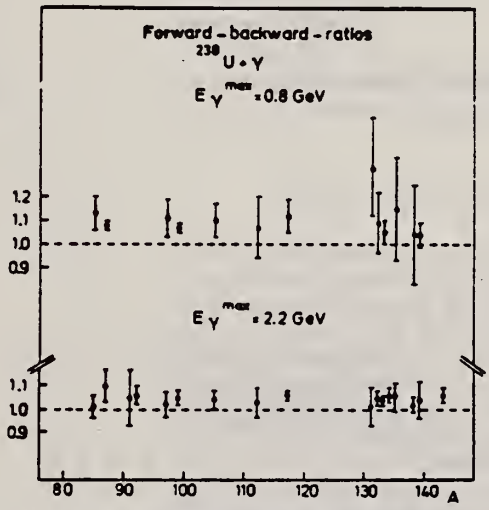

Fig. 11. Forward-backward ratios of isotopes detected in the mica foils in the reaction $^{238}U(\gamma, f)$ at E_γ^{max} = 0.8 GeV and 2.2 GeV.

REF. N.A. Demekhina, V.I. Kasilov, A.V. Mitrofanova, Yu. N. Ranyuk, and P.V. Sorokin
Yad. Fiz. 16, 911 (1972)
Sov. J. Nucl. Phys. 16, 502 (1973)

ELEM. SYM.	A	Z
U	238	92

METHOD

REF. NO. 72 De 12 hmg

REACTION	RESULT	EXCITATION ENERGY	SOURCE TYPE	SOURCE RANGE	DETECTOR TYPE	DETECTOR RANGE	ANGLE
G,F	NOX	THR* 6	C	3* 6	TRK-I		DST

$d\sigma/d\Omega \sim 1+2\ v/V \cos\theta - P\sin^2\theta$

* ENERGIES IN GEV

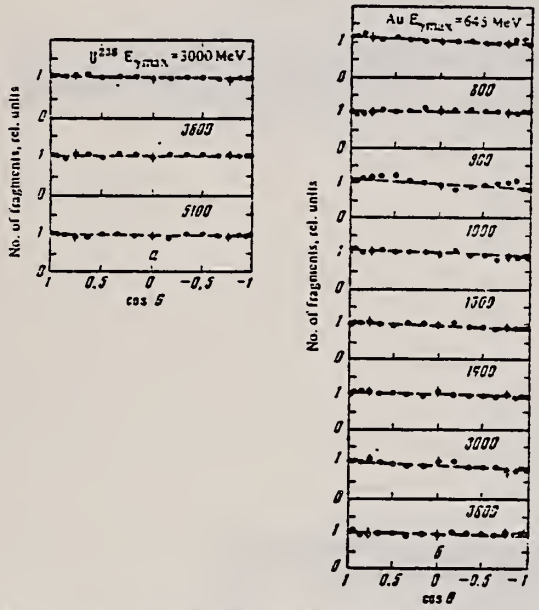

FIG. 2. Angular distributions of fragments from fission of U (a) and Au (b).

Table II

Element	$E_{\gamma\,max}$, MeV	χ^2	$w(\chi^2-\chi^2_Q)$	$a = 2v/V$	$a = 2v/V$ [*]	v, (MeV/nucleon)$^{1/2}$	ε, MeV
U^{238}	3000	0.16	0.99	−0.031±0.025		0.042±0.005	0.160±0.020
	3800	0.55	0.85	0.013±0.017		0.018±0.002	0.045±0.005
	5100	0.59	0.85	0.040±0.017		0.054±0.005	0.306±0.031
Bi^{209}	700	0.93	0.45	0.155±0.017		0.091±0.009	0.851±0.082
	1000	1.14	0.3	0.165±0.017		0.047±0.005	0.227±0.023
	1200	0.76	0.6	0.094±0.020		0.055±0.005	0.314±0.030
	1300	0.91	0.4	0.093±0.018		0.053±0.005	0.311±0.030
	1480	0.62	0.85	0.034±0.018		0.020±0.002	0.116±0.004
Au^{197}	350				0.097±0.010		
	450				0.105±0.010		
	600				0.090±0.010		
	645	0.97	0.55	0.054±0.018		0.044±0.004	0.187±0.016
	700				0.116±0.010		
	800	0.45	0.95	0.008±0.020		0.005±0.001	0.029±0.002
	850				0.121±0.010		
	900	4.50	0.001	0.124±0.018		0.064±0.005	0.400±0.040
	1000	0.95	0.4	0.101±0.017	0.090±0.010	0.052±0.005	0.262±0.025
	1300	0.87	0.4	0.094±0.017		0.049±0.005	0.234±0.024
	1400	0.99	0.5	0.073±0.018		0.039±0.004	0.147±0.015
	3600	1.34	0.15	0.122±0.017		0.065±0.006	0.410±0.040
	3800	0.7	0.65	0.093±0.17		0.048±0.005	0.223±0.022
Ta^{181}	600	0.8	0.5	0.057±0.018		0.044±0.004	0.176±0.018
	700				0.147±0.010		
	1145	5.2	0.001	0.144±0.016		0.072±0.007	0.468±0.047
	1420	1.25	0.15	0.127±0.018		0.064±0.006	0.370±0.037
	5100	2.02	0.001	0.200±0.022		0.100±0.010	0.909±0.090

Note. χ^2 is the value of χ^2 per degree of freedom, $w(\chi^2-\chi^2_Q)$ is the probability of the value of χ^2, $a = 2v/V$ is the anisotropy coefficient, ϵ is the fissioning-nucleus kinetic energy, v is the fissioning-nucleus velocity.

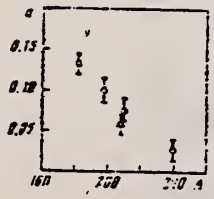

FIG. 3. Anisotropy coefficient as a function of target-nucleus atomic number. Points: O—results of the present work, ● results of Kroon and Forkman [10]

$$a = 2\frac{v}{V}$$

REF.

H. E. Jackson and K. J. Wetzel
Phys. Rev. Letters 28, 513 (1972)

ELEM. SYM.	A	Z
U	238	92

METHOD

REF. NO.: 72 Ja 1 hmg

REACTION	RESULT	EXCITATION ENERGY	SOURCE		DETECTOR		ANGLE
			TYPE	RANGE	TYPE	RANGE	
G,G	ABX	10	D	10	SCD-D		DST
		(10.83)		(10.83)			

RATIO: RAMAN/ELASTIC

We have measured the differential cross sections for the elastic scattering of 10.83-MeV photons by U, Th, and Bi targets and for inelastic scattering to the first excited states of the residual nuclei over a range of scattering angles. The inelastic scattering is found to be significantly weaker than predicted by currently accepted models of the giant dipole resonance.

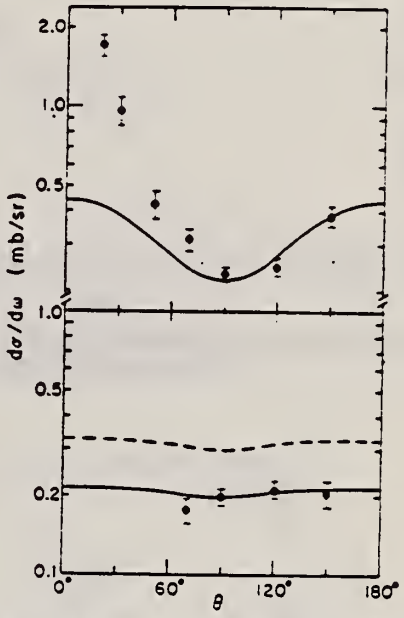

FIG. 2. Differential cross sections for the scattering of 10.83-MeV photons by a U target. The values of the experimental differential cross sections (points) are 0.18 ± 0.02, 0.20 ± 0.02, 0.21 ± 0.02, and 0.20 ± 0.02 mb/sr for Raman scattering at $\theta = 70°$, 90°, 120°, and 150°, respectively, and $d\sigma/d\omega = 1.72 \pm 0.17$, 0.97 ± 0.12, 0.43 ± 0.05, 0.31 ± 0.03, 0.23 ± 0.02, 0.25 ± 0.02, and 0.39 ± 0.04 mb/sr for elastic scattering at 20°, 30°, 50°, 70°, 90°, 120°, and 150°, respectively. The solid curves for both the elastic scattering (upper curve) and nuclear Raman scattering (lower curve) show the angular dependence expected for scattering via a 1⁻ giant dipole state. Elastic scattering at forward angles is enhanced by Delbrück scattering (see Ref. 3). The dashed curve indicates the value of the Raman cross section predicted by theoretical models (see text) if $[d\sigma(90°)/d\omega]_{el} = 0.23$ mb/sr as observed.

REF.

A. M. Khan and J. W. Knowles
Nucl. Phys. A179, 333 (1972)

ELEM. SYM.	A	Z
U	238	92

METHOD

REF. NO. 72 Kh 1 egf

REACTION	RESULT	EXCITATION ENERGY	SOURCE		DETECTOR		ANGLE
			TYPE	RANGE	TYPE	RANGE	
G,F	ABX	THR-9	D	5-9	ION-I		4PI

542

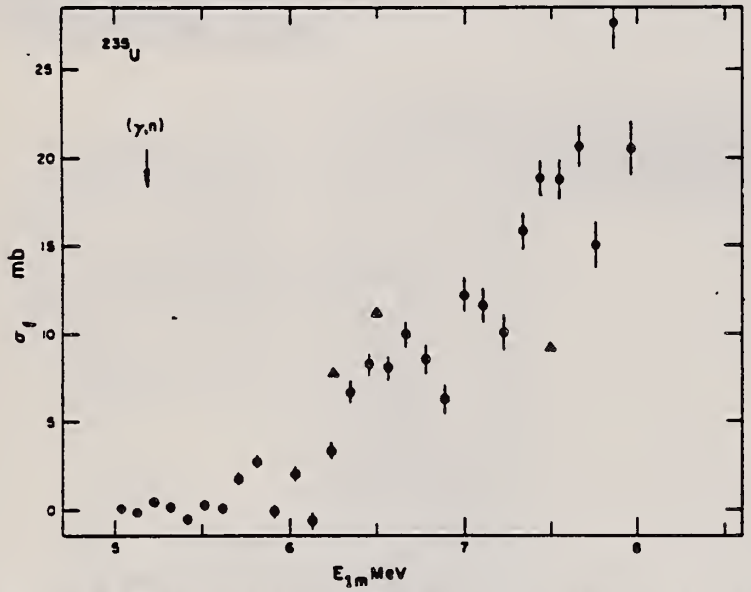

Fig. 11. Absolute photofission cross-section measurements σ_f of ^{235}U as a function of E_{1m}. The points △ are measurements of Bowman *et al.*[13])

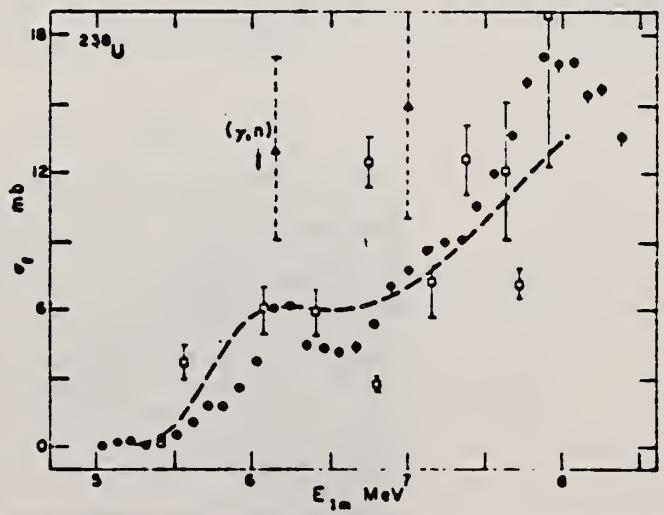

Fig. 10. Absolute photofission cross-section measurements σ_f of ^{238}U as a function of E_{1m}. The broken line represents measurements of Rabotnov *et al.*[8]); the points □ and △ are measurements of Manfredini *et al.*[7]) and Huizenga *et al.*[14]) respectively.

[7] A. Manfredini, L. Fiore, C. Ramorino, H.G. DeCarvalho & W. Wolfli, Nucl. Phys. A127 (1969) 637.

[8] N.S. Rabotnov, G.N. Smirenkin & A.S. Soldatov et al., Proc. Symp. on phys. and chem. of fission, SM 60/81, Vienna, 1965, p.135.

[13] J. R. Huizenga, K.M. Clarke, J.E. Gindler and R. Vandenbosch, Nucl. Phys. 34, (1962) 439.

[14] A.S. Soldatov, Z.A. Aleksandrova, L.D. Gordeeva & G.N. Smirenkin, Sov. J. Nucl. Phys. 1 (1965) 335.

REF.

O.Y. Mafra, S. Kuniyoshi and J. Goldemberg
Nucl. Phys. A186, 110 (1972)

ELEM. SYM.	A	Z
U	238	92

METHOD

REF. NO.: 72 Ma 1 | egf

REACTION	RESULT	EXCITATION ENERGY	SOURCE		DETECTOR		ANGLE
			TYPE	RANGE	TYPE	RANGE	
G,F	ABX	5-9	D	5-9	ION-I		4PI
G,N	ABX	5-9	D	5-9	BF3-I		4PI

TABLE 4
Principal γ-ray energies and uranium and thorium Γ_n/Γ_f ratios

E(MeV)	Uranium Γ_n/Γ_f	Thorium Γ_n/Γ_f
6.07	1.3 ± 0.4	
6.42	1.1 ± 0.5	2.0 ± 0.8
6.73	2.1 ± 0.6	3.2 ± 0.6
6.83	1.9 ± 0.6	
7.23	1.7 ± 1.1	2.9 ± 1.4
7.38	2.1 ± 0.5	5.5 ± 1.0
7.64	2.2 ± 0.8	3.8 ± 0.9
7.72	2.1 ± 0.4	5.1 ± 1.0
7.88	2.3 ± 0.7	5.1 ± 1.0
9.00	2.5 ± 0.7	6.3 ± 2.0

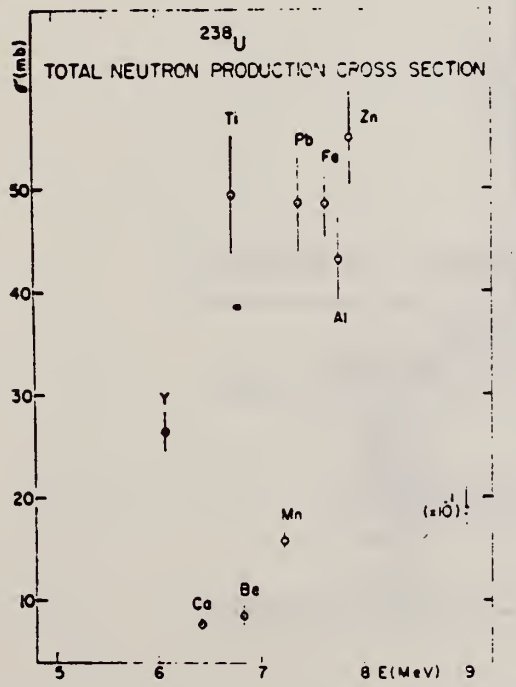

Fig. 8. Total neutron production cross section for ^{238}U. Element symbols indicate the sources of neutron capture γ rays whose energies are listed in table 1

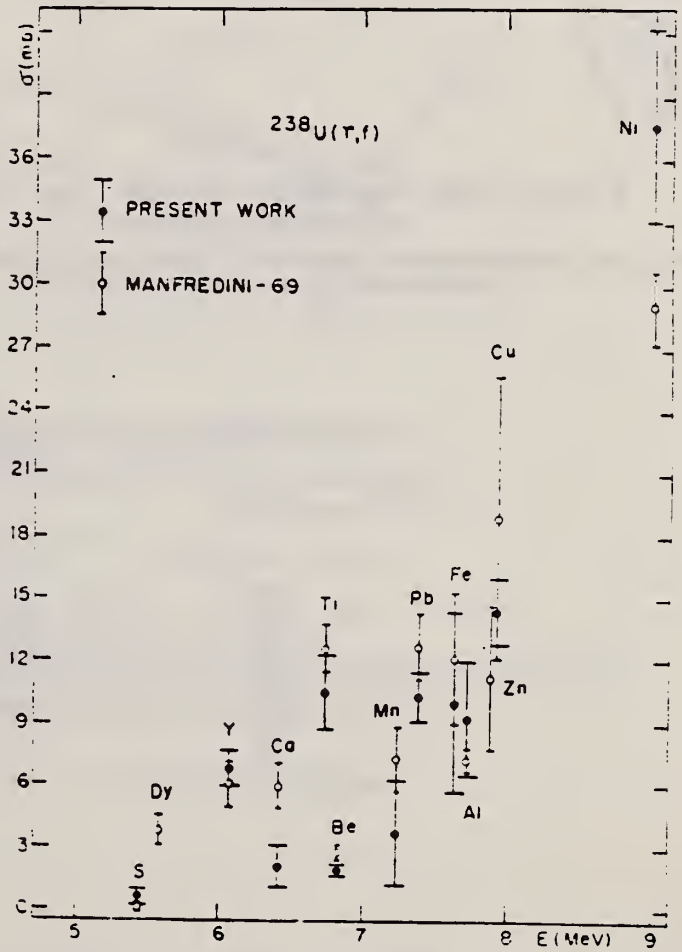

Fig. 9. Photofission cross sections of ^{238}U compared with Manfredini's results. Element symbols indicate the sources of neutron capture γ-rays whose energies are listed in table 1

REF.

B. Schroder, B. Nordgren, A. Alm
Nucl. Phys. A193, 555 (1972)

ELEM. SYM.	A	Z
U	238	92

METHOD

REF. NO. 72 Sc 5 egf

REACTION	RESULT	EXCITATION ENERGY	SOURCE TYPE	SOURCE RANGE	DETECTOR TYPE	DETECTOR RANGE	ANGLE
a G,F	ABY	THR-700	C	150-700	ACT-D		4PI
G,N	ABY	THR-700	C	150-700	ACT-D		4PI

a FISSION PRODUCTS

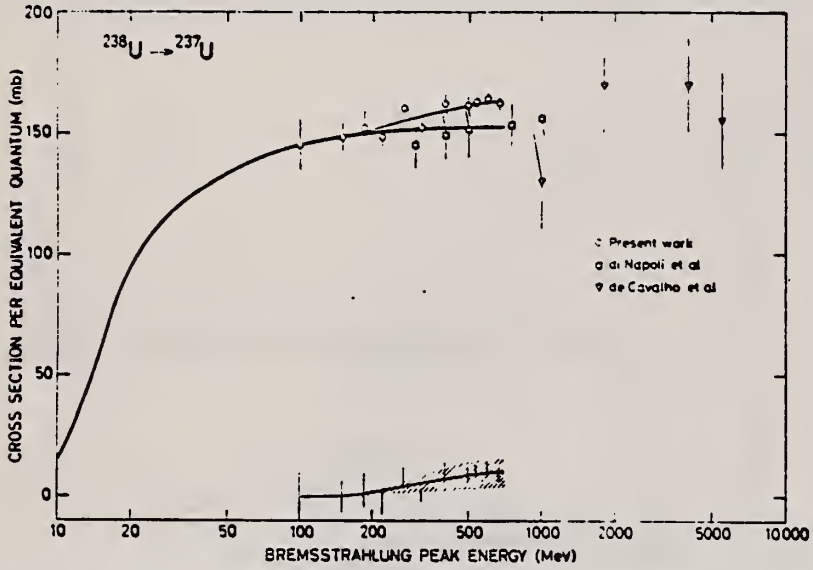

Fig. 1. Cross sections per equivalent quantum from Di Napoli *et al.* [14]), de Carvalho *et al.* [13]) and the present study. The notation is explained in the text.

TABLE 2

Average cross sections and their standard deviations in the energy intervals E = 200-500 MeV and E = 500-700 MeV

Nuclide	Average cross section E = 200-500 MeV	E = 500-700 MeV
^{91}Sr	3.1 ± 0.5	−1.3 ± 2.7
^{92}Sr	2.3 ± 0.1	1.7 ± 0.6
^{97}Zr	3.6 ± 0.2	1.5 ± 0.9
^{105}Ru	3.6 ± 0.4	3.0 ± 1.8
^{132}Te	1.4 ± 0.2	0.6 ± 1.1
^{135}I	1.9 ± 0.2	−1.3 ± 1.1
^{143}Ce	1.5 ± 0.3	
^{237}U	13 ± 5	− 4.0 ± 15

(over)

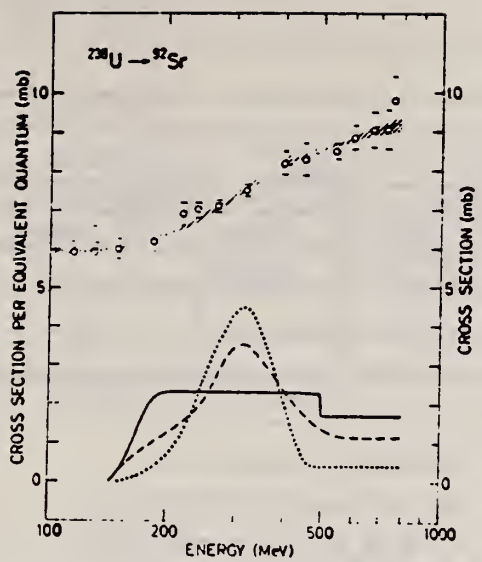

Fig. 2. The σ_0 values for the production of ^{92}Sr. The shaded area represents the variation in the σ_0 values calculated from the three different cross sections (see the text) shown in the bottom of the figure.

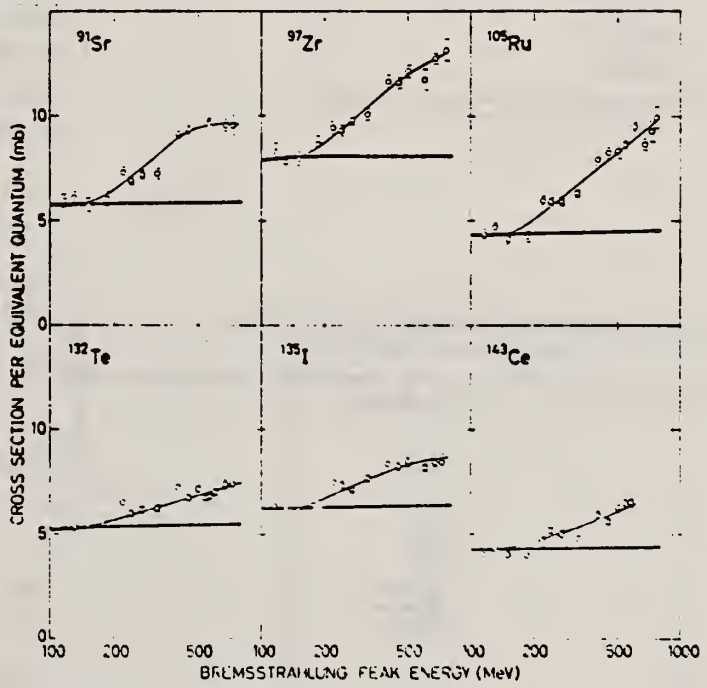

Fig. 4. Cross section per equivalent quantum values for some fission products as a function of the maximum bremsstrahlung energy. The thick solid line gives the contribution to σ_0 from cross sections below 150 MeV and the thin solid line the calculated yields.

REF. A. Alm, T. Kivikas, L.J. Lindgren
PICNS-73, Vol.I, p. 645 Asilomar

ELEM. SYM.	A	Z
U	238	92

METHOD

REF. NO.	
73 A1 5	hmg

REACTION	RESULT	EXCITATION ENERGY	SOURCE		DETECTOR		ANGLE
			TYPE	RANGE	TYPE	RANGE	
G,F	RLY	THR- 7	C	4- 7	ACT-I		4PI

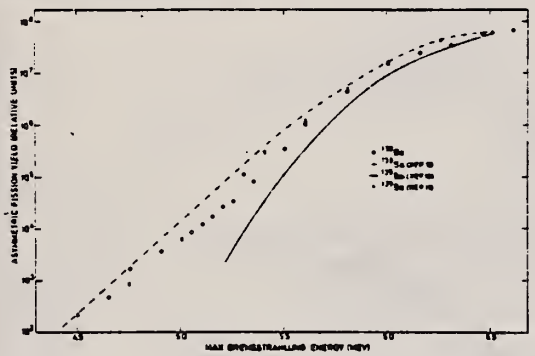

Figure 1. Asymmetric fission yield.
The references are taken from
A Alm et al (to be published)

9. R A Schmitt, R B Duffield
Phys Rev 105(1957)1277
10. T Kivikas, B Forkman
Nucl Phys 64 (1965) 420
11. Kurchatov et al
Sovj Journ Nucl Phys
7 (1968) 326

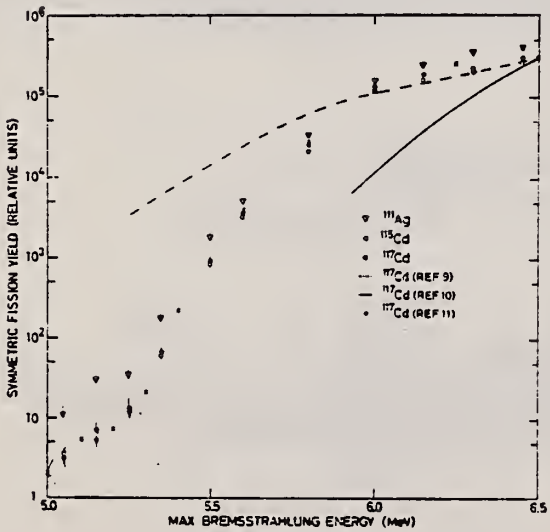

Figure 2. Symmetric fission yield.

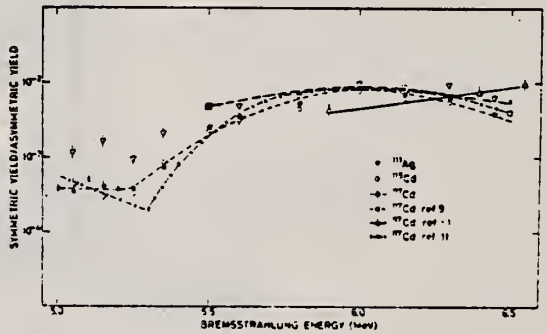

Figure 3. Valley to peak ratio as a function of max bremsstrahlung energy.

REF.

A. Alm and T. Kivikas
Nucl. Phys. A215, 461 (1973)

ELEM. SYM.	A	Z
U	238	92

METHOD

REF. NO. 73 A1 12 egf

REACTION	RESULT	EXCITATION ENERGY	SOURCE		DETECTOR		ANGLE
			TYPE	RANGE	TYPE	RANGE	
G,F	RLY	0- 7	C	4- 7	ACT-I		4PI

Yield tables all normalized at 6 MeV.

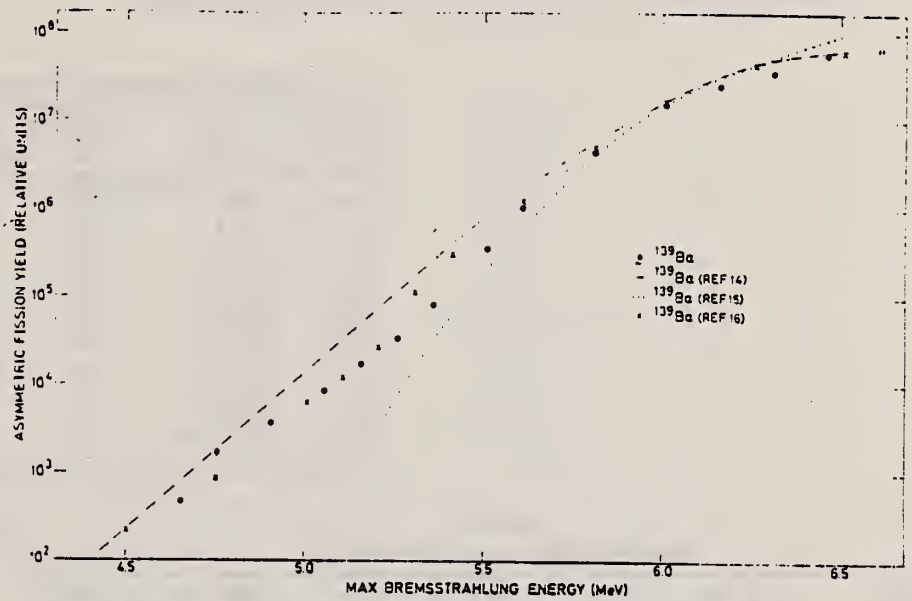

Fig. 1. The yield of the asymmetric fission product ^{139}Ba as a function of maximum bremsstrahlung energy.

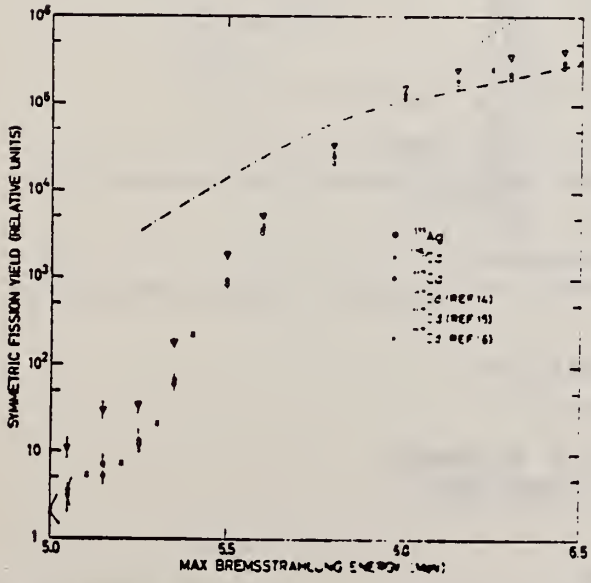

Fig. 2. The yields of the symmetric fission products ^{111}Ag, ^{118}Cd and ^{117}Cd as functions of maximum bremsstrahlung energy.

(over)

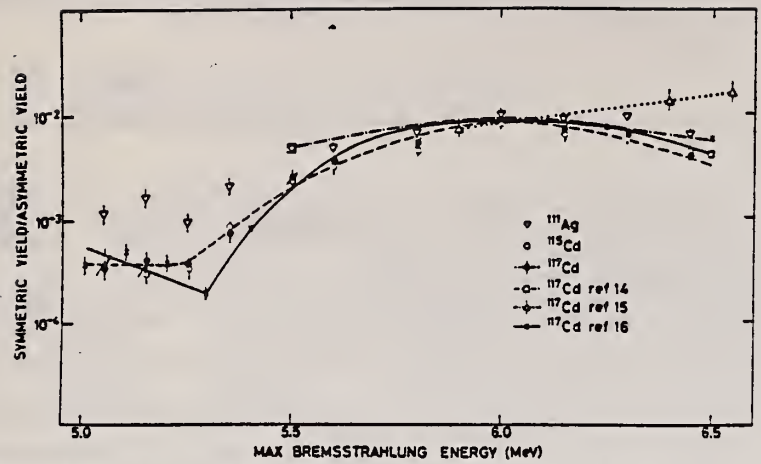

Fig. 3. The ratio between yields of the symmetric fission products ^{111}Ag, ^{115}Cd and ^{117}Cd and the asymmetric fission product ^{139}Ba as functions of maximum bremsstrahlung energy.

TABLE 2

Yields of fission products ^{111}Ag and ^{115,117}Cd, normalized as stated in the text

Energy (MeV)	^{111}Ag (c/min)	Error (%)	^{115}Cd (c/min)	Error (%)	^{117}Cd (c/min)	Error (%)
5.05	10.5	14.8	3.60	23.2	3.20	25.6
5.15	29.8	14.5	5.30	21.3	7.20	24.5
5.25	34.3	13.3	12.0	17.1	13.5	20.3
5.35	1.75×10^{2}	11.9	71.0	15.0	61.5	13.4
5.50	1.79×10^{3}	7.1	8.71×10^{2}	10.0	9.30×10^{2}	10.4
5.60	5.06×10^{3}	5.0	3.35×10^{3}	7.0	3.60×10^{3}	6.0
5.80	3.31×10^{4}	5.0	2.15×10^{4}	5.0	2.58×10^{4}	5.3
6.00	1.58×10^{5}	5.0	1.28×10^{5}	5.0	1.33×10^{5}	5.0
6.15	2.96×10^{5}	5.0	1.66×10^{5}	5.0	1.90×10^{5}	5.0
6.30	3.61×10^{5}	5.0	2.12×10^{5}	5.0	2.38×10^{5}	5.0
6.45	4.01×10^{5}	5.0	2.74×10^{5}	5.0	3.12×10^{5}	5.0

TABLE 3

Valley-to-peak ratio in photofission of ^{238}U

Energy (MeV)	^{111}Ag/^{139}Ba	Error (%)	^{115}Cd/^{139}Ba	Error (%)	^{117}Cd/^{139}Ba	Error (%)
5.05	1.17×10^{-3}	19.8	0.43×10^{-3}	28.2	0.36×10^{-3}	30.0
5.15	1.66×10^{-3}	19.5	0.30×10^{-3}	26.3	0.40×10^{-3}	29.5
5.25	0.95×10^{-3}	18.3	0.33×10^{-3}	22.1	0.38×10^{-3}	25.3
5.35	2.09×10^{-3}	16.9	0.85×10^{-3}	20.0	0.74×10^{-3}	18.4
5.50	4.84×10^{-3}	12.1	2.35×10^{-3}	15.0	2.51×10^{-3}	15.4
5.60	4.92×10^{-3}	10.0	3.05×10^{-3}	12.0	3.50×10^{-3}	11.0
5.80	6.75×10^{-3}	10.0	4.39×10^{-3}	10.0	5.30×10^{-3}	10.3
6.00	9.78×10^{-3}	10.0	7.90×10^{-3}	10.0	8.20×10^{-3}	10.0
6.15	9.80×10^{-3}	10.0	6.05×10^{-3}	10.0	6.95×10^{-3}	10.0
6.30	9.40×10^{-3}	10.0	5.10×10^{-3}	10.0	6.20×10^{-3}	10.0
6.45	6.30×10^{-3}	10.0	4.30×10^{-3}	10.0	4.90×10^{-3}	10.0

[14] R.A. Schmitt and R.B. Duffield, Phys. Rev. 105 (1957) 1277.

[15] T. Kivikas and B. Forkman, Nucl. Phys. 64 (1965) 420.

[16] B.V. Kurchatov, V.I. Novgorodtseva, V.A. Pchelin, G.N. Smirenkin, Yu. M. Tsipenyuk and V.M. Shubko, Sov. J. Nucl. Phys. 7 (1968) 326.

REF.

R.A. Anderl, M.V. Yester, and R.C. Morrison
Nucl. Phys. A212, 221 (1973)

ELEM. SYM.	A	Z
U	238	92

METHOD

REF. NO. 73 An 13 egf

REACTION	RESULT	EXCITATION ENERGY	SOURCE		DETECTOR		ANGLE
			TYPE	RANGE	TYPE	RANGE	
G,F	ABX	5- 8	D	5- 8	SCD-I		4PI

833

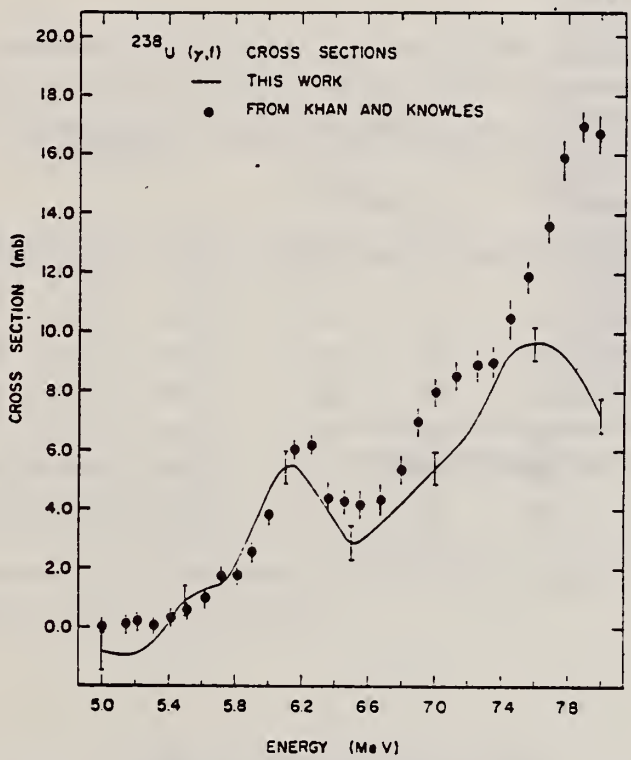

Fig. 3. Comparison of the ^{238}U photofission cross section from this work with that from Khan and Knowles [13]).

[13] A.M. Khan and J.W. Knowles, Nucl. Phys. A179 (1972) 333.

(over)

TABLE 1

Photofission cross sections of ^{238}U and ^{235}U

Energy (MeV)	^{238}U cross section (mb)	^{235}U cross section (mb)
5.0	−0.8±0.6	−0.4±1.9
5.1	−0.9±0.5	0.3±1.6
5.2	−0.9±0.4	1.4±1.3
5.3	−0.5±0.4	2.5±1.0
5.4	0.2±0.5	3.2±0.9
5.5	0.9±0.5	3.6±1.0
5.6	1.2±0.6	3.9±1.1
5.7	1.4±0.6	4.6±1.3
5.8	2.1±0.5	6.0±1.3
5.9	3.2±0.5	7.3±1.3
6.0	4.6±0.5	6.9±1.3
6.1	5.4±0.6	5.1±1.3
6.2	5.2±0.6	3.4±1.3
6.3	4.5±0.6	3.4±1.3
6.4	3.6±0.6	5.4±1.4
6.5	3.1±0.6	8.1±1.4
6.6	3.2±0.6	9.5±1.5
6.7	3.7±0.6	9.4±1.5
6.8	4.3±0.6	8.6±1.5
6.9	4.9±0.6	8.1±1.5
7.0	5.3±0.5	9.5±1.5
7.1	5.9±0.6	12.7±1.5
7.2	6.6±0.6	17.2±1.5
7.3	7.7±0.6	22.6±1.5
7.4	8.9±0.6	26.9±1.5
7.5	9.5±0.6	28.4±1.5
7.6	9.6±0.6	27.0±1.5
7.7	9.5±0.6	23.3±1.4
7.8	9.0±0.5	18.4±1.5
7.9	8.2±0.5	13.6±1.6
8.0	7.2±0.6	10.0±1.8

The relative errors only are given. The ±30% error in the absolute scale has not been included.

REF. T. Bar-Noy and R. Moreh
PICNS-73, Vol.I, p.319 Asilomar

ELEM. SYM.	A	Z
U	238	92

METHOD

REF. NO. 73 Ba 9 hmg

REACTION	RESULT	EXCITATION ENERGY	SOURCE		DETECTOR		ANGLE
			TYPE	RANGE	TYPE	RANGE	
G,G	ABX	7- 12	D	7- 12	SCD-D		140

Table 1. Measured differential cross sections (μb/st.) from ^{238}U target at an angle of 140°. The values at 10.83 MeV were taken from Ref. 2. The calculated values using the GDR parameters of ^{235}U, ^{238}U and a set of tentative parameters found in the present work are shown.

E_γ (MeV)	Experiment		Predicted					
			^{235}U(Ref.5)		^{238}U(Ref.6)		Tentative	
	Elastic	Raman	Elastic	Raman	Elastic	Raman	Elastic	Raman
7.92	2^{+2}_{-1}	3^{+2}_{-1}	8.2	6.9	5.6	5.0	5.7	5
8.53	8±3	10±5	24	15	17	11	18	11
9.00	29±4	20±3	49	28	36	20	36	20
9.30	55±15	25±7	74	43	54	28	55	29
10.06	140±60	80±40	186	125	132	72	145	83
10.83	350±40	200±20	315	275	227	157	295	212
11.39	320±40	260±30	302	324	256	198	332	282

5. C. D. Bowmann, G. F. Auchampaugh and S. C. Fultz, Phys. Rev. 133, B676 (1964).

6. R. Bergere, private communication.

Table 2. The GDR parameters used in the present calculation

Parameters	^{235}U (Ref.5)	^{238}U (Ref.6)	Tentative
E_1	10.85	10.96	11.1
Γ_1	2.45	2.90	2.5
E_2	14.1	14.04	14.2
Γ_2	4.0	4.53	4.6
β	1.25	1.18	1.22

REF. J.T. Caldwell, G.M. Worth, and E.J. Dowdy
PICNS-73, Vol.I, p.651 Asilomar

ELEM. SYM.	A	Z
U	238	92

METHOD

REF. NO. 73 Ca 2 hmg

REACTION	RESULT	EXCITATION ENERGY	SOURCE		DETECTOR		ANGLE
			TYPE	RANGE	TYPE	RANGE	
G,N	NOX	THR- 12	C	8- 12	BF3-I		4PI
G,F	NOX	THR- 12	C	8- 12	BF3-I		4PI

TABLE I

Low Energy Photoneutron and Photofission Parameters Deduced from this Experiment

Isotope	E_c (MeV)	Prompt $\bar{\nu}$	Γ_n/Γ_f	Delayed Neutrons Per Photofission
^{238}U	8	2.683±.094	1.765±.136	0.0355±.0015
^{238}U	10	2.861±.087	2.813±.161	0.0368±.0023
^{238}U	12	3.087±.079	3.250±.150	0.0319±.0023
^{235}U	8	2.675±.095	1.061±.103	0.0101±.0011
^{235}U	10	2.936±.085	1.181±.067	0.0121±.0017
^{235}U	12	3.086±.079	1.224±.079	0.0110±.0020
^{232}Th	8	2.091±.112	1.085±.147	0.0324±.0017
^{232}Th	10	1.980±.115	4.017±.266	0.0309±.0019
^{232}Th	12	2.226±.113	6.781±.577	0.0292±.0038
^{239}Pu	10	3.603±.083	----------	----------
^{239}Pu	12	3.738±.075	0.7±0.4	----------

REF.	ELEM. SYM.	A	Z
P. David, J. Debrus, F. Lubke, H. Mommsen, R. Schoenmackers and G. Stein PICNS-73, Vol.II, p.985 (1973) Asilomar	U	238	92

METHOD	REF. NO.	
	73 Da 6	egf

REACTION	RESULT	EXCITATION ENERGY	SOURCE		DETECTOR		ANGLE
			TYPE	RANGE	TYPE	RANGE	
G,F	ABY	THR* 2	C	1* 2	TRK-I		4PI

ENERGIES IN GEV

The total photofission cross sections of ^{197}Au and ^{238}U were measured for E_{γ}^{max} = 0.8 to 2.2 GeV (fig. 1). The fission cross sections and the fissionabilities are $\sigma_f^{Au} = 1.4 \pm 0.1$ mb, $f^{Au} = (2.1 \pm 0.3)\ 10^{-2}$; $\sigma_f^{U} = 43.2 \pm 4.4$ mb, $f^{U} = 1.04 \pm 0.1$.

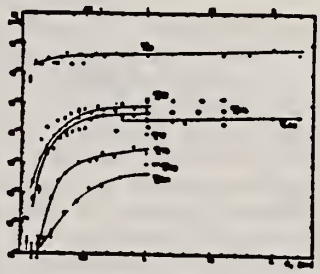

Fig.1:Total photofission cross section σ_q

REF. T. Gozani, R.L. Bramblett, R.O. Ginaven, and D.E. Rundquist
PICNS-73, Vol.I, p.649 Asilomar

ELEM. SYM.	A	Z
U	238	92

METHOD

REF. NO. 73 Go 2 hmg

REACTION	RESULT	EXCITATION ENERGY	SOURCE		DETECTOR		ANGLE
			TYPE	RANGE	TYPE	RANGE	
G,N	RLY	THR- 7	C	5- 7	BF3-I		4PI

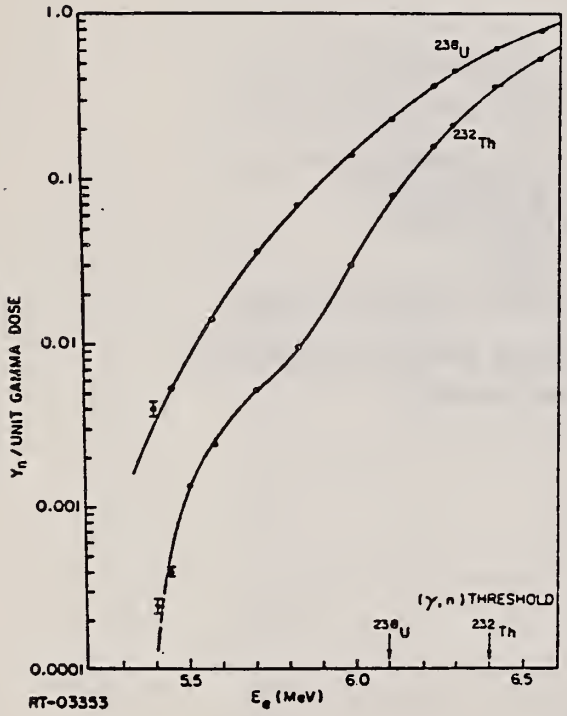

FIG. 1. Prompt neutron yields induced by low-energy electron bremsstrahlung in ^{238}U and ^{232}Th (the statistical errors are shown when larger than the drawn points)

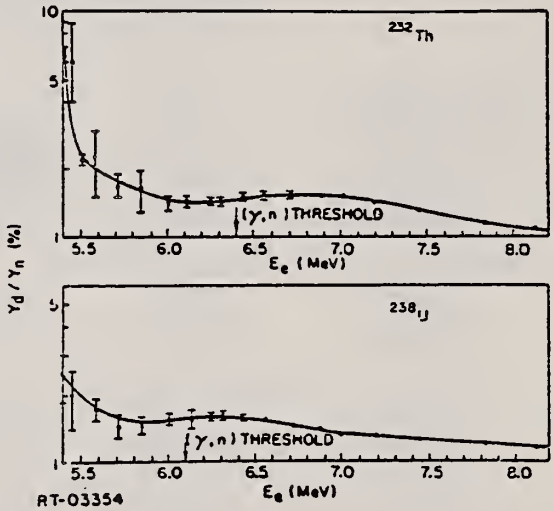

FIG. 2. Bremsstrahlung-averaged delayed neutron fraction

(over)

Since 1968 effort has been devoted at Radiation Technology to measurements of some basic integral quantities related to the low-energy photofission phenomena. The interest in this domain evolves from the application of photoinduced reactions to the nondestructive assay of nuclear materials. The most sensitive energy region for the identification of the various isotopes is around and below the photofission barrier (about 6 MeV). In this region, slight differences in the barrier height or width will cause large differences in the photofission cross sections. The only practical intense source of low-energy photons is bremsstrahlung from low-energy electron accelerators. With such devices the measured quantities are yields. However, in the energy region of importance, especially below the fission barrier, the fission cross section is a very steep function of energy; its integrated product with the bremsstrahlung spectrum, $\phi_B(E,E_e)$, rather closely resembles the fission cross section itself with an effective resolution which broadens as the energy increases. The fission yields were measured[1] simultaneously with the prompt (Y_n) and delayed (Y_d) neutron yields in a moderated neutron detector:

$$Y_n \propto \int_0^{E_e} \left[\nu(E)\sigma_{\gamma,f}(E) + \sigma_{\gamma,n}(E)\right] \phi_B(E,E_e)dE$$

and

$$Y_d \propto \int_0^{E_e} \beta(E)\nu(E)\sigma_{\gamma,f}(E)\phi_B(E,E_e)dE \quad ,$$

where β is the fractional yield of delayed neutrons per prompt neutrons, while the other symbols are the usual ones. The delayed neutron yield, as well as the prompt neutron yield (Fig. 1), indicates the existence of a structure in the subthreshold region of ^{232}Th. This agrees well with Rabotnov *et al.*[2] measurement and our previous fission yield measurement.[1] A plausible explanation[2] for this structure is the existence of a vibrational resonance in this region creating a shallow double hump potential barrier. Ratios of the various yields furnish important integral quantities such as the bremsstrahlung-averaged, effective delayed neutron yield, $\beta(E)$, and averaged number of prompt neutrons, $\nu(E)$, per fission. The former is shown in Fig. 2, which shows a substantial increase toward low excitation energies. Similarly, a certain amount of structure in $\nu(E)$ has been observed in ^{232}Th and ^{238}U in the subthreshold region. This paper presents the techniques used and the complete results obtained, as well as an intercomparison to the small amount of available previous data.

---

[1] T. Gozani *et al.*, Bull. Am. Phys. Soc. 14, 4 (1969).

[2] S. P. Kapitza *et al.*, Soviet Physics - JETP Letters 9, 73 (1969); N. S. Rabotnov *et al.*, Report FEI-170 (1969) - LASL Translation LA-4385-TR (1970).

REF. J.W. Knowles
PICNS-73, Vol.I, p.647 Asilomar

ELEM. SYM.	A	Z
U	238	92

METHOD

REF. NO. 73 Kn 5 hmg

REACTION	RESULT	EXCITATION ENERGY	SOURCE TYPE	SOURCE RANGE	DETECTOR TYPE	DETECTOR RANGE	ANGLE
G,N	ABX	THR- 8	C	5- 8	BF3-I		4PI

INCLUDES G,FN NEUTS

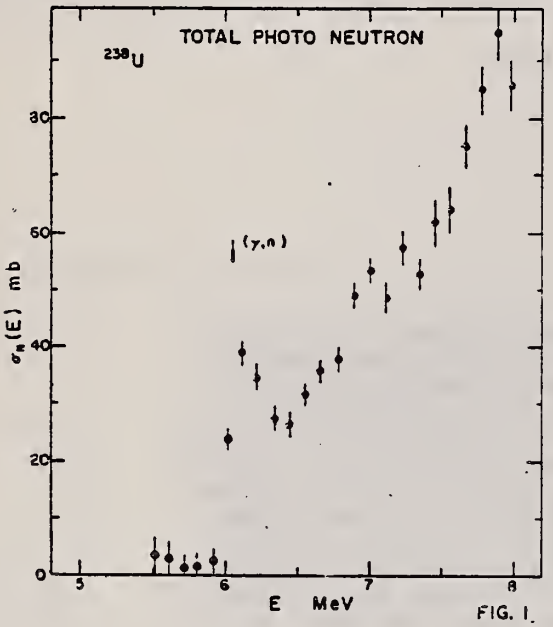

FIG. 1.

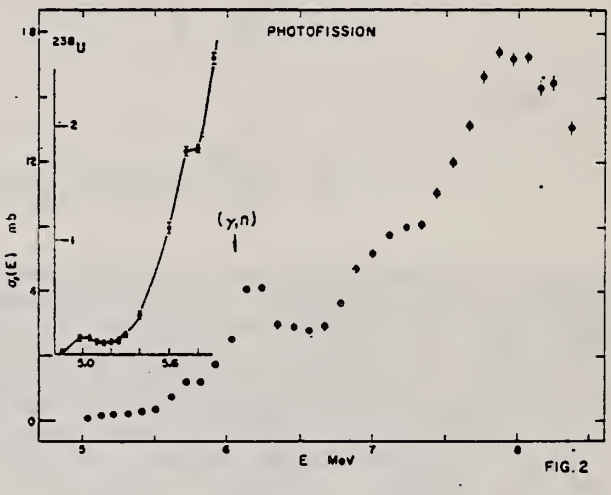

FIG. 2

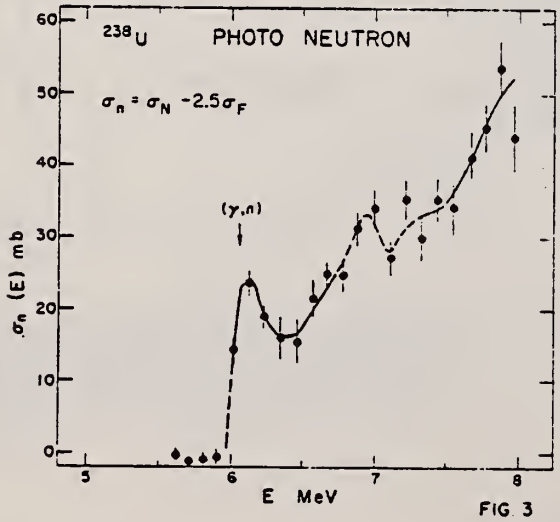

FIG. 3

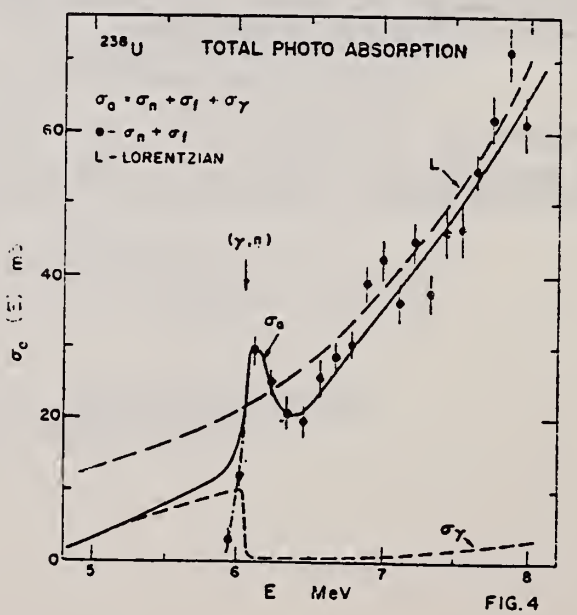

FIG. 4

REF. O.Y. Mafra, M.F. Cesar, S. Kuniyoshi, and J. Goldemberg
PICNS-73, Vol.I, p.643 Asilomar

ELEM. SYM.	A	Z
U	238	92

METHOD

REF. NO.	
73 Ma 8	hmg

REACTION	RESULT	EXCITATION ENERGY	SOURCE		DETECTOR		ANGLE
			TYPE	RANGE	TYPE	RANGE	
G,N	ABX	6- 9	D	6- 9	BF3-I		4PI

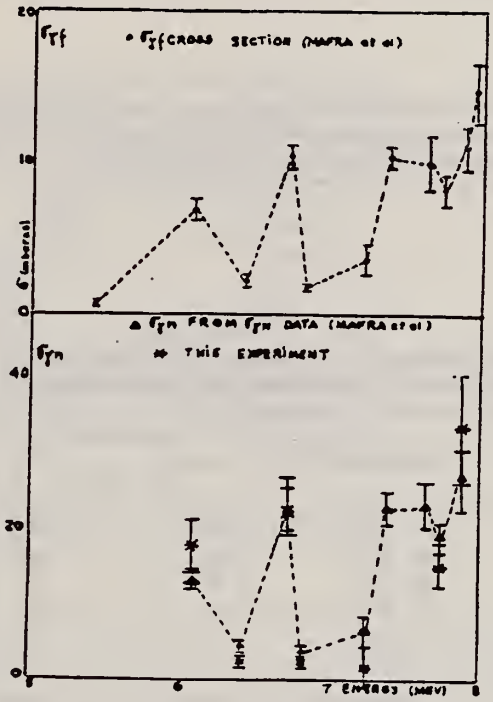

REFERENCES

1. Mafra, O. Y. at al. Nucl.Phys. A186/1 (1972)110

REF. R. Moreh and S. Kahane
Phys. Lett. 47B, 351 (1973)
(See also: 74 Ka 9)

ELEM. SYM.	A	Z
U	238	92

METHOD

REF. NO. 73 Mo 13 egf

REACTION	RESULT	EXCITATION ENERGY	SOURCE		DETECTOR		ANGLE
			TYPE	RANGE	TYPE	RANGE	
G,G	ABX	8	D	8	SCD-D		DST

Saclay data used for nuclear scattering amplitude. 8=7.915

The elastic scattering cross section of 7.9 MeV photons by U and Th was measured in the angular range 25°–140°. It is shown that at this energy the forward elastic scattering is due almost entirely to Delbruck scattering. The results are systematically lower by > 50% than the calculated values. A good agreement with theory was obtained only after excluding the contribution of the real part of the Delbruck scattering amplitude.

Table 1

Measured differential cross sections (μb/sr) for elastic scattering from U and Th targets at various angles. The calculated cross sections with and without the real part of the Delbruck scattering amplitude are also given. The Rayleigh amplitudes were ignored.

Angle (deg.)	Experiment	Calculated without real component	Calculated with real component	Experiment	Calculated without real component	Calculated with real component
25	424 ± 70	490	760	447 ± 90	450	690
35	174 ± 30	170	260	144 ± 40	150	240
45	74 ± 13	70	105	55 ± 15	65	99
60	26 ± 6	26	41	26 ± 9	24	38
75	12.5 ± 3.5	10	21	–	–	–
90	3.5 ± 1.2	4.6	11	3.8 ± 2.7	4.3	10
120	1.7 ± 0.6	1.1	6.2	–	–	–
140	1.5 ± 0.8	1.0	5.5	1.8 ± 1.2	1.0	4.8

REF. David E. Rundquist
PICNS-73, Vol.I, p.619 Asilomar

ELEM. SYM.	A	Z
U	238	92

METHOD

REF. NO. 73 Ru 1 hmg

REACTION	RESULT	EXCITATION ENERGY	SOURCE TYPE	SOURCE RANGE	DETECTOR TYPE	DETECTOR RANGE	ANGLE
G,XN	RLY	THR- 10	C	5- 10	BF3-I		4PI

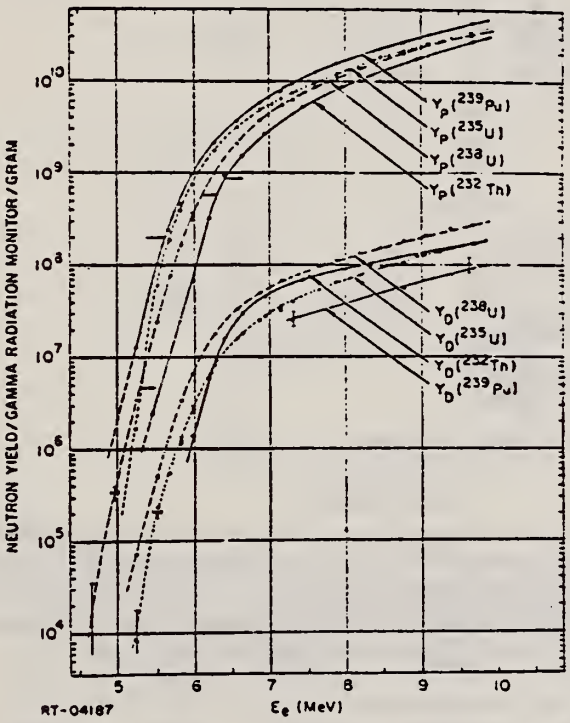

Fig. 1. Prompt and delayed neutron yields in fissile and fertile material produced by bremsstrahlung from electrons of energy E_e

REF. A. Veyssiere, H. Beil, R. Bergere, P. Carlos, A. Lepretre and K. Kernbath
Nucl. Phys. A199, 45 (1973)

ELEM. SYM.	A	Z
U	238	92

METHOD

REF. NO. 73 Ve 1 egf

REACTION	RESULT	EXCITATION ENERGY	SOURCE TYPE	SOURCE RANGE	DETECTOR TYPE	DETECTOR RANGE	ANGLE
G,N	ABX	8- 19	D	8- 19	MOD-I		4PI
G,2N	ABX	8- 19	D	8- 19	MOD-I		4PI
G,F	ABX	8- 19	D	8- 19	MOD-I		4PI

(γ,n) 495+
(γ,2n) 496+
(γ,f) 497+
(γ,tot) 498

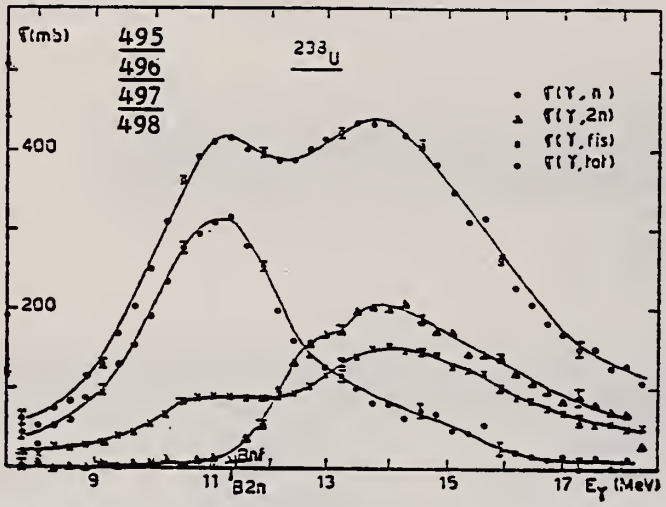

Fig. 4. Partial and total photonuclear cross sections $\sigma(\gamma, n)$, $\sigma(\gamma, 2n)$, $\sigma(\gamma, F)$ and $\sigma_{tot} = \sigma(\gamma, n) + \sigma(\gamma, 2n) + \sigma(\gamma, F)$ of $^{238}_{92}U$.

TABLE 3
Lorentz line parameters and quadrupole moments for ^{232}Th, ^{238}U and ^{237}Np

	E_1 (MeV)	σ_1 (mb)	Γ_1 (MeV)	E_2 (MeV)	σ_2 (mb)	Γ_2 (MeV)	$R = \frac{\frac{1}{2}\pi\sigma_2\Gamma_2}{\frac{1}{2}\pi\sigma_1\Gamma_1}$	Q_0 [a]	Q_0 [b]
$^{232}_{90}Th$	11.08±0.12	268±7	3.37±0.22	14.07±0.14	349±9	4.62±0.16	1.8±0.15	10.2±1	9.66±0.1
$^{238}_{92}U$	10.96±0.09	301±6	2.90±0.14	14.04±0.13	369±6	4.53±0.13	1.9±0.1	11 ±1	11.3 ±0.1
$^{237}_{93}Np$	11.06±0.12	251±7	3.16±0.27	14.21±0.14	380±9	5.12±0.3	2.4±0.3	11.3±1	10.9 ±0.7

[a]) This experiment.
[b]) Ref. [21]).

[21] K.E.G. Löbner et al., Nucl.Data Tables 7, 5 (1970).

TABLE 4
Integrated cross sections of ^{232}Th, ^{238}U and ^{237}Np

	σ_0 [a]) (MeV · b)	σ_{-1} [a]) (mb)	σ_{-1} [a]) (mb · MeV^{-1})	$\sigma_0 = \frac{1}{2}\pi(\sigma_1\Gamma_1+\sigma_2\Gamma_2)$ [b]) (MeV · b)	0.06 NZ/A (MeV · b)	$\frac{\sigma_0}{0.006\,NZ/A}$	$\frac{\sigma'_0}{0.006\,NZ/A}$
$^{232}_{90}Th$	2.50±0.25	198±20	16±2	3.95±0.3	3.31	0.76±0.07	1.19±0.08
$^{238}_{92}U$	2.98±0.15	235±15	19±1.5	3.99±0.15	3.39	0.88±0.05	1.18±0.04
$^{237}_{93}Np$	2.60±0.35	204±30	16±3	4.30±0.4	3.39	0.77±0.12	1.27±0.1

[a]) Values obtained by integrating $\sigma(\gamma, \text{total})$ from 8 to 18 MeV for ^{238}U and from 9 to 16 MeV for ^{232}Th and ^{237}Np.
[b]) Surface under the two Lorentz lines.

REF. T. Bar-Noy and R. Moreh
Nucl. Phys. A229, 417 (1974)

ELEM. SYM.	A	Z
U	238	92

METHOD

REF. NO. 74 Ba 6 egf

REACTION	RESULT	EXCITATION ENERGY	SOURCE		DETECTOR		ANGLE
			TYPE	RANGE	TYPE	RANGE	
G,G	ABX	8- 11	D	8- 11	SCD-D		DST

RAMAN SCTNG

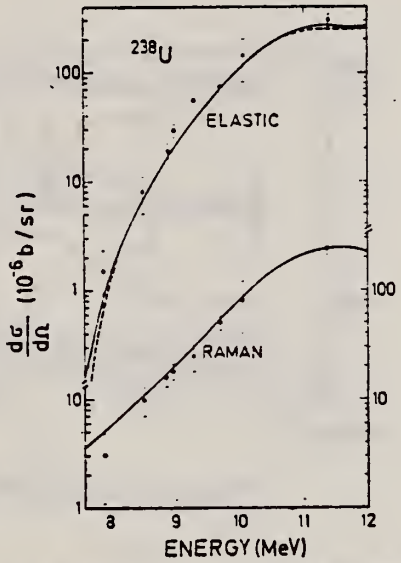

Fig. 3. Differential elastic and Raman photon scattering cross sections for ^{238}U. For the elastic cross section, the solid curve represents the values obtained by including the amplitudes of Thomson, nuclear resonance (according to the SRM) and the imaginary part only of Delbruck scattering (the contribution of the real Delbruck amplitudes was excluded). Dashed curves are similar results with the nuclear resonance amplitudes calculated by the DCM. For Raman scattering, the solid curve represents the results of both the SRM and the DCM.

REF.		ELEM. SYM.	A	Z
	G.M. Gurevich, L.E. Lazareva, V.M. Mazur, and G.V. Solodukhov ZhETF Pis. Red. 20, 741 (1974) JETP Lett. 20, 343 (1974)	U	238	92

METHOD	REF. NO.	
	74 Gu 11	hmg

REACTION	RESULT	EXCITATION ENERGY	SOURCE		DETECTOR		ANGLE
			TYPE	RANGE	TYPE	RANGE	
G,MU-T	ABX	8- 24	C	35	NAI-D		4PI

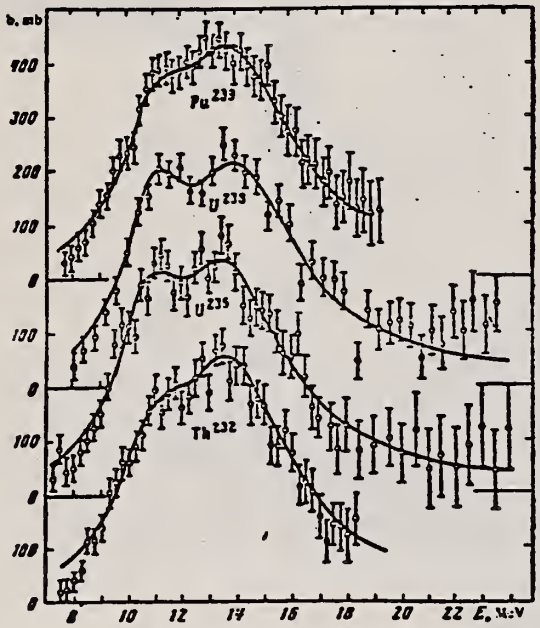

FIG. 1.

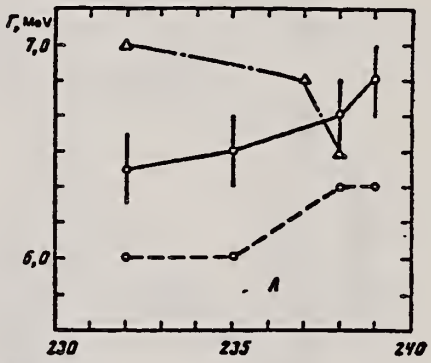

FIG. 2.

TABLE. Parameters for the approximation of the cross section by Lorentz lines.

Nucleus	σ_1 mb	Γ_1 MeV	E_1 MeV	σ_2 mb	Γ_2 MeV	E_2 MeV	$\frac{\sigma_2\Gamma_2}{\sigma_1\Gamma_1}$	β	Q
Th^{232}	247	3.90	10.99	362	4.67	13.9	1.75	0.26	10.0
U^{235}	283	3.23	10.74	354	4.92	13.77	1.91	0.30	11.0
U^{238}	286	2.99	10.97	351	5.10	14.25	2.09	0.31	11.7
Pu^{233}	227	3.47	11.05	362	5.23	14.01	2.40	0.29	11.0

REF.

H.E. Jackson, G.E. Thomas, and K.J. Wetzel
Phys. Rev. C9, 1153 (1974)

ELEM. SYM.	A	Z
U	238	92

METHOD

REF. NO. 74 Ja 2 hmg

REACTION	RESULT	EXCITATION ENERGY	SOURCE		DETECTOR		ANGLE
			TYPE	RANGE	TYPE	RANGE	
G,G	ABX	10	D	10	SCD-D		DST
		(10.83)		(10.83)			

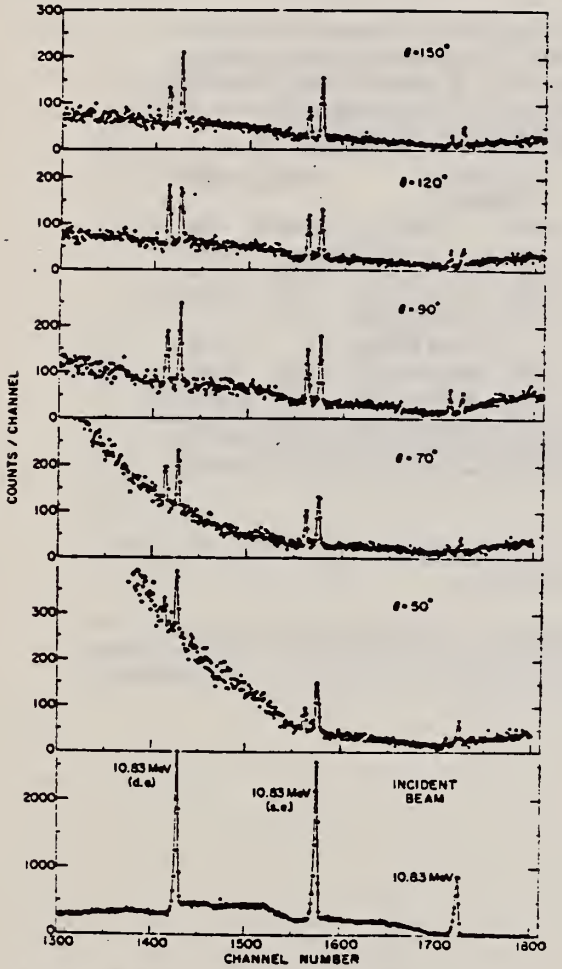

FIG. 2. High-energy portion of the spectra of 10.83-MeV radiation scattered from a U target at several angles and, at the bottom of the figure, a comparable spectrum of incident radiation. This shows the energy calibration of the detector-analyzer system as well as the detector response to 10.83-MeV photons, which is dominated by the double-(two annihilation photons) escape and single-(one annihilation photon) escape peaks. In the scattered spectrum at each angle, the 10.83-MeV photons from elastic scattering, and those of slightly lower energy from inelastic scattering to the 48-keV state, are clearly resolved.

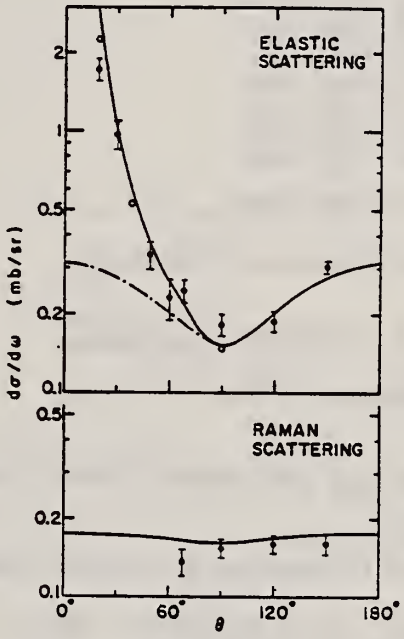

FIG. 5. Angular variation of the elastic and Raman scattering cross sections for uranium at 10.83 MeV. The measured values are shown together with the statistical errors of measurement. The solid curve in each case represents the calculated values. For elastic scattering the broken curve shows the calculated values in the forward direction when Delbrück scattering is neglected. The Delbrück amplitudes of the CERN group (Ref. 18) are used to compute the solid curve; those of the Trondheim group (Ref. 19) give similar values. These are indicated by the open circles at 20°, 50°, and 90°, but at 30° and 70° the two sets of values are so close as to be indistinguishable in the figure. The solid curve in the lower portion of the figure is the prediction of the simple rotator model discussed in the text.

(over)

TABLE I. Differential cross sections measured for elastic and inelastic scattering of 10.83-MeV photons. State or states populated by inelastic scattering are indicated in parentheses below the target. The errors given result from the statistical error in the measurement of the cross section relative to the calibration value, the 90° uranium inelastic cross section.

Nucleus	θ (deg)	$d\sigma/d\omega$ (elastic) (mb/sr)	$d\sigma/d\omega$ (inelastic) (mb/sr)
^{238}U			
(2^+, 45 keV)	20	1.72 ± 0.17	
	30	0.97 ± 0.12	
	50	0.334 ± 0.039	
	60	0.23 ± 0.04	
	70	0.245 ± 0.024	0.136 ± 0.015
	90	0.182 ± 0.017	0.154 ± 0.012
	120	0.189 ± 0.017	0.160 ± 0.013
	150	0.303 ± 0.016	0.160 ± 0.015
^{232}Th			
(2^+, 45 keV)	90	0.129 ± 0.015	0.103 ± 0.007
Pb	20	1.28 ± 0.12	
	30	0.55 ± 0.07	
	50	0.289 ± 0.051	
	60	0.20 ± 0.04	
	70	0.087 ± 0.014	
	90	0.079 ± 0.005	
	120	0.060 ± 0.004	
	150	0.127 ± 0.008	
^{209}Bi			
($\frac{1}{2}^-$, 910 keV)	90	0.101 ± 0.0062	~0
^{181}Ta			
($\frac{9}{2}^+$, 136 keV)	90	0.0370 ± 0.003	0.006 56 ± 0.0015
^{159}Tb			
($\frac{5}{2}^+$, 58 keV)	90	0.0314 ± 0.003	0.0110 ± 0.0016
$\frac{1}{2}^+$, 138 keV)			0.005 11 ± 0.0011

TABLE III. Comparison of calculated and observed values of the 90° cross sections for elastic scattering and of the ratio at 90° of Raman to elastic scattering by various nuclei for 10.83-MeV photons. The parameters used in the calculations are given in Table II.

Target	$d\sigma_{clas}(90°)/d\Omega$ (mb/sr) Calc	Exp	$d\sigma^{(90°)}_{Raman}/d\sigma^{(90°)}_{clas}$ Calc	Exp
Tb	0.036	0.031 ± 0.003	0.80	0.51 ± 0.06
Ta	0.055	0.037 ± 0.003	0.28	0.18 ± 0.04
Pb	0.076	0.079 ± 0.005	0	
Bi		0.101 ± 0.006	0	~0
Th	0.128	0.129 ± 0.015	0.91	0.80 ± 0.08
U	0.157[a]	0.182 ± 0.017	1.03	0.85 ± 0.08

[a] If the Livermore parameters (Ref. 33) for ^{235}U are used then this calculated value would be 0.210 mb/sr.

18 F. Ehlotzky and G.C. Sheppy, Nuovo Cimento 33, 1185 (1964).

19 K. Mork and P. Papatzacos, private communication.

33 C.D. Bowman, G.F. Auchampauch, and S.C. Fultz, Phys. Rev. 133, B676 (1964).

REF. U. Kneissl, G. Kuhl, and A. Weller
Phys. Lett. 49B, 440 (1974)

ELEM. SYM.	A	Z
U	238	92

METHOD

REF. NO. 74 Kn 1 egf

REACTION	RESULT	EXCITATION ENERGY	SOURCE TYPE	SOURCE RANGE	DETECTOR TYPE	DETECTOR RANGE	ANGLE
E,E	RLX	THR- 40	D	15- 40	TRK-I		90

E+,E- YIELDS

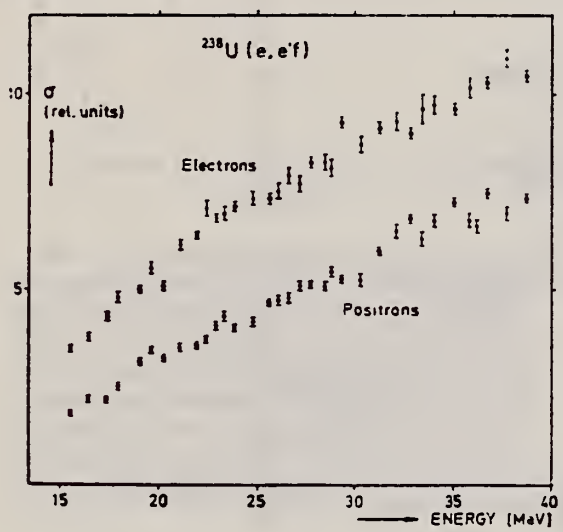

Fig. 1. Excitation function for the U(e, e'f) reaction; open circles measured by glass-detectors, full circles measured by Si-detectors.

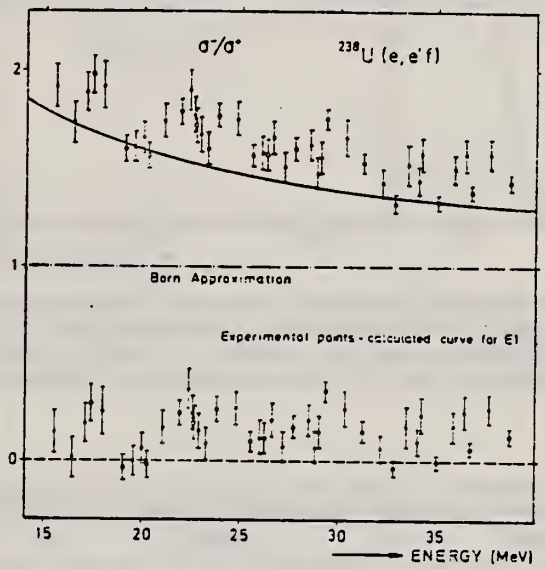

Fig. 2. The ratio σ^-/σ^+ as a function of the incident energy; open circles measured by glass-detectors, full circles measured by Si-detectors.

REF. C. D. Bowman, I. G. Schroder, C. E. Dick, H. E. Jackson
Phys. Rev. C12, 863 (1975)

ELEM. SYM.	A	Z
U	238	92

METHOD

REF. NO. 75 Bo 3 hmg

REACTION	RESULT	EXCITATION ENERGY	SOURCE TYPE	SOURCE RANGE	DETECTOR TYPE	DETECTOR RANGE	ANGLE
G,F	ABX	0- 6	C	3- 6	TRK-I		2PI

2PI= SOLID ANGLE

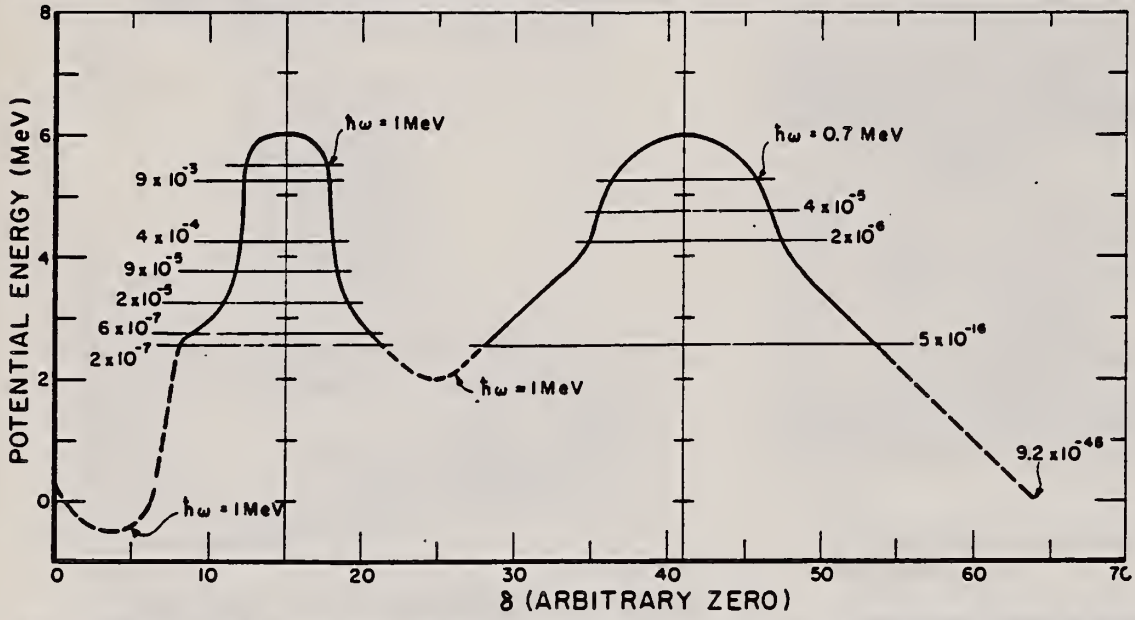

FIG. 3. The potential barrier for ^{238}U. The curve is constructed from barrier penetrabilities derived from this and other experiments. These penetrabilities are given in the figure. The scale for the deformation parameter δ is chosen to simplify calculations as described in the text. The zero for δ has been chosen arbitrarily. The value shown at the far right of the figure of 9.2×10^{-45} is the penetrability corresponding to ground state spontaneous fission.

TABLE II. Experimentally determined barrier penetration parameters.

Energy	P_a	Source	P_b	Source
6.0	0.5	E_a=6 MeV, $\hbar\omega_a$=1 MeV	0.5	E_b=6 MeV, $\hbar\omega_b$=0.7 MeV
5.5	4×10^{-2}			
5.25	9×10^{-3}	from P_aP_b	7×10^{-4}	
4.75	(2×10^{-3})		4×10^{-5}	from P_aP_b
4.25	4×10^{-4}	P_a	2×10^{-6}	P_b
3.75	9×10^{-5}	P_a		
3.25	2×10^{-5}	P_a		
2.75	6×10^{-7}	P_a		
2.56	2×10^{-8}	Russo *et al.* (Ref. 11)	5×10^{-16}	Russo *et al.* (Ref. 11)

(over)

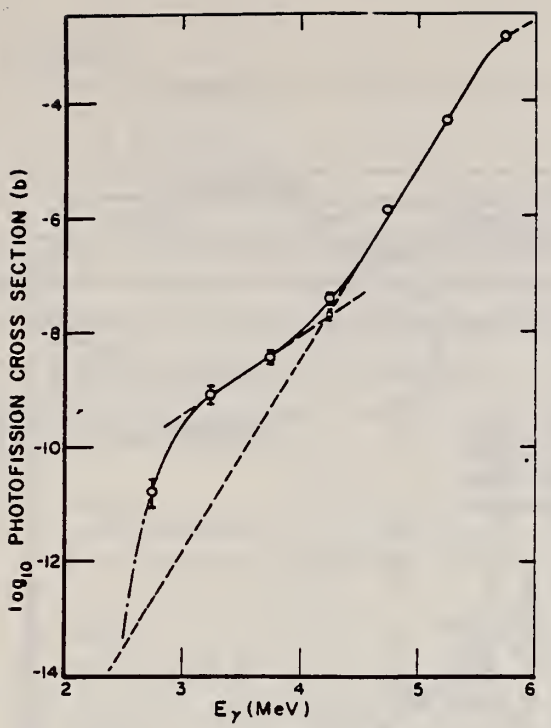

FIG. 2. The photofission cross section of ^{238}U. The two straight dashed lines show the extensions of the regions where either prompt or delayed fission dominates. The dot-dashed curve is included to show the return of the cross section to the dependence on penetration of the full barrier which is predicted to occur below the isomer excitation energy of 2.56 MeV. The uncertainty flags shown do not include systematic uncertainties which are estimated to be of about the same size. When no flags are shown, the uncertainty is only slightly larger than the point size.

TABLE I. A summary of experimental results.

Electron energy (MeV)	Fissions/Ccm^2	x-ray energy (MeV)	Cross section [a] (b)
3.0	0.11 ± 0.06	2.75	$1.9 \pm 1 \times 10^{-11}$
3.5	5.5 ± 1.6	3.25	$8.2 \pm 2.9 \times 10^{-10}$
4.0	41 ± 4	3.75	$3.5^{c} \pm 0.8 \times 10^{-9}$
4.0	33 ± 6		
4.5	$2.0^{b} \times 10^{2}$	4.25	$3.9 \pm 0.9 \times 10^{-8}$
5.0	$7.5^{b} \times 10^{3}$	4.75	$1.3 \pm 0.3 \times 10^{-6}$
5.5	$2.7^{b} \times 10^{5}$	5.25	$4.4 \pm 1.0 \times 10^{-5}$
6.0	$6.3^{b} \times 10^{6}$	5.75	$1.3 \pm 0.3 \times 10^{-3}$

[a] The uncertainty shown is the quadratic sum of the standard deviation resulting from track counting and an estimated ±20% uncertainty in the bremsstrahlung spectrum. An uncertainty discussed in the text of possibly 50% in the scale factor owing to uncertainty in ΔR is not included.

[b] The standard deviation in tract counting for these points is ±10%.

[c] This point is the average of the points measured at NBS and at ANL.

REF. J.T. Caldwell and E.J. Dowdy
Nucl. Sci. & Eng. 56, 179 (1975)

ELEM. SYM.	A	Z
U	238	92

METHOD

REF. NO. 75 Ca 5 egf

REACTION	RESULT	EXCITATION ENERGY	SOURCE		DETECTOR		ANGLE
			TYPE	RANGE	TYPE	RANGE	
G,F	NOX	6- 13	C	8- 13	MOD-I		4PI

NEUTRON MULTIPLICITIES

The prompt- and delayed-neutron multiplicities for photofission of the eight isotopes, ^{232}Th, ^{233}U, ^{234}U, ^{235}U, ^{236}U, ^{238}U, ^{237}Np, and ^{239}Pu, have been measured using bremsstrahlung with end-point energies ranging from 8 to 13 MeV. The measured multiplicities are compared with those from the same compound nucleus formed in neutron-induced fission where such data exist.

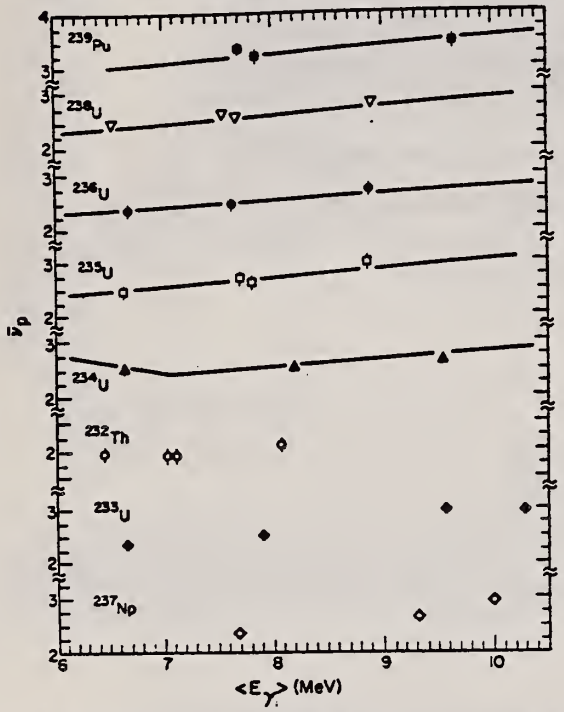

Fig. 5. $\bar{\nu}_p$ versus excitation energy for the eight isotopes studied in this experiment. The full curves shown are from the evaluations of Davey[2] with the excitation energy determined as described in the text. For the lower three isotopes shown, no previous experimental values for $\bar{\nu}_p$ exist.

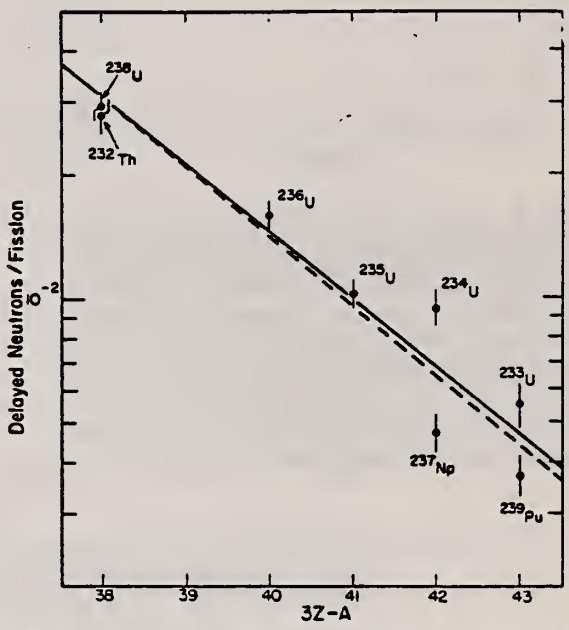

Fig. 6. Delayed neutrons per fission versus the parameter 3Z-A of the compound nucleus. The full curve shown is the least-squares fit to the data shown with $\ln Y_0 = 10.61$, $K = -0.372$. The dashed curve is the least-squares fit to the data provided by Tomlinson[6] with $\ln Y_0 = 11.35$, $K = -0.39$.

TABLE IV

Least-Squares Linear Fit Expressions for $\bar{\nu}_p(\langle E_\gamma \rangle)$

Isotope	$\bar{\nu}_p(\langle E_\gamma \rangle) = \bar{\nu}_0 + d\bar{\nu}_p/dE\,\langle E_\gamma \rangle$	Correlation Coefficient
^{232}Th	$\bar{\nu}_p(\langle E_\gamma \rangle) = 1.310 + 0.090\ \langle E_\gamma \rangle$	0.675
^{233}U	$\bar{\nu}_p(\langle E_\gamma \rangle) = 1.200 + 0.1709\ \langle E_\gamma \rangle$	0.947
^{234}U	$\bar{\nu}_p(\langle E_\gamma \rangle) = 2.222 + 0.0399\ \langle E_\gamma \rangle$	0.741
^{235}U	$\bar{\nu}_p(\langle E_\gamma \rangle) = 0.9034 + 0.2292\ \langle E_\gamma \rangle$	0.967
^{236}U	$\bar{\nu}_p(\langle E_\gamma \rangle) = 1.140 + 0.1788\ \langle E_\gamma \rangle$	0.986
^{238}U	$\bar{\nu}_p(\langle E_\gamma \rangle) = 1.502 + 0.1458\ \langle E_\gamma \rangle$	0.984
^{237}Np	$\bar{\nu}_p(\langle E_\gamma \rangle) = 0.4027 + 0.2505\ \langle E_\gamma \rangle$	0.967
^{239}Pu	$\bar{\nu}_p(\langle E_\gamma \rangle) = 2.526 + 0.0930\ \langle E_\gamma \rangle$	0.777

[2] W.G. Davey, Nucl. Sci. Eng., 44, 345 (1971)

[6] L. Tomlinson, "Delayed Neutrons from Fission: A Compilation and Evaluation of Experimental Data," AERE-R-6993, Atomic Energy Research Establishment, Harwell (1972)

over

TABLE III

Prompt- and Delayed-Neutron Yields

	E_e, MeV	$\langle E_\gamma \rangle$, MeV	$\bar{\nu}_p$	Delayed Neutrons per 100 Fissions
^{232}Th	8	6.44	1.96 ± 0.11	3.10 ± 0.28
(σ = 1.15 ± 0.05)	10	7.02	1.89 ± 0.11	3.06 ± 0.31
	10.2	7.10	1.89 ± 0.11	2.67 ± 0.21
	12	8.06	2.08 ± 0.11	2.59 ± 0.31
				av = 2.80 ± 0.28
^{233}U	8	6.68	2.350 ± 0.112	0.455 ± 0.040
(σ = 1.25 ± 0.05)	10	7.90	2.498 ± 0.108	0.518 ± 0.040
	12	9.55	2.960 ± 0.096	0.640 ± 0.044
	13	10.27	2.870 ± 0.099	0.598 ± 0.051
				av = 0.553 ± 0.044
^{234}U	8	(6.67)[a]	2.536 ± 0.112	---
(σ = 1.13 ± 0.05)	10	8.69	2.499 ± 0.107	0.92 ± 0.06
	12	9.54	2.623 ± 0.105	0.97 ± 0.12
				av = 0.94 ± 0.094
^{235}U	8	6.67	2.456 ± 0.086	0.90 ± 0.08
(σ = 1.20 ± 0.05)	10	7.70	2.697 ± 0.081	0.88 ± 0.08
	10.2	7.81	2.612 ± 0.079	1.13 ± 0.07
	12	8.86	2.963 ± 0.072	1.12 ± 0.08
				av = 1.02 ± 0.08
^{235}U	8	6.66	2.357 ± 0.111	1.43 ± 0.14
(σ = 1.20 ± 0.05)	10	7.63	2.470 ± 0.105	1.73 ± 0.12
	12	8.86	2.744 ± 0.095	1.64 ± 0.10
				av = 1.60 ± 0.13
^{238}U	8	6.53	2.457 ± 0.088	3.06 ± 0.24
(σ = 1.22 ± 0.05)	10	7.54	2.628 ± 0.083	2.76 ± 0.17
	10.2	7.66	2.585 ± 0.082	3.06 ± 0.14
	12	8.88	2.802 ± 0.078	2.75 ± 0.19
				av = 2.91 ± 0.20
^{237}Np	10	7.68	2.35 ± 0.11	0.38 ± 0.04
(σ = 1.20 ± 0.05)	12	9.31	2.65 ± 0.10	0.50 ± 0.04
	13	9.92	2.95 ± 0.10	0.54 ± 0.04
				av = 0.47 ± 0.04
^{239}Pu	10	7.69	3.32 ± 0.08	---
(σ = 1.18 ± 0.10)	10.2	7.84	3.17 ± 0.14	0.37 ± 0.04
	12	9.65	3.43 ± 0.10	0.37 ± 0.04
				av = 0.37 ± 0.04

[a]Estimated value.

REF.

P. A. Dickey and P. Axel
Phys. Rev. Lett. 35, 501 (1975)

ELEM. SYM.	A	Z
U	238	92

METHOD

REF. NO.	
75 Di 2	hmg

REACTION	RESULT	EXCITATION ENERGY	SOURCE		DETECTOR		ANGLE
			TYPE	RANGE	TYPE	RANGE	
G,F	ABX	THR- 8	C	8, 10	TOF-D		135

Variable-energy photons defined to 100 keV were used to study ^{238}U and ^{232}Th from 5 to 8 MeV. The inferred fission transmission indicates (a) that the lowest 1$^-$ fission barrier is about 6.5 MeV in ^{238}U and 6.3 MeV in ^{232}Th, and (b) that there is an energy gap before the rapid opening of additional fission channels above 7 MeV in ^{233}U.

1067

1067

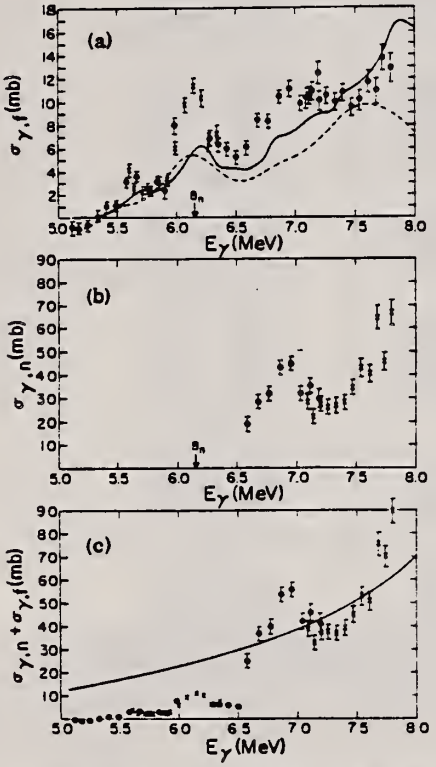

FIG. 1. Photon-induced cross sections for ^{238}U. All of the points come from this experiment. In (b), (c), and the low-energy portion of (a) the different symbols identify different runs; the spacing of points in a single run is equal to the photon-energy resolution. (a) Photofission cross sections. The curves correspond to measurements with poorer resolution; the solid curve is from Ref. 12 and the dashed curve is from Ref. 14. (b) Photoneutron cross sections inferred by measuring only those neutrons with energy above 300 keV. (c) Below 6.6 MeV the points represent $\sigma_{\gamma f}$ only. Above 6.6 MeV, the points are the sum, $\sigma_{\gamma f}+\sigma_{\gamma n}$, with statistical errors shown. The line is the extrapolation of the Lorentzian curves which have been fitted to the giant dipole resonance as reported in Ref. 19.

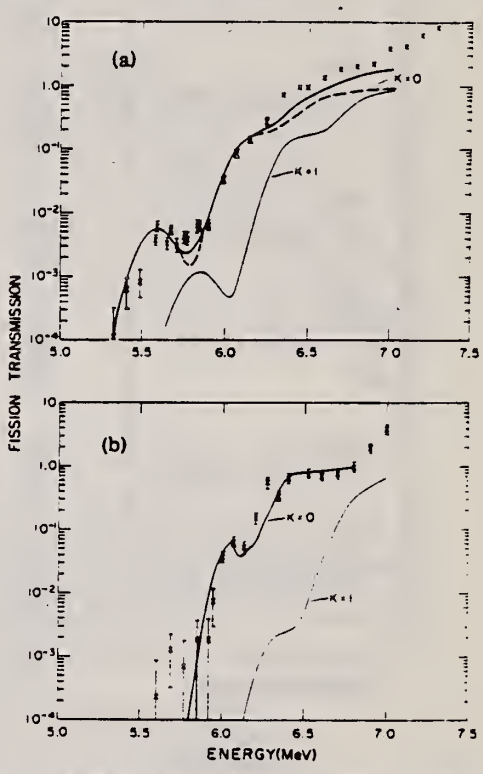

FIG. 3. Fission transmissions: (a) ^{238}U. The upper solid curve is the sum of the $K=0$ and $K=1$ transmissions calculated with the parameters in Table I. The dashed curve shows the $K=0$-barrier contribution when it is noticeably lower than the sum. (b) ^{232}Th. The curves are calculated transmissions for $K=0$ and $K=1$ using the barrier parameters listed in Table I.

(over)

U.S. DEPARTMENT OF COMMERCE
NATIONAL BUREAU OF STANDARDS

TABLE I. Fission-barrier parameters (energies given in MeV).

	J^π	K	E_A	E_{min}	E_B	$\hbar\omega_A$	$\hbar\omega_{min}$	$\hbar\omega_B$
^{238}U	0^+	0	5.9[a]	2.0	6.1[a]	1.0[a]	0.9	0.6[a]
	1^-	0	6.5	2.35	6.1	1.0	0.9	0.6
	1^-	1	6.7	2.55	6.6	1.0	0.9	0.6
^{232}Th	0^+	0	< 5.5[a]	3.0	6.1[a]	0.9[a]	1.5	0.5[a]
	1^-	0	6.3	3.1	6.3	0.9	1.0	0.45
	1^-	1	6.5	3.3	6.9	0.9	1.0	0.5

[a]Values taken from Ref. 4.

[4] B.B. Back et al., Phys. Rev. C9, 1924 (1974)

[12] A.M. Khan et al., Nucl. Phys. A179, 333 (1972)

[14] R.A. Anderl et al., Nucl. Phys. A212, 221 (1973)

[19] A. Veyssiere et al., Nucl. Phys. A199, 45 (1973)

REF. H. E. Jackson, G. E. Thomas, K. J. Wetzel
Phys. Rev. C11, 1664 (1975)

ELEM. SYM.	A	Z
U	238	92

METHOD

REF. NO. 75 Ja 1 hmg

REACTION	RESULT	EXCITATION ENERGY	SOURCE		DETECTOR		ANGLE
			TYPE	RANGE	TYPE	RANGE	
G,G	ABX	11	D	11	SCD-D		DST
		(11.387)		(11.387)			

RATIO RAMAN/ELASTIC

TABLE I. Differential cross sections measured for elastic and inelastic scattering of 11.39-MeV photons. State or states populated by inelastic scattering are indicated in parentheses beside the target. The errors given result from the statistical error in the measurement of the cross section relative to the calibration value, the 90° uranium elastic cross section.

θ (deg)	$d\sigma/d\omega$ (elastic) (mb/sr)	$d\sigma/d\omega$ (inelastic) (mb/sr)
	^{238}U (2$^+$, 45 keV)	
90	0.169 ± 0.011	0.173 ± 0.016
150	0.355 ± 0.041	0.236 ± 0.24
	^{232}Th (2$^+$, 45 keV)	
150	0.331 ± 0.035	0.210 ± 0.022
	^{181}Ta ($\frac{9}{2}^+$, 136 keV) ($\frac{13}{2}^+$, 301 keV)	
90	0.073 ± 0.008	0.020 ± 0.004 0.009 ± 0.004
150	0.145 ± 0.015	0.017 ± 0.004 0.017 ± 0.004
	^{165}Ho ($\frac{9}{2}^+$, 95 keV) ($\frac{11}{2}^+$, 210 keV)	
150	0.141 ± 0.014	0.022 ± 0.004 0.013 ± 0.004
	^{159}Tb ($\frac{5}{2}^+$, 58 keV) ($\frac{7}{2}^+$, 138 keV)	
90	0.062 ± 0.006	0.024 ± 0.003 0.013 ± 0.003
150	0.134 ± 0.012	0.042 ± 0.004 0.019 ± 0.004
	^{141}Pr	
150	0.030 ± 0.008	...

TABLE II. Comparison of calculated and observed values of the cross sections for elastic scattering and of the ratio of Raman to elastic scattering by various nuclei for 11.387-MeV photons at 90 and 150°. The parameters used in the calculations for column 5 are given in Table II. Column 4 describes results obtained by perturbing those parameter to meet the constraint of Eq. (3) (see text).

Target	$d\sigma(\theta)d\Omega$ (mb/sr) Calc.	Exp.	$d\sigma_{Raman}(\theta)/d\sigma_{elastic}(\theta)$		
		$\theta = 150°$			
Pr	0.025	0.030 ± 0.008		0.0	0.0
Tb	0.094	0.134 ± 0.012	0.53	0.57	0.46 ± 0.04
Ho	0.170	0.141 ± 0.014	0.28	0.28	0.25 ± 0.04
Ta	0.160	0.145 ± 0.015	0.23	0.22	0.23 ± 0.04
Th	0.253	0.331 ± 0.035	0.59	0.63	0.64 ± 0.08
U	0.289	0.355 ± 0.041	0.78	0.73	0.67 ± 0.07
		$\theta = 90°$			
Tb	0.062	0.062 ± 0.006	0.76	0.82	0.60 ± 0.07
Ta	0.109	0.074 ± 0.008	0.32	0.30	0.38 ± 0.07
U	0.172	0.169 ± 0.008	1.29	1.15	1.03 ± 0.10

REF. V.E. Zhuchko, A.V. Ignatyuk, Yu. B. Ostapenko, G.N. Smirenkin, A.S. Soldatov, Yu.M. Tsipenyuk
ZhETF Pis. Red. 22, 255 (1975)
JETP Lett. 22, 118 (1975)

ELEM. SYM.	A	Z
U	238	92

METHOD

REF. NO. 75 Zh 1 hmg

REACTION	RESULT	EXCITATION ENERGY	SOURCE TYPE	SOURCE RANGE	DETECTOR TYPE	DETECTOR RANGE	ANGLE
G,F	NOX	THR- 6	C	3- 6	TRK-I		4PI
		(Thr-5.5)		(3.8-5.5)			

For the isotopes ^{232}Th, ^{237}Np, and ^{238}U, in the deep subbarrier region, we observed an abrupt decrease of the slope of the energy dependence of the photofission cross section, called the isomer shelf. An investigation of this phenomenon uncovers a number of new possibilities for the refinement of our concepts concerning the structure of the fission barrier of heavy nuclei.

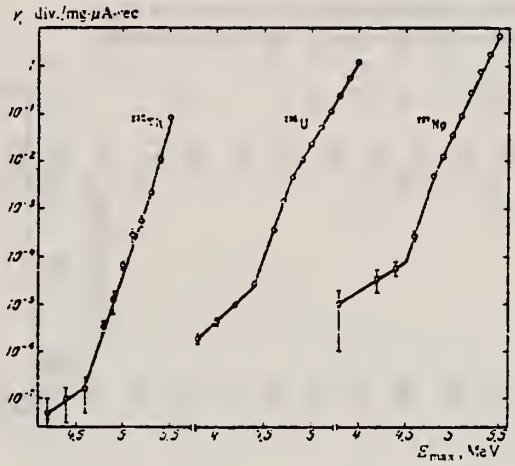

Energy dependence of the photofission yield of ^{232}Th, ^{238}U, and ^{237}Np.

REF.

M.A.A. Al-Janabi, G.W.A. Newton, V.J. Robinson
Radiochem. Radioanal. Letters 25, 345 (1976)

ELEM. SYM.	A	Z
U	238	92

METHOD

REF. NO. 76 Al 6 hmg

REACTION	RESULT	EXCITATION ENERGY	SOURCE		DETECTOR		ANGLE
			TYPE	RANGE	TYPE	RANGE	
G,F	ABY	THR* 3	C	* 3	SCD-D		4PI

*ENERGY, GEV

Radiochemical measurements have been made of fission yields at 3 GeV and forward - backward ratios at 5 GeV in the photofission of natural uranium by bremsstrahlung. The yield results are analysed in terms of a two component mass yield curve, consisting of a low energy assymmetric component and a high energy symmetric component. The relative weights of these components were calculated from cross section data as 30% low energy and 70% high energy, but a better fit was obtained with a much smaller contribution (27%) from the high energy component. A possible explanation is discussed briefly.

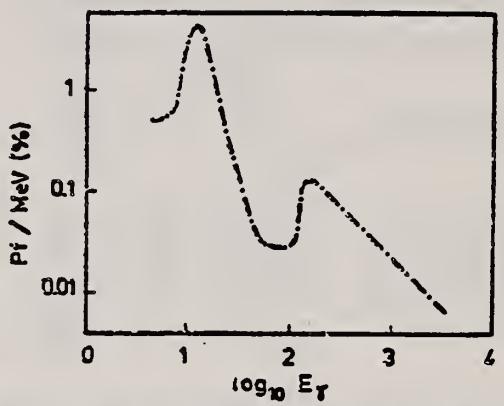

Fig. 1. Probability of photofission as a function of gamma energy for natural uranium irradiated with 3 GeV bremsstrahlung.

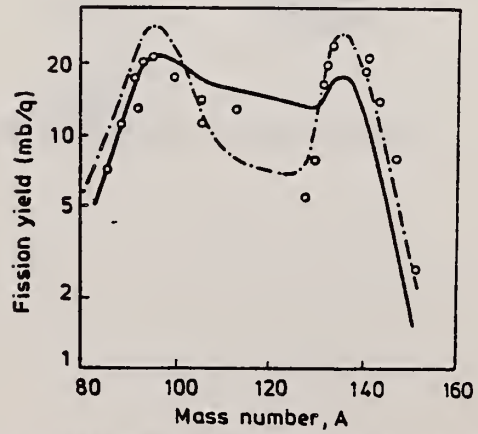

Fig. 3. Predicted mass yield curves compared with experimental data (⊙). The full curve is the one shown in Figure 2; the dash-dot curve was obtained by assuming a higher proportion of the low energy component.

(over)

TABLE 1

Yields of fission products found in natural uranium irradiated with bremsstrahlung of maximum energy of 3 GeV.

Fission product	Half-life	γ-ray energy (keV)	γ- intensity (%)	Yield (mb/g)
^{151}Pm	28 h	340	21.0	2.75
^{147}Nd	11.1 d	531	12.8	8.03
^{143}Ce	33.4 h	293	49.5	13.5
^{141}Ce	32.5 d	145	48.6	21.24
^{140}Ba	12.8 d	537	24.0	18.91
^{135}I	6.7 h	1260	34.0	17.06
^{133}I	20.8 h	530	90.0	23.7
^{132}I	2.3 h	954	22.0	7.7
^{131}I	8.05 d	365	82.4	16.75
^{130}I	12.3 h	418	30.5	2.73
^{126}I	12.8 d	389	34.0	0.5
^{124}I	4.17 d	603	62.0	0.21
^{123}I	13.3 h	159	83.0	0.19
^{132}Te	78 h	228	88.0	19.98
^{129}Sb	4.3 h	813	43.5	7.88
^{127}Sb	3.7 d	686	36.8	5.3
^{113}Ag	5.3 h	298	7.4	12.99
^{105}Rh	36 h	320	19.6	14.36
^{105}Ru	4.4 h	470	17.5	11.44
^{99}Mo	66.7 h	740	13.8	17.37
^{95}Zr	63.98 d	757	54.3	21.07
^{93}Y	10.2 h	947	2.3	20.0
^{91}Sr	9.7 h	1024	34.0	17.62
^{92}Sr	2.7 h	1383	90.0	12.77
^{88}Kr	2.8 h	196	27.2	11.08
^{85m}Kr	4.4 h	151	74.0	6.99

TABLE 3

The calculated kinetic energies of fission fragments and estimated kinetic energy of the pre-fission nucleus obtained from the experimental F/B ratios , 5 GeV Bremsstrahlung energy.

Isotope	K. E. of fragment (MeV) (eqn 3)	Exp. F/B ratio	η 11 (eqn 2)	K. E. of pre-fission nucleus (keV)
^{143}Ce	63.9	1.21	0.048	703
^{141}Ce	65.2	1.24	0.054	312
^{142}La	64.4	1.16	0.037	143
^{139}Ba	66.6	1.14	0.033	121
^{135}Xe	69.4	1.3	0.065	471
^{131}I	72.2	1.3	0.065	542
^{132}I	71.5	1.43	0.089	1000
^{133}I	71.0	1.12	0.028	97
^{135}I	69.4	1.2	0.046	236
^{132}Te	71.5	1.2	0.046	266
^{129}Sb	73.6	1.12	0.028	104
^{113}Ag	85.0	1.15	0.035	213
^{105}Ru	90.6	1.3	0.065	850
^{97}Zr	96.3	1.18	0.041	395
^{92}Y	99.8	1.36	0.076	1480
^{92}Sr	99.8	1.2	0.058	844
^{91}Sr	100.6	1.25	0.056	808
^{88}Kr	103.0	1.07	0.017	79
^{85m}Kr	105.0	1.13	0.03	267
			Mean	470

F/B = ratio of yield in forward to backward direction with respect to beam.

$$\eta_{11} = \frac{(F/B)^{1/2}-1}{(F/B)^{1/2}+1}$$ = ratio of average forward velocity of pre-fusion nucleus to avg velocity of fusion fragment.

REF.		ELEM. SYM.	A	Z
	J.D.T. Arruda Neto, S.B. Herdade, B.S. Bhandari, and I.C. Nascimento Phys. Rev. C14, 1499 (1976)	U	238	92

METHOD	REF. NO.
	76 Ar 3 hmg

REACTION	RESULT	EXCITATION ENERGY	SOURCE		DETECTOR		ANGLE
			TYPE	RANGE	TYPE	RANGE	
G,F	ABX	THR- 60	C	6- 60	TRK-I		DST
E,F	ABY	THR- 60	C	6- 60	TRK-I		4PI

$\frac{d\sigma}{d\Omega}$ (e,f) indicates a large quadrupole component in the energy range 6-9 MeV.

Experimental results are presented for the electrofission and photofission of ^{238}U in the energy range 6 to 60 MeV. The importance of the inclusion of the Coulomb corrections in the calculation of the virtual photon spectrum is emphasized and the relative $E1$ contribution to the electrofission process has been evaluated using the distorted-wave Born-approximation analysis of the experimental data.

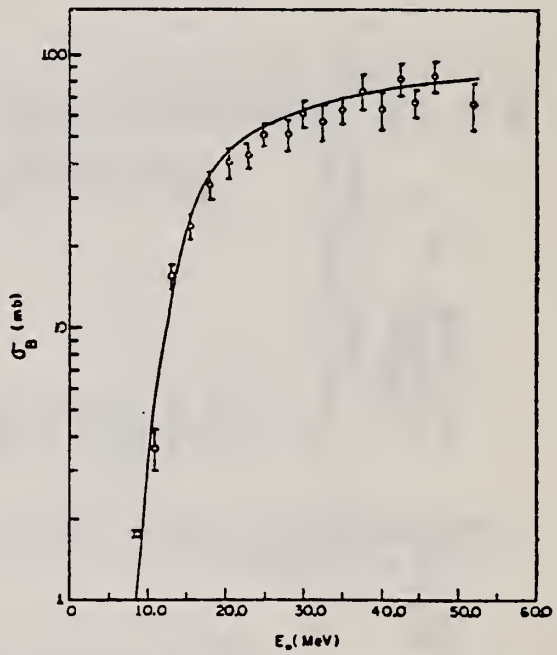

FIG. 2. Bremsstrahlung induced fission yield σ_B of ^{238}U as function of the maximum photon energy E_e. The solid line represents the yield curve obtained by folding in the photofission cross section of ^{238}U (as shown in Fig. 3) with the bremsstrahlung spectrum for a thin radiator (Ref. 17).

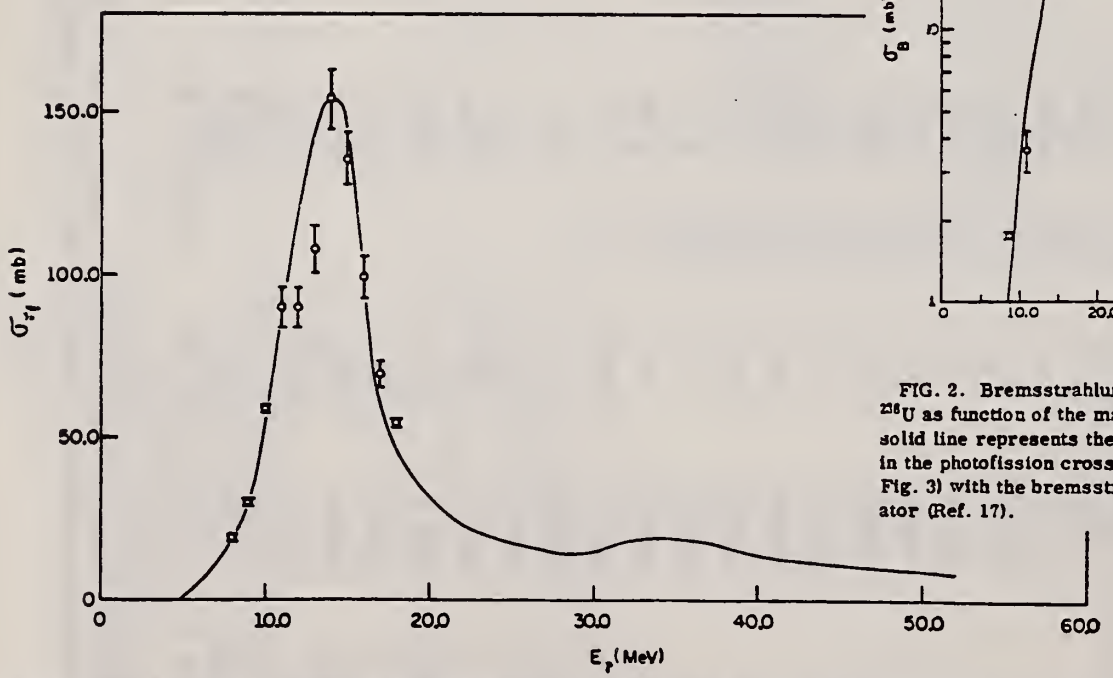

FIG. 3. Photofission cross section $\sigma_{\gamma f}$ of ^{238}U as a function of photon energy E_γ is shown by the solid curve obtained by the unfolding of the bremsstrahlung induced fission yields as described in the text. The experimental points shown are the monochromatic photon cross sections of Veyssière *et al.* (Ref. 29).

(over)

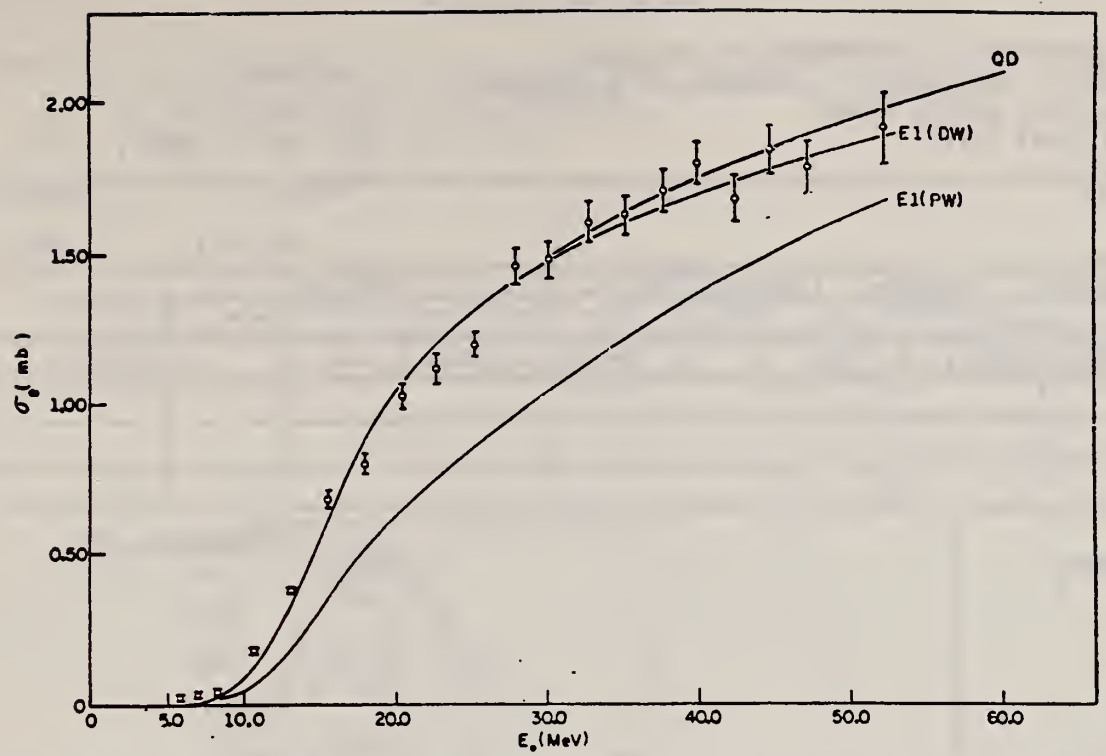

FIG. 4. Electron induced fission yield σ_e of ^{238}U as a function of the incident electron energy E_0. The solid lines labeled by $E1$(DW), $E1$(PW), and QD are the semitheoretical curves as explained in the text.

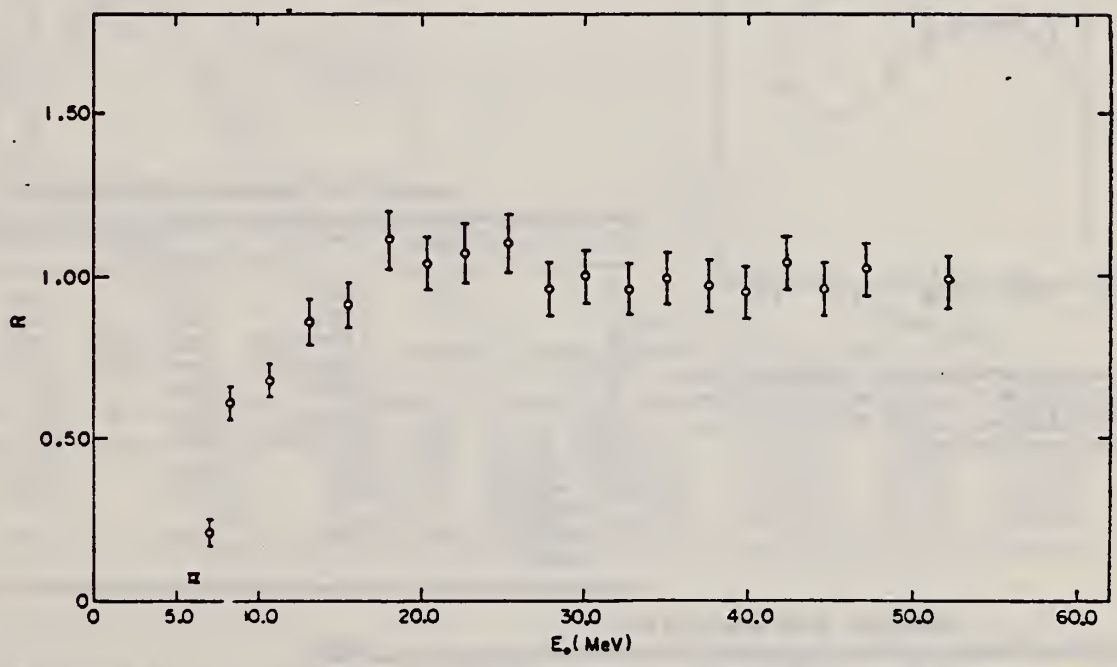

FIG. 5. The relative contribution of the $E1$ excitation with respect to the total electroexcitation process, as defined in Eq. (6) of the text by the ratio R, is plotted as a function of the incident electron energy E_0.

$$R(E_0) = \frac{\sigma_e^{E1}(E_0)}{\sigma_e(E_0)},$$

[17] H.W. Koch and J.W. Motz, Rev. Mod. Phys. 31, 920 (1959).

[29] A. Veyssiere, H. Beil, R. Bergere, P. Carlos, A. Lepretre, K. Kernbath, Nucl. Phys. A199, 45 (1973).

REF. T. Cooper, W. Bertozzi, J. Heisenberg, S. Kowalski, W. Turchinetz, C. Williamson, L. Cardman, S. Fivozinsky, J. Lightbody, Jr., and S. Penner
Phys. Rev. C13, 1083 (1976)

ELEM. SYM.	A	Z
U	238	92

METHOD

REF. NO. 76 Co 3 hmg

REACTION	RESULT	EXCITATION ENERGY	SOURCE TYPE	SOURCE RANGE	DETECTOR TYPE	DETECTOR RANGE	ANGLE
E,E/	FMF	1, 1	D	44-106	MAG-D		DST

LEVELS .045,.148

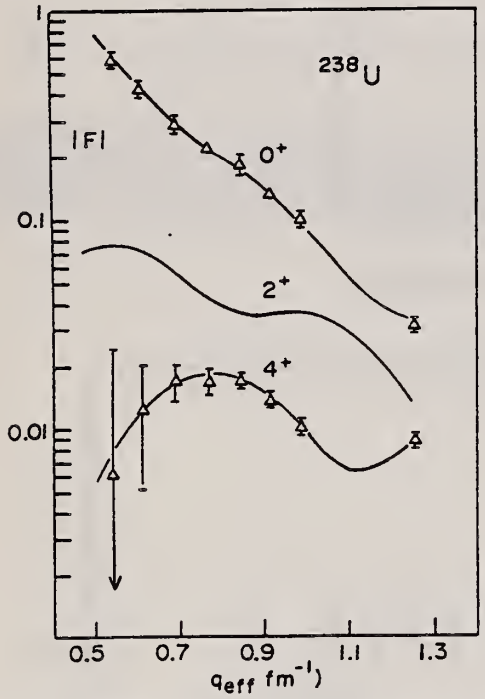

FIG. 3. Measured form factors for the elastic (0^+) and the inelastic 0.045-MeV (2^+) and 0.148-MeV (4^+) states in ^{238}U. The fitted curves are based on a best fit deformed Fermi charge distribution.

TABLE VIII. Deformed Fermi best fit parameters.

	Units	^{152}Sm	^{154}Sm	^{232}Th	^{233}U
c_0	fm	5.8044	5.9387	6.7915	6.8054
t	fm	0.5314	0.5223	0.5713	0.6049
β_2		0.287 ± 0.003	0.311 ± 0.003	0.233 ± 0.002	0.261 ± 0.002
β_4		0.070 ± 0.003	0.087 ± 0.002	0.101 ± 0.003	0.087 ± 0.003
β_6		−0.0120	−0.130	0.0	0.0
$B(E2)$	e^2b^2	3.38 ± 0.07	4.40 ± 0.09	9.21 ± 0.09	11.70 ± 0.15
$B(E4)$	e^2b^4	0.136 ± 0.013	0.221 ± 0.010	1.16 ± 0.05	1.20 ± 0.06
rms radius	fm	5.0922	5.126	5.7723	5.842
ρ_2 Transition radius	fm	6.937	6.950	7.895	7.979
ρ_4 Transition radius	fm	7.757	7.704	8.540	8.748

TABLE VII. Cross sections of ^{238}U.

			Elastic + 2^+			4^+
Energy (MeV)	Angle (deg)	q_{eff} (fm^{-1})	$\frac{d\sigma}{d\Omega}_{exp}$ (mb)	$\frac{d\sigma}{d\Omega}_{best\,fit}$ (mb)	Ratio σ_2^+/σ elastic	$\frac{d\sigma}{d\Omega}_{exp}$ (mb)
44.62	92.42	0.548	0.140×10^{2} ± 3%	0.146×10^{2}	0.016 19	0.131×10^{-2} ± 247%
53.28	92.39	0.611	0.529×10 ± 3%	0.510×10	0.037 21	0.168×10^{-2} ± 111%
65.02	92.39	0.697	0.159×10 ± 5%	0.153×10	0.040 81	0.419×10^{-2} ± 18%
75.12	92.42	0.771	0.701 ± 2%	0.691	0.035 68	0.307×10^{-2} ± 17%
84.93	92.39	0.850	0.378 ± 8%	0.330	0.036 54	0.269×10^{-2} ± 8%
95.33	92.42	0.919	0.163 ± 3%	0.167	0.065 80	0.148×10^{-2} ± 8%
100.42	145.28	1.265	0.982×10^{-3} ± 6%	0.101×10^{-2}	0.121 71	0.397×10^{-4} ± 8%
105.01	92.39	0.990	0.850×10^{-1} ± 6%	0.753×10^{-1}	0.138 30	0.592×10^{-3} ± 14%

REF. G. M. Gurevich, L. E. Lazareva, V. M. Mazur, G. V. Solodukhov, B. A. Tulupov
Nucl. Phys. A273, 326 (1976)

ELEM. SYM.	A	Z
U	238	92

METHOD

REF. NO. 76 Gu 2 egf

REACTION	RESULT	EXCITATION ENERGY	SOURCE		DETECTOR		ANGLE
			TYPE	RANGE	TYPE	RANGE	
G,MUT	ABX	7- 24	C	UKN	NAI-D		4PI

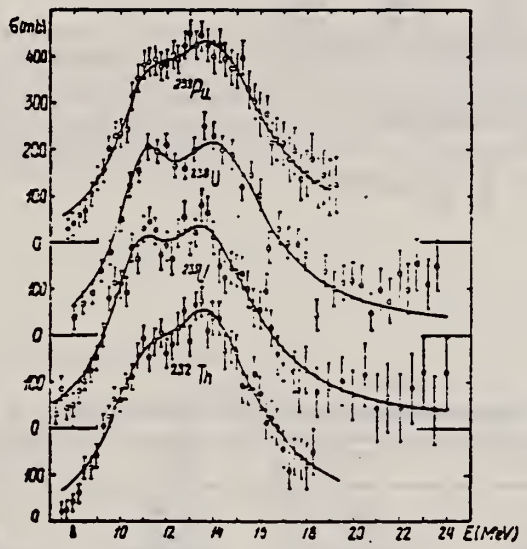

Fig. 2. Total photoabsorption cross sections for ^{232}Th, ^{235,238}U and ^{239}Pu and their respective best two Lorentz line fits.

TABLE 1

Lorentz line parameters for ^{232}Th, ^{235,238}U and ^{239}Pu

Nucleus	E_1 (MeV)	σ_1 (mb)	Γ_1 (MeV)	E_2 (MeV)	σ_2 (mb)	Γ_2 (MeV)
^{232}Th	10.99±0.16	247±26	3.90±0.4	13.9 ±0.13	362±26	4.67±0.38
^{235}U	10.74±0.18	283±39	3.23±0.55	13.77±0.23	354±33	4.92±0.58
^{238}U	10.97±0.13	286±30	2.99±0.48	14.25±0.18	351±25	5.10±0.63
^{239}Pu	11.05±0.13	227±39	3.47±0.57	14.01±0.21	362±31	5.23±0.59

TABLE 2

Deformation parameters and quadrupole moments for ^{232}Th, ^{235,238}U and ^{239}Pu

Nucleus	β_{exp}	β	Q_0 (b)		
			this work	refs. [5,6])	ref. [14])
^{232}Th	0.28±0.03	0.274	10.0±0.8	10.2±1	9.66±0.1
^{235}U	0.30±0.03	0.285	11.0±0.9	12.8±1.3	11.12±0.2
^{238}U	0.31±0.03	0.300	11.7±0.9	11 ±1	11.3 ±0.1
^{239}Pu	0.29±0.03	0.302	11.0±0.9		11.02±0.3

(over)

TABLE 3

Integrated cross sections and mean energies of the dipole absorption

Nucleus	σ_0 (MeV · b)	σ_{-1} (mb)	σ_{-2} (mb · MeV^{-1})	$\bar{E}$ (MeV)	E_H (MeV)	E_M (MeV)	$\bar{E}$ (MeV)
^{232}Th	2.92±0.32	231±24	19±2	13.08	12.64	12.40	12.16
^{235}U	2.99±0.39	238±31	20±2.5	12.91	12.56	12.23	11.90
^{238}U	2.95±0.29	229±22	18±1.8	13.34	12.88	12.80	12.72
^{239}Pu	2.97±0.34	232±26	19±2	13.28	12.80	12.50	12.21

In table 3 various integrated cross sections are defined by the relations

$$\sigma_0 = \int_S^{18} \sigma_{tot}(E)\mathrm{d}E, \qquad \sigma_{-1} = \int_S^{18} \frac{1}{E}\sigma_{tot}(E)\mathrm{d}E, \qquad \sigma_{-2} = \int_S^{18} \frac{1}{E^2}\sigma_{tot}(E)\mathrm{d}E.$$

TABLE 4

Comparison of various integrated cross sections for ^{232}Th, ^{235,238}U and ^{239}Pu

	^{232}Th	^{235}U	^{238}U	^{239}Pu
σ_{0L} (MeV · b)	4.17	4.17	4.16	4.21
0.06 NZ/A (MeV · b)	3.31	3.36	3.39	3.42
$\sigma_0/(0.06\,NZ/A)$	0.88±0.1	0.89±0.12	0.87±0.09	0.87±0.1
$\sigma_{0L}/(0.06\,NZ/A)$	1.26	1.24	1.23	1.23
$\sigma_2\Gamma_2/\sigma_1\Gamma_1$	1.75	1.91	2.09	2.40
σ_{-1L} (mb)	294	298	288	289
$\sigma_{-1L}/A^{4/3}$	0.21	0.21	0.20	0.20
σ_{-2L} (mb · MeV^{-1})	26.3	26.9	25.0	25.3
$\sigma_{-2L} \times 10^3/A^{5/3}$	3.00	3.01	2.74	2.76

[5] C. D. Bowman et al., Phys. Rev. 133 (1964) B676

[6] A. Veyssiere et al., Nucl. Phys. A199 (1973) 45

[14] K.E.G. Lobner et al., Nucl. Data Tables 7 (1970) 495

REF. W.D. James, D.E. Adams, R.A. Sigg, J.T. Harvey, J.L. Meason, J.N. Beck, P.K. Kuroda, H.L. Wright, J.C. Hogan
J. inorg. nucl. Chem. 38, 1109 (1976)

ELEM. SYM.	A	Z
U	238	92

METHOD

REF. NO. 76 Ja 1 egf

REACTION	RESULT	EXCITATION ENERGY	SOURCE TYPE	SOURCE RANGE	DETECTOR TYPE	DETECTOR RANGE	ANGLE
G,F	NOX	THR- 9	C	9	ACT-I		4PI

MASS YIELDS

Abstract—The mass yield distribution of fission products produced in the photofission of ^{238}U using 9 MeV bremsstrahlung have been radiochemically measured for 21 mass chains. The absolute activities of the nuclides measured were determined from gross β counting and total chain yields were measured relative to ^{99}Mo. The peak to valley ratio was found to be about 310, which is comparable with previous results measured at 10 MeV. Fine structure was found to be a prominent feature and occurred around mass number 133, although mass number 134 could not be measured in the present investigation. The fission yields measured in this work have been compared to all known existing values for work in photon energy range of 9 ± 1 MeV.

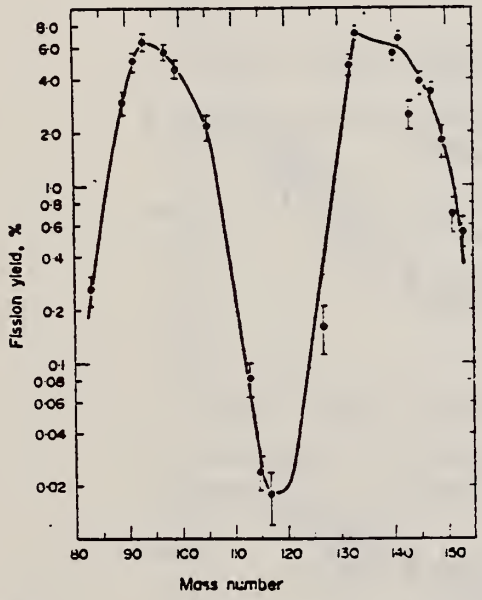

Fig. 1. Mass yield curve for 9 MeV bremsstrahlung fission of depleted uranium.

Table 1. The total fission yields of 21 mass chains measured radiochemically for 9 MeV photofission of ^{238}U. The fission yield data for 10 MeV photofission of Schmitt and Sugarman[1] and Richter and Coryell[2] are also included

Product Nuclide	Half-life (a)	Fission Yields (This Work)	10 MeV Photofission Ref. 1	Ref. 2
^{83}Br	2.4 h	0.26 ± 0.05		0.30 ± 0.04
^{84}Br	31.8 m			0.41 ± 0.07
^{89}Sr	50.5 d	2.96 ± 0.45		
^{91}Y-Sr	58.6 d-9.5 h	5.02 ± 0.55		4.44
^{93}Y	10.2 h	6.52 ± 0.72		
^{97}Zr	16.8 h	5.85 ± 0.45		5.11
^{99}Mo	66.0 h	4.65 ± 0.40	6.6	4.94
^{105}Rh	35.5 h	2.14 ± 0.34		
^{109}Pd	13.5 h			0.085 ± 0.020
^{111}Ag	7.47 d		0.065 ± 0.007	
^{112}Ag	3.13 h		0.047 ± 0.005	0.042 ± 0.002
^{113}Ag	5.3 h	0.082 ± 0.018		
^{115}Cd	53.5 h	0.024 ± 0.006	0.030 ± 0.004	
^{117}Cd	3.4 h	0.018 ± 0.006	0.027 ± 0.007	
^{127}Sb	3.8 d	0.16 ± 0.05		
^{131}I	8.0 d			3.76 ± 0.16
^{132}Te	78 h	4.75 ± 0.65		5.68 ± 0.80
^{133}I	20.8 h	7.14 ± 0.66		6.80 ± 0.60
^{135}I	6.6 h			
^{135}Ba	83.3 m			5.87
^{140}Ba	12.8 d	5.60 ± 0.60	5.7 ± 0.2	5.77 ± 0.47
^{141}Ce	32.5 d	6.80 ± 0.75		
^{143}Ce	33.0 h	2.50 ± 0.45		5.94
^{145}Pr	5.98 h	3.87 ± 0.18		
^{147}Nd	10.99 d	3.38 ± 0.44		
^{149}Pm	53.1 h	1.78 ± 0.36		
^{151}Pm	28.4 h	0.69 ± 0.15		
^{153}Sm	46.5 h	0.55 ± 0.11		

a) The symbols after the half-lives are m : minutes, h : hours, d : days.

REFERENCES

1. R. A. Schmitt and N. Sugarman, *Phys. Rev.* 95, 1260 (1954).
2. H. G. Richter and C. D. Coryell, *Phys. Rev.* 95, 1550 (1954).

REF. F.M. Kiely, B.D. Pate, F. Hanappe, and J. Péter
Z. Physik A279, 331 (1976)

ELEM. SYM.	A	Z
U	238	92

METHOD

REF. NO. 76 Ki 6 egf

REACTION	RESULT	EXCITATION ENERGY	SOURCE		DETECTOR		ANGLE
			TYPE	RANGE	TYPE	RANGE	
G,F	ABY	THR - 580	C	580	TRK-D		4PI

Table 3. Fission cross sections and nuclear fissilities (calculated using several formalisms for σ_{geom}), obtained from coincident track pairs

Element	Z^2/A	σ_f (mb eq. quantum)	$f(=\sigma_f/1.69A^{2/3})$	$\sigma_f/0.33A$
U	35.6	~1.5	$\sim 2.10^{-1}$	$\sim 1.8\times 10^{-1}$
Au	31.7	6.50	1.13×10^{-1}	9.8×10^{-2}
Te	21.1	2.54×10^{-3}	5.92×10^{-5}	5.8×10^{-4}
Ag	20.5	9.09×10^{-4}	2.37×10^{-5}	2.5×10^{-4}

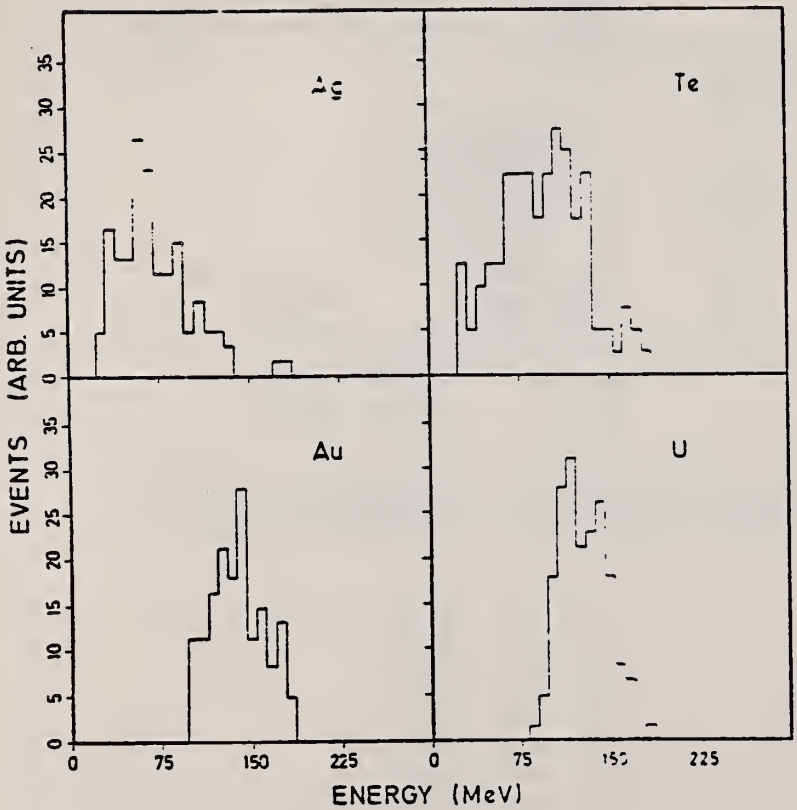

Fig. 3. Fission energy distributions extracted from the present measurements assuming zero centre-of-mass motion for the fissioning systems indicated

REF.

U. Kneissl, G. Kuhl, K. H. Leister, A. Weller
Nucl. Phys. A256, 11 (1976)

ELEM. SYM.	A	Z
U	238	92

METHOD

REF. NO.: 76 Kn 1 egf

REACTION	RESULT	EXCITATION ENERGY	SOURCE		DETECTOR		ANGLE
			TYPE	RANGE	TYPE	RANGE	
E,F	RLX	THR- 40	D	10- 40	TRK-I		2PI

SIGMA(E-)/SIGMA(E+)

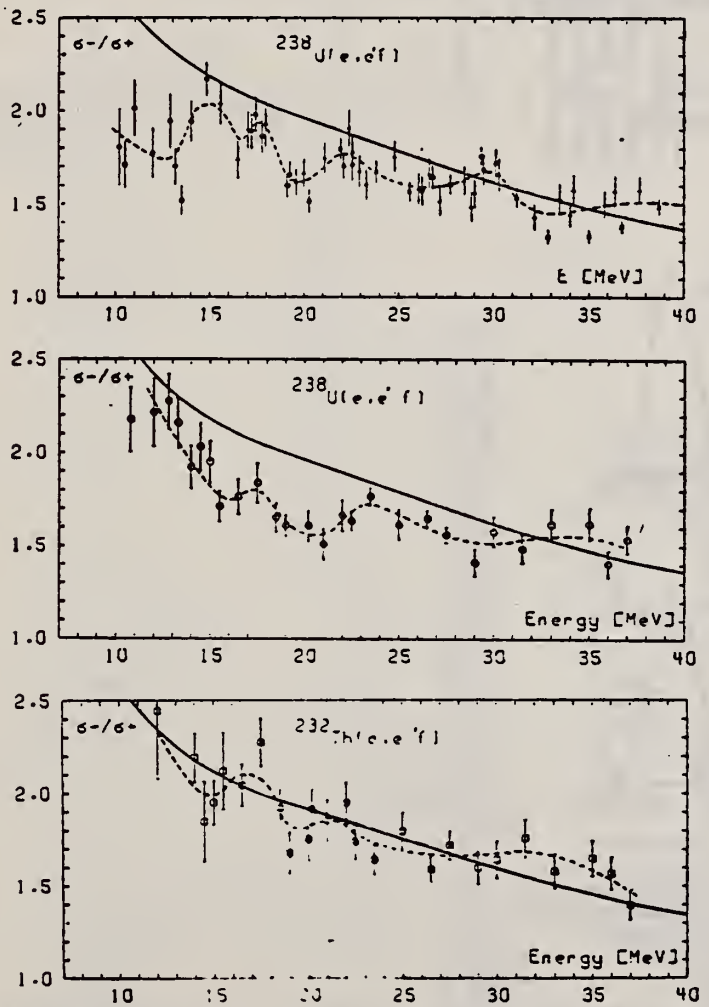

Fig. 2. Experimental results for σ^-/σ^+. Full lines: DW calculations for pure E1 excitation according to ref. [8]). Dashed lines are to guide the eye. The upper part shows the results for uranium (detectors at 90°) with crosses and triangles representing earlier results [7]) with glass detectors and surface barrier detectors, and circles representing new results with glass detectors. The middle and lower parts show the results for uranium and thorium with the 2π arrangement and Macrofol detectors.

[7] U. Kneissl, G. Kuhl, and A. Weller; Phys. Lett. 49B, 440 (1974).

[8] D.S. Onley (Ohio Univ. priv. comm; I.C. Nascimento et al., Nucl. Phys. A246, 210 (75).

REF. A.C. Shotter, J.M. Reid, J.M. Hendry, D. Branford, J.C. McGeorge, J.S. Barton
J. Phys. G: Nucl. Phys. 2, 769 (1976)

ELEM. SYM.	A	Z
U	238	92

METHOD

REF. NO. 76 Sh 12 hg

REACTION	RESULT	EXCITATION ENERGY	SOURCE		DETECTOR		ANGLE
			TYPE	RANGE	TYPE	RANGE	
E,F	RLY	THR-120	D	30-120	SCD-D		90

Abstract. Measurements are presented for the mass and energy distributions of fragments from the fission of ^{235}U and ^{238}U, induced by electrons in the energy range 30–120 MeV. Solid state detectors were used to detect the fragments. Both the mass and energy distributions suggest that the fission process has two distinct components. The change in the distributions for different electron energies indicate that the components are associated with different regions of excitation energy in the fissioning nucleus.

NUCLEAR REACTIONS, FISSION ^{235}U(e,F), ^{238}U(e,F), E = 30, 50, 115 MeV; FF'coin; measured $\sigma(E;E_F,M_F)$. Enriched targets, semiconductor detectors.

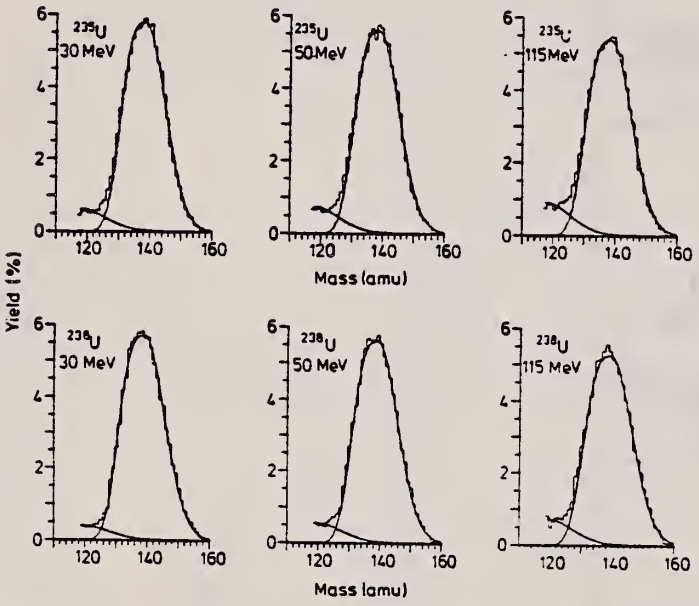

Figure 2. Mass yields for ^{235}U and ^{238}U at 30, 50 and 115 MeV electron energies. Histograms show experimental yields; curves are least-squares fits determining the division of fission into two components. Only the heavy fragment masses are shown.

(over)

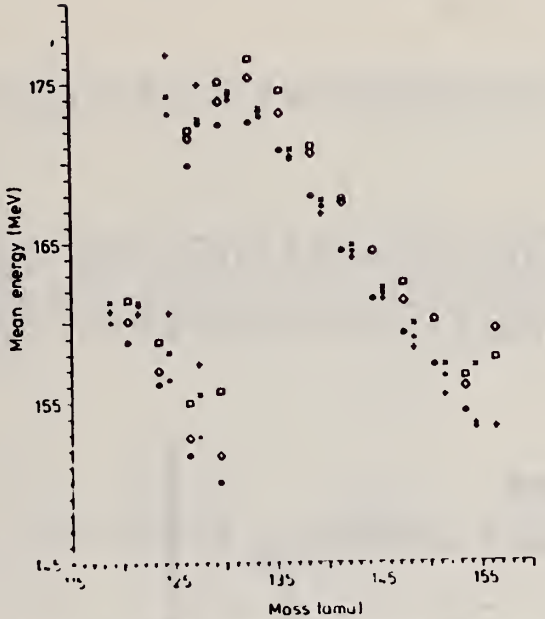

Figure 7. Mean energies of symmetric and asymmetric modes of fission versus heavy fragment mass for ^{235}U and ^{238}U at 30, 50 and 115 MeV electron energies. ●, ^{235}U(30 MeV); +, ^{235}U(50 MeV); ×, ^{235}U(115 MeV). □, ^{238}U(30 MeV); •, ^{238}U(50 MeV); ◇, ^{238}U(115 MeV).

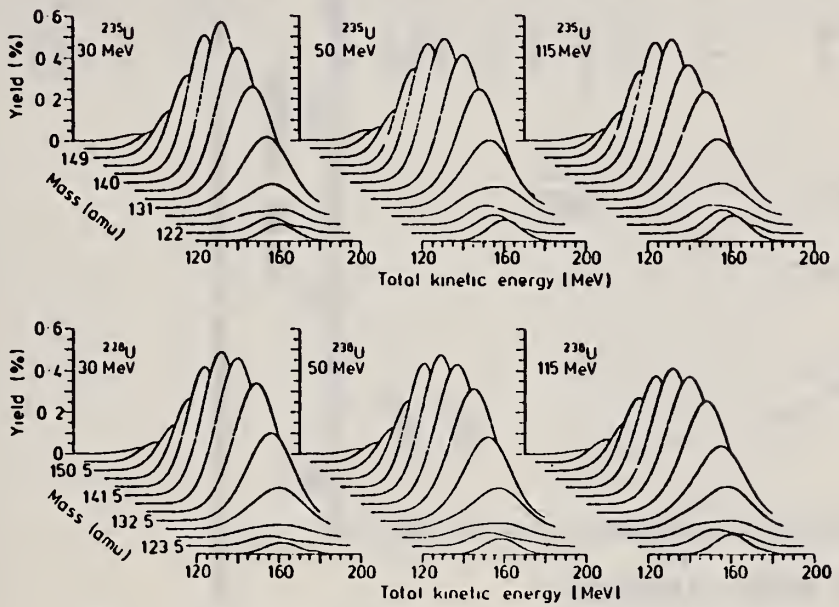

Figure 4. Total kinetic energy yields for ^{235}U and ^{238}U at 30, 50 and 115 MeV electron energies. Curves are least-squares fits to yields for heavy fragment masses in bins of 3 amu. The lowest curve in each set corresponds to symmetric mass division.

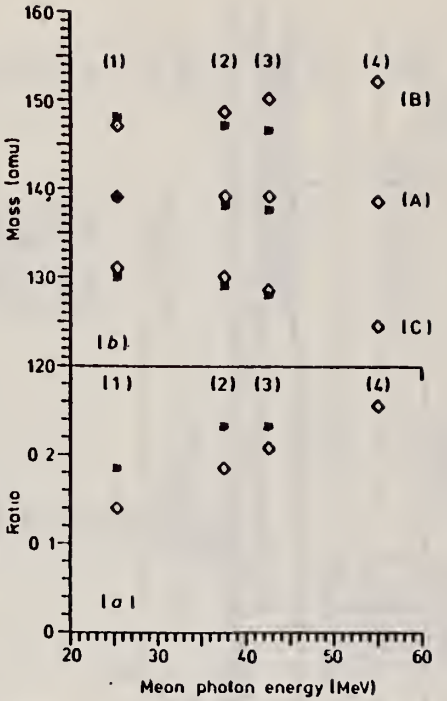

Figure 8. (*a*) Ratio of peak symmetric mass yields to peak asymmetric mass yield against mean photon energy. The data points shown correspond to the difference spectra (1) 50 MeV − 30 MeV; (2) 115 MeV − 30 MeV; (3) 115 MeV − 50 MeV; (4) (115 MeV − 50 MeV) − (50 MeV − 30 MeV). (*b*) (A), mass values of maximum fission yields for the heavy fragment. (B) and (C), mass values corresponding to half of the maximum yields for same difference spectra as (*a*). •, ^{235}U; ◇, ^{238}U.

REF. H. Thierens, D. De Frenne, E. Jacobs, A. De Clercq, P. D'hondt, A. J. Deruytter
Phys. Rev. C14, 1058 (1976)

ELEM. SYM.	A	Z
U	238	92

METHOD

REF. NO. 76 Th 1 hmg

REACTION	RESULT	EXCITATION ENERGY	SOURCE		DETECTOR		ANGLE
			TYPE	RANGE	TYPE	RANGE	
G,F	RLY	THR- 25	C	25	ACT-I		4PI

FISSION PROD YIELD

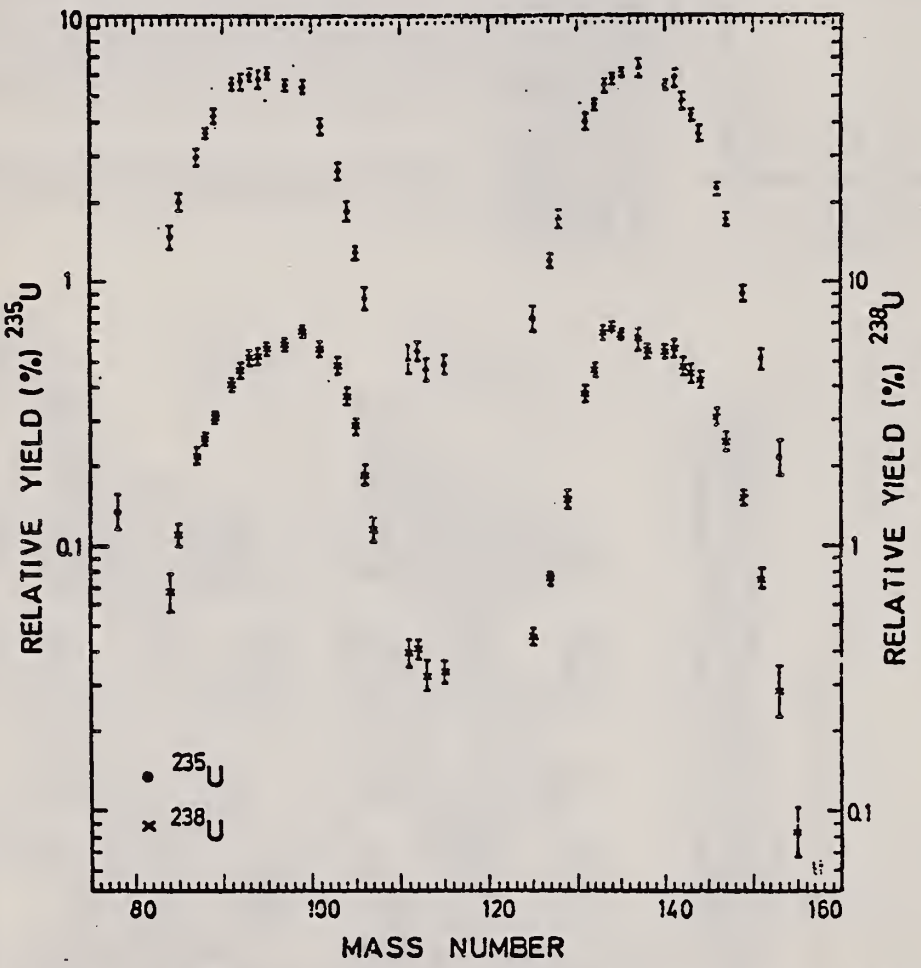

FIG. 1. Postneutron mass distributions for the photofission of ^{235}U and ^{238}U with 25-MeV bremsstrahlung.

(over)

TABLE VII. Independent isomeric yield ratios in fission.

Target	Projectile	Projectile energy (MeV)	Isomeric pair	Spin	$\frac{\sigma_m}{\sigma_m+\sigma_g}$	Ref.
^{233}U	γ (bremsstrahlung)	16	$^{134}Cs^m$-$^{134}Cs^g$	8-4	0.43	37
	n	Thermal	$^{131}Te^m$-$^{131}Te^g$	$\frac{11}{2}-\frac{3}{2}$	0.66±0.03	36
^{235}U	γ (bremsstrahlung)	25	$^{126}Sb^m$-$^{126}Sb^g$	5-8	0.53±0.05	This work
			^{128}Sb(10 min)-^{128}Sb(9 h)	5, 6, 7-8	0.45±0.09	This work
			$^{131}Te^m$-$^{131}Te^g$	$\frac{11}{2}-\frac{3}{2}$	0.58±0.06	This work
	n	Thermal	$^{131}Te^m$-$^{131}Te^g$	$\frac{11}{2}-\frac{3}{2}$	0.64±0.05	36
			$^{133}Te^m$-$^{133}Te^g$	$\frac{11}{2}-\frac{3}{2}$	0.61±0.010	36
^{238}U	γ (bremsstrahlung)	25	^{128}Sb(10 min)-^{128}Sb(9 h)	5, 6, 7-8	0.62±0.22	This work
			$^{131}Te^m$-$^{131}Te^g$	$\frac{11}{2}-\frac{3}{2}$	0.45±0.09	This work
^{239}Pu	n	Thermal	$^{131}Te^m$-$^{131}Te^g$	$\frac{11}{2}-\frac{3}{2}$	0.77±0.04	36

TABLE III. Cumulative chain yields for the photofission of ^{238}U.

Mass chain	Present work	Yield A. Chattopadhyay *et al.*[a] (Ref. 8)	Swindle *et al.* (Ref. 7)
77	•••	0.0673	•••
84	0.67 ±0.12	•••	•••
85	1.10 ±0.11	•••	•••
87	2.20 ±0.16	•••	•••
88	2.56 ±0.10	•••	•••
89	3.06 ±0.16	•••	4.22 ±0.29
91	4.09 ±0.20	4.53	5.35 ±0.37
92	4.63 ±0.27	4.33	•••
93	5.13 ±0.30	4.50	5.84 ±0.41
94	5.21 ±0.36	•••	•••
95	5.55 ±0.30	5.40	•••
97	5.73 ±0.29	5.64	5.75 ±0.40
99	6.48 ±0.28	5.98	•••
101	5.57 ±0.29	•••	•••
103	4.79 ±0.36	4.43	•••
104	3.69 ±0.26	•••	•••
105	2.81 ±0.16	2.61	2.10 ±0.15
106	1.84 ±0.16	2.39	•••
107	1.17 ±0.11	•••	•••
109	•••	•••	0.48 ±0.05
111	0.392±0.048	•••	•••
112	0.408±0.031	0.436	0.21 ±0.02
113	0.324±0.039	•••	•••
115	0.334±0.032	0.475	0.22 ±0.02
125	0.454±0.034	•••	•••
127	0.749±0.035	0.972	1.13 ±0.11
129	1.50 ±0.10	1.81	•••
131	3.74 ±0.27	3.31	2.34 ±0.16
132	4.62 ±0.20	5.07	3.40 ±0.24
133	6.31 ±0.32	6.60	5.61 ±0.39
134	6.59 ±0.33	•••	•••
135	6.26 ±0.20	3.77	4.92 ±0.34
137	6.06 ±0.52	•••	•••
138	5.41 ±0.30	•••	•••
140	5.39 ±0.22	5.53	5.00
141	5.55 ±0.40	6.03	•••
142	4.76 ±0.36	5.40	•••
143	4.51 ±0.33	4.51	5.67 ±0.40
144	4.24 ±0.31	3.18	•••
146	3.05 ±0.17	•••	•••
147	2.46 ±0.18	1.78	2.76 ±0.19
148	•••	0.77	•••
149	1.51 ±0.09	•••	2.09 ±0.15
151	0.758±0.061	•••	1.03 ±0.07
153	0.287±0.061	•••	0.49 ±0.03
155	0.085±0.018	•••	•••
156	•••	0.029	0.095±0.007
157	•••	•••	0.080±0.006

[a]Overall error 8%.

36 D.G. Sarantites, G.E. Gordon, C.D. Coryell, Phys. Rev. 138, B353 (1965).

37 H. Warhanek and R. Vandenbosch, J. Inorg. Chem. 26, 669 (1964).

REF. Yu.A. Vinogradov, V.I. Kasilov, L.E. Lazareva, V.G. Nedorezov, N.V. Nikitina, N.M. Parovik, Yu.N. Ranyuk, P.V. Sorokin
Yad. Fiz. 24, 686 (1976)
Sov. J. Nucl. Phys. 24, 357 (1976)

ELEM. SYM.	A	Z
U	238	92

METHOD

REF. NO. 76 Vi 2 hmg

REACTION	RESULT	EXCITATION ENERGY	SOURCE TYPE	SOURCE RANGE	DETECTOR TYPE	DETECTOR RANGE	ANGLE
G,F	ABY	THR-300	C	50-999	TRK-I		4PI

The 300-MeV and 2-GeV linear electron accelerators at the Physico-technical Institute, Academy of Sciences, Ukrainian SSR, have been used to measure the yields of fragments from photofission for samples of ^{241}Am, ^{243}Am, and ^{238}U in bombardment by bremsstrahlung with various maximum energies $E_{\gamma\,max}$ in the intervals 50–300 and 300–1300 MeV. The relative fissilities of the nuclei have been obtained. Photofission cross-section curves calculated from the experimental data for ^{241}Am and ^{243}Am are compared with the total cross section for hadronic absorption of γ rays by these nuclei in the energy range investigated.

TABLE I. Yield ratios Y_f for photofission fragments (per unit dose, per gram-atom) obtained in irradiation of samples of ^{238}U, ^{241}Am, and ^{243}Am by bremsstrahlung with maximum energies $E_{\gamma\,max}$ = 14.5, 16.6, 30, 39, and 56 MeV.

$E_{\gamma\,max}$, MeV	$Y_f(^{241}Am)/Y_f(^{238}U)$	$Y_f(^{241}Am)/Y_f(^{243}Am)$	$Y_f(^{243}Am)/Y_f(^{238}U)$
14.5	2.42±0.06 (0.15)	2.60±0.10 (0.22)	0.87±0.03 (0.05)
16.6	2.18±0.07 (0.14)	2.65±0.12 (0.22)	0.82±0.03 (0.06)
30	1.93±0.03 (0.12)	2.25±0.05 (0.17)	0.86±0.02 (0.05)
39	1.84±0.02 (0.11)	2.02±0.04 (0.15)	0.91±0.02 (0.06)
56	1.71±0.02 (0.10)	1.99±0.04 (0.15)	0.86±0.02 (0.05)

Note. 1) In the irradiations in the LU-50 MeV accelerator the diameters of the samples were less than the size of the γ-ray beam, and therefore in calculation of the ratios presented in this case we used the ratios of the total weights of the corresponding layers. 2) In order to separate the behavior of the measured ratios with change of the energy $E_{\gamma\,max}$, we have given above only the statistical errors. The errors taking into account the uncertainty in determination of the sample weight, which are systematic in this case, are given in parentheses. 3) The weight of the ^{243}Am layer was determined less reliably and may turn out to be ~10% higher. The ratio $Y_f(^{241}Am)/Y_f(^{243}Am)$ in this case is increased by 10%, and $Y_f(^{243}Am)/Y_f(^{238}U)$ is correspondingly decreased by 10%.

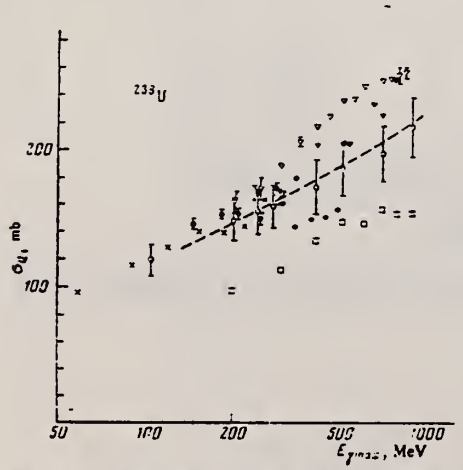

FIG. 5. Photofission cross section per equivalent quantum σ_Q as a function of bremsstrahlung maximum energy $E_{\gamma\,max}$, obtained for ^{238}U in the following studies: ●—Ref. 4; •—Ref. 7, □—Ref. 12, ○—Ref. 13, ▽—Ref. 14, ×—present work. The dashed curve $\sigma_Q(E_{\gamma\,max})$ was obtained by averaging of the data for ^{238}U from Refs. 4, 7, and 12–14.

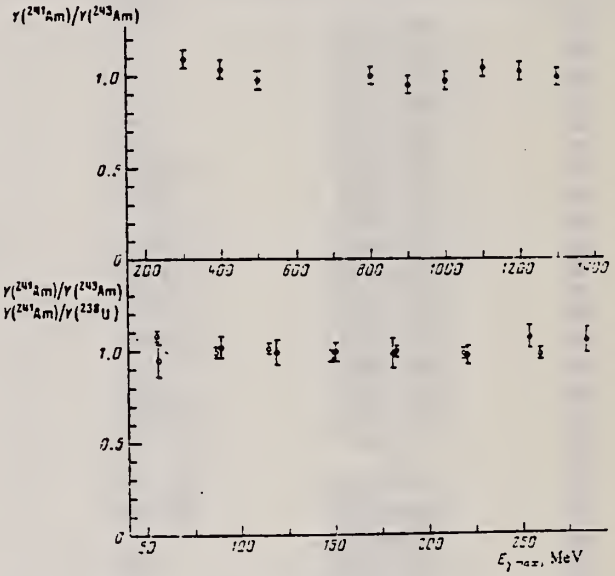

FIG. 3. Ratios of fission fragment yields $Y(^{241}Am)/Y(^{243}Am)$ (●) and $Y(^{241}Am)/Y(^{238}U)$ (○) for various bremsstrahlung maximum energies $E_{\gamma\,max}$ in the range 50–300 and 300–1300 MeV. The values shown are experimental values of the ratios divided by the arithmetic mean for these ratios in this interval of energies $E_{\gamma\,max}$.

[4] J.A. Jungerman et al., Phys. Rev. 106, 585 (1957).

[7] F. Carbonara et al., Nucl. Phys. 73, 385 (1965).

[12] T. Methasiri, Nucl. Phys. A158, 433 (1970).

[13] G.A. Vartapetyan et al., Yad Fiz. 14, 65 (1971); Sov. J. Nucl. Phys. 14, 37 (1972).

[14] Y. Wakuta, J. Phys. Soc. Japan 31, 12 (1971).

U.S. DEPARTMENT OF COMMERCE
NATIONAL BUREAU OF STANDARDS

REF. E. Wolynec, M. N. Martins, and G. Moscati
Phys. Rev. Lett. 37, 585 (1976)

ELEM. SYM.	A	Z
U	238	92

METHOD

REF. NO. 76 Wo 2 hmg

REACTION	RESULT	EXCITATION ENERGY	SOURCE		DETECTOR		ANGLE
			TYPE	RANGE	TYPE	RANGE	
E,A	ABX	THR- 24	D	9- 24	ACT-I		4PI

THORIUM 234 ACTIVITY

Evidence for the α decay of the giant quadrupole resonance is reported. Measurements of the reaction $^{238}U(e,e',\alpha)^{234}Th$ in the region 9-24 MeV are presented. The results imply that the reaction goes dominantly through $E2$ absorption. The amount of $E2$ strength used by the α emission channel exhausts 50% of the isoscalar energy-weighted sum rule.

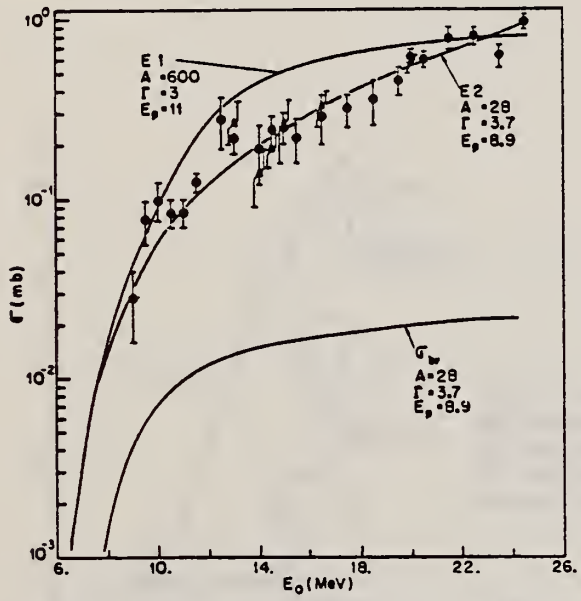

FIG. 3. Experimental cross section for the reaction $^{238}U(e,e',\alpha)^{234}Th$ (circles), versus electron kinetic energy. The triangles refer to the experimental yield for the same reaction induced by electron plus bremsstrahlung. The labeled curves are the calculated values (Breit-Wigner parameters indicated) for the bremsstrahlung yield (curve σ_{br}) and the cross section for (e,e',α) in the cases of a pure $E2$ process (curve $E2$) and a pure $E1$ process (curve $E1$).

REF. V.E. Zhuchko, Yu.B. Ostapenko, A.S. Soldatov, Yu.M. Tsipenyuk
Nucl. Inst. Meth. 136, 373 (1976)

ELEM. SYM	A	Z
U	238	92

METHOD

REF. NO. 76 Zh 2 hg

REACTION	RESULT	EXCITATION ENERGY	SOURCE		DETECTOR		ANGLE
			TYPE	RANGE	TYPE	RANGE	
G,F	ABX	THK-7	C	3-7	TRK-D		90

UNFOLDING SIGMA SOLUT.

Three methods for the solution of experimental subthreshold photofission yield functions for cross-sections of ^{235}U and ^{238}U in the energy range 3.6–7 MeV are presented. Comparison of the resulting cross-sections with the data obtained from reactions with monochromatic photons and charged particles is given.

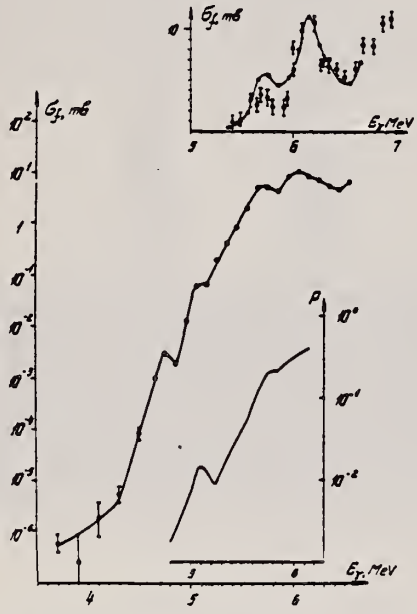

Fig. 3. The photofission cross-section of ^{238}U. In the lower part of the figure: the fission probability for ^{238}U from the (t,pf) reaction[11]). In the upper part: (○) – the results of ref. 13, solid line – our results.

Ref. 13: 75 Di 2 - Dickey, et. al.,
Phys. Rev. Lett. 35, 501 (1975)

REF. V.E. Zhuchko, A.V. Ignatyuk, Yu.B. Ostapenko, G.N. Smirenkin, A.S. Soldatov, Yu.M. Tsipenyuk
JETP Lett. 24, 277 (1976)

ELEM. SYM.	A	Z
U	238	92

METHOD

REF. NO. 76 Zh 3 hg

REACTION	RESULT	EXCITATION ENERGY	SOURCE		DETECTOR		ANGLE
			TYPE	RANGE	TYPE	RANGE	
G,F	RLY	THR-5	C	3-5	TRK-D		DST
		(THR-4.6)		(3-4.6)			

SEE ALSO 71IG1

Extension of work reported in 71IG1

It is established experimentally that the photofission of ^{238}U in the region of the isomer shelf is isotropic. This proves that the shelf in the cross section of the ^{238}U photofission is due to spontaneous fission of the shape isomer, which corresponds to the ground state of the second well.

PACS numbers: 27.90.+b, 24.80.+y

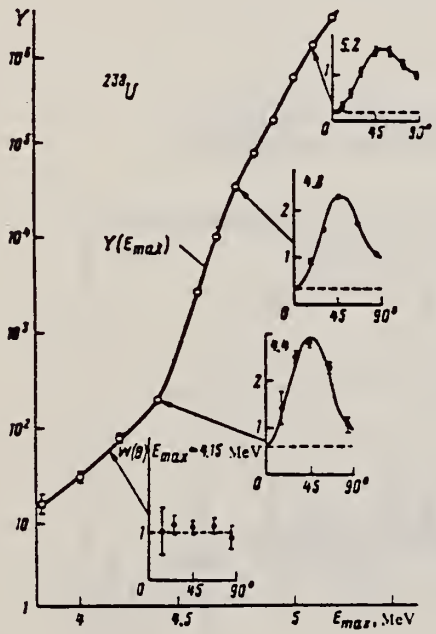

FIG. 1. Dependence of the yield and of the angular distribution of the fragments (in the insert) of the photofission of ^{238}U on the end-point energy of the bremsstrahlung spectrum.

A. Järund and B. Forkman
Z. Physik A281, 39 (1977)

U	238	92	
REF. NO.			
77 Ja 2			egf

REACTION	RESULT	EXCITATION ENERGY	SOURCE TYPE	SOURCE RANGE	DETECTOR TYPE	DETECTOR RANGE	ANGLE
G,NA24	ABY	THR-999	C	400-999	ACT-I		4PI

999=1 GEV

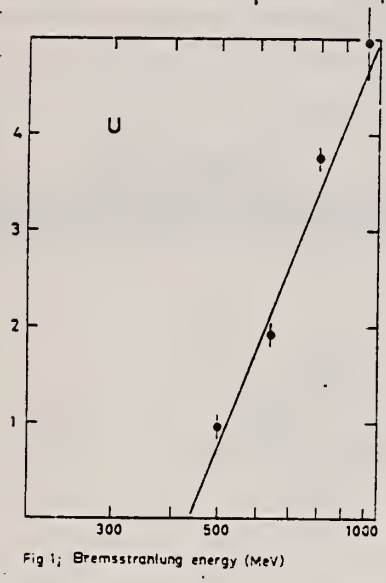

Fig 1; Bremsstrahlung energy (MeV)

Fig. 1a-j. The measured yield as a function of bremsstrahlung end point energy. The error bars give the statistical errors in the numbers of γ-quanta detected. The solid lines are fitted to the yield points with the least-squares method. The yield from Cu (Fig. 1a) is measured in [1] and has been recalculated using the monitor curve of [5]

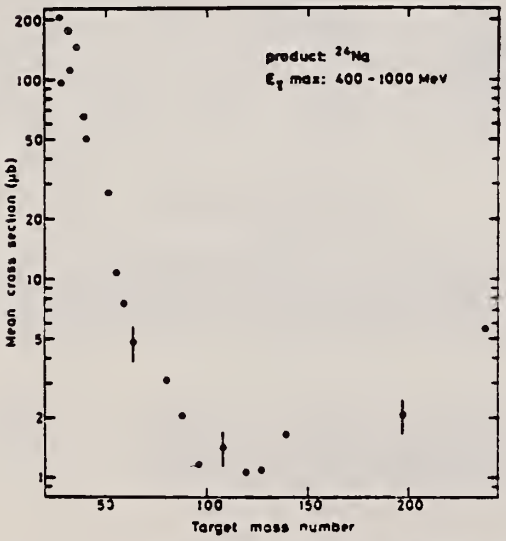

Fig. 2. The mean cross section in the energy range 400 to 1000 MeV calculated from the yields of Figure 1 in this work and of Figures 1 to [illegible]. The error bars given [illegible] bars in some points

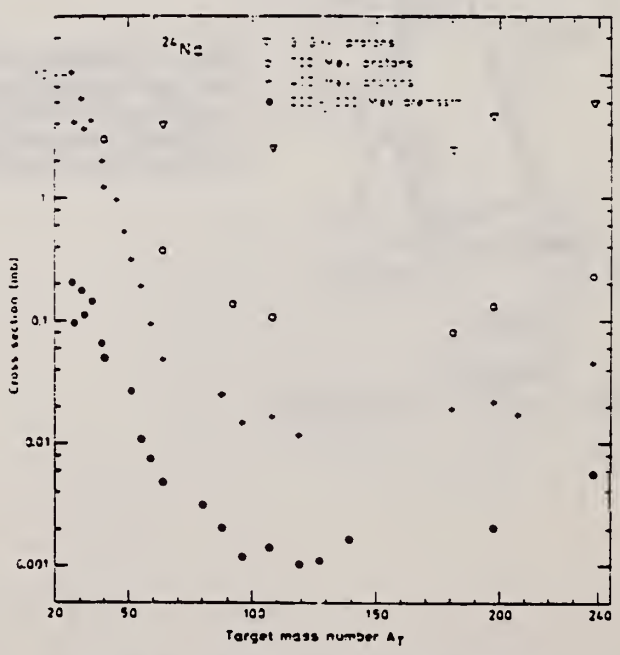

Fig. 4. Mean cross sections of the present work and of [1] (●) compared with the cross sections in proton irradiations: + 400 MeV from [4], ○ 700 MeV from [16] and an extrapolated value from [17], ▽ 3 GeV from [18]

REF. M.N. Martins, E. Wolynec, and G. Moscati
Phys. Rev. C 16, 613 (1977)

ELEM. SYM.	A	Z
U	238	92

METHOD

REF. NO. 77 Ma 4 hmg

REACTION	RESULT	EXCITATION ENERGY	SOURCE		DETECTOR		ANGLE
			TYPE	RANGE	TYPE	RANGE	
E,N	ABX	6-25	D	6-25	ACT-I		4PI

[NUCLEAR REACTIONS $^{238}U(e,e',n)$; $E=6$–25 MeV: measured $\sigma_{e,n}(E)$; DWBA virtual photon analysis, deduced photoabsorption λL.]

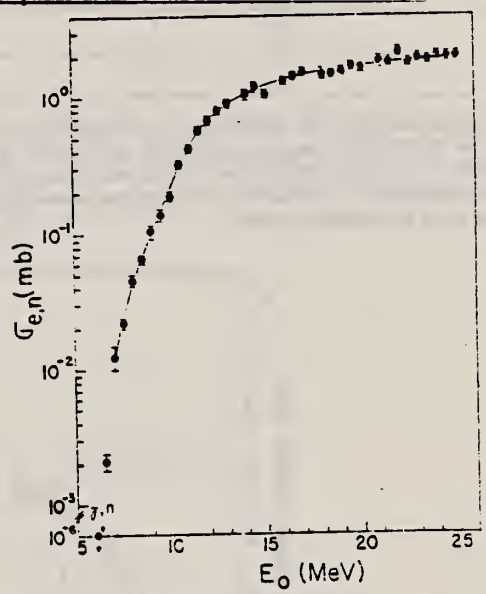

FIG. 4. Experimental cross section for the reaction $^{238}U(e,e',n)^{237}U$ versus electron kinetic energy. The point at 6.0 MeV is an upper limit to the cross section. The full curve is the predicted electrodisintegration cross section for a pure $E1$ process. No free parameters adjusted.

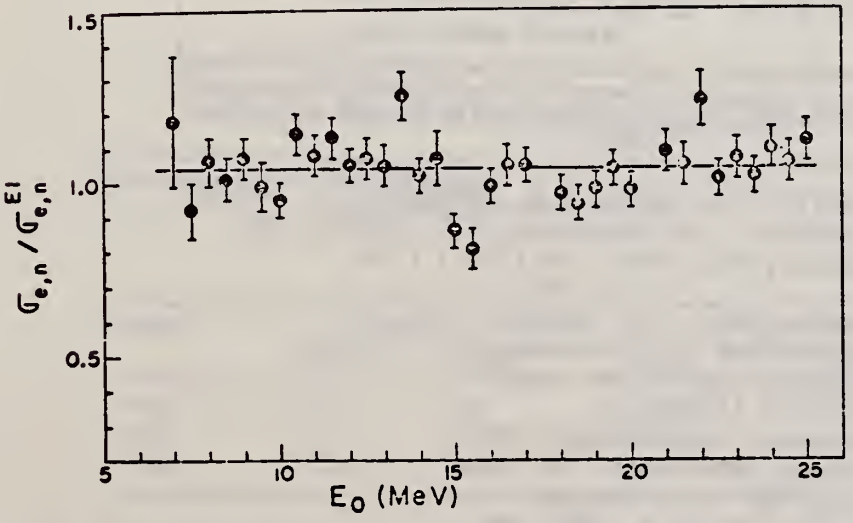

FIG. 5. The ratio of our experimental cross section to the predicted cross section for a pure $E1$ process is shown by the points. The full curve shows the best straight line fit to the points.

REF. A.C. Shotter, D. Branford, J.C. McGeorge and J.M. Reid
Nucl. Phys. A290, 55 (1977)

ELEM. SYM.	A	Z
U	238	92

METHOD

REF. NO. 77 Sh 9

REACTION	RESULT	EXCITATION ENERGY	SOURCE		DETECTOR		ANGLE
			TYPE	RANGE	TYPE	RANGE	
E,G	ABX	C-120	D	20-120	SCD-I		DST

Abstract: Measurements of the electrofission cross section for ^{232}Th, ^{238}U and ^{237}Np have been made for an electron energy range from 20 to 120 MeV. A comparison is made between the electrofission and photofission cross sections using the concept of virtual photons. It is deduced that the electrofission reaction for these elements proceeds through a significant E2 contribution as well as an E1 transition mode.

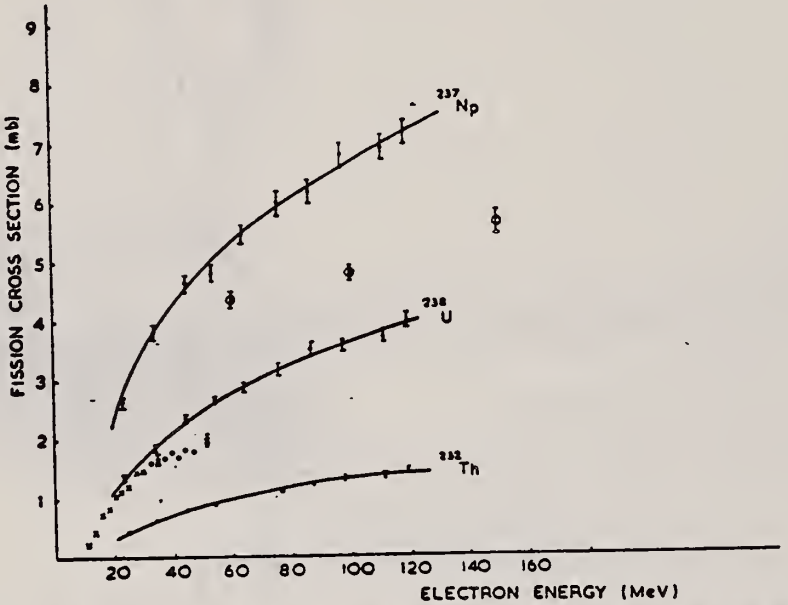

Fig. 1. Total electrofission cross sections versus electron energy. The solid circles are from the present work. Data on ^{238}U from ref. [1]) (open circles) and ref. [3]) (crosses) are also shown. The curves are the best fit to the data as described in the text. The errors shown for the present data are relative only.

[1] L.G. Morretto, R.C. Gatti, S.G. THompson, J.T. Routti, J.H. Heisenberg, L.M. Middleman, M.R. Yearian and R. Hofstadter, Phys. Rev. 179 (1969) 1176

[3] J.D.T. Arruda Neto, S.B. Herdade, B.S. Bhandari and I.C. Niscimento, Universidade de Sao Paulo, report no. IFUSP/P-76 (1976); J.C. Nascimento, S.B. Herdade and J.D.T. Arruda Neto, Proc. Int. Conf. on Photonuclear reactions and applications, Asilomar, 1973, ed. B.L. Berman (Lawrence Livermore Laboratory, Livermore, California) contributed paper, 5D10

over

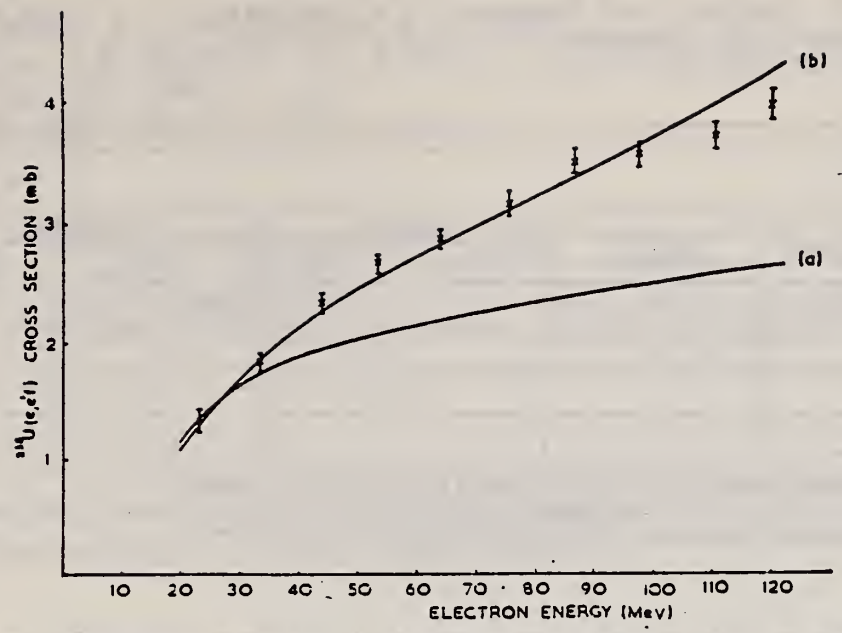

Fig. 3. Electrofission cross section for ^{238}U versus electron energy. The curves (a) and (b) are referred to in the text.

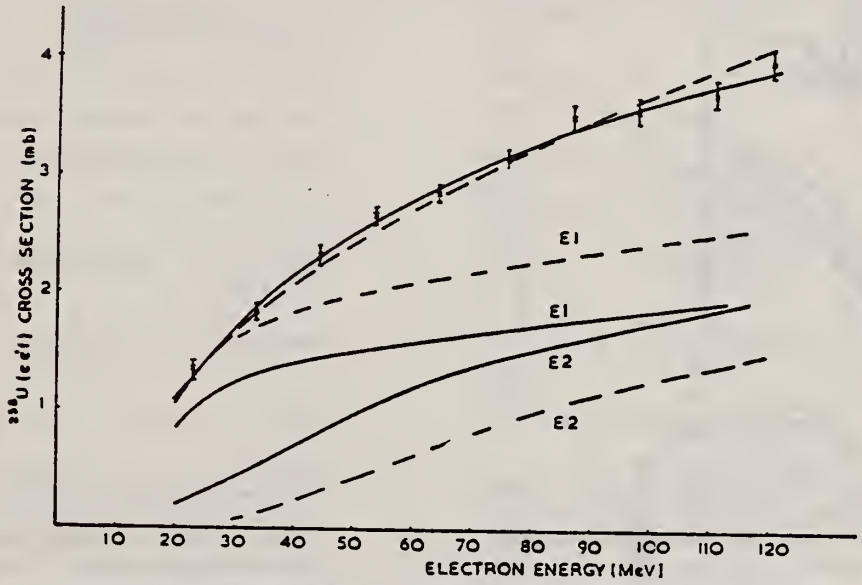

Fig. 5. The ^{238}U(e, e'f) cross sections versus electron energy. The solid and dashed curves through the data are fits to the data as described in the text. The lower solid and dashed curves are the multipole component cross sections of the fitted curves.

TABLE 1

Nucleus	Normalisation		$\int\sigma_{E2(\gamma n)}(E_\gamma)dE_\gamma$	
	9 MeV	22 MeV	9 MeV	22 MeV
^{232}Th	1.17	1.81	2.5 mb · MeV	12.8 mb · MeV
^{238}U	1.00	1.30	6.4 mb · MeV	38.8 mb · MeV
^{237}Np	1.12	1.34	7.9 mb · MeV	52.3 mb · MeV

From table 1 it is observed that the normalisation factors for $E_x = 22$ MeV are higher than would be expected from the absolute experimental errors (± 20%). This may indicate a preferential concentration of E2 strength at 9 MeV.

REF. V.E. Zhuchko, A.V. Ignatyuk, Yu.B Ostapenko, G.N. Smirenkin, A.S. Soldatov and Yu.M. Tsipenyuk
Phys. Lett. 68B, 323 (1977)

ELEM. SYM.	A	Z
U	238	92

METHOD

REF. NO. 77 Zh 1 egf

REACTION	RESULT	EXCITATION ENERGY	SOURCE		DETECTOR		ANGLE
			TYPE	RANGE	TYPE	RANGE	
G,F	ABX	3- 7	C	3- 7	TRK-I		DST

Experimental data on yields and angular distributions of photofission fragments of ^{236}U and ^{238}U are presented. The anomalies caused by delayed fission from the low-lying isomer states of the second well have been clearly observed in the energy dependence of the yields of the isotropic component. Characteristic features of the observed phenomena have been analyzed.

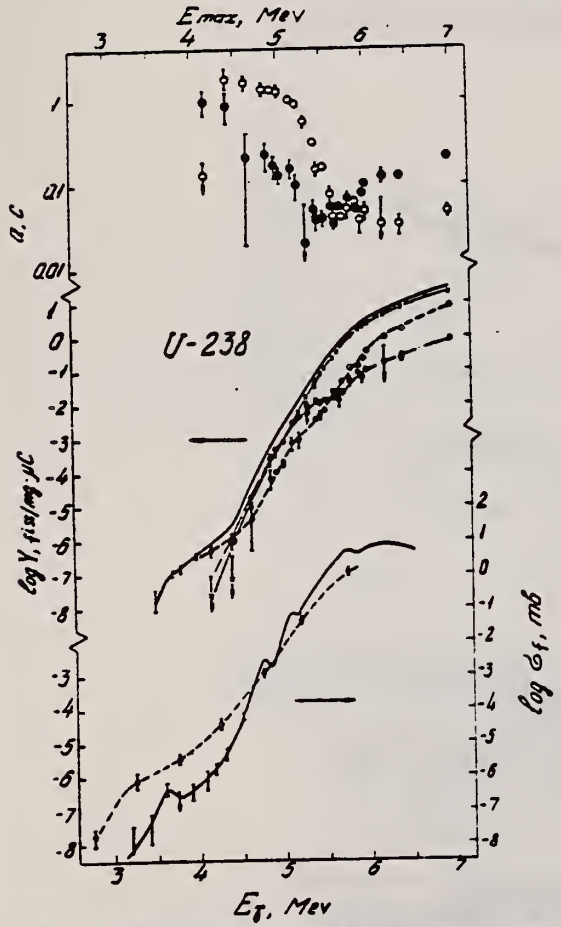

Fig. 1. At the top: the isotropic (•) and quadrupole (○) coefficients of the photofission fragment angular distribution of ^{238}U. At the center: the integral yield $Y(E_{max})$ (solid thick curve) and its angular components: • Y_a, × Y_b and ○ Y_c. At the bottom: the photofission cross section of ^{238}U. The dotted curve is from ref. [1]. All curves are plotted as a function of the electron energy.

REF. B.M. Aleksandrov, A.S. Krivokhatskii, V.L. Kuznetsov, L.E. Lazareva, V.G. Nedorezov, N.V. Nikitina, Yu.N. Ranyuk
Yad. Fiz. 28, 1165 (1978)
Sov. J. Nucl. Phys. 28, 600 (1978)

ELEM. SYM.	A	Z
U	238	92

METHOD

REF. NO.	
78 A1 5	hg

REACTION	RESULT	EXCITATION ENERGY	SOURCE		DETECTOR		ANGLE
			TYPE	RANGE	TYPE	RANGE	
G,F	RLY	THR-999	C	100-999	TRK-D		4PI

999=1.2 GEV

The 300- and 2000-MeV electron linear accelerators have been used to measure the relative fissilities of the nuclei ^{235}U, ^{238}U, ^{237}Np, ^{239}Pu, ^{241}Am, and ^{243}Am. Fragments were detected by glass detectors. Photofission yields were obtained for the nuclei indicated at maximum bremsstrahlung energies 100, 240, 400, and 1200 MeV.

PACS numbers: 25.85.Jg

TABLE I. Relative photofission yields for $E_{\gamma\,max}$ = 100, 240, 400, and 1200 MeV.

Nucleus	Fissility of nuclei in the excitation-energy range ~ 5–12 MeV		Ratios of fragment yields $Y/Y(^{238}U)$ for different maximum energies $E_{\gamma max}$			
	$D_f = \Gamma_f/(\Gamma_f + \Gamma_n)$	Relative fissility	100 MeV	240 MeV	400 MeV	1200 MeV
^{235}U	0.38(b) ·	1.45(a) 1.38(b) 2.13(f)	2.22±0.16	2.15±0.15	1.79±0.13	1.74±0.12
^{238}U	0.22±0.01 *	1.00	1.00	1.00	1.00	1.00
^{237}Np	0.51(b) 0.53(d)	2.53(b) 2.16(c) 2.34(d) 2.93(f)	1.89±0.14	1.92±0.13	1.67±0.12	1.61±0.10
^{239}Pu	0.70(b)	2.70(a) 3.51(b) 3.51(c) 3.45(f)	2.10±0.15	2.10±0.15	1.90±0.13	1.83±0.12
^{241}Am	0.53(e)	1.68(c) ** 2.42(e) 3.27(f)	1.91±0.14	1.77±0.13	1.68±0.10	1.66±0.10
^{243}Am	0.62(e)	2.30(e) 2.59(f)	1.81±0.13	1.81±0.13	1.53±0.11	1.44±0.10

Note. *a*, *b*, *c*, *d*, and *e* denote that the data have been taken respectively from the photofission studies of Refs. 15, 17, 18, 19, and 15. *f* are the average values for the data of a given study on fission by neutrons[20] at nuclear excitation energy ~8 MeV.

*The number given is an average over the results of a large number of studies on photofission of ^{238}U.

**The authors of Ref. 18 point out that the value obtained by them for ^{241}Am is obviously underestimated.

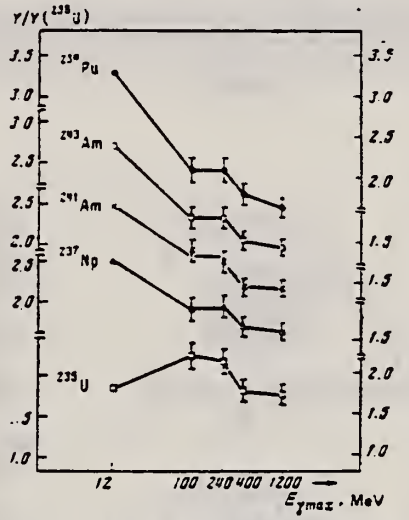

FIG. 2. Relative yields $Y/Y(^{238}U)$ for the nuclei ^{235}U (□), ^{237}Np (△), ^{239}Pu (●), ^{241}Am (×), and ^{243}Am (○) for maximum bremsstrahlung energies $E_{\gamma max}$ ~12, 100, 240, 400, and 1200 MeV.

[15]Yu. A. Vinogradov, V. I. Kasilov, L. E. Lazareva, V. G. Nedorezov, N. V. Nikitina, N. M. Parovik, Yu. N. Ranyuk, and P. V. Sorokin. Yad. Fiz. 24, 636 (1976) Sov. J. Nucl. Phys. 24, 357 (1976).
[16]J. McElhinney and W. E. Ogle, Phys. Rev. 81, 342 (1951).
[17]J. R. Huizenga, Phys. Rev. 109, 484 (1953).
[18]L. Katz, A. P. Baerg, and F. Brown, Proc. of the Second Intern. Conf. on the Peaceful Uses of Atomic Energy, Geneva, 1958, United Nations, Geneva, 1958, Vol. 15, p. 200.
[19]A. Veyssiere, H. Beil, R. Bergere, P. Carlos, A. Lepretre, and K. Kernbath, Nucl. Phys. A199, 45 (1973).

REF. J.D.T. Arruda Neto, S.B. Herdade, B.S. Bhandari & I.C. Nascimento
Phys. Rev. C18, 863 (1978)

ELEM. SYM.	A	Z
U	238	92

METHOD

REF. NO. 78 Ar 11 hmg

REACTION	RESULT	EXCITATION ENERGY	SOURCE		DETECTOR		ANGLE
			TYPE	RANGE	TYPE	RANGE	
E,F	ABX	THR-29	D	5-29	TRK-I		DST
		(THR-28.3)		(5.5-28.3)			

The ^{238}U nucleus was studied measuring the electrofission yield and angular distributions of fission fragments, in the energy range of 5.5 to 28.3 MeV, using a new method of analysis. An $E2$ isoscalar giant resonance was found in the photofission cross section of ^{238}U. This resonance exhausts $(71 \pm 7)\%$ of the energy-weighted sum rule and is located at 9.9 ± 0.2 MeV with a width of 6.8 ± 0.4 MeV. The position of this resonance is in reasonable agreement with the Bohr and Mottelson prediction ($58A^{-1/3}$ MeV). The width of 6.8 ± 0.4 MeV is compatible with a possible triple splitting of the resonance. From the angular distributions of photofission fragments and yield measurements of multipoles other than $E1$, evidence of an $M1$ mixture in the energy region 6–7 MeV was found.

[NUCLEAR REACTIONS, FISSION Electrofission of ^{238}U $(e, e'f)$, $E_0 = 5.5$ to 28.3 MeV, measured electrofission yield and angular distributions of fission fragments. Deduced $E2$ cross section and $E2$ isoscalar giant resonance parameters.]

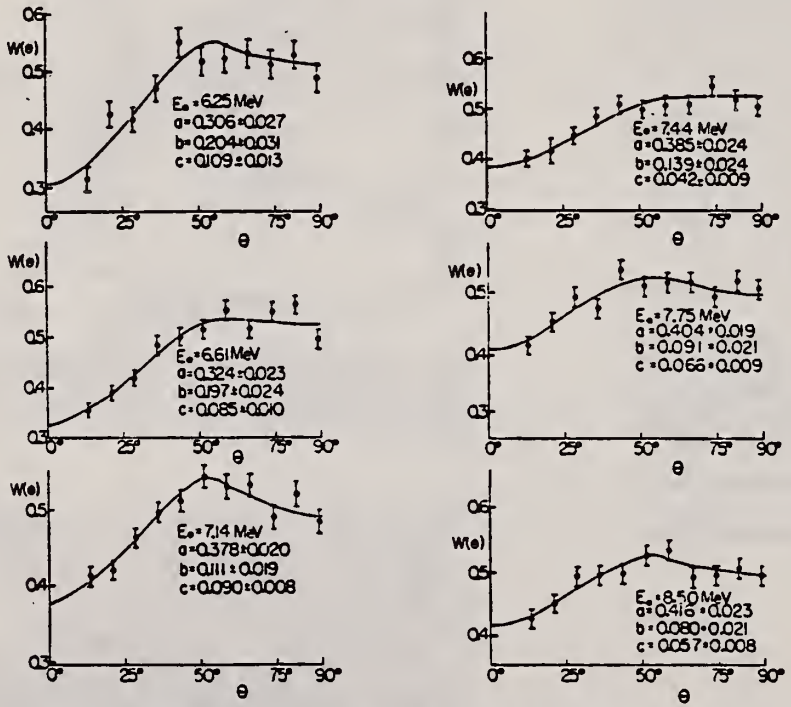

FIG. 1. ^{238}U electrofission fragment angular distributions at several energies, near the fission barrier. The curves are least square fits of the function $W(\theta) = a + b \sin^2\theta + c \sin^2(2\theta)$ to the experimental points.

over

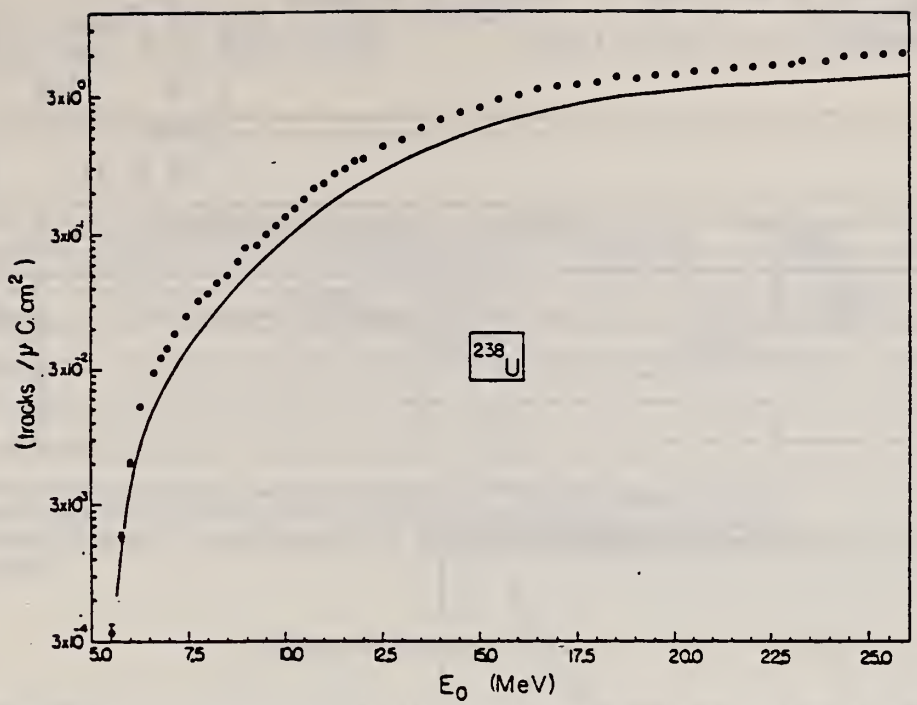

FIG. 2. Experimental electrofission yield for ^{238}U, $Y_{e,e'f}(E_0)$. The continuous curve represents $Y^{\sigma}_{e,e'f}(E_0)$, defined by Eq. (5).

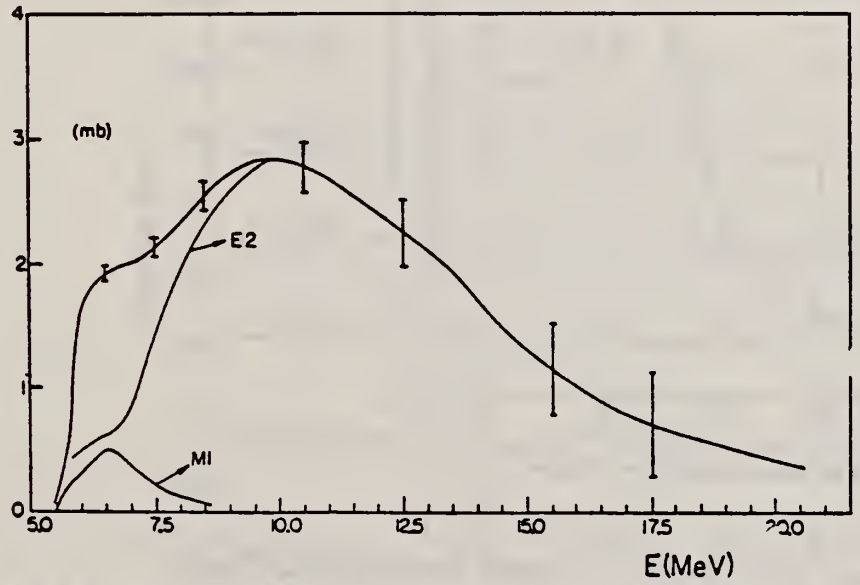

FIG. 5. The $E2$ and $M1$ components of $\sigma^{\text{tot}}_{\gamma,f}$ (mb), as a function of the photon energy. The $M1$ cross section, $\sigma^{M1}_{\gamma,f}(E)$, is represented by a Breit-Wigner curve, with a cutoff at the low-energy tail due to the decrease in the fission probability.

REF. G. Bellia, L. Calabretta, A. Del Zoppo, G. Ingrao, E. Migneco, R.C. Barna, D. De Pasquale
Lettere Al Nuovo Cimento 21, 373 (March 1978)

ELEM. SYM.	A	Z
U	238	92

METHOD

REF. NO. 78 Be 13

hmg 11/18/80

REACTION	RESULT	EXCITATION ENERGY	SOURCE		DETECTOR		ANGLE
			TYPE	RANGE	TYPE	RANGE	
G,F	RLY	THR - 6 (-5.7)	C	3-6 (3.8-5.7)	TRK-I	---	4PI

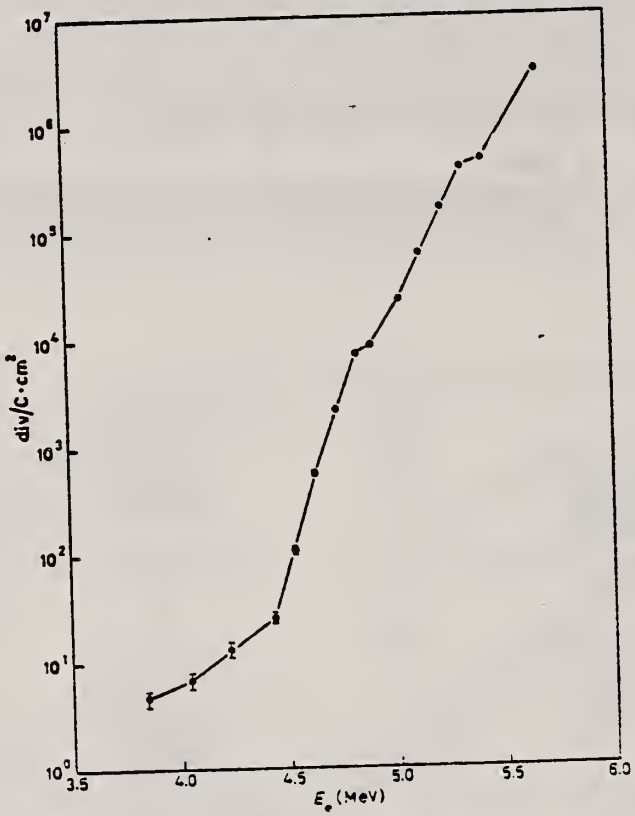

Fig. 1. – ^{238}U photofission yield vs. electron energy: $\bar{d} = 2.31$ mg/cm².

REF. D.H. Dowell, P. Axel and L.S. Cardman
Phys. Rev. C 18, 1550 (1978)

ELEM. SYM.	A	Z
U	238	92

METHOD

REF. NO. 78 Do 4 hg

REACTION	RESULT	EXCITATION ENERGY	SOURCE		DETECTOR		ANGLE
			TYPE	RANGE	TYPE	RANGE	
E,A	ABX	THR- 13	D	13	ACT-I		4PI
				(13.1)			

We performed an experiment which was much more sensitive to the $^{238}U(e,e'\alpha)$ reaction at 13.1 MeV incident electron energy than was a previous experiment which reported surprisingly large cross sections. Our results set an upper limit for the $(e,e'\alpha)$ cross section of about 16 μb, an order of magnitude smaller than that reported earlier.

SIGMA UPPER LIMIT

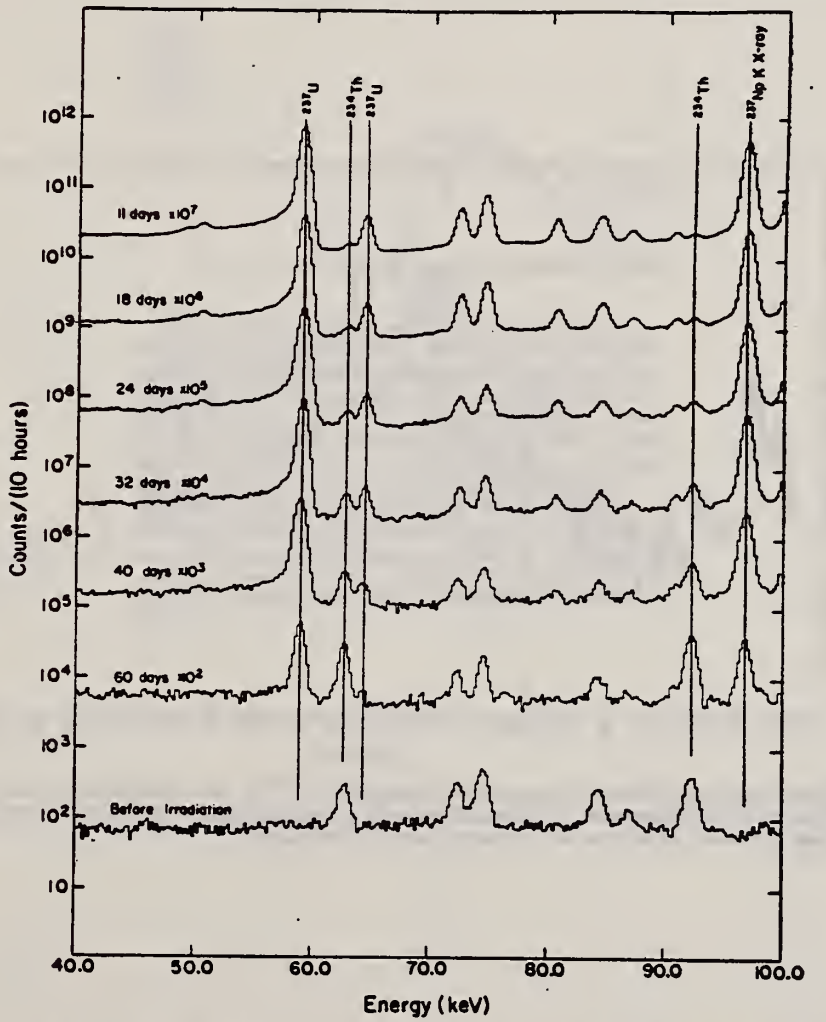

FIG. 1. Observed γ-ray activity from a ^{238}U foil before irradiation (lower spectrum) and at specified intervals after irradiation by 70 mC of charge from a 13.1 MeV electron beam (upper spectra).

REF. W.R. Dodge, E. Hayward, G. Moscati and E. Wolynec
Phys. Rev. C 18, 2435 (1978)

ELEM. SYM.	A	Z
U	238	92

METHOD

REF. NO. 78 Do 6 hg

REACTION	RESULT	EXCITATION ENERGY	SOURCE		DETECTOR		ANGLE
			TYPE	RANGE	TYPE	RANGE	
E,A	SPC	THR- 40	D	40	MAG-D		48
E,P	SPC	7- 40	D	40	MAG-D		48

A search has been made for α particles that might stem from an isoscalar $E2$ giant resonance in ^{238}U near 9 MeV. Using 40 MeV electrons the spectra of protons and α particles emitted in the electrodisintegration of ^{238}U were measured. Peaks in the proton spectrum indicated that the target has an oxygen contamination. The less intense α spectrum contains α particles resulting from the electrodisintegration of ^{16}O, a group that probably stems from ternary fission, and a higher energy feature which may be attributed to the electrodisintegration of ^{238}U. The integrated $^{238}U(e,\alpha)$ cross section is less than 1% of a recently suggested values.

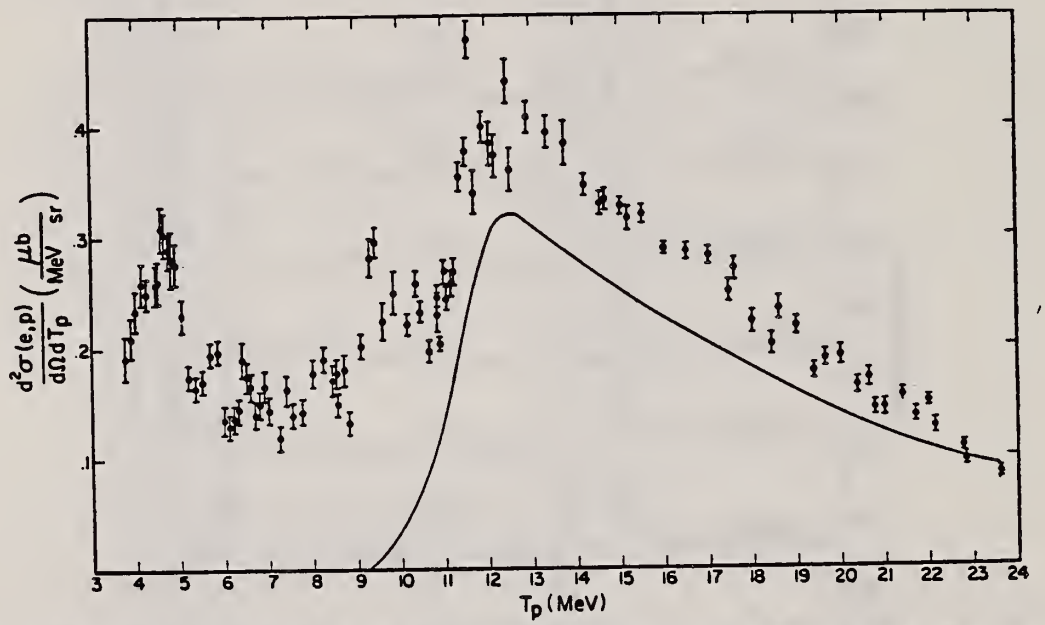

FIG. 1. The proton spectrum obtained in the electrodisintegration of ^{238}U. The peaks below 13 MeV result from the electrodisintegration of a ^{16}O contaminant. The smooth curve is a rough estimate of the proton spectrum from ^{238}U. The absolute values are based on the number of uranium atoms in the target.

over

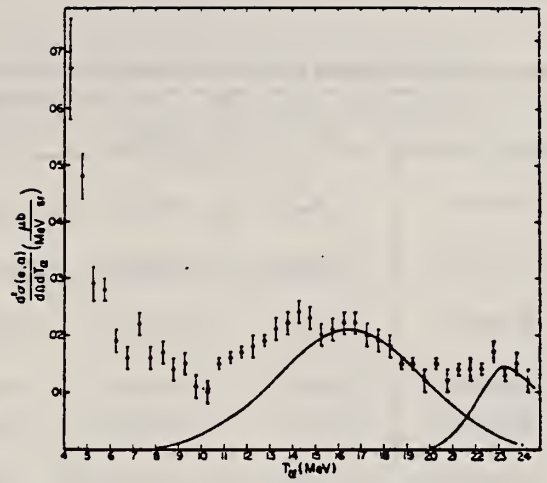

FIG. 2. The α-particle spectrums obtained in the electrodisintegration of ^{238}U. The data have been averaged in half-MeV bins to lessen the error on the individual points. The absolute cross section values are based on the number of ^{238}U atoms in the target. Energy-loss corrections, which amount to 0.5 MeV at 5 MeV and 0.2 MeV at 16 MeV, have not been made. The low energy part of the spectrum results largely from an oxygen contamination of the target. A Gaussian has been fitted through the points between 15 and 20 MeV to map out the part of the spectrum which is thought to result from ternary fission. The higher energy α's near 23 MeV probably stem from the electrodisintegration of ^{238}U.

REF. H. Gäggeler & H.R. Von Gunten
J. Inorg. Nucl. Chem. 40, 1859 (1978)

ELEM. SYM.	A	Z
U	238	92

METHOD

REF. NO. 78 Ga 4 hmg

REACTION	RESULT	EXCITATION ENERGY	SOURCE TYPE	SOURCE RANGE	DETECTOR TYPE	DETECTOR RANGE	ANGLE
G,F	RLY	5-31	C	31	ACT-I		4PI

YIELDS 136CS, 150PM

Table 1. Fractional independent and cumulative yield data from the literature and from this work and corresponding values for Z_p, Z_{UCD}, ΔZ and ν_A

Nuclide	Fract. yield	E_{max} (MeV)	Z_p a)	$\bar{Z}_p$ b)	ν_A c)	Z_{UCD} d)	ΔZ e)	Ref.
^{82}Br	$5.0\cdot10^{-6}$ $4.7\cdot10^{-6}$	23 48	32.45±0.21 32.45±0.21	32.45±0.15	$0^{+0.6}_{-0}$	$31.70^{+0.23}_{-0}$	$0.75^{+0.27}_{-0.15}$	11 12
^{86}Rb	$<1.0\cdot10^{-3}$	25	34.59±0.18 l)	34.59±0.18 l)	0.8±0.5	33.55±0.19	1.04±0.26 l)	2
^{96}Nb	$3.6\cdot10^{-5}$ $(5.7\pm0.7)\cdot10^{-5}$	23 31	38.04±0.24 38.11±0.24	38.08±0.17	1.75±0.4	37.79±0.16	0.29±0.23	11 13
^{99}Nb	$(4.0\pm0.4)\cdot10^{-3}$ f)	31	38.86±0.18 k)	38.86±0.18 k)	1.85±0.4	38.60±0.16	0.26±0.24 k)	13
^{112}Ag	$<1.9\cdot10^{-2}$	48	45.21±0.13 l)	45.21±0.13 l)	2.4±2.0	44.22±0.77	0.99±0.78 l)	12
^{126g}Sb	$(1.2\pm0.5)\cdot10^{-1}$ $(1.3\pm0.5)\cdot10^{-1}$	25 35	49.78±0.08 k) 49.81±0.08 k)	49.80±0.06 k)	$0.1^{+1}_{-0.1}$	$48.74^{+0.35}_{-0.03}$	$1.06^{+0.36}_{-0.07}$ k)	2 2
^{126}Sn	$(7.4\pm0.8)\cdot10^{-1}$ g)	25	50.10±0.17	50.10±0.17	$0.1^{+1}_{-0.1}$	$49.52^{+0.35}_{-0.04}$	$0.58^{+0.39}_{-0.17}$	3
^{126}Sb	$(9.5\pm2.0)\cdot10^{-2}$ h) $(1.0\pm0.2)\cdot10^{-1}$ $(1.0\pm0.2)\cdot10^{-1}$	25 25 35	49.69±0.14 k) 49.72±0.13 k) 49.72±0.13 k)	49.71±0.08 k)	$0.1^{+1}_{-0.1}$	$49.52^{+0.35}_{-0.04}$	$0.19^{+0.36}_{-0.09}$ k)	3 2 2
^{131g}Te ^{131m}Te ^{131}Sb	$(1.1\pm0.4)\cdot10^{-1}$ $(8.6\pm1.3)\cdot10^{-2}$ $(8.0\pm0.8)\cdot10^{-1}$ j)	25 25 25	50.98±0.15 i) 50.98±0.19	50.98±0.12 m)	0.25±0.2	50.74±0.08	0.24±0.14	3 3
^{132}I	$(2.0\pm0.5)\cdot10^{-2}$ $(1.9\pm0.5)\cdot10^{-2}$ $(2.0\pm0.5)\cdot10^{-2}$	25 25 35	51.23±0.17 51.21±0.17 51.23±0.17	51.22±0.10	0.5±0.3	51.22±0.12	0.00±0.16	2 3 2
^{133}I	$(8.0\pm1.5)\cdot10^{-2}$ $(9.0\pm1.5)\cdot10^{-2}$	25 35	51.63±0.14 51.68±0.13	51.66±0.10	0.7±0.35	51.68±0.13	-0.02±0.16	2 2
^{134}I	$2.0\cdot10^{-1}$ $(2.5\pm0.3)\cdot10^{-1}$ $(1.9\pm0.2)\cdot10^{-1}$ $(2.3\pm0.2)\cdot10^{-1}$	21 25 25 35	52.00±0.10 52.11±0.10 51.97±0.09 52.06±0.10	52.03±0.05	0.9±0.35	52.15±0.14	-0.12±0.15	12 3 2 2
^{135}Xe	$(6.6\pm1.0)\cdot10^{-2}$ $(9.0\pm2.0)\cdot10^{-2}$	25 25	52.57±0.13 52.68±0.14	52.62±0.10	1.1±0.3	52.61±0.12	0.01±0.16	3 2
^{136}Cs	$1.8\cdot10^{-3}$ $(4.0\pm1.0)\cdot10^{-3}$ $(8.0\pm1.5)\cdot10^{-3}$ $(3.0\pm0.8)\cdot10^{-3}$ $7.1\cdot10^{-3}$	23 25 25 31 48	52.70±0.17 52.86±0.20 53.01±0.18 52.80±0.21 52.98±0.15	52.88±0.08	1.15±0.3	53.02±0.12	-0.14±0.14	11 3 2 this work 12
^{140}La	$1.1\cdot10^{-3}$	23	54.60±0.19	54.60±0.19	1.3±0.3	54.62±0.12	-0.02±0.22	11
^{150}Pm	$<5.8\cdot10^{-6}$	31	58.49±0.19 l)	58.49±0.19 l)	2.1±0.5	58.79±0.19	-0.31±0.27 l)	this work

a) Most probable charge, calculated from the fractional yields, using the tables of Wolfsberg[16] with $\sigma_Z = 0.62 \pm 0.06$; b) weighted average; c) emitted neutron number from [5]; d) $Z_{UCD} = (Z_f/A_f)X A + \nu_A$); e) $\Delta Z = \bar{Z}_p - Z_{UCD}$; f) yield of 51 min isomer; g) fractional cumulative yield; h) yield of 9 hr isomer; i) calculated from $^{131m+g}$Te; k) lower limit, only one isomer measured; l) upper limit; m) from $^{131m+g}$Te and ^{131}Sb.

Abstract—The fractional independent yields of ^{136}Cs and ^{150}Pm were determined in the photofission of ^{238}U with bremsstrahlung of $E_{max} = 31$ MeV. They were found to be $(3.0 \pm 0.8) \times 10^{-3}$ and $< 5.8 \times 10^{-6}$, respectively. Furthermore, the literature values of fractional independent yields in the photofission of ^{238}U with bremsstrahlung of maximum energies between 21 and 48 MeV are compiled. Most probable charges Z_p were calculated from these data, assuming a Gaussian charge dispersion with a σ_Z of 0.62 ± 0.06. No odd-even corrections were applied. A mean value for ΔZ ($= Z_p - Z_{UCD}$) of 0.05 ± 0.34 was obtained from the limited amount of available data.

REF. W. Gunther, K. Huber, U. Kneissl and H. Krieger
Nucl. Phys. A297, 254 (1978)

ELEM. SYM.	A	Z
U	238	92

METHOD

REF. NO. 78 Gu 2 rs

REACTION	RESULT	EXCITATION ENERGY	SOURCE		DETECTOR		ANGLE
			TYPE	RANGE	TYPE	RANGE	
G,2NF	LFT	THR- 45	C	45	TOF-D		4PI

ISOMER/PROMPT F YLDS

Abstract: A fission isomer with a half-life of 115 ± 5 ns and a yield ratio $Y_{iso}/Y_{prompt} = (2.02 \pm 0.16) \times 10^{-5}$ was observed in bremsstrahlung-induced fission of natural uranium. The isomer is ascribed to ^{236}U populated via a $^{238}U(\gamma, 2n)$ reaction. The integrated cross section for isomeric fission is determined to be $\sigma_{int} = 32 \pm 6\ \mu b \cdot MeV$. Comparing this value with a calculated total isomer production cross section, a branching ratio of the isomer decay of $\Gamma_n/\Gamma_f \approx 6$ can be deduced.

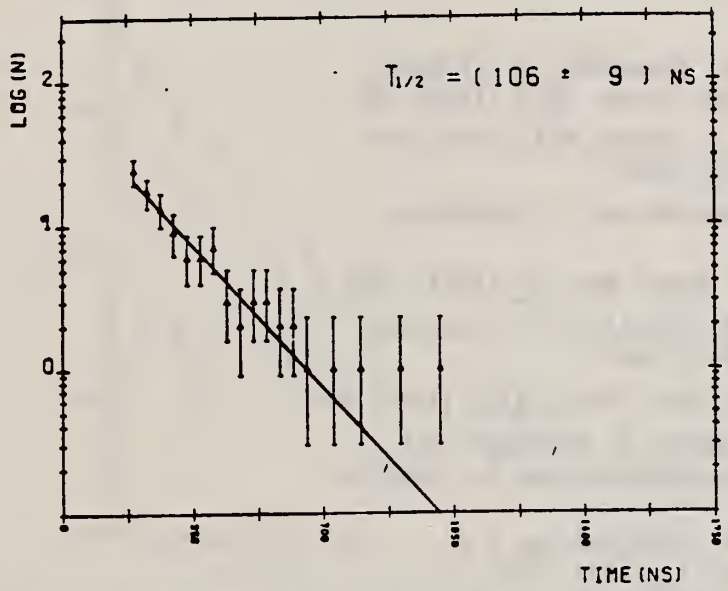

Fig. 2. Example of a measured decay curve (the straight line represents a least-squares fit to the data).

TABLE 1

Experimental results

E_0 (MeV)	Timing	$N_{prompt} \times 10^{-6}$	$T_{1/2}$ (ns)	$(Y_{iso}/Y_{prompt}) \times 10^5$
50	scintill.	5.2	127 ± 11	1.94 ± 0.41
45	trigger	7.7	107 ± 17	1.59 ± 0.47
45	trigger	13.7	118 ± 13	2.09 ± 0.42
45	ferrite	16.0	106 ± 9	2.13 ± 0.37
45	ferrite	14.8	119 ± 10	2.18 ± 0.37
45	ferrite	19.4	111 ± 10	2.02 ± 0.32
		total: 73.8	weighted mean: 115 ± 5	2.02 ± 0.16

over

TABLE 2

Comparison of our results with previous investigations of the ^{236}U form isomer

Reaction	Energy of the projectile (MeV)	$T_{1/2}$ (ns)	$(\sigma_{iso}/\sigma_{prompt}) \times 10^5$	Ref.
^{235}U(d, p)	11.0	130±30	0.96±0.27	[9]
	13.0	110±50	0.31±0.05	[9]
	12.0	130±15	8.6 ±1.3	[10]
	11.0		0.9 ±0.1	[11]
	11.0	130±40	1.46±0.73	[12]
	11.0	116± 7	1.24±0.06	[6]
^{236}U(d, pn)	18.0	105±20		[7]
^{235}U(n, γ)	therm.		<5	[13]
			<4	[14]
			1.0 ±0.2	[15]
	0.5		<2.7	[16]
	2.5		<5	[16]
^{238}U(γ, 2n)	<45	115± 5	2.02±0.16	this work

[6] J. Christiansen, G. Hempel, H. Ingwersen, W. Klinger, G. Schatz and W. Witthuhn, Nucl. Phys. A239 (1975) 253

[7] K.L. Wolf, R. Vandenbosch, P.A. Russo, M.K. Mehta and C.R. Rudy, Phys. Rev. C1 (1970) 2096

[9] N.L. Lark, G. Sletten, J. Pedersen and S. Bjørnholm, Nucl. Phys. A139 (1969) 481

[10] H.C. Britt and B. H. Erkkila, Phys. Rev. C4 (1971) 1441

[11] H.C. Britt, S.C. Burnett, B.H. Erkkila, J.E. Lynn and W.E. Stein, Phys. Rev. C4 (1971) 1444

[12] J. Pedersen and B. Rasmussen, Nucl. Phys. A178 (1972) 449

[13] E. Konecny, H.J. Specht, J. Weber, H. Weigmann, R.L. Ferguson, P. Ostermann, M. Waldschmidt, and G. Siegert, Nucl. Phys. A187 (1972) 426

[14] L.A. Popeko, G.A. Petrov, E.F. Kochubei and T.K. Zvezdkina, Sov. J. Nucl. Phys. 17 (1973) 120

[15] V. Andersen, C.J. Christensen and J. Borggreen, Nucl. Phys. A269 (1976) 338

[16] R. Muller, F. Gonnenwein, F. Kappeler, A. Ernst and J. Scheer, Phys. Lett. 48B (1974) 25

REF. A. Hirsch, C. Creswell, W. Bertozzi, J. Heisenberg, M. V. Hynes, S. Kowalski, H. Miska, B. Norum, F. N. Rad, C. P. Sargent, T. Sasanuma, and W. Turchinetz
Phys. Rev. Lett. 40, 632 (1978)

ELEM. SYM.	A	Z
U	238	92

METHOD

Remarks: B(Ei)=0 in model ($\Delta T=0$), expt limit $[(.75\text{-}2.0)\times10^{-4}]e^2fm^2$.

REF. NO. 78 Hi 1 hmg

REACTION	RESULT	EXCITATION ENERGY	SOURCE TYPE	SOURCE RANGE	DETECTOR TYPE	DETECTOR RANGE	ANGLE
E,E/	LFT	0- 1	D	90-300	MAG-D		DST
		(.680,.827)					

A simple model for nuclear surface vibrations in permanently deformed nuclei does well in reporducing electron scattering cross sections of rotational levels built on a $K^\pi = 0^-$ intrinsic octupole vibration in ^{238}U.

.68,.732,.827 MeV

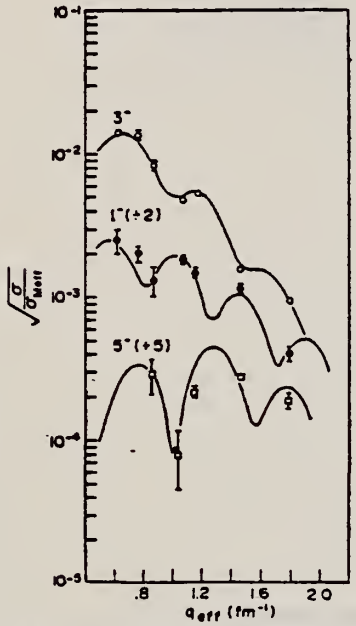

FIG. 2. Experimental data for octupole vibrations in ^{238}U. The curves have been calculated in DWBA using the small vibration expansion and the Hartree-Fock intrinsic density.

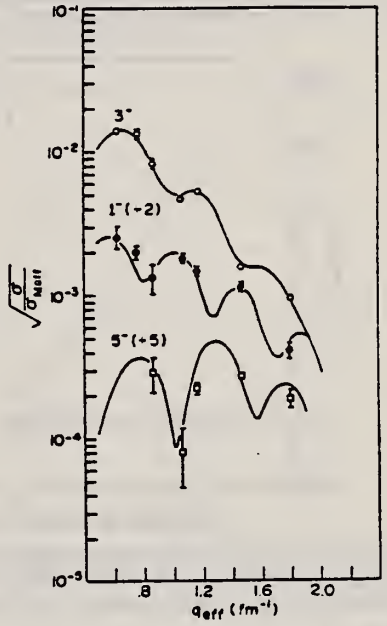

FIG. 3. Experimental data and small vibrational model fit for the three octupole band members observed. The multiple deformed Fermi intrinsic density was used to calculate the vibrational transition charges.

TABLE I. Vibrational parameters.

	HF	MDF	Experiment
$B(E1)$ ($e^2\cdot fm^2$)	0.0	0.0	$(0.75\text{–}2.0)\times10^{-4}$ [a]
$B(E3)$ ($e^2\cdot fm^6$)	5.8×10^5	6.1×10^5	$(6.4\pm0.6)\times10^5$ [b]
			$(5.4\pm0.7)\times10^5$ [c]
$B(E5)$ ($e^2\cdot fm^{10}$)	4.1×10^8	4.1×10^8	...

[a]Ref. 7. [b]Ref. 1. [c]Ref. 2.

[1]E. Gross et al., Phys. Rev. Lett. 35, 565 (1975)
[2]F.K. McGowan et al., Phys. Rev. C 10, 1146 (1974)
[7]F.K. McGowan et al., Bull. Am. Phys. Soc. 16, 493 (1971)

REF. S. Kahane and R. Moreh
Nucl. Phys. A308, 88 (1978)

ELEM. SYM.	A	Z
U	238	92

METHOD

REF. NO. 78 Ka 4 rs

REACTION	RESULT	EXCITATION ENERGY	SOURCE		DETECTOR		ANGLE
			TYPE	RANGE	TYPE	RANGE	
G,G	ABX	8,9	D	8,9	SCD-D		DST

Abstract: The elastic differential scattering cross section of 9.0 MeV photons on ^{239}U has been measured at θ = 1.2°, 1.5°, 25°, 35°, 45°, 60°, 75°, 90°, 120° and 140°. The results show good agreement with theoretical calculations at θ = 1.2° and 1.5°. At 25°, 35°, 45° and 60° a deviation from theory by a factor ≈ 1.8 was observed. This deviation decreased with increasing angle. Those results, together with data at $E \approx 7.9$ MeV in U, were compared with similar data in ^{181}Ta and evidence for the contribution of Coulomb corrections to Delbrück scattering was obtained.

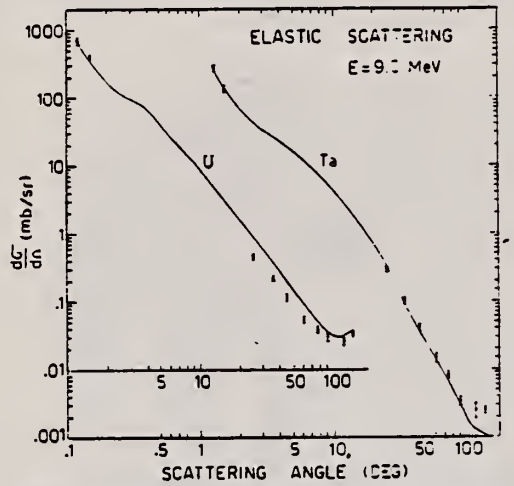

Fig. 2. Differential cross section (mb/sr) for elastic scattering of 9.0 MeV photons from ^{238}U and ^{181}Ta. The solid curve represents the theoretical cross sections obtained by including the coherent contributions of Delbrück, Rayleigh, nuclear resonance, and Thomson scattering amplitudes.

[3] R. Moreh and S. Kahane, Phys. Lett. 47B, (1973) 351
[4] S. Kahane and R. Moreh, Phys. Rev. C9 (1974) 2384
[16] R. Bosch et al., Helv. Phys. Acta 36 (1963) 625

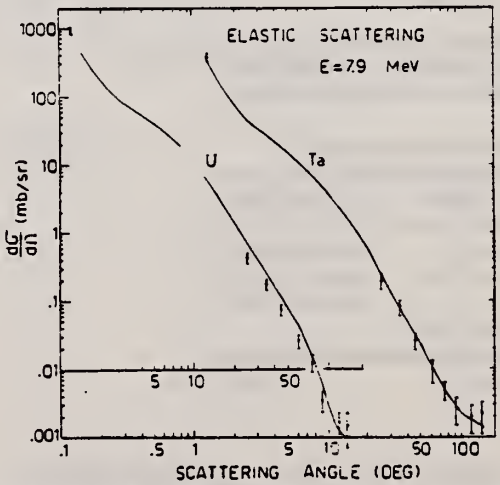

Fig. 3. Differential cross sections for ≈ 7.9 MeV photons. The data at $\theta \approx 1.2°$ [ref. [16]] were measured using E = 7.82 MeV photons from the Ni(n, γ) reaction while those at θ = 25°–140° were obtained [3, 4]) using E = 7.91 MeV photons from the Cu(n, γ) reaction.

TABLE 1

Elastic differential cross section (mb/sr) for 9.0 MeV photons scattered by ^{238}U

θ (deg)	Exp	Calc
1.2	691.0 ± 85.4	693.8
1.5	400.0 ± 19.3	414.5
4.0		69.4
8.0		15.8
15.0		31.2×10^{-1}
25.0	$(461 \pm 38) \times 10^{-3}$	939.0×10^{-3}
35.0	$(216 \pm 17) \times 10^{-3}$	376.0×10^{-3}
45.0	$(113 \pm 12) \times 10^{-3}$	193.0×10^{-3}
60.0	$(54 \pm 7) \times 10^{-3}$	91.0×10^{-3}
75.0	$(39 \pm 5) \times 10^{-3}$	51.0×10^{-3}
90.0	$(30 \pm 4) \times 10^{-3}$	35.0×10^{-3}
120.0	$(26 \pm 3) \times 10^{-3}$	31.0×10^{-3}
140.0	$(33 \pm 3) \times 10^{-3}$	37.0×10^{-3}

REF.	EL EM. SYM.	A	Z
S. Kahane, R. Moreh and O. Shahal Phys. Rev. C 18, 1217 (1978)	U	238	92

METHOD	REF. NO.
	78 Ka 6 hg

REACTION	RESULT	EXCITATION ENERGY	SOURCE		DETECTOR		ANGLE
			TYPE	RANGE	TYPE	RANGE	
G,G	ABX	6- 12	C	6- 12	SCD-D		DST
		(6.84-11.39)		(6.84-11.39)			

Monoenergetic photons at eight energies in the range 6.84–11.39 MeV were elastically scattered from targets of ^{181}Ta, Pb, and ^{238}U at $\theta = 1.21°$–$1.50°$. The differential scattering cross section at such angles was measured relative to the Compton cross section. The photon beam was obtained from the Ni(n,γ) reaction using thermal neutrons. Strong evidence for the contribution of both Rayleigh and the real Delbruck amplitudes and for their destructive interference was obtained.

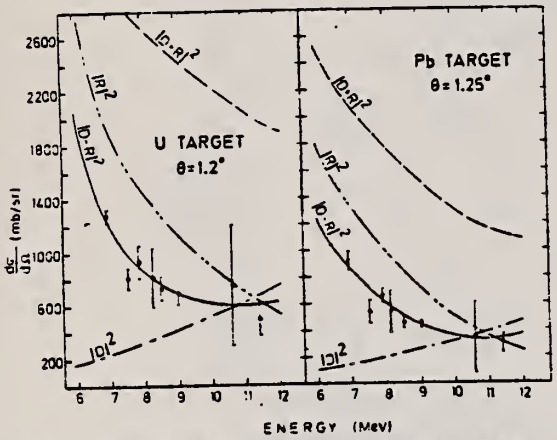

FIG. 3. Differential cross sections for elastic scattering of photons from U and Pb. The solid curves denoted $|D-R|^2$ represent theoretical values obtained by including the Rayleigh, Delbruck, nuclear resonance, and Thomson scattering amplitudes. The dashed curves denoted $|R|^2$ and $|D|^2$ represent almost pure contributions of Rayleigh and Delbruck scattering, respectively. $|D+R|^2$ represents the coherent sum of Delbruck and Rayleigh contributions taken to have the *same* phase. The NR and NT coherent contributions were also included in the dashed curves.

TABLE I. Differential cross section (mb/sr) of elastic photon scattering from U at $\theta = 1.21° \pm 0.26°$ and Pb at $\theta = 1.25° \pm 0.26°$. Columns 4 and 7 give the cross section after excluding the real D amplitudes.

	U ($Z = 92$)			Pb ($Z = 82$)		
E (keV)	Exp.	Theory	No real D	Exp.	Theory	No real D
6837	1274±50	1265	2118	917±68	885	1443
7819	932±120	890	1675	657±53	631	1138
8120	812±220	834	1600	533±160	570	1064
8533	732±90	760	1494	452±45	503	967
8999	691±80	694	1392	443±15	436	868
10596	747±450	604	1169	340±260	333	642
11388	489±114	607	1108	294±70	337	594

REF. L. J. Lindgren; Z. Physik A285, 415 (1978)

ELEM. SYM.	A	Z
U	238	92

METHOD

REF. NO. 78 Li 6 RS

REACTION	RESULT	EXCITATION ENERGY	SOURCE		DETECTOR		ANGLE
			TYPE	RANGE	TYPE	RANGE	
G,F	ABX	5.2-6.4	C	5-6	TRK-D		DST
		5-6					

5.2-6.4 MeV Brems

A measurement of the angular distribution and yield of fission fragments from photofission of ^{238}U has been performed between 5.2 MeV and 6.4 MeV. As γ-source the bremsstrahlung from a microtron has been used. For the detection of the fission fragments, solid state track detectors were used. The yield data were evaluated to approximate cross sections. The data were analyzed within the framework of the double hump barrier model.

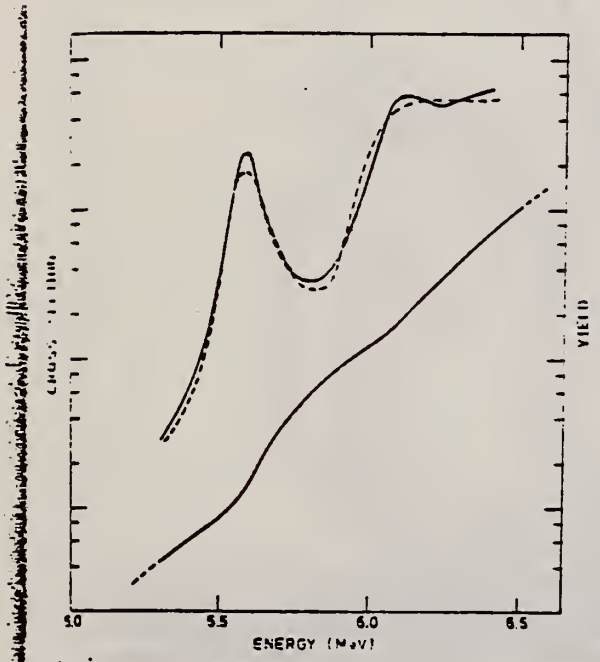

Fig. 3. The solid curves represent the theoretical cross section and the yield. The dashed curve is the evaluated result

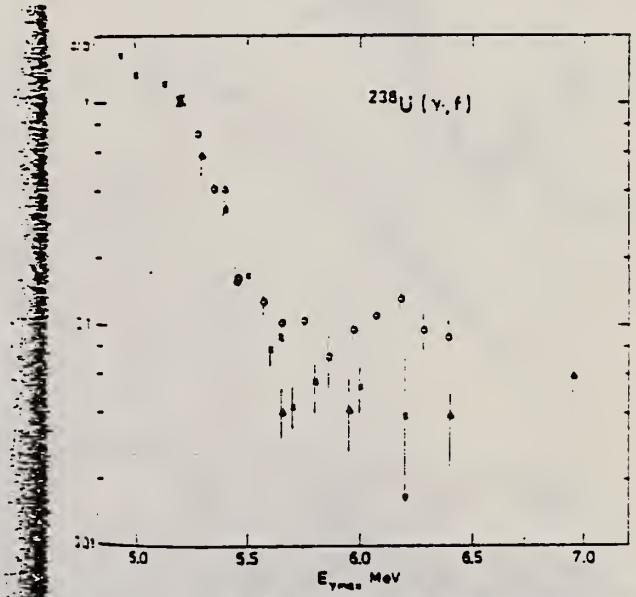

Fig. 4. c/b (e.g. c'/b') as a function of maximum γ-energy. Our measurements (○). Measurements of Ref. 16, 17 (△), (✝) respectively. Errors shown are statistical

over

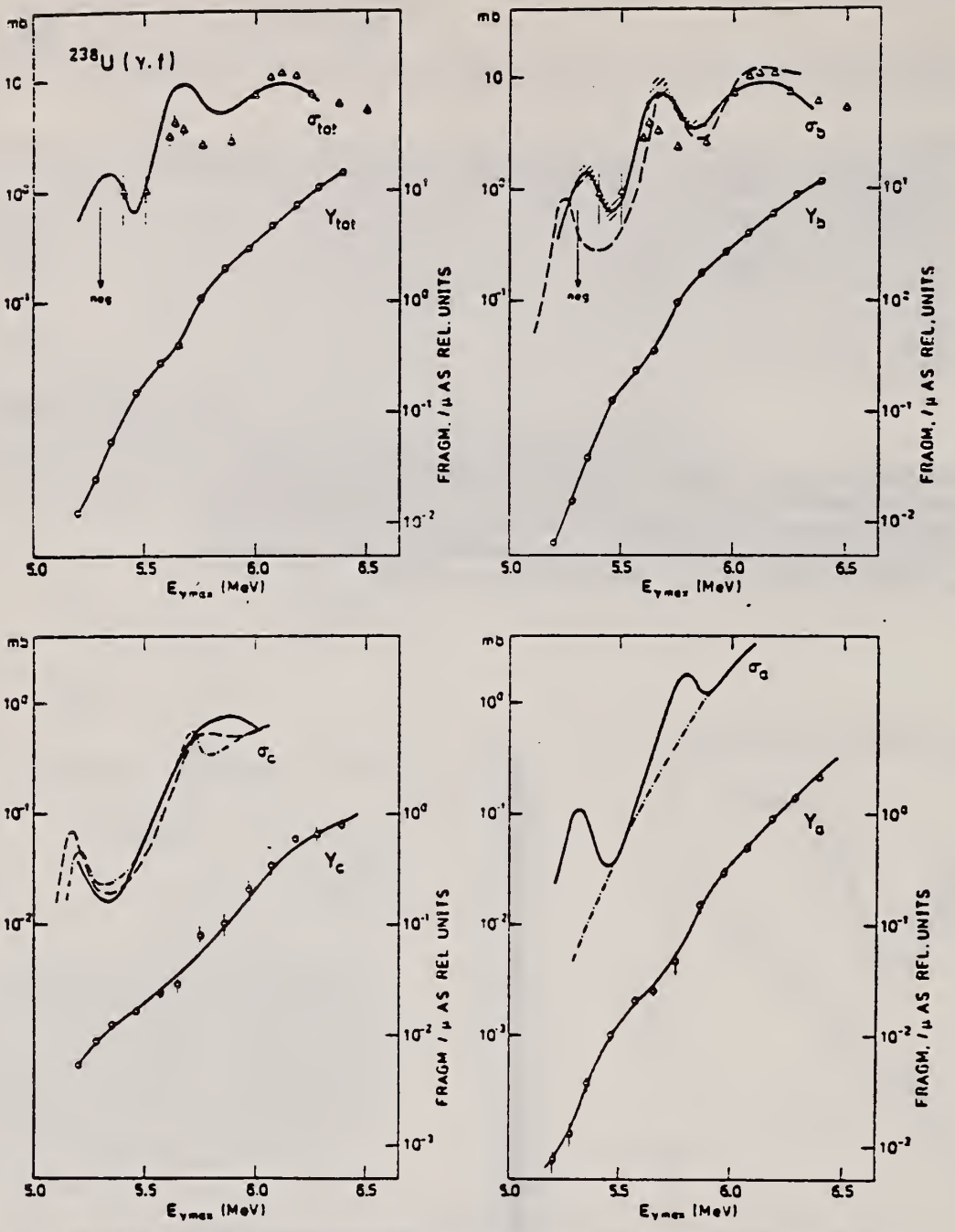

Fig. 2. The figure shows in lower part experimental yields (•) the solid curves are fits to the yield points. The upper part shows corresponding evaluated cross sections (solid curves). The points (•) are data from Axel et al. σ_a: dashed curve gives the final calculated fit. σ_b: dashed curve – a fit with barrier parameters similar to those of Back et al. Dash-dot curve results with the changed resonance parameters. σ_c: dash-dotted curve assumed energy dependence of the cross section which approximately corresponds to the barrier parameters given in Table I. The resonance structure disregarded

REF. J.C. McGeorge, A.G. Flowers, A.C. Shotter and C.H. Zimmerman
J. Phys. G 4, L145 (1978)

ELEM. SYM.	A	Z
U	238	92

METHOD

REF. NO. 78 Mc 5 rs

REACTION	RESULT	EXCITATION ENERGY	SOURCE		DETECTOR		ANGLE
			TYPE	RANGE	TYPE	RANGE	
E,AG	SPC	43	D	43	SCD-D		UNK

Abstract. The unexpectedly large cross section reported by Wolynec *et al* for the $^{238}U(e,\alpha)e'^{234}Th$ reaction has been investigated. Using an activation method the cross section is found to be lower by a factor of at least 6 and the results of a direct alpha-particle counting experiment suggest a factor of at least 20. It is concluded that the alpha-decay mode can, at most, exhaust only a few per cent of the isoscalar energy-weighted sum rule for the giant quadrupole resonance.

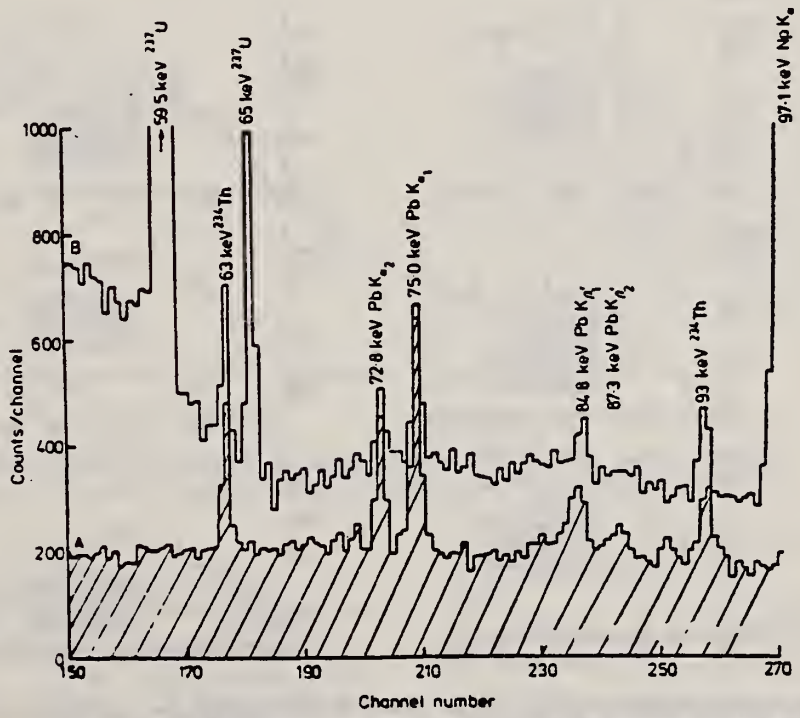

Figure 2. Part of the gamma-ray spectra from ^{238}U (A) before irradiation and (B) after irradiation by 43 MeV electrons.

REF. J.D.T. Arruda Neto, S.B. Herdade, B.S. Bhandari and I.C. Nascimento
Phys. Rev. C 18, 863 (1978)

ELEM. SYM.	A	Z
U	238	92

METHOD

REF. NO. 78 Ne 1 hg

REACTION	RESULT	EXCITATION ENERGY	SOURCE		DETECTOR		ANGLE
			TYPE	RANGE	TYPE	RANGE	
E,F	ABX	THR- 29	D	5- 29	TRK-I		DST

The ^{238}U nucleus was studied measuring the electrofission yield and angular distributions of fission fragments, in the energy range of 5.5 to 28.3 MeV, using a new method of analysis. An $E2$ isoscalar giant resonance was found in the photofission cross section of ^{238}U. This resonance exhausts $(71 \pm 7)\%$ of the energy-weighted sum rule and is located at 9.9 ± 0.2 MeV with a width of 6.8 ± 0.4 MeV. The position of this resonance is in reasonable agreement with the Bohr and Mottelson prediction ($58A^{-1/3}$ MeV). The width of 6.8 ± 0.4 MeV is compatible with a possible triple splitting of the resonance. From the angular distributions of photofission fragments and yield measurements of multipoles other than $E1$, evidence of an $M1$ mixture in the energy region 6–7 MeV was found.

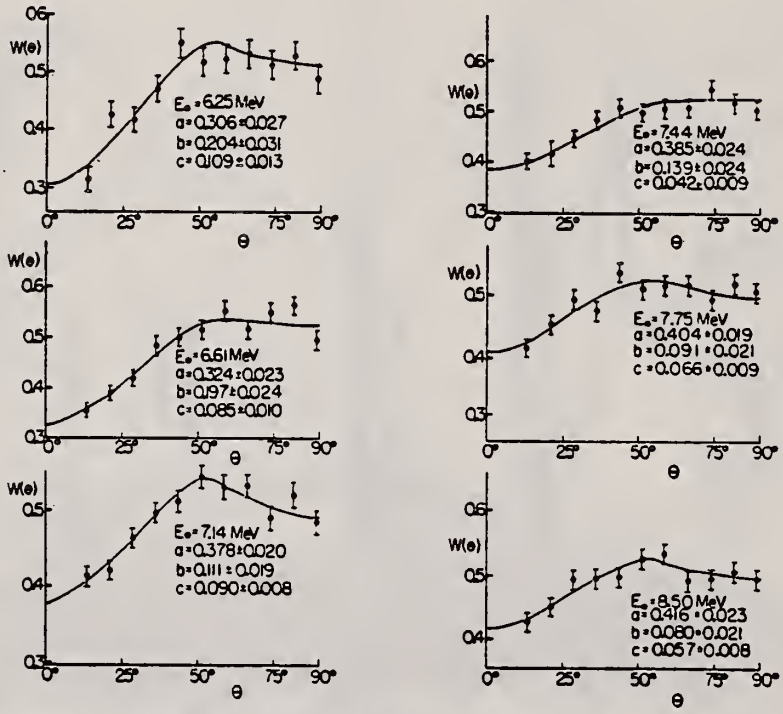

FIG. 1. ^{238}U electrofission fragment angular distributions at several energies, near the fission barrier. The curves are least square fits of the function $W(\theta) = a + b \sin^2\theta + c \sin^2(2\theta)$ to the experimental points.

over

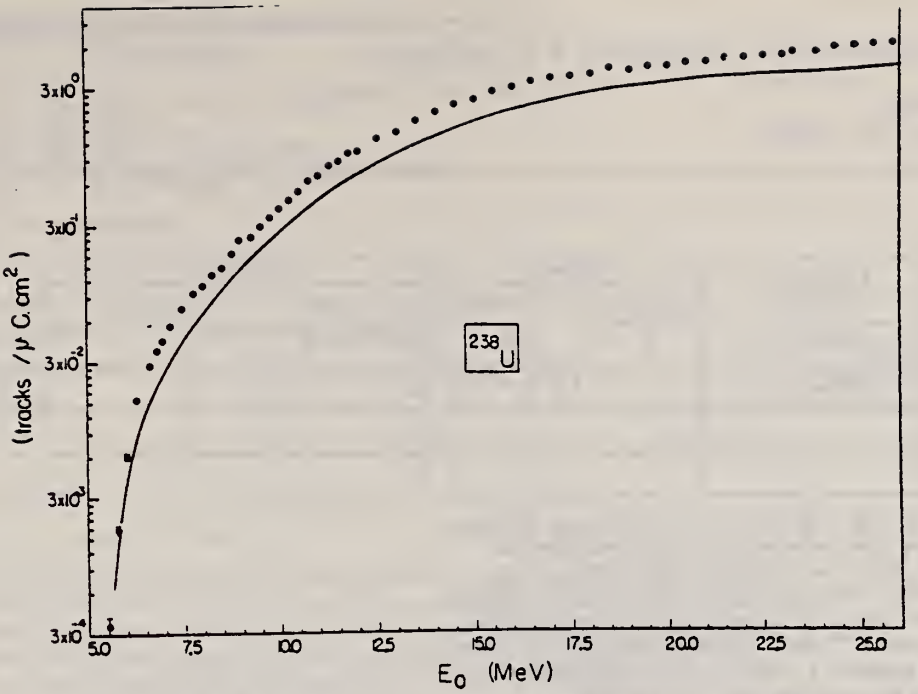

FIG. 2. Experimental electrofission yield for ^{238}U, $Y_{e,e'f}(E_0)$. The continuous curve represents $Y^{*}_{e,e'f}(E_0)$, defined by Eq. (5).

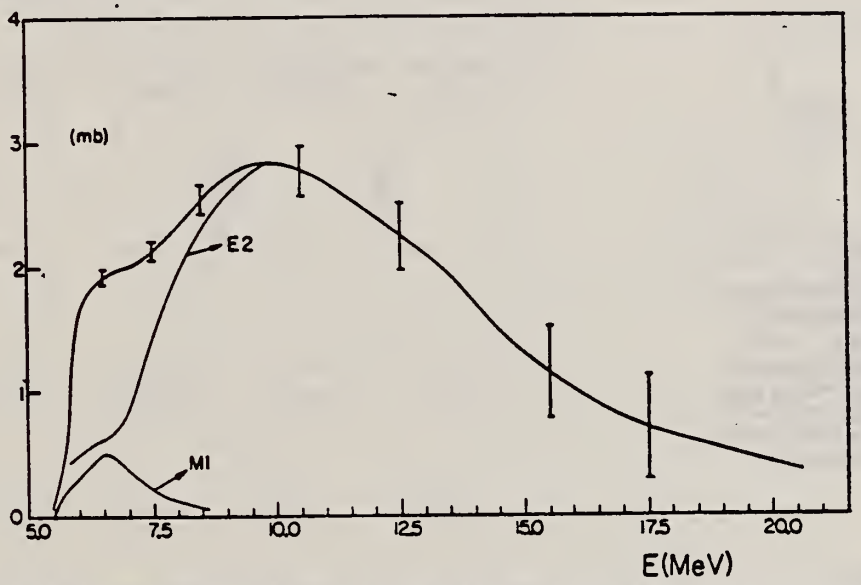

FIG. 5. The $E2$ and $M1$ components of $\sigma^{\text{add}}_{\gamma,f}$ (mb), as a function of the photon energy. The $M1$ cross section, $\sigma^{M1}_{\gamma,f}(E)$, is represented by a Breit-Wigner curve with a cutoff at the low-energy tail due to the decrease in the fission probability.

TABLE II. Isoscalar giant quadrupole resonance in ^{238}U.

Peak (MeV)	Width (MeV)	%EWSR	Reaction	Reference
10–13	···	85	(p,p')	Lewis and Horen (Ref. 4)
8.9 ± 0.3	3.7 ± 1.2	80(50)[a]	$(e,e'\alpha)$	Wolynec *et al* (Ref. 5)
10.5 ± 0.2	$3.9^{+1.1}_{-0.5}$	40	(e,e')	Houk *et al.*[b]
9.9 ± 0.2	6.8 ± 0.4	71	$(e,e'f)$	Present work

[a]The value of 80% was calculated by using expression (84) of Ref. 19 and the rms value of 5.730 fm (Ref. 7) for the ^{238}U nuclear radius. The published value is 50%.
[b]These values are for the parameters of the cross section. The values in Ref. 7 are for the reduced transition probability.

4 M.B. Lewis and D.J. Horen, Phys. Rev. C 10, 1099 (1974)

5 E. Wolynec, M.N. Martins, and G. Moscati, Phys. Rev. Lett. 37, 585 (1976)

7 W.A. Houk, R.W. Moore, F.R. Buskirk, and R. Pitthan, Naval Postgraduate School report (unpublished)

19 J.S. O'Connel, in Proceedings of the international Conference on Photonuclear Reaction and Applications, Asilomar, 1973, edited by B.L. Berman (Lawrence Livermore Laboratory, Univ. of California, 1973). Vol. I, p. 71.

REF. V.E. Zhuchko, Yu.B. Ostapenko, G.N. Smirenkin, A.S. Soldatov, Yu.M. Tsipenyuk
Yad. Fiz. 28, 1185 (1978)
Sov. J. Nucl. Phys. 28, 611 (1978)

ELEM. SYM.	A	Z
U	238	92

METHOD

REF. NO. 78 Zh 6 hg

REACTION	RESULT	EXCITATION ENERGY	SOURCE		DETECTOR		ANGLE
			TYPE	RANGE	TYPE	RANGE	
G,F	ABX	THR-5	C	3-5	TRK-D		4PI
		(THR-4.6)		(3.5-4.6)			

Yield measurements are reported for photofission of ^{232}Th, ^{236}U, ^{238}U, and ^{237}Np in the deep sub-barrier energy region 3.5–4.6 MeV where anomalies in the cross section—isomeric shelfs—were previously observed [Phys. Rev. C, 12, 863 (1975)]; Pis'ma. Zh. Eksp. Teor. Fiz. 22, 255 (1975), [JETP Lett. 22, 118 (1975)]. The various sources of background arising in this energy region, which is only with difficulty accessible for measurements, are analyzed in detail. Analysis of the anomalies in the behavior of the integrated photofission yields in the case of the two nuclei ^{236}U and ^{238}U most favorable for study indicates a resonance nature of the cross sections for delayed fission and a substantially more complicated physics of the phenomenon than the simplified interpretation of Bowman [Phys. Rev. C, 12, 863 (1975)].

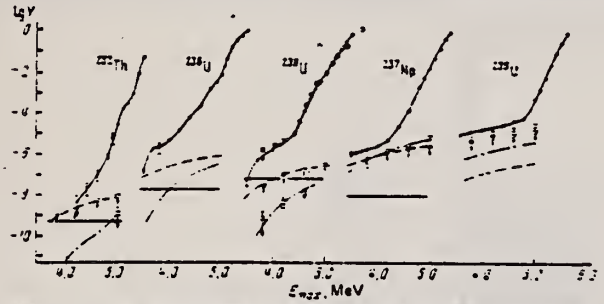

FIG. 2. The round points are the results of measurement of the yields $Y(E_{max})$ in fissions/mg-μC of the photofission reaction: ●—present work and Ref. 7; ○—Ref. 8. ⁻ and dashed lines—respectively the experimental and theoretical estimates of the background due to fissions by neutrons from the reaction Be(γ,n); ○ and dot-dash lines—the same for the D(γ,n) reaction. The shaded sections show the level of background from spontaneous fission and fission induced by cosmic rays.

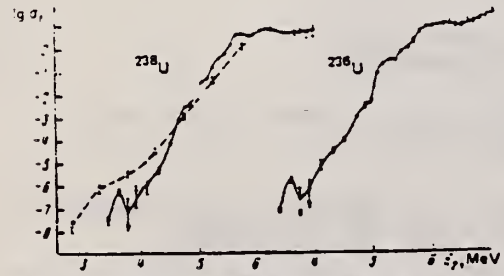

FIG. 3. Photofission cross sections $\sigma_f(E_\gamma)$ in mb for ^{236}U and ^{238}U: ●—results of the present work and Ref. 7; ○ data of Ref. 2.

REF. V.E. Zhuchko, Yu.B. Ostapenko, G.N. Smirenkin, A.S. Soldatov, Yu.M. Tsipenyuk
Yad. Fiz. 28, 1170 (1978)
Sov. J. Nucl. Phys. 28, 602 (1978)

ELEM. SYM.	A	Z
U	238	92

METHOD

REF. NO. 78 Zh 7 hg

REACTION	RESULT	EXCITATION ENERGY	SOURCE TYPE	SOURCE RANGE	DETECTOR TYPE	DETECTOR RANGE	ANGLE
G,F	ABX	THR-7	C	4-7	TRK-D		4PI
				(4.4-7.)			

The bremsstrahlung beam of the microtron at our Institute has been used to measure photofission yields of nine nuclei—^{232}Th, ^{233,235,236,238}U, ^{237}Np, ^{239,241}Pu, and ^{241}Am in the energy region 4.4–7.0 MeV. The method of minimization of the directed deviation was used to reproduce the photofission cross sections from the integrated yields. The following problems are discussed in terms of the experimental data: resonance structure of the cross sections, effects of a two-humped shape of the fission barrier, and comparison of the fissility in the (γ,f) and (n,f) reactions and in direct reactions.

PACS numbers: 25.85.Jg

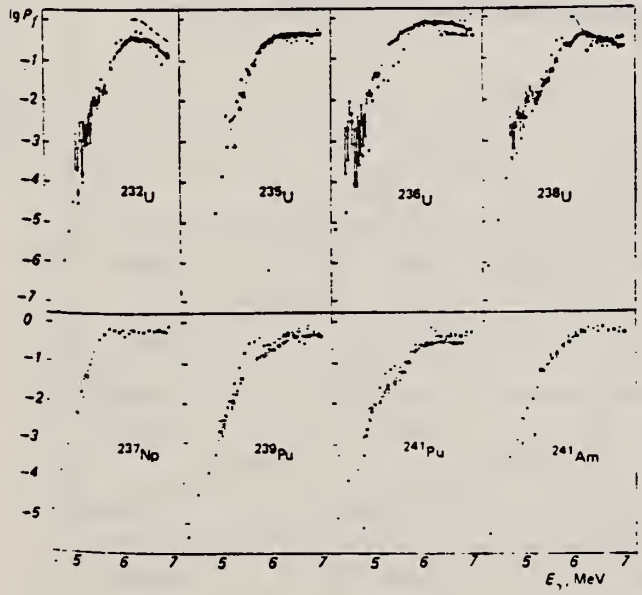

FIG. 4. Fissility P_f in the reactions (γ,f)—●, (n,f)—△ (Ref. 14), and in direct reactions—○.[2] The dashed curve shows the results of evaluation of P_f in accordance with Eq. (9).

(over)

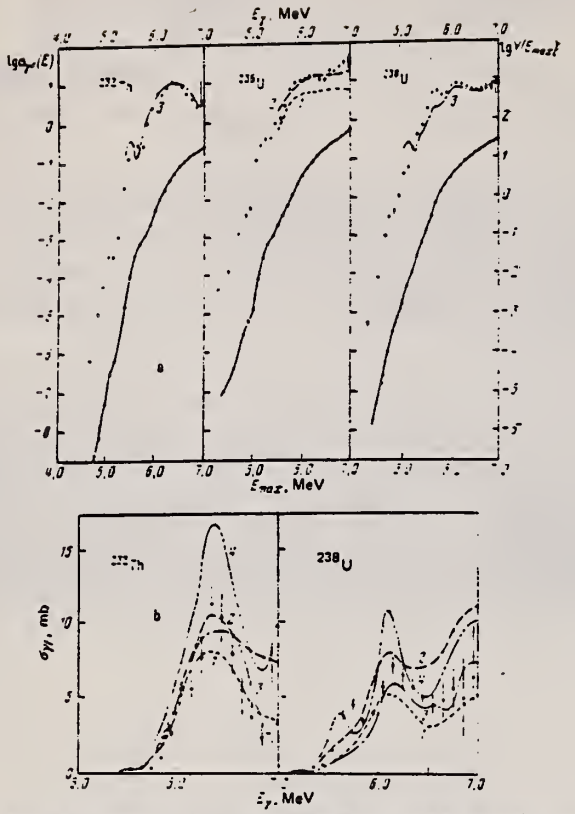

FIG. 2. Yields $Y(E_{max})$, fissions/mg-μC (lower curve), and cross sections $\sigma_{\gamma f}(E_\gamma)$, mb (upper curve). of the photofission reaction for even-even isotopes—a; comparison of the functions $\sigma_{\gamma f}(E_\gamma)$ obtained in the present work for ^{232}Th and ^{238}U with data obtained in quasimonochromatic γ rays—b. Curves: solid lines (and points)—results of the present work, 1—data of Ref. 5, 2—data of Ref. 6, 3—data of Ref. 7, 4—data of Ref. 8.

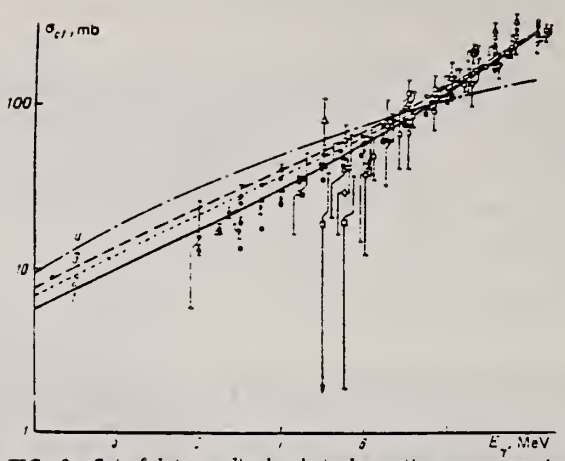

FIG. 6. Set of data on dipole photoabsorption cross sections σ_{c1}. The solid line (1)—the present work—is the result of fitting the data of Ref. 6 by Eq. (2) in the region $E_\gamma = 6$–10 MeV. Curves 2 and 3 are an extrapolation of the fit from Ref. 16 (2) and Ref. 17 (3) for ^{238}U; curve 4 is an estimate by means of Axel's formula.[15] Points: □, ■—^{232}Th: △, ▲—^{235}U: ◆—^{236}U: ○, ●—^{238}U; ▽, ▼—^{237}Np; ◇—^{239}Pu. The hollow points are from Refs. 16 and 17: the solid points are from Ref. 6.

REF. J. Aschenbach, R. Haag, H. Krieger
Z. Phys. A292, 285 (1979)

ELEM. SYM.	A	Z
U	238	92

METHOD

REF. NO. 79As4 hg

REACTION	RESULT	EXCITATION ENERGY	SOURCE		DETECTOR		ANGLE
			TYPE	RANGE	TYPE	RANGE	
E,F	ABX	THR-65	D	7-65	TRK-D		DST

Absolute electrofission cross sections for ^{238}U and ^{232}Th in the energy region $E_e = 7 - 65$ MeV and fission fragment angular distributions for $E_e = 7 - 30$ MeV have been measured. The angular distributions show strong anisotropies for low energies. The relative dipole and quadrupole contributions as a function of excitation energy are discussed in terms of the low lying fission transition states above the fission barriers. The cross sections show significant deviations from the results of some earlier measurements, in particular in the energy region above the giant dipole resonance. From the difficulties of absolute electrofission cross section measurements and the ambiguities in their interpretation it is concluded that by this time the quantitative analysis of electrofission cross sections with respect to the contributions of the giant quadrupole resonances to the fission decay channel should be regarded as rather tentative.

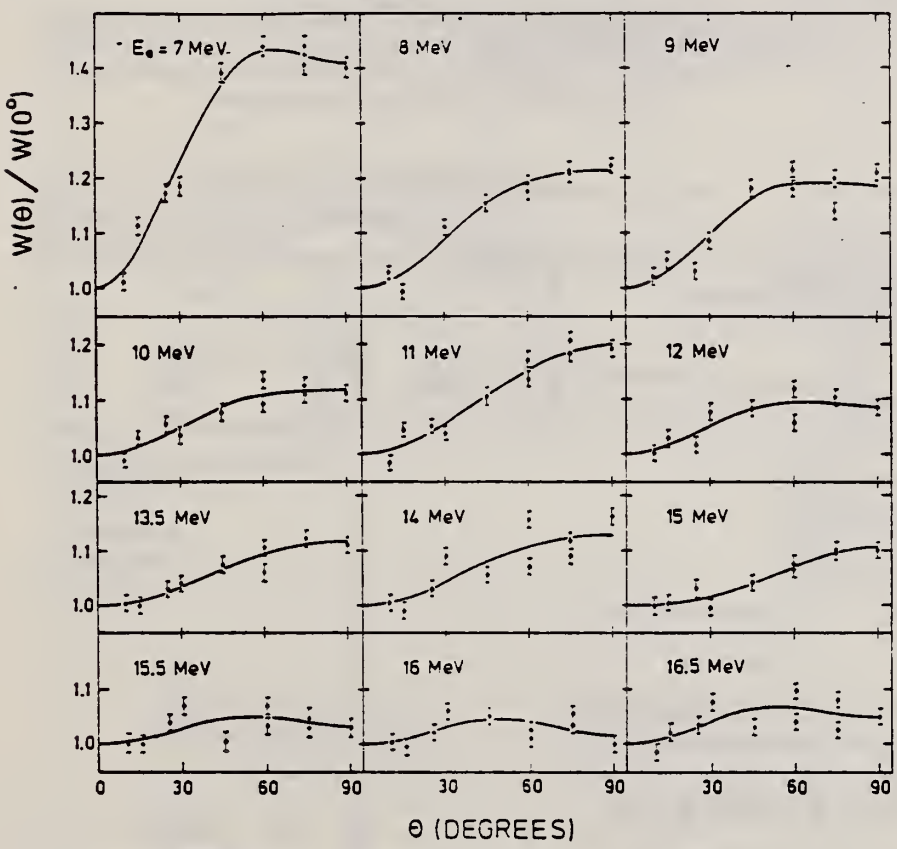

Fig. 1. Fragment angular distributions in the electrofission of ^{238}U

$$W(\theta) = a + b \cdot \sin^2\theta + c \cdot \sin^2(2\theta) \qquad (1)$$

where a and b are mixed coefficients, arising both from dipole and quadrupole fission, whereas c is a pure quadrupole term describing the 45° anisotropy. The solid curves in Fig. 1 represent the least squares fit results to the experimental data according to the above angular distribution formula.

over

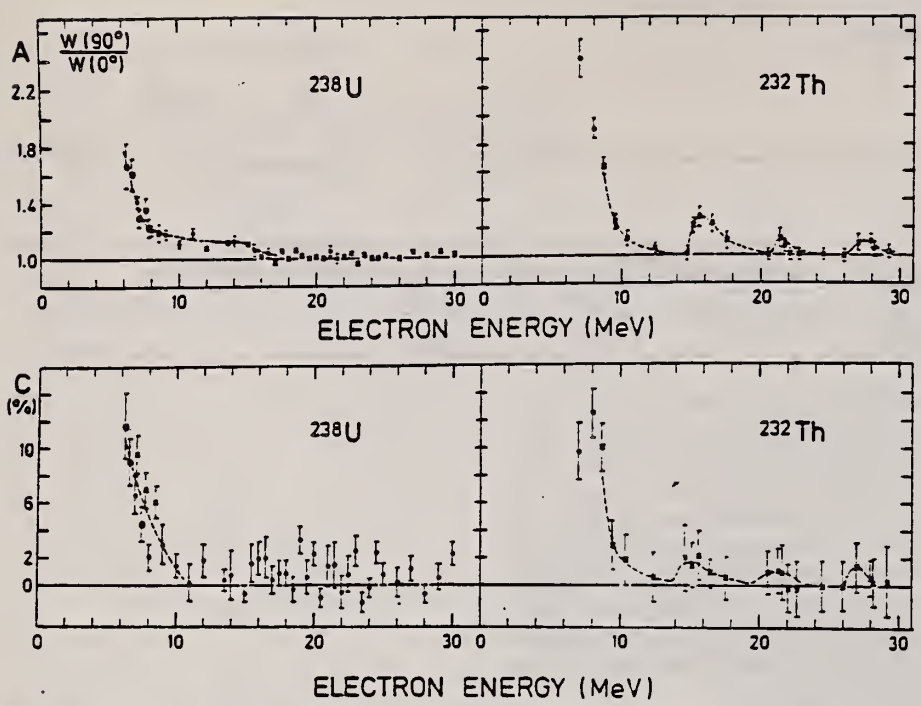

Fig. 2. Top: Anisotropies $A = W(90°)/W(0°)$ corresponding to the least squares fit results from Fig. 1 in the electrofission of ^{238}U and ^{232}Th. Bottom: Relative quadrupole contributions C as described in the text. Circles this work, squares [8], crosses [6]

$$C = (8c/15)/(a + 2b/3 + 8c/15) \qquad (2)$$

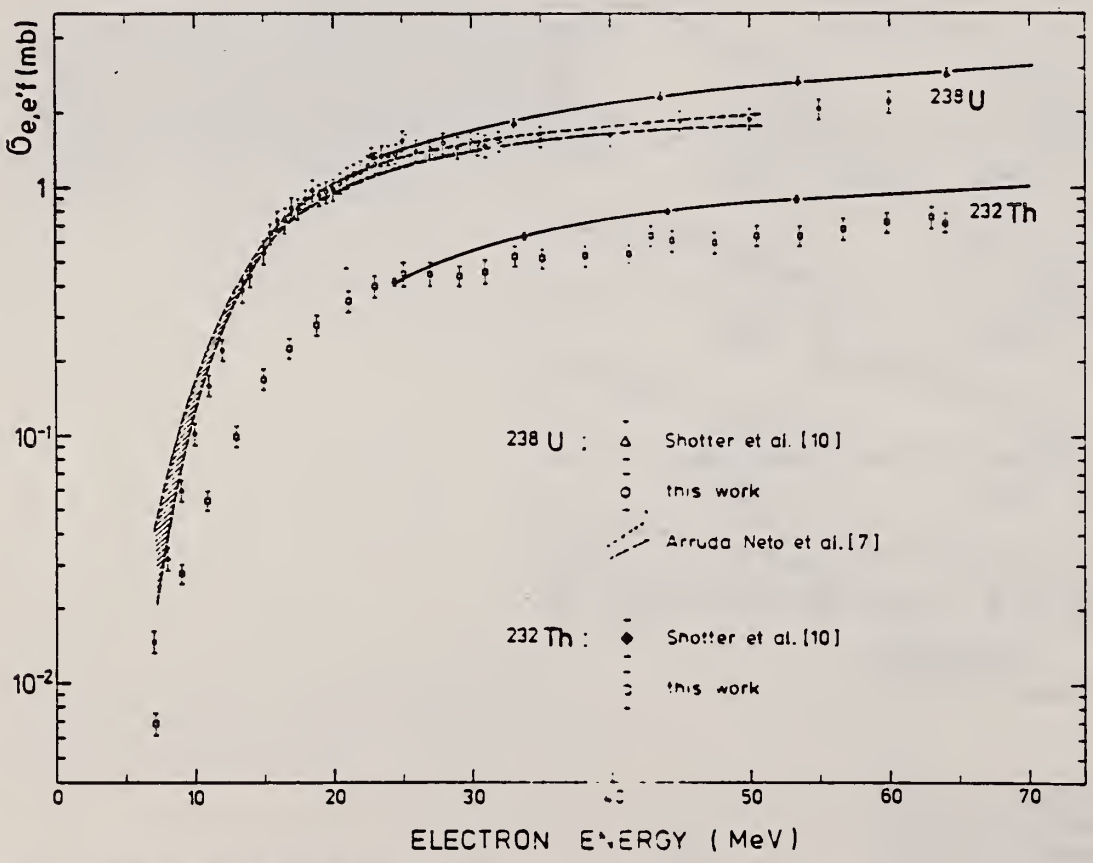

Fig. 4. Absolute electrofission cross sections of ^{238}U and ^{232}Th from this work in comparison with the data of Shotter et al. [10] and Arruda Neto et al. [7]

REF. G. Bellia, A. Del Zoppo, E. Migneco, R.C. Barna, D. De Pasquale
Phys. Rev. C20, 1059 (1979)

ELEM. SYM.	A	Z
U	238	92

METHOD

REF. NO. 79 Be 11 hg

REACTION	RESULT	EXCITATION ENERGY	SOURCE		DETECTOR		ANGLE
			TYPE	RANGE	TYPE	RANGE	
G,F	ABY	3-6	C	3-6	UKN		4PI

Photofission yield measurements on ^{232}Th and ^{235,236,238}U, showing the "shelf effect," have been analyzed in terms of a double-humped fission barrier. From the characteristic of the shelf it was possible to evaluate the excitation energy E_{II} of the shape isomer. In the framework of the double-humped barrier, with the competition between γ decay to the shape isomer and tunneling through the outer barrier of a compound state in the second well, it was possible to deduce fission branching ratios in agreement with those known in the literature. In particular for ^{232}Th a three-humped fission barrier is proposed, the second deep minimum causing the shelf effect and the third one the narrow resonances detected in this isotope.

[NUCLEAR REACTIONS, FISSION ^{232}Th, ^{235,236,238}U photofission yields measurements analyzed in the frame of a double-humped fission barrier model. Excitation energies and fission branching ratios for shape isomers deduced. A three-humped fission barrier proposed for ^{232}Th.]

FISSION BARRIER ANAL

Analysis of data from 77 Zh 1 and 78 Bo 8

TABLE I. Experimental energy values E_{end} for investigated nuclei. The E_{II} values for ^{232}Th and ^{235}U are evaluated from Eq. (5) with pairing gap $\Delta_{P_{II}} = \Delta_{P_I}$. Energy values are in MeV.

	E_{end}	E_{II}	$\Delta_{P_{II}}$	Δ_{P_I} [a]
^{232}Th	3.5–3.9 [b]	2.2–2.6 [c]	...	1.3
^{235}U	3.5–3.9 [b]	2.8–3.2 [c]	...	0.7
^{236}U	3.5 [d]	2.3 [e]	1.2	1.2
^{238}U	3.6 [f]	2.56 [g]	1.04	1.1

[a] Δ_{P_I} values are from Ref. 11.
[b] Reference 5.
[c] This work.
[d] Reference 3.
[e] Reference 16.
[f] See Fig. 1.
[g] Reference 15.

TABLE II. Summary of second barrier parameters for investigated nuclei. Energy values are in MeV.

	V_B	$\hbar\omega_B$
^{232}Th [a]	6.18	0.47
^{235}U [b]	5.9	0.52
^{236}U	6.0 [c]	0.7 [d]
^{238}U [e]	6.0	0.63

[a] Reference 8.
[b] Reference 10.
[c] Reference 16.
[d] Reference 22.
[e] Reference 15.

TABLE III. List of experimental E_{th} values (MeV) and branching ratios R.

	E_{th}	R (literature)	R (this work)
^{232}Th	4.4	...	$(1.0-4) \times 10^{-5}$
^{235}U	4.6	...	$(0.4-1.6) \times 10^{-2}$
^{236}U	4.2	0.11 [a]	0.1
^{238}U	4.2	$2 \cdot 10^{-2}$ [b]	0.01

[a] Reference 16.
[b] Reference 15.

TABLE IV. Fission barrier parameters of ^{232}Th for a double-humped and a triple-humped barrier. Energy values are in MeV.

	V_A	$\hbar\omega_A$	V_{II}	$\hbar\omega_{II}$	V_B	$\hbar\omega_B$	V_{III}	$\hbar\omega_{III}$	V_C	$\hbar\omega_C$
double [a] humped	5.5	0.9	4.35	0.36	6.15	0.47				
triple humped	5.5	0.9	2.0	1.0	6.18	2.0	4.96	0.36	6.0	2.0

[a] Reference 8.

REF. E. Jacobs, A.De Clercq, H. Thierens, D. De Frenne, P. D'hondt, P. DeGelder, A.J. Deruytter
Phys. Rev. C20, 2249 (1979)

ELEM. SYM.	A	Z
U	238	92

METHOD

REF. NO. 79 Ja 5 hg

REACTION	RESULT	EXCITATION ENERGY	SOURCE TYPE	SOURCE RANGE	DETECTOR TYPE	DETECTOR RANGE	ANGLE
G,F	NOX	THR-70	C	12-70	SCD-D		90

Energy correlation measurements with semiconductor detectors were performed for the photofission of ^{238}U with 12-, 15-, 20-, 30-, and 70-MeV bremsstrahlung. The behavior of the mass distribution with changing total kinetic energy of the fragments and with changing excitation energy of the compound nucleus is deduced. The distribution of the total fragment kinetic energy as a function of the fragment mass and as a function of the average excitation energy of the ^{238}U compound nucleus is studied. The results are discussed in terms of the two mode and fragment-shell hypotheses.

ENERGY, MASS FRAG DST

[NUCLEAR REACTIONS, FISSION ^{238}U(γ,F), $E\gamma_{max}$ = 12, 15, 20, 30, 70 MeV; measured fragment energies E_1, E_2; deduced $N(\mu, E_K)/\langle E_{exc}(E_e)\rangle$.]

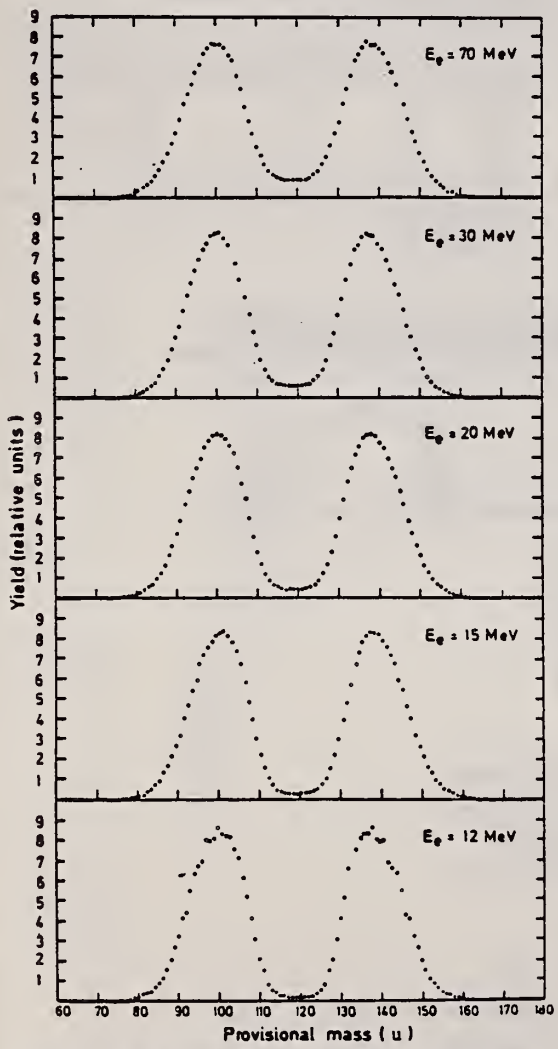

FIG. 1. Provisional mass μ distribution for the photofission of ^{238}U with 12-, 15-, 20-, 30-, and 70-MeV bremsstrahlung.

TABLE I. Parameters of the overall kinetic energy and mass distributions for the photofission of ^{238}U with 12-, 15-, 20-, 30-, and 70-MeV bremsstrahlung.

E_e (MeV)	12	15	20	30	70
$\langle E_{exc}(E_e)\rangle$ (MeV)	9.7	11.6	13.4	14.7	19.9
NEV	24 $\times 10^3$	135 $\times 10^3$	292 $\times 10^3$	171 $\times 10^3$	127 $\times 10^3$
$\langle E_K\rangle$ (MeV)	171.78 ± 0.56	171.41 ± 0.13	170.88	170.37 ± 0.25	169.41 ± 0.30
$\sigma(E_K)$ (MeV)	11.06 ± 0.24	10.93 ± 0.10	10.98 ± 0.08	11.08 ± 0.15	11.42 ± 0.35
$\langle \mu_L\rangle$ (u)	99.24 ± 0.18	99.21 ± 0.10	99.39 ± 0.13	99.82 ± 0.12	99.61 ± 0.27
$\langle \mu_L\rangle_{1/4}$ (u)	100.03	99.90	99.90	100.12	99.75
$\langle \mu_H\rangle$ (u)	138.76 ± 0.16	138.79 ± 0.09	138.61 ± 0.08	138.18 ± 0.20	138.39 ± 0.20
$\langle \mu_H\rangle_{1/4}$ (u)	137.97	138.10	138.10	137.88	138.25
$\sigma(\mu_L) = \sigma(\mu_H)$ (u)	6.41 ± 0.16	6.63 ± 0.18	6.80 ± 0.16	6.84 ± 0.15	7.40 ± 0.70
FW(3/4)(u)	11.07	11.00	11.07	10.98	11.36
P/V	55 ±11	31 ±2	19.2 ±0.6	13.7 ±0.5	8.5 ±0.3

TABLE II. $\langle \mu_L\rangle_{1/4}$ values for different E_K cuts for the photofission of ^{238}U with 12-, 15-, 20-, 30-, and 70-MeV bremsstrahlung. $\langle \mu_L\rangle_{1/4}$ is the midpoint between the $\frac{1}{4}$-maximum points in the light fragment mass distribution.

E_K (MeV) \ E_e (MeV)	12	15	20	30	70
129–157	92.56 ± 0.15	93.00 ± 0.07	93.13 ± 0.05	93.55 ± 0.07	93.61 ± 0.07
158–169	95.30 ± 0.07	96.01 ± 0.03	96.19 ± 0.02	96.56 ± 0.03	96.34 ± 0.03
170–182	100.38 ± 0.06	100.33 ± 0.03	100.44 ± 0.02	100.63 ± 0.03	100.37 ± 0.03
183–205	104.43 ± 0.06	104.29 ± 0.03	104.38 ± 0.02	104.43 ± 0.03	104.09 ± 0.03
195–210	105.91 ± 0.14	105.91 ± 0.06	105.91 ± 0.05	105.98 ± 0.07	105.72 ± 0.10

TABLE III. $\langle \mu_H\rangle_{1/4}$ values for different E_K cuts for the photofission of ^{238}U with 12-, 15-, 20-, 30-, and 70-MeV bremsstrahlung. $\langle \mu_H\rangle_{1/4}$ is the midpoint between the $\frac{1}{4}$-maximum points in the heavy fragment mass distribution.

E_K (MeV) \ E_e (MeV)	12	15	20	30	70
129–157	145.44 ± 0.15	145.00 ± 0.07	144.87 ± 0.05	144.46 ± 0.07	144.39 ± 0.07
158–169	142.20 ± 0.07	141.99 ± 0.03	141.81 ± 0.02	141.44 ± 0.03	141.66 ± 0.03
170–182	137.62 ± 0.06	137.67 ± 0.03	137.56 ± 0.02	137.37 ± 0.03	137.63 ± 0.03
183–205	133.57 ± 0.06	133.71 ± 0.03	133.62 ± 0.02	133.57 ± 0.03	133.91 ± 0.03
195–210	132.19 ± 0.14	132.19 ± 0.06	132.09 ± 0.05	132.02 ± 0.07	132.28 ± 0.10

(over)

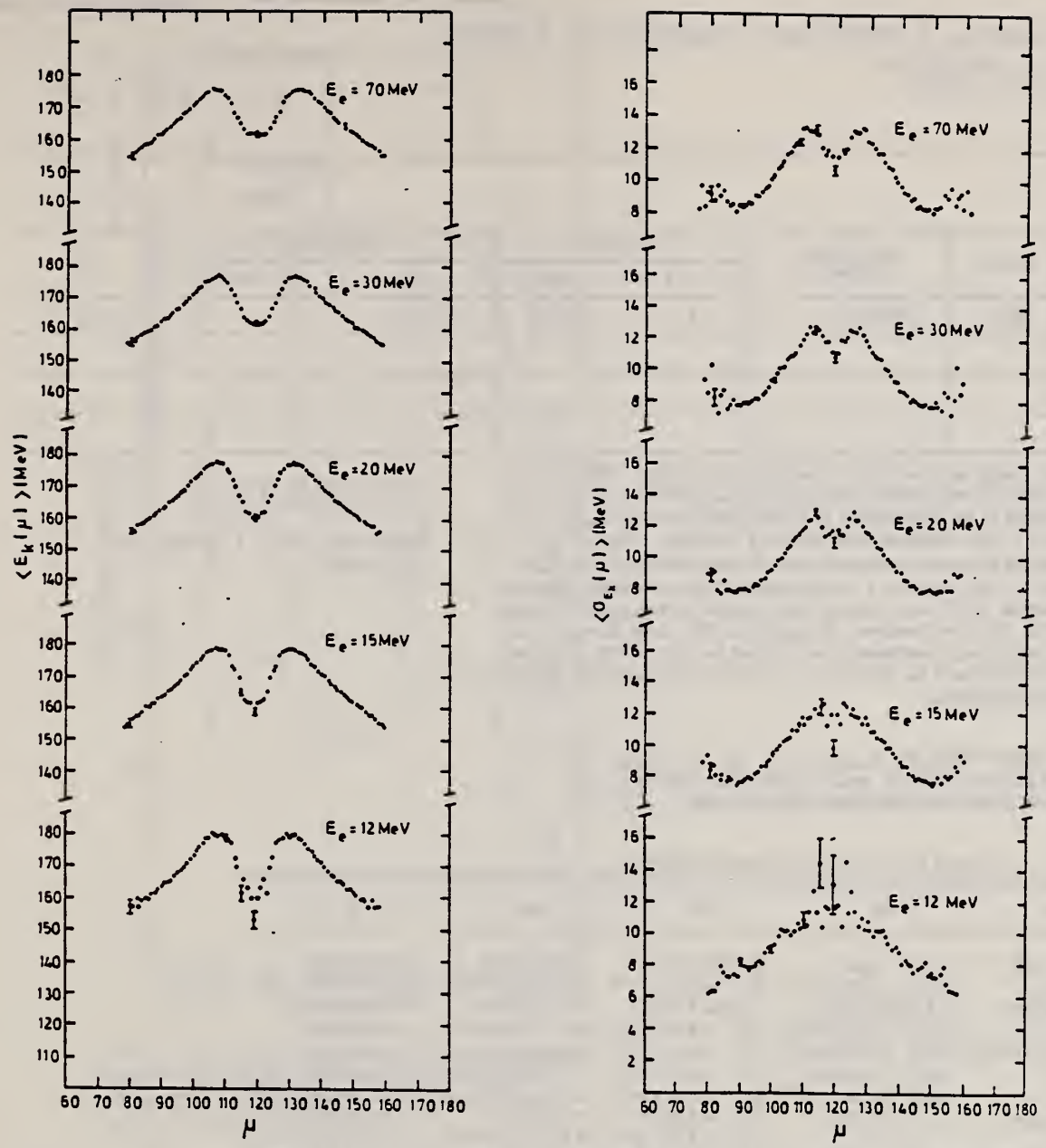

FIG. 2. Average total fragment kinetic energy $\langle E_K(\mu) \rangle$ and its dispersion $\sigma_{E_K}(\mu)$ as a function of the fragment mass μ for photofission of ^{238}U with 12-, 15-, 20-, 30-, and 70-MeV bremsstrahlung.

TABLE V. Peak-to-valley ratio values for different E_K cuts for the photofission of ^{238}U with 12-, 15-, 20, 30-, and 70-MeV bremsstrahlung.

E_K (MeV) \ E_e (MeV)	12	15	20	30	70
129–157	14.6 ± 1.3	8.28 ± 0.27	5.52 ± 0.12	4.14 ± 0.10	2.66 ± 0.06
158–169	60 ± 9	28.2 ± 1.1	10.1 ± 0.2	11.4 ± 0.3	7.49 ± 0.16
170–182	115 ± 15	85 ± 7	59 ± 3	36.2 ± 1.5	18.8 ± 0.6
183–205	238 ± 168	371 ± 58	257 ± 28	194 ± 32	76 ± 8

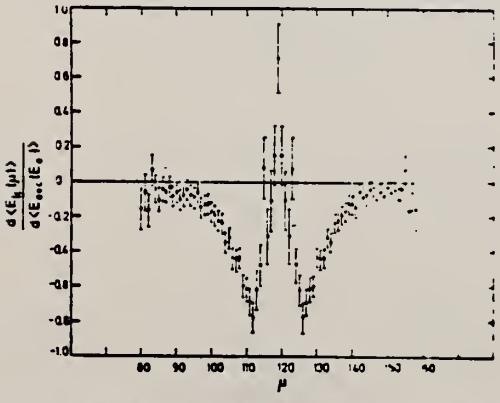

FIG. 3. Change of the average total fragment kinetic energy with the average excitation energy of the compound nucleus, $d\langle E_K(\mu)\rangle / d\langle E_{exc}(E_e)\rangle$ as a function of the fragment mass.

TABLE IV. Dispersion, $\sigma(\mu_L) = \sigma(\mu_H)$, for the light and heavy fragment mass distribution for different E_K cuts for the photofission of ^{238}U with 12-, 15-, 20-, 30-, and 70-MeV bremsstrahlung.

E_K (MeV) \ E_e (MeV)	12	15	20	30	70
129–157	7.35 ± 0.10	8.24 ± 0.05	8.70 ± 0.04	9.00 ± 0.05	9.78 ± 0.05
158–169	6.20 ± 0.05	6.54 ± 0.02	6.82 ± 0.02	7.00 ± 0.02	7.52 ± 0.02
170–182	5.34 ± 0.05	5.49 ± 0.02	5.60 ± 0.02	5.65 ± 0.02	6.01 ± 0.02
183–205	3.78 ± 0.04	3.93 ± 0.02	3.98 ± 0.02	3.98 ± 0.02	4.35 ± 0.03
195–210	2.85 ± 0.10	3.02 ± 0.04	3.19 ± 0.04	3.34 ± 0.05	4.16 ± 0.10

REF. E. Jacobs, H. Thierens, D. DeFrenne, A. DeClercq, P. D'hondt, P. DeGelder, A. J. Deruytter
Phys. Rev. C19, 422 (1979)

ELEM. SYM.	A	Z
U	238	92

METHOD

REF. NO. 79Ja7 hg

REACTION	RESULT	EXCITATION ENERGY	SOURCE		DETECTOR		ANGLE
			TYPE	RANGE	TYPE	RANGE	
G,F	RLY	THR-70	C	12-70	ACT-I		4PI

Cumulative yields for about 40 mass chains and fractional independent yields of ^{128}Sn, ^{128}Sb^{g}, ^{131}Te^{g}, ^{131}Te^{m}, ^{132}I^{g}, ^{132}I^{m}, ^{134}I, ^{134}Cs, ^{135}Xe, and ^{136}Cs were determined for the photofission of ^{238}U with 12-, 15-, 20-, 30-, and 70-MeV bremsstrahlung. Changes in the characteristics of the mass distribution are studied. An enhanced yield in the mass region 133-134, decreasing with increasing end-point energy of the bremsstrahlung (E_e), is observed. From the determined independent yields the most probable charges $Z_p(E_e)$ are calculated using the value 0.85 for the width parameter c of the charge distribution as deduced from our results for mass chain 134. The determined $Z_p(E_e)$ values are very well described by the empirical relation of Nethaway except for the mass chain 136. This discrepancy for mass chain 136, which decreases with increasing end-point energy of the bremsstrahlung, is attributed to an abnormal low yield of ^{136}Cs. Fragment shell effects are discussed. From the isomeric ratios for ^{131}Te^{g}-^{131}Te^{m} and ^{132}I^{g}-^{132}I^{m} average initial fragment spins are calculated using a statistical model analysis.

MASS CHAIN YIELDS

Data for Fig. 1 given in Table II

[NUCLEAR REACTIONS, FISSION ^{238}U(γ,F), $E_{\gamma\,max}$=12, 15, 20, 30, 70 MeV; measured: fragment γ-ray spectra; deduced: mass distributions, most probable charges, isomeric ratios, average initial fragment spins.]

TABLE IV. Fractional independent yields.

Isotope \ E_e (MeV)	12	15	20	30	70
^{128}Sn [a]	0.77 ±0.12	0.67 ±0.11	0.700 ±0.090	0.702 ±0.090	0.615 ±0.076
^{128}Sb^{g}	• • •	(4.9 ±1.9)×10^{-2}	(6.2 ±2.3)×10^{-2}	(8.5 ±2.4)×10^{-2}	0.188 ±0.030
^{131}Sb [a]	0.915 ±0.071	0.855 ±0.050	0.829 ±0.046	0.798 ±0.049	0.761 ±0.061
^{131}Te^{g}	• • •	(7.8 ±4.8)×10^{-2}	(8.5 ±4.5)×10^{-2}	(9.3 ±4.3)×10^{-2}	0.109 ±0.041
^{131}Te^{m}	(2.9 ±0.7)×10^{-2}	(5.7 ±1.1)×10^{-2}	(7.7 ±1.1)×10^{-2}	0.100 ±0.013	0.110 ±0.013
^{132}I^{g}	• • •	(5.7 ±1.4)×10^{-3}	(7.4 ±1.5)×10^{-3}	(1.17 ±0.21)×10^{-2}	(2.82 ±0.51)×10^{-2}
^{132}I^{m}	• • •	(3.9 ±1.2)×10^{-3}	(5.7 ±0.9)×10^{-3}	(1.26 ±0.17)×10^{-2}	(2.13 ±0.39)×10^{-2}
^{134}I	0.169 ±0.041	0.213 ±0.024	0.227 ±0.028	0.255 ±0.023	0.275 ±0.025
^{134}Cs	• • •	• • •	(4.0 ±1.5)×10^{-5}	(8.6 ±3.4)×10^{-5}	(1.33 ±0.14)×10^{-3}
^{135}Xe	(3.5 ±1.5)×10^{-2}	(4.4 ±1.7)×10^{-2}	(5.1 ±1.2)×10^{-2}	(6.0 ±1.2)×10^{-2}	(7.7 ±1.3)×10^{-2}
^{136}Cs	(4.6 ±1.1)×10^{-4}	(1.06 ±0.11)×10^{-3}	(1.86 ±0.16)×10^{-3}	(3.62 ±0.32)×10^{-3}	(1.15 ±0.12)×10^{-2}

[a] Fractional cumulative yield.

TABLE VI. Isomeric ratios $\sigma_m/(\sigma_g+\sigma_m)$.

Isomeric pair \ E_e (MeV)	15	20	30	70
^{131}Te^{m}-^{131}Te^{g}	0.43 ±0.15	0.48 ±0.14	0.52 ±0.12	0.50 ±0.10
^{132}I^{m}-^{132}I^{g}	0.41 ±0.09	0.44 ±0.06	0.51 ±0.06	0.44 ±0.05

over

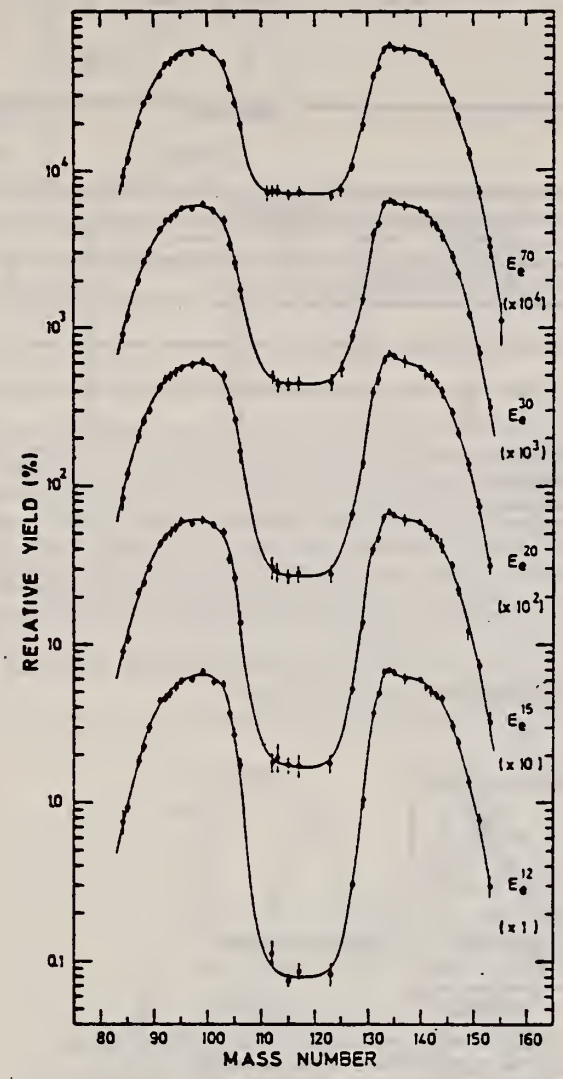

FIG. 1. Post neutron mass distributions for the photofission of ^{238}U with 12-, 15-, 20-, 30-, and 70-MeV bremsstrahlung. The yields have been multiplied by the scale factor given in parentheses.

REF. I.S. Koretskaya, V.L. Kuznetsov, L.E. Lazareva, V.G. Nedorezov, N.V. Nikitina
Yad. Fiz. 30, 910 (1979)
Sov. J. Nucl. Phys. 30, 472 (1979)

ELEM. SYM.	A	Z
U	238	92

METHOD

REF. NO. 79 Ko 11 hg

REACTION	RESULT	EXCITATION ENERGY	SOURCE		DETECTOR		ANGLE
			TYPE	RANGE	TYPE	RANGE	
G,F	ABX	THR-26	C	7-26	SPK-D		Ø

A 35-MeV synchrotron has been used to measure photofission yields in the range of bremsstrahlung maximum energy $E_{\gamma max} \simeq 7$–26 MeV for samples of ^{241}Am and ^{243}Am. The fission fragments were detected by multiwire spark counters. From the yield curves we have obtained the fission cross sections and fissilities of ^{241}Am and ^{243}Am in the region of the $E1$ giant resonance.

PACS numbers: 25.85.Jg, 24.30.Cz, 27.90. + b

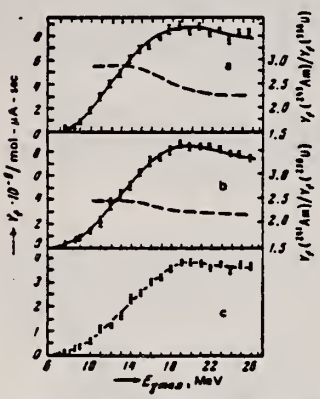

FIG. 1. Photofission yields of ^{238}U (a), ^{241}Am (b), and ^{243}Am (c) for various maximum energies $E_{\gamma\ max}$. The dashed lines show the yield ratios $Y_f(^{241}\text{Am})/Y_f(^{238}\text{U})$ and $Y_f(^{241}\text{Am})/Y_f(^{238}\text{U})$ (right-hand scale).

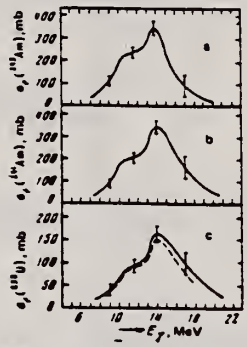

FIG. 2. Photofission cross sections of ^{238}U (a), ^{241}Am (b), and ^{243}Am (c) in the region of the $E1$ giant resonance. In Fig. a the dashed line shows the σ_f curve measured for ^{238}U in Ref. 9.

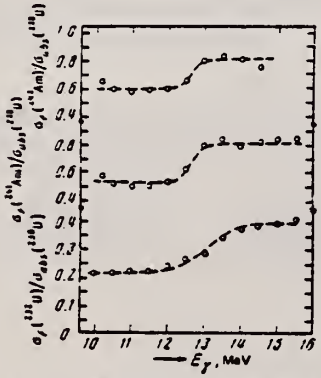

FIG. 4. Fissilities D_f of the nuclei ^{238}U, ^{241}Am, and ^{243}Am in the region of the peak of the $E1$ giant resonance.

REF. J. C. McGeorge, A. C. Shotter, D. Branford, J. M. Reid
Nucl. Phys. A326, 108 (1979)

ELEM. SYM.	A	Z
U	238	92

METHOD

REF. NO. 79Mc2 hg

REACTION	RESULT	EXCITATION ENERGY	SOURCE		DETECTOR		ANGLE
			TYPE	RANGE	TYPE	RANGE	
E,F	NOX	THR-110	D	110	SCD-D	110-165	90

Abstract: Fission of ^{232}Th, ^{237}Np, ^{209}Bi, ^{235}U and ^{238}U induced by 110 MeV electrons has been studied by means of surface barrier detectors. The resulting mass and kinetic energy distributions are presented. Comparison with the liquid drop model predictions shows reasonable agreement in the case of ^{209}Bi. The data are analysed in terms of a two component model of fission and the mean total kinetic energies of the components are shown to depend linearly on $Z_1Z_2(A_1^{1/3}+A_2^{1/3})$. Interesting differences are found when the present results are compared with the recent photofission experiments of Areskoug *et al.* and features in both sets of data correlate with changes of fragment deformation implied by the calculations of Wilkins *et al.*

MASS AND EGY DISTRIB

E NUCLEAR REACTIONS ^{237}Np, ^{232}Th, ^{209}Bi, ^{238}U, ^{235}U(e, f), E = 110 MeV; measured fission fragment E, deduced mass.

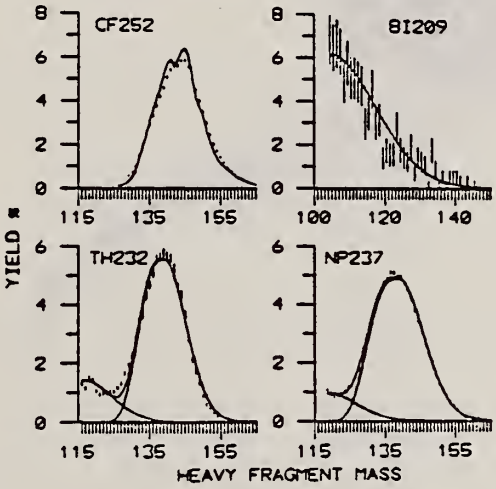

Fig. 1. The HFM yield distributions for electrofission of ^{209}Bi, ^{232}Th and ^{237}Np and spontaneous fission of ^{252}Cf. Statistical uncertainties are shown where larger than the size of the points in this and succeeding diagrams. The solid line in the ^{252}Cf case represents the experimental results of Schmidt *et al.* [12]). In the ^{209}Bi case the solid line represents a Gaussian fit to the data while the solid lines in the other two cases are the result of a two component analysis (see text).

TABLE 2

Target	Mean total KE (MeV) present work	semi-empirical [ref. [14])] a)	b)	Width present work
^{238}U	171.8±3.4	168.5	169.4	11.6±0.1
^{235}U	171.3±3.4	169.1	170.1	10.8±0.1
^{232}Th	167.0±3.3	163.4	163.5	9.6±0.1
^{237}Np	174.3±3.0	171.9	173.3	11.5±0.1
^{209}Bi	140 ±4	146.5	143.9	11.5±0.4

a) $0.1071Z^2/A^{1/3}+22.2$.
b) $0.1240Z^2/A^{1/3}$.

over

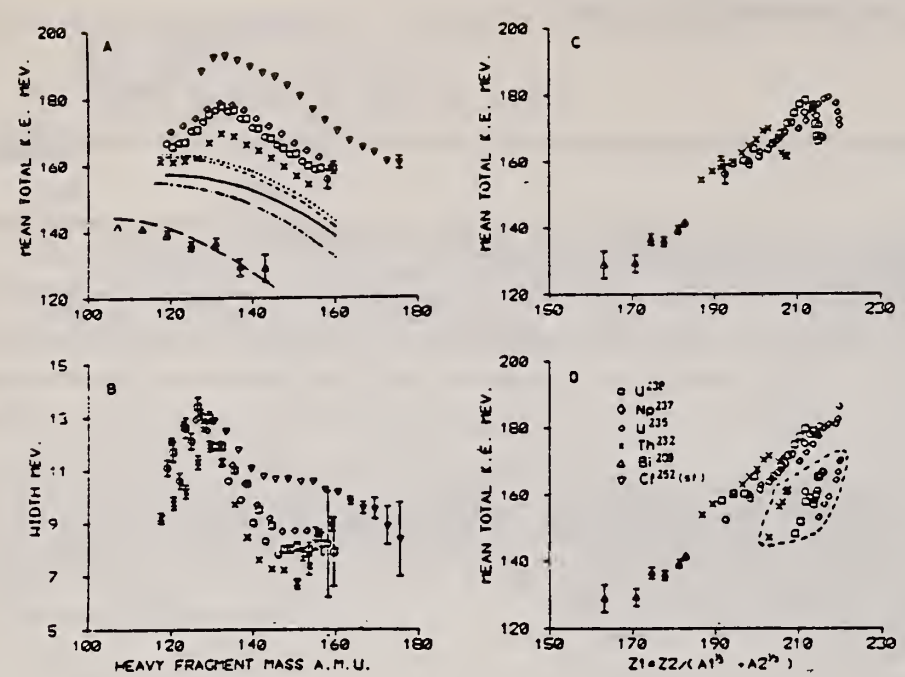

Fig. 3 Total fragment kinetic energy data from electrofission of ^{238}U, ^{235}U, ^{237}Np, ^{232}Th, ^{209}Bi and for spontaneous fission of ^{252}Cf. (A) Mean TKE versus HFM. The lines represent the LDM calculations of Nix and Swiatecki [13]) – solid ^{238}U, short dash ^{235}U, long dash ^{209}Bi, dot ^{237}Np and dot dash ^{232}Th. (B) Width of the TKE distribution versus heavy fragment mass. (C) Mean total fragment kinetic energy versus $Z_1Z_2/(A_1^{1/3}+A_2^{1/3})$. (D) Mean total fragment kinetic energy of the symmetric (enclosed by the dashed line) and asymmetric components versus $Z_1Z_2/(A_1^{1/3}+A_2^{1/3})$. In (A)(C) and (D) the relative uncertainties between targets are ±3 MeV and the absolute uncertainties are ±4 MeV.

REF. A.C. Shotter, C.H. Zimmerman, J.M. Reid, J.C. McGeorge, A.G. Flowers
Nucl. Phys. A330, 325 (1979)

ELEM. SYM.	A	Z
U	238	92

METHOD

REF. NO. 79 Sh 10 hg

REACTION	RESULT	EXCITATION ENERGY	SOURCE		DETECTOR		ANGLE
			TYPE	RANGE	TYPE	RANGE	
E,N	ABX	6-120	C	20-120	ACT-D		4PI

Abstract: The total cross section for the reaction $^{238}U(e, n)^{237}U$ has been measured for electron energies between 20 MeV and 120 MeV. The cross section is analysed into E1 and E2 multipole components. A value of Γ_n/Γ_f for the E2 component is deduced assuming that the strength of this component is concentrated between 9 and 11 MeV in excitation energy.

VIRT PHOT. ANALYSIS

E

NUCLEAR REACTIONS $^{238}U(e, n)$, $E = 20-120$ MeV; measured $\sigma(E)$. ^{238}U resonance deduced Γ_n/Γ_f for E2 component. Separated target. ^{237}U residual activity detected by Ge (Li).

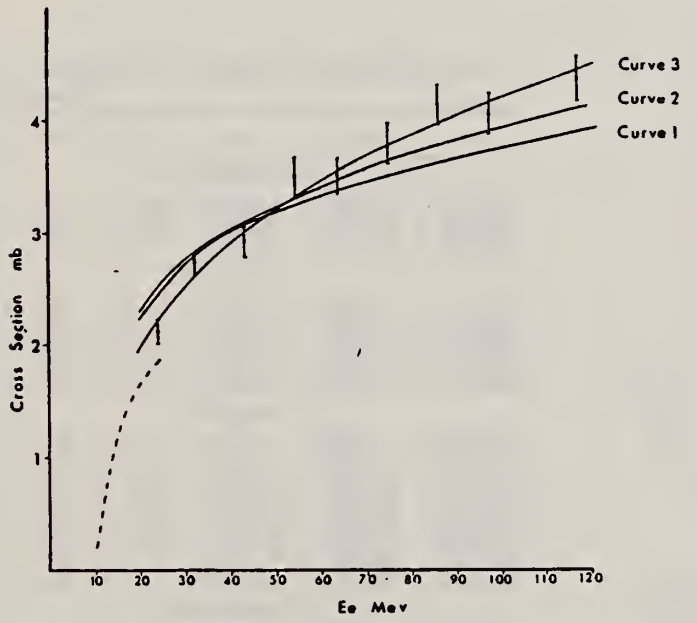

Fig. 2. Cross section for the reaction $^{238}U(e, n)^{237}U$ versus incident electron energy. The dashed curve is a line through the data of ref. [9]). Curves 1 and 2 are best fits to the data with an E1 process only; $\sigma_{>17(\gamma,n)} = 0$ mb and 10 mb respectively. Curve 3 is best fit to the data with an E1 and E2 process.

TABLE 1
Results

E_R (MeV)	$\sigma_{>17(\gamma,n)}$ (mb)	$S(\gamma,n)$ (MeV · mb)	N	$\frac{S(\gamma,n)}{\text{sum rule}}$ (%)	$\frac{S(\gamma,n)}{\int_7^{17}\sigma_{(\gamma,n)}(E_\gamma)dE_\gamma}$ (%)	$\frac{S(\gamma,n)/S(\gamma,f)}{[=\Gamma_n/\Gamma_f \text{ for } f=0]}$	$\frac{\Gamma_n/\Gamma_f}{[\text{for } f=0.2]}$
9	0	3.9	1.15	16	0.3	0.6	0.8
	10	2.9	1.15	12	0.25	0.45	0.6
11	0	5.9	1.15	16	0.5	0.6	0.8
	10	4.4	1.15	12	0.4	0.45	0.6

$$S(\gamma,n) = \int \sigma_{E2(\gamma,n)}(E_\gamma)dE_\gamma, \quad S(\gamma,f) = \int \sigma_{E2(\gamma,f)}(E_\gamma)dE_\gamma.$$

Table 1 gives the values of $S(\gamma, n)$ expressed as : (a) ratios to the energy integrated experimental $\sigma_{(\gamma,n)}(E_\gamma)$ cross section (deduced to be 1160 MeV · mb for energy integration 7 to 17 MeV from the $\sigma_{(\gamma,n)}(E_\gamma)$ data given in ref. [10]), and (b) ratios to the

REF. J. Visser, G.A. Brinkman, Cees N.M. Bakker
Int. J. Appl. Rad. & Isotopes 30, 745 (1979)

ELEM. SYM.	A	Z
U	238	92

METHOD

REF. NO. 79 Vi 1 hg

REACTION	RESULT	EXCITATION ENERGY	SOURCE		DETECTOR		ANGLE
			TYPE	RANGE	TYPE	RANGE	
G,SPL	ABY	THR-300	C	300	ACT-I		4PI

Cross section per equivalent quantum: ^{209}At (15.8±0.8) mb
^{210}At (17.9±0.8) mb

Photospallation cross sections of ^{232}Th with bremsstrahlung beams of 0.25, 0.30 and 0.35 GeV maximum energies have been determined for ^{209}At (66, 87 and 280 μb), ^{210}At (74, 98 and 230 μb) and ^{211}Rn (28, 40 and 130 μb). These yields are an order of magnitude lower than predicted by the Rudstam CDMD formula, possibly as a consequence of the rather thick Cu converter that was used. Irradiation of UO_2 at 0.3 GeV resulted in cross sections for ^{209}At: 15.8 μb and for ^{210}At: 17.9 μb. Cumulative photofission cross sections have been determined for $A = 135$ at 0.25 GeV (1.96 mb) and at 0.35 GeV (2.53 mb). Half-lives were measured for ^{207}Po (6.7 h) and ^{211}Rn (14.6 h).

REF. V.E. Zhuchko, Yu.B. Ostapenko, G.N. Smirenkin, A.S. Soldatov
Yu.M. Tsipenyuk
Yad. Fiz. 30, 634 (1979)
Sov. J. Nucl. Phys. 30, 326 (1979)

ELEM. SYM.	A	Z
U	238	92

METHOD

REF. NO.	
79 Zh 3	hg

REACTION	RESULT	EXCITATION ENERGY	SOURCE		DETECTOR		ANGLE
			TYPE	RANGE	TYPE	RANGE	
G,F	YLD	THR-7	C	5-7	TRK-D		DST
				(5.2-6.4)			

We report the method and results of measurements of angular distributions of fragments in the (γ,f) reaction for ^{232}Th, ^{236}U, and ^{238}U carried out in connection with the investigation of the properties of deep sub-barrier photofission: the isomeric shelf phenomenon, disappearance of the angular anisotropy ($^{236,238}U$), and the absence of this effect and of the sub-barrier enhancement of quadrupole photofission in ^{232}Th. The experimental data presented permit an understanding of the nature and relation of these properties in terms of the concept of a two-humped fission-barrier structure.

PACS numbers: 25.85.Jg

TABLE I. Parameters of the angular distributions of photofission fragments.

E_{max}, MeV	N, no.	$J\Delta t$, μC	$c \pm \Delta c$	$b \pm \Delta b$	$a \pm \Delta a$
		^{232}Th (δ=200 mg/cm^2)			
5.0	552	$8.9 \cdot 10^6$	0.000±0.06	1.000±0.06	0.250±0.060
5.2	738	$1.0 \cdot 10^7$	0.000±0.08	1.000±0.08	0.225±0.100
6.4	46 950	510	0.06±0.03	0.94±0.03	0.06±0.04
6.4 •	29 340	10 900	0.014±0.002	0.956±0.003	0.028±0.006
		^{236}U (δ=1.7 mg/cm^2)			
4.3	168	$9.6 \cdot 10^6$	0.72±0.25	0.28±0.26	1.71±0.35
4.75	2543	$2.0 \cdot 10^7$	0.17±0.20	0.83±0.20	0.18±0.15
5.0	3441	$0.5 \cdot 10^7$	0.10±0.10	0.90±0.10	0.20±0.15
5.1 •	852	$0.9 \cdot 10^7$	0.04±0.02	0.96±0.05	0.187±0.048
5.25	23 630	$0.1 \cdot 10^7$	0.06±0.03	0.94±0.03	0.12±0.04
5.5	16 580	$1.5 \cdot 10^7$	0.11±0.08	0.89±0.08	0.42±0.08
5.8 •	4623	$0.17 \cdot 10^7$	0.040±0.012	0.960±0.024	0.503±0.028
		^{238}U (δ=0.8 mg/cm^2)			
4.5	612	$8.9 \cdot 10^6$	1.000±0.3	0.000±0.3	2.800±0.35
5.0	3917	$1.0 \cdot 10^7$	0.200±0.1	0.800±0.1	0.250±0.15
5.3	12 800	$2.0 \cdot 10^7$	0.150±0.07	0.850±0.07	0.500±0.13
5.5 •	12 700	$1.6 \cdot 10^7$	0.048±0.006	0.952±0.014	0.479±0.016
5.75 •	7695	$2.0 \cdot 10^7$	0.027±0.005	0.973±0.013	0.432±0.015
6.0 •	7681	$4.0 \cdot 10^7$	0.042±0.005	0.958±0.013	0.166±0.013
6.25 •	9831	$2.0 \cdot 10^7$	0.069±0.005	0.931±0.013	0.110±0.013
6.5 •	10 150	$1.0 \cdot 10^7$	0.112±0.006	0.888±0.013	0.080±0.014
6.75 •	10 090	5000	0.199±0.008	0.801±0.014	0.051±0.015
7.0 •	7762	2500	0.257±0.008	0.743±0.014	0.071±0.015
7.25 •	4790	1000	0.320±0.009	0.680±0.014	0.038±0.015
		^{238}U (δ=200 mg/cm^2)			
4.15	130	$12.8 \cdot 10^6$	1.000±0.2	0.000±0.2	0.230±0.20
4.4	434	$9.5 \cdot 10^6$	0.940±0.35	0.060±0.35	2.500±0.50
4.8	7252	$1.0 \cdot 10^7$	0.490±0.04	0.510±0.04	2.800±0.03
5.4	449 050	$0.4 \cdot 10^7$	0.020±0.02	0.980±0.02	0.340±0.02
5.4 •	5761	$0.5 \cdot 10^7$	0.094±0.011	0.906±0.015	0.308±0.026

Note. N is the total number of tracks recorded by the detectors; $J\Delta t$ is the integral of the current of accelerated electrons at the bremsstrahlung target; δ is the thickness of the fissile target. The results marked by an asterisk were obtained by the circular glass plate technique[2]; the remaining results are in the 4π geometry.

$$W(\theta)=a+b\sin^2\theta+c\sin^2 2\theta$$

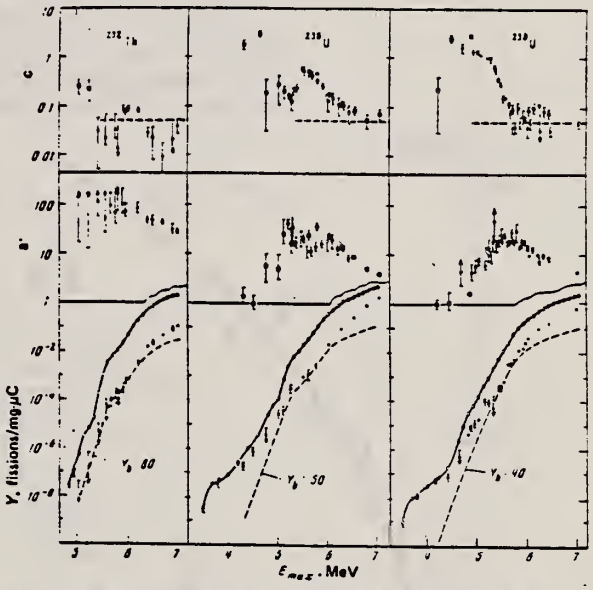

FIG. 3. In the upper and central parts we have shown the parameters of the angular distributions of fragments from photofission of ^{232}Th, ^{236}U, and ^{238}U as a function of E_{max}. Points: ■—results of the present work, ●—results of Refs. 2 and 15, ○—results of Ref. 13. In the lower part: the hollow circles and their connecting solid lines are the total yield of photofissions of the corresponding nuclei,[6,10] the solid circles are the isotropic component of the yield—Y_a, and the dashed line is the component Y_b which has been normalized to Y_a in the region of maximum anisotropy. The dashed line in the upper part of the figure shows the asymptotic value of the coefficient $c \approx c/b \approx 0.05$ for energies above the barrier [see Eq. (3)].

REF. J.D.T. Arruda Neto, S.B. Herdade, I.C. Nascimento
Nucl. Phys. A334, 297 (1980)

ELEM. SYM.	A	Z
U	238	92

METHOD

REF. NO. 80 Ar 4 hg

REACTION	RESULT	EXCITATION ENERGY	SOURCE		DETECTOR		ANGLE
			TYPE	RANGE	TYPE	RANGE	
E,F	ABX	THR-9	D	5-9	TRK-D		DST

Abstract: A formalism for the joint analysis of angular distributions of electro- and photofission fragments is presented, utilizing the vitual-photon spectrum technique in DWBA. This formalism is applied to the study of angular distributions for the electrofission of ^{238}U, measured near the fission barrier, to obtain information about the low-lying levels (J^{π}, K) of the transition nucleus. The (2^+, 0), (1^-, 0), and (1^-, 1) levels, previously detected in photofission experiments, were confirmed. Evidences of a significant contributions of (1^-, 1), (2^+, 1)and (2^+, 2) levels are also presented.

E NUCLEAR REACTION ^{238}U(e, e'f), E = 5.5–9 MeV; measured fission fragment $\sigma(\theta)$; ^{238}U deduced low-lying fissioning levels. Natural target.

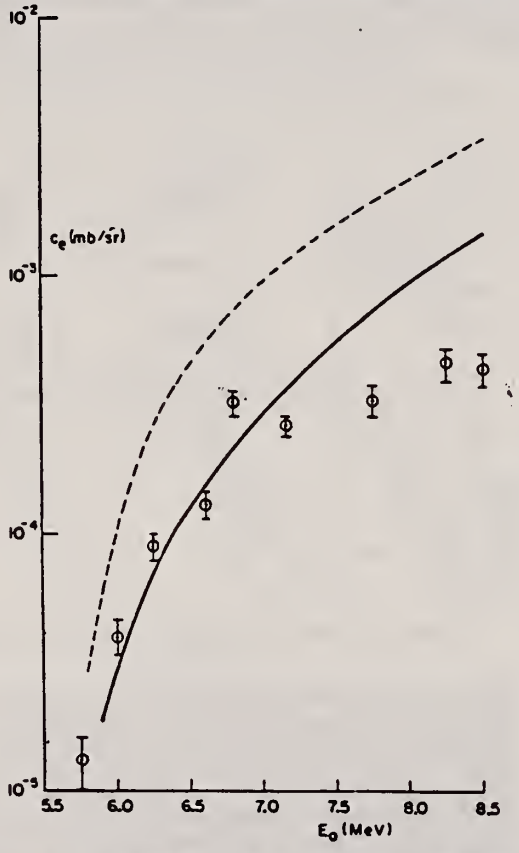

Fig. 6. The circles with error bars represent C_e^{exp} (see text), obtained by least square fits of the function $W(\theta) = A_e + B_e \sin^2\theta + C_e \sin^2 2\theta$ to the experimental ^{238}U electrofission fragment angular distributions. The dashed curve is the result of the integral of eq. (22), with $\sigma_{\gamma,f}(2^+, 0) = \sigma_{\gamma,f}^{add}$. The continuous curve represents the same integral with $\sigma_{\gamma,f}(2^+, 0) = \sigma_{\gamma,f}^{(F2)}$.

$$C_e(E_0) = \frac{15}{32\pi}\int_0^{E_0} \sigma_{\gamma,f}^{(2^+,0)}(E) N^{(E2,*)}(E, E_0)\frac{dE}{E}. \qquad (22)$$

(OVER)

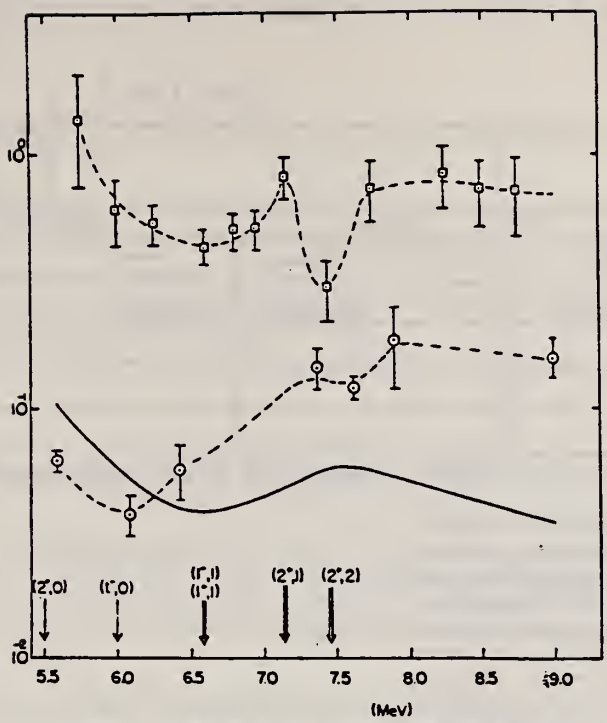

Fig. 7. The points in circles and the continuous curve represent the ratios C_γ/B_γ of ^{238}U photofission fragment angular distributions as a function of the photon energy, taken from Dowdy and Krysinski [10]) and Rabotnov *et al.* [4]), respectively. The points in squares represent the ratios C_e/B_e of ^{238}U electrofission fragment angular distributions as a function of the electron incident energy, from this work. The dashed curves are only to guide eyes. The single arrows indicate in the energy scale the mean values of fission channels thresholds taken from the litterature [4, 10, 13, 14]), and double arrows from the conclusions of this work.

$$C_e(E_0) = \frac{15}{32\pi}\int_0^{E_0} \sigma_{\gamma,f}^{(2^+,0)}(E) N^{(E2,*)}(E, E_0)\frac{dE}{E}. \qquad (22)$$

TABLE 1

Low-lying levels in the ^{238}U transition nucleus, identified in photofission and electrofission

(L^π, K)	Energy (MeV)		Threshold (MeV)			
	[a])	[b])	[c])	[d])	[e])	[f])
$(2^+, 0)$	5.5		5.0	4.5 ± 3.3	5.95	
$(1^-, 0)$	6.2	6.5	5.7	5.98 ± 0.06	6.70	
$(1^-, 1)$	6.6 to 7.0	6.7	7.0	6.63 ± 0.04	6.80	6.6
$(2^+, 1)$						7.2
$(2^+, 2)$						7.4

[a]) Anderl *et al.*, 1973; Compton scattering γ-rays [ref. [13])].
[b]) Dickey and Axel, 1975; bremsstrahlung monochromator [ref. [14])].
[c]) Rabotnov *et al.*, 1970; bremsstrahlung [ref. [4])].
[d]) Dowdy and Krysinsky, 1971; neutron capture γ-rays [ref. [10])].
[e]) Lindgren *et al.*, 1978, bremsstrahlung [ref. [7])].
[f]) Present work; electrons (virtual photons).

REF. V. Bellini, V. Emma, S. Lo Nigro, C. Milone, G.S. Pappalardo, G. Bologna
Il Nuovo Cimento 55A, 182 (1980)

Card 1 of 2

ELEM. SYM.	A	Z
U	238	92

METHOD

REF. NO. 80 Be 5 hg

REACTION	RESULT	EXCITATION ENERGY	SOURCE		DETECTOR		ANGLE
			TYPE	RANGE	TYPE	RANGE	
G,F	ABX	100-999	C	100-999	TRK-D		4PI

Calculation and reported cross section valves assumed for cross sections below 150 MeV.

Summary. — The cross-section per equivalent quantum in the fission induced in ^{238}U by a quasi-monochromatic photon beam has been measured. The photon beam was obtained by coherent bremsstrahlung from 1000 MeV electrons striking a diamond single crystal. In the experiment the energies of the main peak of the photon spectrum assumed sixteen different values in the range from 220 MeV to 500 MeV. The fission fragments have been detected by means of glass sandwiches containing thin targets of UF_4. The cross-section per photon from 100 MeV to 1000 MeV has been deduced from the experimental yields applying an appropriate unfolding method after having subtracted from the yields the contribution due to photons with energies below 100 MeV. The obtained cross-section clearly shows a resonance centred at a photon energy 320 MeV with a FWHM ≃125 MeV and a peak value of 70 mb. This resonance is in good agreement with the first baryon resonance in pion photoproduction. The energy dependence of the photofission cross-section for ^{238}U can be explained by both assuming that the photomesonic absorption mechanism prevails over the quasi-deuteron interaction in producing fission above 150 MeV and that the nuclear fissility increases with the energy.

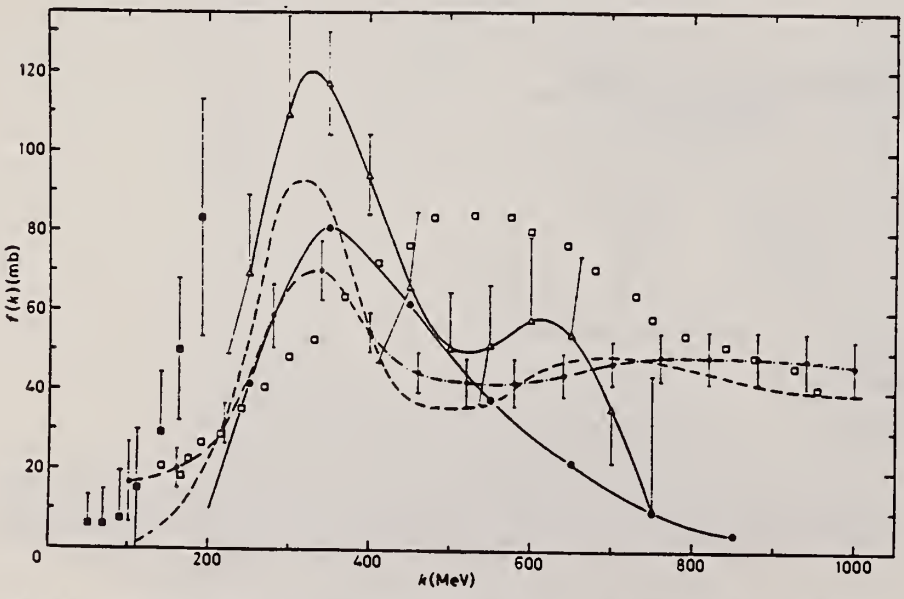

Fig. 2. – Fission cross-section per photon $f(k)$ of ^{238}U *vs.* the photon energy k. Experimental data: ■ ref. (6), □ ref. (10), ● ref. (11), ▲ ref. (12). The dashed curve represents the cross-section assumed in ref. (14). The dash-dotted curve is the cross-section obtained in the present work.

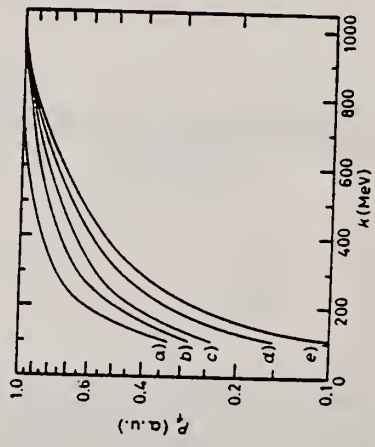

Fig. 3. – Nuclear fissility P_f *vs.* the photon energy k. The curves are normalized at $k = 1000$ MeV: *a*) ^{238}U, *b*) Bi, *c*) Pb, *d*) Au, *e*) Ta.

(OVER)

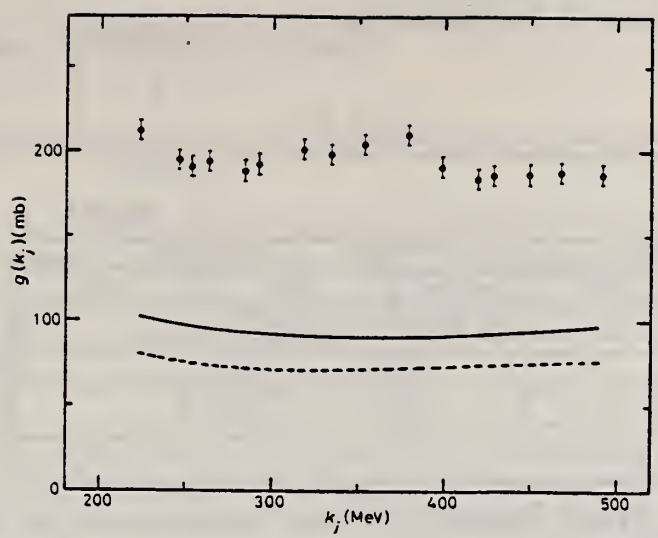

Fig. 3. – Photofission yields per equivalent quantum of ^{238}U as a function of the first peak energy k_j of photons. • our experimental results. The continuous curve represents the $g_0(k_j)$ contribution due to photons with energies $k \lesssim 100$ MeV. The dashed curve represents the contribution arising from the photons in the giant-resonance region only.

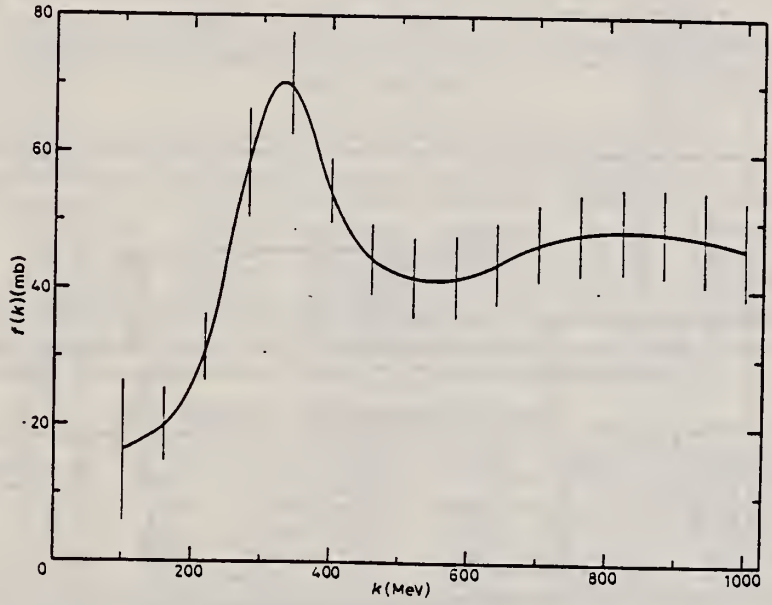

Fig. 5. – Photofission cross-section of ^{238}U estimated by our unfolding method.

TABLE II. – *Estimated f_i cross-sections of ^{238}U and corresponding errors.*

k (MeV)	$f(k)$ (mb)	k (MeV)	$f(k)$ (mb)
100	16.3 ± 10.4	580	41.8 ± 6.2
160	19.9 ± 5.1	640	43.9 ± 5.9
220	31.4 ± 5.1	700	46.8 ± 5.7
280	58.5 ± 8.3	760	48.3 ± 5.9
340	69.8 ± 7.4	820	48.7 ± 6.3
400	54.4 ± 4.8	880	48.6 ± 6.7
460	44.5 ± 5.2	940	47.8 ± 6.9
520	41.9 ± 6.2	1000	46.1 ± 7.1

REF. V. Bellini, V. Emma, S. Lo Nigro, C. Milone, G.S. Pappalardo, G. Bologna
Il Nuovo Cimento 55A, 182 (1980)

Card 2 of 2

EL EM. SYM.	A	Z
U	238	92

METHOD

REF. NO. 80 Be 5 hg

REACTION	RESULT	EXCITATION ENERGY	SOURCE		DETECTOR		ANGLE
			TYPE	RANGE	TYPE	RANGE	
G,F	ABX	100-999	C	100-999	TRK-D		4PI

Calculation and reported cross section valves assumed for cross sections below 150 MeV.

TABLE I. – *Photofission cross-section per equivalent quantum for* ^{238}U *as a function of the first peak energy* k_j *of photons.* $g(k_j)$ *represent the experimental values;* $g_c(k_j)$ *are the values obtained after having subtracted to* $g(k_j)$ *the contribution due to photons with energies* $k \leq 100$ MeV.

k_j (MeV)	$g(k_j)$ (mb)	$g_c(k_j)$ (mb)
223	212.2 ± 6.4	100.2 ± 6.4
246	195.1 ± 5.9	98.7 ± 5.9
253	191.2 ± 5.7	96.6 ± 5.7
263	194.1 ± 5.8	101.5 ± 5.8
284	188.5 ± 5.7	96.6 ± 5.7
292	192.5 ± 5.8	101.6 ± 5.8
318	200.7 ± 6.0	110.3 ± 6.0
334	197.8 ± 5.9	107.1 ± 5.9
353	203.8 ± 6.1	112.6 ± 6.1
379	210.4 ± 6.3	119.3 ± 6.3
398	190.7 ± 5.7	98.4 ± 5.7
419	184.1 ± 5.5	90.5 ± 5.5
428	186.2 ± 5.6	91.9 ± 5.6
449	186.8 ± 5.6	91.9 ± 5.6
467	188.0 ± 5.6	91.9 ± 5.6
491	186.7 ± 5.3	90.0 ± 5.3

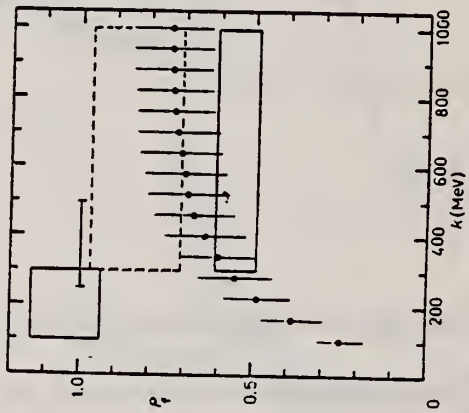

Fig. 6. – Nuclear fissility of ^{238}U as a function of the photon energy k. Experimental data: • present work; region delimited by the dashed lines, ref. (8); regions delimited by the continuous lines, ref. (13). The horizontal segment represents the average value of P, reported in ref. (12).

REF. J. T. Caldwell, E. J. Dowdy, B . L. Berman, R. A. Alvarez, P. Meyer
Phys. Rev. C21, 1215 (1980)

ELEM. SYM.	A	Z
U	238	92

METHOD

REF. NO. 80Cal

egf

REACTION	RESULT	EXCITATION ENERGY	SOURCE		DETECTOR		ANGLE
			TYPE	RANGE	TYPE	RANGE	
G,1N	ABX	5-18	D	5-18	BF3 - [illegible]	I	4PI
G,2N	ABX	9-18	D	5-18	BF3 - [illegible]	I	4PI
G,F	ABX	5-18	D	5-18	BF3 - [illegible]	I	4PI

The photoneutron cross sections $\sigma(\gamma,n)$ and $\sigma(\gamma,2n)$, and total photofission cross sections $\sigma(\gamma,F)$ have been measured for ^{235}U, ^{236}U, ^{238}U, and ^{232}Th from threshold to 18.3 MeV using monoenergetic photons from the annihilation in flight of fast positrons and neutron-multiplicity detection in an efficient 4π neutron detector. Use of the ring-ratio technique allowed both the average photofission neutron energy for each nucleus to be obtained as a function of photon energy and, for ^{236}U and ^{238}U, the determination of the partial cross sections for first-chance $\sigma(\gamma,f)$ and second-chance $\sigma(\gamma,nf)$ photofission as well. Information extracted from the data includes integrated cross sections and their moments, giant-resonance parameters, deformation and radius parameters, and relative and absolute neutron and fission probabilities.

SEE ALSO 80CA2

[NUCLEAR REACTIONS $^{235,236,238}U$ and ^{232}Th $(\gamma,n,2n,F)$, E_γ = 5–18.3 MeV; measured 4π neutron yield, neutron multiplicities, and average energies for monoenergetic photons; $\sigma(E_\gamma,1n)$, $\sigma(E_\gamma,2n)$, $\sigma(E_\gamma,F)$, integrated cross sections and moments, GDR parameters, nuclear shape parameters, neutron and fission probabilities.]

TABLE II. Parameters of Lorentz-curve fits to the giant dipole resonance.[a]

Nucleus	$E_m(1)$ (MeV)	$\sigma_m(1)$ (mb)[b]	$\Gamma(1)$ (MeV)	$E_m(2)$ (MeV)	$\sigma_m(2)$ (mb)[b]	$\Gamma(2)$ (MeV)
^{235}U	10.90 ± 0.05	328 ± 19	2.30 ± 0.15	13.96 ± 0.09	459 ± 10	4.75 ± 0.32
^{236}U	10.92 ± 0.04	271 ± 16	2.55 ± 0.17	13.78 ± 0.08	415 ± 10	4.88 ± 0.24
^{238}U	10.77 ± 0.04	311 ± 20	2.37 ± 0.13	13.80 ± 0.09	459 ± 9	5.13 ± 0.35
^{232}Th	11.03 ± 0.04	302 ± 19	2.71 ± 0.13	13.87 ± 0.08	449 ± 9	4.77 ± 0.28

[a] Lorentz parameters defined by Eq. (1); the fitting interval for all cases is 9 to 18 MeV.
[b] Uncertainties for σ_m given here are relative. The absolute uncertainties are 7%.

TABLE IV. Nuclear shape parameters.

Nucleus	R_A[a]	η[b]	ϵ[c]	β_2[d]	Q_0 (b)[e]	Q_0 (b)[f]	Q_0 (b)[g]
^{235}U	0.35	1.308	0.595	0.315	12.0	10.6 ± 0.2	11.0 ± 0.5
^{236}U	0.34	1.287	0.556	0.295	11.2	10.75 ± 0.7	10.3 ± 0.4
^{238}U	0.31	1.309	0.596	0.316	12.1	11.3 ± 0.1	11.1 ± 0.5
^{232}Th	0.38	1.283	0.547	0.290	10.7	9.8 ± 0.1	9.8 ± 0.4

[a] Area ratio, defined by Eq. (6).
[b] Deformation parameter, computed from Eq. (3).
[c] Nuclear eccentricity, computed from Eq. (4).
[d] Deformation parameter, computed from Eq. (7).
[e] Intrinsic quadrupole moment, computed from Eq. (8), with R_0 taken to be 1.20 fm.
[f] Intrinsic quadrupole moment, taken from Ref. 47.
[g] "Best value" for Q_0, computed from Eq. (8), with R_0 taken to be 1.15 fm (see text).

TABLE V. Integrated cross sections.[a]

Nucleus	$\sigma_{int}(\gamma,n)$ (MeV b)	$\sigma_{int}(\gamma,2n)$ (MeV b)	$\sigma_{int}(\gamma,F)$ (MeV b)	$\frac{\frac{1}{2}\pi[\sigma_m(1)\Gamma(1)+\sigma_m(2)\Gamma(2)]}{0.06NZ/A}$[b]
^{235}U	1.14	0.20	2.16	1.37
^{236}U	1.26	0.45	1.45	1.26
^{238}U	1.36	1.13	1.09	1.43
^{232}Th	1.66	1.45	0.37	1.41

[a] $\sigma_{int}(\gamma,x) = \int \sigma(\gamma,x)dE_\gamma$, integrated from threshold to the maximum experimental energy $E_{\gamma max}$ = 18.3 MeV.
[b] Uncertainties given here are relative. The absolute uncertainties are 7%.

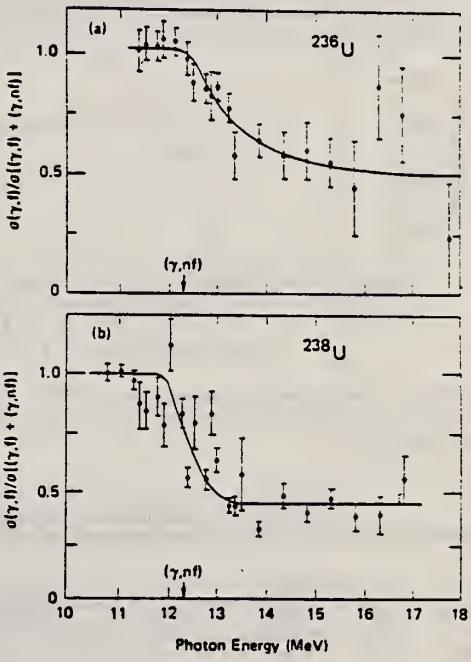

FIG. 12. Ratios of the first-chance photofission cross section $\sigma(\gamma,f)$ to the total photofission cross section $\sigma(\gamma,F) = \sigma[(\gamma,f)+(\gamma,nf)]$: (a) for ^{236}U, (b) for ^{238}U.

over

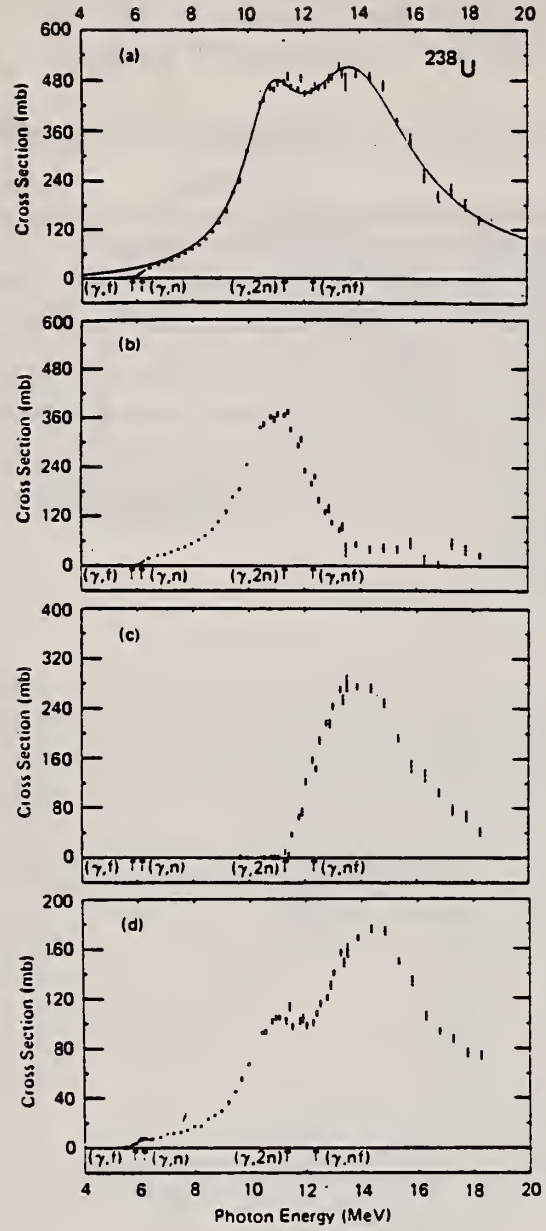

FIG. 4. Photonuclear cross sections for ^{238}U: (a) $\sigma(\gamma, \text{tot})$, with a Lorentz-curve fit; (b) $\sigma(\gamma, n)$; (c) $\sigma(\gamma, 2n)$; (d) $\sigma(\gamma, F)$.

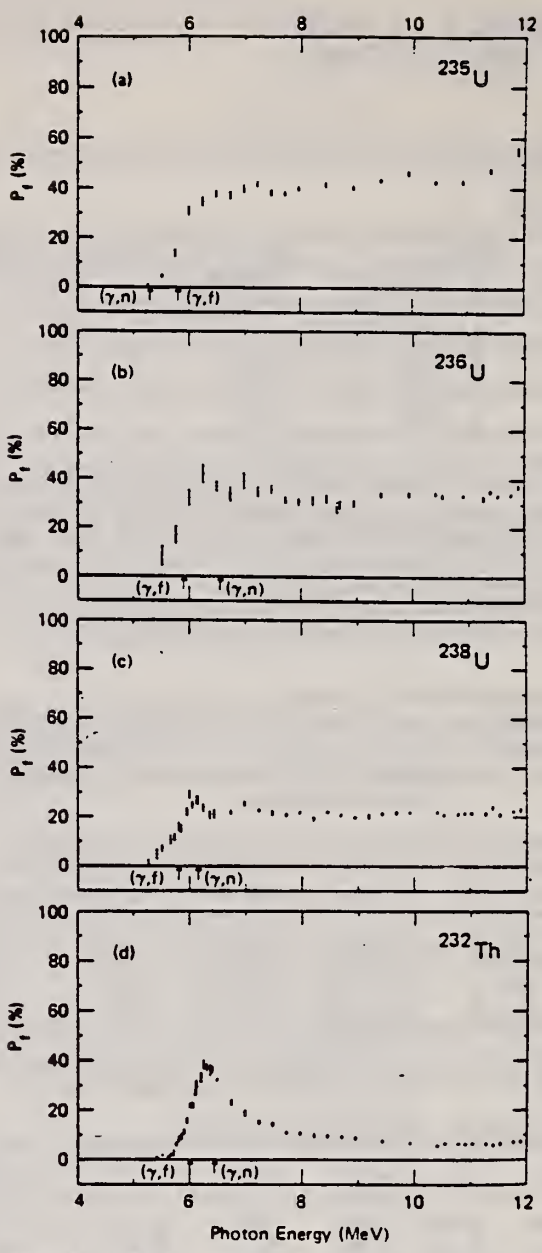

FIG. 15. Fission probability P_f from the ratio of $\sigma(\gamma, f)$ to the value at each energy of the two-component Lorentz-curve fits to the GDR shown in Figs. 2–5: (a) for ^{235}U, (b) for ^{236}U, (c) for ^{238}U, (d) for ^{232}Th.

TABLE VI. Integrated cross-section moments.[a]

Nucleus	σ_{-1} (mb)	$\sigma_{-1}A^{-4/3}$ (mb)	σ_{-2} (mb MeV^{-1})	$\frac{\sigma_{-2}}{0.00225A^{5/3}}$	$\frac{\sigma_{-2}K}{0.05175^{5/3}}$	$\frac{0.05175A^{5/3}}{\sigma_{-2}}$ (MeV)
^{235}U	278	0.191	23.1	1.15	1.36	20.1
^{236}U	252	0.173	21.0	1.04	1.21	22.2
^{238}U	286	0.194	24.0	1.17	1.38	19.7
^{232}Th	276	0.194	22.8	1.16	1.35	19.9

[a] $\sigma_{-1} = \int \sigma(\gamma, \text{tot})\, E_\gamma^{-1}\, dE_\gamma$ and $\sigma_{-2} = \int \sigma(\gamma, \text{tot}) E_\gamma^{-2}\, dE_\gamma$, integrated from threshold to $E_{\gamma\max} = 18.3$ MeV.

REF. J. T. Caldwell, E. J. Dowdy, R. A. Alvarez, B. L. Berman, P. Meyer
Nucl. Sci. Eng. 73, 153 (1980)

ELEM. SYM.	A	Z
U	238	92

METHOD

REF. NO. 80Ca2 egf

REACTION	RESULT	EXCITATION ENERGY	SOURCE		DETECTOR		ANGLE
			TYPE	RANGE	TYPE	RANGE	
G,F	NOX	5-18	D	5-18	BF3 - I	D	4PI
G,F	NOX	11-17	D	5-18	BF3 - I	D	4PI
G,F	NOX	5-17	D	5-18	BF3 - I	D	4PI

The prompt neutron multiplicities for photofission of the four isotopes ^{235}U, ^{236}U, ^{238}U, and ^{232}Th have been measured with monoenergetic photons over the energy range from 5.5 to 18 MeV using the annihilation in flight of fast positrons. The delayed neutron yield has been measured for all four isotopes at 10.9- and 16.8-MeV photon energies. The ratio of first- to second-chance fission has been measured as a function of energy up to 17-MeV excitation energy for ^{236}U and ^{238}U photofission.

PROMPT N MULT
DELAYED N YLD
RATIO 1-/2- CHANCE F

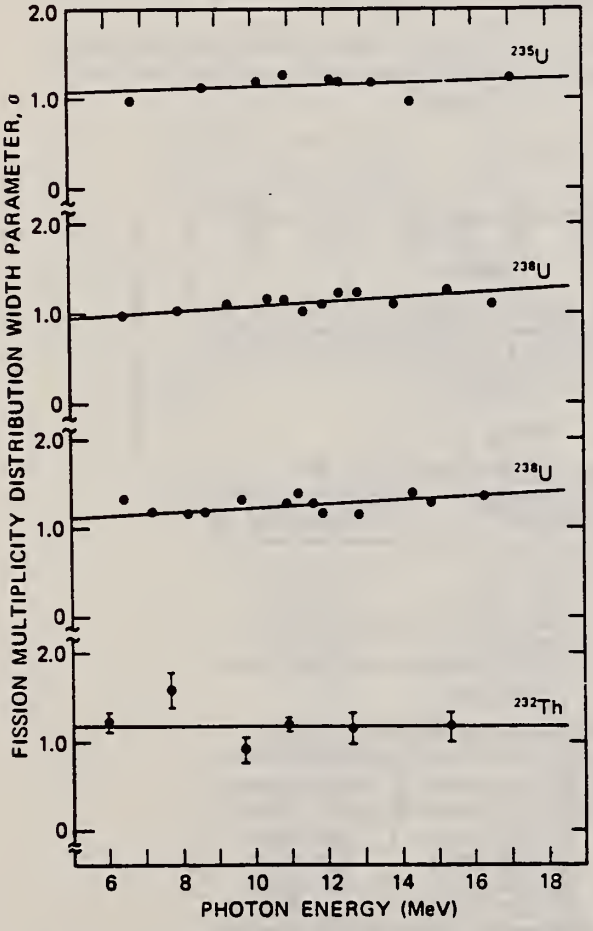

Fig. 6. Prompt neutron multiplicity width parameter data as a function of excitation energy. Solid circles are experimental data, and straight lines are the least-squares fits to these data (see Table II).

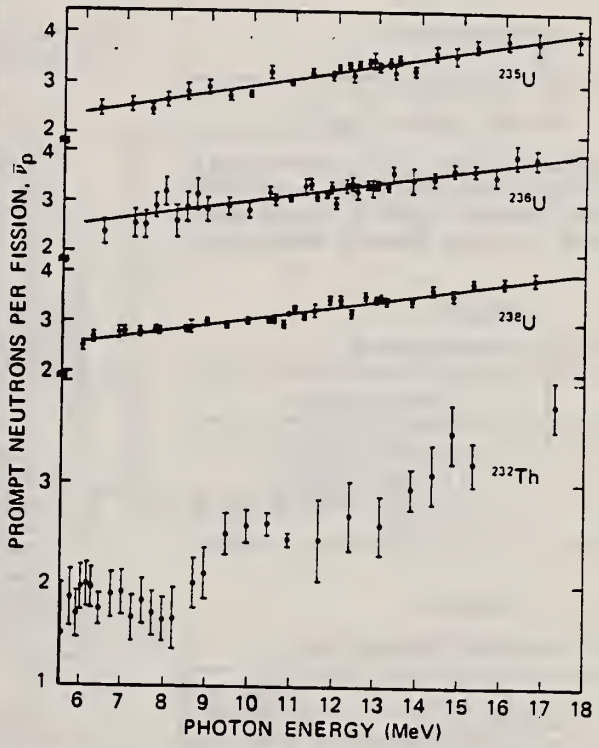

Fig. 7. Prompt neutron $\bar{\nu}_p$ data as a function of excitation energy. Solid circles are experimental data, and the straight lines are the least-squares fits (see Table IV) to these data. A single straight line fit was not obtainable for ^{232}Th.

over

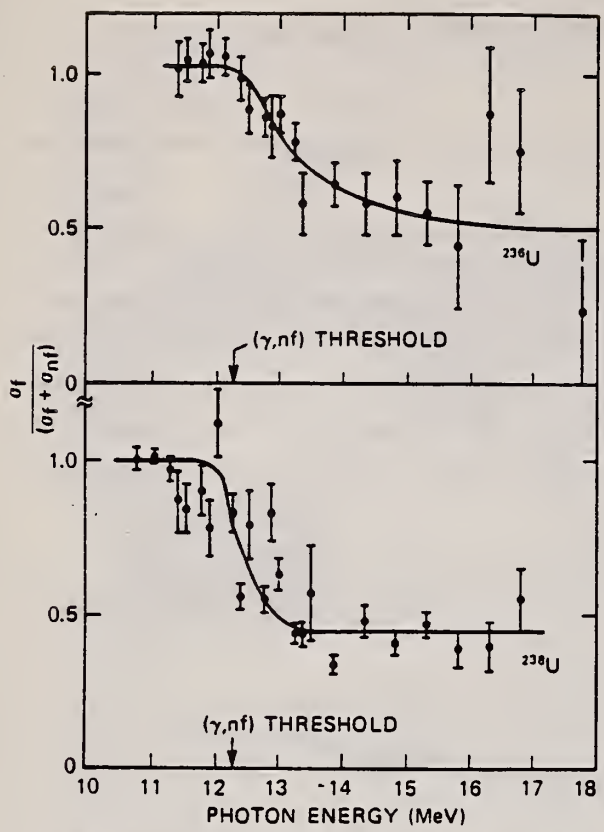

Fig. 8. Experimental $\sigma_f/(\sigma_f + \sigma_{nf})$ data as a function of excitation energy (solid circles). The smooth curves drawn through the data are intended to guide the eye and are not based on analytic fits to the data. Threshold values are from Ref. 15.

TABLE II

Multiplicity Width Parameter

Isotope	Least-Squares Fit
^{235}U	$\sigma = 1.009 + 0.0110\ E$
^{236}U	$\sigma = 0.840 + 0.0253\ E$
^{238}U	$\sigma = 1.003 + 0.0227\ E$
^{232}Th	$\sigma = 1.183$

TABLE IV

Prompt Neutrons per Photofission, $\bar{\nu}_p(E)$

Isotope	Least-Squares Fit	Correlation Coefficient
^{235}U	$\bar{\nu}_p = 1.610 + 0.133\ E$ (all data)	0.965
^{236}U	$\bar{\nu}_p = 1.881 + 0.116\ E$ (all data)	0.906
^{238}U	$\bar{\nu}_p = 1.862 + 0.123\ E$ (all data)	0.969
^{232}Th	$\bar{\nu}_p = 2.826 - 0.143\ E$ $(6.0 < E < 8.2$ MeV)	0.819
	$\bar{\nu}_p = 0.453 + 0.175\ E$ $(E > 8.5$ MeV)	0.927

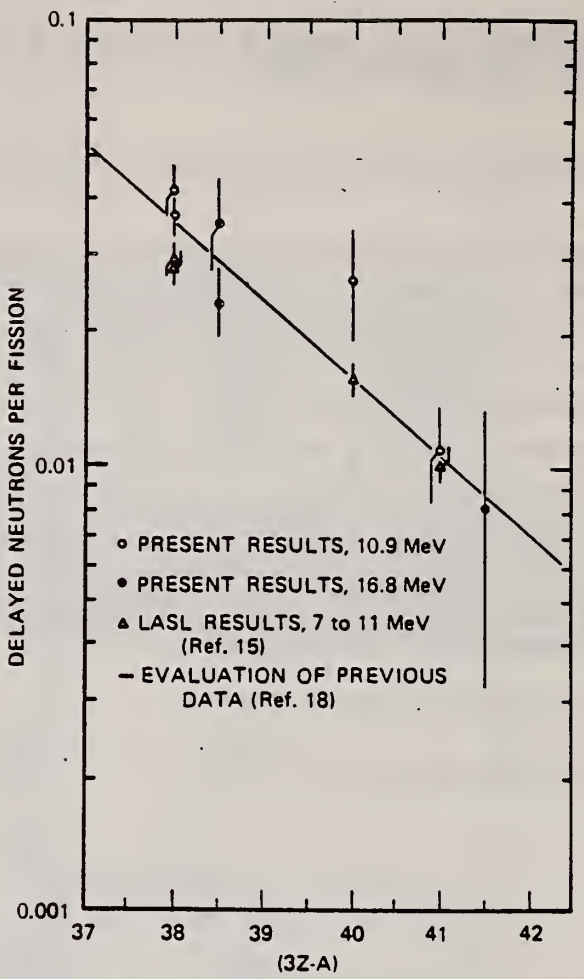

Fig. 9. Yield of delayed neutron from photofission as a function of $3Z\text{-}A$. Solid line is an evaluated least-squares fit to existing data as of 1975 (Ref. 18). Solid circles are the present results. Solid squares are from Ref. 15.

TABLE V

Prompt Neutrons per Photofission at 8.5 MeV

Isotope	From Ref. 15	Present Data
^{235}U	2.85 ± 0.09	2.74 ± 0.10
^{236}U	2.66 ± 0.11	2.71 ± 0.10
^{238}U	2.74 ± 0.09	2.91 ± 0.10
^{232}Th	2.07 ± 0.11	1.94 ± 0.08

TABLE VII

Comparison of Values of $\bar{\nu}_p$ for Photofission of ^{238}U

Excitation Energy	From Ref. 34	Present Results
9.7	2.85 ± 0.11	3.06 ± 0.08
11.6	3.39 ± 0.12	3.29 ± 0.07
13.4	3.44 ± 0.11	3.51 ± 0.07
14.7	3.57 ± 0.11	3.67 ± 0.07

REF. D. De Frenne, H. Thierens, E. Jacobs, P. De Gelder, A. De Clercq, P. D'hondt, A.J. Deruytter
Phys. Rev. C21, 629 (1980)

ELEM. SYM.	A	Z
U	238	92

METHOD

REF. NO. 80 De 2 hg

REACTION	RESULT	EXCITATION ENERGY	SOURCE TYPE	SOURCE RANGE	DETECTOR TYPE	DETECTOR RANGE	ANGLE
G,F	RLY	THR-20	C	20	ACT-I		4PI

Fractional independent or cumulative chain yields of 35 fission products were determined for the photofission of ^{238}U with 20-MeV bremsstrahlung, using direct γ spectrometry of irradiated uranium samples, γ-ray spectrometry of fission product catcher foils, and chemical separation techniques. For the mass chains 131–136 the width parameter c of the charge distribution was obtained. An average value of 0.93 ± 0.06 was deduced for c. A comparison of this c value with the results for other low-energy fissioning systems indicates that the width of the charge distribution is practically independent of the excitation energy of the compound nucleus. Using the average c value, the most probable charges Z_p(20 MeV) were calculated for 8 light and 12 heavy mass chains. A comparison of the deduced Z_p(20 MeV) behavior with the expectations of the unchanged charge density hypothesis shows the higher charge-to-mass ratio of the light fragments compared to the heavy ones and the influence of the closed 50-proton shell on the charge distribution. The Z_p(20 MeV) values determined are very well reproduced by the empirical relation of Nethaway except in the vicinity of the Z = 50 line.

MASS YLD 88 TO 139

[NUCLEAR REACTIONS, FISSION $^{238}U(\gamma,F)$, $E_{\gamma max}$=20 MeV; measured: fragment γ-ray spectra; deduced: charge distributions, width and most probable charges.]

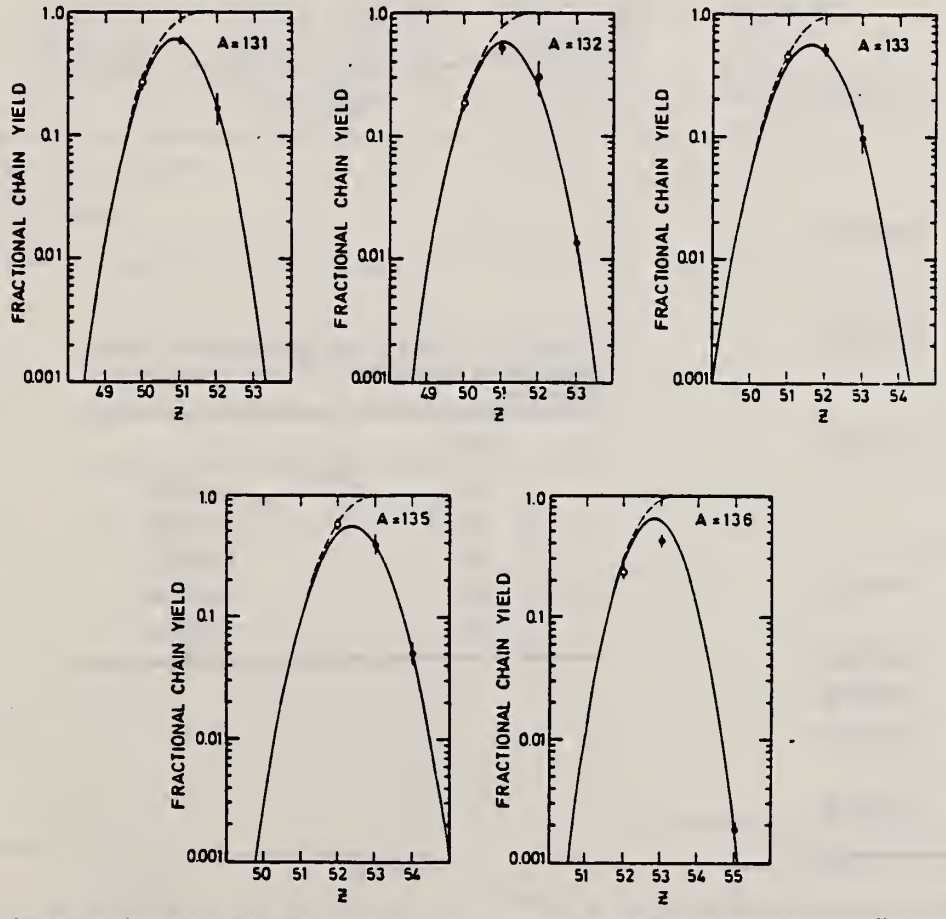

FIG. 1. Charge distribution for the mass chains 131, 132, 133, 135, and 136 for the photofission of ^{238}U with 20-MeV bremsstrahlung. ○ is the experimentally determined fractional cumulative chain yield (FCY) and ● is the experimentally determined fractional independent chain yield (FIY). A least-squares fit to the data based on expression (2) is represented by the full line (FIY) or by the dotted line (FCY).

(OVER)

TABLE II. Fractional independent and cumulative chain yields and deduced Z_p (20 MeV) values for the photofission of ^{238}U.

M_{post}	Product	Fractional chain yield	Z_p(20 MeV)
88	^{88}Br	0.740 ± 0.080(c)	35.10 ± 0.16
90	^{90}Kr	0.838 ± 0.093(c)	$35.90^{+0.22}_{-0.36}$
91	^{91}Kr	0.665 ± 0.087(c)	36.17 ± 0.20
93	^{93}Rb	0.736 ± 0.129(c)	$37.11^{+0.24}_{-0.34}$
94	^{94}Sr	0.884 ± 0.099(c)	$37.76^{+0.29}_{-0.64}$
95	^{95}Sr	0.848 ± 0.071(c)	$37.87^{+0.19}_{-0.28}$
96	^{96}Nb	$(1.1 \pm 0.5) \times 10^{-4}$	$38.17^{+0.16}_{-0.20}$
100	^{100}Zr	0.870 ± 0.108(c)	$39.81^{+0.27}_{-0.82}$
128	^{128}Sn	0.700 ± 0.090(c)	50.17 ± 0.20
131	$^{131}Sn^{g}$	0.096 ± 0.013	50.86 ± 0.09
	$^{131}Sn^{m}$	0.159 ± 0.024	
	^{131}Sb	0.573 ± 0.057	
	$^{131}Te^{g}$	$(8.5 \pm 4.5) \times 10^{-2}$	
	$^{131}Te^{m}$	$(7.7 \pm 1.1) \times 10^{-2}$	
132	^{132}Sn	0.181 ± 0.019(c)	$51.10^{+0.05}_{-0.04}$
	$^{132}Sb^{g}$	0.169 ± 0.037	
	$^{132}Sb^{m}$	0.339 ± 0.051	
	^{132}Te	0.299 ± 0.096	
	$^{132}I^{g}$	$(7.4 \pm 1.5) \times 10^{-3}$	
	$^{132}I^{m}$	$(5.7 \pm 0.9) \times 10^{-3}$	
133	^{133}Sb	0.450 ± 0.046(c)	$51.62^{+0.06}_{-0.09}$
	$^{133}Te^{g}$	0.147 ± 0.040	
	$^{133}Te^{m}$	0.348 ± 0.034	
	^{133}I	$(9.5 \pm 2.6) \times 10^{-2}$	
134	$^{134}I^{g}$	0.118 ± 0.018	52.07 ± 0.08
	$^{134}I^{m}$	0.109 ± 0.010	
	^{134}Cs	$(4.0 \pm 1.5) \times 10^{-5}$	
135	^{135}Te	0.567 ± 0.062(c)	$52.40^{+0.10}_{-0.12}$
	^{135}I	0.393 ± 0.078	
	^{135}Xe	0.051 ± 0.012	
136	^{136}Te	0.230 ± 0.028(c)	$52.87^{+0.02}_{-0.01}$
	$^{136}I^{g}$	0.109 ± 0.017	
	$^{136}I^{m}$	0.304 ± 0.039	
	^{136}Cs	$(1.86 \pm 0.16) \times 10^{-3}$	
137	^{137}I	0.679 ± 0.080(c)	$53.15^{+0.10}_{-0.12}$
	^{137}Xe	0.266 ± 0.056	
138	^{138}I	0.300 ± 0.036(c)	$53.87^{+0.10}_{-0.08}$
139	^{139}Xe	0.812 ± 0.084(c)	$53.95^{+0.22}_{-0.26}$
140	^{140}Xe	0.594 ± 0.061(c)	54.40 ± 0.07
	^{140}Cs	0.416 ± 0.053	
144	^{144}Ba	0.788 ± 0.084(c)	$56.07^{+0.11}_{-0.18}$
	^{144}La	0.237 ± 0.078	

(c) = Fractional cumulative chain yield.

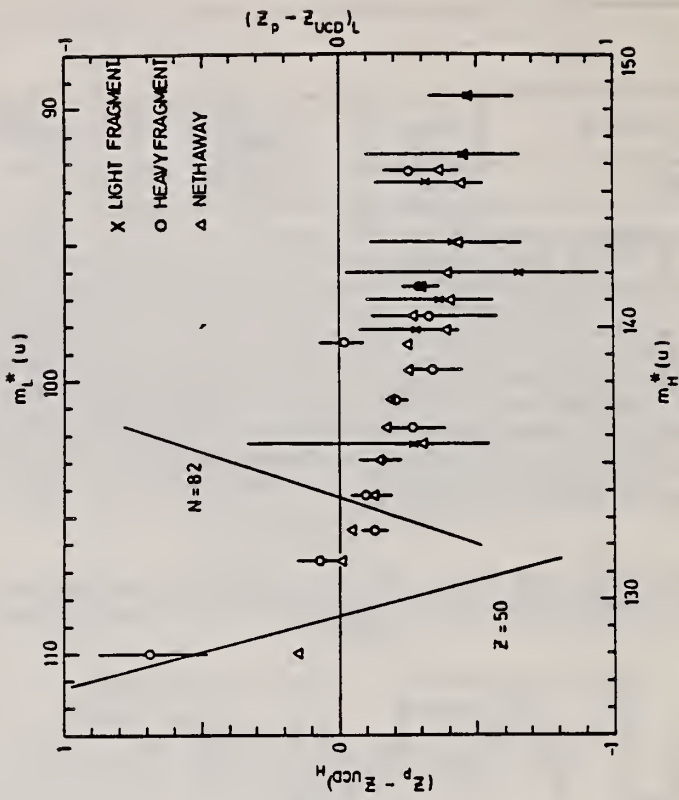

FIG. 2. Z_p-Z_{UCD} versus fragment mass number for the photofission of ^{238}U with 20-MeV bremsstrahlung. The Z_p values calculated following Nethaway (Ref. 9) are indicated by the triangles.

TABLE III. Values of the width parameter c determined for the photofission of ^{238}U with 20-MeV bremsstrahlung.

M_{post}	c
131	$0.90^{+0.25}_{-0.18}$
132	$0.95^{+0.08}_{-0.07}$
133	$1.05^{+0.22}_{-0.23}$
134	0.86 ± 0.09
135	$1.06^{+0.24}_{-0.26}$

REF. W. Günther, K. Huber, U. Kneissl, H. Krieger, H.J. Maier
Z. Phys. A 295, 333 (1980)

ELEM. SYM.	A	Z
U	238	92

METHOD

REF. NO. 80 Gu 4 hg

REACTION	RESULT	EXCITATION ENERGY	SOURCE		DETECTOR		ANGLE
			TYPE	RANGE	TYPE	RANGE	
G,F	RLY	THR-55	C	15-55	SCD-D		90

M,E DST, SYM/ASYM YLD

Measurements are presented for the mass and energy distributions of fragments from the photofission of ^{232}Th, ^{235}U, ^{238}U and ^{239}Pu. The experiments were performed for bremsstrahlung endpoint energies between 15 and 55 MeV, using silicon surface barrier detectors. The results are discussed with respect to the competition between the symmetric and asymmetric fission modes.

Table 2. Most probable heavy masses, most probable total kinetic energies and their variances (The variances have been corrected for the detector resolution and for γ- and electron pile up)

Nucleus	$[m]_{heavy}$	$[E_k]_{syst}$ a)	$[E_k]_{syst}$ b)	$[E_k]_{exp}$	σ_{E_k}
^{232}Th	(141.7 ± 2) amu	163.3 MeV	163.5 MeV	(159.5 ± 4) MeV	(9.0 ± 0.8) MeV
^{235}U	(138.5 ± 2) amu	169.1 MeV	170.1 MeV	(168 ± 3) MeV	(11.1 ± 1) MeV
^{238}U	(140.3 ± 2) amu	168.5 MeV	169.4 MeV	(164.5 ± 4) MeV	(11.7 ± 1) MeV
^{239}Pu	(137.2 ± 2) amu	174.7 MeV	176.6 MeV	(174 ± 3) MeV	(11.9 ± 1) MeV
^{252}Cf[c]				185.5 MeV	11.6 MeV

[a] $[E_k] = (0.1071 \cdot Z^2 \cdot A^{-1/3} + 22.2)$ MeV
[b] $[E_k] = (0.1240 \cdot Z^2 \cdot A^{-1/3})$ MeV
[c] Calibration measurement

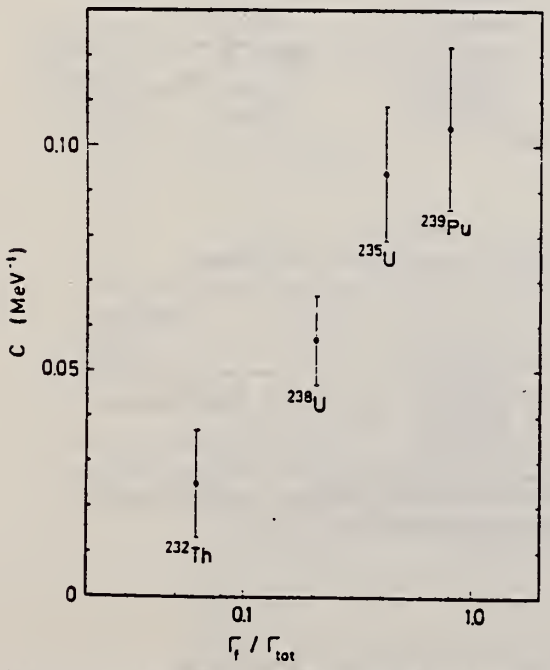

Fig. 5. Saturation parameter c as a function of the fission probability Γ_f / Γ_{tot}

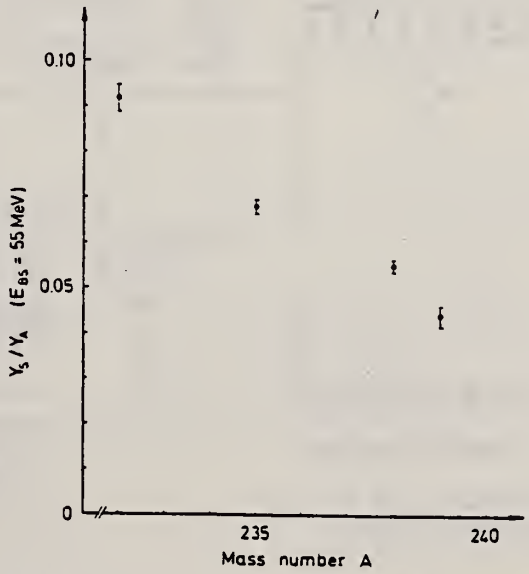

Fig. 6. Y_s, Y_A at $E_{BS} = 55$ MeV as a function of the mass number A

(OVER)

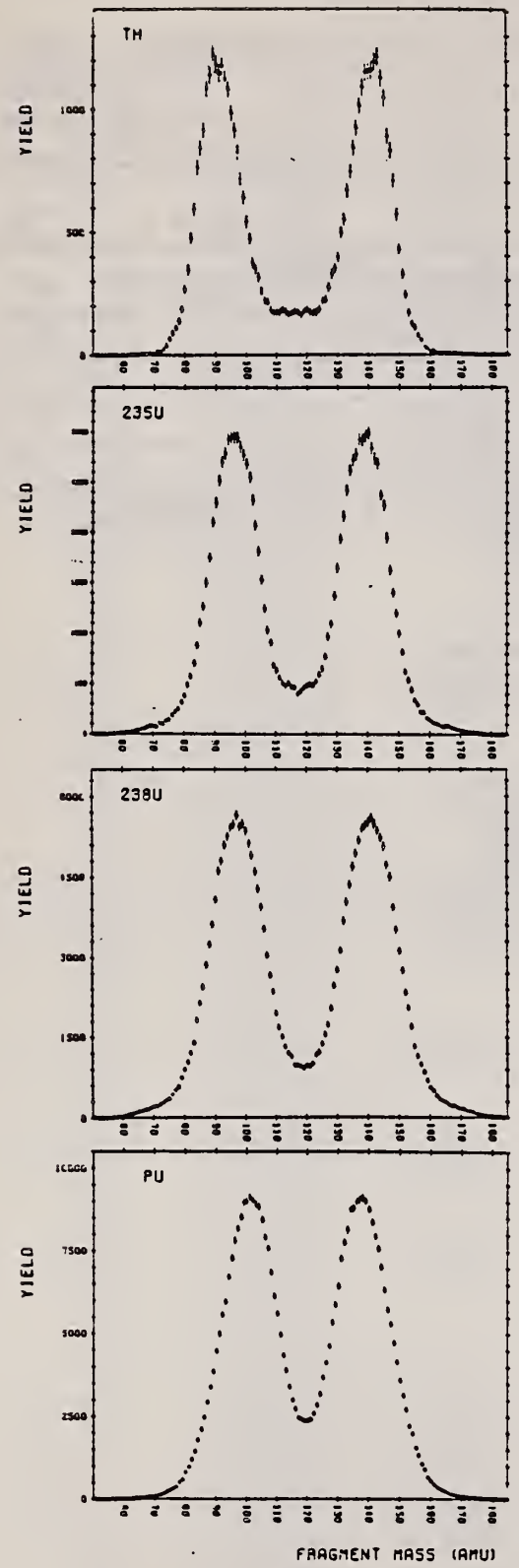

Fig. 1. Mass distributions for the photofission of ^{232}Th, ^{235}U, ^{238}U and ^{239}Pu (Bremsstrahl endpoint energy E_{BS} = 45 MeV)

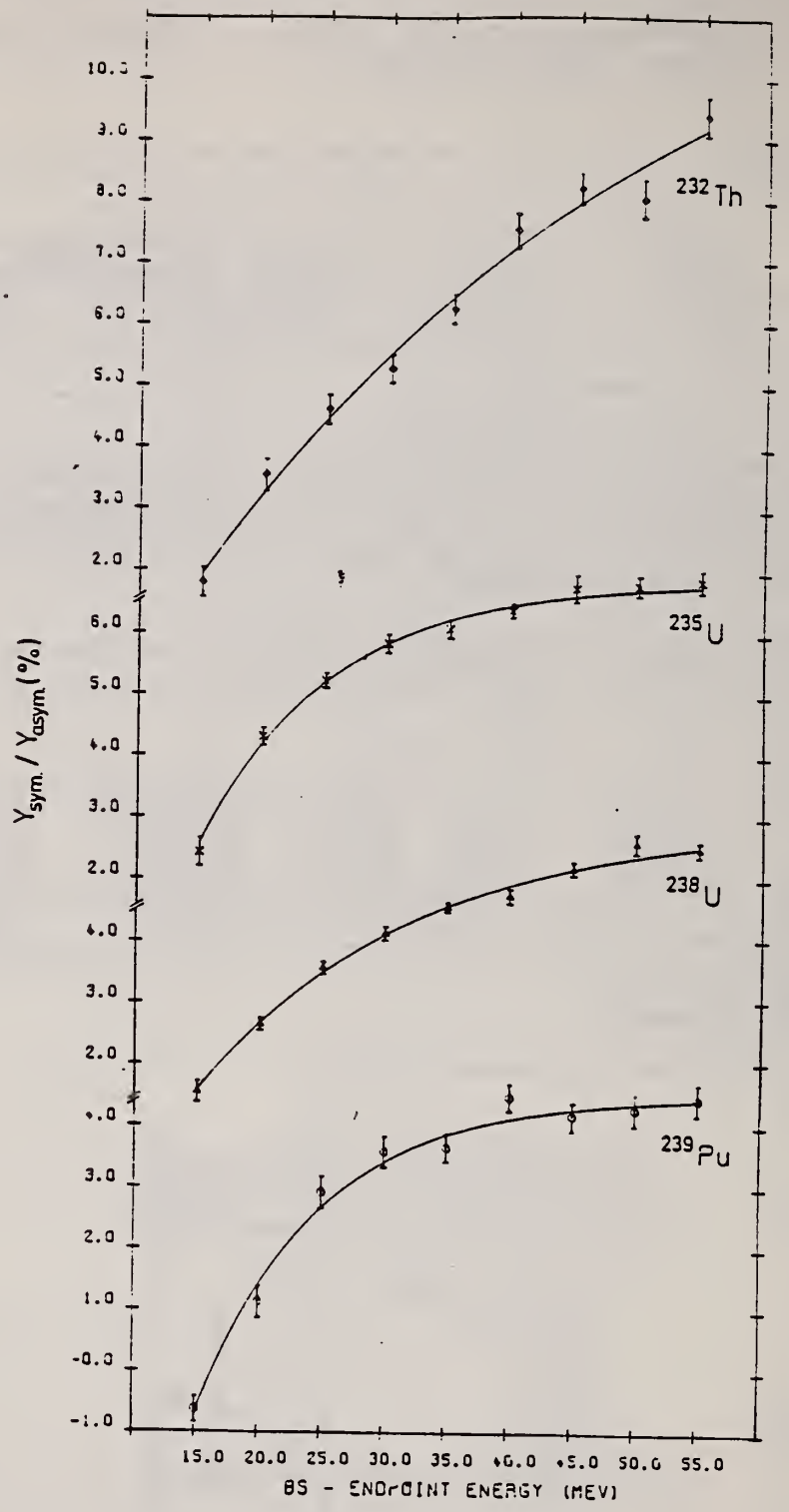

Fig. 4. Symmetric to asymmetric fission yield ratio as a function of E_{BS}. The lines are fits with an empirical function Y_s. $Y_s = a + be^{-c E_{BS}}$ (s. text)

REF. W. Günther, K. Huber, U. Uneissl, H. Krieger, H. Ries, H. Ströher, W. Wilke, H.J. Maier
Nucl. Phys. A350, 1 (1980)

ELEM. SYM.	A	Z
U	238	92

METHOD

REF. NO. 80 Gu 5 hg

REACTION	RESULT	EXCITATION ENERGY	SOURCE		DETECTOR		ANGLE
			TYPE	RANGE	TYPE	RANGE	
G,2N	RLY	THR-45	C	45	SPK-I		90

Abstract: Half-lives and yields in photonuclear reactions have been measured for shape isomers in U and Pu isotopes by pulsed-beam techniques bombarding ^{235,238}U and ^{239,240,242}Pu targets with bremsstrahlung. Isomeric fission cross sections have been deduced from the measured isomeric to prompt yield ratios within an evaporation model using absolute prompt fission data. The results are compared with data from particle-induced reactions.

YLD FISSION ISOMERS

E NUCLEAR REACTIONS ^{240}Pu^{235}U(γ, xn), ^{238}U, ^{239}Pu(γ, 2n), ^{242}Pu(γ, n); bremsstrahlung; measured $T_{1/2}$, isomeric to prompt yield ratios, ^{236}U, ^{237}Pu, ^{239}Pu, ^{241}Pu levels, deduced σ for isomeric fission. Natural and enriched targets.

TABLE 2

Results of isomeric fission experiments performed at Giessen

Reaction	Isomer	Half-life	Y_{iso}/Y_{pr}	Detector
^{232}Th(γ, xn)			$<10^{-6}$	PPAD
^{235}U (γ, xn)			$<10^{-7}$	PPAD
^{238}U (γ, 2n)	^{236}U	115 ± 5 ns	$(2.02\pm0.16)\times10^{-5}$	Si
		118 ± 7 ns	$(2.10\pm0.16)\times10^{-5}$	PPAD
^{239}Pu (γ, 2n)	^{237m_1}Pu	77 ± 16 ns	$(6.4\pm1.7)\times10^{-6}$	Si
		87 ± 11 ns	$(4.9\pm0.7)\times10^{-6}$	PPAD
	^{237m_2}Pu	1050 ± 400 ns	$(0.83\pm0.22)\times10^{-6}$	Si
^{240}Pu (γ, n)	^{239m_1}Pu	6.5 ± 0.4 μs	$(7.9\pm0.4)\times10^{-5}$	PPAD
^{240}Pu(γ, xn)	?	4.5 ± 1.5 ns	$<1.1\times10^{-4}$	PPAD
^{242}Pu(γ, n)	^{241m_1}Pu	20.5 ± 2.5 μs	$(9.2\pm0.8)\times10^{-5}$	PPAD
	^{241m_2}Pu	34 ± 7 ns	$(3.7\pm0.7)\times10^{-5}$	PPAD

TABLE 6

Isomeric fission cross sections for (γ, 2n) reactions (this work)

Reaction	E_0 (MeV)	$Y_{iso}/Y_{pr}\times10^{-5}$	σ_{iso}^{max} (μb)	E_{max} (MeV)
^{238}U(γ, 2n)	45	2.02 ± 0.16	9.9 ± 1.9	16†
		2.10 ± 0.16	10.3 ± 2.0	16†
^{239}Pu(γ, 2n)^{237m_1}Pu	45	0.64 ± 0.017		17.5†
^{239}Pu(γ, 2n)^{237m_2}Pu	45	0.49 ± 0.07 0.083 ± 0.022	5.7 ± 1.7	17.5† 17.5†

† The shape of the cross section was calculated (see text).

REF. W. Mückenheim, P. Rullhusen, F. Smend, M. Schumacher
Phys. Lett. 92B, 71 (1980)

ELEM. SYM.	A	Z
U	238	92

METHOD

REF. NO. 80 Mu 4 hg

REACTION	RESULT	EXCITATION ENERGY	SOURCE		DETECTOR		ANGLE
			TYPE	RANGE	TYPE	RANGE	
G,G	ABX	2,4	D	2-4	UKN-D		DST
		(2.254,3.254)		(2.5-3.5)			

LFT, 2 LEV., 2.254, 3.254

Elastic photon scattering investigated at energies of 2.5–3.5 MeV using radioactive sources has revealed a large probability for observing photoexcitation of nuclear levels. This finding removes inconsistencies in previously investigated properties of Delbrück scattering and provides a new access to nuclear resonance fluorescence.

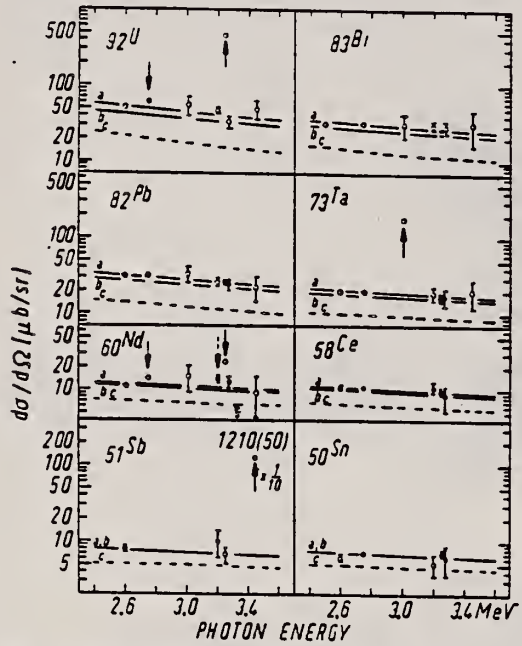

Fig. 1. Elastic differential cross sections versus photon energy. Unless error bars are given, the error intervals are at most equal to the diameter of the circles. Predicted differential cross sections: (a) including Coulomb corrections in addition to lowest-order D-, T-, R- and N-amplitudes, (b) including lowest-order D-, T-, R- and N-amplitudes, (c) including T-, R- and N-amplitudes.

Table 1
Levels observed via photoexcitation. ΔE: width of exciting photon line. D: predicted level spacing at 3 MeV. I^π: spin–parity. $(d\sigma/d\Omega)_{res}$: elastic differential cross section for resonance fluorescence by the identified isotope or element measured for $\theta = 90°$. Γ_0: partial width of the level for γ-transition to the ground state. Γ: total level width. $g = (2I_{ex}+1)/(2I_g+1)$. $W(\theta)$: angular correlation function.

Isotope	Level (MeV)	ΔE (eV)	D (eV)	I^π	$(d\sigma/d\Omega)_{res}$ (μb/sr)	$W(\theta)g\Gamma_0^2/\Gamma$ (meV)	Γ_0/Γ	Γ_0 (meV)
^{238}U	2.754	451	10^3	(1, 2)	13 ± 4	0.145	≲ 0.77	≳ 0.084 a)
	3.254	57		1⁻	399 ± 5	0.79	0.24	1.5
^{181}Ta	3.010	81	5×10^2	–	165 ± 17	0.40	≲ 0.72	≳ 0.56 b)
^{nat}Nd	2.754	451		–	2.6 ± 0.5	–	–	
	3.202	63	2×10^3	–	3.3 ± 1.5	–	–	
	3.254	57		–	12.8 ± 1.0	–	–	
^{121}Sb	3.452	35	10^3	(3/2, 5/2)⁺	2100 ± 50	2.8	0.60	4.7 b)

a) $I = 1$ assumed. b) $gW(0) = 1$ assumed.

REF. R. Pitthan, F.R. Buskirk, W.A. Houk, R.W. Moore
Phys. Rev. C21, 28 (1980)

ELEM. SYM.	A	Z
U	238	92

METHOD

REF. NO. 80 Pi 3 hg

REACTION	RESULT	EXCITATION ENERGY	SOURCE		DETECTOR		ANGLE
			TYPE	RANGE	TYPE	RANGE	
E,E/	ABX	5-40	D	87	MAG-D		DST

The deformed, fissionable nucleus ^{238}U was studied with inelastic scattering of 87.5 MeV electrons between 5 and 40 MeV excitation energy with inelastic momentum transfers ranging from 0.32 fm^{-1} to 0.58 fm^{-1} for an excitation energy of 15 MeV. Resonance cross sections extracted were compared with distorted-wave Born-approximation calculations using the Goldhaber-Teller, Steinwedel-Jensen, and Myers-Swiatecki models of the giant resonance. It is demonstrated that up to the first minimum of the form factor the cross section is nearly completely determined by one parameter, the transition radius R_{tr}. Using the known systematics of various multipole resonances in other, nonfissionable nuclei as a guide, it was found that the assumed ground state radius of ^{238}U had to be enlarged by about 10% for all multipolarities, to bring the strength found into agreement with the systematics and with other experiments in ^{238}U. In particular, while the model-independent values for position and width of the giant dipole resonance agree well with photon experiments, a scaled version of the Myers-Swiatecki model had to be used to produce agreement in strength. Similarly a scaled Goldhaber-Teller model was used for the isoscalar $E2$ resonance at 9.9 MeV. The situation for the isovector states above the giant dipole resonance, $E2$, and $E3$ (or $E0$) is even more complicated. It is argued that with proper caution and consideration of other available data the use of the collective models mentioned above may give valuable insight into the charge distribution of ^{238}U at higher excitation energies.

[NUCLEAR REACTIONS ^{238}U(e,e'), $E_0 = 87.5$ MeV. Measured $d^2\sigma/d\Omega dE_x$, bound and continuum states (giant resonances). Deduced multipolarity, reduced matrix element $B(E\lambda)$, radiative width Γ_γ^0, sum rule exhaustion of giant resonances, total width of continuum and clustered states.]

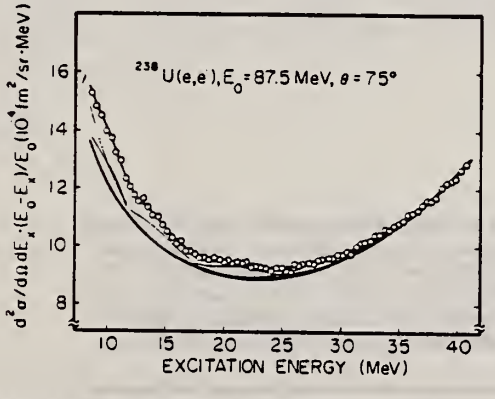

FIG. 2. Spectrum of 87.5 MeV electrons scattered inelastically from ^{238}U at 75°. The total fitted background consisting of radiation tail, general room background, and experimental scattering is represented by the lowest heavy line. The fitted resonances (lines between background and data points) and the composite fitted cross section (top line) are indicated. Note the suppressed scale; the resonant cross section is only a small fraction of the underlying radiation tail. The raising line at the very left is due to the tail of the ghost peak. The cross section has not been corrected for the constant dispersion of the magnetic spectrometer in order to show the data as measured. It is evident that not much can be learned from the data without background subtraction (see Fig. 3).

J-PI BEL LFT

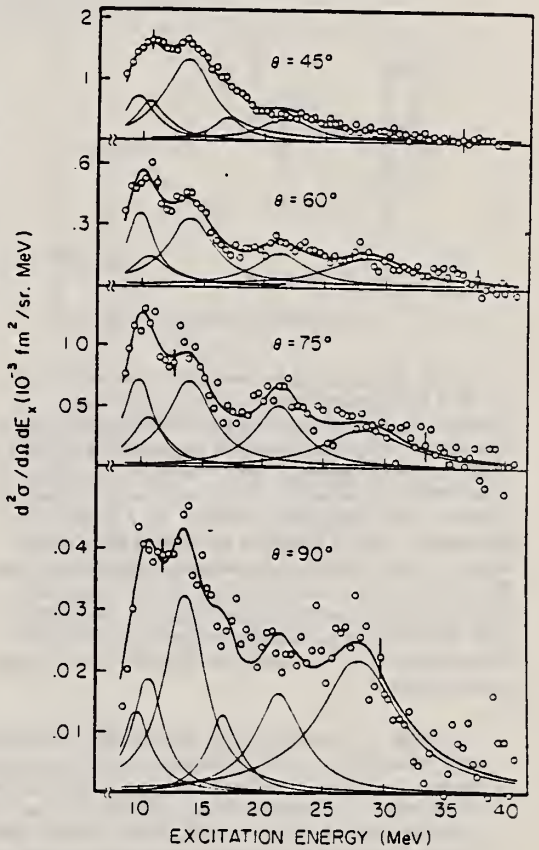

FIG. 3. 87.5 MeV electrons scattered inelastically from ^{238}U at 45°, 60°, 75°, and 90°. The fitted background, consisting of radiation tail, general room background, and instrumental scattering, has been subtracted. Comparison of part c with Fig. 2 shows that after subtraction of background many more details show up. The data have been corrected for the constant dispersion of the magnetic spectrometer in order to show the cross sections of the various resonances in their true relation. The relative differences in peak height for different resonances at different angles show that several multipolarities contribute.

(OVER)

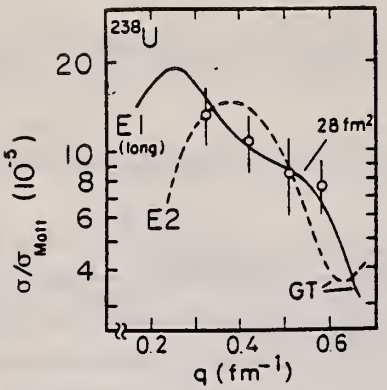

FIG. 9. Comparison between experimental and DWBA ($GT, c_{tr}/c = 1$) form factor for the GDR branch at 11 MeV (oscillation along long axis). The data are extremely well described by the calculation.

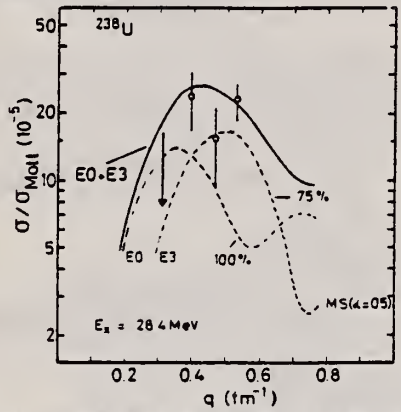

FIG. 15. Comparison between the cross section of the 28.4 MeV resonance and DWBA calculations. Choosing $c_{tr}/c = 1.1$ in agreement with the parametrization for the other resonances is *compatible* with 100% of the isovector monopole plus 75% of the isovector octupole EWSR in this region. It should be emphasized, however, that assumption of 90% of the $E3$ EWSR (on the basis of the GT model) to be present fits the data nearly as well without any monopole contribution. Similar to Fig. 13 the upper limit at 0.30 fm^{-1} was estimated from the statistical error of the 45° data at 28.4 MeV and the width as determined from other angles. We think that the χ^2 fit would be sensitive to any larger cross section.

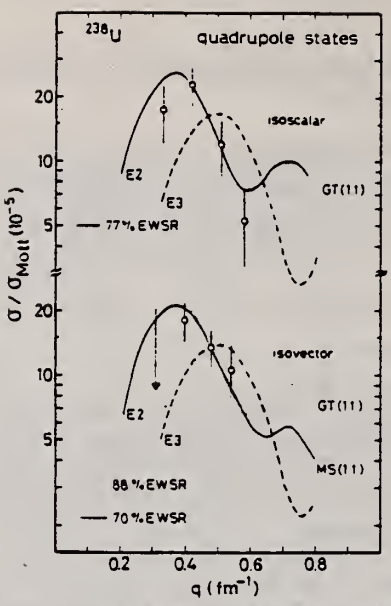

E_x=9.9 MeV

E_x=21.6 MeV

FIG. 14. Comparison between the experimental data of Figs. 12 and 13 and DWBA calculations based on modified GT and MS models. If we follow the underlying hypothesis of this paper, namely the assumption of a spatially larger ^{238}U in the excited state as compared to the ground state, the data are well described by the DWBA calculations *and* are in agreement with other experiments and what we would expect from Figs. 4 and 5.

TABLE II. Summary of the quantitative results of this paper. While the excitation energy and the width of the resonant structures found is relatively insensitive to multipolarity and models used, the strength is not. For each resonance, two values are given. The upper value corresponds to a straight application of the GT model to the data. The lower value corresponds to the assumption of an ^{238}U nucleus which is spatially enlarged by approximately 10% as compared to the ground state. In addition, the MS model (Refs. 52, 53) was used for the isovector excitations. These assumptions lead to a greater consistency of the strength with other available data in lighter nuclei (Ref. 8) and for ^{238}U.

E_x (MeV)	$E\lambda$	Model (c_{tr}/c)	$E_x(A^{-1/3})$ MeV	ΔT	Γ (MeV)	$B(E\lambda)$ ($fm^{2\lambda}$)	Γ_γ^0 (eV)	SPU	R (%) [a]
9.9 ± 0.2	$E2$	GT(1.0)	62	0	$2.9^{+0.8}_{-0.4}$	3700	56	17	38 ± 10
		GT(1.1)				7500	114	35	77 ± 20
10.8 ± 0.3	$E1$	GT(1.24)	67	1	3.2 ± 0.4	28	1.3×10^4	5	36 ± 4
		MS(1.35) [b]				30	1.3×10^4	5	39 ± 4
13.9 ± 0.3	$E1$	GT(0.9)	86	1	$4.5^{+0.3}_{-0.4}$	49	4.6×10^4	10	81 ± 8
		MS(1.0) [b]				50	4.7×10^4	10	83 ± 8
21.6 ± 0.6	$E2$	GT(1.0)	133	1	5.0 ± 0.6	3600	2.7×10^3	17	51 ± 8
		MS(1.1) [c]				5000	3.7×10^3	23	70 ± 11
28.4 ± 1.2	$E3$	GT(1.0)	176	1	8.1 ± 1.1	6.2×10^5	5.4×10^2	78	91 ± 15
		MS(1.1) [d]				5.1×10^5	6.6×10^2	64	75 ± 12

[a] $R = E_x \times B(E\lambda)/\mathrm{EWSR}(E\lambda, \Delta T) \times 100$.
[b] $\alpha(238,1) = 0.9$.
[c] $\alpha(238,2) = 1.0$.
[d] $\alpha(238,3) = 0.5$.

REF. R. Alba, G. Bellia, L. Calabretta, A. Del Zoppo, E. Migneco, G. Russo, R.C. Barna, D. De Pasquale
Il Nuovo Cimento 62A, 145 (1981)

ELEM. SYM.	A	Z
U	238	92

METHOD

REF. NO. 81 A1 7 hg

REACTION	RESULT	EXCITATION ENERGY	SOURCE TYPE	SOURCE RANGE	DETECTOR TYPE	DETECTOR RANGE	ANGLE
G,F	RLY	THR-6	C	5-6	TRK-I		DST
				(5.1-6.03)			

Differential photofission yields are fitted by: $\frac{dY_f}{d\Omega}(\theta)=a+b\sin^2\theta+c\sin^2 2\theta$

Summary. — Measurements of photofission fragment angular distributions of ^{238}U between 5.1 and 6.0 MeV are presented. As γ-source the intense bremsstrahlung beam from the Catania University Microtron is used. The results are analysed within the framework of the double-humped barrier model with a potential constructed with three smoothly joined parabolae and a damping term in the second well. The values of the fission barrier parameters for the involved 2^-0, 1^-0 and 1^-1 channels are extracted and a comparison with the theoretical predictions and experimental results in the literature is made. Delayed-fission contributions for the involved channels are taken into account in the 1^-1 channel parameter determination.

TABLE I. – *The ^{238}U parameters describing the double-humped barriers for the transition states involved as obtained from the best fit of our experimental data.*

Channel	Γ_A	$\hbar\omega_A$	Γ_{II}	$\hbar\omega_{II}$	Γ_B	$\hbar\omega_B$
2^-0	5.9±0.2	1.2±0.1	2.16±0.03	0.84±0.01	6.0 ±0.05	0.65±0.02
1^-0	6.6±0.1	1.1±0.1	2.98±0.03	0.40±0.01	6.0 ±0.05	0.56±0.02
1^-1	6.6±0.1	1.1±0.05	3.0 ±0.03	0.50±0.01	6.64±0.05	0.67±0.02

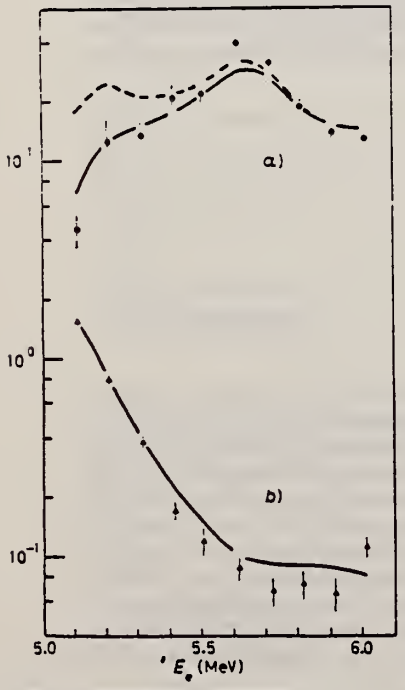

Fig. 4. – (▲) and (●) are, respectively, our c/b and b/a ratios as functions of electron energy. The curves are the c/b and b/a values as they result from the ratio of the separate yield curve fitting. The dashed curve represents the b/a ratio without delayed contributions in Γ_a^{th}.

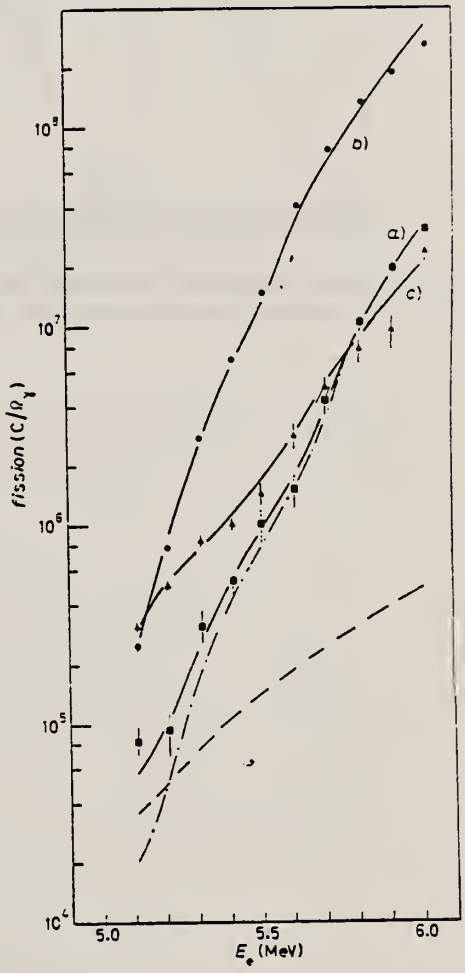

Fig. 5. – The figure shows the experimental yields (■) Γ_a^{exp}, (●) Γ_b^{exp} and (▲) Γ_c^{exp} as functions of the electron energy. The solid curves *a*), *b*) and *c*) represent the best fits to the experimental points. —·—·— is the calculated prompt-photofission contribution for the 1^-1 channel in Γ_a^{th} and ——— is the calculated total delayed-photofission yield due to the 1^-1, 1^-0, 2^-0 and 2^-2 channels.

(over)

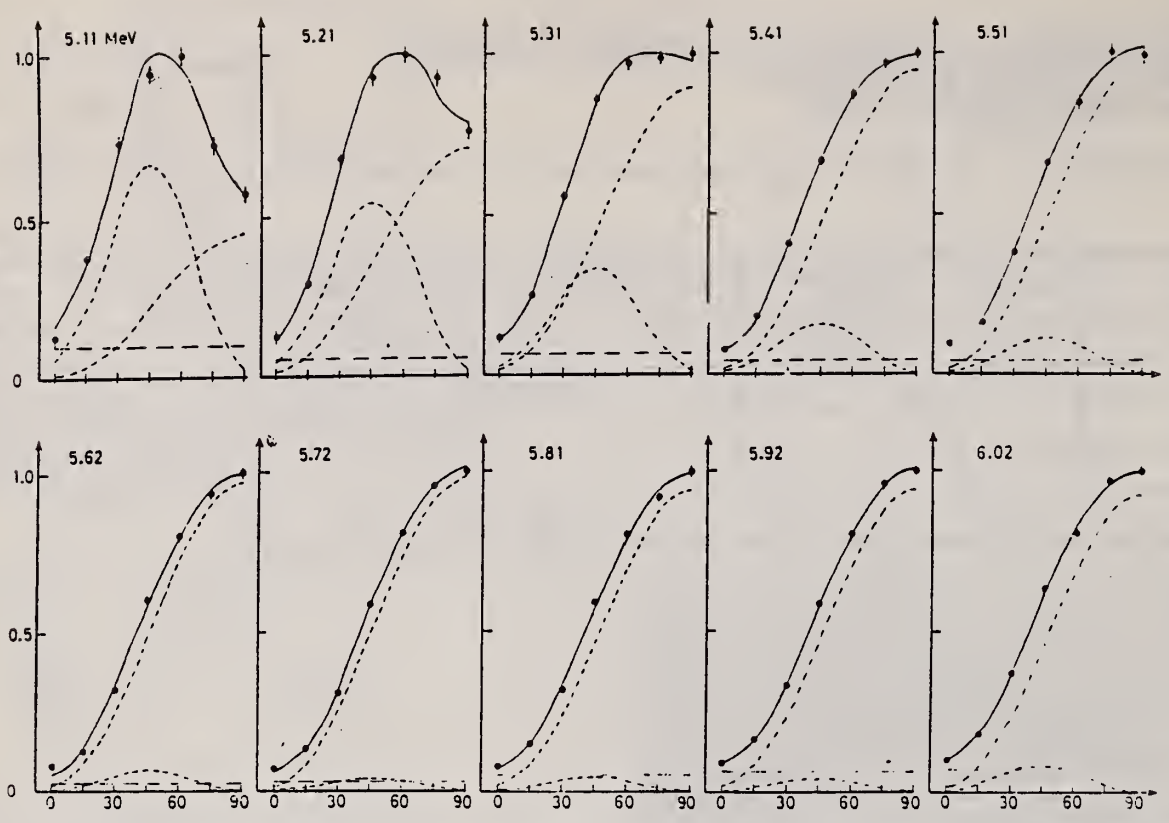

Fig. 3. – Angular distributions normalized to the maximum value. The dashed curves represent the isotropic, dipole and quadrupole components as obtained from the best fit. Their sum is represented by the solid curve.

REF. A.P. Antipenko, I.A. Grishaev, V.I. Kasilov, N.I. Lapin, S.F. Shcherbak
Sov. J. Nucl. Phys 33, 163 (1981)
Yad. Fiz. 33, 310 (1981)

ELEM. SYM.	A	Z
U	238	92

METHOD

REF. NO. 81 An 9 hg

REACTION	RESULT	EXCITATION ENERGY	SOURCE		DETECTOR		ANGLE
			TYPE	RANGE	TYPE	RANGE	
E,F	RLY	THR - 999	C	600-999	TRK - I		DST

999=1.6GEV, COH BRMS

Yields of fragments from photofission of ^{238}U have measured in the energy range $E_{\gamma max} = 600$–1600 MeV under the influence of photons produced in a silicon single crystal by electrons. The ^{238}U fission fragment yields are measured as a function of the orientation of the silicon crystal with respect to the direction of the electron beam. The energy dependences of the ratio of ^{238}U fission fragment yields for an oriented and an unoriented silicon crystal are presented.

PACS-numbers: 25.85.Jg, 61.80.Mk, 27.90. + b

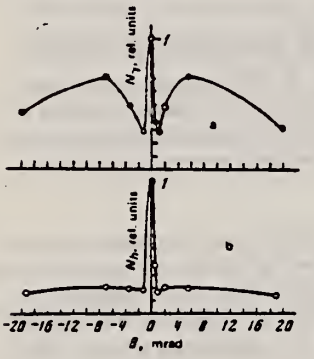

FIG. 2. Orientation dependence of the yield of photons from a silicon single crystal bombarded by 1000-MeV electrons (a) and of the yield of fission fragments from an amorphous ^{234}U target bombarded by photons from the crystal (b).

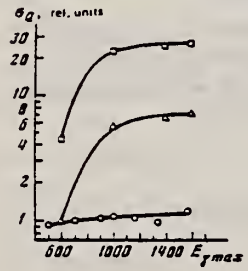

In Fig. 3 we have shown the yield of ^{238}U fragments as a function of the photon energy $E_{\gamma\ max}$. The upper curve corresponds to the case in which the [111] crystal axis is oriented along the electron beam direction. The middle curve is with the crystal rotated around the $[11\bar{2}]$ axis in the $\{11\bar{2}\}$ plane by an angle of 19 mrad. The lower curve corresponds to the fission fragment yields for the case in which the ^{238}U target is irradiated by bremsstrahlung produced by electrons in an ordinary amorphous tantalum target.[7] The yield values are given in relative units.

REF. V.I. Kasilov, N.I. Lapin
Yad. Fiz. 34, 865 (1981)
Sov. J. Nucl. Phys. 34, 483 (1981)

ELEM. SYM.	A	Z
U	238	92

METHOD

REF. NO. 81 Ka 5 egf

REACTION	RESULT	EXCITATION ENERGY	SOURCE		DETECTOR		ANGLE
			TYPE	RANGE	TYPE	RANGE	
G,F	RLY	4*1	C	*1	TRK-I		DST

COH BRMS 999=1.26 GEV

An enhancement in the yield of fragments was detected at 90° for the fission of ^{238}U induced by photons generated by the motion of high-energy electrons through a single crystal of silicon. These results allow one to select the optimum conditions with which to obtain maximum yields for nuclear particles.

PACS numbers: 25.85.Jg

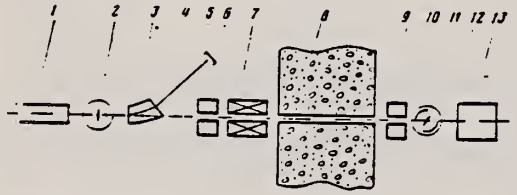

FIG. 1. Schematic of the experimental setup: 1—electron accelerator, 2—silicon single crystal, 3—bending magnet, 4—electron pipe, 5—secondary-emission monitor, 6—collimator, 7—clearing magnet, 8—shielding, 9—collimator, 10—fission chamber, 11—^{238}U target, 12—track detectors, 13—quantameter.

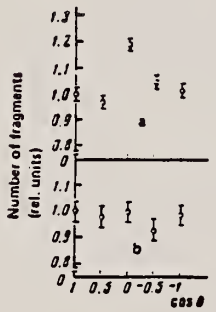

FIG. 2. Angular distributions of ^{238}U fission fragments.

Figure 2 shows the angular distribution of fragments from ^{238}U fission induced by photons generated in the silicon single crystal when the ⟨111⟩ axis coincided with the electron beam direction [Fig. 2(a)] and by photons generated in the amorphous gold target [Fig. 2(b)].

The photon energy spectrum corresponding to an axial motion for the electrons in the silicon single crystal was taken from Ref. 4, while data on the angular distributions for ^{238}U photofission fragments were taken from Refs. 1–3. In Ref. 4 it was shown that for axial motion of electrons through a silicon single crystal the number of photons with energies from 7 to 15 MeV increased by twenty times in comparison with an amorphous target of equivalent thickness.

Calculated values of $[Y_f(90°)/Y_f(0°)]_{am}$ and $[Y_f(90°/Y_f(0°)]_{cr}$ were found to be 1.03 ± 0.05 and 1.23 ± 0.11, respectively; these values agree well with the experimental results obtained in the present study.

REF. A. Leprètre, H. Beil, R. Bergère, P. Carlos, J. Fagot, A. De Miniac, A. Veyssière
Nucl. Phys. A367, 237 (1981)

ELEM. SYM.	A	Z
U	238	92

METHOD

REF. NO. 81 Le 1 egf

REACTION	RESULT	EXCITATION ENERGY	SOURCE		DETECTOR		ANGLE
			TYPE	RANGE	TYPE	RANGE	
G,SN	ABX	25-140	D	25-140	MOD-I		4PI
G,XN	ABX	25-140	D	25-140	MOD-I		4PI

Abstract: The total photonuclear absorption cross section for Sn, Ce, Ta, Pb and U has been studied from 25 to 140 MeV using a continuously variable monochromatic photon beam obtained from the annihilation in flight of monoenergetic positrons. The basic experimental results are a set of data giving sums of inclusive multiple photoneutron production cross sections of the form $\sigma^{(i)}(E_\gamma) = \sum_{i=j}\sigma(\gamma, in: E_\gamma)$ for neutron multiplicities ranging from $i = 1$ to 12. From these data the total photonuclear absorption cross section $\sigma(\text{tot}: E_\gamma)$ has been deduced. It is concluded that Levinger's modified quasideuteron model describes the total cross sections reasonably well. When these data are combined with lower energy data and integrated to 140 MeV they indicate the need for an enhancement factor K for the Thomas–Reiche–Kuhn sum rule of 0.76 ± 0.10. No evidence was found that would indicate an A-dependence for the enhancement factor.

E PHOTONUCLEAR REACTIONS Sn, Ce, Ta, Pb, U(γ, xn), $E_\gamma = 25$–140↓ MeV; measured $\sigma(E_\gamma)$ summed for $x = 1$–12; deduced $\sigma(E_\gamma$, total), integrated σ, interaction models. Monochromatic photons.

(G,SN) NO G,1N IN G,SN

$$\sigma^{(i)}(E_\gamma) = \sum_{i=j}\sigma(\gamma, in: E_\gamma).$$

TABLE 3
Integrated cross sections

	Sn	Ce	Ta	Pb	U	U
$\sigma_0 = 0.06NZ/A$ (MeV · b)	1.74	2.04	2.61	2.97	3.40	3.40
$E_{\gamma 0}$(MeV)	29.7	25	25	25	18	18.30
$M = \int_{B_{1n}}^{E_{\gamma 0}} \sigma_{GDR}(E_\gamma)\,dE_\gamma$ (MeV · b)	2.0 ± 0.15 [a]	2.13 ± 0.15 [b]	2.90 ± 0.23 [b]	3.48 ± 0.23 [c]	2.98 ± 0.15 [d]	3.58 [a]
(σ_0 unit)	1.15 ± 0.09	1.04 ± 0.07	1.11 ± 0.09	1.17 ± 0.08	0.88 ± 0.05	1.05
$N = \int_{E_{\gamma 0}}^{140\text{ MeV}} \sigma^{(2)}(E_\gamma)\,dE_\gamma$ (MeV · b)	0.96 ± 0.1	1.27 ± 0.1	1.73 ± 0.15	1.69 ± 0.15	2.59 ± 9.2	2.59 ± 0.2
(σ_0 unit)	0.55 ± 0.06	0.63 ± 0.05	0.66 ± 0.06	0.57 ± 0.05	0.76 ± 0.06	0.76 ± 0.06
$M + N$ (MeV · b)	2.96 ± 0.2	3.40 ± 0.2	4.63 ± 0.3	5.17 ± 0.3	5.57 ± 0.3	6.17 ± 0.3
(σ_0 unit)	1.70 ± 0.12	1.67 ± 0.10	1.77 ± 0.10	1.74 ± 0.10	1.64 ± 0.10	1.81 ± 0.10
$(M + N)$ + evaluation of the $\int_{E_{\gamma 0}}^{140\text{ MeV}} \lvert\sigma^{(1)} - \sigma^{(2)}\rvert\,dE_\gamma$ contribution $= (1 + K)$ (σ_0 unit)	1.74 ± 0.15	1.71 ± 0.15	1.81 ± 0.15	1.78 ± 0.15	1.68 ± 0.15	1.85 ± 0.15
$\int \sigma_L(E_\gamma)\,dE_\gamma$ (σ_0 unit)	1.28 [a]	1.24 [b]	1.30 [b]	1.35 [a]	1.18 [d]	1.43 [e]

[a]) Ref. [26]). [b]) Ref. [27]). [c]) Ref. [5]). [d]) Ref. [28]). [e]) Ref. [29]).

The symbols M and N are defined in the text. The last row gives the integrated cross sections for the Lorentz line fit, $\sigma_L(E_\gamma)$ to the GDR data, published in the above references.

(OVER)

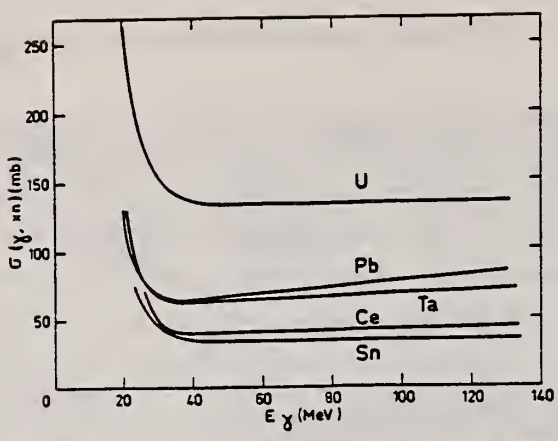

Fig. 11. The general behaviour of the "smoothed" average neutron yield cross sections $\sigma(\gamma, xn) = \sum_i i\sigma(\gamma, in : E_\gamma)$ for the Sn, Ce, Ta, Pb and U nuclei studied in the present paper (see text).

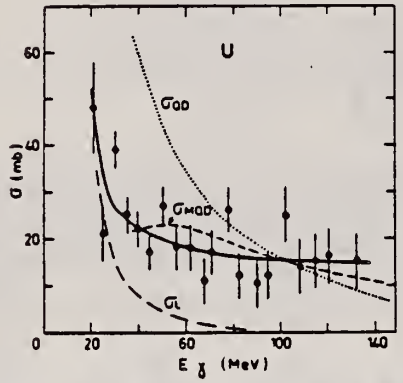

Fig. 15. Total photonuclear absorption cross sections $\sigma(\text{tot}: E_\gamma) \approx \sigma^{(2)}(E_\gamma)$ from the present paper, represented by the experimental points and the corresponding full lines, are shown for Pb, Sn, Ce, Ta and U. These experimental results for photon energies E_γ between 20 and 140 MeV are compared with: (a) Lorentz line fits to the GDR data of the appropriate nucleus represented by the dot-dash $\sigma_L(E_\gamma)$ plots. (b) Quasideuteron cross sections, $\sigma_{QD}(E_\gamma) = (4.6NZ/A)\sigma_D(E_\gamma)$ for the appropriate nuclei, represented by the dotted $\sigma_{QD}(E_\gamma)$ plots. Here $\sigma_D(E_\gamma)$ is the photodisintegration cross section of deuterium. (c) Modified quasideuteron cross sections, $\sigma_{QDM}(E_\gamma) = (8.NZ/A)\sigma_D(E_\gamma) \exp(-D/E_\gamma)$ with $D = 60$ MeV, represented by the dashed $\sigma_{MQD}(E_\gamma)$ plots. Pertinent GDR data for Pb, Sn, Ce, Ta and U were taken from refs. [5.26–28]).

REF. W. Mückenheim, P. Rullhusen, F. Smend, M. Schumacher, G. Endres, H. Langhoff
Z. Phys. A300, 43 (1981)

ELEM. SYM.	A	Z
U	238	92

METHOD

REF. NO. 81 Mu 3 egf

REACTION	RESULT	EXCITATION ENERGY	SOURCE		DETECTOR		ANGLE
			TYPE	RANGE	TYPE	RANGE	
G,GL	LFT	3	D	3	SCD-D		DST

L=0-10 3=3.254 MEV

Using ^{56}Co sources. a 3.254 MeV level in ^{238}U was photoexcited by a γ-line emitted in the decay of the 4.100 MeV level in ^{56}Fe. 10 γ-transitions deexciting this 3.254 MeV level were identified. Spin and parity were determined to be 1^-. By moving the ^{56}Co source in a high speed centrifuge the profile of the 3.254 MeV emission line was investigated. By applying a new variety of Doppler shift analysis a lifetime of $\tau_{Fe} = 55 \pm 25$ fs was obtained for the 4.100 MeV level in ^{56}Fe. The cross section for nuclear resonance fluorescence yields a lifetime of $\tau_U = 0.33 \pm 0.12$ ps for the 3.254 MeV level in ^{238}U.

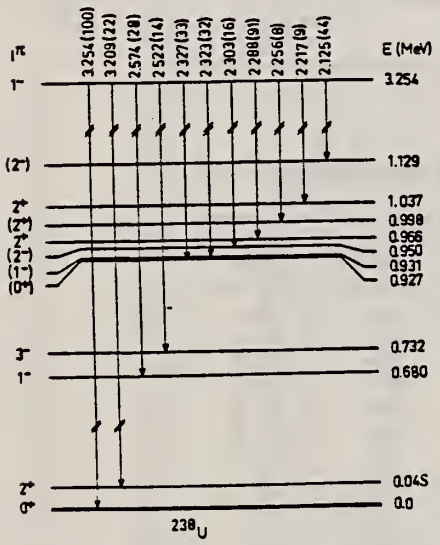

Fig. 2. Decay scheme of the 3.254 MeV level in ^{238}U. The transition energies and the relative intensities in parentheses are given on the top of each line. The relative intensities are obtained from the differential cross sections $(d\sigma\, d\Omega)_i$ for nuclear resonance scattering through the 3.254 MeV level (Table 1) after correcting for the angular correlation functions $W(\theta)$ of the photons

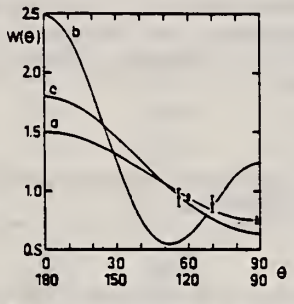

Fig. 3. Angular correlation functions $W(\theta)$ for the spin sequences (a) 0-1-0, (b) 0-2-0 and (c) 0-3-0, compared with the experimental results for the 3.254 MeV γ-lines exciting and deexciting the 3.254 MeV level in ^{238}U, respectively

Table 1. Differential cross sections $(d\sigma\, d\Omega)_i$ for nuclear resonance scattering through the 3.254 MeV level of ^{238}U leading to final-state levels with energies E_i. For $E_i = 0$ the elastic differential cross sections are given after subtracting the predicted coherent contributions

E_γ (MeV)	E_i (MeV)	$(d\sigma/d\Omega)_i^{\theta=90°}$ (μb sr)	$(d\sigma\, d\Omega)_i^{\theta=120}$ (μb sr)	I^a
3.254	0.0	399 (5)	505 (8)	0
3.209	0.045	118 (4)	117 (5)	2
2.574	0.680	183 (6)	142 (7)	1
2.522	0.732	77 (5)	77 (5)	3
2.327	0.927	133 (8)	164 (6)	0
2.323	0.931	193 (8)	174 (6)	1
2.303	0.950	78 (6)	85 (6)	2
2.288	0.966	473 (10)	485 (10)	2
2.256	0.998	34 (6)	52 (5)	2
2.217	1.037	48 (7)	50 (5)	2
2.125	1.129	230 (10)	237 (10)	2

a) Spins used for calculating the branching ratios of Fig. 3

REF. M. Schumacher, F. Smend, W. Mückenheim, P. Rullhusen, H.G. Börner
Z. Phys. A300, 193 (1981)

ELEM. SYM.	A	Z
U	238	92

METHOD

REF. NO. 81 Sc 6 egf

REACTION	RESULT	EXCITATION ENERGY	SOURCE		DETECTOR		ANGLE
			TYPE	RANGE	TYPE	RANGE	
G,G	ABX	2,3		2,7	SCD-D		90

2.75,6.42 MEV

Elastic scattering by nuclei in the range of mass numbers between 64 and 238 has been studied with monochromatic photons in the energy range between 2 and 8 MeV. These photons were provided either by a Ti(n,γ) source installed in the tangential through channel of the Grenoble high flux reactor, or by ^{24}Na and ^{56}Co sources produced by deuteron bombardment of Al or Fe at the Göttingen cyclotron. The photoexcitation of 23 nuclear levels has been observed and the decay properties and groundstate widths of the majority of these levels have been determined. For the lead scattering target the coherent elastic differential cross section has been studied in detail. There is evidence that below the photo-neutron threshold the elastic scattering via virtual photoexcitation of the nucleus can be approximated by extrapolating the real part of the Giant Dipole Resonance amplitude along a Lorentzian curve. Coulomb corrections to Delbrück scattering seem to play a small role at 6.5 MeV.

Table I. Differential cross sections for elastic scattering $(d\sigma/d\Omega)^{exp}$ of photons from ^{56}Co and ^{24}Na sources by different scattering targets, in units of μb/sr. Errors in the last digits are given in parentheses.

Θ deg	Scattering targets	2.599[a] (MeV)	2.754[b] (MeV)	3.010[a] (MeV)	3.202[a] (MeV)	3.254[a] (MeV)	3.273[a] (MeV)	3.452[a] (MeV)
90	^{238}U	52.7(25)	57.5(25)[c]	56(16)	47(4)	456 (10)[c]	34(6)	49(14)
	^{209}Bi	33.1(30)	32 (2)	33(11)	32(4)	25.6(20)	29(6)	33(15)
	^{nat}Pb	31.5(23)	31.0(16)	35 (8)	27(3)	26.6(22)	25(4)	23 (8)
	^{nat}Tl	31.5(33)	-	27(12)	32(5)	24 (3)	22(7)	34(15)
	^{nat}Hg	30.0(27)	-	24(10)	28(5)	25.5(18)	26(8)	20 (8)
	^{nat}W	22.5(11)	-	17 (7)	19(3)	18.4(15)	18(5)	21 (6)
	^{181}Ta	20.0(15)	19.2 (6)	193(20)[c]	20(4)	17.3(21)	18(5)	21 (8)
	^{165}Ho	15.9(13)	-	17(10)	13(6)	15.6(20)	18(8)	-
	^{nat}Nd	11.4 (7)	14.2 (5)[d]	15 (7)	14(3)	24.2(12)[d]	13(3)	9 (6)
	^{nat}Ce	11.1 (9)	11.0 (5)	-	11(3)	9.5(13)	8(4)	-
	^{127}J	8.4(10)	8.6 (5)	-	9(2)	7 (1)	5(3)	-
	^{nat}Sb	8.0(11)	-	-	10(4)	6.8(19)	-	1,270(50)[c]
	^{nat}Sn	6.5 (7)	7.0 (5)	-	5(2)	7.6 (8)	6(3)	-
	^{nat}Cd	6.2 (5)	-	-	6(2)	6.6 (8)	7(3)	-
120	^{238}U	55.1(25)	64 (4)[c]	43(15)	55(5)	574 (10)[c]	48(5)	48(11)
	^{181}Ta	27.5(15)	25.0 (9)	227(20)[c]	22(5)	21 (2)	22(8)	-
	^{nat}Nd	17.9(30)	17.0 (9)[d]	-	-	29.8(47)[d]	-	-

[a] ^{56}Co source in Fe lattice [b] ^{24}Na source in Al lattice (part of data have been published elsewhere)
[c] Transitions to excited states observed in addition to the ground-state transition
[d] Photoexcitation of nuclear level identified from the size of the differential cross section

(OVER)

Table 2. Elastic differential cross sections $d\sigma/d\Omega(\Theta=90°)$ in μb/sr measured with the Ti(n,γ) source and compared with theoretical predictions. n: predicted number of levels in a $\Delta E=25$ eV interval at 6.5 MeV. Errors in the last digits are given in parentheses

Scattering target	6.418 MeV		6.555 MeV		6.759 MeV		7.168 MeV		n
	exp.	th.	exp.	th.	exp.	th.	exp.	th.	
^{238}U	23 (12)	10.3	-	-	-	-	-	-	45
^{209}Bi	-	-	219(39)[b,c]	8.0	12 (4)	7.4	1.5(3)·10^5 [b,c]	5.7	0.1
^{nat}Pb	7.0(15)	8.6	-	-	6.5(11)	7.4	-	-	0.05
^{nat}Tl	2,586 (92)[a,c]	7.5	-	-	13 (3)[b]	6.0	-	-	0.4
^{nat}Hg	12 (3)	7.8	74(17)[b]	6.5	6.7(15)	6.4	-	-	3.4
^{nat}W	159 (10)[a,c]	6.6	306(33)[a,c]	6.3	20 (2)[a,c]	5.6	-	-	13
^{181}Ta	68 (4)[a,c]	6.3	-	-	10.1(12)[b,c]	5.3	-	-	28
^{165}Ho	15 (3)[b]	4.7	-	-	9.5(14)[b]	3.9	-	-	18
^{nat}Ce	4.1(21)	4.1	-	-	17 (1)[b,c]	3.6	-	-	0.04
^{nat}Sn	4.2(13)	3.0	-	-	2.5 (5)	2.7	-	-	1.9
^{nat}Mo	1,474 (44)[a,c]	2.5	407(39)[a,c]	2.5	8.5(15)[b,c]	2.3	817(258)[b,c]	2.0	0.5
^{nat}Zn	2.4 (8)	1.6	-	-	1.8 (5)	1.5	-	-	0.3

[a] Transitions to excited states observed [b] Photoexcitation identified from size of differential cross section
[c] Photoexcitation reported in [11]

Table 4. Properties of levels observed by photoexcitation. $(d\sigma/d\Omega)^{NRF}$: experimental differential cross section per identified isotope or element for resonance scattering through $\Theta=90°$. I^π: spin-parity of excited level; $W(\Theta)$: angular correlation function; $g=(2I_{ex}+1)/(2I_g+1)$; Γ_0: radiative groundstate transition width, Γ: total level width. Errors in the last digits are given in parentheses

Isotope	E_γ (MeV)	$(d\sigma/d\Omega)^{NRF}$ (μb/sr)	I^π	Γ_0/Γ [e]	$W(\Theta)g\Gamma_0^2/\Gamma$ (meV)	Γ_0 [f] (meV)	Γ_0 [g] (meV)
^{238}U	2.754	13 (4)	(1)	0.77	0.145	0.084	-
^{238}U	3.254	421 (5)	1$^-$	0.24	0.83	1.5	0.52(15)[d]
^{209}Bi	6.555	2.1 (4)·10^2	-	-	0.74	0.74[b]	-
^{209}Bi	7.168	1.7 (3)·10^5	9/2$^+$[a]	1.00	710	786	820 (40)[a]
^{203}Tl	6.418	8.75(30)·10^3	1/2[a]	0.28	30	102	82 (15)[a]
Tl	6.759	7 (3)	-	-	-	-	-
Hg	6.555	68 (17)	-	-	-	-	-
^{186}W	6.418	5.2 (3)·10^2	1$^-$[a]	0.32	1.75	2.4	-
^{184}W	6.555	9.8 (10)·10^2	(1)	0.52	3.44	2.9	-
^{184}W	6.759	46 (10)	(1)	0.58	0.17	0.13	-
^{181}Ta	3.010	174 (17)	-	0.72	0.42	0.59	-
^{181}Ta	6.418	62 (4)	-	0.73	0.2	0.27[c]	-
^{181}Ta	6.759	4.8 (12)	-	-	0.018	0.018[b]	-
^{165}Ho	6.418	10.3 (30)	-	-	0.035	0.035[b]	-
^{165}Ho	6.759	5.6 (14)	-	-	0.021	0.021[b]	-
Nd	2.754	2.6 (5)	-	-	-	-	-
Nd	3.254	14.0 (10)	-	-	-	-	-
Ce	6.759	13.4 (10)	-	-	-	-	-
^{121}Sb	3.452	2.20 (5)·10^3	-	0.60	2.9	4.9[b]	-
^{100}Mo	6.418	1.53 (4)·10^4	1$^-$[a]	0.88	52	26	25 (8)[a]
^{94}Mo	6.555	4.4 (4)·10^3	(1)	0.33	15	21	-
Mo	6.759	6.2 (15)	-	-	-	-	-
Mo	7.168	8.2 (26)·10^2	-	-	-	-	-

[a] [11] [b] $W(\Theta)g\Gamma_0/\Gamma=1$ assumed [c] $W(\Theta)g=1$ assumed
[d] [28] (a small correction has been applied to the data of [28])
[e] Upper limits in case not all the transitions to lower levels were observed
[f] Present work [g] Previous work

REF. H. Ströher, R.D. Fischer, J. Drexler, K. Huber, U. Kneissl, R. Ratzek, H. Ries, W. Wilke, H.J. Maier
Phys. Rev. Lett. 47, 318 (1981)

ELEM. SYM.	A	Z
U	238	92

METHOD

REF. NO. 81 St 5 hg

REACTION	RESULT	EXCITATION ENERGY	SOURCE		DETECTOR		ANGLE
			TYPE	RANGE	TYPE	RANGE	
E,F	ABX	THR-35	D	10-35	SPK-I		90
E+,F	ABX	THR-27	D	10-27	SPK-I		90

ALSO RATIO E,F/E+,F

The controversial results for the fission decay of the isoscalar giant quadrupole resonance in ^{238}U have been investigated by electron- and positron-induced fission experiments (E_e = 10–35 MeV). The measured cross-section ratio σ^-/σ^+ and absolute cross sections were analyzed with use of available distorted-wave Born-approximation virtual-photon spectra. Within this analysis no fission decay of the giant quadropole resonance could be detected, in contrast to a recent inclusive electrofission work.

PACS numbers: 25.85.Jg, 24.30.Cz, 27.90.+b

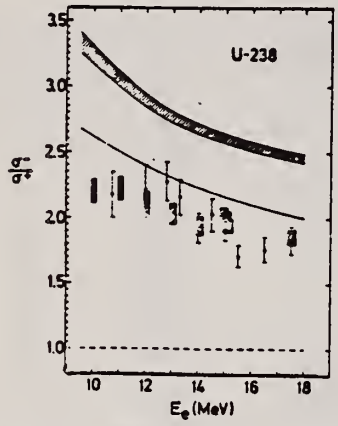

FIG. 1. Ratio σ^-/σ^+ as a function of bombarding energy E_e. Hatched rectangles: results for a thick target; full rectangles: results for a thin target; full points: previous results (Ref. 16) taken with track detectors; broken line: plane-wave calculation; full line: DWBA calculation for a pure $E1$ excitation; hatched area: DWBA prediction including the $E2$ strength of Ref. 6.

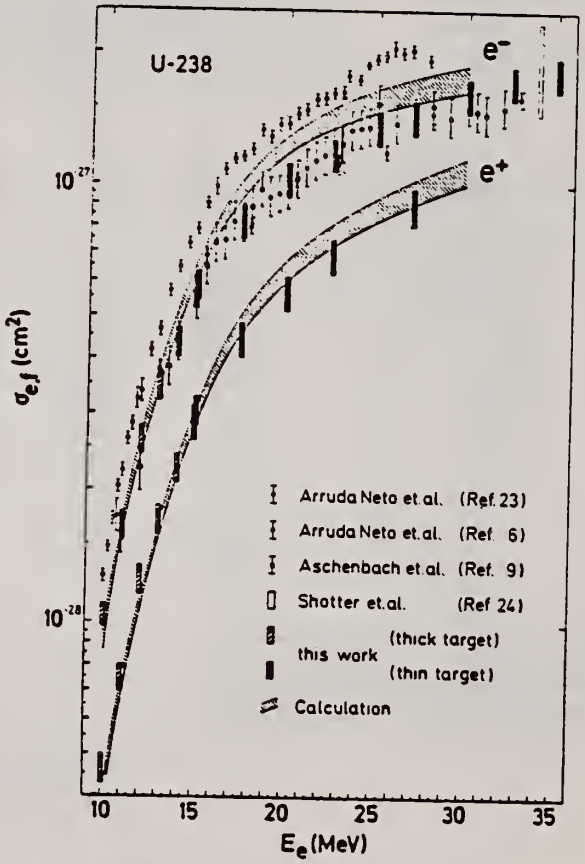

FIG. 2. Comparison of absolute electron- and positron-induced fission cross sections for ^{238}U. The error bars of the present results include both systematic and statistical errors. (Hatched areas: DWBA calculation for a pure $E1$ excitation including the systematic uncertainties in the $\sigma_{\gamma f}$ values of Ref. 14.)

REF. A.S. Voronin, I.S. Koretskaya, V.L. Kuznetsov, V.G. Nedorezov, N.V. Nikitina, V.I. Noga, S.A. Pashchuk, Yu.N. Ranyuk, S.M. Solov'ev
Yad. Fiz. 34, 1439 (1981)
Sov. J. Nucl. Phys. 34, 797 (1981)

ELEM. SYM.	A	Z
U	238	92

METHOD

REF. NO.: 81 Vo 3 | egf

REACTION	RESULT	EXCITATION ENERGY	SOURCE TYPE	SOURCE RANGE	DETECTOR TYPE	DETECTOR RANGE	ANGLE
E,F	ABX	4-275	D	97-275	TRK-I		45
G,F	RLY	4-275	D	184-275	TRK-I		45

RELATIVE BRMS/E YLD

Results are presented of cross-section measurements for the fission of ^{232}Th, ^{233}U, ^{235}U, ^{236}U, ^{238}U, ^{237}Np, and ^{239}Pu by electrons with energies between 100 and 275 MeV; photofission and electrofission cross-section ratios for the same nuclei are given as well.

PACS numbers: 25.85.Jg, 27.90. + b, 25.85.Ge

TABLE II. Electrofission cross sections (mb) for nuclei with $Z \geq 90$ measured for electron energies between 100 and 275 MeV.

E_e, MeV	Nucleus ^{232}Th	^{233}U	^{235}U	^{236}U	^{238}U	^{237}Np	^{239}Pu
97	1.24	8.12	5.66	4.55	3.23	6.22	7.26
134	1.47	9.17	6.08	4.74	3.42	6.63	7.98
149	1.42	9.75	6.17	5.50	3.89	7.16	8.39
166	1.63	10.36	7.01	5.29	4.15	7.70	9.18
184	1.78	9.61	7.13	5.64	4.17	7.92	8.92
201	1.54	9.84	6.53	6.10	4.56	7.49	9.31
217	1.73	10.91	7.73	6.14	4.77	7.09	9.56
240	1.91	10.25	7.26	5.92	4.49	7.84	9.43
253	1.85	9.89	7.00	6.17	4.76	7.80	9.78
275	2.22	10.50	8.15	6.66	5.26	9.63	10.50

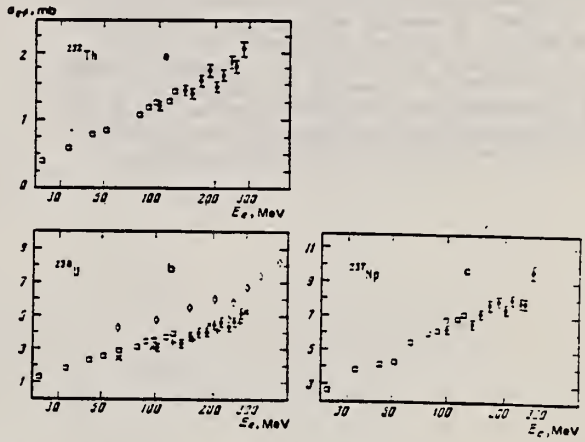

FIG. 2. Electrofission cross section for ^{232}Th (a), ^{238}U (b), and ^{237}Np (c). The points represent data as follows: □—Ref. 3, ●—present work, ◇—Ref. 1, ×—Ref. 2, and ---Ref. 4.

TABLE IV. Cross sections (mb) for photo- and electrofission ($\sigma_{Qf}\Delta t + \sigma_{ef}$) obtained in measurements with aluminum radiators with a thickness of $0.023t_0$ for ^{235}U, ^{236}U, ^{238}U, and ^{237}Np and of $0.011t_0$ for ^{239}Pu.

E_e, MeV	Nucleus ^{235}U	^{236}U	^{238}U	^{237}Np	^{239}Pu	E_e, MeV	Nucleus ^{235}U	^{236}U	^{238}U	^{237}Np	^{239}Pu
184	13.33	10.48	7.57	13.49	11.65	240	14.02	10.57	3.43	11.62	13.23
201	14.10	11.50	8.32	12.79	12.48	253	14.17	10.96	8.11	11.94	12.90
217	14.36	10.76	8.67	12.95	12.98	275	15.22	12.00	9.29	12.92	13.63

TABLE V. Cross-section ratios for photo- and electrofission (σ_{Qf}/σ_{ef}) for energies between 184 and 275 MeV.

Nucleus	σ_{Qf}/σ_{ef}	Nucleus	σ_{Qf}/σ_{ef}
^{235}U	40±8	^{237}Np	24±5
^{236}U	35±7	^{239}Pu	30±6
^{238}U	35±7		
	Average	33±3	
	Theoretical	35.3	

REF. T.R. Yeh, H. Lancman
IEEE Trans. Nucl. Sci. NS-28, 1289 (1981)

ELEM. SYM.	A	Z
U	238	92

METHOD

REF. NO. 81 Ye 1 egf

REACTION	RESULT	EXCITATION ENERGY	SOURCE		DETECTOR		ANGLE
			TYPE	RANGE	TYPE	RANGE	
G,F	ABX	5-11	D	5-11			4PI

Summary

High intensity proton beams from the Dynamitron at Brooklyn College are used to generate monochromatic gamma rays from known (p,γ) resonances in various nuclei. The gamma rays, whose energy varies continuously as a function of the angle with the proton beam, are used in turn to measure photofission cross sections in ^{238}U and ^{232}Th. The number of suitable (p,γ) resonances is sufficient to cover the 5 - 13 MeV range of excitation energy with an average step of ~100 keV. For a resonance of average strength the yield is 10^3 photons per μA of protons on target. The energy spread is typically 20 - 40 keV and a gamma ray energy resolution of 200 eV can easily be reached. This resolution is adequate for investigating structure in the photofission cross sections resulting from class II states in the second well of the fission barrier.

PHOTONS FROM P,G

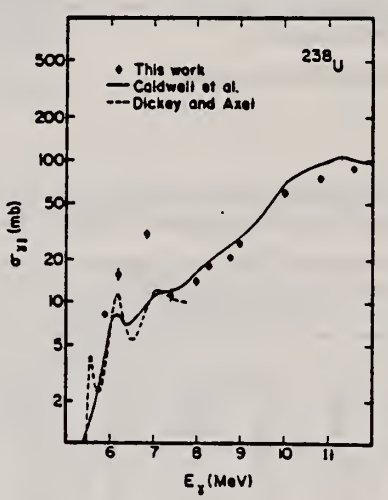

Fig. 3 Averaged photofission cross section $\sigma_{\gamma f}(E_\gamma)$ for ^{238}U. The results of Caldwell et al[10] and Dickey and Axel[4] are shown for comparison.

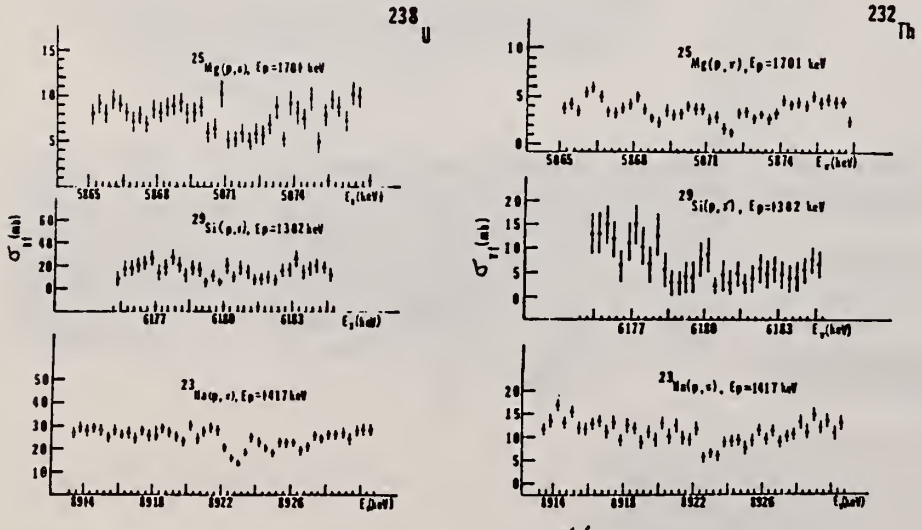

Fig. 2 Photofission fragment yields at several (p,γ) resonances.

(over)

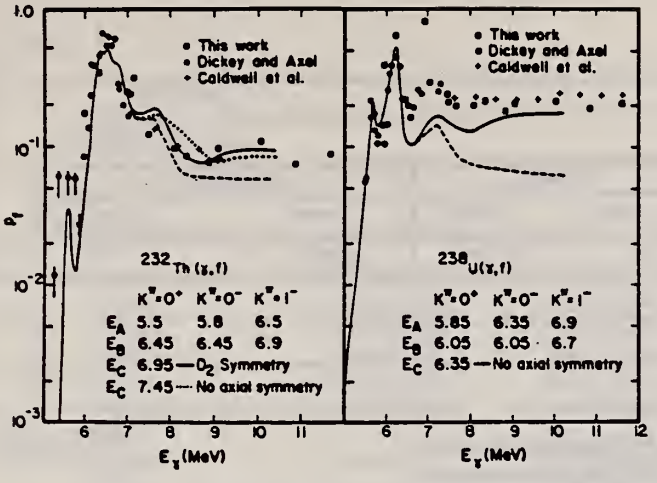

Fig. 5 Comparison of the fission probabilities of ^{238}U and ^{232}Th with results of statistical model calculations.

REF. D. DeFrenne, H. Thierens, B. Proot, E. Jacobs, P. DeGelder, A. DeClercq, W. Westmeier
Phys. Rev. C26, 1356 (1982)

ELEM. SYM.	A	Z
U	238	92

METHOD

REF. NO. 82 De 4 egf

REACTION	RESULT	EXCITATION ENERGY	SOURCE		DETECTOR		ANGLE
			TYPE	RANGE	TYPE	RANGE	
G,F	RLY	5-30	C	12-30	ACT-I		4PI

FRAG YLDS

A systematic study of the charge distribution for bremsstrahlung-induced photofission of ^{235}U and ^{238}U with the end point energies ranging from 12 to 30 MeV was performed using direct γ-ray spectrometry of irradiated uranium samples or of fission product catcherfoils, and also employing chemical separation techniques. For both fissioning systems the width of the charge distribution was found to be practically independent of the average excitation energy and the values obtained are in very good agreement with those reported in the literature for low-energy fission. The deviation of the most probable charge Z_p from the unchanged charge density value Z_{UCD} as a function of the fragment mass shows the influence of the 50-proton shell in the charge distributions and a higher charge-to-mass ratio of the light fragments independent of the compound nucleus excitation energy. For the necessary conversion of postneutron into preneutron masses, neutron emission curves, $\nu(m^*)$, were deduced from previously measured postneutron and provisional mass distributions. Calculations following the scission-point model of Wilkins *et al.* and the predictions of the empirical relation of Nethaway reproduce very well the experimentally determined Z_p behavior, except in the mass region affected by the $Z=50$ closed shell.

NUCLEAR REACTIONS, FISSION ^{235,238}U(γ,F), $E_{\gamma max}$ = 12, 15, 20, 30 MeV; measured product γ-ray spectra, deduced charge distributions, width, and most probable charges; calculated $\nu(m^*)$ from measured provisional and postneutron mass distributions.

TABLE V. Values of the width parameter c determined for the photofission of ^{238}U. M_{post} denotes the postneutron mass.

M_{post} \ E_e (MeV)	12	15	20	30
131		1.09±0.22	1.19±0.27	1.43±0.32
132	1.23±0.29	0.97±0.06	0.94±0.05	1.05±0.05
133	0.75±0.16	1.12±0.21	1.03±0.19	1.31±0.32
134	0.65±0.02	0.63±0.03	0.69±0.05	0.64±0.32
135	0.82±0.22	0.90±0.23	1.06±0.21	1.06±0.04
136	0.67±0.02	0.68±0.02	0.73±0.03	0.70±0.04
$\langle c \rangle$	0.82±0.21	0.90±0.23	0.94±0.20	1.03±0.31
$\langle E_{exc} \rangle$ (MeV)	9.7	11.6	13.4	14.7

(OVER)

TABLE III. Fractional independent and cumulative chain yields for the photofission of ^{238}U. (c) denotes the fractional cumulative chain yield.

Nuclide \ E_e (MeV)	12	15	20	30
$^{88}Br(c)$	0.810±0.085	0.788±0.073	0.740±0.080	0.788±0.078
$^{90}Kr(c)$	0.853±0.107	0.803±0.101	0.838±0.093	0.772±0.098
$^{91}Kr(c)$	0.725±0.107	0.655±0.063	0.665±0.087	0.683±0.133
$^{93}Rb(c)$	0.862±0.190	0.625±0.162	0.736±0.130	
$^{94}Sr(c)$	0.870±0.090	0.864±0.083	0.884±0.099	0.797±0.084
$^{95}Sr(c)$	0.881±0.078	0.823±0.080	0.848±0.071	0.875±0.092
^{96}Nb		$(7.3 \pm 2.5)\times10^{-5}$	$(1.1 \pm 0.5)\times10^{-4}$	$(2.4 \pm 0.6)\times10^{-4}$
$^{100}Zr(c)$	0.915±0.116	0.915±0.116	0.870±0.108	0.920±0.115
^{124}Sb		$(1.36 \pm 0.63)\times10^{-3}$	$(2.07 \pm 0.36)\times10^{-3}$	$(3.98 \pm 0.59)\times10^{-3}$
$^{126}Sb^{g}$	$(1.18 \pm 0.09)\times10^{-2}$	$(1.45 \pm 0.07)\times10^{-2}$	$(1.81 \pm 0.10)\times10^{-2}$	$(2.96 \pm 0.12)\times10^{-2}$
$^{126}Sb^{m}$		$(1.07 \pm 0.24)\times10^{-2}$	$(1.30 \pm 0.32)\times10^{-2}$	$(1.78 \pm 0.24)\times10^{-2}$
$^{128}Sn(c)$	0.770±0.120	0.670±0.110	0.700±0.090	0.702±0.090
$^{128}Sb^{g}$		$(4.9 \pm 1.9)\times10^{-2}$	$(6.2 \pm 2.3)\times10^{-2}$	$(8.5 \pm 2.4)\times10^{-2}$
$^{129}Sn^{A}(\frac{11}{2}^{-})(c)$	0.475±0.056	0.363±0.044	0.297±0.036	0.304±0.036
$^{129}Sn^{B}(\frac{3}{2}^{+})(c)$	0.316±0.043	0.263±0.034	0.277±0.033	0.250±0.030
$^{130}Sn(c)$	0.453±0.036	0.410±0.031	0.400±0.046	0.380±0.040
$^{130}Sb^{A}(5^{+})$	0.20 ±0.10	0.14 ±0.07	0.17 ±0.10	0.18 ±0.11
$^{130}Sb^{B}(8^{-})$	0.292±0.034	0.229±0.023	0.296±0.017	0.329±0.014
$^{131}Sn(c)$	0.380±0.035	0.349±0.028	0.334±0.050	0.341±0.021
^{131}Sb	0.507±0.075	0.506±0.054	0.494±0.058	0.457±0.054
$^{131}Te^{g}$		$(7.8 \pm 4.8)\times10^{-2}$	$(8.5 \pm 4.5)\times10^{-2}$	$(9.3 \pm 4.3)\times10^{-2}$
$^{131}Te^{m}$	$(2.9 \pm 0.7)\times10^{-2}$	$(5.7 \pm 1.1)\times10^{-2}$	$(7.7 \pm 1.1)\times10^{-2}$	0.100±0.013
^{132}Sn	0.249±0.021	0.222±0.017	0.181±0.019	0.182±0.017
$^{132}Sb^{g}$	0.186±0.049	0.202±0.023	0.169±0.037	0.217±0.033
$^{132}Sb^{m}$	0.328±0.055	0.312±0.075	0.339±0.051	0.317±0.118
^{132}Te	0.24 ±0.12	0.25 ±0.11	0.31 ±0.10	0.28 ±0.17
$^{132}I^{g}$		$(5.7 \pm 1.4)\times10^{-3}$	$(7.4 \pm 1.5)\times10^{-3}$	$(1.17 \pm 0.21)\times10^{-2}$
$^{132}I^{m}$		$(3.9 \pm 1.2)\times10^{-3}$	$(5.7 \pm 0.9)\times10^{-3}$	$(1.26 \pm 0.17)\times10^{-2}$
$^{133}Sb(c)$	0.487±0.032	0.498±0.032	0.450±0.046	0.492±0.054
$^{133}Te^{g}$	0.173±0.031	0.156±0.041	0.147±0.040	0.135±0.039
$^{133}Te^{m}$	0.302±0.026	0.267±0.035	0.348±0.034	0.277±0.034
^{133}I	$(3.5 \pm 2.0)\times10^{-2}$	$(7.4 \pm 2.1)\times10^{-2}$	$(9.5 \pm 2.6)\times10^{-2}$	0.101±0.031
^{134}Sb	0.136±0.008	0.102±0.006	0.102±0.006	$(9.3 \pm 0.7)\times10^{-2}$
^{134}Te	0.695±0.012	0.685±0.030	0.671±0.034	0.665±0.030
^{134}I	0.169±0.041	0.213±0.024	0.227±0.028	0.255±0.023
^{134}Cs			$(4.0 \pm 1.5)\times10^{-5}$	$(8.6 \pm 3.4)\times10^{-5}$
$^{135}Te(c)$	0.532±0.113	0.530±0.088	0.567±0.060	0.538±0.090
^{135}I	0.433±0.128	0.426±0.105	0.393±0.078	0.402±0.102
^{135}Xe	0.035±0.015	0.044±0.017	0.051±0.012	0.060±0.012
^{136}Te	0.285±0.017	0.228±0.018	0.230±0.028	0.167±0.026
$^{136}I^{g}$	0.113±0.044	0.138±0.044	0.109±0.017	0.144±0.056
$^{136}I^{m}$	0.269±0.015	0.256±0.015	0.304±0.039	0.364±0.051
^{136}Cs	$(4.6 \pm 1.1)\times10^{-4}$	$(1.06 \pm 0.11)\times10^{-3}$	$(1.86 \pm 0.16)\times10^{-3}$	$(3.62 \pm 0.32)\times10^{-3}$
$^{137}I(c)$	0.713±0.103	0.709±0.063	0.679±0.080	0.577±0.072
^{137}Xe	0.249±0.106	0.234±0.051	0.266±0.056	0.42 ±0.18
$^{138}I(c)$	0.311±0.027	0.334±0.048	0.300±0.036	0.292±0.034
$^{139}Xe(c)$	0.923±0.107	0.812±0.095	0.812±0.084	
$^{140}Xe(c)$	0.686±0.050	0.637±0.051	0.594±0.065	0.587±0.059
^{140}Cs	0.314±0.055	0.363±0.056	0.416±0.053	0.413±0.064
$^{144}Ba(c)$	0.756±0.068	0.789±0.054	0.788±0.084	0.790±0.067
^{144}La	0.244±0.067	0.244±0.061	0.237±0.078	0.210±0.025

REF. D.H. Dowell, L.S. Cardman, P. Axel, G. Bolme, S.E. Williamson
Phys. Rev. Lett. 49, 113 (1982)

ELEM. SYM.	A	Z
U	238	92

METHOD

REF. NO. 82 Do 5 egf

REACTION	RESULT	EXCITATION ENERGY	SOURCE		DETECTOR		ANGLE
			TYPE	RANGE	TYPE	RANGE	
E,E/F	ABX	5-12	D	46-67	SCI-D		DST

The $^{238}U(e,e'f)$ cross section was measured for excitations between 5 and 11.7 MeV. The sum of the $E2$ and $E0$ strength functions was extracted with the aid of available $^{238}U(\gamma,f)$ data. The present results show that the $E2/E0$ strength in the fission channel is spread almost uniformly from 7 to 11.7 MeV. The $E2/E0$ strength that is found in the fission channel corresponds to 10% of the isoscalar $E2$ sum rule; if the fission probability is 0.22, this energy region contains 45% of this sum.

PACS numbers: 25.85.Ge, 24.30.Cz, 27.90.+b

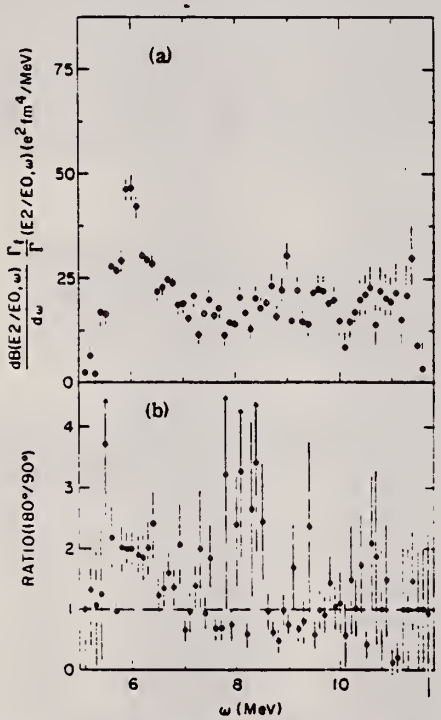

FIG. 2. The $E2/E0$ strength in the fission channel as determined from the present experiment, and the measured angular asymmetry.

REF. H. Ströher, R.D. Fischer, J. Drexler, K. Huber, U. Kneissl, R. Ratzek, H. Ries, W. Wilke, H.J. Maier
Nucl. Phys. A378, 237 (1982)

ELEM. SYM.	A	Z
U	238	92

METHOD

REF. NO.: 82 St 4 | egf

REACTION	RESULT	EXCITATION ENERGY	SOURCE		DETECTOR		ANGLE
			TYPE	RANGE	TYPE	RANGE	
E+,F	ABX	4-27	D	10-27	SPK-I		90
E,F	ABX	4-35	D	10-35	SPK-I		90

Abstract: Absolute cross sections for electron- and positron-induced fission of ^{238}U have been measured in the energy range 10–35 MeV. The cross sections were compared with the corresponding photo-fission cross sections using DWBA virtual-photon spectra. The reliability of the virtual-photon formalism to extract E2 strength from inclusive electrodisintegration experiments is critically discussed.

E NUCLEAR REACTIONS. Fission $^{238}U(e^-, F)$, (e^+, F), $E = 10$–35 MeV, measured absolute σ. Natural targets.

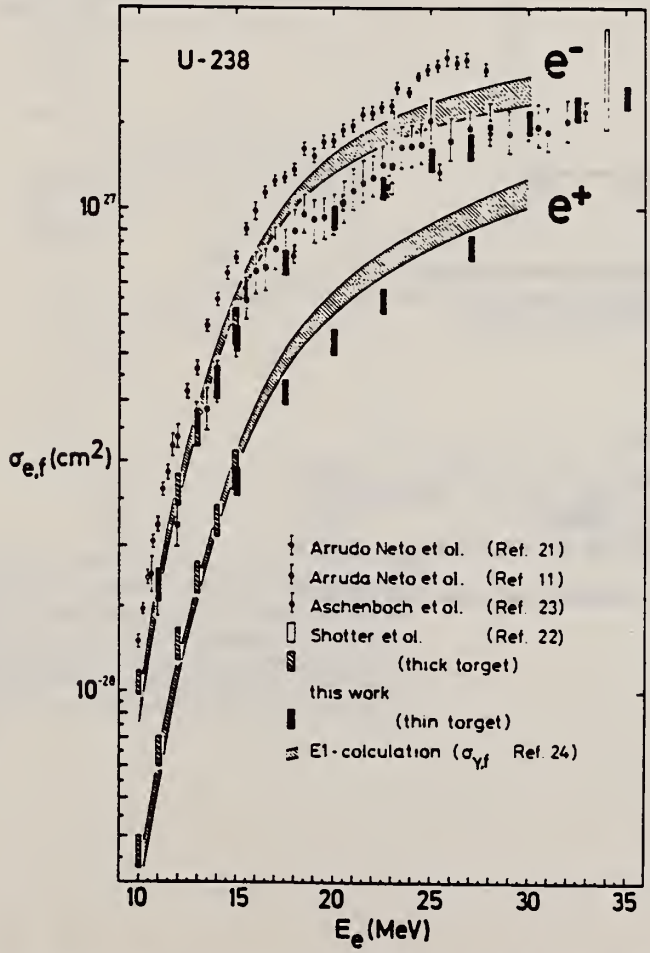

Fig. 3. Comparison of absolute electrofission cross sections (for details see text). Improved determinations of the target thickness and the detector efficiencies led to a reduction of the systematic errors of our cross sections when compared with the data reported in our previous letter [27]).

(OVER)

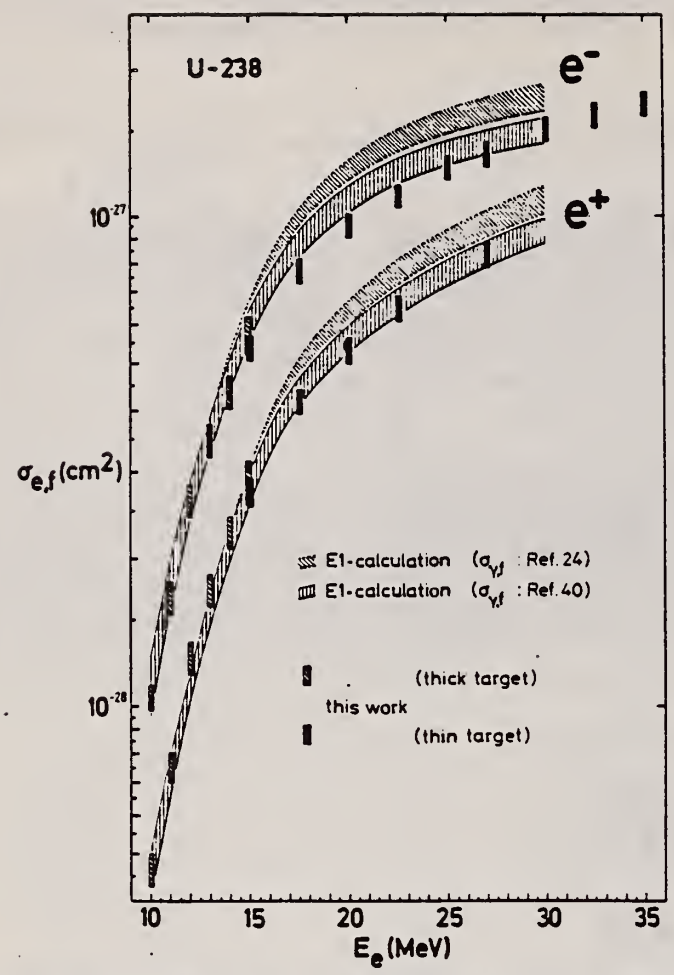

Fig. 8. Giessen electrofission results for ^{238}U compared with DWBA predictions using Livermore [34]) and Saclay [40]) photofission data. The hatched areas represent the quoted statistical errors of the photofission cross sections and the uncertainties of their extrapolations above 18 MeV.

11) J.D.T. Arruda Neto and B.L. Berman, Nucl. Phys. A349 (1980) 483

21) J.D.T. Arruda Neto, S.B. Berdade, B.S. Bhandari and I.C. Nascimento, Phys. Rev. C14 (1976) 1499 76Ar3
22) A.C. Shotter, D. Branford, I.C. McGeorge and J.M. Reid, Nucl. Phys. A290 (1977) 55 77Sh9
23) J. Aschenbach, R. Haag and H. Krieger, Z. Phys. A292 (1979) 285 79As4
24) J.T. Caldwell, E.J. Dowdy, B.L. Berman, R.A. Alvarez and P. Meyer, Phys. Rev. C21 (1980) 1215 80Ca1

40) A. Veyssière, H. Beil, R. Bergère, P. Carlos, A. Leprêtre and K. Kernbath, Nucl. Phys. A199 (1973) 45 73Ve1

REF. U. Zurmühl, P. Rullhusen, F. Smend, M. Schumacher, H.G. Börner
Phys. Lett. 114B, 99 (1982)

ELEM. SYM.	A	Z
U	238	92

METHOD

REF. NO. 82 Zu 2 egf

REACTION	RESULT	EXCITATION ENERGY	SOURCE		DETECTOR		ANGLE
			TYPE	RANGE	TYPE	RANGE	
G,G	ABX	3-6	D	3-6	SCD-D		90

SOURCE 141PR(N,G)

A procedure is presented to determine total photoabsorption cross sections σ_t by resonant scattering of γ-rays. It is shown that σ_t follows along the GDR lorentzian line down to 3.5 MeV. Indications for nonstatistical deviations from the lorentzian line are observed.

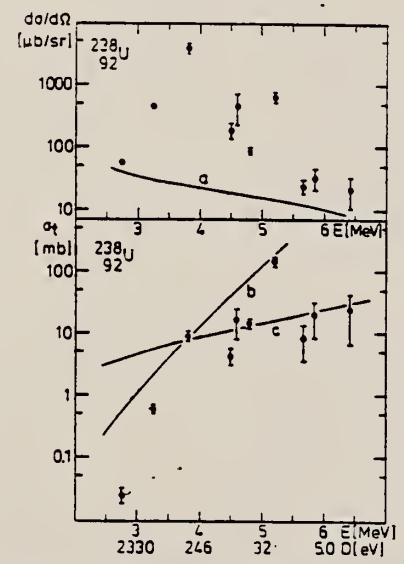

Fig. 1. Upper part: differential cross section for elastic photon scattering by ^{238}U through $\theta = 90°$ versus energy. Curve a: predicted differential cross sections for nonresonant elastic scattering. Lower part: total photoabsorption cross section for ^{238}U versus energy. Curve b: total photoabsorption cross section predicted by the Weisskopf model with hindrance factor 3×10^{-5}. Curve c: extrapolated lorentzian according to ref. [10].

U
A=239

U
A=239

REF. D. K. McDaniels, P. Varghese, I. Bergqvist, D. Drake
PICNS-73, Vol. II, p.951 (1973) Asilomar

ELEM. SYM.	A	Z
U	239	92

METHOD

REF. NO. 73 Mc 6 egf

REACTION	RESULT	EXCITATION ENERGY	SOURCE TYPE	SOURCE RANGE	DETECTOR TYPE	DETECTOR RANGE	ANGLE
N,G	RLX	13- 19	D	7- 14	NAI-D		UKN

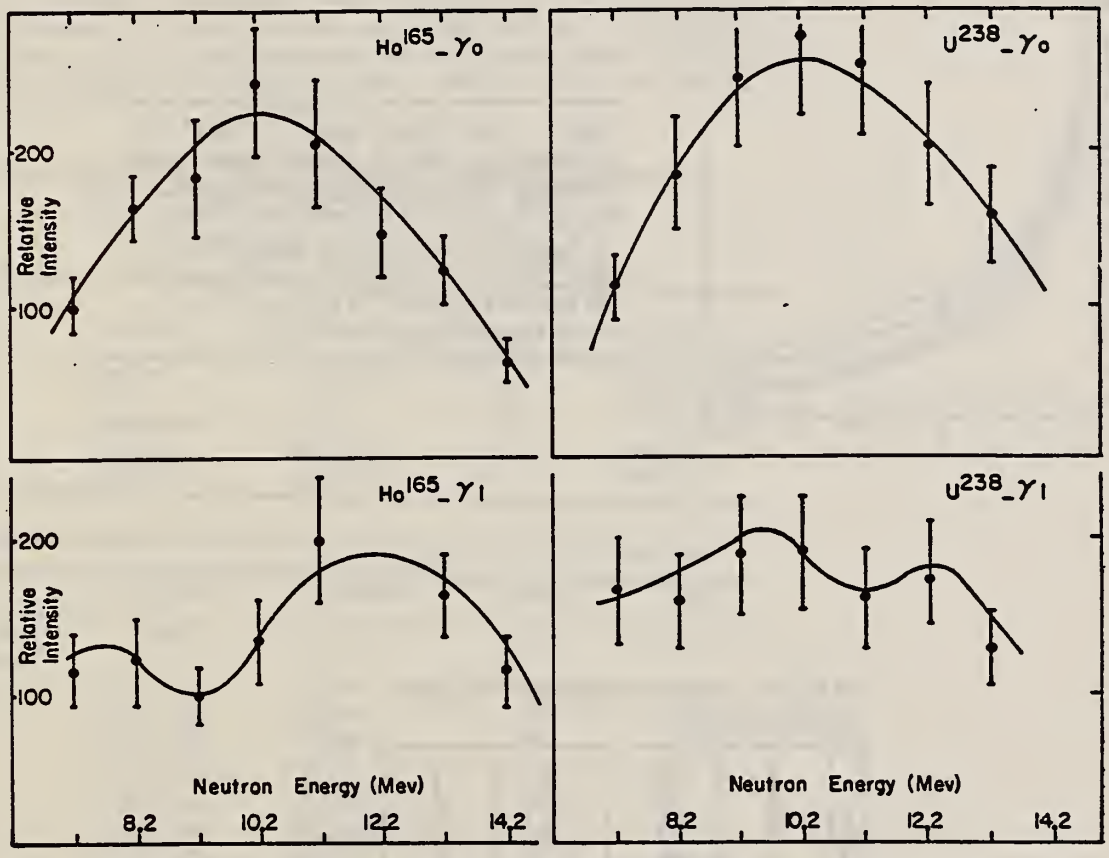

FIG. 1. The total (n,γ) cross section for ^{165}Ho and ^{238}U targets. The upper figs. show the data for transitions to the ground states of the final nucleus. The lower figs. show the data for transitions corresponding to the first peak found in the observed spectra below the one belonging to the ground state transition.

REF. M. Ya. Kondrat'ko, V. N. Korinets, and K. A. Petrzhak
Sov. Atomic Energy 40, 83 (1976)
Atomnaya Energiya 40, 72 (1976)

ELEM. SYM.	A	Z
U	239	92

METHOD

REF. NO. 76 Ko 8 hmg

REACTION	RESULT	EXCITATION ENERGY	SOURCE TYPE	SOURCE RANGE	DETECTOR TYPE	DETECTOR RANGE	ANGLE
G,F	RLY	THR- 24	C	10- 24	ACT-I		4PI

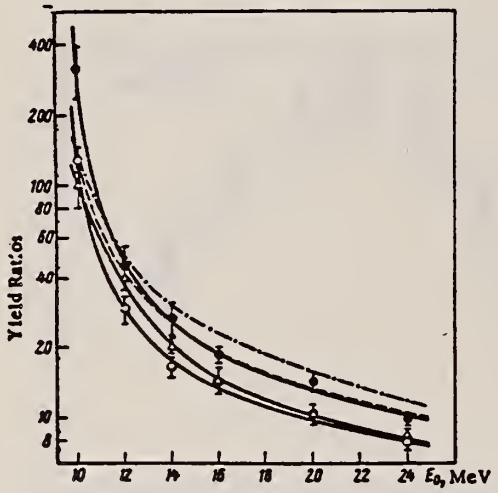

Fig. 1. Yield ratios "peak to trough" for photofission. Data of present paper for the reaction ^{233}U (γ, f): ○) $Y_{110}Ba/Y_{115}Cd$; ●) $Y_{140}Ba/Y_{113}Ag$; for the reaction ^{239}Pu (γ, f): △) $Y_{140}Ba/Y_{117}Cd$. Data in [1] for the reaction ^{235}U (γ, f): – – –) $Y_{140}Ba/Y_{115}Cd$; in [6] for the reaction ^{238}U (γ, f): —·—·—·) $Y_{140}Ba/Y_{115}Cd$.

TABLE 2. Relative Yields of ^{239}Pu Photofission Products

E_0, MeV	$Y_{111}Ag/Y_{140}Ba$	$Y_{113}Ag/Y_{140}Ba$	$Y_{115}Cd/Y_{140}Ba$	$Y_{117}Cd/Y_{140}Ba$
10	0,046±0,005	0,020±0,006	0,013±0,002	0,010±0,002
12	0,075±0,005	0,031±0,003	0,027±0,002	0,024±0,003
14	0,100	0,058	0,059	0,049
16	0,144	0,081	0,073	0,071
20	0,176	0,099	0,102	0,094
24	0,202	0,121	0,127	0,127

REF. W. Gunther, K. Huber, U. Kneissl, H. Krieger, H. J. Maier
Phys. Rev. C19, 433 (1979)

ELEM. SYM.	A	Z
Pu	239	94

METHOD

REF. NO. 79 Gü 1 hg

REACTION	RESULT	EXCITATION ENERGY	SOURCE		DETECTOR		ANGLE
			TYPE	RANGE	TYPE	RANGE	
G,2n	RLY	12-45	C	45	SCD-I		4PI

ISOMERIC/PROMPT YLD

The half-lives and yield ratios Y_{iso}/Y_{prompt} for the two ^{237}Pu fission isomers have been investigated in the photonuclear reaction ^{239}Pu(γ,2n). The observed half-lives ($t_{1/2} = 77 \pm 16$ ns, 1050 ± 400 ns) agree well with the data from particle induced fission. The measured yield ratios were $(Y_{iso}/Y_{prompt})_f^{short} = (6.4 \pm 1.7) \times 10^{-6}$ and $(Y_{iso}/Y_{prompt})_f^{long} = (0.83 \pm 0.22) \times 10^{-6}$. From a statistical model analysis of the isomeric fission yield ratio ($Y_{short}/Y_{long} = 7.7 \pm 2.9$) a spin assignment of the two shape isomers was attempted. The analysis provided, in the context of the statistical model, the most probable spin values $I = 11/2$ for the exicted, long lived state and $I = 5/2$ for the short lived ground state in the second minimum of ^{237}Pu. Comparing these spin values with single particle calculations, we tend to classify the excited state as the $[615]_{11/2+}$ Nilsson orbit and the short lived state as the $[862]_{5/2+}$ state.

[NUCLEAR REACTIONS ^{239}Pu(γ,2n), bremsstrahlung 45 MeV; measured $t_{1/2}$, Y_{iso}/Y_{pr} for ^{237}Pu^{m1,m2} deduced isomeric ratio, spins.]

TABLE II. Results.

Pulse length (ns)	$T_{1/2}$(ns)	$Y_{iso}/Y_{pr} \times 10^6$	$N_{pr} \times 10^{-6}$	Assignment
50	80 ± 20	6.2 ± 1.8	21.4	^{237}Pu^{m1}
	11 ± 6	...	21.4	^{238}Pu^{m}(?)
	long-lived	< 1.5	21.4	
1000	72 ± 26	10.9 ± 8.5	236.0	^{237}Pu^{m1}
	1050 ± 400	0.83 ± 0.22	...	^{237}Pu^{m2}

TABLE III. Comparison with previous results from particle induced reactions.

	$T_{1/2}$ (ns)	Reaction	Method	Ref.
Short-lived component	≈60	(α,2n)	R [a]	5
	100 ± 30	(d,2n)	R	9
	120 ± 50	(α,2n)	P [b]	10
	100 ± 50	(α,2n)	P	7
	120 ± 50	(α,n)	P	7
	82 ± 8	(α,2n)	P	11
	88 ± 35 [d]	(d,2n), (α,2n)	P	11
	114 ± 12	(d,2n)	P	6
	45 ± 10	(α,2n)	P	13
	110 ± 9	(α,2n)	P	14
	77 ± 16 [c]	(γ,2n)	P	this work
Long-lived component	900 ± 150	(d,2n)	P	8
	1120 ± 80 [d]	(α,2n), (d,2n)	P	11
	950 ± 300	(d,2n)	P	6
	1310 ± 260	(d,2n)	P	14
	1050 ± 400	(γ,2n)	P	this work

[a] Recoil techniques.
[b] Pulsed beam techniques.
[c] Weighted average of short and long beam pulse experiments.
[d] Weighted average of (d,2n) and (α,2n) results.

NEPTUNIUM
Z=93

In 1940, while at the University of California, Edwin McMillan was investigating the properties of a fission product of uranium. He found a substance associated with it that had a half-life of 2.3 days and he at once suspected that this might be the element with atomic number 93 that Fermi and his co-workers had looked for earlier.

In the spring of 1940, Philip Abelson came to Berkeley for a short vacation; he was at the Carnegie Institution in Washington, where, unknown to McMillan, he had also begun to work on the 2.3-day half-life substance. McMillan and Abelson found they had a common interest and decided to work together on the problem. They were soon able to demonstrate that they were dealing with the first transuranium element number 93. McMillan decided to name it neptunium since it was the element next to uranium, just as the planet Neptune was next to Uranus.

Np
A=237

Np
A=237

REF. L. Katz, A. P. Baerg, and F. Brown
Peaceful Uses of Atomic Energy, Switzerland 1958

ELEM. SYM.	A	Z
Np	237	93

METHOD: Fission chamber

[Page 1 of 2]

REF. NO.: 58 Ka 2 | EGF

REACTION	RESULT	EXCITATION ENERGY	SOURCE		DETECTOR		ANGLE
			TYPE	RANGE	TYPE	RANGE	
. G,F	ABX	5-18	C	5-18	ION-I		DST

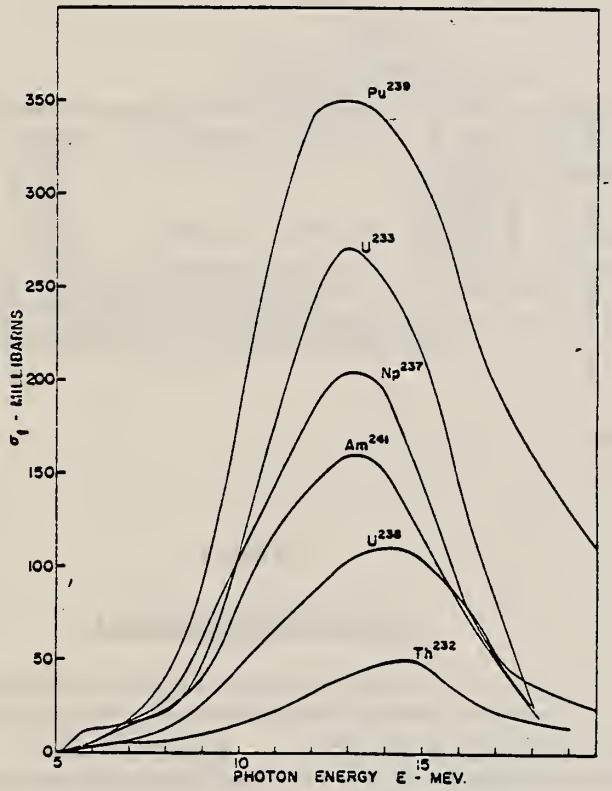

Fig. 5 - Photofission cross sections versus photon energy

REF.

L. Katz, A. P. Baerg, and F. Brown
Peaceful Uses of Atomic Energy, Switzerland 1958

ELEM. SYM.	A	Z
Np	237	93

METHOD

Fission chamber

REF. NO. 58 Ka 2 EGF

REACTION	RESULT	EXCITATION ENERGY	SOURCE		DETECTOR		ANGLE
			TYPE	RANGE	TYPE	RANGE	

Fig. 7 - Low-energy-yield curves: fissions per roentgen-nucleus versus maximum bremsstrahlung energy. (The solid and dotted lines are samples of smoothed yield curves which fit the experimental data.)

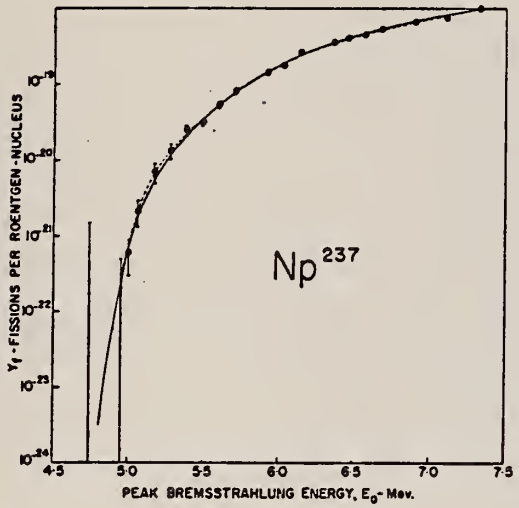

Table 4

Angular Distributions

Nuclide	Ratio, (Counts at 90°)/(Counts at 0°)[a] E_0 = 8.0 Mev[b]	E_0 = 10.0 Mev	E_0 = 20.0 Mev
U-233	1.048 ± 0.07	1.032 ± 0.04	0.994 ± 0.03
U-235	1.024 ± 0.05		
Np-237	1.024 ± 0.10		
Pu-239	1.002 ± 0.06	1.013 ± 0.05	0.952 ± 0.03
Am-241	0.958 ± 0.07		

(a) The ratio is the number of counts observed at 90° per unit X-ray dose divided by the number observed at 0° for the same dose.

(b) E_0 is the maximum energy of the bremsstrahlung spectrum.

REF.

A. P. Baerg, R. M. Bartholomew, F. Brown, L. Katz, and S. B. Kowalski
Can. J. Phys. 37, 1418 (1959) (A.E.C.L. No. 896)

ELEM. SYM.	A	Z
Np	237	93

METHOD

Betatron with ionization chamber detector, enriched samples.

REF. NO. 59 Ba 4 EGF

REACTION	RESULT	EXCITATION ENERGY	SOURCE		DETECTOR		ANGLE
			TYPE	RANGE	TYPE	RANGE	
G,F	RLY	THR - 20	C	6-20	ION-I		DST

TABLE I

Angular distributions
Ratio, counts at 90°/counts at 0°*

Nuclide	E_0† = 6.0	E_0 = 6.5	E_0 = 8.0	E_0 = 10.0	E_0 = 20.0
U-233			1.048±0.07	1.032±0.04	0.994±0.03
U-235			1.024±0.05		
Np-237			1.024±0.10		
Pu-239‡	1.034±0.26	0.927±0.12	1.002±0.06	1.013±0.05	0.952±0.03
Am-241			0.958±0.07		

*The ratio is the number of counts observed at 90° per unit X-ray dose divided by the number observed at 0° for the same dose.
†E_0 is the maximum energy in million electron volts of the bremsstrahlung spectrum.
‡The 45°/0° ratio at E_0 = 6.5 Mev was 1.09±0.23.

Ref. J.R. Huizenga, K.M. Clarke, J.E. Gindler, R. Vandenbosch
Nuclear Phys. 34, 439 (1962)

Elem. Sym.	A	Z
Np	237	93

Method: Monoergic γ's from $F^{19}(p,\alpha\gamma)O^{16}$ reaction; fission fragment ionization chamber.

Ref. No.: 62 Hu 1 | JHH

Reaction	E or ΔE	E_o	Γ	$\int \sigma dE$	Jπ	Notes
$Np^{237}(\gamma, f)$	6.14 7.0					

TABLE 3

Photofission cross sections obtained with mono-energetic gamma rays from the $F^{19}(p, \alpha\gamma)O^{16}$ reaction

Target	$\sigma_{7.0}/\sigma_{6.14}$	$\sigma_{7.0}$(mb)	$\sigma_{6.14}$(mb)	B_f(MeV) [a]	E_f(MeV) [b]
Th^{232}	1.00 ± 0.13	9 ± 3	9 ± 3	6.34	5.5
U^{238}	1.12 ± 0.15	15 ± 5	13 ± 4	6.04	5.3
U^{236}	0.80 ± 0.10	28 ± 9	35 ± 11	6.40	5.2
U^{235}	2.06 ± 0.33	33 ± 10	16 ± 5	5.24	5.5
U^{234}	10.0 ± 5.0	52 ± 16	5^{+10}_{-5}	6.77	5.1
U^{233}	3.24 ± 0.79	44 ± 14	13 ± 4	5.99	5.4
Np^{237}	1.43 ± 0.21	45 ± 14	31 ± 10	6.76	5.3

[a] From the compilation of ref. [20]
[b] From the compilation of ref. [26]

Ref 20: Everling, König, Mattauch & Wapstra - Nuclear Phys. 18, 529 (1960)

Ref 26: Vandenbasch & Seaborg - Phys. Rev. 110, 507 (1958)

REF.	ELEM. SYM.	A	Z
R. Bergere, H. Beil, P. Carlos, A. Veyssiere, A. Lepretre PICNS-72, p. 273 Sendai	Np	237	93

METHOD	REF. NO.	
	72 Be 15	hvm

REACTION	RESULT	EXCITATION ENERGY	SOURCE		DETECTOR		ANGLE
			TYPE	RANGE	TYPE	RANGE	
G,N	ABX	9- 17	D	9- 17	MOD-I		4PI
G,2N	ABX	9- 17	D	9- 17	MOD-I		4PI
G,F	ABX	9- 17	D	9- 17	MOD-I		4PI

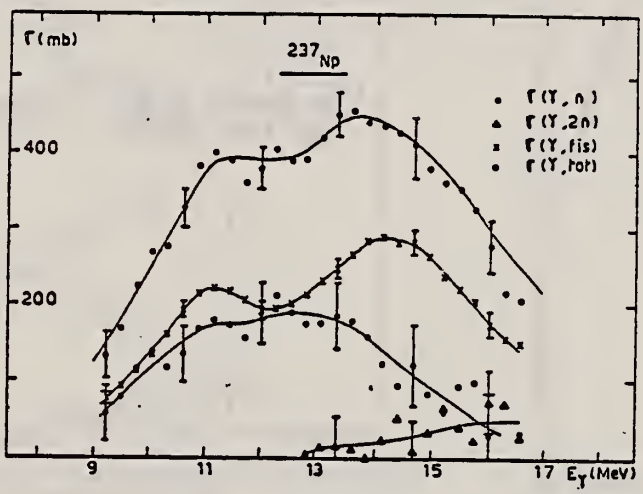

Fig. 5

TABLE 1

LORENTZ LINE PARAMETRS AND INTRINSIC QUADRUPOLE MOMENTS

Target nucleus	E_1 MeV	σ_1 mb	Γ_1 MeV	E_2 MeV	σ_2 mb	Γ_2 MeV	$R = \frac{\pi/2\,\sigma_2\,\Gamma_2}{\pi/2\,\sigma_1\,\Gamma_1}$	Q_0 barns *	Q_0 barns **
$^{232}_{90}Th$	11.08 ±0.12	268 ± 7	3.37 ±0.22	14.07 ±0.14	349 ± 9	4.62 ±0.16	1.8 ± 0.15	10.2 ± 1	9.66 ±0.1
$^{238}_{92}U$	10.96 ±0.09	301 ± 6	2.90 ±0.14	14.04 ±0.13	369 ± 6	4.53 ±0.13	1.9 ± 0.1	11 ± 1	11.3 ±0.1
$^{237}_{93}Np$	11.06 ±0.12	251 ± 7	3.16 ±0.27	14.21 ±0.14	380 ± 9	5.12 ±0.3	2.4 ± 0.3	11.3 ± 1	10.9 ±0.7

I/ LORENTZ LINES PARAMETERS

* this experiment

** —. E.E.G. [illegible], E. [illegible], V. [illegible]. - Nuclear data tables, Vol. 7, 5 (1970).

REF. M.Ya. Kondrat'ko, V.N. Korinets, K.A. Petrzhak, and O.A. Teodorovich
At. Energ. 35, 211 (1972)
Sov. J. At. Energy 35, 862 (1973)

EL.EM. SYM.	A	Z
Np	237	93

METHOD

REF. NO. 72 Ko 9 egf

REACTION	RESULT	EXCITATION ENERGY	SOURCE TYPE	SOURCE RANGE	DETECTOR TYPE	DETECTOR RANGE	ANGLE
G,F	RLY	THR- 24	C	10- 24	ACT-I		4PI

FISSION PROD YIELDS

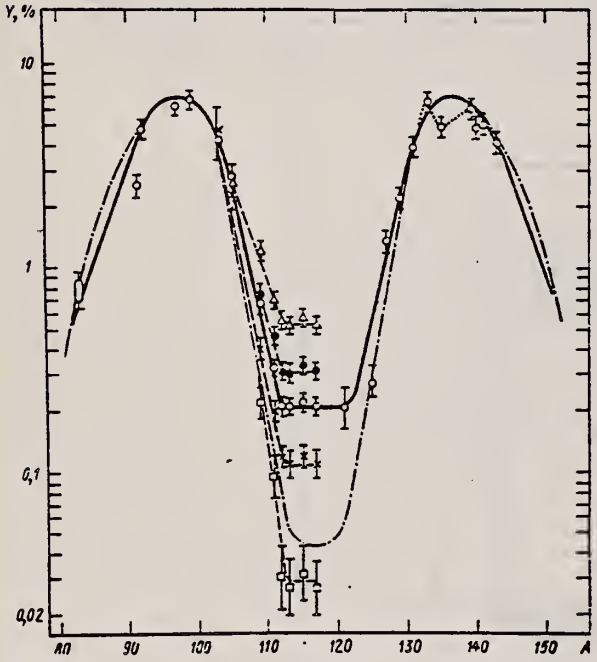

Fig. 1. Curves of the distribution of yields of fission fragments. Data of the present study for Np^{237} (γ, f): (– □ –) 10 MeV; (– × –) 12 MeV; (– ○ –) 14 MeV; (– ● –) 16 MeV; (– Δ –) 24 MeV; (– · – · –) data of (12) for Np^{237} (n, f).

[12] R. Stella et al., J. Inorg. Nucl. Chem., 31, 3739 (1969).

TABLE 1. Yields of Fragments for Photofission of Np^{237} (%)

Isotope	Maximum bremsstrahlung energy $E_{\gamma 0}$, MeV					
	24	20	16	14	12	10
Br^{87}	—	—	—	0,70±0,05 0,88±0,06	—	—
Sr^{91}	—	—	—	2,55±0,18	—	—
Sr^{92}	—	—	—	4,70±0,48	—	—
Zr^{97}	—	—	—	6,23±0,66	—	—
Mo^{99}	—	—	—	6,84±0,49	—	—
Ru^{103}	4,47±0,35	4,88±0,87	—	4,25±0,43	4,72±0,84	—
Ru^{105}	2,65±0,18	2,87±0,18	—	2,86±0,22	2,34±0,34	—
Pd^{109}	1,20±0,11	0,88±0,09	0,73±0,06	0,63±0,04	0,40±0,07	0,22±0,03
Ag^{111}	0,70±0,06	0,53±0,04	0,47±0,03	0,52±0,03	0,20±0,02	0,095±0,010
Pd^{112}	0,55±0,05	0,47±0,04	0,31±0,03	0,21±0,02	0,13±0,02	0,031±0,008
Ag^{113}	0,51±0,04	0,40±0,03	0,31±0,03	0,21±0,02	0,11±0,02	0,027±0,005
Cd^{115}	0,56±0,04	0,43±0,03	0,33±0,03	0,22±0,02	0,12±0,02	0,032±0,008
Cd^{117}	0,53±0,04	0,40±0,03	0,32±0,03	0,21±0,02	0,11±0,02	0,027±0,007
Sn^{121}	—	—	—	0,21±0,05	—	—
Sn^{125}	—	—	—	0,32±0,03	—	—
Sb^{127}	—	—	—	1,36±0,08	—	—
Sb^{129}	—	—	—	2,18±0,21	—	—
I^{131}	—	—	—	3,90±0,27	—	—
I^{133}	—	—	—	6,54±0,30	—	—
I^{135}	—	—	—	4,91±0,33	—	—
Ba^{139}	5,49±0,32	6,02±0,35	5,64±0,33	6,08±0,36	5,44±0,32	6,37±0,23
Ba^{140}	4,82±0,24	4,83±0,24	4,96±0,23	4,90±0,20	4,94±0,25	4,98±0,26
Ce^{141}	—	—	—	4,99±0,31	—	—
Ce^{143}	—	—	—	4,06±0,42	—	—

REF. A. Veyssiere, H. Beil, R. Bergere, P. Carlos, A. Lepretre and K. Kernbath
Nucl. Phys. A199, 45 (1973)

ELEM. SYM.	A	Z
Np	237	93

METHOD

REF. NO.	
73 Ve 1	egf

REACTION	RESULT	EXCITATION ENERGY	SOURCE		DETECTOR		ANGLE
			TYPE	RANGE	TYPE	RANGE	
G,N	ABX	9- 17	D	9- 17	MOD-I		4PI
G,2N	ABX	9- 17	D	9- 17	MOD-I		4PI
G,F	ABX	9- 17	D	9- 17	MOD-I		4PI

(γ,n) 499+
(γ,2n) 500+
(γ,f) 501+
(γ,tot) 502

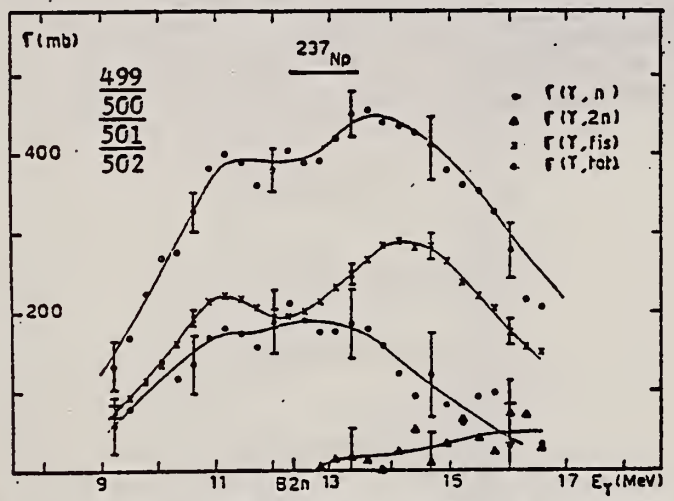

Fig. 7. Partial and total photonuclear cross sections $\sigma(\gamma, n)$, $\sigma(\gamma, 2n)$, $\sigma(\gamma, F)$ and $\sigma_{tot} = \sigma(\gamma, n) + \sigma(\gamma, 2n) + \sigma(\gamma, F)$ of $^{237}_{93}Np$.

TABLE 3

Lorentz line parameters and quadrupole moments for ^{232}Th, ^{238}U and ^{237}Np

	E_1 (MeV)	σ_1 (mb)	Γ_1 (MeV)	E_2 (MeV)	σ_2 (mb)	Γ_2 (MeV)	$R = \frac{\frac{1}{2}\pi\sigma_2\Gamma_2}{\frac{1}{2}\pi\sigma_1\Gamma_1}$	Q_0 [a]	Q_0 [b]
$^{232}_{90}Th$	11.08±0.12	268±7	3.37±0.22	14.07±0.14	349±9	4.62±0.16	1.8±0.15	10.2±1	9.66±0.1
$^{238}_{92}U$	10.96±0.09	301±6	2.90±0.14	14.04±0.13	369±6	4.53±0.13	1.9±0.1	11 ±1	11.3 ±0.1
$^{237}_{93}Np$	11.06±0.12	251±7	3.16±0.27	14.21±0.14	380±9	5.12±0.3	2.4±0.3	11.3±1	10.9 ±0.7

[a]) This experiment.
[b]) Ref. [21]).

[21] K.E.G. Löbner et al., Nucl. Data Tables 7, 5 (1970).

TABLE 4

Integrated cross sections of ^{232}Th, ^{238}U and ^{237}Np

	σ_0 [a]) (MeV · b)	σ_{-1} [a]) (mb)	σ_{-2} [a]) (mb · MeV^{-1})	$\sigma'_0 = \frac{1}{2}\pi(\sigma_1\Gamma_1 + \sigma_2\Gamma_2)$ [b]) (MeV · b)	0.06 NZ/A (MeV · b)	$\frac{\sigma_0}{0.006\ NZ/A}$	$\frac{\sigma'_0}{0.006\ NZ/A}$
$^{232}_{90}Th$	2.50±0.25	198±20	16±2	3.95±0.3	3.31	0.76±0.07	1.19±0.08
$^{238}_{92}U$	2.98±0.15	235±15	19±1.5	3.99±0.15	3.39	0.88±0.05	1.18±0.04
$^{237}_{93}Np$	2.60±0.35	204±30	16±3	4.30±0.4	3.39	0.77±0.12	1.27±0.1

[a]) Values obtained by integrating $\sigma(\gamma, \text{total})$ from 8 to 18 MeV for ^{238}U and from 9 to 16 MeV for ^{232}Th and ^{237}Np.
[b]) Surface under the two Lorentz lines.

REF. K.N. Ivanov and K.A. Petrzhak
At. Energ. 36, 404 (1974)
Sov. J. At. Energy 36, 515 (1974)

ELEM. SYM.	A	Z
Np	237	93

METHOD

REF. NO. 74 Iv 2 egf

REACTION	RESULT	EXCITATION ENERGY	SOURCE		DETECTOR		ANGLE
			TYPE	RANGE	TYPE	RANGE	
G,F	RLY	5- 12	C	5- 12	TRK-I		4PI

YIELD REL U-238

The curves for the relative photofission yield functions $Y_i(E_{\gamma m})/Y_{^{238}U}(E_{\gamma m})$ were obtained from experimental ratios by least-square analysis. This method of analysis smooths out observed structure but maxima are seen in the curves (with an accuracy of ±0.16 MeV) at the following values of maximum bremsstrahlung energy:

Nucleus	Position of Maximum, MeV
^{232}Th	5.3; 6.3; 6.6; 7.5; 10.8.
^{235}U	5.1; 6.6; 8.4.
^{237}Np	5.5; 6.0; 7.1; 8.35; 9.8.
^{239}Pu	6.5.

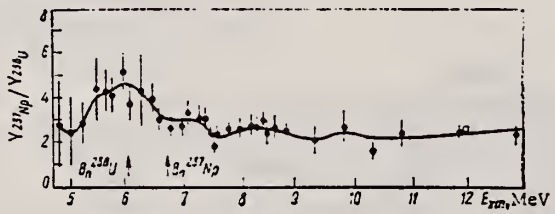

Fig. 3

Fig. 3. Relative photofissility of ^{237}Np: ●) present work; □) data from [5].

[5] J. Huizenga et al., Phys. Rev. 95, 1009 (1954).

REF. J.T. Caldwell and E.J. Dowdy
Nucl. Sci. & Eng. 56, 179 (1975)

ELEM. SYM.	A	Z
Np	237	93

METHOD

REF. NO. 75 Ca 5 egf

REACTION	RESULT	EXCITATION ENERGY	SOURCE		DETECTOR		ANGLE
			TYPE	RANGE	TYPE	RANGE	
G,F	NOX	6- 13	C	8- 13	MOD-I		4PI

NEUTRON MULTIPLICITIES

The prompt- and delayed-neutron multiplicities for photofission of the eight isotopes, ^{232}Th, ^{233}U, ^{234}U, ^{235}U, ^{236}U, ^{238}U, ^{237}Np, and ^{239}Pu, have been measured using bremsstrahlung with end-point energies ranging from 8 to 13 MeV. The measured multiplicities are compared with those from the same compound nucleus formed in neutron-induced fission where such data exist.

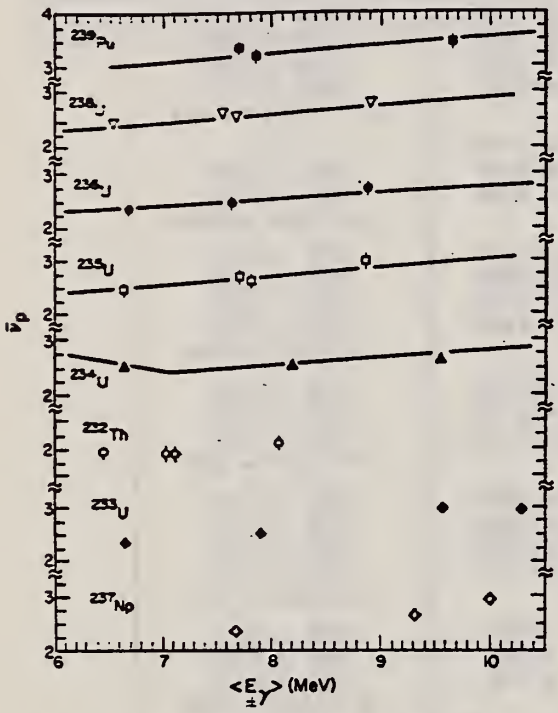

Fig. 5. $\bar{\nu}_p$ versus excitation energy for the eight isotopes studied in this experiment. The full curves shown are from the evaluations of Davey[2] with the excitation energy determined as described in the text. For the lower three isotopes shown, no previous experimental values for $\bar{\nu}_p$ exist.

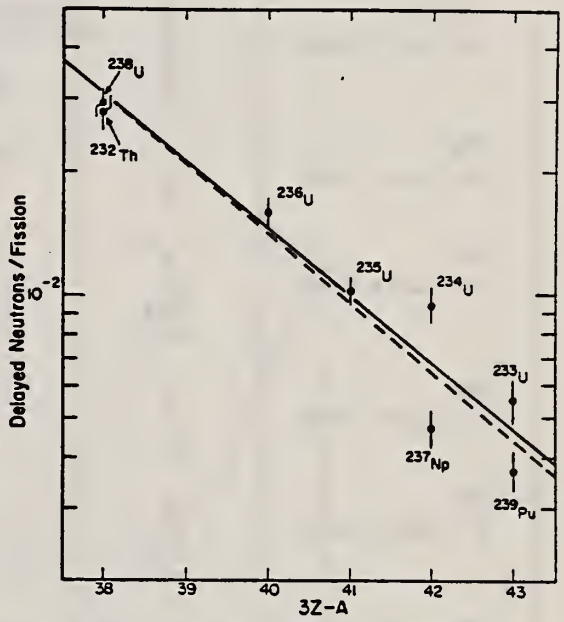

Fig. 6. Delayed neutrons per fission versus the parameter 3Z-A of the compound nucleus. The full curve shown is the least-squares fit to the data shown with $\ln Y_0 = 10.61$, $K = -0.372$. The dashed curve is the least-squares fit to the data provided by Tomlinson[6] with $\ln Y_0 = 11.35$, $K = -0.39$.

TABLE IV

Least-Squares Linear Fit Expressions for $\bar{\nu}_p(\langle E_\gamma \rangle)$

Isotope	$\bar{\nu}_p(\langle E_\gamma \rangle) = \bar{\nu}_0 + d\bar{\nu}_p/dE\,\langle E_\gamma \rangle$	Correlation Coefficient
^{232}Th	$\bar{\nu}_p(\langle E_\gamma \rangle) = 1.310 + 0.090\ \langle E_\gamma \rangle$	0.675
^{233}U	$\bar{\nu}_p(\langle E_\gamma \rangle) = 1.200 + 0.1709\ \langle E_\gamma \rangle$	0.947
^{234}U	$\bar{\nu}_p(\langle E_\gamma \rangle) = 2.222 + 0.0399\ \langle E_\gamma \rangle$	0.741
^{235}U	$\bar{\nu}_p(\langle E_\gamma \rangle) = 0.9034 + 0.2292\ \langle E_\gamma \rangle$	0.967
^{236}U	$\bar{\nu}_p(\langle E_\gamma \rangle) = 1.140 + 0.1788\ \langle E_\gamma \rangle$	0.986
^{238}U	$\bar{\nu}_p(\langle E_\gamma \rangle) = 1.502 + 0.1458\ \langle E_\gamma \rangle$	0.984
^{237}Np	$\bar{\nu}_p(\langle E_\gamma \rangle) = 0.4027 + 0.2505\ \langle E_\gamma \rangle$	0.967
^{239}Pu	$\bar{\nu}_p(\langle E_\gamma \rangle) = 2.526 + 0.0930\ \langle E_\gamma \rangle$	0.777

[2] W.G. Davey, Nucl. Sci. Eng., 44, 345 (1971)

[6] L. Tomlinson, "Delayed Neutrons from Fission: A Compilation and Evaluation of Experimental Data," AERE-R-6993, Atomic Energy Research Establishment, Harwell (1972)

over

TABLE III

Prompt- and Delayed-Neutron Yields

	E_e, MeV	$\langle E_\gamma \rangle$, MeV	$\bar{\nu}_p$	Delayed Neutrons per 100 Fissions
^{232}Th	8	6.44	1.96 ± 0.11	3.10 ± 0.28
(σ = 1.15 ± 0.05)	10	7.02	1.89 ± 0.11	3.06 ± 0.31
	10.2	7.10	1.89 ± 0.11	2.67 ± 0.21
	12	8.06	2.08 ± 0.11	2.59 ± 0.31
				av = 2.80 ± 0.28
^{233}U	8	6.68	2.350 ± 0.112	0.455 ± 0.040
(σ = 1.25 ± 0.05)	10	7.90	2.498 ± 0.108	0.518 ± 0.040
	12	9.55	2.960 ± 0.096	0.640 ± 0.044
	13	10.27	2.870 ± 0.099	0.598 ± 0.051
				av = 0.553 ± 0.044
^{234}U	8	(6.67)[a]	2.536 ± 0.112	---
(σ = 1.13 ± 0.05)	10	8.69	2.499 ± 0.107	0.92 ± 0.06
	12	9.54	2.623 ± 0.105	0.97 ± 0.12
				av = 0.94 ± 0.094
^{235}U	8	6.67	2.456 ± 0.086	0.90 ± 0.08
(σ = 1.20 ± 0.05)	10	7.70	2.697 ± 0.081	0.88 ± 0.08
	10.2	7.81	2.612 ± 0.079	1.13 ± 0.07
	12	8.86	2.963 ± 0.072	1.12 ± 0.08
				av = 1.02 ± 0.08
^{236}U	8	6.66	2.357 ± 0.111	1.43 ± 0.14
(σ = 1.20 ± 0.05)	10	7.63	2.470 ± 0.105	1.73 ± 0.12
	12	8.86	2.744 ± 0.095	1.64 ± 0.10
				av = 1.60 ± 0.13
^{238}U	8	6.53	2.457 ± 0.088	3.06 ± 0.24
(σ = 1.22 ± 0.05)	10	7.54	2.628 ± 0.083	2.76 ± 0.17
	10.2	7.66	2.585 ± 0.082	3.06 ± 0.14
	12	8.88	2.802 ± 0.078	2.75 ± 0.19
				av = 2.91 ± 0.20
^{237}Np	10	7.68	2.35 ± 0.11	0.38 ± 0.04
(σ = 1.20 ± 0.05)	12	9.31	2.65 ± 0.10	0.50 ± 0.04
	13	9.92	2.95 ± 0.10	0.54 ± 0.04
				av = 0.47 ± 0.04
^{239}Pu	10	7.69	3.32 ± 0.08	---
(σ = 1.18 ± 0.10)	10.2	7.84	3.17 ± 0.14	0.37 ± 0.04
	12	9.65	3.43 ± 0.10	0.37 ± 0.04
				av = 0.37 ± 0.04

[a]Estimated value.

REF. V.E. Zhuchko, A.V. Ignatyuk, Yu. B. Ostapenko, G.N. Smirenkin, A.S. Soldatov, Yu. M. Tsipenyuk
ZhETF Pis. Red. 22, 255 (1975)
JETP Lett. 22, 118 (1975)

EL EM. SYM.	A	Z
Np	237	93

METHOD

REF. NO. 75Zh 1 hmg

REACTION	RESULT	EXCITATION ENERGY	SOURCE		DETECTOR		ANGLE
			TYPE	RANGE	TYPE	RANGE	
G,F	NOX	THR- 6	C	3- 6	TRK-I		4PI
		(Thr-5.5)		(3.8-5.5)			

For the isotopes ^{232}Th, ^{237}Np, and ^{238}U, in the deep subbarrier region, we observed an abrupt decrease of the slope of the energy dependence of the photofission cross section, called the isomer shelf. An investigation of this phenomenon uncovers a number of new possibilities for the refinement of our concepts concerning the structure of the fission barrier of heavy nuclei.

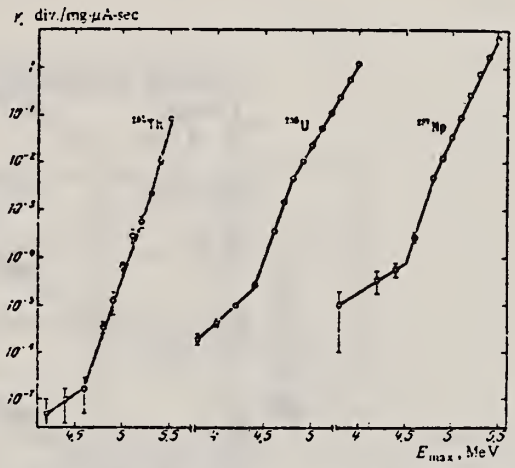

Energy dependence of the photofission yield of ^{232}Th, ^{238}U, and ^{237}Np.

REF. T. Bar-Noy and R. Moreh
Nucl. Phys. A275, 151 (1977)

ELEM. SYM.	A	Z
Np	237	93

METHOD

REF. NO. 77 Ba 7 egf

REACTION	RESULT	EXCITATION ENERGY	SOURCE		DETECTOR		ANGLE
			TYPE	RANGE	TYPE	RANGE	
G,G	ABX	8- 12	D	8- 12	SCD-D		DST

Abstract: Differential cross sections for elastic and inelastic Raman scattering from the deformed heavy nuclei ^{159}Tb, ^{165}Ho and ^{237}Np were measured at five energies between 8.5 and 11.4 MeV. Angular distributions at four angles between 90° and 140° for both elastic and inelastic scattering at 9.0 and 11.4 MeV were also measured. The monoenergetic photons were obtained from thermal neutron capture in Ni and Cr. All the angular distributions and the elastic and Raman scattering at the higher energies are in good overall agreement with theoretical predictions. The theory is based on a modified simple rotator model of the giant dipole resonance in which the effect of Delbrück scattering was included. A trend of both the elastic and Raman scattering at lower energies to be stronger than expected was suggested by the data. However, the ratio between the Raman and elastic scattering seem to be in good agreement with theory throughout the whole energy range. This shows that there is no need to introduce a direct nonresonant component to the imaginary part of the elastic scattering amplitude to explain the experimental data.

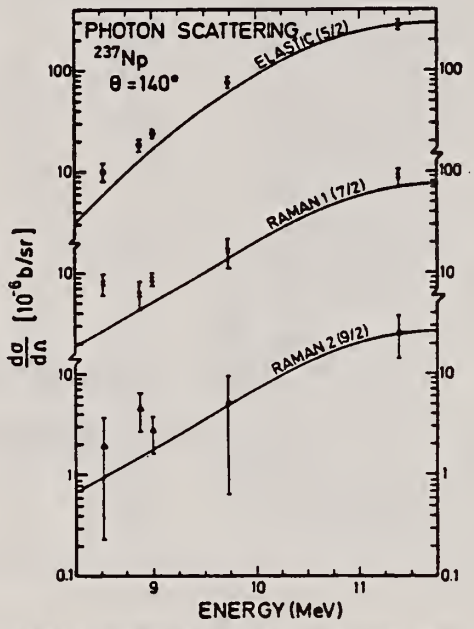

Fig. 3. Elastic and Raman inelastic differential scattering cross sections from ^{237}Np at 140°. The elastic curve is obtained by including the amplitudes of Thomson, Delbrück and nuclear resonance. The inelastic Raman curves represent the results of eq. (10).

over

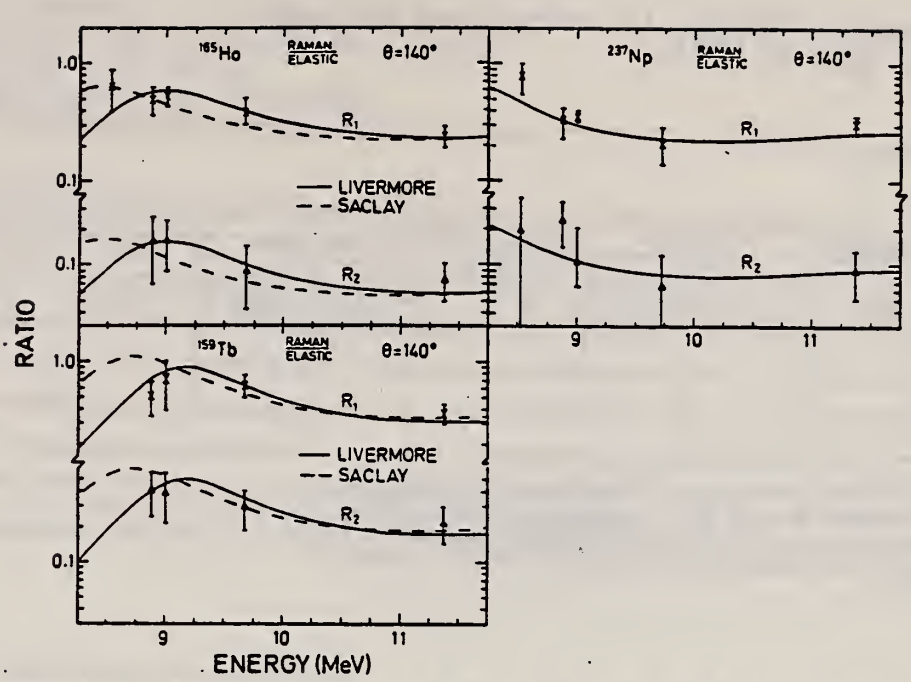

Fig. 6. Ratios of Raman/elastic scattering cross sections at 140° for ^{237}Np, ^{165}Ho and ^{159}Tb targets. Here, R_1 and R_2 refer to the first and second Raman lines. In the solid and dashed lines, the nuclear resonance amplitudes were obtained using parameters extracted from fits made to the Livermore and Saclay measurements respectively. (See text, table 3 and caption to fig. 3.)

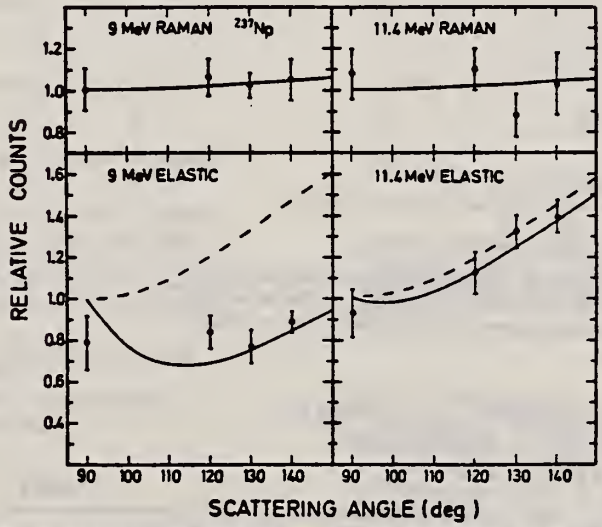

Fig. 7. Angular distributions of elastic and inelastic Raman scattered lines from ^{237}Np. The solid elastic curves include the amplitudes of Thomson, Delbrück and nuclear resonance; the dashed curves exclude the Delbrück contribution. The theoretical cross sections were all normalized to unity at $\theta = 90°$. The experimental points were normalized to fit the theoretical curves. The nuclear resonance amplitudes were obtained by using parameters extracted from the (γ, n) data of the Saclay group [23]). The Raman inelastic curve has the form $W(\theta) = 1 + \frac{1}{13}\cos^2\theta$.

REF. A.C. Shotter, D. Branford, J.C. McGeorge and J.M. Reid
Nucl. Phys. A290, 55 (1977)

ELEM. SYM.	A	Z
Np	237	93

METHOD

REF. NO. 77 Sh 9

REACTION	RESULT	EXCITATION ENERGY	SOURCE		DETECTOR		ANGLE
			TYPE	RANGE	TYPE	RANGE	
E,G	ABX	C-120	D	20-120	SCD-I		DST

Abstract: Measurements of the electrofission cross section for ^{232}Th, ^{238}U and ^{237}Np have been made for an electron energy range from 20 to 120 MeV. A comparison is made between the electrofission and photofission cross sections using the concept of virtual photons. It is deduced that the electrofission reaction for these elements proceeds through a significant E2 contribution as well as an E1 transition mode.

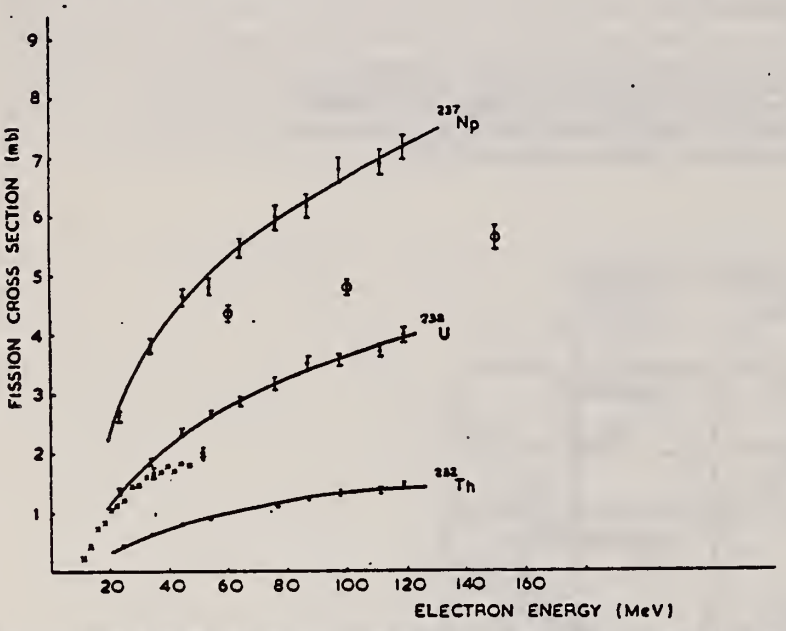

Fig. 1. Total electrofission cross sections versus electron energy. The solid circles are from the present work. Data on ^{238}U from ref. [1]) (open circles) and ref. [3]) (crosses) are also shown. The curves are the best fit to the data as described in the text. The errors shown for the present data are relative only.

[1] L.G. Morretto, R.C. Gatti, S.G. THompson, J.T. Routti, J.H. Heisenberg, L.M. Middleman, M.R. Yearian and R. Hofstadter, Phys. Rev. 179 (1969) 1176

[3] J.D.T. Arruda Neto, S.B. Herdade, B.S. Bhandari and I.C. Niscimento, Universidade de Sao Paulo, report no. IFUSP/P-76 (1976); J.C. Nascimento, S.B. Herdade and J.D.T. Arruda Neto, Proc. Int. Conf. on Photonuclear reactions and applications, Asilomar, 1973, ed. B.L. Berman (Lawrence Livermore Laboratory, Livermore, California) contributed paper, 5D10

USCOMM-NBS-DC

TABLE 1

Nucleus	Normalisation		$\int\sigma_{E2(\gamma n)}(E_\gamma)dE_\gamma$	
	9 MeV	22 MeV	9 MeV	22 MeV
^{232}Th	1.17	1.81	2.5 mb · MeV	12.8 mb · MeV
^{238}U	1.00	1.30	6.4 mb · MeV	38.8 mb · MeV
^{237}Np	1.12	1.34	7.9 mb · MeV	52.3 mb · MeV

From table 1 it is observed that the normalisation factors for E_g = 22 MeV are higher than would be expected from the absolute experimental errors (± 20 %). This may indicate a preferential concentration of E2 strength at 9 MeV.

REF.	ELEM. SYM.	A	Z
B.M. Aleksandrov, A.S. Krivokhatskii, V.L. Kuznetsov, L.E. Lazareva, V.G. Nedorezov, N.V. Nikitina, Yu.N. Ranyuk Yad. Fiz. 28, 1165 (1978) Sov. J. Nucl. Phys. 28, 600 (1978)	Np	237	93

METHOD	REF. NO.	
	78 A1 5	hg

REACTION	RESULT	EXCITATION ENERGY	SOURCE		DETECTOR		ANGLE
			TYPE	RANGE	TYPE	RANGE	
G,F	RLY	THR-999	C	100-999	TRK-D		4PI

The 300- and 2000-MeV electron linear accelerators have been used to measure the relative fissilities of the nuclei ^{235}U, ^{238}U, ^{237}Np, ^{239}Pu, ^{241}Am, and ^{243}Am. Fragments were detected by glass detectors. Photofission yields were obtained for the nuclei indicated at maximum bremsstrahlung energies 100, 240, 400, and 1200 MeV.

999=1.2 GEV

PACS numbers: 25.85.Jg

TABLE I. Relative photofission yields for $E_{\gamma max}$=100, 240, 400, and 1200 MeV.

Nucleus	Fissility of nuclei in the excitation-energy range ~ 5–12 MeV		Ratios of fragment yields $Y/Y(^{238}U)$ for different maximum energies $E_{\gamma max}$			
	$D_f = \Gamma_f/(\Gamma_f + \Gamma_n)$	Relative fissility	100 MeV	240 MeV	400 MeV	1200 MeV
^{235}U	0.33(b)	1.45(a) 1.58(b) 2.15(f)	2.22±0.16	2.15±0.15	1.79±0.13	1.74±0.12
^{238}U	0.22±0.01 *	1.00	1.00	1.00	1.00	1.00
^{237}Np	0.51(b) 0.53(d)	2.53(b) 2.16(e) 2.34(d) 2.93(f)	1.89±0.14	1.92±0.13	1.67±0.12	1.61±0.10
^{239}Pu	0.70(b)	2.70(a) 3.51(b) 3.51(c) 3.45(f)	2.10±0.15	2.10±0.15	1.50±0.13	1.63±0.12
^{241}Am	0.53(e)	1.68(e) ** 2.42(e) 3.27(f)	1.91±0.14	1.77±0.13	1.48±0.10	1.44±0.10
^{243}Am	0.62(e)	2.80(e) 2.59(f)	1.81±0.13	1.81±0.13	1.53±0.11	1.44±0.10

Note. *a*, *b*, *c*, *d*, and *e* denote that the data have been taken respectively from the photofission studies of Refs. 16, 17, 18, 19, and 15. *f* are the average values for the data of a given study on fission by neutrons[20] at nuclear excitation energy ~8 MeV.

*The number given is an average over the results of a large number of studies on photofission of ^{238}U.

**The authors of Ref. 18 point out that the value obtained by them for ^{241}Am is obviously underestimated.

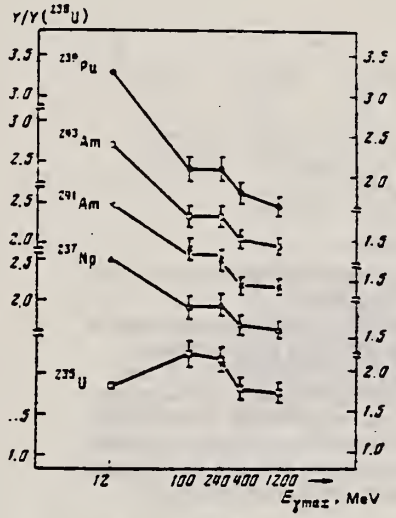

FIG. 2. Relative yields $Y/Y(^{238}U)$ for the nuclei ^{235}U (□), ^{237}Np (△), ^{239}Pu (●), ^{241}Am (×), and ^{243}Am (○) for maximum bremsstrahlung energies $E_{\gamma max}$ ~12, 100, 240, 400, and 1200 MeV.

[15]Yu. A. Vinogradov, V. I. Kasilov, L. E. Lazareva, V. G. Nedorezov, N. V. Nikitina, N. M. Parovik, Yu. N. Ranyuk, and P. V. Sorokin, Yad. Fiz. 24, 686 (1976) Sov. J. Nucl. Phys. 24, 357 (1976).
[16]J. McElhinney and W. E. Ogle, Phys. Rev. 81, 342 (1951).
[17]J. R. Huizenga, Phys. Rev. 109, 484 (1953).
[18]L. Katz, A. P. Baerg, and F. Brown, Proc. of the Second Intern. Conf. on the Peaceful Uses of Atomic Energy, Geneva, 1958, United Nations, Geneva, 1958, Vol. 15, p. 200.
[19]A. Veyssiere, H. Beil, R. Bergere, P. Carlos, A. Lepretre, and K. Kernbath, Nucl. Phys. A199, 45 (1973).

REF. V.E. Zhuchko, Yu.B. Ostapenko, G.N. Smirenkin, A.S. Soldatov, Yu.M. Tsipenyuk
Yad. Fiz. 28, 1185 (1978)
Sov. J. Nucl. Phys. 28, 611 (1978)

ELEM. SYM.	A	Z
Np	237	93

METHOD

REF. NO. 78 Zh 6 hg

REACTION	RESULT	EXCITATION ENERGY	SOURCE		DETECTOR		ANGLE
			TYPE	RANGE	TYPE	RANGE	
G,F	RLY	THR-5	C	3-5	TRK-D		4PI
		(THR-4.6)		(3.5-4.6)			

Yield measurements are reported for photofission of ^{232}Th, ^{236}U, ^{238}U, and ^{237}Np in the deep sub-barrier energy region 3.5–4.6 MeV where anomalies in the cross section—isomeric shelfs—were previously observed [Phys. Rev. C, 12, 863 (1975)]; Pis'ma. Zh. Eksp. Teor. Fiz. 22, 255 (1975), [JETP Lett. 22, 118 (1975)]. The various sources of background arising in this energy region, which is only with difficulty accessible for measurements, are analyzed in detail. Analysis of the anomalies in the behavior of the integrated photofission yields in the case of the two nuclei ^{236}U and ^{238}U most favorable for study indicates a resonance nature of the cross sections for delayed fission and a substantially more complicated physics of the phenomenon than the simplified interpretation of Bowman [Phys. Rev. C, 12, 863 (1975)].

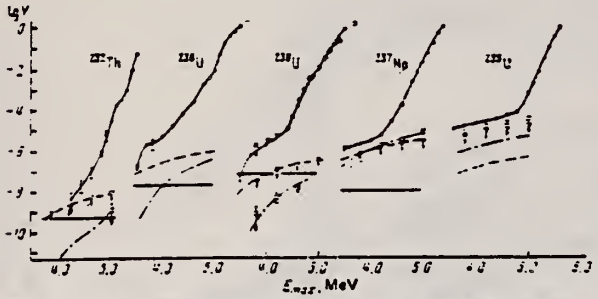

FIG. 2. The round points are the results of measurement of the yields $Y(E_{max})$ in fissions/mg-μC of the photofission reaction: ●—present work and Ref. 7; ○—Ref. 8. ⊤ and dashed lines—respectively the experimental and theoretical estimates of the background due to fissions by neutrons from the reaction Be(γ,n); ⊏ and dot-dash lines—the same for the D(γ,n) reaction. The shaded sections show the level of background from spontaneous fission and fission induced by cosmic rays.

REF. V.E. Zhuchko, Yu.B. Ostapenko, G.N. Smirenkin, A.S. Soldatov, Yu.M. Tsipenyuk
Yad. Fiz. 28, 1170 (1978)
Sov. J. Nucl. Phys. 28, 602 (1978)

ELEM. SYM.	A	Z
Np	237	93

METHOD

REF. NO. 78 Zh 7 hg

REACTION	RESULT	EXCITATION ENERGY	SOURCE		DETECTOR		ANGLE
			TYPE	RANGE	TYPE	RANGE	
G,F	ABX	THR-7	C	4-7	TRK-D		4PI
				(4.4-7.)			

The bremsstrahlung beam of the microtron at our Institute has been used to measure photofission yields of nine nuclei—^{232}Th, ^{233,235,236,238}U, ^{237}Np, ^{239,241}Pu, and ^{241}Am in the energy region 4.4–7.0 MeV. The method of minimization of the directed deviation was used to reproduce the photofission cross sections from the integrated yields. The following problems are discussed in terms of the experimental data: resonance structure of the cross sections, effects of a two-humped shape of the fission barrier, and comparison of the fissility in the (γ,f) and (n,f) reactions and in direct reactions.

PACS numbers: 25.85.Jg

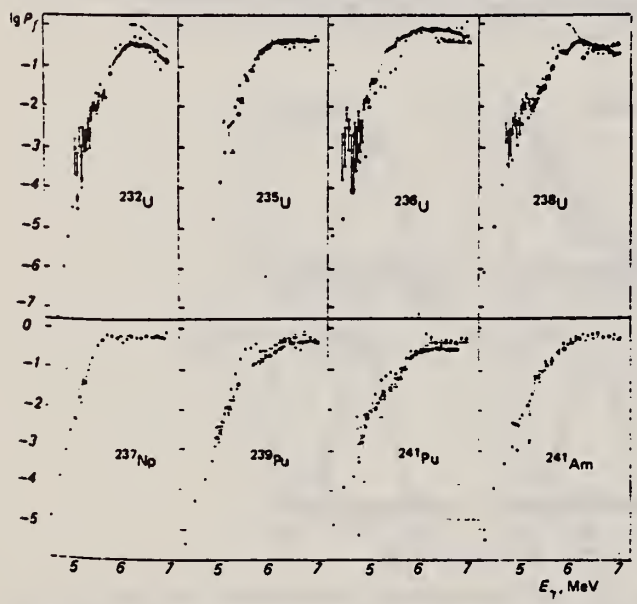

FIG. 4. Fissility P_f in the reactions (γ,f)—●, (n,f)—△ (Ref. 14), and in direct reactions—○.[2] The dashed curve shows the results of evaluation of P_f in accordance with Eq. (9).

(over)

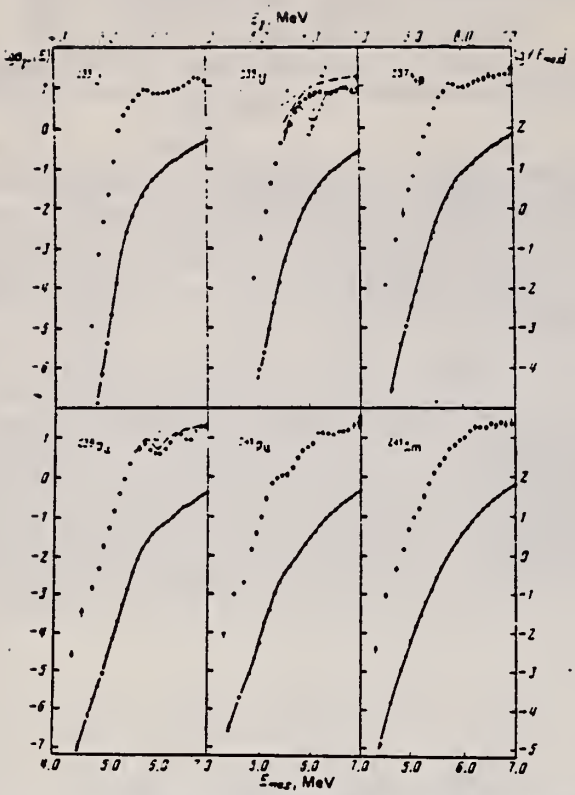

FIG. 3. Yields $Y(E_{max})$, fissions/mg-μC, and cross sections $\sigma_{\gamma f}(E_\gamma)$, mb, for odd isotopes. The designations are the same as in Fig. 2.

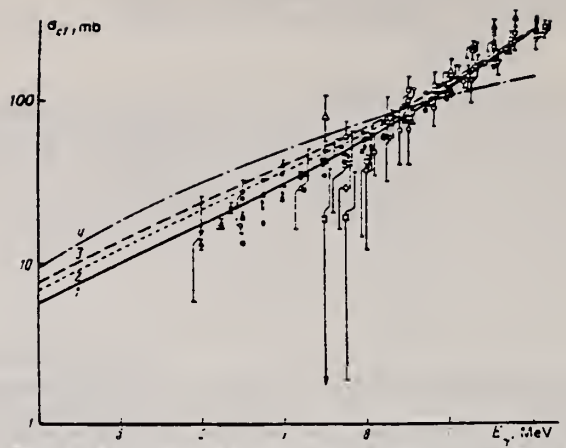

FIG. 6. Set of data on dipole photoabsorption cross sections σ_{c1}. The solid line (1)—the present work—is the result of fitting the data of Ref. 6 by Eq. (2) in the region $E_\gamma = 6$–10 MeV. Curves 2 and 3 are an extrapolation of the fit from Ref. 16 (2) and Ref. 17 (3) for ^{238}U; curve 4 is an estimate by means of Axel's formula.[15] Points: □, ■—^{232}Th: △, ▲—^{235}U; ◆—^{236}U; ○, ●—^{238}U; ▽, ▼—^{237}Np; ◇—^{239}Pu. The hollow points are from Refs. 16 and 17; the solid points are from Ref. 6.

REF. J. C. McGeorge, A. C. Shotter, D. Branford, J. M. Reid
Nucl. Phys. A326, 108 (1979)

ELEM. SYM.	A	Z
Np	237	93

METHOD

REF. NO. 79Mc2 hg

REACTION	RESULT	EXCITATION ENERGY	SOURCE		DETECTOR		ANGLE
			TYPE	RANGE	TYPE	RANGE	
E,F	NOX	THR-110	D	110	SCD-D	120-210	90

Abstract: Fission of ^{232}Th, ^{237}Np, ^{209}Bi, ^{235}U and ^{238}U induced by 110 MeV electrons has been studied by means of surface barrier detectors. The resulting mass and kinetic energy distributions are presented. Comparison with the liquid drop model predictions shows reasonable agreement in the case of ^{209}Bi. The data are analysed in terms of a two component model of fission and the mean total kinetic energies of the components are shown to depend linearly on $Z_1Z_2(A_1^{1/3}+A_2^{1/3})$. Interesting differences are found when the present results are compared with the recent photofission experiments of Areskoug *et al.* and features in both sets of data correlate with changes of fragment deformation implied by the calculations of Wilkins *et al.*

MASS AND EGY DISTRIB

E NUCLEAR REACTIONS ^{237}Np, ^{232}Th, ^{209}Bi, ^{238}U, ^{235}U(e, f), E = 110 MeV; measured fission fragment E, deduced mass.

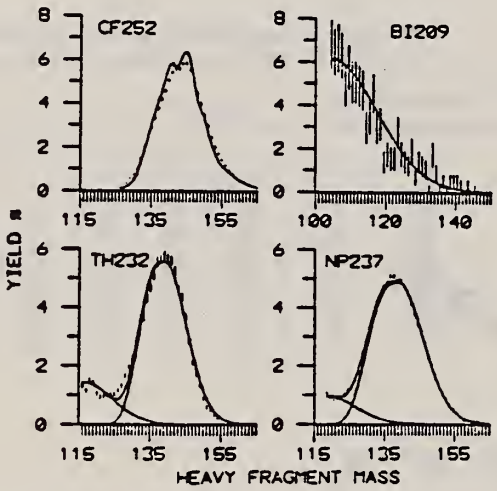

Fig. 1. The HFM yield distributions for electrofission of ^{209}Bi, ^{232}Th and ^{237}Np and spontaneous fission of ^{252}Cf. Statistical uncertainties are shown where larger than the size of the points in this and succeeding diagrams. The solid line in the ^{252}Cf case represents the experimental results of Schmidt *et al.* [12]). In the ^{209}Bi case the solid line represents a Gaussian fit to the data while the solid lines in the other two cases are the result of a two component analysis (see text).

TABLE 2

Target	Mean total KE (MeV)			Width
	present work	semi-empirical [ref. [14])]		present work
		a)	b)	
^{238}U	171.8±3.4	168.5	169.4	11.6±0.1
^{235}U	171.3±3.4	169.1	170.1	10.8±0.1
^{232}Th	167.0±3.3	163.4	163.5	9.6±0.1
^{237}Np	174.3±3.0	171.9	173.3	11.5±0.1
^{209}Bi	140 ±4	146.5	143.9	11.5±0.4

a) $0.1071Z^2/A^{1/3}+22.2$.
b) $0.1240Z^2/A^{1/3}$.

over

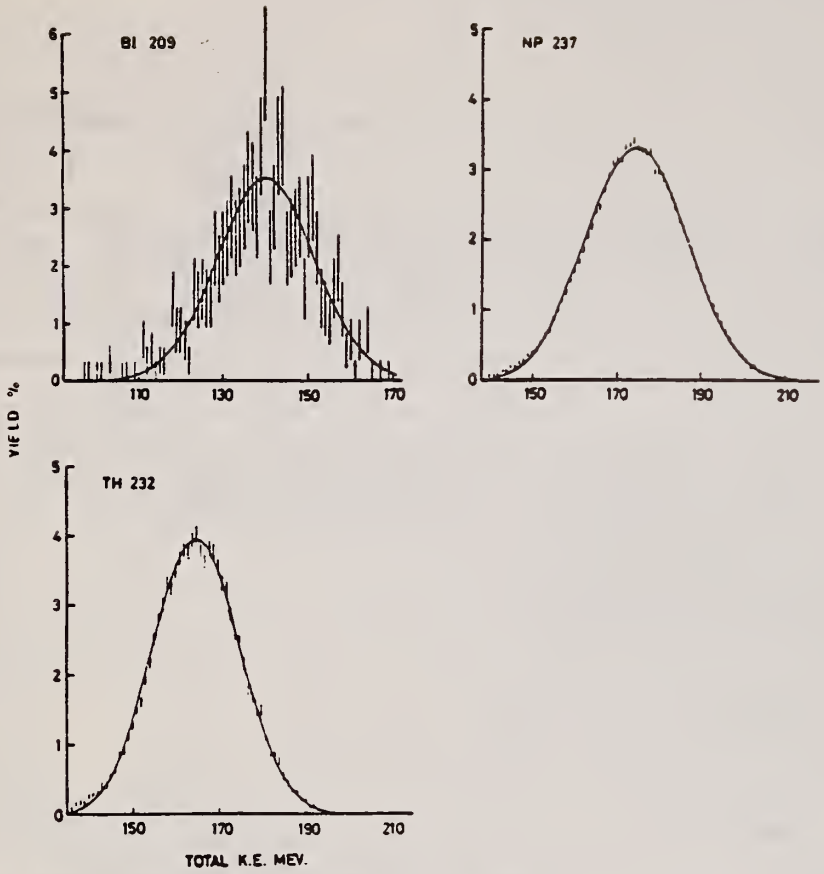

Fig. 2. Total fragment kinetic energy distributions in the electrofission of ^{209}Bi, ^{237}Np and ^{232}Th. The solid lines result from fitting a single Gaussian to the data in the ^{209}Bi case and a double Gaussian in the other cases.

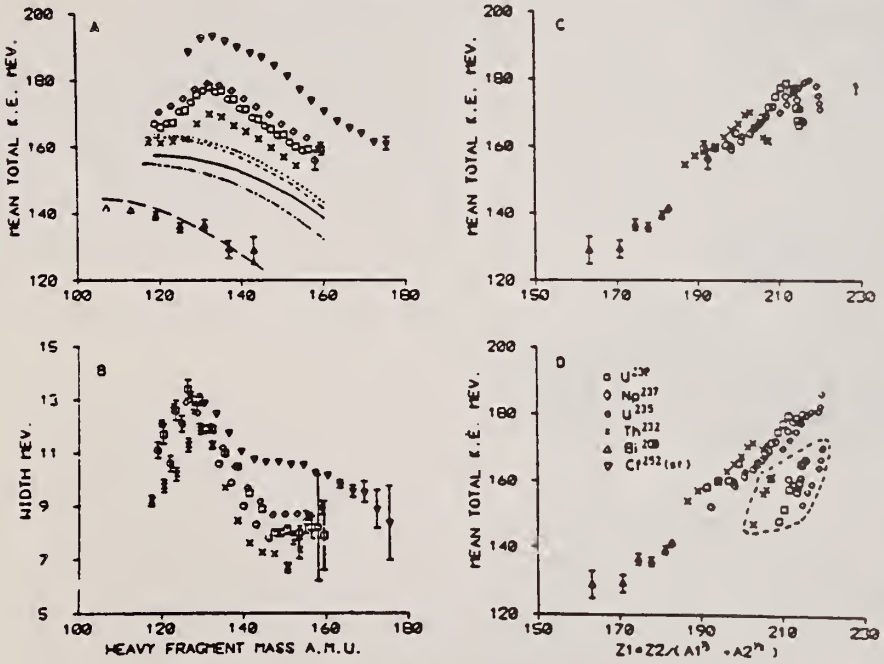

Fig. 3. Total fragment kinetic energy data from electrofission of ^{238}U, ^{235}U, ^{237}Np, ^{232}Th, ^{209}Bi and for spontaneous fission of ^{252}Cf. (A) Mean TKE versus HFM. The lines represent the LDM calculations of Nix and Swiatecki [13]) – solid ^{238}U, short dash ^{235}U, long dash ^{209}Bi, dot ^{237}Np and dot dash ^{232}Th. (B) Width of the TKE distribution versus heavy fragment mass. (C) Mean total fragment kinetic energy versus $Z_1Z_2/(A_1^{1/3}+A_2^{1/3})$. (D) Mean total fragment kinetic energy of the symmetric (enclosed by the dashed line) and asymmetric components versus $Z_1Z_2/(A_1^{1/3}+A_2^{1/3})$. In (A)(C) and (D) the relative uncertainties between targets are ±3 MeV and the absolute uncertainties are ±4 MeV.

REF. A.S. Voronin, I.S. Koretskaya, V.L. Kuznetsov, V.G. Nedorezov, N.V. Nikitina, V.I. Noga, S.A. Pashchuk, Yu.N. Ranyuk, S.M. Solov'ev
Yad. Fiz. 34, 1439 (1981)
Sov. J. Nucl. Phys. 34, 797 (1981)

ELEM. SYM.	A	Z
Np	237	93

METHOD

REF. NO. 81 Vo 3 egf

REACTION	RESULT	EXCITATION ENERGY	SOURCE		DETECTOR		ANGLE
			TYPE	RANGE	TYPE	RANGE	
E,F	ABX	4-275	D	97-275	TRK-I		45
G,F	RLY	4-275	D	184-275	TRK-I		45

RELATIVE BRMS/E YLD

Results are presented of cross-section measurements for the fission of ^{232}Th, ^{233}U, ^{235}U, ^{236}U, ^{238}U, ^{237}Np, and ^{239}Pu by electrons with energies between 100 and 275 MeV; photofission and electrofission cross-section ratios for the same nuclei are given as well.

PACS numbers: 25.85.Jg, 27.90. + b, 25.85.Ge

TABLE II. Electrofission cross sections (mb) for nuclei with $Z \geq 90$ measured for electron energies between 100 and 275 MeV.

E_e, MeV	Nucleus						
	^{232}Th	^{233}U	^{235}U	^{236}U	^{238}U	^{237}Np	^{239}Pu
97	1.24	8.12	5.66	4.55	3.23	6.22	7.26
134	1.47	9.17	6.08	4.74	3.42	6.63	7.98
149	1.42	9.75	6.17	5.50	3.89	7.16	8.39
166	1.63	10.36	7.01	5.29	4.15	7.70	9.18
184	1.78	9.61	7.13	5.64	4.17	7.92	8.92
201	1.54	9.84	6.53	6.10	4.56	7.49	9.31
217	1.78	10.91	7.73	6.14	4.77	7.09	9.56
240	1.91	10.25	7.26	5.92	4.49	7.84	9.43
253	1.85	9.89	7.09	6.17	4.78	7.30	9.78
275	2.22	10.50	8.15	6.66	5.26	9.68	10.50

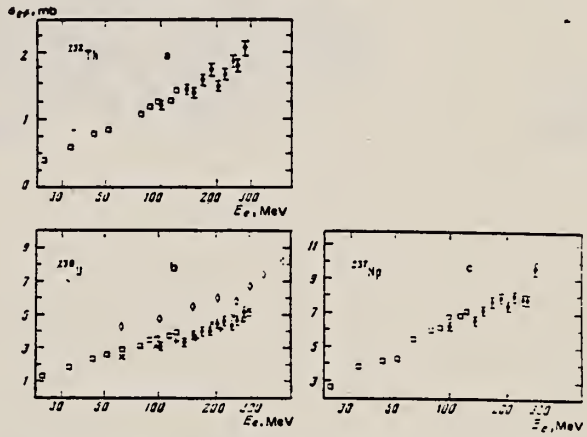

FIG. 2. Electrofission cross section for ^{232}Th (a), ^{238}U (b), and ^{237}Np (c). The points represent data as follows: □—Ref. 3, ♦—present work, ○—Ref. 1, ×—Ref. 2, and ·—Ref. 4.

TABLE IV. Cross sections (mb) for photo- and electrofission ($\sigma_{Qf}\Delta t + \sigma_{ef}$) obtained in measurements with aluminum radiators with a thickness of $0.023t_0$ for ^{235}U, ^{236}U, ^{238}U, and ^{237}Np and of $0.011t_0$ for ^{239}Pu.

E_e, MeV	Nucleus					E_e, MeV	Nucleus				
	^{235}U	^{236}U	^{238}U	^{237}Np	^{239}Pu		^{235}U	^{236}U	^{238}U	^{237}Np	^{239}Pu
184	13.33	10.48	7.57	13.40	11.65	240	14.02	10.57	8.43	11.82	13.23
201	14.10	11.50	8.82	12.70	12.46	253	14.17	10.98	8.11	11.94	12.90
217	14.36	10.76	8.67	12.94	12.98	275	15.22	12.00	9.29	12.92	13.63

TABLE V. Cross-section ratios for photo- and electrofission (σ_{Qf}/σ_{ef}) for energies between 184 and 275 MeV.

Nucleus	σ_{Qf}/σ_{ef}	Nucleus	σ_{Qf}/σ_{ef}
^{235}U	40±8	^{237}Np	24±5
^{236}U	35±7	^{239}Pu	30±6
^{238}U	35±7		
	Average	33±3	
	Theoretical	35.3	

PLUTONIUM
Z=94

When McMillan left Berkeley in 1940, he was convinced that another element was present in his neptunium fractions. Glenn Seaborg continued these studies and with N. C. Wahl and J. W. Kennedy separated from neptunium the new element identified as having an atomic number of 94. The discovery was reported to the journals early in 1941 but was not published until 1946. Seaborg's group isolated a new isotope in the spring of 1941. This was prepared by neutron bombardment of U^{238} and was the basis for the plutonium nuclear bomb. The Manhattan Project began concentrated work on the new element at Chicago. Analogous to neptunium, the element was named plutonium for Pluto, the planet next beyond Neptune in the solar system.

Pu
A=238

Pu
A=238

S. P. Kapitza, N. S. Rabotnov, G. N. Smirenkin, A. S. Soldatov
L. N. Usachev, Yu. M. Ysipenyuk
ZhETF Pis. Red. 9, 128 (1969); JETP Letters 9, 73 (1969)

ELEM. SYM.	A	Z
Pu	238	94

METHOD

REF. NO.	
69 Ka 1	hmg

REACTION	RESULT	EXCITATION ENERGY	SOURCE		DETECTOR		ANGLE
			TYPE	RANGE	TYPE	RANGE	
G,F	ABX	THR-8	C	5-8	TRK-I		DST

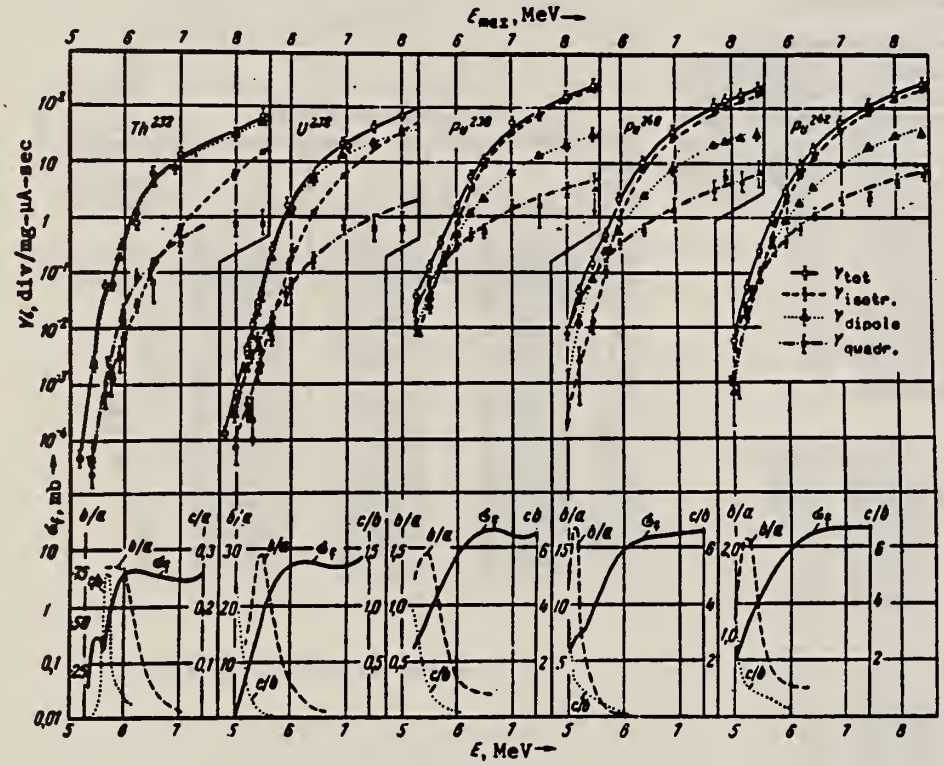

Fig. 2. Results of measurements of the fragment yields corresponding to different components of the angular distribution, as functions of the end-point energy of the bremsstrahlung spectrum (upper plots) and fission cross section and values of the ratios b/a and c/b as functions or the energy of the γ quanta, obtained as a result of the reduction of the experimental data (lower plots).

REF. N.S. Rabotnov, G.N. Smirenkin, A.S. Soldatov, L.N. Usachev, S.P. Kapitza, and Yu. M. Tsipenyuk
Yad. Fiz. 11, 508 (1970)
Sov. J. Nucl. Phys. 11, 285 (1970)

ELEM. SYM.	A	Z
Pu	238	94

METHOD

REF. NO.	
70 Ra 1	hmg

REACTION	RESULT	EXCITATION ENERGY	SOURCE		DETECTOR		ANGLE
			TYPE	RANGE	TYPE	RANGE	
G,F	ABX	THR-9	C	5-10	TRK-D		DST

SEE 68RA1, 69KA1

Table II. Parameters of angular distributions of the fragments

E_{max}, MeV	a	b	c	Y, fission / mg·μ·sec
		Th^{234}		
5.2	—	—	—	$4.5\cdot10^{-6}$
5.4	0.009±0.009	0.991±0.027	0.020±0.027	0.0024
5.65	0.011±0.005	0.989±0.007	−0.005±0.006	0.059
5.75	0.015±0.010	0.985±0.033	0.033±0.033	0.062
5.9	0.010±0.005	0.990±0.016	0.004±0.015	0.20
5.95	0.014±0.005	0.986±0.009	0.074±0.009	0.32
6.2	0.012±0.003	0.988±0.010	0.079±0.010	0.79
6.5	0.022±0.005	0.978±0.015	0.022±0.014	3.4
6.7	0.023±0.002	0.977±0.009	0.009±0.008	9.8
6.9	0.032±0.007	0.968±0.024	0.029±0.022	7.7
7.0	0.036±0.004	0.964±0.013	0.038±0.012	13.5
7.3	0.056±0.006	0.944±0.020	0.031±0.017	19.5
7.7	0.088±0.005	0.912±0.015	0.024±0.013	40.5
8.0	0.109±0.006	0.891±0.014	0.026±0.012	55
8.5	0.164±0.004	0.836±0.008	0.017±0.006	71
10.0	0.304±0.009	0.696±0.014	−0.031±0.014	—
		U^{238}		
5.0	0.052±0.100	0.948±0.164	1.296±0.205	0.00671
5.2	0.100±0.035	0.900±0.061	0.910±0.080	0.0062
5.3	0.020±0.035	0.980±0.065	0.566±0.076	0.0120
5.4	0.007±0.024	0.993±0.059	0.512±0.066	0.0.0
5.45	0.038±0.009	0.962±0.017	0.155±0.021	0.014
5.65	0.034±0.005	0.966±0.011	0.040±0.010	0 27
5.95	0.078±0.005	0.922±0.014	0.039±0.014	1.7
6.5	0.127±0.004	0.873±0.009	0.034±0.008	6.0
6.95	0.213±0.004	0.787±0.008	0.037±0.008	25.0
7.5	0..61±0.006	0.636±0.010	0.024±0.011	47.0
8.0	0.501±0.005	0.599±0.006	0.014±0.007	74.0
9.25	0.570±0.006	0.430±0.007	0.013±0.007	—
		Pu^{239}		
5.25	0.408±0.103	0.592±0.139	1.112±0.139	0.011
5.5	0.330±0.065	0.670±0.095	1.513±0.112	0.15
5.75	0.414±0.047	0.586±0.066	0.654±0.065	0.37
6.0	0.526±0.011	0.474±0.016	0.370±0.018	1.7
6.25	0.666±0.008	0.334±0.011	0.180±0.013	5.9
6.5	0.733±0.012	0.267±0.016	0.090±0.018	11
7.0	0.772±0.011	0.228±0.016	0.068±0.017	56
7.5	0.785±0.012	0.215±0.017	0.012±0.019	80
8.0	0.813±0.013	0.187±0.017	0.029±0.018	164
8.5	0.828±0.015	0.172±0.020	0.021±0.022	270
		Pu^{240}		
5.0*	0.000±0.200	0.000±0.200	1±0.200	0.0041
5.2	0.115±0.097	0.885±0.111	2.58±0.15	0.047

*In this case W(ϑ) is described by a pure quadrupole distribution, ~$\sin^2 2\vartheta$, and therefore the coefficient c is meaningless in the employed normalization and is assumed equal to unity.

Table II (cont.)

E_{max}, MeV	a	b	c	Y, Y, fission / mg·μ·sec
		Pu^{242}		
5.45	0.102±0.014	0.898±0.056	1.147±0.070	0.15
5.7	0.222±0.034	0.778±0.052	0.710±0.052	0.49
5.95	0.533±0.010	0.467±0.011	0.331±0.013	2.3
6.4	0.670±0.012	0.330±0.012	0.096±0.013	11.5
6.95	0.689±0.025	0.311±0.027	0.087±0.029	40
7.7	0.716±0.012	0.284±0.016	0.055±0.017	115
7.9	0.725±0.012	0.275±0.016	0.074±0.018	145
8.2	0.762±0.010	0.238±0.014	0.056±0.015	189
8.5	0.779±0.020	0.221±0.027	0.057±0.029	230
8.7	0.791±0.009	0.209±0.012	0.042±0.014	230
9.5	0.822±0.011	0.178±0.014	0.019±0.016	690
5.0	0.542±0.304	0.458±0.372	3.702±0.424	0.0055
5.25	0.448±0.053	0.552±0.068	0.965±0.082	0.056
5.45	0.418±0.046	0.582±0.059	1.018±0.069	—
5.5	0.310±0.022	0.690±0.029	0.734±0.033	0.26
5.75	0.488±0.008	0.512±0.010	0.422±0.012	1.0
6.0	0.598±0.011	0.402±0.016	0.207±0.018	2.7
6.25	0.669±0.012	0.331±0.017	0.138±0.019	8.8
6.5	0.700±0.009	0.300±0.013	0.122±0.014	17
7.0	0.750±0.005	0.250±0.007	0.075±0.008	50
7.5	0.754±0.005	0.246±0.007	0.046±0.004	105
8.0	0.766±0.006	0.234±0.008	0.057±0.009	175
8.5	0.814±0.005	0.186±0.007	0.012±0.008	225

$$W(\theta) = a + b \sin^2\theta + c \sin^2 2\theta$$

[over]

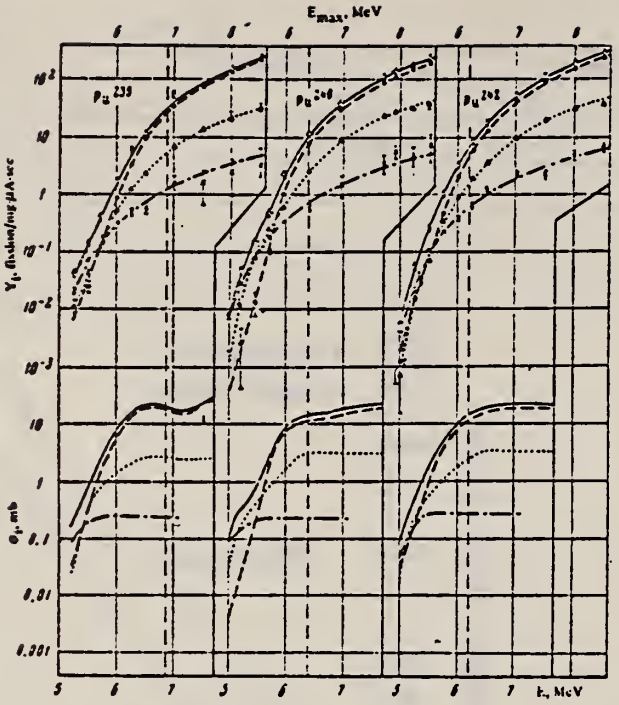

Angular components of the yield. Knowledge of the coefficients a, b, and c makes it possible to determine the contribution of the individual components of the yield Y_a, Y_b, and Y_c, the angular dependence of which corresponds to three components in the expression (2): isotropic, dipole, and quadrupole. Their meaning can be understood from the following definitions:

$$Y = Y_a + Y_b + Y_c; \quad \frac{dY}{d\Omega} = \frac{1}{4\pi\nu} Y W(\theta);$$

$$Y_a = \frac{a}{\nu} Y; \quad Y_b = \frac{2}{3}\frac{b}{\nu} Y; \quad Y_c = \frac{8}{15}\frac{c}{\nu} Y. \qquad (4)$$

Plots of Y_i and E_{max} are shown in Fig. 3 together with the data on the total yield. The experimental points $Y_i(E_{max})$ were determined by means of formulas (4) from the coefficients $W(\vartheta)$ listed in Table II and from the total yield. The error of Y_i indicated in Fig. 3 does not include the error in the measurement of $Y(E_{max})$ (~10%).

REF.

A. Shapiro and W. F. Stubbins
Nucl. Sci. & Engr. 45, 47 (1971)

ELEM. SYM.	A	Z
Pu	238	94

METHOD

REF. NO. 71 Sh 4 egf

REACTION	RESULT	EXCITATION ENERGY	SOURCE		DETECTOR		ANGLE
			TYPE	RANGE	TYPE	RANGE	
G,F	ABX	7-11	C	4-12,	SPK-I		2PI

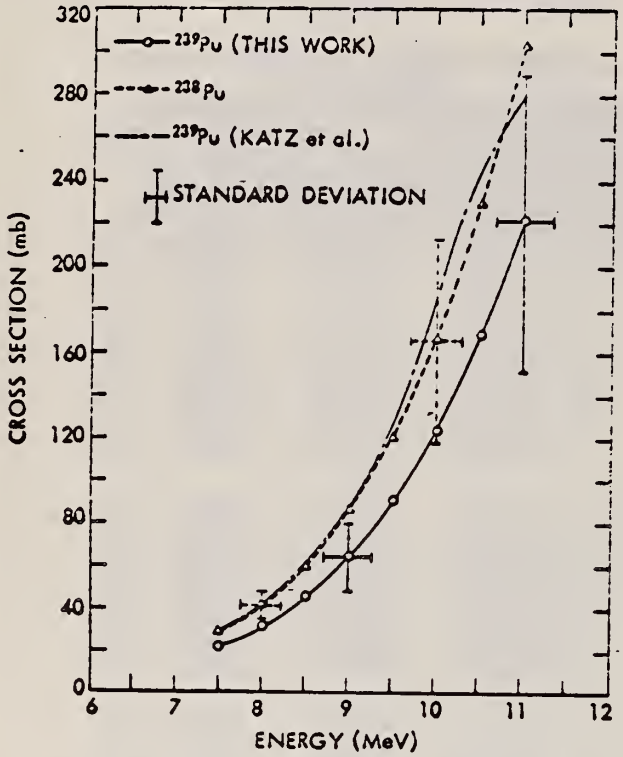

Fig. 3. Photofission cross section of ^{238}Pu and ^{239}Pu deduced from the Penfold-Leiss analysis. The dash-dot curve for ^{239}Pu is taken from Ref. 6.

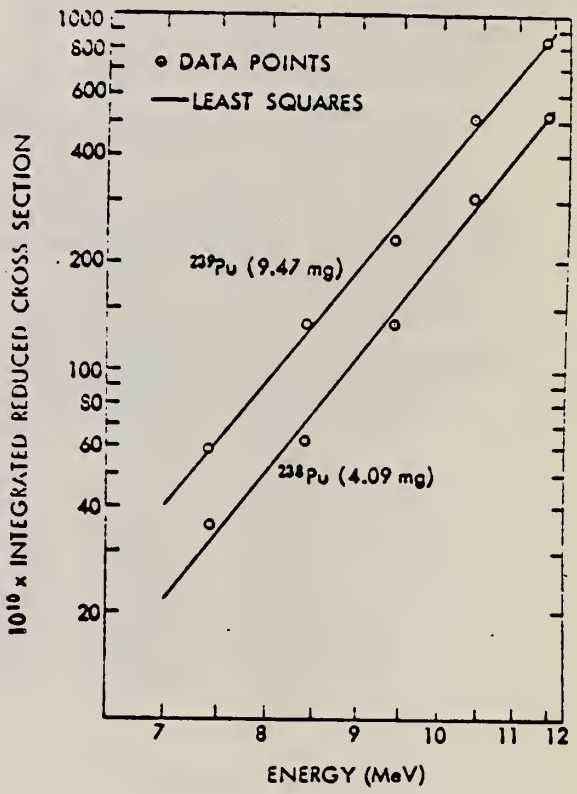

Fig. 2. Integrated reduced cross section vs energy. [The reduced cross section has a dimension of (energy)$^{-1}$, so the reduced cross section integrated with respect to energy is unitless.]

6 L. Katz, A. P. Baerg, and F. Brown, Proc. U.N. Intern. Conf. Peaceful Uses At. Energy, 2nd, Geneva, 1958, 15, 188 (1958).

TABLE I

Photofission Cross Sections Deduced by Penfold-Leiss Analysis

(Indicated errors are standard deviations)

Energy (MeV)	Cross Section (mb)	
	^{238}Pu	^{239}Pu
7.5	28 ± 5	21 ± 4
8.0	41 ± 8	31 ± 6
8.5	59 ± 13	45 ± 10
9.0	85 ± 21	64 ± 16
9.5	120 ± 32	90 ± 24
10.0	166 ± 47	123 ± 35
10.5	229 ± 68	168 ± 50
11.0	303 ± 94	221 ± 69

Pu
A=239

Pu
A=239

REF.

L. Katz, K. G. McNeill, M. LeBlanc and F. Brown
Can. J. Phys. 35, 470 (1957)

ELEM. SYM.	A	Z
Pu	239	94

METHOD

REF. NO.	
57 Ka 1	JOC

REACTION	RESULT	EXCITATION ENERGY	SOURCE		DETECTOR		ANGLE
			TYPE	RANGE	TYPE	RANGE	
G,XN	ABX	6 - 23	C	6 - 23	BF3-I		4PI

Fig. 4. (γ,N) yield and cross section curves for Pu^{239}.

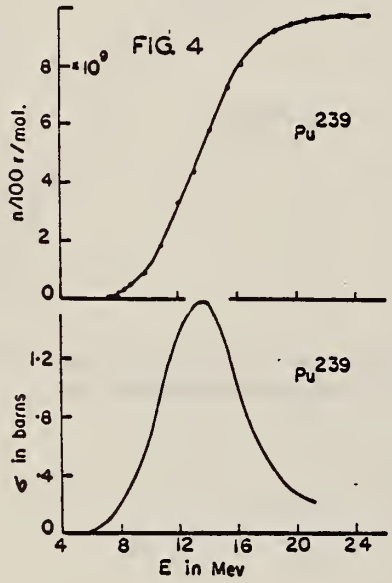

REF.
L. Katz, A. P. Baerg, and F. Brown
Peaceful Uses of Atomic Energy, Switzerland 1958

ELEM. SYM.	A	Z
Pu	239	94

METHOD
Fission chamber

[Page 1 of 2]

REF. NO.
58 Ka 2

EGF

REACTION	RESULT	EXCITATION ENERGY	SOURCE		DETECTOR		ANGLE
			TYPE	RANGE	TYPE	RANGE	
G,F	ABX	5-18	C	5-18	.ION-I		DST

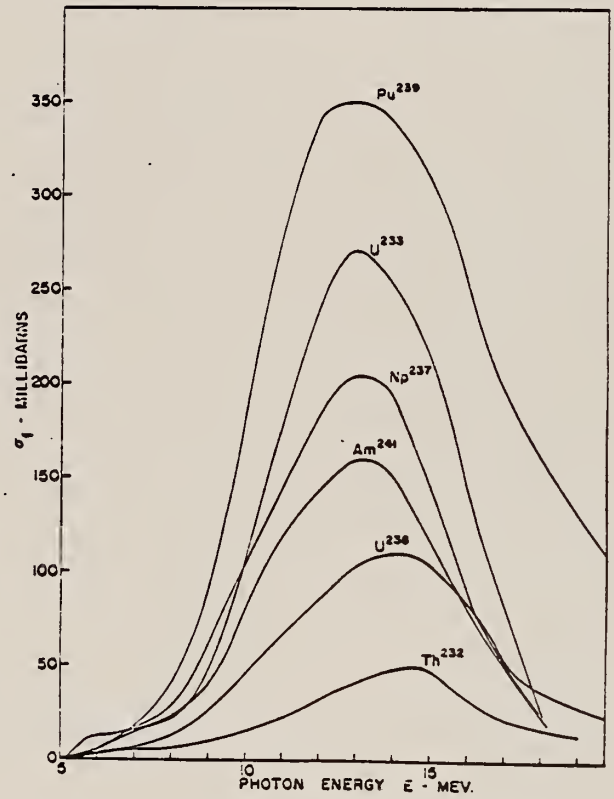

Fig. 5 - Photofission cross sections versus photon energy

REACTION	RESULT	EXCITATION ENERGY	SOURCE		DETECTOR		ANGLE
			TYPE	RANGE	TYPE	RANGE	

Fig. 7 - Low-energy-yield curves: fissions per roentgen-nucleus versus maximum bremsstrahlung energy. (The solid and dotted lines are samples of smoothed yield curves which fit the experimental data.)

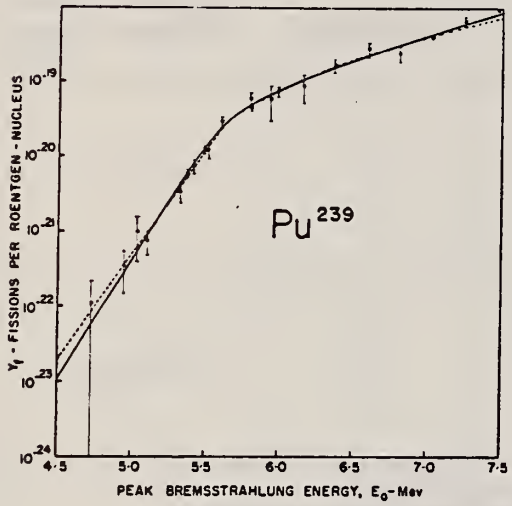

Table 4

Angular Distributions

Nuclide	Ratio, (Counts at 90°)/(Counts at 0°)[a] E_0 = 8.0 Mev[b]	E_0 = 10.0 Mev	E_0 = 20.0 Mev
U-233	1.048 ± 0.07	1.032 ± 0.04	0.994 ± 0.03
U-235	1.024 ± 0.05		
Np-237	1.024 ± 0.10		
Pu-239	1.002 ± 0.06	1.013 ± 0.05	0.952 ± 0.03
Am-241	0.958 ± 0.07		

(a) The ratio is the number of counts observed at 90° per unit X-ray dose divided by the number observed at 0° for the same dose.

(b) E_0 is the maximum energy of the bremsstrahlung spectrum.

REF.

A. P. Baerg, R. M. Bartholomew, F. Brown, L. Katz, and S. B. Kowalski
Can. J. Phys. 37, 1418 (1959) (A.E.C.L. No. 896)

ELEM. SYM.	A	Z
Pu	239	94

METHOD

Betatron with ionization chamber detector, enriched samples.

REF. NO. 59 Ba 4 EGF

REACTION	RESULT	EXCITATION ENERGY	SOURCE		DETECTOR		ANGLE
			TYPE	RANGE	TYPE	RANGE	
G,F	RLY	THR - 20	C	6-20	ION-I		DST

TABLE I

Angular distributions
Ratio, counts at 90°/counts at 0°*

Nuclide	E_0† = 6.0	E_0 = 6.5	E_0 = 8.0	E_0 = 10.0	E_0 = 20.0
U-233			1.048±0.07	1.032±0.04	0.994±0.03
U-235			1.024±0.05		
Np-237			1.024±0.10		
Pu-239‡	1.034±0.26	0.927±0.12	1.002±0.06	1.013±0.05	0.952±0.03
Am-241			0.958±0.07		

*The ratio is the number of counts observed at 90° per unit X-ray dose divided by the number observed at 0° for the same dose.
†E_0 is the maximum energy in million electron volts of the bremsstrahlung spectrum.
‡The 45°/0° ratio at E_0 = 6.5 Mev was 1.09±0.23.

TABLE IV

Relative fissionabilities, U-238 = 100 at 20 Mev

E_0	U-234	U-235	U-236	U-238	Pu-239	Pu-240
6.0		0.45±0.05	0.303±0.013	0.387±0.040		
6.5	1.165±0.033	1.134±0.025	1.159±0.026	1.08±0.07	0.239±0.024	1.145±0.051
7.0	2.515±0.053	2.282±0.038	2.358±0.037	2.14±0.14	4.50±0.22	2.528±0.075
8.0	6.285±0.085	5.519±0.067	5.285±0.056	4.87±0.24	11.35±0.34	6.09±0.12
9.0		11.00±0.33	8.94±0.13	8.65±0.26		
10.0	17.30±0.53	18.75±0.30	14.29±0.20	14.41±0.28	45.1±2.2	
14.0		88.0±4.5	43.11±0.53	57.7±1.4		
15.0	84.3±1.9	119.0±0.9	73.58±0.78	70.5±1.8	255.0±7.6	82.3±1.8
20.0	127.5±2.5	180.8±2.2	109.1±1.0	100±2.5	352±10	120.8±2.3

REF. O. P. Nikotin and K. A. Petrzhak
Atomnaya Energiya 20, 268 (1966)
UDC 539.173.84, p. 300

ELEM. SYM.	A	Z
Pu	239	94

METHOD

REF. NO.: 66 Ni 1 egf

REACTION	RESULT	EXCITATION ENERGY	SOURCE		DETECTOR		ANGLE
			TYPE	RANGE	TYPE	RANGE	
G,F	RLY	THR-15	C	10-15	TRK-D	0-1	4PI
						(.1-1.0)	

Delayed Neutrons from Photofission ($E_{\gamma\,max}$ = 15 MeV)

DELAYED N YIELDS

Total yield of delayed neutrons, neutrons/100 fissions	Neutron group	$T_{1/2}$, sec	Relative yield of group, %	Absolute yield of group, neutrons per 100 fissions
3,8±0,6 (Th^{232})	1	55,6±1,5	4,40±0,20	0,17±0,03
	2	20,3±0,8	16,3±1,0	0,62±0,10
	3	5,45±0,50	15,9±1,5	0,60±0,10
	4	1,98±0,20	37,5±3,0	1,43±0,30
	5	0,43±0,10	17,2±2,0	0,66±0,10
	6	0,18±0,03	$8,7^{+2,0}_{-4,0}$	$0,33^{+0,10}_{-0,20}$
0,96±0,13 (U^{235})	1	54,7±2,5	5,4±0,5	0,052±0,010
	2	20,3±1,0	20,0±2,0	0,193±0,040
	3	5,45±0,60	15,2±2,0	0,146±0,030
	4	2,01±0,25	36,9±4,0	0,354±0,070
	5	0,50±0,10	13,9±2,0	0,134±0,030
	6	0,19±0,04	$8,6^{+2,0}_{-5,0}$	$0,083^{+0,025}_{-0,050}$
3,1±0,4 (U^{238})	1	56,2±0,8	1,98±0,08	0,061±0,010
	2	21,3±0,3	15,7±0,5	0,489±0,070
	3	5,50±0,20	17,5±0,7	0,545±0,070
	4	2,15±0,10	31,1±0,8	0,970±0,150
	5	0,70±0,06	17,7±0,9	0,552±0,080
	6	0,19±0,02	$16,1^{+2,0}_{-5,0}$	$0,502^{+0,120}_{-0,200}$
0,36±0,06 (Pu^{239})	1	54,0±3,0	6,05±0,60	0,022±0,004
	2	20,6±1,0	20,6±2,0	0,075±0,018
	3	5,7±0,7	18,3±3,0	0,066±0,015
	4	1,94±0,30	29,5±4,0	0,105±0,020
	5	0,58±0,10	14,9±3,0	0,054±0,012
	6	0,20±0,04	$10,6^{+2,0}_{-5,0}$	$0,038^{+0,012}_{-0,025}$

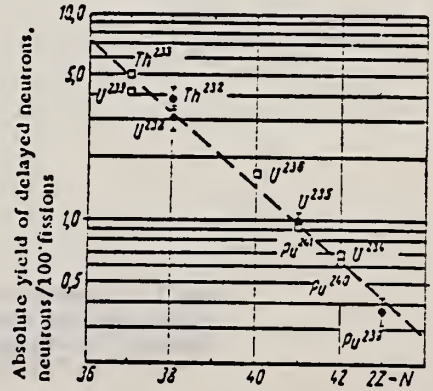

Fig. 3. Absolute yields of delayed neutrons from fission of nuclei: □) [7]; ●) present authors.

REF.

N.S. Rabotnov, G.N. Smirenkin, A.S. Soldatov, L.N. Usachov, S.P. Kapitza and Yu. M. Tsipenyuk
Nuclear Phys. 77, 92 (1966)

ELEM. SYM.	A	Z
Pu	239	94

METHOD: Microtron

REF. NO.: 66 Ra 2 JDM

REACTION	RESULT	EXCITATION ENERGY	SOURCE TYPE	SOURCE RANGE	DETECTOR TYPE	DETECTOR RANGE	ANGLE
G,F	NOX	5-7	C	5-8			DST

$W(\theta) = a + b \sin^2\theta$

TABLE 1

Angular anisotropy of ^{239}Pu photofission b/a as a function of E_{max} and E^*

E_{max} (MeV)	b/a	E^* (MeV)
5.4	0.103 ± 0.028	5.15
5.65	-0.192 ± 0.010	5.38
5.9	-0.161 ± 0.012	5.52
6.4	-0.016 ± 0.025	5.70
6.9	-0.011 ± 0.015	a)
7.9	0.016 ± 0.008	a)

a) For $E_{max} = 6.9$ and 7.9 MeV the values of the mean excitation energies which are not required for the subsequent analysis were not calculated.

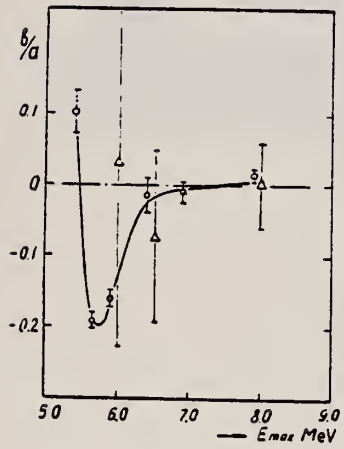

Fig. 1. Dependence of the angular anisotropy of ^{239}Pu photofission on the bremsstrahlung spectrum boundary energy E_{max}. △-results of ref. [5]), ○-results of the present measurements.

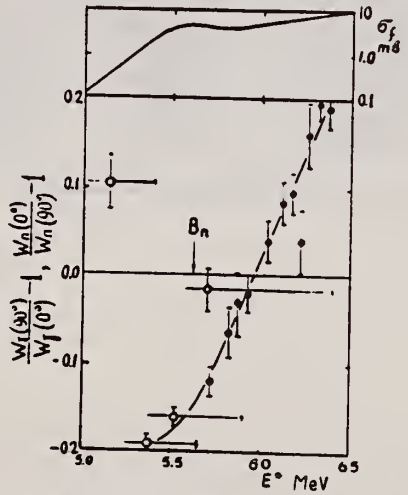

Fig. 2. Comparison of the angular anisotropy of the fragments from the ^{239}Pu$(\gamma, f)[W_\gamma(90°)/W_\gamma(0°)-1]$(○) and ^{239}Pu$(n, f)[W_n(0°)/W_n(90°)-1]$ (●) reactions. The data are represented as a function of the excitation energy of the ^{239}Pu compound nucleus E^* (see text). The energy dependence of the ^{239}Pu photofission cross section [4]) is presented in the upper part of the figure.

REF. N. S. Rabotnov, G. N. Smirenkin, A. S. Soldatov, L. N. Ysachev, S. P. Kapitza and Yu. M. Tsipeniuk
Phys. Letters 26B, 218 (1968)

ELEM. SYM.	A	Z
Pu	239	94

METHOD

REF. NO.	
68 Ra 1	EGF

REACTION	RESULT	EXCITATION ENERGY	SOURCE		DETECTOR		ANGLE
			TYPE	RANGE	TYPE	RANGE	
G,F	NOX	THR-8	C	5-8	FRG-I		DST

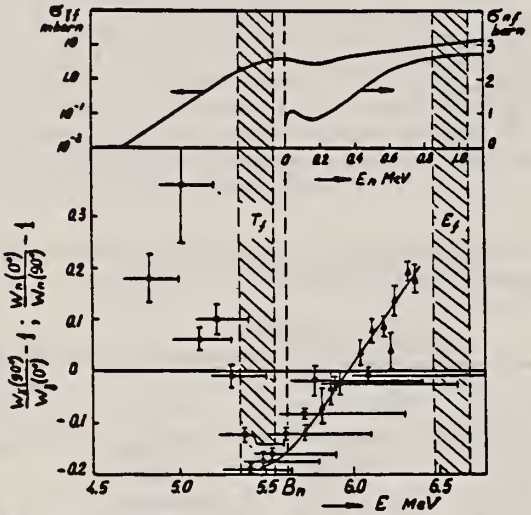

Fig. 2. Energy dependence of the anisotropy for the ^{239}Pu photofission and the ^{238}Pu(n,f) reaction. The neutron data are taken from ref. 4. In the upper part of the figure the energy dependence of the cross sections as measured in refs. 1 and 4 is shown. The shaded regions indicate approximately the positions of the observable and the real fission thresholds for the compound nucleus ^{239}Pu; E_n is the neutron binding energy in ^{239}Pu.

REF.	ELEM. SYM.	A	Z
A. S. Soldatov, Yu. M. Tsipenyuk, G.N. Smirenkin Yad. Fiz. 11, 992 (1970) Sov. J. Nucl. Phys. 11, 552 (1970)	Pu	239	94

METHOD	REF. NO.	
	70 So 2	hmg

REACTION	RESULT	EXCITATION ENERGY	SOURCE		DETECTOR		ANGLE
			TYPE	RANGE	TYPE	RANGE	
G,F	ABX	5-8	C	5-8	FRG-D		DST

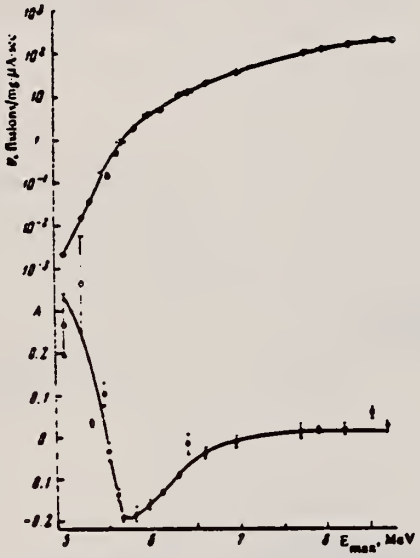

FIG. 1. Yield Y and angular anisotropy A in photofission of Pu^{239} as a function of maximum bremsstrahlung energy E_{max}.

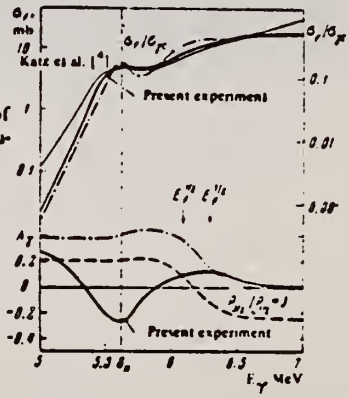

FIG. 2. Energy dependence of the cross section $\sigma_f(E_\gamma)$ and angular anisotropy $A_\gamma(E_\gamma)$ for monochromatic photons. The solid curves are experiment, and the dashed and dot-dash curves are theory.

REF. W. Gunther, K. Huber, U. Kneissl, H. Krieger, H. J. Maier
Phys. Rev. C19, 433 (1979)

ELEM. SYM.	A	Z
Pu	239	94

h OD

REF. NO. 79 Gu 1 hg

REACTION	RESULT	EXCITATION ENERGY	SOURCE		DETECTOR		ANGLE
			TYPE	RANGE	TYPE	RANGE	
G,2n	RLY	12-45	C	45	SCD-I		4PI

ISOMERIC/PROMPT YLD

The half-lives and yield ratios Y_{iso}/Y_{prompt} for the two ^{237}Pu fission isomers have been investigated in the photonuclear reaction ^{239}Pu(γ,2n). The observed half-lives ($t_{1/2} = 77 \pm 16$ ns, 1050 ± 400 ns) agree well with the data from particle induced fission. The measured yield ratios were $(Y_{iso}/Y_{prompt})_f^{short} = (6.4 \pm 1.7) \times 10^{-6}$ and $(Y_{iso}/Y_{prompt})_f^{long} = (0.83 \pm 0.22) \times 10^{-6}$. From a statistical model analysis of the isomeric fission yield ratio ($Y_{short}/Y_{long} = 7.7 \pm 2.9$) a spin assignment of the two shape isomers was attempted. The analysis provided, in the context of the statistical model, the most probable spin values $I = 11/2$ for the exicted, long lived state and $I = 5/2$ for the short lived ground state in the second minimum of ^{237}Pu. Comparing these spin values with single particle calculations, we tend to classify the excited state as the $[615]_{11/2+}$ Nilsson orbit and the short lived state as the $[862]_{5/2+}$ state.

[NUCLEAR REACTIONS ^{239}Pu(γ, 2n), bremsstrahlung 45 MeV; measured $t_{1/2}$, Y_{iso}/Y_{pr} for ^{237}Pu^{m1,m2} deduced isomeric ratio, spins.]

TABLE II. Results.

e length (ns)	$T_{1/2}$(ns)	$Y_{iso}/Y_{pr} \times 10^6$	$N_{pr} \times 10^{-6}$	Assignment
50	80 ± 20	6.2 ± 1.8	21.4	^{237}Pu^{m1}
	11 ± 6	•••	21.4	^{238}Pu^{m}(?)
	long-lived	< 1.5	21.4	
1000	72 ± 26	10.9 ± 8.5	236.0	^{237}Pu^{m1}
	1050 ± 400	0.83 ± 0.22	•••	^{237}Pu^{m2}

TABLE III. Comparison with previous results from particle induced reactions.

	$T_{1/2}$ (ns)	Reaction	Method	Ref.
Short-lived component	≈60	(α,2n)	R [a]	5
	100 ± 30	(d,2n)	R	9
	120 ± 50	(α,2n)	P [b]	10
	100 ± 50	(α,2n)	P	7
	120 ± 50	(α,n)	P	7
	82 ± 8	(α,2n)	P	11
	88 ± 35 [d]	(d,2n), (α,2n)	P	11
	114 ± 12	(d,2n)	P	6
	45 ± 10	(α,2n)	P	13
	110 ± 9	(α,2n)	P	14
	77 ± 16 [c]	(γ,2n)	P	this work
Long-lived component	900 ± 150	(d,2n)	P	8
	1120 ± 80 [d]	(α,2n), (d,2n)	P	11
	950 ± 300	(d,2n)	P	6
	1310 ± 260	(d,2n)	P	14
	1050 ± 400	(γ,2n)	P	this work

[a] Recoil techniques.
[b] Pulsed beam techniques.
[c] Weighted average of short and long beam pulse experiments.
[d] Weighted average of (d,2n) and (α,2n) results.

REF.

A. Shapiro and W. F. Stubbins
Nucl. Sci. & Engr. 45, 47 (1971)

ELEM. SYM.	A	Z
Pu	239	94

METHOD

REF. NO.: 71 Sh 4 egf

REACTION	RESULT	EXCITATION ENERGY	SOURCE		DETECTOR		ANGLE
			TYPE	RANGE	TYPE	RANGE	
G,F	ABX	7-11	C	4-12	SPK-I		2PI

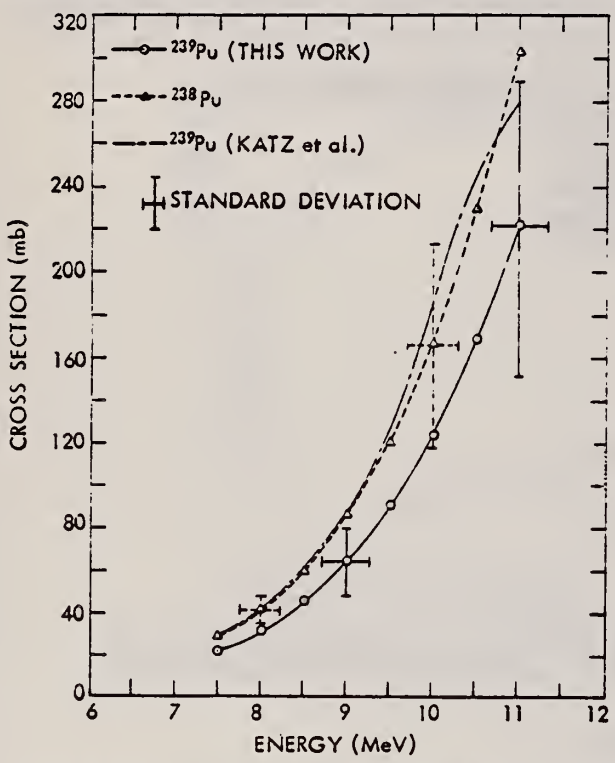

Fig. 3. Photofission cross section of ^{238}Pu and ^{239}Pu deduced from the Penfold-Leiss analysis. The dash-dot curve for ^{239}Pu is taken from Ref. 6.

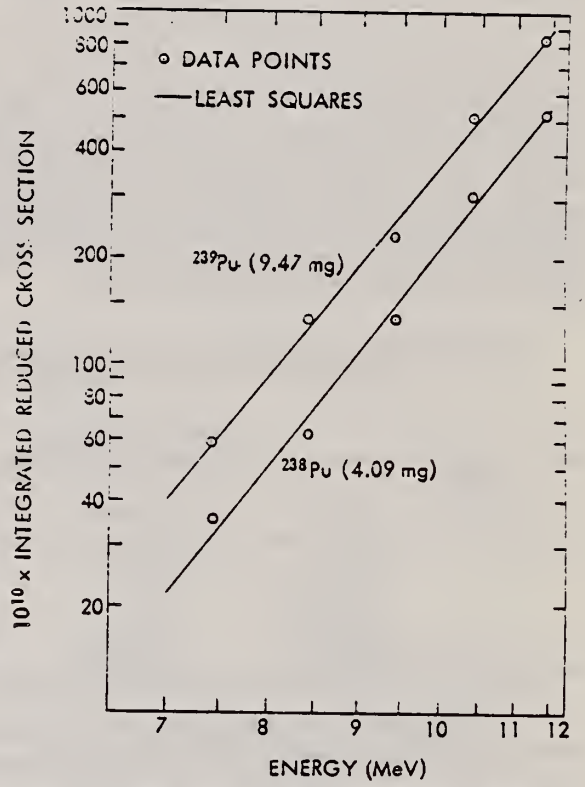

Fig. 2. Integrated reduced cross section vs energy. [The reduced cross section has a dimension of (energy)$^{-1}$, so the reduced cross section integrated with respect to energy is unitless.]

6 L. Katz, A. P. Baerg, and F. Brown, Proc. U.N. Intern. Conf. Peaceful Uses At. Energy, 2nd, Geneva, 1958, 15, 188 (1958).

TABLE I

Photofission Cross Sections Deduced by Penfold-Leiss Analysis

(Indicated errors are standard deviations)

Energy (MeV)	Cross Section (mb)	
	^{238}Pu	^{239}Pu
7.5	28 ± 5	21 ± 4
8.0	41 ± 8	31 ± 6
8.5	59 ± 13	45 ± 10
9.0	85 ± 21	64 ± 16
9.5	120 ± 32	90 ± 24
10.0	166 ± 47	123 ± 35
10.5	229 ± 68	168 ± 50
11.0	303 ± 94	221 ± 69

REF.

B. Tamain, B. Pfeiffer, H. Wollnik, E. Konecny
Nucl. Phys. A173, 465 (1971)

ELEM. SYM.	A	Z
Pu	239	94

METHOD

REF. NO.	
71 Ta 1	egf

REACTION	RESULT	EXCITATION ENERGY	SOURCE		DETECTOR		ANGLE
			TYPE	RANGE	TYPE	RANGE	
G,F	LFT	THR-53	C	53	SCD-I		90

DELAYED FISSION

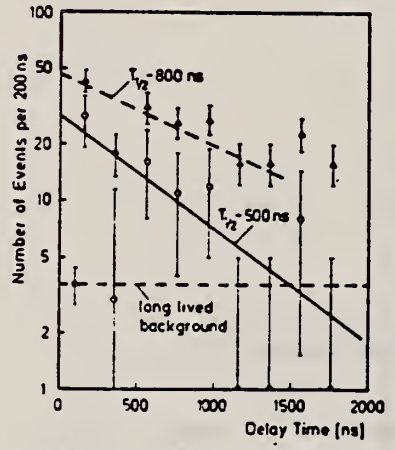

Fig. 7. Decay curve for delayed fission of $^{239}Pu+\gamma$. △ refers to raw data, ⊙ includes correction for the long-lived component. By dashed line the number of background events is shown as determined from fission pulses measured between beam pulses outside the 2 μs time range which was recorded by the TPHC.

REF. R.L. Bramblett, T. Gozani, R.O. Ginaven, D.E. Rundquist
Nucl. Technology 13, 33 (1972)

ELEM. SYM.	A	Z
Pu	239	94

METHOD

REF. NO.	
72 Br 8	egf

REACTION	RESULT	EXCITATION ENERGY	SOURCE		DETECTOR		ANGLE
			TYPE	RANGE	TYPE	RANGE	
G,XN	RLY	THR-11	C	5-11	BF3-I		4PI

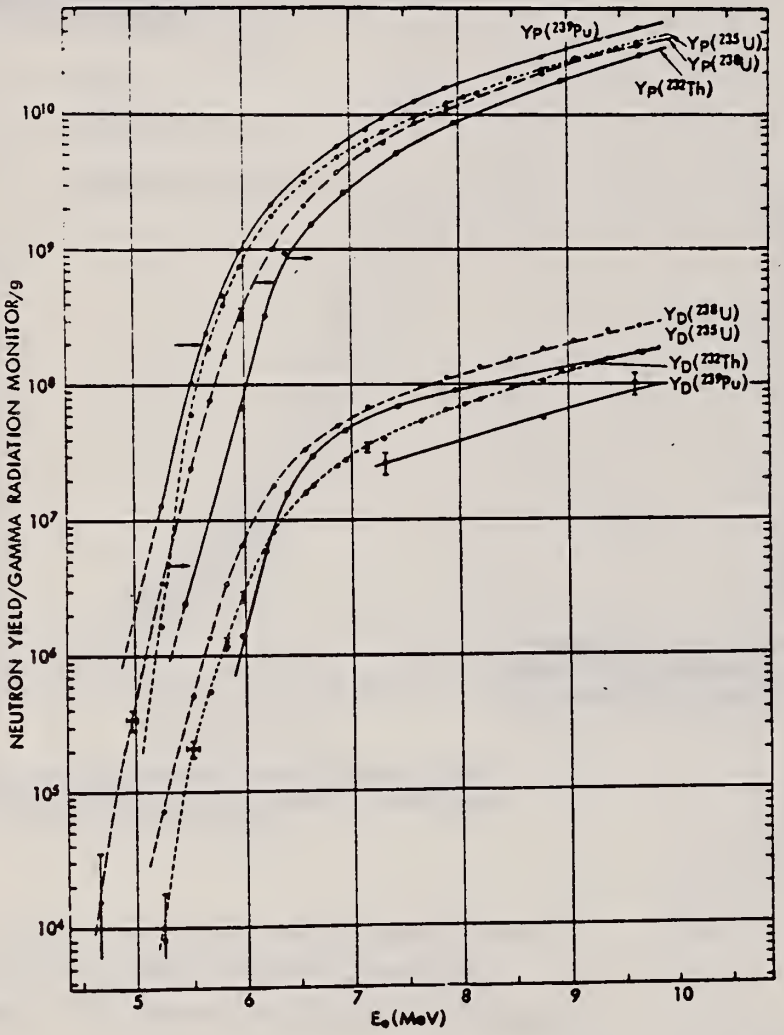

Fig. 8. Prompt- and delayed-neutron yields induced by electron bremsstrahlung for ^{232}Th, ^{235}U, ^{238}U, and ^{239}Pu.

REF. J.T. Caldwell, G.M. Worth, and E.J. Dowdy
PICNS-73, Vol.I, p.651 Asilomar

ELEM. SYM.	A	Z
Pu	239	94

METHOD

REF. NO. 73 Ca 2 hmg

REACTION	RESULT	EXCITATION ENERGY	SOURCE		DETECTOR		ANGLE
			TYPE	RANGE	TYPE	RANGE	
G,N	NOX	THR- 12	C	10, 12	BF3-I		4PI
G,F	NOX	THR- 12	C	10, 12	BF3-I		4PI

TABLE I

Low Energy Photoneutron and Photofission
Parameters Deduced from this Experiment

Isotope	E_c (MeV)	Prompt $\bar{\nu}$	Γ_n / Γ_f	Delayed Neutrons Per Photofission
^{238}U	8	2.633±.094	1.765±.136	0.0355±.0015
^{238}U	10	2.661±.087	2.813±.161	0.0358±.0023
^{238}U	12	3.087±.079	3.250±.150	0.0319±.0026
^{235}U	8	2.675±.095	1.051±.103	0.0101±.0011
^{235}U	10	2.936±.085	1.161±.067	0.0121±.0017
^{235}U	12	3.086±.079	1.224±.079	0.0110±.0020
^{232}Th	8	2.091±.112	1.086±.147	0.0324±.0017
^{232}Th	10	1.980±.115	4.017±.266	0.0309±.0019
^{232}Th	12	2.226±.113	6.764±.577	0.0292±.0038
^{239}Pu	10	3.603±.083	----------	----------
^{239}Pu	12	3.738±.075	0.7±0.4	----------

REF. David E. Rundquist
PICNS-73, Vol.I, p.619 Asilomar

ELEM. SYM.	A	Z
Pu	239	94

METHOD

REF. NO. 73 Ru 1 hmg

REACTION	RESULT	EXCITATION ENERGY	SOURCE		DETECTOR		ANGLE
			TYPE	RANGE	TYPE	RANGE	
G,XN	RLY	THR- 10	C	5- 10	BF3-I		4PI

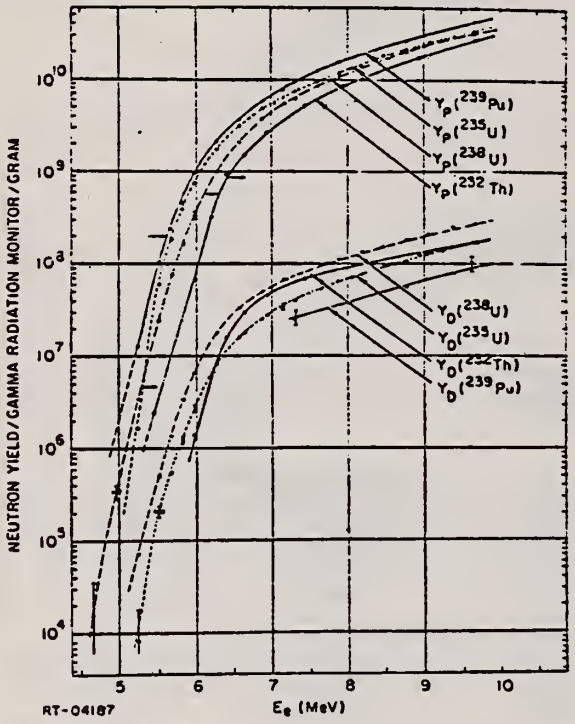

Fig. 1. Prompt and delayed neutron yields in fissile and fertile material produced by bremsstrahlung from electrons of energy E_e

REF.

G.M. Gurevich, L.E. Lazareva, V.M. Mazur, and G.V. Solodukhov
ZhETF Pis. Red. 20, 741 (1974)
JETP Lett. 20, 343 (1974)

ELEM. SYM.	A	Z
Pu	239	94

METHOD

REF. NO.	
74 Gu 11	hmg

REACTION	RESULT	EXCITATION ENERGY	SOURCE		DETECTOR		ANGLE
			TYPE	RANGE	TYPE	RANGE	
G,MU-T	ABX	7- 20	C	35	NAI-D		4PI

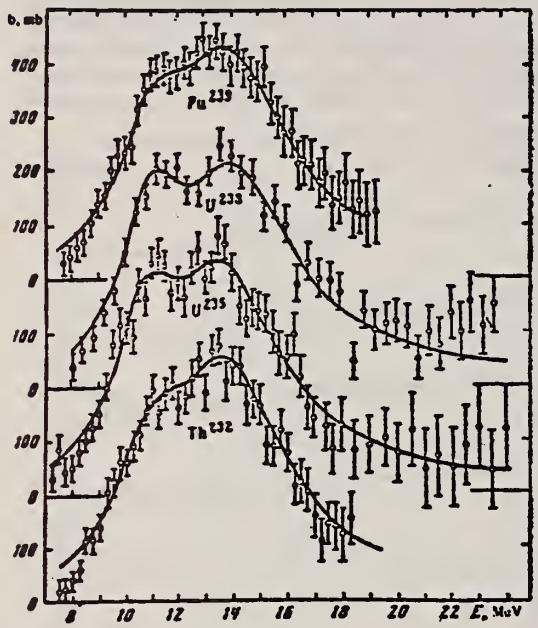

FIG. 1.

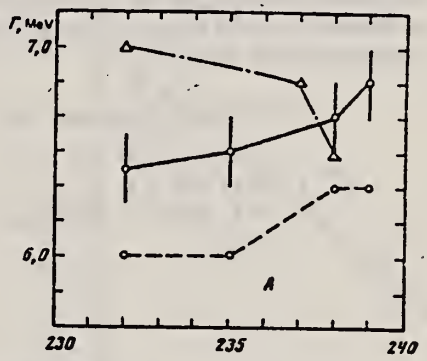

FIG. 2.

TABLE. Parameters for the approximation of the cross section by Lorentz lines.

Nucleus	σ_1 mb	Γ_1 MeV	E_1 MeV	σ_2 mb	Γ_2 MeV	E_2 MeV	$\frac{\sigma_2\Gamma_2}{\sigma_1\Gamma_1}$	β	Q
Th^{232}	247	3.90	10.99	362	4.67	13.9	1.75	0.28	10.0
U^{235}	283	3.23	10.74	354	4.92	13.77	1.91	0.30	11.0
U^{238}	286	2.99	10.97	351	5.10	14.25	2.09	0.31	11.7
Pu^{239}	227	3.47	11.05	362	5.23	14.01	2.40	0.29	11.0

REF.		ELEM. SYM.	A	Z
	K.N. Ivanov and K.A. Petrzhak At. Energ. 36, 404 (1974) Sov. J. At. Energy 36, 515 (1974)	Pu	239	94

METHOD	REF. NO.	
	74 Iv 2	egf

REACTION	RESULT	EXCITATION ENERGY	SOURCE		DETECTOR		ANGLE
			TYPE	RANGE	TYPE	RANGE	
G,F	RLY	5- 12	C	5- 12	TRK-I		4PI

YIELD REL U-238

The curves for the relative photofission yield functions $Y_i(E_{\gamma m})/Y_{^{238}U}(E_{\gamma m})$ were obtained from experimental ratios by least-square analysis. This method of analysis smooths out observed structure but maxima are seen in the curves (with an accuracy of ±0.16 MeV) at the following values of maximum bremsstrahlung energy:

Nucleus	Position of Maximum, MeV
^{232}Th	5.3; 6.3; 6.6; 7.5; 10.8.
^{235}U	5.1; 6.6; 8.4.
^{237}Np	5.5; 6.0; 7.1; 8.35; 9.8.
^{239}Pu	6.5.

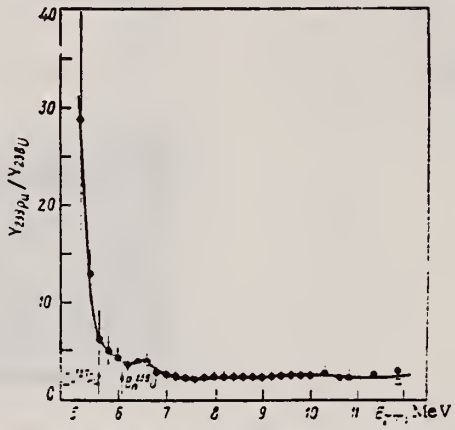

Fig. 4. Relative photofissility of ^{239}Pu: ●) present work; □) data from [5].

[5] J. Huizenga et al., Phys. Rev. 95, 1009 (1954).

REF. J.T. Caldwell and E.J. Dowdy
Nucl. Sci. & Eng. 56, 179 (1975)

ELEM. SYM.	A	Z
Pu	239	94

METHOD

REF. NO. 75 Ca 5 egf

REACTION	RESULT	EXCITATION ENERGY	SOURCE		DETECTOR		ANGLE
			TYPE	RANGE	TYPE	RANGE	
G,F	NOX	6- 13	C	8- 13	MOD-I		4PI

The prompt- and delayed-neutron multiplicities for photofission of the eight isotopes, ^{232}Th, ^{233}U, ^{234}U, ^{235}U, ^{236}U, ^{238}U, ^{237}Np, and ^{239}Pu, have been measured using bremsstrahlung with end-point energies ranging from 8 to 13 MeV. The measured multiplicities are compared with those from the same compound nucleus formed in neutron-induced fission where such data exist.

NEUTRON MULTIPLICITIES

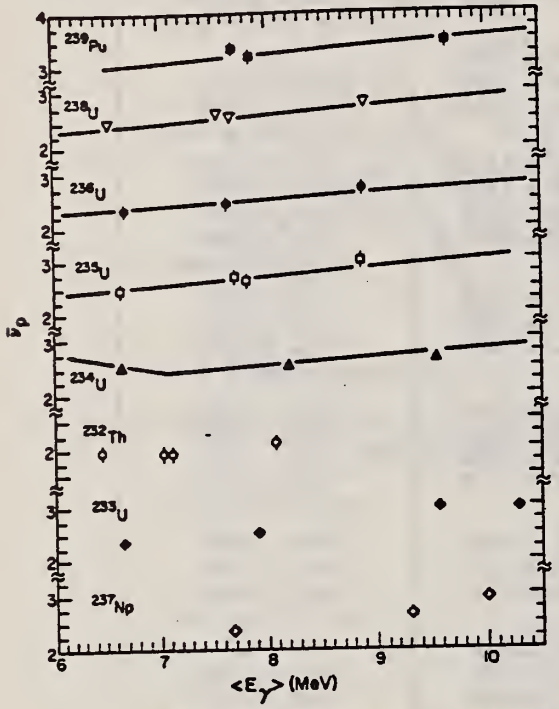

Fig. 5. $\bar{\nu}_p$ versus excitation energy for the eight isotopes studied in this experiment. The full curves shown are from the evaluations of Davey[2] with the excitation energy determined as described in the text. For the lower three isotopes shown, no previous experimental values for $\bar{\nu}_p$ exist.

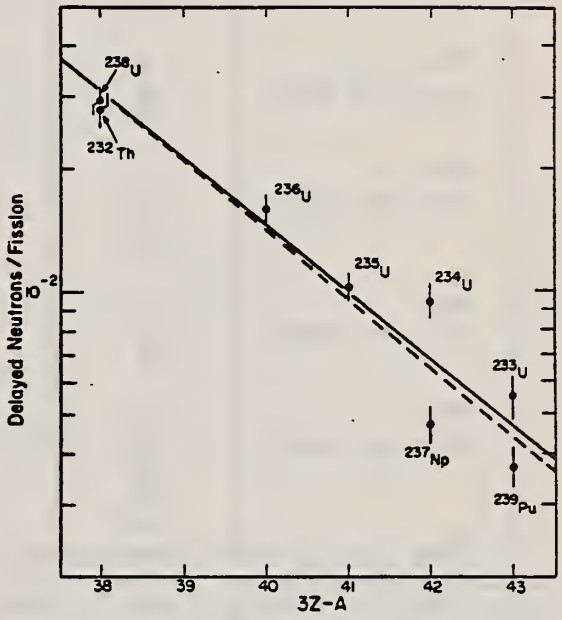

Fig. 6. Delayed neutrons per fission versus the parameter 3Z-A of the compound nucleus. The full curve shown is the least-squares fit to the data shown with $\ln Y_0 = 10.61$, $K = -0.372$. The dashed curve is the least-squares fit to the data provided by Tomlinson[6] with $\ln Y_0 = 11.35$, $K = -0.39$.

TABLE IV

Least-Squares Linear Fit Expressions for $\bar{\nu}_p(\langle E_\gamma \rangle)$

Isotope	$\bar{\nu}_p(\langle E_\gamma \rangle) = \bar{\nu}_0 + d\bar{\nu}_p/dE\,\langle E_\gamma \rangle$	Correlation Coefficient
^{232}Th	$\bar{\nu}_p(\langle E_\gamma \rangle) = 1.310 + 0.090\ \langle E_\gamma \rangle$	0.675
^{233}U	$\bar{\nu}_p(\langle E_\gamma \rangle) = 1.200 + 0.1709\ \langle E_\gamma \rangle$	0.947
^{234}U	$\bar{\nu}_p(\langle E_\gamma \rangle) = 2.222 + 0.0399\ \langle E_\gamma \rangle$	0.741
^{235}U	$\bar{\nu}_p(\langle E_\gamma \rangle) = 0.9034 + 0.2292\ \langle E_\gamma \rangle$	0.967
^{236}U	$\bar{\nu}_p(\langle E_\gamma \rangle) = 1.140 + 0.1788\ \langle E_\gamma \rangle$	0.986
^{238}U	$\bar{\nu}_p(\langle E_\gamma \rangle) = 1.502 + 0.1458\ \langle E_\gamma \rangle$	0.984
^{237}Np	$\bar{\nu}_p(\langle E_\gamma \rangle) = 0.4027 + 0.2505\ \langle E_\gamma \rangle$	0.967
^{239}Pu	$\bar{\nu}_p(\langle E_\gamma \rangle) = 2.526 + 0.0930\ \langle E_\gamma \rangle$	0.777

[2] W.G. Davey, Nucl. Sci. Eng., 44, 345 (1971)

[6] L. Tomlinson, "Delayed Neutrons from Fission: A Compilation and Evaluation of Experimental Data," AERE-R-6993, Atomic Energy Research Establishment, Harwell (1972)

TABLE III

Prompt- and Delayed-Neutron Yields

	E_e, MeV	$\langle E_\gamma \rangle$, MeV	$\bar{\nu}_p$	Delayed Neutrons per 100 Fissions
^{232}Th	8	6.44	1.96 ± 0.11	3.10 ± 0.28
(σ = 1.15 ± 0.05)	10	7.02	1.89 ± 0.11	3.06 ± 0.31
	10.2	7.10	1.89 ± 0.11	2.67 ± 0.21
	12	8.06	2.08 ± 0.11	2.59 ± 0.31
				av = 2.80 ± 0.28
^{233}U	8	6.68	2.350 ± 0.112	0.455 ± 0.040
(σ = 1.25 ± 0.05)	10	7.90	2.498 ± 0.108	0.518 ± 0.040
	12	9.55	2.960 ± 0.096	0.640 ± 0.044
	13	10.27	2.870 ± 0.099	0.598 ± 0.051
				av = 0.553 ± 0.044
^{234}U	8	(6.67)[a]	2.536 ± 0.112	---
(σ = 1.13 ± 0.05)	10	8.69	2.499 ± 0.107	0.92 ± 0.06
	12	9.54	2.623 ± 0.105	0.97 ± 0.12
				av = 0.94 ± 0.094
^{235}U	8	6.67	2.456 ± 0.086	0.90 ± 0.08
(σ = 1.20 ± 0.05)	10	7.70	2.697 ± 0.081	0.88 ± 0.08
	10.2	7.81	2.612 ± 0.079	1.13 ± 0.07
	12	8.86	2.963 ± 0.072	1.12 ± 0.08
				av = 1.02 ± 0.08
^{236}U	8	6.66	2.357 ± 0.111	1.43 ± 0.14
(σ = 1.20 ± 0.05)	10	7.63	2.470 ± 0.105	1.73 ± 0.12
	12	8.86	2.744 ± 0.095	1.64 ± 0.10
				av = 1.60 ± 0.13
^{238}U	8	6.53	2.457 ± 0.088	3.06 ± 0.24
(σ = 1.22 ± 0.05)	10	7.54	2.628 ± 0.083	2.76 ± 0.17
	10.2	7.66	2.585 ± 0.082	3.06 ± 0.14
	12	8.88	2.802 ± 0.078	2.75 ± 0.19
				av = 2.91 ± 0.20
^{237}Np	10	7.68	2.35 ± 0.11	0.38 ± 0.04
(σ = 1.20 ± 0.05)	12	9.31	2.65 ± 0.10	0.50 ± 0.04
	13	9.92	2.95 ± 0.10	0.54 ± 0.04
				av = 0.47 ± 0.04
^{239}Pu	10	7.69	3.32 ± 0.08	---
(σ = 1.18 ± 0.10)	10.2	7.84	3.17 ± 0.14	0.37 ± 0.04
	12	9.65	3.43 ± 0.10	0.37 ± 0.04
				av = 0.37 ± 0.04

[a]Estimated value.

REF.

G. M. Gurevich, L. E. Lazareva, V. M. Mazur,
G. V. Solodukhov, B. A. Tulupov
Nucl. Phys. A273, 326 (1976)

ELEM. SYM.	A	Z
Pu	239	94

METHOD

REF. NO.: 76 Gu 2 | egf

REACTION	RESULT	EXCITATION ENERGY	SOURCE		DETECTOR		ANGLE
			TYPE	RANGE	TYPE	RANGE	
G,MUT	ABX	7- 20	C	UKN	NAI-D		4PI

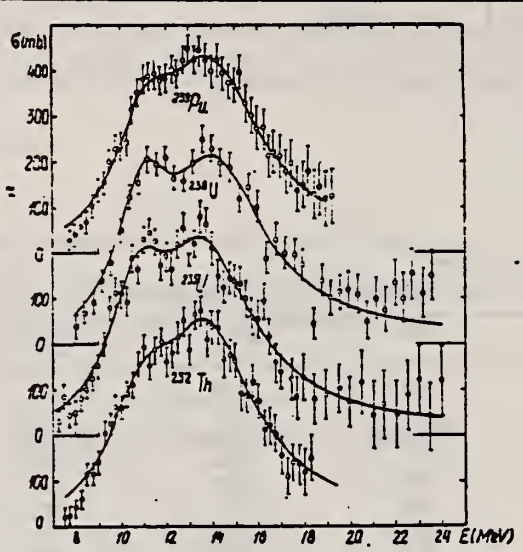

Fig. 2. Total photoabsorption cross sections for ^{232}Th, ^{235,238}U and ^{239}Pu and their respective best two Lorentz line fits.

TABLE 1

Lorentz line parameters for ^{232}Th, ^{235,239}U and ^{239}Pu

Nucleus	E_1 (MeV)	σ_1 (mb)	Γ_1 (MeV)	E_2 (MeV)	σ_2 (mb)	Γ_2 (MeV)
^{232}Th	10.99±0.16	247±26	3.90±0.4	13.9 ±0.13	362±26	4.67±0.38
^{235}U	10.74±0.18	283±39	3.23±0.55	13.77±0.23	354±33	4.92±0.58
^{238}U	10.97±0.13	286±30	2.99±0.48	14.25±0.18	351±25	5.10±0.63
^{239}Pu	11.05±0.13	227±39	3.47±0.57	14.01±0.21	362±31	5.23±0.59

TABLE 2

Deformation parameters and quadrupole moments for ^{232}Th, ^{235,238}U and ^{239}Pu

Nucleus	β_{exp}	$\bar{\beta}$	Q_0 (b)		
			this work	refs. [5,6])	ref. [14])
^{232}Th	0.28±0.03	0.274	10.0±0.8	10.2±1	9.66±0.1
^{235}U	0.30±0.03	0.285	11.0±0.9	12.8±1.3	11.12±0.2
^{238}U	0.31±0.03	0.300	11.7±0.9	11 ±1	11.3 ±0.1
^{239}Pu	0.29±0.03	0.302	11.0±0.9		11.02±0.3

(over)

TABLE 3

Integrated cross sections and mean energies of the dipole absorption

Nucleus	σ_0 (MeV · b)	σ_{-1} (mb)	σ_{-2} (mb · MeV^{-1})	$\bar{E}$ (MeV)	E_H (MeV)	E_M (MeV)	E^* (MeV)
^{232}Th	2.92±0.32	231±24	19±2	13.08	12.64	12.40	12.16
^{235}U	2.99±0.39	238±31	20±2.5	12.91	12.56	12.23	11.90
^{238}U	2.95±0.29	229±22	18±1.8	13.34	12.88	12.80	12.72
^{239}Pu	2.97±0.34	232±26	19±2	13.28	12.80	12.50	12.21

In table 3 various integrated cross sections are defined by the relations

$$\sigma_0 = \int_s^{18} \sigma_{tot}(E)dE, \qquad \sigma_{-1} = \int_s^{18} \frac{1}{E}\sigma_{tot}(E)dE, \qquad \sigma_{-2} = \int_s^{18} \frac{1}{E^2}\sigma_{tot}(E)dE.$$

TABLE 4

Comparison of various integrated cross sections for ^{232}Th, ^{235,238}U and ^{239}Pu

	^{232}Th	^{235}U	^{238}U	^{239}Pu
σ_{0L} (MeV · b)	4.17	4.17	4.16	4.21
0.06 NZ/A (MeV · b)	3.31	3.36	3.39	3.42
$\sigma_0/(0.06\ NZ/A)$	0.88±0.1	0.89±0.12	0.87±0.09	0.87±0.1
$\sigma_{0L}/(0.06\ NZ/A)$	1.26	1.24	1.23	1.23
$\sigma_2\Gamma_2/\sigma_1\Gamma_1$	1.75	1.91	2.09	2.40
σ_{-1L} (mb)	294	298	288	289
$\sigma_{-1L}/A^{4/3}$	0.21	0.21	0.20	0.20
σ_{-2L} (mb · MeV^{-1})	26.3	26.9	25.0	25.3
$\sigma_{-2L} \times 10^3/A^{5/3}$	3.00	3.01	2.74	2.76

[5] C. D. Bowman et al., Phys. Rev. 133 (1964) B676

[6] A. Veyssiere et al., Nucl. Phys. A199 (1973) 45

[14] K.E.G. Lobner et al., Nucl. Data Tables 7 (1970) 495

REF. B.M. Aleksandrov, A.S. Krivokhatskii, V.L. Kuznetsov, L.E. Lazareva, V.G. Nedorezov, N.V. Nikitina, Yu.N. Ranyuk
Yad. Fiz. 28, 1165 (1978)
Sov. J. Nucl. Phys. 28, 600 (1978)

ELEM. SYM.	A	Z
Pu	239	94

METHOD

REF. NO. 78 A1 5 hg

REACTION	RESULT	EXCITATION ENERGY	SOURCE TYPE	SOURCE RANGE	DETECTOR TYPE	DETECTOR RANGE	ANGLE
G,F	RLY	THR-999	C	100-999	TRK-D		4PI

The 300- and 2000-MeV electron linear accelerators have been used to measure the relative fissilities of the nuclei ^{235}U, ^{238}U, ^{237}Np, ^{239}Pu, ^{241}Am, and ^{243}Am. Fragments were detected by glass detectors. Photofission yields were obtained for the nuclei indicated at maximum bremsstrahlung energies 100, 240, 400, and 1200 MeV.

999=1.2 GEV

PACS numbers: 25.85.Jg

TABLE I. Relative photofission yields for $E_{\gamma max}$=100, 240, 400, and 1200 MeV.

Nucleus	Fissility of nuclei in the excitation-energy range ~ 5–12 MeV: $D_f = \Gamma_f/(\Gamma_f + \Gamma_n)$	Relative fissility	Ratios of fragment yields $Y/Y(^{238}U)$ for different maximum energies $E_{\gamma max}$: 100 MeV	240 MeV	400 MeV	1200 MeV
^{235}U	0.38(b)	1.45(a) 1.38(b) 2.15(f)	2.22±0.16	2.15±0.15	1.79±0.13	1.74±0.12
^{238}U	0.22±0.01 *	1.00	1.00	1.00	1.00	1.00
^{237}Np	0.51(b) 0.53(d)	2.53(b) 2.16(c) 2.34(d) 2.93(f)	1.89±0.14	1.92±0.13	1.67±0.12	1.61±0.10
^{239}Pu	0.70(b)	2.70(a) 3.51(b) 3.51(c) 3.45(f)	2.10±0.15	2.10±0.15	1.80±0.13	1.63±0.12
^{241}Am	0.53(e)	1.68(c) ** 2.42(e) 3.27(f)	1.91±0.14	1.77±0.13	1.48±0.10	1.44±0.10
^{243}Am	0.62(e)	2.80(e) 2.59(f)	1.81±0.13	1.81±0.13	1.53±0.11	1.44±0.10

Note. *a*, *b*, *c*, *d*, and *e* denote that the data have been taken respectively from the photofission studies of Refs. 16, 17, 18, 19, and 15. *f* are the average values for the data of a given study on fission by neutrons[20] at nuclear excitation energy ~8 MeV.

*The number given is an average over the results of a large number of studies on photofission of ^{238}U.

**The authors of Ref. 18 point out that the value obtained by them for ^{241}Am is obviously underestimated.

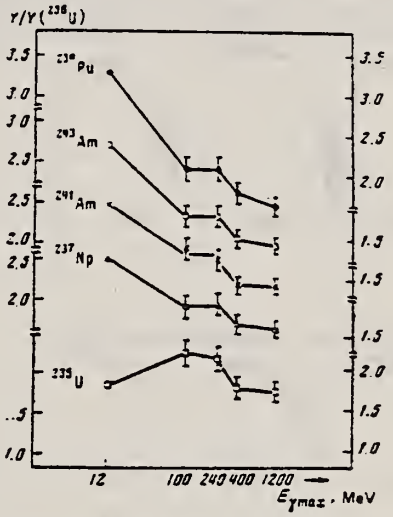

FIG. 2. Relative yields $Y/Y(^{238}U)$ for the nuclei ^{235}U (□), ^{237}Np (△), ^{239}Pu (●), ^{241}Am (×), and ^{243}Am (○) for maximum bremsstrahlung energies $E_{\gamma max}$ ~12, 100, 240, 400, and 1200 MeV.

[15]Yu. A. Vinogradov, V. I. Kasilov, L. E. Lazareva, V. G. Nedorezov, N. V. Nikitina, N. M. Parovik, Yu. N. Ranyuk, and P. V. Sorokin. Yad. Fiz. 24, 686 (1976) Sov. J. Nucl. Phys. 24, 357 (1976).
[16]J. McElhinney and W. E. Ogle, Phys. Rev. 81, 342 (1951).
[17]J. R. Huizenga, Phys. Rev. 109, 484 (1958).
[18]L. Katz, A. P. Baerg, and F. Brown, Proc. of the Second Intern. Conf. on the Peaceful Uses of Atomic Energy, Geneva, 1958, United Nations, Geneva, 1958, Vol. 15, p. 200.
[19]A. Veyssiere, H. Beil, R. Bergere, P. Carlos, A. Lepretre, and K. Kernbath, Nucl. Phys. A199, 45 (1973).

REF. V.E. Zhuchko, Yu.B. Ostapenko, G.N. Smirenkin, A.S. Soldatov, Yu.M. Tsipenyuk
Yad. Fiz. 28, 1170 (1978)
Sov. J. Nucl. Phys. 28, 602 (1978)

ELEM. SYM.	A	Z
Pu	239	94

METHOD

REF. NO. 78 Zh 7 hg

REACTION	RESULT	EXCITATION ENERGY	SOURCE TYPE	SOURCE RANGE	DETECTOR TYPE	DETECTOR RANGE	ANGLE
G,F	ABX	THR-7	C	4-7	TRK-D		4PI
				(4.4-7.)			

The bremsstrahlung beam of the microtron at our Institute has been used to measure photofission yields of nine nuclei—^{232}Th, ^{233,235,236,238}U, ^{237}Np, ^{239,241}Pu, and ^{241}Am in the energy region 4.4–7.0 MeV. The method of minimization of the directed deviation was used to reproduce the photofission cross sections from the integrated yields. The following problems are discussed in terms of the experimental data: resonance structure of the cross sections, effects of a two-humped shape of the fission barrier, and comparison of the fissility in the (γ,f) and (n,f) reactions and in direct reactions.

PACS numbers: 25.85.Jg

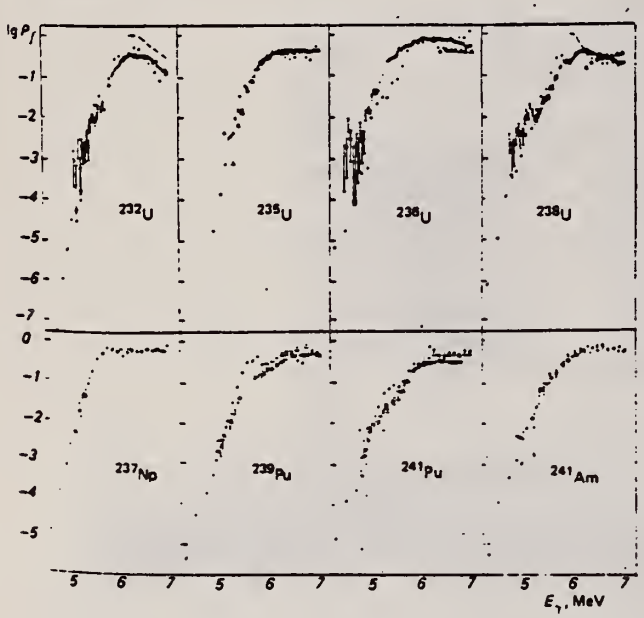

FIG. 4. Fissility P_f in the reactions (γ,f)—●, (n,f)—Δ (Ref. 14), and in direct reactions—○.[2] The dashed curve shows the results of evaluation of P_f in accordance with Eq. (9).

(over)

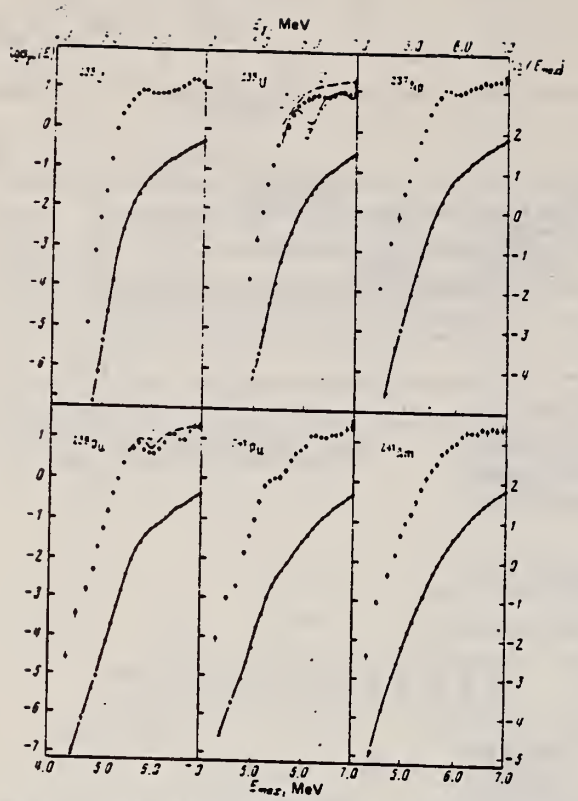

FIG. 3. Yields $Y(E_{max})$, fissions/mg-μC, and cross sections $\sigma_{\gamma f}(E_\gamma)$, mb, for odd isotopes. The designations are the same as in Fig. 2.

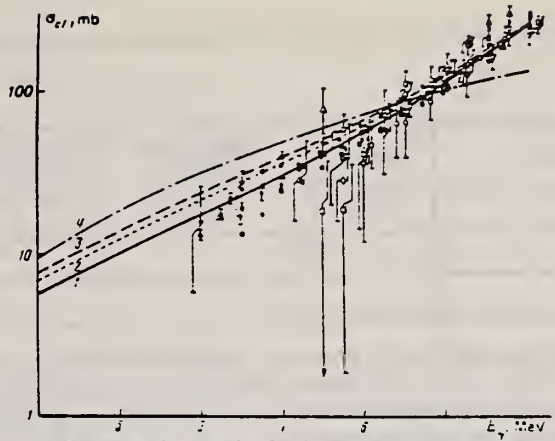

FIG. 6. Set of data on dipole photoabsorption cross sections σ_{ct}. The solid line (1)—the present work—is the result of fitting the data of Ref. 6 by Eq. (2) in the region $E_\gamma = 6$–10 MeV. Curves 2 and 3 are an extrapolation of the fit from Ref. 16 (2) and Ref. 17 (3) for ^{238}U; curve 4 is an estimate by means of Axel's formula.[15] Points: □, ■—^{232}Th; △, ▲—^{235}U; ♦—^{236}U; ○, ●—^{238}U; ▽, ▼—^{237}Np; ◇—^{239}Pu. The hollow points are from Refs. 16 and 17; the solid points are from Ref. 6.

REF. W. Günther, K. Huber, U. Kneissl, H. Krieger, H.J. Maier
Z. Phys. A 295, 333 (1980)

ELEM. SYM.	A	Z
Pu	239	94

METHOD

REF. NO. 80 Gu 4 hg

REACTION	RESULT	EXCITATION ENERGY	SOURCE		DETECTOR		ANGLE
			TYPE	RANGE	TYPE	RANGE	
G,F	RLY	THR-55	C	15-55	SCD-D		90

Measurements are presented for the mass and energy distributions of fragments from the photofission of ^{232}Th, ^{235}U, ^{238}U and ^{239}Pu. The experiments were performed for bremsstrahlung endpoint energies between 15 and 55 MeV, using silicon surface barrier detectors. The results are discussed with respect to the competition between the symmetric and asymmetric fission modes.

M,E DST, SYM/ASYM YLD

Table 2. Most probable heavy masses, most probable total kinetic energies and their variances (The variances have been corrected for the detector resolution and for γ- and electron pile up)

Nucleus	$[m]_{heavy}$	$[E_k]_{tot}$		$[E_k]_{exp}$	σ_{E_k}
		a)	b)		
^{232}Th	(141.7 ± 2) amu	163.3 MeV	163.5 MeV	(159.5 ± 4) MeV	(9.0 ± 0.8) MeV
^{235}U	(138.5 ± 2) amu	169.1 MeV	170.1 MeV	(168 ± 3) MeV	(11.1 ± 1) MeV
^{238}U	(140.3 ± 2) amu	168.5 MeV	169.4 MeV	(164.5 ± 4) MeV	(11.7 ± 1) MeV
^{239}Pu	(137.2 ± 2) amu	174.7 MeV	176.6 MeV	(174 ± 3) MeV	(11.9 ± 1) MeV
^{252}Cf[c]				185.5 MeV	11.6 MeV

[a] $[E_k] = (0.1071 \cdot Z^2/A^{1/3} + 22.2)$ MeV
[b] $[E_k] = (0.1240 \cdot Z^2/A^{1/3})$ MeV
[c] Calibration measurement

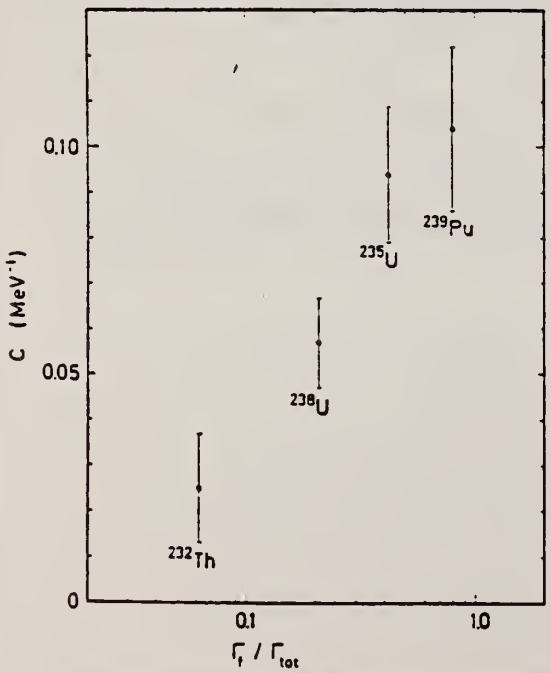

Fig. 5. Saturation parameter c as a function of the fission probability Γ_f/Γ_{tot}

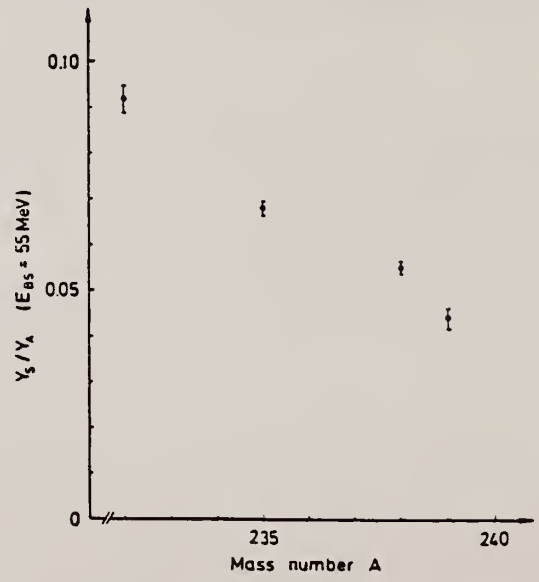

Fig. 6. Y_S/Y_A at $E_{BS} = 55$ MeV as a function of the mass number A

(OVER)

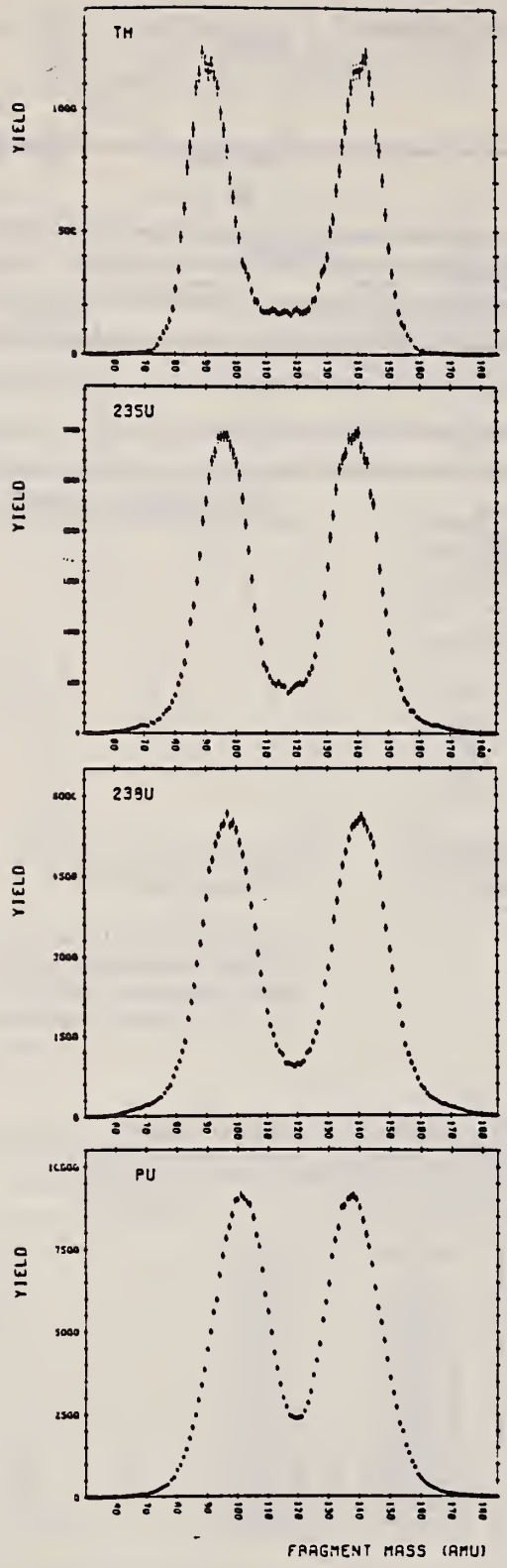

Fig. 1. Mass distributions for the photofission of ^{232}Th, ^{235}U, ^{238}U and ^{239}Pu (Bremsstrahl endpoint energy E_{BS} = 45 MeV)

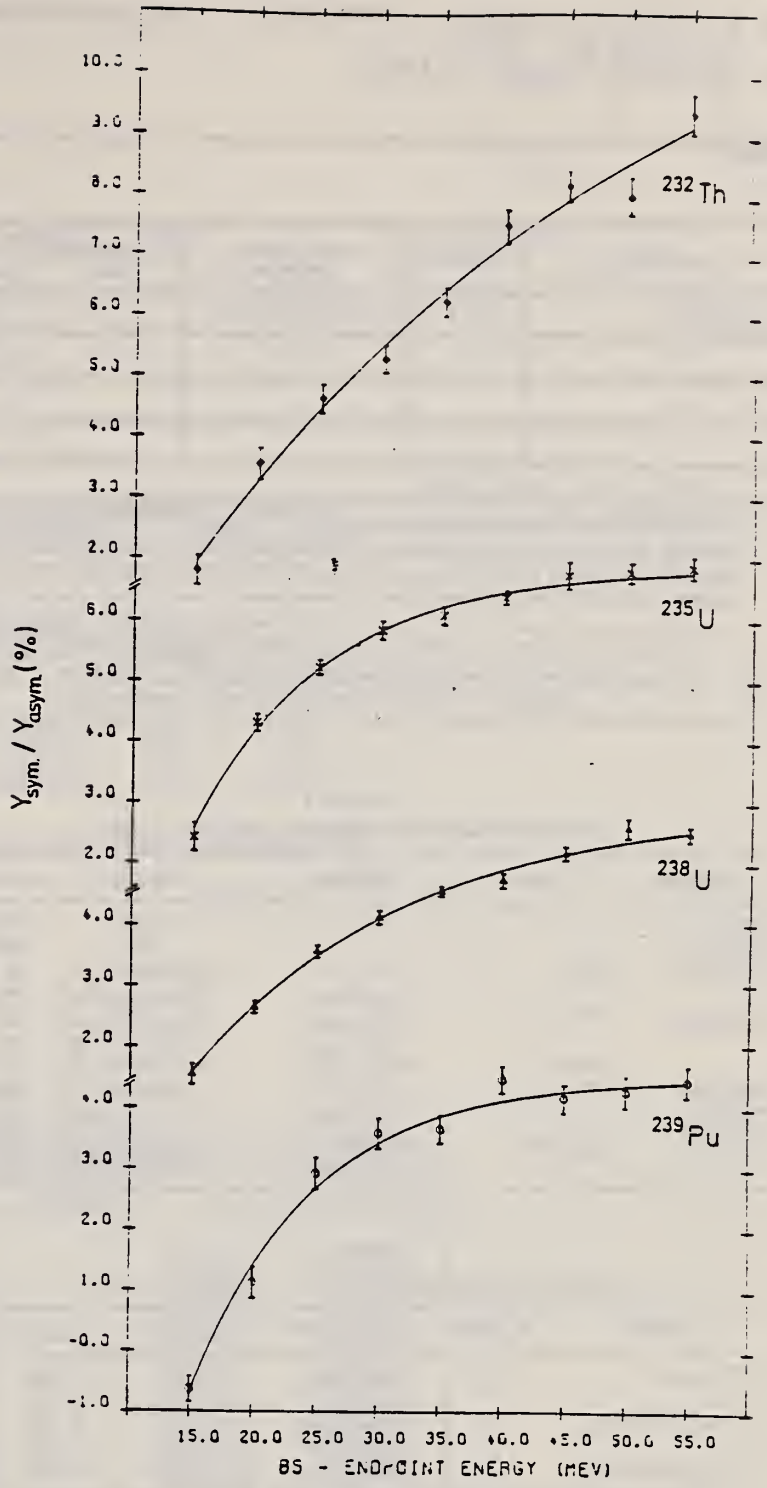

Fig. 4. Symmetric to asymmetric fission yield ratio as a function of E_{BS}. The lines are fits with an empirical function Y_S, $Y_A = a + be^{-cE_{BS}}$ (s. text)

REF. W. Günther, K. Huber, U. kneissl, H. Krieger, H. Ries, H. Ströher, W. Wilke, H.J. Maier
Nucl. Phys. A350, 1 (1980)

ELEM. SYM.	A	Z
Pu	239	94

METHOD

REF. NO. 80 Gu 5 hg

REACTION	RESULT	EXCITATION ENERGY	SOURCE		DETECTOR		ANGLE
			TYPE	RANGE	TYPE	RANGE	
G,2N	RLY	THR-45	C	45	SPK-I		90

YLD FISSION ISOMERS

Abstract: Half-lives and yields in photonuclear reactions have been measured for shape isomers in U and Pu isotopes by pulsed-beam techniques bombarding ^{235,238}U and ^{239,240,242}Pu targets with bremsstrahlung. Isomeric fission cross sections have been deduced from the measured isomeric to prompt yield ratios within an evaporation model using absolute prompt fission data. The results are compared with data from particle-induced reactions.

E NUCLEAR REACTIONS ^{240}Pu^{235}U(γ, x n), ^{238}U, ^{239}Pu(γ, 2n), ^{242}Pu(γ, n); bremsstrahlung; measured $T_{1/2}$, isomeric to prompt yield ratios, ^{236}U, ^{237}Pu, ^{239}Pu, ^{241}Pu levels, deduced σ for isomeric fission. Natural and enriched targets.

TABLE 2

Results of isomeric fission experiments performed at Giessen

Reaction	Isomer	Half-life	Y_{iso}/Y_{pr}	Detector
^{232}Th(γ, x n)			$<10^{-6}$	PPAD
^{235}U (γ, x n)			$<10^{-7}$	PPAD
^{238}U (γ, 2n)	^{236}U	115 ± 5 ns	$(2.02\pm0.16)\times10^{-5}$	Si
		118 ± 7 ns	$(2.10\pm0.16)\times10^{-5}$	PPAD
^{239}Pu (γ, 2n)	^{237m_1}Pu	77 ± 16 ns	$(6.4\pm1.7)\times10^{-6}$	Si
		87 ± 11 ns	$(4.9\pm0.7)\times10^{-6}$	PPAD
	^{237m_2}Pu	1050 ± 400 ns	$(0.83\pm0.22)\times10^{-6}$	Si
^{240}Pu (γ, n)	^{239m_1}Pu	6.5 ± 0.4 μs	$(7.9\pm0.4)\times10^{-5}$	PPAD
^{240}Pu(γ, x n)	?	4.5 ± 1.5 ns	$<1.1\times10^{-4}$	PPAD
^{242}Pu(γ, n)	^{241m_1}Pu	20.5 ± 2.5 μs	$(9.2\pm0.8)\times10^{-5}$	PPAD
	^{241m_2}Pu	34 ± 7 ns	$(3.7\pm0.7)\times10^{-5}$	PPAD

TABLE 6

Isomeric fission cross sections for (γ, 2n) reactions (this work)

Reaction	E_0 (MeV)	$Y_{iso}/Y_{pr}\times10^{-5}$	σ_{iso}^{max} (μb)	E_{max} (MeV)
^{238}U(γ, 2n)	45	2.02 ± 0.16	9.9 ± 1.9	16†
		2.10 ± 0.16	10.3 ± 2.0	16†
^{239}Pu(γ, 2n)^{237m_1}Pu	45	0.64 ± 0.017		17.5†
		0.49 ± 0.07	5.7 ± 1.7	17.5†
^{239}Pu(γ, 2n)^{237m_2}Pu	45	0.083 ± 0.022		17.5†

† The shape of the cross section was calculated (see text).

REF. M.Ya. Kondrat'ko, A.V. Mosesov, K.A. Petrzhak, O.A. Teodorovich
Sov. J. At. Ener. 50, 41 (1981)
At. Energ. 50, 34 (1981)

ELEM. SYM.	A	Z
Pu	239	94

METHOD

REF. NO. 81 Ko 4 hg

REACTION	RESULT	EXCITATION ENERGY	SOURCE		DETECTOR		ANGLE
			TYPE	RANGE	TYPE	RANGE	
G,F	RLY	THR-28	C	28	ACT-D		4PI

FISS PROD, MASS DIST

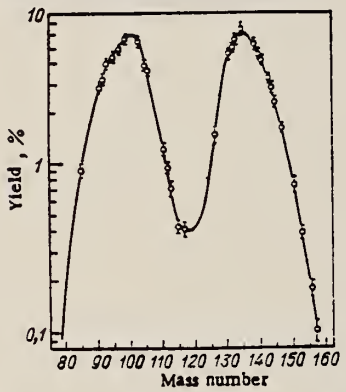

Fig. 1. Mass distribution of the photofission products of ^{239}Pu for a maximum bremsstrahlung energy of E_0 = 28 MeV.

TABLE 2. Fractional Individual Yields and Data on the Charge Distribution of the Photofission Products of ^{239}Pu (E_0 = 28 MeV)

Nuclide	Fractional individual yield f_i	Most probable charge $Z_p(\sigma=0.59)$	ΔZ_p relative to ^{238}U (n_σ, f)*
^{99}Nb	0,011±0,002	39,15	+1,03
^{132}I	0,217±0,044	52,05	+1,52
^{135}Xe	0,412±0,025	53,42	+1,51
^{136}Cs	0,123±0,009	53,82	+1,49
^{140}La	0,032±0,006	55,41	+1,49

*Average value with respect to heavy products amounts to 1,50.

TABLE 1. Yields of Photofission Products of ^{239}Pu (E_0 = 28 MeV)

Nuclide	Method of determination	Cumulative yield, %	Estimate of total yield of chain, %	Nuclide	Method of determination	Cumulative yield, %	Estimate of total yield of chain, %
^{83m}Kr	a	0,851±0,068	0,931±0,075	^{127}Sb	a	1,43±0,15	1,46±0,15
^{85}Kr	»	1,62±0,21	—	^{131}I	»	4,67±0,15	4,67±0,15
^{91}Sr	a, c	2,89±0,23	2,91±0,23	^{132}I	»	4,96±0,16	5,00±0,16
^{92}Y	»	3,20±0,16	3,20±0,16	^{133}I	»	5,43±0,21	5,64±0,22
^{93}Y	b	4,02±0,20	4,04±0,20	^{135}Xe	»	6,32±0,26	6,55±0,27
^{95}Zr	a	4,39±0,13	4,40±0,13	^{139}Ba	c	5,18±0,26	5,21±0,26
^{97}Zr	»	4,63±0,17	4,93±0,18	^{140}La	a, b, c	4,55±0,18	4,55±0,18
^{99}Mo	»	5,76±0,22	5,76±0,22	^{141}Ce	a, b	4,23±0,14	4,23±0,14
^{103}Ru	»	5,55±0,28	5,55±0,28	^{143}Ce	a, b, c	3,26±0,13	3,26±0,13
^{105}Ru	»	3,96±0,20	3,96±0,20	^{144}Ce	a	2,83±0,11	2,86±0,11
^{106}Ru	»	3,70±0,26	3,73±0,26	^{145}Pr	c	2,33±0,15	2,33±0,15
^{111}Ag	b, c	1,242±0,075	1,242±0,075	^{147}Nd	a, b, c	1,642±0,064	1,642±0,064
^{112}Ag	a	0,955±0,057	0,956±0,057	^{151}Pm	b, c	0,745±0,074	0,748±0,074
^{113}Ag	b, c	0,710±0,069	0,720±0,070	^{153}Sm	»	0,385±0,027	0,385±0,027
^{115}Cd	a, b	0,394±0,027	0,421±0,030	^{156}Sm	»	0,161±0,018	0,179±0,021
^{117m}Cd	b	0,165±0,017	0,412±0,035	^{157}Eu	c	0,098±0,015	0,099±0,015
^{117}Cd	»	0,227±0,016					

*a) Gross-spectra, γ-spectrometer: b) radiochemical analysis, γ-spectrometer c) radiochemical analysis, 4π-counter.

REF. A.S. Voronin, I.S. Koretskaya, V.L. Kuznetsov, V.G. Nedorezov, N.V. Nikitina, V.I. Noga, S.A. Pashchuk, Yu.N. Ranyuk, S.M. Solov'ev
Yad. Fiz. 34, 1439 (1981)
Sov. J. Nucl. Phys. 34, (1981)

ELEM. SYM.	A	Z
Pu	239	94

METHOD

REF. NO. 81 Vo 3 egf

REACTION	RESULT	EXCITATION ENERGY	SOURCE		DETECTOR		ANGLE
			TYPE	RANGE	TYPE	RANGE	
E,F	ABX	4-275	D	97-275	TRK-I		45
G,F	RLY	4-275	D	184-275	TRK-I		45

RELATIVE BRMS/E YLD

Results are presented of cross-section measurements for the fission of ^{232}Th, ^{233}U, ^{235}U, ^{236}U, ^{238}U, ^{237}Np, and ^{239}Pu by electrons with energies between 100 and 275 MeV; photofission and electrofission cross-section ratios for the same nuclei are given as well.

PACS numbers: 25.85.Jg, 27.90. + b, 25.85.Ge

TABLE II. Electrofission cross sections (mb) for nuclei with $Z \geq 90$ measured for electron energies between 100 and 275 MeV.

E_e, MeV	Nucleus						
	^{232}Th	^{233}U	^{235}U	^{236}U	^{238}U	^{237}Np	^{239}Pu
97	1.24	8.12	5.60	4.55	2.23	6.22	7.26
134	1.47	9.17	6.08	4.74	3.42	6.63	7.98
149	1.62	9.75	6.17	5.50	3.59	7.16	8.39
166	1.63	10.36	7.01	5.29	4.15	7.70	9.18
184	1.78	9.61	7.13	5.04	4.17	7.92	8.92
201	1.54	9.84	6.53	6.10	4.56	7.49	9.31
217	1.73	10.91	7.73	6.14	4.77	7.99	9.56
240	1.91	10.25	7.26	5.92	4.29	7.84	9.43
253	1.85	9.89	7.00	6.17	4.76	7.80	9.78
275	2.22	10.50	8.15	6.66	5.26	9.63	10.50

TABLE IV. Cross sections (mb) for photo- and electrofission ($\sigma_{Qf}\Delta t + \sigma_{ef}$) obtained in measurements with aluminum radiators with a thickness of $0.023t_0$ for ^{235}U, ^{236}U, ^{238}U, and ^{237}Np and of $0.011t_0$ for ^{239}Pu.

E_e, MeV	Nucleus					E_e, MeV	Nucleus				
	^{235}U	^{236}U	^{238}U	^{237}Np	^{239}Pu		^{235}U	^{236}U	^{238}U	^{237}Np	^{239}Pu
184	13.33	10.48	7.57	13.49	11.65	240	14.02	10.57	8.43	11.62	13.23
201	14.10	11.50	8.82	12.79	12.46	253	14.17	10.96	8.11	11.94	12.90
217	14.36	10.76	8.67	12.94	12.98	275	15.22	12.00	9.29	12.32	13.63

TABLE V. Cross-section ratios for photo- and electrofission (σ_{Qf}/σ_{ef}) for energies between 184 and 275 MeV.

Nucleus	σ_{Qf}/σ_{ef}	Nucleus	σ_{Qf}/σ_{ef}
^{235}U	40±8	^{237}Np	24±5
^{236}U	35±7	^{239}Pu	30±6
^{238}U	35±7		
Average	33±3		
Theoretical	35.3		

Pu
A=240

Pu
A=240

A. P. Baerg, R. M. Bartholomew, F. Brown, L. Katz, and S. B. Kowalski
Can. J. Phys. 37, 1418 (1959) (A.E.C.L. No. 896)

Pu	240	94

METHOD

Betatron with ionization chamber detector, enriched samples.

REF. NO. 59 Ba 4 | EGF

REACTION	RESULT	EXCITATION ENERGY	SOURCE		DETECTOR		ANGLE
			TYPE	RANGE	TYPE	RANGE	
G,F	RLY	THR - 20	C	6-20	ION-I		DST

TABLE II

Angular distributions

Relative fission fragment yields as a function of peak bremsstrahlung energy E_0 and angle θ to X-ray beam

E_0, Mev	Angle θ 0	25	45	60	90
Th-232					
6.5	1.00±0.3				20±5
7.0	1.00±0.04		4.1±0.2	6.7±0.3	8.4±0.3
7.5	1.00±0.1		5.1±0.4	6.0±0.4	7.9±0.5
8.0	1.00±0.09		2.4±0.2	3.6±0.3	5.1±0.3
9.0	1.00±0.1				3.4±0.3
10.0	1.00±0.04	1.16±0.05	1.67±0.08	1.97±0.08	2.4±0.1
14.0	1.00±0.05				1.43±0.08
20.0	1.00±0.05				1.13±0.06
U-238					
6.0	1.00±0.3				6.0±1.4
6.3	1.00±0.1		3.6±0.4		5.9±0.6
6.5	1.00±0.2				4.5±0.7
7.0	1.00±0.08	1.5±0.1	2.0±0.2	2.4±0.2	2.9±0.2
8.0	1.00±0.06				2.1±0.1
9.4	1.00±0.023	1.094±0.029	1.224±0.029	1.274±0.034*	1.452±0.033
10.0	1.00±0.04				1.38±0.04
14.0	1.00±0.04				1.08±0.04
20.0	1.00±0.03				1.05±0.03
	*θ = 65° in this case				
U-236					
6.0	1.00±0.25				4.6±0.8
6.5	1.00±0.1		2.06±0.2		2.55±0.25
7.0	1.00±0.06		1.65±0.10		2.11±0.12
8.0	1.00±0.04		1.39±0.06		1.66±0.07
9.0	1.00±0.04	1.10±0.07	1.15±0.04	1.31±0.08*	1.46±0.05
10.0	1.00±0.03		1.07±0.03		1.28±0.04
14.0	1.00±0.02				1.03±0.02
	*θ = 65° in this case				
U-234					
6.5	1.00±0.1		1.41±0.14		1.98±0.20
7.0	1.00±0.05		1.19±0.06		1.53±0.08
8.0	1.00±0.03		1.11±0.03		1.30±0.04
10.0	1.00±0.03				1.12±0.03
15.0	1.00±0.03				1.01±0.03
Pu-240					
6.5	1.00±0.10		1.49±0.15		1.55±0.16
7.0	1.00±0.06		1.03±0.06		1.35±0.08
8.0	1.00±0.03		1.01±0.03		1.21±0.04
15.0	1.00±0.02				1.01±0.02

The values quoted are counts observed for unit X-ray dose normalized to unit yield at θ = 0°. No corrections have been applied.

REF.

A. P. Baerg, R. M. Bartholomew, F. Brown, L. Katz, and S. B. Kowalski
Can. J. Phys. 37, 1418 (1959) (A.E.C.L. No. 896)

ELEM. SYM.	A	Z
Pu	240	94

METHOD

[Page 2 of 2]

Betatron with ionization chamber detector, enriched samples.

REF. NO.	
59 Ba 4	EGF

REACTION	RESULT	EXCITATION ENERGY	SOURCE		DETECTOR		ANGLE
			TYPE	RANGE	TYPE	RANGE	

TABLE IV

Relative fissionabilities, U-238 = 100 at 20 Mev

E_0	U-234	U-235	U-236	U-238	Pu-239	Pu-240
6.0		0.45±0.05	0.303±0.013	0.387±0.040		
6.5	1.165±0.033	1.134±0.025	1.159±0.026	1.08±0.07	0.239±0.024	1.145±0.051
7.0	2.515±0.053	2.282±0.038	2.358±0.037	2.14±0.14	4.50±0.22	2.528±0.075
8.0	6.285±0.085	5.519±0.067	5.285±0.056	4.87±0.24	11.35±0.34	6.09±0.12
9.0		11.00±0.33	8.94±0.13	8.65±0.26		
10.0	17.36±0.53	18.75±0.30	14.29±0.20	14.41±0.28	45.1±2.2	
14.0		88.0±4.5	43.11±0.53	57.7±1.4		
15.0	84.3±1.9	119.0±0.9	73.58±0.78	70.5±1.8	255.0±7.6	82.3±1.8
20.0	127.5±2.5	180.8±2.2	109.4±1.0	100±2.5	352±10	120.8±2.3

TABLE VI

Corrected values of α in $W(\theta) = 1+\alpha \sin^2\theta$

E_0	Th-232	U-238	U-236	U-234	Pu-240
6.0		6.6±2	6.0±2.3		
6.3		6.7±1.1			
6.5	>25	4.4±1.0	2.1±0.4	2.3±0.6	0.65±0.20
7.0	11.0±0.8	2.05±0.24	1.33±0.17	0.90±0.16	0.49±0.12
7.5	10.3±1.6				
8.0	4.9±0.6	1.3±0.1	0.79±0.09	0.44±0.08	0.29±0.07
9.0	2.8±0.4		0.51±0.07		
9.4		0.44±0.04			
10.0	1.61±0.12	0.41±0.05	0.32±0.06	0.17±0.07	
14.0	0.46±0.09	0.09±0.04	0.04±0.03		
15.0				0.02±0.04*	0.01±0.03*
20.0	0.14±0.06	0.05±0.03			

*These values, which do not differ from zero, have not been corrected for isotopic composition.

REF. N. S. Rabotnov, G. N. Smirenkin, A. S. Soldatov, L. N. Ysachev, S. P. Kapitza and Yu. M. Tsipeniuk
Phys. Letters 26B, 218 (1968)

ELEM. SYM.	A	Z
Pu	240	94

METHOD

REF. NO. 68 Ra 1 EGF

REACTION	RESULT	EXCITATION ENERGY	SOURCE		DETECTOR		ANGLE
			TYPE	RANGE	TYPE	RANGE	
G,F	NOX	THR-8	C	5-8	FRG-I		DST

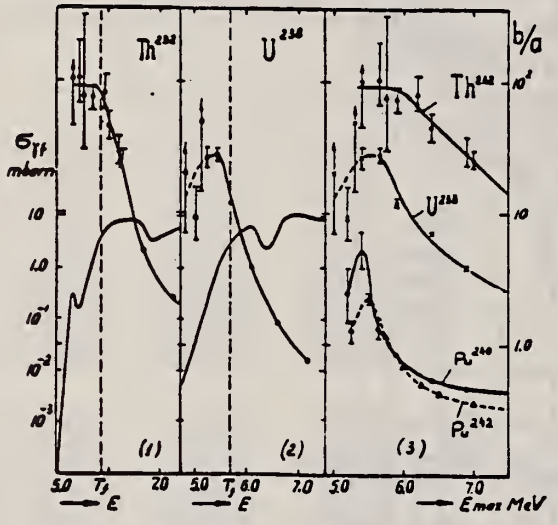

Fig. 1. The measured value of b/a as a function of energy. Photofission cross sections taken from ref. 1 are also shown for ^{232}Th and ^{238}U. E is the average excitation energy of the fissioning nuclei and T_f the observable fission threshold.

REF.

S. P. Kapitza, N. S. Rabotnov, G. N. Smirenkin, A. S. Soldatov, L. N. Usachev, Yu. M. Ysipenyuk
ZhETF Pis. Red. 9, 128 (1969); JETP Letters 9, 73 (1969)

ELEM. SYM.	A	Z
Pu	240	94

METHOD

REF. NO.	
69 Ka 1	hmg

REACTION	RESULT	EXCITATION ENERGY	SOURCE		DETECTOR		ANGLE
			TYPE	RANGE	TYPE	RANGE	
G,F	ABX	THR-8	C	5-8	TRK-I		DST

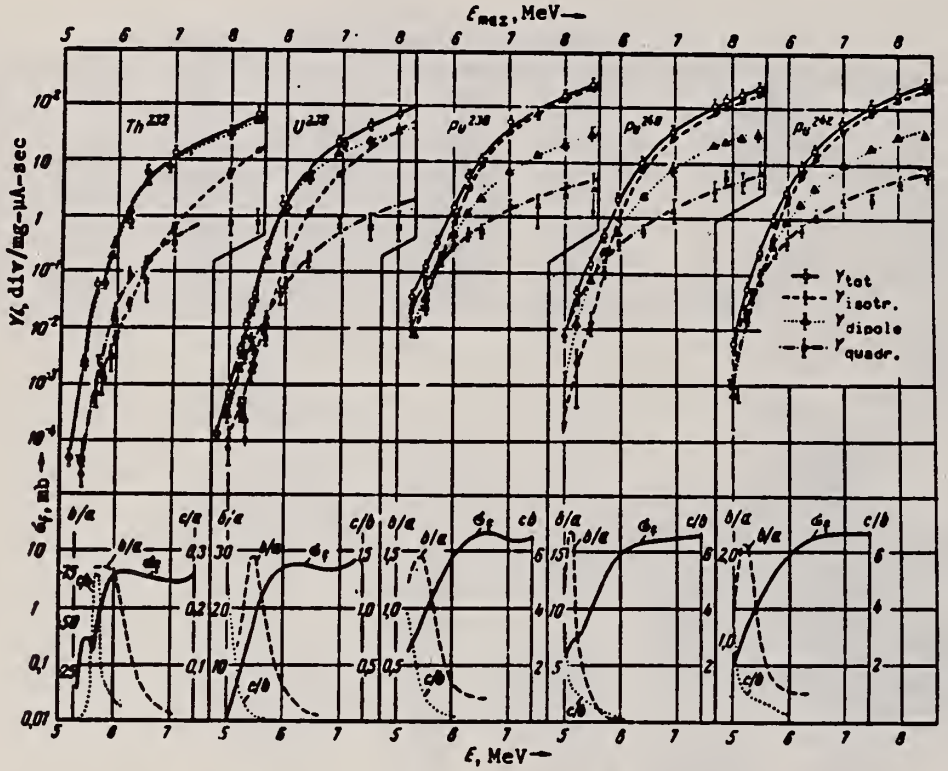

Fig. 2. Results of measurements of the fragment yields corresponding to different components of the angular distribution, as functions of the end-point energy of the bremsstrahlung spectrum (upper plots) and fission cross section and values of the ratios b/a and c/b as functions of the energy of the γ quanta, obtained as a result of the reduction of the experimental data (lower plots).

REF. N.S. Rabotnov, G.N. Smirenkin, A.S. Soldatov, L.N. Usachev, S.P. Kapitza, and Yu. M. Tsipenyuk
Yad. Fiz. 11, 508 (1970)
Sov. J. Nucl. Phys. 11, 285 (1970)

ELEM. SYM.	A	Z
Pu	240	94

METHOD

REF. NO. 70 Ra 1 hmg

REACTION	RESULT	EXCITATION ENERGY	SOURCE TYPE	SOURCE RANGE	DETECTOR TYPE	DETECTOR RANGE	ANGLE
G,F	ABX	THR-9	C	5-10	TRK-D		DST

SEE 68RA1, 69KA1

Table II. Parameters of angular distributions of the fragments

E_{max}, MeV	a	b	c	Y, fission mg·μ-sec
		Th^{232}		
5.2	—	—	—	$4.5\cdot10^{-6}$
5.4	0.009±0.009	0.991±0.027	0.030±0.025	0.024
5.65	0.011±0.005	0.989±0.007	−0.005±0.006	0.059
5.75	0.015±0.010	0.985±0.033	0.013±0.033	0.062
5.9	0.010±0.005	0.990±0.016	0.004±0.015	0.20
5.95	0.014±0.004	0.986±0.009	0.071±0.010	0.32
6.2	0.012±0.003	0.988±0.010	0.079±0.010	0.79
6.5	0.022±0.005	0.978±0.015	0.022±0.014	5.4
6.7	0.021±0.002	0.977±0.009	0.009±0.008	9.8
6.9	0.032±0.007	0.968±0.024	0.020±0.022	7.7
7.0	0.036±0.004	0.961±0.013	0.038±0.012	13.5
7.3	0.056±0.006	0.944±0.020	0.041±0.017	19.5
7.7	0.088±0.005	0.912±0.015	0.024±0.013	40.5
8.0	0.109±0.006	0.891±0.013	0.026±0.012	35
8.5	0.164±0.004	0.836±0.008	0.017±0.008	71
10.0	0.304±0.009	0.696±0.014	−0.031±0.014	—
		U^{238}		
5.0	0.052±0.100	0.948±0.164	1.206±0.205	0.00071
5.2	0.100±0.035	0.900±0.060	0.910±0.060	0.0052
5.3	0.020±0.035	0.980±0.064	0.566±0.076	0.0120
5.4	0.007±0.024	0.993±0.050	0.412±0.066	0.0.0
5.45	0.038±0.009	0.962±0.017	0.155±0.021	0.014
5.65	0.034±0.005	0.966±0.011	0.040±0.009	0.27
5.95	0.078±0.005	0.922±0.004	0.039±0.014	1.7
6.4	0.127±0.005	0.873±0.009	0.035±0.008	6.0
6.95	0.213±0.005	0.787±0.008	0.057±0.008	24.0
7.5	0.264±0.006	0.636±0.010	0.021±0.011	47.0
8.0	0.401±0.005	0.599±0.006	0.014±0.007	74.0
9.25	0.570±0.006	0.430±0.007	0.013±0.007	—
		Pu^{239}		
5.25	0.408±0.103	0.592±0.139	1.412±0.139	0.011
5.5	0.330±0.063	0.670±0.085	1.513±0.112	0.14
5.75	0.414±0.047	0.586±0.056	0.651±0.055	0.47
6.0	0.526±0.011	0.474±0.016	0.370±0.018	1.7
6.25	0.666±0.008	0.334±0.011	0.180±0.013	5.9
6.5	0.733±0.012	0.267±0.016	0.090±0.018	11
7.0	0.772±0.011	0.228±0.016	0.068±0.017	36
7.5	0.785±0.012	0.215±0.017	0.032±0.019	80
8.0	0.813±0.013	0.187±0.017	0.029±0.018	160
8.5	0.828±0.015	0.172±0.020	0.023±0.022	270
		Pu^{240}		
5.0*	0.000±0.200	0.000±0.200	1±0.200	0.0051
5.2	0.115±0.097	0.885±0.111	2.58±0.15	0.047

*In this case W(ϑ) is described by a pure quadrupole distribution, ~$\sin^2 2\vartheta$, and therefore the coefficient c is meaningless in the employed normalization and is assumed equal to unity.

Table II (cont.)

E_{max}, MeV	a	b	c	Y, Y, fission mg·μ-sec
		Pu^{242}		
5.15	0.102±0.014	0.898±0.056	1.147±0.070	0.15
5.7	0.222±0.014	0.778±0.052	0.710±0.052	0.49
5.95	0.533±0.010	0.467±0.011	0.331±0.013	2.3
6.4	0.670±0.012	0.330±0.012	0.096±0.013	11.5
6.95	0.689±0.025	0.311±0.027	0.067±0.029	30
7.7	0.716±0.012	0.284±0.016	0.055±0.017	115
7.9	0.725±0.012	0.275±0.016	0.074±0.018	145
8.2	0.762±0.010	0.238±0.014	0.046±0.015	180
8.5	0.779±0.020	0.221±0.027	0.057±0.029	230
8.7	0.791±0.009	0.209±0.012	0.032±0.014	230
9.5	0.822±0.011	0.178±0.014	0.019±0.016	680
5.0	0.832±0.303	0.168±0.372	3.702±0.424	0.0055
5.25	0.448±0.053	0.552±0.068	0.965±0.052	0.056
5.75	0.418±0.016	0.582±0.050	1.018±0.069	—
5.5	0.310±0.022	0.690±0.029	0.735±0.033	0.26
5.75	0.488±0.008	0.512±0.010	0.422±0.012	1.9
6.0	0.598±0.011	0.402±0.016	0.207±0.018	2.7
6.25	0.660±0.012	0.340±0.017	0.138±0.019	8.8
6.5	0.700±0.009	0.300±0.013	0.122±0.014	17
7.0	0.740±0.005	0.260±0.007	0.075±0.008	50
7.5	0.754±0.005	0.246±0.007	0.076±0.008	105
8.0	0.766±0.008	0.234±0.008	0.017±0.009	175
8.5	0.814±0.005	0.186±0.007	0.052±0.008	225

$$W(\theta) = a + b \sin^2\theta + c \sin^2 2\theta$$

[over]

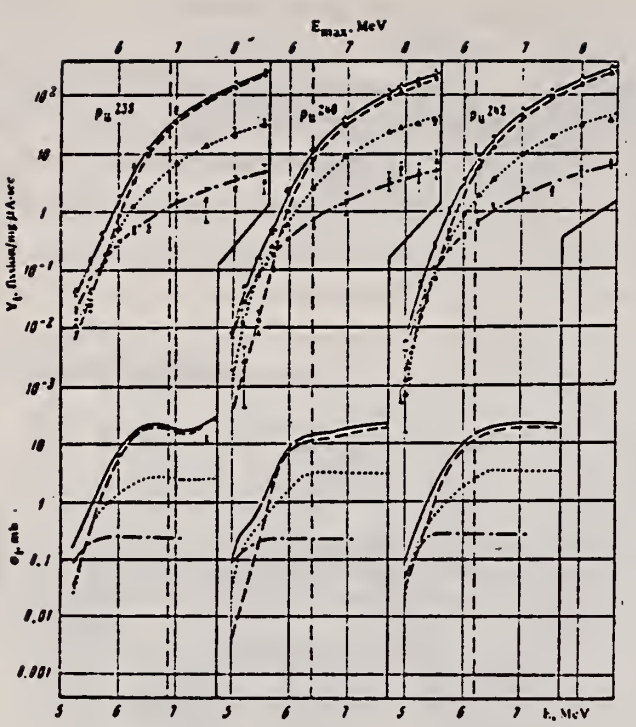

Angular components of the yield. Knowledge of the coefficients a, b, and c makes it possible to determine the contribution of the individual components of the yield Y_a, Y_b, and Y_c, the angular dependence of which corresponds to three components in the expression (2): isotropic, dipole, and quadrupole. Their meaning can be understood from the following definitions:

$$Y = Y_a + Y_b + Y_c; \quad \frac{dY}{d\Omega} = \frac{1}{4\pi\nu} YW(\vartheta);$$

$$Y_a = \frac{a}{\nu} Y; \quad Y_b = \frac{2}{3}\frac{b}{\nu} Y; \quad Y_c = \frac{8}{15}\frac{c}{\nu} Y. \qquad (4)$$

Plots of Y_i and E_{max} are shown in Fig. 3 together with the data on the total yield. The experimental points $Y_i(E_{max})$ were determined by means of formulas (4) from the coefficients $W(\vartheta)$ listed in Table II and from the total yield. The error of Y_i indicated in Fig. 3 does not include the error in the measurement of $Y(E_{max})$ ($\sim 10\%$).

REF. W. Günther, K. Huber, U. Kneissl, H. Krieger, H. Ries, H. Ströher, W. Wilke, H.J. Maier
Nucl. Phys. A350, 1 (1980)

ELEM. SYM.	A	Z
Pu	240	94

METHOD

REF. NO. 80 Gu 5 hg

REACTION	RESULT	EXCITATION ENERGY	SOURCE		DETECTOR		ANGLE
			TYPE	RANGE	TYPE	RANGE	
G,XN	RLY	THR-45	C	45	SPK		4PI

YLD FISSION ISOMERS

Abstract: Half-lives and yields in photonuclear reactions have been measured for shape isomers in U and Pu isotopes by pulsed-beam techniques bombarding ^{235,238}U and ^{239,240,242}Pu targets with bremsstrahlung. Isomeric fission cross sections have been deduced from the measured isomeric to prompt yield ratios within an evaporation model using absolute prompt fission data. The results are compared with data from particle-induced reactions.

E NUCLEAR REACTIONS ^{240}Pu^{235}U(γ, xn), ^{238}U, ^{239}Pu(γ, 2n), ^{242}Pu(γ, n); bremsstrahlung; measured $T_{1/2}$, isomeric to prompt yield ratios, ^{236}U, ^{237}Pu, ^{239}Pu, ^{241}Pu levels, deduced σ for isomeric fission. Natural and enriched targets.

TABLE 2

Results of isomeric fission experiments performed at Giessen

Reaction	Isomer	Half-life	Y_{iso}/Y_{pr}	Detector
^{232}Th(γ, xn)			$<10^{-6}$	PPAD
^{235}U (γ, xn)			$<10^{-7}$	PPAD
^{238}U (γ, 2n)	^{236}U	115 ± 5 ns	$(2.02\pm0.16)\times10^{-5}$	Si
		118 ± 7 ns	$(2.10\pm0.16)\times10^{-5}$	PPAD
^{239}Pu (γ, 2n)	^{237m_1}Pu	77 ± 16 ns	$(6.4\pm1.7)\times10^{-6}$	Si
		87 ± 11 ns	$(4.9\pm0.7)\times10^{-6}$	PPAD
	^{237m_2}Pu	1050 ± 400 ns	$(0.83\pm0.22)\times10^{-6}$	Si
^{240}Pu (γ, n)	^{239m_1}Pu	6.5 ± 0.4 μs	$(7.9\pm0.4)\times10^{-5}$	PPAD
^{240}Pu(γ, xn)	?	4.5 ± 1.5 ns	$<1.1\times10^{-4}$	PPAD
^{242}Pu(γ, n)	^{241m_1}Pu	20.5 ± 2.5 μs	$(9.2\pm0.8)\times10^{-5}$	PPAD
	^{241m_2}Pu	34 ± 7 ns	$(3.7\pm0.7)\times10^{-5}$	PPAD

TABLE 5

Isomeric fission cross sections for (γ, n) reactions

Reaction	E_0 (MeV)	$Y_{iso}/Y_{pr}\times10^5$	σ_{iso}^{max} (μb)	E_{max} (MeV)	Ref.
^{235}U(γ, n)	45	≤0.01	<0.05	11.4†	this work
^{240}Pu(γ, n)	15.5		170 ± 60	11.5	Gangrsky *et al.* [3])
	45	7.9 ± 0.4	49 ± 3	12.3†	this work
^{242}Pu(γ, n)^{241m_1}Pu	12.5	115 ± 25	200 ± 60	10.5	Gangrsky *et al.* [3])
	40	9.2 ± 0.8	54 ± 5	12.0†	this work
^{242}Pu(γ, n)^{241m_2}Pu	48	3.7 ± 0.7			
^{241}Am(γ, n)	13	40 ± 10	150 ± 50	11.2	Gangrsky *et al.* [3])
	41	13 ± 1.5	60 ± 8	12.0	Kuznetsov *et al.* [4])
^{243}Am(γ, n)	12.5	70 ± 20	130 ± 50	10.6	Gangrsky *et al.* [3])
	41	18.5 ± 2.5	80 ± 10	12.0	Kuznetsov *et al.* [4])

† The shape of the cross section was calculated (see text).

REF. H. Thierens, A. De Clercq, E. Jacobs, D. De Frenne, P. D'hondt, P. De Gelder, A.J. Deruytter
Phys. Rev. C23, 2104 (1981)

ELEM. SYM.	A	Z
Pu	240	94

METHOD

REF. NO. 81 Th 1 hg

REACTION	RESULT	EXCITATION ENERGY	SOURCE TYPE	SOURCE RANGE	DETECTOR TYPE	DETECTOR RANGE	ANGLE
G,F	ABX	THR-30.	C	12-30	SCD-D		4PI

Energy correlation measurements were performed for ^{240}Pu(s.f.), ^{239}Pu(n_{th},f), and the photofission of ^{240}Pu with 12-, 15-, 20-, and 30-MeV bremsstrahlung. The photofission cross section for ^{240}Pu was determined up to 30 MeV, which permitted the calculation of the average excitation energy $\langle E_{exc}\rangle$ of the compound nucleus. The average total kinetic energy $\langle E_k\rangle$ of the fragments for ^{240}Pu(s.f.) was found to be 1.2±0.5 MeV higher than for ^{239}Pu(n_{th},f). A decrease of $\langle E_k\rangle$, with $\langle E_{exc}\rangle$, $d\langle E_k\rangle/d\langle E_{exc}\rangle = -0.37\pm0.08$, is observed in the photofission of ^{240}Pu. Fragment shell effects are present in the kinetic energy and mass distributions for ^{240}Pu(s.f.). Changes in the measured distributions with increasing excitation energy of the compound nucleus ^{240}Pu are discussed in the framework of the scission point model of Wilkins *et al.*

ENERGY, MASS DISTRIB

PACS numbers: 25.85. − w, 24.75. + i

[RADIOACTIVITY Fission ^{240}Pu(s.f.).
NUCLEAR REACTIONS Fission ^{239}Pu(n_{th},f), ^{240}Pu(γ,f), $E_{\gamma max}$=12, 15, 20, 30 MeV; measured: photofission yields, fragment energies E_1, E_2; deduced: $\sigma(\gamma,f)$, $N(\mu,E_k)/\langle E_{exc}(E_\gamma)\rangle$.]

TABLE I. Parameters of the overall kinetic energy and mass distributions for ^{240}Pu(s.f.), ^{239}Pu(n_{th},f), and the photofission of ^{240}Pu.

	^{240}Pu(s.f)	^{239}Pu(n_{th},f)	^{240}Pu(γ,f) E_γ=12 MeV	E_γ=15 MeV	E_γ=20 MeV	E_γ=30 MeV
NEV	7262	101×10^3	12×10^3	51×10^3	355×10^3	113×10^3
$\langle E_k\rangle$ (MeV)	177.25 ± 0.30	175.57	173.99 ± 0.24	173.25 ± 0.24	172.46 ± 0.20	172.22 ± 0.31
$\langle E_k^*\rangle$ (MeV)	178.85 ± 0.30	177.69	176.39 ± 0.24	175.80 ± 0.24	175.15 ± 0.20	174.98 ± 0.31
σ_{E_k} (MeV)	11.99 ± 0.20	11.84	11.86 ± 0.14	11.94 ± 0.15	12.22 ± 0.12	12.37 ± 0.10
$\langle\mu_L\rangle$ (u)	101.53 ± 0.20	100.68	100.50 ± 0.14	100.48 ± 0.09	100.57 ± 0.08	100.72 ± 0.14
$\langle\mu_H\rangle$ (u)	138.47 ± 0.20	139.32	139.50 ± 0.14	139.52 ± 0.09	139.43 ± 0.08	139.28 ± 0.14
$\sigma_{\mu_L}=\sigma_{\mu_H}$ (u)	5.70 ± 0.12	6.69	7.16 ± 0.10	7.36 ± 0.08	7.64 ± 0.06	7.82 ± 0.08
$\langle m_L^*\rangle$ (u)	101.26 ± 0.20	100.33	100.12 ± 0.14	100.08 ± 0.09	100.16 ± 0.08	100.29 ± 0.14
$\langle m_H^*\rangle$ (u)	138.74 ± 0.20	139.67	139.88 ± 0.14	139.92 ± 0.09	139.84 ± 0.08	139.71 ± 0.14
σ/V	400 ±180	100 ±9	27 ±3	20.6 ±1.3	13.1 ±0.4	9.3 ±0.3
S_{exc} (MeV)	0	6.5	9.4	11.1	12.6	13.3

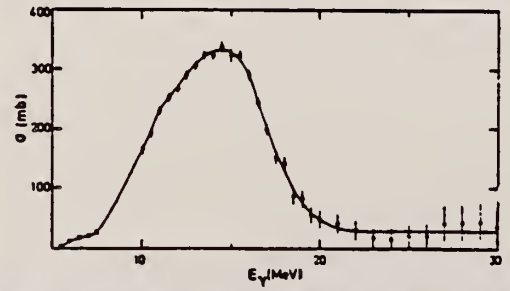

FIG. 1. Photofission cross section of ^{240}Pu, including second and multiple chance fission.

[16] J. T. Caldwell, E. J. Dowdy, B. L. Berman, R. A. Alvarez, and P. Meyer, Phys. Rev. C 21, 1215 (1980).

(OVER)

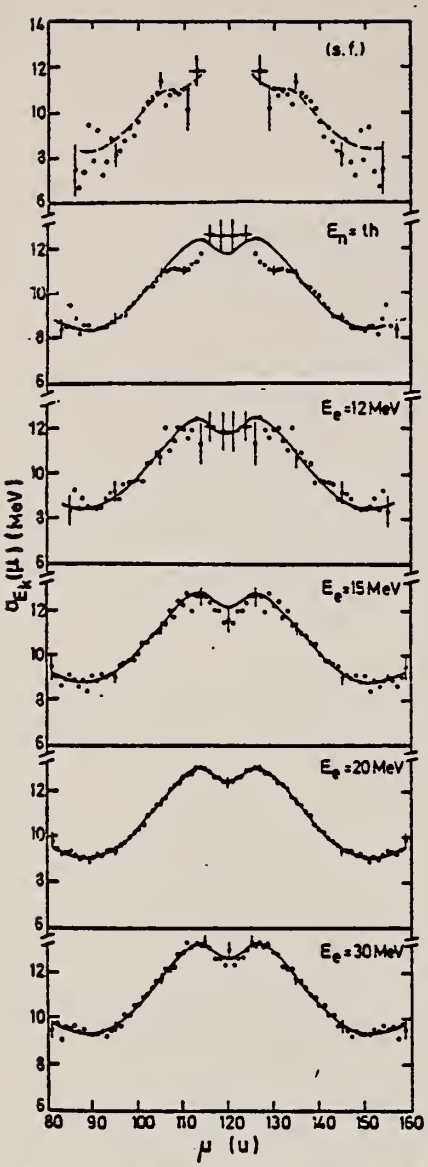

FIG. 6. Variance $\sigma_{E_k}(\mu)$ of the total kinetic energy distributions, as a function of the provisional fragment mass for ^{240}Pu(s.f.), ^{239}Pu(n_{th},f), and the photofission of ^{240}Pu. The end-point energy of the bremsstrahlung is indicated by E_e.

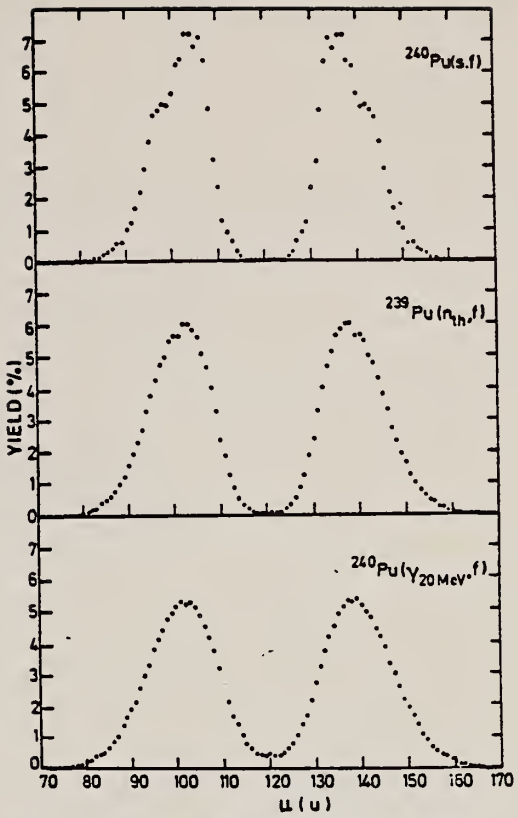

FIG. 7. Provisional mass distribution for ^{240}Pu(s.f.), ^{239}Pu(n_{th},f) and the photofission of ^{240}Pu with 20-MeV bremsstrahlung.

Error bars show statistical uncertainty only. Cross section normalized to that of Caldwell et al. (16)

Pu
A=241

Pu
A=241

REF. V.E. Zhuchko, Yu.B. Ostapenko, G.N. Smirenkin, A.S. Soldatov,
Yad. Fiz. 28, 1170 (1978)
Sov. J. Nucl. Phys. 28, 602 (1978)

ELEM. SYM.	A	Z
Pu	241	94

METHOD

REF. NO. 78 Zh 7 hg

REACTION	RESULT	EXCITATION ENERGY	SOURCE		DETECTOR		ANGLE
			TYPE	RANGE	TYPE	RANGE	
G,F	ABX	THR-7	C	4-7	TRK-D		4PI
				(4.4-7.)			

The bremsstrahlung beam of the microtron at our Institute has been used to measure photofission yields of nine nuclei—^{232}Th, ^{233,235,236,238}U, ^{237}Np, ^{239,241}Pu, and ^{241}Am in the energy region 4.4–7.0 MeV. The method of minimization of the directed deviation was used to reproduce the photofission cross sections from the integrated yields. The following problems are discussed in terms of the experimental data: resonance structure of the cross sections, effects of a two-humped shape of the fission barrier, and comparison of the fissility in the (γ,f) and (n,f) reactions and in direct reactions.

PACS numbers: 25.85.Jg

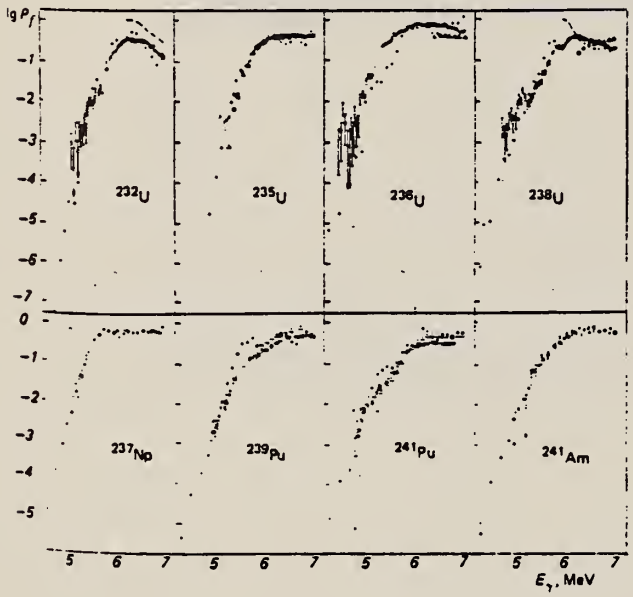

FIG. 4. Fissility P_f in the reactions (γ,f)—●, (n,f)—△ (Ref. 14), and in direct reactions—○.[2] The dashed curve shows the results of evaluation of P_f in accordance with Eq. (9).

(over)

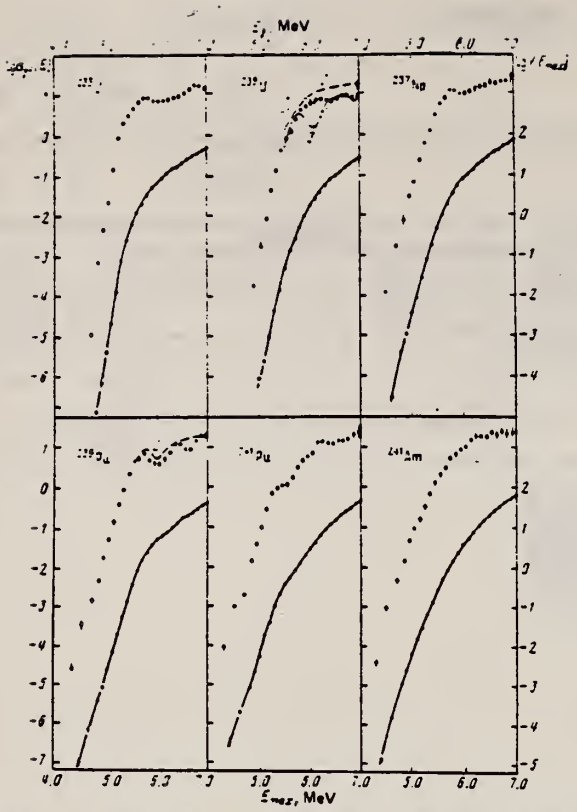

FIG. 3. Yields $Y(E_{max})$, fissions/mg-μC, and cross sections $\sigma_{\gamma f}(E_\gamma)$, mb, for odd isotopes. The designations are the same as in Fig. 2.

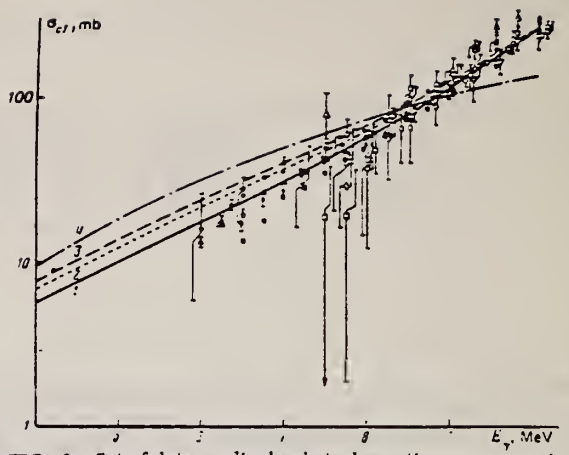

FIG. 6. Set of data on dipole photoabsorption cross sections σ_{cl}. The solid line (1)—the present work—is the result of fitting the data of Ref. 6 by Eq. (2) in the region $E_\gamma = 6$–10 MeV. Curves 2 and 3 are an extrapolation of the fit from Ref. 16 (2) and Ref. 17 (3) for ^{238}U; curve 4 is an estimate by means of Axel's formula.[15] Points: □, ■—^{232}Th; △, ▲—^{235}U; ♦—^{236}U; ○, ●—^{238}U; ▽, ▼—^{237}Np; ◇—^{239}Pu. The hollow points are from Refs. 16 and 17; the solid points are from Ref. 6.

Pu
A=242

Pu
A=242

Pu
A=242

REF. N. S. Rabotnov, G. N. Smirenkin, A. S. Soldatov, L. N. Ysachev, S. P. Kapitza and Yu. M. Tsipeniuk
Phys. Letters 26B, 218 (1968)

ELEM. SYM.	A	Z
Pu	242	94

METHOD

REF. NO. 68 Ra 1 EGF

REACTION	RESULT	EXCITATION ENERGY	SOURCE		DETECTOR		ANGLE
			TYPE	RANGE	TYPE	RANGE	
G,F	NOX	THR-8	C	5-8	FRG-I		DST

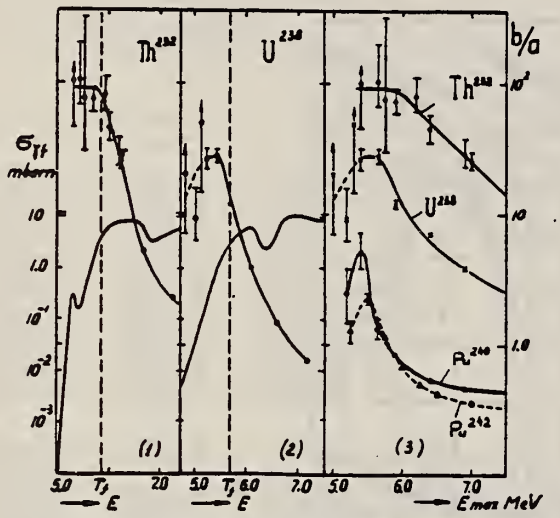

Fig. 1. The measured value of b/a as a function of energy. Photofission cross sections taken from ref. 1 are also shown for ^{232}Th and ^{238}U. E is the average excitation energy of the fissioning nuclei and T_f the observable fission threshold.

S. P. Kapitza, N. S. Rabotnov, G. N. Smirenkin, A. S. Soldatov, L. N. Usachev, Yu. M. Ysipenyuk
ZhETF Pis. Red. 9, 128 (1969); JETP Letters 9, 73 (1969)

ELEM. SYM.	A	Z
Pu	242	94

METHOD

REF. NO.	
69 Ka 1	hmg

REACTION	RESULT	EXCITATION ENERGY	SOURCE		DETECTOR		ANGLE
			TYPE	RANGE	TYPE	RANGE	
G,F	ABX	THR-8	C	5-8	TRK-I		DST

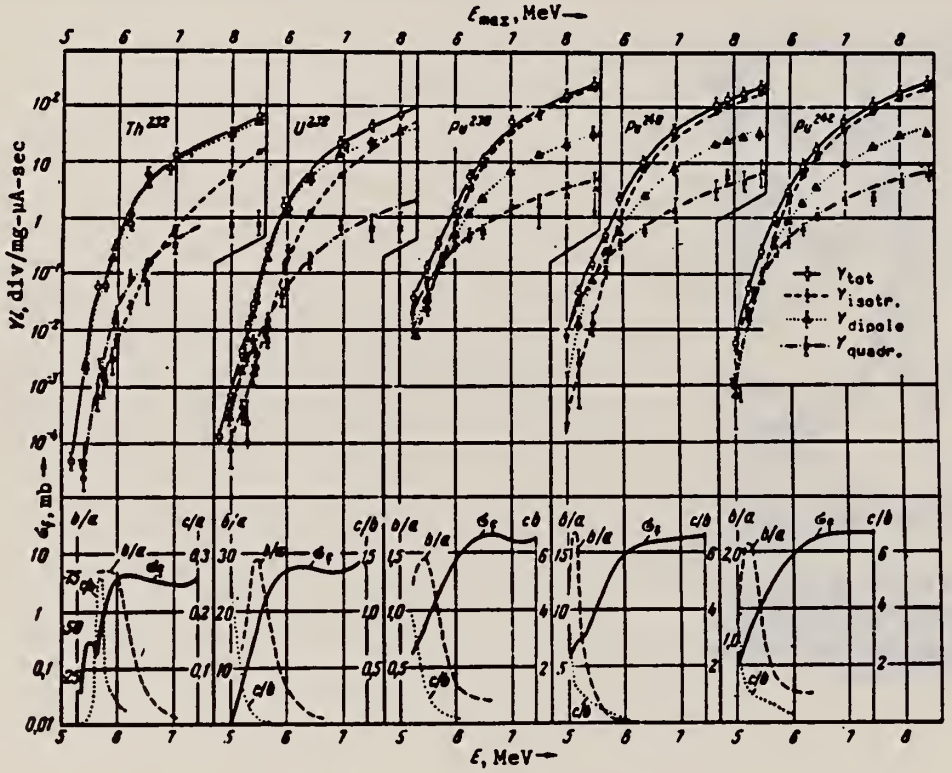

Fig. 2. Results of measurements of the fragment yields corresponding to different components of the angular distribution, as functions of the end-point energy of the bremsstrahlung spectrum (upper plots) and fission cross section and values of the ratios b/a and c/b as functions of the energy of the γ quanta, obtained as a result of the reduction of the experimental data (lower plots).

REF. N.S. Rabotnov, G.N. Smirenkin, A.S. Soldatov, L.N. Usachev, S.P. Kapitza, and Yu. M. Tsipenyuk
Yad. Fiz. 11, 508 (1970)
Sov. J. Nucl. Phys. 11, 285 (1970)

ELEM. SYM.	A	Z
Pu	242	94

METHOD

REF. NO. 70 Ra 1 hmg

REACTION	RESULT	EXCITATION ENERGY	SOURCE TYPE	SOURCE RANGE	DETECTOR TYPE	DETECTOR RANGE	ANGLE
G,F	ABX	THR-9	C	5-10	TRK-D		DST

SEE 68RA1, 69KA1

Table II. Parameters of angular distributions of the fragments

E_{max}, MeV	a	b	c	Y, fission, mg·μ·sec
		Th^{232}		
5.2	—	—	—	$4.5\cdot10^{-4}$
5.4	0.009±0.009	0.991±0.027	0.030±0.025	0.0024
5.65	0.011±0.005	0.989±0.007	−0.005±0.006	0.059
5.75	0.015±0.010	0.985±0.033	0.015±0.033	0.062
5.9	0.010±0.005	0.990±0.016	0.084±0.014	0.20
5.95	0.014±0.004	0.986±0.009	0.074±0.010	0.32
6.2	0.012±0.003	0.988±0.010	0.079±0.010	0.79
6.5	0.022±0.005	0.978±0.015	0.022±0.014	3.4
6.7	0.023±0.002	0.977±0.009	0.060±0.008	9.8
6.9	0.032±0.007	0.968±0.024	0.029±0.022	7.7
7.0	0.036±0.005	0.965±0.013	0.038±0.012	13.5
7.3	0.056±0.006	0.944±0.020	0.031±0.017	19.5
7.7	0.088±0.005	0.912±0.015	0.029±0.013	30.5
8.0	0.109±0.006	0.891±0.013	0.026±0.012	35
8.5	0.164±0.004	0.836±0.008	0.017±0.008	71
10.0	0.301±0.009	0.696±0.014	−0.031±0.014	—
		U^{238}		
5.0	0.052±0.100	0.948±0.164	1.296±0.295	0.00071
5.2	0.100±0.035	0.900±0.061	0.910±0.090	0.0042
5.3	0.020±0.035	0.980±0.065	0.566±0.076	0.0120
5.4	0.007±0.025	0.993±0.050	0.412±0.066	0.0.0
5.45	0.038±0.009	0.962±0.017	0.155±0.021	0.044
5.65	0.034±0.005	0.966±0.011	0.050±0.010	0.27
5.95	0.078±0.005	0.922±0.014	0.039±0.014	1.7
6.1	0.127±0.004	0.873±0.009	0.045±0.008	6.0
6.35	0.213±0.004	0.787±0.008	0.037±0.008	24.0
7.5	0..64±0.006	0.836±0.010	0.024±0.011	47.0
8.0	0.501±0.005	0.599±0.006	0.014±0.007	74.0
9.25	0.570±0.006	0.430±0.007	0.013±0.007	—
		Pu^{239}		
5.25	0.408±0.103	0.592±0.139	1.412±0.139	0.011
5.5	0.330±0.063	0.670±0.081	1.513±0.112	0.14
5.75	0.414±0.047	0.586±0.056	0.654±0.055	0.47
6.0	0.526±0.011	0.474±0.016	0.370±0.018	1.7
6.25	0.666±0.008	0.334±0.011	0.180±0.013	5.9
6.5	0.733±0.012	0.267±0.016	0.080±0.018	11
7.0	0.772±0.011	0.228±0.016	0.068±0.017	56
7.5	0.785±0.012	0.215±0.017	0.012±0.019	80
8.0	0.813±0.013	0.187±0.017	0.029±0.018	160
8.5	0.828±0.015	0.172±0.020	0.023±0.022	270
		Pu^{240}		
5.0*	0.000±0.200	0.000±0.200	1±0.200	0.0041
5.2	0.115±0.097	0.885±0.111	2.58±0.15	0.047

*In this case W(ϑ) is described by a pure quadrupole distribution, ~$\sin^2 2\vartheta$, and therefore the coefficient c is meaningless in the employed normalization and is assumed equal to unity.

Table II (cont.)

E_{max}, MeV	a	b	c	Y, Y. fission, mg·μ·sec
		Pu^{241}		
5.15	0.102±0.014	0.898±0.056	1.147±0.070	0.15
5.7	0.222±0.014	0.778±0.042	0.710±0.052	0.39
5.95	0.533±0.010	0.467±0.011	0.331±0.013	2.3
6.1	0.670±0.012	0.330±0.012	0.096±0.013	11.5
6.25	0.689±0.025	0.311±0.027	0.067±0.029	30
7.7	0.716±0.012	0.284±0.016	0.055±0.017	115
7.9	0.725±0.012	0.275±0.016	0.074±0.018	145
8.2	0.762±0.010	0.238±0.014	0.016±0.015	180
8.5	0.779±0.029	0.221±0.027	0.057±0.029	240
8.7	0.791±0.009	0.209±0.012	0.012±0.014	220
9.5	0.822±0.011	0.178±0.014	0.019±0.016	680
5.0	0.532±0.304	0.468±0.372	3.702±0.524	0.0055
5.25	0.548±0.051	0.452±0.068	0.965±0.082	0.056
5.5	0.518±0.038	0.482±0.059	1.018±0.069	—
5.5	0.310±0.022	0.690±0.029	0.734±0.033	0.26
5.75	0.488±0.008	0.512±0.010	0.422±0.012	1.0
6.0	0.598±0.011	0.402±0.018	0.207±0.018	2.7
6.25	0.669±0.012	0.331±0.017	0.138±0.019	8.8
6.5	0.700±0.009	0.300±0.013	0.122±0.014	17
7.0	0.740±0.005	0.260±0.007	0.075±0.008	50
7.5	0.754±0.005	0.246±0.007	0.076±0.008	105
8.0	0.766±0.006	0.234±0.008	0.047±0.009	175
8.5	0.814±0.005	0.186±0.007	0.032±0.008	225

$$W(\theta) = a + b \sin^2\theta + c \sin^2 2\theta$$

[over]

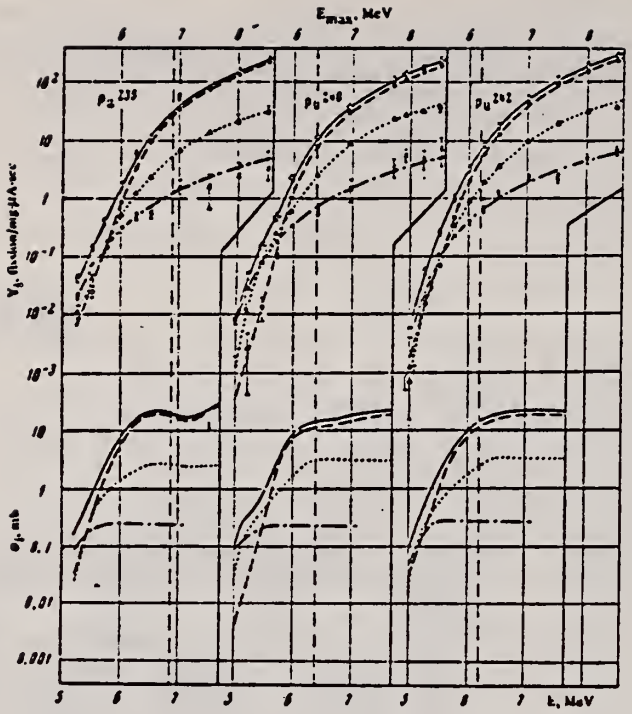

Angular components of the yield. Knowledge of the coefficients a, b, and c makes it possible to determine the contribution of the individual components of the yield Y_a, Y_b, and Y_c, the angular dependence of which corresponds to three components in the expression (2): isotropic, dipole, and quadrupole. Their meaning can be understood from the following definitions:

$$Y = Y_a + Y_b + Y_c; \quad \frac{dY}{d\Omega} = \frac{1}{4\pi\nu} YW(\vartheta);$$

$$Y_a = \frac{a}{\nu} Y; \quad Y_b = \frac{2}{3}\frac{b}{\nu} Y; \quad Y_c = \frac{8}{15}\frac{c}{\nu} Y. \qquad (4)$$

Plots of Y_i and E_{max} are shown in Fig. 3 together with the data on the total yield. The experimental points $Y_i(E_{max})$ were determined by means of formulas (4) from the coefficients $W(\vartheta)$ listed in Table II and from the total yield. The error of Y_i indicated in Fig. 3 does not include the error in the measurement of $Y(E_{max})$ ($\sim 10\%$).

REF. W. Günther, K. Huber, U. Kneissl, H. Krieger, H. Ries, H. Ströher, W. Wilke, H.J. Maier
Nucl. Phys. A350, 1 (1980)

ELEM. SYM.	A	Z
Pu	242	94

METHOD

REF. NO. 80 Gu 5 hg

REACTION	RESULT	EXCITATION ENERGY	SOURCE TYPE	SOURCE RANGE	DETECTOR TYPE	DETECTOR RANGE	ANGLE
G,N	RLY	THR-48	C	40,48	SPK -T		4PI

Abstract: Half-lives and yields in photonuclear reactions have been measured for shape isomers in U and Pu isotopes by pulsed-beam techniques bombarding ^{235,238}U and ^{239,240,242}Pu targets with bremsstrahlung. Isomeric fission cross sections have been deduced from the measured isomeric to prompt yield ratios within an evaporation model using absolute prompt fission data. The results are compared with data from particle-induced reactions.

YLD FISSION ISOMERS

E NUCLEAR REACTIONS ^{240}Pu^{235}U(γ, xn), ^{238}U, ^{239}Pu(γ, 2n), ^{242}Pu(γ, n); bremsstrahlung; measured $T_{1/2}$, isomeric to prompt yield ratios, ^{236}U, ^{237}Pu, ^{239}Pu, ^{241}Pu levels, deduced σ for isomeric fission. Natural and enriched targets.

TABLE 2

Results of isomeric fission experiments performed at Giessen

Reaction	Isomer	Half-life	Y_{iso}/Y_{pr}	Detector
^{232}Th(γ, xn)			$<10^{-6}$	PPAD
^{235}U (γ, xn)			$<10^{-7}$	PPAD
^{238}U (γ, 2n)	^{236}U	115 ± 5 ns	$(2.02\pm0.16)\times10^{-5}$	Si
		118 ± 7 ns	$(2.10\pm0.16)\times10^{-5}$	PPAD
^{239}Pu (γ, 2n)	^{237m_1}Pu	77 ± 16 ns	$(6.4\pm1.7)\times10^{-6}$	Si
		87 ± 11 ns	$(4.9\pm0.7)\times10^{-6}$	PPAD
	^{237m_2}Pu	1050 ± 400 ns	$(0.83\pm0.22)\times10^{-6}$	Si
^{240}Pu (γ, n)	^{239m_1}Pu	6.5 ± 0.4 μs	$(7.9\pm0.4)\times10^{-5}$	PPAD
^{240}Pu(γ, xn)	?	4.5 ± 1.5 ns	$<1.1\times10^{-4}$	PPAD
^{242}Pu(γ, n)	^{241m_1}Pu	20.5 ± 2.5 μs	$(9.2\pm0.8)\times10^{-5}$	PPAD
	^{241m_2}Pu	34 ± 7 ns	$(3.7\pm0.7)\times10^{-5}$	PPAD

TABLE 5

Isomeric fission cross sections for (γ, n) reactions

Reaction	E_0 (MeV)	$Y_{iso}/Y_{pr}\times10^5$	σ_{iso}^{max} (μb)	E_{max} (MeV)	Ref.
^{235}U(γ, n)	45	≤ 0.01	< 0.05	11.4†	this work
^{240}Pu(γ, n)	15.5		170 ± 60	11.5	Gangrsky *et al.* [3])
	45	7.9 ± 0.4	49 ± 3	12.3†	this work
^{242}Pu(γ, n)^{241m_1}Pu	12.5	115 ± 25	200 ± 60	10.5	Gangrsky *et al.* [3])
	40	9.2 ± 0.8	54 ± 5	12.0†	this work
^{242}Pu(γ, n)^{241m_2}Pu	48	3.7 ± 0.7			
^{241}Am(γ, n)	13	40 ± 10	150 ± 50	11.2	Gangrsky *et al.* [3])
	41	13 ± 1.5	60 ± 8	12.0	Kuznetsov *et al.* [4])
^{243}Am(γ, n)	12.5	70 ± 20	130 ± 50	10.6	Gangrsky *et al.* [3])
	41	18.5 ± 2.5	80 ± 10	12.0	Kuznetsov *et al.* [4])

† The shape of the cross section was calculated (see text).

REF. W. Gunther, K. Huber, U. Kneissl, H. Krieger, H. Ries, H. Stroher, W. Wilke
Nucl. Phys. A359, 397 (1981)

ELEM. SYM.	A	Z
Pu	242	94

METHOD

REF. NO. 81 Gu 1 hg

REACTION	RESULT	EXCITATION ENERGY	SOURCE		DETECTOR		ANGLE
			TYPE	RANGE	TYPE	RANGE	
G,NF	RLY	THR-80	C	40,48	SPK-I		4PI

Abstract: The half-lives and yield ratios for the two ^{241}Pu fission isomers have been measured in the ^{242}Pu(γ, n) reaction. The observed half-life for the long-lived isomer ($T_{1/2}$ = 20.5±2.2 μs) is in agreement with previous data, and the existence of a short-lived 34±7 ns isomer in ^{241}Pu could be confirmed. The measured yield ratios are $Y_{iso}/Y_{pr} = (9.2\pm0.8)\times10^{-5}$ and $Y_{iso}/Y_{pr} = (3.7\pm0.7)\times10^{-5}$, respectively. From a statistical model analysis of the isomeric fission yield ratio, $Y_{iso}^{long}/Y_{iso}^{short} = 2.5\pm0.6$, a spin assignment for the two isomers is attempted. Possible spin combinations are compared with single-particle shell-model calculations and with available spectroscopic data for the other even-odd Pu isotopes.

ISOMER YIELD RATIO

E NUCLEAR REACTIONS ^{242}Pu(γ, n), E = 40–48 MeV bremsstrahlung; measured $T_{1/2}$, isomeric to prompt yield ratio; ^{241}Pu levels deduced isomeric ratio, spins. Enriched target.

TABLE I
Comparison of results obtained for ^{241m_1,m_2}Pu

Reaction	Half-life	Y_{iso}/Y_{pr}	σ(μb)	Ref.
^{241}Pu(d, pn)	27 ±3 μs			[16]
^{240}Pu(d, p)			0.9±0.4	[16]
^{242}Pu(γ, n)	23 ±1 μs	(1.15±0.25)×10^{-3}		[14]
^{242}Pu(γ, n)	20.5±2.2 μs	(9.2 ±0.8)×10^{-5}		this work
^{240}Pu(d, p)	30 ±5 ns		0.5±0.09	[15]
^{242}Pu(γ, n)	34 ±7 ns	(3.7 ±0.7)×10^{-5}		this work

AMERICIUM
Z=95

The nature and similarity in the chemical properties of uranium, neptunium, and plutonium led Seaborg to realize that as a group, the transuranium elements resembled the rare earths, and that the higher transuranium elements should have properties similar to the heavier rare earths. Using this idea as a guide, element 96 was found almost at once in a sample of Pu^{239} that had been bombarded with helium ions in the cyclotron at Berkely. Element 95 was found in the fall of 1944 as a result of neutron irridiation of Pu^{239}. For nearly a year attempts at chemical separation failed and Seaborg reports that the yet unnamed elements were refered to as "pandemonium" and "delirium". The first pure compound of element 95 was obtained by B. B. Cunningham in 1945 and by analogue with europium, was named americium.

Am
A=241

Am
A=241

REF.

L. Katz, A. P. Baerg, and F. Brown
Peaceful Uses of Atomic Energy, Switzerland 1958

ELEM. SYM.	A	Z
Am	241	95

METHOD

Fission chamber

REF. NO. 58 Ka 2 EGF

REACTION	RESULT	EXCITATION ENERGY	SOURCE		DETECTOR		ANGLE
			TYPE	RANGE	TYPE	RANGE	
G,F	ABX	5-18	C	5-18	ION-I		DST

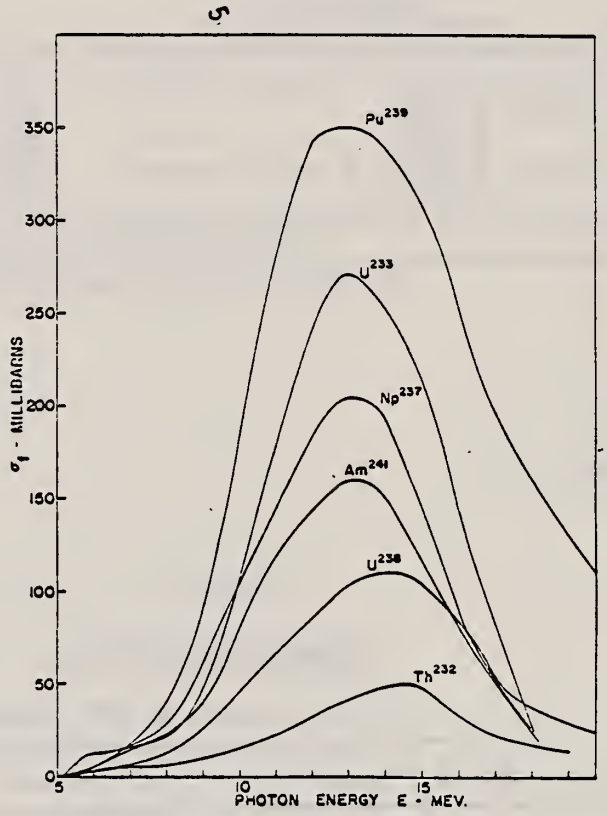

Fig. 5 - Photofission cross sections versus photon energy

REF.

L. Katz, A. P. Baerg, and F. Brown
Peaceful Uses of Atomic Energy, Switzerland 1958

ELEM. SYM.	A	Z
Am	241	95

METHOD

Fission chamber

REF. NO.	
58 Ka 2	EGF

REACTION	RESULT	EXCITATION ENERGY	SOURCE		DETECTOR		ANGLE
			TYPE	RANGE	TYPE	RANGE	

Fig. 7 - Low-energy-yield curves: fissions per roentgen-nucleus versus maximum bremsstrahlung energy. (The solid and dotted lines are samples of smoothed yield curves which fit the experimental data.)

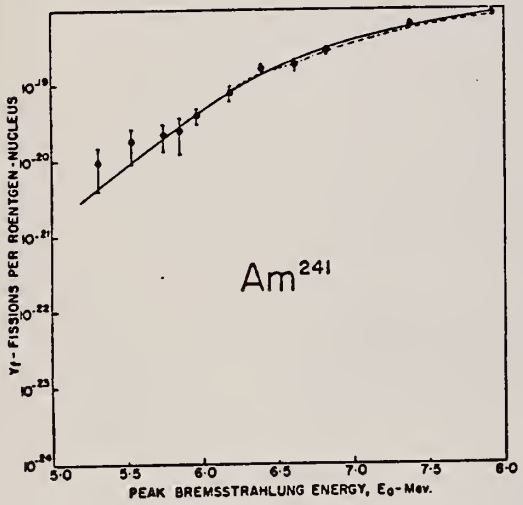

Table 4

Angular Distributions

Nuclide	Ratio, (Counts at 90°)/(Counts at 0°)[a] E_o = 8.0 Mev[b]	E_o = 10.0 Mev	E_o = 20.0 Mev
U-233	1.048 ± 0.07	1.032 ± 0.04	0.994 ± 0.03
U-235	1.024 ± 0.05		
Np-237	1.024 ± 0.10		
Pu-239	1.002 ± 0.06	1.013 ± 0.05	0.952 ± 0.03
Am-241	0.958 ± 0.07		

(a) The ratio is the number of counts observed at 90° per unit X-ray dose divided by the number observed at 0° for the same dose.

(b) E_o is the maximum energy of the bremsstrahlung spectrum.

A. P. Baerg, R. M. Bartholomew, F. Brown, L. Katz, and S. B. Kowalski
Can. J. Phys. 37, 1418 (1959) (A.E.C.L. No. 896)

Am	241	95

METHOD

Betatron with ionization chamber detector, enriched samples.

REF. NO. 59 Ba 4 EGF

REACTION	RESULT	EXCITATION ENERGY	SOURCE		DETECTOR		ANGLE
			TYPE	RANGE	TYPE	RANGE	
G,F	RLY	THR - 20	C	6-20	ION-I		DST

TABLE I

Angular distributions
Ratio, counts at 90°/counts at 0°*

Nuclide	E_0† = 6.0	E_0 = 6.5	E_0 = 8.0	E_0 = 10.0	E_0 = 20.0
U-233			1.048±0.07	1.032±0.04	0.994±0.03
U-235			1.024±0.05		
Np-237			1.024±0.10		
Pu-239‡	1.034±0.26	0.927±0.12	1.002±0.06	1.013±0.05	0.952±0.03
Am-241			0.958±0.07		

*The ratio is the number of counts observed at 90° per unit X-ray dose divided by the number observed at 0° for the same dose.
†E_0 is the maximum energy in million electron volts of the bremsstrahlung spectrum.
‡The 45°/0° ratio at E_0 = 6.5 Mev was 1.09±0.23.

REF. Yu. P. Gangrskii, B.N. Markov, and Yu. M. Tsipenyuk
Yad. Fiz. 11, 54 (1970)
Sov. J. Nucl. Phys. 11, 30 (1970)

ELEM. SYM.	A	Z
Am	241	95

METHOD

REF. NO. 70 Ga 1 hmg

REACTION	RESULT	EXCITATION ENERGY	SOURCE		DETECTOR		ANGLE
			TYPE	RANGE	TYPE	RANGE	
G,NF	THR	THR-14	C	10-13	SPK-D		4PI

PROMPT AND DELAYED F

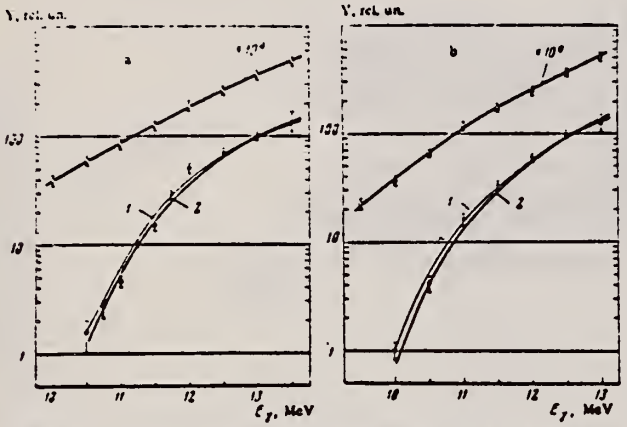

FIG. 2. Yield (Y) of prompt (O) and delayed (O) fission fragments as a function of bremsstrahlung end-point energy (E_γ) in bombardment of: a—Am^{241}, b—Am^{243}. Curves 1 were calculated for T = 0.7 MeV, and curves 2 for T = 1.5 MeV.

By combining the delayed fission fragment yields calculated in this way as a function of γ-ray energy with the experimental data (see Figs. 2a and b), we can determine the thresholds of the reactions leading to spontaneously fissile isomers. These thresholds turned out to be 9.95 ± 0.15 MeV for the reaction $Am^{241}(\gamma, n)Am^{240mf}$ and 9.55 ± 0.15 MeV for the reaction $Am^{243}(\gamma, n)Am^{242mf}$. The thresholds of the reactions leading to the ground states of Am^{240} and Am^{242} obviously are equal to the neutron binding energies in these nuclei, which are respectively 6.70 ± 0.20 and 6.27 ± 0.03 MeV.[8] The difference in the thresholds can evidently be considered as the excitation energy of the isomeric states, which is equal to 3.25 ± 0.25 MeV for Am^{240mf} and 3.30 ± 0.20 MeV for Am^{242mf}. Both these results agree within experimental error with the previously measured excitation energies, which are respectively 3.15 ± 0.25 MeV (Am^{240mf}[3]) and 2.9 ± 0.4 MeV (Am^{242mf}[9]).

In our work we measured also the yield ratios of delayed and prompt fission fragments, which turned out to be $(4 \pm 1) \times 10^{-4}$ for Am^{241} for a γ-ray energy of 13 MeV and $(7 \pm 2) \times 10^{-4}$ for Am^{243} for an energy of 12.5 MeV. By means of Eq. (1) we obtained the following ratios of cross sections for these energies: $(1.0 \pm 0.25) \times 10^{-3}$ for Am^{241} and $(1.3 \pm 0.4) \times 10^{-3}$ for Am^{243}. Knowing the value of the Am^{241} photofission cross section,[6] we can determine the cross section for formation of the isomer Am^{240mf}, which turned out to be 150 ± 40 μb. If we use the value $\Gamma_f/(\Gamma_n + \Gamma_f) = 0.32$,[6] then the isomeric ratio for the reaction $Am^{241}(\gamma, n)Am^{240}$ will be $(5 \pm 1.2) \times 10^{-4}$, which is close to the values obtained in reactions with charged particles and neutrons. In the case of Am^{242mf}, detailed calculation of the isomeric ratio is impossible because of the lack of absolute values of σ_f and $\Gamma_f/(\Gamma_n + \Gamma_f)$.

[3] S. Bjørnholm, J. Borggreen, L. Westgaard, and V. A. Karanukhov, Nucl. Phys. A95, 513 (1967).
[6] L. Katz, A.P. Baerg, and F. Brown, PUAE, 15, 188 (P/200), 1958.
[8] J. H. E. Mattauch, W. Thiele, and A. H. Wapstra, Nucl. Phys. 67, 1 (1965).
[9] G. N. Flerov, A. A. Pleve, S. M. Polikanov, et al., Nucl. Phys. A97, 444 (1967).

REF.	ELEM. SYM.	A	Z
Yu.A. Vinogradov, V.I. Kasilov, L.E. Lazareva, V.G. Nedorezov, N.V. Nikitina, N.M. Parovik, Yu.N. Ranyuk, P.V. Sorokin Yad. Fiz. 24, 686 (1976) Sov. J. Nucl. Phys. 24, 357 (1976)	Am	241	95

METHOD	REF. NO.
	76 Vi 2 hmg

REACTION	RESULT	EXCITATION ENERGY	SOURCE		DETECTOR		ANGLE
			TYPE	RANGE	TYPE	RANGE	
G,F	ABX	THR-999	C	50-999	SPK-I		4PI

999= 1.3 GEV

The 300-MeV and 2-GeV linear electron accelerators at the Physico-technical Institute, Academy of Sciences, Ukrainian SSR, have been used to measure the yields of fragments from photofission for samples of ^{241}Am, ^{243}Am, and ^{235}U in bombardment by bremsstrahlung with various maximum energies $E_{\gamma max}$ in the intervals 50–300 and 300–1300 MeV. The relative fissilities of the nuclei have been obtained. Photofission cross-section curves calculated from the experimental data for ^{241}Am and ^{243}Am are compared with the total cross section for hadronic absorption of γ rays by these nuclei in the energy range investigated.

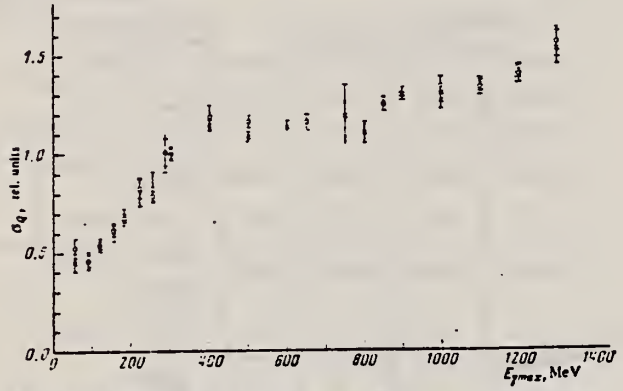

FIG. 2. Relative photofission cross sections σ_Q per equivalent quantum, obtained for the isotopes ^{241}Am (×) and ^{243}Am (○) in the energy range $E_{\gamma max}$ = 55–1300 MeV.

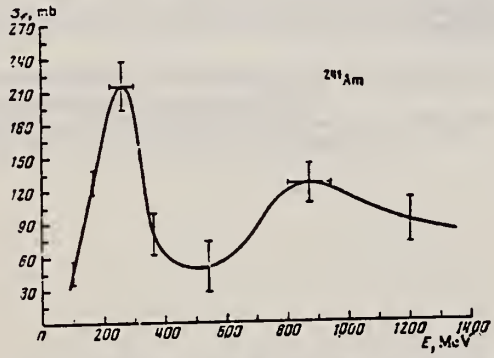

FIG. 4. Photofission cross section of the isotope ^{241}Am for γ rays with energies 50–1300 MeV, calculated from the curve in Fig. 2 for a photon spectrum ~ $1/E$.

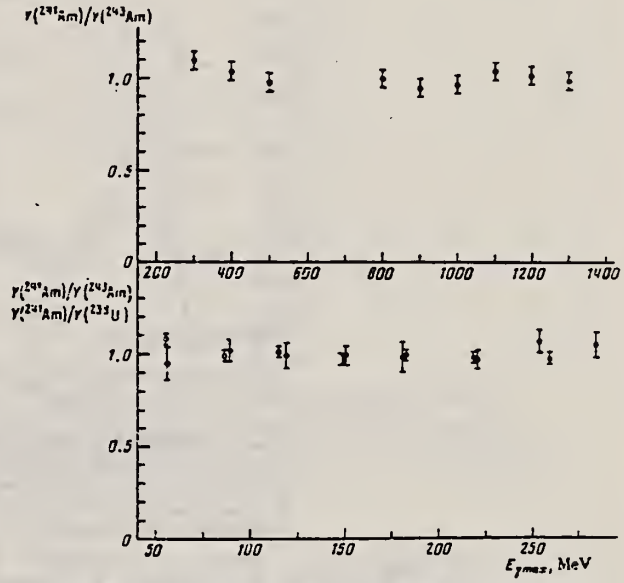

FIG. 3. Ratios of fission fragment yields $Y(^{241}Am)/Y(^{243}Am)$ (●) and $Y(^{241}Am)/Y(^{235}U)$ (○) for various bremsstrahlung maximum energies $E_{\gamma max}$ in the range 50–300 and 300–1300 MeV. The values shown are experimental values of the ratios divided by the arithmetic mean for these ratios in this interval of energies $E_{\gamma max}$.

(over)

TABLE I. Yield ratios Y_f for photofission fragments (per unit dose, per gram-atom) obtained in irradiation of samples of ^{238}U, ^{241}Am, and ^{243}Am by bremsstrahlung with maximum energies $E_{\gamma max} = 14.5$, 16.6, 30, 39, and 56 MeV.

$E_{\gamma max}$, MeV	$Y_f(^{241}Am)/Y_f(^{238}U)$	$Y_f(^{243}Am)/Y_f(^{238}U)$	$Y_f(^{243}Am)/Y_f(^{241}Am)$
14.5	2.32±0.08 (0.15)	2.50±0.10 (0.22)	0.97±0.03 (0.06)
16.6	2.18±0.07 (0.14)	2.65±0.12 (0.23)	0.82±0.03 (0.06)
30	1.93±0.03 (0.12)	2.25±0.05 (0.17)	0.86±0.02 (0.05)
39	1.84±0.02 (0.11)	2.02±0.04 (0.15)	0.91±0.02 (0.06)
56	1.71±0.02 (0.10)	1.99±0.04 (0.15)	0.86±0.02 (0.05)

Note. 1) In the irradiations in the LU-50 MeV accelerator the diameters of the samples were less than the size of the γ-ray beam, and therefore in calculation of the ratios presented in this case we used the ratios of the total weights of the corresponding layers. 2) In order to separate the behavior of the measured ratios with change of the energy $E_{\gamma max}$, we have given above only the statistical errors. The errors taking into account the uncertainty in determination of the sample weight, which are systematic in this case, are given in parentheses. 3) The weight of the ^{243}Am layer was determined less reliably and may turn out to be ~10% higher. The ratio $Y_f(^{241}Am)/Y_f(^{243}Am)$ in this case is increased by 10%, and $Y_f(^{243}Am)/Y_f(^{238}U)$ is correspondingly decreased by 10%.

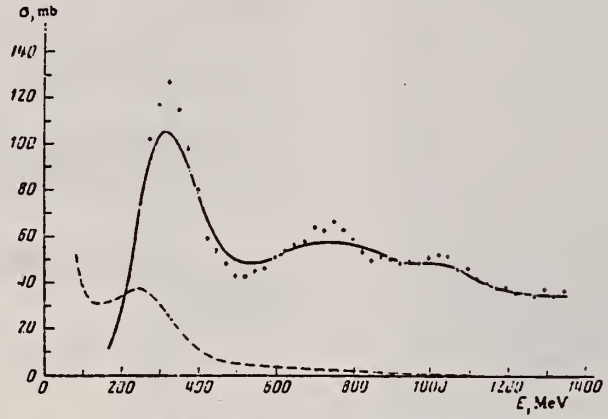

FIG. 6. Quasideuteron cross section $\sigma_{qd} = 10.3(ZN/A)\sigma(\gamma + d \to p + n)$, calculated for the ^{241}Am nucleus (dashed curve); the total hadronic cross section for hydrogen $\sigma_{\gamma p}$ measured in Ref. 22, multiplied by $A = 241$ (points); the total hadronic absorption cross section for γ rays $A\sigma_{\gamma p}$ for ^{241}Am (solid curve).

REF. B.M. Aleksandrov, A.S. Krivokhatskii, V.L. Kuznetsov, L.E. Lazareva, V.G. Nedorezov, N.V. Nikitina, Yu.N. Ranyuk
Yad. Fiz. 28, 1165 (1978)
Sov. J. Nucl. Phys. 28, 600 (1978)

ELEM. SYM.	A	Z
Am	241	95

METHOD

REF. NO. 78 A1 5 hg

REACTION	RESULT	EXCITATION ENERGY	SOURCE TYPE	SOURCE RANGE	DETECTOR TYPE	DETECTOR RANGE	ANGLE
G,F	RLY	THR-999	C	100-999	TRK-D		4PI

The 300- and 2000-MeV electron linear accelerators have been used to measure the relative fissilities of the nuclei ^{235}U, ^{238}U, ^{237}Np, ^{239}Pu, ^{241}Am, and ^{243}Am. Fragments were detected by glass detectors. Photofission yields were obtained for the nuclei indicated at maximum bremsstrahlung energies 100, 240, 400, and 1200 MeV.

999=1.2 GEV

PACS numbers: 25.85.Jg

TABLE I. Relative photofission yields for $E_{\gamma\,max}$=100, 240, 400, and 1200 MeV.

Nucleus	Fissility of nuclei in the excitation-energy range ~9–12 MeV: $D_f = \Gamma_f/(\Gamma_f + \Gamma_n)$	Relative fissility	Ratios of fragment yields $Y/Y(^{238}U)$ for different maximum energies $E_{\gamma max}$: 100 MeV	240 MeV	400 MeV	1200 MeV
^{235}U	0.38(b)	1.45(a) 1.38(b) 2.15(f)	2.22±0.16	2.15±0.15	1.79±0.13	1.74±0.12
^{238}U	0.22±0.01 *	1.00	1.00	1.00	1.00	1.00
^{237}Np	0.51(b) 0.53(d)	2.33(b) 2.16(c) 2.34(d) 2.93(f)	1.89±0.14	1.92±0.13	1.67±0.12	1.61±0.10
^{239}Pu	0.70(b)	2.70(a) 3.51(b) 3.51(e) 3.45(f)	2.10±0.15	2.10±0.13	1.80±0.13	1.53±0.12
^{241}Am	0.53(e)	1.68(c) ** 2.42(e) 3.27(f)	1.91±0.14	1.77±0.13	1.48±0.10	1.44±0.10
^{243}Am	0.62(e)	2.80(e) 2.59(f)	1.81±0.13	1.81±0.13	1.53±0.11	1.44±0.10

Note. *a*, *b*, *c*, *d*, and *e* denote that the data have been taken respectively from the photofission studies of Refs. 16, 17, 18, 19, and 15. *f* are the average values for the data of a given study on fission by neutrons[20] at nuclear excitation energy ~8 MeV.

*The number given is an average over the results of a large number of studies on photofission of ^{238}U.

**The authors of Ref. 18 point out that the value obtained by them for ^{241}Am is obviously underestimated.

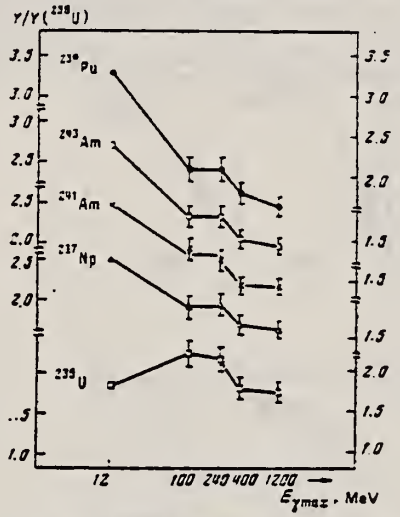

FIG. 2. Relative yields $Y/Y(^{238}U)$ for the nuclei ^{235}U (□), ^{237}Np (△), ^{239}Pu (●), ^{241}Am (×), and ^{243}Am (○) for maximum bremsstrahlung energies $E_{\gamma max}$ ~12, 100, 240, 400, and 1200 MeV.

[15]Yu. A. Vinogradov, V. I. Kasilov, L. E. Lazareva, V. G. Nedorezov, N. V. Nikitina, N. M. Parovik, Yu. N. Ranyuk, and P. V. Sorokin. Yad. Fiz. 24. 686 (1976) Sov. J. Nucl. Phys. 24, 357 (1976).
[16]J. McElhinney and W. E. Ogle, Phys. Rev. 81, 342 (1951).
[17]J. R. Huizenga, Phys. Rev. 109, 484 (1958).
[18]L. Katz, A. P. Baerg, and F. Brown, Proc. of the Second Intern. Conf. on the Peaceful Uses of Atomic Energy, Geneva, 1958, United Nations, Geneva, 1958, Vol. 15. p. 200.
[19]A. Veyssiere, H. Beil, R. Bergere, P. Carlos, A. Lepretre, and K. Kernbath, Nucl. Phys. A199. 45 (1973).

REF. V.E. Zhuchko, Yu.B. Ostapenko, G.N. Smirenkin, A.S. Soldatov, Yu.M. Tsipenyuk
Yad. Fiz. 28, 1170 (1978)
Sov. J. Nucl. Phys. 28, 602 (1978)

ELEM. SYM.	A	Z
Am	241	95

METHOD

REF. NO. 78 Zh 7 hg

REACTION	RESULT	EXCITATION ENERGY	SOURCE		DETECTOR		ANGLE
			TYPE	RANGE	TYPE	RANGE	
G,F	ABX	THR-7	C	4-7	TRK-D		4PI
				(4.4-7.)			

The bremsstrahlung beam of the microtron at our Institute has been used to measure photofission yields of nine nuclei—^{232}Th, ^{233,235,236,238}U, ^{237}Np, ^{239,241}Pu, and ^{241}Am in the energy region 4.4–7.0 MeV. The method of minimization of the directed deviation was used to reproduce the photofission cross sections from the integrated yields. The following problems are discussed in terms of the experimental data: resonance structure of the cross sections, effects of a two-humped shape of the fission barrier, and comparison of the fissility in the (γ,f) and (n,f) reactions and in direct reactions.

PACS numbers: 25.85.Jg

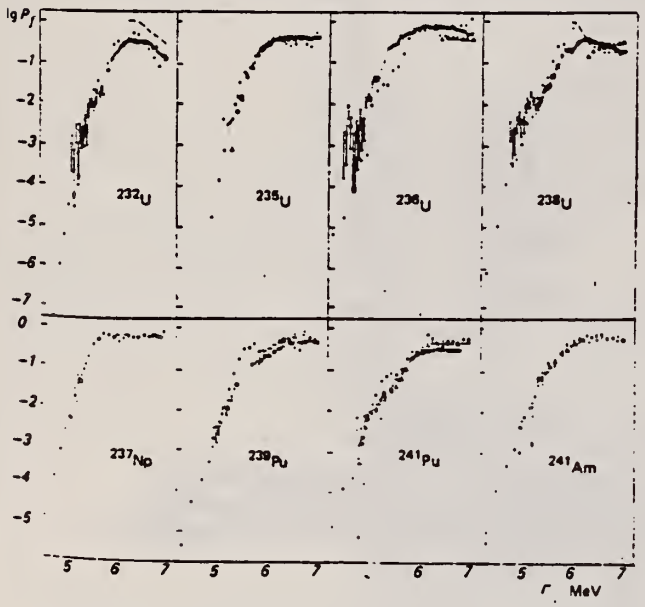

FIG. 4. Fissility P_f in the reactions (γ,f)—●, (n,f)—△ (Ref. 14), and in direct reactions—○.[2] The dashed curve shows the results of evaluation of P_f in accordance with Eq. (9).

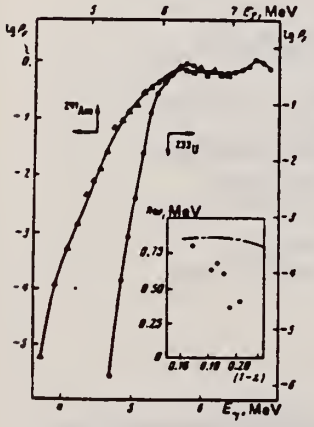

FIG. 8. Comparison of energy dependences of the fissilities of ^{233}U and ^{241}Am. In the insert is a comparison of the effective curvature parameters (10) (points) with calculations according to the liquid-drop model[25] (dot-dash curve).

(over)

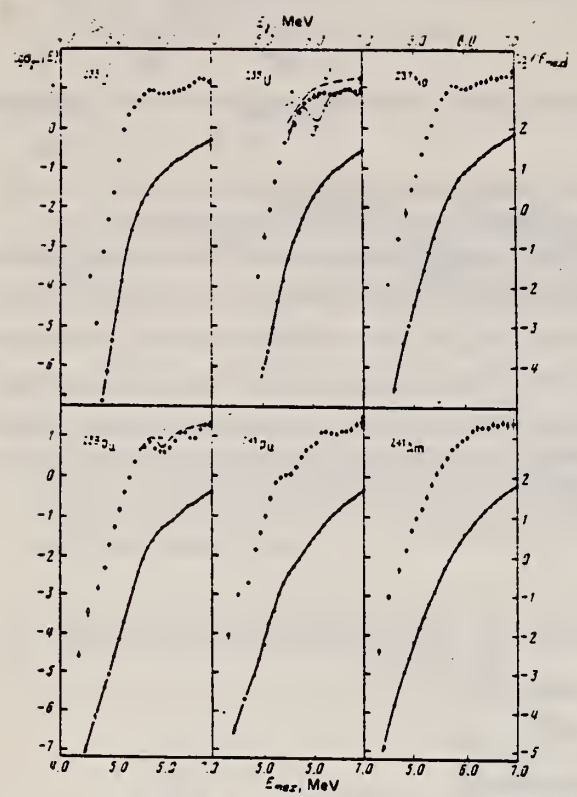

FIG. 3. Yields $Y(E_{max})$, fissions/mg-μC, and cross sections $\sigma_{\gamma f}(E_\gamma)$, mb, for odd isotopes. The designations are the same as in Fig. 2.

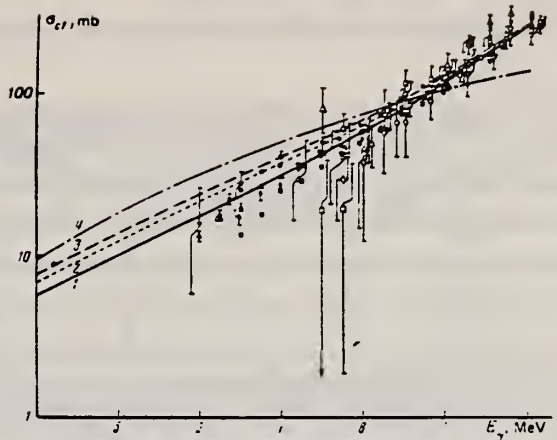

FIG. 6. Set of data on dipole photoabsorption cross sections σ_{c1}. The solid line (1)—the present work—is the result of fitting the data of Ref. 6 by Eq. (2) in the region $E_\gamma = 6$–10 MeV. Curves 2 and 3 are an extrapolation of the fit from Ref. 16 (2) and Ref. 17 (3) for ^{238}U; curve 4 is an estimate by means of Axel's formula.[15] Points: □, ■—^{232}Th; △, ▲—^{235}U; ♦—^{236}U; ○, ●—^{238}U; ▽, ▼—^{237}Np; ◇—^{239}Pu. The hollow points are from Refs. 16 and 17; the solid points are from Ref. 6.

REF. I.S. Koretskaya, V.L. Kuznetsov, L.E. Lazareva, V.G. Nedorezov, N.V. Nikitina
Yad. Fiz. 30, 910 (1979)
Sov. J. Nucl. Phys. 30, 472 (1979)

ELEM. SYM.	A	Z
Am	241	95

METHOD

REF. NO. 79 Ko · 9 hg

REACTION	RESULT	EXCITATION ENERGY	SOURCE		DETECTOR		ANGLE
			TYPE	RANGE	TYPE	RANGE	
G,F	ABX	THR-26	C	7-26	SPK-D		Ø

A 35-MeV synchrotron has been used to measure photofission yields in the range of bremsstrahlung maximum energy $E_{\gamma max} = 7$–26 MeV for samples of ^{241}Am and ^{243}Am. The fission fragments were detected by multiwire spark counters. From the yield curves we have obtained the fission cross sections and fissilities of ^{241}Am and ^{243}Am in the region of the $E1$ giant resonance.

PACS numbers: 25.85.Jg, 24.30.Cz, 27.90. + b

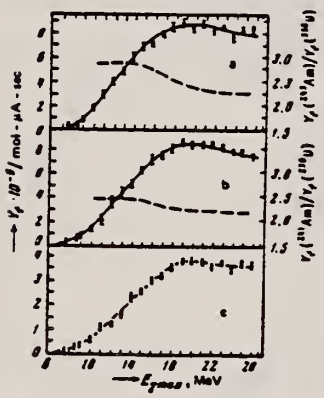

FIG. 1. Photofission yields of ^{238}U (a), ^{241}Am (b), and ^{243}Am (c) for various maximum energies $E_{\gamma\ max}$. The dashed lines show the yield ratios $Y_f(^{241}\text{Am})/Y_f(^{238}\text{U})$ and $Y_f(^{241}\text{Am})/Y_f(^{238}\text{U})$ (right-hand scale).

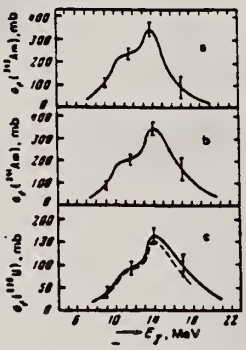

FIG. 2. Photofission cross sections of ^{238}U (a), ^{241}Am (b), and ^{243}Am (c) in the region of the $E1$ giant resonance. In Fig. a the dashed line shows the σ_f curve measured for ^{238}U in Ref. 9.

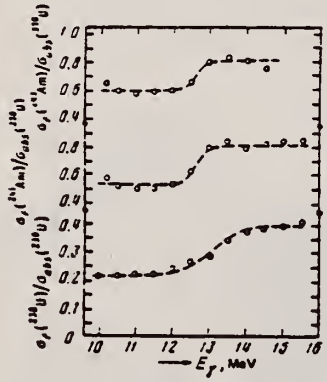

FIG. 4. Fissilities D_f of the nuclei ^{238}U, ^{241}Am, and ^{243}Am in the region of the peak of the $E1$ giant resonance.

REF. V. L. Kuznetsov, L. E. Lazareva, V. G. Nedorezov, N. V. Nikitina, N. M. Parovic
Nucl. Phys. A324, 29 (1979)

ELEM. SYM.	A	Z
Am	241	95

METHOD

REF. NO. 79Ku3 hg

REACTION	RESULT	EXCITATION ENERGY	SOURCE		DETECTOR		ANGLE
			TYPE	RANGE	TYPE	RANGE	
G,F	ABY	THR-80	C	10-80	SPK-I		4PI

Abstract: The ratio of delayed to prompt fission yields has been measured for ^{241}Am and ^{243}Am samples irradiated by a bremsstrahlung photon pulsed beam over the energy range $E_{\gamma max}$ = 10–80 MeV. The relative probabilities of ^{240mf}Am and ^{242mf}Am isomer production and the cross sections of the ^{241}Am(γ, n)^{240mf}Am and ^{243}Am(γ, n)^{242mf}Am reactions were deduced from the yields measured in the El giant resonance region.

DELAYED/PROMPT F YLD

E NUCLEAR REACTIONS, FISSION ^{241}Am, ^{243}Am(γ, F), E = 10–80 MeV bremsstrahlung; measured isomer/prompt yield ratio; deduced production σ for ^{240mf},^{242mf}Am. Enriched targets.

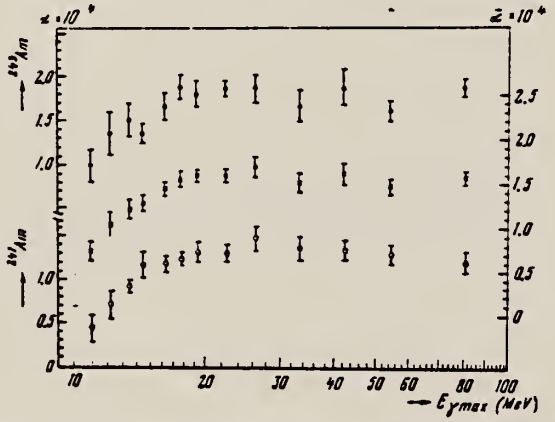

Fig. 2. Ratio (x) of the ^{240mf}Am and ^{242mf}Am isomer yields to the prompt fission yields of ^{241}Am and ^{243}Am, respectively, for various bremsstrahlung limiting energies over the range from ≈ 10–80 MeV. The crosses are the mean values $\bar{x} = \frac{1}{2}[x(^{241}\text{Am}) + x(^{243}\text{Am})]$ (right scale).

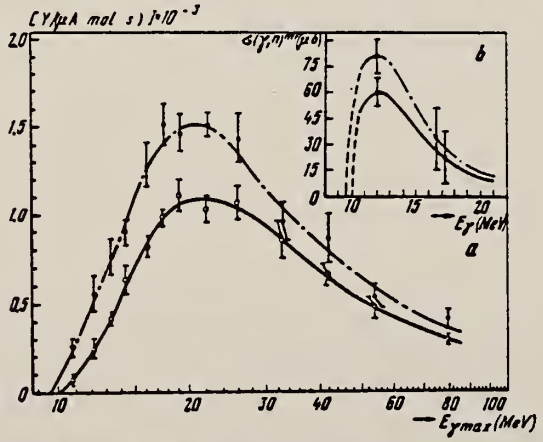

Fig. 3. (a) Yields of ^{240mf}Am and ^{242mf}Am isomers as a function of $E_{\gamma max}$, rms error bars are shown. (b) Cross sections of ^{241}Am(γ, n)^{240mf}Am and ^{243}Am(γ, n)^{242mf}Am calculated from smoothed yield curves shown in fig. 3a.

Am
A=243

Am
A=243

REF. Yu. P. Gangrskii, B.N. Markov, and Yu. M. Tsipenyuk
Yad. Fiz. 11, 54 (1970)
Sov. J. Nucl. Phys. 11, 30 (1970)

ELEM. SYM.	A	Z
Am	243	95

METHOD

REF. NO. 70 Ga 1 hmg

REACTION	RESULT	EXCITATION ENERGY	SOURCE		DETECTOR		ANGLE
			TYPE	RANGE	TYPE	RANGE	
G,NF	THR	THR-14	C	10-13	SPK-D		4PI

PROMPT AND DELAYED F

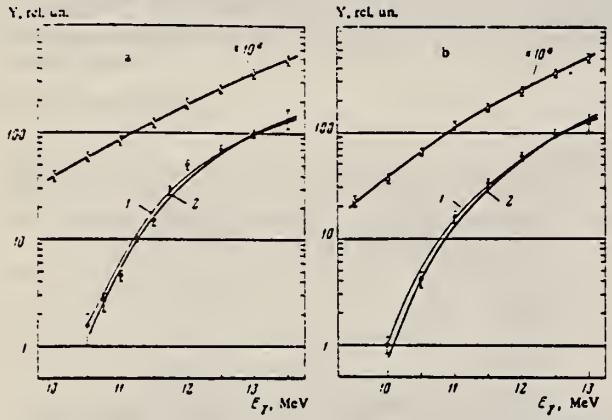

FIG. 2. Yield (Y) of prompt (○) and delayed (○) fission fragments as a function of bremsstrahlung end-point energy (E_γ) in bombardment of: a–Am^{241}, b–Am^{243}. Curves 1 were calculated for T = 0.7 MeV, and curves 2 for T = 1.5 MeV.

By combining the delayed fission fragment yields calculated in this way as a function of γ-ray energy with the experimental data (see Figs. 2a and b), we can determine the thresholds of the reactions leading to spontaneously fissile isomers. These thresholds turned out to be 9.95 ± 0.15 MeV for the reaction $Am^{241}(\gamma, n)Am^{240mf}$ and 9.55 ± 0.15 MeV for the reaction $Am^{243}(\gamma, n)Am^{242mf}$. The thresholds of the reactions leading to the ground states of Am^{240} and Am^{242} obviously are equal to the neutron binding energies in these nuclei, which are respectively 6.70 ± 0.20 and 6.27 ± 0.03 MeV.[8] The difference in the thresholds can evidently be considered as the excitation energy of the isomeric states, which is equal to 3.25 ± 0.25 MeV for Am^{240mf} and 3.30 ± 0.20 MeV for Am^{242mf}. Both these results agree within experimental error with the previously measured excitation energies, which are respectively 3.15 ± 0.25 MeV (Am^{240mf}[3]) and 2.9 ± 0.4 MeV (Am^{242mf}[9]).

In our work we measured also the yield ratios of delayed and prompt fission fragments, which turned out to be $(4 \pm 1) \times 10^{-4}$ for Am^{241} for a γ-ray energy of 13 MeV and $(7 \pm 2) \times 10^{-4}$ for Am^{243} for an energy of 12.5 MeV. By means of Eq. (1) we obtained the following ratios of cross sections for these energies: $(1.0 \pm 0.25) \times 10^{-3}$ for Am^{241} and $(1.3 \pm 0.4) \times 10^{-3}$ for Am^{243}. Knowing the value of the Am^{241} photofission cross section,[6] we can determine the cross section for formation of the isomer Am^{240mf}, which turned out to be 150 ± 40 μb. If we use the value $\Gamma_f/(\Gamma_n + \Gamma_f) = 0.32$,[6] then the isomeric ratio for the reaction $Am^{241}(\gamma, n)Am^{240}$ will be $(5 \pm 1.2) \times 10^{-4}$, which is close to the values obtained in reactions with charged particles and neutrons. In the case of Am^{242mf}, detailed calculation of the isomeric ratio is impossible because of the lack of absolute values of σ_f and $\Gamma_f/(\Gamma_n + \Gamma_f)$.

[3] S. Bjørnholm, J. Borggreen, L. Westgaard, and V.A. Karanukhov, Nucl. Phys. A95, 513 (1967).
[6] L. Katz, A.P. Baerg, and F. Brown, PUAE, 15, 188 (P/200), 1958.
[8] J. H. E. Mattauch, W. Thiele, and A. H. Wapstra, Nucl. Phys. 67, 1 (1965).
[9] G. N. Flerov, A. A. Pleve, S. M. Polikanov, et al., Nucl. Phys. A97, 444 (1967).

REF. Yu.A. Vinogradov, V.I. Kasilov, L.E. Lazareva, V.G. Nedorezov, N.V. Nikitina, N.M. Parovik, Yu.N. Ranyuk, P.V. Sorokin
Yad. Fiz. 24, 686 (1976)
Sov. J. Nucl. Phys. 24, 357 (1976)

ELEM. SYM.	A	Z
Am	243	95

METHOD

REF. NO. 76 Vi 2 hmg

REACTION	RESULT	EXCITATION ENERGY	SOURCE TYPE	SOURCE RANGE	DETECTOR TYPE	DETECTOR RANGE	ANGLE
G,F	ABX	THR-999	C	50-999	SPK-I		4PI

The 300-MeV and 2-GeV linear electron accelerators at the Physico-technical Institute, Academy of Sciences, Ukrainian SSR, have been used to measure the yields of fragments from photofission for samples of ^{241}Am, ^{243}Am, and ^{235}U in bombardment by bremsstrahlung with various maximum energies $E_{\gamma\,max}$ in the intervals 50–300 and 300–1300 MeV. The relative fissilities of the nuclei have been obtained. Photofission cross-section curves calculated from the experimental data for ^{241}Am and ^{243}Am are compared with the total cross section for hadronic absorption of γ rays by these nuclei in the energy range investigated.

999= 1.3 GEV

TABLE I. Yield ratios Y_f for photofission fragments (per unit dose, per gram-atom) obtained in irradiation of samples of ^{238}U, ^{241}Am, and ^{243}Am by bremsstrahlung with maximum energies $E_{\gamma max}$=11.5, 16.6, 30, 39, and 56 MeV.

$E_{\gamma\,max}$, MeV	$Y_f(^{241}Am)/Y_f(^{238}U)$	$Y_f(^{243}Am)/Y_f(^{238}U)$	$Y_f(^{241}Am)/Y_f(^{243}Am)$
11.5	2.42±0.03 (0.15)	2.80±0.10 (0.22)	0.87±0.03 (0.06)
16.6	2.18±0.07 (0.14)	2.65±0.12 (0.22)	0.82±0.03 (0.06)
30	1.93±0.03 (0.12)	2.25±0.05 (0.17)	0.86±0.02 (0.05)
39	1.84±0.02 (0.11)	2.02±0.04 (0.15)	0.91±0.02 (0.06)
56	1.71±0.02 (0.10)	1.99±0.04 (0.15)	0.86±0.02 (0.05)

Note. 1) In the irradiations in the LU-50 MeV accelerator the diameters of the samples were less than the size of the γ-ray beam, and therefore in calculation of the ratios presented in this case we used the ratios of the total weights of the corresponding layers. 2) In order to separate the behavior of the measured ratios with change of the energy $E_{\gamma max}$, we have given above only the statistical errors. The errors taking into account the uncertainty in determination of the sample weight, which are systematic in this case, are given in parentheses. 3) The weight of the ^{243}Am layer was determined less reliably and may turn out to be ~10% higher. The ratio $Y_f(^{241}Am)/Y_f(^{243}Am)$ in this case is increased by 10%, and $Y_f(^{243}Am)/Y_f(^{238}U)$ is correspondingly decreased by 10%.

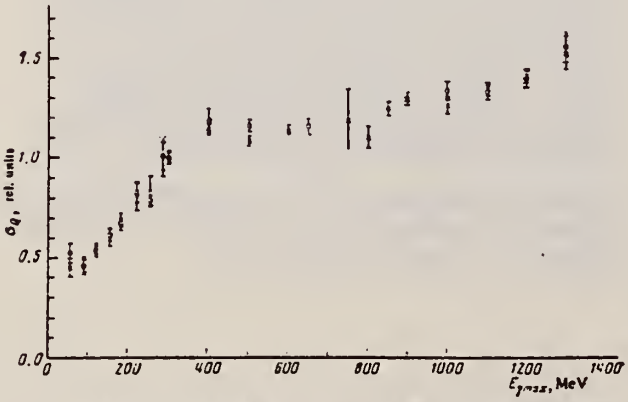

FIG. 2. Relative photofission cross sections σ_Q per equivalent quantum, obtained for the isotopes ^{241}Am (×) and ^{243}Am (○) in the energy range $E_{\gamma max}$=55–1300 MeV.

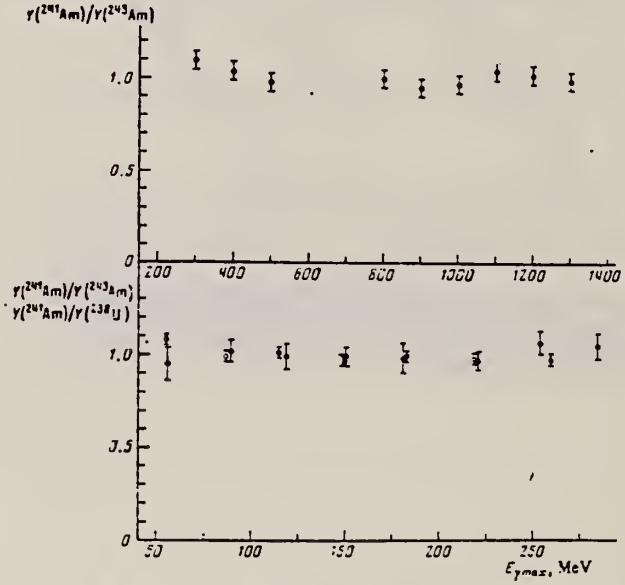

FIG. 3. Ratios of fission fragment yields $Y(^{241}Am)/Y(^{243}Am)$ (●) and $Y(^{241}Am)/Y(^{238}U)$ (○) for various bremsstrahlung maximum energies $E_{\gamma max}$ in the range 50–300 and 300–1300 MeV. The values shown are experimental values of the ratios divided by the arithmetic mean for these ratios in this interval of energies $E_{\gamma max}$.

REF. B.M. Aleksandrov, A.S. Krivokhatskii, V.L. Kuznetsov, L.E. Lazareva, V.G. Nedorezov, N.V. Nikitina, Yu.N. Ranyuk
Yad. Fiz. 28, 1165 (1978)
Sov. J. Nucl. Phys. 28, 600 (1978)

ELEM. SYM.	A	Z
Am	243	95

METHOD

REF. NO. 78 A1 5 hg

REACTION	RESULT	EXCITATION ENERGY	SOURCE TYPE	SOURCE RANGE	DETECTOR TYPE	DETECTOR RANGE	ANGLE
G,F	RLY	THR-999	C	100-999	TRK-D		4PI

The 300- and 2000-MeV electron linear accelerators have been used to measure the relative fissilities of the nuclei ^{235}U, ^{238}U, ^{237}Np, ^{239}Pu, ^{241}Am, and ^{243}Am. Fragments were detected by glass detectors. Photofission yields were obtained for the nuclei indicated at maximum bremsstrahlung energies 100, 240, 400, and 1200 MeV.

999=1.2 GEV

PACS numbers: 25.85.Jg

TABLE I. Relative photofission yields for $E_{\gamma max}$=100, 240, 400, and 1200 MeV.

Nucleus	Fissility of nuclei in the excitation-energy range ~5–12 MeV: $D_f = \Gamma_f/(\Gamma_f + \Gamma_n)$	Relative fissility	Ratios of fragment yields $Y/Y(^{238}U)$ for different maximum energies $E_{\gamma max}$: 100 MeV	240 MeV	400 MeV	1200 MeV
^{235}U	0.38(b)	1.45(a) 1.88(b) 2.15(f)	2.22±0.16	2.15±0.15	1.79±0.13	1.74±0.12
^{238}U	0.22±0.01 *	1.00	1.00	1.00	1.00	1.00
^{237}Np	0.51(b) 0.53(d)	2.33(b) 2.16(c) 2.34(d) 2.93(f)	1.89±0.14	1.92±0.13	1.67±0.12	1.61±0.10
^{239}Pu	0.70(b)	2.70(a) 3.51(b) 3.51(c) 3.45(f)	2.10±0.15	2.10±0.15	1.80±0.13	1.63±0.12
^{241}Am	0.53(e)	1.68(c) ** 2.42(e) 3.27(f)	1.91±0.14	1.77±0.13	1.48±0.10	1.44±0.10
^{243}Am	0.62(e)	2.80(e) 2.59(f)	1.81±0.13	1.81±0.13	1.53±0.11	1.44±0.10

Note. *a*, *b*, *c*, *d*, and *e* denote that the data have been taken respectively from the photofission studies of Refs. 16, 17, 18, 19, and 15. *f* are the average values for the data of a given study on fission by neutrons[20] at nuclear excitation energy ~8 MeV.

*The number given is an average over the results of a large number of studies on photofission of ^{238}U.

**The authors of Ref. 18 point out that the value obtained by them for ^{241}Am is obviously underestimated.

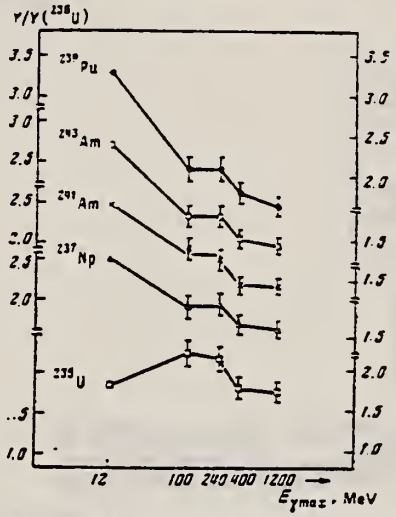

FIG. 2. Relative yields $Y/Y(^{238}U)$ for the nuclei ^{235}U (□), ^{237}Np (△), ^{239}Pu (●), ^{241}Am (×), and ^{243}Am (○) for maximum bremsstrahlung energies $E_{\gamma max}$ ~12, 100, 240, 400, and 1200 MeV.

[15]Yu. A. Vinogradov, V. I. Kasilov, L. E. Lazareva, V. G. Nedorezov, N. V. Nikitina, N. M. Parovik, Yu. N. Ranyuk, and P. V. Sorokin. Yad. Fiz. 24, 686 (1976) Sov. J. Nucl. Phys. 24, 357 (1976).
[16]J. McElhinney and W. E. Ogle, Phys. Rev. 81, 342 (1951).
[17]J. R. Huizenga, Phys. Rev. 109, 484 (1958).
[18]L. Katz, A. P. Baerg, and F. Brown, Proc. of the Second Intern. Conf. on the Peaceful Uses of Atomic Energy, Geneva, 1958, United Nations, Geneva, 1958, Vol. 15, p. 200.
[19]A. Veyssiere, H. Beil, R. Bergere, P. Carlos, A. Lepretre, and K. Kernbath, Nucl. Phys. A199, 45 (1973).

REF. I.S. Koretskaya, V.L. Kuznetsov, L.E. Lazareva, V.G. Nedorezov, N.V. Nikitina
Yad. Fiz. 30, 910 (1979)
Sov. J. Nucl. Phys. 30, 472 (1979)

ELEM. SYM.	A	Z
Am	243	95

METHOD

REF. NO. 79 Ko 11 hg

REACTION	RESULT	EXCITATION ENERGY	SOURCE		DETECTOR		ANGLE
			TYPE	RANGE	TYPE	RANGE	
G,F	ABX	THR-26	C	7-26	SPK-D		Ø

A 35-MeV synchrotron has been used to measure photofission yields in the range of bremsstrahlung maximum energy $E_{\gamma max} \approx 7$–26 MeV for samples of ^{241}Am and ^{243}Am. The fission fragments were detected by multiwire spark counters. From the yield curves we have obtained the fission cross sections and fissilities of ^{241}Am and ^{243}Am in the region of the $E1$ giant resonance.

PACS numbers: 25.85.Jg, 24.30.Cz, 27.90. + b

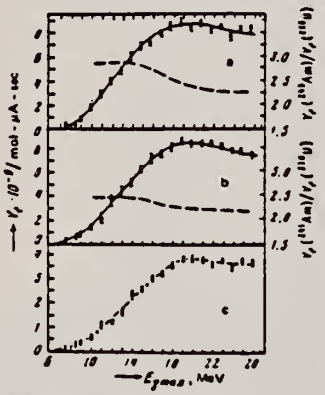

FIG. 1. Photofission yields of ^{238}U (a), ^{241}Am (b), and ^{243}Am (c) for various maximum energies $E_{\gamma\ max}$. The dashed lines show the yield ratios $Y_f(^{241}\text{Am})/Y_f(^{238}\text{U})$ and $Y_f(^{243}\text{Am})/Y_f(^{238}\text{U})$ (right-hand scale).

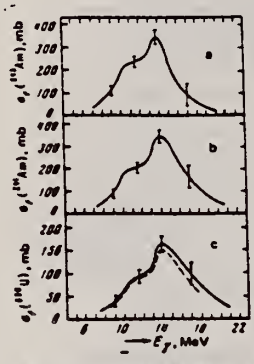

FIG. 2. Photofission cross sections of ^{238}U (a), ^{241}Am (b), and ^{243}Am (c) in the region of the $E1$ giant resonance. In Fig. a the dashed line shows the σ_f curve measured for ^{238}U in Ref. 9.

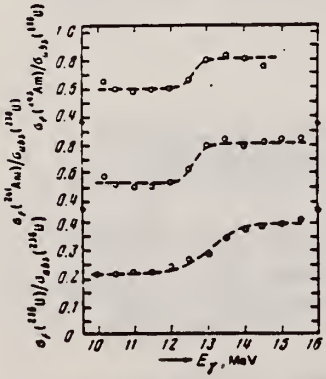

FIG. 4. Fissilities D_f of the nuclei ^{238}U, ^{241}Am, and ^{243}Am in the region of the peak of the $E1$ giant resonance.

REF. V. L. Kuznetsov, L. E. Lazareva, V. G. Nedorezov, N. V. Nikitina, N. M. Parovic
Nucl. Phys. A324, 29 (1979)

EL.EM. SYM.	A	Z
Am	243	95

METHOD

REF. NO. 79Ku3 hg

REACTION	RESULT	EXCITATION ENERGY	SOURCE TYPE	SOURCE RANGE	DETECTOR TYPE	DETECTOR RANGE	ANGLE
G,F	ABY	THR-80	C	10-80	SPK-I		4PI

Abstract: The ratio of delayed to prompt fission yields has been measured for ^{241}Am and ^{243}Am samples irradiated by a bremsstrahlung photon pulsed beam over the energy range $E_{\gamma max}$ = 10–80 MeV. The relative probabilities of ^{240mf}Am and ^{242mf}Am isomer production and the cross sections of the ^{241}Am(γ, n)^{240mf}Am and ^{243}Am(γ, n)^{242mf}Am reactions were deduced from the yields measured in the E1 giant resonance region.

DELAYED/PROMPT F YLD

E NUCLEAR REACTIONS, FISSION ^{241}Am, ^{243}Am(γ, F), E = 10–80 MeV bremsstrahlung; measured isomer/prompt yield ratio; deduced production σ for ^{240mf,242mf}Am. Enriched targets.

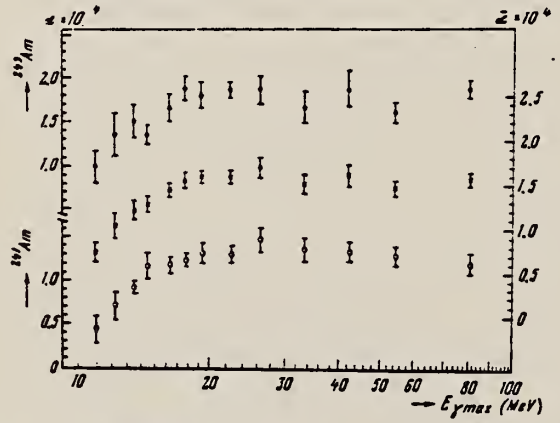

Fig. 2. Ratio (z) of the ^{240mf}Am and ^{242mf}Am isomer yields to the prompt fission yields of ^{241}Am and ^{243}Am, respectively, for various bremsstrahlung limiting energies over the range from ≈ 10–80 MeV. The crosses are the mean valucs $\bar{z} = \frac{1}{2}[z(^{241}\text{Am}) + z(^{243}\text{Am})]$ (right scale).

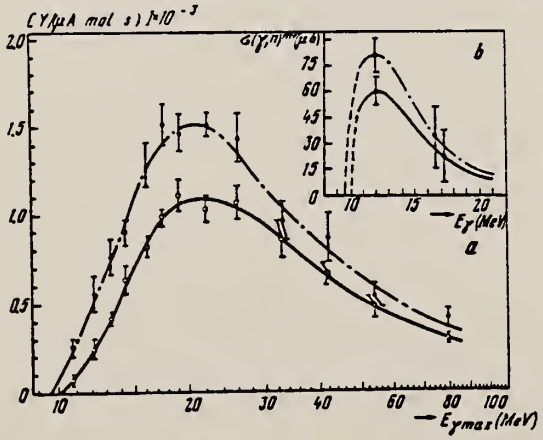

Fig. 3. (a) Yields of ^{240mf}Am and ^{242mf}Am isomers as a function of $E_{\gamma max}$, rms error bars are shown. (b) Cross sections of ^{241}Am(γ, n)^{240mf}Am and ^{243}Am(γ, n)^{242mf}Am calculated from smoothed yield curves shown in fig. 3a.

DEFINITIONS OF ABBREVIATIONS AND SYMBOLS

Note: In this list definitions are given for various photoneutron reactions in which the following symbols are used: N, NL, nN, SN and XN. Corresponding definitions apply for reactions involving other nuclear particles where the symbols N (neutron) is replaced by, e.g. P, D, T, HE, A etc. Where unknown reactions result in the production of a specific radionuclide, the chemical symbol and mass number is listed as the reaction product, e.g. a G,NA22 reaction in ^{59}Co.

A	alpha particle
ANAL	analysis
ABI	absolute integrated cross-section data
ABX	absolute cross-section data
ABY	absolute yield data. Often means cross-section per equivalent quantum is listed.
ACT	measurement of induced radioactivity of the target
ASM	asymmetric, asymmetry
AVG	average
BBL	bubble chamber
BEL B(EL)	reduced electric radiative transition probability
BF3	BF_3 neutron counter with moderator e.g., Halpern detector, long counter
BML	reduced magnetic radiative transition probability, B(ML)
BREAKS	levels located by "breaks" in the yield curve
BRKUP	breakup
BRMS	bremsstrahlung
BTW	between
C	continuous. Used to describe a photon source or a detector response function. Contrast with D = discrete.
CCH	cloud chamber
CF	compared with
CHRGD	charged
CMPT	Compton
COIN COINC	coincidence, coincide
COH	coherent
CK	Cerenkov
D	deuteron or discrete. When discrete, it is used to describe a photon source or a detector response function. Contrast with C = continuous.
DLTE	energy loss
DLTQ	momentum transfer
DST	distribution
DT BAL	detailed balance
E	electron
E/	inelastically scattered electron
E+	positron
EDST	energy distribution or spectrum
E/N	used only to indicate a coincidence experiment as in (E,E/N).

	N stands for any outgoing particle measured in coincidence with an inelastically scattered electron. Distinguish from eg., (E,N) which is used to represent an electron induced reaction when only the outgoing particle N is detected.
EMU	emulsions (photographic plates)
EXCIT	excited
F	fission
FMF	form factor
FM-1	inverse femtometers
FRAG	fragment
G	photon
G/	inelastically scattered photon
G-WIDTH	gamma-ray transition width
HAD	hadrons, hadron production
HE He3	^{3}He particle
INT	interaction, integral, intensity
INC	includes
ION	ionization chamber
ISOB	isobaric
ISM	isomer
J	multiplicity of particle defined by following symbol e.g. (G,PJN) with remark J = 2,3,5,7
JPI J-PI	spin and parity of a nuclear state
K	second multiplicity index, e.g. (G,JPKN) with both J & K positive integers greater than 1
KE	kinetic energy
L	may be an integer or zero that always follows a reaction product symbol. This is used to indicate transitions to specific states in the residual nuclide. When the letter is used as in (G,NL) the cross section given is that for the sum of transitions to two or more specific final states.
LFT	excited state lifetime
LIM	limit
LV,LVS	level, levels
LQD	liquid
MAG	magnetic spectrometer
MEAS	measurement(s)
MGC	magnetic Compton spectrometer
MGP	magnetic pair spectrometer
MOD	moderated neutron detector not employing a BF_3 counter, e.g. rhodium foil, Szilard-Chalmers reaction, ^{3}He, ^{6}Li reactions, GD loaded liquid scintillator, etc.
MSP	mass spectrometer
MULT	multiple, multipole, multiplicity
MU-T	used only in combination with G to indicate a total photon absorption cross section measurement, i.e. (G,MU-T)
N	neutron (see also XN and SN). The notation (G,N) is used to indicate a reaction in which only a single neutron is emitted, i.e. the reaction that can, in many cases, be measured by observing the radioactive decay of the residual nuclide.

nN	where n is any integer. (G,nN) indicates the sum over all reaction cross sections in which n neutrons are emitted.
NAI	NaI(Tl) spectrometer
NEUT	neutron(s)
NOX	no cross-section data
P	proton (see also XP)
PART	particle(s)
PHOT	photon(s)
PI	pion, usually written as PI+, PI-, PIO to indicate charge
POL	polarized or polarization
Q-SQUAR	momentum transfer squared (q^2)
RCL	recoil
REL	relative
RLI	relative integrated cross-section data
RLX	relative cross-section data
RSP	reaction spectrometer
RLY	relative yield data
SCTD	scattered
SCD	semiconductor (solid state) detector
SCI	scintillator detector other than NaI, e.g., CsI, KI, organic (liquid or solid), stilbene, He
SEP	separation
SEP ISOTP	separated isotope used
SIG	SIGMA (cross section)
SN	sum of neutron producing reactions, $\sigma(\gamma,SN)=\sigma(\gamma,N) + \sigma(\gamma,NP) + \sigma(\gamma,2N) + \sigma(\gamma,3N)$ + etc.
SPC	photon or particle energy spectrum
SPK	spark chamber
SPL	spallation
STAT	statistical
SYM	symetric, symmetry
T	triton
TEL	counter telescope
THR	threshold for reaction or threshold detector, e.g., $^{29}Si(n,p)^{29}Al$.
TOF	time-of-flight detector
TRK	tracks of particles or fragments observed in solid materials (glass, mylar, etc.)
TRNS	transition
UKN UNK	unknown
VIB	vibrational
VIR PHOT	virtual photon(s)
XN	all neutrons, total neutron yield, $\sigma(\gamma,XN) = \sigma(\gamma,N) + 2\sigma(\gamma,2N) + 3\sigma(\gamma,3N) + \sigma(\gamma,NP)$ + etc.
XP	all protons, total proton yield $\sigma(\gamma,XP) = \sigma(\gamma,P) + \sigma(\gamma,NP) + 2\sigma(\gamma,2P)$ + etc.
XX XXX	reaction products defined in REMARKS
YLD	yield

4PI	a 4π geometry was used or a method like radioactivity or a total absorption measurement
999	energy defined in REMARKS
$	indicates the measurement involved beams or targets that were either polarized or aligned, or that the polarization of the reaction products was determined. The polarized particle is indicated in REMARKS.
* or @	symbols used to indicate that the units associated with the numerals on one or both sides of the symbol in a specific column are not MeV. The units are defined in REMARKS.

NBS-114A (REV. 2-8C)

U.S. DEPT. OF COMM. BIBLIOGRAPHIC DATA SHEET (See instructions)	1. PUBLICATION OR REPORT NO.	2. Performing Organ. Report No.	3. Publication Date

4. TITLE AND SUBTITLE

Photonuclear Data-Abstract Sheets
1955-1982

5. AUTHOR(S)

E.G. Fuller and Henry Gerstenberg

6. PERFORMING ORGANIZATION (If joint or other than NBS, see instructions)

NATIONAL BUREAU OF STANDARDS
DEPARTMENT OF COMMERCE
WASHINGTON, D.C. 20234

7. Contract/Grant No.

8. Type of Report & Period Covered

9. SPONSORING ORGANIZATION NAME AND COMPLETE ADDRESS (Street, City, State, ZIP)

10. SUPPLEMENTARY NOTES

☐ Document describes a computer program; SF-185, FIPS Software Summary, is attached.

11. ABSTRACT (A 200-word or less factual summary of most significant information. If document includes a significant bibliography or literature survey, mention it here)

These abstract sheets cover most classes of experimental photonuclear data leading to information of the electromagnetic matrix element between the ground and excited states of a given nucleus. This fifteen volume work contains nearly 7200 abstract sheets and covers 89 chemical elements from hydrogen through americium. It represents a twenty-seven year history of the study of electromagnetic interactions. The sheets are ordered by target element, target isotope, and by an assigned bibliographic reference code. Information is given on the type of measurement, excitation energies studied, source type and energies, detector type, and angular ranges covered in the measurement. For a given reference, the relevant figures and tables are mounted on a separate sheet for each nuclide studied.

12. KEY WORDS (Six to twelve entries; alphabetical order; capitalize only proper names; and separate key words by semicolons)

data-abstract sheets, elements, experimental, isotopes, nuclear physics, photonuclear reactions

13. AVAILABILITY

☐ Unlimited

☒ For Official Distribution. Do Not Release to NTIS

☐ Order From Superintendent of Documents, U.S. Government Printing Office, Washington, D.C. 20402.

☐ Order From National Technical Information Service (NTIS), Springfield, VA. 22161

14. NO. OF PRINTED PAGES

15. Price

USCOMM-DC 6043-P80